THE EFFECTS OF STRUCTURE ON THE PROPERTIES OF AN ITALIAN PLEISTOCENE CLAY

by

FEDERICA COTECCHIA

Bsc, Msc, DIC

June 1996

A thesis submitted to the University of London
(Imperial College of Science, Technology and Medicine)
in partial fulfilment of the requirements for the degree of
Doctor in Philosophy in the Faculty of Engineering

To my father

Entities are not to be multiplied beyond necessity

William of Ockham

ABSTRACT

The prediction of the stress-strain response of natural clays can be derived from generalized models of behaviour if the role of the soil's structure is properly interpreted. The thesis provides a novel approach to the analysis of structural effects enabling both natural and reconstituted clays to be included within a general framework of soil behaviour. Two main types of structure are defined and a classification of clays is proposed which distinguishes clay types on the basis of their structure and behaviour.

Results are presented of an extensive laboratory and field investigation of a Pleistocene stiff clay in its natural and reconstituted states, including constant-rate-of-strain oedometer and triaxial tests. To investigate the complete framework of behaviour the stiff clay was studied over a wide stress range by means of high pressure apparatus built during the research. The geological history of the natural clay is reconstructed and results of scanning electron microscopy and chemical micro-analysis are used to illustrate the clay's structural features both before and after compression. The relationships between the clay's structure, its geological history and its mechanical behaviour are demonstrated.

The analysis of both the new data and existing data from the literature enable general patterns of stress-strain behaviour to be identified, demonstrating that clays follow common deformation mechanisms. Sensitivity is highlighted as the parameter quantifying the mechanical effects of structure giving rise to differences in behaviour. The analysis of one-dimensional consolidation according to a theory which allows for the strain-rate dependency of soils, demonstrates that clay's strain-rate dependency is not affected by structure. An analysis of the triaxial test results, which accounts for the effects of localization, shows that many aspects of the critical state framework apply to the natural clay. A frictional flow rule applies to both natural and reconstituted clays over a large range of strains including yield A new normalization of the data shows that up to yield the natural clay behaviour is isotropically hardening with both volume and change in structure. The parameters which normalize the clay behaviour with respect to volume and structure respectively are identified.

ACKNOWLEDGEMENTS

I would like to thank my supervisor Prof.R.J.Chandler for his faith in my work, his helpful suggestions and assistance throughout my PhD. His continuous reassurance and his not giving up with my "Italian" English allowed me to proceed with my research.

I express my gratitude also to Dr.M.R.Coop for his invaluable help which allowed me to understand the significance of a doctorate and for his help in solving the many problems which endangered my PhD during my periods in Bari. His support has always been precious to me. I also thank him and Prof.R.N.Taylor for lending me the load cell which I used in the CRS testing programme and for the use of the high pressure triaxial at City University.

To Prof. F.Veniale goes all my gratitude as his help and enthusiastic explanations let me enter the world of mineralogy and micro-morphology of clays. The SEM laboratories where the micro-analyses of Pappadai clay were carried out were : the CNR-SEM Laboratory at the Earth Science Department of Milan University, the SEM Laboratory at the Politecnico di Bari, directed by Prof.F.Zezza, the SEM Laboratory of the Faculty of Medicine of Bari University, directed by Prof.Mazzarella, and the SEM Laboratory of the University of East Anglia directed by Dr.K.Tovey. To Prof.Zezza, Mr.Macri', Prof.Mazzarella, Dr.Tovey and Mr.Bennet I express my gratitude.

A would also like to thank Prof.B.G.Clarke who came personally to supervise the Self Boring Pressuremeter testing for PM In Situ Techniques, and who took care of the data processing. The Self Boring Pressuremeter testing was sponsored by Cogefar Impresit, to whom I express my thanks.

Particular thanks go to Mr.S.Ackerley who helped me very much at the start of my research, revealing me all the tricks of laboratory electronics and apparatus set-up. His explanations have been precious also for my work in the laboratory in Bari. I am also grateful to Mr.A.Bolsher, Mr.G.Keefe and Mr.L.Spall for their technical support. I express my gratitude to Mr.T.Orlandi and Mr.S.Schiavone for their technical support in the laboratory in Bari, for their help with the index testing on Pappadai clays and supervising my tests while I was away. At the Istituto di Geologia Applicata e Geotecnica I express my thanks to Mrs.E.Carbone and Mrs.M.R.Paiano for their great help in the editing of the thesis, as well as to all the other members of staff who gave me support at this final stage of the work.

I am grateful to my friends at Imperial College who shared with me all the problems in the laboratory work and the worries in the development of the research. I will never forget my

friends Dennis Ganendra, Nasha Kovacevic, Fernando Marinho, Chris Menkiti, Esad Porovic and Marinos Skempas, who were with me since the start of the PhD, and Lidija Zdravkovic, Trevor Addenbrooke, Fiona Chow, Keiran Denean and Mohamed Barrakat who later joined the group. I will always be grateful to my friends Jamie Standing and Andrew Ridley who helped me at the start of the research, when I was lost in the laboratory; I express to them my sincere appreciation of their friendship.

Thanks are also due to my old friends Rocco Lagioia and Francesca Santaloia, who came to Imperial College and shared with me the problems of this split life between England and Italy, as well as giving me support every time I needed it.

I also thank Prof.R.Belviso who showed interest towards my work and understanding for my periods of leave from the Istituto di Geologia Applicata e Geotecnica.

There are no words to thank my mother and my sister for all the support they gave me in these five years, for their patience in coping with all my worries and needs. Finally I thank my father whose enthusiastic, rigorous and broad approach to the problems of Engineering Geology and Soil Mechanics and to the understanding of Earth Science will always be an example for me in my research work.

TABLE OF CONTENTS

	page
ABSTRACT	i
ACKNOWLEDGMENTS	iii
TABLE OF CONTENTS	v
LIST OF FIGURES	xiii
LIST OF TABLES	xxxii
LIST OF SYMBOLS AND ABBREVIATIONS	xxxiv
INTRODUCTION	1
ORGANIZATION OF THE THESIS	4
Chapter 1 Microstructure of clays and micro-behaviour	
1.1. Introduction	7
1.2. Clay minerals and particles	7
1.3. Interaction between clay particles and water	8
1.4. Interaction between clay particles	9
1.5. Soil structure and remoulding	10
1.6. Classification of fabrics	12
1.7. Fabrics of remoulded clays	14
1.8. Effects of the deposition conditions on the clay fabric	14
1.9. Effects of one-dimensional compression on the clay fabric	15
1.10. Other structural changes occurring during geological compaction	17
1.11. Proposed soil structure classification	18
Chapter 2 Mechanical behaviour of clays and proposals for a general behavioural framework	
2.1. Introduction	37
2.2. The behaviour of reconstituted clays	37
2.2.1. The Critical State Framework	37
2.2.2. The existence of a Critical State or state of permanence	39

2.2.3. The State Boundary Surface on the wet side of the framework 40
2.2.4. Shearing behaviour on the dry side of the framework 40
2.2.5. The total State Boundary Surface 41
2.2.6. Frictional behaviour of clay and the Cam Clay model 42
2.2.7. "Basically" frictional deformation 43
2.3. Strain softening and localization of strain on the dry side 44
2.3.1. The study of localization phenomena 45
2.4. Effects of structure on the behaviour of reconstituted Behaviour of low plasticity reconstituted soils 47
2.4.2. Behaviour of anisotropically consolidated reconstituted soils 48
2.4.3. Effects of ageing on the behaviour of reconstituted clays 49
2.5. Behaviour of natural clays 50
2.5.1. The sedimentation compression curve 51
2.5.2. Natural sedimentation compression curve and the ICL 52
2.5.3. A basic classification of clays 52
2.5.4. Construction of a Sensitivity framework 54
2.5.5. Compression behaviour of sensitive clays 57
2.5.6. The shearing behaviour of natural soft clays 58
2.5.7. The shearing behaviour of cemented soils 63
2.5.8. Suggestions for a general framework of behaviour 65
2.5.9. The shearing behaviour of stiff clays 67

Chapter 3 Geological characteristics and basic geotechnical properties of the Pappadai clays

3.1. Introduction 93
3.2. Geological background 93
3.3. In situ and laboratory investigations 95
3.4. Lithological and palaeontological interpretations 96
3.5. Physical and mineralogical properties 97
3.6. Mineralogy of the Pappadai clay 99
3.7. Microstructural features arising from the clay geological history 100
3.8. Pappadai: post-deposition history 101
3.8.1. Pappadai: the first two stages of the clay history 101

3.8.2. Pappadai: desiccation and shallow mechanical weathering 102
3.8.3. Modelling the history of the clay 103
3.9. Conclusions 106

Chapter 4 Measurement of the in situ stresses, shear moduli and undrained shear strengths of the Pappadai clays

4.1. Objectives of the in situ measurements 123
4.2. The self-boring pressuremeter test 123
4.3. Analysis of the SBP test data 125
4.3.1. Lateral stress σ_h 125
4.3.2. Shear modulus G 126
4.3.3. Undrained shear strength c_u 127
4.4. Equipment used at Pappadai 129
4.5. SBP testing at Pappadai 130
4.6. Test results 132
4.6.1. In situ horizontal stresses 132
4.6.2. In situ undrained shear strengths 133
4.6.3. In situ shear moduli 135
4.7. State history of the Pappadai clay 136
4.7.1. Present e-q-p' state of the clay in situ 136
4.7.2. Modelling the e-q-p' state history of Pappadai clay 137
4.7.3. Modelling σ'_h in the four stages of the clay history 138
4.8. Conclusions 144

Chapter 5 Volume-stress state and microstructure of the Pappadai clay

5.1. Introduction 191
5.2. Undisturbed sampling of Pappadai clay 191
5.3. In situ stress state and σ'_p of the undisturbed clay 192
5.4. Index properties and mineralogy of the natural clay 192
5.5. Storage of the undisturbed clay samples 192
5.6. Volume-stress state of the undisturbed clay samples 193

5.6.1. Volumetric state of the clay in the laboratory 193
5.6.2. e-w and S_r-w relationship of the natural clay 194
5.6.3. Measurements of suction by means of the filter paper technique 195
5.6.4. Measurements of suction in the triaxial apparatus 196
5.6.5. Suction measurements using the pressure plate apparatus 197
5.6.6. Measurements of the clay swelling pressure in the oedometer 197
5.6.7. Discussion of e-p_k data 197
5.7. Sampling state path 198
5.8. Reconstituted Pappadai clay 202
5.8.1. Reconstitution of the clay 202
5.8.2. Consolidation of the clay from slurry 203
5.9. Microstructure of the Pappadai clay 204
5.9.1. Investigation of the clay fabric by means of the SEM 204
5.9.2. Equipment and techniques used 205
5.9.3. Undisturbed clay - Results 206
5.9.4. Reconstituted clay - Results 210
5.10. Investigation of bonding 212
5.10.1.Macrostructure of the Pappadai clay after swelling 213
5.10.2.Chemical micro-analysis: Procedures 214
5.10.3.Chemical micro-analysis of the undisturbed clay: Results 214
5.10.4 Chemical micro-analysis to the reconstituted clay: Results 217
5.11. Conclusions 217

Chapter 6 Oedometric compression and consolidation behaviour of Pappadai clay

6.1. Introduction 293
6.1.1. Objectives of the oedometer testing programme 293
6.1.2. Testing programme 294
6.2. Apparatus and equipment used in the programme 295
6.2.1. Oedometer cells 295
6.2 2. Application of the vertical load 299
6.2.3. Measuring system 300
6.3. Testing Procedures 301
6.3.1. Procedures followed in the soil testing 301

6.3.2. Apparatus compliance 304
6.4. Processing the data: Methods used and Literature review 306
6.4.1. Corrections applied to the raw data 306
6.4.2. Terzaghi's analysis of consolidation 307
6.4.3. Limitations of the Terzaghi model 309
6.4.4. Wissa's analysis of consolidation 313
6.5. Discussion of the OED test results 315
6.5.1. Consolidation curves 316
6.5.2. Compression curves and yield stresses 317
6.5.3. Dependency of the state of the clay on strain-rate 318
6.5.4. Swelling data recorded in the OED tests 318
6.5.5. Oedometric stiffness in OED tests 319
6.5.6. Behaviour of the Pappadai clay during creep 319
6.5.7. State-paths during primary consolidation and strain-rate effects 320
6.5.8. Variation of M with strain-rate during primary consolidation 321
6.5.9. OED test c_v values and inconsistencies of Terzaghi's model 322
6.5.10.Permeability coefficients from the OED tests 323
6.5.11.OED test on reconstituted clay 323
6.6. Discussion of the CRS test results and comparison with the OED test results 324
6.6.1. Clay stiffness M_0 at the start of CRS loading 325
6.6.2. Strain rates in the CRS tests 325
6.6.3. Pore water pressure response in CRS compression 326
6.6.4. Janbu and Senneset's (1979) correction 327
6.6.5. Behaviour of the natural clay in the e-σ'_v -$d\varepsilon_v/dt$ and ε_v -σ'_v -$d\varepsilon_v/dt$ space 328
6.6.6. Reconstituted clay behaviour in the e-σ'_v-$d\varepsilon_v/dt$ and ε_v -σ'_v-$d\varepsilon_v/dt$ space 332
6.6.7. Comparison of the strain-rate dependency of natural and reconstituted clay 332
6.6.8. Yield of natural and reconstituted clay 333
6.6.9. Effects of swelling before compression on the compression behaviour of the natural clay 333
6.6.10.Oedometric stiffness 335
6.6.11.Compression indexes 337
6.6.12.Coefficient of consolidation 338

6.6.13.Coefficient of permeability 339
6.6.14.Swelling behaviour pre- and post-yield 341
6.6.15.State of the natural and reconstituted clay at high stresses 342
6.7. Framework for the oedometric compression behaviour of clays 343
6.7.1. Relationship between the geological history, the structure of the clay and its present state in the I_v-σ'_v plane 343
6.7.2. A general Sensitivity framework for clays 345
6.7.3. Sensitivity and structural stability of natural stiff clays 347
6.7.4. The basic mechanics of natural and reconstituted clays pre- and post-yield 347
6.7.5. Normalization of the oedometric stiffness of Pappadai clay 350

Chapter 7 Changes in the microstructure of the clay during oedometric compression

7.1. Introduction 447
7.2. Clay samples examined by means of the SEM 447
7.3. Fabric of natural clay after oedometric yield 448
7.4. Fabric of natural clay under very high stresses 450
7.5. Fabric of reconstituted clay after compression to very high stresses 453
7.6. Effects of oedometric compression on the mineralogy of the clay 454
7.7. Conclusions 455

Chapter 8 Pappadai clay: triaxial testing programme

8.1. Introduction 493
8.1.1. Objectives of the triaxial testing programme 493
8.1.2. Testing programme 494
8 2 Apparatus 496
8.2.1. Calibration and accuracy 500
8.3. Test procedures 501
8.4. Data processing procedures 503
8.5. Behaviour of the reconstituted clay 505

8.5.1. Isotropic and K_0 compression 506
8.5.2. Stress-strain behaviour 507
8.5.3. Flow rule and stress ratio at critical state 508
8.5.4. Critical state line 509
8.5.5. State Boundary Surface 510
8.5.6. Normalized gross yield surface 510
8.6. Behaviour of the natural clay 511
8.6.1. Isotropic and K_0 compression 511
8.6.2. Undrained stress-strain behaviour 513
8.6.3. Drained stress-strain behaviour 516
8.6.4. Critical states 518
8.6.5. Flow rule 520
8.6.6. Current yield surface of the clay 522
8.6.7. Normalization of clay behaviour with respect to volume 523
8.6.8. Normalization with respect to volume and structural changes 525
8.6.9. Normalized stiffnesses of natural and reconstituted clay 527
8.6.10.Intrinsic anisotropy 528
8.7. Behavioural framework of the natural clay 529

Chapter 9 Conclusions

9.1. A framework for the behaviour of clays 585
9.1.1. A novel approach to the structural effects on clay behaviour 585
9.1.2. Classification of clays 586
9.1.3. Framework of clay behaviour in the I_v-σ'_v plane 587
9.1.4. Similarities in the patterns of behaviour of clays 590
9.1.5. The differences between the behaviour of clays 593
9.2. Geological history, structural features and v-p′ state history of Pappadai clay 596
9.3. Structural changes occurring in the clay with compression 598
9.4. Strain-rate dependency of clays 599
9.5. Future work 600

REFERENCES 603

Appendix 6.1. Design of the loading ram in the high pressure oedometer A.1

Appendix 6.2. Use of the Gibson and Lo model (1961) to interpret the behaviour of soil during creep and the strain-rate dependency of the soil A.3

Appendix 6.3. Theoretical solution of CRS one-dimensional consolidation A.7

LIST OF FIGURES

Fig.1.1 Structure of the main clay minerals (after Veniale 1983).

Fig.1.2 (a) Charge distribution on the clay particle surface; (b) internal surface structure of a structural unit of Kaolinite (after Veniale 1983).

Fig.1.3 Scheme of the different water layers surrounding the clay particle (after Veniale 1971).

Fig.1.4 (a) Terzaghi-Casagrande honeycomb fabric (after Terzaghi 1925); (b) Open fabric of undisturbed marine clay (after Casagrande 1936-a).

Fig.1.5 (a) Relation between liquidity index and undrained shear strength of remoulded clays; (b) Relation between liquidity index and consolidation pressure for natural and remoulded clays (after Skempton and Northey 1952) and constant sensitivity lines.

Fig.1.6 (a) Cardhouse fabric in saltwater deposit (b) cardhouse fabric in freshwater deposit; (c) remoulded fabric (after Lambe 1953).

Fig.1.7 Idealized clay fabrics (after Sides and Barden 1970).

Fig.1.8 Assemblages and pore classes in the open fabric of a reconstituted clay (after Griffith and Joshy 1990).

Fig.1.9 (a) Kaolin slurry (w=117%); (b) "bridge" between domains (after V.Cotecchia et al.1982-b).

Fig.1.10 Pyrite framboids (after O'Brien and Slatt 1990).

Fig.1.11 (a) and (b): pore spaces partially or completely filled with calcite crystals; (c), (d) and (e): irregular grains of calcite and flakes of gypsum deposited within the interlayering of laminated clays (cross section) (after Veniale 1985).

Fig.1.12 Oedometer compression of a kaolin slurry (w_0=6c3%=w_{LL}): (a) σ'_V=4.9kPa; (b) σ'_V=49kPa; (c) σ'_V=490kPa; (d) σ'_V=4900kPa; (e) scheme of the complex architecture of the fabric in (a); pictures after V.Cotecchia et al.(1982-b).

Fig.1.13 Fiumicino clay, normally consolidated in situ : (a) fabric on a vertical fracture through an undisturbed sample from 18m depth; (b) fabric on a vertical fracture through a sample compressed to σ'_v = 4704kPa; (c) fabric scheme applying to the clay compressed to very high stresses (after Sfondrini 1975).

Fig.2.1 Reconstituted London clay: isotropic compression and swelling curves (data from Henkel 1956; after Schofield and Wroth 1968).

Fig.2.2 Reconstituted Lower Cromer Till: (a) constant η lines; (b) normalized swelling lines (after Gens and Potts 1982).

Fig.2.3 Normally consolidated reconstituted Weald Clay: failure states in drained and undrained shearing (data from Parry 1960; after Atkinson and Bransby 1978).

Fig.2.4 Overconsolidated reconstituted kaolin: normalized undrained stress paths (data from Loudon 1967; after Atkinson and Bransby 1978).

Fig.2.5 Remoulded London Clay at failure (data from Parry 1958; after Schofield and Wroth 1968).

Fig.2.6 Condition of specimens at yield in relation to the critical state line (after Schofield and Wroth 1968).

Fig.2.7 Normally consolidated reconstituted kaolin: normalized stress paths (data from Balasubramaniam 1969; after Atkinson and Bransby 1978).

Fig.2.8 The state boundary surface and the elastic wall in the Critical State Framework (after Atkinson and Bransby 1978).

Fig.2.9 (a) Idealized behaviour of samples of normally consolidated and overconsolidated soil in undrained compression tests; (b) Idealized behaviour of overconsolidated soil in undrained compression tests with partial drainage (after Atkinson and Richardson 1987).

Fig.2.10 Stereophotogrammetric measurements during a plane strain test: (a) incremental displacements; (b) shear intensities; (c) volumetric strains; (d) stress-strain curve (after Desrues 1990).

Fig.2.11 Reconstituted Lower Cromer Till: stress paths on isotropically normally consolidated samples (a) in the normalized *t*-p' plane (after Gens 1982) and (b) in the normalized q-p' plane (data from Gens 1982).

Fig.2.12 Normalized stress paths for K_0 and isotropically consolidated samples of remoulded organic clay (after Pickles 1988).

Fig.2.13 Reconstituted Lower Cromer Till: plastic strain ratios along constant η lines (data from Gens 1982).

Fig.2.14 Reconstituted Lower Cromer Till: (a) stress paths for drained tests on K_0 consolidated samples; (b) undrained stress paths on samples consolidated at $\eta=1$ (after Gens 1982).

Fig.2.15 Reconstituted Lower Cromer Till: drained triaxial compression on a K_0 normally consolidated sample (data after Gens 1982).

Fig.2.16 Ageing effects on clay behaviour.

Fig 2 17 Influence of ageing on compression behaviour of a reconstituted clay (after Leonards and Ramiah 1959)

Fig.2.18 Mechanical behaviour of normally consolidated aged kaolin (data from N.Ninis 1990; after Burland 1990).

Fig.2.19 In situ I_v-σ'_v states for natural clays (after Burland 1990).

Fig.2.20 Boom Clay (W_{LL} = 65%): high pressure oedometer test on block sample from Mol (data from Horseman 1987; after Burland 1990).

Fig.2.21 Normally consolidated argillaceous sediments : (a) in situ states (after Skempton 1970); (b) sedimentation compression curves.

Fig.2.22 Sedimentation Compression Curves:(a) Gosport Clay, (b) Bothkennar Clay (after Burland 1990).

Fig.2.23 The sensitivity framework for soft clays: sedimentation compression curves of clays of equal sensitivity.

Fig.2.24 Bothkennar clay: oedometric compressions on undisturbed and reconstituted clay (W_{LL}=85.4%; W_{PL}=41%) (after Burland 1990).

Fig.2.25 Behaviour of natural soft clays: (a) undrained stress-strain behaviour and stress paths of James Bay B-6 marine clay (after Jamiolkowsky et al.1985, data from Lefebvre et al.1983); (b) current yield curves of undisturbed specimens and yield curves of specimens compressed beyond isotropic gross yield (after Tavenas and Lerouil 1985).

Fig.2.26 Bothkennar Clay: Normalized probing stress paths and current SBS (after Smith et al.1992).

Fig.2.27 Winnipeg Clay: (a) current yield envelopes; (b) current yield envelopes normalized with respect to the preconsolidation pressure (after Graham et al.1983); (c) current yield envelope normalized with respect to the equivalent pressure p'_{SCC} (p'_e in the figure; after Graham et al.1988).

Fig.2.28 Mechanical behaviour of Norwegian clays (data from Lacasse et al.1985; after Burland 1990).

Fig.2.29 Corinth marl: (a) drained stress paths and current yield curve; (b) undrained stress paths and current yield curve (after Anagnostopulos et al.1991).

Fig.2.30 Mechanical behaviour of Cemented Carbonate Sand: (a) stress paths; (b) normalized stress paths at low and intermediate confining pressures; (c) normalized stress paths at high confining pressures (after Coop and Atkinson 1993).

Fig.2.31 Behavioural frameworks for reconstituted soils, cemented soils and soft sensitive clays.

Fig.2.32 London Clay: undrained stress paths and failure envelope (after Sandroni 1977).

Fig.2.33 London Clay at Ashford Common: normalized strength envelopes (after Burland 1990).

Fig.2.34 Todi Clay: (a) undrained stress-strain behaviour; (b) post-rupture shear stresses and stress ratios (after Burland 1990).

Fig.2.35 London Clay: undrained stress path corrected for localization (after Sandroni 1977).

Fig.3.1 Simplified geology of southern Italy.
Fig.3.2 Geology of the study area, showing the Bradano Trough and Pleistocene marine terraces (from Ciaranfi *et al.* 1988). Key: 1, Middle-Upper Pleistocene calcarenites; 2, Monte Marano Sands; 3, upper-cycle blue clays; 4, Gravina Calcarenites; 5, paleo coastline; 6, location of Pappadai; 7, Cretaceous limestone.
Fig.3.3 Sections showing the position of the upper-cycle blue clays; the locations of the sections are shown in Fig. 32. Key: 1, Pleistocene calcarenites; 2, upper-cycle blue clays; 3, Gravina Calcarenites; 4, Cretaceous Basement; 5, faults. (From Italian Geological Survey, Anon. 1967.)
Fig.3.4 (a) Reconstruction of the Montemesola Basin at the commencement of deposition of the upper-cycle blue clays (from Ciaranfi *et al.* 1971); (b) Section A-A showing location of Pappadai.
Fig.3.5 Location of boreholes. Key: 1, alluvium; 2, Quaternary calcarenites; 3, Pappadai clay; 4, lines of section; 5, Borehole A; 6, shaft; 7, individual boreholes.
Fig.3.6 Sections A-A and B-B, Fig. 35.
Fig.3.7 Grading curves for Pappadai Clay.
Fig.3.8 (a) Laminations between 25-32m depth; (b) coarse bedding, 6-8m depth.
Fig.3.9 Pappadai Clay: palaeontological associations.
Fig.3.10 Geotechnical profiles, borehole A.
Fig.3.11 Plasticity index versus carbonate content, Pappadai Clay.
Fig.3.12 Clay-size fraction versus carbonate content, Pappadai Clay.
Fig.3.13 Combined geotechnical data, other boreholes.
Fig.3.14 Mineralogy of Pappadai Clay; data from borehole A.
Fig.3.15 (a) Sketch showing geological section of the Montemesola Basin; (b) Pappadai : in situ conditions at the end of stage 1 and at present.
Fig.3.16 (a) Values of LI logged for the Pappadai clays; (b) values of voids ratio in an ideal clay deposit after normal consolidation and erosion; (c) London clay: water content profile (after Chandler and Apted 1987); (d) Taranto clay: water content profile (after V.Cotecchia et al.1977).
Fig.3.17 The four stages of the geological history at Pappadai - borehole A.
Fig.3.18 Relation between liquidity index and effective overburden pressure of natural clays, after Skempton (1970), and SCC of Pappadai clay.
Fig.3.19. Pore pressure profiles in existing stratum used in calculating the LI profiles shown in Fig.3.20. Key: 1, at end of deposition; 2, after erosion of 120 m of sediment; 3, after desiccation; 4, present day profile.

Fig.3.20. Liquidity index profiles resulting from the modelling of the Pappadai clay history.

Fig.4.1 Scheme of a pressuremeter (after Clarke 1992-a).

Fig.4.2 The Cambridge self-boring pressuremeter (after Windle and Wroth 1977).

Fig.4.3 Pressuremeter cavity (after Mair and Wood 1987).

Fig.4.4 Measurement of the lift-off pressure (after Mair and Wood 1987).

Fig.4.5 Possible cavity deformations at lift-off.

Fig.4.6 Stress-strain conditions for an element of soil in cylindrical symmetry.

Fig.4.7 Deformation of soil during the expansion of a cylindrical cavity (after Mair and Wood 1987).

Fig.4.8 Stresses around expanding cavity in elastic soil.

Fig.4.9 SBP test curves in terms of cavity strain and volume change (after Mair and Wood 1987).

Fig.4.10 (a) Ideal soil behaviour; (b) relation between t and ε_c during the pressuremeter expansion for a soil as in (a); (c) measurement of c_u (after Mair and Wood 1987) for an elastic-perfectly plastic soil (see (a)).

Fig.4.11 τ-ε_c curve resulting from a SBP test curve (after Mair and Wood 1987).

Fig.4.12 SBP testing : (a) possible failure planes; (b) inclination of the failure planes with respect to the lamination planes for the three modes of failure shown in (a).

Fig.4.13 Possible t-ε_c paths during a SBP test.

Fig.4.14 Loading of a laminated soil element in laboratory tests : (a) plane strain, (b) hollow cylinder and (c) triaxial test.

Fig.4.15 SBP testing at Pappadai : (a) SBP probe, (b) rotary rig.

Fig.4.16 SBP testing at Pappadai : control and data logging system at the surface.

Fig.4.17 Drilling operations at Pappadai.

Fig.4.18 SBP testing at Pappadai : p-ε_c curves.

Fig.4.19 SBP testing at Pappadai : measured horizontal stresses σ_h; for each data point the test number is indicated.

Fig.4.20 SBP testing at Pappadai : measured undrained shear strengths c_u.

Fig.4.21 SBP testing at Pappadai : measured limit pressures.

Fig.4.22 SBP testing at Pappadai : t-ε_c curves resulting from the Palmer analysis.

Fig.4.23 SBP testing at Pappadai : unload-reload loops.

Fig.4.24 SBP testing at Pappadai : relation between the reload cavity moduli G_{ur} and the cavity strain at the start of the unload-reload loop.

Fig.4.25 Horizontal effective stresses down borehole A.

Fig.4.26 K_0 values down borehole A.

Fig.4.27 q-p' states down borehole A.
Fig.4.28 In situ states in the four stages of the clay history : (a) e-σ'_v states; (b) LI-σ'_v states.
Fig.4.29 (a) Variation of K_0 with OCR and (b) e-σ'_v curves for undisturbed Haney Clay (after Campanella and Vaid 1972).
Fig.4.30 Coefficient *a*, relating K_0 with OCR, versus plasticity index (after Ladd et al.1977).
Fig.4.31 OC clays : effects on the clay stress history of the further bonding acquired by the clay after virgin compression.

Fig.4.32 e-p' states down borehole A in the four stages of the geological history.
Fig.4.33 q-p' states down borehole A in the four stages of the geological history.
Fig.4.34 Values of OCR down borehole A in the four stages of the geological history.
Fig.4.35 Values of K_0 down borehole A in the four stages of the geological history..
Fig.4.36 Relationship between K_0 and OCR (Table 4.7) reported in the literature for soft OC clays (clay type 2 in Table 2.1) and K_0-OCR values applying to the Pappadai clays down borehole A.
Fig.4.37 q-p' states down borehole A in the four stages of the clay history as resulting from the modelling, and present q-p' states as resulting from the in situ measurements.
Fig.5.1 Block sampling of Pappadai clay.
Fig.5.2 Grading curves of the natural and reconstituted Pappadai clay.
Fig.5.3 Block sample of Pappadai clay.
Fig.5.4 Samples of undisturbed clay tested at IC : (a) filter paper test on the clay block before storage; (b) division of the block sample into small cubes.
Fig.5.5 Undisturbed Pappadai clay: (a) e-w and (b) S_r-w relations.
Fig.5.6 Undisturbed Pappadai clay: e-p_k and e-σ'_v relationships.
Fig.5.7 Filter paper measurements on the undisturbed clay before storage.
Fig.5.8 Pore water pressure response of a saturated soil to undrained isotropic loading (after Baldi et al.1988).
Fig.5.9 Fuse wire technique (after Bishop and Henkel 1962).
Fig.5.10 Drying test on overconsolidated kaolin (after Ridley 1993).
Fig.5.11 Drying test on undisturbed London Clay (after Marinho 1994).
Fig.5.12 Oedometric compression curves of London clay (after Marinho 1994).
Fig.5.13 Pappadai clay: initial and final states of the block sampling stress path.
Fig.5.14 Stages of a block sampling path.
Fig.5.15 Total and effective stress paths during block sampling.

Fig.5.16 One-dimensional compression of reconstituted Pappadai clay from slurry in the consolidometer.

Fig.5.17 SEM : (a) modes of operation (manual of Cambridge 500 SEM); (b) sample preparation methods (Smart and Tovey 1981).

Fig.5.18 Undisturbed Pappadai clay: global view of the fabric on a vertical fracture; group 1 (Table 5.9).

Fig 5.19 Undisturbed Pappadai clay: vertical fracture, densely packed well orientated fabric; group 1 (Table 5.9).

Fig 5.20 Undisturbed Pappadai clay: vertical fracture, densely packed well orientated fabric; group 1 (Table 5.9).

Fig 5.21 Undisturbed Pappadai clay: vertical fracture, densely packed, well orientated fabric; group 2 (Table 5.9).

Fig 5.22 Undisturbed Pappadai clay: well orientated fabric; horizontal fracture, group 1 (Table 5.9).

Fig 5.23 Undisturbed Pappadai clay: well orientated fabric; horizontal fracture, group 1 (Table 5.9).

Fig 5.24 Undisturbed Pappadai clay: (Foraminifera shells) (a) globigerinae, group 1; (b) globigerinae, group 2; (c) coccosphera group2; (d) foraminifera group 2 (Table 5.9).

Fig 5.25 Undisturbed Pappadai clay: voids created by interbedded foraminifera, group 1 (Table 5.9).

Fig 5.26 Undisturbed Pappadai clay: clay particles and coccoliths; horizontal fracture; group 1 (Table 5.9).

Fig 5.27 Undisturbed Pappadai clay: clay particles; horizontal fracture, group 1 (Table 5.9).

Fig 5.28 Undisturbed Pappadai clay: Smectite particles in random fabric of "spongy" appearance; coccoliths group 1 (Table 5.9).

Fig 5.29 Undisturbed Pappadai clay: strata of orientated domains, bending from sub-horizontal directions to sub-vertical directions and crossing each other; vertical fracture, group 1 (Table 5.9).

Fig 5.30 Undisturbed Pappadai clay: strata of orientated domains in horizontal directions in edge to face contact with strata of domains in sub-vertical directions; vertical fracture, group 1 (Table 5.9).

Fig 5.31 Undisturbed Pappadai clay: complex architecture, smectite particles, spongy appearance, group 1 (Table 5.9).

Fig 5.32 Undisturbed Pappadai clay: complex laminae and chaotic fabric, group 1 (Table 5.9).

Fig 5.33 Undisturbed Pappadai clay: random fabric, group 1 (Table 5.9).

Fig 5.34 Undisturbed Pappadai clay: interbedding of piles of iso-orientated sub-horizontal domains and strata of openly spaced sub-vertical domain aggregates. Intense presence of coccoliths; the coccoliths are immersed within particle aggregates having both iso-orientated and flocculated fabrics. Vertical fracture, group 2 (Table 5.9).
Fig 5.35 Undisturbed Pappadai clay: lamination plane; horizontal fracture, group 2 (Table 5.9).
Fig 5.36 Undisturbed Pappadai clay: sub-horizontal stacks surrounded by densely packed chaotic flocculated aggregates and open arrangements of domains in edge to face contact; vertical fracture, group 1 (Table 5.9).
Fig 5.37 Undisturbed Pappadai clay: edge to edge and edge to face contacts; vertical fracture, group 1 (Table 5.9).
Fig 5.38 Undisturbed Pappadai clay: calcite crystals within a stack of iso-orientated clay particles; vertical fracture, group 1 (Table 5.9).
Fig 5.39 Undisturbed Pappadai clay: lath shaped illite, horizontal fracture, group 2 (Table 5.9).
Fig 5.40 Undisturbed Pappadai clay: framboide pyrite crystal, vertical fracture, group 1 (Table 5.9).
Fig. 5.41 Reconstituted Pappadai clay: global view of the fabric on a vertical fracture; group 1 (Table 5.9).
Fig. 5.42 Reconstituted Pappadai clay: sand size constituents immersed in the clay fabric, group 1 (Table 5.9).
Fig. 5.43 Reconstituted Pappadai clay: Flocculated random fabric between horizontal strata of iso-orientated domains; vertical fracture, group 1 (Table 5.9).
Fig. 5.44 Reconstituted Pappadai clay: mediumly orientated fabric, horizontal fracture; group 1 (Table 5.9).
Fig. 5.45 Reconstituted Pappadai clay: different flocculated arrangements; vertical fracture, group 1 (Table 5.9).
Fig. 5.46 Fabric of one-dimensionally normally consolidated KSS (after Menkiti 1995).
Fig. 5.47 Reconstituted Pappadai clay: interparticle contacts within a flocculated aggregate; remains of a coccolith are seen in the bottom left of the picture; the large clay particles appear damaged along the contour and on the surface; vertical fracture, group 1 (Table 5.9).
Fig. 5.48 Undisturbed Pappadai clay: free swelling of the undisturbed natural clay.
Fig. 5 49 Undisturbed Pappadai clay: free swelling of the natural clay after drying at 120°C for 24 hours.
Fig. 5.50 Undisturbed Pappadai clay: interbedding of strata of iso-orientated domains and flocculated fabric (fabric similar to the one shown in Fig 1 12 (e)); vertical fracture, group 3 (Table 5.9).

Fig. 5.51 Undisturbed Pappadai clay: fossil shell interbedded within random fabric; sub-vertical fracture , group 3 (table 5.9).

Fig. 5.52 Undisturbed Pappadai clay: "bridge" between two particle domains; sub-vertical fracture, group 3 (Table 5.9).

Fig. 5.53 Undisturbed Pappadai clay: sub-vertical fracture, group 3 (Table 5.9).

Fig. 5.54 Undisturbed Pappadai clay: sub-vertical fracture, group 3 (Table 5.9).

Fig. 5.55 Undisturbed Pappadai clay: vertical fracture, group 2 (Table 5.9).

Fig. 5.56 Undisturbed Pappadai clay: vertical fracture, group 2 (Table 5.9).

Fig. 5.57 Reconstituted Pappadai clay (compressed to 20 MPa): vertical fracture, group 3 (Table 5.9).

Fig. 5.58 Reconstituted Pappadai clay (compressed to 20 MPa): iso-orientated particles, group 3, (Table 5.9).

Fig.5.59 State history of the natural and reconstituted Pappadai clay.

Fig.5.60 In situ states of natural normally consolidated clays (after Skempton 1970) and sedimentation compression curves (SCC) of the natural and reconstituted Pappadai clay.

Fig.6.1. Oedometer cell Design 1.

Fig.6.2. Oedometer cell Design 2 : (a) scheme; (b) cell set up within the high pressure oedometer.

Fig.6.3. Oedometer cell Design 3 : (a) scheme; (b) cell set up within the OED loading frame.

Fig.6.4. OED tests : loading frames with the oedometer cells Design 1 and 3.

Fig.6.5. Application of the vertical load to the specimen in the oedometer cell Design 3 : (a) OED tests; (b) high pressure CRS tests.

Fig.6.6. High pressure CRS test carried out with the oedometer cell Design 2.

Fig.6.7. High pressure CRS test carried out with the oedometer cell Design 3; the detail sketch shows the connection between the loading ram and the load cell.

Fig.6.8. High pressure oedometer with cell Design 2 : application of the vertical load.

Fig.6.9. Oedometer cell Design 3 : eccentricity of the vertical load in the high pressure CRS tests (a) and in the OED tests (b); system (a) is safer against buckling of the loading ram.

Fig.6.10. High pressure oedometer : measurement of the vertical load with both an external and an internal load cell.

Fig.6.11. Typical equilibration stage at the start of the CRS tests (test CRS5).

Fig.6.12. Typical equilibration stage after an unloading step in the CRS tests (test CRSR1).

Fig.6.13. High pressure oedometer with cell Design 2 : compliance tests; no filter paper discs were present; (a) loading; (b) unloading.

Fig.6.14. High pressure oedometer with cell Design 2 : compliance tests; filter paper discs were present; (a) loading; (b) unloading.

Fig.6.15. High pressure oedometer with cell Design 2 : compliance test; cycled filter paper discs were present; (a) loading; (b) unloading.

Fig 6.16. High pressure oedometer with cell Design 3 : compliance tests; no filter paper discs were present; (a) loading from 300N; (b) loading from 1000N; (c) unloading.

Fig.6.17. High pressure oedometer with cell Design 3* : compliance tests; no filter paper discs were present; (a) loading from 30N; (b) loading from 300N; (c) loading from 1000N; (d) unloading.

Fig.6.18. Terzaghi model : U%-T_v relationship (after Head 1986).

Fig.6.19. Casagrande curve fitting method (after Head 1986).

Fig.6.20. OC clay subjected to a load increment which includes σ'_p : (a) measured consolidation degree; (b) average consolidation degree U_s predicted by the Terzaghi model. Key : C_r recompression index; C_c compression index; σ'_p preconsolidation stress; σ'_{v0} initial vertical stress (after Mesri and Rokhsar 1974).

Fig.6 21. Consolidation of a clay stratum under a stress increment which includes σ'_p (after Mesri and Godlewski 1979).

Fig.6 22. Average strain ε_v and base effective stress σ'_{vb} versus time for a single stage-loading test on an OC soil specimen (after Lerouil et al.1983).

Fig.6 23. Ageing effects on both the compression curve and the c_v-σ'_v relationship of an OC marine clay (after Lowe et al.1969).

Fig.6 24. State path followed by a soft sensitive clay during an end of primary oedometer test (EOP) (after Lerouil et al.1985).

Fig.6 25. Strain rate dependency of the behaviour of a soft sensitive clay (after Lerouil et al.1985).

Fig.6 26. Values of YSR (OCR in the figure) measured on firm to stiff marine clays by means of both OED and CRS tests (after Hanzawa et al.1990); the S-Oed data are from OED tests and the SC-Oed data are from CRS tests.

Fig.6 27. Model representation of soil skeleton in the 1D consolidation model of Gibson and Lo (1961).

Fig.6.28. Consolidation curves and strain rates logged in the OED tests on the undisturbed Pappadai clay.

Fig.6.29. Test OED5 : raw settlements and base pore water pressures.

Fig.6 30. Test OED6 : raw settlements and base pore water pressures

Fig.6.31. OED tests on the undisturbed clay : compression and swelling curves. σ'_y as measured by means of the Casagrande construction (1936); the OED9 specimen was subjected to SEM analysis after compression.

Fig.6.32. OED tests on the undisturbed and reconstituted clay : C_c values.

Fig.6.33. OED tests on the undisturbed clay : compression curves, duration of the loading steps and current strain rates. σ'_y as measured in the linear plots immediately before the points of minimum stiffness.

Fig.6.34. OED tests on the undisturbed clay: compression curves, duration of the loading steps and current strain rates.

Fig.6.35. Natural Pappadai clay : effects of swelling before compression on the OED compression curve and effects of the compression beyond yielding on the swelling index.

Fig.6.36. OED tests on the natural clay: measured oedometric stiffnesses M.

Fig.6.37. OED tests on the natural clay : c_α values.

Fig.6.38. Natural Pappadai clay : variation of c_α with the compression index C_c (a) and the oedometric stiffness M (b).

Fig.6.39. Natural Pappadai clay : c_α-σ'_v-M relationship.

Fig.6.40. Tests OED 5 (a) and OED6 (b): strain rates; σ'_v as resulting from eq.(6.17).

Fig.6.41. OED tests : black are both the compression curves relating the states at the end of the loading steps and the intermediate state paths (tests OED 5 and 6) during consolidation and creep. The red curves represent compressions at constant strain rate (isotacae).

Fig.6.42. OED loading steps : average values of the oedometric stiffness M and variations of M during the single loading steps (tests OED 5 and 6; Appendix 6.3).

Fig.6.43. OED loading steps : values of c_v from the Terzaghi model and c_v variations in the single loading steps (tests OED 5 and 6; Appendix 6.3).

Fig.6.44 Discrepancy between the average consolidation degrees U_s% and U_p% of the Terzaghi model.

Fig.6.45. Terzaghi model : values of c_v (test OED 5) derived from either the average consolidation degree U_s% or the base pore water pressure (u_b).

Fig.6.46. Terzaghi model : values of c_v (tests OED 6) derived from either the average consolidation degree U_s% or the base pore water pressure (u_b); legend as for Fig.6.45.

Fig.6.47. OED loading steps : k values from the Terzaghi model and variations of k in the single loading steps (tests OED 5 and 6 Appendix 6.3).

Fig.6.48. Reconstituted clay : (a) consolidation curves; (b) strain rates.

Fig.6.49. Natural and reconstituted clay : OED compression curves. The strain rates at the state points of the OEDR curve are reported.

Fig.6.50. Natural and reconstituted clay : values of k from the Terzaghi model.
Fig.6.51. Reconstituted clay : comparison between the measured consolidation curves and the Terzaghi predictions.
Fig.6.52. CRS tests on the undisturbed clay: strain rates; (a) slow tests, (b) all the tests and (c) test CRS6.
Fig.6.53. CRS tests on the reconstituted clay : strain rates.
Fig.6.54. CRS tests on the undisturbed clay : (a) measured base excess pore water pressures u_b; (b) identification of the yield stress in the slow tests.
Fig.6.55. CRS tests on the reconstituted clay : (a) measured base excess pore water pressures u_b; (b) identification of the yield stress in the slow tests.
Fig.6.56. Effects on u_b of the strain rate changes in test CRS6. Correction of u_b in test CRS1.
Fig.6.57. CRS tests on the undisturbed clay : (a) u_b/σ_v ratios; (b) identification of the yield stress in the slow tests.
Fig.6.58. CRS tests on the reconstituted clay: u_b/σ_v ratios.
Fig.6.59. Correction coefficients α_m and α_c from Janbu and Senneset (1979).
Fig.6.60. Compression curves from tests CRS 7 and 9 before and after the α_m correction .
Fig.6.61. Undisturbed clay : CRS compression curves.
Fig.6.62. Undisturbed clay : slow CRS test compression curves (average strain rate 3E-3% min).
Fig.6.63. Effects of the change in strain rate (test CRS6) on the clay state path.
Fig.6.64. Effects of the correction of the base pore water pressure u_b on the CRS1 compression curve.
Fig.6.65. Undisturbed clay : CRS compression curves and isotacae resulting from the study of the OED test data (see Fig.6.41).
Fig.6.66. Undisturbed Pappadai clay : isotacae.
Fig.6.67. Undisturbed Pappadai clay : isotacae and CRS6 compression curve.
Fig.6.68. Reconstituted clay : CRS compression curves.
Fig.6.69 Reconstituted clay : CRS compression curves.
Fig.6.70. Framework of strain-rate dependency of the natural and reconstituted Pappadai clay.
Fig.6.71. Framework of strain-rate dependency of the natural and reconstituted Pappadai clay.
Fig.6.72. Effect of swelling before compression on the CRS compression of the natural clay.
Fig.6.73. M values from CRS tests calculated according to Wissa's solution and to the solution in App.6.3 : (a) slow tests; (b) fast tests.
Fig.6.74. Oedometric stiffness M of the natural clay as resulting from the OED and CRS test results.

Fig.6.75. Values of M and c_v observed during the CRS compression of reconstituted kaolin clay (after Davison and Atkinson 1990).

Fig.6.76. Exponential M-σ'_v relationships applying to (a) the natural clay and (b) the reconstituted clay.

Fig.6.77. Oedometric stiffness M of the reconstituted clay as resulting from the OED and CRS tests.

Fig.6.78. M-σ'_v data recorded for the natural and the reconstituted clay.

Fig.6.79. M-e data recorded for the natural and the reconstituted clay.

Fig.6.80. Comparison between the values of M in constant strain-rate compressions and the M values exhibited by the clay in the OED loading steps.

Fig.6.81. Variation of M during test CRS6 (undisturbed clay).

Fig.6.82. Variation of M during test CRSR3 (reconstituted clay).

Fig.6.83. Natural and reconstituted Pappadai clay : values of C_c measured in the OED and CRS tests.

Fig.6.84. Natural and reconstituted Pappadai clay : values of c_v measured in the CRS tests.

Fig.6.85. Natural clay : comparison between the c_v values measured in the OED and the CRS tests.

Fig.6.86. Natural clay : values of k measured in the OED and CRS tests.

Fig.6.87. Comparison between the k-e relationships applying to the natural and the reconstituted clay.

Fig.6.88. Constancy of k before yielding.

Fig.6.89. k-e relationships for clays.

Fig.6.90. Compression behaviour of the natural and the reconstituted clay.

Fig.6.91. Natural and reconstituted clay : swelling index.

Fig.6.92. The ICL, the SCL (Burland 1990) and the normalized compression curves of natural clays of different origin and structure. Data from Webb (1964), Burland (1990), F.Cotecchia (1990), Rampello et al.(1993), Smith et al.(1993), Coop et al.(1995), Burland et al.(1996).

Fig.6.93. M-e relationship applying to both the reconstituted and the natural Pappadai clay beyond yield.

Fig.6.94. Idealized e-σ'_v (a) and M-σ'_v (b) behaviour of the natural and the reconstituted clay in oedometric compression; calculation of the normalizing factor M_{NCeq} (c).

Fig.6.95. (a) Test OEDRb on the reconstituted clay and (b) test OED10 on the undisturbed clay.

Fig.6.96. Oedometric stiffness of the reconstituted clay normalized with respect to volume.

Fig.6.97. Oedometric stiffness of the natural clay normalized with respect to volume.

Fig.6.98. Oedometric stiffness of the natural clay normalized with respect both to volume and to the structural changes.

Fig.7.1 Natural clay compressed to a σ'_v of 3 MPa: global view of the fabric on a vertical fracture: the fabric appears densely packed but poorly orientated; group 1 (Table 5.9).

Fig.7.2 Natural clay compressed to a σ'_v of 3 MPa: vertical fracture; stacks of domains are inclined in different directions; empty macro-voids confined by fossil shells; group 1 (Table 5.9).

Fig.7.3 Natural clay compressed to a σ'_v of 3 MPa: vertical fractures; (a) stacks of domains following different directions confine areas of more open either random or more regularly flocculated fabric; at points the fabric is chaotic; various coccospheres can be seen on the right side of the picture; (b) the fabric is denser and with a higher degree of orientation than in (a); group 1 (Table 5.9).

Fig.7.4 Natural clay compressed to a σ'_v of 3 MPa: vertical fractures; undamaged shells of globigerinae; group 1 (Table 5.10).

Fig.7.5 Natural clay compressed to a σ'_v of 3 MPa: horizontal fractures; in (a) a medium to low fabric orientation is shown; in (b) both intact and broken fossil shells appear; in (c) the fabric is chaotic, stacks of particles being interbedded with random particles and "chaotic masses" of particles; group 1 (Table 5.9).

Fig.7.6 Natural clay compressed to a σ'_v of 3 Mpa: vertical fracture; a long horizontal stack is interbedded between flocculated and chaotic fabric; group 1 (Table 5.10).

Fig.7.7 Natural clay compressed to a σ'_v of 3 MPa: vertical fracture; the fabric is more open and flocculated in the centre of the picture; "chaotic masses" of particles are seen in the bottom half and in the top right of the picture; group 1 (Table 5.9).

Fig.7.8 Natural clay compressed to a σ'_v of 3 MPa: vertical fracture; chaotic densely packed fabric; coccoliths are shown; group 1 (Table 5.9).

Fig.7.9 Natural clay compressed to a σ'_v of 3 MPa: vertical fracture; two stacks of iso-orientated particles confine a chaotic mass of particles; group 1 (Table 5.9).

Fig.7.10 (a) Undisturbed natural clay before compression; (b) undisturbed natural clay compressed to a σ'_v of 3 MPa; vertical fractures; group 3 (Table 5.9).

Fig.7.11 Natural clay compressed to a σ'_v of 22 MPa: fabric on a vertical fracture; the clay is crossed by horizontal extension fractures; group 1 (Table 5 9).

Fig.7.12 Natural clay compressed to a σ'_v of 22 MPa. vertical fracture; open horizontal fracture limited by two stacks of iso-orientated particles which are interbedded between flocculated fabrics; complex, but regular architecture; group 1 (Table 5.9).

Fig.7.13 Natural clay compressed to a σ'_v of 22 MPa; vertical fracture; interbedding of denser iso-orientated fabric and more open flocculated one; group 1 (Table 5.9).

Fig.7.14 Natural clay compressed to a σ'_v of 22 MPa: vertical fracture; stacks of c.p.o. fabric within less orientated fabric; group 1 (Table 5.9).

Fig.7.15 Natural clay compressed to a σ'_v of 22 MPa; horizontal fractures; highly orientated fabric; in (a) a fissility plane is shown; group 1 (Table 5.9).

Fig.7.16 Natural clay compressed to a σ'_v of 22 MPa: vertical fracture; the fabric is highly orientated, with many stacks of c.p.o. fabric; group 1 (Table 5.9).

Fig.7.17 Natural clay compressed to a σ'_v of 22 MPa: vertical fracture; honeycomb resistant fabric; truss of domains in edge to face contact which sustain the horizontal stack of iso-orientated particles shown in Fig.7.16; group 1 (Table 5.9).

Fig.7.18 Natural clay compressed to a σ'_v of 22 MPa; details of orientated fabric; (a) vertical fracture; (b) and (c) horizontal fracture; group 1 (Table 5.9).

Fig.7.19 Natural clay compressed to a σ'_v of 22 MPa; vertical fractures; details of flocculated fabric; many large voids between domains in edge to face contact; the particle outlines appear slightly fringed; group 1 (Table 5.9).

Fig.7.20 Reconstituted clay compressed to a σ'_v of 22 MPa; global view of the fabric on a vertical fracture; very densely packed fabric; some globigerina fossil shells can be seen; group 1 (Table 5.9).

Fig.7.21 Reconstituted clay compressed to a σ'_v of 22 MPa: fabric on fractures inclined to the horizontal; group 1 (Table 5.9).

Fig.7.22 Reconstituted clay compressed to a σ'_v of 22 MPa; vertical fracture; stacks of iso-orientated particles following different directions interbedded with both areas of flocculated fabric and random chaotic fabric; group 1 (Table 5.9).

Fig.7.23 Reconstituted clay compressed to a σ'_v of 22 MPa: (a) highly dense fabric on vertical fractures; group 1 (Table 5.9).

Fig.7.24 Reconstituted clay compressed to a σ'_v of 22 MPa: areas of chaotic fabric where the small particles are either stuck on the surface of the domains or penetrate into them; (a) densely packed fabric; (b) macrovoid in areas of relatively more open fabric; group 1 (Table 5.9).

Fig.7.25 Reconstituted clay compressed to a σ'_v of 22 MPa: domains grown at the expenses of the small particles; the particle surfaces appear damaged and their outlines fringed; group 1 (Table 5.9).

Fig.7.26 Comparison between the fabrics on vertical fractures of sample D (a), and of sample E (b) (see Table 5.9); the higher orientation of the fabric of sample D with respect to sample E is evident while the clay of sample E appears more densely packed; group 3 (Table 5.9).

Fig.8.1. Half ball connection between the sample top platen and the load cell : triaxial apparatus A (a) and C (b).

Fig.8.2. Triaxial apparatus A.

Fig.8.3. Triaxial apparatus A : data logging system.

Fig.8.4. Triaxial apparatus B.

Fig.8.5. Triaxial apparatus E.

Fig.8.6. (a) Specimen with pre-formed failure plane at axial displacement Δh (eq.8.2); after Chandler 1966); (b) bulging and progressive shear band formation before the development of a failure surface.

Fig.8.7. Reconstituted clay : isotropic compression and swelling states.

Fig.8.8. Anisotropic strains recorded during the isotropic stress compression of the reconstituted clay (test TR1).

Fig.8.9. Anisotropic compression of the reconstituted clay (test TR5).

Fig.8.10. Reconstituted clay : states in isotropic and anisotropic compression and swelling.

Fig.8.11. Reconstituted clay : stress-strain behaviour of isotropically normally consolidated specimen.

Fig.8.12. Reconstituted clay : stress-strain behaviour of anisotropically consolidated specimen.

Fig.8.13. Reconstituted clay : stress-strain behaviour of isotropically overconsolidated specimen (R=2.4), before and after correction for localization (q_{loc}.,q/p'_{loc} , u_{ploc}).

Fig.8.14. Reconstituted clay : stress-strain behaviour of isotropically overconsolidated specimen (R=4.5), before and after correction for localization (q_{loc}., q/p'_{loc}., u_{ploc}).

Fig.8.15. Reconstituted clay : flow rules.

Fig.8.16. Reconstituted clay : plastic strain ratios in isotropic compression.

Fig.8.17. Reconstituted clay : stress paths and critical state line.

Fig.8.18. Reconstituted clay : v-p' state paths and critical state line.

Fig.8.19. Reconstituted clay : normalized stress paths and state boundary surface.

Fig.8.20. Reconstituted clay : normalized yield curve and plastic strain vectors.

Fig.8.21. Undisturbed clay : isotropic compression and swelling states.

Fig.8.22. Undisturbed clay : strain ratios in isotropic compression.

Fig.8.23. Undisturbed clay : isotropic and K_0 compression lines.

Fig.8.24. K_0 compression of the undisturbed clay : (a) radial strains; (b) stress path.

Fig.8.25. Natural and reconstituted Pappadai clay : isotropic and K_0 compression and swelling behaviour.

Fig.8.26. Undisturbed clay : typical differences between the measurements of pore water pressure at the base and at mid-height of the specimen.

Fig.8.27. Undisturbed clay (YSRis=7.5) : undrained stress-strain behaviour before and after correction for localization ($q_{loc.}$, $q/p'_{loc.}$, $u_{ploc.}$).

Fig.8.28. Undisturbed clay (YSRis=4.52) : undrained stress-strain behaviour before and after correction for localization ($q_{loc.}$, $q/p'_{loc.}$, $u_{ploc.}$).

Fig.8.29. Undisturbed clay (YSRis=3.22) : undrained stress-strain behaviour before and after correction for localization ($q_{loc.}$, $q/p'_{loc.}$, $u_{ploc.}$).

Fig.8.30. Undisturbed clay (YSRis=2.42) : undrained stress-strain behaviour before and after correction for localization ($q_{loc.}$, $q/p'_{loc.}$, $u_{ploc.}$).

Fig.8.31. Undisturbed clay (YSRis=2.167) : undrained stress-strain behaviour before and after correction for localization ($q_{loc.}$, $q/p'_{loc.}$, $u_{ploc.}$).

Fig.8.32. Undisturbed clay (YSRis=1.95) : undrained stress-strain behaviour before and after correction for localization ($q_{loc.}$, $q/p'_{loc.}$, $u_{ploc.}$).

Fig.8.33. Undisturbed clay (YSRis=1.74) : undrained stress-strain behaviour before and after correction for localization ($q_{loc.}$, q/p'_{loc}, u_{ploc}).

Fig.8.34. Undisturbed clay (YSRis=1.4) : undrained stress-strain behaviour before and after correction for localization (q_{loc}, q/p'_{loc}, u_{ploc}).

Fig.8.35. Undisturbed clay compressed beyond isotropic yield : undrained stress-strain behaviour before and after correction for localization (q_{loc}, q/p'_{loc}).

Fig.8.36. Shape of undisturbed clay specimens after shearing to large strains.

Fig.8.37. Undisturbed clay after undrained shearing to large strains : specimen TN2.

Fig.8.38. Undisturbed clay after undrained shearing to large strains : specimen TN1.

Fig.8.39. Undisturbed clay (YSRis=4.52) : drained stress-strain behaviour and strain rates.

Fig.8.40. Undisturbed clay (YSRis=9.04) : (a) drained stress-strain behaviour before and after correction for localization (q/p'_{loc}, $\varepsilon_v{}^p{}_{loc}$); (b) stress-strain curve according to the local strain measurements; (c) local dilation at the formation of the failure surface.

Fig.8.41. TN20 specimen : location of both the local strain transducers and the mid-height probe after the failure surface formation.

Fig.8.42. Undisturbed clay (YSRis=2.825) : drained stress-strain behaviour before and after correction for localization ($q\ p'_{loc}$, $\varepsilon_v{}^p{}_{loc}$).

Fig.8.43. Undisturbed clay (YSRis=1.5) : drained stress-strain behaviour.

Fig.8.44. Undisturbed clay compressed beyond isotropic yield : drained stress-strain behaviour.

Fig.8.45. Undisturbed clay after drained shearing to large strains : specimen TN15.

Fig.8.46. Flow rule of the undisturbed clay in undrained shear.

Fig.8.47. Flow rule of the undisturbed clay in drained shear.

Fig.8.48. Undrained shearing : fictitious dilation of the specimen causing a drop of pore water pressure after the formation of the failure surface.

Fig.8.49. Undisturbed clay : undrained stress paths and critical state line.

Fig.8.50. Undisturbed clay : v-p' state paths and critical states.

Fig.8.51. Isotropic and K_0 normal compression lines and critical state lines (constant η lines) of the natural and reconstituted Pappadai clay.

Fig.8.52. Behaviour of the undisturbed Pappadai clay in relation to the location of yield with respect to both the straight line of gradient 1.08 and the critical state line.

Fig.8.53. Plastic strain ratios during the K_0 compression of the undisturbed clay.

Fig.8.54. Current yield curve of the undisturbed clay : the yield states have been normalized with respect to two alternative values of p'_{yIS}.

Fig.8.55. Stress paths normalized with respect to the equivalent pressure p^*_e : (a) natural clay specimens consolidated to states before isotropic yield; (b) natural clay specimens consolidated to states beyond isotropic yield and reconstituted clay specimens.

Fig.8.56. Normalized stress paths of the natural clay consolidated to states before isotropic yield and dry and wet sides of the natural clay framework of behaviour.

Fig.8.57. Natural clay : stress paths normalized with respect to volume by means of the pressure p'_{NC}.

Fig.8.58. Natural clay : stress paths normalized with respect to volume by means of the yield pressure p'_{vIS}.

Fig.8.59. Natural clay : stress paths normalized with respect to volume and structure by means of the pressure p'_{NC} and the stress ratio $X_{NC}(=p'_{NC}/p^*_e)$.

Fig.8.60. Natural clay : stress paths normalized with respect to volume and structure by means of the yield pressure p'_y and the stress ratio $X_y=(p'_{yIS}\ p^*_e)$.

Fig.8.61. Reconstituted clay : shear stiffness measurements.

Fig.8.62. Natural clay : shear stiffness measurements.

Fig.8.63. Relationship between the normalized shear stiffness and the yield stress ratio for both the natural and the reconstituted clay.

Fig.8.64. Horizontally trimmed specimen of undisturbed clay : stress-strain behaviour before and after correction for localization (q_{loc}, q p'_{loc}, u_{ploc}).

Fig A.6 1 1 Loading ram of the oedometer cell Design 3 : boundary conditions assumed in the calculation of the Euler stress.

Fig.A.6.3.1. Pore water pressures in the oedometer specimen.

Fig.A.6.3.2. Integration of the CRS consolidation integral (A.6.3.4) : (a) integration proposed by Wissa et al.(1971) and (b) integration proposed in App.A.6.3.

Fig.A.6.3.3. Correction factors α_m and α_c proposed by Janbu and Senneset (1979).

LIST OF TABLES

Table 1.1 Classification of structures and sensitivities of clays.

Table 2.1 Structure-related classification of clays

Table 3.1. Summary of the index properties of the Pappadai clay, Borehole A.

Table 3.2. Ground levels at the borehole locations in the Pappadai valley.

Table 3.3. Values of C_c used in the modelling.

Table 4.1 SBP tests : lift-off pressures and average horizontal pressures σ_h

Table 4.2 SBP tests : measured values of shear strength and limit pressure.

Table 4.3. SBP tests : unload-reload loops; average secant cavity moduli G_{ur} and reload moduli $G_{ur}(.1\%)$ and $G_{ur}(.2\%)$.

Table 4.4. Normalized average secant cavity moduli.

Table 4.5. Normalized reload cavity moduli.

Table 4.6 Present volume-stress state of the clay down borehole A.

Table 4.7. K_0 values used in the modelling of the clay state-history.

Table 5.1 In situ stress state of the clay block samples.

Table 5.2 Undisturbed Pappadai clay: (a) index properties; (b) mineralogical composition.

Table 5.3 Measurements on specimens of undisturbed Pappadai clay.

Table 5.4 Undisturbed Pappadai clay: w-e-S_r values after storage.

Table 5.5 K_0-YSR values measured for Pappadai clay and London clay.

Table 5.6. Reconstituted Pappadai clay: mineralogical composition.

Table 5.7 Reconstituted Pappadai clay: Index properties.

Table 5.8 Reconstituted Pappadai clay: consolidation from slurry.

Table 5.9 Samples subject to scanning electron microscopy.

Table 6.1. Oedometer tests on Pappadai clay.

Table 6.2. Dimensions of the oedometer specimens.

Table 6.3. Characteristics of the automatic measuring systems used in the oedometer tests; the annotation * refers to the pore water pressure transducer used in the fast tests.

Table 6.4. CRS tests : bedding errors and non-repeatable compliances of the high pressure oedometer.

Table 6.5. CRS tests : possible strain measurement errors.

Table 6.6. e_i-σ'_{v_i} states at the start of the continuous CRS compressions.

Table 6.7. Values of σ'_y measured for the natural Pappadai clay.

Table 6.8. S_t(YSR=1)-σ'_y σ^*_e data for various natural clays.

Table 6.9. Values of the equivalent oedometric stiffness M_{NCeq} and of the stress ratio σ'_y / σ^*_e used in the normalization of the oedometric stiffnesses.

Table 7.1. Mineralogical composition of the natural and reconstituted clay before and after oedometric compression

Table 8.1. Triaxial tests on reconstituted Pappadai clay.

Table 8.2. Triaxial tests on undisturbed Pappadai clay.

Table 8.3. Triaxial tests on the undisturbed clay : inclination of the failure surfaces.

Table 8.4. Triaxial tests on the undisturbed clay : yield and final stress ratios.

Table 8.5. Triaxial tests on the undisturbed clay : corrections applied to the final pore water pressure values and corrected final stress ratios.

LIST OF SYMBOLS AND ABBREVIATIONS

1D	one-dimensional
a	parameter of the soil model from Gibson and Lo (1961)
A	coefficient of the basically frictional flow rule (eq.2.4)
A	pore pressure parameter from Skempton (1954)
A	coefficient of the G -R relationship
A	area of the loading ram in the high pressure oedometer (Design 3)
a	parameter of the K_0-OCR relationship applying to soils during unloading
B	pore pressure parameter from Skempton (1954)
b	parameter of the soil model from Gibson and Lo (1961)
Ca	Calcium
c_α	coefficient of secondary compression : $\Delta e/\Delta \log(t)$
C_c	compression index
C_c^*	intrinsic compression index
CF	clay fraction
Chl	chlorite
c.p.o.	complete preferred orientation
CRS	constant rate of strain
CS	critical state
C_s	swelling index
C_s^*	intrinsic swelling index
C_s^*/ C_s	swelling sensitivity
CSF	Critical State Framework
CSL	Critical State Line
c_u	undrained shear strength
c_v	coefficient of 1D consolidation
D	diameter of the specimen
Dol	dolomite
D1	Design 1
D2	Design 2
D3	Design 3
D3*	Design 3*

d_0	immediate oedometer settlement (Casagrande curve fitting)
D	diameter of the loading ram
E	Young's modulus
e	voids ratio
e_0	voids ratio after the equilibration stage in the CRS oedometer tests
e_{100}	voids ratio on the ICL for 100kPa vertical pressure
e_{1000}	voids ratio on the ICL for 1000kPa vertical pressure
e_y	voids ratio at gross yield
Fd	feldspar
G	shear modulus
G_0	shear modulus at very small strains
G_i	initial cavity modulus in SBP testing
G_s	specific gravity : γ_s/γ_ω
G_{ur}	cavity modulus from unload-reload loops - SBP testing
H	longest drainage path at the start of consolidation
h	initial height of the specimen
h_0	height of the triaxial specimen after consolidation, before shearing
I	Illite
I	moment of inertia : $\pi D^4/64$
ICL	intrinsic compression line
I_v	void index : $(e - e_{100})/(e_{100} - e_{1000})$
k	coefficient of permeability
K	Kaolinite
K_0	σ'_v/σ'_h
L	length of the loading ram checked for safety (oedometer cell Design 3)
LCT	Lower Cromer Till
LI	liquidity index
LL	liquid limit
LP	plastic limit
M	oedometric stiffness : $d\sigma'_v/d\varepsilon_v$
M_b	stiffness of the elastic element of the Kelvin body in the soil model from Gibson and Lo (1961)
M_{NC}	oedometric stiffness beyond yield
M_{NCeq}	equivalent oedometric stiffness calculated as shown in Fig.6.94(c)

m_v	coefficient of oedometric compressibility
$\mathcal{M}$	stress ratio q/p' at critical state
$\mathcal{M}_1$	final shearing stress ratio q/p' corrected for localization of strain and membrane effects
$\mathcal{M}_2$	final shearing stress ratio q/p' corrected for localization of strain, membrane and pore water presure effects
$\mathcal{M}_{nat}$	stress ratio q p' related to zero volumetric strain rate in the flow rule (eq.2.4) when this applies to the natural clay
M	$(2n + 1)\pi/2$
m	exponent of G_0-R relationship
N	specific volume on the isotropic normal compression line of the natural clay for p'=1kPa
N*	specific volume on the isotropic normal compression line of the reconstituted clay for p'=1kPa
NC	normally consolidated
NCL_{is}	isotropic compression curve beyond yield
NCL_{oed}	oedometric compression curve beyond yield
n	exponent of the G_0-R relationship
OC	overconsolidated
OCR	overconsolidation ratio : σ'_p/σ'_v
OED	step loading oedometer
P	Pappadai clay sample "prism"
p	cavity pressure - SBP testing
PI	plasticity index
p_k	suction
p_l	limit pressure - SBP testing
p'	mean normal effective stress : $(\sigma'_1 + 2\,\sigma'_3)/3$ for axial symmetry
p'_0	mean effective stress at the start of shearing in triaxial testing
p'_{CS}	mean effective stress at critical state
p^*_e	p' on the isotropic compression line of the reconstituted clay from the current specific volume
p'_{NC}	p' on the NCL_{is} line of the natural clay for the current specific volume
p'_p	isotropic preconsolidation stress
p'_{SCC}	p' on the SCC corresponding to the current volume

p'_y	mean effective stress at gross yield in isotropic compression
p'_{yK0}	mean effective stress at gross yield in K_0 compression
p^*_y	p′ on the NCL_{is} line of the reconstituted clay for the specific volume at gross yield
P	basal vertical steel rod in the CRS oedometer
q	deviatoric stress : $\sigma_1 - \sigma_3$ for axial symmetry
q_{CS}	deviatoric stress at critical state
q_{loc}	deviatoric stress corrected for localization
q/p'_{peak}	stress ratio at peak
q p'_y	stress ratio at yield
q/p'_{CS}	stress ratio at critical state
Qz	quartz
R	overconsolidation ratio : p'_p/p'
r	average strain rate in CRS oedometer testing
r	radial distance - SBP testing
S	compression measured during oedometric consolidation
SBP	self-boring pressuremeter
SBS	state boundary surface
SCC	sedimentation compression curve (Terzaghi 1944)
SCL	sedimentation compression line (Burland 1990)
SEM	scanning electron microscope
Sm	Smectite
S_r	saturation degree
S_t	sensitivity
S_t(YSR=1)	sensitivity of the clay consolidated to gross yield
S_∞	compression measured at the end of an oedometric consolidation step
s′	$(\sigma'_1 + \sigma'_3)/2$
t	$(\sigma_1 - \sigma_3)/2$
t	time in minutes
T_v	Terzaghi's time factor : $c_v t/H^2$
T	vertical steel rod in the CRS oedometer
u	excess pore water pressure
u_0	in situ pore water pressure
u_l	in situ hydrostatic pore water pressure profile

u_2	in situ pore water pressure profile equal to u_1 above 30 m depth and assuming zero pore water pressure below 30 m depth
u_b	excess base pore water pressure
u_{base}	pore water pressure at the base of the specimen in triaxial testing
u_p	plastic excess pore water pressure
u_{probe}	pore water pressure at mid-height of the specimen in triaxial testing
$u_{p\,oc}$	plastic excess pore water pressure corrected for localization
U_p	average degree of consolidation calculated from the pore water pressure measurements
U_s	average degree of consolidation calculated from the compression measurements
V	volume of the specimen
V_0	volume of the triaxial specimen after consolidation, before shearing
v	specific volume
V_c	volume of the cavity - SBP testing
$\mathcal{V}$	$\mathcal{W}H$
v	vertical displacement within the Wissa's integration of consolidation
w	water content
X	z/H
X_{NC}	p^*_e/p'_{NC}
X_Y	p^*_y/p'_y
YSR	yield stress ratio : σ'_y/σ'_v
YSR_{is}	p'_y/p'
y	radial displacement at radius r - SBP testing
Z	vertical height in situ
z	depth from the drainage boundary
α_c	correction coefficient for c_v (Janbu and Senneset 1979)
α_m	correction coefficient for σ'_v (Janbu and Senneset 1979)
β	viscosity in the soil model from Gibson and Lo (1961) : $1/\mu$
Δ	increment
ε_1	maximum principal strain
ε_2	intermediate principal strain
ε_3	minimum principal strain
ε_a	axial strain

ε_{av}	average strain in the CRS test specimen
ε_c	cavity strain - SBP testing
ε_h	principal stress in the horizontal direction
ε_p	permanent strain component
ε_r	radial strain
ε_s	shear strain : $2(\varepsilon_1 - \varepsilon_3)/3$ for axial symmetry
ε_s^p	plastic shear strain
ε_t	transient strain component in Wissa's solution of CRS consolidation
ε_t^*	transient strain component in the solution of CRS consolidation in App.6.3
ε_v	volumetric strain : $(\varepsilon_1 + 2\,\varepsilon_3)$
ε_v^p	plastic volumetric strain
ε_x	normal strain in the x direction
ε_y	normal strain in the y direction
ε_z	normal strain in the z direction
ϕ_f	friction angle satisfying the dilatancy equation for loose packings or high confining stresses
ϕ_μ	friction angle satisfying the dilatancy equation for dense packings at low confining stresses
ϕ'_{CS}	critical state friction angle
ϕ'_{ULT}	ultimate friction angle
γ	bulk unit weight
γ_d	dry bulk unit weight
γ_w	unit weight of water
γ_s.	unit weight of the soil grains
η	stress ratio q/p′
κ	gradient of the swelling lines in the v-lnp′ plane according to the CSF
κ^*	gradient of the swelling lines in the v-lnp′ plane for the reconstituted clay
λ	gradient of the constant η lines in the v-lnp′ plane according to the CSF
λ^*	gradient of the constant η lines in the v-lnp′ plane for the reconstituted clay
Γ	specific volume on the critical state line for p′ =1kPa
Γ^*	specific volume on the critical state line of the reconstituted clay for p′ =1kPa
μ	parameter of the soil model from Gibson and Lo (1961)
ν'	Poisson's ratio

ρ	cavity radius - SBP testing
σ	total stress
σ'	effective stress
σ_1	maximum principal stress
σ_2	intermediate principal stress
σ_3	minimum principal stress
σ'_{av}	average vertical effective stress in the CRS test specimen
σ_h	in situ horizontal stress
σ_{h1}	lift-off pressure
σ_{h2}	lift-off pressure
σ_{h3}	lift-off pressure
σ_e	Euler stress
σ_r	radial stress
σ_v	vertical stress
σ_θ	circumferential stress
σ'_h	horizontal effective stress
σ'_{hp}	horizontal preconsolidation pressure
σ'_p	one-dimensional preconsolidation stress
σ'_v	vertical effective stress
σ'_{v0}	vertical effective stress after the equilibration stage in the CRS oedometer tests
σ'_y	vertical effective stress at gross yield in one-dimensional compression
σ^*_e	vertical pressure on the ICL corresponding to the specific volume at 1D gross yield
$\sigma'_v\ \sigma^*_e$	factor normalizing the effects of structure on the clay behaviour
τ	shear stress
$\boldsymbol{\tau}$	time parameter in Wissa's integration

INTRODUCTION

The present research is within that part of Soil Mechanics which deals with the basics of the mechanical response of soils and the laws governing their behaviour, particularly the mechanical behaviour of clays.

The Critical State Framework (CSF) (Roscoe et al.1958; Schofield and Wroth 1968), developed in the Sixties from research on the behaviour of reconstituted soils (Rendulic 1936; Hvorslev 1937; Henkel 1960), was a main development in the understanding of the behaviour of soils, above all because it demonstrated the importance of using a rational framework to represent the stress-strain-strength laws of soils. The soil response was expressed in terms of effective stress invariants and volume, and key features of its behaviour were identified.

The belief that it is important to extend the methodological approach typified by critical state soil mechanics to the study of the response of both natural and reconstituted soils, and to endeavour to relate their behaviour in a general framework, underlies the research presented in this thesis. The fundamental concepts underlying the Critical State Soil Mechanics Theory are discussed in Section 2.2.

The CSF, combined with strain-hardening plasticity laws, was the basis for mathematical modelling of soil behaviour (Schofield and Wroth 1968, Roscoe and Burland 1968). The provision of models of use in engineering practice has since given great impulse to Soil Mechanics research, requiring systematic programmes of highly accurate laboratory tests. Nonetheless at present models are often constructed to conform with the mechanical response of the specific soil studied, and are not based on general fundamental laws of behaviour. In fact while the mathematical description of observed aspects of soil behaviour has developed, the understanding of both the origins of that behaviour and the intrinsic phenomena being modelled has not improved greatly.

The investigation of the phenomena giving rise to the soil response is instead here believed to generate a more fundamental understanding of the mechanics of soils, which is the basis of the construction of a simplified general framework of soil behaviour. Such a framework allows the behaviour of different natural and reconstituted soils and their models to be seen within a single picture. In this manner the causes of the differences in behaviour between soils can be understood

and the identification of the common features of behaviour of different soils may be applied to models of general validity.

In this thesis it is suggested that different natural and reconstituted clays, despite their different origins and structures, have basic common laws of behaviour. The structure of the clays and their common features of behaviour should then be further investigated to create models of clay behaviour of more general validity than is presently possible

A comprehensive study of the geological characteristics of the soil is a necessary background to the work outlined above since it aids the understanding of the origins of the soil behaviour. Many studies report the geological characteristics and the mechanical response of the soil without truly exploring the connections between the two.

As the importance of a simplified common framework of soil behaviour is not generally considered, often insufficient effort is made to recognize similarities between the behaviour of different soils. Obviously similar laws of behaviour may be differently exhibited by soils of different composition and microstructure Rational normalization of soil response with respect to composition has successfully simplified the picture of the behaviour of natural and reconstituted clays (Skempton and Northey 1952; Skempton 1970; Burland 1990). However differences can exist in the normalized behaviour of clays of different microstructure, different structures giving rise to differences in the mechanical responses.

The problem is then to rationalize the effects of structure on the clay behaviour. However the existence of similarities in many basic aspects of the mechanics of soils of different structure (Lerouil and Vaughan 1990) suggests that differences in structure modify only part of the soil's behaviour, and that aspects common to all clays should be investigated first to define the basis of the general framework of behaviour of clays.

This thesis presents an experimental study of the behaviour of an Italian clay, the Pappadai clay (Chapter 3). The research developed as a comparison of a study of the clay at the macro-level and the micro-level

In order to identify the factors controlling the properties of the clay, a comprehensive study of the origin, composition, deposition conditions and geological history of the clay was carried out using both literature data and original experimental work This study also addressed the development of the structure of the natural clay during its geological history

Subsequently a broad experimental programme, both in situ and in the laboratory, examined the clay behaviour at the macro-level. In an in situ investigation the current effective stress state of the natural clay, the final result of its total geological history, was established. In the laboratory, the macro-behaviour of both the natural and the reconstituted Pappadai clay was investigated, aiding the understanding of the phenomena occurring at the micro-level. To investigate how the clay structure determined the observed behaviour, a comparison between the response of the natural and of the reconstituted clay was made, and, at the same time, the microstructure of the two clays, before and after testing, was investigated by means of the scanning electron microscope (SEM).

The present work can thus be considered an inter-related study of the factors determining the behaviour of Pappadai clay, see below :

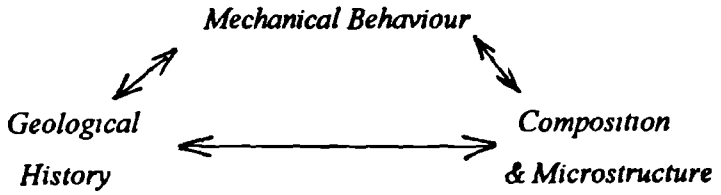

linking in cause and effect terms the geological history of the soil, its composition and structure, and its mechanical behaviour.

The behaviour of the natural and reconstituted clay were also compared with the behaviour of other clays in the context of the general framework of behaviour of soils. Both the understanding of how the behaviour of the natural and reconstituted Pappadai clay are related to their respective structures, and the appropriate representation of the clay behaviour in a common picture were then used as the basis of a proposed general scheme of soil response and a definition of the parameters on which the effects of structure on the clay behaviour depend.

ORGANIZATION OF THE THESIS

The use of the word structure in Soil Mechanics is often misleading and is not based on general agreement, so as the distinction often made between "structured" and "non-structured" clays does not correspond to the meaning of the word structure used by those studying clays at the micro-level. The first chapter of this thesis reviews the microstructural features of clays, attempting to follow a rigorous approach to the description of clay structure and shows how clay structure necessarily determines the clay's behaviour. The discussion in the first chapter leads to a definition of two categories of structure subsequently addressed

A literature review of the mechanical behaviour of soils in Chapter 2 illustrates the basic deformation mechanisms which are believed to be common to clays. The basis of a general framework of behaviour of clays is proposed and a classification of clays is developed which distinguishes between categories of clays which exhibit basic differences in behaviour.

Pappadai clay is described in Chapter 3 The lithological characteristics, the index properties and the mineralogy of the different clay strata are shown, and using data from the literature together with new information the deposition conditions and the geological history of the Pappadai clays are reconstructed. The occurrence of diagenesis in the clay is recognized, and the e-σ'_v state history of the clay is modelled.

In Chapter 4 the self-boring pressuremeter testing carried out at Pappadai is described, and the in situ effective stresses are derived from the test results and piezometer readings. The values of in situ undrained shear strengths and shearing stiffnesses are also reported. The results of a study of the e-q-p' state history of the clay suggest the development of further bonding in the clay once virgin compression is complete. This pattern of behaviour of the Pappadai clay enables it to be placed in one of the structural categories proposed earlier.

In Chapter 5 the e-S_r-p_k states of the natural and reconstituted clay samples are presented. The sampling stress path of the natural clay is reconstructed, and the features of the microstructure of the natural and reconstituted clay are shown. These were observed with the scanning electron microscope and in some cases the SEM used had the facility for chemical micro-analysis.

In Chapter 6 the results of an oedometer testing programme on both the natural and the reconstituted clay are presented. The consolidation behaviour is analyzed in detail and related to

the structural features of the clay The limitations of the theories of consolidation generally adopted to interpret consolidation behaviour are reviewed The strain-rate dependency and the creep behaviour of the soil are considered and the complementary roles of the structural stiffness and viscosity in controlling the clay's response is demonstrated. The strain-rate dependency is shown to be similar for both the natural and reconstituted clays. A framework of compression behaviour of clays is derived, which represents the behaviour of the clay types classified in Chapter 2. A parameter representative of the effects of structure on the clay behaviour is defined.

In Chapter 7 the microstructure of the natural and reconstituted clay after oedometric compression is examined and the effects of yielding on the microstructure is recognized. The difference in microstructure between natural and reconstituted clay at high stresses is examined.

Chapter 8 discusses the results of a triaxial testing programme, and the behaviour of both the natural and the reconstituted clay in the v-q-p' space is outlined. A frictional flow rule is shown to apply to the elasto-plastic behaviour of the two clays. The differences in shearing behaviour between the natural and reconstituted clay are identified, and are related to the clay structure. A framework of clay behaviour in v-q-p' space is thus derived.

The principal conclusions which are drawn from the work described are summarized in Chapter 9. The framework of clay behaviour anticipated in Chapter 2 is shown to be supported by the results of the research on Pappadai clay. Key areas of future research are then identified.

CHAPTER 1

MICROSTRUCTURE OF CLAYS AND MICRO-BEHAVIOUR

1.1. Introduction

In most branches of engineering, materials are regarded as continua. This is generally so in soil mechanics. This approach is particularly appropriate for clays, given the small size of the clay particles and the complexity of their interaction. But an understanding of the particulate nature of the soil, and the phenomena occurring at the micro-level are important because the soil behaviour is the expression of both its particulate nature and its geological history. The present chapter reviews the nature of both the clay particles and the microstructure of clay.

The nature of clay minerals and their modification as a result of geological processes are among the main factors which determine the structure of the clay and the clay behaviour, the subject of the present research. The mineralogy of the Pappadai clay was examined in detail, as discussed in Chapter 3, and usefully defined the degree of diagenesis of this clay.

The microstructure of both the natural and the reconstituted Pappadai clay are reported in Chapters 5 and 7. As an introduction to the structural studies of the Pappadai clay, this chapter considers the definitions of fabric, bonding and structure following a literature review and in the light of the objective of the research, that is the relation of the clay behaviour to its structure. Finally, the structural changes of clay under load are reviewed briefly.

1.2. Clay minerals and particles

Clay minerals are hydrated layered silicates of aluminium and magnesium. The mineral structural units have an alternating crystalline structure consisting of siliceous layers and aluminium-magnesium layers (Fig.1.1), in which substitution of some of the cations with other isomorphous ones (e g. Fe2+, Fe3+) can occur. The sequence of layers in the structural unit will differ for different clay minerals as indicated in Fig.1.1.

The clay particle is formed of a sequence of structural units whose distance (basal spacing) is more or less stable depending on the strength of the link between the units. Kaolinite is the most

stable as hydroxal links exist between the units Illites are sedimentary micas in which potassium links are present in the basal spacing inducing a rather stable base dimension. They show different possible degradation and stability levels in relation to different levels of interlayer potassium hydration Chlorites also have a rather stable base dimension because of brucite-octohedral links Smectites, derived from the extreme degradation of rock silicates, are the least stable clay minerals as the basal link is provided by hydrated cations, e g Na+, Ca+, Mg+ (Fig 1 1) (Veniale 1983, Blyth and De Freitas 1984).

With extreme degradation processes illites and chlorites can become smectites (Fig 1.1). Conversely, through diagenetic processes (aggradation), smectites can loose their swelling capacity acquiring a stronger inter-unit link and becoming "intergrades" or "mixed-layer" minerals. These are the results of an intermediate stage in the diagenetic process that can finally transform smectites into illites and chlorites (Fig.1.1). Aggradation and degradation of the clay minerals typically occur respectively during deposition-compaction and unloading-weathering processes, and these phenomena can modify significantly the clay behaviour.

Theoretically fine grained soils possess greater free energy than a soil formed of larger crystals of the same composition (Veniale 1983). Consequently a clay does not represent a potential equilibrium condition, the particle behaviour being governed by particle surface forces rather than gravity. Moreover, a clay particle is a "non perfect" crystal: unbalanced links can be present along the edges due to fracturing, while the basal planes are negatively charged as result of the isomorphous substitutions occurring in the structural units (Fig.1 2) These unbalanced charges govern the behaviour of the clay particles and their bonding.

1.3. Interaction between clay particles and water

When submerged, the clay particles interact with the pore water, i.e. with an electrolyte solution. The closest water molecules are attracted by the surface of the clay particles and form a thin "bound" or solid layer of water molecules which cannot be removed even by heating (Fig.1.3). Beyond the bound-water film, water molecules and hydrated cations are attracted by the particle and form a layer of high viscosity water: the absorbed water (Fig 1.3). This can be removed by heating, but because of its high viscosity it is not moved by hydraulic gradients. The charged particle surface and the cations located in the absorbed water layer together form the "double layer". Both the thickness of the double layer and the unbalanced nature of the particle surface charges depend on the mineralogy of the particle and the pore water chemistry

1 4 Interaction between clay particles

The clay particles do not interact directly. It is the association of the single clay particle with its own double layer, from here onwards called the "single particle-water system", which controls the interaction with the other single particle-water systems at deposition. Such interaction is governed by the combined effect of gravity, electrostatic forces, Van der Waal forces, osmotic pressures and pore water surface tension (Sfondrini 1975). The electrostatic forces are related to the charge distribution within the particle-water systems, while the Van der Waal forces depend on the dielectric constant of the soil-water system (Sides and Barden 1970). The complexity of the particle interactions in clays is thus evident.

When an increment of overburden pressure or other external stress is applied to the clay sediment the particle interactions change as the soil mass reaches a new equilibrium state. Models have been proposed which assume that the clay particles are not in contact and the external forces are equilibrated by the repulsion between the particles (Bolt 1956; Leroux 1975). In the last thirty years instruments such as the Transmission Electron Microscope and the Scanning Electron Microscope (SEM) have allowed two and three-dimensional imaging of clay particle arrangements (e.g. Smart and Tovey 1981). The existence of direct contacts between clay particles and groups of particles has been established, so that a mechanical stress can be transmitted at the interparticle contacts. But even if the available models provide theoretical descriptions of the interparticle stresses, how the physico-chemical interactions and the mechanical stresses are actually combined to provide equilibrium in clays has not been yet established (V.Cotecchia et al.1982-a).

As early as 1925 Terzaghi postulated that during consolidation highly viscous absorbed water, coating clay particle surface, is squeezed out from between points of contact (Fig.1.4(a)), and the resulting close approach of particles leads to high attractive forces. In this way Terzaghi addressed the microstructure of naturally sedimented clays. He accounted for remoulding as disruption of the interparticle contacts, by which absorbed water fills in around the old contacts and the strength of the clay is reduced. This "breakage of contacts" was seen as the cause of different strengths between the natural and the remoulded clay. Terzaghi later (1944) defined as sensitivity S_t the ratio between the undrained strength of the undisturbed clay and the undrained strength of the remoulded clay at the same water content. Since then, sensitivity has been regarded as the parameter embodying the differences of the microstructures of the natural and the remoulded clay.

Casagrande (1936-a) (Fig I 4(b)) explained marine clay sensitivity on the basis of a load-carrying skeleton consisting of highly compressed bond clay trapped between silt and fine sand particles during consolidation. Remoulding was visualized by Casagrande as the destruction of the load carrying skeleton

Skempton and Northey (1952) carried out an experimental study of the effects of the leaching action of fresh water on the volume and strength of natural and reconstituted clays. Leaching of marine clays had been recognized as cause of sensitivity in the Norwegian and Canadian quick clays. Skempton and Northey inferred that the change in chemistry of the pore water at leaching was affecting the double layers, and they measured a variation of the liquid limit of the clay after leaching. But since they observed that the leaching process was not affecting either the volume or the strength of the clay, they deduced that the clay particles had to be in effective contact before leaching. So Skempton and Northey (1952), as had earlier Terzaghi (1925) and Casagrande (1936-a), considered that the strength of the natural clay was related to a microstructure formed of particles in open arrangement and effectively in solid contact, established through the interpenetration of the films of bound water. In these studies the term microstructure was in general used to address the features of the clay at the micro-level. It is thus worth re-establishing what is understood by the "structure" of the clay

1.5. Soil structure and remoulding

V.Cotecchia et al.(1982-a) reviewed microstructural models and definitions presented in the literature to date; from here onwards their paper is addressed for terminology. Two fundamental factors determine the clay response, the arrangement of the particles and the inter-particle forces, which together let the clay sustain the external forces. Among all the definitions of structure presented in the literature (V.Cotecchia et al.1982-a), that of Lambe and Withmann (1969) seems the most appropriate, "the term soil structure refers to the orientation and distribution of the particles in a soil mass, called fabric, and the forces between adjacent soil particles". The terms fabric and microfabric, structure and microstructure, will be considered synonymous from here on.

While the fabric of a clay can be visualized and quantified as defined above, the particle interactions cannot be defined. If a saturated clay is under positive effective stresses with positive or zero pore water pressure, normal and tangential frictional stresses can be transmitted at the inter-particle contacts. In addition, electrostatic and Van der Waal forces, and viscous stresses

within the absorbed water layer, will act between uncemented particles. If cemented links exist between the particles, part of the load may be concentrated at these links. The combination of all the interparticle forces which are not of a purely frictional nature, e g. normal and tangential frictional contact stresses, will be defined as bonding.

It follows that bonding is not necessarily a solid link, and should be considered as a concept rather than an absolute value; but bonding is of great help in characterizing different structures. The bonding which develops in a clay depends on the physico-chemical environment, e g. chemistry of the suspension, pressure, temperature, organic content, and on the mechanical boundary conditions, e.g. the consolidation strain path and the deposition and consolidation rate (Mitchell and Houston 1969; Mitchell 1976; Sides and Barden 1970; Sfondrini 1975).

Following the definition of structure given above, the term remoulding should now be discussed. To remould a clay the material is worked to weaken its bonding. Remoulding can require the clay to be mixed with water; for stiff clays it is in general necessary to create a slurry to remould the clay. Even the clays which are "heavily remoulded", so as to have sensitivity 1, as with any other clay have a structure, but this has fabric and bonding which are "stable", as the clay strength does not change with disturbance. The Atterberg limits are measured on the heavily remoulded clay and reflect both the amount and type of minerals present in the clay, and such properties as cation-exchange capacity and total surface area (Skempton 1953).

Skempton and Northey (1952) referred to clays consolidated from a slurry as being remoulded. They considered that the process of formation of the clay slurry (reconstitution) and very rapid consolidation of the slurry in the laboratory created non-sensitive clays. By consolidating and shearing these remoulded clays Skempton and Northey demonstrated that the curves relating the undrained strength and the liquidity index (LI) for the different clays were very close (Fig.1 5(a)). They so observed that the strength of clays normally consolidated from a slurry in the laboratory is a function only of the liquidity index of the clay. This reinforced the distinction between the stable microstructure created in the laboratory by reconsolidating the clay from slurry and that resulting from the natural deposition process.

Skempton and Northey found that various sensitive natural clays from different environments had a more open structure than the clays consolidated from slurry in the laboratory, showing that the liquidity index of the natural clays is always higher than that of remoulded clay compressed to the same vertical pressure (Fig.1.5(b)). Skempton and Northey concluded that factors other than leaching and thixotropy account for the state of natural clays. It appears that the bonding created

during the very slow process of the natural formation of clays can be so strong as to impart to the intact clay a more open fabric and higher sensitivity than that of the remoulded clay under the same load (Fig.1.5(b)).

Clays consolidated from slurry in the laboratory can exhibit a sensitivity higher than 1 as the sensitivity of a one-dimensionally consolidated reconstituted clay depends on the initial water content, the load increment ratio and the loading rate (Mitchell and Houston 1969). In general, high loading rates, as applied in conventional oedometer tests, induce very low sensitivities, approaching 1. Burland (1990) defined as "reconstituted" the clays remoulded to form a slurry at water contents about the liquid limit and consolidated using the conventionally high laboratory loading rates. He thus distinguished the reconstituted clays, which then have S_t about 1, from the resedimented clays (Lerouil et al.1984), where the consolidation process is much slower, and from the remoulded clays disturbed to perhaps only a limited extent. The term reconstituted clay will be used in the following as suggested by Burland (1990).

1 6. Classification of fabrics

The models of microstructure were for too long oversimplistic, until the first use of polarizing and transmission electron microscopes. The models gave great emphasis to the existence of flocculated particle arrangements that were then considered a general feature of sensitive clays. Rosenqvist (1963) observed that the undisturbed fabric of Norwegian marine clays corresponded closely to the schematic picture of a clay mineral network dominated by edge to face contacts Both edge to face and edge to edge particle contacts were observed by Push (1966) which were similar to the card-house scheme (Fig.1.6(a)) already proposed by Lambe in 1953. The flocculated arrangement was considered responsible for the stronger and less compressible behaviour of natural clays and the deflocculated state was associated with remoulded clay (Fig.1.6(c)).

These rather simple schemes were not concerned with interparticle forces. However many purely theoretical studies were carried out to quantify the interparticle forces and deduce the resulting clay particle arrangements in given colloidal suspensions, as reviewed by V.Cotecchia et al.(1982-a). The results of these studies, together with improved applications of electron microscopy, revealed that the generally accepted concepts of flocculated and dispersed structures were too simple (Sides and Barden 1970). Nowadays, because of the increasingly sophisticated techniques and theoretical analyses involved in the study of the micromorphology of clays, this

has become a specialism distinct from classic Soil Mechanics Many fabric classifications are proposed in the literature, and quantitative interpretations of the fabric of clays are now possible using image processing of SEM pictures.

Sides and Barden (1970) provided a classification of the fundamental fabrics that, because it is concise, is considered helpful and will be referred to subsequently. Fig 1 7 shows schemes (a), (b) and (c) which represent flocculated fabrics, the term flocculated referring to a soil in which the net electrical force between the adjacent particles during deposition was attractive. The term "cardhouse" refers to the essentially single-particle arrangement of Fig 1.7(a), but little evidence of it is reported in the literature. The term "bookhouse" (Fig.1.7(b)) refers to a much more common structure The groups or aggregates of particles, in which the particles are approximately parallel are called domains. Domains are nowadays generally recognized as the fundamental unit of the clay fabric as they are casually formed in the suspension during deposition (V.Cotecchia et al.1982-a). Salt flocculated implies small domains containing few particles. An even more open fabric is the honeycomb (Fig.1.7(c)).

The term "dispersed" is used by Sides and Barden for a soil in which the net electrical force between adjacent particles during deposition was one of repulsion. Thus dispersed implies a rather close packed fabric, as in Fig(1.7(d)). But Sides and Barden considered that a more realistic representation of a dispersed fabric is the turbostratic fabric (Fig.1.7(e)), in which some edge to face contacts between domains are present. Areas of high degree of overall orientation, complete preferred orientation (c.p o.), is the stack represented in Fig 1.7(f).

The simple two-dimensional schemes of fabric are often difficult to recognize in the three-dimensional visualisation given by the SEM. Moreover the clay fabric is strongly affected by the presence of sand and silt grains, which induce turbulence even in a dispersed fabric (O'Brien and Slatt 1990; Lupini et al.1983; Hawkins and McDonald 1992). Sides and Barden pointed out that the main difficulty in classifying fabrics is to distinguish a turbostratic from a compressed bookhouse fabric. The first implies large domains with a gradual change in orientation, with the boundary between domains often diffuse and indistinct and with no inter-domain macro-voids. The compressed bookhouse fabric is formed of smaller domains having rather well defined boundaries with sudden and marked changes in orientation and large inter-domain macro-voids.

1 7 Fabrics of remoulded clays

Griffith and Joshy (1990) observed with the SEM the fabric of an illitic clay slurry at the liquid limit They described it as formed by three orders of aggregates and pores in a flocculated arrangement (Fig 1 8). In this scheme, the assemblages of domains interact through connectors which give the entire fabric a honeycomb appearance. Such a fabric is very distant from the simplified scheme of the fabric of the remoulded clay reported by Lambe (1953), Fig.1 6(c) According to the schemes in Fig 1.6, widely accepted in the past, the fabric of the remoulded clay was considered not to be aggregated and the intact fabric of sensitive clays was considered flocculated. But the intact sensitive and the remoulded clay can both have flocculated particle arrangements (Griffith and Joshy 1990; V.Cotecchia et al.1982-b). In fact what is fundamentally different between the structure of the remoulded clay and that of the intact sensitive clay is not necessarily the type of fabric, but the nature, stability and strength of the bonding.

V.Cotecchia et al.(1982-b) recognized flocculated domains in both a slurry of kaolin and a slurry of bentonite in distilled water; the flocculated fabric of the kaolin slurry is shown in Fig 1.9. They showed how the dimensions of the domains decrease with increasing mixing water content; a connecting bridge between assemblages, formed by smaller domains and sometimes by single particles, is shown in the SEM pictures (Fig.1 9(b)).

Differences between the natural and the remoulded clay fabric also arise from the distribution of the sand and silt grains In well graded clayey soils one fraction does not dominate the fabric and clay bands flow around the sand and silt grains When the clay fraction is small with respect to the silt and sand fractions, remoulding can give rise to segregation of the sand and clay. Lupini et al (1983) showed that segregation occurred in remoulded Lower Cromer Till, producing unusual effects on the stiffness and strength of the soil.

1 8. Effects of the deposition conditions on the clay fabric

Reviewing now the fabrics and the sensitivities observed for sedimented clays as the effects of particular deposition conditions, it may be observed that identical clay particles sedimented in solutions of different salinity form clays of different activity. In this case not only are the fabrics and the strengths of the sedimented clays different, but also the strengths of the equivalent remoulded clays are different, giving rise to different sensitivities (Lerouil et al.1984)

Sides and Barden (1970) studied the fabrics of kaolinite, illite and montmorillonite resulting from slurries containing chemical dispersing and flocculating agents. They observed that kaolinite formed in a flocculating environment at 30 kPa vertical pressure was not very different from that formed in a dispersing environment, both having a high degree of orientation. The fabric of the flocculated illite was far more random than the flocculated kaolin. So Sides and Barden concluded that the dispersing and the flocculating agents have a much greater influence on the arrangement of smaller colloidally active particles. They recalled cases of illitic clays deposited in a saline marine environment for which fairly random open fabrics had been observed and a case of illitic clay deposited in dispersing conditions created by the presence of organic matter whose fabric was highly oriented.

Distinguishing the origins of the features of a natural fabric is a very complex task, even for a sediment of recent deposition. The fabric at deposition will be here termed "primary fabric". Confined areas of different primary fabric can exist as a consequence of either the local presence of chemical agents, organic matter, or a local perturbation of the mechanical deposition. O'Brien and Slatt (1990) showed that lamination indicates that deposition occurred in still conditions, with no post-depositional mixing, while the existence of pyrite framboids (Fig.1.10) is an indicator of anaerobic sulphide diagenesis developing in the early stages of consolidation, implying the existence of a confined, reducing environment.

1.9 Effects of one-dimensional compression on the clay fabric

The subsequent modification of the primary fabric by one-dimensional consolidation is very complex. Primary fabrics which are random can be preserved during burial if chemical compounds precipitate during deposition and act as cementing between the particles. In Fig.1.11 SEM pictures by Veniale (1985) show precipitated calcite and gypsum crystals. But cementing can not be always recognised as they may exist in an amorphous state. The measurement of high content of possible cement compounds in the clay is not enough to establish its cemented nature. Hawkins and McDonald (1992) showed that great part of the carbonate content measured in a calcareous mudrock can be concentrated in the silt and sand fractions, so being detritic rather than a precipitate. In general a cemented nature of a clay cannot be inferred from a high carbonate content.

It is a general belief that one-dimensional consolidation orientates the uncemented clay particles to lie normally to the consolidation stress (Tchalenko 1967). However, although an increase in the

average degree of orientation of the clay particles is observed in many clays with increasing vertical stress, this may result from the development of areas of highly oriented fabric and the preservation of areas of non-oriented fabric. Griffith and Joshy (1990) observed by means of SEM that after compression of a slurry to 490 kPa vertical stress (Fig.1.8), the connectors in the fabric had been destroyed and much of the inter-assemblage porosity was lost. But at this pressure the reorientation involved only part of the fabric, and a random fabric was still preserved inside the assemblages. Consolidation to 1500 kPa vertical stress induced reorientation of the particles within the aggregations, though some areas of random orientation could still be recognized.

V.Cotecchia et al.(1982-b) reported SEM pictures (Fig.1.12) showing the effects of one-dimensional consolidation on the kaolin slurry in Fig. 1.9. At 4.9 kPa (Fig.1 12(a)) the fabric was already much more compacted than that at the liquid limit although, not discussed by the authors, a complex fabric architecture can be identified consisting of horizontal strata of c.p.o. fabric (Section 1.6) interbedded between areas of flocculated fabric. These strata resemble horizontal slabs sustained by a truss of domains in edge to face contacts (Fig.1.12(e)). Further compression induced further development of the strata of c.p.o. fabric, the stacks, and the fabric developed through interpenetration of the domains (V.Cotecchia et al 1982-b). The level of orientation achieved by compression to 490 kPa was not increased significantly with compression to 4900 kPa. The further loading only increased the density of the clay, while edge-to-face contacts between domains were preserved.

Sfondrini (1975) proposed a scheme for fabric development in oedometric compression, i.e. during the application of high loading energy. First he suggested that there exists a lower bound stress below which the fabric of the clay is determined by the internal forces. Above this value the external forces determine the fabric of the clay. Sfondrini discussed the case of Fiumicino clay, an illitic clay that after deposition in a brackish lagoon and normal consolidation to 180 kPa still has a bookhouse fabric (Fig 1.13(a)), showing that the in situ consolidation preserved much of the primary fabric. Sfondrini found that under oedometric compression in the laboratory the strain was concentrated in some areas of the sample, preserving the porosity of others. Sfondrini identified a stage when strata of c.p.o. fabric, referred to as "stacks" above, and that Sfondrini called "complex laminae", formed between a honeycomb fabric (Fig 1.13(b)). The picture and the scheme in Fig.1.13(b) resemble the fabric architecture described for compressed kaolin, Fig 1.12(e).

The complex laminae are predominantly formed of particles in face contact, which progressively grow with increased loading. Similar fabrics develop in stiff clays which have been subject to both high consolidation and high shearing stresses in situ. Sfondrini (1975) observed that samples of Scaly Clays are crossed by frequent slip surfaces which cut strata of c p o particles. These strata are interbedded in a more random fabric. Also in clay samples sheared to residual V.Cotecchia et al.(1982-b) observed the presence of strata of c.p.o. fabric on the sides of the shearing plane, interbedded in a honeycomb fabric.

It seems then that both one-dimensional consolidation and shearing result in heterogeneous straining and the formation of complex laminae or stacks. The data shown in Figs.1.12 and 1.13 will be frequently referred to in the study of the Pappadai clay fabric in Chapters 5 and 7.

1.10. Other structural changes occurring during geological compaction

When a clay is compressed due to burial, structural phenomena occur which can significantly modify the clay's structure. The physico-chemical equilibrium inside the clay microstructure changes with time since it is influenced by such factors as the electrostatic and the magnetic interactions between crystals, the ion concentration in the pore water, the vapour tension, the osmotic pressure, temperature and the conditions of the buried organic material. Either externally induced variations of any of these factors or the development of chemical reactions within the sediment can cause substantial changes of both the bonding and the fabric of the clay with time.

"Ageing" is defined as the stage in which the clay rests after burial following primary consolidation. Usually in Soil Mechanics the main phenomena occurring during ageing are considered to be creep deformations and the thixotropic processes. Thixotropy is a reversible process (Skempton and Northey 1952) which develops during periods of rest of the clay and induces an increase of strength and sensitivity that is lost on remoulding. The physico-chemical phenomena involved in it are still obscure. Skempton and Northey visualised thixotropy as developing by inter-penetration of the double layers and the bound water surrounding particles. Mitchell and Houston (1969) assumed that for deflocculated remoulded clay thixotropy was triggered by a tendency for aggregation, which then develops in a reorganization of fabric and double layers. Thixotropic hardening develops in nature for any clay at rest and in general it induces sensitivities of 1.5-2, developing mostly in the first year of rest of the sediment (Skempton and Northey 1952).

Here we distinguish thixotropy from diagenetic phenomena which require a longer time to develop, and are predominantly irreversible. Diagenesis can produce modifications and creation of crystals, the alteration and crystallisation of organic matter, the strengthening of the clay bonding and changes of fabric. Mild diagenesis can start in the early stages of burial, as the vertical pressure increases and the soil-water system becomes hydraulically confined, as is the case for the alteration of organic matter triggering the formation of pyrite and greigite previously discussed. Some diagenesis can also occur in clay under high pressures while it is still consolidating Generally the diagenetic processes which cause the major structural changes, strengthen the clay bonding and increase the clay strength all develop at high pressures after consolidation, i.e. in the clay at rest. In the following such diagenetic processes will be referred to as "long-term diagenesis".

The aggradation of the swelling minerals, previously discussed, is a common diagenetic process. The formation of authigenic cement between the clay particles can also occur after consolidation at high pressures as part of the long-term diagenesis. Cement can precipitate if a supersaturated solution fills the pores (Sfondrini 1975), as in clays rich of either calcareous fossils or detritus, when an authigenic carbonate cement can be formed as a result of the segregation of calcite in either its crystalline or amorphous forms (Veniale 1985). Long-term diagenesis can modify the clay fabric and bonding to such an extent as to significantly affect its mechanical behaviour

The occurrence of diagenetic phenomena can be identified if the mineralogy and chemical composition of the soil is seen in the context of the geological history of the deposit. The direct visualisation of the fabric of the clay greatly helps this reconstruction (O'Brien and Slatt 1990).

1.11. Proposed soil structure classification

The structure of a clay is then the result of the combination of all the geological phenomena that have occurred since deposition. Further microstructural changes can occur in an overconsolidated clay after unloading. But it is apparent from the above discussion that a description of all the processes affecting the microstructure of a clay can never be complete and that the soil structure should be thought of as continuously developing, being affected by most of the environmental factors involving the clay.

Here a classification is proposed which divides the clay structures into two groups, as defined in Table 1.1. Structures are distinguished on the basis of their history. Each group includes

structures of different characteristics, but which can give rise to similar basic features of clay behaviour, as will be discussed in Chapter 2. This classification of structures will then be used for a classification of clays which will be useful in the construction of a general framework of behaviour.

The group of processes which comprises those that determine the clay structure during deposition and following virgin compression is defined as group 1 in Table 1.1. The resulting structure is here called the "sedimentation structure" (see Table 1.1) and can exist only in clays which are normally consolidated (NC).

Group 2 in table 1 1 comprises all the processes developing after virgin compression, that is those occurring during ageing, e g. thixotropy and long-term diagenesis, and in any subsequent geological event which affects the clay both at the micro and the macro-level, e.g. unloading, weathering, etc. The clay affected by the processes of the second group may or may not be overconsolidated by geological unloading, i.e. it can have OCR equal to or above 1, but nonetheless its structure will be different from the sedimentation structure and results from both the phenomena giving rise to this structure and phenomena of the second group. The structure of clays affected by the phenomena in the second group will be defined as the "post-sedimentation structure" (see Table 1.1).

The processes giving rise to the sedimentation structure give rise to the "sedimentation sensitivity", which is the sensitivity that a NC clay has if its structure has not undergone changes after virgin compression. The processes of the second group can give rise to an "acquired sensitivity". The sensitivity of a clay that after virgin compression had its structure changed from the sedimentation structure into the post-sedimentation structure, is the result of the superimposition of the acquired sensitivity on the sedimentation sensitivity and is here defined as "post-sedimentation sensitivity". These definitions will be applied to structures of natural and reconstituted clays whose behaviour is reviewed in the following chapters.

<table>
<tr><td rowspan="2">GEOLOGICAL PROCESSES</td><td>GROUP 1
Processes at deposition and during virgin compression:
flocculation, dispersion, cementation, fabric compaction, mild diagenesis in clay still compressing</td><td>GROUP2
Processes after virgin compression:
thixotropy, long-term diagenesis, authigenic cementation (in the clay at rest), weathering, geological unloading, leaching</td></tr>
<tr><td colspan="2">POST-SEDIMENTATION STRUCTURE
(inherited from Group1 and Group2)</td></tr>
<tr><td rowspan="2">STRUCTURES</td><td>SEDIMENTATION STRUCTURE</td><td></td></tr>
<tr><td colspan="2"></td></tr>
<tr><td rowspan="2">SENSITIVITIES</td><td>SEDIMENTATION SENSITIVITY</td><td>ACQUIRED SENSITIVITY</td></tr>
<tr><td colspan="2">POST-SEDIMENTATION SENSITIVITY
(inherited from Group1 and Group 2)</td></tr>
</table>

Table 1.1 ***Classification of structures and sensitivities of clays***

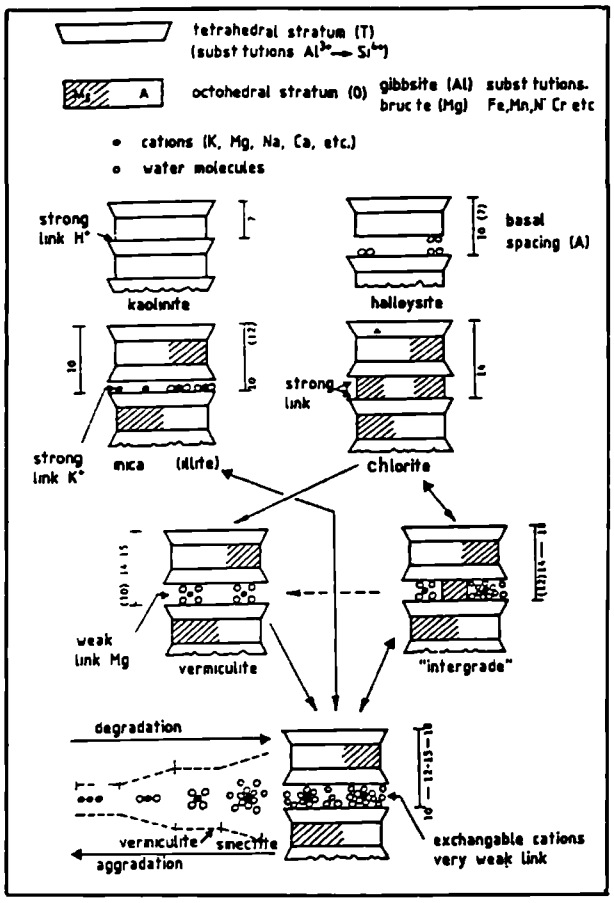

Fig.1.1 Structure of the main clay minerals (after Veniale 1983).

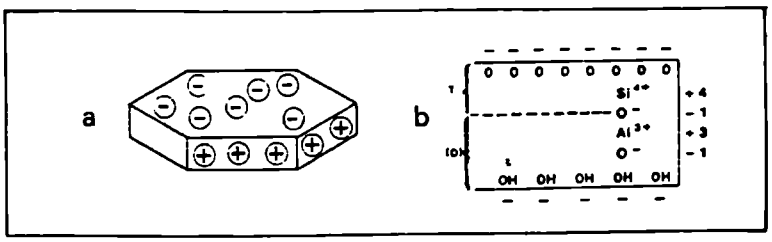

Fig.1.2 (a) Charge distribution on the clay particle surface; (b) Internal surface structure of a structural unit of Kaolinite (after Veniale 1983).

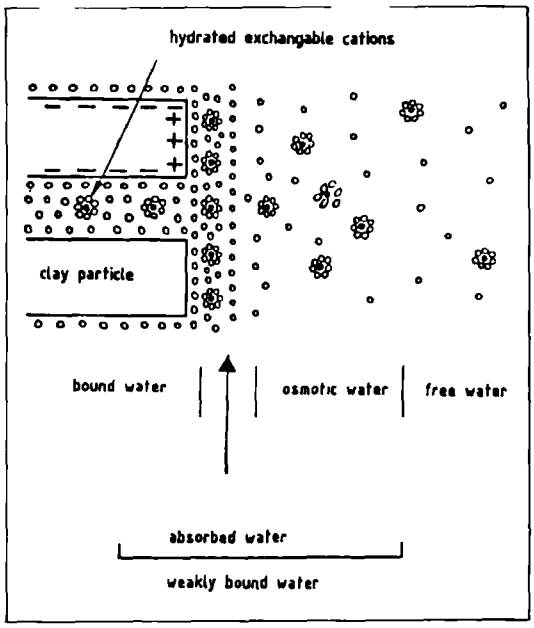

Fig.1.3 Scheme of the different water layers surrounding the clay particle (after Veniale 1983).

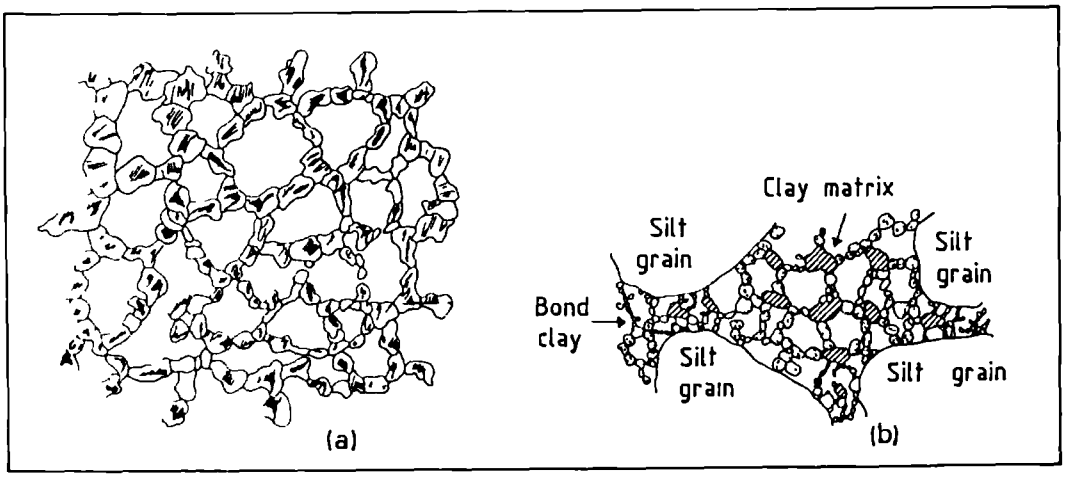

Fig.1.4 (a) Terzaghi-Casagrande honeycomb fabric (after Terzaghi 1925); (b) Open fabric of undisturbed marine clay (after Casagrande 1936-a).

a)

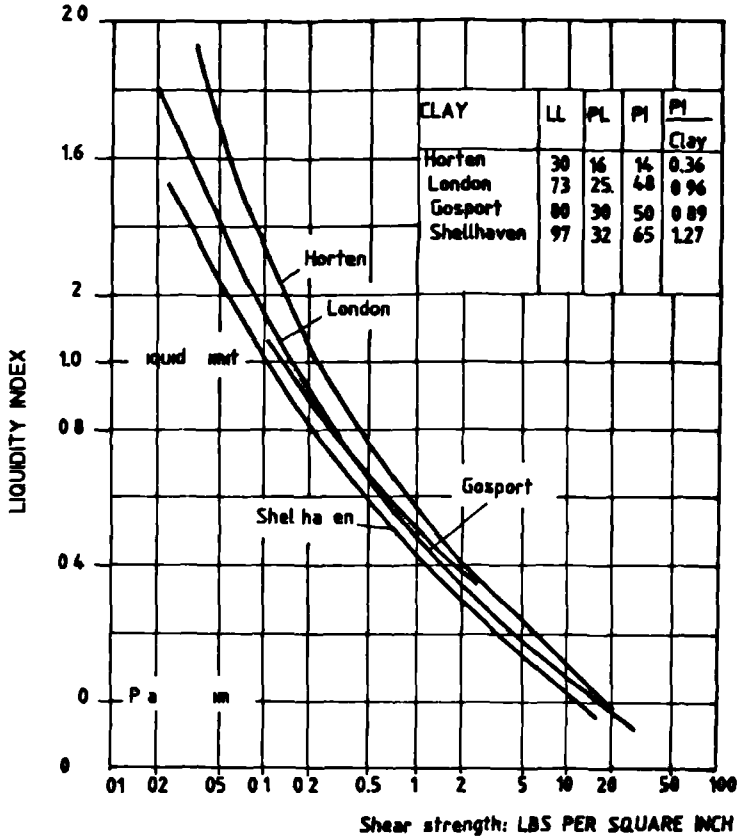

b)

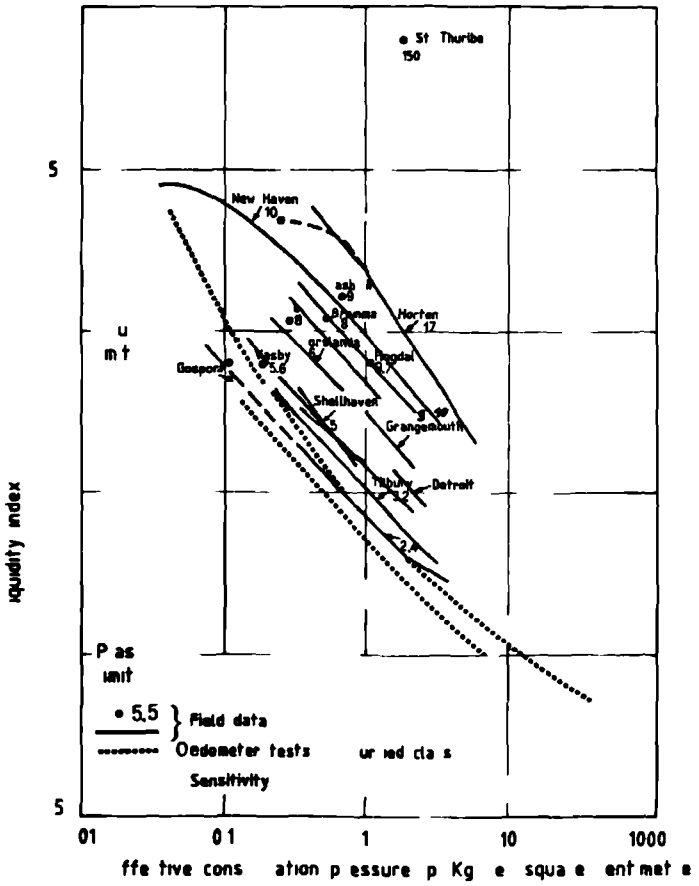

LOCATION	AVERAGE	
	SENSITIVITY	LIQUID LIMIT
St Thuribe	c. 150	33
Horten, Norway	7	32
New Haven,	c. 10	93
Hodal	9.7	64
Vasby	9.0	79
Bromma	8.0	69
Angso	8.0	87
Torslanda	6.0	67
Vasby	5.6	125
Shellhaven	5.5	105
Gosport-mud	4.4	80
Grange-mouth	4.3	41
Tilbury	3.2	00
Gosport-deep	2.4	80
Detroit	2.3	3
London	c. 9	77

Fig 1 5 (a) Relation between liquidity index and undrained shear strength of remoulded clays, (b) Relation between liquidity index and consolidation pressure for natural and remoulded clays (after Skempton and Northey 1952) and constant sensitivity lines

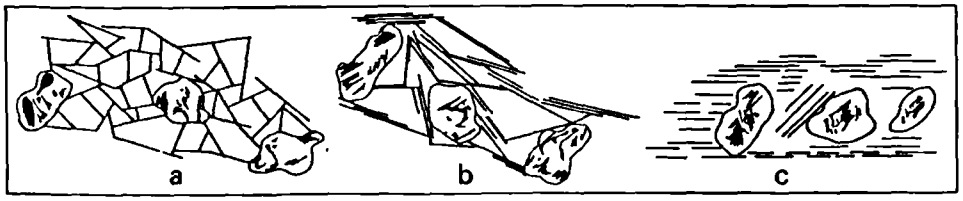

Fig.1.6 (a) Cardhouse fabric in saltwater deposit (b) cardhouse fabric in freshwater deposit; (c) remoulded fabric (after Lambe 1953).

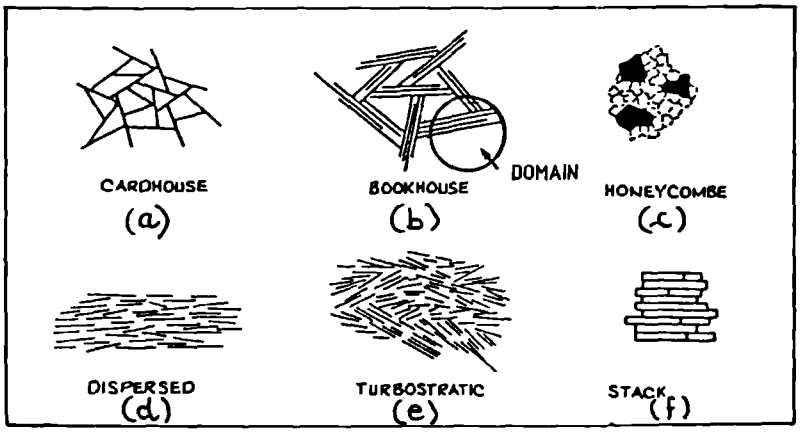

Fig.1.7 Idealized clay fabrics (after Sides and Barden 1970).

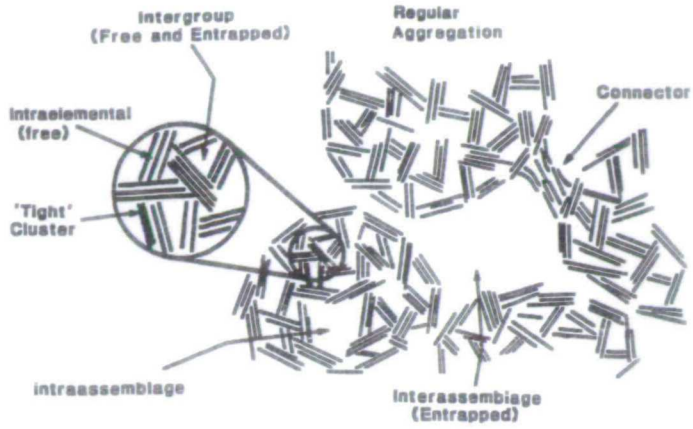

Fig.1.8 Assemblages and pore classes in the open fabric of a reconstituted clay (after Griffith and Joshy 1990).

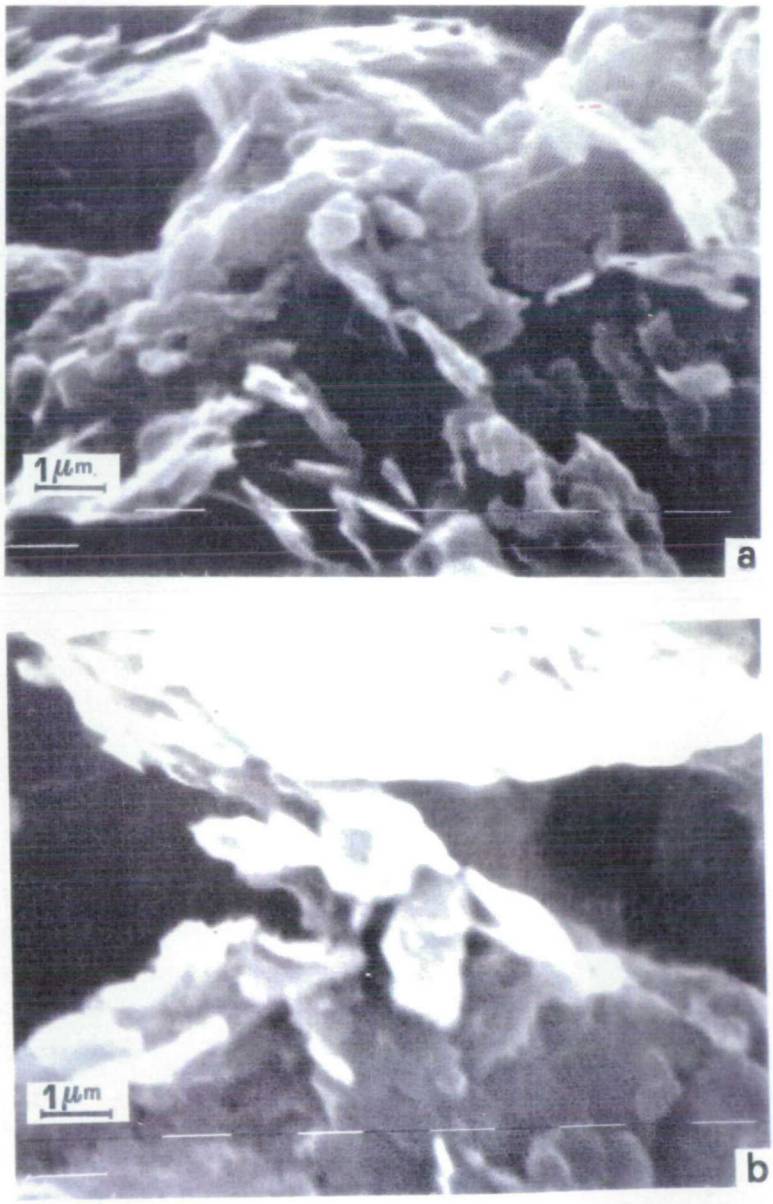

Fig.1.9 (a) Kaolin slurry (w=117%); (b) "bridge" between domains (after V.Cotecchia et al.1982-b).

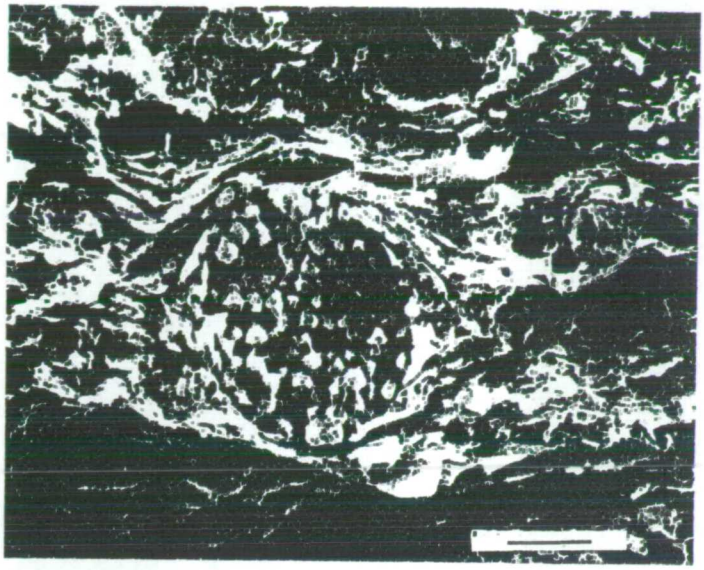

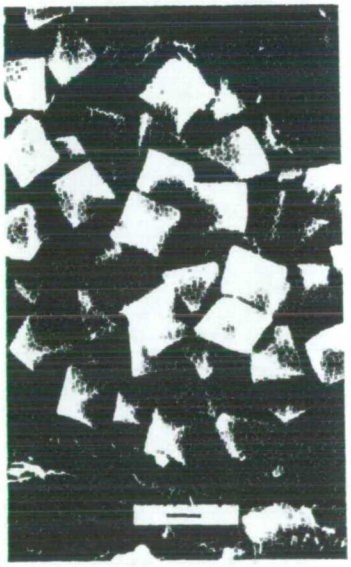

Fig.1.10 Pyrite framboids (after O'Brien and Slatt 1990).

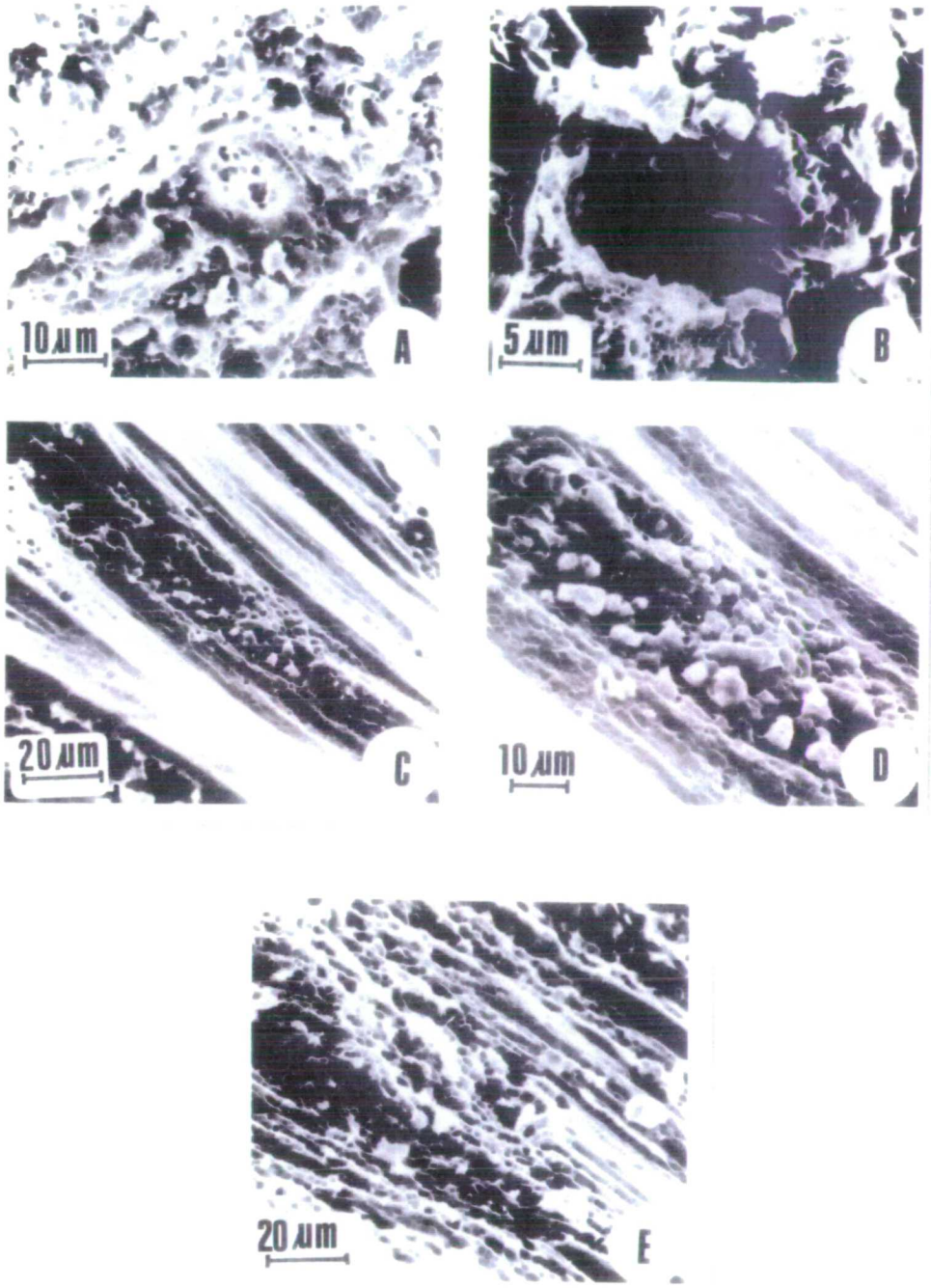

Fig.1.11 (a) and (b): pore spaces partially or completely filled with calcite crystals; (c), (d) and (e): irregular grains of calcite and flakes of gypsum deposited within the interlayering of laminated clays (cross section) (after Veniale 1985).

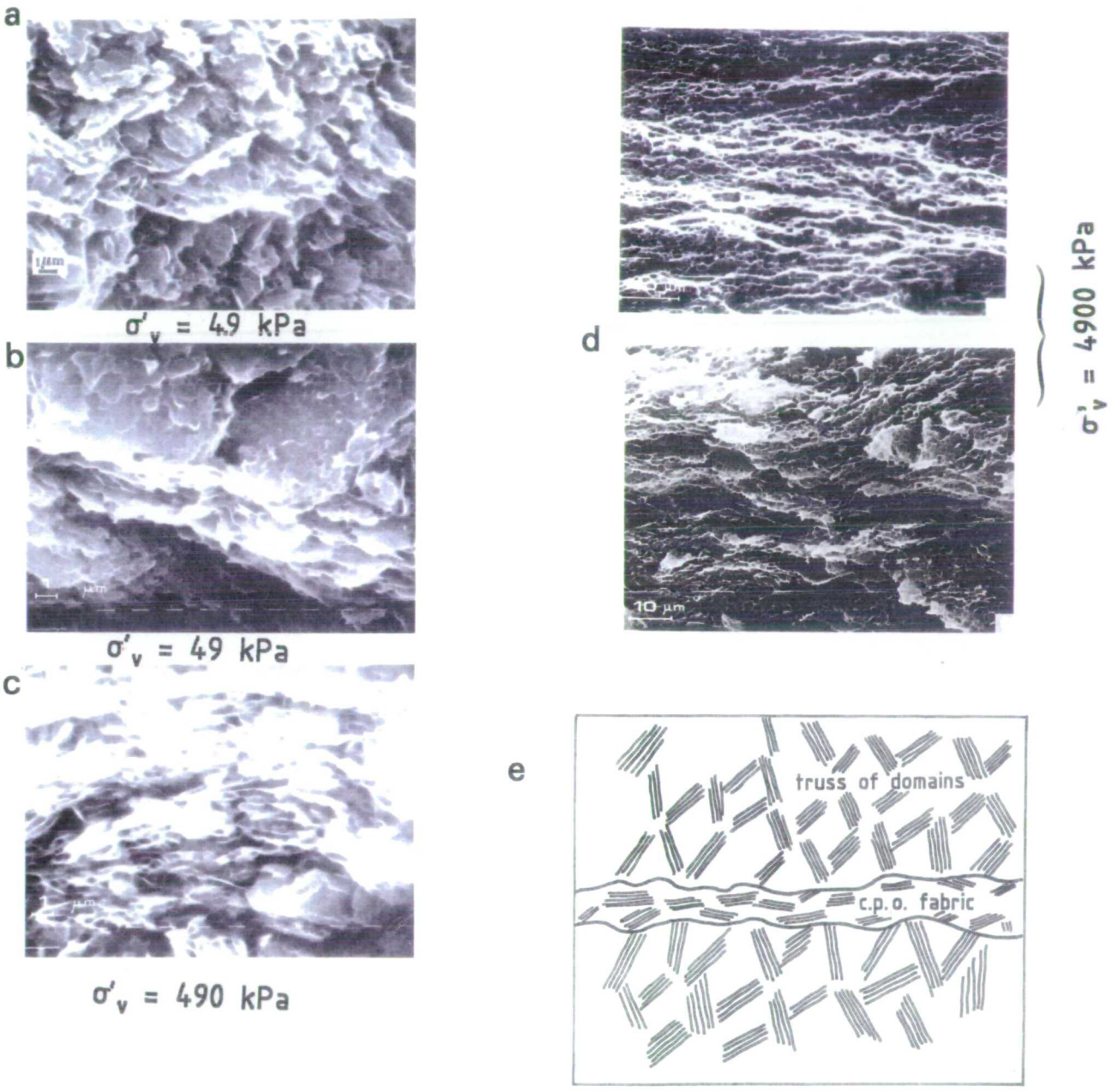

Fig.1.12 Oedometer compression of a kaolin slurry (w_0=63%=w_{LL}): (a) σ'_V=4.9kPa; (b) σ'_V=49kPa; (c) σ'_V=490kPa; (d) σ'_V=4900kPa; (e) scheme of the complex architecture of the fabric in (a); pictures after V.Cotecchia et al.(1982-b).

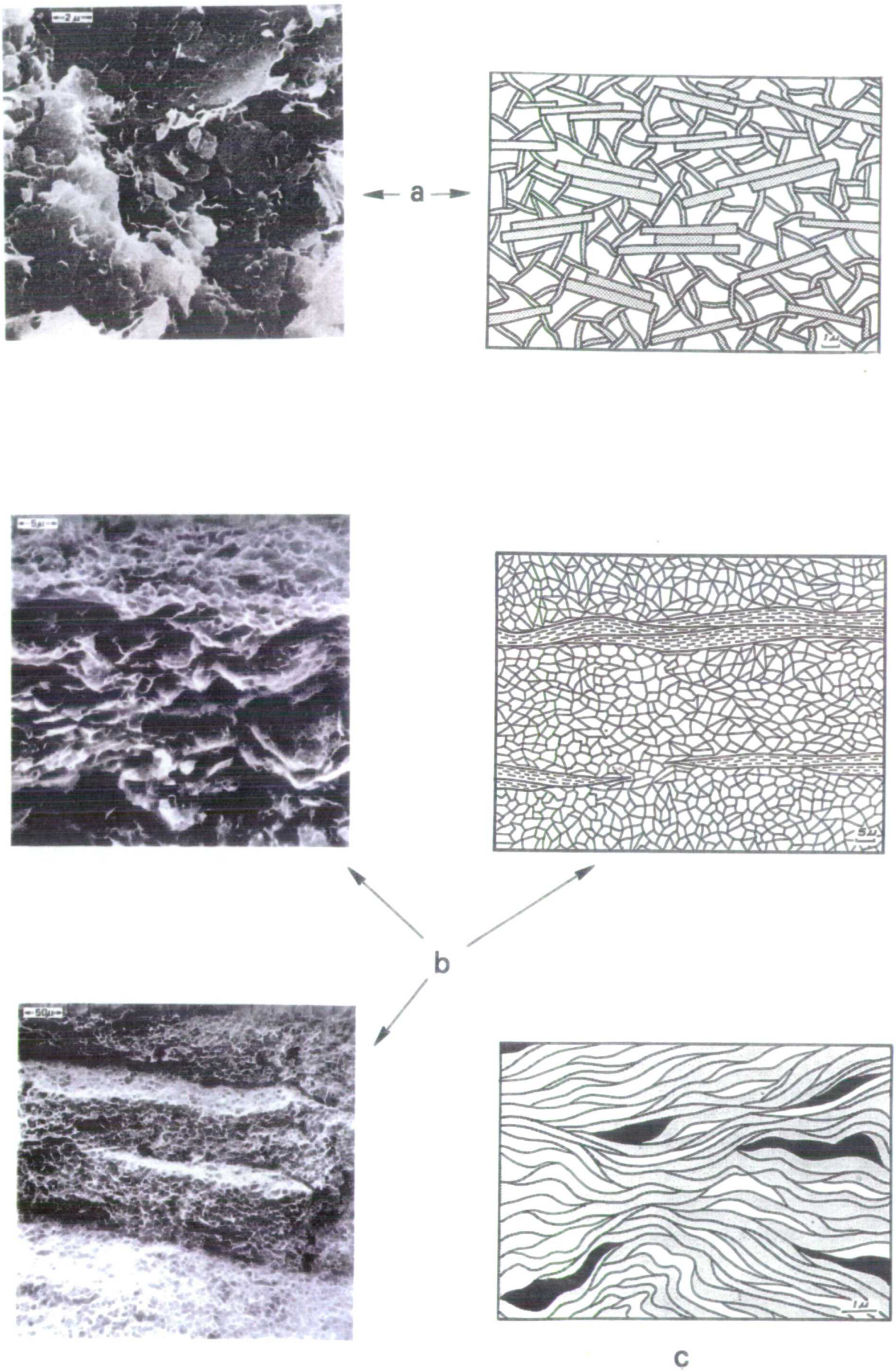

Fig.1.13 Fiumicino clay, normally consolidated in situ : (a) fabric on a verical fracture through an undisturbed sample from 18m depth; (b) fabric on a vertical fracture through a sample compressed to σ'_v = 4704kPa; (c) fabric scheme applying to the clay compressed to very high stresses (after Sfondrini 1975).

CHAPTER 2

MECHANICAL BEHAVIOUR OF CLAYS AND PROPOSALS FOR A GENERAL BEHAVIOURAL FRAMEWORK

2.1. Introduction

In this chapter the basic features of a general framework for the behaviour of clays are proposed based upon a literature review of the behaviour of both reconstituted clays and natural clays. The validity of the proposals reported in the present chapter was further investigated in the research.

Given the definition of structure in Chapter 1, the behaviour of all reconstituted and natural clays is determined by their fabric and bonding. Despite the differences in structure between different clays there are some common features of behaviour. These can be identified if the Critical State Framework (CSF), which represents the behaviour of reconstituted clays, is compared with the response of natural clays. Whether the basic features of the CSF and the basic deformation mechanisms underlying it apply both to anisotropically consolidated reconstituted clays and to natural clays is discussed in the following sections, accordingly.

A classification of clays is proposed in Section 2.5.3 on the basis of both the geological history and the one-dimensional compression of the clay in the I_v-σ'_v plane. Although the eight clay types defined in the classification have different origins, fabric and bonding, they all have either a sedimentation or a post-sedimentation structure as defined in Table 1.1. The definition of these clay types is taken as a starting point for the construction of a general framework of behaviour of clays.

2.2. The behaviour of reconstituted clays

2.2.1. The Critical State Framework

Most of the research on the mechanical behaviour of clays has been based on laboratory testing on either reconstituted or remoulded clay. The features of the structure of remoulded and reconstituted clays have been discussed in Sections 1.5 and 1.7. In both the cases series of specimens of equal mechanical properties can be created on which a defined stress-strain history

can be applied So the testing of remoulded-reconstituted clay specimens was a rational start to investigate the clay behaviour. A large part of this research investigated the clay response for axially-symmetric stress paths.

The Critical State Framework (Roscoe et al.1958, Roscoe and Poorooshasb 1963, Schofield and Wroth 1968) was the first rationalization of the results of the research on reconstituted clays, and it addressed concepts fundamental to the general behaviour of soils. The most important concept underlying the framework is that the soil behaviour depends both on specific volume (v) and the effective stress invariants (q; p'). The state of the clay is represented as a point in the v-q-p' space at any stage of its state history. The framework considers the clay behaviour along axi-symmetric stress paths and shows that the clay behaviour with respect to the effective stresses is the same for different constant volumes apart from a scaling factor and that the clay behaviour can be normalized with respect to volume (Rendulic 1936; Hvorslev 1937; Roscoe et al 1958; Roscoe and Poorooshabs 1963; Schofield and Wroth 1968).

Using results of the type shown in Fig.2.1 the isotropic virgin compression and the isotropic swelling of the reconstituted clay were represented in the v-lnp' plane as straight lines, of gradient λ and κ respectively. The volumetric behaviour was described as elasto-plastic during virgin compression and as non-linear elastic during isotropic swelling (Schofield and Wroth 1968). In one-dimensional compression the linearity of the virgin compression line in the v-logσ'_v plane and the constant value of K_0 ($=\sigma'_h/\sigma'_v$) (Jaky 1944; Brooker and Ireland 1965; Schmidt 1966) were both consistent with a state path plotting as a straight line in the v-lnp' plane. The one-dimensional compression line:

$$\eta = q/p' = 3(1-K_0)/(1+2K_0) \qquad (2.1)$$

appeared to be closely parallel to the isotropic compression line. All the lines at constant stress ratio η ($=q/p'$) were assumed parallel in the v-lnp' plane, so as to plot positions which are geometrically similar for changing volume, and the swelling from any η line was considered to be uniquely related to the change of p' and to follow lines of constant gradient κ. The experimental results obtained by Gens (1982) for reconstituted Lower Cromer Till (Fig 2 2) are an example of later experimental evidence that confirmed that these CSF assumptions were well justified.

2 2 2. The existence of a critical state or state of permanence

The existence of a critical state (CS), reached by the soil at large distortions, at which the soil can undergo distortions at both constant volume and effective stress, was first defined by Casagrande (1936-a). Roscoe et al.(1958) also observed critical states at large strains in simple shear tests. Results of triaxial tests on isotropically normally consolidated reconstituted clay (Parry 1960) also showed that the clay reached a final state of constant volume and effective stress. For a given specific volume, the critical state was found to occur at a unique effective stress and the locus of the critical states in v-q-p' space coincided with the line $q/p' = \mathcal{M}$; $v = \Gamma - \lambda \ln p'$ (Parry 1960; Fig.2.3).

Schofield and Wroth (1968) described the critical state as flow of the soil like a frictional fluid, with the energy dissipated as friction. They intended "loosely" to define friction as a basic property of the soil that determines its response. The gradient of the critical state line in the q-p' plane, $\mathcal{M}$, is a simple constant modelling frictional behaviour at the macroscopic scale. It defines the deviatoric stress, q_{cs}, needed to keep the soil flowing at the critical state for a given p'_{cs}.

The data in Fig.2.3 are for both undrained and drained shearing tests on isotropically normally consolidated clay. The framework assumed that the critical state is reached during shearing of both isotropically normally consolidated and overconsolidated specimens, as shown in Figs.2.4 and 2.5. The stress paths in Fig.2 4 are normalized with respect to volume by means of an equivalent pressure p'_e, which will be discussed later and be referred to as p^*_e. The $\eta = \mathcal{M}$ line lies parallel to the other constant η lines Contractant and strain hardening behaviour is shown by the soil yielding in shear on the right side of the critical state line, and dilation with strain softening is exhibited by the soil yielding on the left side of the critical state line (Figs.2.5 and 2.6(d)). Thus the critical state line is a key locus, separating two different shear behaviour modes.

Schofield and Wroth claimed that the ultimate fully remoulded condition of the critical state would always occur if the process of uniform distortion were carried out on until the soil flowed as a frictional fluid. However they acknowledged that specimens only approach the critical state after severe distortion, when strain may no longer be homogeneous, so that the conditions in the specimen cannot be expected to define accurately a point on the critical state line. Only those portions of the specimen which are strained reach the critical state.

2 2 3. The State Boundary Surface on the wet side of the framework

Rendulic (1936) and later Henkel (1960) showed that the stress-strain behaviour during shearing of isotropically normally consolidated clay can be normalized with respect to volume. Undrained stress paths at different volumes and constant volume contours from drained stress path data all exhibited a similar shape in the effective stress plane. Thus in the v-q-p' space the stress paths during shearing of the isotropically normally consolidated clay lie on a unique surface, the "Roscoe" surface, that stretches from the virgin isotropic compression line to the critical state line. The η lines were assumed to lie on the Roscoe surface as it was presumed that no stress path crossed it. This surface was then termed the "state boundary surface" (SBS) by Roscoe and Poorooshabs (1963), as it was considered to confine the domain of the possible states for the clay. Normalizing the stress states on the boundary surface with respect to volume by means of the mean effective stress p^*_e on the isotropic compression line corresponding to the same volume, Roscoe and Poorooshasb (1963) defined a two-dimensional representation of the Roscoe surface. The normalized Roscoe surface for kaolin is shown in Fig.2.7 (Balasubramaniam 1969).

2.2.4. Shearing behaviour on the dry side of the framework

On the dry side of the framework the difficulty of observing stress paths approaching critical state was attributed by Schofield and Wroth to the instability triggered by strain softening. As heterogeneous strains usually occur in specimens, they considered strain softening to give rise to localization of strain which causes the difficulties to recognize the arrival to critical state on the dry side.

The effects of dilation on the peak strength of granular soils were analyzed by Rowe (1962) in detail. He assumed friction to be the property of the soil which governed its strength, and chose the friction between the mineral surfaces at the interparticle contacts as the friction constant ϕ_μ for the soil. He modelled mathematically the sliding of particles during the deformations of the assemblage and, following Taylor (1948) and Skempton and Bishop (1950), he calculated the work done by the effective stresses as dissipated in frictional heat. So Rowe derived the stress dilatancy equation.

$$\sigma'_1 / [\sigma'_3 (1 + (dV/V)/d\varepsilon_1)] = \tan^2 (45 + \phi_\mu/2) \qquad (2.2)$$

which shows that both friction and the dilation rate determine the peak strength, the peak occurring when the dilation rate is maximum. The stress-dilatancy theory explained the peak failure, although it did not explain how the dilation rates vary in the v-q-p' space. For dense packings at low confining stresses eq.(2.2) was shown to work with $\phi_{p_{max}}$ but with increasing voids ratio or confining pressure dilatancy at failure gradually reduced, and a parameter ϕ_f had to be considered, which accounted for overall frictional effects. For a range of soils that would plot on the wet side of the critical state framework, Rowe recognized the occurrence of failure at constant volume and stress. Therefore Rowe identified a critical state, which he described as a state when continuous local dilations and contractions occur.

From the experimental observations reported by Rowe, heterogeneity of strain appears always to be active in the soil during large distortions, as strain is continuously redistributed among particle groups. The peak strength can therefore be seen as the maximum average of the strengths exhibited by differently strained particle groups. When strain softening starts in some of the particle groups, the redistribution of strain tends to strain localization. Therefore Rowe, in agreement with Schofield and Wroth (1968), regarded the strain softening behaviour as the trigger of the formation of the failure surface post-peak, and not vice-versa.

2.2.5. The total State Boundary Surface

The normalization that Hvorslev (1937) applied to the direct shear strengths showed that the peak strength behaviour in the v-q-p' space can be normalized with respect to the volume at failure. A similar normalization was found by Parry (1960) to be successful for peak strength values recorded for triaxial stress paths on isotropically consolidated clay. In the v-q-p' space the peak states lie on the "Hvorslev" surface (Fig.2.8).

The Hvorslev normalization demonstrates that the effects of dilatancy on the peak strength outlined by Rowe (1962) can be normalized with respect to volume at peak. Within the CSF, state paths for overconsolidated soils are assumed to reach the Hvorslev surface and then travel on it towards the critical state, while exhibiting large plastic deformations. The Roscoe surface and the Hvorslev surface together thus define the complete state boundary surface (SBS) (Roscoe et al.1958; Roscoe and Poorooshasb 1963) for isotropically consolidated reconstituted clay (Fig.2.8).

2 2 6 Frictional behaviour of clay and the Cam Clay model

Cam Clay (Schofield and Wroth 1968) was intended to be a simple model to interpret soil behaviour at large strains within the critical state framework. The model assumed elastic behaviour below the SBS, where the state paths move along elastic walls defined by the κ lines as shown in Fig 2 8. The model thus assumed yield to occur on the SBS and considered the soil behaviour to be isotropically hardening with volume after yield, the yield curves in the v-q-p' space being similar. The yield stress states normalized with respect to the corresponding isotropic preconsolidation pressures p'_p give the yield curve of the clay in the plane of normalized stresses q/p'_p-p'/p'_p.

During plastic deformation, the behaviour was assumed to be simply frictional, $\mathcal{M}$ being the constant expressing the frictional properties of the soil. Consequently the model assumed the work associated with the plastic strains to be dissipated as frictional loss:

$$q\, d\varepsilon_s^p + p'\, d\varepsilon_v^p = \mathcal{M}\, p'\, d\varepsilon_s^p \qquad (2.3)$$

where ε_v and ε_s are the strain invariants, the superscript p referring to the plastic component. Both eqs.(2 2) and (2.3) model the effects of volumetric strain assuming a purely frictional deformation mechanism, although the relative modelling approaches are fundamentally different. The importance of eq.(2.3) is in the fact that it demonstrates in a simple way how the assumption of frictional mechanism of deformation, which will later be referred to as frictional deformation, explains the stress-strain behaviour of the soil on both sides of the critical state line. On the right side the soil yields at q/p' less than $\mathcal{M}$. If a frictional mechanism of deformation applies, then for equation (2.3) the soil necessarily has to contract and strain harden, and indeed soils yielding on the right side exhibit this behaviour. Schofield and Wroth (1968) termed the domain where the soil yields at stress ratios q/p' lower than the critical stress ratio $\mathcal{M}$, where the soil contracts, as the "wet zone", using the phrase "weak at yield" (Fig.2.6(a)). For reconstituted clays, in the v-p' plane the wet domain happens to be concentrated to the right of the critical state line (Fig.2.6(d)).

On the left side of the critical state line the soil yields at q/p' values higher than $\mathcal{M}$, and the constitutive law (eq 2 3) then requires the soil to dilate, as actually observed. Schofield and Wroth termed dry zone the domain where the soil yields at stress ratios higher than the stress ratio at critical state. The wet and dry behaviour modes are then truly related only to the difference between the yield stress ratio q/p'_y and the basic friction ratio $\mathcal{M}$ (Figs 2 6(a) and (b)).

Equation (2.3) defines the flow rule of the soil model Cam Clay assumes that the soil is a stable plastic material and applies the associated flow and the normality rule. The yield locus equation is then defined by integrating equation (2 3), assuming that the yield curve lies on an elastic wall and intersects the critical state line; four parameters are required to describe fully the stress-strain behaviour of the soil: λ , κ, Γ, $\mathcal{M}$.

Other critical state based models (Roscoe and Burland 1968; van Eekelen and Potts 1978; Nova and Wood 1979; Pender 1978) have been formulated which assume the soil to yield on the SBS and to be strain hardening with volume, but which modify the soil flow rule used in the Cam Clay model. However, it is now generally accepted that soil is already at yield after very small strains, and that its true yield surface involves a region of very small extent (Atkinson et al.1990; Jardine 1992). The onset of plastic straining is observed at shear strain as low as 0.01%. Atkinson et al. (1990) and Jardine (1992) have shown that the elastic boundary of soils is a kinematic yield surface inside the SBS which is dragged with the current stress point through the stress space. However, mathematical modelling continues to introduce more realistic representations of the soil stress-strain behaviour within the powerful simplicity of the critical state framework.

2.2.7. "Basically" frictional deformation

Analyzing the extent to which the behaviour of different natural and reconstituted clays fits the CSF provides a start for the definition of a framework of more general validity. The applicability of the concept of critical state to the behaviour of the soil has first to be evaluated. The concept was criticized by Bishop et al.(1965) on the grounds that critical state does not necessarily coincide with the final shearing state of clays. But the fundamental role of the critical state is that it defines how the fabric of a specimen is modified by shearing, either dilating or contracting, rather than in the definition of the ultimate soil deformation mode. The following sections examine the extent to which the movement towards a critical state determines a clay's mode of deformation at large strains as contractant or dilatant, as expressed by eq.(2.3).

Eq.(2.3) interprets the clay behaviour as solely frictional and it is not necessarily an accurate mathematical expression of the flow rule even for reconstituted soils which do arrive at a critical state and which exhibit a seemingly frictional behaviour. This is because the frictional component of behaviour may be more or less dominant depending on the influence of structure on the soil

stress-strain behaviour and eq (2 3) is more than anything a simple tool to interpret the soil behaviour. However it is of considerable value, as a similar equation of the type :

$$q\,p' = \mathcal{M} - A\,d\varepsilon_v^p/d\varepsilon_s^p \qquad \text{with} \qquad A(q,p')>0 \qquad (2\ 4)$$

will be shown to be generally applicable in the following sections. Also when the stress-strain behaviour of the soil can be interpreted according to equation (2.4) it may be considered that a frictional deformation mechanism applies, although the deformation is influenced by structure and is not therefore solely frictional. The plastic deformation mechanism expressed by eq.(2.4) will be called "basically" frictional.

The stress at which large straining starts, defined by Lerouil and Vaughan (1990) as "primary yield", will be defined as either "gross yield" or simply "yield" in the following. Within the critical state framework these yield points are all located on the SBS. It is possible that this is not so for clays having a microstructure different from the one of the isotropically consolidated reconstituted clay. The applicability of these aspects of the framework to the behaviour of clays and their plastic deformation mechanism will be examined in the following sections.

2.3. Strain softening and localization of strain on the dry side

Fig.2.9(a) shows the clay behaviour conforming to eq.(2.3) during undrained shearing. Dilatancy induces reduced pore water pressures and a related increase of strength up to a critical state, while strain-softening develops as a reduction of the stress ratio q/p'. In the following by strain-softening it will be addressed the reduction of the stress ratio q/p' with increasing shear strain (Atkinson and Richardson 1987; Burland 1990).

In general, even for isotropically consolidated reconstituted clays greater strain softening than expected from Fig.2.9(a) is observed in undrained shearing, as shown in Fig.2.9(b), so that a peak strength and a failure surface occur, and the specimen does not appear to reach critical state.

Atkinson and Richardson (1987) interpreted this behaviour assuming that a frictional deformation mechanism is still active in the clay. They assumed that the strain-softening, starting at point R (Fig.2.9), causes localization of strain and pore water pressure gradients across the specimen

The critical state develops in the shear band, but at higher volume and lower strength than expected due to the local drainage.

Atkinson and Richardson presented tests supporting this interpretation Strain softening appears to start at about the peak pore water pressure in Fig.2.9(a). In the tests from Atkinson and Richardson strain softening started at about the peak pore water pressure as for the CSF, and only thereafter did the behaviour diverge from the CSF. The interpretation of the undrained failure mechanism from Atkinson and Richardson is consistent with the differences of water content measured by various authors at the end of the tests between the soil in the shear band and that in rest of the specimen (Bishop and Henkel 1962; Sandroni 1977). Also, in general, it is found that both the drained peak strengths and the undrained peak stress ratio states (q/p'_{peak}) lie together on the Hvorslev surface. The formation of a localized structure of deformation seems to affect the clay behaviour after the SBS is reached; localization thus affects the undrained peak strength, but not the SBS.

No discrepancies therefore exist between the clay behaviour observed on the dry side of the CSF and the behaviour defined by CSF if the interpretations of Atkinson and Richardson (1987), Rowe (1962) and Schofield and Wroth (1968), regarding the development of heterogeneities of strain and strain localization in clays, are correct.

Heterogeneities of strain are likely to increase with increasing strain. If the soil is strain-hardening, continuous redistribution of strain in the soil is likely to develop without the formation of localized structures of deformation. However once the critical state is reached and strain-hardening complete, sudden instability during shearing has been observed (Wroth 1958; Rowe 1962). Indeed, in clays which are straining at critical state the formation of local areas of iso-oriented fabric is possible, causing local strength reduction towards the residual strength state, and localization of strain after the critical state has been reached. In contrast, if a soil is strain-softening, the strain-softening law should induce concentration of strain in the zones that soften first. So, once strain-softening has started it is expected that with increasing strain there will be progressive localized deformation.

2.3.1. The study of localization phenomena

The investigation of localization phenomena has been usually carried out by visual observation of the failure surface formation (Bishop et al. 1965; Chandler 1966; Sandroni 1977), but this does

not necessarily identify when localized distortion first influences the failure mechanism. Localization during undrained shearing has also been investigated through the study of the distribution of pore water pressures across the specimen (Sandroni 1977).

The experimental study of localization has required the development of highly refined measurement techniques to catch the localization phenomenon at its very early stage. It has been observed that heterogeneities are always present in real soil as localization has been observed also in "rheological" tests, where boundary conditions inducing heterogeneities are carefully avoided (Desrues 1992).

Fig.2.10 shows a drained plane-strain test performed by Desrues (1992) on a fine sand, during which the strain increments were detected by the false relief stereo-photogrammetric technique. Non-homogeneous deformations are evident before peak, and localized dilation appears to increase with the shearing strain. At peak the maximum strains are concentrated at the heart of the specimen. It appears that when the peak strength occurs, most of the soil is dilating and the maximum dilation rate is acting in the most severely strained zones. Only after that the soil specimen starts to strain-soften as a whole does a unique localized structure develops. A movement of the two blocks on the sides of the shear band is evident in the drop after peak (stage 5-6 of the test in Fig. 2.10). This test therefore confirms the above interpretation of the influence of strain softening on the strain localization phenomena.

Desrues reported that both during tests on loose specimens and during tests at high pressures, both showing a contractant strain-hardening behaviour, the bulging deformation of the specimen was related to heterogeneities distributed through the whole specimen, and that in these conditions the eventual formation of a unique localized deformation structure can occur only at very large strains. Mokni (1992), using an X-ray attenuation technique to quantify the density distribution in specimens, demonstrated that in triaxial tests on dense specimens the occurrence of localized strain patterns could be delayed by up to twice the strain at peak strength if very refined specimen preparation and test procedures were used. Even so, Desrues (1992) concluded that post-peak strain softening in drained tests is the result of, and not the cause of, the emergence of a complete kinematically compatible mechanism of localized deformation. However the writer finds that this conclusion is not consistent with the data, which instead seem to confirm that localization of strain does not develop with strain-hardening, but is triggered by strain-softening

Testing has been carried out on marls by Tillard et al.(1992) to examine the mechanics of deformation in these materials. It would be expected that strong bonding influences the

development of localization The data of Tillard et al seem to confirm that the shear band formation arises from the condensation of heterogeneities, mainly triggered by the intrinsic strain-softening.

Further confirmation of the critical state concept is seen in the data from Desrues (1992) and in the work from Mokni (1992). Desrues reported that the density within the shear band tends to a limiting value for large localized strains. Mokni, by using tomodensitometry techniques on drained triaxial tests, showed that the final constant volume in the shear band was the same for specimens starting from different densities and equal consolidation pressures, and that loose specimens could be strained to large strains reaching the same density but remaining homogeneous.

2.4. Effects of structure on the behaviour of reconstituted clayey soils

2.4.1. Behaviour of low plasticity reconstituted soils

Gens, in 1982, published a comprehensive study of the behaviour of reconstituted Lower Cromer Till (LCT), and found it to behave according to the CSF in the v-p' plane (Fig. 2.2) and to reach critical states during shearing, both isotropically and K_0 consolidated and over a large range of overconsolidation ratios (OCR:1-20). Isotropically consolidated LCT reached stable critical state conditions in undrained shear and, for OCRs above four, during drained shear exhibited maximum dilation rates at peak, and then tended to move towards critical state.

However this soil does not satisfy Rendulic's generalized principle that the three stress paths shown in Fig 2.11(a) should plot as a unique curve in the normalized stress plane. In Fig.2.11(a) the stress paths are reported as plotted by Gens in the normalized stress plane t/p_e-p'/p_e; t is equal to half the deviator stress q and p_e is the equivalent pressure p^*_e defined in Section 2.2.3. In Fig.2.11(b) the stress paths in Fig.2.11(a) have been replotted in the normalized stress plane q/p'_p-p'/p'_p, p'_p being the isotropic preconsolidation stress invariant.

The stress paths of constant η were found to plot above the normalized shearing stress paths, as shown in Fig.2.11(b). Given the definition of the SBS as the limit of the states possible for the soil, the surface defined by the constant η tests in Fig.2.11(b) should coincide with the SBS. It follows that for low plasticity soils similar to LCT, large plastic deformations can develop below the SBS. Indeed this is a characteristic of the behaviour of many granular soils, as well as low

plasticity clays (Georgiannou et al 1990, Coop 1990) For these soils gross yield points for drained stress paths plot on the undrained stress path appropriate to the current state (Gens and Potts 1982), in contrast to that predicted by the Cam Clay model. The surface defined by undrained stress paths, on which drained yielding occurs, has been called the local bounding surface by Georgiannou et al.1990, Rossato et al 1992 and Smith et al.1992.

2 4.2. Behaviour of anisotropically consolidated reconstituted soils

For soils of higher plasticity the shearing stress paths seem to plot close to the SBS, and large plastic deformations seem to occur at the SBS. The data presented by Pickles (1988) for a reconstituted organic clay are reported in Fig.2.12. Test B6 is a probing test to follow the SBS and starts from the K_0 normally consolidated state. The comparison of this stress path with those starting from the isotropic state shows that the stress paths do not plot as far below the SBS as for LCT, and to a first approximation they are close to defining a unique Roscoe surface. For the undrained extension path with constant radial stress (U6) Pickles suggested that large plastic deformations were only recorded on approaching the extension side of the SBS. Thus, the behaviour of this clay largely fits within the critical state framework.

Along stress paths of constant η Gens (1982) recorded constant plastic strain ratios $d\varepsilon_v^p/d\varepsilon_s^p$ (Fig. 2.13), which is consistent with a basically frictional deformation mechanism (eq.2.4). In Fig 2.13 the dilation rates recorded by Gens in the constant η stress paths have been plotted against the stress ratios It can be seen from the figure that neither the flow rule of Cam Clay (eq.2.3) nor that of Modified Cam Clay fit the observed behaviour, and the introduction of a coefficient A different from 1 in eq. 2.4 gives a line which best fits the data. The plastic strain ratios exhibited by LCT along the constant stress ratio lines represent the behaviour of the different soil structures which develop during the different virgin compressions (η= constant).

Data from Gens (1982), Pickles (1988) and Rossato et al.(1992) illustrate the responses of reconstituted anisotropic soil specimens, which show how structure can influence the soil behaviour. The K_0 virgin compression line of the soils plots in the upper part of the SBS (Figs 2 11 and 2 12) and during undrained shearing after K_0 consolidation the soil often exhibits a peak deviatoric stress, but the behaviour remains contractant and strain-hardening until the critical state is reached (Figs.2.12 and 2.14(a)). So, although the behaviour shown by the K_0 consolidated soil is different from that of the isotropically consolidated soil, it is still of a frictional type, that is contractant and strain-hardening to critical state. The K_0-consolidation

structure imposes a shape to the undrained stress-strain curve different from that of the isotropically consolidated clay. The undrained compression stress path on K_o-consolidated soil follows the SBS very closely (Figs.2.12 and 2.14). It appears that the SBS must have a "cupola shape" in the normalized stress plane, incorporating the states at high deviatoric stress experienced by the K_o-consolidated clay.

In Fig.2.14(a) the drained stress paths recorded by Gens on K_o-consolidated LCT at different OCRs are plotted, and it appears that shearing behaviour after K_o-consolidation can be normalized with respect to volume. The stress paths of K_o-overconsolidated specimens (Fig.2.14(a)) rise to the SBS and follow it while strain hardening to the critical state. The drained test in Fig.2.14(a), performed by Gens on the K_o normally consolidated LCT, Fig.2.15, has been used by the writer with eq.(2.4) to calculate the coefficient A at various points (see Fig 2.15(b)). The coefficient is seen to remain almost constant during shearing, again agreeing with a frictional deformation mechanism.

In Fig.2.14(b), the stress paths followed by LCT consolidated with η equal to 1 show that the strongly anisotropic soil structure allows the soil to exist outside the surface defined by the constant η state paths, though the soil still exhibits a contractant strain hardening behaviour up to the critical state. It follows that a frictional deformation mechanism applies to reconstituted clays with different consolidation structures, although the stress-strain response changes with the consolidation structure, affecting both the shape and size of the SBS.

2.4.3. Effects of ageing on the behaviour of reconstituted clays

Ageing (see Section 1.10) can also give rise to changes in the behaviour of reconstituted clay. Fig.2.16 shows the effects of creep on the clay behaviour. The clay at A moves to an overconsolidated state B, and then its behaviour follows that expected for an OC clay in the CSF (Fig.2.16: oedometric compression BCE in (a) and (b) and shearing stress paths BA^*CS in (c)). In contrast thixotropic hardening during ageing can cause inconsistencies between the clay response after ageing and the CSF. The thixotropic modification of bonding (see Section 1.10) increases the clay strength and consequently the yield state of the clay is shifted to the right of the original SBS (point D in Fig.2.16; Fig.2.17 from Leonards and Ramiah 1959). During oedometric compression from B to D, K_o falls below the K_o value of the NC clay. Beyond D a modification of the acquired bonding occurs as the clay state joins the original virgin compression line. The instability of the acquired bonding is reflected by the acquired sensitivity (see Table 1.1)

of the clay, which makes the normalized peak strength rise from A^* to A^{**} in Fig 2 16(c) The acquired interparticle bonding then increases the size of the SBS of the clay. Nonetheless the clay still conforms to a basically frictional deformation mechanism, as the following example shows.

Burland (1990) reported the results of an undrained triaxial test performed on aged K_0-consolidated kaolin by Mr.N.Ninis at the Imperial College laboratory. The observed behaviour was that of a structure developing as a response to anisotropic consolidation and ageing phenomena. The aged kaolin exhibited a peak strength, but contracted and strain hardened as expected with frictional deformation. Straining continued at a constant stress ratio with a constant pore pressure. Localization of strain started once a constant stress ratio was reached (see Fig.2.18). The maximum (and ultimate) stress ratio reached during the test is the critical stress ratio q/p'_{cs} for kaolin. Localization of strain then commenced after the critical state had been reached, as recognized as possible in Section 2.3.

2.5. Behaviour of natural clays

The microstructure of natural clays is the result of their composition and geological history as explained in Chapter 1. Consequently studies of their mechanical behaviour have typically treated individual materials as special cases, reflecting their variable and complex origins. Lerouil and Vaughan (1990) gave an extensive review of natural soil behaviour to support the idea that, while the origins of natural structures may be complex, the effects themselves are repetitive for different soils. Similarly Burland (1990) put as a long term objective of his Rankine lecture the aim of stimulating efforts to bring to natural soils the same unity and coherence which critical state soil mechanics in its broadest sense had brought to reconstituted soils.

In the previous Section 2.4 basic concepts underlying the critical state framework have been shown to apply to the behaviour of reconstituted clays, no matter what structure had developed due to consolidation and thixotropy. Structure has, however, been shown to affect the SBS of the reconstituted clay, giving it a "cupola" shape (Figs 2.11 and 2.12) so as to bound the response of the sedimentation structures developing during anisotropic virgin compression. Moreover, it has been shown that structural modifications during ageing can increase the size of the SBS of the reconstituted clay.

The problem then is to understand whether the natural structure can modify the basic deformation mechanisms identified for reconstituted clays, and whether the basic features of the CSF, as shown in the scheme in Fig 2.6, apply to the behaviour of natural clays.

2 5.1. The sedimentation compression curve

Terzaghi (1944) defined the e-σ'_v curve followed by the clay during virgin compression in situ as the sedimentation compression curve (SCC) of the clay. The SCC of a clay reflects the response of the structure developing in the clay during virgin compression, that is the sedimentation structure defined in Section 1.11 (Table 1.1). Both the sedimentation structure of the clay and the clay SCC then depend on the mineralogy of the clay, its pore water chemistry and the deposition and consolidation conditions (see Chapter 1).

The clay when reconstituted and consolidated in the laboratory has a stable sedimentation structure, which gives the clay a sensitivity of about 1. As different laboratory reconstitution and consolidation procedures can give rise to different structures and different SCCs, Burland (1990) proposed that the technique of reconstitution and consolidation should be standardized by preparing the clay at a water content of 1.2-1 5 times the liquid limit, and then consolidate it in the oedometer. Burland defined the mechanical properties of the reconstituted clay as "intrinsic" and for the associated parameters used the superscript *.

The mineralogy and pore water chemistry of a clay are reflected in its Atterberg limits (Skempton 1953), and Skempton and Northey (1952) showed that normalizing the clay water contents with respect to the Atterberg limits by means of the liquidity index LI, the SCCs of reconstituted clays of different mineralogy coincide (see Section 1.5; Fig 1.5(b)). The manner in which the structure of the reconstituted clay determines the normally consolidated states of the clay is then always similar. Burland (1990) used the void index I_v :

$$I_v = (e - e_{100})/(e_{100} - e_{1000}) \qquad (2.5)$$

rather than the liquidity index to normalize the clay volumetric state with respect to composition. He defined the resulting equation of the unique SCC of the reconstituted clays in the I_v-σ'_v plane (Fig.2.19) as the "Intrinsic Compression Line" (ICL).

2 5 2 Natural sedimentation compression curve and the ICL

Skempton and Northey (1952) showed that the stability of the reconstituted clay structure is such that the SCC plots to the left of the natural clay SCC, as shown in Fig.1 5(b) The SCCs of the different clays shown in Fig.2.19 plot on the right of the ICL, accordingly, and their different locations are the direct effect of differences in their structure.

Lerouil and Vaughan (1990) defined the space to the right of the ICL as "structure permitted space". This definition is not strictly correct given the meaning of structure defined in Section 1.5, but it emphasizes that the structure of the natural soil can allow it to exist outside the SBS of the reconstituted soil.

2.5.3. A basic classification of clays

In Table 2.1 the natural clays, whose state may or not plot in the structure permitted space, have been classified in relation to both their geological history and current structure, Table 1.1, and in relation to key elements of their mechanical response, as explained in the following. For the purposes of the present discussion the clay sensitivity S_t will be redefined as the ratio of the undrained strength of the natural clay to the undrained strength of the reconstituted clay consolidated to the same voids ratio. The terms OCR and YSR are used in Table 2.1 as suggested by Burland (1990). He recommended that the term yield stress, σ'_y in oedometric compression, should be used in general to denote the stress beyond which large volumetric changes occur (gross yield), while the preconsolidation pressure, σ'_p, be reserved for the true geological preconsolidation. Similarly the term yield stress ratio ($YSR=\sigma'_y/\sigma'_v$) can be used instead of overconsolidation ratio ($OCR=\sigma'_p/\sigma'_v$), which should be reserved for describing a known stress history.

In general, natural soft clays tend to be normally or lightly overconsolidated from geological evidence, i.e. OCR about 1, and their structure is not strong, as for the clay type 1 in Table 2.1. Their structure neither has been cemented during deposition and compression, nor has it acquired bonding after virgin compression (see Section 1.10). It follows that these soft clays have an in situ stress σ'_v which lies close to their SCC, while their σ'_p and σ'_y in K_0 compression almost coincide as YSR is about equal to OCR.

If soft clays overconsolidated by geological unloading (OC) exist, these are represented by clay type 2 in Table 2.1. Their gross yield stress σ'_y still plots on the SCC and coincides with σ'_p.

In Table 2 1 it is specified whether the clays included in the different clay types have either a sedimentation or a post-sedimentation sensitivity (see Table 1.1) when compressed up to the gross yield stress σ'_y (S_t(YSR=1)). For soft clays (both clay types 1 and 2) the sensitivity at yield is the sedimentation sensitivity. Both this sensitivity S_t(YSR=1) and the distance between the SCC of the soft clay and the ICL are measures of the greater strength of the natural sedimentation structure with respect to the strength of the reconstituted clay. The distance between the SCC and the ICL can be expressed as the ratio of the clay gross yield stress σ'_y to the "equivalent" pressure σ^*_e, which is the vertical effective stress on the ICL corresponding to the gross yield voids ratio of the clay. The significance of the relationship between the sensitivity at gross yield S_t(YSR=1) and the ratio σ'_y/σ^*_e will be considered in detail later. As for soft clays the preconsolidation pressure σ'_p equals the gross yield stress σ'_y, the ratio σ'_y/σ^*_e may be otherwise expressed as σ'_p/σ^*_e.

Leached clays (type 8 in Table 2.1.) are soft, but they differ from the soft clays of Table 2.1 as their structure has changed since virgin compression, making their ICL move in the e-σ'_v plane, or the clay's SCC move in the I_v-σ'_v plane. For the leached clay, both the sedimentation sensitivity and the distance between the SCC and the ICL increase after virgin compression, although the yield state and the SCC of the clay remain close to one another.

The NC stiff clays reported as type 3 in Table 2.1 are clays which have become stiff while compressing along the SCC to high values of σ'_v (e g. Skempton 1970), though they have preserved their sedimentation structure and have a YSR about equal to OCR. Apparently their structure was not affected by any phenomena of group 2 in Table 1.1. If these clays had been geologically unloaded, with their structure unaffected by any other process of group 2 than simple unloading, they would fall in type 4 in Table 2.1. These clays have a YSR close to the OCR and, when recompressed to gross yield (YSR=1), their structure is still a sedimentation structure, exhibiting a sedimentation sensitivity. Clay types 3 and 4 are probably uncommon in nature, as it is unlikely that in a clay buried for a long time under high pressures diagenesis would not occur. For clay types 3 and 4 the distance between the clay SCC and the ICL is still indicative of the higher strength of the clay arising from the natural sedimentation process.

NC clays which were cemented at deposition are stiff, and have a cemented sedimentation structure, as for some marls and mudstones (Anagnostopoulos et al.1991). These are clay type 5

in Table 2.1. During oedometric compression they exhibit a stiff response up to a σ'_y higher than the preconsolidation pressure σ'_p, and they have a YSR higher than the OCR. In this case the "sedimentation sensitivity" is a measure of the effects of structure on the soil behaviour and the distance between the SCC of the soil and the ICL is not the parameter which relates to the soil's structural strength.

For clays having a post-sedimentation structure due to either thixotropy, diagenesis, authigenic cementation or other phenomena in group 2 in Table 1.1, the structural changes after virgin compression gave rise to an increase of the yield stress σ'_y with respect to σ'_p, (e.g. Hanzawa et al. 1990) shifting the clay yield state to the right of the clay SCC as observed by Leonards and Ramiah (1959) in relation to thixotropy. Thus for clay types 6 and 7 the difference between the OCR and YSR expresses the strength acquired by the clay due to structural changes that occurred after virgin compression.

Both for clays cemented at deposition (type 5) and for clays having a YSR higher than OCR due to changes in structure after virgin compression (types 7 and 8) the sensitivity at gross yield S_t(YSR=1) and the ratio σ'_y/σ^*_e relate to the effects of structure on the clay behaviour. In contrast both the distance of the clay's SCC from the ICL and the clay's stress ratio σ'_p/σ^*_e are not related to these effects.

The behaviour of Boom Clay, shown in Fig.2.20, confirms this interpretation. Boom Clay is a stiff clay from Mol, Belgium, which geologically is only lightly overconsolidated. The clay is from a great depth and is very stiff, and Horseman et al.(1987) found difficulty in reconciling the preconsolidation pressure measured in the oedometer with the geological evidence. But a post-sedimentation structure is likely to have developed, if only because of long-term diagenetic phenomena, giving rise to the difference between the YSR and OCR for Boom Clay. This clay therefore is a probable example of clay type 6 in Table 2.1. The SCC of Boom Clay plots close to the in situ state, due to the low OCR of the clay, and therefore it plots close to the ICL (see Fig.2.20). However the compression behaviour of this clay is significantly different from that of the reconstituted clay.

2.5.4. Construction of a sensitivity framework

The understanding of one-dimensional compression behaviour of soft clays results mainly from the work of Skempton and Northey (1952), Skempton (1970) and Burland (1990).

Skempton and Northey (1952), plotting the in situ states of sixteen soft NC clays together with the compression curves of the reconstituted clays in the LI-σ'_v plane recognized the existence of a general correlation between the sensitivities and the liquidity indexes of the clays at any given pressure (see Fig.1.5(b)). They observed that in the general LI-σ'_v plot the sensitivities increased with LI for a given σ'_v They used this correlation to evaluate the influence of the structural stability on sensitivity.

Here this approach is used to quantify the effects of structure on the clay behaviour and add to the understanding of the general compression behaviour of soft clays. Plotting lines through the data corresponding to the same sensitivity value in Fig.1.5(b) (red lines) seems to suggest that there is a unique sedimentation compression curve for soft clays of different origins but equal sensitivity. This SCC appears parallel to the compression curve of the reconstituted clay in the normalized plane LI-σ'_v. That is there is a unique relationship between the sensitivity S_t (YSR=1) of soft clays (sedimentation sensitivity) and the ratio σ'_p/σ^*_e, as all the soft clays of equal sedimentation sensitivity have equal σ'_p/σ^*_e. This constant ratio is independent of the origins of the sedimentation structure giving rise to the sensitivity; the sensitivity S_t(YSR=1) and the ratio σ'_p/σ^*_e are two reciprocally dependant parameters, both representing the effects of the sedimentation structure of soft clays on their current behaviour. Note that for normally consolidated soft clays the sedimentation sensitivity S_t(YSR=1) is equal to the current sensitivity S_t of the clay. Given the few data in Fig.1.5(b), more experimental evidence is required to confirm this interpretation.

In 1970 Skempton presented a considerable field evidence on the virgin compression of natural clays. These clays were of different characteristics, origins and levels of compaction, and were normally consolidated or lightly overconsolidated from the geological evidence. For most he confirmed that their normally consolidated nature was evident also from oedometer test results. All the clays had sensitivities less than 10, had less than 10% organic content and less than 25% carbonate content, and plotted just above the A-line in the Casagrande plasticity chart. The sedimentation compression curves of these clays all plotted in the LI-logσ'_v plane within a band, as shown in Fig.2.21 (a), lying almost parallel to each other over the medium stress range, tending to converge at very large stresses, Fig. 2.21 (b).

Burland (1990) replotted most of the natural clay states from Skempton (1970) together with the ICL and some further field data in the I_v-σ'_v plot. From Fig.2.19 it can be seen that regression

lines through each of the data sets are parallel to the ICL. Detailed data from Gosport and Bothkennar are given in Fig 2.22 (a) and (b) respectively. For sites characterized by predominantly constant deposition conditions, even with changing clay mineral composition, the data in the normalized I_v-σ'_v plane fall close to a continuous SCC parallel to the ICL.

A different value of sensitivity is associated with each of the sedimentation compression curves in Figs 2 19 and 2.21 Skempton pointed out (Fig 2.21) that the clays with high sensitivity, e g. Drammen and Algaven, lie towards the upper part of the band, while those with a low sensitivity, e.g. Gosport and Tilbury, lie towards the lower part of the band. Given the small range of sensitivity selected by Skempton (S_t :1-10) the band is rather narrow. The field data from Gosport are shown to lie close to the ICL in Fig 2.22(b), which is consistent with the low sensitivity of the clay.

In Fig.2.19 Burland fitted a regression line, defining a unique sedimentation compression curve, that he called the "Sedimentation Compression Line" (SCL). The analysis of the data regressed by the Burland's SCL shows that they refer to clays of medium sensitivity, in the range 4 to 9. The SCL plots in the middle of the sedimentation compression data of the selected clays and can be seen as the SCC for clays having a sedimentation sensitivity approximately 5-6. In other words the SCL is a particular SCC which expresses the sedimentation behaviour of clays of "normal" sensitivity.

Burland pointed out that in Fig 2.19 the SCL and the ICL are approximately parallel, the effective overburden pressure carried by the natural clay being approximately 5 times that carried by the reconstituted clay Thus the ratio of the stresses at the SCL to those at the ICL at the same voids ratio is constant, and approximately equal to the sensitivity of the clays whose SCC coincides with the SCL. A grid of parallel sedimentation compression curves SCC in the I_v-logσ'_v plot may therefore be identified, shown in Fig.2.23, and which represents the sensitivity framework for soft clays, the lower boundary being defined by the ICL. One sensitivity value S_t is associated with each SCC; this value is the sensitivity of all the clays plotting on that SCC, which can have different structural features, but all have a "sedimentation structure" as defined in Table 1.1.

Skempton's data also include NC stiff clays, such as the S.Joaquin and the Milazzo clay. These clays seem to be of type 3 in Table 2.1, and plot consistently with the other data in the general plot in Fig.2.23. The sensitivity framework thus includes clays of type 3. It is also to be expected

that overconsolidated clays exhibiting a YSR equal to the OCR, clay types 2 and 4, when compressed up to the gross yield stress σ'_y will fit the grid of constant sensitivity lines

In contrast both NC cemented clays (type 5) and stiff clays having a post-sedimentation structure and acquired sensitivity (types 6 and 7), have a YSR greater than OCR and so the clay recompressed to the yield point does not lie on the SCC; its sensitivity is greater than the sedimentation sensitivity. The position of the SCC of these clays in the I_v-σ'_v plane is not representative of their current behaviour, though is the location of the yield state in the I_v-σ'_v plane indicative of the strength of their current structure. The behaviour of stiff clays of types 5, 6 and 7 does not fit the scheme in Fig 2.23. In Section 6.7.2 it will be shown whether these clay types fit a framework similar to the one in Fig.2.23, but in which the constant sensitivity lines are seen as one-dimensional yield profiles, not necessarily coincident with the clay's SCCs, and the parameters of the framework are seen as the sensitivity S_t at gross yield (S_t(YSR=1)) and the ratio σ'_y/σ^*_o, which is not necessarily equal to σ'_p/σ^*_o. At present the general sensitivity framework defined in Fig.2.23 can be considered relevant only to the behaviour of soft clays and, perhaps, of stiff clays having YSR equal to OCR, i.e. the clay types 1, 2, 3 and 4 in Table 2.1.

2.5.5. Compression behaviour of sensitive clays

The loading energy applied either during oedometric compression in the laboratory or by loading in the field may be sufficient to modify the fabric and the bonding of soft clays (Burland 1990) during compression. At stresses higher than the preconsolidation pressure, the clay moves away from the SCC towards the ICL, (Lerouil et al 1979, Lerouil et al.1985, Tavenas and Lerouil 1985, Jamiolkowsky et al.1985, Burland 1990). A typical example of this behaviour is shown in Fig.2.24 for Bothkennar Clay; an OCR=1.7 had been estimated for this soft clay from geological evidence.

A high post-yield compressibility shows that the clay sedimentation structure has significant metastable elements whose contribution to the clay structural strength is lost during compression. However, regarding microstructural changes which occur post-yield as destructuring (Lerouil et al.1979; Lerouil and Vaughan 1990) is not correct as the use of this term implies that structure only exists in the undisturbed natural clay, and not when compressed post-yield or reconstituted. Burland (1990) pointed out that the alteration of structure beyond yield is progressive for soft clays. But, even if the voids ratio of the clay reduces to that of the reconstituted clay, it cannot be established whether the structure of the natural clay becomes similar to that of the reconstituted.

In Chapters 5 and 7 it will be shown that complex structural changes occur in clay during compression, which may result in the creation of new fabrics.

Fig 2.20 shows that stiff clays can exhibit high compressibility beyond yield, though the stability of the structure of highly overconsolidated clays and how it modifies after yield is not established as the response of clays at high stresses has never been fully investigated. For many highly OC clays, such as Gault Clay and London Clay, the YSR and the OCR have yet to be measured

The ratio of the swelling index of natural stiff clays and to that of the reconstituted clay C_s^*, i.e. the swelling sensitivity C^*_s/C_s (Schmertmann 1969), has been regarded as an indicator of how strong is the bonding of the stiff clay (Burland 1990), and the progressive increase of the swelling index at different stages during compression has been seen as an indicator of the progressive weakening of bonding. However the post-yield compression of stiff clays is generally not known.

Among the long-term objectives of the research presented in this thesis is the definition of a general framework of behaviour of clays. Large part of the research therefore focused on the understanding of the behaviour of stiff clays at high stresses, which are the ones least investigated in the literature. The research also investigated the physical phenomena, the effects of which are described in the behavioural framework. In particular the question of what microstructural changes occur at yield in the clay was addressed. A direct analysis by means of the SEM of both the natural and the reconstituted clay at different stages during compression was therefore carried out, which showed to what extent the natural structure of the clay is modified beyond yield (see Chapters 5 and 7). The strength and stability of the clay structure was deduced by the analysis of the clay response during both compression to high stresses and swelling (Chapter 6), but the nature of bonding was also directly investigated by means of SEM studies together with chemical micro-analysis.

2.5.6. Shearing behaviour of natural soft clays

The review of natural soil behaviour presented by Lerouil and Vaughan in 1990 suggested that the concepts of yielding and overconsolidation traditionally used to describe the effects of stress history on the strength of reconstituted clays may be equally applicable to the effects of structure The present review provides evidence of the similarities of behaviour of reconstituted soils related to OCR, and the trends of behaviour of natural soils related not to OCR, but to YSR. This

distinction is, of course, meaningless for soils having OCR equal to YSR. The behaviour of natural soft clays (see Table 2.1) will be examined first.

Tavenas and Lerouil (1985) and Jamiolkowsky et al.(1985) reported the behaviour of a range of natural sensitive soft clays (Fig.2.25). In many respects the behaviour of these clays was similar to that of reconstituted clays anisotropically consolidated and aged. As for the clays in Fig.2.25, peak deviatoric stresses are also recorded during undrained shearing of either anisotropic or aged reconstituted clay specimens. Also, the peak states of the clays in Fig.2.25 coincide with the gross yield states and plot on the state boundary envelope as observed for the reconstituted clays In contrast, after gross yield the behaviour of the natural clays in Fig 2 25 is different from that of the reconstituted clays as the stress paths move inwards from the state boundary envelope in the normalized stress plane. The normalizing factor σ'_p in the plots in Fig.2.25 is the preconsolidation pressures of the undisturbed clay considered.

Smith (1992) carried out a large number of probing stress paths starting from the in situ state of the soft Bothkennar Clay. In Fig.2.26 the stress paths are shown normalized with respect to p^*_e (p'e in the figure). Smith et al. (1992) observed that gross yield during undrained shearing occurred at peak on the state boundary envelope (Fig.2.26). In contrast, on the drained stress paths they were able to distinguish the gross yield points from the boundary points, and identified a yield curve slightly inside the state boundary envelope in the normalized stress plane. Thus they recognized a difference between the behaviour of the natural and reconstituted clay at yield. However, defining the location of the gross yield point within that portion of the state path which has highest curvature requires a degree of judgement (Graham et al.1988). The difference between the behaviour of the natural and of the reconstituted clay at yield recognized by Smith et al. is therefore related to their choice of the yield points. Between the yield points which they defined and the boundary states of Bothkennar clay the stress increase was of only few kPa, and the voids ratio decrease was of the order of 0.03. Thus, in a simplified framework the gross yield points of Bothkennar clay can be still considered to be on the state boundary envelope, as in the CSF.

The shape of the state boundary envelope of Bothkennar clay resembles a cupola (Fig 2 26) as with anisotropically consolidated reconstituted clays. However, the behaviour of Bothkennar clay is still different from that expected for reconstituted clay because it is not stable, but rather it is brittle along all the stress paths, the stress paths being redirected inwards after touching the state boundary envelope in the normalized stress plane (Fig 2 26).

Unlike the stable reconstituted clay, both the soft clays in Fig.2.25 and Bothkennar clay exhibit a considerable reduction (about 50%) in tangent shear modulus and bulk stiffness normalized with respect to volume, and a loss of normalized shear strength, beyond yield. The SBS, normalized with respect to the pressure p^*_e on the ICL relative to the current volume, contracts inwards as straining continues beyond yield. Reducing sensitivities are measured for the clay while its state migrates towards the left of the I_v-σ'_v plane, consistent with the sensitivity framework defined in Fig.2.23.

It is thus necessary to distinguish the framework of behaviour of the clay which is not compressed, either isotropically or anisotropically, beyond yield before shearing, from that representing the behaviour of the clay compressed to stresses both before and beyond yield before shearing. In the first case the framework represents the response of the current structure of the clay, as it is in situ, i.e. not yielded. This framework is here defined the "current" behavioural framework of the clay. In the second case the framework includes the effects of the changes in structure occurring in the clay due to yielding before shearing. This framework is here defined as the "natural" clay framework or the framework of the natural clay.

In fact, the complete current SBS of the clay needs to be defined from the boundary states of undisturbed samples from the same profile having different initial voids ratios but similar geological histories in situ. They must have been consolidated along the same SCC in situ. In contrast the SBS of the natural clay results from the response of specimens trimmed from the same undisturbed sample and compressed both to states before and beyond yield before shearing. The one-dimensional compression index C_c from oedometer tests on sensitive clays is relevant to the natural clay framework, but not to the current one, as it defines how the boundary state of the natural clay beyond gross yield moves far from the "current" SBS of the clay.

In the current behavioural framework of a normally consolidated soft clay the ratio σ'_y/σ^*_e is constant as is the ratio of the in situ undrained shear strength to that of the reconstituted clay at the same voids ratio, that is the sensitivity S_t, according to the sensitivity framework discussed in Section 2 5 4. Since the current undrained peak strength states lie on the current SBS of the clay, the constancy of the above ratios indicates that the size of the constant volume sections of the current SBS of the undisturbed clay increases with the corresponding sections of the SBS of the reconstituted clay That is the current SBS of a normally consolidated soft clay is isotropically hardening with volume. This is demonstrated by the example reported below.

Graham et al.(1983) plotted the yield loci of undisturbed samples of Winnipeg clay from different depths (Fig.2.27(a)). This is a lightly overconsolidated pro-glacial fresh-water clay of high plasticity. In this case, the yield states were boundary states. The yield curves were broadly similar in shape and increased in size with the preconsolidation pressure, demonstrating that the current SBS of Winnipeg clay was isotropically hardening. Normalizing the curves with respect to the in situ pre-consolidation stress, Graham et al. (1983) obtained a unique yield envelope (Fig.2.27(b)). On the right hand side it seems cupola shaped. When Graham et al. (1988) normalized the yield stresses by the pressures on the SCC for the same voids ratio as the yield point p'_{scc} (Fig.2.27(c)), the SBS appeared to resemble the SBS of the reconstituted clay even more.

In conclusion, for natural soft clays the current SBS is isotropically hardening and of similar shape to the SBS of the reconstituted clay. Both the size and the location of the current SBS depend on either of the two parameters: $\sigma'_y/\sigma^*_e = \sigma'_p/\sigma^*_e$ or S_t(YSR=1). So far these conclusions are relevant only to the clay types 1 and 2 in Table 2.1 and cannot yet be extended to the other clay types in the table.

The tests on the very sensitive Norwegian clays, from Onsoy and Ellinsgrud, reported by Burland (1990) and shown in Fig.2.28, provide further information about the behaviour of soft clays before and beyond yield. The clays plot above the SCL at different values of I_v and each have a YSR slightly greater than one. Their stress paths (Fig 2.28(c)), the same as those for Bothkennar clay (Fig.2.26), are typical of sensitive slightly overconsolidated soft clays. After a highly stiff response up to a peak normalized deviator stress, the stiffness reduces dramatically, but the behaviour is contractant and strain hardening in terms of q/p' along the whole stress path. The term wet, as defined by Schofield and Wroth (1968) (see Fig.2.6) seems appropriate to describe the deformation mechanism of these natural soft clays.

It is evident that at yield the manner in which the structure determines the behaviour of the clay changes, but a basically frictional deformation mechanism is active from the start of the shearing path. Beyond yield, the frictional deformation mechanism is dominant, so that clay softening due to the weakening of structure is more than compensated for by the hardening effects of contractancy. While non sensitive clays strain harden to critical state along the SBS, sensitive clays appear to strain harden to a final constant stress ratio q/p' while moving away from the SBS. The final constant friction angle reached by the clay has been denoted as ϕ'_{ult} in Fig.2.28.

After reaching a maximum stress ratio the natural clay continues to strain at constant stress ratio, but with decreasing normalized strength (Smith 1992; Lerouil and Vaughan 1990). Indeed, if the state paths of a natural sensitive clay had to reach the intrinsic critical state, they would have to travel a long way and cross the ICL (Burland 1990). However, the definition of the ultimate volumetric state of the natural clay is uncertain as the behaviour at very large strains has not been investigated.

The strain ratios recorded in the tests on Bothkennar Clay (Smith 1992) reduced very slowly while q and p' were approaching a constant value, but the tests were stopped at 20% strain, too low to estimate the ultimate state of the clay. Smith et al.(1992) suggested that two of their stress paths seemed to approach a tentative critical state line to the right of the ICL. In the writer's opinion, four stress paths in Fig.2.26 move towards the same final point, which is at q/p' of 1.4, the stress ratio at critical state of the reconstituted clay measured by Allman and Atkinson (1992). The Bothkennar clay specimens whose structure had been altered by consolidation beyond yield reach the same final stress ratio of 1.4 (Smith 1992), reinforcing the idea that the ultimate stress ratio of the clay is the critical state $(q/p')_{cs}$. Thus the natural Bothkennar clay appears to strain harden to the stress ratio at critical state, although the final v-q-p' state of the clay cannot be assessed. Large shearing strains can even induce strain localization, so that assessing the final state of natural clays is, in general, very difficult.

Natural soft clays overconsolidated by unloading in the laboratory show a behaviour related to OCR similar to that of reconstituted clays (Lerouil and Vaughan 1990). Samples with low OCRs, below 2-3, sheared under drained conditions, contract while reaching a constant q/p'. After yield they still contract while straining at constant stress ratio q/p' to large strains similarly to the clays from Ellinsgrud and Onsoy, which have a YSR slightly above 1 due to geological processes. The term wet seems appropriate to describe the deformation mechanism of the slightly overconsolidated soft clays (YSR<3). At high values of OCR the clay exhibits a stiff response up to a peak stress ratio higher than the final one while dilating. The peak stress ratio is at least in part related to the yielding of structure. Maximum dilation rates have been observed at strains larger than at peak and various authors have proposed that, in these cases, the peak strength is governed by structure rather than dilation (Lerouil and Vaughan 1990; Aversa et al.1993). However for moderately high values of OCR, and when the structural brittleness is less dominant, a contribution of dilation to the peak strength is observed

The undrained stress path reported in Fig 2 28(c) is for a Norweg an soft clay from Emmerstad having a YSR of 4 Burland pointed out that the shape of this stress path is unusual as it rises

above the ultimate failure line, bends to the right approaching a peak and then follows a loop. But comparing the shape of this stress path with that exhibited by a reconstituted specimen at an OCR about 4, it appears that they are similar up to the peak deviator stress. As with reconstituted clay (Fig.2.9), in the natural clay strain softening and plastic dilation start at about the same point, and a peak deviator stress is approached with some dilation. With strain softening localization occurs which causes the drop in deviator stress, while the pore water pressure tends to a constant value. This stress path travels towards the left and reaches the ultimate stress ratio line. Again, the specimen from Emmerstad K_o-consolidated beyond yield reached the same ultimate stress ratio as the undisturbed specimen.

Structure may more or less dominate the peak strength of the natural clays at high YSRs, but as a result of strain softening the state paths approach the same ultimate stress ratio as on the wet side. The peak stress ratios, both along drained and undrained stress paths, identify the Hvorslev surface of the natural clay (Figs 2.25(b) and 2.27(b)).

2.5.7. The shearing behaviour of cemented soils

Before analysing the behaviour of stiff clays it is worth reviewing the large body of research on cemented granular soils (Maccarini 1987; Coop and Atkinson 1993) and marls (Anagnostopoulos et al.1991), i.e. soils for which solid bonding is the dominant structural feature. In these cases the process of bond alteration is relatively simple and is known as the breakage of the solid cement bonds.

When compressed to low values of YSR these soils show a contractant strain-hardening behaviour (Figs.2.29 and 2.30). As with soft clays, cemented soils on the right hand side of the framework have their structural brittleness compensated by the frictional strain-hardening behaviour of the contracting particle arrangement. As shearing progresses the marl tested by Anagnostopoulos et al. tends to a state of constant volume and constant stress-ratio ($c'=0$, $\phi'=33.4°$ in the figure). Anagnostopoulos et al.(1991) (Fig 2 29) show that this stress ratio coincides with the ultimate stress ratio reached by the reconstituted soil, i e $\phi'=33\ 4°=\phi'_{ult}$, but neither Maccarini (1987) nor Lerouil and Vaughan (1990) or Anagnostopoulos et al (1991) either point out this tendency to a final constant stress ratio or specify it as the critical state In the writer's opinion the post-yield soil behaviour on the right side of the framework can be explained as basically frictional, although the plastic deformation mechanism is also affected by the brittle breakage of bonding.

Anagnostopoulos et al.(1991) identified a unique elliptical yield curve in the q-p′ plane from both drained and undrained triaxial test results, which is the current yield curve of the undisturbed soil, defined as initial yield surface in Fig.2.29. However they did not specify the location of the SBS of the marl they tested. On the right side of the framework this seems to lie above the yield locus. On the left side yield occurs at about peak stress ratio, and to a first approximation it coincides with the boundary state. The tests in Fig.2.29 were stopped at an early stage and the large strain behaviour of the marl was not investigated.

Coop and Atkinson (1993) presented a complete set of test results on both artificial and naturally cemented carbonate sand, and on the same soil uncemented. Aiming to investigate the whole framework for cemented materials, tests were carried out up to very high pressures inducing different degrees of debonding before shearing (Fig.2.30(a)). They also plotted the SBS and the location of the critical state line of the uncemented soil (Fig 2.30(b)) They recognized three classes of behaviour. The first refers to isotropic consolidation stresses beyond yield. For this class, the shearing behaviour is similar to that of the uncemented soil at similar stresses. With increasing consolidation stress the normalized stress paths tend to contract towards the SBS of the uncemented soil as the compression curve approaches the normal compression line of the uncemented soil (Fig 2.30(c)). Thus the effects of the cemented structure on the mechanical behaviour of the soil can be erased by the breakage of the bonding during compression. Bonding affects the deformation mechanism up to yield, but beyond yield a continuously contractant strain-hardening behaviour was recorded up to a final state coincident with the critical state of the uncemented soil. The normalized stress paths in Fig.2.30(c) show that the shape of the SBS becomes more rounded and less elongated with the progression of debonding.

The second class of behaviour is seen at intermediate stresses but low values of YSR. Yielding always occurs during shear and the drained stress-strain curve can even exhibit a peak, but the behaviour is strain hardening and contractant up to the same critical state (Fig 2 30(b)) as the reconstituted material. This is shown by the data as Coop and Atkinson carried out the tests up to very large strains (40%). Consequently they established that after yield the soil exhibited a frictional behaviour. They identified a unique plane, inclined at the gradient of the critical state line $(q/p')_{cs}$ down which the stress paths travel towards the critical state point This plane has been indicated by the writer with the CS-gradient line in Fig 2 30(b) and (c) In the figures also the current SBS and the yield curve of the soil have been tentatively drawn

The third class refers to specimens consolidated to lower stresses, that is high values of YSR. Peak stresses occur at low strains well outside the SBS of the uncemented soil. It can be concluded that both soft clays and cemented soils seem to reach ultimate stress ratio close to the ratio at critical state at significantly smaller strains than are required to bring the soil to constant volume. The two stress paths to the left of the line of CS-gradient in Fig.2.30(b) show a looped shape, drop to the CS-gradient line by strain-softening and travel down this line. Their similarity to the stress path for the clay from Emmerstad (Fig.2.28(c)) emphasizes the similarity of the behaviour of two extremely different families of natural soils: soft clays and cemented sands.

2.5.8. Suggestions for a general framework of behaviour

An overall framework of behaviour results from the above discussion, outlined in Fig.2.31. This will be first discussed for the cemented soil, for example clay type 5 in Table 2.1.

The yield point in isotropic compression can be considered as a parameter representing the maximum stress that the soil structure can sustain as a result of the bond strength. When compressed at low YSRs, the soil structure results in a stiff response, but yield and breakage of the cemented bonds occurs at stress ratios lower than the stress ratio at critical state (vector a in Fig.2.31(a); Fig.2.31(c)). Beyond the yield stress ratio the particle arrangements start to contract and strain-harden to the critical state (Fig.2.31(c)) and a basically frictional deformation mechanism (eq 2 4) becomes dominant. The zone where the soil yields at stress ratios below the line of critical stress ratio q/p'_{cs} (the CS-ratio line in the figure) coincides with the wet side of the framework. This is shown in Fig.2.31(c), where the stress paths are normalized with respect to volume by the use of the equivalent pressure p^*_e.

At high YSRs the bonds are intact and sustain high shearing stresses, so that the soil exhibits a stiff response up to high stress ratios. The soil can be loaded to a stress ratio higher than the critical stress ratio (vector b in Fig.2.31(a)). The breakage of the cemented bonds leaves the unbonded particles under a stress state q-p′ such as to induce dilation, even at volume-stress states to the right of the critical state line of the reconstituted soil in the v-p′ plane. Under these stress ratios the bonding alteration appears to be more sudden, imparting considerable brittleness to the soil In Figs 2.29 and 2.30 the yield loci appear rather flat, and yielding of the cemented soil is dominated by the strength of the bonds which is little affected by the mean stress. A tentative boundary envelope in Fig 2.30(b) is apparently far above the yield curve Therefore the SBS of the cemented soil has been drawn above the locus of current yield points in Fig 2 31(c)

From the simple scheme in Fig.2 31(c) it appears that the behaviour of the cemented soil is determined by the location, size and shape of the yield curve with respect to the line of critical stress ratio q/p'_{cs}, since the intersection of this line with the yield locus divides the wet and the dry sides of the framework. The similarity between the sketch (c) in Fig.2.31, outlining the behaviour of cemented soil, sketch (b) for reconstituted soil and Fig 2.6 (a) and (b), which defines the frictional behaviour of the reconstituted clay in the CSF, is evident. A basically frictional deformation mechanism is active in the cemented soil beyond yield as it is in the reconstituted one. For reconstituted soils the behaviour after gross yield is frictional, and defines a stable SBS on which the final states lie. In the natural cemented soil gross yielding is below the SBS, and frictional behaviour becomes progressively dominant with increasing strain.

The behaviour of soft clays is sketched in Fig 2.31(d). The similarity between the schemes (b), (c) and (d) in the figure, representing the behaviour of reconstituted soils, cemented soils and soft clays respectively, emphasizes the general applicability of a behavioural framework in which the soil deformation is basically frictional beyond yield (as loosely expressed by eq 2.4).

The yield curve of the soft clay is located below the line of critical stress gradient in the normalized stress plane for low YSRs, and above it for high YSRs. Dry and wet zones are located correspondingly at low YSRs and at high YSRs. For soft clays, the sensitive open structure gives a very brittle post-yield behaviour both on the wet and the dry side, so that yield can be considered a boundary state.

For the reconstituted clay yielding is stable, beyond yield the state paths move on the SBS and the behaviour is isotropically hardening. In contrast for both natural soft clays and cemented soils the state of the soil moves quickly inside the current SBS after touching it. Therefore the SBS of the natural soil, including the soil behaviour both before and beyond yield (see Section 2 5 6), is not normalized by the use of the equivalent pressure p^*_e, as shown in Figs.2.26 and 2 30 Whether the SBS and the yield curves of natural soft clays and cemented soils can be normalized with respect to volume by means of other normalizing factors has yet to be demonstrated. The validity of the behavioural features sketched in Fig 2 31 will be further discussed in Chapter 8 and 9

2.5.9. The shearing behaviour of stiff clays

The experimental evidence for the behaviour of stiff clays presented in the literature is not sufficient to allow the application of the above behavioural framework to these clays.

Sandroni (1977) carried out a series of undrained triaxial tests on London clay to investigate the pore water pressure distribution in the specimen and the development of localisation of strain. In the specimens consolidated to high YSRs the pore water pressures always dropped after the peak stress ratio, but before the peak deviator stress. The states at peak pore pressure plotted close to the states of maximum stress ratio, which defined the peak failure envelope (Fig.2.32), as would be the case for the reconstituted clay (Fig.2.9). Sandroni (1977) reported that soon after the peak pore pressure the formation of a shear band could be seen in the specimens which still proceeded towards peak strength. At the same time he observed the development of differences in pore water pressure within the specimen, the maximum pore pressure difference occurring after the peak deviator stress. Consistently at the end of the test he measured different water contents in the shear band and the surrounding clay.

Thus, stiff clays at high YSRs seem to exhibit a behaviour both at strains corresponding to the peak stress ratio and during strain softening which is similar to the corresponding behaviour of reconstituted clay in undrained shearing on the dry side of the CSF (Section 2.2.4 and 2.3). The peak strength of both the stiff and the reconstituted clay at high YSRs is affected by the localization of strain triggered by strain-softening.

For London Clay at Ashford Common Bishop et al.(1965) (Fig.2.33) observed drained peak strengths at high YSRs, with the maximum dilation rate occurring after peak and with localization of strain. Both the drained peak strengths and the undrained peak stress ratios of London clay were found to plot on the state boundary surface, which is a straight line in the normalized stress plane, i e. is a Hvorslev surface located above the SBS of the reconstituted London clay, Fig 2 33. Bishop et al. suggested that the strength of London clay is dominated by the strength of the clay structure However frictional deformation mechanisms can be active at peak failure for stiff clays, as shown for Ancona Clay by Canestrari and Scarpelli (1993)

Burland (1990) reported the results of a triaxial test on Todi Clay, an overconsolidated fluvio-lacustrine clay, Fig 2.34. On the basis of local strain measurements he recognized that a failure plane formed in the specimen at peak But in the writer's opinion the stress-strain curve related to the local strain measurements shows that the straining rates of the two blocks on the sides of the

shear band reduced gradually after that the maximum pore pressure state and the maximum stress ratio were reached, that is when strain-softening started, as highlighted in Fig.2.34 by the writer. Localization developed with strain-softening, affecting the peak deviatoric stress. Viggiani et al.(1993) arrived at the same conclusions through a detailed analysis of the differences between the local strain measurements on the two blocks and the overall strain measurement. So the process of strain-localization in Todi clay is consistent with the processes observed by Atkinson and Richardson (1987) and Sandroni (1977).

Chandler (1968) proposed a correction for the cross specimen area in the computation of the axial stress when deformation develops by sliding of two rigid blocks along a failure surface. This allows, to a first approximation, the normal and tangential stresses acting on the failure surface to be computed. Sandroni (1977) pointed out that after the peak deviator stress the stress state computed by the application of the area correction reaches a frictional strength that he called "remoulded" (line a in Fig 2.35 $c'=0$, $\phi'=20°$), after which the pore water pressure is constant But the stress ratio that he associated with this condition for the London Clay samples is actually equal to the stress ratio at critical state of reconstituted London Clay In fact, by "remoulded" Sandroni referred to a clay reconstituted from a slurry. It follows that during strain-softening beyond the undrained peak strength the clay seems to reach a constant volume at critical state in the shear band. Sandroni recorded a further decrease of strength at large strains, which he interpreted as due to the arrival to a residual state on the failure surface.

Burland (1990) studied the post-peak behaviour of Todi Clay and London Clay by expressing the stress path followed by the clay in the shear zone in terms of τ and σ'. He called the strength reached on the failure plane when the constant stress-constant volume state had been reached the "post-rupture" strength. For both Todi Clay and London Clay the post-rupture strength is intermediate between the peak strength and the residual strength. The post-rupture strength envelope is very close to the intrinsic critical state failure envelope in the low and intermediate stress range. This observation is consistent with the interpretation reported by Sandroni, and with the CSF assumption that critical state is reached in the zones of the specimen where strain localizes. With increasing consolidation stress the post-rupture strength envelope seems to diverge from the intrinsic critical state line

Rampello et al (1993) reported the results of triaxial tests on Vallericca Clay, an overconsolidated marine clay They suggested the existence of a natural critical state line in structure permitted space, lying parallel to both the ICL and intrinsic critical state line However both the natural and the reconstituted specimens on the dry side of the recon tituted critical state

line did not reach their appropriate critical state lines, as localization of strain intervened. Also the natural specimens on the right side of the critical state line, subject to both drained and undrained shearing, reached v-p' states which do not define a unique critical state line. It can be concluded that the location of the final state after shearing of natural clays remains an open question both for stiff clays and for soft clays.

Burland (1990) reported the normalized plots of the boundary envelops measured by Webb (1964) for different depths of London Clay at Ashford Common (Fig.2.33). Since the Ashford Common depth profile is quite uniform, the plots portray different sections of the left side of the current SBS of London Clay, just as the yield loci reported by Graham et al.(1983) represented different sections of the current SBS of Winnipeg Clay (Fig.2.27). Burland pointed out that the failure envelopes at different depths A to E are almost identical, suggesting that the small differences in strength are related to differences in I_v. However, the failure envelope of the deepest level F, lies significantly above the others, indicating a structural difference of the clay at this depth. Levels A to E are structurally homogeneous, and from Fig 2 33 it can be deduced that the current SBS of the London Clay can be normalized with respect to volume.

It can be concluded that for both soft clays and stiff clays the effects of the natural structure are such as to affect the size of the current SBS, but in a way that can be normalized with respect to volume.

Various authors have investigated, from a study of the stiff clay behaviour at the macrolevel, whether the difference between the strength of the natural clay and that of the reconstituted clay arise from the existence of a strong bonding in the clay or are due solely to the fabric differences which cause displacement of the natural clay framework at higher specific volumes in the v-q-p' space (Rampello et al 1993; Coop et al.1995). This approach is not considered correct, first because the microstructural features of a clay can be deduced only from a study of the clay microstructure Second because the strength of clays, and more generally their behaviour, is a combined effect of fabric and bonding, where a given fabric can exist thanks to the associated bonding and vice versa, as discussed in Chapter 1 The effects of fabric and those of bonding cannot be separated and is the structure as a whole which determines the clay's behaviour If the SBS of a natural clay is above that of the reconstituted clay, the only deduction that can be made is that the two clays have different structural strength Nonetheless, whatever the structure, different clays exhibit fundamentally similar features of behaviour, of which a tentative description has been made

From this section it can be seen that there have been few attempts to construct a framework of behaviour of stiff clays. In the following chapters data from laboratory and field tests will be carefully examined with a view to constructing such a framework. This will be developed bearing in mind the patterns of behaviour seen for other natural soils such as cemented soils and soft clays, which have been discussed in more detail in this chapter and for which more data are available in the literature.

CLAY	TYPE	OCR	YSR\OCR	STRUCTURE*	COMMENTS	SENSITIVITY at gross yield in oedometric compression: S_t(YSR=1) ($\sigma'_v = \sigma'_y$)
SOFT	1	≈1	≈1	SEDIMENTATION STRUCTURE	NC or lightly OC clay. Processes of group 1° generated clay structure and clay SCC. In situ state of clay ($e - \sigma'_v$) plots close to SCC and $\sigma'_v \approx \sigma'_p \approx \sigma'_y$.	sedimentation sensitivity
	2	>1	≈1	POST-SEDIMENTATION STRUCTURE	OC clay. Only geological unloading caused the clay sedimentation structure change into post-sedimentation σ'_y plots on SCC, $\sigma'_p \approx \sigma'_y$	sedimentation sensitivity
STIFF	3	≈1	≈1	SEDIMENTATION STRUCTURE	NC clay compressed to high σ'_v in virgin compression. Some diagenesis occurred but while clay was compressing σ'_v is close to SCC and $\sigma'_v \approx \sigma'_p \approx \sigma'_y$	sedimentation sensitivity
	4	>1	≈1	POST-SEDIMENTATION STRUCTURE	OC clay compressed to high σ'_v, as for clays n 3. Only geological unloading caused sedimentation structure change into post sedimentation as for clays n 2.	sedimentation sensitivity
	5	≈1	>1	SEDIMENTATION STRUCTURE	NC clay cemented at deposition σ'_v plots on SCC but $\sigma'_y > \sigma'_p \approx \sigma'$	sedimentation sensitivity
	6	≈1	>1	POST-SEDIMENTATION STRUCTURE	NC clay undergoing processes of group 2° while at rest under the overburden pressure	post-sedimentation sensitivity
	7	>1	>1	POST-SEDIMENTATION STRUCTURE	OC clay undergoing geological unloading and other processes of group 2°	post-sedimentation sensitivity
LEACHED	8	≈1	≈1	POST-SEDIMENTATION STRUCTURE	NC clay undergoing leaching after virgin compression	post-sedimentation sensitivity

Table 2.1. *Structure - related classification of clays*

** see table 1.1*

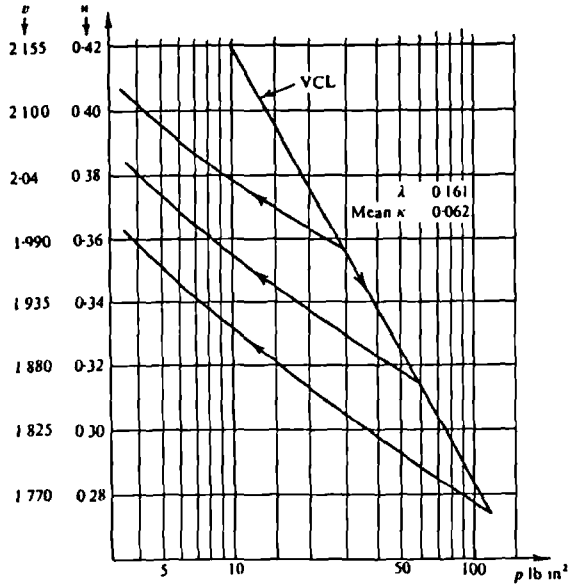

VCL: virgin compression line

Fig.2.1 Reconstituted London clay: isotropic compression and swelling curves (data from Henkel 1956; after Schofield and Wroth 1968).

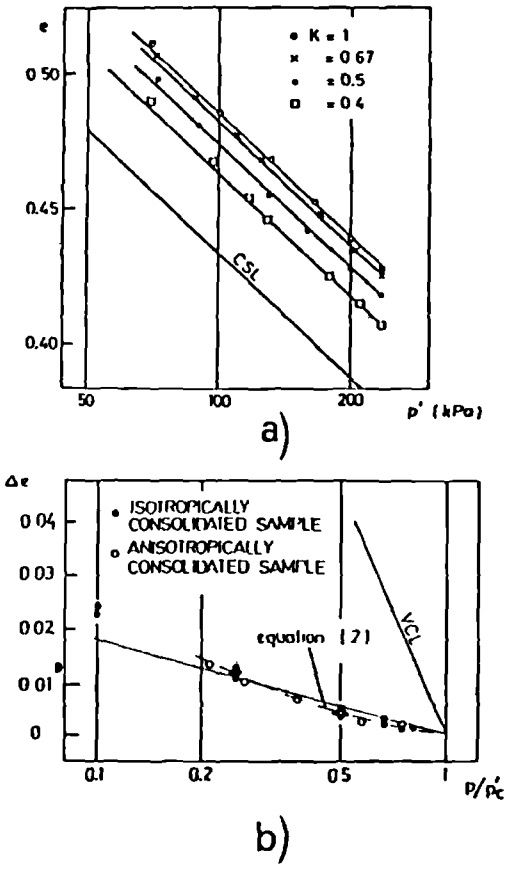

Fig.2.2 Reconstituted Lower Cromer Till: (a) constant η lines; (b) normalized swelling lines (after Gens and Potts 1982).

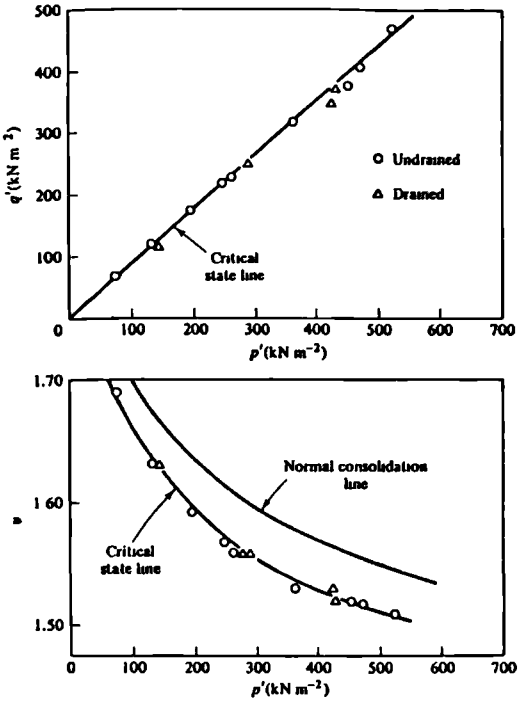

Fig.2.3 Normally consolidated reconstituted Weald Clay: failure states in drained and undrained shearing (data from Parry 1960; after Atkinson and Bransby 1978).

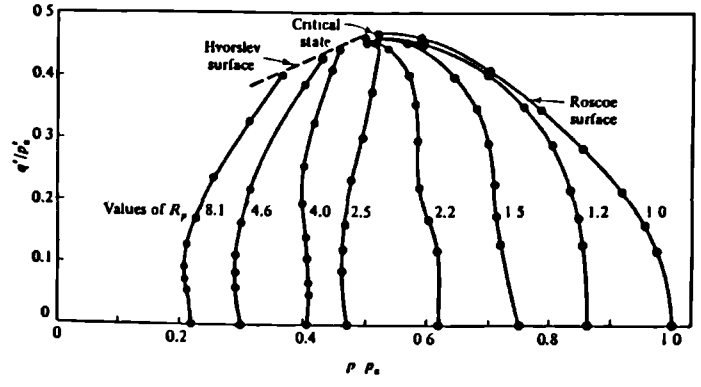

Fig.2.4 Overconsolidated reconstituted kaolin: normalized undrained stress paths(data from Loudon 1967; after Atkinson and Bransby 1978).

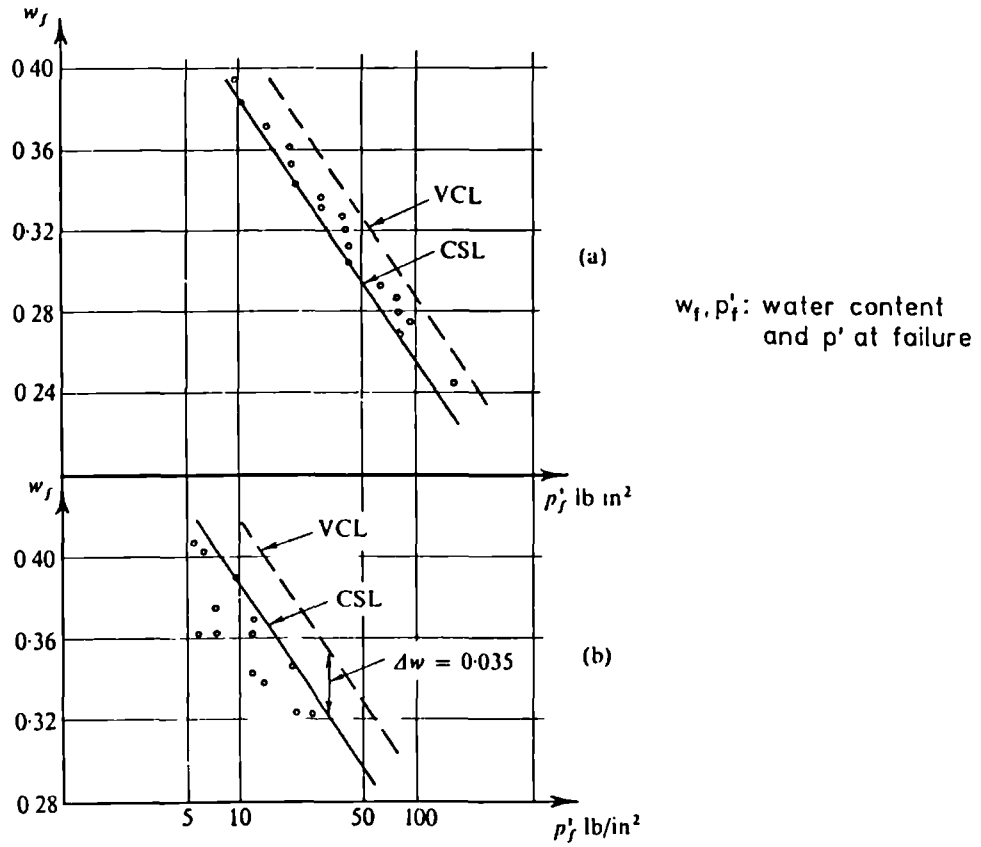

Fig.2.5 Remoulded London Clay at failure (data from Parry 1958; after Schofield and Wroth 1968).

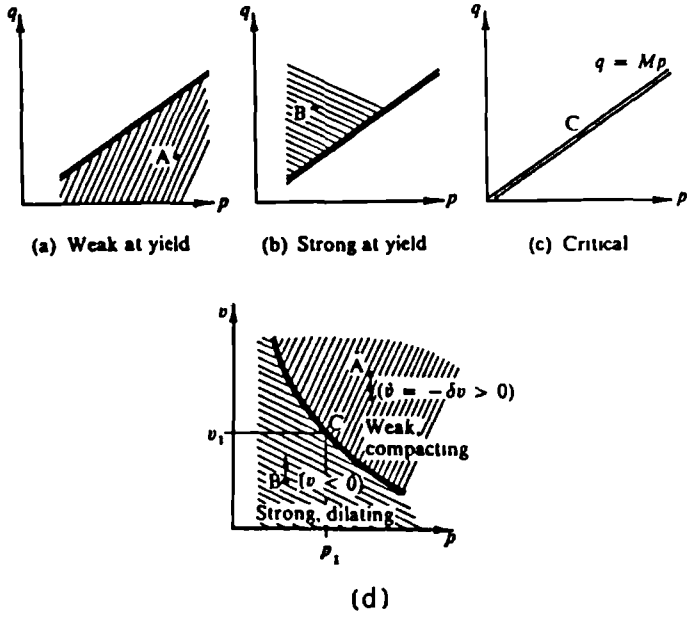

Fig.2.6 Condition of specimens at yield in relation to the critical state line (after Schofield and Wroth 1968).

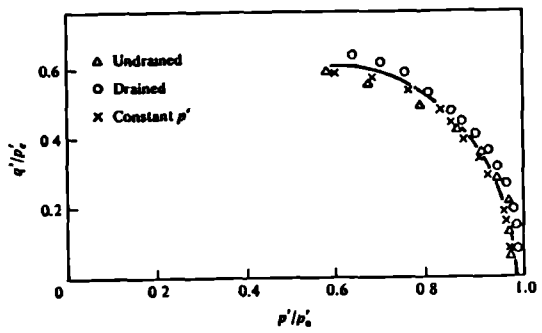

Fig.2.7 Normally consolidated reconstituted kaolin: normalized stress paths (data from Balasubramaniam 1969; after Atkinson and Bransby 1978).

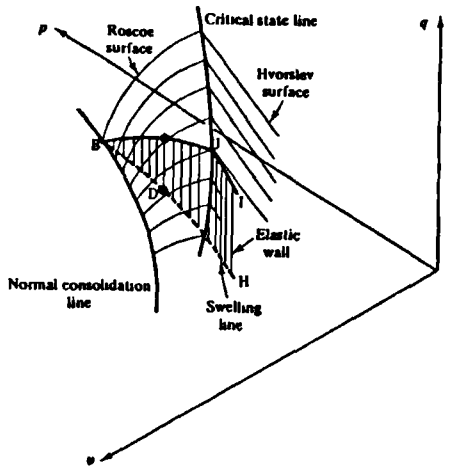

Fig.2.8 The state boundary surface and the elastic wall in the Critical State Framework (after Atkinson and Bransby 1978).

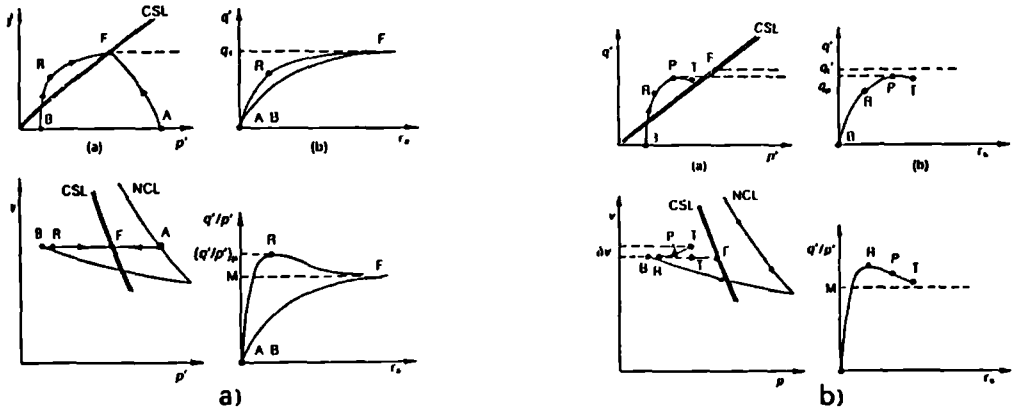

Fig.2.9 (a) Idealized behaviour of samples of normally consolidated and overconsolidated soil in undrained compression tests; (b) Idealized behaviour of overconsolidated soil in undrained compression tests with partial drainage (after Atkinson and Richardson 1987).

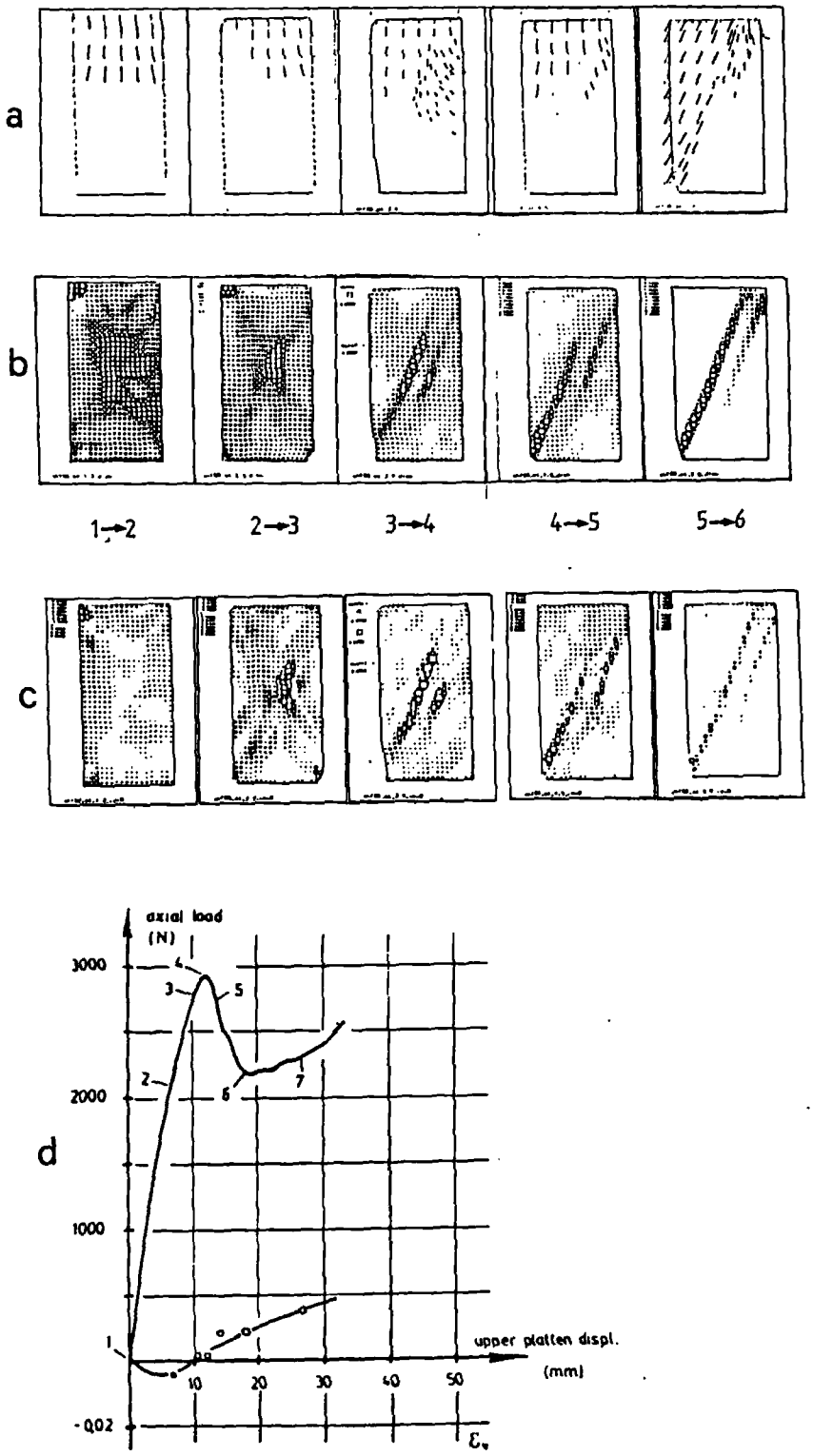

Fig.2.10 Stereophotogrammetric measurements during a plane strain test: (a) incremental displacements; (b) shear intensities; (c) volumetric strains; (d) stress-strain curve (after Desrues 1990).

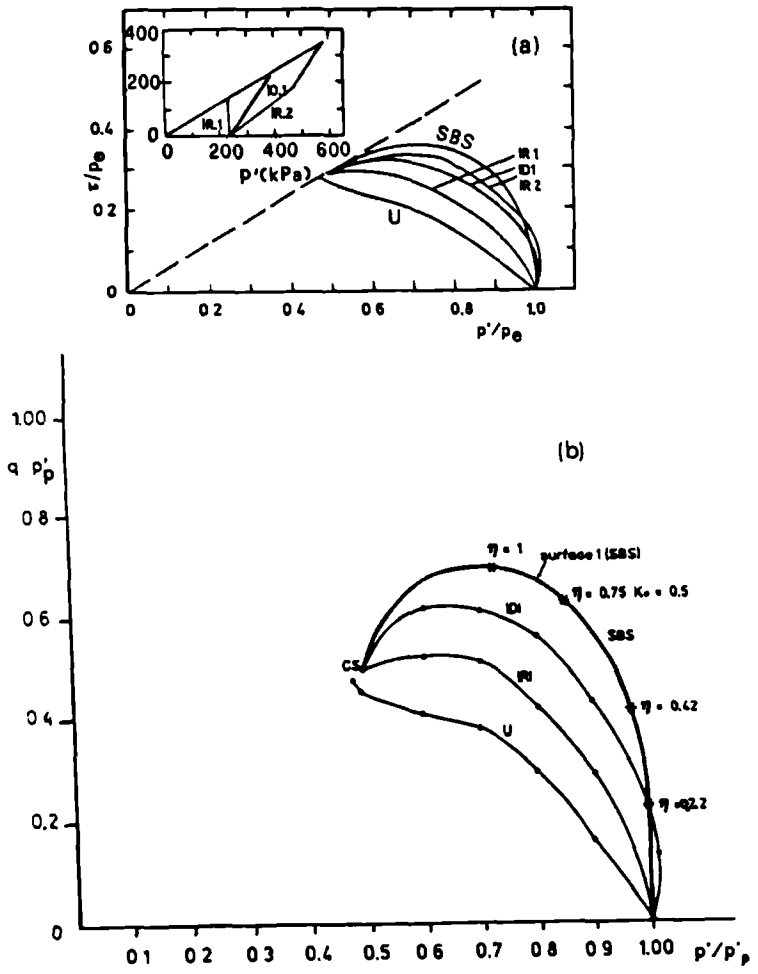

Fig 2 11 Reconstituted Lower Cromer Till: stress paths on isotropically normally consolidated samples (a) in the normalized ℓ-p' plane (after Gens 1982) and (b) in the normalized q-p' plane (data from Gens 1982).

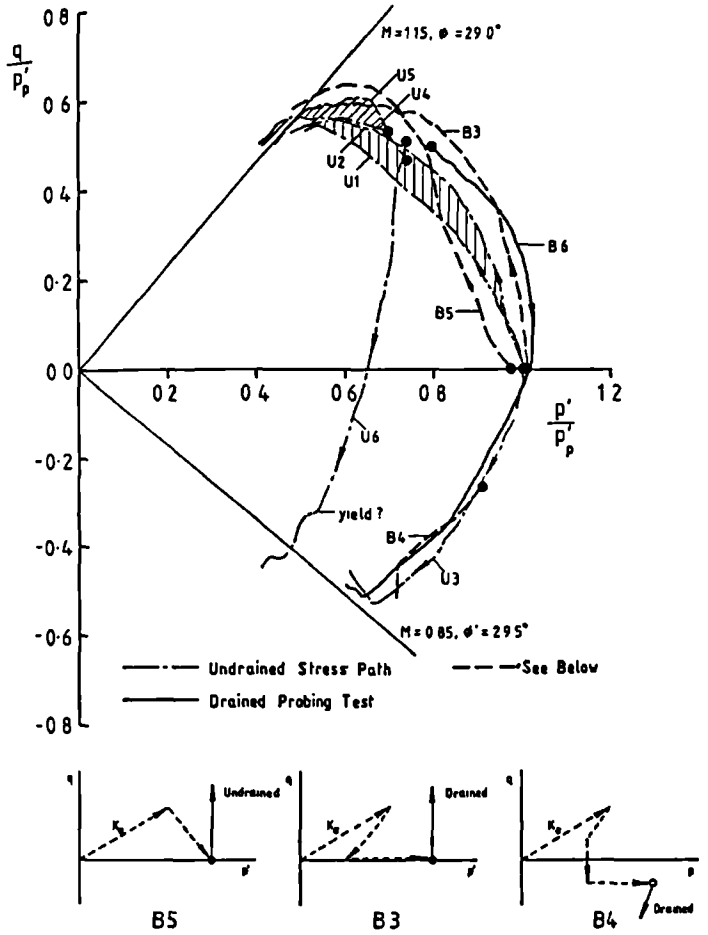

Fig 2.12 Normalized stress paths for K_0 and isotropically consolidated samples of remoulded organic clay (after Pickles 1988)

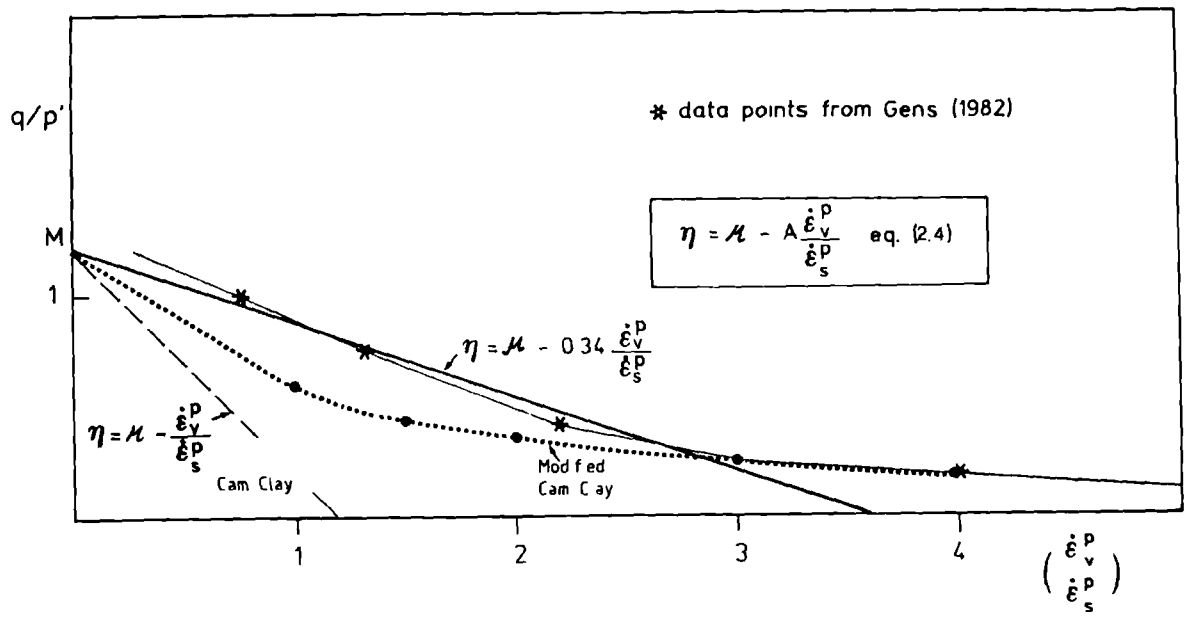

Fig.2.13 Reconstituted Lower Cromer Till: plastic strain ratios along constant η lines (data from Gens 1982).

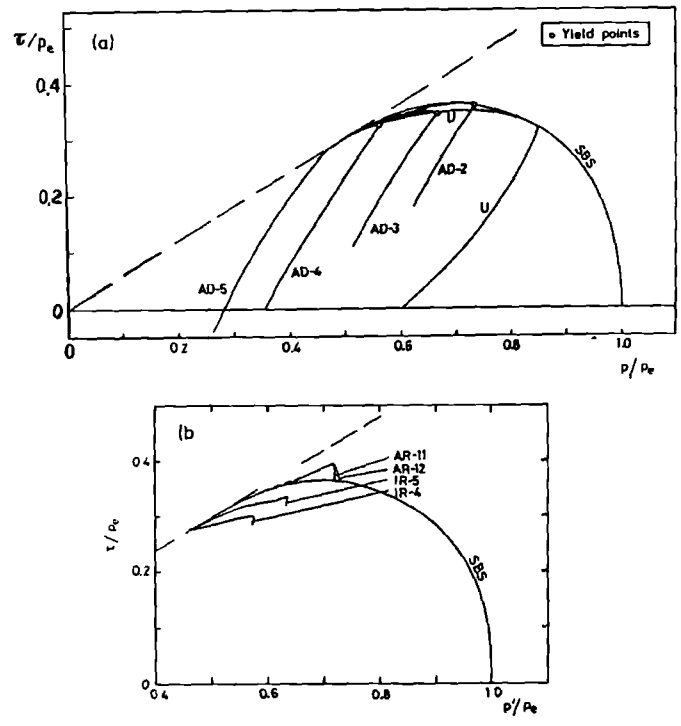

Fig 2.14 Reconstituted Lower Cromer Till: (a) stress paths for drained tests on K_0 consolidated samples; (b) undrained stress paths on samples consolidated at η=1 (after Gens 1982)

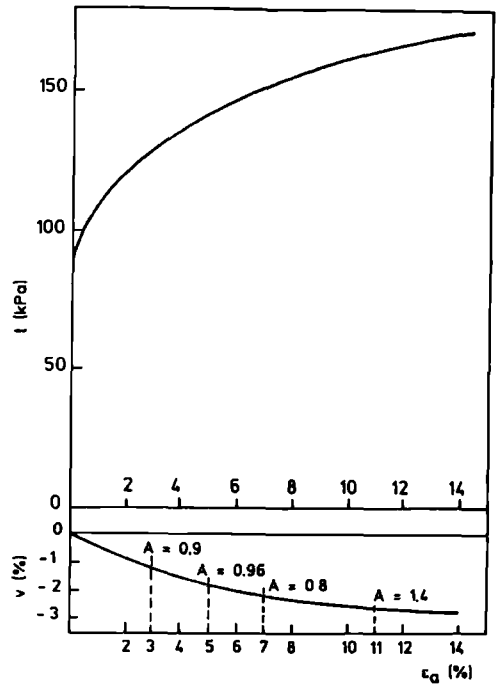

Fig.2.15 Reconstituted Lower Cromer Till: drained triaxial compression on a K_0 normally consolidated sample (data after Gens 1982).

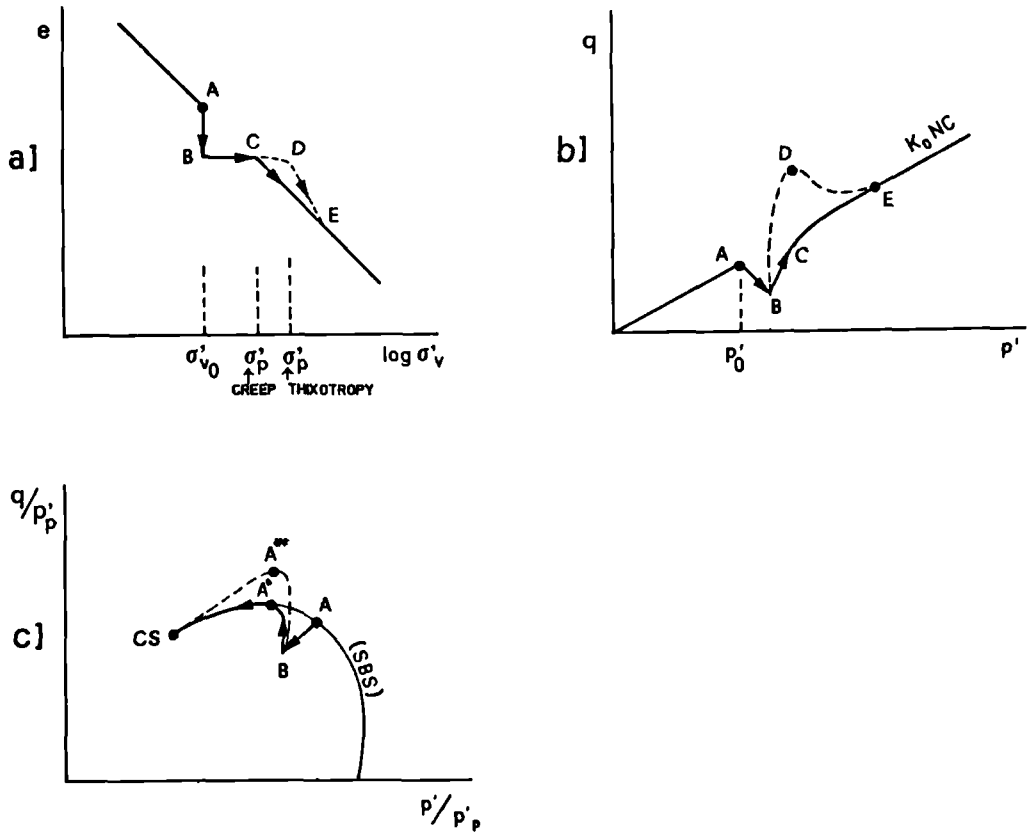

Fig.2.16 Ageing effects on clay behaviour.

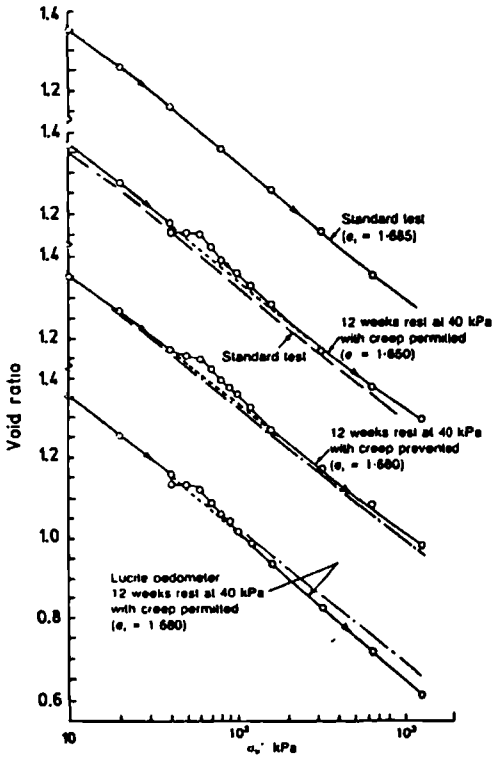

Fig.2.17 Influence of ageing on compression behaviour of a reconstituted clay (after Leonards and Ramiah 1959).

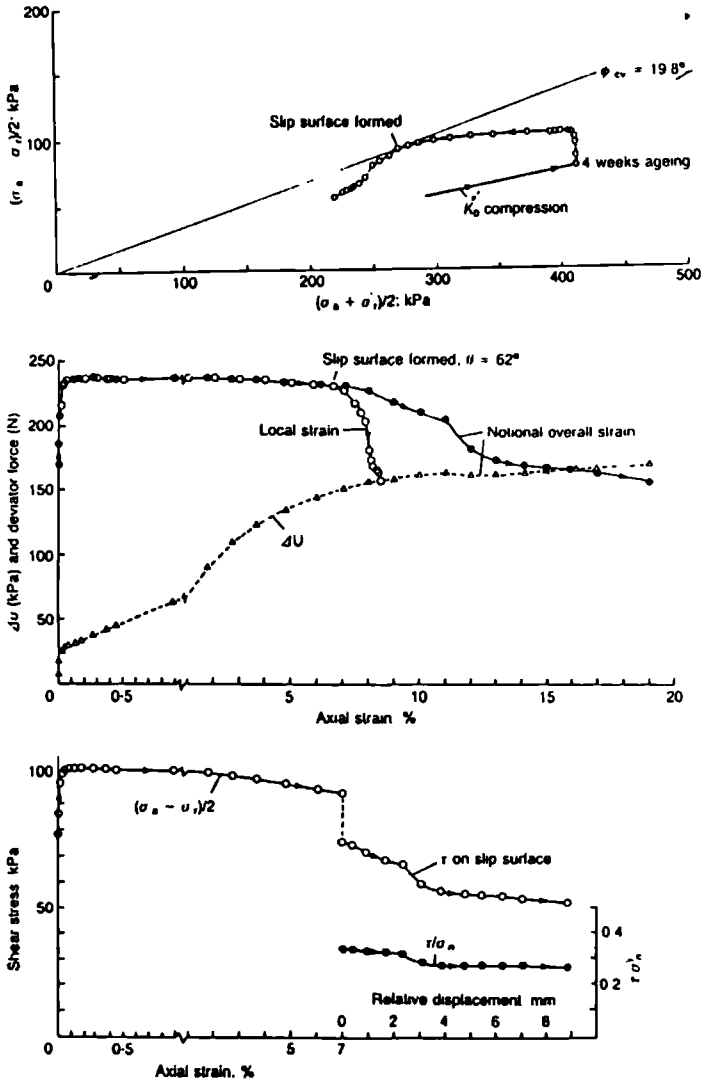

Fig.2.18 Mechanical behaviour of normally consolidated aged kaolin (data from N.Ninis 1990; after Burland 1990).

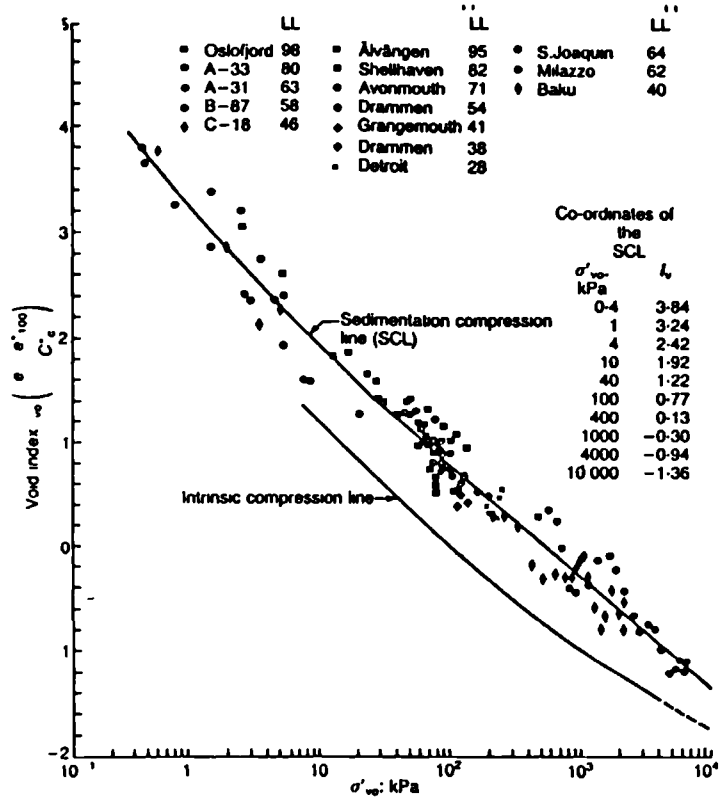

Fig.2.19 In situ I_v-σ'_v states for natural clays (after Burland 1990).

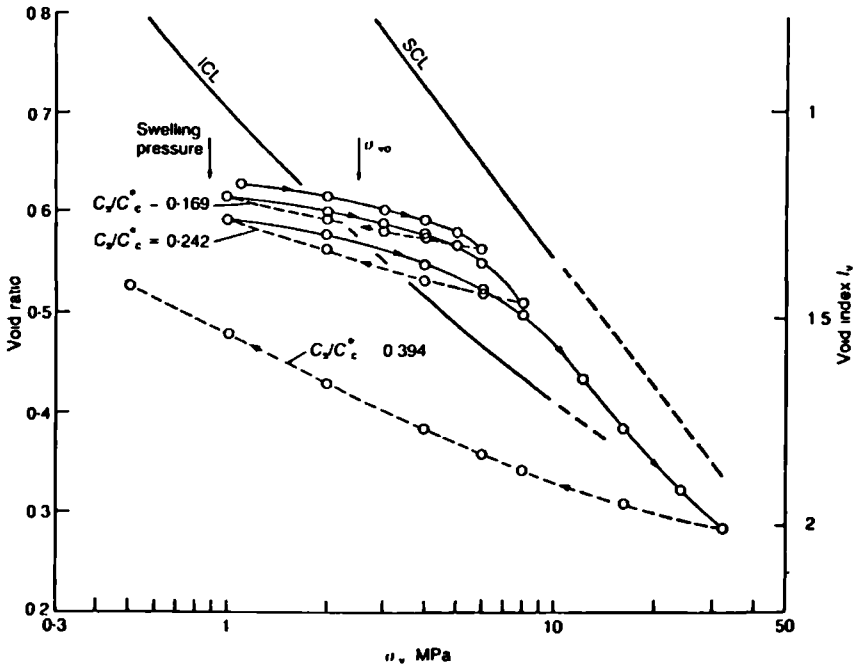

Fig.2.20 Boom Clay (W_{LL} = 65%): high pressure oedometer test on block sample from Mol (after Burland 1990).

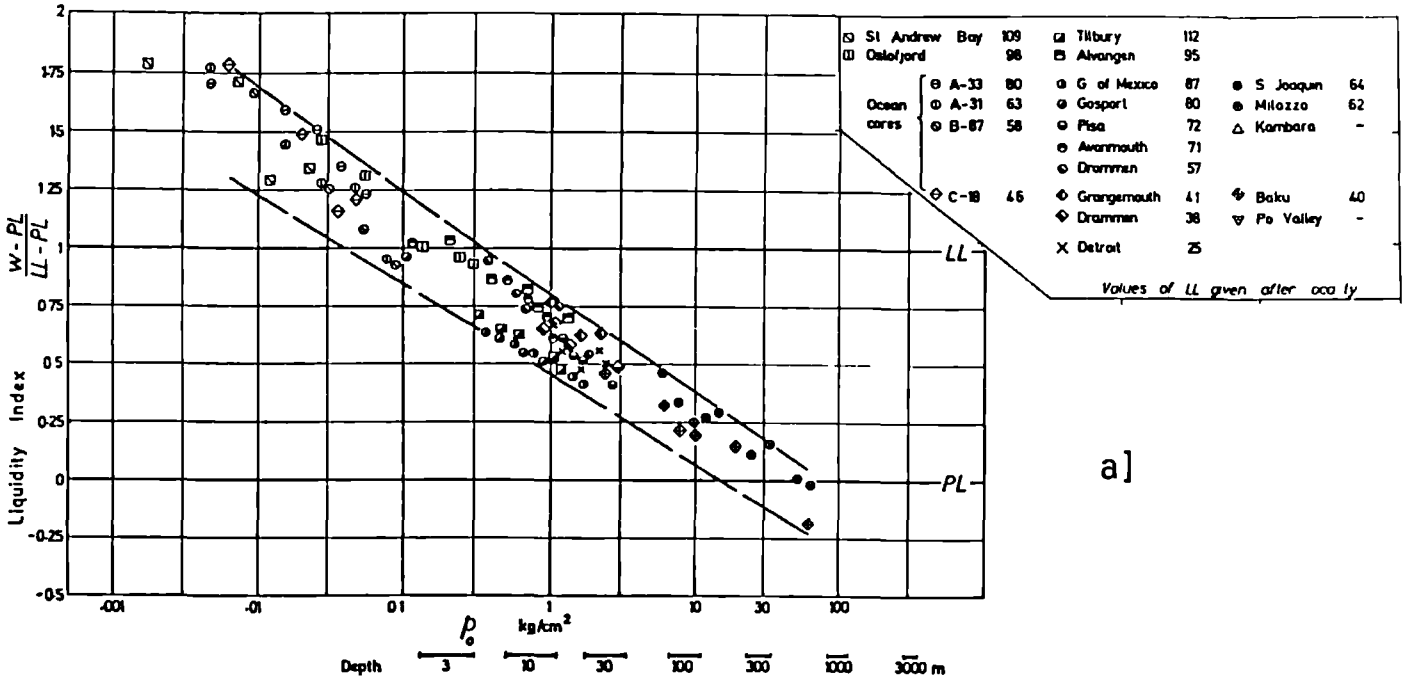

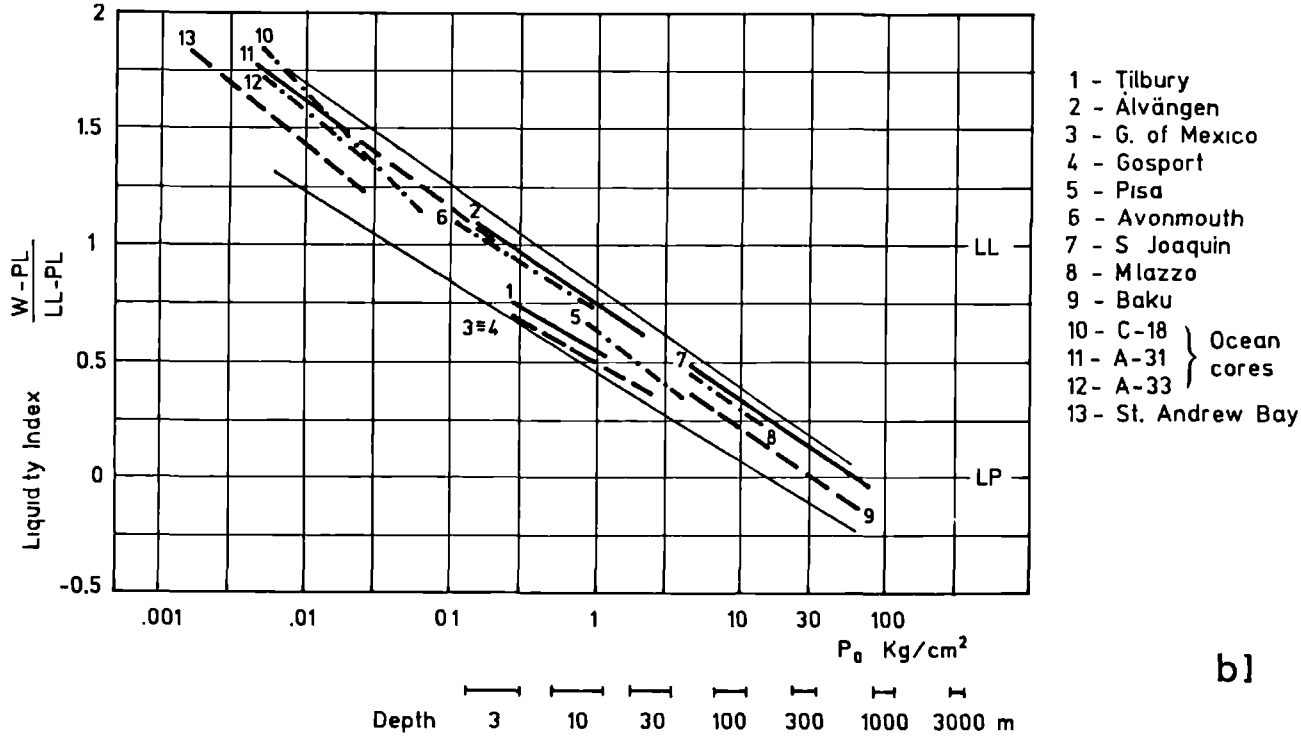

Fig.2.21 Normally consolidated argillaceous sediments : (a) in situ states (after Skempton 1970); (b) sedimentation compression curves.

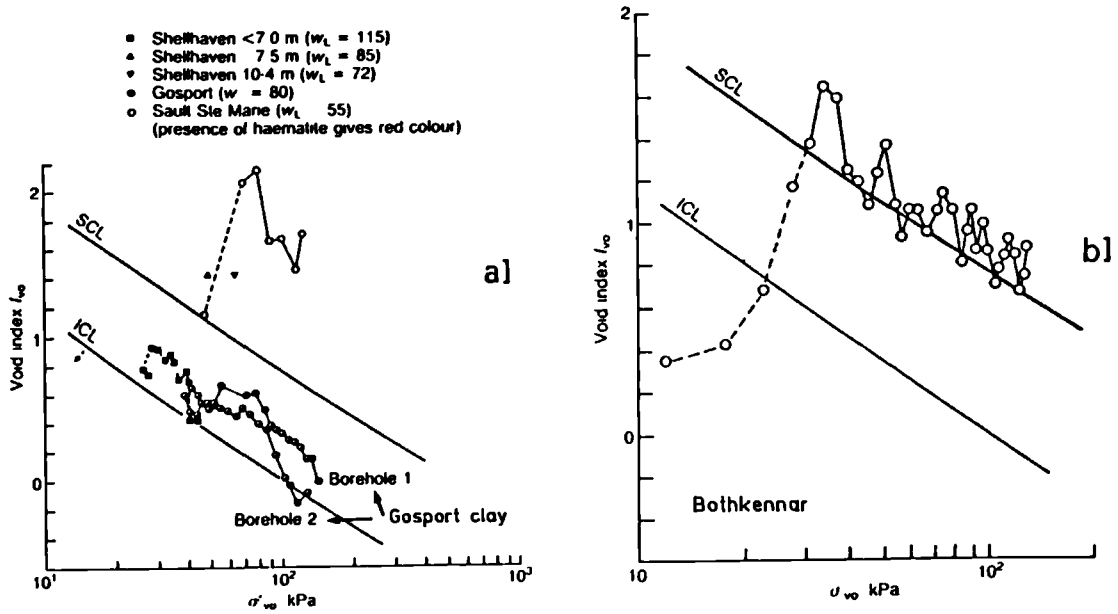

Fig.2.22 Sedimentation Compression Curves:(a) Gosport Clay, (b) Bothkennar Clay (after Burland 1990).

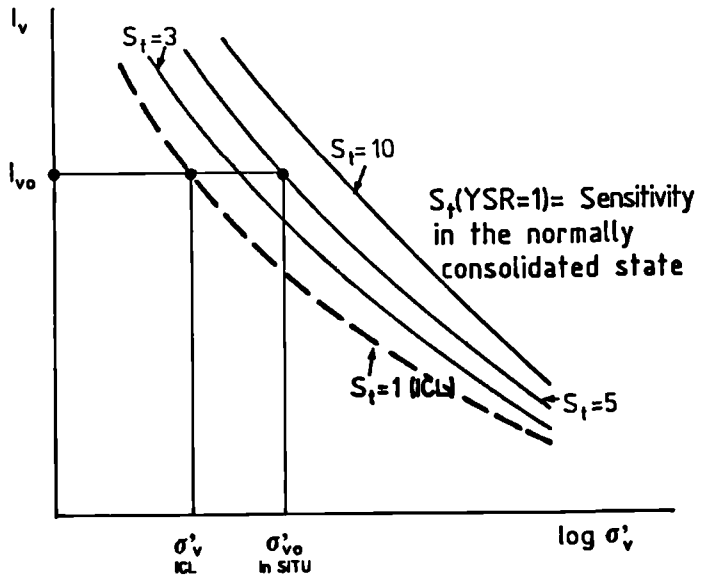

Fig.2.23 The sensitivity framework for soft clays: sedimentation compression curves of clays of equal sensitivity.

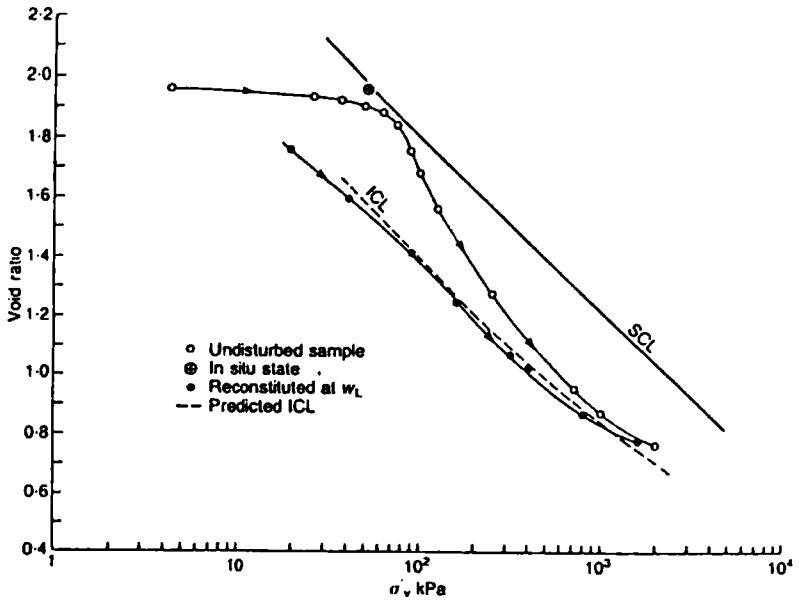

Fig.2.24 Bothkennar clay: oedometric compressions on undisturbed and reconstituted clay (W_{LL}=85.4%; W_{PL}=41%) (after Burland 1990).

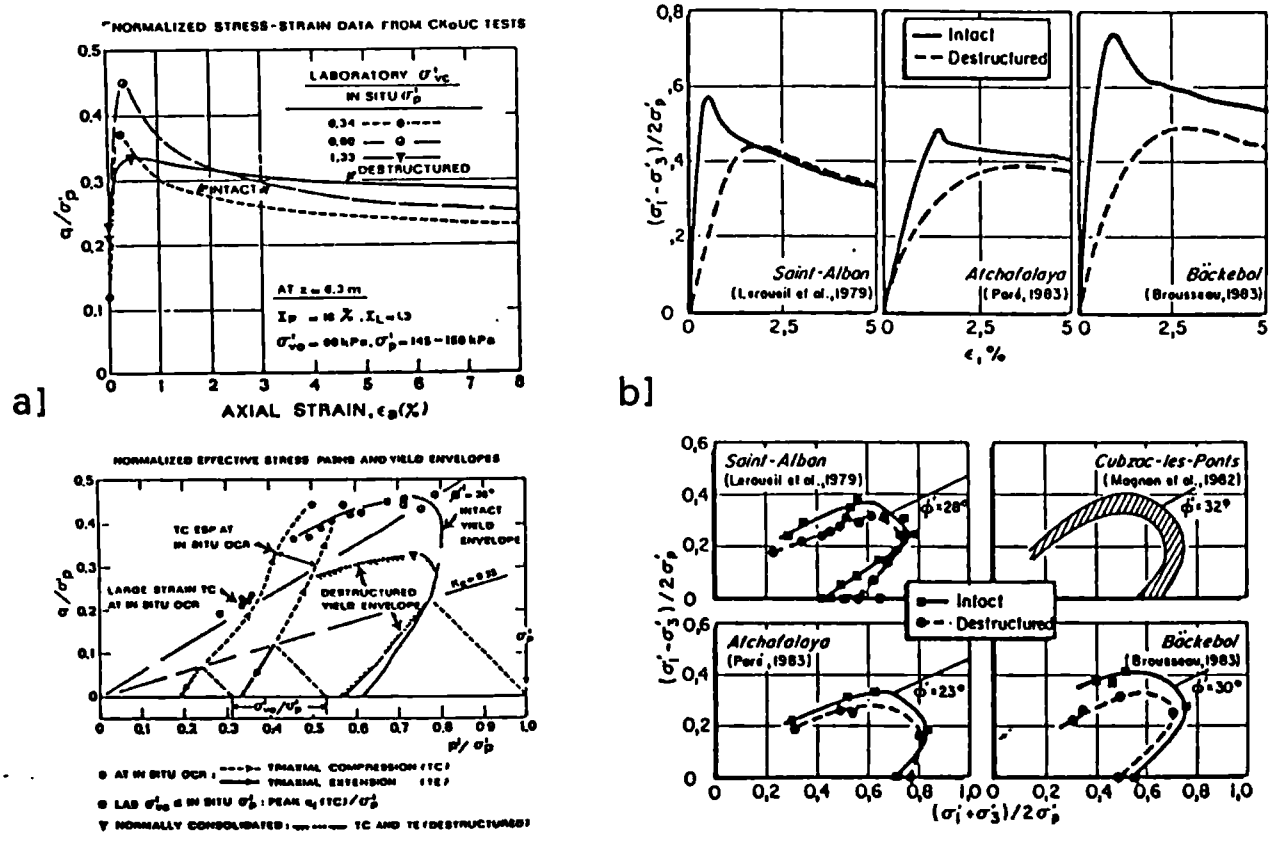

Fig.2.25 Behaviour of natural soft clays: (a) undrained stress-strain behaviour and stress paths of James Bay B-6 marine clay (after Jamilkowsky et al.1985, data from Lefebvre et al.1983); (b) current yield curves of undisturbed specimens and yield curves of specimens compressed beyond isotropic gross yield (after Tavenas and Lerouil 1985).

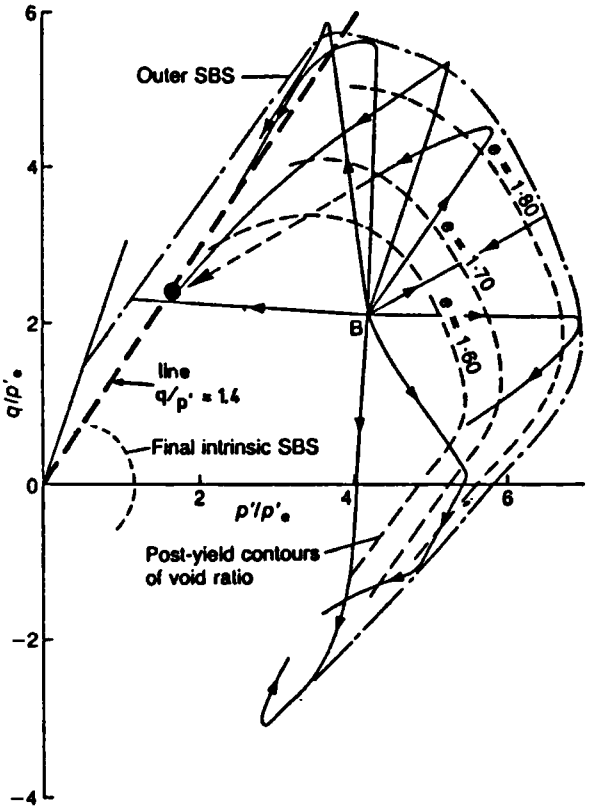

Fig.2.26 Bothkennar Clay: Normalized probing stress paths and current SBS (after Smith et al.1992).

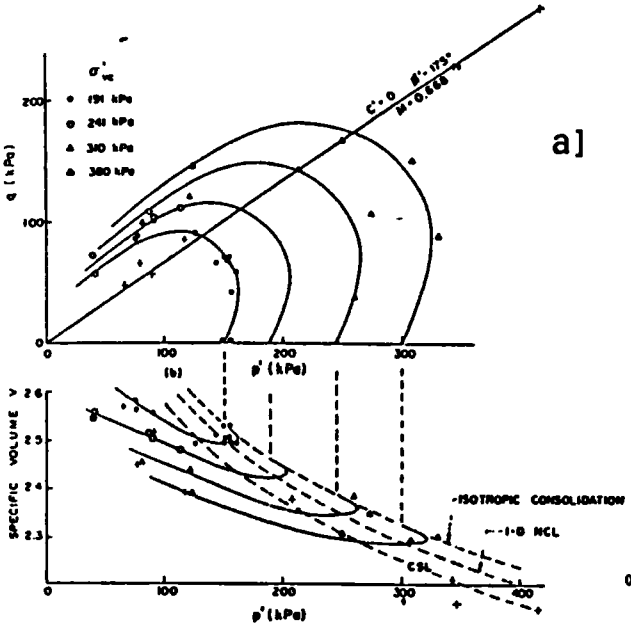

σ'_{vc}: preconsolidation pressure

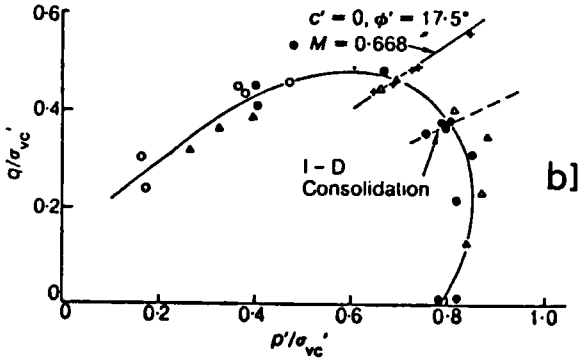

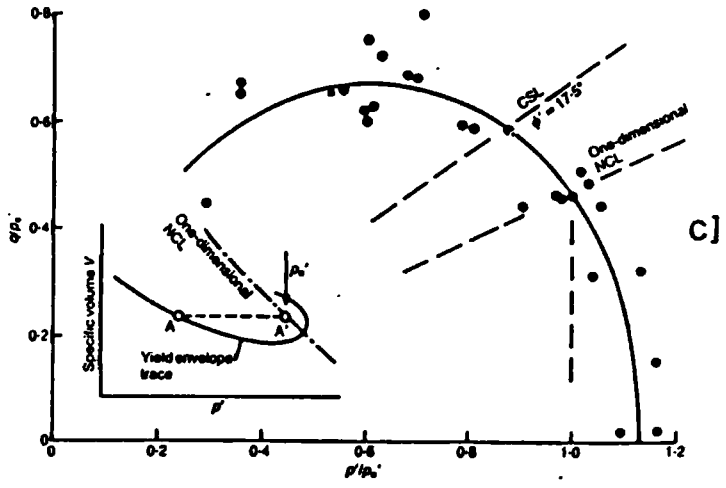

Fig.2.27 Winnipeg Clay: (a) current yield envelopes; (b) current yield envelopes normalized with respect to the preconsolidation pressure (after Graham et al.1983); (c) current yield envelope normalized with respect to the equivalent pressure p'_{scc} (p'_e in the figure; after Graham et al.1988).

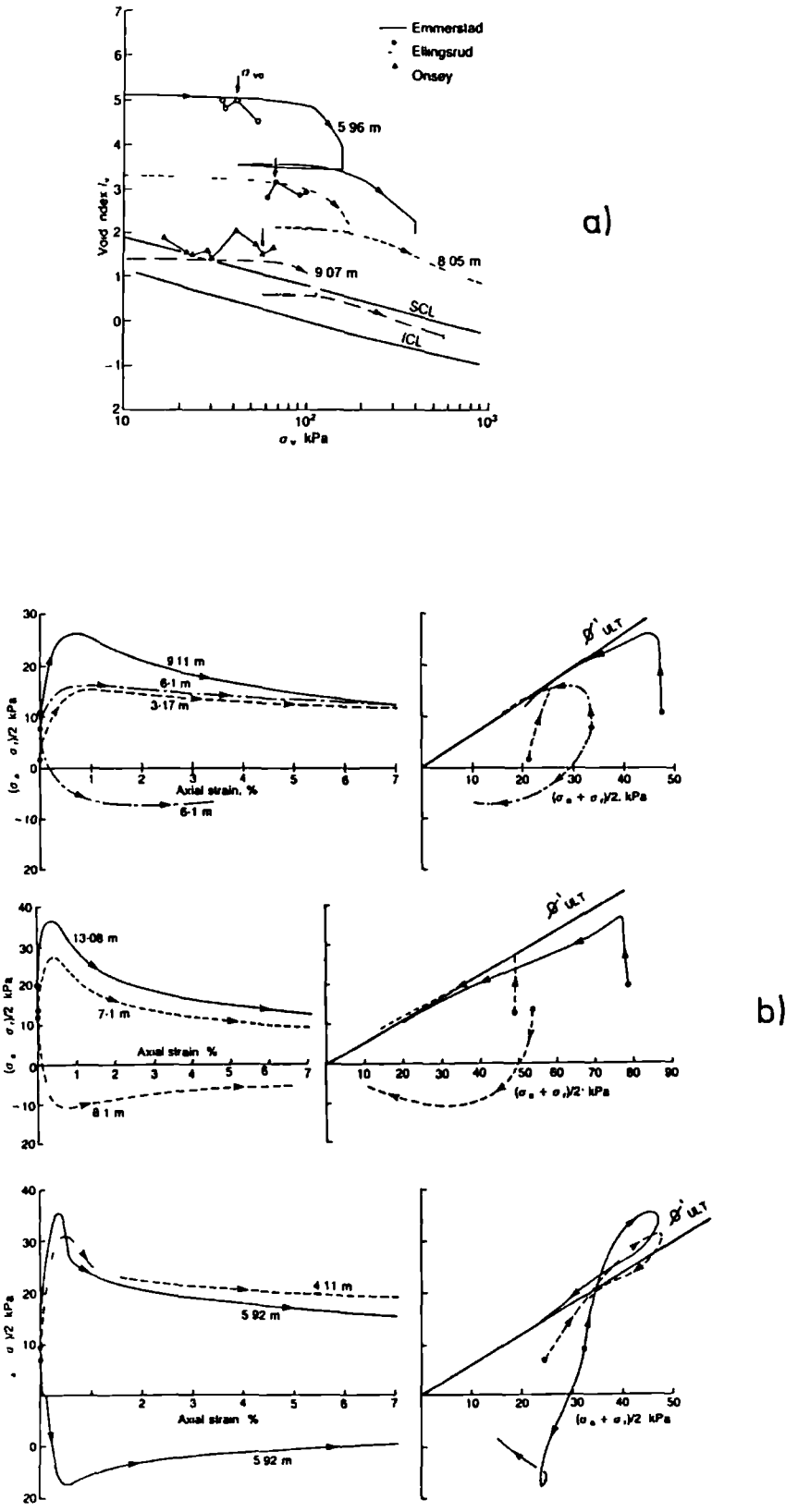

Fig.2.28 Mechanical behaviour of Norwegian clays (data from Lacasse et al.1985; after Burland 1990).

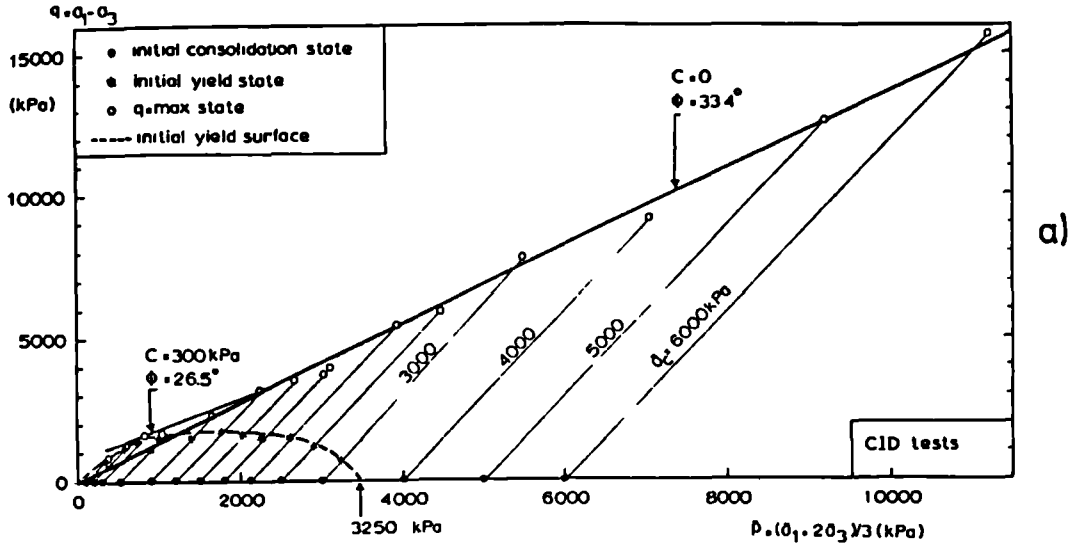

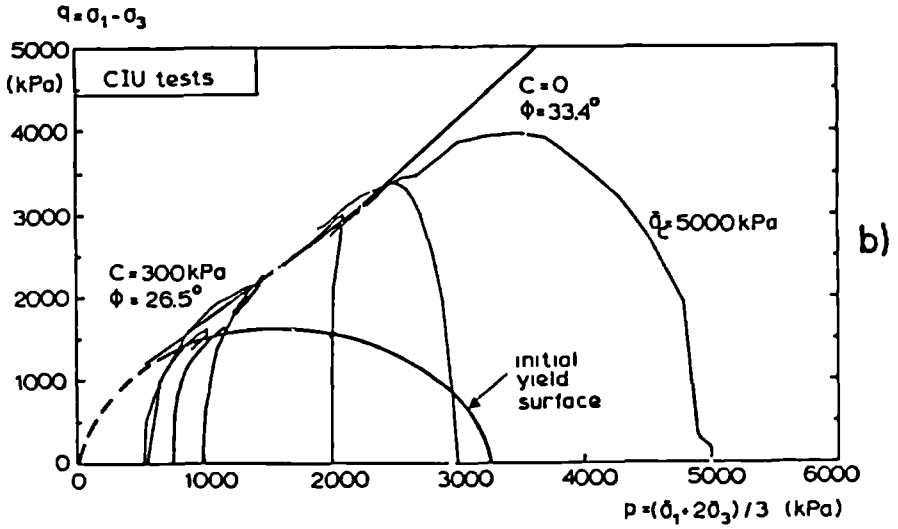

Fig.2.29 Corinth marl: (a) drained stress paths and current yield curve; (b) undrained stress paths and current yield curve (after Anagnostopulos et al.1991).

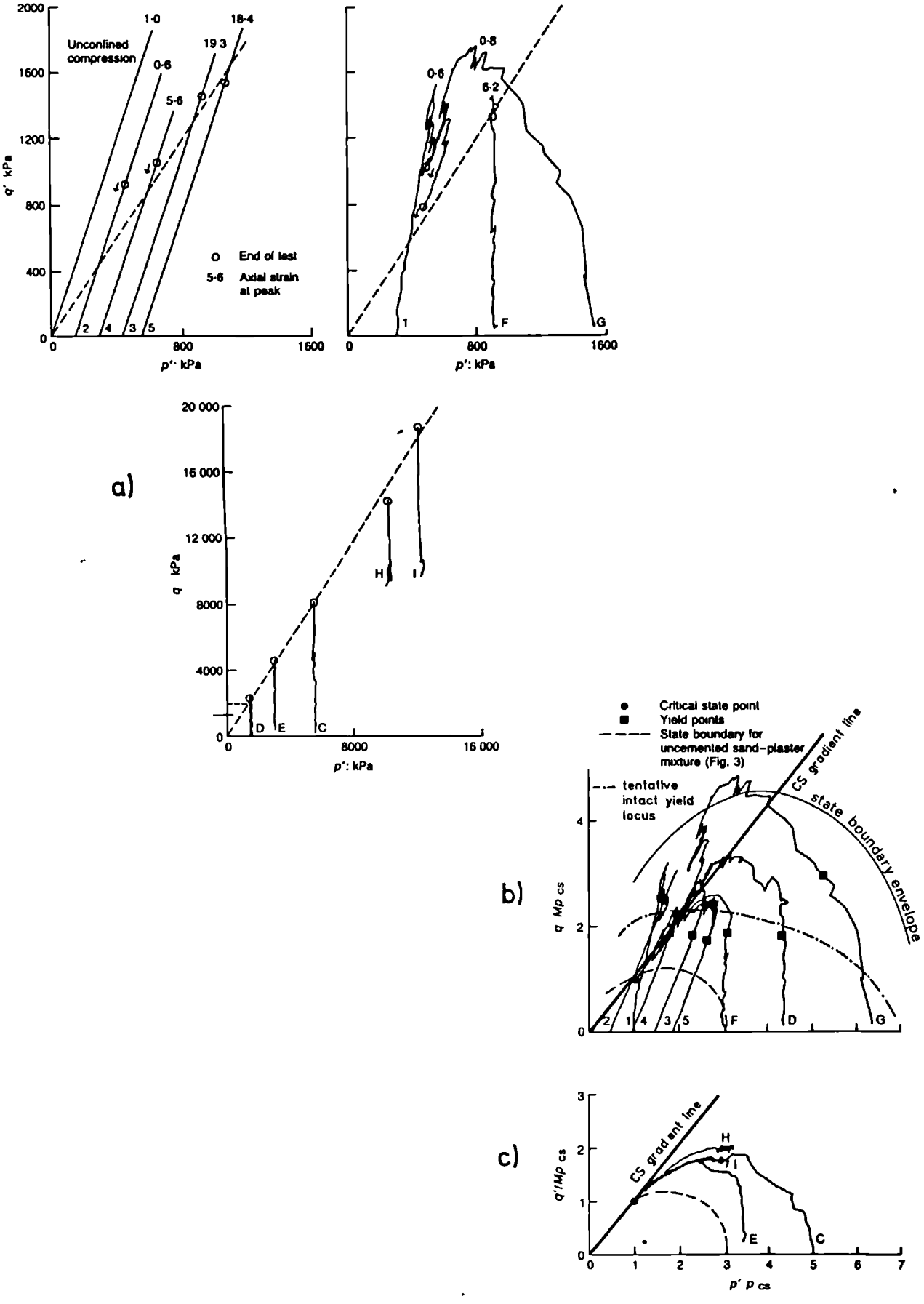

Fig.2.30 Mechanical behaviour of Cemented Carbonate Sand: (a) stress paths; (b) normalized stress paths at low and intermediate confining pressures; (c) normalized stress paths at high confining pressures (after Coop and Atkinson 1993).

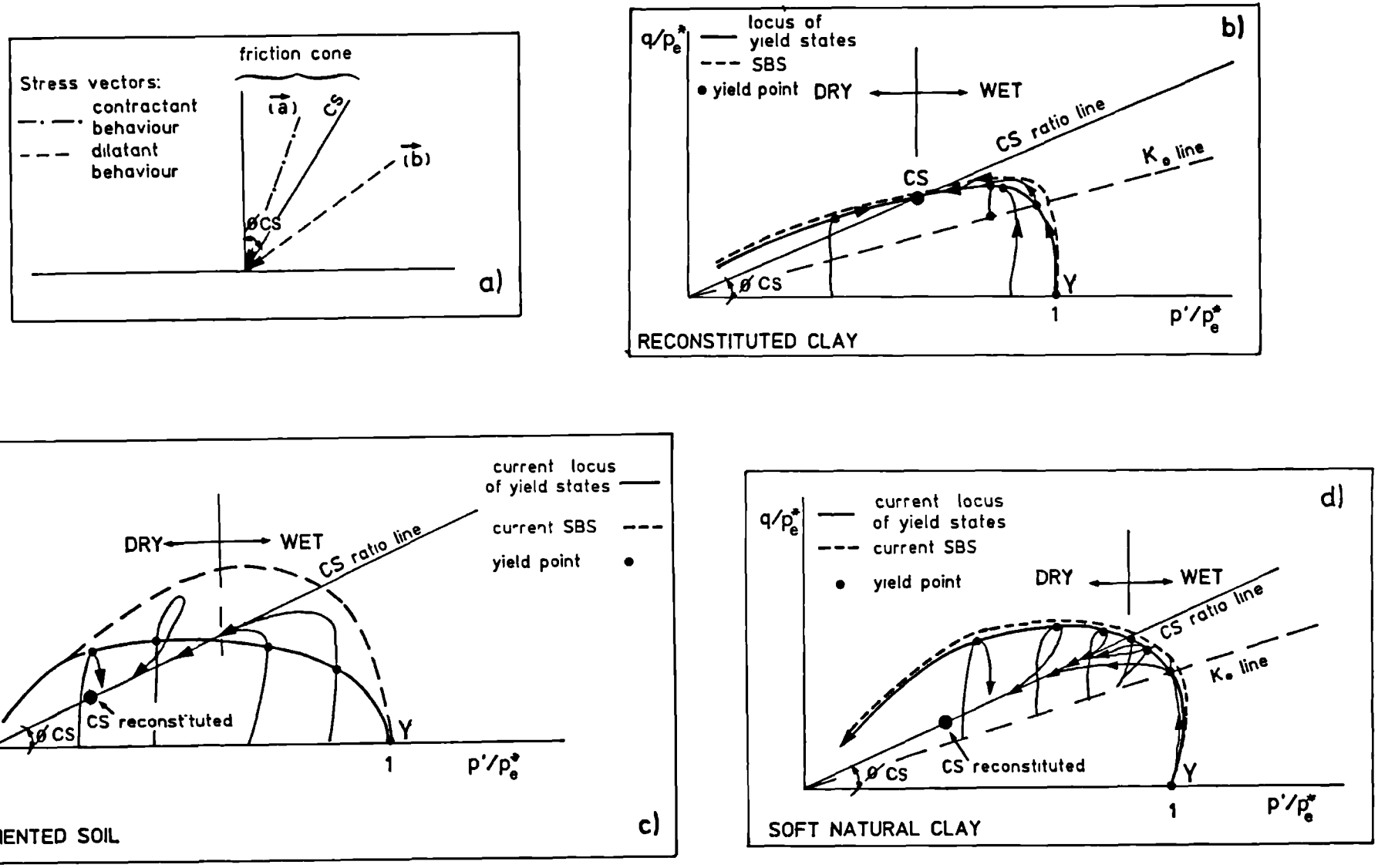

Fig.2.31 Behavioural frameworks for reconstituted soils, cemented soils and soft sensitive clays.

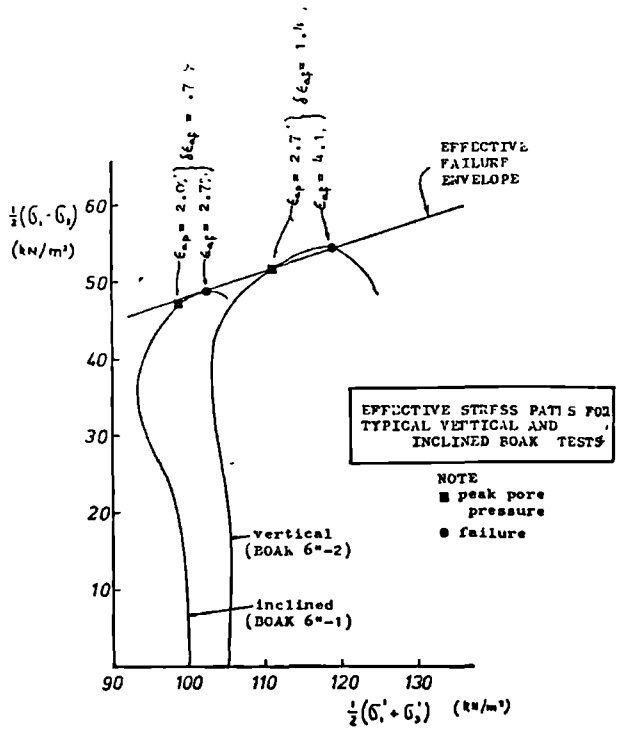

Fig.2.32 London Clay: undrained stress paths and failure envelope (after Sandroni 1977).

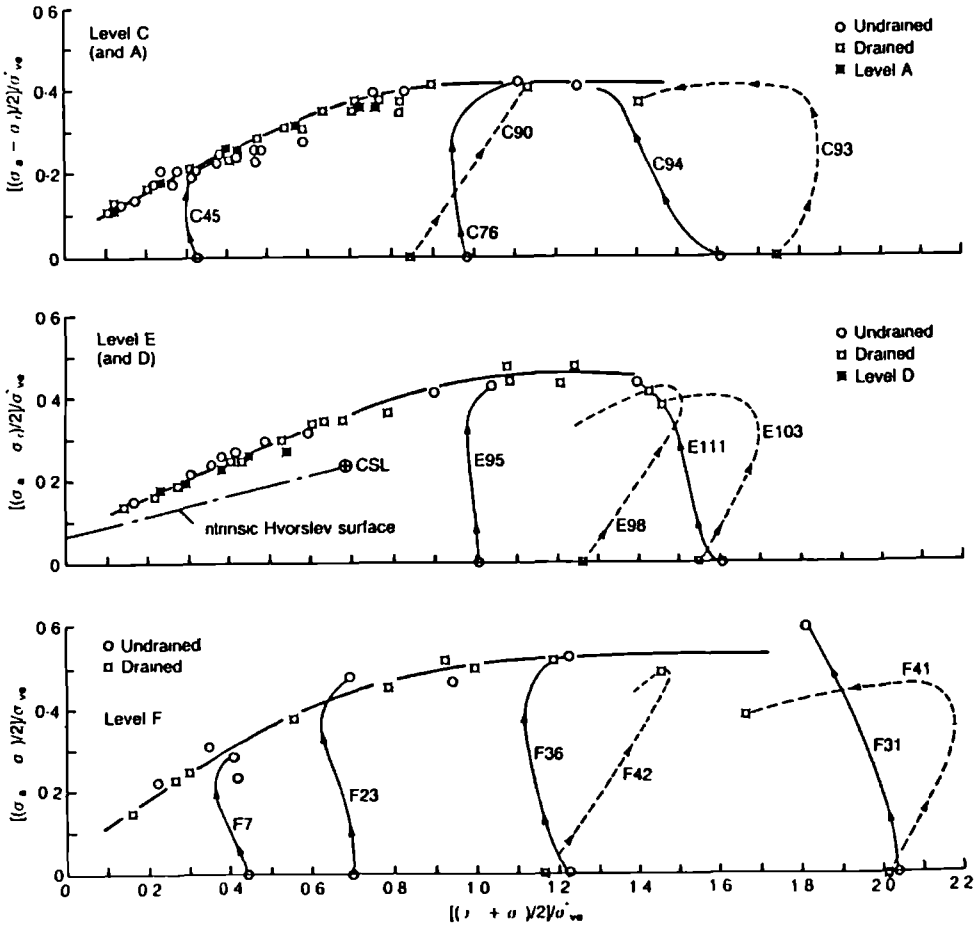

Fig.2.33 London Clay at Ashford Common: normalized strength envelopes (after Burland 1990).

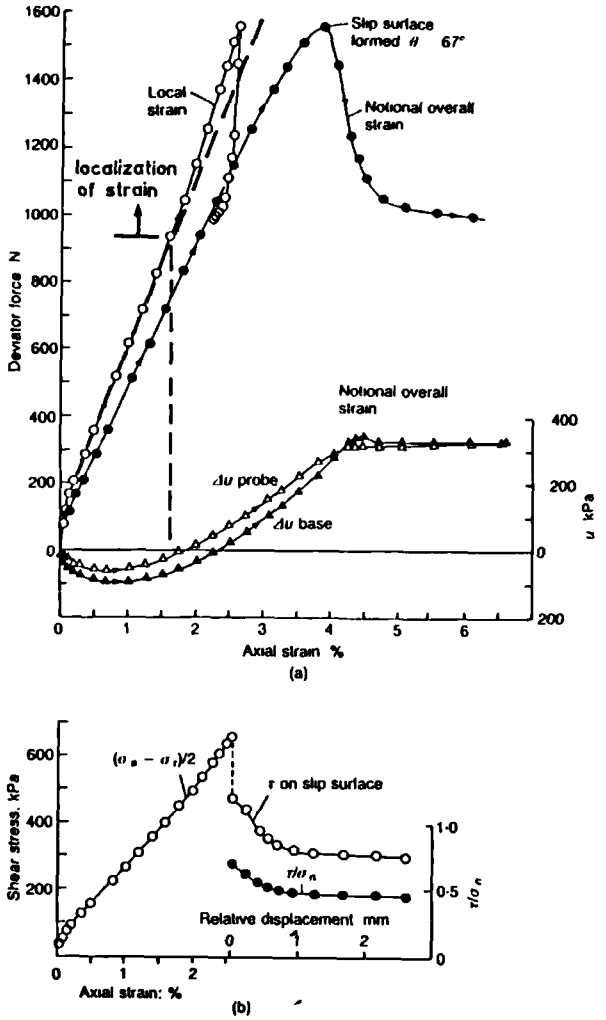

Fig.2.34 Todi Clay: (a) undrained stress-strain behaviour; (b) post-rupture shear stresses and stress ratios (after Burland 1990).

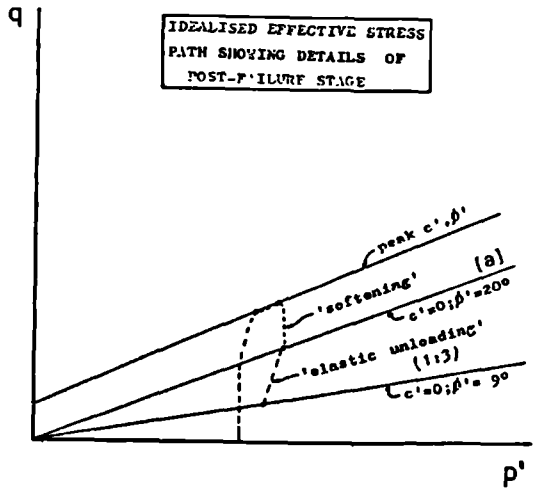

Fig.2.35 London Clay: undrained stress path corrected for localization (after Sandroni 1977).

CHAPTER 3

GEOLOGICAL CHARACTERISTICS AND BASIC GEOTECHNICAL PROPERTIES OF THE PAPPADAI CLAYS

3.1. Introduction

This chapter reports the geological history and present characteristics of the natural stiff clay which was subjected to experimental investigation in the research The clay studied is part of the sub-Apennine blue clays present in the Pappadai valley (subsequently referred to as Pappadai clay). The valley is located in the Montemesola Basin, near Taranto, southern Italy, as shown in Figs.3.1 and 3.2. This valley has been the subject of intensive field investigations for the construction of a dam across the valley (V.Cotecchia et al 1993), during the course of which many continuously cored boreholes were drilled. Some of the data presented here are the result of these investigations, but a more recent continuously cored boring provided further extensive information.

The lithological profile of the clay deposit was examined in great detail. The index properties and mineralogical properties were measured in the laboratory on numerous clay samples, which describe the variations of the properties of the clay for various vertical profiles through the deposit.

The results of the analysis were related to the geological history of the sediments, which was reconstructed in some detail. A palaeontological analysis complemented the study of the literature data about the clay history. The known details of the clay history were of use to examine the current water content profile of the Pappadai clay deposit. Since the clay appears to have developed a structure which involves significant bonding, as shown in the following chapters, the origins of the clay bonding were searched for in the study of the clay history

3.2. Geological Background

The sub-Apennine blue clays are marine deposits of widespread distribution in southern Italy (Fig 3.1) that were deposited in one or other of two sedimentary cycles (Del Prete and Valentini 1971) The lower-cycle blue clays are of Lower or Middle Pliocene age and are found in basins

within the tectonically active Apennine Chain, and correspondingly have been disturbed significantly in situ. Upper-cycle blue clays occur in the Bradano Trough, and also on the Apulian Cretaceous platform to the east. They were deposited during a marine transgression in Upper Pliocene - Lower Pleistocene times, following the formation of the Bradano Trough during the Upper Pliocene (Ogniben 1969). These upper-cycle clays differ from those of the lower-cycle, typically having higher proportions of clay and being far less disturbed tectonically. Since the upper-cycle blue clays were deposited initially in isolated basins over an extensive area (Ricchetti 1967; Ciaranfi et al.1971), they exhibit some variability.

In the south-eastern part of the Bradano Trough and in Apulia the upper-cycle blue clays lie unconformably on a dolomite basement of Cretaceous age. Directly overlying the Cretaceous bedrock are the Gravina Calcarenites, fine to coarse weakly cemented sands, on which, as the depositional basin deepened, the sub-Apennine blue clays were deposited (Fig 3 2). The blue clays are composed of sediments derived from the erosion of Apennine rocks and were deposited continuously throughout the upper-cycle transgression Subsequently, uplift resulted in a regression, and, where the uplift was more rapid, sands and conglomerates (Monte Marano Sands; Irsina Conglomerates) were deposited (Fig.3.2) (Ciaranfi et al. 1988). This marks the start of the regression and the top of the sedimentary cycle, though still within the Lower-Middle Pleistocene, with an age of 1.0 - 1.1 million years. At this time some of the depositional basins, notably those of Taranto and Montemesola (Fig.3.3), were still submerged, and the sands and conglomerates were not deposited. This regression eventually resulted in the erosion of a sequence of Upper Pleistocene marine terraces on which calcarenites were deposited. Thus locally, following some erosion, the more recent calcarenites were deposited directly on the upper-cycle blue clays.

Ciaranfi et al (1971) present morphological, geochemical and palaeontological data which show that depositional conditions in the Montemesola Basin differed from those in the Taranto Basin at the time of deposition of the Pappadai clay. Their reconstruction of the morphology of the Montemesola Basin before clay deposition is shown in Fig 3.4. The high percentage (70°₀) of plankton in the central area of the Montemesola Basin, as against 30°₀ for comparable locations within the Taranto Basin, indicates that in the Montemesola Basin the sea was more protected and comparatively still (at least in the initial stages of deposition), resulting in a reducing environment at the sea bed Moreover, the benthic fauna identified in the Montemesola Basin is that associated with a deep-water habitat, while that in the Taranto Basin is apparently related to more open marine conditions. Finally, the presence in the clay of authigenic sulphates (greigite and pyrite) confirms that there was organic matter present in a reducing environment with little

water circulation at the time of deposition. The deposition of Pappadai clay thus occurred in comparatively deep and still marine reducing conditions

The total thickness of the sediments deposited in the Pappadai valley can be estimated from geological evidence to have been of the order of 170m. In the Montemesola basin the maximum height of the Lower Pleistocene sea-bed, as indicated by the highest marine terraces in the immediate area, is 230-240m above sea level (a.s.l.; Fig.3.2), while the top of the Gravina Calcarenites occur at 61m a.s.l. at Pappadai, as shown later. The post-Calabrian calcarenites deposited on the eroded blue clays rarely exceeded 10m in thickness (Ciaranfi et al.1988). It is thus possible to make a reasonably accurate estimate of the geological history of the Pappadai blue clay for comparison with the measured engineering properties. This is discussed later.

3.3. In situ and laboratory investigations at Pappadai

Evidence from the investigation of the Pappadai valley (V.Cotecchia et al.1993) strongly suggests that the area has not been affected significantly by tectonic activity, and it will be presumed that locally the Pappadai clay is both unfaulted and horizontally bedded.

The locations of the various boreholes from which data were obtained are shown in Fig.3.5. Undisturbed samples taken at various depths in these boreholes provide an indication of the variation of the properties within the deposit. The natural water contents, index properties, particle-size distributions and specific gravities were measured in the laboratory according to BS 1377.

Subsequently a continuously-cored deep borehole was drilled (borehole A, Figs.3 5 and 3 6), in which piezometers were installed at depths of 12 m and 27m. This borehole allowed the opportunity for a detailed visual description of the soil and for samples to be taken at closely spaced depths. These samples were used for the determination of particle-size distributions, index properties and specific gravities. In addition, the carbonate contents were measured by gasometric techniques using a calcimeter. These laboratory investigations were carried out in the laboratory of the Politecnico di Bari. Mineralogical analysis was carried out at the Mineralogy Department of the University of Pavia with the supervision of Prof Veniale, by X-ray diffractometry on dry powder at 60°C, and also after both glycolation and heating to 550°C. Thus the carbonate contents have been obtained by two different techniques

In a shaft excavated close to borehole A (Figs.3.5 and 3.6) high quality undisturbed block samples of clay were taken at about 25 metre depth. A palaeontological analysis was carried out on these block samples using both simple and polarising optical microscopes, while the clay fabric was examined using a Cambridge 500 scanning electron microscope, as shown in Section 5.9. Detailed studies of the mechanical properties of these block samples are reported in Chapters 6 and 8.

3.4. Lithological and palaeontological interpretations

All the site investigation boreholes encountered yellow-brown clays which, with depth, gradually merged into grey clay, Fig.3.6. The sequence encountered, based on borehole A, is as follows. The base of the Pappadai clay, and therefore the top of the Gravina Calcarenites, is found at a depth of 50m (61m a.s.l), confirming the geological section of the Montemesola Basin reported by the Italian Geological Survey (Anon 1967, Fig 3 3)

At 49m depth a dark clay shows that the upward passage from the calcarenite to high clay-fraction soils develops in less than a metre. Above 47m depth the more typical grey Pappadai clay appears, and between 47m and 33m depth this is composed of a massive clayey matrix where the deposition bedding cannot easily be recognized, though the sequence is occasionally interrupted by depositional discontinuities These seemingly random discontinuities are presumably the consequence of non-uniform deposition, since they involve coarser material such as calcareous sand or gravel, fossil shells and black silt. There is some evidence of periodic, rhythmic changes in sedimentation since every six metres or so lower clay fractions are recorded The consequence of these rhythmic changes can be seen in the grading curves in Fig.3 7, which fall within one or other of two separate envelopes. The curves comprising each envelope do not relate to a particular depth interval, but appear to be the result of a process of alternating deposition of coarser and finer material. The particle-size distributions shown in Fig 3 7 do not include samples with particularly coarse bedding (greater than 2-3 mm)

Between depths 33m - 25m the grey clay is particularly uniform, massive and very stiff Depositional discontinuities composed of coarser calcareous material are almost absent, but marked laminations can be seen, Fig.3.8(a). The origin of these laminations, probably due to pulses of coarser inorganic sediment or systematic alternation of the conditions of sedimentation (e g. O'Brien and Slatt 1990), cannot be established in detail It is presumed that for these horizontal laminations to occur, a qu et deposition environment must have existed, with l ttle

water circulation. Consequently, the clay in this stratum should exhibit comparatively uniform mechanical properties.

Between 25m and 20m depth the lamination is poorly defined or absent, and coarse bedding with dark, almost black veins occasionally occur. There are oxidation features around those depositional discontinuities that incorporate coarser material. With decreasing depth, depositional discontinuities are more frequent, and the soil becomes far more heterogeneous, Fig.3.8(b).

This increasing lack of uniformity is evidently the result of depositional changes, and is accompanied by increasing oxidation as the ground surface is approached, shown by a gradual colour change of the clay from grey to yellow-brown.

These vertical variations through the depth of the Pappadai clay identify changes in sedimentary conditions from a shallower to a deeper sea, then again reverting to more turbulent conditions of deposition. It appears that the clay between 25 and 33m depth was deposited at the stage of maximum quiet and during a period of particularly uniform deposition. The palaeontological analysis of this clay shows that both foraminifera and nannofossils are abundant and well preserved, while their palaeontological association (Fig 3.9) identifies the age of the clay as Lower Pleistocene (1.2 - 1.3 million years). The lack of benthic fossils suggests an anaerobic depositional environment with little water circulation, confirming the observations of Ciaranfi et al.(1971). The absence of *Hyalinea baltica* and the presence of *Bulimina* and *Anomalina* are consistent with a sea water depth during deposition greater than 100m.

The decrease in sediment uniformity with reducing depth probably coincides with the merging of the Montemesola and the Taranto Basins in the later stages of the Lower Pleistocene transgression (Fig.3.4(b)).

3.5. Physical and Mineralogical Properties

Figure 3.10 and Table 3 1 give the profiles of Atterberg limits, specific gravity G_s, carbonate content (gasometric technique), clay fraction and activity in borehole A It will be seen that the liquid and plastic limits vary in parallel with the clay fraction, and that the activity of the clay gradually decreases down the profile, while carbonate content increases. It appears that there was a general reduction in the quantity of calcareous sediment with time, presumably reflecting the gradually changing nature of the source of the sed ment

There is no indication of significantly different physical properties between the grey clay and the yellow-brown clay, the average liquid and plastic limits (LL, PL) of both being 55% and 30% respectively. In the more clayey strata the liquid and plastic limits are respectively about 63% and 33% (Table 3.1); it will be seen that the Pappadai clay is most uniform at depths between 20 and 33 m.

The average clay fraction of 50% is quite a high value for the blue clays of both the Bradano Trough and the Apulian region (Del Prete and Valentini, 1971; Cotecchia et al 1977), while its variation with depth reflects the changing depositional conditions

The carbonate content measurements in borehole A not only confirm the alternating deposition of coarse and fine material, but also identify the coarser sediment as being calcareous or dolomitic In the more plastic clay the carbonate content lies between 28% and 33% in the lower part of the profile, between 25% and 32% at mid-depth, and between 22% and 27 % in the upper part; there is a general decrease of carbonate content up the profile. Locally, in the coarser layers, the carbonate content increases to values of 40% to 50%. These results suggest that the high values of carbonate content often recorded in the literature for the sub-Apennine blue clays, which can be in the range 30% to 50%, relate to coarse calcareous-dolomitic sediment. This point is emphasised by the relationship of both the clay fraction and the plasticity index to the carbonate content, with the clay fraction and plasticity index reducing with increasing carbonate content, as shown in Figs 3.11 and 3.12. Similar results were reported by Hawkins and McDonald (1992) for the Jurassic Fuller's Earth in Avon, England.

Even in the more clayey strata the carbonate content of the massive stiff clay may still be concentrated in sandy or silty bedding or in fossil fragments. But since the carbonate content may also exist as a cement, either precipitated at deposition or formed authigenically during sedimentary compaction, the nature of the carbonate content can only be satisfactorily established using chemical micro-analysis As might be expected, the variations of specific gravity with depth follow the variations in carbonate content, though the values of specific gravity reflect the dominance of the clay fraction

The data from borehole A can be compared with other profiles within the Pappadai valley, given in Fig 3 13 The valley has been divided into three zones of similar topographic position (Fig 3 5) It is found that the overall average liquid limit is 55% and the average plasticity index is 33% Again, the data show greater consistency at 8 t 93m a s l ere the m t un f rm c ay

stratum has previously been identified. Above and below this depth the data are consistently more scattered, indicating a less uniform deposition environment. Most of the clay samples may be classified as clays of high plasticity, though there are lower clay-fraction medium plasticity clays, while two samples from borehole A are best regarded as compressible silt.

The clay-fraction plot always shows values of around 50%, with a small scatter. There is no significant gradient of clay fraction with depth, except perhaps a slight reduction with depth in area 1. Between 80 and 93m a.s.l. the data lie in a narrower band of reduced scatter, again consistent with the apparently quieter deposition environment at this depth. The alternating deposition of coarser and finer sediment identified in borehole A can be recognized in the global clay-fraction plot of Fig.3.13. It may be concluded that the particle-size distribution profiles across the valley confirm the pattern observed in borehole A An overall decrease in activity with depth may also be recognized.

3.6. Mineralogy of the Pappadai clay

The mineralogical composition of clay samples from borehole A, determined by X-ray diffractometry, are shown in Fig.3.14. If the calcite and dolomite contents given are summed they are in good agreement with the values of carbonate content measured by gasometric technique shown in Fig 3.10.

It can be seen from Fig 3.14 that the dominant clay minerals are illite and kaolinite, with subordinate chlorite and smectite. The amount of smectite is quite large at shallow depths (Ciaranfi et al.1971; De Marco et al 1981, Dell'Anna and Laviano 1991), but it reduces below 10m depth (100 m a.s.l.), while the proportion of mixed-layer minerals, together with chlorite and illite, increases with depth Reduction with depth of the proportion of swelling minerals is generally recognized as the effect of geological compaction (e.g. O'Brien and Slatt 1990), a major physical diagenetic process responsible for the final structure of many argillaceous rocks. In the present case it must be remembered that overlying sediments, now removed, will have been in part responsible for these changes, which are reflected in the reduction of activity with depth

3.7. Microstructural features arising from the geological history of the clay

In this section the microstructural features which were likely to develop in Pappadai clay during its geological history are proposed based upon the deposition conditions and subsequent compression history of the clay outlined in the previous sections. The analysis concerns the clay present between 80 and 86m a s l. the depths where the clay samples tested in the laboratory were taken, as reported in the following Chapters 5, 6 and 8. The existence in the clay of the microstructural features here suggested was assessed in the direct investigation of the clay microstructure developed by means of the SEM, as reported in Section 5.9.

As discussed in Sections 3.2 and 3.4. the stillness of the depositional environment and the lamination of the clay both suggest that the particle arrangement created at deposition was not altered by immediate post-depositional mixing The high percentages of illite, chlorite and smectite, and the high electrolyte content of the suspension, make it likely that the sediment settled out as aggregates or flocules O'Brien and Slatt 1990), giving rise to a bookhouse fabric, although in some areas other physico-chemical factors could promote local dispersion of the smaller size particles (Sides and Barden 1970)

Reorientation of the bookhouse fabric may have occurred during the compression of the clay during burial so that the present fabric of the clay is expected to be a compacted bookhouse fabric. Particle reorientation during fabric compaction is generally not a uniform process, as shown by Sfondrini (1977) (see Section 1 9). therefore areas of open flocculated sedimentation fabric may be expected to exist in the clay

The progressive reduction with increasing depth of the content of swelling minerals, and the corresponding increase of intergrades see Section 1 2), which both the mineralogical analyses and the activity profile have shown to occur at Pappadai (Sections 3 5 and 3 6), suggest that some aggradation of the clay minerals has occurred in the clay, and that therefore the Pappadai clay has undergone diagenesis Aggradation of the clay minerals generally takes place at high pressures. It could therefore occur in the Pappadai clay both in the final stages of virgin compression and in the longer term long-term diagenesis, see Section 1 10) During diagenesis transient changes of pressure and temperature in the clay may have caused changes of fabric (Sfo drini 1977) and the crea n f further bonding in add tion to the observed mineralogical changes

In conclusion, based upon the data presented so far it is suggested that the clay at 80-86 m a.s.l., i.e. the clay forming the block samples tested in the laboratory, had a bookhouse fabric at deposition, which was compacted during virgin compression and underwent diagenesis when at high pressures. Due to the diagenetic processes, the clay may have acquired sensitivity at high pressures and may be therefore expected to have a higher strength than the reconstituted clay. The carbonates present in the clay may form bonding between the clay particles. Both the analysis with the SEM and the chemical micro-analysis of the clay structure reported in Chapter 5 will show whether the hypotheses presented in this section are correct and whether carbonates are cementing agents between the particles of the Pappadai clay.

3 8. Pappadai: post-deposition history

In the present section a reconstruction of the stress history of the clay is proposed, which is then checked by comparing the results of the modelling of the stress history, carried out in terms of LI-σ'_v paths, with the observed profiles of liquidity index (Fig.3.13). Fig 3 15(b) reports the geometric and piezometric conditions characterizing the in situ Pappadai clay stratum at present. Point X in the figure is within the clay stratum (80-86 m a s.l) for which both the microstructure and the mechanics were studied in the research. Therefore the state of the clay at point X will be often referred to in the following in relation to the different stages of the clay history.

3 8 1 Pappadai: the first two stages of the clay history

At the location of borehole A the present ground level is 111m a s l , and the Pappadai clay crops out at the surface (Figs.3.5 and 3.15). The highest surface level of the clay in the neighbourhood of Pappadai is a marine terrace 14km north-east with its surface at 230m a s l. (Figs.3.2 and 3.15(a)). If the sediment surface at the time of deposition was horizontal, and if there have been no subsequent relative changes in level between the two locations, then it follows that about 170 metres of sub-Apennine blue clays were deposited at Pappadai in the Lower Pleistocene. The virgin compression of these clays is here defined as stage 1 of the geological history During the Middle-Upper Pleistocene, alternating transgressions and regressions caused erosion, and about 120 metres of clays were removed (Fig 3 15) The unloading due to erosion is defined as stage 2 of the Pappadai clay history

In reality this unloading was interrupted by minor reloading cycles associated with the deposition and erosion of Quaternary calcarenites, whose maximum thickness was about 10 metres (Ricchetti 1967). These loading cycles are presumed to have caused only temporary and reversible changes of voids ratio, so they are unimportant in the evolution of the present state of the clay.

At point X, Figs.3.6 and 3.15, at 84 m a.s.l. in borehole A, the present in situ vertical effective stress is known as a Casagrande piezometer (see Section 3.3) there indicates a pore water pressure of 84kPa. Assuming an average bulk unit weight of 19kN/m$^{3(*)}$, the present σ'_v at X is about 430 kPa. At the end of stage 1 the value of σ'_v at X was about 1320kPa, Fig 3 15(b). As will be seen, this is the maximum value of σ'_v occurred at this point in the geological history, i e the σ'_p at X. Given this σ'_p the OCR at X is equal to 3 1, and this also applies to the clay tested in the laboratory, which was taken from an equivalent depth to point X

3.8.2 Pappadai: desiccation and shallow mechanical weathering

In Fig.3 16(a) the liquidity indexes (LI) logged at Pappadai are plotted against depth. In Fig.3.16(b) line 1 is an ideal stratum of normally consolidated clay and line 2 the profile of the same stratum after swelling due to erosion of ΔH. This is very different from that observed at Pappadai, where an "S" shaped LI profile can be recognized.

Thus it appears that the events were in fact more complicated, and it is necessary to postulate the occurrence of further geological events at Pappadai The decrease of LI with decreasing depth, Fig.3.16(a), can be explained by an increase of suction accompanying the draw-down of the water table. Desiccation will result in suctions greater at shallower depths, resulting in greater compressions near ground surface. Such a desiccation cycle probably occurred at Pappadai, assumed to be stage 3 of the Pappadai clay history

At the shallowest depths LI increases again (Fig 3 16(a)) Thus a further geological event caused a significant further increase of water content at shallow depth Chandler (1972), and Chandler and Apted (1988) showed that weathering can cause increase of volume with no effect on the

(*)This value has been chosen as an average accounting for the measurements on the undisturbed samples of index properties reported in Fig 3 13 The likely error of ±2% is acceptable since the calculations of the present stress state has to be compared with the modelling of the geological t p hs f r the cl y s h aff ted by mu h great r un rta nti .

plasticity index of the clay. Mechanical weathering may thus be the cause of the high voids ratios of the shallow Pappadai clays, which have similar index properties to the grey clays, but are yellowish.

The ground levels of the boreholes whose data are shown in Fig.3 16(a) vary as shown in Table 3.2. Borehole A has ground level at 111m a.s.l., within Area 2. However, most boreholes have ground levels below 105m a.s.l., so much of the data in the figure apply to erosion greater than that at borehole A. Moreover, for the boreholes at lower elevations desiccation affected the strata at levels lower than in borehole A. For these reasons the S-shaped line through most of the data in Fig.3.16(a), the dashed line, differs from that which refers to the zone surrounding borehole A alone, the solid line in the figure. S-shaped LI profiles are recognized also in London Clay and in the sub-Apennine blue clays of the Taranto Basin, as shown in Figs.3.16(c) and (d).

In borehole A mechanical weathering is evident mainly above 7-8m depth. Fig.3.8(b) shows weathered clay in which zones of coarser grading probably result from the infilling of cracks opened during desiccation and weathering. Below 7-8m depth in borehole A the clay is chemically but not mechanically weathered. Oxidation is concentrated in the zones where coarser soils are located; but these coarser soils seem to be of depositional origin. Opening of fractures around those areas where coarser soil is present probably occurred during desiccation, giving rise to preferential seepage paths, allowing oxidation to develop. It follows that the deep weathering of the Pappadai clays, observed to depth of 20 metres, was a chemical weathering resulting from the presence of coarser material of depositional origin, while at shallow depth also a mechanical weathering occurred. The rising of the water table after desiccation and the occurrence of mechanical weathering at shallow depths has been therefore considered as a fourth stage of the geological history at Pappadai.

3.8.3 Modelling the history of the clay

Both the geometric and piezometric conditions in situ at the end of the four stages of the clay history are represented in Fig 3 17. The changes of LI resulting from each of the four stages of the clay history were modelled, and the final LI values compared with those measured in situ

In developing the model it was assumed that the clay remained saturated, that the loading was purely one-dimensional, and that the soil had uniform properties (LL = 60%, PL = 28%, bulk

unit weight γ = 18 8kN/m^3, G_s = 2.746). The values chosen are consistent with the index data for the more clayey strata at Pappadai.

The compression of the normally consolidated clay was modelled, assuming the LI of the clay at a depth of one metre to be 1.1 , as suggested by Skempton (1970) At one metre depth $\sigma'_v \approx$ 9kPa, with a void ratio of 1.738

The compression index during stage 1 was assumed to be constant up to σ'_v of 1000kPa, and then to gradually reduce following the curvature of the sedimentation compression curve SCC. The values assumed for the compression index C_c are shown in Table 3.3 These values were chosen from the intrinsic compression index C^*_c calculated from the relationships .

$C_c^* = G_s\, PI/2 = 0.44$ (Schofield and Wroth 1968) (3 1)

$C_c^* = 0.256\, e_{LL} - 0\ 04 = 0.382$ (Burland 1990) (3 2)

The values of C_c were then slightly adjusted to follow the general trend of the SCCs of Skempton (1970) (Fig. 2.21) as shown in Fig 3.18, assuming the clay to have a low-medium sensitivity S_t during stage 1 according to the sensitivity framework in Fig 2 23 The values of C_c used also assume that during virgin compression cementing did not develop in the clay. Line 1 in Fig 3.19 shows the pore pressures at the end of stage 1 for borehole A; in Fig 3 20 line 1 shows the calculated LIs. The in situ pore water pressures at any stage of the clay history and at present will be indicated as u_0 in the following.

The increase of voids ratios during stage 2 was calculated using the different preconsolidation states reached by the clay at different depths at the end of stage 1. A swelling index C_s equal to 1/10 of the corresponding compression index was used, assuming that the clay had been neither cemented nor strongly bonded during virgin compression. A strongly bonded sedimentation structure would have resulted in C_s values lower than those used, whereas the influence of swelling minerals on the clay behaviour would cause higher values of C_s Line 2 in Fig 3 19 represents the pore pressures at the end of stage 2 and line 2 in Fig 3 20 shows the calculated LIs

To model desiccation during stage 3, the ground water table was lowered to a depth of 50m, giving a suction about 3 00kPa at ground level The enhanced negative pore pressures developed

due to surface evaporation were assumed to vary parabolically with depth, according to the equation:

$$u_0 = 1.22\ Z^2 + \beta Z + \gamma \qquad (3.3)$$

where the depth Z is indicated in Fig.3.17. The use of these high values of suction was found necessary to match the measured water content profile which suggests that at depth some irreversible specific volume change had occurred at this stage The high suctions imply that the water table was lowered as a consequence of evaporation from an unvegetated surface, since desiccation solely caused by vegetation yields maximum suctions of about 1500kPa. Line 3 in Fig.3.19 represents the suction profile.

A gradually increasing recompression index C_r was used in the calculations. C_r was taken as initially equal to C_s, and then increasing to 2.5-3 times C_s when the vertical effective stress was about 2/3 of the preconsolidation pressure. Beyond σ'_p the recompression curve was assumed to lie on the original sedimentation compression curve SCC. At depths above 22-23 metres in borehole A the recompression of stage 3 caused an increase of σ'_p. The values of LI at the end of stage 3 are plotted as line 3 in Fig.3.20.

At the end of stage 4 the water table is assumed to have risen to 20m depth, as shown in Fig.3.17 The unloading paths due to the rise of the water table started from the final voids ratios of stage 3 and followed swelling indices equal or higher than the initial value of C_s The swelling indices were set to increase with decreasing depth from 20m depth upwards, in order to take into account the weakening of the clay bonding which had arisen from the compression beyond yield and weathering, which will be of greater importance at shallow depths because of the mechanical weathering. The resulting values of LI are shown as line 4 in Fig 3.20. Line 4 follows an S-shape, showing an encouraging qualitative agreement with Fig 3.16(a), and it appears that the occurrence of both a desiccation cycle and near-surface weathering explains the complex LI profile observed in Fig.3 16(a).

This model does not take into account the influence of either diagenesis or any other structural phenomena that may have affected the clay state history Nonetheless from the comparison of the results in Fig 3 20 and the data in Fig 3 16(a) it is reasonable to conclude that the present LI profile at Pappadai is consistent with a single cycle of erosion, ground water lowering and weathering, followed by a rise in ground water to the present level

Comparison of the LI values in Figs.3.16(a) and 3.20 shows that for the clay located below 23 m depth in borehole A the recompression during stage 3 did not cause an increase of σ'_p and OCR, as anticipated in Section 3.8.1 with reference to the OCR of the clay at point X (Fig.3.15).

Below 23m depth the calculated LI data are close to the measured ones, showing that the SCC assumed for Pappadai clay (Fig 3 18) is generally correct, and that the depths of deposition and erosion deduced from the geological evidence are realistic. The assumption that the Pappadai clay was not cemented at deposition and during virgin compression is thus presumably correct It follows that the present high strength of the Pappadai clay cannot be attributed to a cemented sedimentation structure, as for clays type 5 in Table 2.1.

It is concluded that the clay at present is overconsolidated by geological events and therefore has a post-sedimentation structure. The clay is stiff and falls in one of the two categories 4 or 7 in Table 2.1, depending on whether processes of group 2, such as long-term diagenesis, caused the clay's YSR to increase with respect to the OCR or not, and the clay to exhibit a post-sedimentation sensitivity or a sedimentation sensitivity when recompressed to YSR of 1 (S_t(YSR=1)). The study presented in Sections 4.7 and 4 8, in Chapter 5 and Chapter 6 will demonstrate which of the two clay types, 4 or 7 in Table 2 1, is representative of the Pappadai clay, and whether long-term diagenesis has occurred in the clay.

3.9. Conclusions

The Pappadai clay has been shown to be a marine clay of Lower Pleistocene age (about 1 3 million years old). The engineering index properties of the clay have been examined through much of a sedimentary cycle within the depositional basin The cycle commenced at the beginning of the marine transgression with the deposition of a calcarenite over a Cretaceous basement, sedimentation rapidly changing to clay (the Pappadai clay), deposited under strongly reducing conditions. A period of maximum quiet in sedimentation terms occurred about mid-depth of the sequence, giving rise to the formation of a massive, uniform, stiff clay

More disturbed sedimentation succeeded, and rather less uniform clays occur at shallower depths This cycle of deposition is documented by detailed depth profiles of the engineering index properties, together with the measurement of carbonate content and a systematic examination of the clay mineralogy through the deposit

The deposition was truncated by a regression which resulted in the erosion of about 120 m of sediment, so that the deposit has been overconsolidated by a known geological loading. Subsequently there was at least one period of groundwater lowering which has resulted in the clay being oxidised to a depth of about 20 m, rather greater on the interfluves and somewhat less in the valley floor. Piezometric levels now stand above the depth of oxidization, so that present day ground water levels are presumed to be higher than in the past.

This geological cycle of sedimentation, erosion, oxidation following ground water lowering and subsequent rise in ground water level has been modelled, and results in a predicted water content - depth profile that is qualitatively very similar to that at Pappadai.

Sample DEPTH m	Sample POSITION m a s.l.	CF %	LL %	PI %	SPECIFIC GRAVITY	ACTIVITY	CARBONATE CONTENT %
1.6	110.4	40	51.1	28.7	2.70	0.72	22 4
4	108	50	55 0	31 5	2.74	0 63	27 2
5.4	106.6	51	57.3	32.7	2.74	0 64	27.7
8.5	103.5	60	67.3	37.0	2.74	0.62	25 1
10.5	101.5	55	61 3	33.9	2.74	0 62	27.1
13.9	98.1	37	40.9	19.3	2.75	0.52	38.1
16	96	46	49 6	27.5	2.74	0.60	35.6
18.3	93.7	41	45.3	24.2	2.74	0 59	32 9
20.8	91 2	51	55.3	30.7	2.74	0 60	31.6
21.5	90.5	60	60.3	33.7	2.74	0 56	29.8
22.2	89 8	52	60.4	33.8	2.75	0.65	25 6
25.8	86 2	58	65.6	35.7	2.73	0 62	26.3
31	80.9	57	56 4	29.9	2.74	0.52	31.5
33.7	78.3	37	45.1	19.9	2.75	0.54	47 6
34.2	77.8	58	63.4	33.4	2.72	0 58	28 4
36.5	75 5	50	57.0	32.4	2.75	0 65	32 5
38.8	73.2	38	44.1	21.6	2.74	0.57	48.2
39.8	72 2	50	59 1	31.1	2.74	0.62	33 0
41.3	70.7	57	61.0	28 0	2 71	0 49	30 6
44.4	67.6	40	45 4	22.9	2.73	0 57	32.8
46.4	65.6	54	52.0	25 6	2 72	0 47	34 0
47.6	64.4	47	62.8	32.0	2.71	0.68	28 5
48.6	63 4	55	61 9	29.9	2.71	0 54	30 0
50.7	61 3	29	30 5	12.3	2 75	0 42	68 8
50.7	61 3	22	32.9	11.2	2.75	0 51	71 1

Table 3 1. Summary of the index properties of the Pappadai clay, Borehole A.

Area1			Area2			Area3		
Borehole	Depth (m)	Ground lev. (m a s.l.)	Boreho e	Depth (m)	Ground lev. (m a.s.l.)	Boreho e	Depth (m)	Ground lev. (m a.s l.)
S3	25	88.1	S1	15	95.47	S3E	20	107.9
S4	30	96.2	S2	28	95.1	S15E	20	100.7
S5	30	99.6	S14E	20	90 7	SS1	20	106 0
			SF2	35	114.0	SS2	20	96 0
			SF3	35	116.0	SS3	10	99.0
			SF4	30	110.0	SS4	10	90.0
			SF5	20	96.0	SS5	10	86.0
			CR1	10	91.0			

Table 3.2. Ground levels at the borehole locations in the Pappadai valley.

Cc	σ v kPa
0 42	10-1100
0 38	1100-1500
0 36	1500-1950
0 33	1950-2500

Table 3 3 Values of C_c used in the mode ling

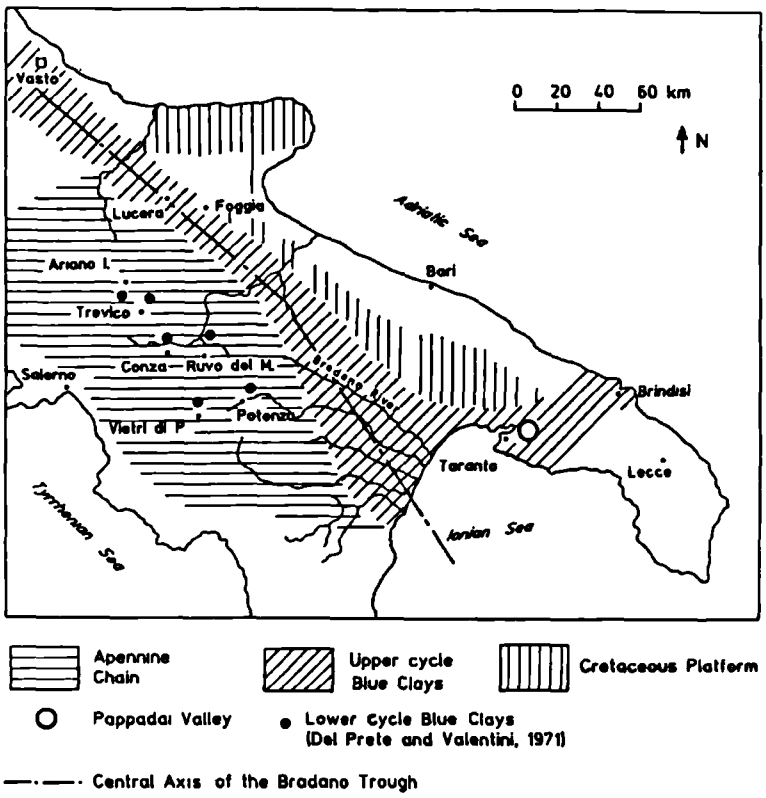

Fig.3.1 Simplified geology of southern Italy.

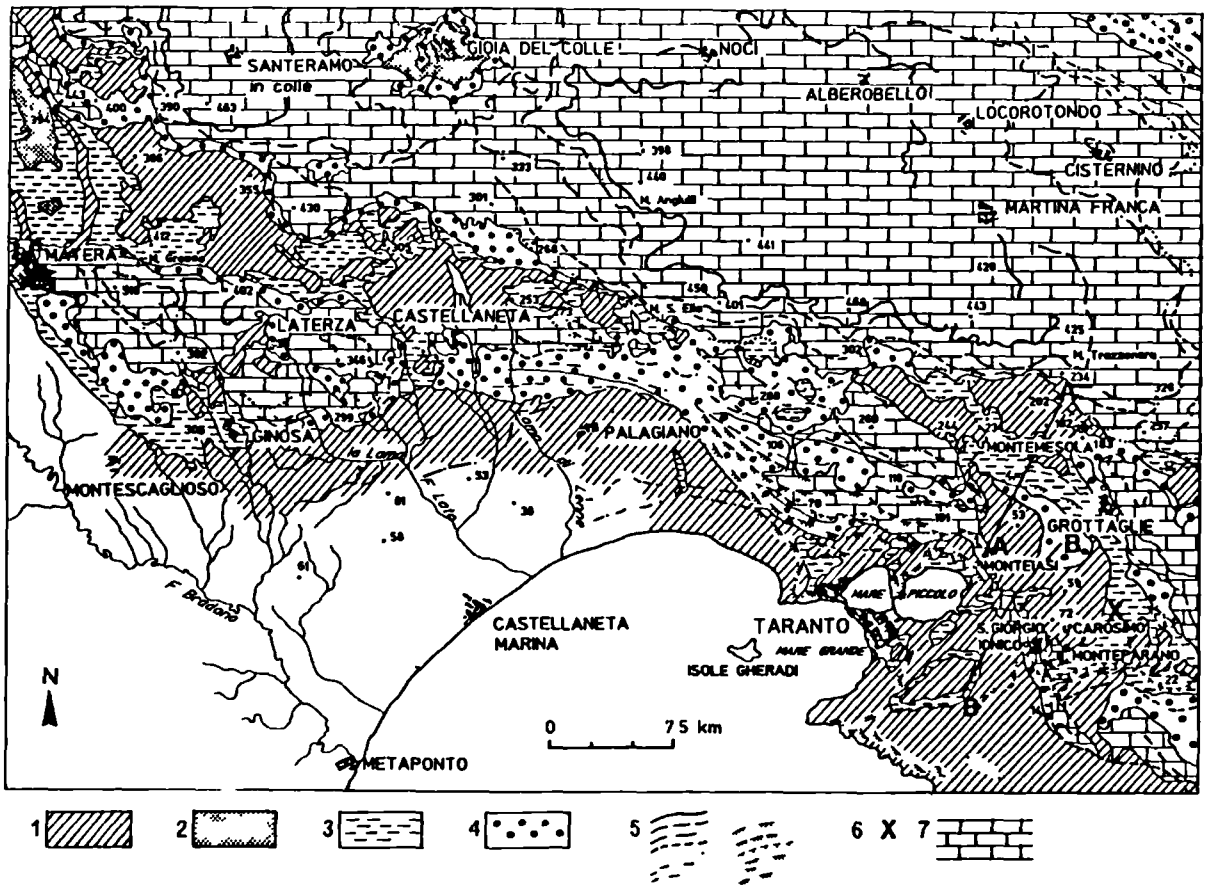

Fig.3.2 Geology of the study area, showing the Bradano Trough and Pleistocene marine terraces (from Ciaranfi *et al.* 1988). Key: 1, Middle-Upper Pleistocene calcarenites; 2, Monte Marano Sands; 3, upper-cycle blue clays; 4, Gravina calcarenites; 5, paleo coastline; 6, location of Pappadai; 7, Cretaceous limestone.

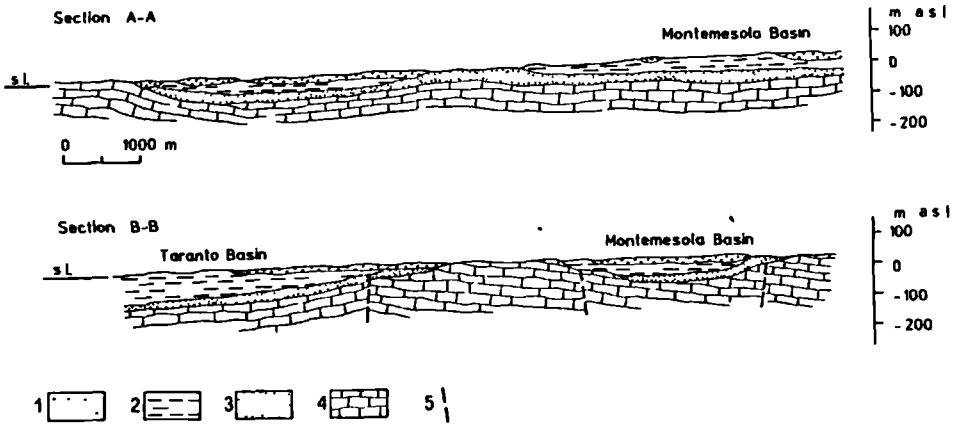

Fig.3.3 Sections showing the position of the upper-cycle blue clays; the locations of the sections are shown in Fig.3.2.Key: 1, Pleistocene calcarenites; 2, upper-cycle blue clays; 3, Gravina Calcarenites; 4, Cretaceous Basement; 5, faults. (From Italian Geological Survey, Anon. 1967.)

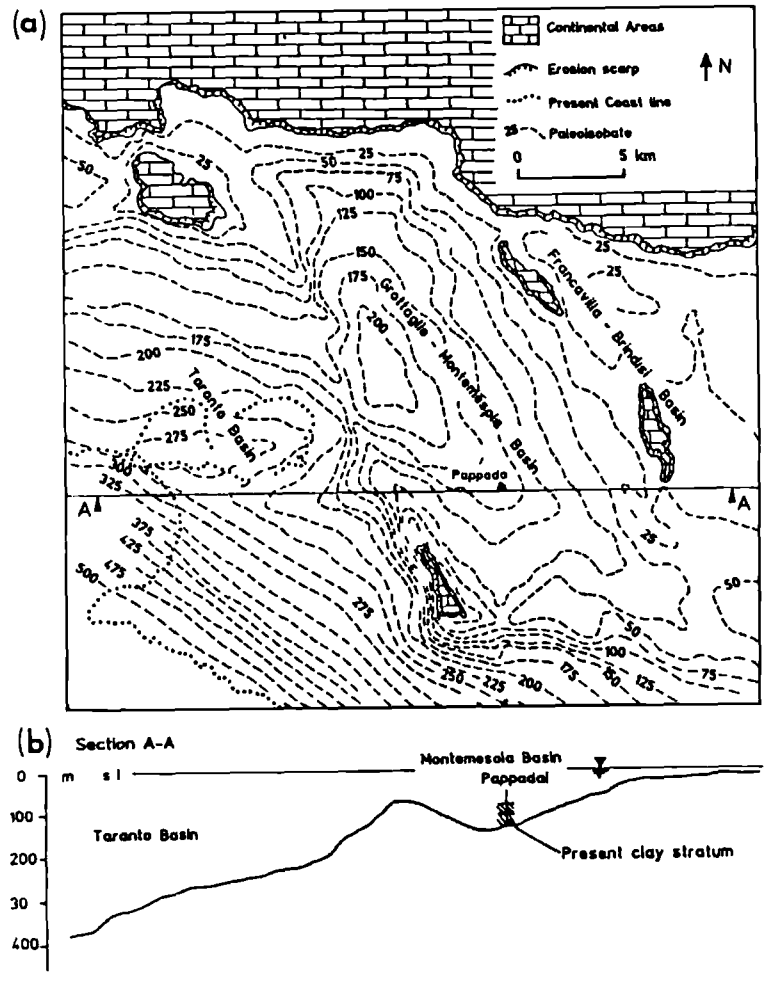

Fig.3.4 (a) Reconstruction of the Montemesola Basin at the commencement of deposition of the upper-cycle blue clays (from Ciaranfi *et al.* 1971); (b) Section A-A showing location of Pappadai.

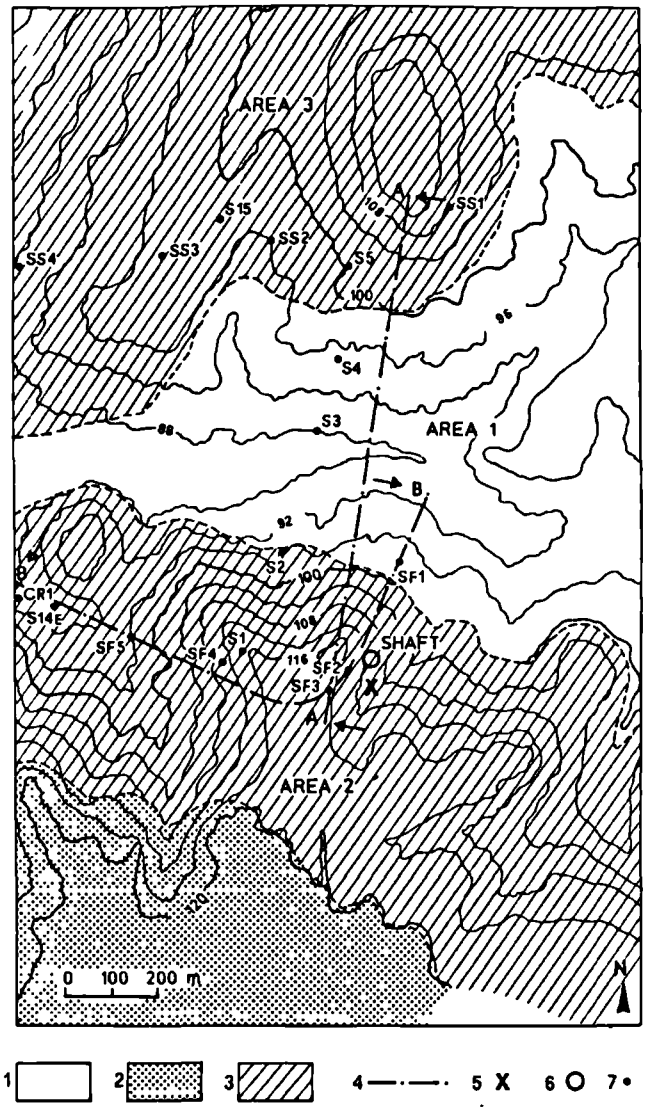

Fig.3.5 Location of boreholes. Key: 1, alluvium; 2, Quaternary calcarenites; 3, Pappadai clay; 4, lines of section; 5, Borehole A; 6, shaft; 7, individual boreholes.

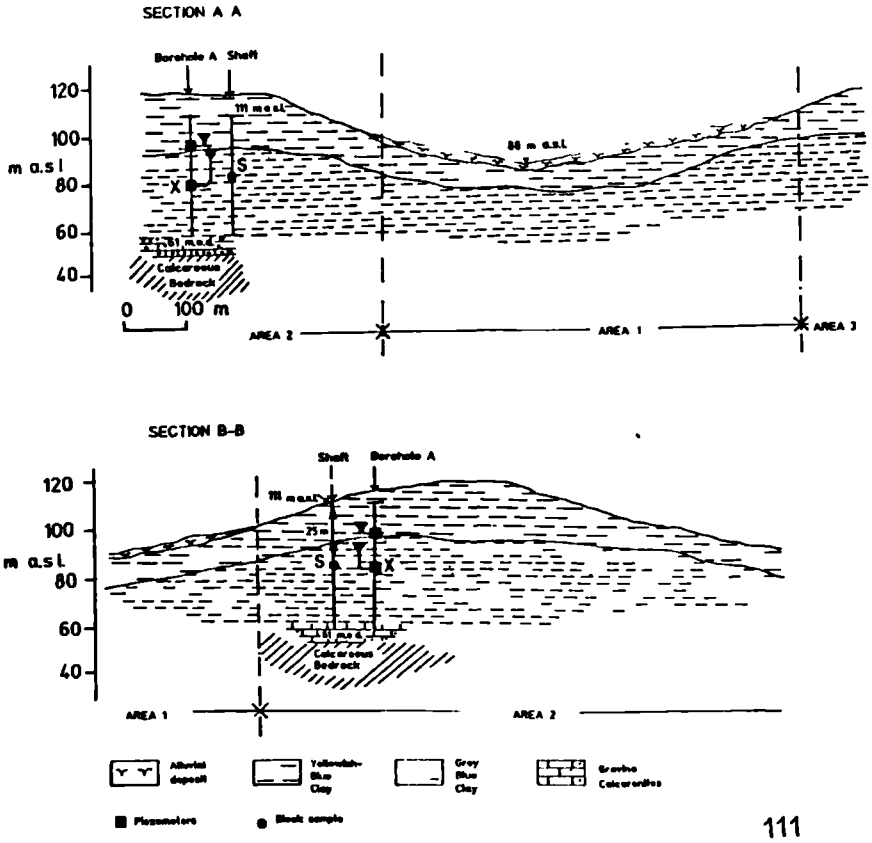

Fig.3.6 Sections A-A and B-B, Fig. 3.5

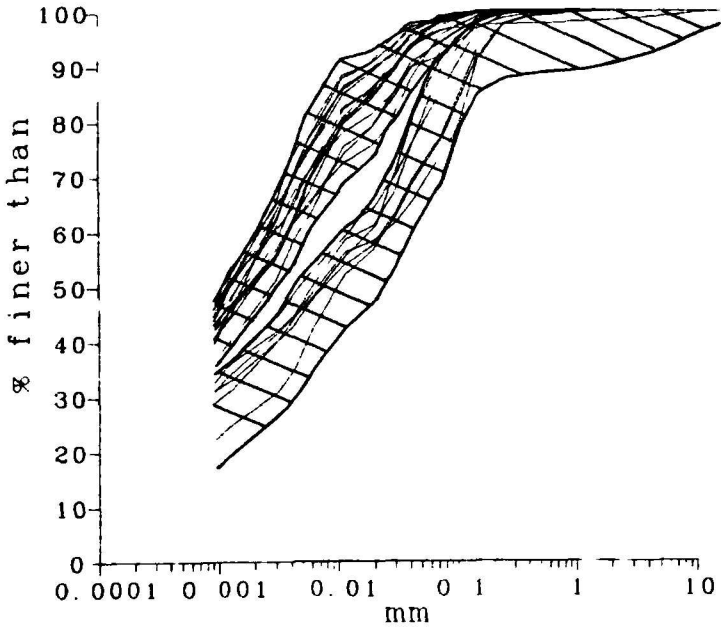

Fig.3.7 Grading curves for Pappadai Clay.

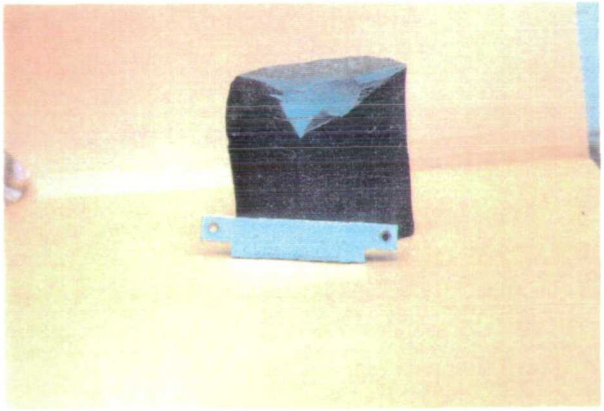

a)

b)

Fig.3.8 (a) Laminations between 25-32m depth; (b) coarse bedding, 6-8m depth.

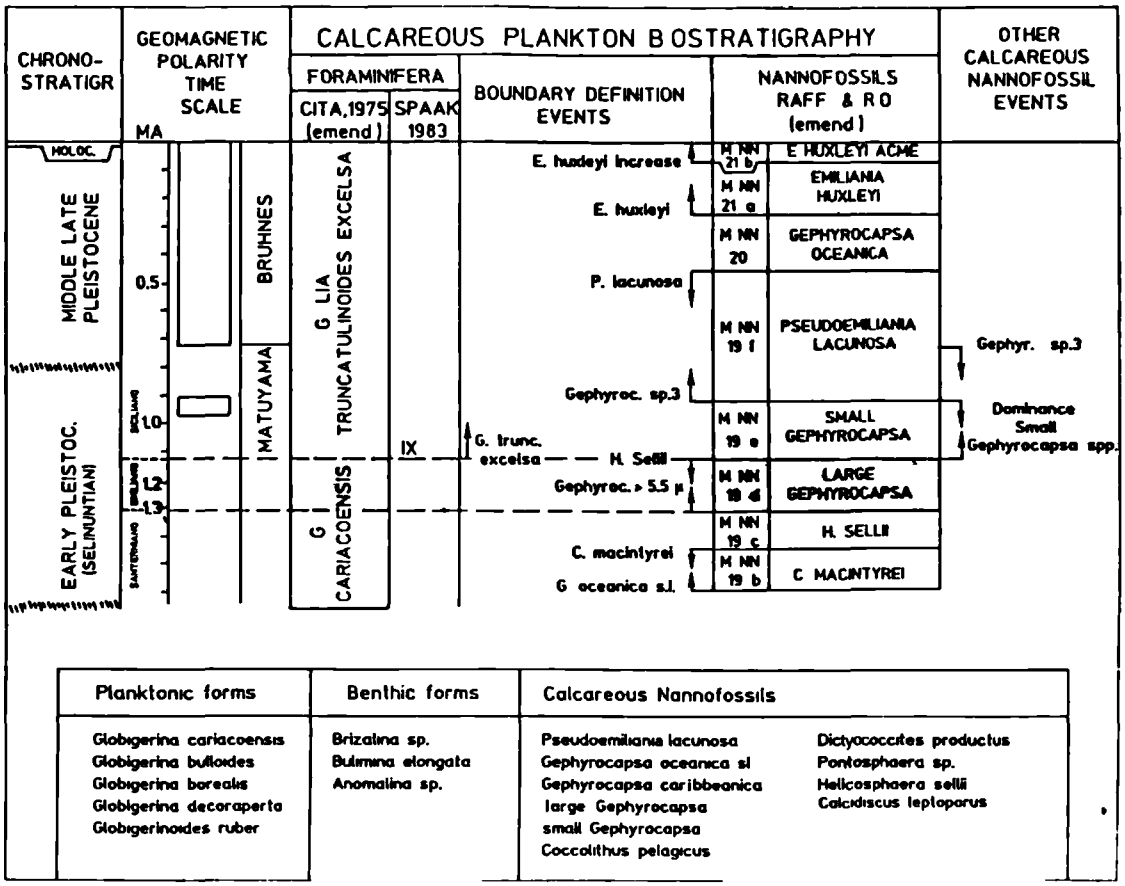

Fig.3.9 Pappadai Clay: palaeontological associations.

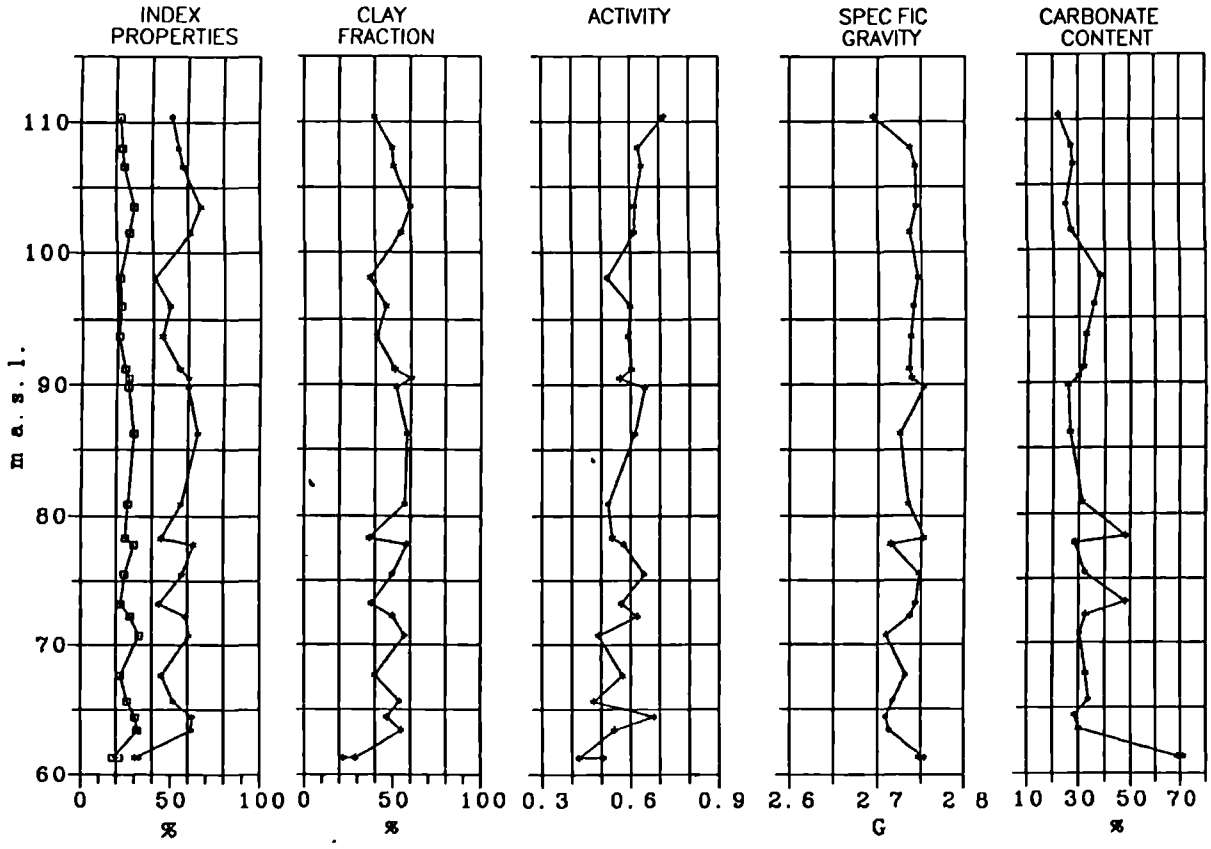

Fig.3.10 Geotechnical profiles, borehole A.

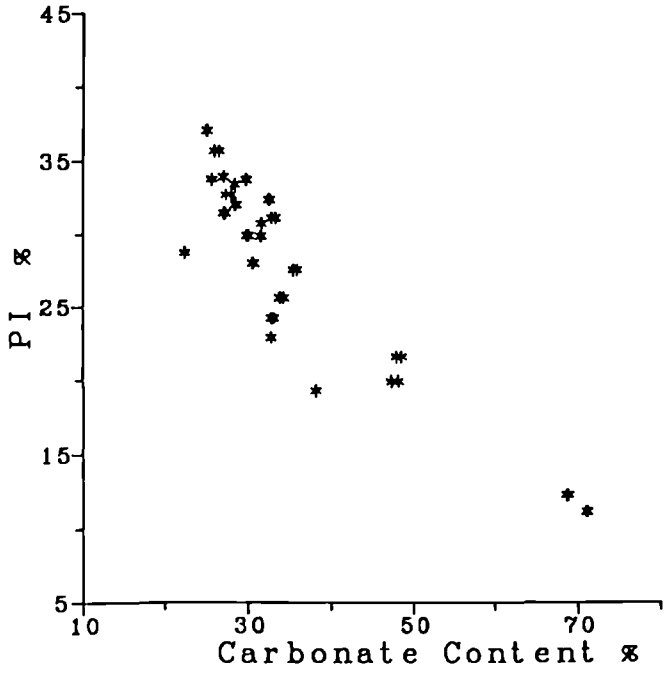

Fig.3.11 Plasticity index versus carbonate content, Pappadai Clay.

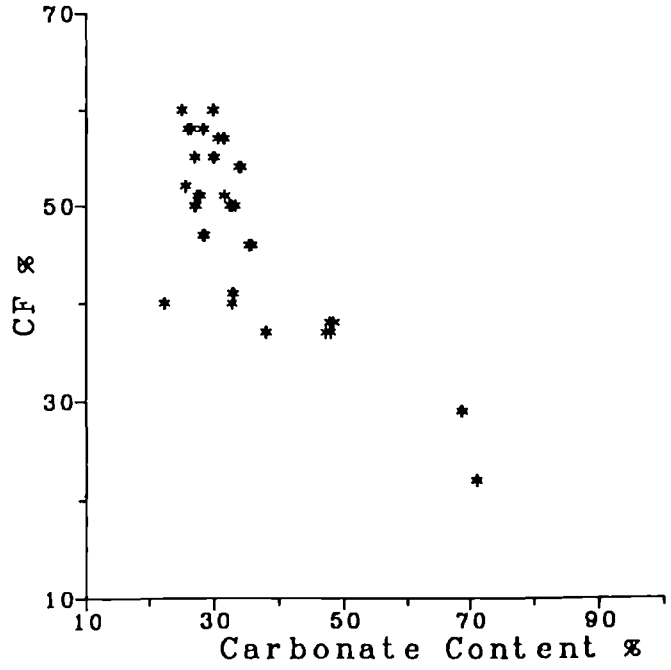

Fig.3.12 Clay-size fraction versus carbonate content, Pappadai Clay.

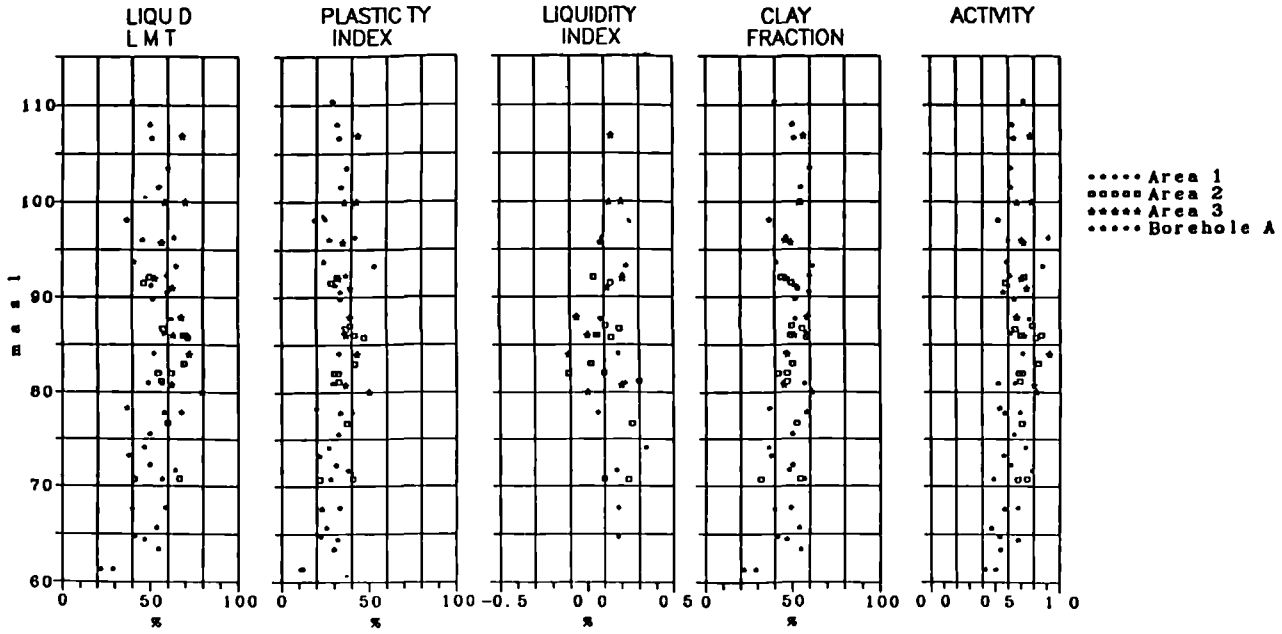

Fig.3.13 Combined geotechnical data, other boreholes.

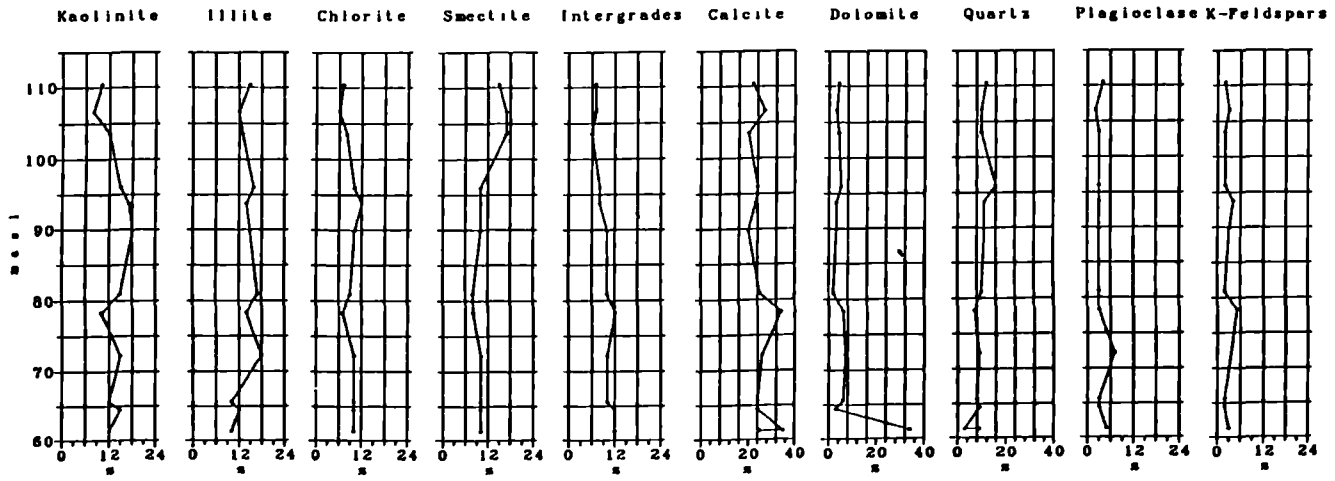

Fig.3.14 Mineralogy of Pappadai Clay; data from borehole A.

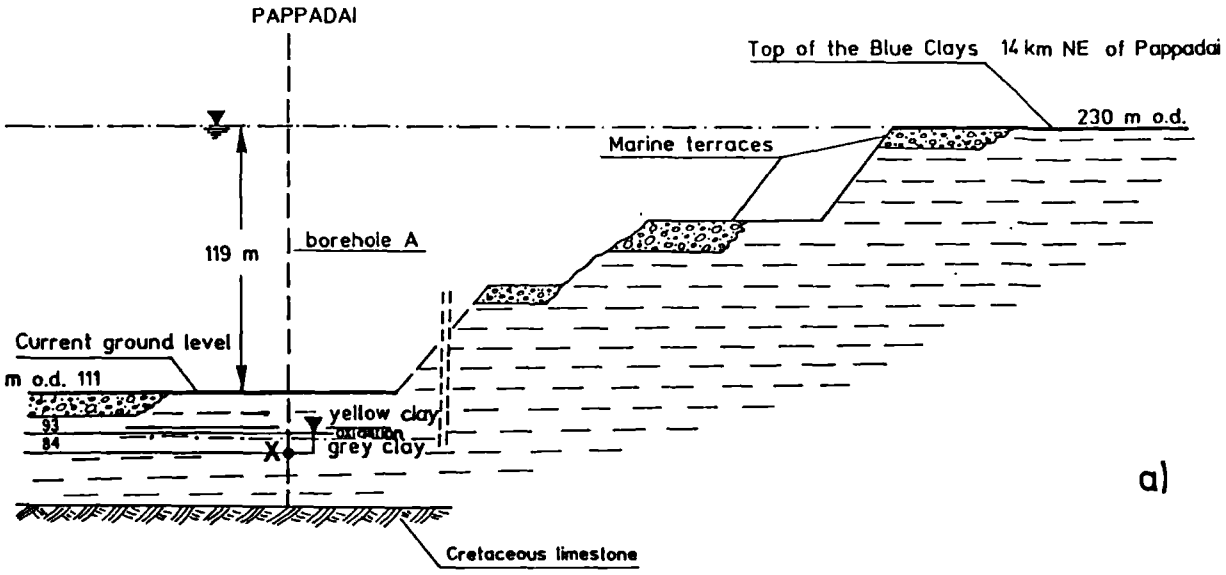

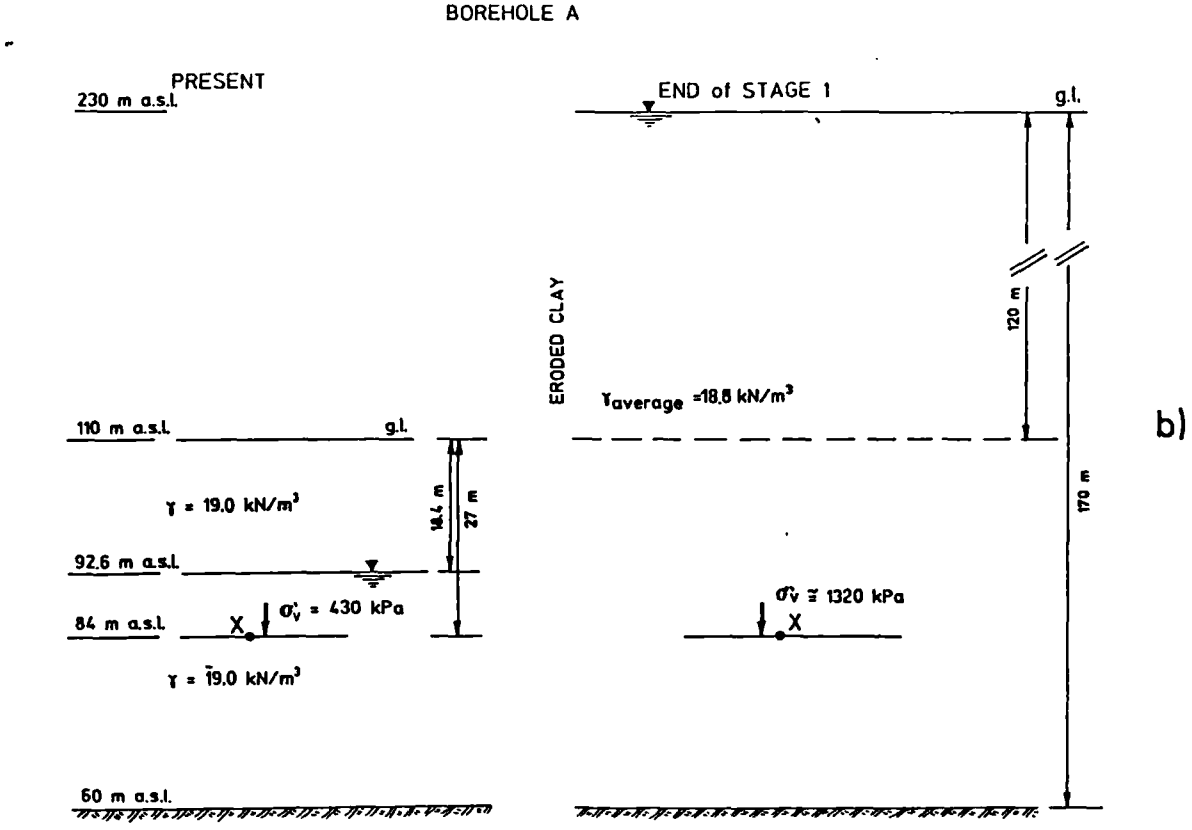

Fig.3.15 (a) Sketch showing geological section of the Montemesola Basin; (b) Pappadai : in situ conditions at the end of stage 1 and at present.

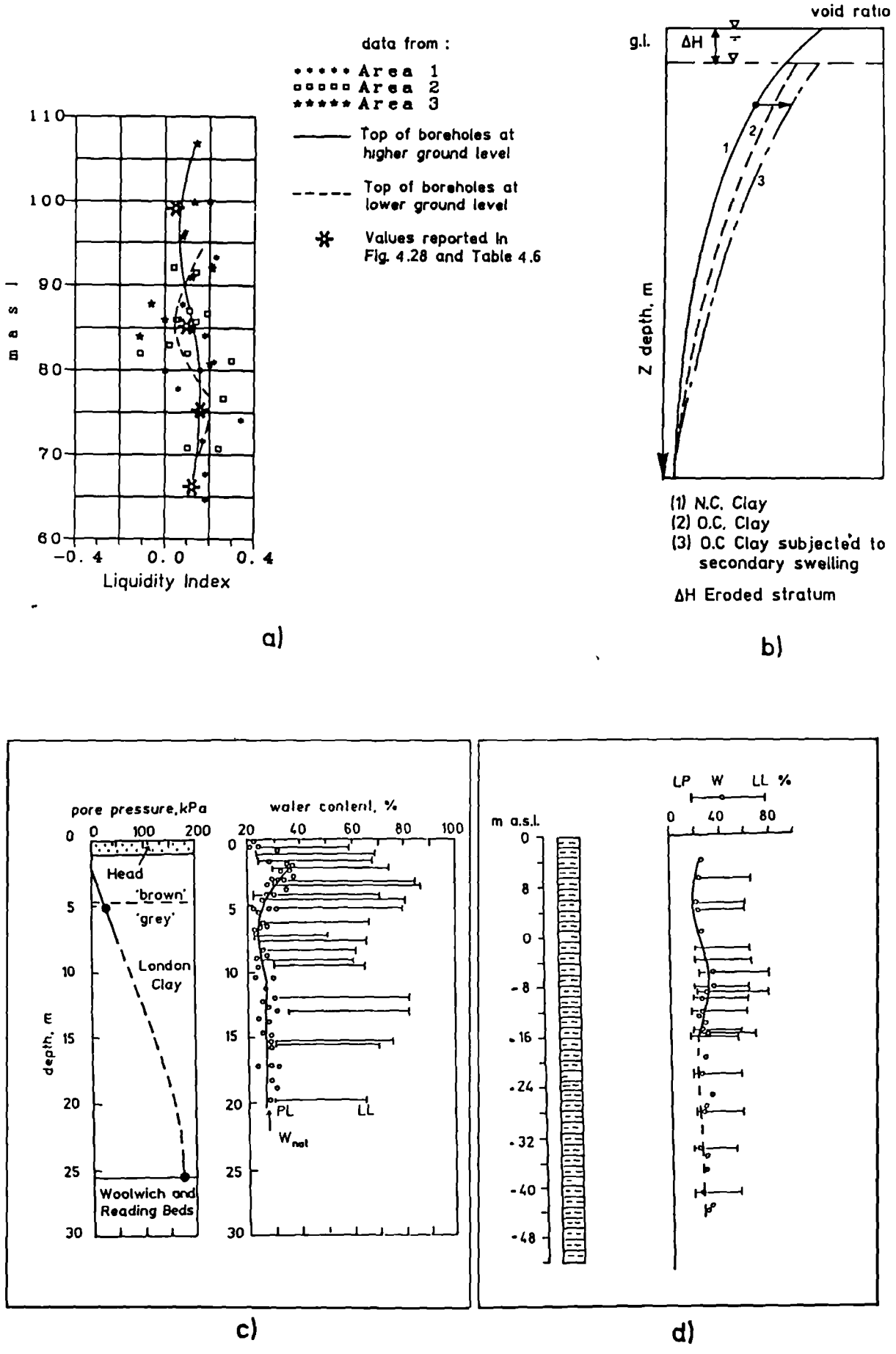

Fig.3.16 (a) Values of LI logged for the Pappadai clays; (b) values of voids ratio in an ideal clay deposit after normal consolidation and erosion; (c) London clay: water content profile (after Chandler and Apted 1987); (d) Taranto clay: water content profile (after V.Cotecchia et al.1977).

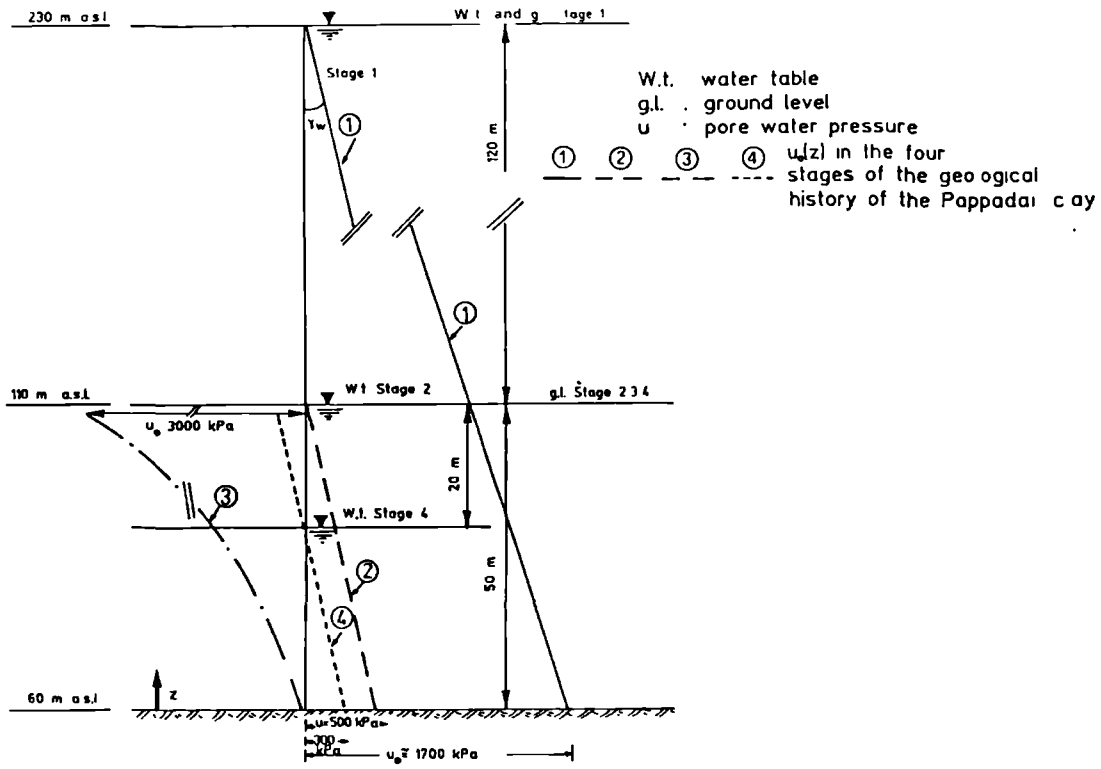

Fig.3.17 The four stages of the geological history at Pappadai - borehole A.

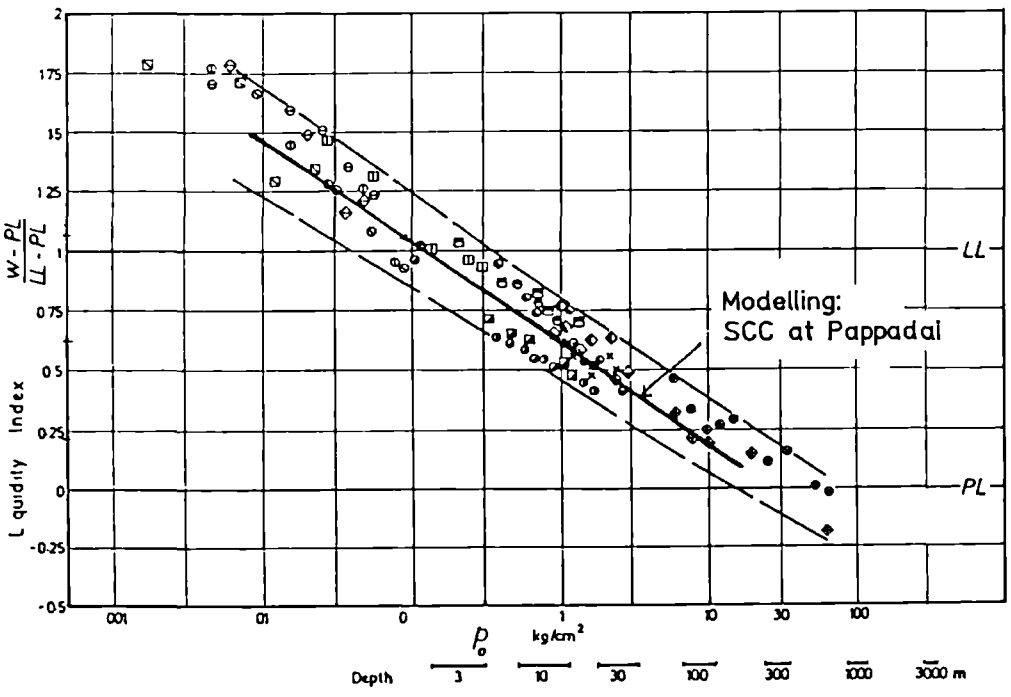

Fig 3.18 Relation between liquidity index and effective overburden pressure of natural clays, after Skempton (1970), and SCC of Pappadai clay.

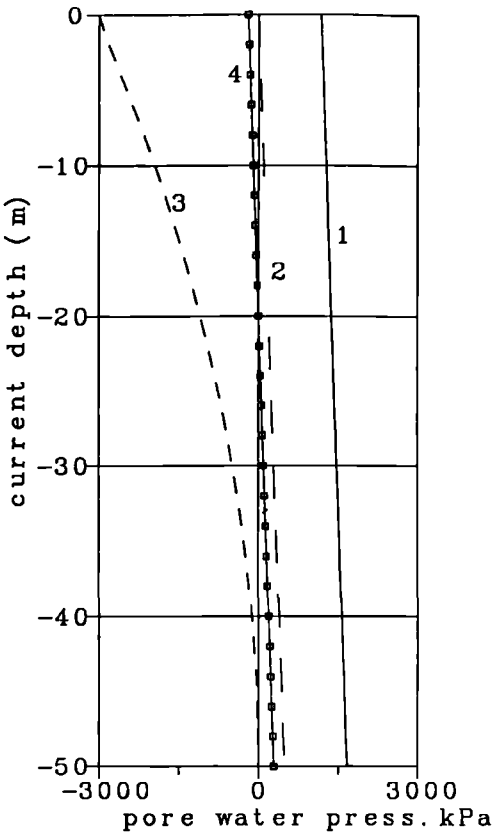

Fig.3.19. Pore pressure profiles in existing stratum used in calculating the LI profiles shown in Fig.3.20 Key: 1, at end of deposition; 2, after erosion of 120 m of sediment; 3, after desiccation; 4, present day profile.

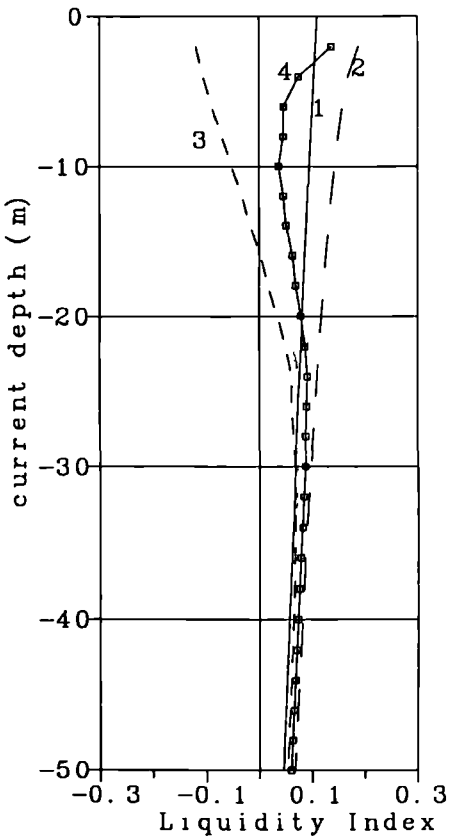

Fig.3.20. Liquidity index profiles resulting from the modelling of the Pappadai clay history.

CHAPTER 4

MEASUREMENT OF THE IN SITU STRESSES, SHEAR MODULI AND UNDRAINED SHEAR STRENGTHS FOR THE PAPPADAI CLAYS

4.1. Objectives of the in situ measurements

A series of self-boring pressuremeter tests (SBP) was carried out to compliment the laboratory tests in order to measure the in situ horizontal stress σ_h, the shear modulus G and the undrained shear strength c_u at Pappadai. The tests were carried out at various depths down borehole A, which is shown in Figs 3.5 and 3 6.

These tests are part of the investigation of the basic framework of the mechanical behaviour of the Pappadai clay. The horizontal stress σ_h measured in situ, together with the vertical stress σ_v, the pore water pressure u_0 and the voids ratio e, were used to define the present clay states e-q-p', which are the consequence of the clay's mechanical response to the geological loading-unloading events described in Section 3.8. Assuming the stresses in the clay to be axi-symmetric during the whole geological history, the e-q-p' state paths followed by the clay since deposition are investigated. These are modelled according to the e-σ'_v paths discussed in Section 3 8, and are then compared with the current e-q-p' state of the clay in situ (Section 4 7). This enables the validity of the assumed framework of behaviour of the clay to be checked and the clay response to the geological events to be interpreted. The in situ and laboratory shearing behaviour of the clay will be compared in Chapter 8 in light of the state path that the clay would undergo at sampling, as discussed in Chapter 5.

4.2. The self-boring pressuremeter test

During in situ pressuremeter tests a cylindrical cavity is expanded by means of a cylindrical device designed to apply a uniform fluid pressure to the walls of a borehole (e g Clarke 1992, Fig.4.1). It is theoretically possible to analyze pressuremeter tests to give fundamental parameters of soil behaviour, but the validity of the analysis and the parameters measured depend on the installation and measuring procedure (Clarke 1992).

The self-boring pressuremeter (SBP) was developed to minimize the disturbance of the in situ soil during installation of the device (Jezequel et al. 1968; Windle and Wroth 1977). The pressuremeter is directly drilled into the ground and, since in theory its installation does not affect the surrounding soil, the in situ horizontal stress σ_h may be measured and the test closely represents the soil response to the expansion of a cavity from the in situ stress conditions. It is assumed that the cavity expands as an infinitely long cylinder, and theories of cavity expansion are used to derive the in situ stiffness and strength.

A detailed description of the SBP equipment, installation and testing procedure are given by Mair and Wood (1987). The Cambridge SBP (Windle and Wroth 1977), used at Pappadai, is illustrated in Fig.4.2. During installation a twin-rod drilling system is used; the outer non-rotating rod pushes the cutting shoe of the drilling head into the ground, whilst the cutter is turned by the inner rods. The drilling rams can be part of a rotary drilling rig. The cutter trims the plug of soil forced into the shoe as the SBP advances, while the cuttings are flushed away by a flushing medium which is pumped through the inner rods and back through the instrument to the surface.

Behind the cutting head is a flexible membrane designed to expand into the surrounding soil. After installation, this membrane is inflated by gas pressure controlled from the surface via a gas cable. Its expansion is measured by three separate strain-gauged feeler arms spaced at 120 degrees around its mid plane. The gas pressure inside the membrane and the pore pressure in the soil in contact with the membrane are measured by means of pressure transducers mounted within the pressuremeter. The normal stress applied to the borehole wall is corrected for the membrane stiffness.

Installation of the SBP in clays may generate appreciable excess pore pressures (Mair and Wood 1987) and some relaxation time has to be allowed after installation before starting the test Tests can be either stress-controlled or strain-controlled, the test procedure being designed according to the main parameters to be measured. For undrained tests in clays, strain rates about 1°o/min have to be used to avoid drainage effects (Mair and Wood 1987)

In practice, even with skilled operators, some degree of disturbance is inevitable (Clarke 1992) Slight variations in the drilling technique can cause either under-drilling, or over-drilling or obliquity of the SBP in the ground with respect to the borehole axis Consequently measurements of horizontal stress, cavity strain and undrained shear strength may be affected To establish the accuracy of the measurements it is helpful to compare profiles of pressuremeter test data for the same soil in similar conditions For the Pappadai clay the pressuremeter test data presented in this

chapter are the only ones measured to date, so the validity of the test results can be established only by referring to the drilling records and comparing the profiles obtained for the different parameters.

4.3. Analysis of the SBP test data

4.3.1. Lateral stress σ_h

The volume of the cavity is defined as V_c, the current radius as ρ, while p is the cavity pressure, as shown in Fig 4.3. The cavity strain ε_c is defined as:

$$\varepsilon_c = (\rho - \rho_0)/\rho_0 \qquad (4\ 1)$$

The pressure inside the membrane can expand the membrane only when p is higher than σ_h. The lift-off pressure is that at which membrane expansion commences The displacements recorded by the feeler arms are corrected for mechanical compliance, membrane stiffness, compression and thinning, giving the lift-off pressure at zero cavity strain, as shown in Fig 4.4.

In general it is assumed that the three lift-off pressures σ_{h1}, σ_{h2}, σ_{h3} can differ and still represent the anisotropic in situ horizontal stresses in three different directions. But if

$$\sigma_{h1} > \sigma_{h2} > \sigma_{h3} \qquad (4\ 2)$$

then at the first lift-off the cavity is no longer circular, and the cavity deformation which occurs before the other horizontal stresses are measured must be allowed for As shown in Fig 4 5, the ideal measurement of horizontal stress by the SBP test is correct only for an axially symmetric state of stress.

In general it is assumed that the anisotropic deformation, shown in Fig 4 5(2) does not affect significantly the horizontal stresses to be measured, even so, if the soil stresses are not isotropic, the measured horizontal stresses are not necessarily the horizontal principal stresses Other complicating factors are discussed by Mair and Wood (1987) It is normal practice then to consider the average lift-off pressure as the in situ σ_h In the following, the inspection method (Clarke 1992-a) has been used to estimate the lift-off pressures (Fig 4 4)

4.3.2. Shear modulus

The initial conditions are shown in Fig.4.3. The cavity expansion problem is solved using equations of equilibrium, compatibility, and stress-strain laws. In practice, use is often made of simple models of the soil behaviour since the unknowns in the assumptions and installation techniques do not warrant greater sophistication (Clarke 1992-a, Mair and Wood 1987).

The soil is assumed to be homogeneous and isotropic and the cavity is assumed to be infinitely long and to expand cylindrically. So the soil is subjected to plane strain deformation, with no deformation in the vertical direction The soil is deformed under conditions of overall axial symmetry and the vertical stress σ_v, the radial stress σ_r and the circumferential stress σ_θ are principal stresses, as shown in Fig 4 6. These assumptions are approximated because in the real SBP test the presence of a friction stress at the cavity wall can make the vertical, radial and circumferential stresses not principal, the stresses in the ground not necessarily are axi-symmetric and deformation close to plane strain probably occurs only in the middle third of the pressuremeter.

If the radial displacement at radius r is y (Fig 4.7), the radial and circumferential strains are:

$$\varepsilon_\theta = y/r \; ; \; \varepsilon_r = dy/dr \qquad (4\ 3)$$

It is assumed that at the start the soil behaviour is elastic (Mair and Wood 1987) In this case

$$\Delta \sigma_\theta = - \Delta \sigma_r \qquad (4\ 4)$$

and for small deformations :

$$-\varepsilon_\theta = y_c \rho / r^2 = \varepsilon_r \qquad (4\ 5)$$

so that the volume strain is zero, drained and undrained conditions coincide and the vertical total and effective stresses σ_v and σ'_v, do not change

The variation of the stresses σ_r and σ_θ with increasing cavity pressure is as represented in Fig 4 8 (Mair and Wood 1987). Then the stiffness G at the cavity wall is .

$$G = \rho dp / (2 \rho_0 d\varepsilon_c) \qquad (4.6)$$

The stiffness at the start of the test is indicated as G_i, and equals dpV_o/ dV_c (Mair and Wood 1987). G_i is an initial tangent stiffness modulus directly determined from the pressuremeter expansion curve assuming an initial linear elastic behaviour for the clay. However, as discussed in Section 2.2.6, soil behaviour is generally elastic only at very small strains, which cannot be detected by SBP testing. So G_i should more correctly be considered a test parameter rather than a value for the soil shear modulus.

G_i is also strongly affected by the disturbance inevitable to the soil during installation, therefore it may give poor estimate of the intact soil stiffness. To avoid the disturbance effects the soil stiffness is estimated from unload-reload cycles carried out during the test as shown in Fig.4.9, and is called G_{ur}. Given the hysteretic behaviour of the clay, G_{ur} varies with the loop strain range, mean effective stress and stress range. These ranges should be always quoted for any G_{ur} measurement (Clarke 1992-b). Also the stress and strain variations occurring in the ground at different radius from the pressuremeter are different and G_{ur} is not constant in the soil Clarke (1992-a) considered the deformation in the ground as dependent on an average shear modulus and defined the modulus from the SBP test as this average modulus or "cavity modulus".

4.3.3. Undrained shear strength

For a linear elastic soil (Fig.4.10(a)) t $(=(\sigma_1-\sigma_2)/2)$ at the cavity wall is

$$t = (\sigma_r-\sigma_\theta)/2 = p - p_0 \qquad (4.7)$$

and its change with ε_c is as represented in Fig 4.10(b). The soil will reach the undrained shear strength first at the cavity wall (see Fig 4.8) and, if it is linear elastic up to the peak deviatoric stress (Fig.4.10(a)), c_u coincides with the pressure increase at the end of the linear portion of the test curve, as indicated in Fig 4.10(b)

However real test curves are not linear from early strains and it is difficult to identify the yield point on the p-ε_c curve. Nonetheless the soil is still modelled as linear elastic up to the maximum strength. The analysis of the cavity expansion problem in undrained conditions for an elastic-perfectly plastic soil results in the following relationship between the cavity pressure and cavity expansion

$$p = \sigma_h + c_u (1+\ln(G/c_u)) + c_u \ln(\Delta V_c/V_c) \qquad (4\ 8)$$

the limit pressure p_l being:

$$p_l = \sigma_h + c_u (1+\ln(G/c_u)) \qquad (4\ 9)$$

For these soils the cavity pressure plotted against $\ln(\Delta V_c/V_c)$ gives a straight line of gradient c_u in the plastic stage (Gibson and Anderson 1961; Fig.4.10(c)) from which c_u is derived

If the soil is not assumed to be elastic-perfectly plastic, but a strain softening law applies to its behaviour, for homogeneous and undrained soil conditions the t-ε_c curve can be deduced from the analysis of Palmer (1972). The relationship between t and the cavity expansion dV_c then is:

$$t = dp / d\ln(\Delta V_c/V_c) \qquad (4.10)$$

It follows that c_u is the maximum gradient of the curve p-$\ln(\Delta V_c/V_c)$ as indicated in Fig 4 11 It is apparent that the Gibson and Anderson analysis is a particular case of the Palmer analysis and if applied to the latter part of the loading curve for strain-softening soils it gives an average post-peak strength (Clarke 1992).

In order to compare the strength measured in the SBP testing on the Pappadai clay with the strength measured in the laboratory, the failure conditions occurring in situ during SBP tests were examined first. Three different failure conditions may occur in the ground during the SBP test, which give values of the undrained strength c_u expressed as follows :

$$c_u = \sigma_r - \sigma_\theta \qquad (4.11) \text{ case (1)}$$

$$c_u = \sigma_v - \sigma_\theta \qquad (4\ 12) \text{ case (2)}$$

$$c_u = \sigma_r - \sigma_v \qquad (4.13) \text{ case (3)}$$

The failure plane in the three cases would be different, as schematically shown in Fig 4 12(a), and the values of c_u corresponding to the different cases may be different, accordingly Eqs 4 8 and 4.10 are appropriate to estimate the strength corresponding to the failure condition 'case 1" (eq 4.11), but if the value of K_o is very low, the condition expressed by case (2) may apply,

while, if K_0 is very high, the passive failure expressed by eq.(4.13) may develop, as schematically shown in Fig.4.12(b).

Fig.4.13 shows possible changes of the three descriptors t_1 ($=\sigma_r - \sigma_\theta$), t_2 ($=\sigma_v - \sigma_\theta$) and t_3 ($=\sigma_r - \sigma_v$) during the expansion of the cavity for the two cases when K_0 is less than 1 and when it is higher than 1. Failure occurs when one of the three descriptors reaches the maximum value allowed by the soil strength properties. The analysis of the SBP test data described above results in a correct definition of the soil strength c_u only if the descriptor t_1 reaches the maximum value before t_2 and t_3. The case when K_0 is extremely low, so that t_2 reaches the possible maximum value as first (case 2) is unlikely ever to happen for a frictional material because of the limit provided to K_0 by the normally consolidated state On the contrary in highly OC soils the case when failure occurs as in case (3) is possible.

The laboratory tests that most closely reproduce the conditions present in the soil during SBP tests are the plane strain compression test on a soil element trimmed horizontally in the ground (Fig.4.14(a)) or the hollow cylinder test on a soil specimen trimmed vertically (Fig.4.14(b)). In the triaxial compression on an horizontally trimmed soil specimen, plane strain deformation would be not respected (Fig.4.14(c)). This will be discussed in greater detail in Section 8.6.10, when comparing the undrained shear strength resulting from triaxial tests with the c_u from the SBP tests.

4 4. Equipment used at Pappadai

At Pappadai the SBP tests were performed by PM In situ Techniques Ltd (U.K.) and Geo SRl (Bari, Italy). The SBP tests were carried out by Dr.B G Clarke whose experience in pressuremeter testing resulted in the high quality of the SBP test data In the following some of the diagrams reporting the SBP tests are from the report presented by PM In situ Techniques about the SBP testing at Pappadai.

A Cambridge-type SBP (Windle and Wroth 1977) was used (Fig 4 15 a), similar to that shown in Fig 4.2. The 84mm diameter probe consisted of a drill head which contains a drill bit and bearing, a pressuremeter and a guard cell It is nominally one metre long, with the pressuremeter expanding section being 500mm long, i.e. a ratio of pressuremeter length to diameter of about 6 The centre of the pressuremeter is 400mm from the leading edge of the probe

In general, the design of the SBP and the rig to be used depend on the grading, level of cementation, stiffness and strength of the soil being tested (Clarke and Allan 1989). So, for example, for the SBP in Fig.4 2 the design limits the strength of the soil into which the cutting shoe can be pushed. For very stiff/very dense soils and weak rocks a rock pressuremeter (RSBP), having full-face cutter of the same diameter as the pressuremeter is used (Clarke and Allan 1989). The rock is ground rather than chipped, using a series of tungsten tips, and some over-drilling occurs during installation.

The probe used at Pappadai was a RSBP type, but with a cutting head similar to that in Fig 4.2. This robust configuration allowed high compression stresses to be applied via the drilling rods during installation, so that the high resistance of the clay to the insertion of the cutting shoe and the friction at the cavity wall could be overcome. A MK 900F1 crawler-mounted rotary rig, shown in Fig.4.15(b), was used to advance the hole to the test depth and also to drill the probe into the ground. Outer rods of 50mm diameter and RW size rotating inner rods were used Water was used as the flushing fluid

The adiprene membrane and the pressure source usually used with the SBP (Figs 4 2 and 4 15(a)) give a designed pressure capacity of 4Mpa, which limits testing to clays having an undrained shear strength lower than 700kPa The RSBP used at Pappadai has a pressure capacity of 20Mpa, but a 10MPa pressure transducer was used to increase the sensitivity. Given the toughness of the membrane and the absence of rock fragments in the soil profile, a chinese lantern was not used to protect the probe

One gas pressure transducer and three feeler arms were used, but a soil pore pressure transducer was absent. The feeler arms were Hall-effect transducers of the type described by Clarke and Allan (1989). The control and data logging system, shown in Fig 4 16, consisted of a unit to amplify the signals from the transducers and convert them to a digital signal, a computer to log the data and a unit which controlled the rate at which the membrane was pressurized.

4 5 SBP testing at Pappadai

The SBP tests were carried out in borehole A (Fig 3 6), which is about 80 metres distant fr m the shaft where the laboratory samples were taken (Fig 3 5) Borehole A is sufficiently distant from the shaft to assume that the effects of the shaft excavation on the in situ effective stresses down the boreh le were not s gnificant Significant differences are presumed unlikely in the ground

conditions in borehole A and in the shaft pre- excavation; the ground surface of the borehole and of the shaft are both at 111m a.s.l., as shown in Figs.3.6.

As discussed in Section 4.2, the SBP test is designed according to the main parameters to be measured, in the present case the horizontal stress σ_h and the undrained shear strength c_u. Priority was given to the measurement of c_u rather then the shear modulus G, firstly because the present research investigated the mechanical behaviour of the clay at strains close to or beyond gross yield. Secondly, because, given the uncertainties concerning the interpretation of the cavity modulus, the latter is considered a test parameter rather than a fundamental soil property, and therefore not of particular interest in the understanding of the clay's behaviour. So as not to break the continuity of the t-ϵ_c curve (Fig 4.11) and avoid the risk of drainage occurring, unload-reload loops were carried out only towards the end of most of the tests.

Typical site operations were carried out as follows (Fig.4.17):

1 The borehole was advanced to within one metre of a test position.
2 The probe was lowered to the base of the hole using the rig.
3 The probe was self-bored to the test position using the rig.
4 About half an hour relaxation time was allowed.
5 A test was carried out.
6 The probe was self-bored to the next position (if this was not possible, the probe was removed).
7 A second test was carried out.
8 The probe was removed using the rig.
9 The operations were repeated until the borehole was complete.

For each test the membrane was expanded at a controlled rate, initially controlled by the gas pressure. Once the membrane begun to expand the rate of expansion was set at 1%/min. During unload-reload cycles and during the initial part of the final unloading the rate of expansion/contraction was again controlled by the gas pressure.

Pairs of tests were performed at close depths to check the results. Ten tests were carried out, but there were no results for test 1 because of problems during installation, the depths of the tests are shown in Table 4.1.

During the installation before tests 2 and 3 the probe was probably partly pushed in, as flushing was inefficient and the clay tended to clog inside the probe Consequently, given the inexperience

with the material being tested, in the first two tests the probe was advanced while applying some excess vertical force.

Tests 4 and 5 were carried out at the same depth, test 4 being performed at the end of a shift and test 5 twelve hours later at the beginning of another, after the probe had been left in the hole overnight. Some over-drilling probably occurred during the installation before test 4. No drilling problems were recorded during the installations before tests 6 to 10. During the last test the membrane was brought to 5MPa, but then it burst.

4.6. Test Results

Figs.4.18 (a) to (i) show the results from the tests in form of cavity pressure-cavity strain ε_c. The data have been corrected for mechanical compliance and membrane thinning and compression during expansion. During tests 2, 3 and 4 unload-reload cycles were carried out at intermediate strains, below 5% cavity strain, as is conventional practice The test curves for tests 4 and 5 are anomalous for clays, and resemble those observed for sands. They presumably reflect the over-drilling that occurred during the installation of the probe The curve for test 5 shows the response of soil which has already been failed. Tests 6 and 7 appear to be the most successful

4.6.1 In situ horizontal stresses

By the use of the inspection method, as defined in Section 4.3 2, the lift-off pressures were identified. The curves from each of the feeler arms were inspected independently, giving three lift-off pressures for each test. These are reported in Table 4 1, together with their average (σ_h).

The quality of the test results can be judged only considering the overall trend of the data and drilling records As discussed in Section 4 3 1, it is difficult to discern the causes of differences between the lift-off pressures measured during a test and to judge the reliability of the single measurement The stress state q-p' in the ground is then usually assessed by use of the average of the lift-off pressures If the lift-off pressures differ because of errors in the measurements which cannot be identified, the errors may have a lesser effect on the average measurement than on the individual ones.

The average lift-off pressures (σ_h) are plotted in Fig.4.19. The repeatability of the measurement in the different directions is indicative of stresses truly acting in the ground after installation, although these measurements can also be affected by disturbance of the soil at the cavity wall. The tests for which at least two arms have measured similar horizontal stresses have been indicated in Table 4.1. For each test also the maximum difference between the lift-off pressures σ_{hi} and their average σ_h is reported in the table (denoted as max.error %), which is calculated as:

$$[(\sigma_{hi} - \sigma_h)_{max} / \sigma_{hi}] \, 100 \qquad (4\ 14)$$

The table shows that tests 6 and 9 gave very consistent lift-off pressures. Tests 6 and 9 were performed at depths close to tests 7 and 8, in each of which the average lift-off pressure was close to that in the other test at similar depth, as shown in Fig.4.19. This suggests that the average stresses from tests 7 and 8 are reliable. The average stresses σ_h from the pairs of tests 6-7 and 8-9 then represent the horizontal stresses at (24-25)m and (35-36.1)m depths.

The average stresses from tests 2, 3 and 10 plot close to a straight line through the average stresses from tests 6, 7, 8 and 9, line (a) in Fig 4 19. The fact that the stresses from tests 2 and 3 are high is probably due to the excess pushing during installation (Section 4 5).

In contrast, the results from tests 4 and 5 at 23m depth plot to the left of line (a) and give undrained shear strengths which are particularly high. This is usually observed in tests when over-drilling occurred during installation, consistent with the drilling records for test 4 (see Section 4 5). So the lift-off pressures from tests 4 and 5 are discarded from the analysis.

In conclusion the average horizontal stresses from tests 2, 3, 6, 7, 8, 9 and 10 shown in Fig.4.19 are considered representative of the horizontal stresses present along borehole A before excavation. The stresses from tests 2 and 3 are probably too high as result of some disturbance during installation.

4.6.2 In situ undrained shear strengths

The undrained shear strengths were initially calculated according to the Gibson and Anderson (1961) method, discussed in Section 4 3 2 For each test the data for each feeler arm were plotted in form of cavity pressure against $\ln(\Delta V_c/V)$, as in Fig 4 10(c), and c_u was taken as the gradient in the latter part of the curve From the same plot the limit pres ure p was calculated These c_u

values are reported in Table 4.2 and plotted in Fig.4 20; the limit pressures are plotted in Fig.4.21. In the figures the average measurements for each test are also reported

The limit pressure (p_l) increases linearly with depth. p_l is a test parameter rather than a basic in situ soil parameter, given the uncertainties about the applicability to the soil being tested of the model assumed to derive p_l. However, the linear increase in Fig.4.21 may be an indication of uniformity of the mechanical properties along the profile. p_l exceeds 4000kPa below 25m depth, showing that for the Pappadai clays the conventional Cambridge SBP is under-designed.

For each of the pairs of tests 2-3, 6-7 and 8-9 the c_u results are very consistent. The consistency between the three arm measurements for each of tests 6 and 7, for which also the conditions at lift-off were considered reliable, makes these tests the most reliable along the profile. The very high strength values implied by tests 4 and 5 confirm that over-drilling occurred before these tests and that their results must be discarded.

In Fig.4.20 the undrained shear strengths observed by Ghionna et al (1983) in sub-Apennine blue clays in the Taranto area are reported. These strengths are also derived from the latter part of the curve p-ln($\Delta V_c/V_c$), and are higher than those for Pappadai But for strain softening soils, such as the Pappadai clays (see Chapter 8), the c_u values derived from the Gibson and Anderson analysis are average post-peak strengths To identify the peak strengths of these clays the t-ϵ_c curves were used, t being derived from eq (4.10). These curves are shown in Figs 4.22(a) to (i) For tests 2 to 5 the unload-reload loops interrupt the curve at the strain levels where the peak strength develops. This confirms that if c_u has to be measured for a strain-softening soil it is convenient to carry out the unload-reload loops at larger strains. An average peak c_u about 200kPa for test 2 and about 280kPa for test 3 were extrapolated for around 2% cavity strain from these curves. These values are indicated in Fig 4.20. Strain-hardening type curves resulted from tests 4 and 5.

Very well defined t-ϵ_c curves were derived for tests 6 and 7, giving peak strengths of 430kPa and 520kPa respectively. In Chapter 8 these two values are shown to be consistent with the laboratory measurements of c_u on clay from the block sample taken at a depth similar to that of these two tests In Fig 4 22(e) the c_u value from the Gibson and Anderson analysis is reported, this is close to the average post-peak strength, as suggested by Clarke (1992) The peak c_u value plotted in F g 4 20 for 24 2 and 24 9 m depth are thus considered correct, reflecting very successful insertion procedure.

The peak strengths of the Pappadai clay are close to the average post-peak strengths recorded for Taranto clays by Ghionna et al.(1983). The t-ϵ_c plots from tests 8 and 9 are not as easily interpreted as tests 6 and 7. For test 10 a peak c_u equal to 750kPa can be identified; during the last part of this test the membrane was expanded at about its limit capacity. For tests 2, 3, 8 and 10 the peak strengths have been defined using data selectively from some of the feeler arm test curves.

Using all the peak strength measurements outlined above a linear peak strength profile is obtained for borehole A, Fig.4.20.

4 6.3. Shear moduli

Since, even during good quality insertion there is inevitable disturbance of a soil annulus around the cavity, thus the soil shear modulus is underestimated, and was not calculated for the present tests.

In Fig.4.23 the p-ϵ_c plots of the unload-reload loops performed during the tests are reported In Table 4 3 for each test both the stress ranges and the strain ranges of the unload-reload loops are reported. For each loop the average secant cavity modulus G_{ur} over the whole cycle was calculated along with the cavity modulus on reload over both 0.1% (G_{ur} (.1%)) and 0.2% (G_{ur} (.2%)) cavity strain The data are reported in Table 4.3. To calculate G_{ur}, ρ was assumed equal to the average radius over the stress range of the unload-reload loop and for both G_{ur} (.1%) and G_{ur} (2%) ρ was assumed equal to the radius at the start of reloading.

The tests for which similar cavity moduli were measured from all three arms are indicated in Table 4.3. The moduli G_{ur} and the corresponding stress and strain ranges are reported in Table 4.4, and the G_{ur}(.1%) and G_{ur}(.2%) values are reported in Table 4.5.

The differences between the secant moduli in Table 4 4 are at least in part the effect of the differences between both the strain ranges and the mean effective stress relative to the loops The secant moduli have been normalized with respect to both the effective horizontal stress σ'_h (Clarke 1992-b), and the mean effective stress p' at the start of the expansion

The moduli from tests 2 and 3 are much lower than the others and this difference increases when the moduli are normalized because of the high horizontal stresses measured for tests 2 and 3 But

these stresses probably overestimate those in situ, and for this reason the normalization is not successful. Normalization with respect to p' reduces the difference from the moduli of the other three tests reported in the table.

In Table 4.5 the G_{ur}(.1%) and G_{ur}(.2%) values are reported with their normalized values with respect to both the effective horizontal stress and the mean effective stress. Again the modulus from 12m depth is much lower than the others both before and after normalization. The normalized moduli from tests 6 and 7 are similar while those from tests 8 and 9 are higher. The differences between the normalized shear moduli from tests 6 to 9 in Tables 4 4 and 4.5 are in part effect of the dependency of the shear modulus on YSR, since YSR changes with depth (Viggiani and Atkinson 1995).

Moreover, also the fact that the unload-reload loops commenced at different cavity strains probably causes the differences between the normalized shear moduli. As shown in Fig 4 24, the normalized cavity moduli reduce with the increase of strain reached before unloading In general, the clay stiffness progressively reduces with straining because the clay structure is progressively disturbed and weakened. For unload-reload loops carried out following large cavity strains the cavity moduli are lower because they are related to the stiffness of a partly weakened clay structure.

Considering the uncertainties regarding the significance of the cavity modulus and its relation to the clay's shear modulus G, only an order of magnitude can be deduced from the SBP tests for G at 25m depth, that is about 150MPa. This value will be compared with that resulting from the laboratory testing discussed in Chapter 8.

4.7. State history of the Pappadai clay

4.7.1. Present e-q-p' state of the clay in situ

In Table 4 6 the data defining the voids ratio-stress states of the clay in borehole A are reported The voids ratios reported in Table 4 6 were calculated from the LI values chosen along the solid line in Fig 3 16(a) The possible errors affecting the horizontal stre ses σ_h in Table 4 6 have been discussed in Section 4 6.1.

The vertical total stresses have been calculated assuming an average total unit weight of about 19 kN/m^3; see Section 3.8. The pore water pressures in Table 4 6 were deduced from the piezometer readings reported in Chapter 3. In the Casagrande piezometer at 27m depth in borehole A a piezometric level of 18.5m below ground level was measured (Fig.3.6), while in the Casagrande piezometer at 12m depth no water was recorded. The piezometric conditions above 27m depth were thus assumed to be hydrostatic with a water table at 18.5m below ground level. The pore water pressures at 11 and 12m depth are therefore assumed to be negative.

At both 35.1-36.1m and 43.6m depth the pore pressures must be within a range from 0kPa to values which are hydrostatic with respect to the water table at 18 5m, because the pore pressures below the clay stratum are known to be zero. At these depths the calculation of the effective stresses was carried out considering both zero pore water pressure values and hydrostatic pore water pressures, as reported in Table 4.6. The first pore water pressure values are referred to as u_1 in the following figures, and the second pore water pressure values as u_2.

The effective horizontal stresses are plotted in Fig.4.25 and the K_0 values in Fig.4 26. The assumptions regarding the pore water pressures have little effect on K_0. For Pappadai clay K_0 in situ is always higher than 1, and reduces with depth. At 25m depth, which coincides with the depth down the shaft (Fig.3.6) of the block sample tested in the laboratory, K_0 is about 1.5-1.7. The in situ stress states are represented in terms of q and p' in Fig.4 27.

4.7.2. Modelling the e-q-p' state history of Pappadai clay

The state paths followed by the Pappadai clay since deposition were modelled assuming one-dimensional loading. In Section 3.8 the four stages defining the history of the clay and that part of the modelling concerning the LI-σ'_v paths followed by the clay in these four stages were discussed. In the following, the corresponding e-p' and q-p' paths are discussed The K_0 values assumed in the modelling were derived from both the CSF of clay behaviour and empirical K_0-OCR relationships reported in the literature, as discussed in the following

The in situ states at the end of stage 1, which were shown as line 1 in the LI-depth plot in Fig 3 20, are represented by line 1 in Fig 4 28(a) as voids ratio e against σ'_v and in Fig 4 28(b) as LI against σ'_v. Similarly the in situ states at the end of stages 2, 3 and 4 are represented by lines 2, 3 and 4 in the LI-depth plot in Fig 3 20 and in the e-σ'_v and LI-σ'_v plots in Fig 4 28 As pointed out in Section 3 8, the development of additional bonding d e either to diagenesis or to

cementation, which might have affected the clay behaviour during its geological history, were not considered in any of the modelling. Lines 4 in Figs.3.20 and 4.28 represent the present clay profile for the model clay.

The LIs and the voids ratios in Table 4 6 are also plotted in Fig 4.28. This figure then shows that the voids ratios resulting from the modelling are reasonably close to the measured ones, supporting the geological history reconstructed for the clay and the assumption that the sedimentation structure of Pappadai clay was uncemented (see Section 3 8) The opposite assumption, that the clay became cemented during sedimentation, would have given a much less steep SCC in the e-σ'_v plane, and much higher final voids ratios. The differences between the calculated and measured present e-σ'_v states in situ (Fig 4.28(a)) are higher than the differences between the calculated and measured LI-σ'_v states (Fig 4.28(b)) because of the differences between the index properties assumed for the model clay and the index properties of the natural Pappadai clay.

In Section 3.7 it was proposed that the Pappadai clay underwent diagenesis at the end of virgin compression or later, as will be confirmed by the analyses reported in the following. However diagenesis was not included in the modelling and this may be another cause of the differences existing between the calculated LI-σ'_v states of the clay at present and the LI-σ'_v states measured in situ.

4.7.3. Modelling σ'_h in the four stages of the clay history

To model the horizontal stresses during the four stages of the clay history, the expressions for K_0 conforming to the CSF were first considered. For one-dimensional compression of a horizontally isotropic soil, both the vertical strain ε_z and effective stress σ'_z are principal, the same as the horizonatal strains ε_x, ε_y and the horizontal stresses σ'_x and σ'_y. During the compression the loading conditions are as follows:

$$\varepsilon_h - \varepsilon_x = \varepsilon_y = 0 \qquad (4\ 15)$$

$$\sigma'_h = \sigma'_x = \sigma'_y \qquad (4\ 16)$$

Consequently the strain invariants ε_v and ε_s (see Section 2 2 6) are

$$\varepsilon_v = \varepsilon_z \text{ and } \varepsilon_s = 2\,\varepsilon_s/3 \qquad (4.17)$$

and are then related as follows

$$(\varepsilon_s/\varepsilon_v) = 2/3 \qquad (4.18)$$

Therefore a one-dimensional compression path is strain controlled as expressed in eq.(4.18). For the Cam Clay model, the stress ratio q/p' is necessarily constant during one-dimensional compressions of normally consolidated (NC) clays, as during virgin compression the plastic volumetric strain is :

$$d\varepsilon_v^p/dp' = d\varepsilon_v/dp' - \kappa/p' \qquad (4.19)$$

and $$d\varepsilon_v/dp' = \lambda / p' \qquad (4.20)$$

It then follows that :

$$d\varepsilon_v^p/d\varepsilon_s = (d\varepsilon_v/dp' - \kappa/p') / (d\varepsilon_s/dp') \qquad (4\ 21)$$

and from equations (4.18) and (4 20) :

$$d\varepsilon_v^p / d\varepsilon_s = 3(\lambda - \kappa) / (2\,\lambda) \qquad (4.22)$$

If the strain ratio from eq (4.22) is substituted either in eq (2 3) or in the general expression of the "basically" frictional plastic deformation mechanism (eq 2.4; Section 2 2 7), it follows that :

$$q/p' = M - 3/2\ A\ (\lambda - \kappa) / \lambda \qquad (4\ 23)$$

Thus for basically frictional behaviour (eq.2 4), one-dimensionally compressed NC clays are necessarily subjected to a constant stress ratio q/p' and constant K_o. The expression of K_o resulting from eq (4 23) is of the type

$$K_o = (a - b \sin\phi'_{cs}) / (c + d \sin\phi'_{cs}) \qquad (4.24)$$

where a, b, c and d are coefficients depending on λ and κ. K_0 then depends on the basic frictional property of the soil, the critical state friction angle ϕ'_{cs} . The higher is ϕ'_{cs} the lower is K_0. The relationship between K_0 and ϕ'_{cs} in eq.(4.24) is consistent with the empirical expressions reported in the literature for reconstituted and natural soft NC clays, such as:

$K_0 = 1 - \sin\phi'_{cs}$ Jaky (1944) (4.25)

$K_0 = 0.95 - \sin\phi'_{cs}$ Brooker and Ireland (1965) (4.26)

$K_0 = 1 - 1.2\sin\phi'_{cs}$ Schmidt (1966) (4.27)

$K_0 = (1 - \sin\phi'_{cs}) \pm 0.05$ Ladd et al (1977) (4.28)

To simulate the lateral stress response of Pappadai clay during stage 1 eq (4 25) was used in the modelling with a friction angle of 23°, as measured for the reconstituted Pappadai clay, Chapter 8. The formulae and the values of the earth pressure coefficients used in the various stages of the modelling are reported in Table 4.7.

With one-dimensional unloading, an increase of K_0 with increasing OCR was observed by Brooker and Ireland (1965), Campanella and Vaid (1972) and Ladd et al. (1977) The relationship between K_0 and OCR was found to be independent of the maximum vertical normal-consolidation pressure (Schmdt 1966), but different for unloading and reloading (Fig 3 29; Campanella and Vaid 1972). Thus, as emphasized by Wroth (1984), the precise geological history of a deposit and not just the OCR has to be known in order to derive K_0.

For the Cam Clay model during one-dimensional unloading K_0 increases for decreasing σ'_v and increasing OCR, consistent with what is observed Since the behaviour of OC clay is non-linear elastic, $\sigma'_z (=\sigma'_v)$ and σ'_h during unloading are such that:

$$d\sigma'_h = \nu' (1- \nu') d\sigma'_v \quad (4\ 29)$$

where ν', the Poisson's ratio, is a function of σ'_v

It follows that .

$$\sigma'_h = \sigma'_{hp} + \int_{\sigma'_p}^{\sigma'_v} \nu'/(1-\nu')d\sigma'_v \qquad (4.30)$$

$$\sigma'_v = \sigma'_p - \Delta\sigma'_v \qquad (4.31)$$

where v_p-σ'_p-σ'_{hp} is the preconsolidation state of the clay. The earth pressure coefficient is then :

$$K_0 = [K_{0NC}\sigma'_p + \int_{\sigma'_p}^{\sigma'_v} \nu'/(1-\nu')d\sigma'_v] \; / (\sigma'_p - \Delta\sigma'_v) \qquad (4.32)$$

The K_0 increase then depends on the relationship between ν' and OCR or YSR. Following the Cam Clay model it can be demonstrated that ν' decreases for increasing OCR. Given the Cam Clay assumption that the soil follows a κ line in one-dimensional unloading, the shear modulus G is a function of ν' and κ as follows :

$$G = 3(1-2\nu')\, p'v \,/\, (2(1+\nu')\kappa) \qquad (4\ 33)$$

The overconsolidation ratio R (= p'_p/p') can be introduced into eq.(4.33) as v is equal to :

$$v = v_p + \kappa \ln R \qquad (4\ 34)$$

and substituting expression (4.34) in eq.(4.33), the value of the Poisson's ratio ν' in terms of G and R can be derived:

$$\nu' = [\alpha\,(v_p + \kappa \ln R) - G\,R] \;/\; [\,2\alpha\,(v_p + \kappa \ln R) + G\,R\,] \qquad (4\ 35)$$

where α equals $3p_p'/(2\kappa)$.

For reconstituted and natural clays the relationship between the shear modulus at very small strains G_0 and R reported by Viggiani and Atkinson (1995) is

$$G_0 = A\, p'^{n} R^{m} \qquad A>0,\ 0<n<1,\ 0<m<1 \qquad (4\ 36)$$

Substituting G_0 from eq (4 36) for G in eq (4 35), the result is

$$\nu' = \frac{\alpha\,(v_p + \kappa \ln R) - A\, p'^{n}_p\, R^{m+1-n}}{\alpha\,(v_p + \kappa \ln R) + A\, p'^{n}_p\, R^{m+\ n}} \qquad (4\ 37)$$

It follows that ν' decreases with increasing R and then with increasing OCR, as previously assessed, this influencing the relationship between K_0 and OCR (eq. 4 32). Eqs.(4.32) and (4.35) show that during unloading the increase of K_0 with OCR depends on the relationship between G and OCR, and that the increase in K_0 is greater with stiffer material.

The empirical relationships between K_0 and OCR reported in the literature refer to the unloading of soft clays. Given the effects of the relationship between G and OCR on the values of K_0 (eqs.4.32 and 4.35), the empirical K_0-OCR relationships for soft clays may not apply to stiff clays, in particular to clays which have become stiff before unloading Thus the behaviour of soft clays is likely to differ from that of stiff, strongly bonded clays In Fig 4 31 the possible stress paths followed by a natural clay during loading-unloading cycles are drawn schematically. At point P in the figure, that is the preconsolidation state, the clay is presumed to have an uncemented "sedimentation structure", as for Pappadai clay, and, if no changes occur while at rest, during unloading it follows the path P-A. This path would conform to the relationship between K_0 and OCR reported in the literature for first time unloading of soft clays (Schmidt 1966; Ladd et al.1977; Mayne and Kulhaway 1982) :

$$K_0 (OC) = K_0(NC)\ OCR^a \qquad (4\ 38)$$

An increase of stiffness at the end of the virgin compression, arising from a strengthening of the clay structure due to the acquisition of bonding, would result in higher K_0 values during unloading, since the increase in K_0 is greater for stiffer materials, as demonstrated in eqs. (4 32) and (4.35). The clay would then follow a stress path P-B. During reloading, due for example to desiccation as in stage 3 of the Pappadai clay history , the stress path may follow any of paths A-Y-D, B-Y'-D or B-Y"-D in Fig 4.31. Path B-Y"-D explains a decrease of K_0 that has been observed during recompression of strongly bonded soils such as marls (Chandler 1967) and cemented sands (Maccarini 1987, Coop and Atkinson 1993)

Equation (4.38) was used in the modelling of the behaviour of Pappadai clay during unloading Both Schmidt (1966) and Mayne and Kulhaway (1982) have proposed expressions of a as a function of $\sin\phi'$ while Ladd et al (1977) proposed the relationship between a and PI reported in F g 4 30 In the model "a" was deduced from Fig 4 30 for PI equal to 33% as reported in Table 4 7

For the Pappadai clay the increase of bonding after virgin compression was not considered, and so during stage 3 the lateral stress response was modelled assuming a stress path of the type A-Y-D. In particular, the equation proposed by Mayne and Kulhaway (1982) for reloading :

$$K_0 = (1-\sin\phi')(OCR/OCR_{max}^{0.61} + 3/4\ (1-OCR/OCR_{max})) \qquad (4.39)$$

was used. During stage 4 unloading was modelled using eq.(4.38) as indicated in Table 4.7. In conclusion, the whole of the modelling was carried out without allowing for any possible effects of the acquired strength of the "post-sedimentation" structure (see Table 1 1) of the Pappadai clay.

The in situ states through the 50m clay stratum at borehole A calculated for each of the stages of the geological history at Pappadai is shown in Fig 4.32 as voids ratio against mean effective stress p'. The corresponding stress states q-p' are plotted in Fig 4.33. In Fig.4.34 the OCRs calculated for each stage of the geological history are plotted against depth The calculated K_0 profiles are plotted for each of the stages of the clay history in Fig 4 35, and against the OCRs at each stage in Fig.4.36. The calculated state profiles can then be compared with the in situ measurements in each of these plots.

In Fig.4.35 the measured K_0 values are higher than those calculated at any stage of the clay history, and consequently the measured in situ states plot to the right of those calculated for stage 4, Fig.4.32 So at present the Pappadai clays have higher mean effective stresses and higher negative deviatoric stresses than would be expected for clays which behave according to eqs.(4.38) and (4.39), as predicted for a clay which acquired structural strength after virgin compression, state B in Fig.4 31.

In Fig.4.37 are plotted the stress states calculated at the end of each stage of the clay history for the depths where the tests in Table 4.6 were carried out. The stress paths followed by the model clay at each of these depths are also plotted. These stress paths are the solid lines in the figure, and show the inclination of the unloading paths according to eq (4 38) The unloading paths which connect the estimated preconsolidation pressures at the test depths and the stress states measured in situ are also plotted, these are the dashed lines in the figure Because of the higher K_0 values, the dashed unloading paths are much steeper than the calculated ones (solid lines) Comparing Fig 4 37 with Fig 4 31 it appears that the Pappadai clay followed unloading paths similar to P-B rather than P-A in Fig 4.31 This shows that at unloading the clay was stiffer than during the virgin compression Thus it is demonstrated that at the end of virgin compression the

Pappadai clay structure was strengthened and made stiffer, perhaps due to long-term diagenesis (Table 1.1), as was previously anticipated when reviewing the possible causes of discrepancy from the model results in Fig.4.28.

In Fig.4.37 the unloading paths from the preconsolidation states to the present in situ stress states are parallel if at 44m depth the effective stresses are calculated with zero pore pressure (u_2), which is likely to be the case at this depth. At 35-36m depth the pore pressure is likely to be intermediate between hypotheses (u_1) and (u_2).

4.8 . Conclusions

The modelling of the history of the Pappadai clay presented in this chapter suggests that the clay was uncemented during deposition and virgin compression and that its SCC was not far from line 1 in Fig 4.28.

At the present time the K_o values measured in situ are higher than those calculated by modelling the clay history, and relying on the K_o - OCR relationships reported in the literature for clays overconsolidated in the laboratory. The clay states in the q-p' plane plot to the right of those to which the clay would have arrived at if it had behaved as a reconstituted clay during unloading (Fig 4.37). Eqs.(4.32) and (4 35) show that the K_o value of overconsolidated clays increases with increasing clay stiffness on unloading It is thus considered that the Pappadai clay experienced values of K_o during unloading which were higher than those expected because the clay stiffness and strength increased at the end of virgin compression This finding is a further confirmation that a post-sedimentation structure stronger than the original sedimentation structure developed in the Pappadai clay once virgin compression was complete as a consequence of ageing and long-term diagenesis, as initially proposed in Section 3 7. Thus the Pappadai clay is a stiff clay of category 7 in Table 2.1, as will be definitively confirmed in Section 6.7 1.

The effects of an increase of clay strength and stiffness after virgin compression on the q-p' paths followed by the clay during unloading from its preconsolidation state, are shown in Fig 4 31. These compare very well with the q-p' paths followed by the Pappadai clay in its unloading history, as shown in Fig 4 37 The shift of the clay states in the q-p' plane are consistent with a general increase of the size of the state boundary surface of the natural clay beyond that of the original SBS of the normally consolidated clay This is investigated in Chapter 8

It follows that the relationship between K_0 and the geological OCR reported in the literature may not apply to stiff clays such as types 5, 6 and 7 in Table 2.1. In Fig 4.36 the K_0 value logged at 25m depth is plotted against both the geological OCR of the clay and its YSR, the latter being measured during oedometric compression, Chapter 6. For the Pappadai clay YSR is higher than OCR. Eq.(4.39) thus appears to work with the YSR, but not with the OCR, suggesting that the diagenetic increase of structural strength of the Pappadai clay is reflected in an increase of σ'_y. It appears that after the occurrence of structural changes in the clay it is the yield stress ratio YSR that determines the clay behaviour, not OCR. YSR may be substituted for OCR and a similar relationship between K_0 and YSR probably applies to the different clays in Table 2.1, but expressed in terms of YSR rather than OCR.

In the following chapters other aspects of the behaviour of the natural Pappadai clay are investigated in an attempt to verify if the use of the YSR of a natural clay is analogous to the use of OCR as a controlling factor for the behaviour of reconstituted clays

Test	Depth m	arm 1 kPa	arm 2 kPa	arm 3 kPa	average kPa(σ_h)	*/-	max. error (%)
2	11.0	295	930	740	655	-	55
3	12.0	395	960	805	720	-	45
4	23.0	415	415	390	405	*	3.7
5	23.0	335	205	205	250	*	34
6	24.2	710	635	710	685	*	7.3
7	24.9	750	640	960	785	-	22
8	35.1	805	805	995	870	*	14
9	36.1	820	875	820	840	*	4
10	43.6	1220	575	850	880	-	38

* *very consistent readings of the three feeler arms*
\- *inconsistencies exist between the feeler arm readings*

Table 4 1 SBP tests : lift-off pressures and average horizontal pressures σ_h

Test	Depth	Arm 1		Arm 2		Arm 3	
		Shear Strength kN/m^2	Limit Pressure kN/m^2	Shear Strength kN/m^2	Limit Pressure kN/m^2	Shear Strength kN/m^2	Limit Pressure kN/m^2
2	11.0	180	2015	160	1975	150	1980
3	12.0	110	1890	130	1935	115	1870
4	23.1	1070	4100	1105	3690	1075	3320
5	23.1	1050	4065	1395	3950	1285	3475
6	24.2	290	3460	255	3420	320	3475
7	24.9	300	3460	190	3250	195	3265
8	35.1	680	5670	540	5250	645	5240
9	36.1	510	5340	460	5125	885	5295
10	43 6	820	6110	965	6435	1095	6885

Table 4 2 SBP tests . measured values of shear strength and limit pressure

TEST	DEPTH m	CYCLE	PRESSURE RANGE kN/m²	Arm 1				Arm 2				Arm 3			
				Strain Range %	G_{ur} MPa	G_{ur} (.1%) MPa	G_{ur} (.2%) MPa	Strain Range %	G_{ur} MPa	G_{ur} (.1%) MPa	G_{ur} (.2%) MPa	Strain Range %	G_{ur} MPa	G_{ur} (.1%) MPa	G_{ur} (.2%) MPa
	11.0	1	805-1425	0.193 1.980	18	58	46	0.146-1 395	21	74	56	0 049 1395	24	108	68
		2	1175 1595	4.546 6 051	19	38	22	4.450-5.957	19	61	45	3.725-5 127	19	71	47
3	12.0	1	1085 1315	0.170-0.367	59	85	57	0.268-0 788	34	39	32	0.331-0 691	34	44	35
		2	1265-1483	1.296-1.761	28	47	36	2.095-2.572	32	42	34	2.148 2 734	24	41	33
4	23 1	1	525-715	0 409-0.699	40	45	36	0.788-1.224	27	31	27	0.917-1.402	24	29	25
		2	725-935	1.416-1.735		48	37	2.418-2.929		32	27	2.877-3 490		26	23
5	23 1	1	340-490	0.245-0.396	56	59	44	0.747-1.112	24	31	25	0.675-1 066	22	28	24
6	24 2	1	2535-2985	11.800-12.787	57	96	65	8.744-11.376	58	92	59	11.007-13.513	58	90	60
7	24.9	1	2400 2970	10 274-11.115	48	97	72	12.594-14.053	44	97	65	11.650-12 874	46	97	70
8	35.1	1	3515-4215	6.807-7.895	69	121	99	6.533-10.038	58	123	95	12.673-14 928	48	147	97
9	36.1	1	3005-4110	3 709-4.900	79	156	125	4.844-6. 331	76	160	126	14.133-16.346	65	192	139

Pressure Range range of pressure of modulus cycle
Strain Range range of strain of modulus cycle
G_{ur} average shear modulus from whole of cycle
G_{ur} (.1%) reload modulus over 0.1% cavity strain
G_{ur} (.2%) reload modulus over 0.2% cavity strain
☐ values used in Tables 4.4 and 4.5

Table 4.3. SBP tests : unload-reload loops; average secant cavity moduli G_{ur} and reload moduli G_{ur}(.1%) and G_{ur}(.2%).

Test N°	DEPTH (m)	$\Delta\varepsilon_c$%	Gur (MPa)	Gur / σ'_h	Gur / p'
2	11	1.7	21	28	36
2	11	1.5	19	26	33
3	12	0.5	28	36	45
6	24.2	1	58	92	104
7	24.9	0.9	46	64	74
9	36	1.2	73	104	104

Table 4.4. Normalized average secant cavity moduli.

Test N°	Depth	Gur(.1%) (MPa)	$\frac{Gur(1\%)}{\sigma'_h}$	$\frac{Gur(1\%)}{P'}$	Gur(.2%) (MPa)	$\frac{Gur(.2\%)}{\sigma'_h}$	$\frac{Gur(2\%)}{P'}$
3	12	43	55	69	34	43	55
6	24.2	92.6	147	166	61	98	109
7	24.9	97	134	156	69	96	111
8	35.1	130	164	178	97	123	133
9	36.1	169	224	234	130	172	178

Table 4 5. Normalized reload cavity moduli.

depth	m	11	12	24.2	24.9	35.1		36.1		43.6	
u	kPa	-72.5	-62.7	56.8	63.7	163	0	173	0	247	0
σ_v	kPa	213	233	469.5	483	681	681	700	700	846	846
σ'_v	kPa	285.5	296	412	419	518	681	527	700	599	846
σ_h	kPa	655	720	685	785	870	870	840	840	880	880
σ'_h	kPa	727.5	782.7	628	721	707	870	667	840	633	880
Ko		2.5	2.6	1.5	1.72	1.36	1.27	1.26	1.2	1.05	1.04
q	kPa	-442	-487	-216	-302	-189	-189	-140	-140	-34	-34
p'	kPa	580	620	556	620	644	807	620	793	622	868
e		0.86	0.86	0.88	0.88	0.93		0.93		0.88	
L.I.		0.07	0.07	0.10	0.10	0.13		0.13		0.11	

Table 4.6 Present volume-stress state of the clay down borehole A.

STAGE	Ko FORMULA	PARAMETERS	K_o
1	Eq. (4.25)	$\phi'_{cs} = 23°$	0.61
2	Eq. (4.38)	a = 0.38	$0.61 \times OCR^{0.38}$
3	Eq. (4.39)	$\phi'_{cs} = 23°$	$0.61\left(0.75+0.25\ OCR/OCR_{max}^{0.61}\right)$
4	Eq. (4.38)	a = 0.38	$0.61 \times OCR^{0.38}$

Table 4.7. K_0 values used in the modelling of the clay state-history.

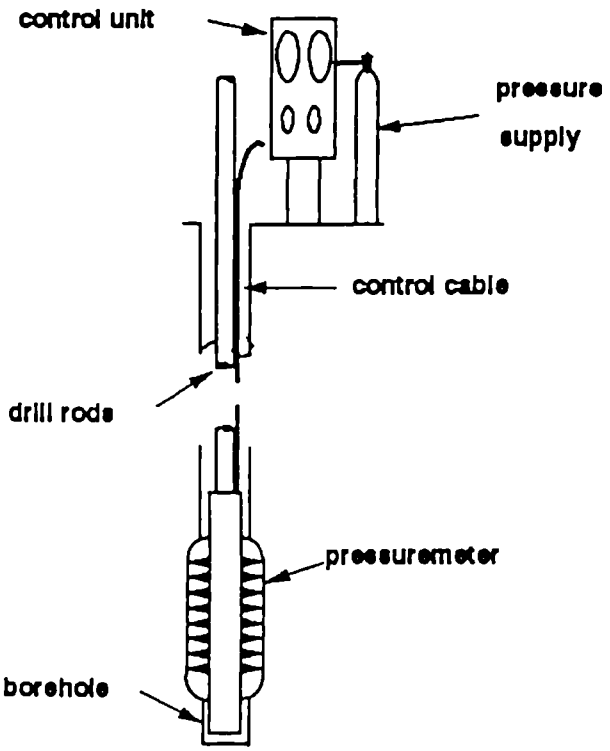

Fig.4.1 Scheme of a pressuremeter (after Clarke 1992).

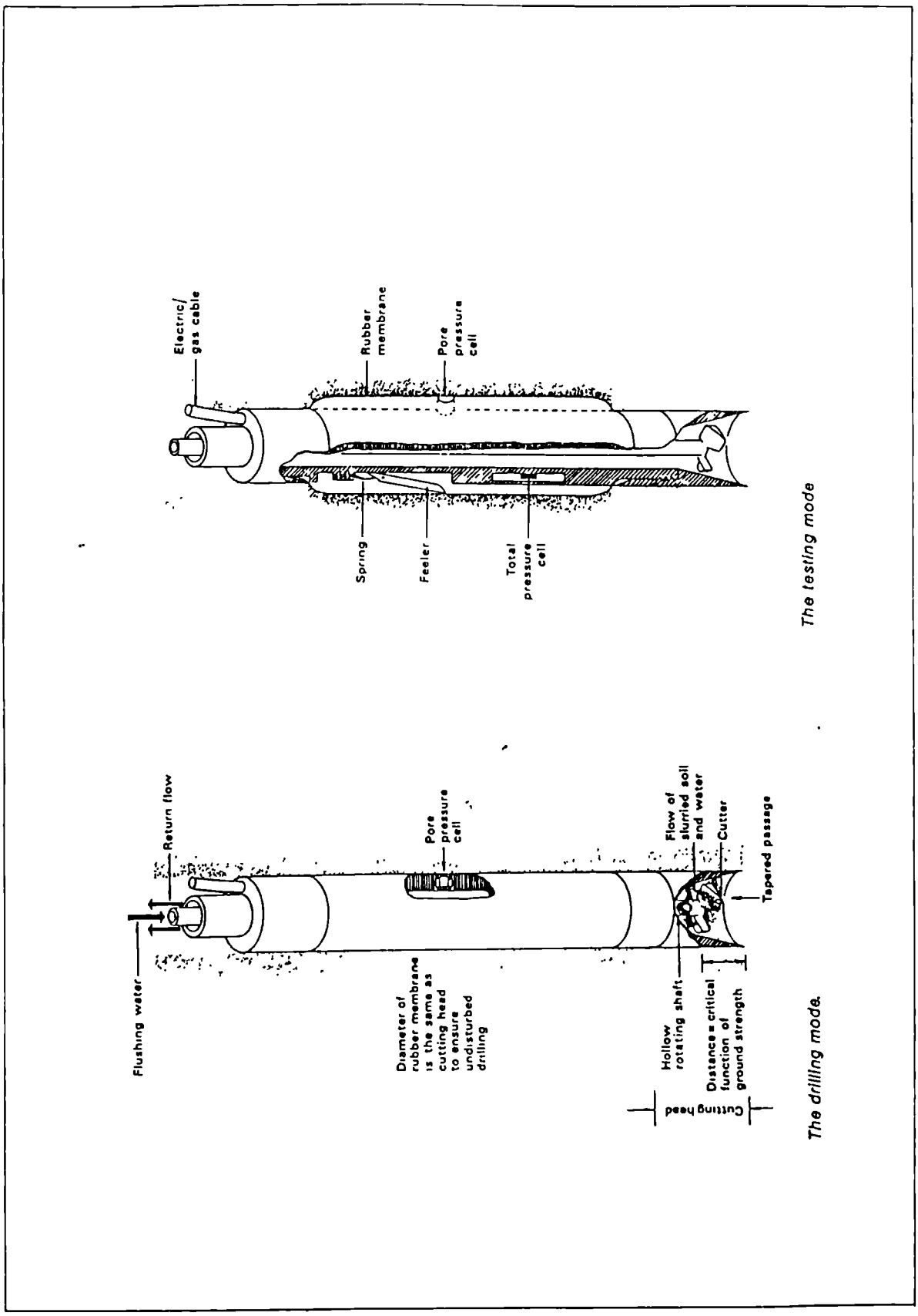

Fig.4.2 The Cambridge self-boring pressuremeter (after Windle and Wroth 1977).

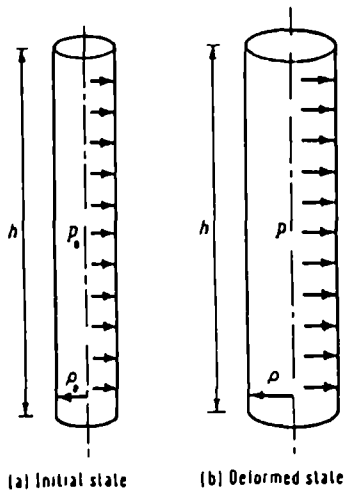

Fig.4.3 Pressuremeter cavity (after Mair and Wood 1987).

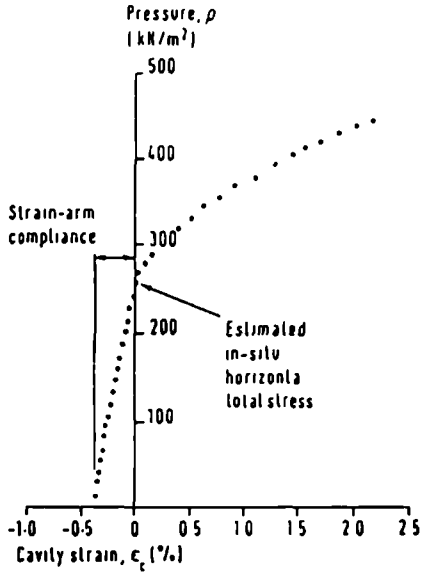

Fig.4.4 Measurement of the lift-off pressure (after Mair and Wood 1987).

ϱ_i : cavity radius at installation

P_{o1}, P_{o2}, P_{o3}: lift-off pressures

1)

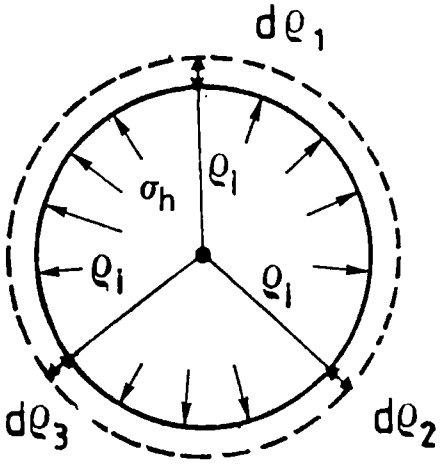

AXIALLY SYMMETRIC STATE OF STRESS

$d\varrho_1 = d\varrho_2 = d\varrho_3$

$P_{o1} = P_{o2} = P_{o3} = \sigma_h$

2)

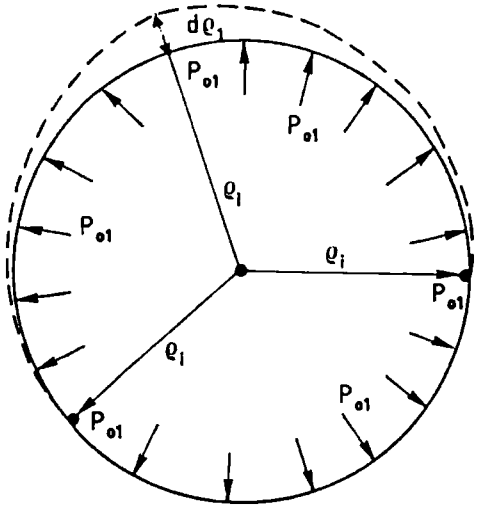

ANISOTROPIC STATE OF STRESS

$P_{o1} < P_{o2} < P_{o3}$

Fig.4.5 Possible cavity deformations at lift-off.

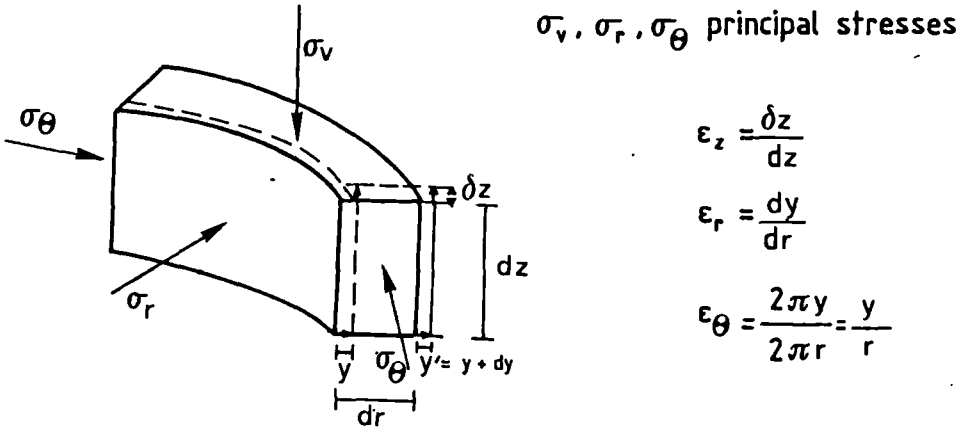

Fig.4.6 Stress-strain conditions for an element of soil in cylindrical symmetry.

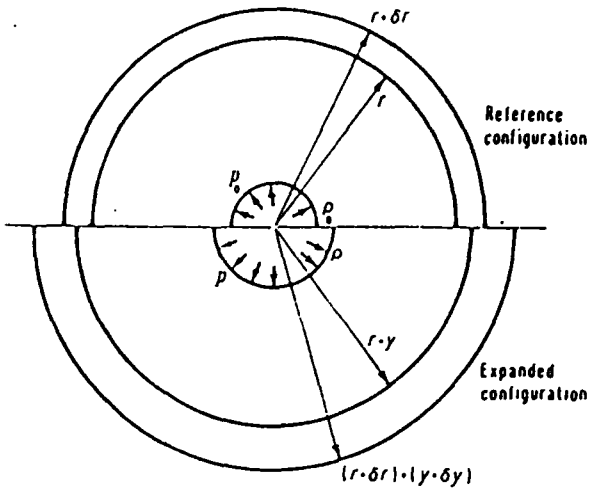

Fig.4.7 Deformation of soil during the expansion of a cylindrical cavity (after Mair and Wood 1987).

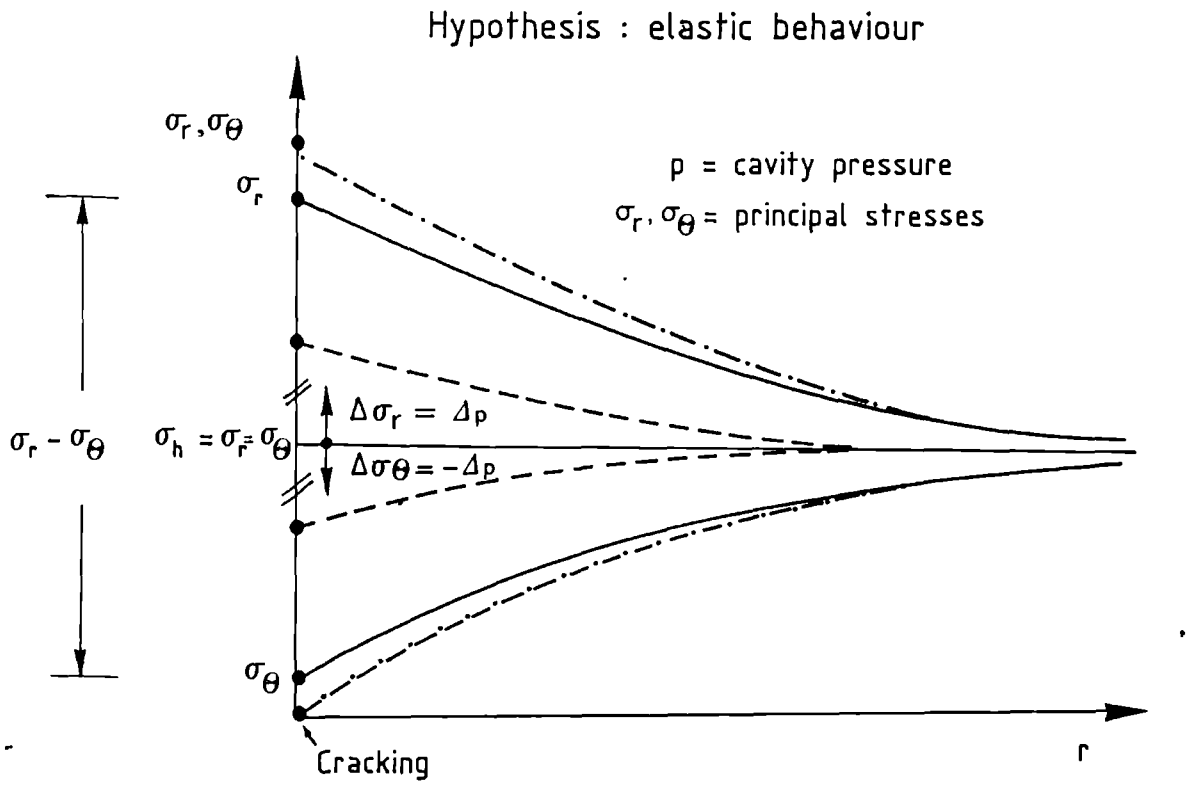

Fig.4.8 Stresses around expanding cavity in elastic soil.

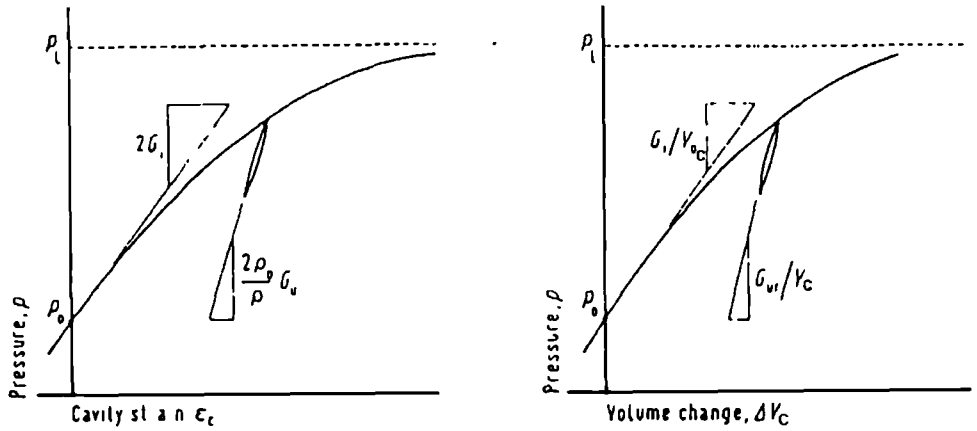

Fig.4.9 SBP test curves in terms of cavity strain and volume change (after Mair and Wood 1987).

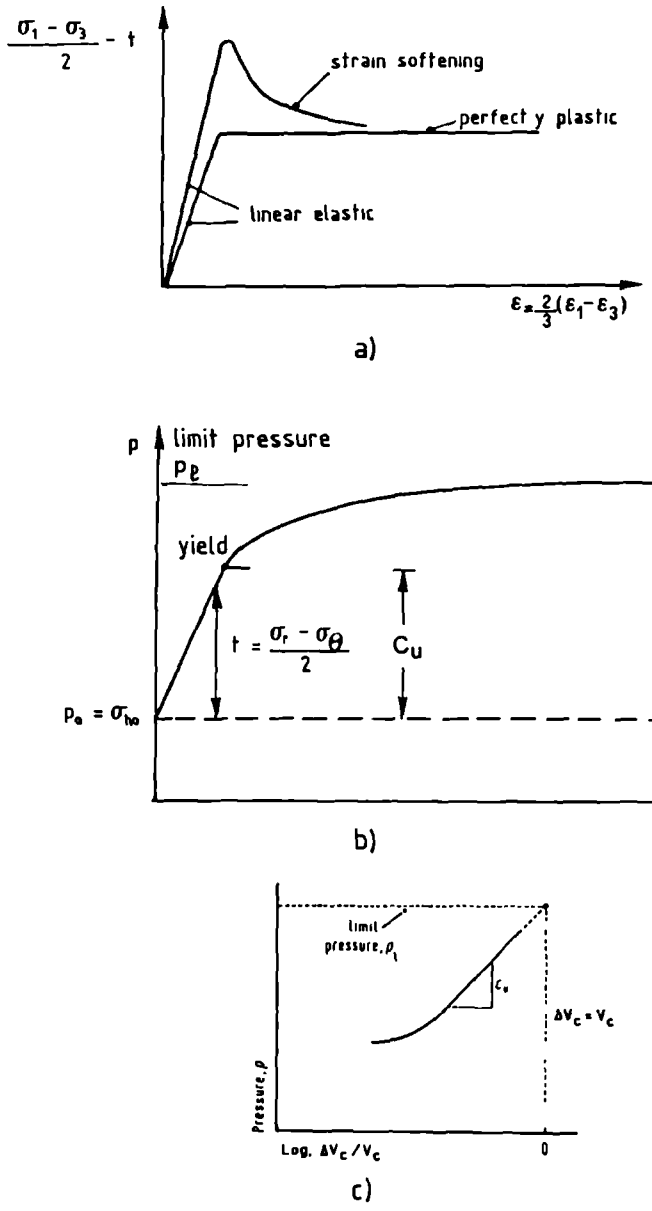

Fig.4.10 (a) Ideal soil behaviour; (b) relation between τ and ε_c during the pressuremeter expansion for a soil as in (a); (c) measurement of c_u (after Mair and Wood 1987) for an elastic-perfectly plastic soil (see (a)).

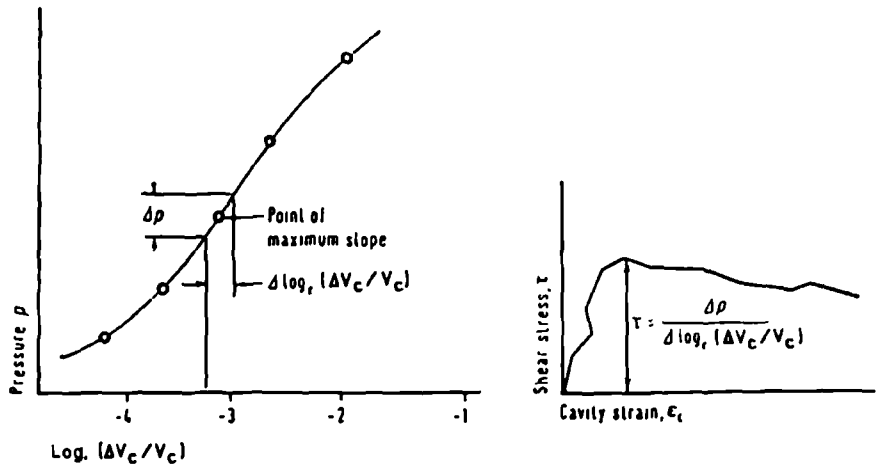

Fig.4.11 τ-ε_c curve resulting from a SBP test curve (after Mair and Wood 1987).

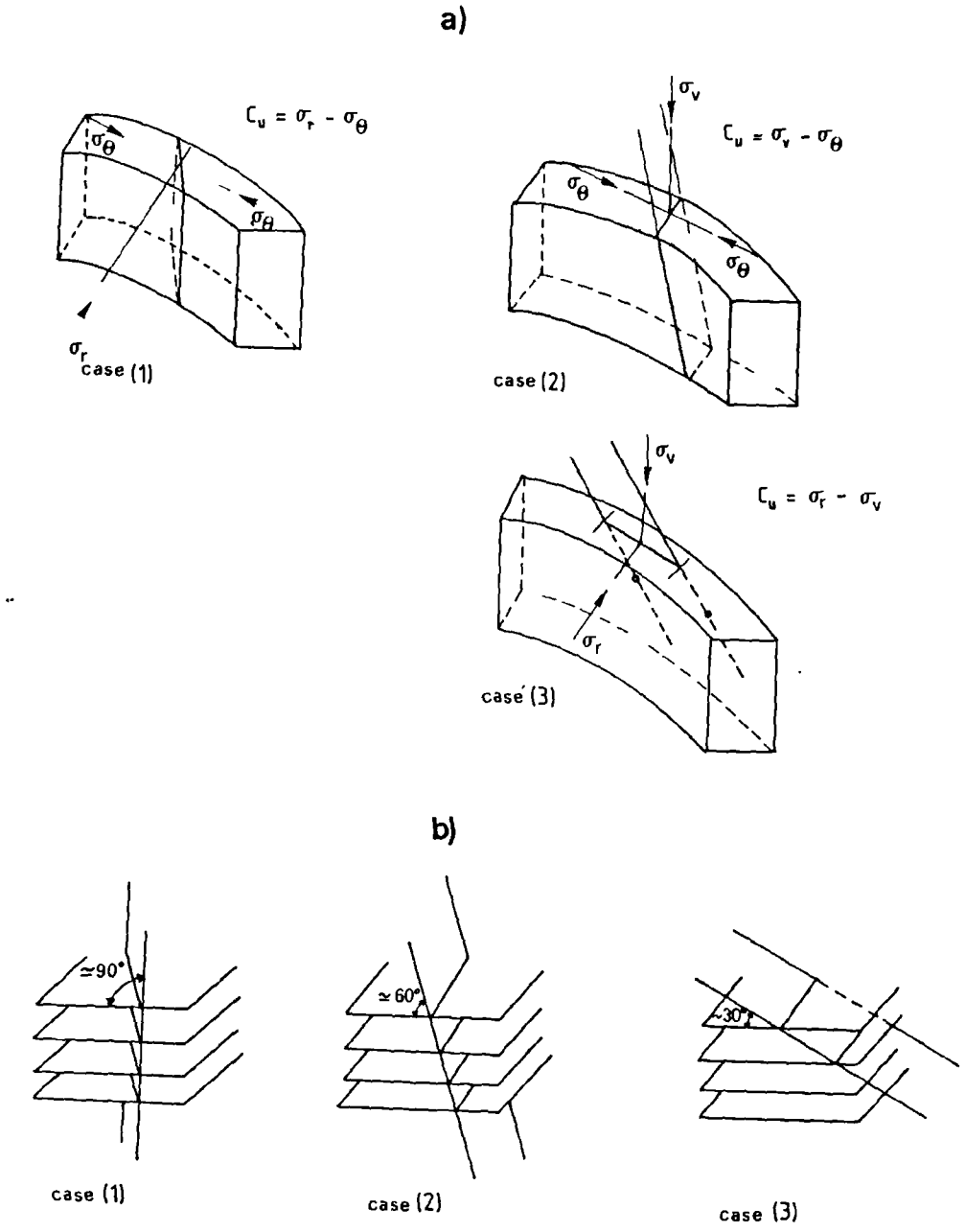

Fig.4.12 SBP testing : (a) possible failure planes; (b) inclination of the failure planes with respect to the lamination planes for the three modes of failure shown in (a).

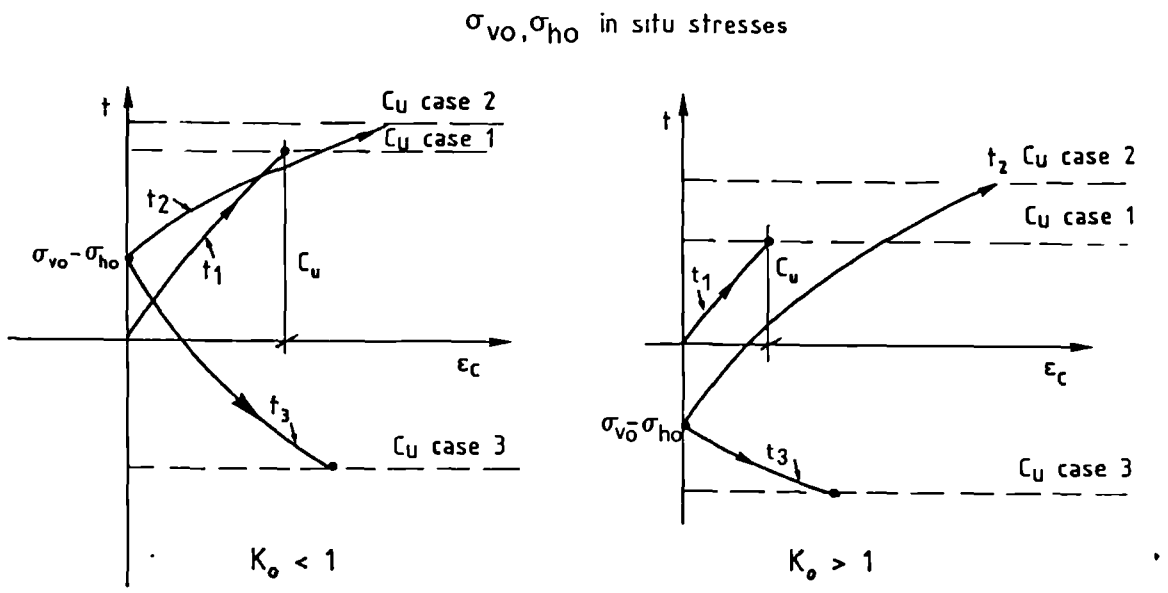

Fig.4.13 Possible t-ε_c paths during a SBP test.

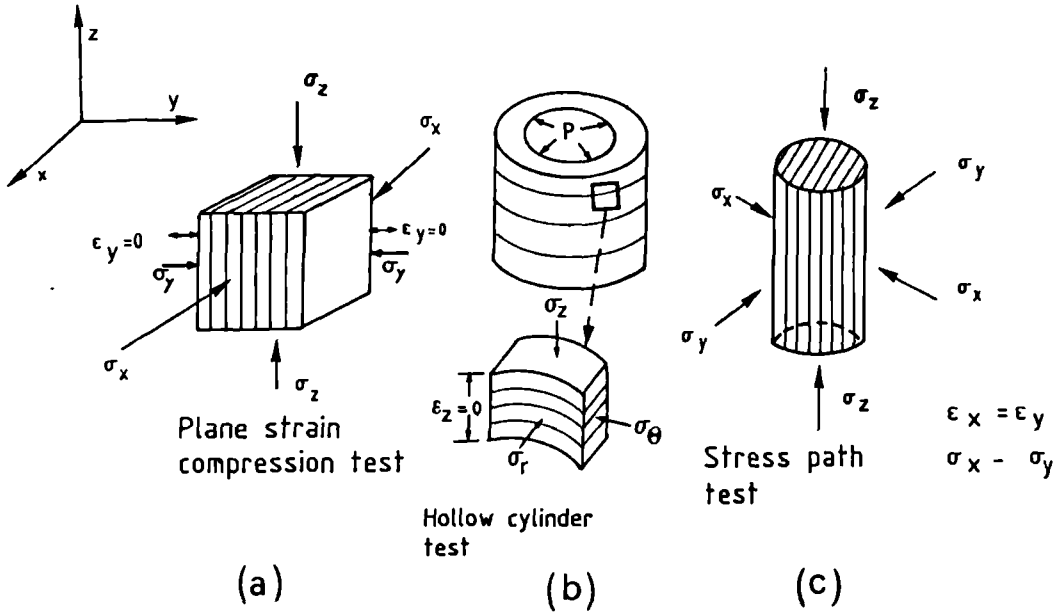

Fig.4.14 Loading of a laminated soil element in laboratory tests : (a) plane strain, (b) hollow cylinder and (c) triaxial test.

a)

b)

Fig.4.15 SBP testing at Pappadai : (a) SBP probe, (b) rotary rig.

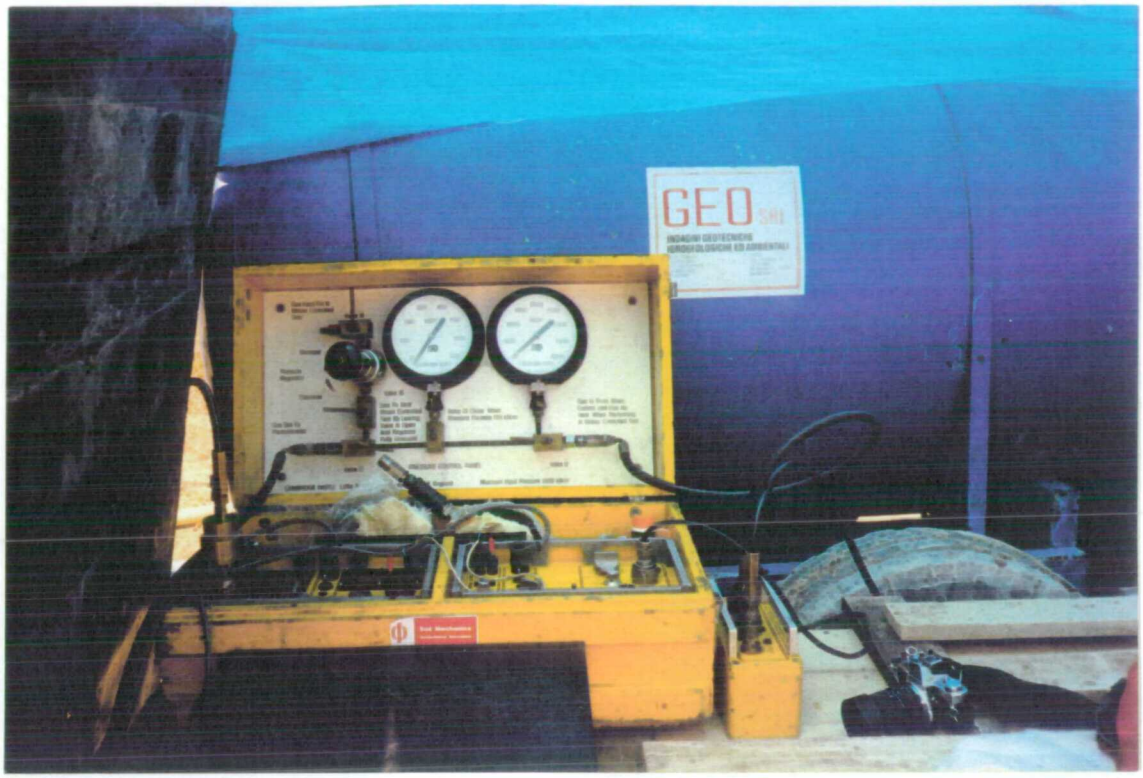

Fig.4.16 SBP testing at Pappadai : control and data logging system at the surface.

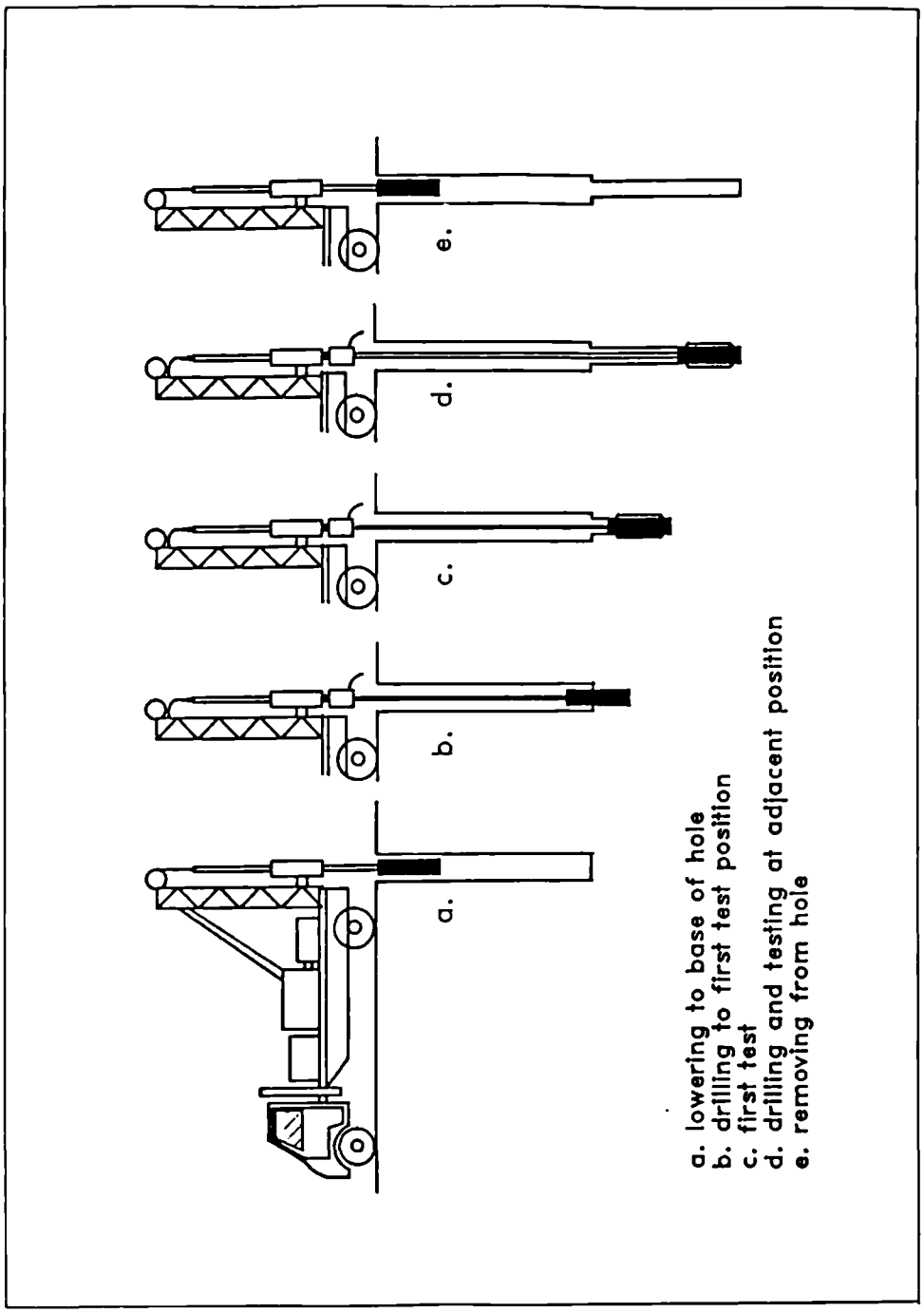

Fig.4.17 Drilling operations at Pappadai.

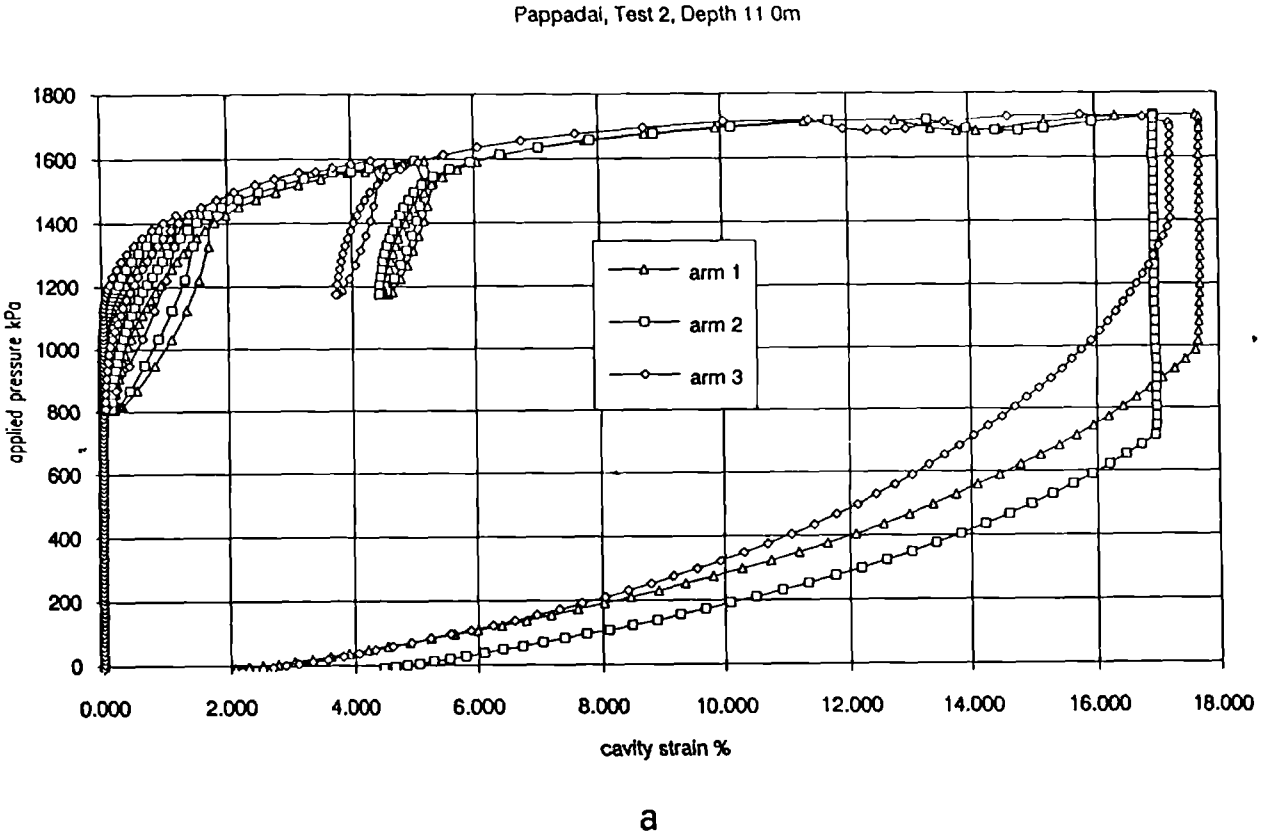

a

Fig.4.18 SBP testing at Pappadai : p-ϵ_c curves.

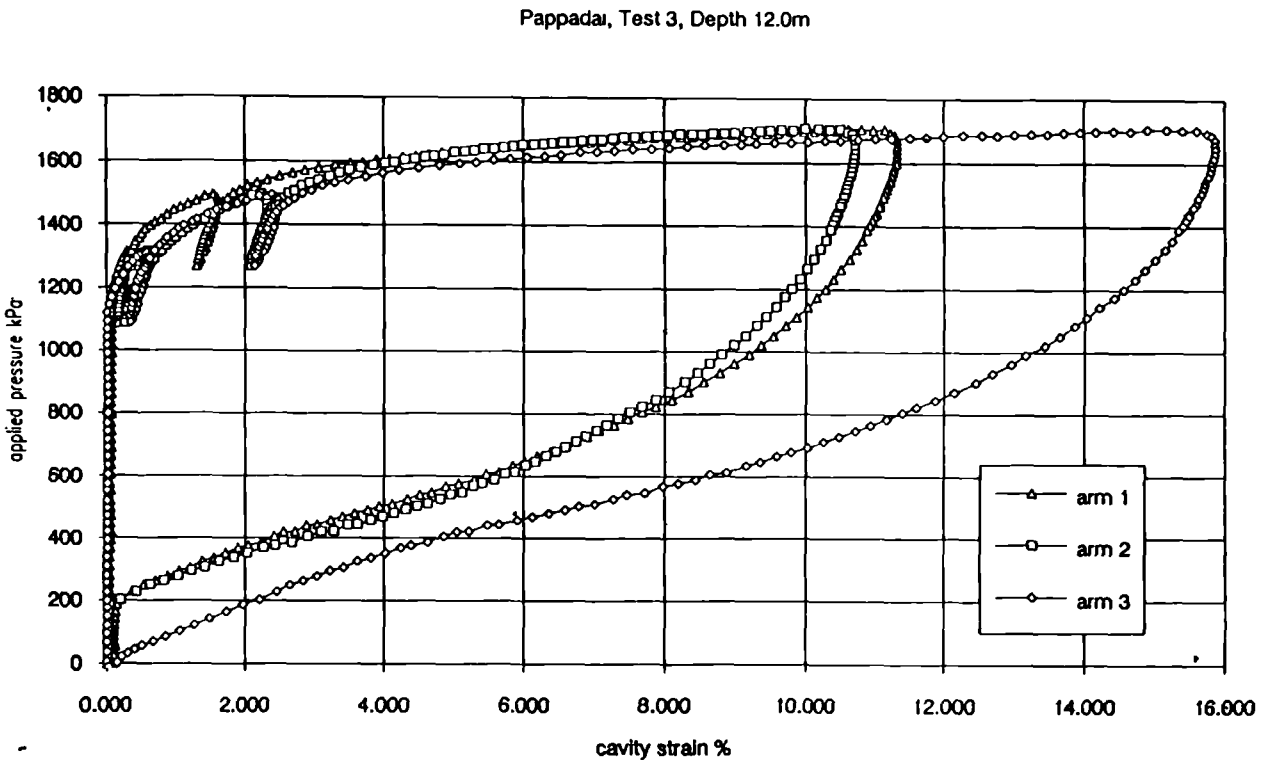

b

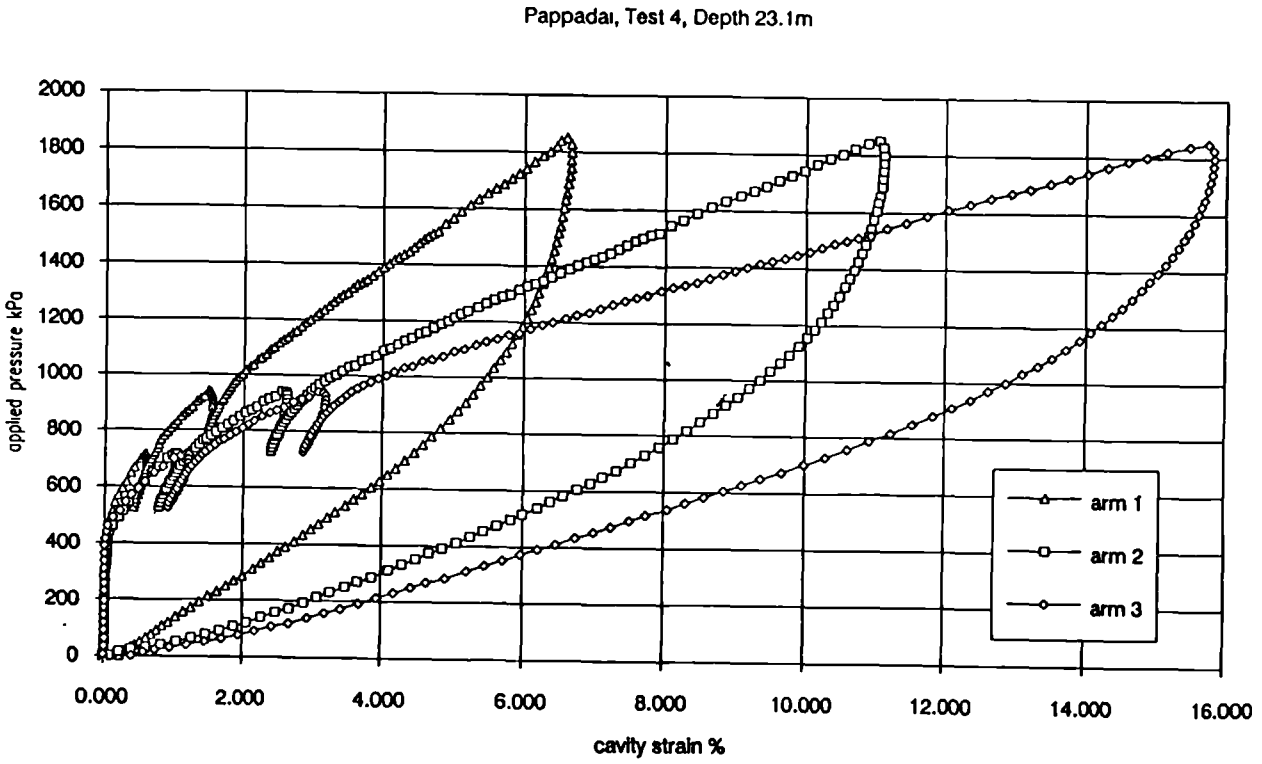

c

Fig.4.18 SBP testing at Pappadai : p-ϵ_c curves.

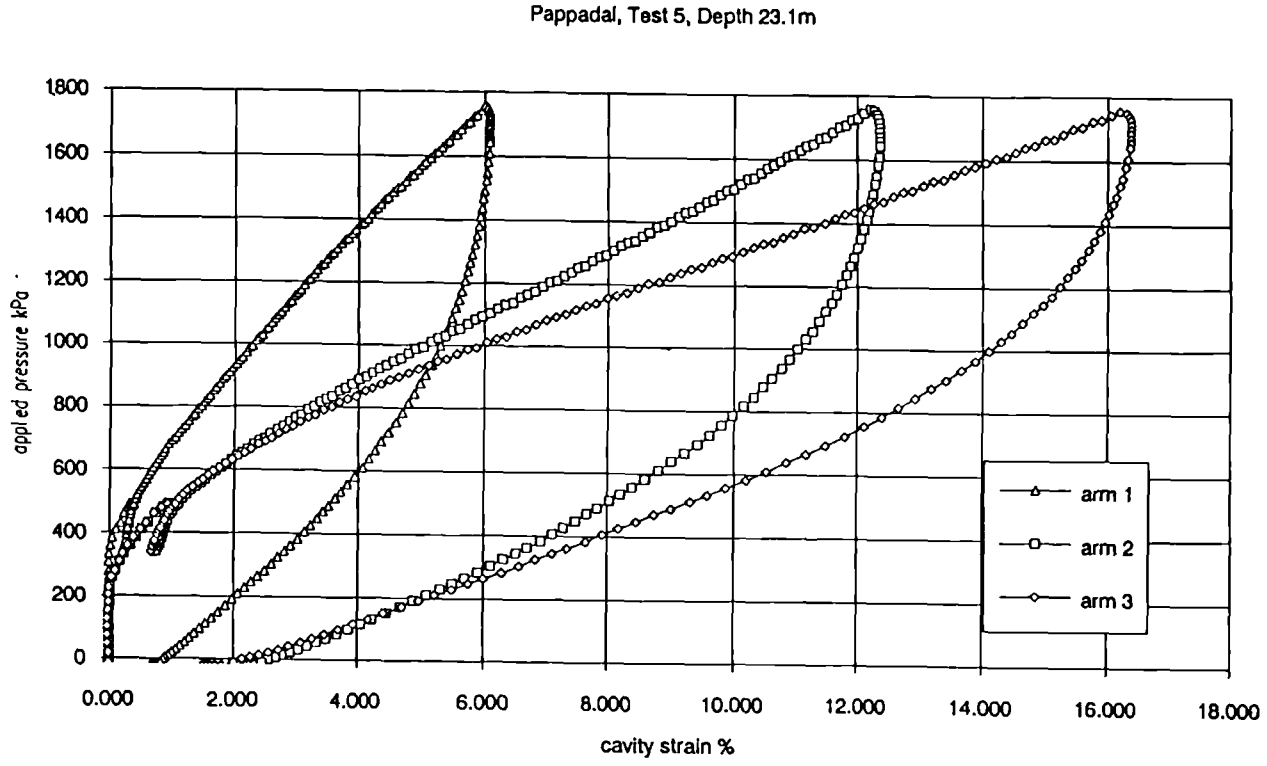

d

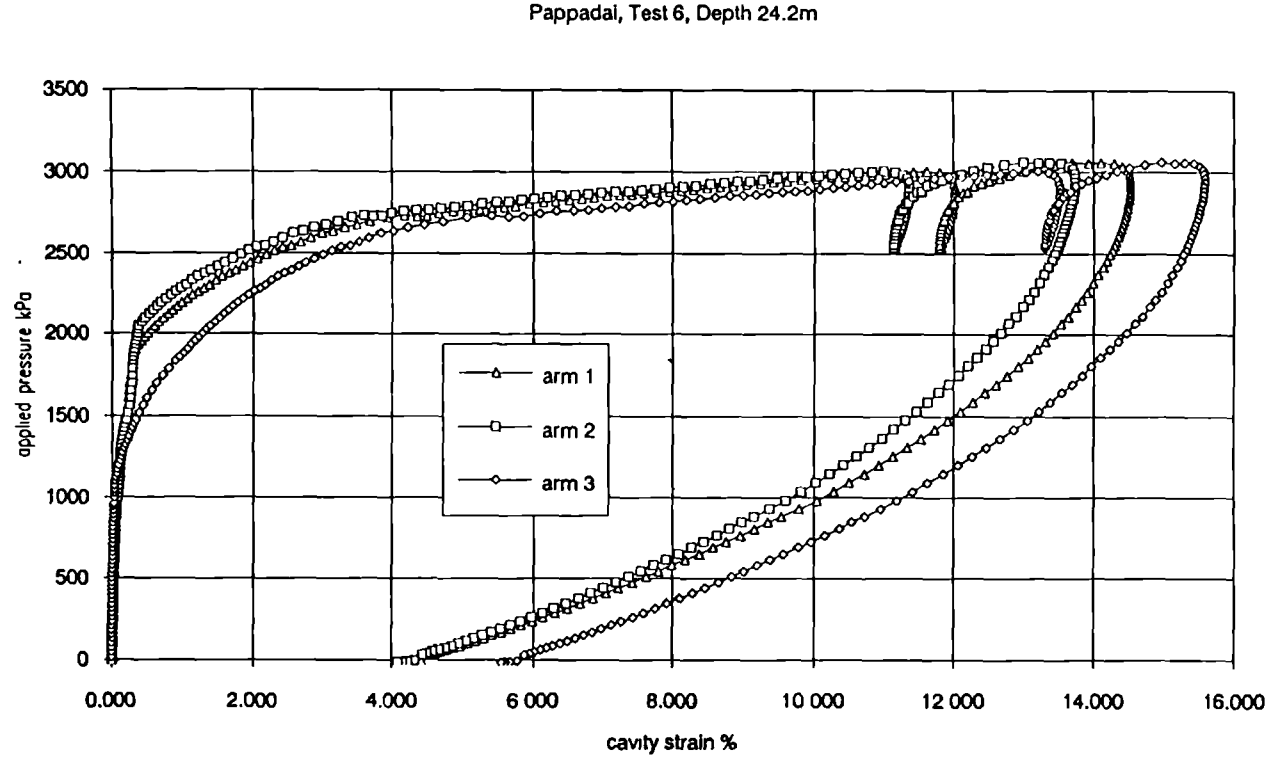

e

Fig.4.18 SBP testing at Pappadai : p-ε_c curves.

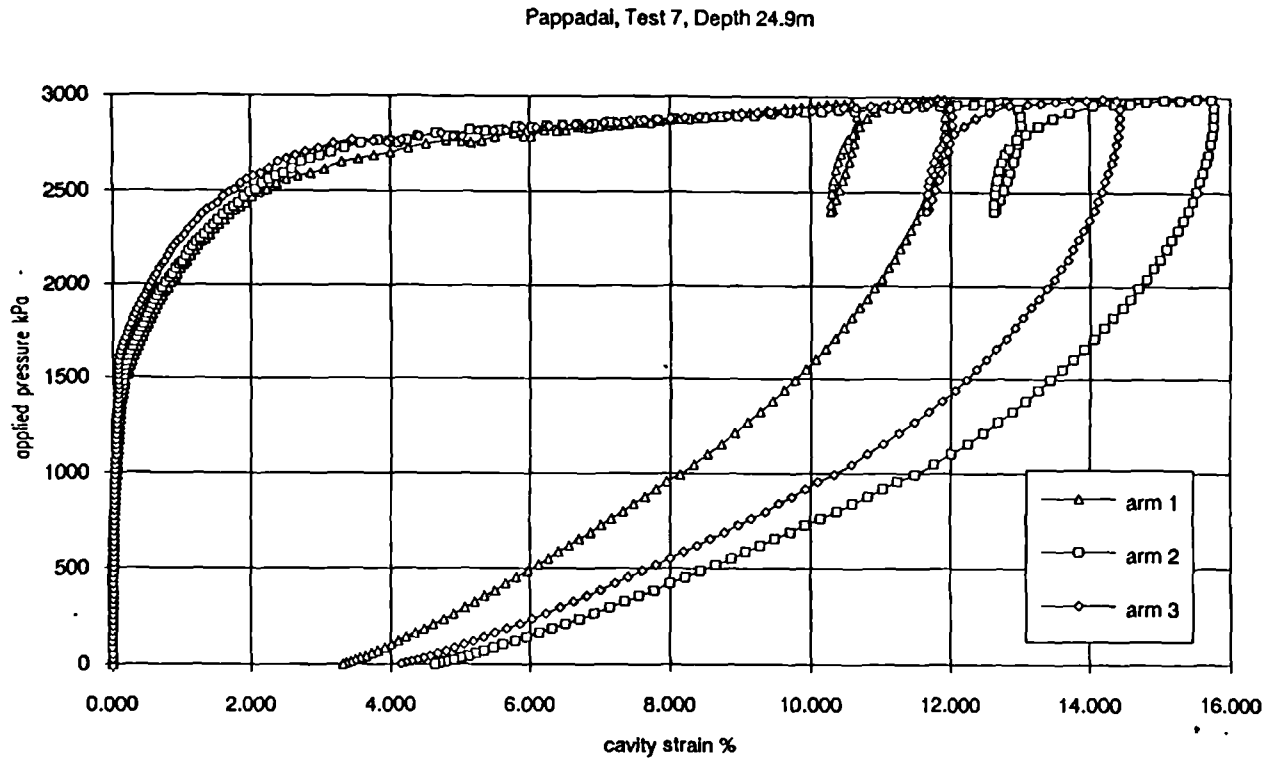

f

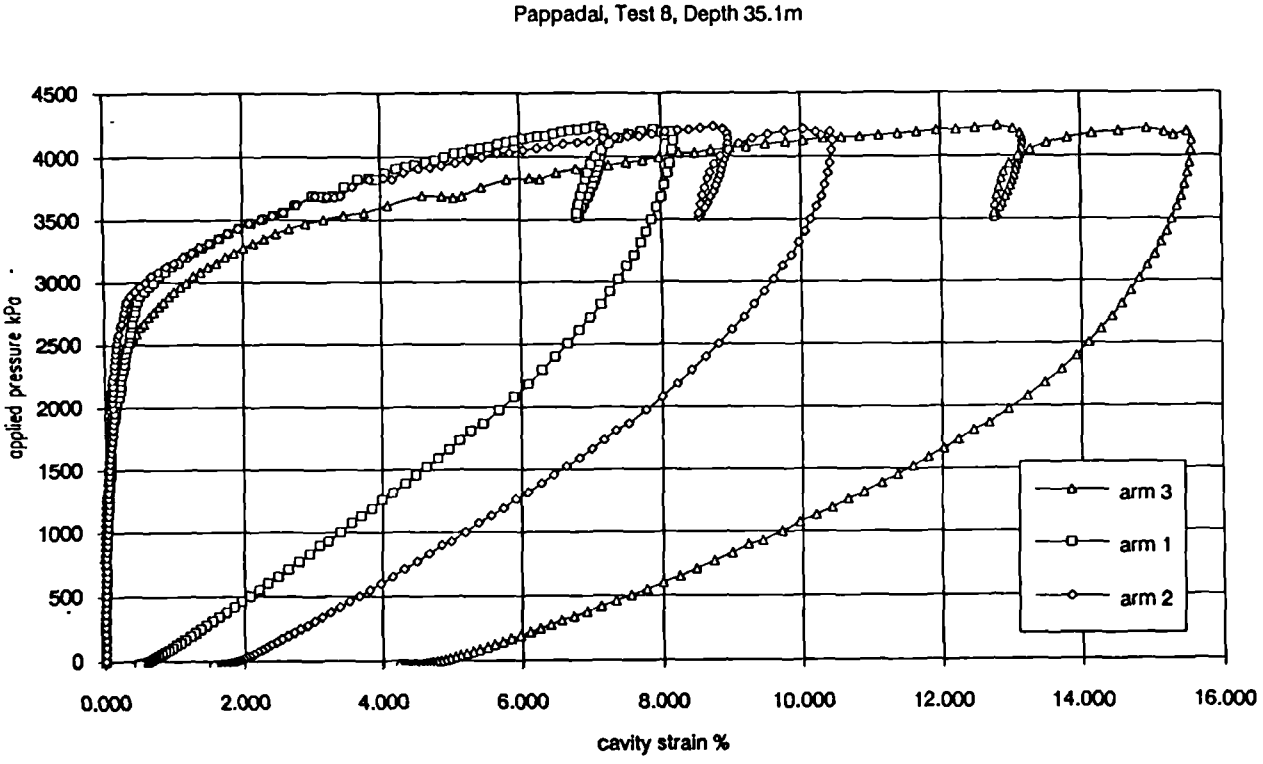

g

Fig.4.18 SBP testing at Pappadai : p-ε_c curves.

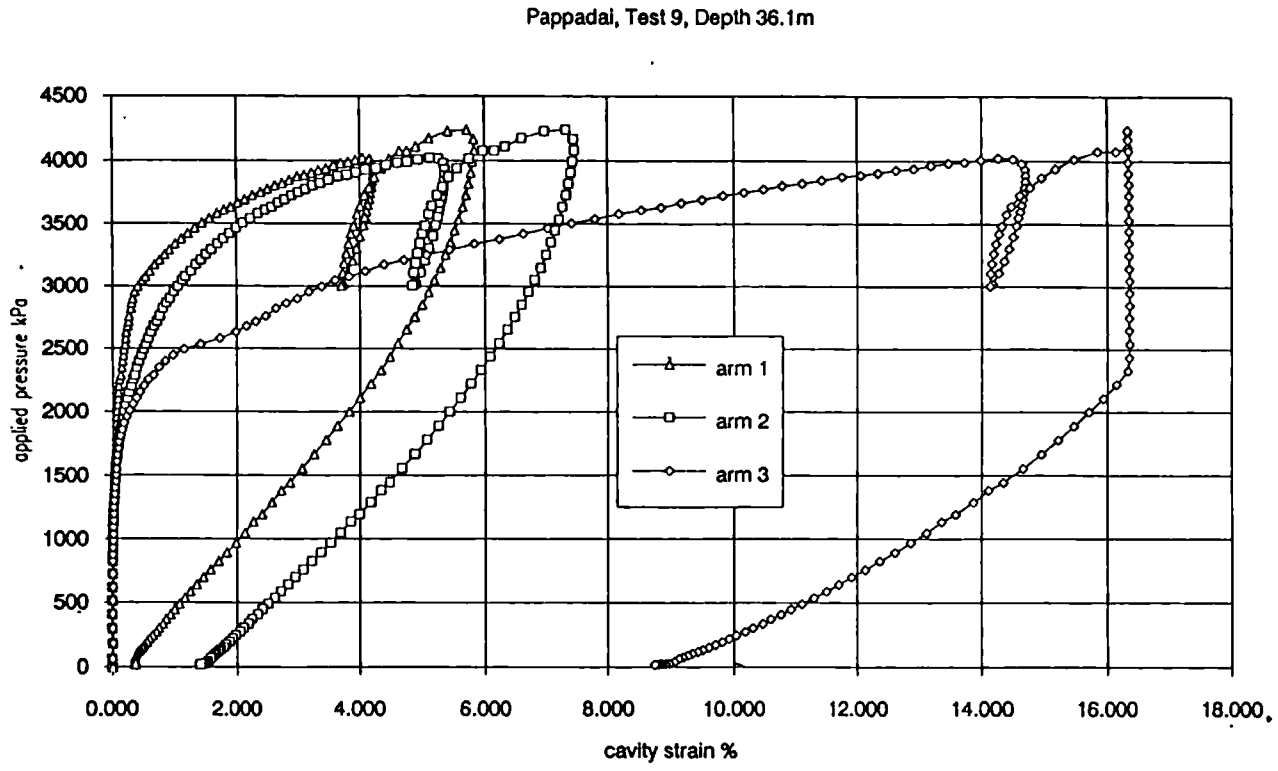

h

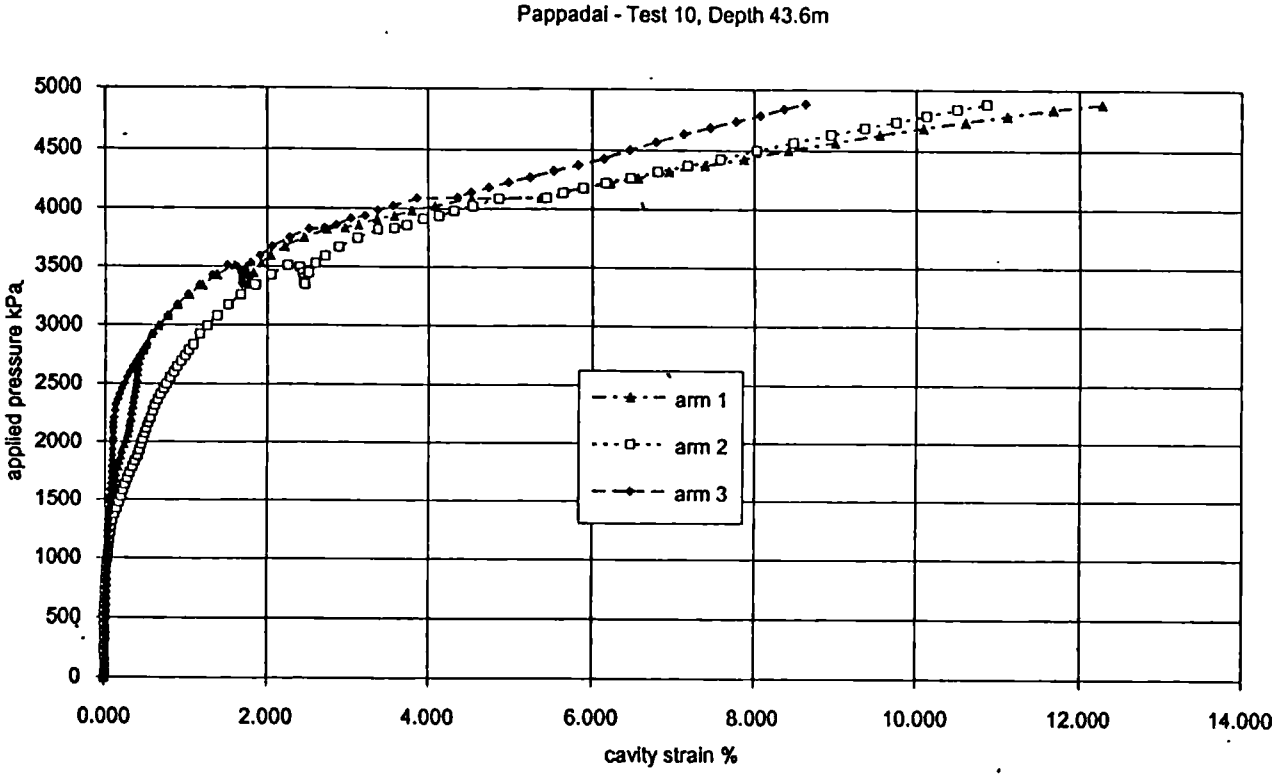

i

Fig.4.18 SBP testing at Pappadai : p-ϵ_c curves.

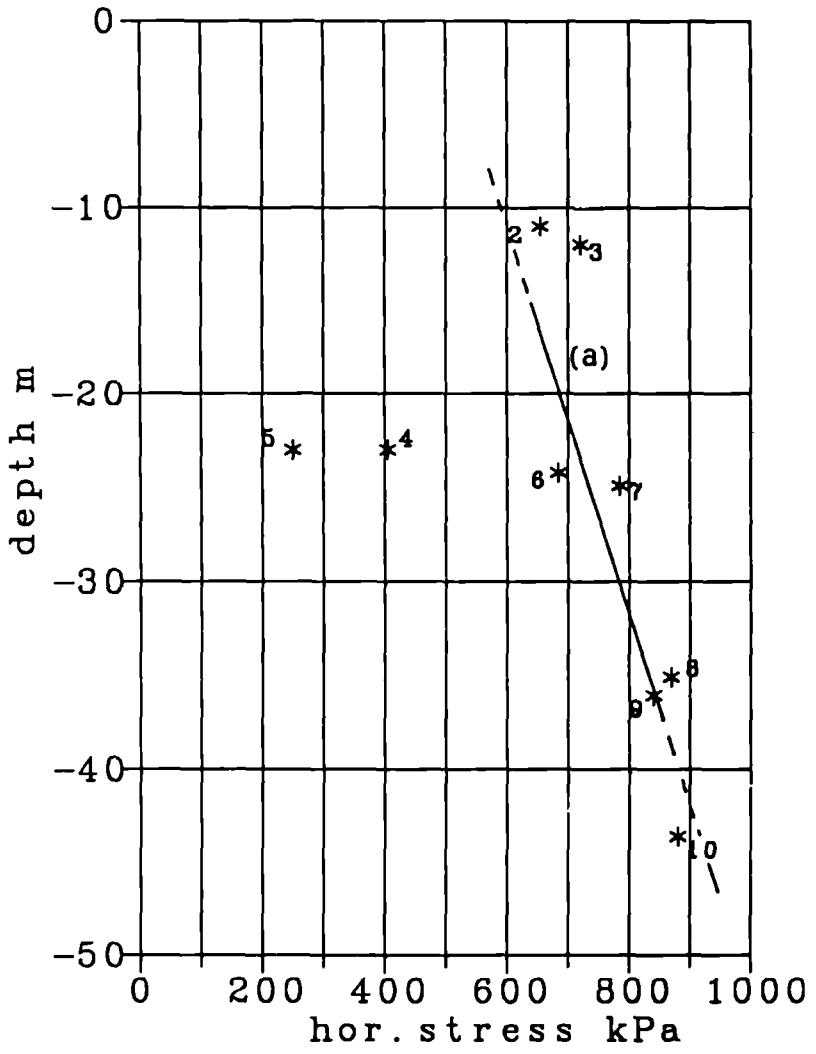

Fig.4.19 SBP testing at Pappadai : measured horizontal stresses σ_h; for each data point the test number is indicated.

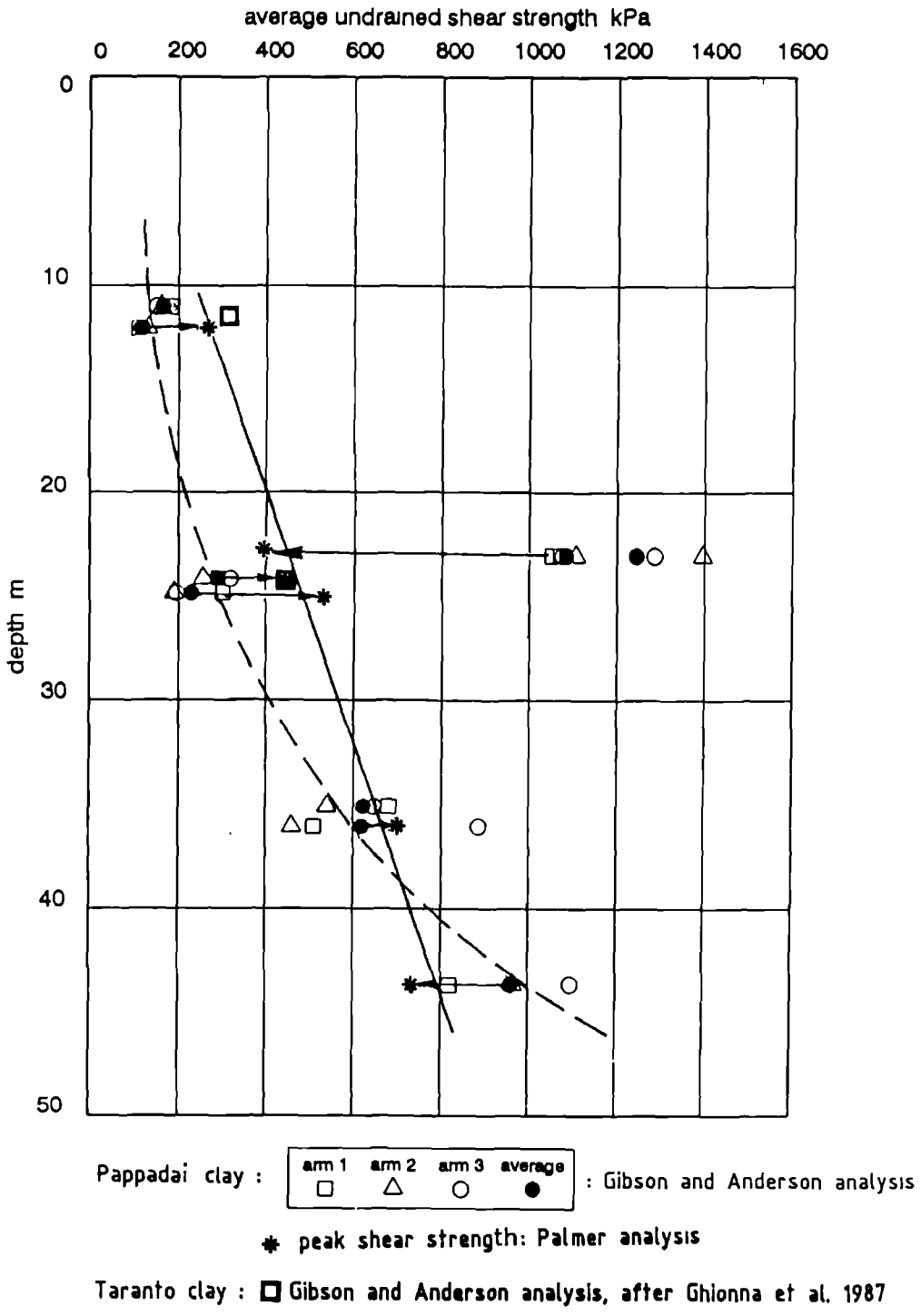

Fig 4.20 SBP testing at Pappadai : measured undrained shear strengths c_u.

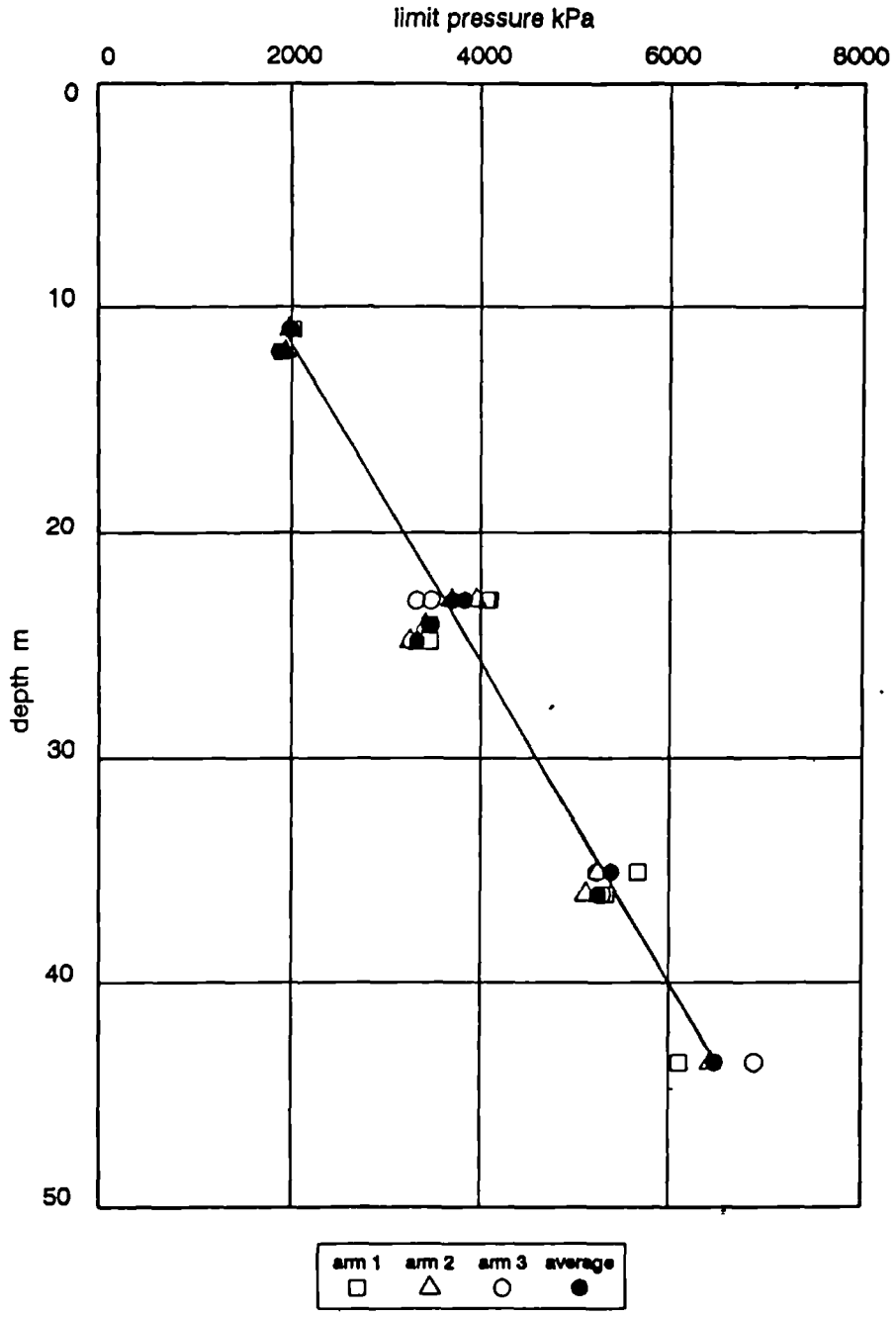

Fig.4.21 SBP testing at Pappadai : measured limit pressures.

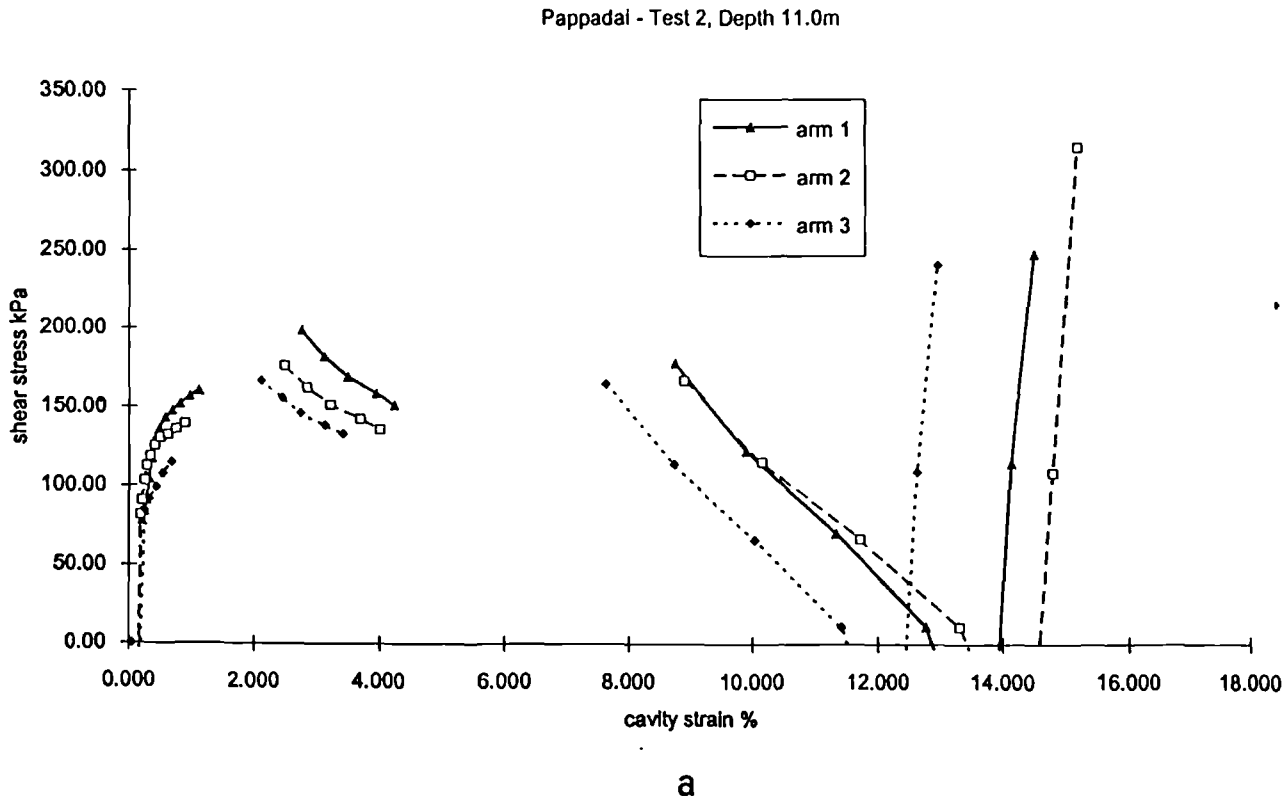

Fig.4.22 SBP testing at Pappadai : t-ε_c curves resulting from the Palmer analysis.

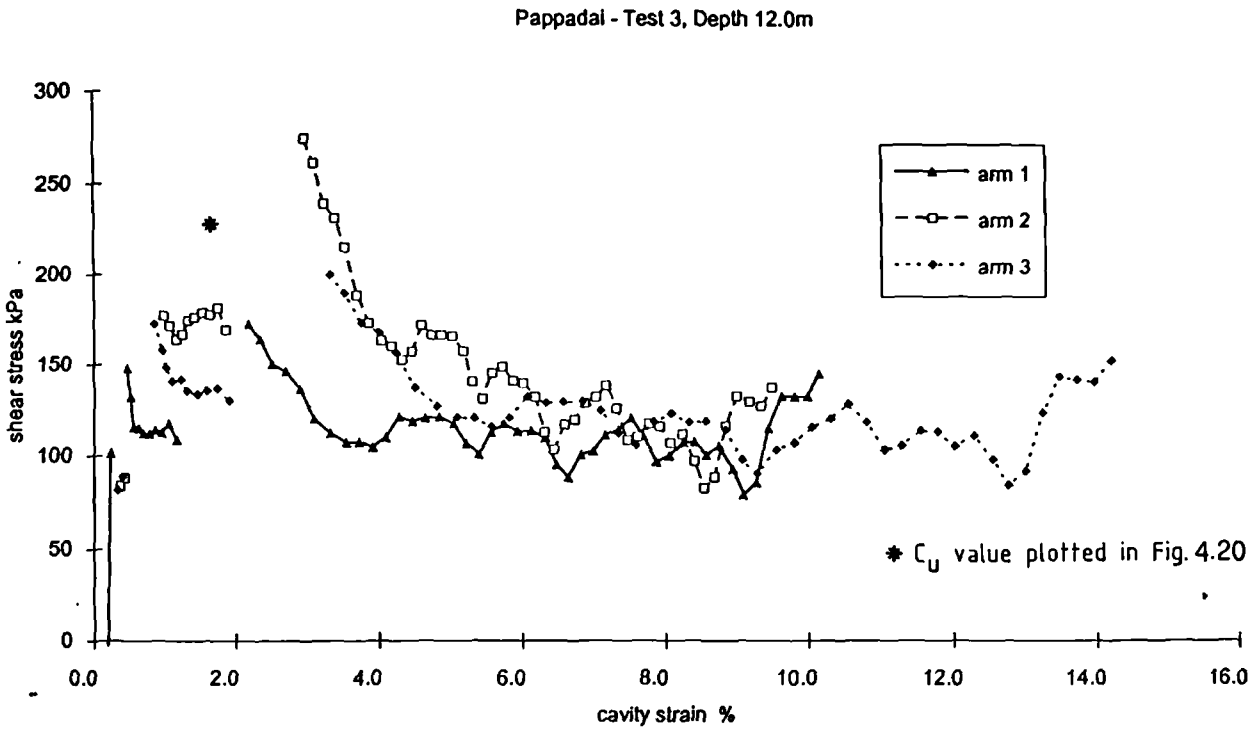

b

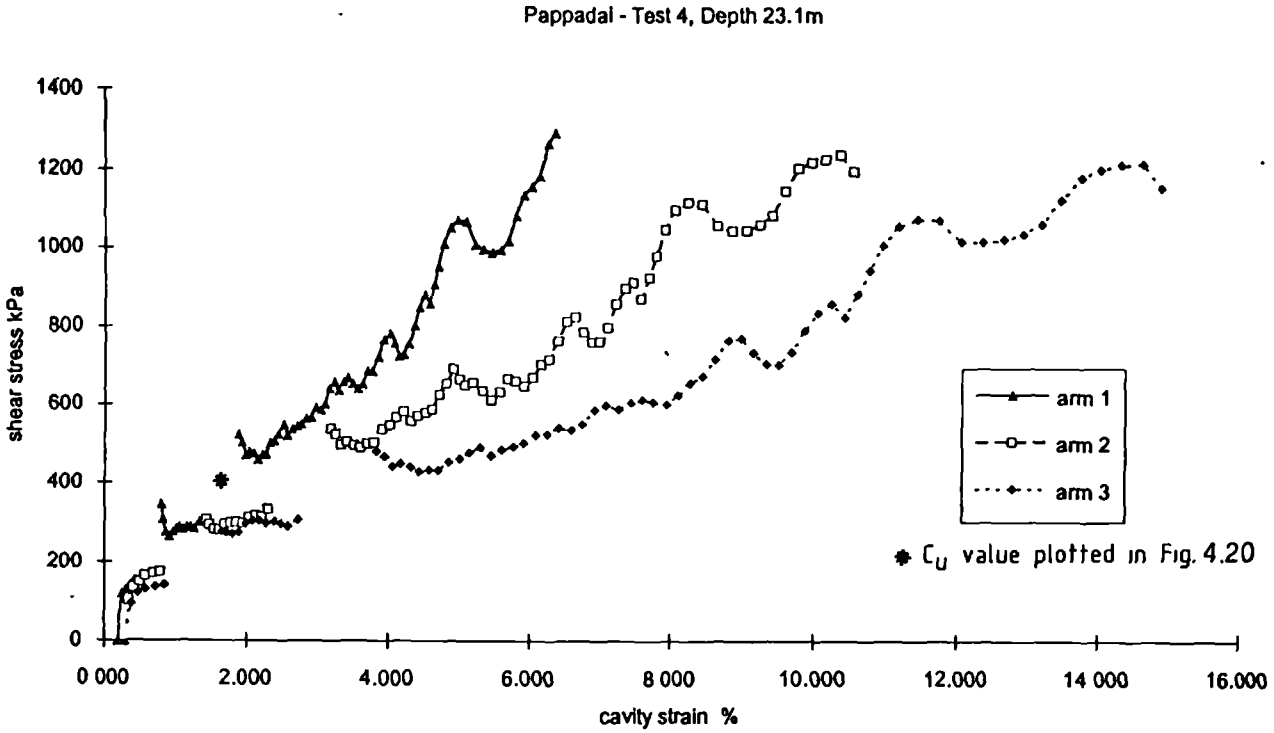

c

Fig.4.22 SBP testing at Pappadai : $\mathcal{L}$-ε_c curves resulting from the Palmer analysis.

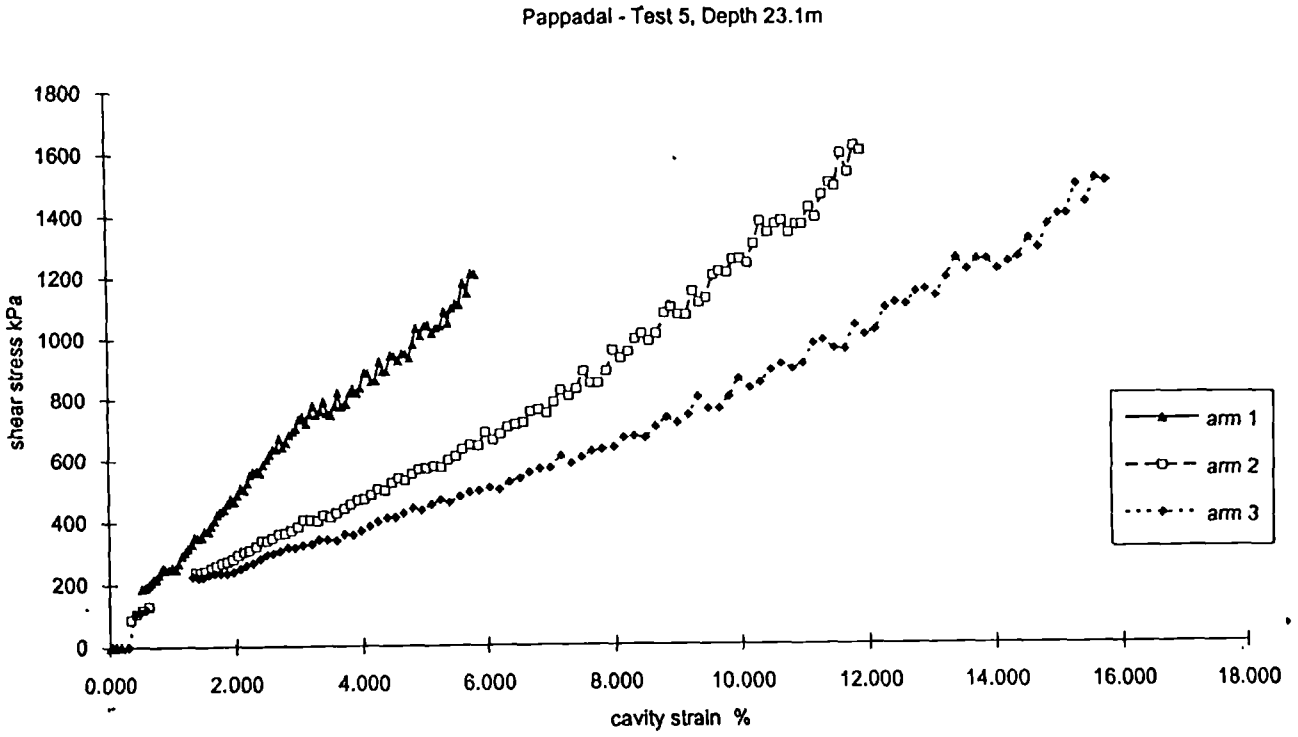

d

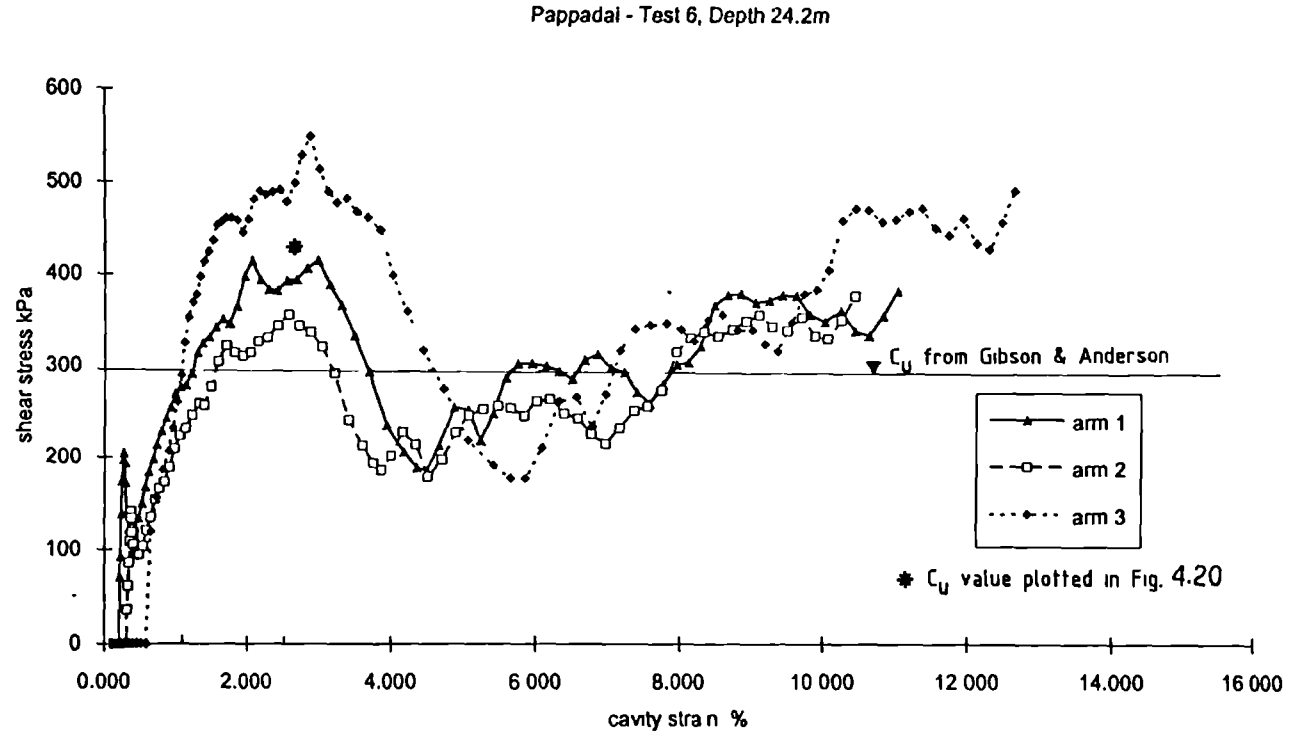

e

Fig.4.22 SBP testing at Pappadai : $\mathcal{L}$-ε_c curves resulting from the Palmer analysis.

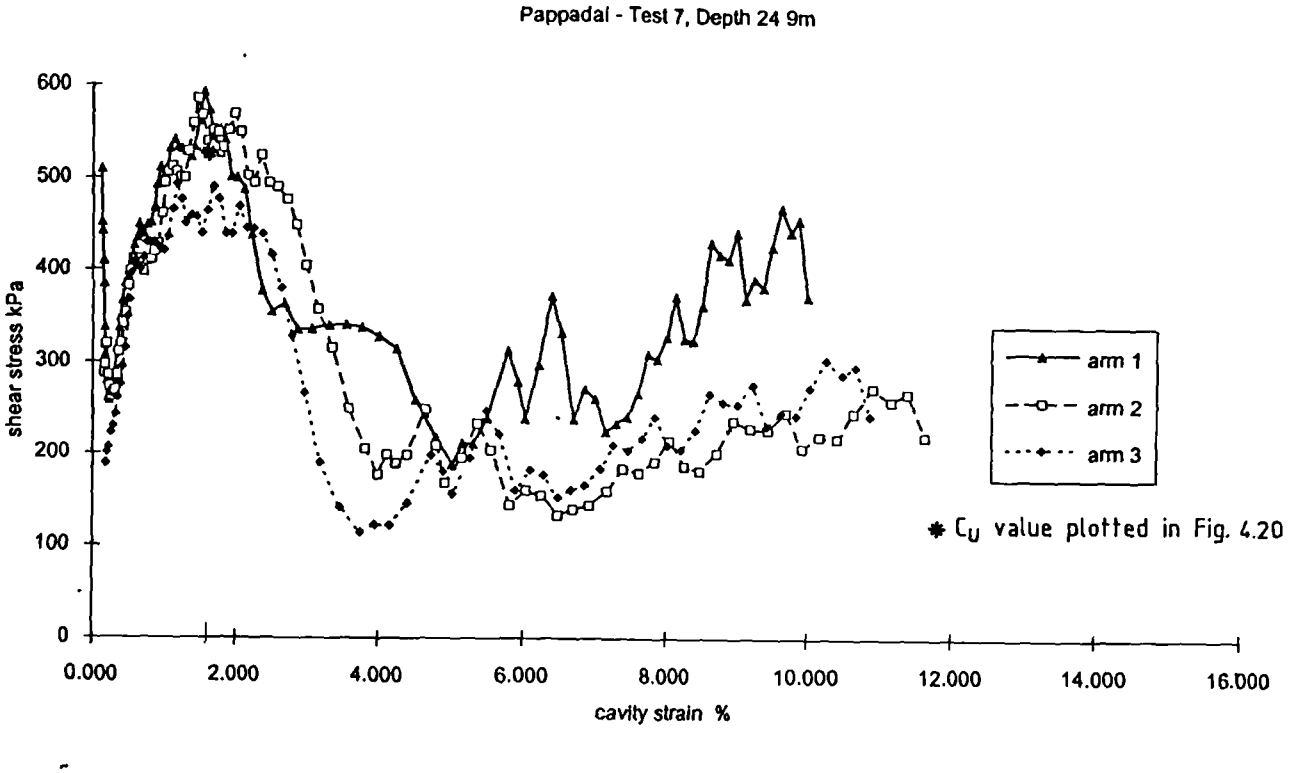

f

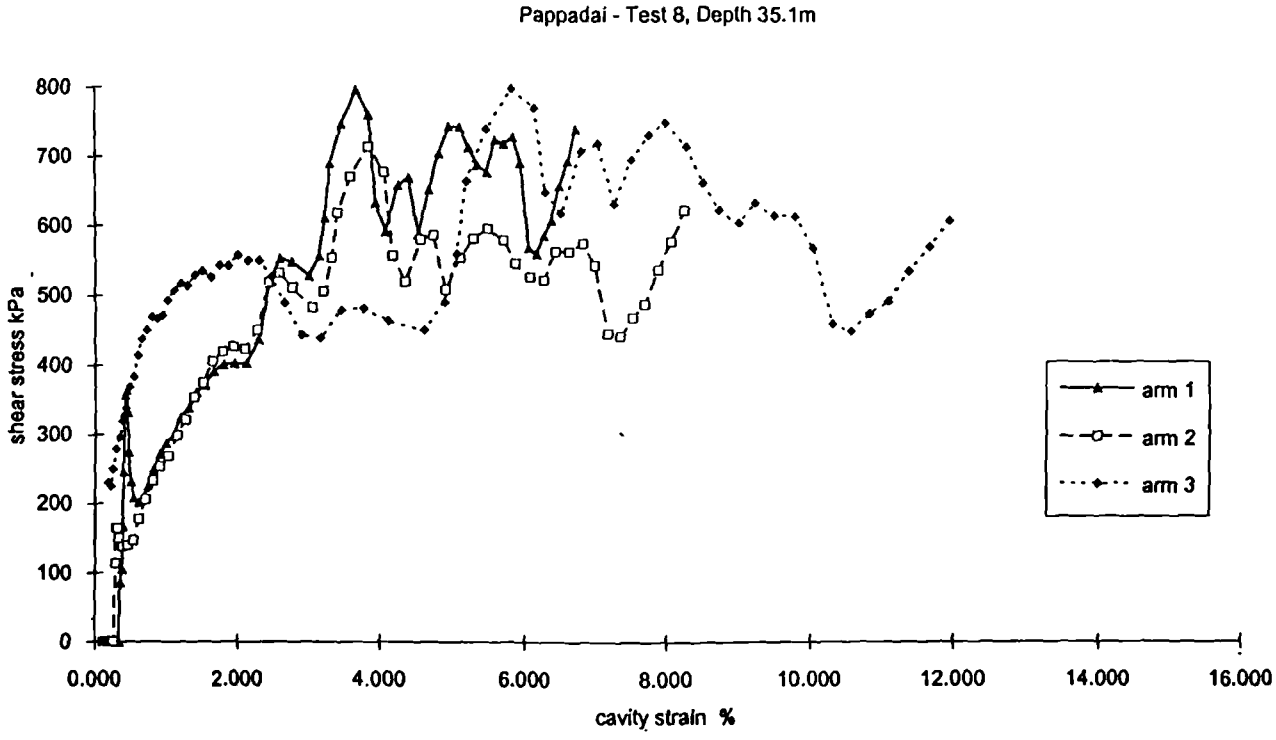

g

Fig.4.22 SBP testing at Pappadai : $\mathcal{L}$-ε_c curves resulting from the Palmer analysis.

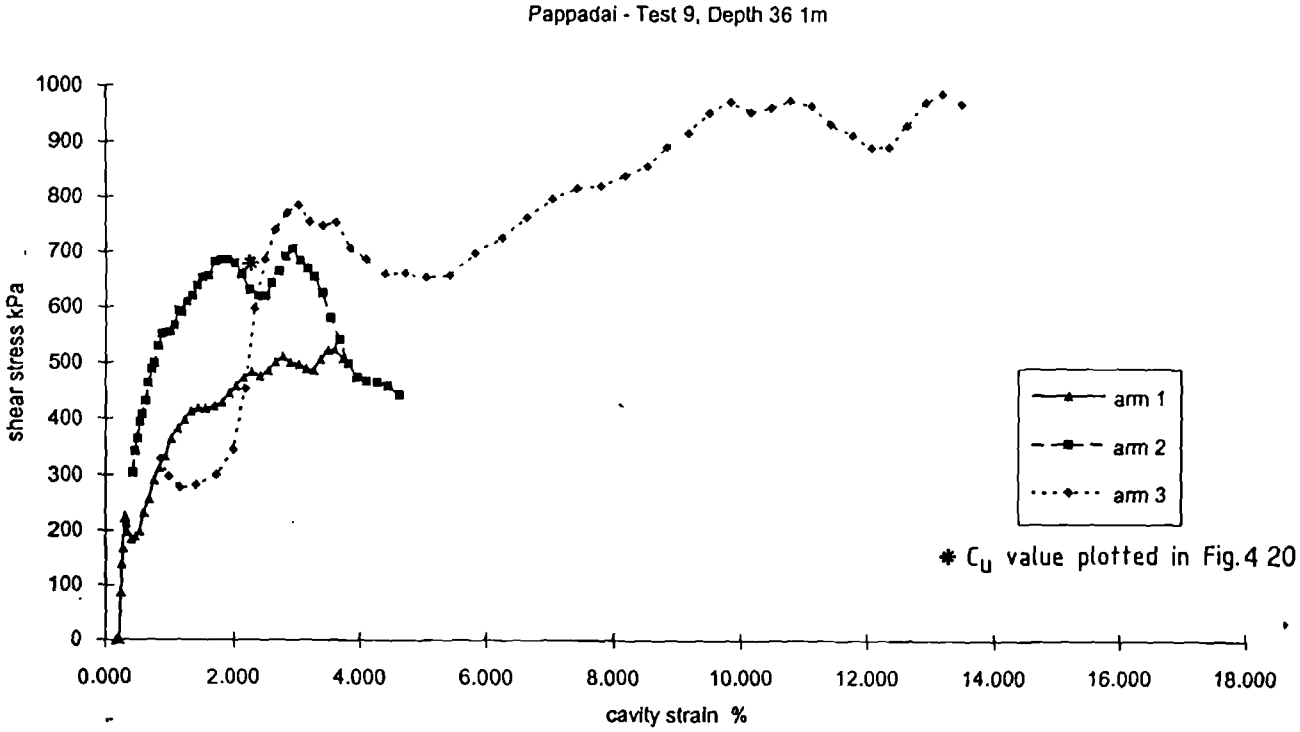

h

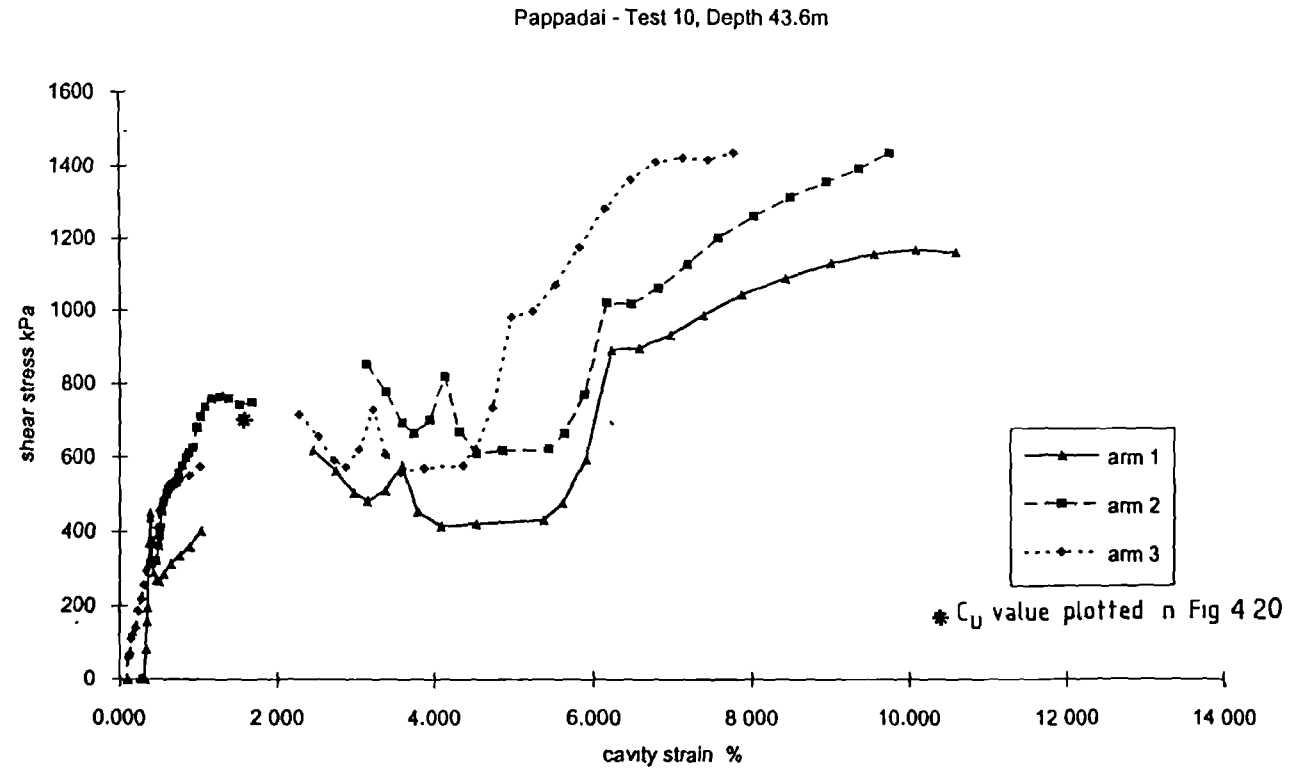

i

Fig 4 22 SBP testing at Pappadai : ϵ-ε_c curves resulting from the Palmer analysis.

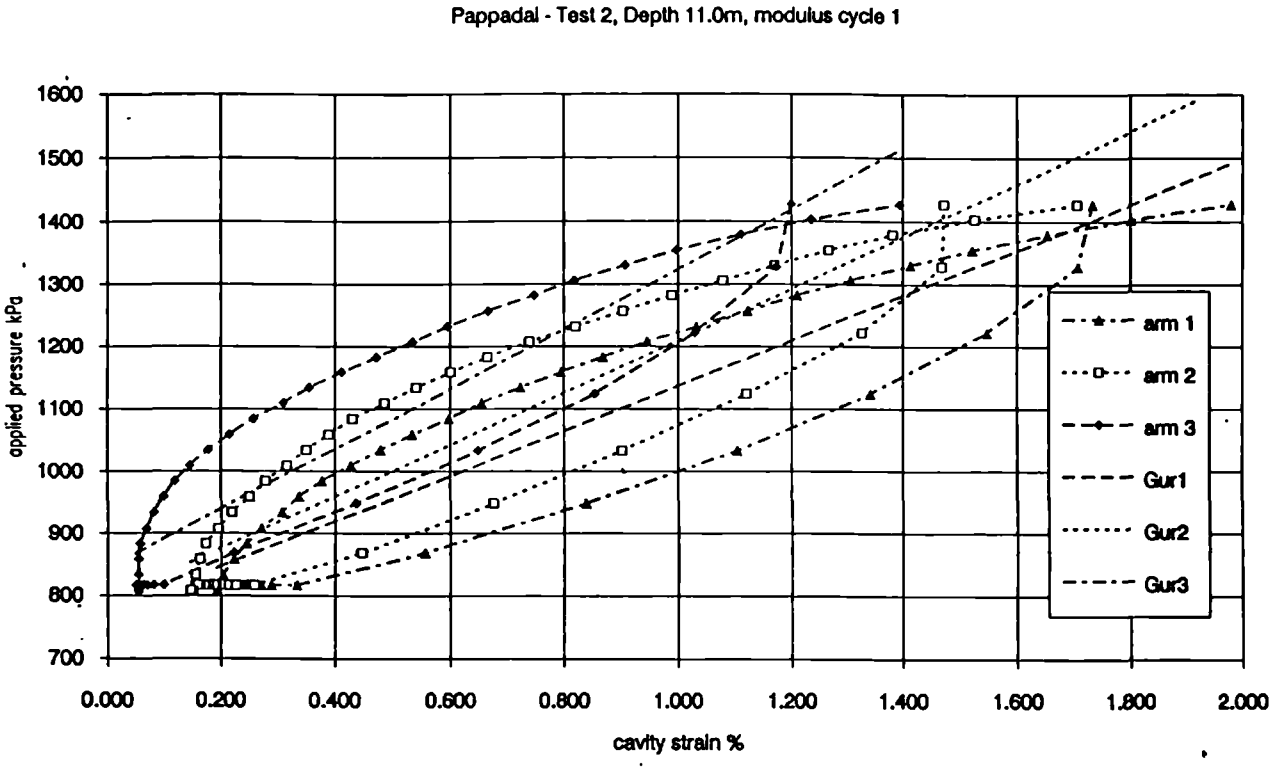

a

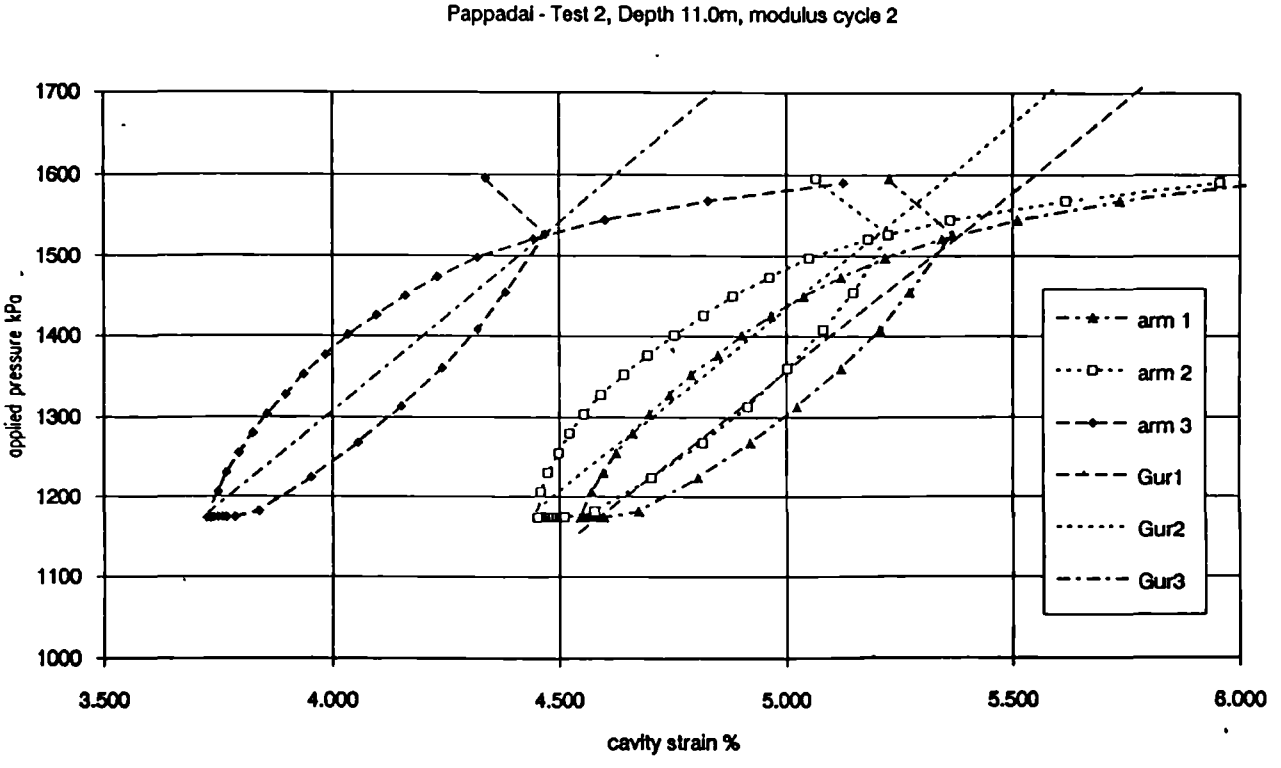

a

Fig.4.23 SBP testing at Pappadai : unload-reload loops.

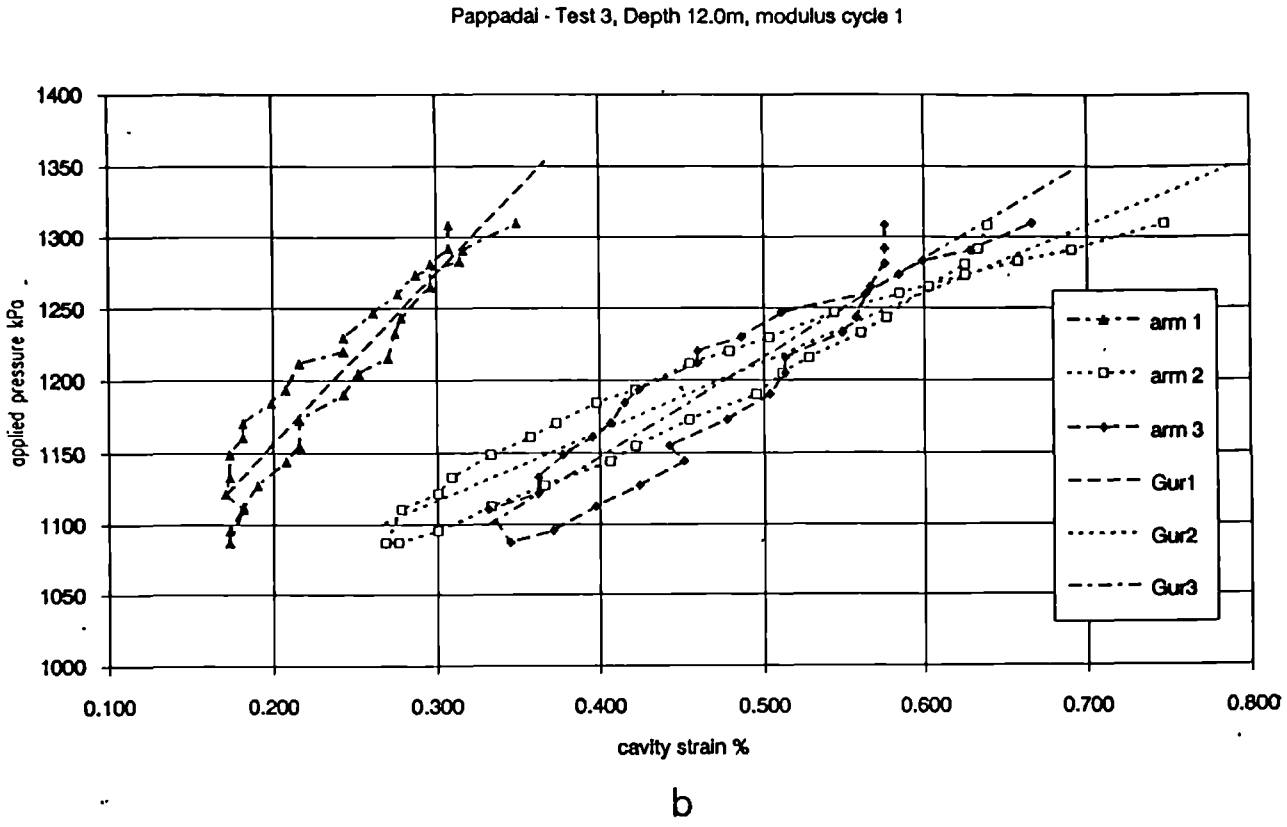

b

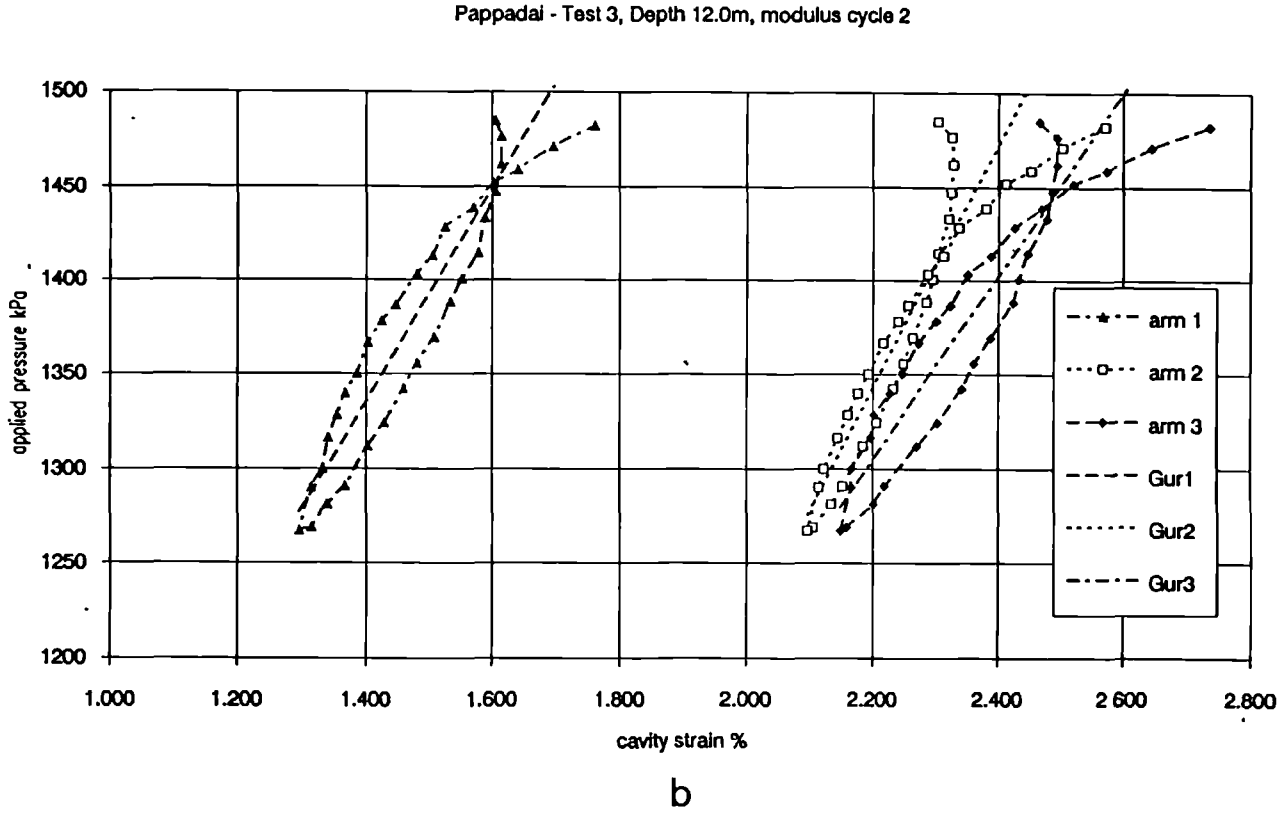

b

Fig 4 23 SBP testing at Pappadai : unload-reload loops.

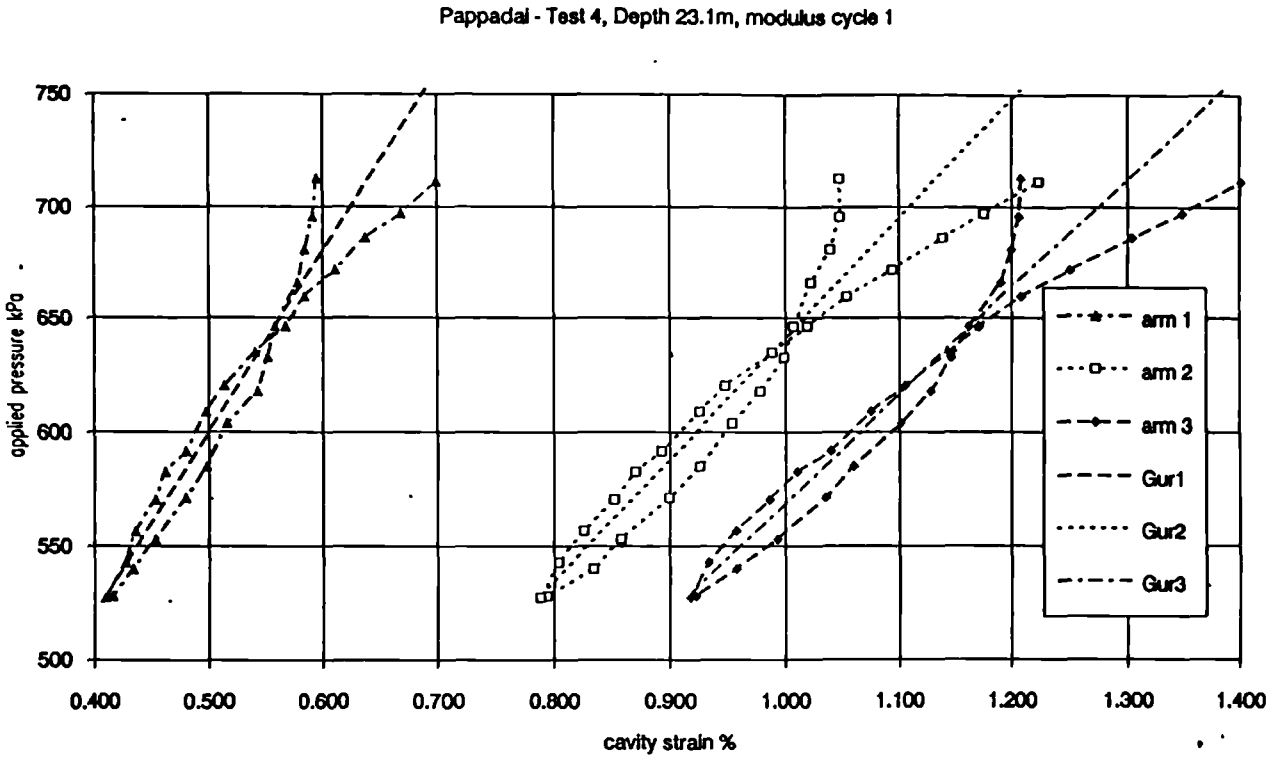

C

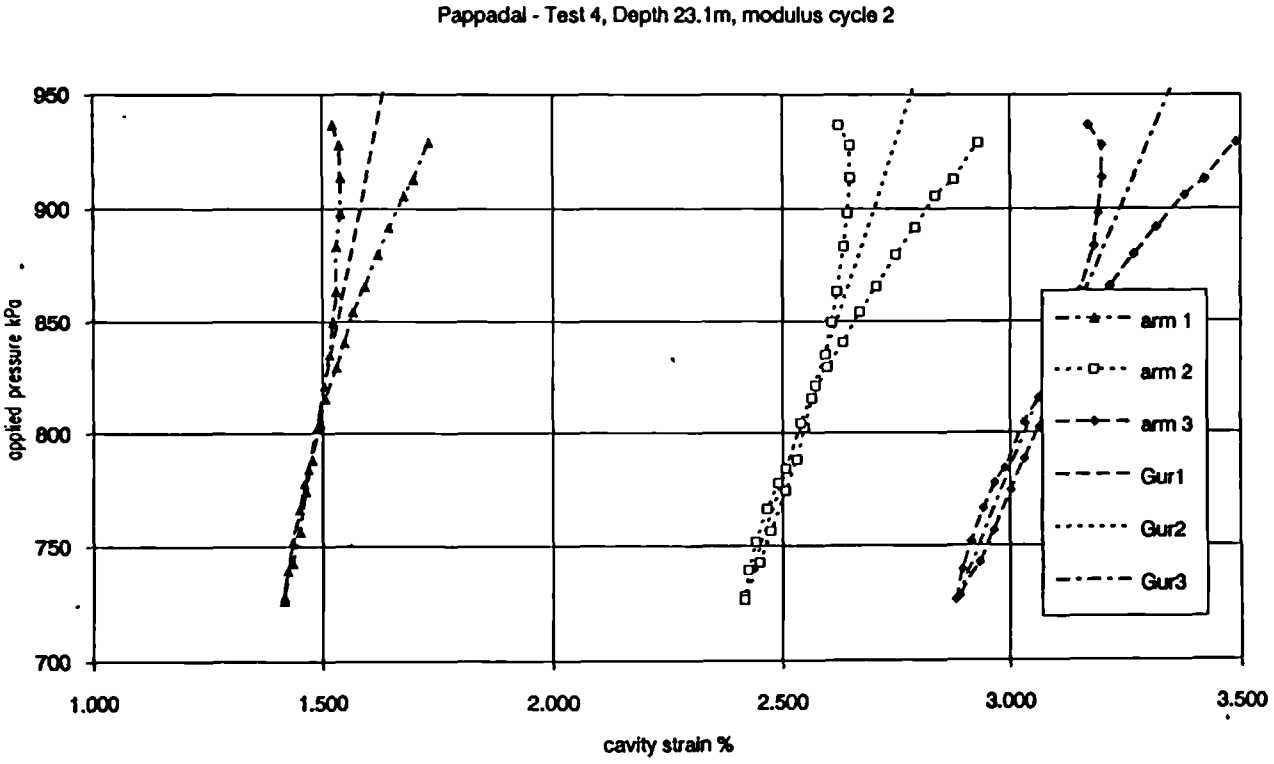

C

Fig.4.23 SBP testing at Pappadai : unload-reload loops.

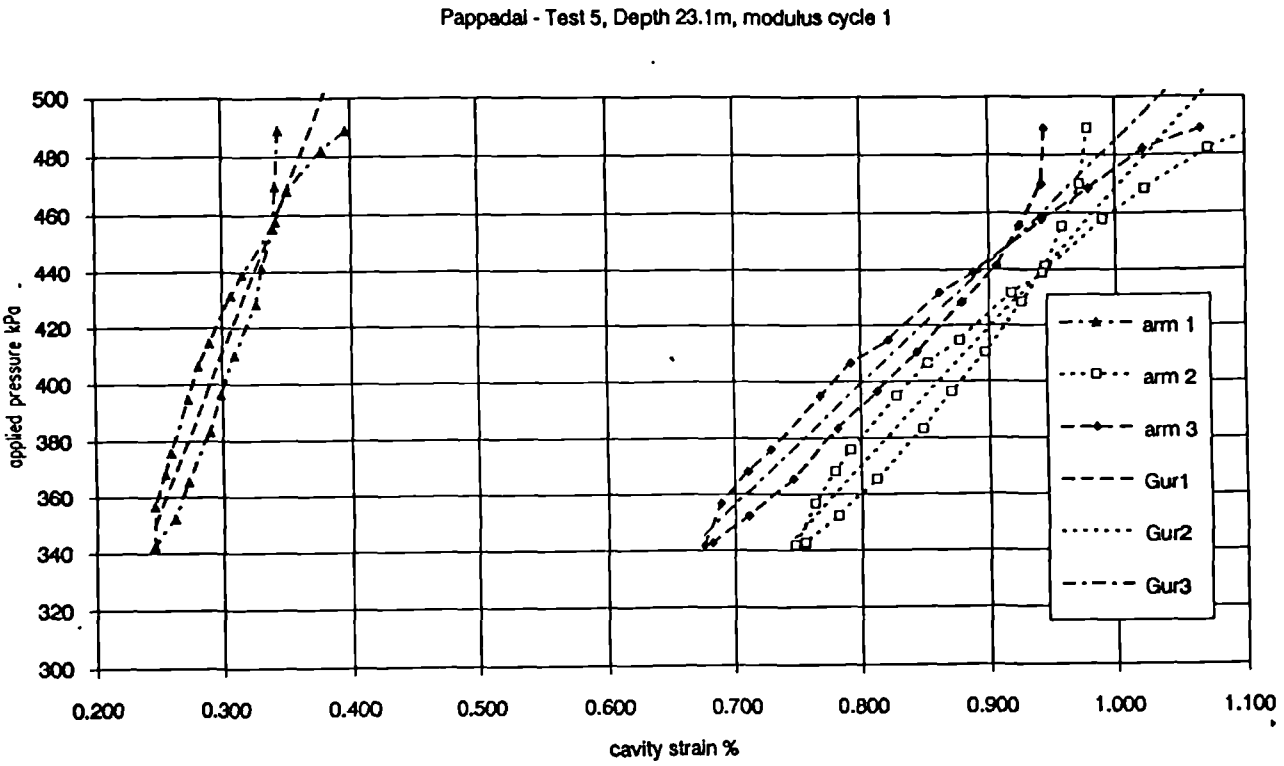

d

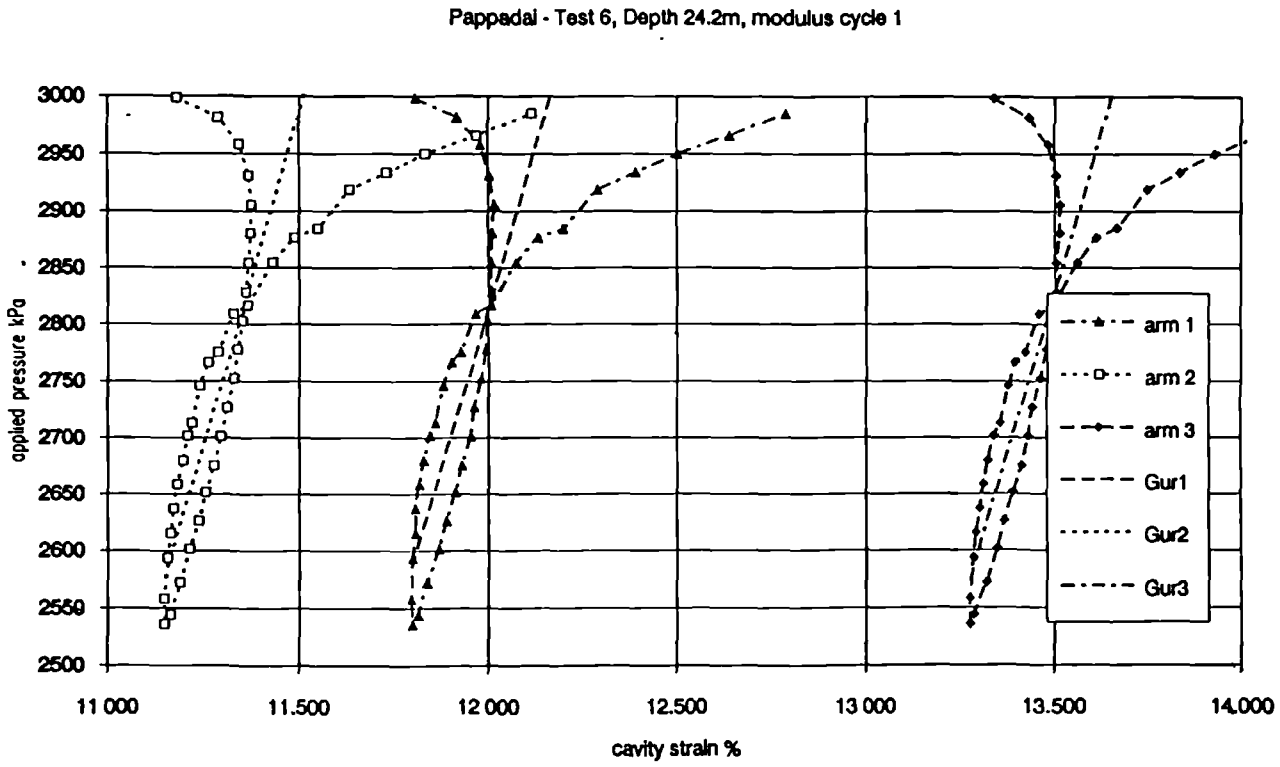

e

Fig.4 23 SBP testing at Pappadai : unload-reload loops.

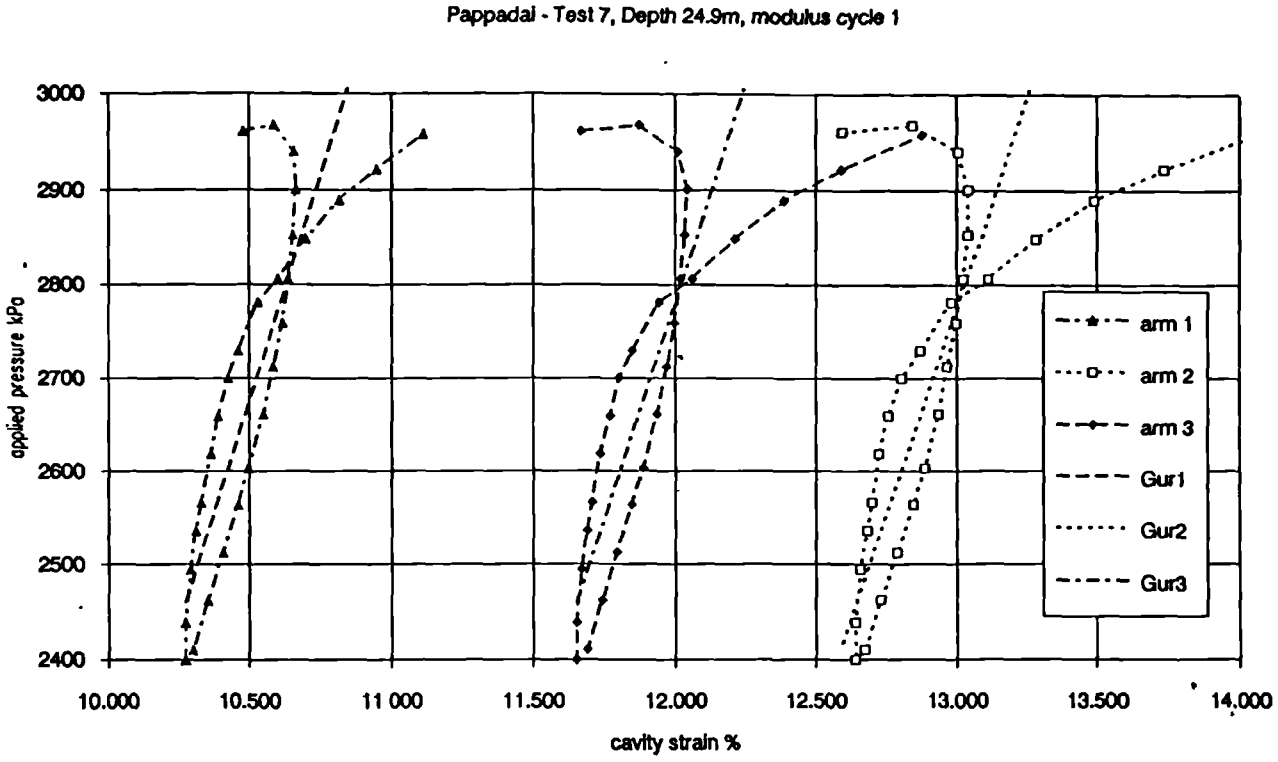

f

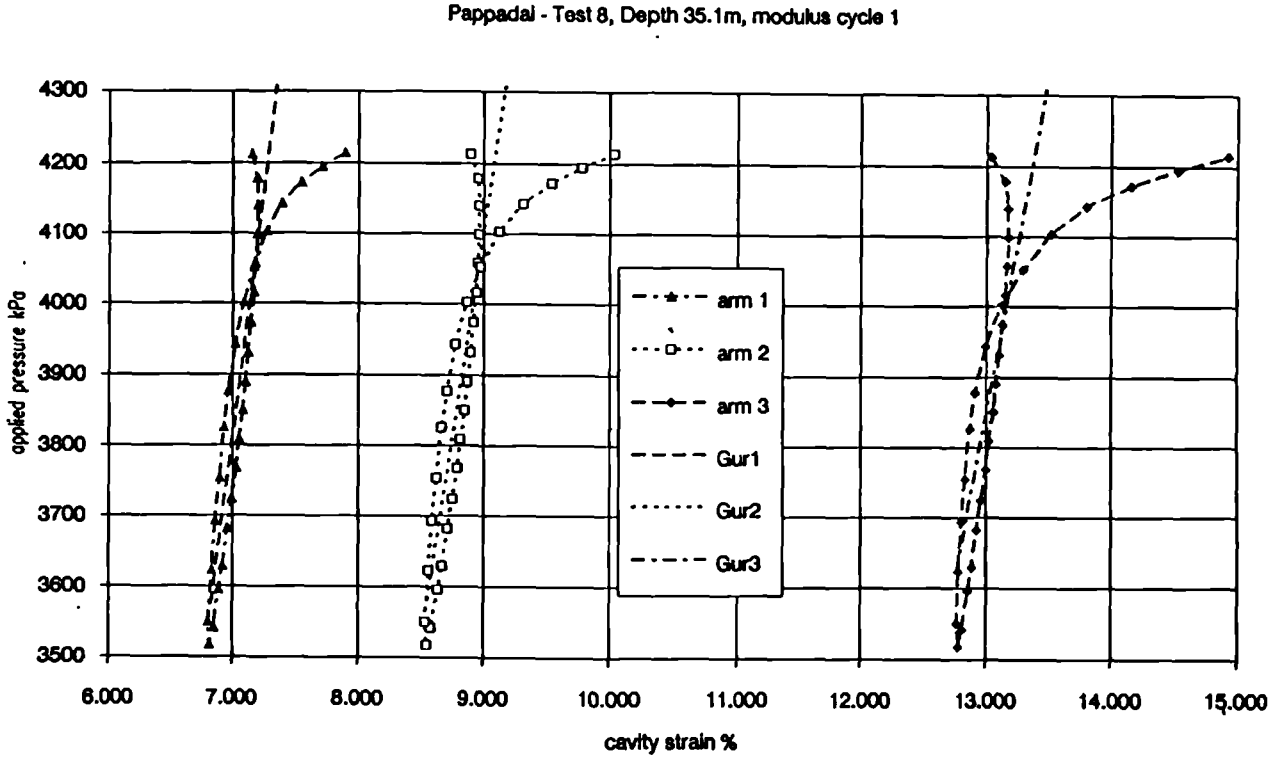

g

Fig.4.23 SBP testing at Pappadai : unload-reload loops.

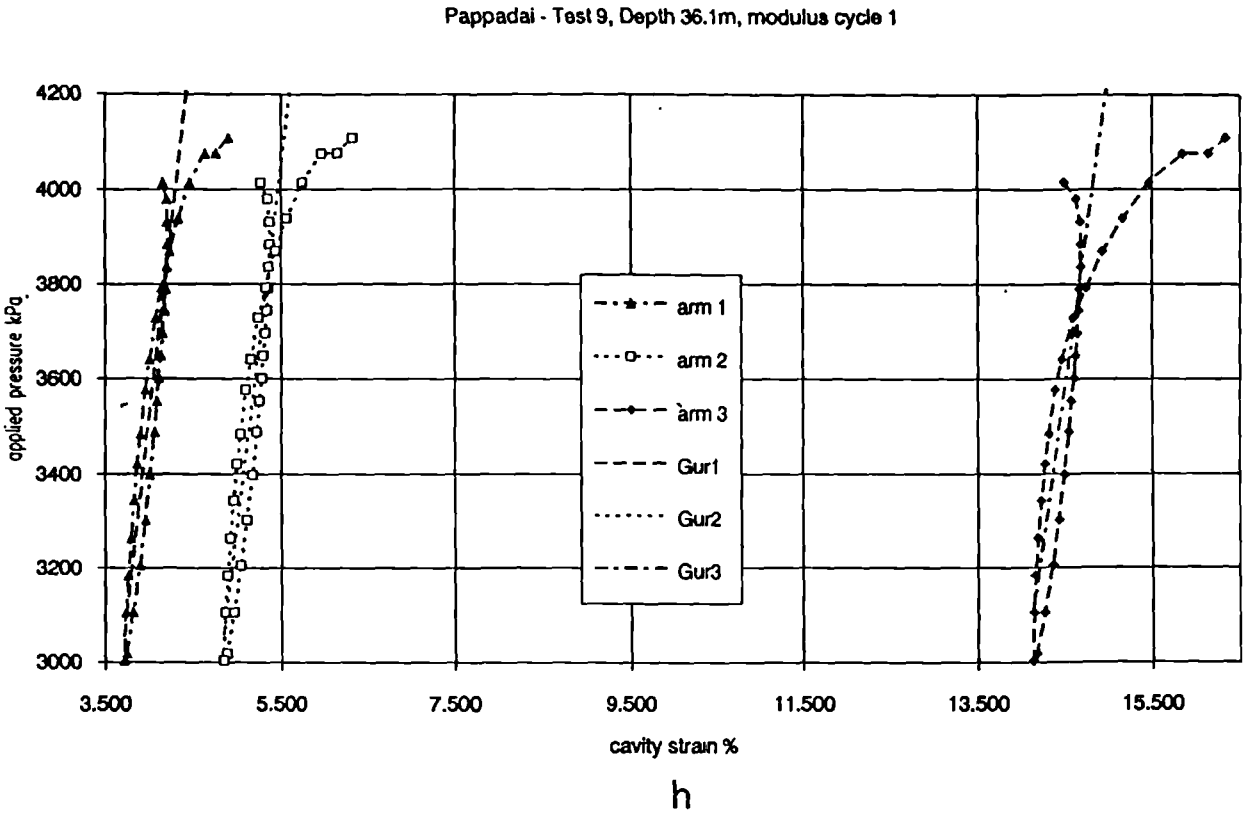

Fig.4.23 SBP testing at Pappadai : unload-reload loops.

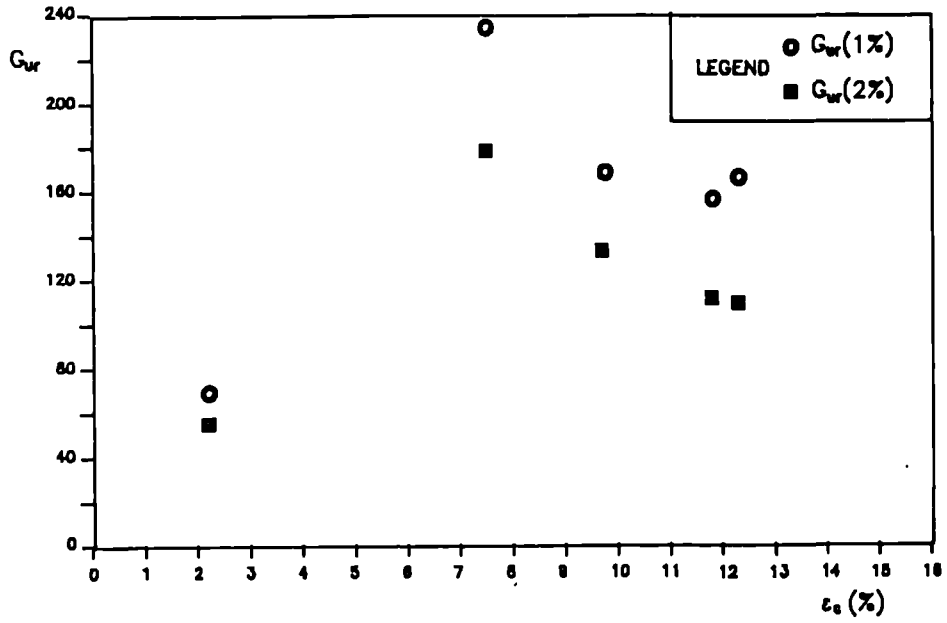

Fig.4.24 SBP testing at Pappadai : relation between the reload cavity moduli G_{ur} and the cavity strain at the start of the unload-reload loop.

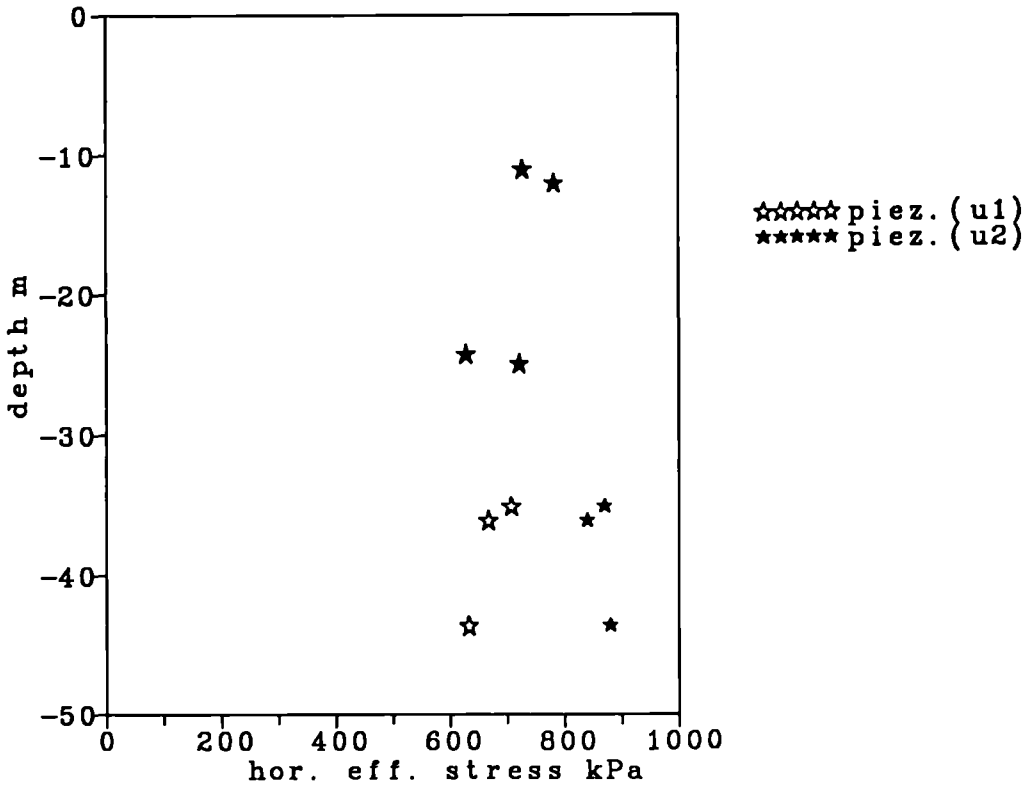

Fig.4.25 Horizontal effective stresses down borehole A.

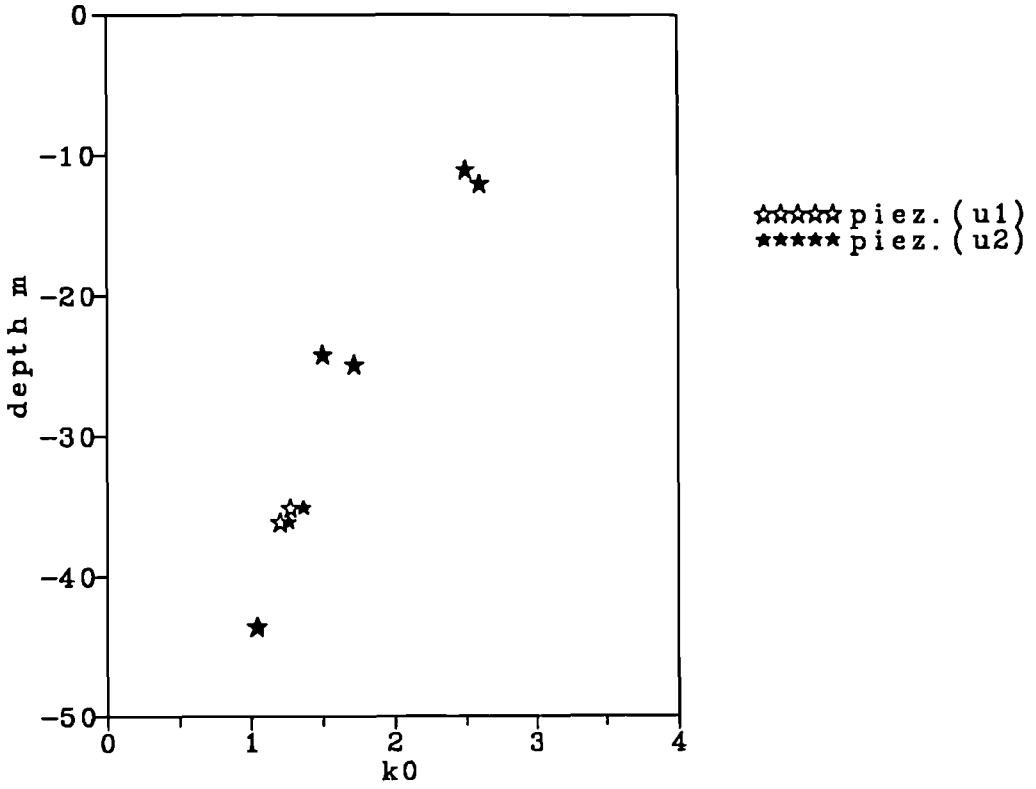

Fig.4 26 K_0 values down borehole A.

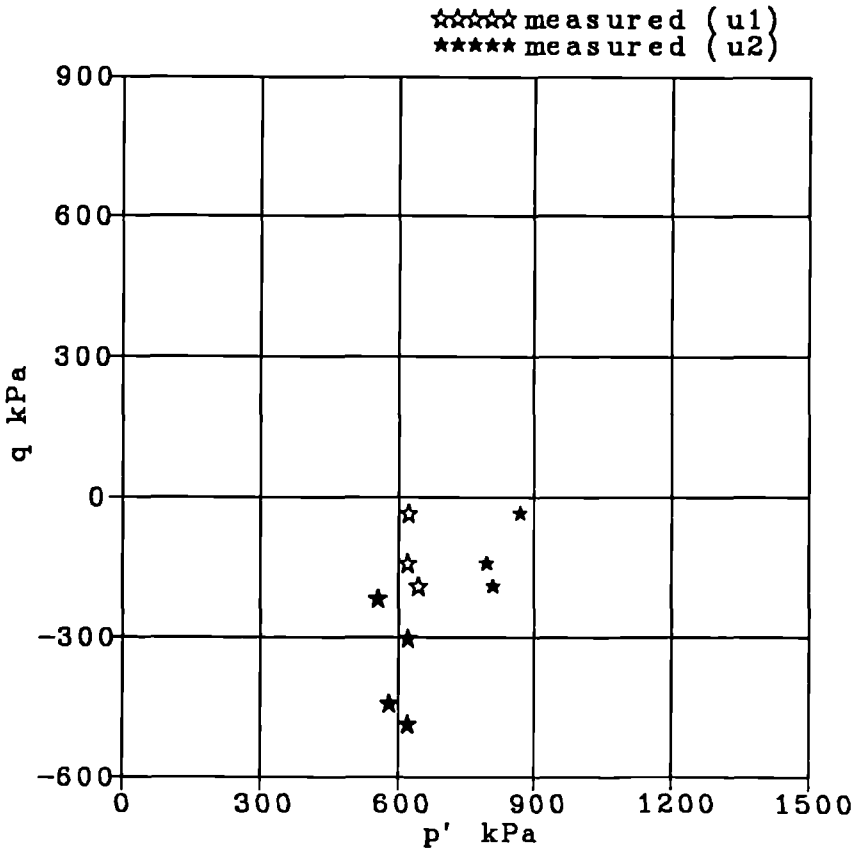

Fig 4.27 q-p' states down borehole A

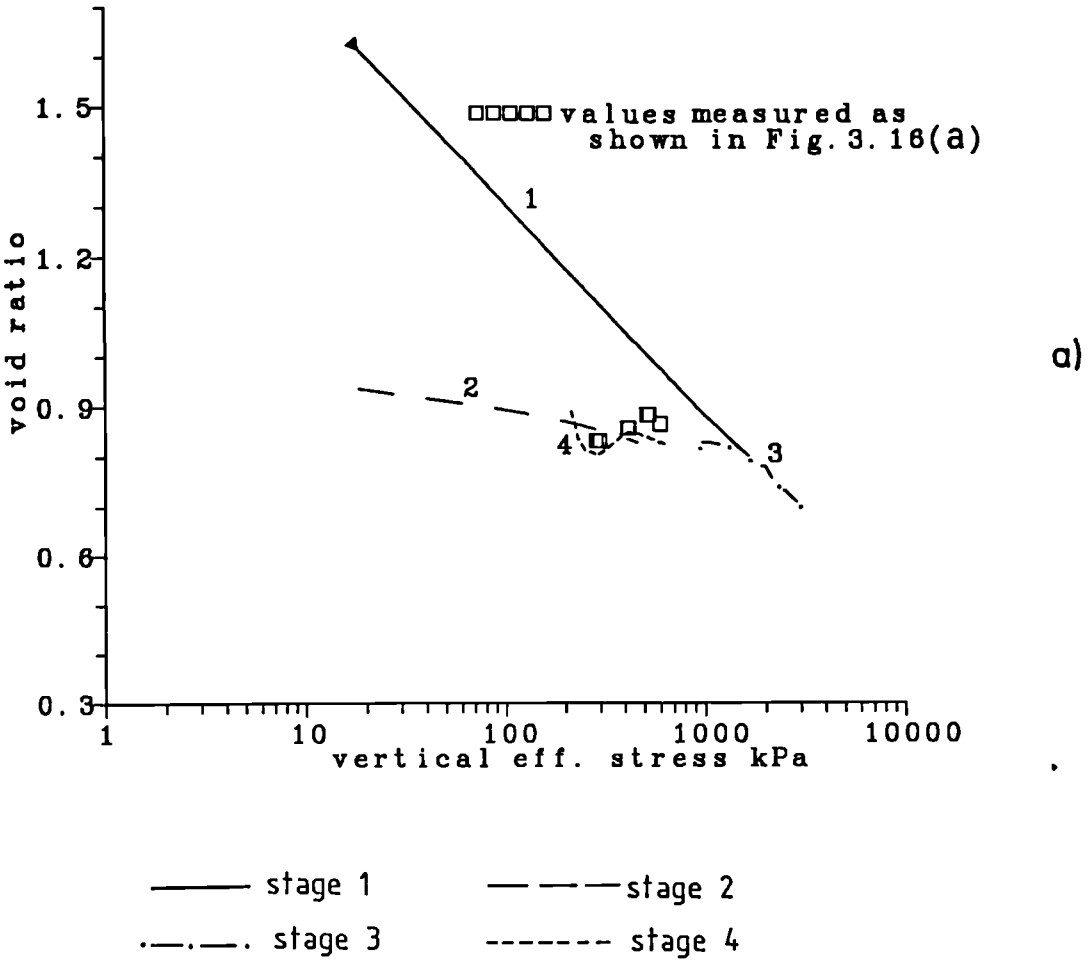

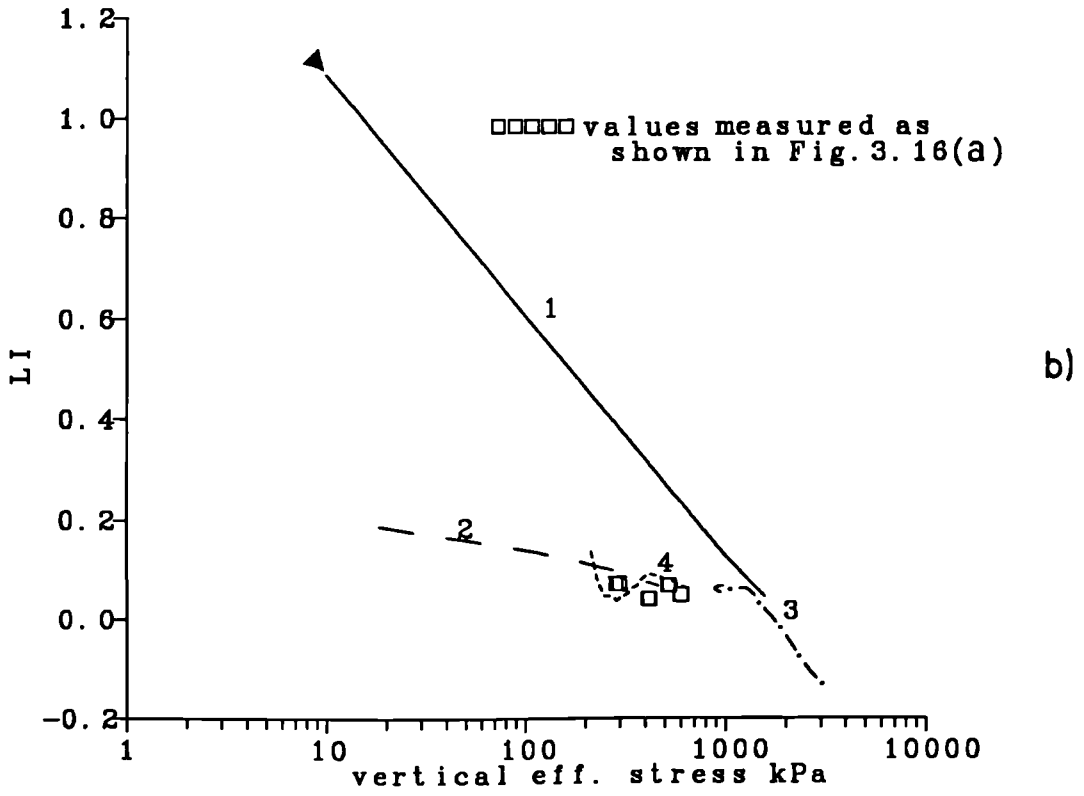

Fig.4.28 In situ states in the four stages of the clay history : (a) e-σ'_v states; (b) LI-σ'_v states.

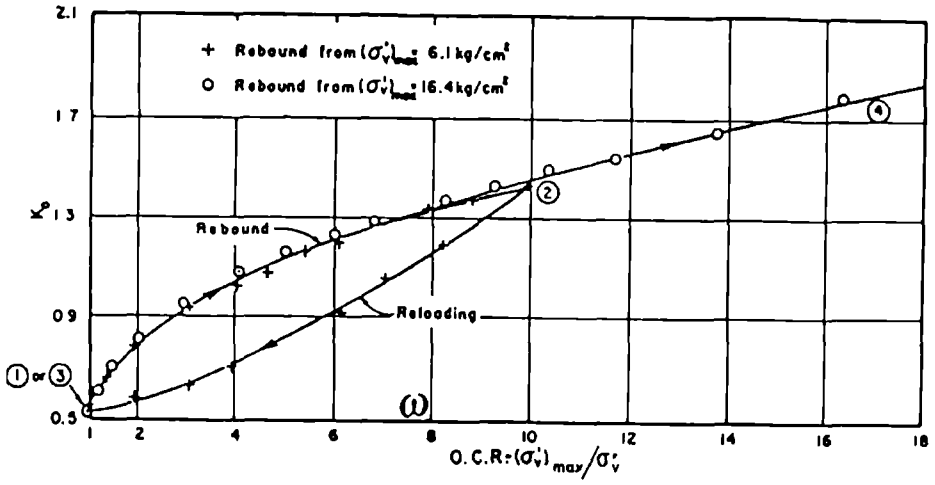

a)

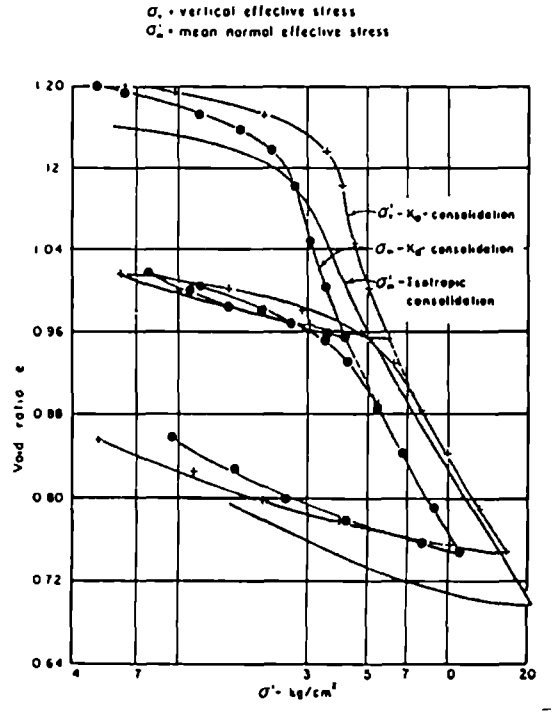

b)

Fig.4.29 (a) Variation of K_0 with OCR and (b) e-σ'_v curves for undisturbed Hancy Clay (after Campanella and Vaid 1972)

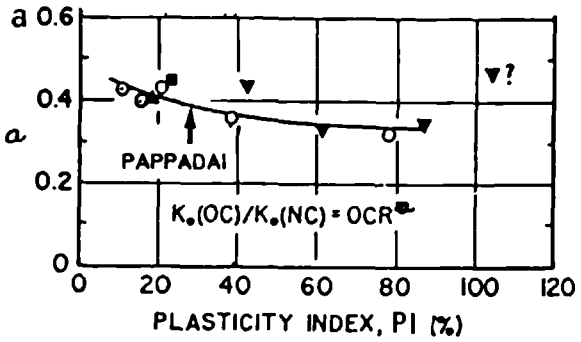

Fig.4.30 Coeffecient a, relating K_0 with OCR, versus plasticity index (after Ladd et al.1977).

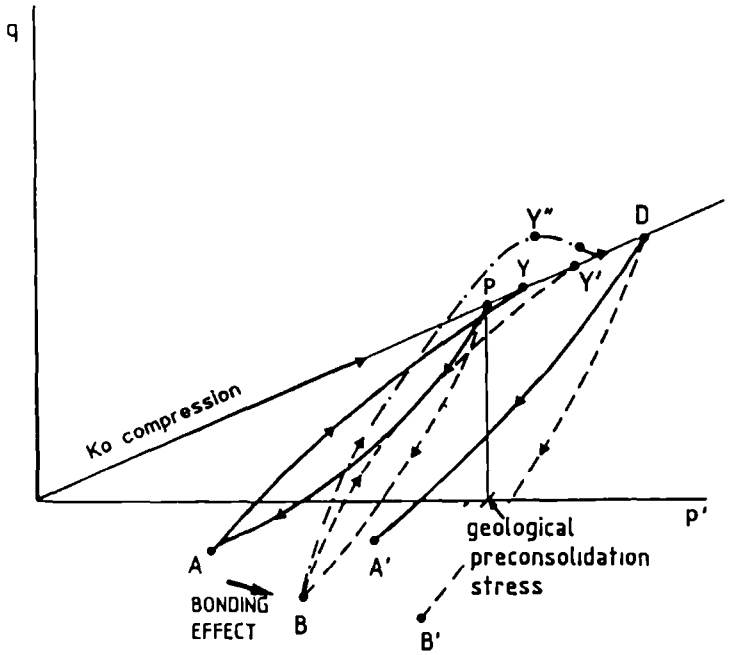

P-A-Y-D-A' : stress path followed by a soft clay or a medium bonded clay

P-B-Y'-D-B' }
P-B-Y"-D-B' } Stress path followed by a clay which has acquired futher bonding after virgin compression to P.

Fig.4.31 OC clays : effects on the clay stress history of the further bonding acquired by the clay after virgin compression.

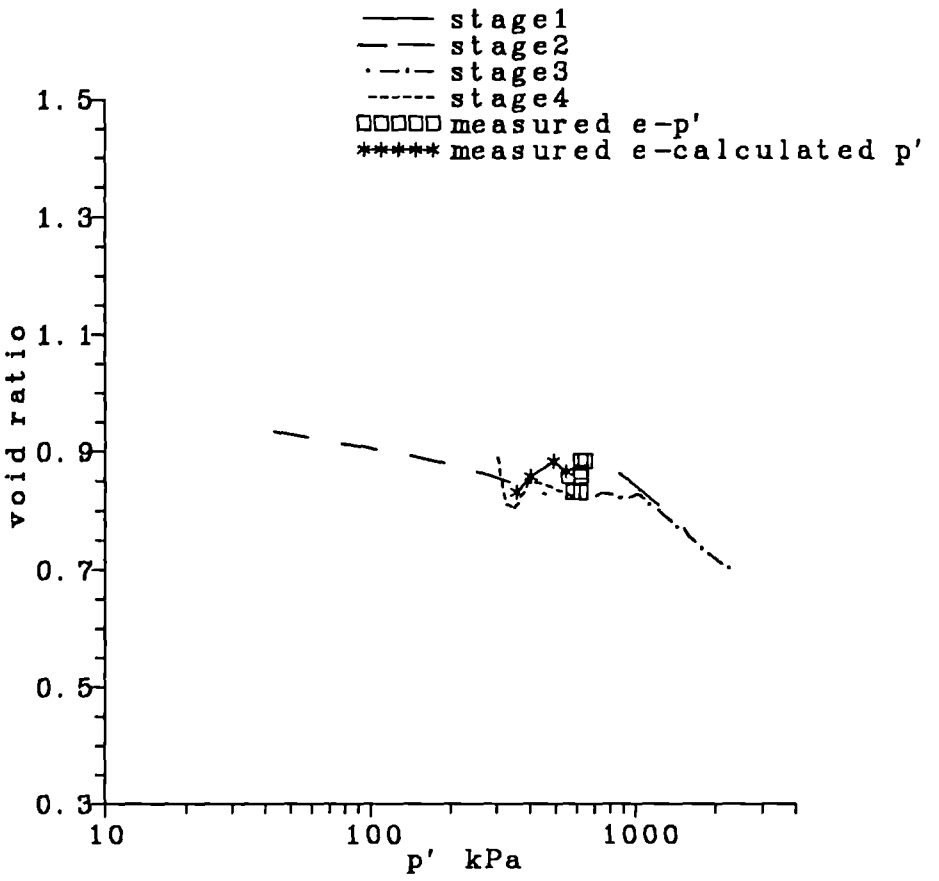

Fig.4.32 e-p' states down borehole A in the four stages of the geological history.

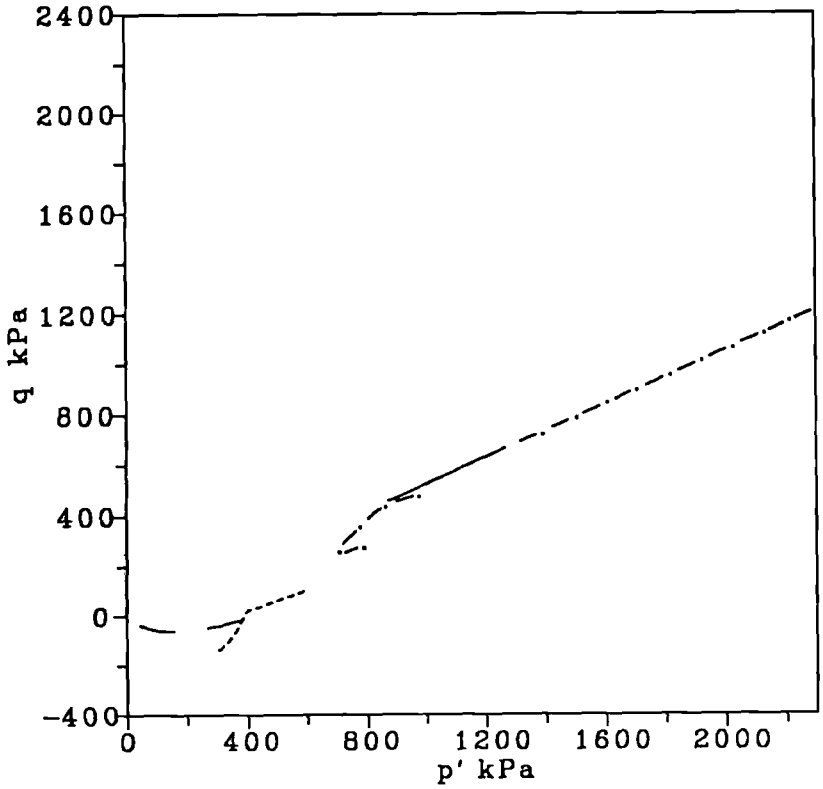

Fig.4 33 q-p' states down b rehole A in the f ur stages of the geol g cal history; legend as for Fig.4.32.

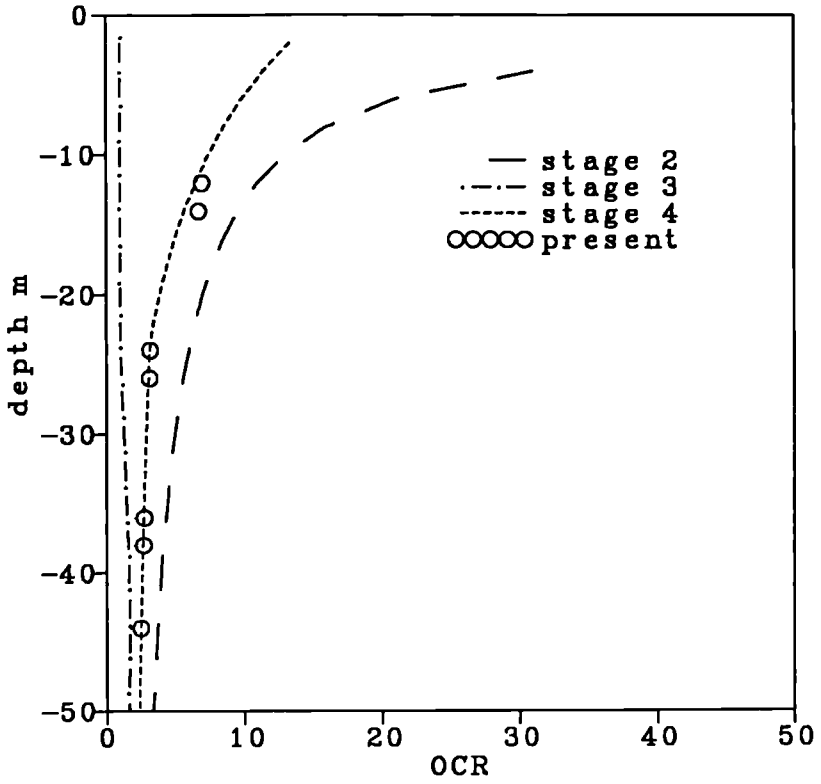

Fig.4.34 Values of OCR down borehole A in the four stages of the geological history.

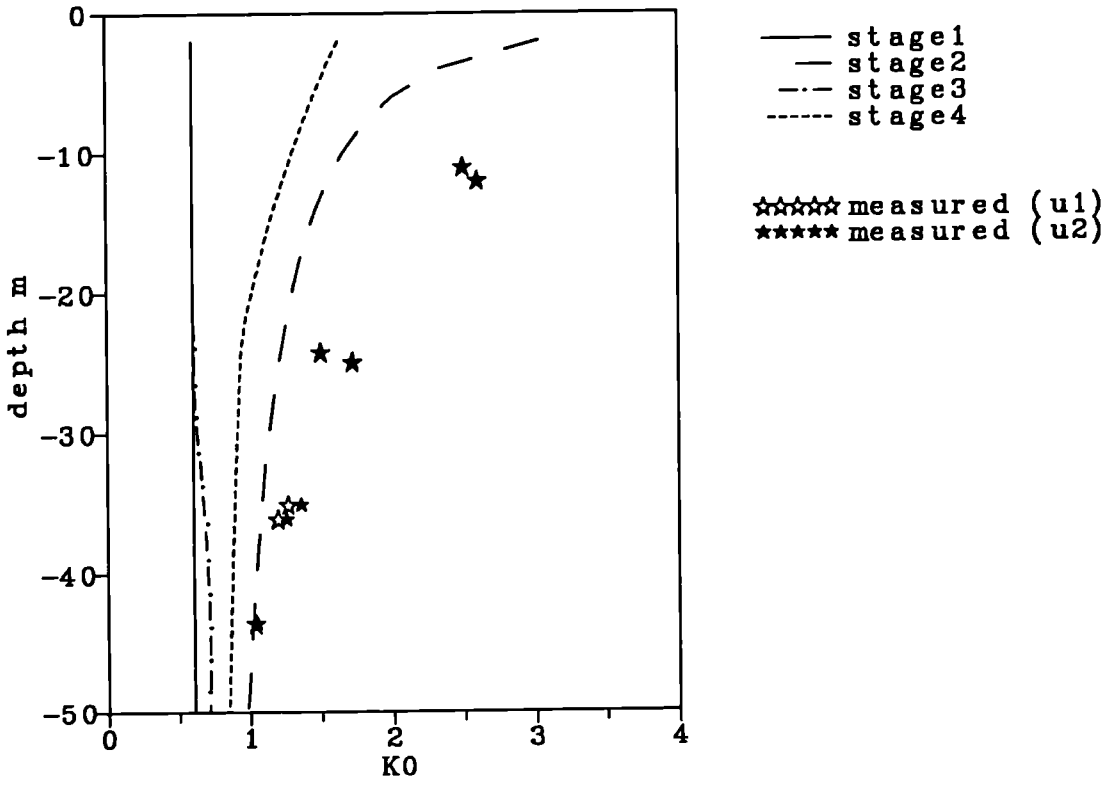

Fig.4.35 Values of K_0 down borehole A in the four stages of the geological history.

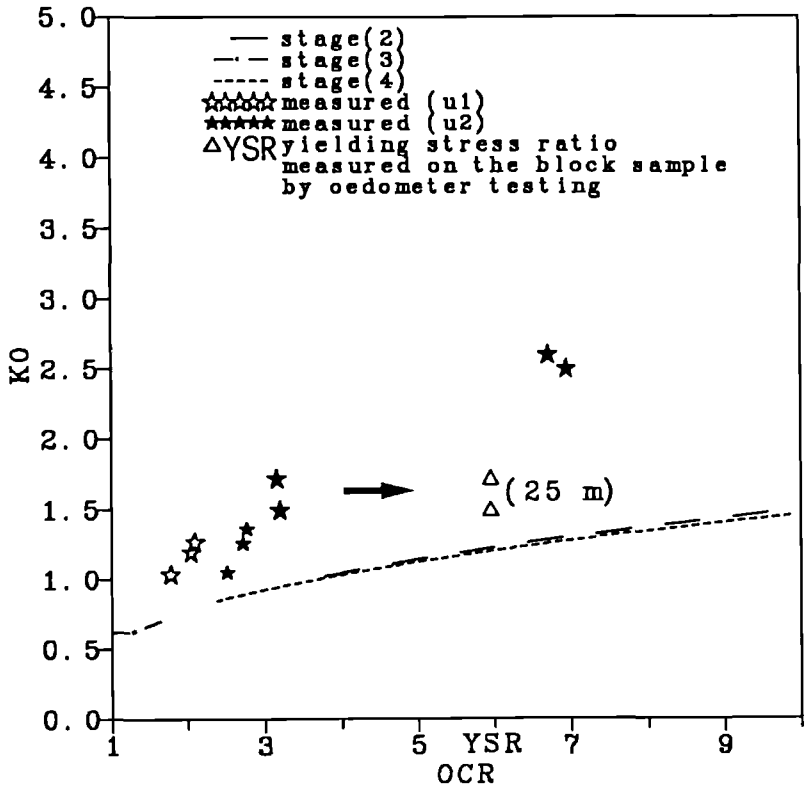

Fig.4.36 Relationship between K_0 and OCR (Table 4.7) reported in the literature for soft OC clays (clay type 2 in Table 2.1) and K_0-OCR values applying to the Pappadai clays down borehole A.

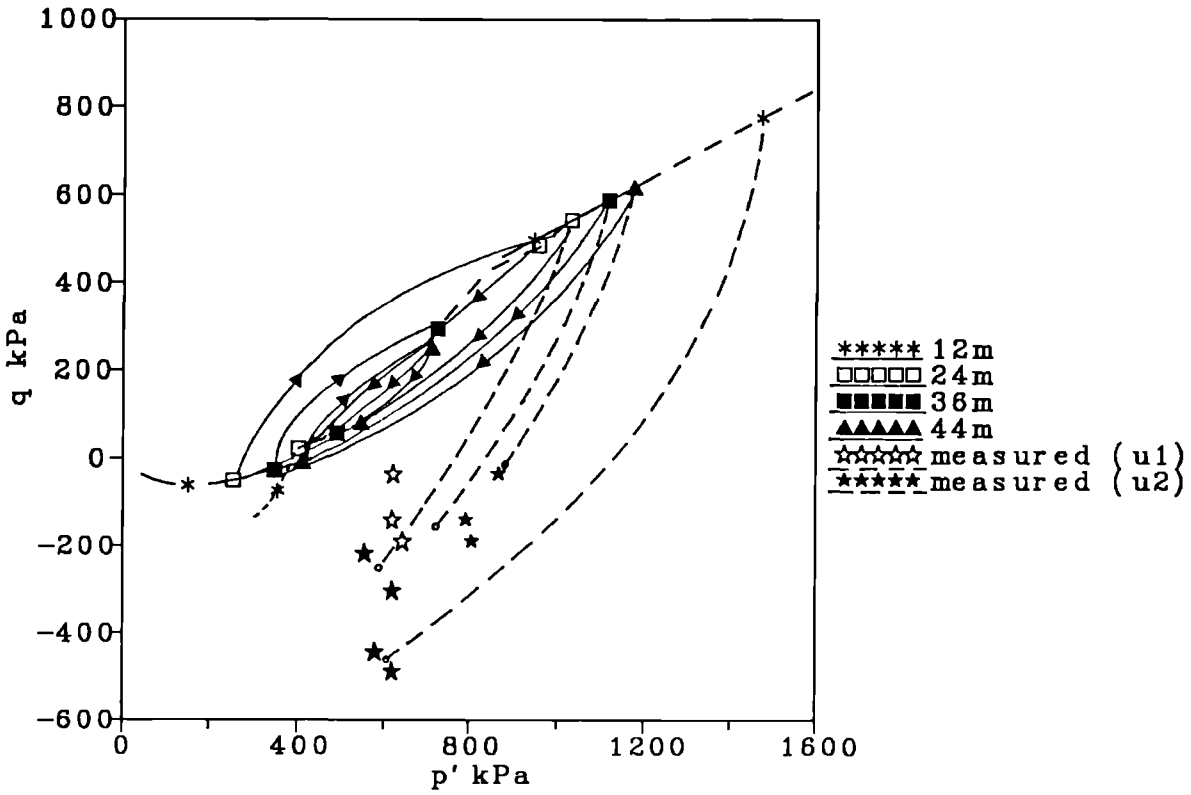

Fig.4.37 q-p' states down borehole A in the four stages of the clay history as resulting from the modelling, and present q-p' states as resulting from the in situ measurements

CHAPTER 5

VOLUME-STRESS STATE AND MICROSTRUCTURE OF THE PAPPADAI CLAY

5.1. Introduction

This chapter presents the index properties and the volume-stress states of the samples of natural and reconstituted Pappadai clay which were tested within the present research.

For the natural clay, the sampling operations are described and the original in situ volume-stress state of the clay at the sampling point is defined. The measurements of the suction (p_k) in the clay in the laboratory and its degree of saturation are reported so as to characterize the effects of sampling and storage on the original volume-stress state for the natural clay. The relationships between the water content, voids ratio, saturation degree and suction for the natural Pappadai clay are also discussed.

The techniques adopted to reconstitute and then consolidate the clay are described.

The analysis of the microstructure of both the natural and the reconstituted clay prior to testing is then presented. The clay microstructure was studied by means of SEM and chemical micro-analysis applications; SEM pictures and X-ray diffractograms are referred to in discussing the features of the fabric and bonding of the clay.

5.2. Undisturbed sampling of Pappadai clay

In November 1990 two undisturbed block samples were taken at the base of a shaft being excavated at Pappadai. The location of the shaft is indicated in Figs 3 5 and 3.6. The outflow tunnel of the artificial reservoir, which was under construction at Pappadai (see Section 3 1) when sampling was carried out, today crosses the above mentioned shaft, in which the systems controlling the water outflow are located.

The shaft, 7 metres in diameter, had been excavated down to about 25 m depth and lined before sampling In the few days between excavation and sampling, the base of the shaft was covered with gravel to restrain the loss of moisture content from the clay Before preparing the block

samples a 10 cm thick layer of clay was removed from the base of the shaft Two cubes, of 40cm side, were then trimmed by means of a hand operated chain-saw, as shown in Fig 5 1.

5.3. In situ stress state and σ'_p of the undisturbed clay

As discussed in Section 4.5, the effective stresses measured down borehole A by SBP testing (Table 4 6) are considered representative of the stresses at the corresponding depths down the shaft before excavation. In particular, the stresses were measured at 25m depth in borehole A wishing to measure a stress state close to the original in situ state for the clay subjected to block sampling down the shaft. The pore water pressure at 25 m depth down both borehole A and the shaft was considered hydrostatic in relation to the pore water pressure measured at 27m depth down borehole A, as shown in Table 4 6.

The original in situ state of stress for the clay forming the block samples was calculated as reported in Table 5.1, σ'_v being equal to 414kPa, σ'_h equal to 654kPa and K_0 equal to 1.58. The clay preconsolidation pressure σ'_p was calculated as 1310kPa following the same procedure used to calculate σ'_p at point X in Fig.3 15 (see Section 3.8 1) The OCR of the clay forming the block samples is thus about 3.2.

5.4. Index properties and mineralogy of the natural clay

The grading, the index properties, the specific gravity, the organic and carbonate content of the clay forming the block samples were all measured, the data being shown in Fig 5.2 and Table 5.2(a). These data match the measurements reported in Figs 3 10 and 3 13

The mineralogical composition of the clay at 25m depth in borehole A, reported in Table 5 2(b), was measured by X-ray diffraction on powdered clay. In the table the term smectite refers to all the swelling minerals present in the clay, including the intergrades (see Section 1 2)

5.5 St rage of the undisturbed clay samples

In this research project testing was carried out in the geotechnical laboratories of both the Politecnico di Bari and Imperial College (IC) Part of the undisturbed clay was then stored at IC

and part in Bari. The procedures adopted to store the block samples preserved the original moisture content and saturation degree of the clay quite well over the years, as shown by the data presented in the following sections.

In the shaft, the block samples were wrapped in cling film and waxed, as shown in Fig 5.3. Once in the laboratory in Bari, layers of clay a few centimetres thick were removed from the sides of the block. One block, 30 cm cube, was wrapped in cling film, waxed, and packed in a wooden box, lined with polystyrene, and was then sent to Imperial College. The remaining clay blocks were wrapped in cling film, waxed and stored in an underground cellar in Bari, where a low temperature and high humidity are present year round.

At Imperial College the clay block was first subjected to a suction test using the filter paper technique, as described in the Section 5.6 3. The block was then cut into cubes as sketched in Fig.5.4. Each cube was wrapped into two layers of cling film and wax, sealed into plastic bags and then stored with wet sand in sealed plastic boxes

5.6. Volume-stress state of the undisturbed clay samples

In this section the bulk unit weight γ, the voids ratio e, the saturation degree S_r of the undisturbed clay and the suction p_t immediately after sampling and after storage are presented (Table 5 3) The relationships between the values of e, w ,S_r and p_t of the clay are discussed. The stress path experienced by the clay at sampling was also reconstructed on the basis of the state of stress measured in the clay immediately after sampling, as discussed in Section 5.7.

5.6.1. Volumetric state of the clay in the laboratory

The measurements of bulk unit weight γ, dry bulk unit weight γ_d, w, e and S_r reported in the first line of Table 5.3 were carried out in Bari soon after sampling, and show that the clay was saturated in situ. Values of S_r below 100 occurred as a result of storage. The liquidity index of the clay in situ was equal to 0 074.

The other values reported in Table 5.3 were measured on specimens before testing For each specimen the name of the relative test and of the sample it belonged to are indicated in the table For the samples stored at IC the block number is reported as in Fig 5 4, while the samples stored

in Bari are referred to as "prism" (P). Not all the specimens tested during the research are reported in Table 5.3 as some measurements (see Tables 6.1 and 8.2.) were not as accurate as those in Table 5.3. For these specimens the voids ratio and the saturation degree at the start of the test were deduced on the bases of the relationship w-e-S_r obtained from Table 5.3, which is discussed in the following.

The measurements were carried out following BS 1377 - Methods of test for Soil. The specific gravity G_s of Pappadai clay was measured as 2.746.

The data in Table 5.3 define the following ranges:

w : (30.19-32.5)%

γ : (18.8-19.06) kN/m^3

γ_d: (14.28-14.63)kN/m^3

e : (0 840-0-888)

S_r : (98-100)%

5.6.2. e-w and S_r-w relationships of the natural clay

The drying occurring during storage was the main cause of variation in the measurement values, as shown by the plots e-w and S_r-w in Fig 5.5.

In the figure the results reported by Marinho (1994) for one drying test on a sample of undisturbed Pappadai clay ("prism") are also shown. These demonstrate that the decrease of voids ratio with drying is rather small (Δe=0.09 for ΔS_r=80%) for Pappadai clay The voids ratio rapidly becomes constant with decreasing water content (Fig.5 5(a)), while the S_r-w points plot along a straight line (Fig.5 5(b)) except for the data points corresponding to high S_r values

The e-w and S_r-w points from Table 5.3 plot around the initial data points from Marinho (1994) (Fig 5.5) and extend the investigated range of water contents towards the higher values The data show that, for w above 31%, a significant voids ratio decrease occurs, while the saturation degree remains in the range 99%-100% Below 31% water content, the rate of voids ratio decrease reduces and the S_r-w relationship approaches a steep straight line When the water content is below 30 5% desaturation is the main drying effect

Fig.5.5 shows that a high saturation degree of the Pappadai clay was rather preserved over the three years and half of testing. The storage of the clay in Bari gave rise to the minimum loss of moisture content, probably because of both the larger size of the clay samples (prisms) and the lower temperature of the storage room. The smaller samples at IC apparently dried rather more, though the water content did not drop below 30% and S_r below 98%.

The ranges of w-e-S_r reported in Table 5.4 were derived from the plots in Fig.5.5 and summarize the variations of w-e-S_r possible for the Pappadai clay samples due to drying during storage. The values in Table 5.4 were used to define the state of the clay specimens when the measurement of either w, e or S_r was not accurate (see Table 6.1 and 8.2). For the tests discussed in the following chapters the initial voids ratio e was estimated to be correct to the nearest ±0 01.

5.6.3. Measurements of suction by means of the filter paper technique

The filter paper technique, described by Chandler and Gutierrez (1986), was used to measure the clay suction p_k both before and after storage (Table 5.3 and Fig.5.6). The calibration equation for the Whatman No.42 filter paper is :

$$p_k = \gamma_w 10^{(5\ 85-0.0622w)} \qquad (5.1)$$

For high degrees of saturation the filter paper technique measures the matrix suction (First Expansive Soil Conference 1965; Chandler and Gutierrez 1986; Ridley 1993), given that the water in the filter paper is continuous and in equilibrium with the soil pore water. But for both clay of low saturation degree and clay with very high suction (1000kPa), continuity of the filter paper with the soil pore water is not possible (Schreiner 1988; Ridley 1993) and a suction intermediate between the matrix and the total suction is measured

The matrix suction of the clay block was measured at IC by means of a test carried out as shown in Fig 5 4(a) Sixteen filter papers were put on one of the faces of the clay block, before cutting it into smaller cubes, and the block and the filter papers were kept sealed for one month The p_k measured by the sixteen filter papers are reported in Fig.5.7. The average of these p_k values, 650kPa (first row of Table 5 3) represents the suction of the clay soon after sampling (S_r =100%). The other filter paper test results in Table 5 3 refer to the clay cubes and prisms after storage

5 6.4. Measurements of suction in the triaxial apparatus

For some triaxial specimens the clay suction was measured in triaxial apparatus (Table 5.3), which are described in Chapter 8. The clay suction can be measured in the triaxial by an isotropic undrained compression if both the clay and the pore pressure measuring system are saturated. A typical response of saturated clay specimens during the compression is shown in Fig 5.8 (Baldi at al.1988).

If either the clay is not fully saturated or some air is trapped in the system, after an initial increase the pore pressure gradually decreases with time as the air tends to dissolve into the water, and it may only reach a constant value after very long time. Consequently the pore volume changes, the effective stresses increase and the pore water pressure decreases, and the effective stress is higher than the original clay matrix suction. The error in the suction measurement is higher when testing stiff clays than soft clays since the compression of the air gives rise to a greater increase in the effective stress in the stiffer soil.

Cavitation often occurred in the pore water pressure measuring system during setting up and undrained loading of the specimens, due to the high suction present in the Pappadai clay. To reduce the likelihood of cavitation of the system the procedure used to set up the specimen was as follows.

1) A high air entry porous stone (1500kPa) was put on the base pedestal;
2) A thin wire was put on the porous stone (Fig 5.9) to avoid contact between the specimen and the porous stone during the setting up; the gap due to the wire was filled with some water so that the specimen did not touch the water surface; the volume of air trapped was not thought significant. Application of the cell pressure caused the squeezing of the wire into the clay and the compression of the air and water present in the gap (Bishop and Henkel 1962),
3 The sample setting-up was carried out in the shortest time possible, and the cell pressure was applied quickly to avoid cavitation in the drainage lines.
4 A cell pressure much higher than the clay suction was applied during the undrained compression.

The use of a high cell pressure in the undrained isotropic compression of the specimen was found to be critical for successful p_k measurements During tests TN2, TN9 and TN11 and TN12 (Table 5 3) the cell pressures were respectively 200 kPa, 200 kPa, 170 kPa and 170 kPa, and

the p_k measurements required the use of a high pressure apparatus, see Chapter 8. The B values relative to the initial state of the clay were measured in these tests, Table 5.3.

5.6.5 Suction measurements using the pressure plate apparatus

For two specimens the suction was measured using the pressure plate (Ridley 1993), as reported in Table 5.3. These suction measurements were carried out with the kind help of Dr.Ridley.

5.6.6 Measurements of the clay swelling pressure in the oedometer

In some of the step-loading oedometer tests (OED), which will be described in Chapter 6, the swelling pressure of the intact clay was measured. Although the clay swelling pressure may differ from the clay matrix suction due to water-particle interactions at the micro-level, in Table 5.3 the swelling pressures have been assumed to be measurements of the clay matrix suction.

To measure the swelling pressure the swelling of the oedometer specimen was restrained at the start of the test by incremental loading. The load was increased if the vertical displacement recorded in the loading step was lower than the compliance of the apparatus. The maximum pressure of the loading sequence for which the settlement was lower than the apparatus compliance and the pressure corresponding to the first loading step for which the clay underwent consolidation were considered to define an interval of pressures which comprised the swelling pressure (Table 5.3).

5.6.7. Discussion of the e-p_k data

The p_k values reported in Table 5.3 and plotted in Fig 5 6 against e are in the range (600kPa - 950kPa), which is rather small if the differences between the measuring techniques are considered

The test results from Marinho (1994), also plotted in Fig 5 6, show to what extent suction can give rise to volumetric strain in the undisturbed Pappadai clay The p_k data in Table 5 3 plot on the left side of the data from Marinho.

In Fig.5.6 one of the oedometer compression curves measured for the undisturbed clay (see Chapter 6) is also plotted (Marinho 1994). It appears that when the yield state of Pappadai clay is approached in the drying test, the increase of suction does not give rise to the volumetric strain recorded during the oedometric loading. At this stage the rate of saturation decrease increases as the w-S_r data approach the straight line in Fig.5.5(b). It follows that the structure of the Pappadai clay does not yield as a consequence of drying.

The data in Fig.5.6 may be interpreted in two alternative ways. The first interpretation is that the air entry value of the natural Pappadai clay happens to be just before yield. Alternatively, the increase of suction is not able to cause the clay to yield so that air entry necessarily occurs before yield. In Chapter 7 the changes in structure occurring at yield during oedometric compression are shown to be quite complex. If these structural changes cannot be induced by an increase of suction, then yield is one of the factors controlling the drying behaviour of the clay and different air entry values must exist, depending on yield stress and stress history

Little study has been made on the drying behaviour of overconsolidated clays. Ridley (1993) reported the results of a drying test on reconstituted kaolin (Fig.5.10) which had been compressed to 1000 kPa and swelled. It appears that the main desaturation of kaolin starts when the clay suction is about 900 kPa, i e. just before yield, while the air entry value for kaolin is about 700kPa when normally consolidated from slurry. This test then seems to support the second interpretation of the drying behaviour of OC clays presented above. Marinho (1994) reported test results for undisturbed London clay (Fig.5.11 and 5.12). The clay yield pressure is not identified by the oedometer test results in Fig.5.12. Plots (c) and (d) in Fig.5.11 show that only when very high suction values are reached do the gradients of the voids ratio-suction and saturation-suction graphs decrease and increase respectively. Also these results are then consistent with the second interpretation presented above, although the drying behaviour of OC clays is not conclusively explained by this limited evidence. The investigation of the relation between the gross yielding process and the desaturation process for OC clays seems worthy of future research

5.7. Sampling state path

The q-p' state of the Pappadai clay before sampling (Table 5 1) and the state of the clay in the laboratory (first line in Table 5.3, p_k = 650 kPa) are plotted in Fig 5 13 as points A and B In the following, a qualitative reconstruction of the sampling stress path experienced by the clay block samples is proposed and the sampling disturbance is discussed

Skempton (1961) and Skempton and Sowa (1963), assuming block sampling to be "perfect sampling" (Ladd and Lambe 1963), the soil to be saturated, using the pore water pressure parameter A_s from Skempton (1954-a) and assuming the stress state in situ to be axi-symmetric, the vertical stress being a principal stress, defined the pore water pressure change at block sampling as :

$$\Delta u = 1/3\ (\Delta\sigma_v+2\Delta\sigma_h) + (A_s-1/3)\ |\Delta\sigma_v-\Delta\sigma_h| \qquad (5.2)$$

In eq. (5.2) $|\Delta\sigma_v-\Delta\sigma_h|$ is the absolute value of the difference between the stress variations, that is the deviator of the stress change at sampling. In the given hypothesis of perfect sampling $\Delta\sigma_v$ is actually equal to the opposite of the vertical stress in situ σ_v and $\Delta\sigma_h$ is equal to the opposite of horizontal stress in situ σ_h. Therefore, according to eq (5 2), the suction p_k in a saturated clay sample is:

$$p_k = \sigma'_v\ (K_0 - A_s\ (K_0 - 1)) \qquad (5.3)$$

if the values of K_0 in situ is higher than 1 and σ'_v is the effective vertical stress in situ It follows that:

$$K_0 = (p_k/\sigma'_v-As) / (1-A_s) \qquad (5.4)$$

.

Eq (5.4) has been generally used to derive the in situ stress state of overconsolidated clays from the suction measurements in the laboratory (e g. Skempton 1961; Bishop et al. 1965; Chandler and Apted 1988)

In Fig.5.13 the values of p_k for the Pappadai clay block sample, as resulting from eq.(5.3) assuming different A_s values, are shown. Skempton (1961) considered 0.3 to be an appropriate value of A_s for the London clay from Bradwell Differences in A_s of about 0 1 give rise to differences in p_k of the same order of magnitude as the typical error in suction measurement in the laboratory. The accuracy in the estimation of A_s has then little influence on the relationship between K_0 and p_k in eq (5 3) (Bishop et al.1965) Fig 5 13 then shows that the effective isotropic stress p_k present in the Pappadai clay after block sampling was only slightly higher than the stress which would be expected for perfect sampling assuming A_s equal to 0 3

Nonetheless, during block sampling the clay undergoes a stress path which is more complex than that for perfect sampling. Block sampling of Pappadai clay consisted of two stages, stage (a) being the excavation to reach the sample position and stage (b) the sample extraction from the base of the shaft.

During excavation the soil element A in Fig.5.14 undergoes an undrained extension (Fig.5.14(b)). The radial total stress may reduce as a result of the vertical extension of the soil element. The shear stress τ_{vh} (Fig. 5.14(b)) is different from zero and restrains the vertical extension of the soil. However τ_{vh} decreases from the walls to the centre of the shaft, thus in the block sampling at Pappadai, which was carried out at the centre of the shaft, τ_{vh} could be assumed as zero, σ_v and σ_h remaining principal stresses during sampling. In the following (Fig 5 14(b)) the principal total and effective stresses at the end of stage (a) are defined as σ_{va} and σ_{ha}, σ'_{va} and σ'_{ha} respectively.

The total stress state after excavation is.

$$q = -\sigma_{ha} \qquad (5\ 5)$$

$$p = 2/3\ \sigma_{ha} \qquad (5\ 6)$$

In Fig 5.15, point A (q_A; p'_A) represents the effective stress state in situ before excavation. The total stress path during stage (a) is shown as A-B assuming that u_0 in situ is zero and that :

$$(\sigma_h - \sigma_{ha}) < \sigma_v \qquad (5\ 7)$$

The effect of the variation of σ_{ha} on the total stress path during stage (a) is shown in the detail plot in Fig.5.15. The excess pore water pressure developing in the clay during stage A is (Skempton 1954-a):

$$\Delta u(\text{stage a}) = (A_s\text{-}2/3)\ \sigma_v - (\sigma_h\text{-}\sigma_{ha})(1\ 3+A_s) \qquad (5\ 8)$$

if eq. (5.7) applies. Therefore the effective stress state after excavation is

$$q = -\sigma_{ha} \qquad (5\ 9)$$

$$p' = \sigma_{ha}(1/3 - A_s) + \sigma_h\ (1/3 + A_s) + \sigma_v(2/3 - A\ ) - u_0 \qquad (5\ 1\ )$$

If A_s is positive, but lower than 0.33, the effective stress path during stage (a) is similar to A-B' in Fig.5.15.

During stage (b) at Pappadai only a thin layer of clay located at the periphery of the block was distorted during trimming and the distortion of the clay inside the block could be considered negligible. Thus during stage (b) the clay underwent a "perfect sampling" from the stress state developed at the end of stage (a) (Fig.5.14(c)). The excess pore water pressure developing during stage (b) was then :

$$\Delta u(\text{stage b}) = (A_s - 1)\,\sigma_{hs} \qquad (5.11)$$

the effective stress p_t at the end of stage (b) being :

$$p_t = \sigma_h\,(1/3+A_s)+2\sigma_{hs}\,(1/3-A_s)+\sigma_v\,(2/3-A_s)-u_0 \qquad (5.12)$$

if A_s was constant during stage (a) and (b) (path B'C' in Fig.5.15). The analysis presented here thus shows that the effective stress-strain paths followed by the Pappadai clay at sampling, which were rather uniform across the block sample, can be specified (Fig 5 15) if the values of A_s during stages (a) and (b), and the change in σ_h during stage (a) are defined

As the clay is an elasto-plastic material, block sampling may cause significant plastic distortions. The passive compression during stage (a) (path AB' in Fig.5.15) may even produce passive failure of the clay if K_0 is very high. The disturbance is lower for lower K_0 values, for A_s values below 0.33, and for higher passive strengths.

Fig.5.15 shows that even if the clay is not strongly distorted during stage (a) and if the A_s changes along the whole sampling stress path are small, the final p_t may be different from p_t for perfect sampling. If A_s is lower than 0.33, p_t after block sampling (p_{tb}) is higher than the p_t after perfect sampling (p_{tp}). In this case eq (5.3) overestimates the K_0 in situ, and for Pappadai clay, assuming A_s close to 0.3 (Skempton 1961), K_0 would have been estimated as 1 77 from eq (5 3) as compared to the measured value of 1 58

K_0 values measured for London clay block samples were compared with the K_0 of Pappadai clay (Table 5.5). For samples of London clay from Bradwell, which had a YSR equal to that of the Pappadai clay (YSR~6), a K_0 very close to the K_0 measured at Pappadai was obtained

(Skempton 1961). Larger differences between the K_0 values were measured for London Clay samples of similar YSR from Ashford Common and Bradwell.

5.8 Reconstituted Pappadai clay

The Pappadai clay was reconstituted and one-dimensionally consolidated at Imperial College. First the undisturbed natural clay was heavily remoulded and mixed with water to form a slurry and then the slurry was consolidated in the oedometer In the following the procedure adopted to create the slurry and consolidate it are discussed

5 8.1. Reconstitution of the clay

To reconstitute the clay the particles must be disaggregated Prolonged swelling in water does not disaggregate the particles of the natural Pappadai clay and a heavy and thorough remoulding is required. Given the large amount of clay which had to be reconstituted for consolidation in a large consolidometer (see Section 5.8.2), the clay was disaggregated by means of a motor-driven grinder.

Large pieces of undisturbed clay were cut into very small pieces, dried at 60°C and then ground, reducing the clay into powder. The clay-water mixture was thoroughly worked to complete the disaggregation of the powder grains and squeeze the clay lumps forming by flocculation of the clay particles in the suspension. Before consolidation the clay slurry was deaired The slurry was stirred for 48 hours in a stirring apparatus which worked under vacuum The deaired slurry was then poured into the consolidometer.

Following the procedure defined by Burland (1990) the water content of the clay slurry was planned to be about 1.5 times the liquid limit of the clay, i e. 97 5%; in the event the water content of the clay slurry before deposition in the consolidometer was measured as 101%

When the reconstitution of the Pappadai clay was carried out, grinding was considered a procedure suitable for the objectives of the research Only in a later stage of the research was it realized that grinding may affect the grading of the clay, the features of the clay particles, and the clay mineralogy In Fig 5 2 the gradings of the natural and reconstituted Pappadai clay are

compared. It is possible that grinding reduced the coarse silt fraction of the clay, as grinding can crush carbonate sand and silt grains.

In Table 5.6 the mineralogical composition of the reconstituted Pappadai clay, as measured by X-ray diffraction, is reported. Comparison between this composition and that measured for the undisturbed clay (Table 5.2(b)), shows that in the reconstituted clay both the carbonate content and the swelling mineral content are lower than in the natural clay, while the content of the non swelling minerals is higher. Data in the literature show that different duration of dry grinding may induce different structural alterations of the clay minerals (Wiewiora et al.1993). During the first few minutes of grinding delamination and structural break-down of the clay mineral may occur Prolonged grinding may cause a reaggradation of the ground powder, with an increase of the non-swelling minerals. The differences in swelling and non-swelling minerals between the natural and reconstituted clay might then be due to grinding. The difference in carbonate content may suggest that carbonates were leached out during the reconstitution and consolidation of the clay. The effects of grinding on the clay particles will be further discussed in Section 5 9.4.

However, even if the grading and the mineralogical composition of the reconstituted Pappadai clay were affected by grinding, its Atterberg limits were not sensibly different from those of the natural clay and grinding did not change the clay plasticity index PI, as shown in Table 5.7

5.8.2. Consolidation of the clay from slurry

The clay slurry was poured into a consolidometer of 397.6 cm^2 cross sectional area and 280mm height. In order to ensure uniform one-dimensional deformations in the consolidometer the internal surface of the consolidometer was covered with grease to reduce the side friction

The initial voids ratio of the clay slurry was 2.773. The clay slurry was left to settle down in hydrostatic conditions, with no base drainage, until the settlement rate was sufficiently low. The settlement of the slurry, 20mm, was correlated to an average vertical stress down the consolidometer due to the submerged self weight, 0 6kPa (Fig 5 16) The vertical stresses applied during the compression of the reconstituted clay are reported in Table 5 8 and the compression curve of the slurry is plotted in Fig 5.16.

The voids ratio at the end of the compression in the consolidometer was about 1 13 At this stage the free water was removed from the top of the sample, and the clay was quickly unloaded

Although swelling was restrained, a voids ratio increase was recorded after unloading (Tables 6 1 and 8.1).
The SEM pictures of the reconstituted clay (Section 5.9.4) show that unloading caused the opening of horizontal fissures in the clay, which gave rise to the voids ratio increase.

5.9 Microstructure of the Pappadai clay

In this section the microstructure of both the undisturbed and the one-dimensionally consolidated reconstituted Pappadai clay are illustrated. The clay fabric was examined using the SEM. The particle arrangements as well as the type of interparticle contacts were detected using high enlargements. A chemical micro-analysis was used to investigate the compounds forming different portions of the clay structure, and to examine if cementing agents form part of the clay bonding

For the undisturbed clay the analysis revealed the fabric and bonding which have developed as a result of the geological history, reconstructed in Chapter 3. In addition, the investigation revealed the differences between the microstructures of the natural and the reconstituted clay. These findings may help to document more objectively and to interpret the differences between the mechanical behaviour of the two clays.

In several studies in the literature (Burland 1990, Rampello 1993, Rampello et al. 1993, Coop at al.1995) the characteristics of the clay microstructure are derived from the clay mechanical response, and are supported by direct observation of the clay at the micro-level. Thus, the validity of such interpretations is not rigorously checked The reasons why deducing the microstructural features of a clay from its mechanical behaviour is limited have been discussed extensively in Chapter 1 Thus the analysis of the clay microstructure should be a main element in all studies aiming to define a general relationship between structure and behaviour of clays.

5 9 1 Investigation of the clay fabric by means of the SEM

The physical principles background of SEM as well as the systems and techniques used for SEM applications are amply documented in the literature (Smart and Tovey 1981, Smart and Tovey 1982, Wenk 1976).

Basically, in the scanning electron microscope an electron gun shoots a narrow electron beam against a sample surface under vacuum. Three magnetic lenses compress the size of the beam so that the size of the area being scanned is reduced. The electrons are reflected at the impact with the sample constituents in a way that depends on the topography of these constituents, as schematically shown in Fig.5.17(a). A receiver-decoder of the reflected electrons produces a message which is then converted into magnified images of the area being scanned.

The SEM techniques are so sophisticated that specialized operators have to carry out the SEM application, though the objectives may require the method to be used in different ways In this work the SEM applications were carried out in specialized laboratories, the writer preparing the clay samples to be scanned, and supervising the operators during the SEM application.

For clay in particular the method of preparation of the SEM specimens and the extraction of pore water is important. The clay has to be dried in the way which least affects its fabric (Smart and Tovey 1982), and the methods of SEM sample preparation are outlined in Fig.5.17(b). With impregnated samples only two-dimensional analyses of the clay fabric may be carried out. Alternatively, fractured samples allow three-dimensional analysis. The sample preparation techniques used for the Pappadai clay and the way the SEM applications were designed are discussed in the following section

5.9.2. Used equipment and technique

The microscopic analysis investigated fractured dried clay samples to examine the clay particle arrangements and inter-particle contacts in three dimensions. SEM applications on impregnated clay were not carried out since the scanning of flat sections through the clay does not show the particle inclinations and the architecture of the particle aggregates

Three different sets of samples were prepared from both the intact and the reconstituted clay The samples being examined are listed in Table 5 9. Each set was examined in a different SEM laboratory, as reported in the table. The clay was examined both before and after oedometer testing Samples A and B in Table 5 9 were from the undisturbed and reconstituted clay before testing, respectively. Samples C, D and E were from the clay after testing, as specified in the table. The SEM results for samples A and B are reported in Sections 5 9 3 and 5 9 4 The volume-stress state for the clay forming samples A has been defined in Section 5 6 (Table 5 3)

The state of the reconstituted clay forming samples B has been described in Section 5.8.2, e g the clay is normally compressed to σ'_v equal to 200kPa. Samples C, D and E will be shown in Chapter 7 where, by comparison with samples A and B, the structural changes occurring in the clay during oedometric compression will be shown.

The first set of samples in Table 5 9, i.e. group 1, was examined with the help of Prof.Veniale at the CNR-SEM Laboratory at the Dipartimento di Scienze della Terra, Università di Milano The samples were prepared by freeze-drying. The clay at the original water content was immersed into nitrogen and then transferred to a vacuum chamber so that the water could sublimate and the clay could dry with no significant volume change Air drying may give rise to shrinkage and affect the clay fabric, and should be avoided, especially when testing soft clays such as samples B in Table 5.9. After freeze-drying the samples were fractured along sub-horizontal and sub-vertical surfaces which were then gold coated High resolution pictures were taken of these samples

The samples of group 2 were only of the A type (Table 5.9) and were air dried, fractured and gold coated These samples were examined in the SEM Laboratory of the Medicine Faculty of the Università di Bari, directed by Prof Mazzarella. These pictures are also of high resolution.

The samples forming group 3 in Table 5.9 were freeze-dried and carbon coated. These were examined in the SEM Laboratory of the Istituto di Geologia Applicata e Geotecnica of the Politecnico di Bari, directed by Prof.Zezza In this case, carbon coating was used because a chemical micro-analysis was also carried out during the SEM application. The carbon coating gave rise to rather poor resolution SEM pictures.

For all the SEM applications Cambridge 500 microscopes were used

5.9.3. Undisturbed Pappadai clay - Results

In this section the SEM results for samples A from group 1 and 2 in Table 5 9 are discussed. The SEM pictures of these samples are in Figs 5.18 to 5 40. For each picture the sample group is specified in the figure caption and will not be mentioned in the text

Fig.5.18 is a global view of the fabric on a vertical fracture through the undisturbed clay The fabric appears densely packed The remains of numerous foraminifera can be recognized Their

fossil shells form macro-pores, of about 0.03mm diameter, which are noticeable even at this magnification.

Enlargements of two areas of this picture are shown in Figs.5.19 and 5.20. The fabric still appears densely packed at this higher magnification and numerous sub-horizontal strata of iso-orientated edges of particles can be seen (Figs.5.19, 5.20 and 5.21). Some strata are more densely packed than others, as can be seen by comparing regions A and B in Fig.5.20. On the horizontal fractures, shown in Figs.5.22 and 5.23, particle faces are predominantly seen, strongly suggesting that part of the clay fabric is horizontally orientated.

Many Globigerinae and detritic crystals are interbedded within the clay particles. Enlargements of globigerinae are shown in Figs.5.24(a) and (b). Three rare examples of coccospheres can be seen in Fig.5.24(c) and other beautiful examples of foraminifera interbedded in the clay are in Fig.5.24(d). Although the clay has been preconsolidated up to σ'_p of about 1310kPa, these fossil shells are still almost intact. Foraminifera and crystals as shown in Figs 5.23 and 5.24 constitute the largest particles, e.g 0.1-0.2mm, which can be observed in the Pappadai clay. The fact that the foraminifera shells are seldom broken and usually empty suggests that during consolidation the clay deformation has mainly risen from changes of the particle arrangements and slipping of the clay particles around the fossil shells and crystals. In Fig 5.25 the enlargement of a typical void created by fossil shells is shown The presence of the many fossils does indeed affect the orientation of the Pappadai clay fabric (Figs.5.24 and 5 25).

The large variety of particles present in the Pappadai clay can be seen in Figs 5.26, 5.27 and 5.28. The width of the clay particles varies from 1 to 5 μm. Large kaolinite particles, having perimeters of regular geometry, as well as illite particles, which have a more rounded outline, can be recognized in Figs. 5.26 and 5.27 The very small smectite particles in Fig.5.28 give the fabric a characteristic spongy appearance.

The enlargements of the clay fabric on vertical fractures shown in Figs 5 29 and 5 30 show that most of the clay particles form domains, in which they are in face to face contact Both small and large domains can be seen Iso-orientated densely packed domains forming strata which lie in sub-horizontal directions are seen (Fig 5 29). However many of these strata also bend towards sub-vertical directions. Sub-vertical strata truncating the horizontal ones are also observed Indeed in Figs.5.29 and 5 30 many domains which are either in edge to face or in edge to edge contact are shown. These may form large voids, of 10-20μm diameter. In addition there are stacks of domains interbedded with zones of rand m fabric, and within confined zones the fabric

is even chaotic. The Pappadai clay fabric, which appears well packed and more-or-less orientated at low magnification, is far less well orientated when seen at larger magnification.

Strongly variable particle arrangements can be found adjacent to each other, as flocculated aggregates are interbedded with strata of orientated domains. Higher magnifications of the fabric on vertical fractures through the clay are shown in Figs.5.31 to 5 33. Stacks of platy particles are observed in Fig. 5.31, and domains merge with each other to form large strata However areas where the fabric is chaotic, and where the particles are mainly in edge-to-face contact are shown in Figs.5.32 and 5.33.

Observing the particle arrangement in this detail is necessary for a correct interpretation of the structure formation and mechanical behaviour of the clay. Following the fabric classification reported in Chapter 1 (Sides and Barden 1970), the Pappadai clay fabric may be considered to be the result of the one-dimensional consolidation of a primary bookhouse fabric Indeed both the edge to face contacts between the domains, as well as the local random fabric may be considered to be relics of a flocculated fabric formed at deposition. In Section 3 7 it was suggested that a primary bookhouse fabric was formed in the Pappadai clay at deposition, on the basis of the study of the deposition environment Now this hypothesis seems to be confirmed The difficulty of distinguishing between compacted bookhouse and turbostratic fabrics has been fully discussed in Chapter 1. Despite this conflict, the features of the Pappadai clay seem to conform very closely to the fabric expected from the compaction of arrangements of flocculated particles.

The schemes in Figs. 1.12(e) and 1.13 were compared with the Pappadai clay fabric observed in the SEM pictures in order to investigate the fabric changes occurred in the clay during its geological history. The schemes in Fig. 1.13 represent the fabric evolution during one-dimensional compression of a flocculated fabric as proposed by Sfondrini (1977) These schemes seem to model well the successive features of the Pappadai clay fabric. As discussed in Section 1.9, Sfondrini proposed that during one-dimensional consolidation a general reorientation of particles and growth of domains occur, but some zones of the clay undergo more strain than others so that in some areas packed iso-orientated particles form "complex laminae" or stacks, while in other areas open random fabric is preserved What is observed for the Pappadai clay conforms to the discontinuous fabric attributed by Sfondrini (1977) to clay consol dated one-dimensionally to medium-high stresses In particular "complex laminae" between chaotic fabric are easily recognisable in Figs 5 31 and 5 32

Particle arrangements similar to those represented in the sketches in Fig.1.12(e) for the kaolin slurry examined by V.Cotecchia et al.(1982-b), and in Fig 1.13(b) for the natural Fiumicino clay (Sfondrini 1977), are seen in the Pappadai clay (Figs.5.31 and 5.34). Horizontal "complex laminae" are systematically interbedded within strata formed by a truss of domains in edge to face contact (see Fig.1.12(e)). This fabric type is recognized also in the reconstituted clay (Section 5.9.4) and in the undisturbed clay after oedometric compression to very high stresses (Chapter 7).

In Figs.5.34 and 5.35 the abundance of nannofossils within the Pappadai clay can be appreciated. These are mainly coccoliths of 3 to 5μm diameter. They may be found both lying between parallel domains and flocculated with the clay particles. In Fig.5.35 a horizontal fracture through the clay coated by nannofossils is shown. Such fracture is likely to be part of the characteristic lamination planes within the Pappadai clay shown in Chapter 3.

Single particle aggregates are examined in Figs.5.36 and 5.37 Domains and single particles are either in edge to face or edge to edge contact In Fig 5 37 a stack of orientated particles lies above large particles in "honeycomb" arrangement.

Particles having one edge floating within the pores can be seen, but in general the fabric is formed by particles in mechanical contact. However the SEM analysis does not reveal the bonding present at the contacts. In general in the Pappadai clay, neither crystals nor other constituents are seen at the contacts between the clay particles, confirming that carbonate crystals did not precipitate during the sedimentation of the clay. But the possibility of a carbonate bonding developing later in the history of the clay cannot be excluded

Calcite crystals which seem to form bonding between the particles within an isolated zone are seen only in Fig.5.38. These crystals may be authigenic. Authigenic crystallisation of compounds is a diagenetic process which may develop during compaction of the clay under burial within a relatively dry environment. In particular the crystals in Fig 5 38 lie within a zone where consolidation induced perfect particle orientation and probably gave rise to conditions prompting the diagenetic phenomenon. Other diagenetic effects can also be recognized in the clay fabric In Fig 5.39 lath-shaped illite can be recognized, the result of a diagenetic transformation of smectite into an illite-type mineral within a confined environment (Veniale 1993). In Fig 5 40 a framboid pyrite crystal is shown, which suggests that sulphide diagenesis occurred in the clay in reducing conditions.

The SEM analysis seems to confirm that diagenetic phenomena occurred in the Pappadai clay, as previously deduced from the mineralogical profile of the clay deposit (Section 3 6). In this case part of the features of the fabric may have arisen from diagenesis. In fact, during the mineralogical transformations, the clay fabric could be deformed by local changes of pressure and temperature, as anticipated in Section 1.10. The resulting fabric may be completely different from that existing before diagenesis (Sfondrini 1977) and additional bonding may also be present. Thus, according to the definitions given in Section 1.11 and reported in Table 1.1, a "post-sedimentation" structure developed in the Pappadai clay as a consequence of both unloading and diagenesis. In this section the fabric forming this post-sedimentation structure has been shown.

The results presented in this section for the freeze-dried and air-dried samples are consistent. They show that air-drying does not damage the fabric of a stiff clay such as Pappadai clay, perhaps because air-drying does not produce significant shrinkage of the clay, as shown in Fig.5.6.

5.9.4. Reconstituted Pappadai clay - Results

The reconstituted clay, one-dimensionally consolidated to σ'_v equal to 200kPa, is examined in this section. Samples B from group 1, Table 5.9 ,are analysed

Fig.5 41 shows a vertical fracture through the clay In the top half of the picture the fabric seems orientated since sub-horizontal strata formed by particle edges can be seen. However in the lower part of the picture the fabric is less orientated. Here both sand grains and casts of sand-size particles are present, and the fabric appears strongly affected by these constituents (Fig 5 42). In Fig 5 42 clay particles cover the sand grains and the surrounding fabric follows their perimeter The disturbance induced by sand and silt grains on the fabric orientation is as apparent as for the undisturbed clay, Figs.5.24 and 5 25 for example

The sand particles appear to be sub-rounded crystalline grains, components rarely seen in the undisturbed clay. Moreover foraminifera shells and detritic crystals are not seen as frequently as in the undisturbed clay. This may be the effect of the grinding carried out during the reconstitution of the clay Indeed what is observed by SEM is consistent with the hypothes s that grinding has affected the grading, as suggested by the comparison of the grading curves for the natural and reconstituted clay in F g 5 2 Grinding may ha e mod fied the coarse s il const tuents of the Pappadai clay, crushing the carbonate shells and und ng the detrit c crysta s

In Figs.5.43 to 5.45 the reconstituted fabric appears less densely packed than the undisturbed clay fabric (Figs.5.18 to 5.21). This difference between the packing of the two clays is related to the difference between their preconsolidation pressures. The reconstituted clay is normally consolidated to σ'_v equal to 200kPa, while the undisturbed clay was preconsolidated to 1310kPa and swelled to 414kPa, though swelling gave rise to quite a small increase of the pore volume.

The reconstituted clay underwent a rapid unloading in the oedometer following compression to 200kPa, but the presence of open fissures between some domains (Fig 5.43) shows that the unloading was not at constant volume, even if no drainage was permitted The fissures mainly developed either at the contact between the faces of parallel domains or at the contact between clay domains and sand grains. It may be that in these contact areas the electrostatic and electromagnetic forces between the clay particles, i e the bonding of the reconstituted clay, is weakest So during undrained unloading the clay volume seems to increase, and cavitation occurs, mainly in those zones where bonding is weak. Open fissures were not observed in the undisturbed clay after the undrained unloading due to sampling, which is consistent with the fact that the natural structure sustained very high suctions (see Section 5.6.) and has a strong bonding, as will be discussed later. This interpretation of the clay response to unloading will be supported by other results in Chapter 7.

The pictures of a sub-vertical fracture in Fig.5.43 and of a sub-horizontal one in Fig 5 44, show a mediumly orientated open fabric. Thin strata formed by well orientated domains are interbedded with large zones of open random fabric. Voids of 7μm diameter occur within the flocculated fabric shown in Fig.5.45. Differences may exist between the flocculation modes in different zones of the random fabric. This shows that also in the reconstituted clay one-dimensional consolidation gives rise to non-uniform fabric changes. Thus the fabric evolution during one-dimensional consolidation proposed by Sfondrini (1977) and discussed in Chapter 1 (Fig 1 13) seems to apply both to the natural and the reconstituted Pappadai clay

It is suggested that this fabric transformation process occurs generally during one-dimensional consolidation of normally-consolidated clays This hypothesis will be discussed in more detail in Chapter 7 in light of the fabric observed in the reconstituted Pappadai clay after oedometric compression to high stresses

The systematic succession of stacks of domains and honeycomb strata shown in Fig 1 12(e) was recognized in some areas of the undisturbed fabric (Fig 5 31), and now it is recognized in some

zones of the reconstituted fabric (Fig.5.43). The pictures in Fig.5.46 show that a similar fabric can be observed also in other reconstituted clayey soils (Menkiti 1995). The repetitive presence of this fabric within one-dimensionally consolidated clays will also be further discussed in Chapter 7.

Although the one-dimensional consolidation of the clay induces a non-uniform fabric as discussed above, it does induce a progressive increase of the average orientation of the clay particles The areas of random fabric are more extensive in the reconstituted clay than in the undisturbed one. However, although the undisturbed clay is in general more densely packed than the reconstituted clay, in some areas its fabric is as open as in the reconstituted. Indeed, in some zones, the undisturbed fabric is even more chaotic than the reconstituted and in general it is more complex as processes have occurred in the natural clay which do not apply to the reconstituted clay, diagenesis being one of these

At higher magnifications it can be seen that while a large number of coccoliths exist in the undisturbed clay, only few are observed in the reconstituted clay and these are often broken (Fig.5.47). As previously suggested for the foraminifera, also the nannofossils may have been damaged by the grinding operations. The shape of the reconstituted clay particles, shown in Fig.5.47, may also be compared with that of the corresponding particles in the undisturbed clay (Figs.5.26 and 5.27). The outlines of the reconstituted clay particles are not as regular as those of the undisturbed clay particles, appearing to have damaged surfaces. These differences may be related to the fact that grinding has affected the mineralogical structure of some of the clay particles, an hypothesis suggested in Section 5.8. on the basis of the results of the X-ray diffraction analyses of powdered undisturbed and reconstituted Pappadai clay. In conclusion, there is considerable evidence which suggests that grinding affects the mineralogical properties and the grading of the clay, and future research should take account of this problem

5.10 Investigation of bonding

Part of the high carbonate content of the Pappadai clay may be acting as a bonding agent although the SEM has shown that a large part of it is concentrated in fossil shells and detritic crystals In this section data supporting the existence of a carbonate bonding in the undisturbed Pappadai clay are presented However, as well as the carbonate bonding, other types of bonding also exist in the clay The existence of electrostatic and electromagnetic bonding in any clay has

been discussed in Section 1.4. In addition, diagenetic bonding other than cementation may exist in the natural Pappadai clay, but this cannot be demonstrated in the present research.

5.10.1 Macrostructure of the Pappadai clay after swelling

The qualitative results of the two very simple tests reported in this section suggest that the clay bonding may consist in part of a weak cementation.

Two small undisturbed initially saturated clay specimens were prepared, they had a water content equal to 31.8%. One of the specimens was left to swell freely inside a glass of water for two months. Apart from some softening at the sample surface, the clay macrostructure did not change during the test (Fig.5.48). The dissipation of the high suctions present in the clay caused a very limited volume increase and did not loosen the clay particles. The clay remained intact and after swelling a strong bonding was still present since considerable mechanical disturbance was necessary for remoulding. Similar effects are usually observed for cemented soils.

The other specimen was first dried at 120C° and then left to swell freely submerged in water for two months as well. When immersed, the clay absorbed water as effect of the very high pressure gradients present in the specimen and air bubbles were seen coming out of the specimen. After few minutes the specimen split along parallel horizontal lamination planes (Fig.5.49). Open fissures developed along the lamination planes. In between these laminations the clay strata appeared to remain intact. The pile of thin clay strata underwent no further change during the following two months. A possible reason for this behaviour is that at the contact between the clay and the sand of the lamination planes bonding had been weakened during drying due to the different shrinkage behaviour of the clay strata and the silty laminations.

The test results then show that the bonding of the Pappadai clay restrains swelling unless it is mechanically disturbed, as may be expected for cemented bonding Nonetheless, if it exists, this cementation is very weak, as it is apparently destroyed by extensive drying at the contact between the clay and the silt-sand laminations In practice the lamination planes have been found to be critical zones for the strength response of the sub-Apennine blue clays in situ, as in deep tunnelling the clay strata first loose their stability by slipping along the lamination planes, this being the main failure mode exhibited during the tunnelling operations (V Cotecchia and Tafuni 1996).

5.10.2. Chemical micro-analysis: Procedures

The chemical micro-analysis defines the chemical composition of microscopic zones within the material. It is carried out using a system composed of a scanning electron microscope and an X-ray receiver and diffractometer. In principle, an energy dispersive X-ray analysis is carried out. Inside the electron microscope the impact of the electron beam with the material generates the X-rays which are analyzed, revealing the composition of the spot being scanned.

The minimum diameter of the area which can be analyzed chemically is about 1μm The area being scanned is displayed on the screen of the scanning electron microscope so that what is being analyzed can be recognized within the fabric. The chemical micro-analysis was carried out together with the SEM analysis of the clay fabric for the samples forming group 3 in Table 5 9. The chemical composition of locations within single clay particles, at interparticle contacts, within stacks of particles, within fossils, within crystals and bridges crossing the clay pores were investigated.

In the following sections the diffractograms obtained from these experiments are shown, together with the pictures of the area being examined. Even though the resolution of the SEM pictures is not good, they still usefully document the locations to which the diffractograms refer. The size of the peaks in the diffractograms show to a good approximation the relative proportions of the elements present.

Some of the gold coated samples from group 2 in Table 5.9 were also chemically scanned The pictures of these samples are of good resolution and, although the X-ray diffractograms are affected by the gold coating, they support the conclusions drawn from the analysis of the other samples.

5 10.3 Chemical micro-analysis of the undisturbed clay : Results

In Fig 5.50 the fabric on a vertical fracture through the clay for a carbon coated sample is shown Diffractogram (a) is logged on a clay particle It shows the typical composition of mica (Si, Al and K), but in addition a high proportion of calcium is detected Calcium seems to be superimposed on the clay mineral Diffractogram (b) in the figure refers to a constituent which resembles pyrite. The identification of pyrite is confirmed by the size of the peaks related to su phur (S) and iron (Fe) in the diffract gram In Fig 5 51 what appears t be a f ss shell was

scanned chemically. Diffractogram (a) shows that the size of the peak related to calcium is by far the largest.

These three examples show that the diffractograms do give a reasonable estimate of the relative proportions of the different elements at the location being scanned, and that they may be used to define to a first approximation the chemical composition of the different parts of the clay fabric.

However, sometimes the diffractograms may not represent the chemical composition of what is actually seen on the screen. For example, when the area being scanned appears to be a continuous particle aggregate, the electron beam may in fact be penetrating an inter-particle void which cannot be seen by SEM. So care is necessary in defining the chemistry of the particle aggregates.

Diffractogram (b) in Fig.5.51 shows mica particles adjacent to a fossil shell, but that a lot of calcium is present within the particles. In Fig 5 52 a flocculated fabric, formed by domains in edge to face contact surrounding a 5μm diameter pore, is investigated in detail. Diffractogram (a) shows that for the "bridge" between the two domains indicated in the figure the basic chemical composition is that of mica plus a considerable proportion of calcium. A large quantity of calcium is also present in the adjacent particles (diffractogram (b)), although its maximum concentration is logged within the "bridge".

In Fig.5.53 iso-orientated domains forming sub-horizontal strata are seen on an inclined fracture through the clay. Diffractogram (a) is typical of the domains in the picture Again, together with mica components, the presence of a significant amount of calcium can be seen. The enlargement of a particle aggregate from Fig 5.53 is shown in Fig 5.54. Diffractogram (a) refers to one particle and is very similar to what was observed for the particle domain in Fig 5.53. Calcium is detected throughout the fabric, but its presence increases within the pore voids, as shown by diffractograms (b), Figs. 5.53 and 5.54, and at the edge-to-face contacts between particles and domains, as shown by diffractogram (c) in Fig 5.54.

In Fig.5.55 the results for the gold coated samples, e g group 2 in Table 1, are shown Diffractograms (a) and (b) are very similar and represent the composition of two particles in edge to face contact, indicated in the pictures Although two major bands indicating gold dominate the diffractogram, again the basic composition is of mica plus a significant amount of calcium The ratio between the sizes of the peaks for silicon and calcium (Si/Ca) is about 2 6 in the diffractograms referring to single clay particles both in Figs 5 54, for the carbon-coated specimen, and in Fig 5 55, for the gold-coated specimen

Given the differences in the ways the two tests were carried out, this consistency is an encouraging reflection of the relevance of the results so far presented. Diffractograms (c) and (d) in Fig.5.55 again show that a concentration of calcium systematically occurs at the edge-to-face contacts between particles and domains, although similar concentrations are sometimes detected for single particles (diffractogram (e)). Similar results are obtained from the analysis of the particle aggregate in Fig.5.56.

The results presented above show that calcium alone is detected only when scanning detrital crystals or fossil shells, but that calcium is widespread within the Pappadai clay fabric. The calcium content is about 30% of the silicon content in areas where clay particles are scanned and it rises to about 60% at the inter-particle contacts However this calcium content is in general not crystalline, since it cannot be seen by SEM. Calcium then seems to form a film of amorphous, or cripto-crystalline, calcite which covers the clay particles and the inter-particle contacts, being thicker at the contacts.

The calcite film does coincide with a carbonate bonding which at places may even form a "binding" between the clay particles of the natural Pappadai clay The formation of this carbonate binding did not occur during deposition and virgin compression, firstly because in general precipitation of calcite from a solution creates calcite crystals rather than amorphous calcite; secondly because the modelling reported in Sections 3 8 and 4 7 showed that the Pappadai clay must have an uncemented sedimentation structure during virgin compression. It follows that the calcite films were formed at a later stage, either at the end of virgin compression or during long-term diagenesis (see Section 1.10). In both the cases, calcite precipitated from the pore fluid after it had become supersaturated. The formation of authigenic calcite has indeed been observed in soils rich of carbonate fossils (Sfondrini 1977, O'Brien and Slatt 1990), and in Pappadai clay calcite crystals which have been partially dissolved were found, as shown in Fig 5 23.

In conclusion, the existence in the Pappadai clay of a carbonate bonding acquired by the clay when under high σ'_v has been demonstrated. This bonding is such as to bind the clay particles and almost give rise to weak cementation, as anticipated in the previous section on the basis of the clay response to swelling The structure of the Pappadai clay during unloading was thus stronger than its original sedimentation structure (see Table 1 1), as proposed in Section 4 7 on the basis of the discrepancy between the K_o values exhibited by the natural OC clay and the K_o values expected for a model clay which did not undergo strengthening by further bonding in its geolog cal history

5.10.4. Chemical micro-analysis of the reconstituted clay : Results

For samples B of group 3 (Table 5.9) the carbon coating was not well done and the chemical micro-analysis gave unreliable results. However, with the reconstituted clay reliable measurements of the chemical composition were carried out on the clay after consolidation in the oedometer to σ'_v equal to 22MPa. If no significant changes of the clay composition occurred during the oedometric compression, these results may also be relevant to the reconstituted clay prior to compression.

The pictures of the reconstituted fabric at high pressures and the corresponding diffractograms are shown in Fig.5.57. This clay fabric will be discussed in Chapter 7, but here the fact that the clay particles are very densely packed must be taken into account because it is consequently difficult to scan a single clay particle or constituent, and the diffractograms are less precisely targeted.

The diffractograms for the single clay particles are similar to those obtained for the natural clay However many clay-size constituents either have a very high calcium content (Fig 5 57 diffractogram (b)), or are formed only of calcium (Fig 5.58 diffractogram (a)). This finding may be consistent with the fact that the many fossils present in the intact clay have been broken into smaller pieces during grinding, and that few fossils can be recognized within the reconstituted fabric. So the chemical micro-analysis is consistent with the fact that the reconstitution process affected the clay grading

5.11 Conclusions

The SEM shows that the natural Pappadai clay is generally densely packed, but non-uniformly orientated. Fabric elements formed by orientated particle domains do exist, but they may lie in different directions, crossing each other, and be interbedded with a flocculated fabric, where clay particles and domains are both in edge-to-edge and edge-to-face contact. At places, the fabric is non-orientated because of the presence of fossil shells and detritic crystals

The random fabric and the flocculated aggregates are relics of an original bookhouse fabric, formed in the Pappadai clay at deposition, and compacted during consolidation. The bookhouse fabric was non-uniformly rearranged during consolidation Some zones were highly compressed, the particles being reoriented in a c p o fabric to f rm stacks or as otherw se defined b\

Sfondrini (1977), "complex laminae". Other zones were less compressed, the flocculated fabric there being preserved. Then, during virgin compression, localization of strain took place in the Pappadai clay fabric; the schemes of fabric transformation, during one-dimensional consolidation up to medium-high stresses, proposed by Sfondrini and reported in Fig.1.13, have so been shown to apply to the Pappadai clay case history.

The reconstituted clay fabric also conforms to the schemes of Sfondrini (Fig 1.13), as zones of rather orientated fabric alternate with zones of flocculated fabric. However, in the reconstituted clay, the changes from one type of fabric to the other are less chaotic than in the natural clay, and in general the fabric is rather open.

Some structural features observed by SEM confirm that the natural Pappadai clay was subjected to diagenesis and indeed part of the complexity of its fabric may have arisen from diagenetic phenomena. The existence of a calcite film covering the natural clay particles and inter-particle contacts was revealed by the chemical micro-analysis which demonstrated that a carbonate bonding currently exists in the natural clay. Calcite forms a continuous fragile coating of the particle aggregates, and gives place to an interparticle connection which most probably works as a fragile weak cementation here defined as carbonate "binding". The clay acquired this carbonate binding under high stresses.

In Fig.5.59 the state history of the natural Pappadai clay and that of the reconstituted one are compared in the LI-σ'_v plane In the figure the microstructural events occurring at different stages of the state history of the natural clay are also specified.

The virgin compression line for the reconstituted clay, i e the ICL, is below the SCC of the natural clay. The value of e_{100} measured for the reconstituted Pappadai clay, that is about 1 30, is higher than the value deduced from the relationship between e_{100} and the liquid limit proposed by Burland (1990), that is 1.128. Similar discrepancies have also been observed for other clays of various types (Coop and Cotecchia 1995).

It has been shown in Section 2 5 4 that for each SCC in the LI-σ'_v plane only one value of sensitivity applies In the LI-σ' plot of natural SCCs (Skempton 1970), reported in Fig 2 21, the compression curve for the reconstituted Pappadai clay lies at the lower boundary of the band formed by the SCCs, (see Fig. 5.60) as it should for the low sensitivity of the clay and following the sensitivity framework shown in Fig 2 23 The SCC of the natural Pappadai c ay l es ju t

below the middle of the band in Fig.5.60, showing that this clay had a low to medium sensitivity sedimentation structure during virgin compression.

Both the microstructural changes due to diagenesis at the end of virgin compression, and the changes due to the loading-unloading cycles the natural clay subsequentely underwent gave rise to the post-sedimentation structure considered in the previous sections, and places the natural Pappadai clay in the clay category 7 in Table 2.1.

The mechanical response of the two clays represented by points A and $\bar{B}$ in Fig 5.59 is shown in the following Chapters 6 and 8, where comparison will be made between the behaviour of a typical reconstituted structure and that of a post-sedimentation natural structure.

Depth m	pore water pressure kPa	σ'v kPa	σ'h kPa	q kPa	p' kPa	K0
25.4	68.7	414	654	-240	574	1.58

Table 5.1 In situ stress state of the clay block samples.

γ_s KN / m³	26.94
LIQUID LIMIT %	64.8
PLASTIC LIMIT %	29.8
ORGANIC CONTENT %	2k3
CARBONATE CONTENT %	28

a

Qz	Fd	Ca	Dol	K	Cl	I	Sm
3	1	22	6	12	14	20	22

b

Table 5.2 Undisturbed Pappadai clay: (a) index properties; (b) mineralogical composition

TEST	DATE	SAMPLE	W	γ_{wet}	γ_d	e	S_r	Suction kPa	Technique
	11/90	BLOCK SAMPLE	31.7	18.94	14.38	0.87	99.9	650	F.P.
OED1	12/90	P	31.17	18.95	14.44	0.863	99.2	600 600-1257	F.P. Sw., pr
OED2	12/90	1 T	30.198	19.00	14.59	0.844	98	617 636-1016	F.P. Sw , pr.
OED3	12/90	1 T	30.28	19.06	14.65	0.842	99	825 620-1270	F.P Sw ,pr
	5/91	P	31.35	18 96	14.43	0.864	99.6	902	F.P.
CRS 1	7/91	P	31.12	18.96	14.45	0.860	99		
CRS 2	7/91	P	31	18.96	14.47	0.860	99	725 670	Press.Plate Sw., pr
CRS 3	7/91	P	31.22	18.90	14.41	0.87	98.5		
TN 9	7/91	P	31.5	18.9	14.37	0.872	99.1 B=0 95	900	TRX
CRS 4	9/91	P	31.8	18 9	14.34	0.876	99.6		
TN 2	9/91	P	31.3	18.9	14.4	0.873	98.5 B=0 96	933	TRX
TN 3	10/91	P	30 6	18.9	14.47	0.857	96		
CRS 5	10/91	6B	31.00	18.95	14.46	0.86	99	813	Pressure Plate
TN 5	10 91	P	31.97	18 92	14.34	0.878	99.9		
TN 7	11 91	8B	30.79	18.90	14.45	0.862	98	920	F P
CRS 6	11 91	1 M	31.7	18.88	14.34	0.878	99	693	
CRS 7	11/91	5B	30.156	19.05	14.62	0.8407	98 5		
CRS 8	11 91	5B	30.8	19.01	14 53	0.854	99		
CRS 9	11/91	P	30.542	19 043	14.58	0.847	99		
	1/92	8B	31.15	18 92	14.42	0.865	99		
Sw.pr.test.	2/92	P	32.50	19.01	14.33	0.876	100	900	Sw pr.
	2 92	P	31.55	18.95	14 41	0.867	>99.8		
OED 7	2/92	P	32	18.82	14.25	0.887	99		
OED 5	3/92	P	32.18	18.89	14.28	0.882	100		
TN 11	4/92	P	32.3	18.89	14.28	0.884	100 B=1	820	TRX
OED 6	4/92	P	31.69	18.89	14.34	0.876	99		
TN 18	5/92	P	31.33	18.816	14.33	0.877	98		
CRS 11	7/92	3B	31.18	18.96	14.45	0.864	99		
TN 14	7 92	3B	30.756	18.89	14 45	0.862	98		
TN 12	10/92	3T	31.33	18.92	14 40	0.868	99	950	TRX
TN 20	12 92	2T	32.61	18.89	14.25	0 888	100		

Table 5 3 Measurements on specimens of undisturbed Pappadai clay.

w	e	S_r
31.5 - 32.5	0.87 - 0.885	99.5 - 100
31 - 31.5	0.86 - 0.87	99 - 99.5
30 - 31	0.84 - 0.86	98 - 99

Table 5.4 Undisturbed Pappadai clay: w-e-S_r values after storage.

K_o	YSR	STIFF CLAY
1.58	5.9	PAPPADAI CLAY
1.54	6	LONDON CLAY from BRADWELL (Skempton 1961)
2.29	11	"
2.26	25	"
2.1	11	LONDON CLAY from ASHFORD COMMON (Bishop et al. 1965)
2.6	27	"

Table 5.5 K_o-YSR values measured for Pappadai clay and London clay.

Qz	Fd	Ca	Dol	K	Chl	I	Sm
4	1	12	2	16	20	29	16

Table 5.6. Reconstituted Pappadai clay: mineralogical composition.

L.L. %	P.L. %	P.I. %
62.6	27.5	35.1

Table 5.7 Reconstituted Pappadai clay: Index properties.

Loading	σ'v (kPa)	Settlement mm
Hydrostatic Settling	0.6	20
Top cap weight & Suction due to base drainage	13.3	28.034
Weight	25.8	64.394
Weight	50.8	75.384
Weight	100.8	86.204
Weight	200.8	94.864

Table 5.8 Reconstituted Pappadai clay: consolidation from slurry.

Sample Group	SAMPLES					Sample Preparation	Coating	Laboratory
1	A	B	C	D	E	Freeze Drying	Gold	SEM Laboratory - CNR c/o Dpt. Scienze della Terra - Milano University
2	A					Air Drying	Gold	SEM Laboratory - Medicine Faculty Bari University
3	A	B	C	D	E	Freeze Drying	Carbon	SEM Laboratory - Istituto di Geologia Applicata e Geotecnica - Politecnico di Bari

Legend : A Natural Pappadai Clay - Undisturbed - before testing
B Reconstituted " - One-dimensionally compressed to σ'v = 200 kPa
C Natural " - " " " σ'v = 3 MPa
D " " - " " " σ'v = 22 MPa
E Reconstitute " - " " " σ'v = 22 MPa

Table 5.9 Samples subject to scanning electron microscopy.

Fig.5.1 Block sampling of Pappadai clay.

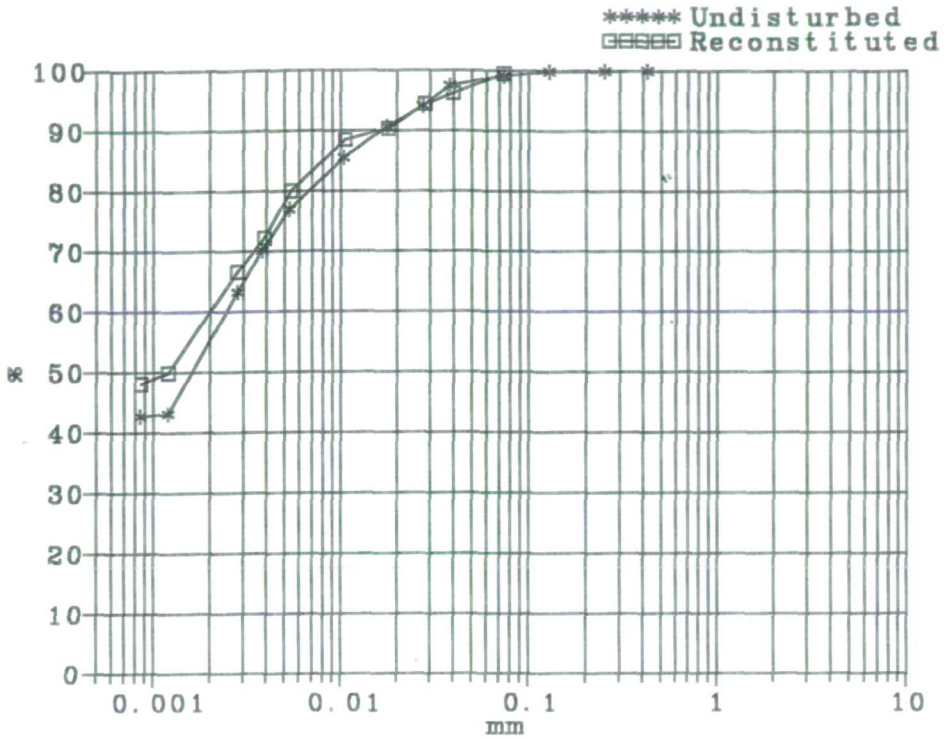

Fig.5.2 Grading curves of the natural and reconstituted Pappadai clay.

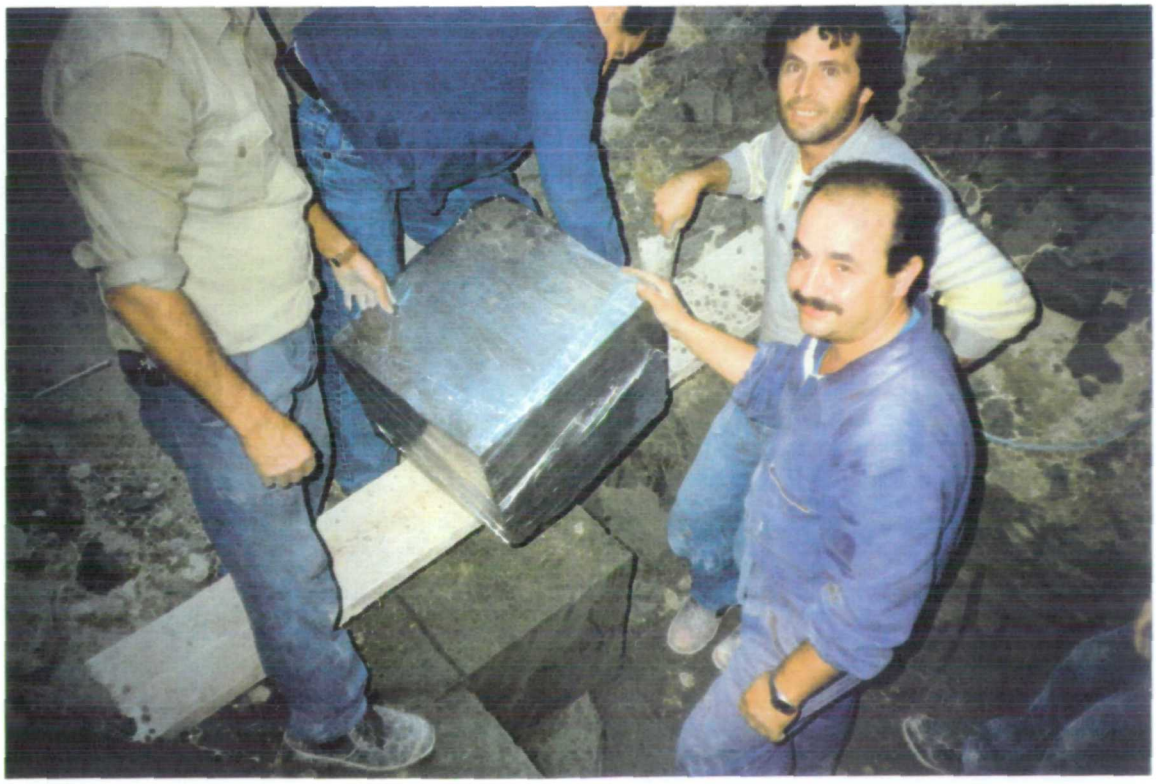

Fig.5.3 Block sample of Pappadai clay.

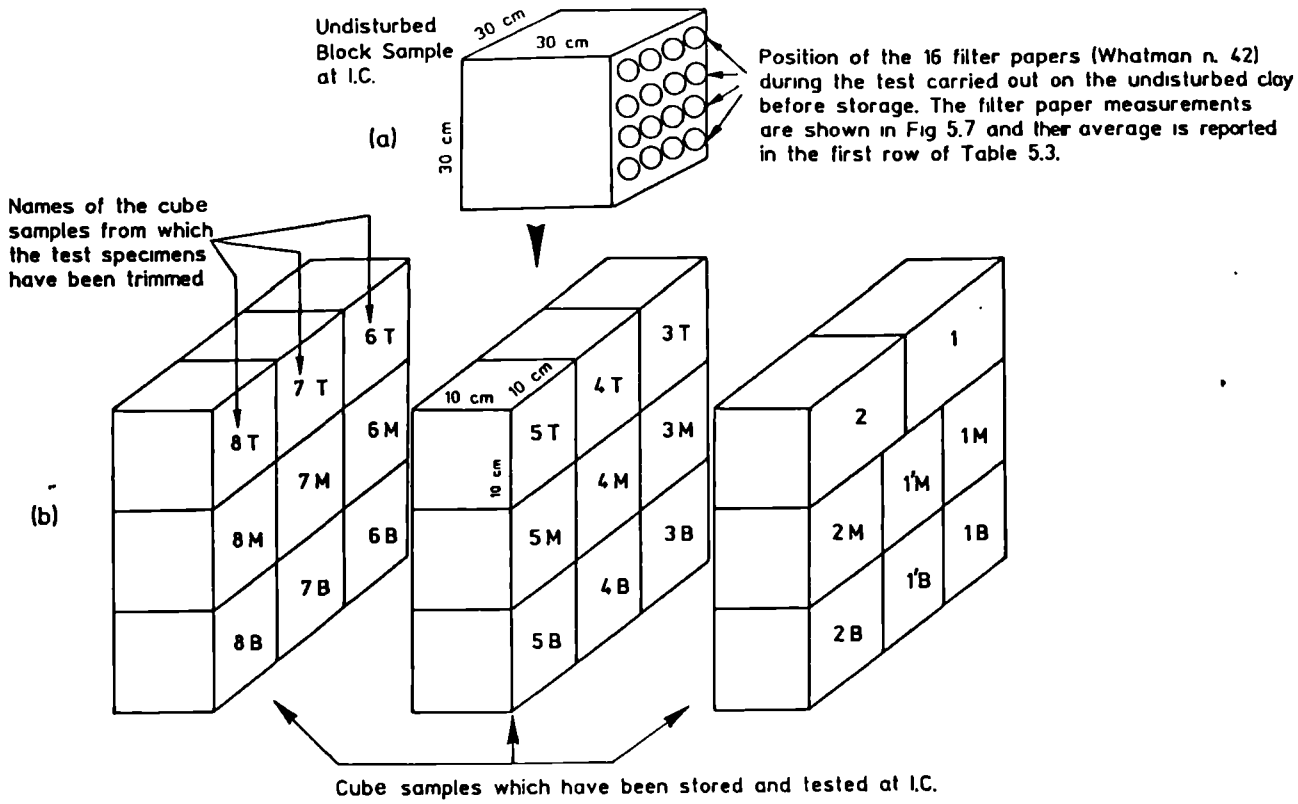

Fig.5.4 Samples of undisturbed clay tested at IC : (a) filter paper test on the clay block before storage; (b) division of the block sample into small cubes.

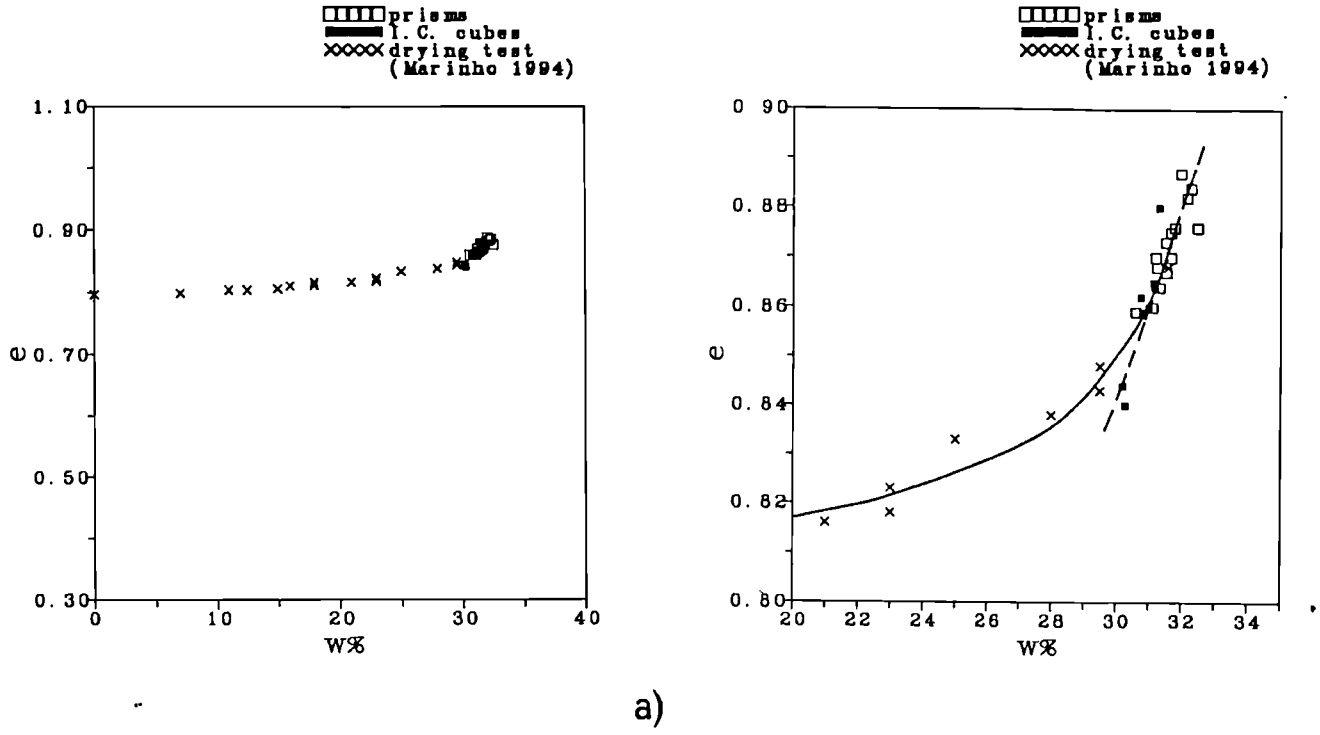

a)

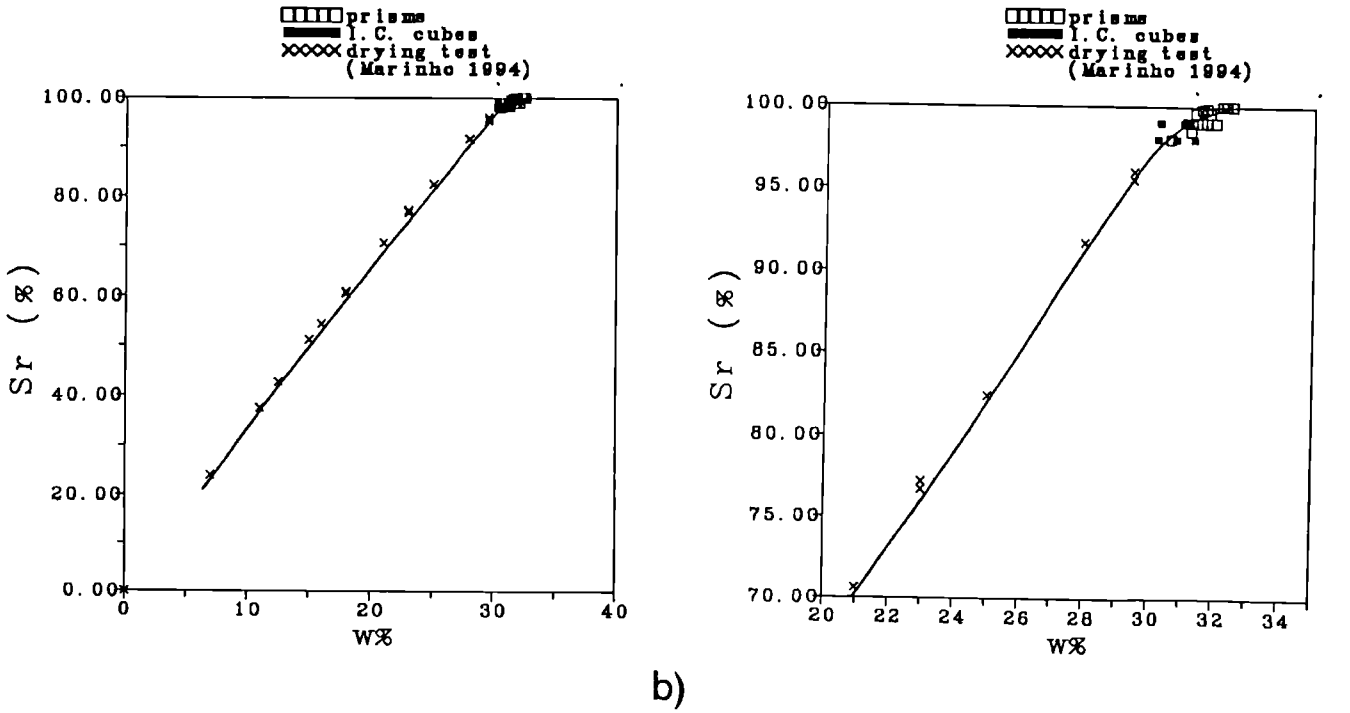

b)

Fig 5.5 Undisturbed Pappadai clay: (a) e-w and (b) S_r-w relations.

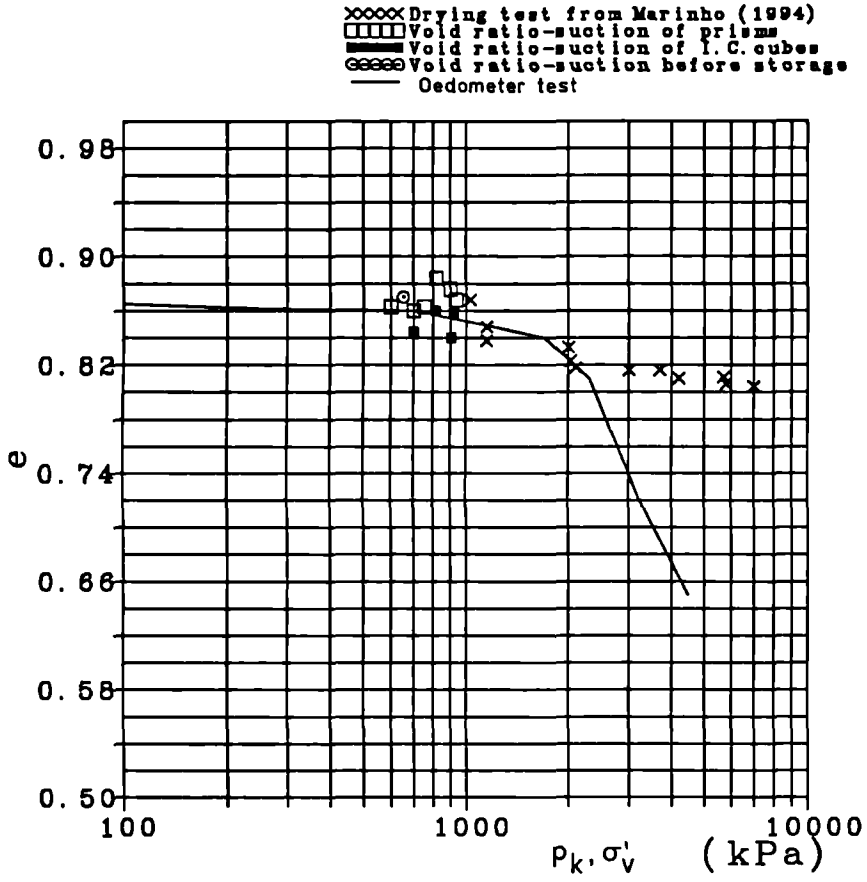

Fig.5.6 Undisturbed Pappadai clay: e-p_k and e-σ'_v relationships.

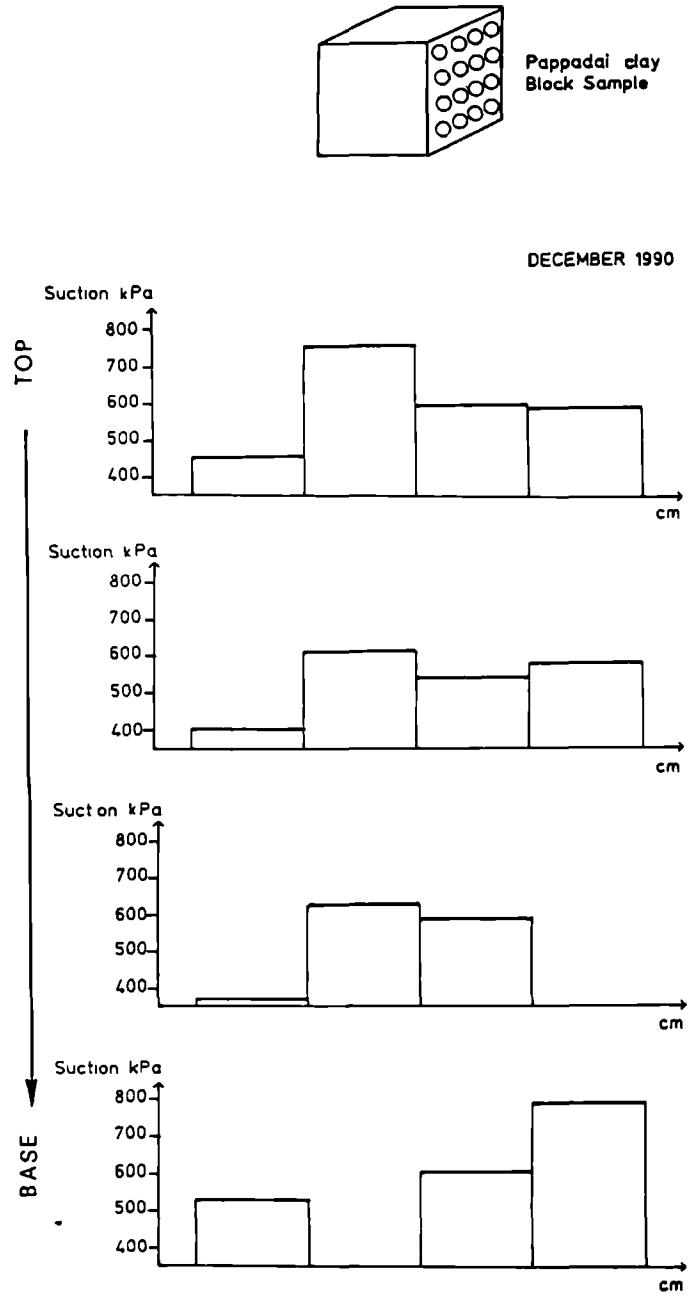

Fig.5.7 Filter paper measurements on the undisturbed clay before storage.

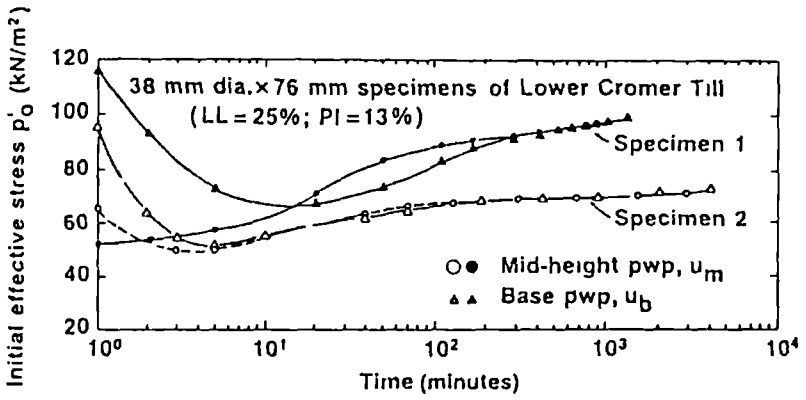

Fig.5.8 Pore water pressure response of a saturated soil to undrained isotropic loading (after Baldi et al.1988).

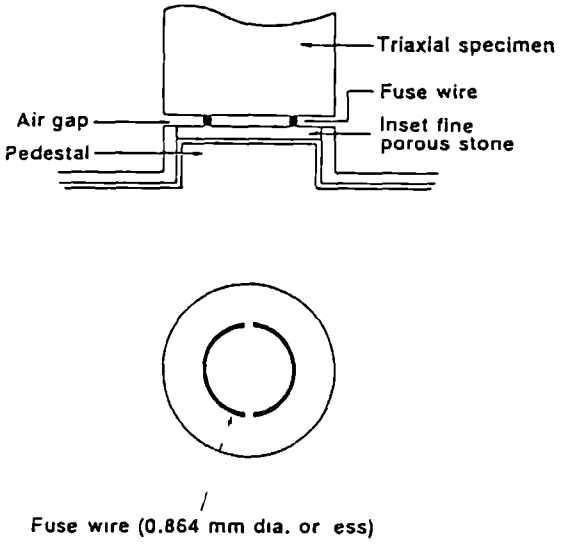

Fig.5.9 Fuse wire technique (after Bishop and Henkel 1962).

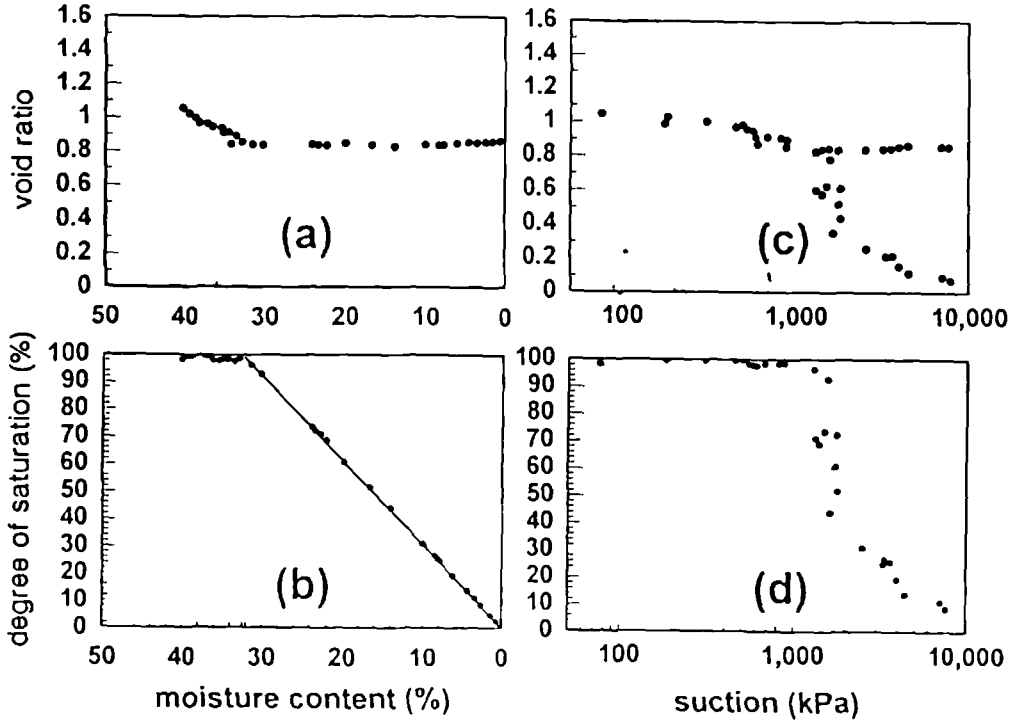

Fig.5.10 Drying test on overconsolidated kaolin (after Ridley 1993).

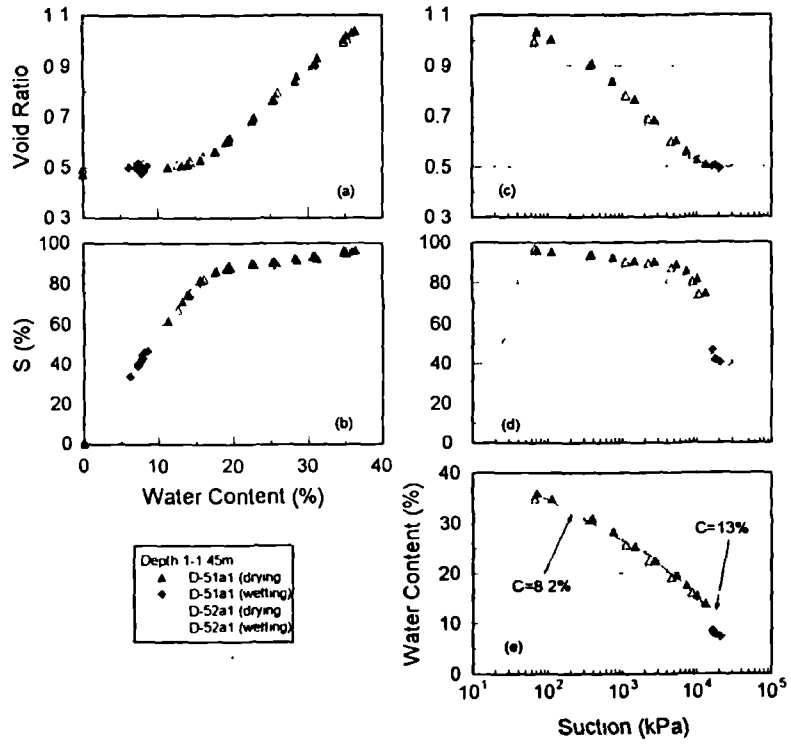

Fig.5.11 Drying test on undisturbed London Clay (after Marinho 1994).

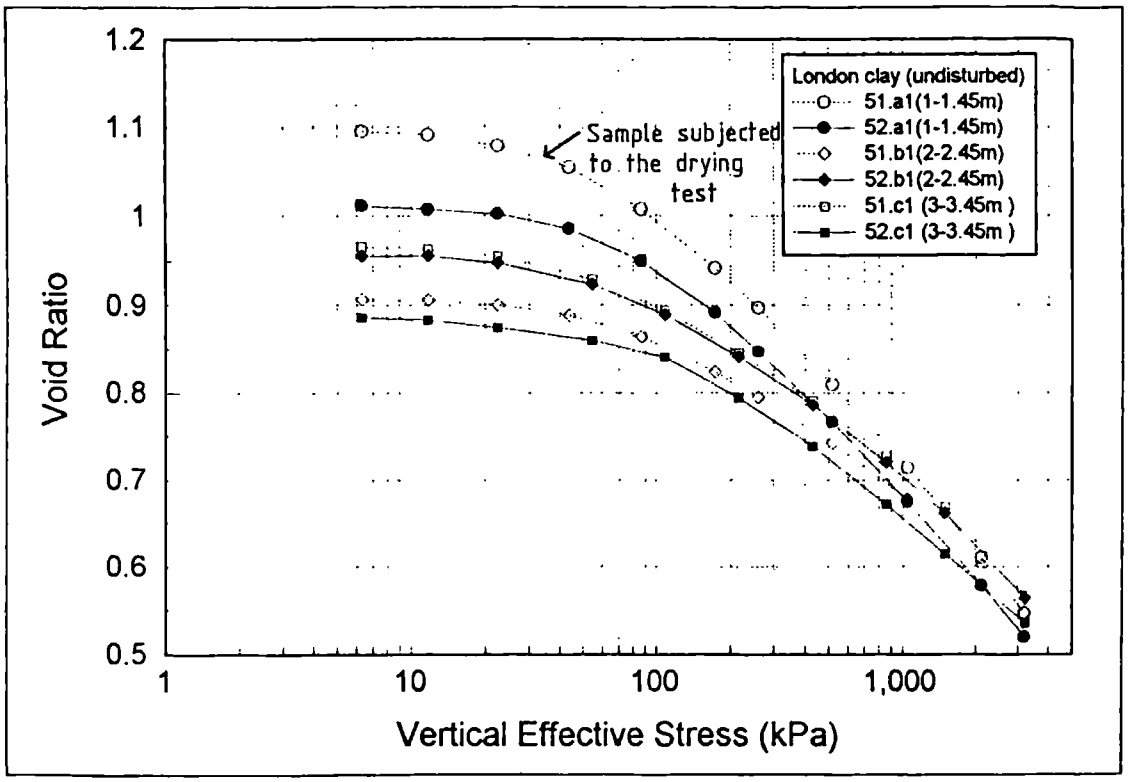

Fig.5.12 Oedometric compression curves of London clay (after Marinho 1994).

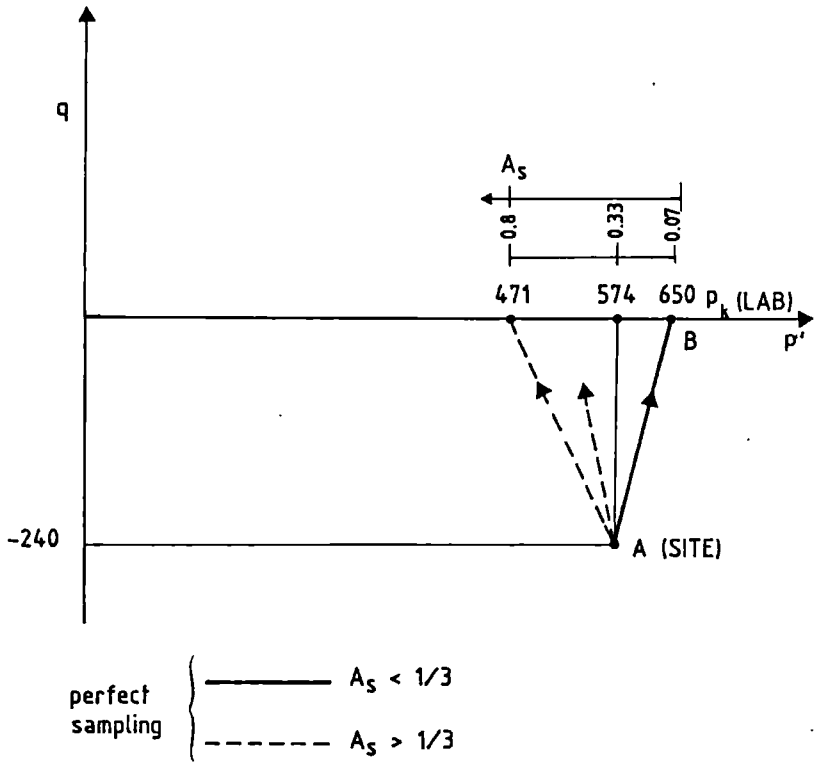

Fig.5.13 Pappadai clay: initial and final states of the block sampling stress path.

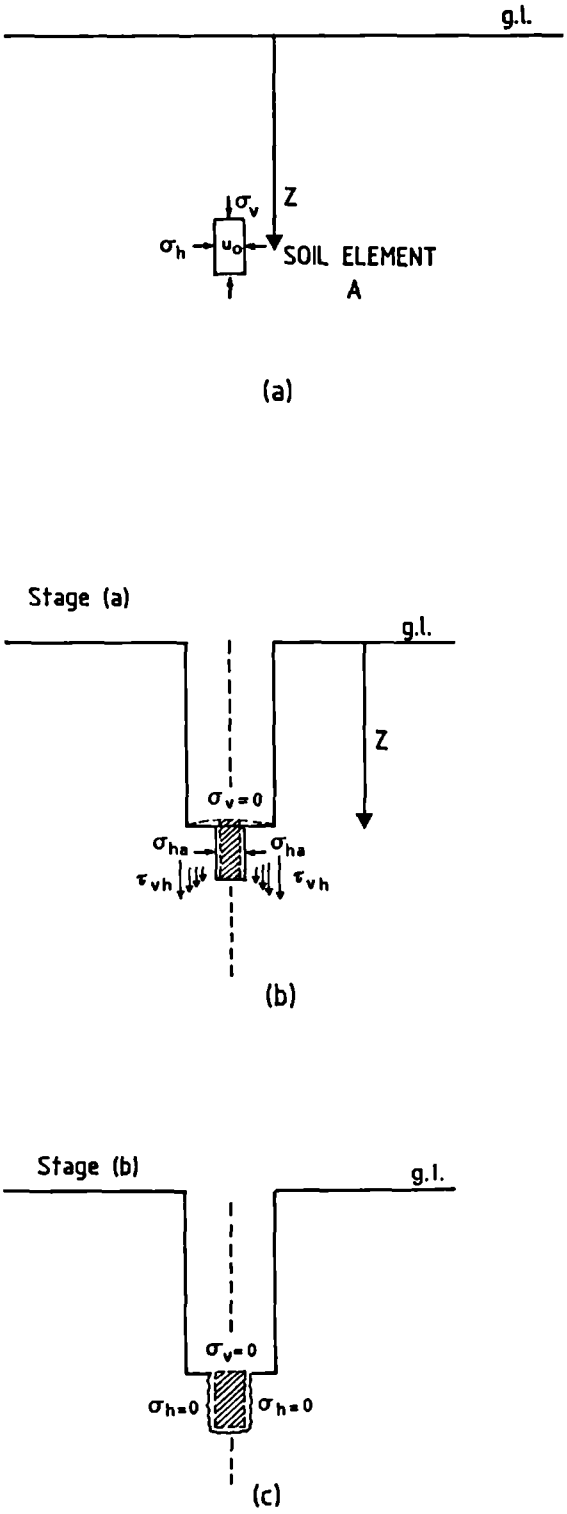

Fig.5.14 Stages of a block sampling path.

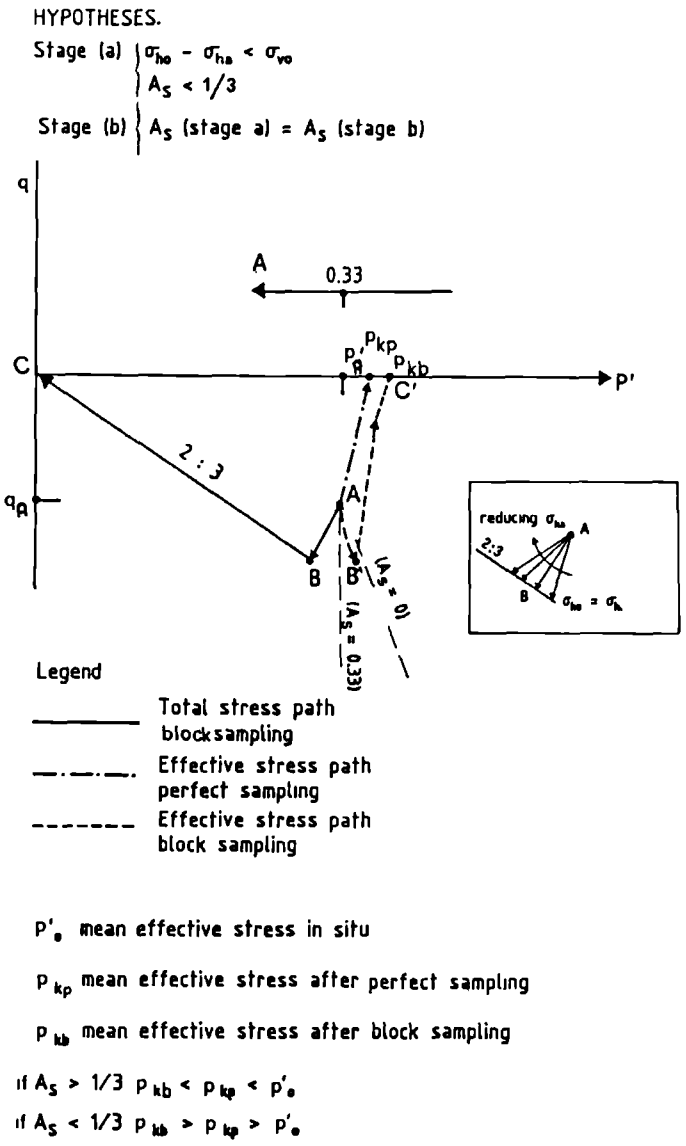

Fig. 5.15 Total and effective stress paths during block sampling.

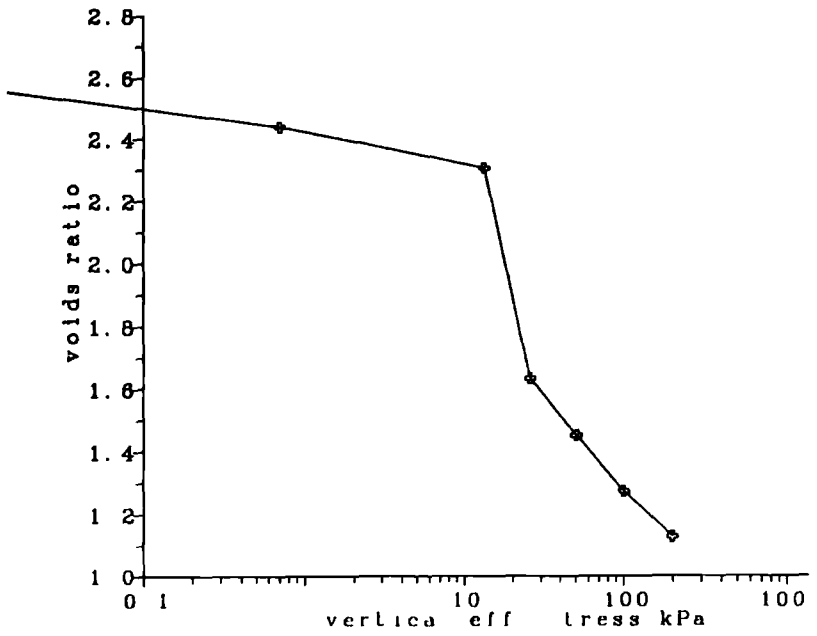

Fig. 5.16 One dimensional compression of reconstituted Pappadai clay from slurry in the consolidometer.

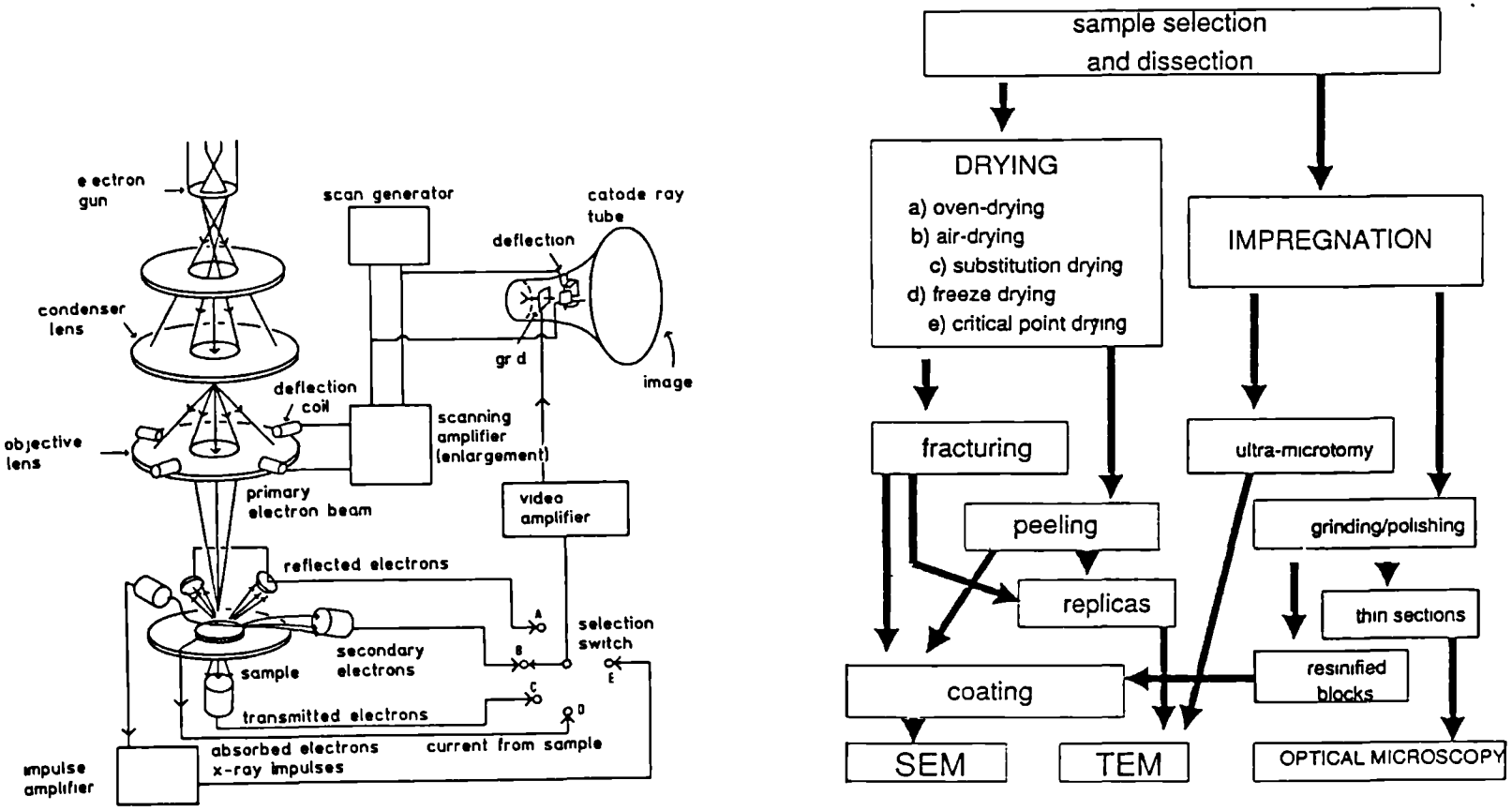

Fig.5.17 SEM : (a) modes of operation (manual of Cambridge 500 SEM); (b) sample preparation methods (Smart and Tovey 1981).

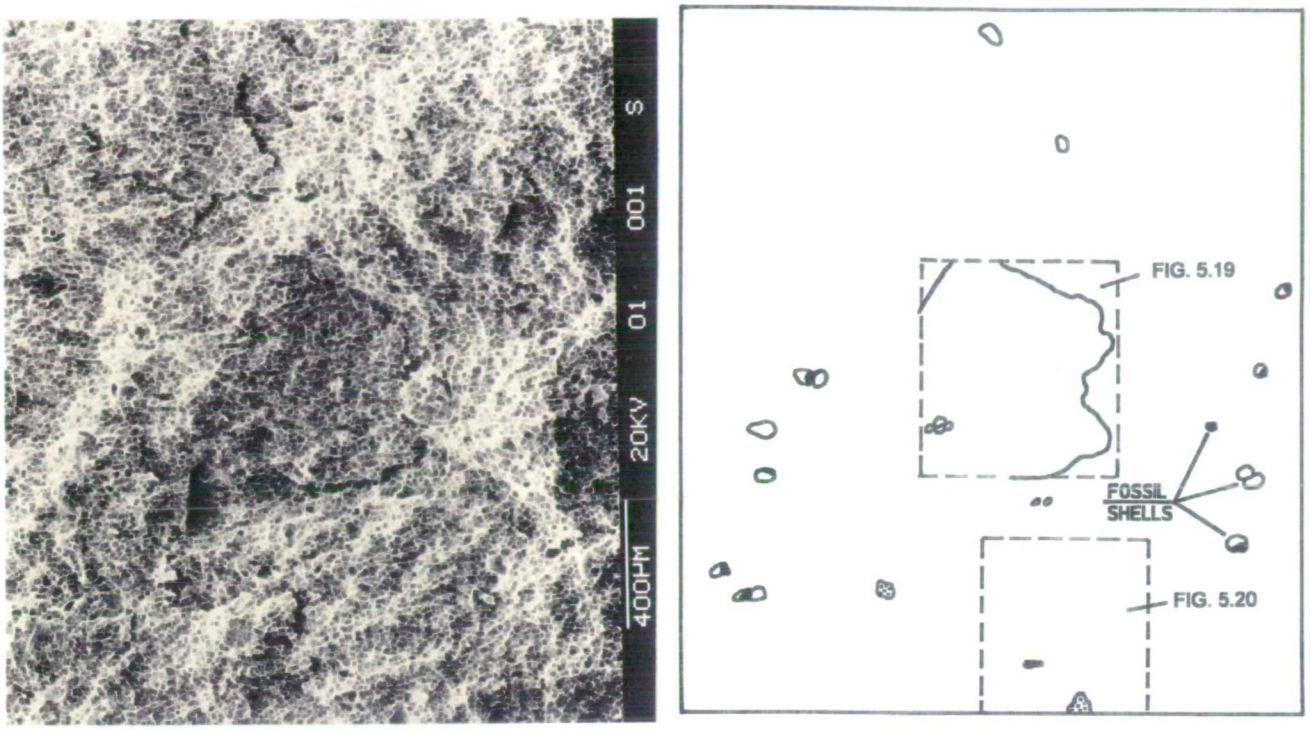

Fig. 5.18 - Undisturbed Pappadai Clay: Global view of the fabric on a vertical fracture; group 1 (Table 5.9)

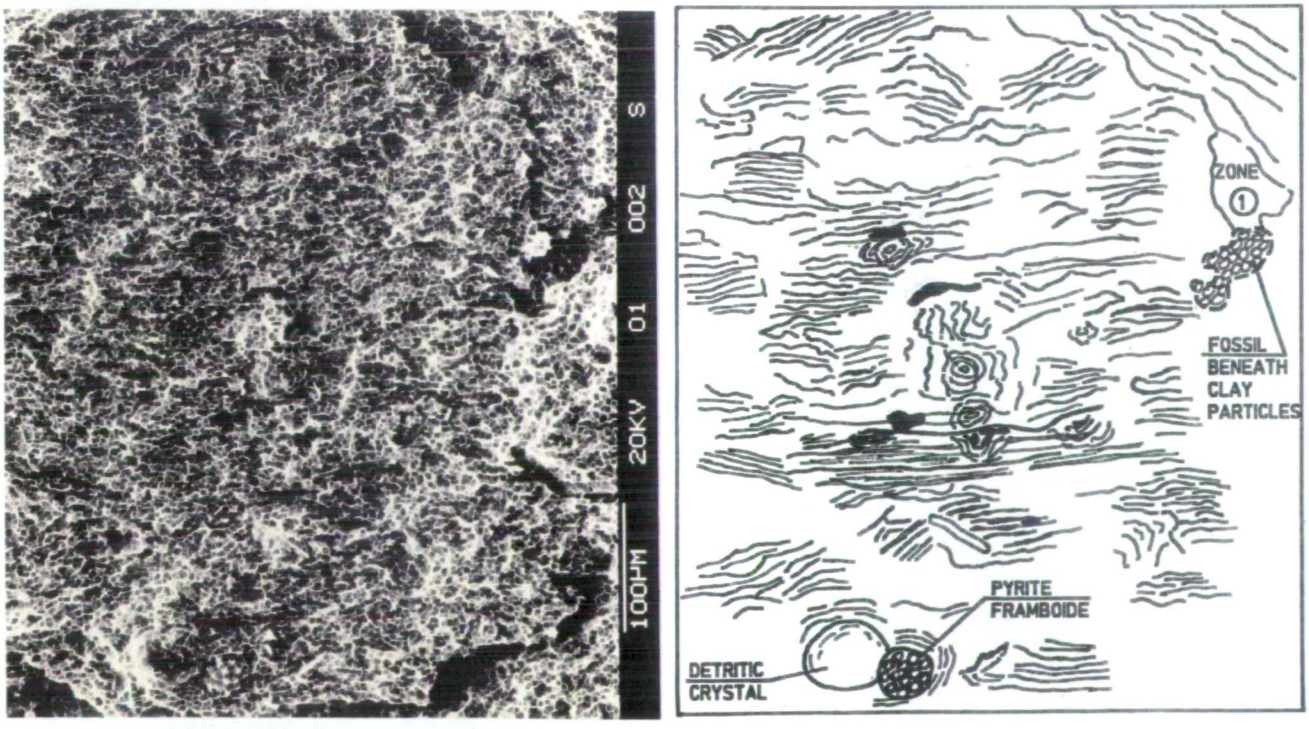

Fig. 5.19 - Undisturbed Pappadai Clay: Vertical fracture densely packed well orientated fabric; group 1 (Table 5.9)

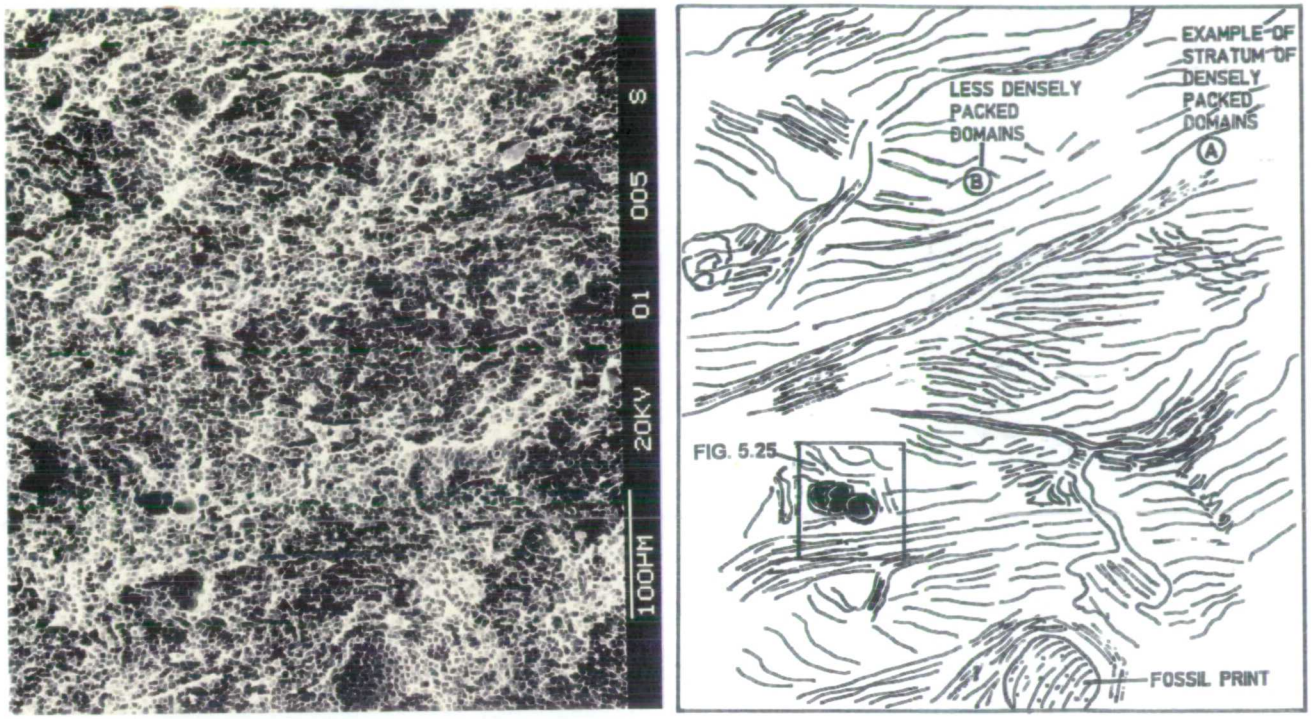

Fig. 5.20 - Undisturbed Pappadai Clay: Vertical fracture, densely packed well orientated fabric; group 1 (Table 5.9)

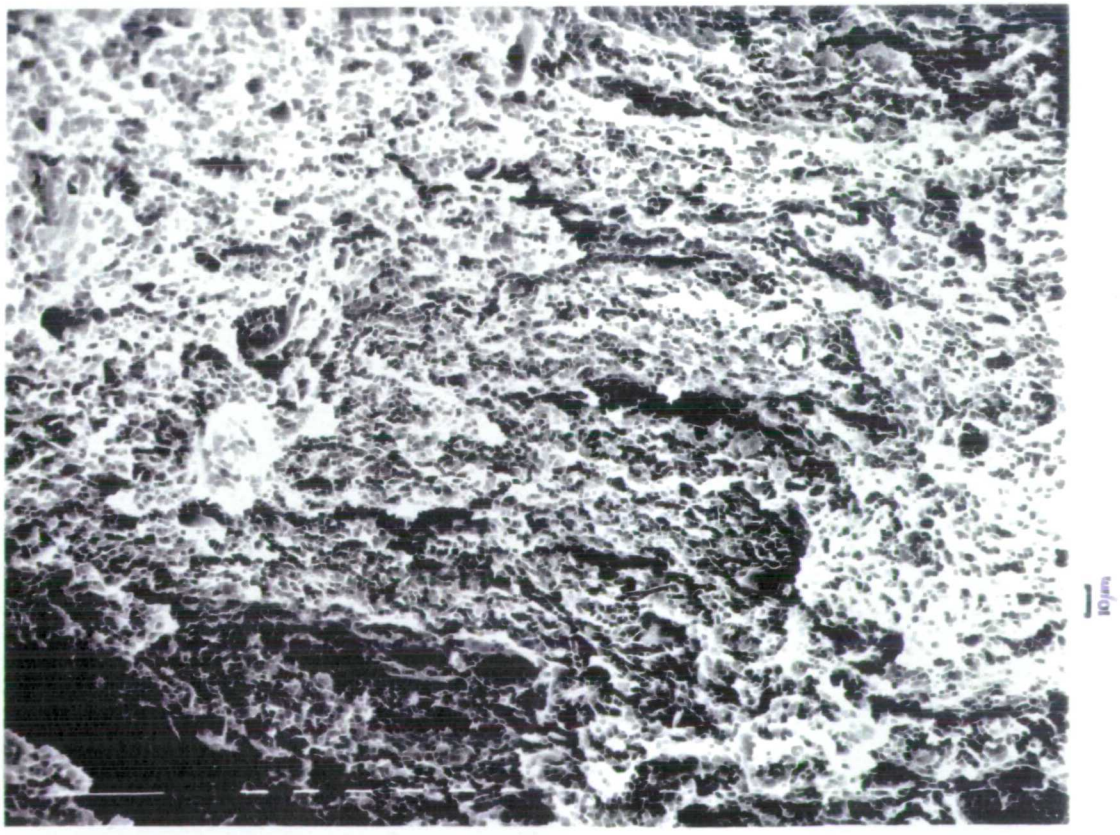

Fig. 5.21 - Undisturbed Pappadai Clay: Vertical fracture,densely packed well orientated fabric; group 2 (Table 5.9)

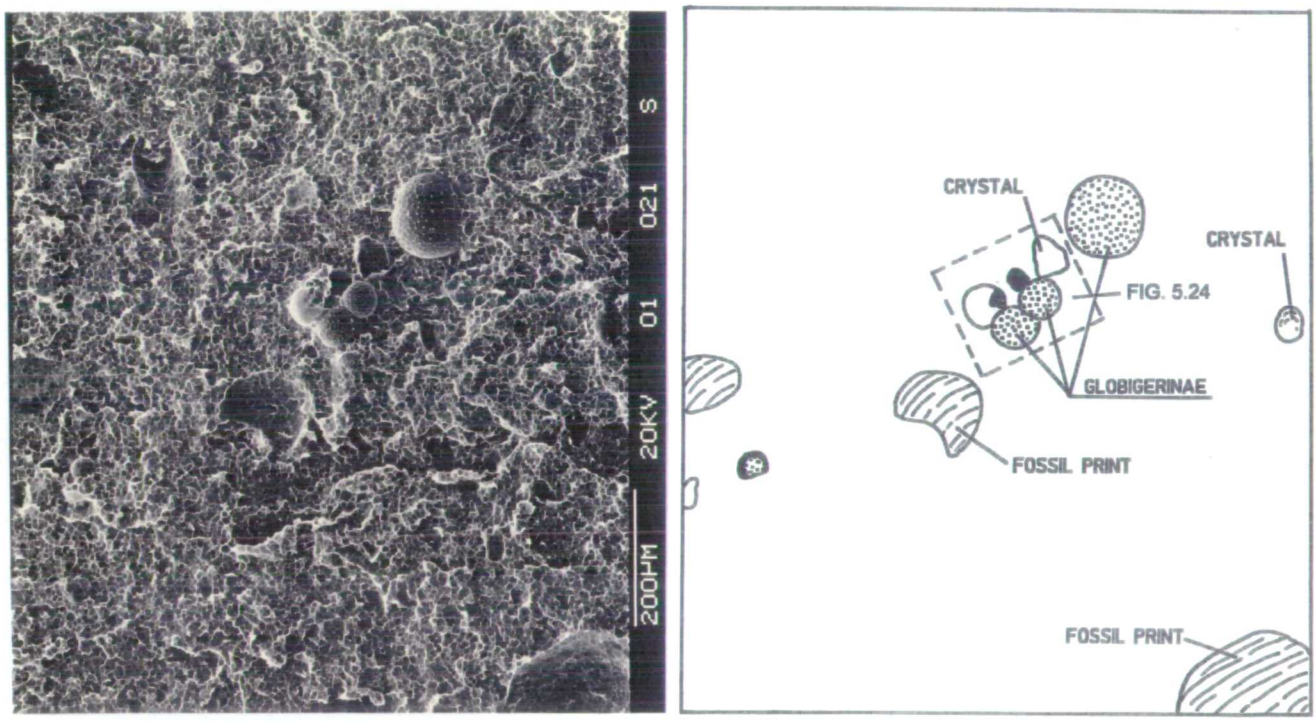

Fig. 5.22 - Undisturbed Pappadai Clay: Well orientated fabric; horizontal fracture, group 1 (Table 5.9)

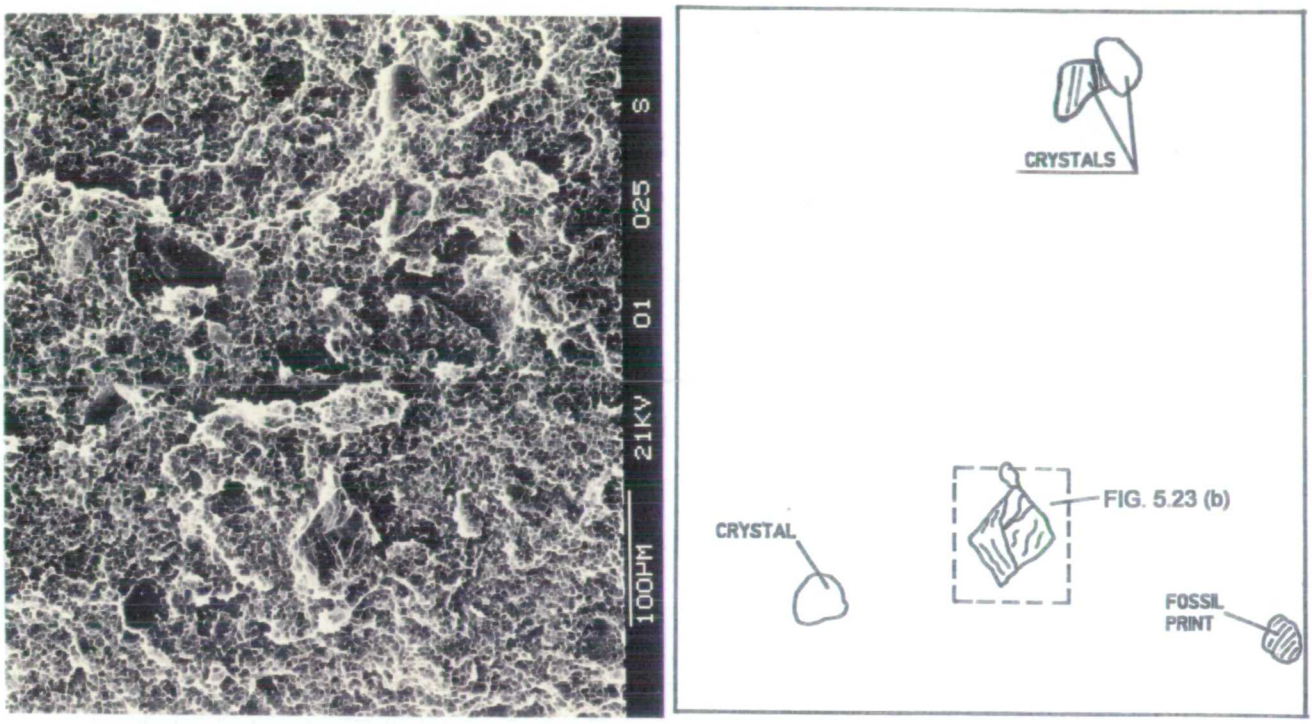

(a)

(b)

Fig. 5.23 - Undisturbed Pappadai Clay: Well orientated fabric; horizontal fracture, group 1 (Table 5.9)

Fig. 5.24 a - Undisturbed Pappadai Clay: Foraminifera shells; globigerina, group 1 (Table 5.9).

Fig. 5.24 b - Undisturbed Pappadai Clay: Foraminifera shells; globigerina, group 2 (Table 5.9)

Fig. 5.24 c - Undisturbed Pappadai Clay: Coccosphera, group 2 (Table 5.9).

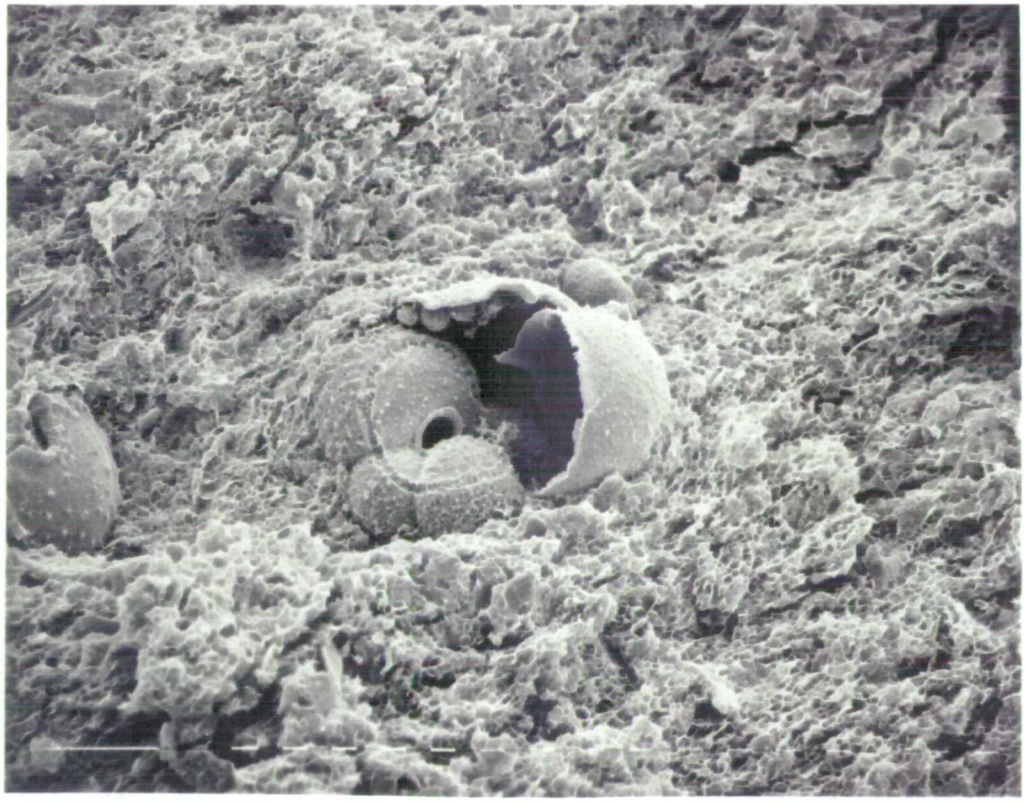

Fig. 5.24 d - Undisturbed Pappadai Clay; Foraminifera; group 2 (Table 5.9).

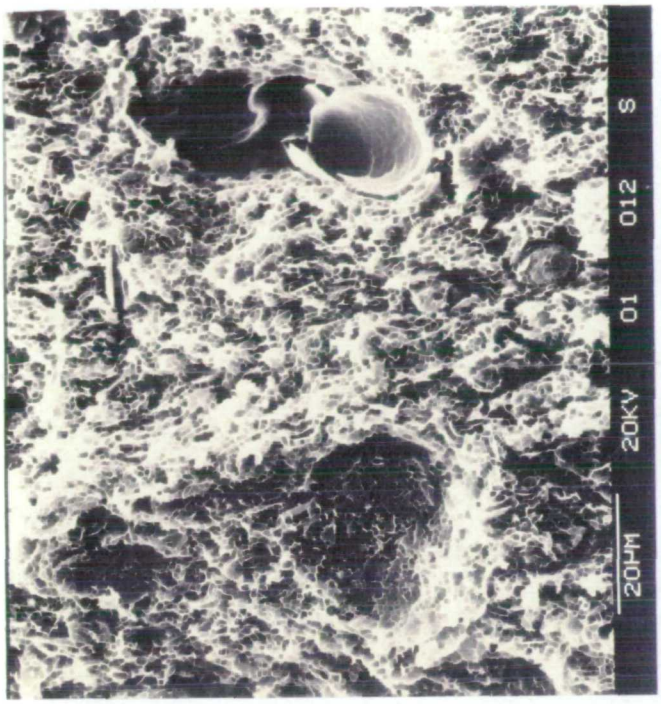

Fig. 5.25 - Undisturbed Pappadai Clay: Voids created by interbedded foraminifera; group 1 (Table 5.9)

Fig. 5.26 - Undisturbed Pappadai Clay: clay particles and coccoliths; horizontal fracture; group 1 (Table 5.9)

Fig. 5.27 - Undisturbed Pappadai Clay: clay particles; horizontal fracture, group 1 (Table 5.9).

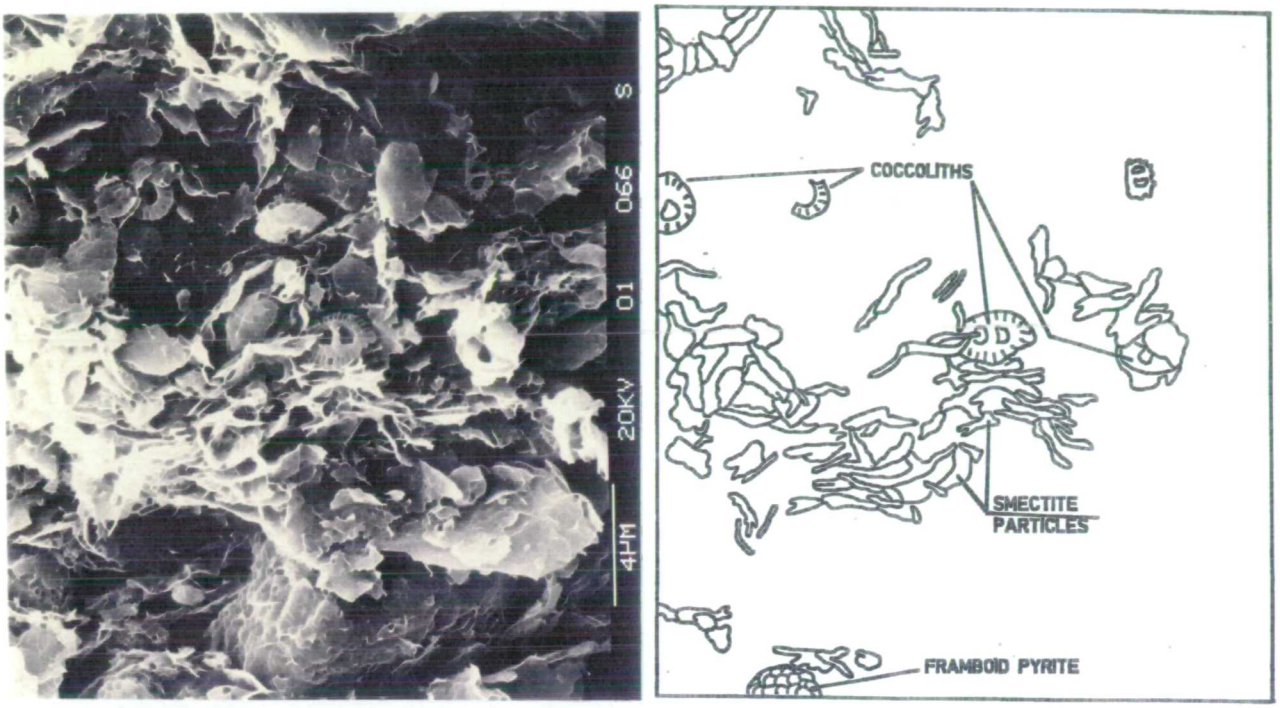

Fig. 5. 28 - Undisturbed Pappadai Clay: Smectite particles in random fabric of "spongy" appearance; coccoliths; group 1 (Table 5.9).

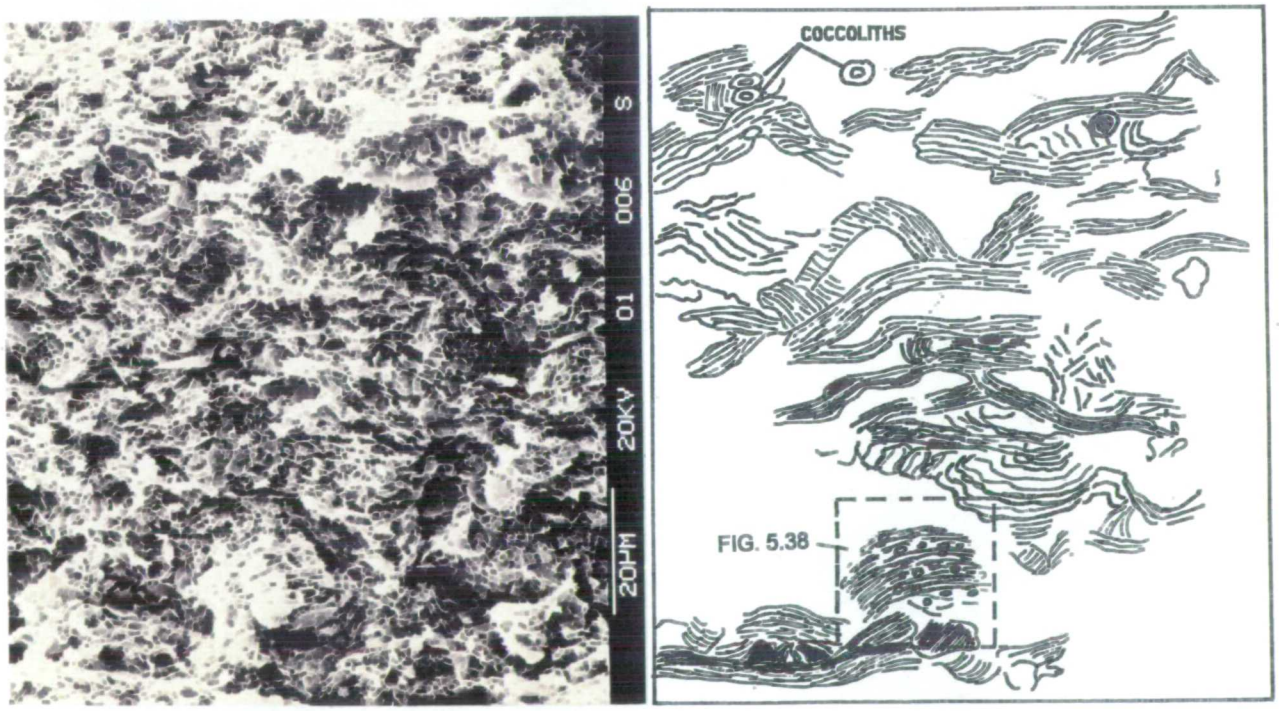

Fig. 5.29 - Undisturbed Pappadai Clay: Strata of orientated domains, bending from sub-horizontal directions to sub-vertical directions and crossing each other; vertical fracture, group 1 (Table 5.9)

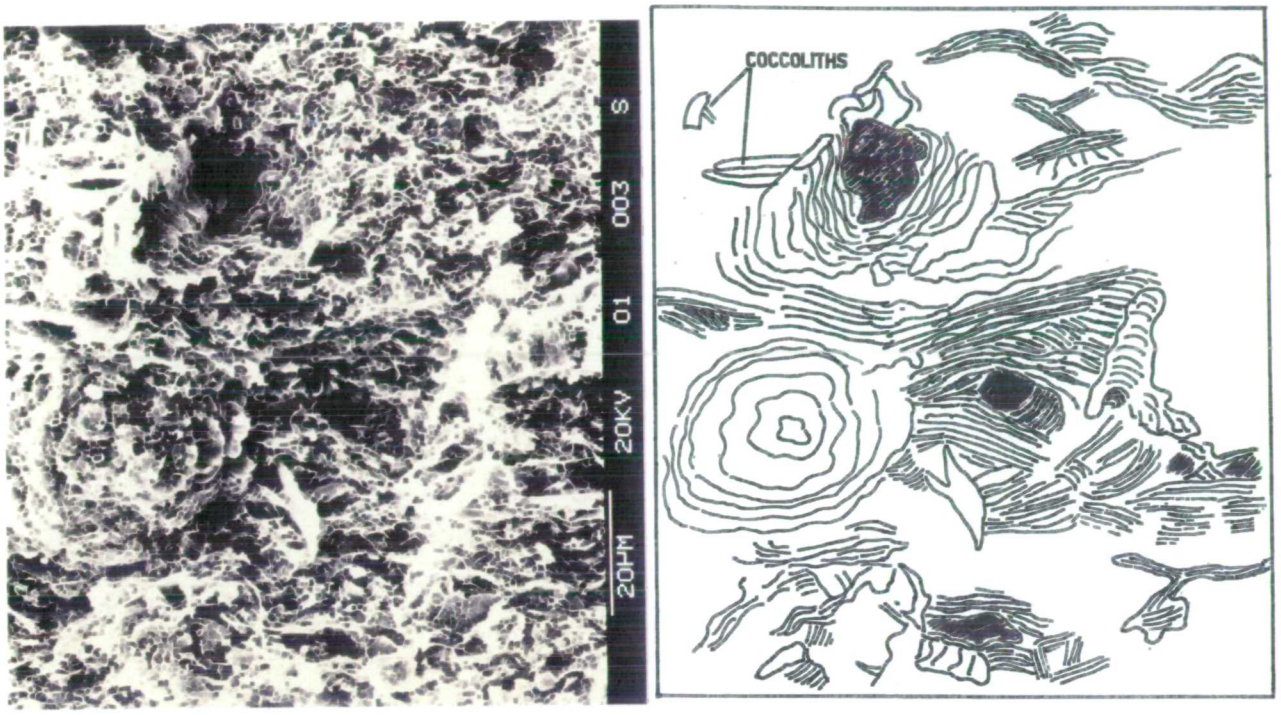

Fig. 5.30 - Undisturbed Pappadai Clay: Strata of orientated domains in horizontal directions in edge to face contact with strata of domains orientated in sub-vertical direction; vertical fracture, group 1 (Table 5.9)

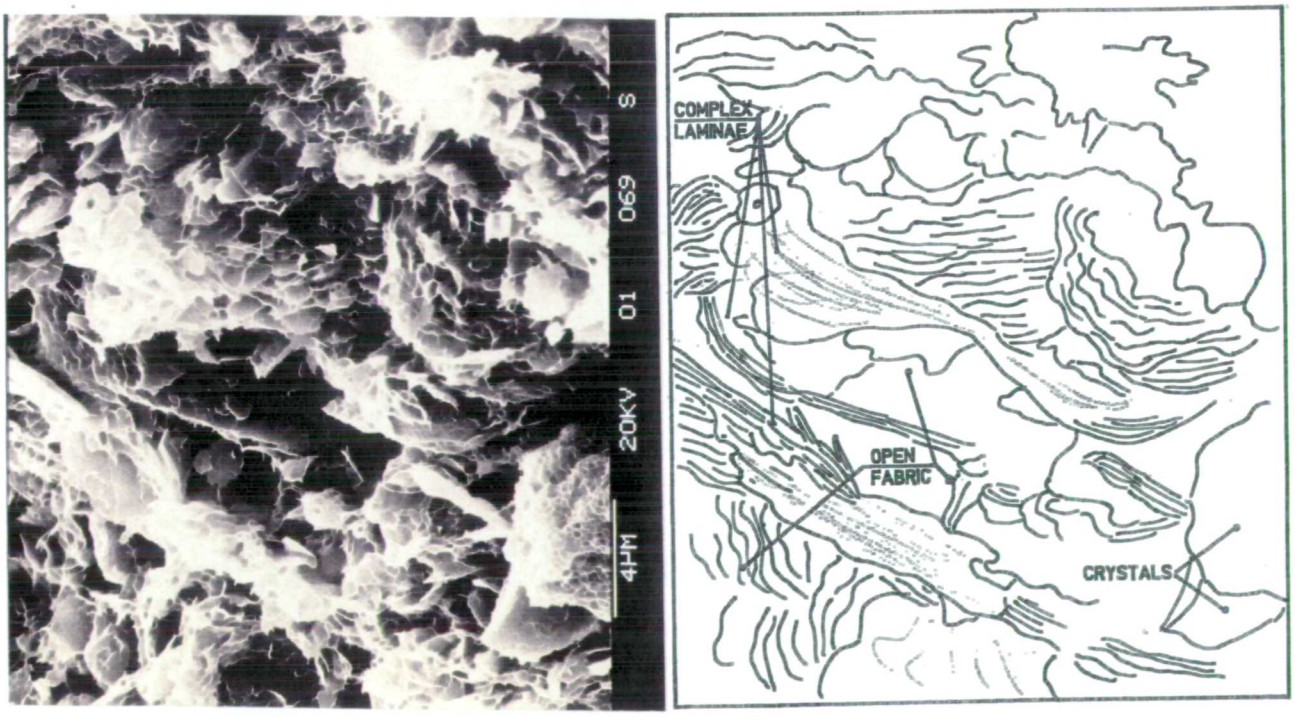

Fig. 5.31 - Undisturbed Pappadai Clay: Complex architecture,smectite particles, spongy appearance, group 1 (Table 5.9)

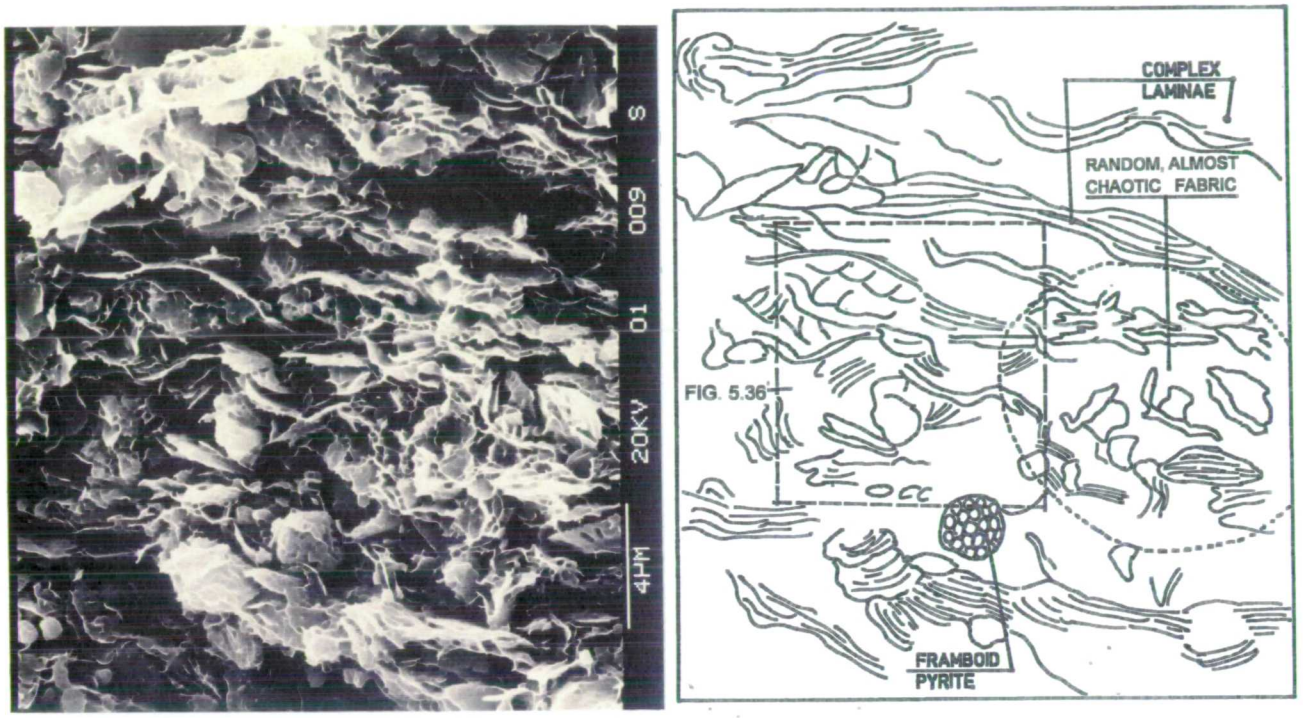

Fig. 5.32 - Undisturbed Pappadai Clay: Complex laminae and chaotic fabric, group 1 (Table 5.9)

Fig. 5.33 - Undisturbed Pappadai Clay: Random fabric, group 1 (Table 5.9)

Fig. 5.34 - Undisturbed Pappadai Clay: Interbedding of piles of iso-orientated sub-horizontal domains and strata of openly spaced sub-vertical domain aggregates. Note the intense presence of coccoliths; the coccoliths are immersed within particle aggregates having both iso-orientated and flocculated fabrics. Vertical fracture, group 2, (Table 5.9).

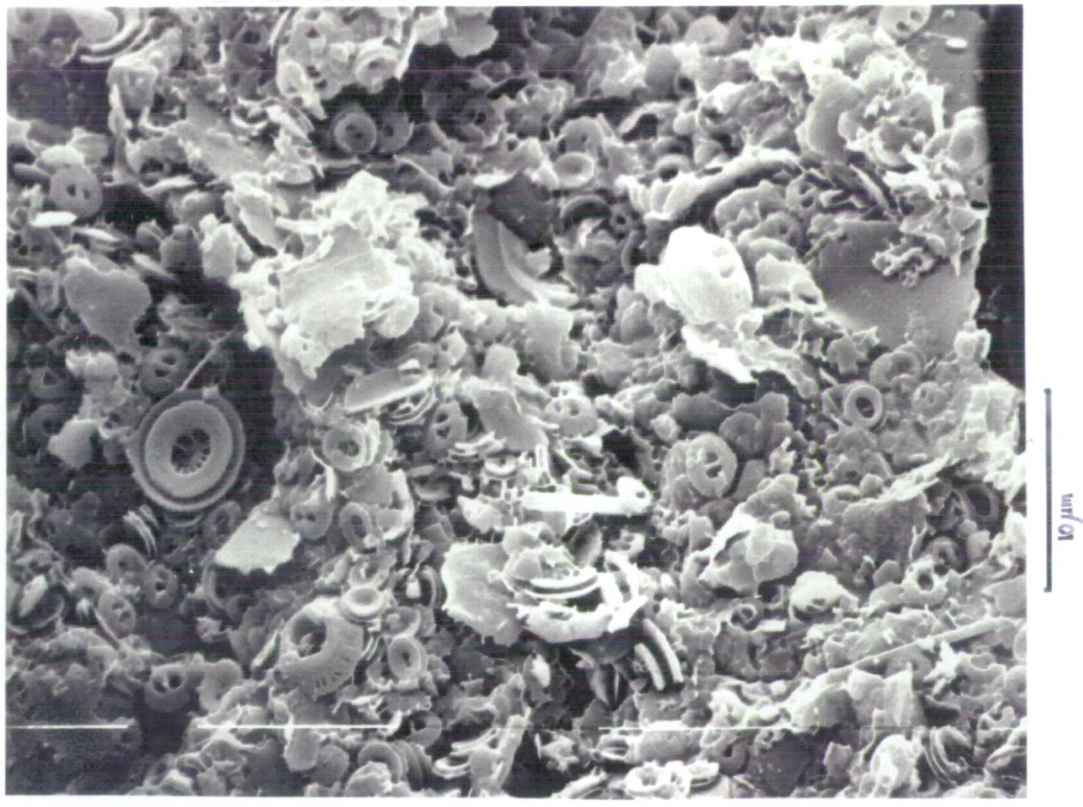

Fig. 5.35 - Undisturbed Pappadai Clay: Lamination plane; horizontal fracture, group 2 (Table 5.9).

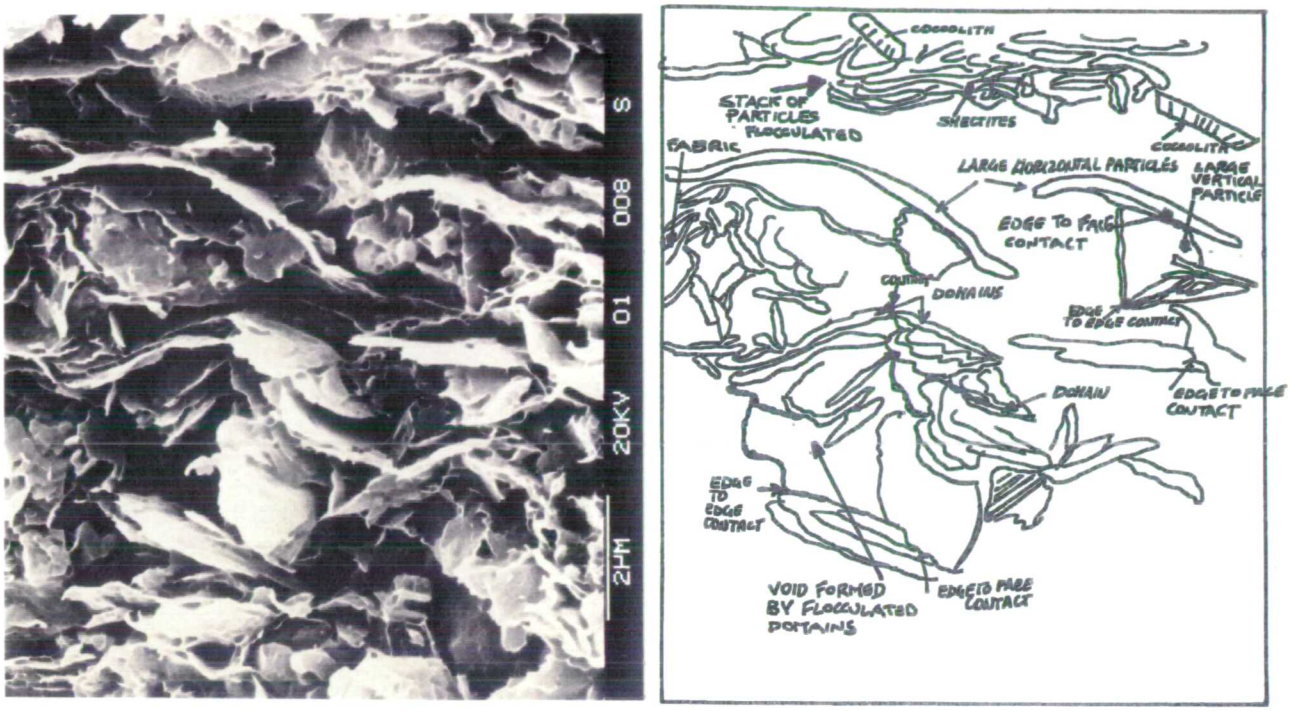

Fig. 5.36 - Undisturbed Pappadai Clay: horizontal stacks surrounded by densely packed chaotic flocculated aggregates and open arrangements of domains in edge to face contact; vertical fracture, group 1 (Table 5.9).

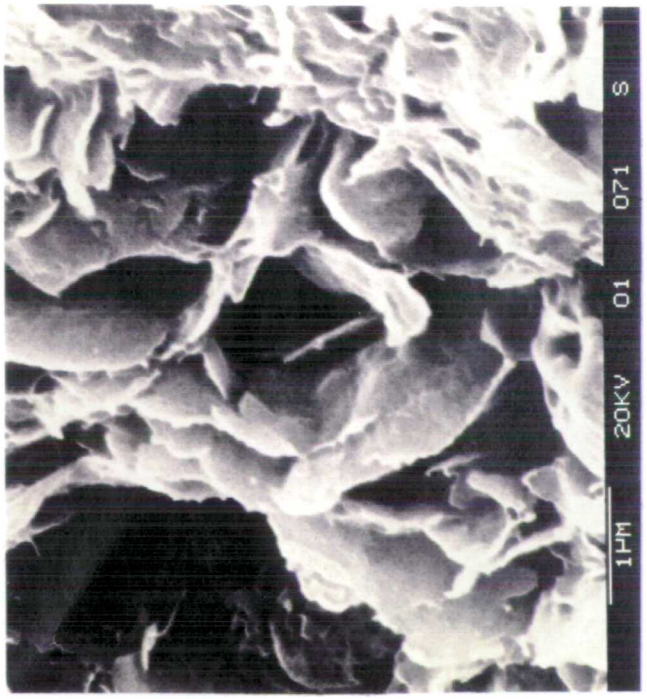

Fig. 5.37 - Undisturbed Pappadai Clay: Edge to edge and edge to face contacts; vertical fracture, group 1 (Table 5.9)

Fig. 5.38 - Undisturbed Pappadai Clay: Calcite crystals within a stack of iso-orientated clay particles; vertical fracture, group 1 (Table 5.9)

Fig. 5.39 - Undisturbed Pappadai Clay: Lath shaped illite, horizontal fracture, group 2 (Table 5.9)

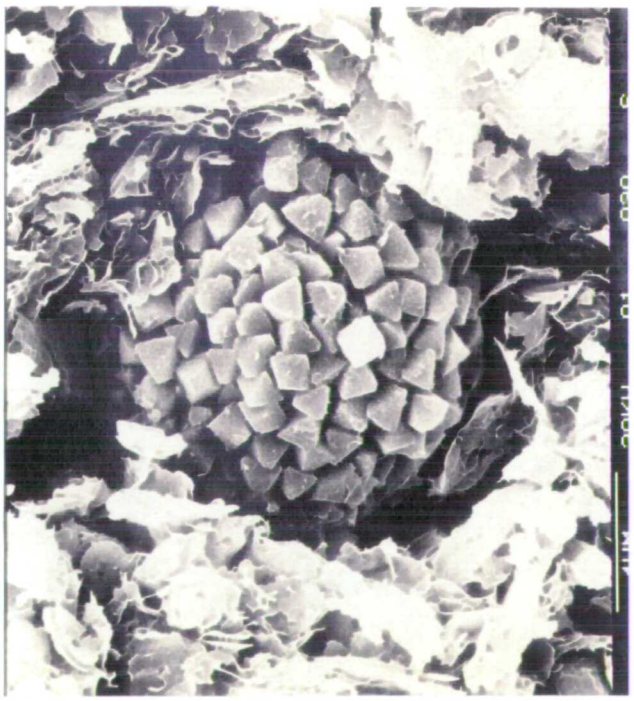

Fig. 5.40 - Undisturbed Pappadai Clay: Framboide Pyrite crystal; vertical fracture, group 1 (Table 5.9)

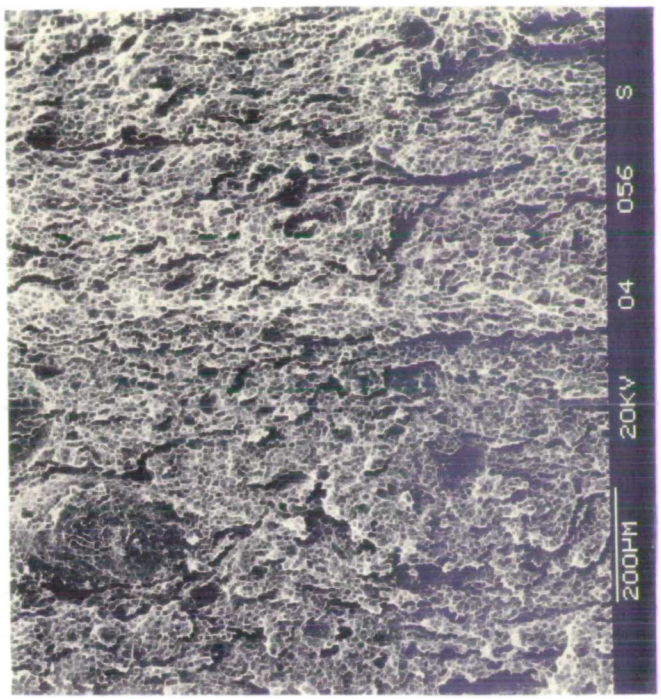

Fig. 5.41 - Reconstituted Pappadai Clay: Global view of the fabric on a vertical fracture; group 1 (Table 5.9)

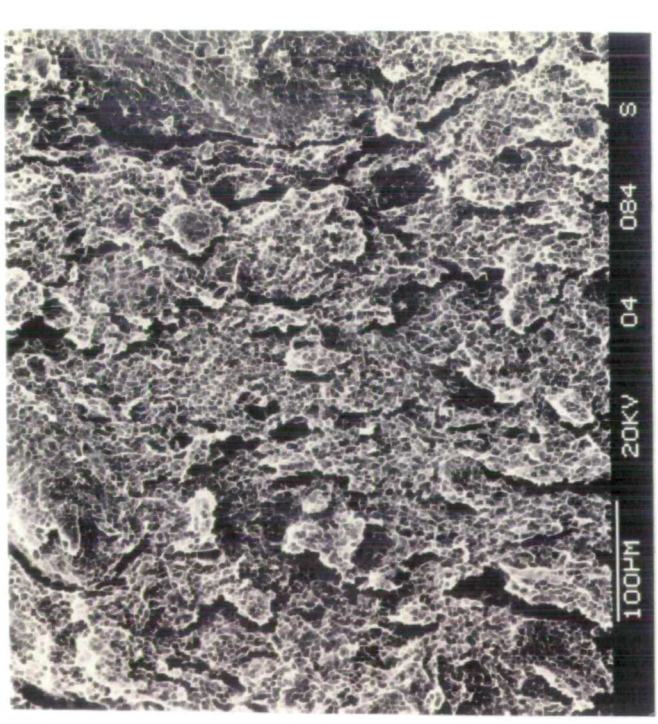

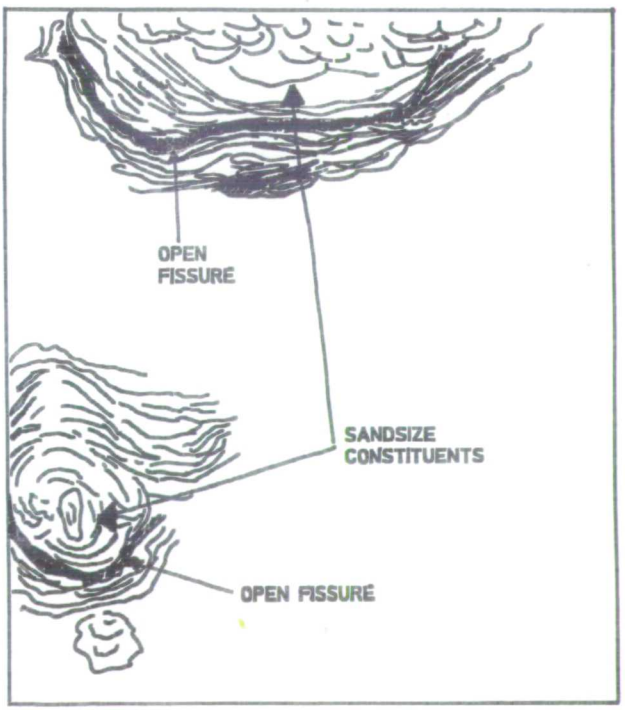

Fig. 5.42 - Reconstituted Pappadai Clay: Sand size constituents immersed in the clay fabric; group 1 (Table 5.9)

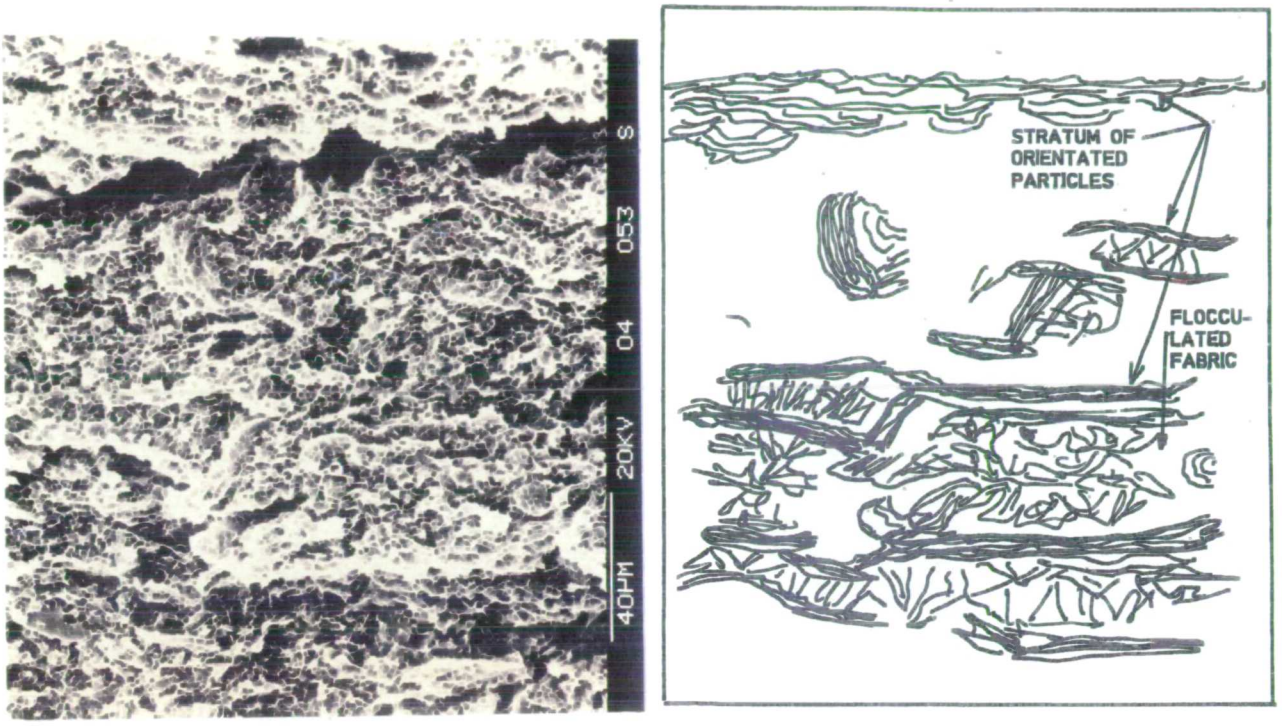

Fig. 5.43 - Reconstituted Pappadai Clay: Flocculated random fabric between horizontal strata of iso-orientated domains; vertical fracture; group 1 (Table 5.9)

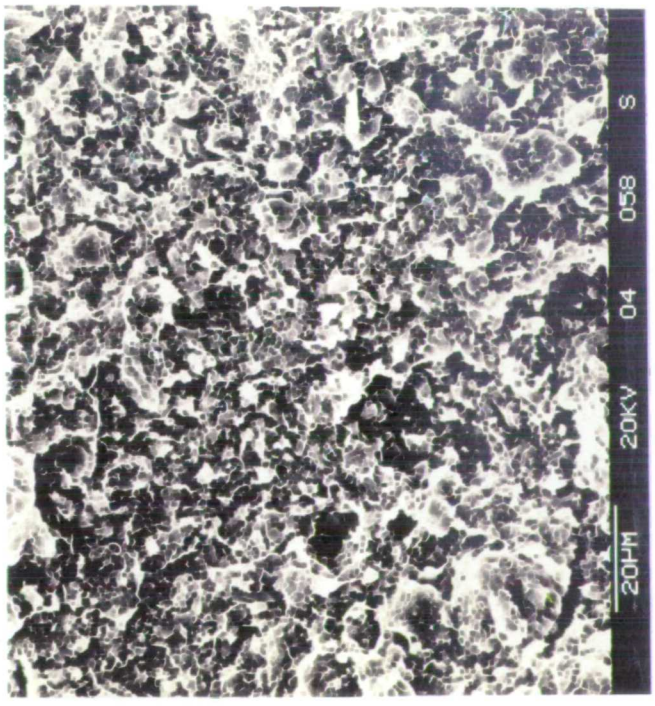

Fig. 5.44 - Reconstituted Pappadai Clay: Mediunly orientated fabric; horizontal fracture; group 1 (Table 5.9).

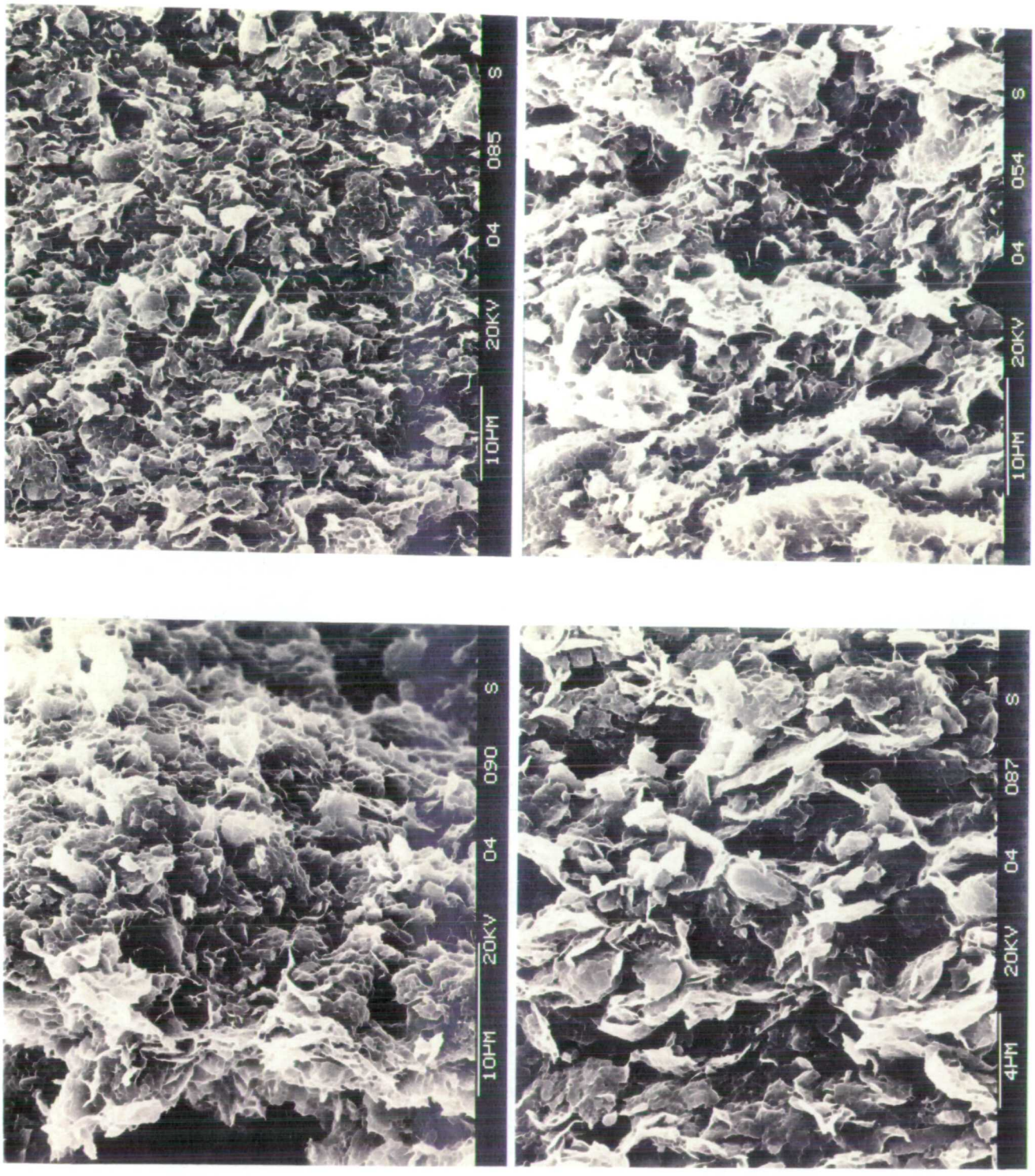

Fig. 5.45 - Reconstituted Pappadai Clay: Different flocculated arrangements; vertical fractures, group 1 (Table 5.9)

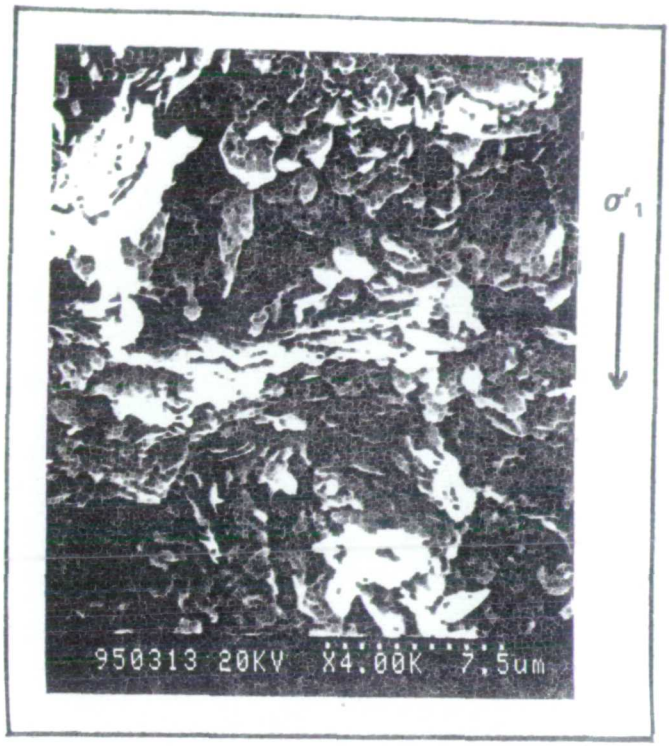

(a) Vertical section

(c) Horizontal section

Fig. 5.46 - Fabric of one-dimensionally normally consolidated KSS (after Menkiti, 1995)

Fig. 5.47 - Reconstituted Pappadai Clay: Interparticle contacts within a flocculated aggegate; remains of a coccolith are seen in the bottom left of the picture; the large clay particles appear damaged along the contour and on the surface; vertical fracture, group 1 (Table 5.9).

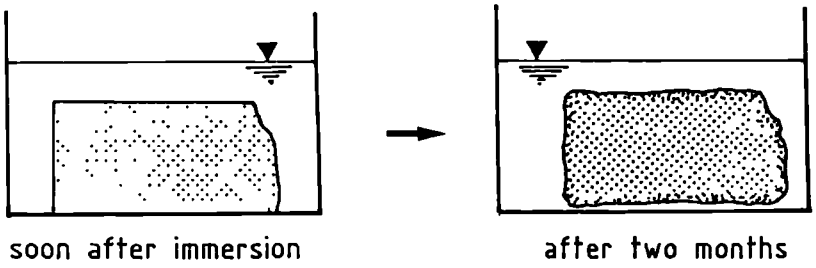

Fig. 5.48 Undisturbed Pappadai clay: free swelling of the undisturbed natural clay.

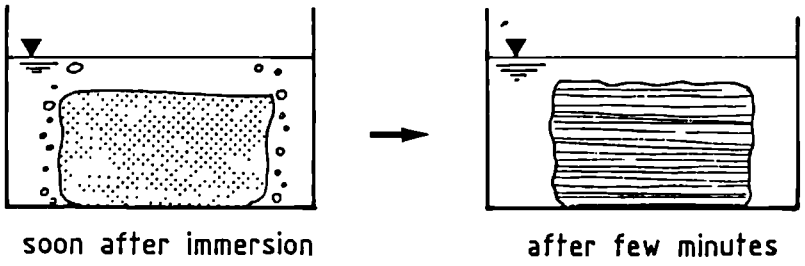

Fig 5.49 Undisturbed Pappadai clay: free swelling of the natural clay after drying at 120°C for 24 hours

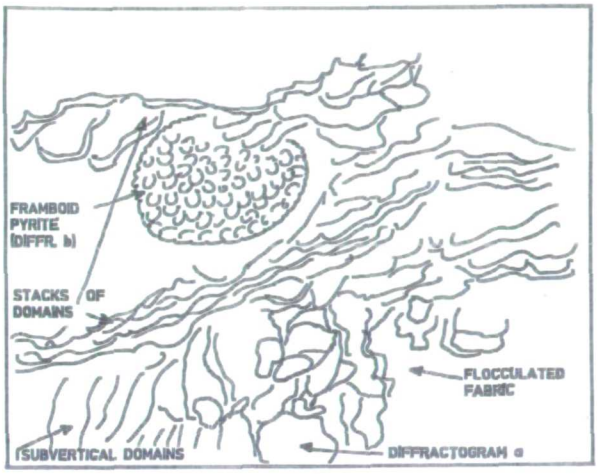

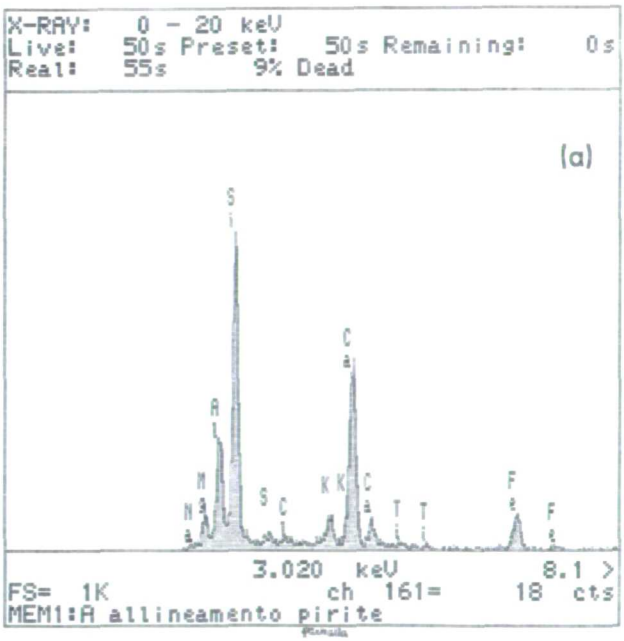

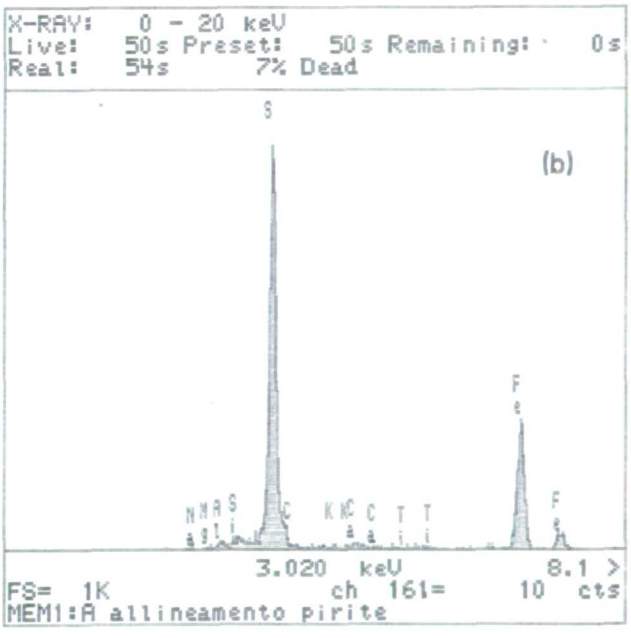

Fig. 5.50 - Undisturbed Pappadai Clay: Interbedding of strata of iso-orientated domains and flocculated fabric (fabric similar to the one shown in Fig. 1,12 e ; vertical fracture, group 3 (Table 5.9).

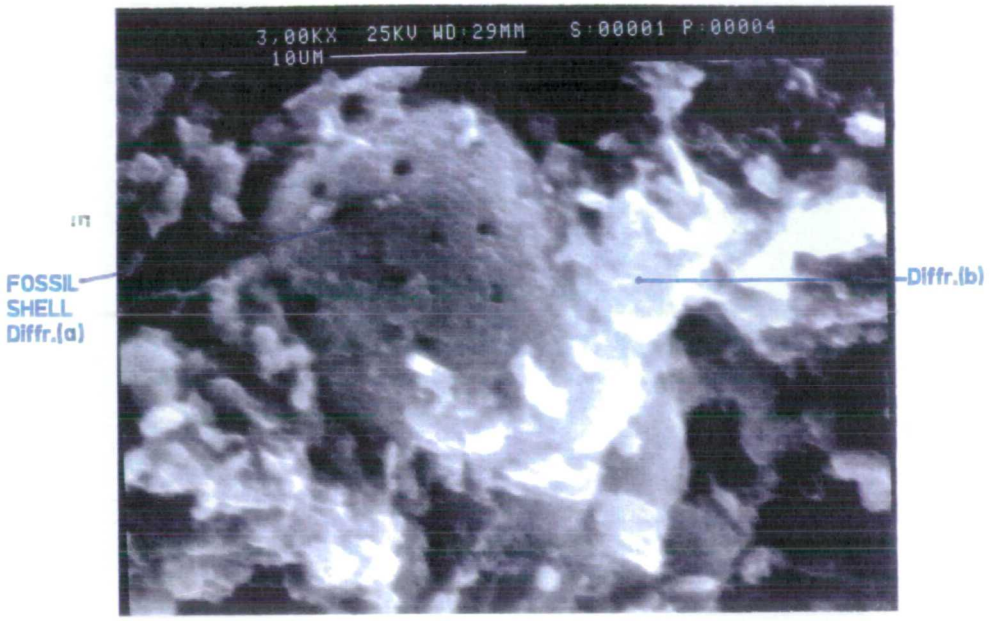

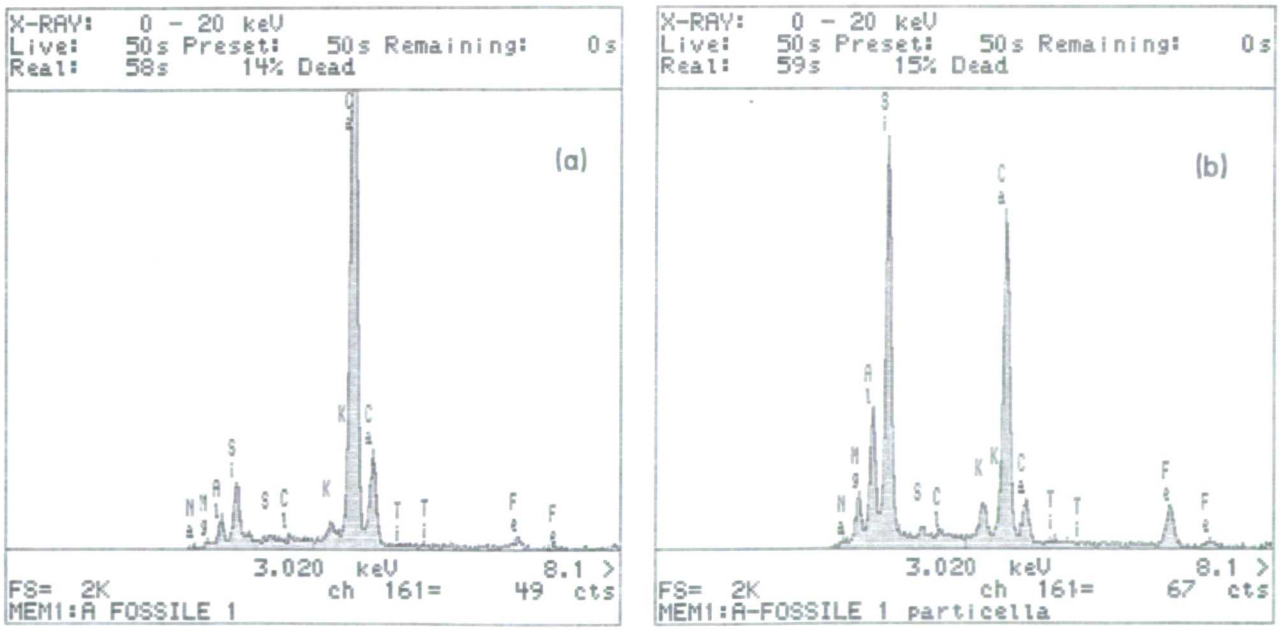

Fig. 5.51 - Undisturbed Pappadai Clay: Fossil shell interbedded within random fabric; sub-vertical fracture, group 3 (Table 5.9)

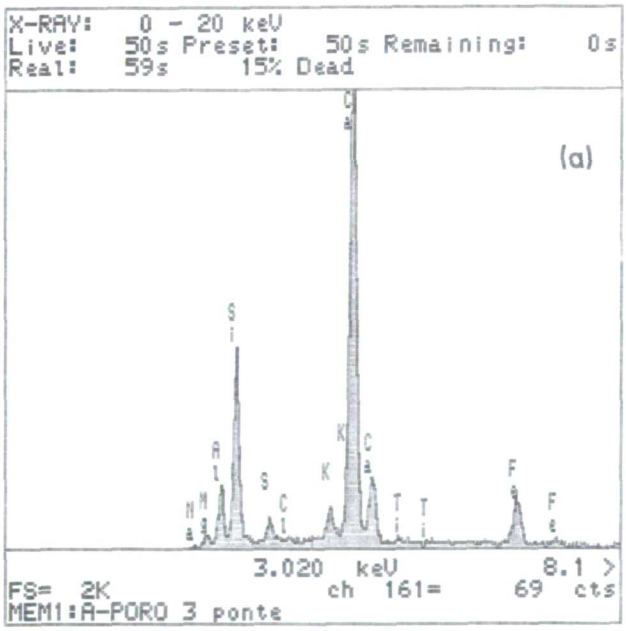

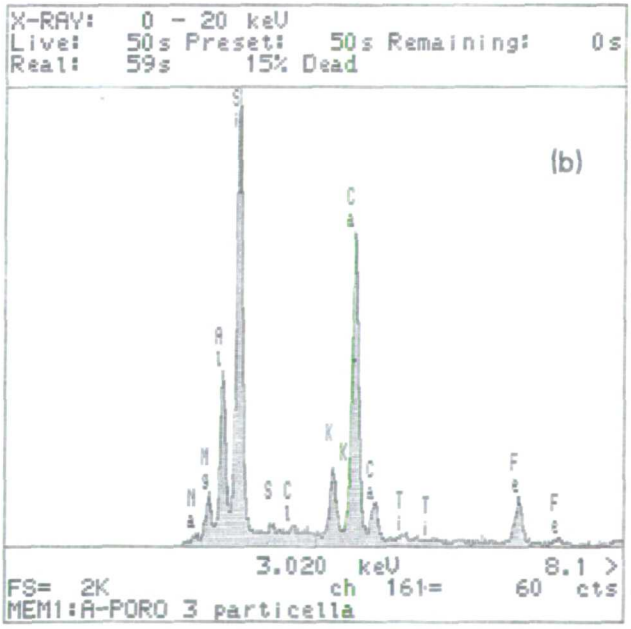

Fig. 5.52 - Undisturbed Pappadai Clay: "Bridge" between two particle domains; sub-vertical fracture, group 3 (Table 5.9)

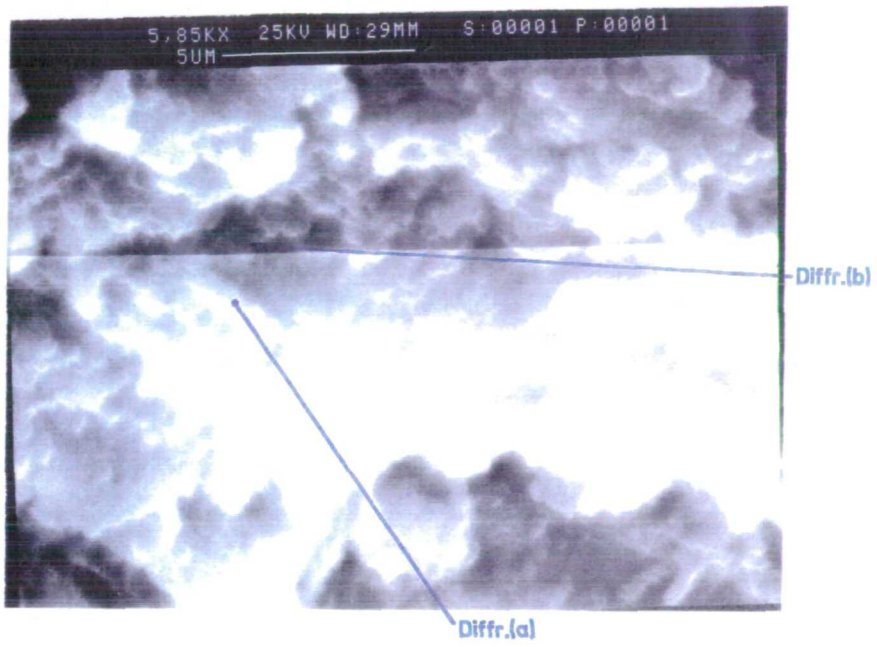

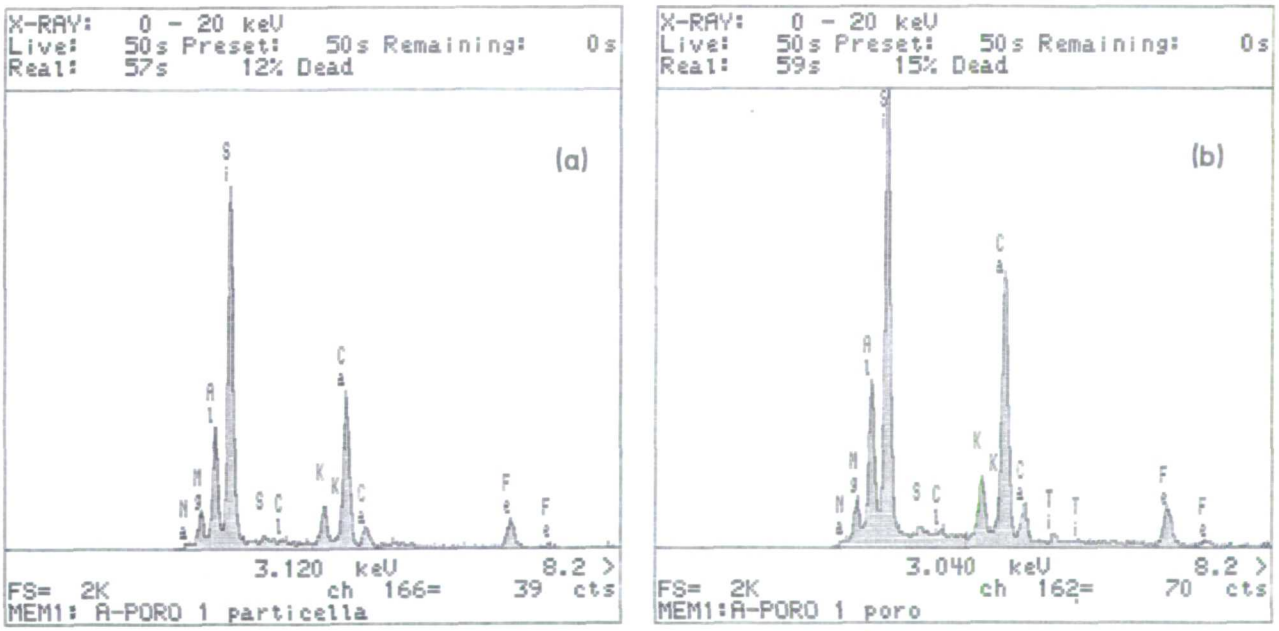

Fig. 5.53 - Undisturbed Pappadai Clay: sub-vertical fracture, group 3 (Table 5.9)

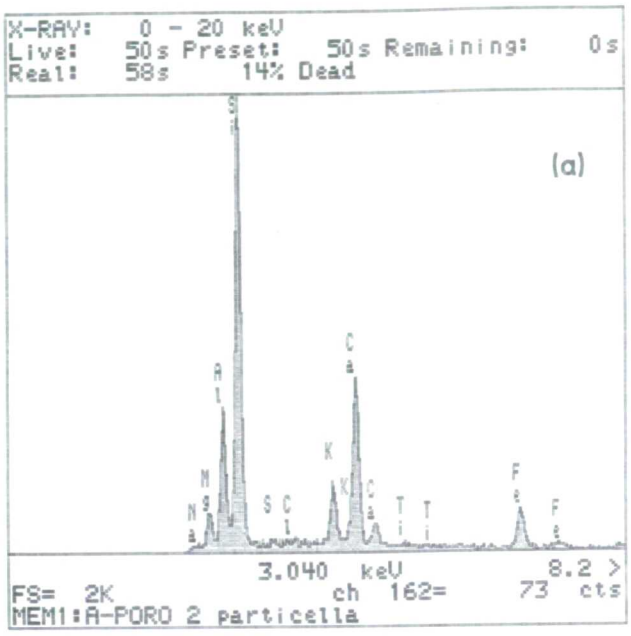

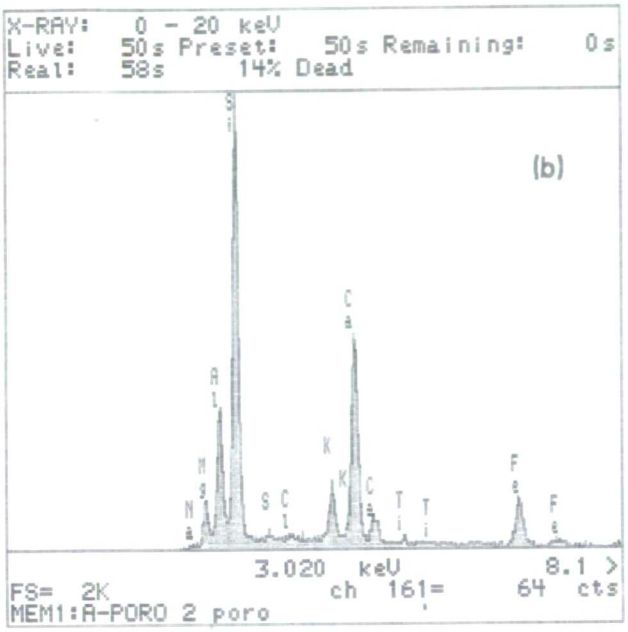

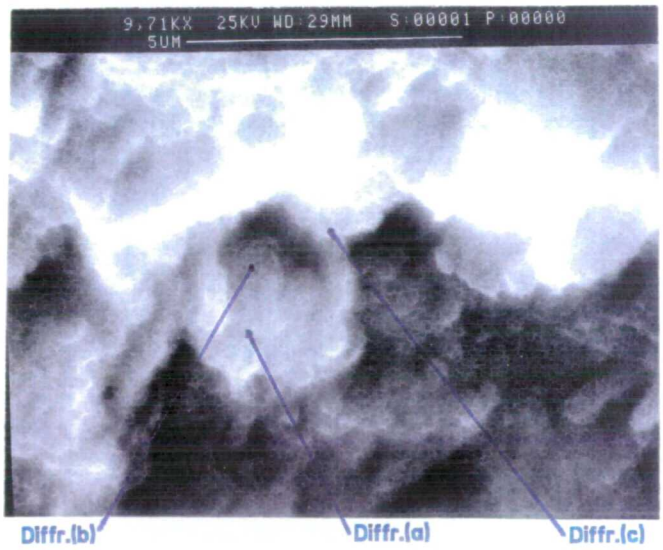

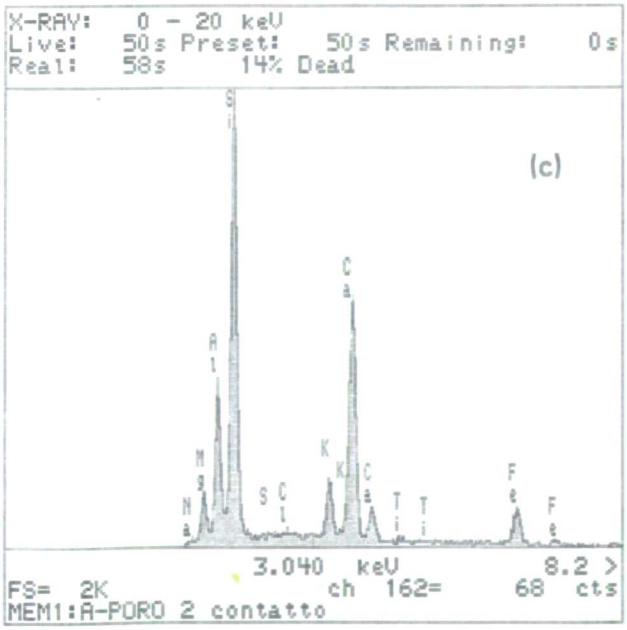

Fig. 5.54 - Undisturbed Pappadai Clay: sub-vertical fracture, group 3 (Table 5.9)

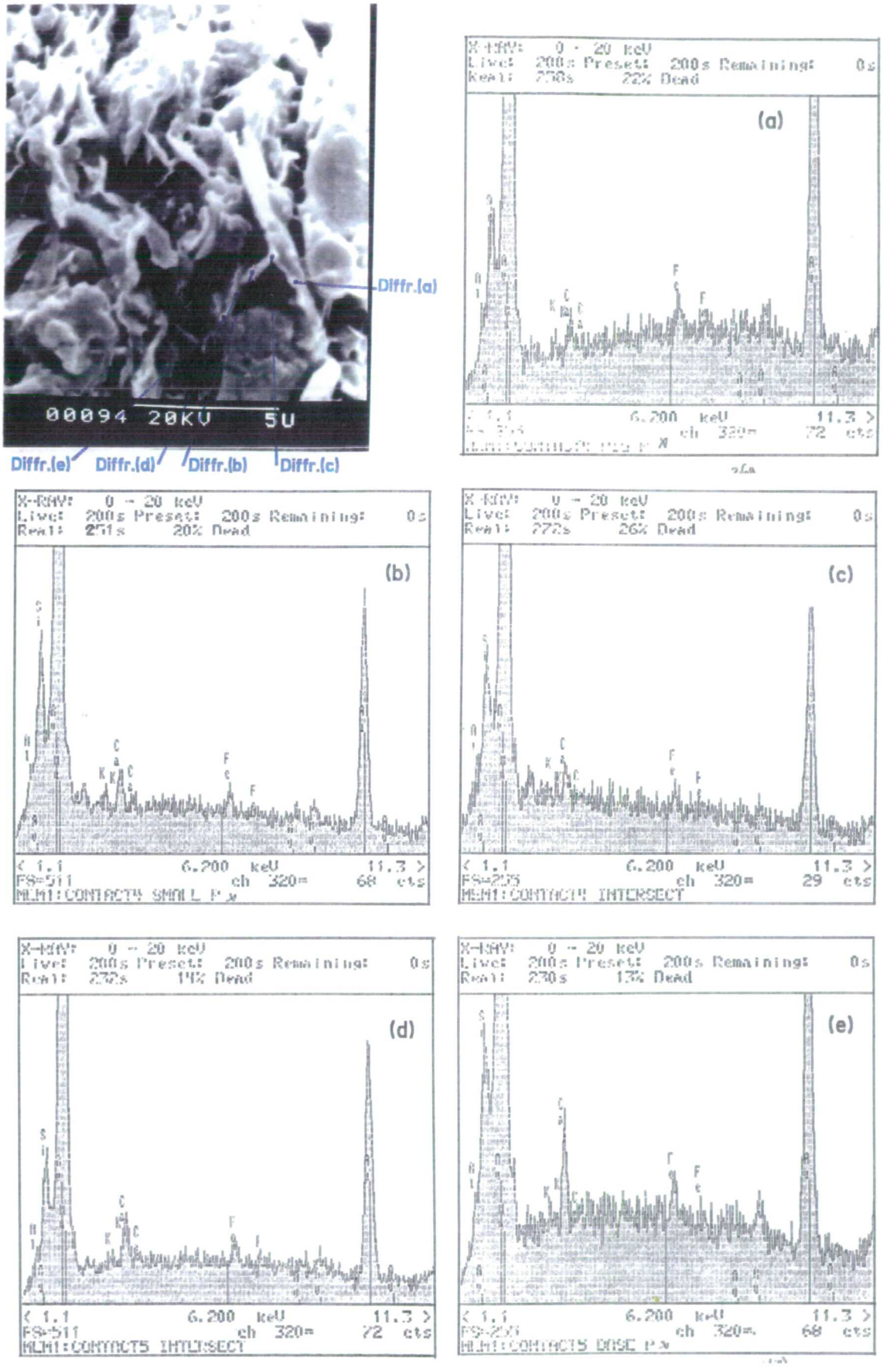

Fig. 5.55 - Undisturbed Pappadai Clay: vertical fracture, group 2 (Table 5.9)

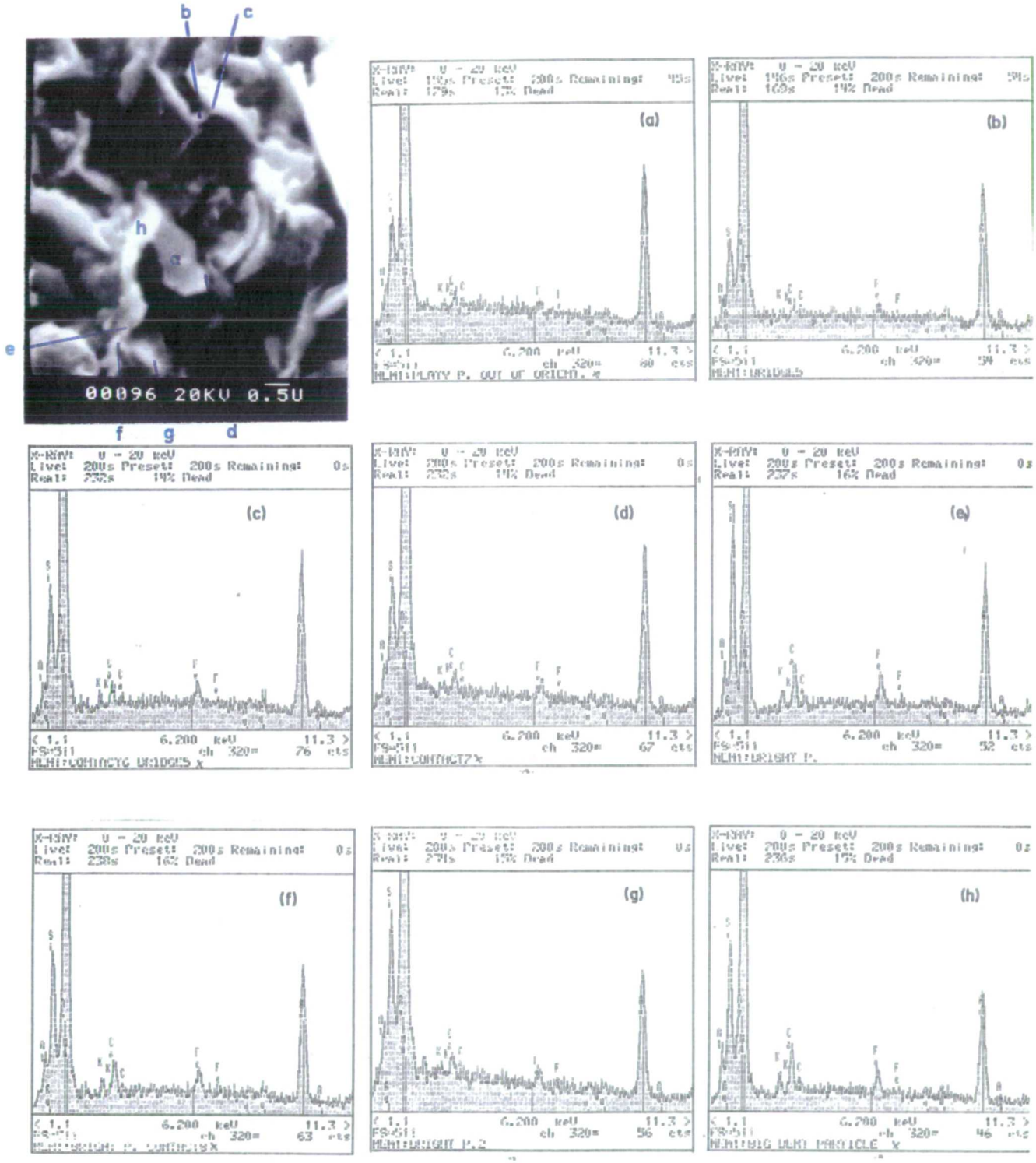

Fig. 5.56 - Undisturbed Pappadai Clay: vertical fracture, group 2 (Table 5.9)

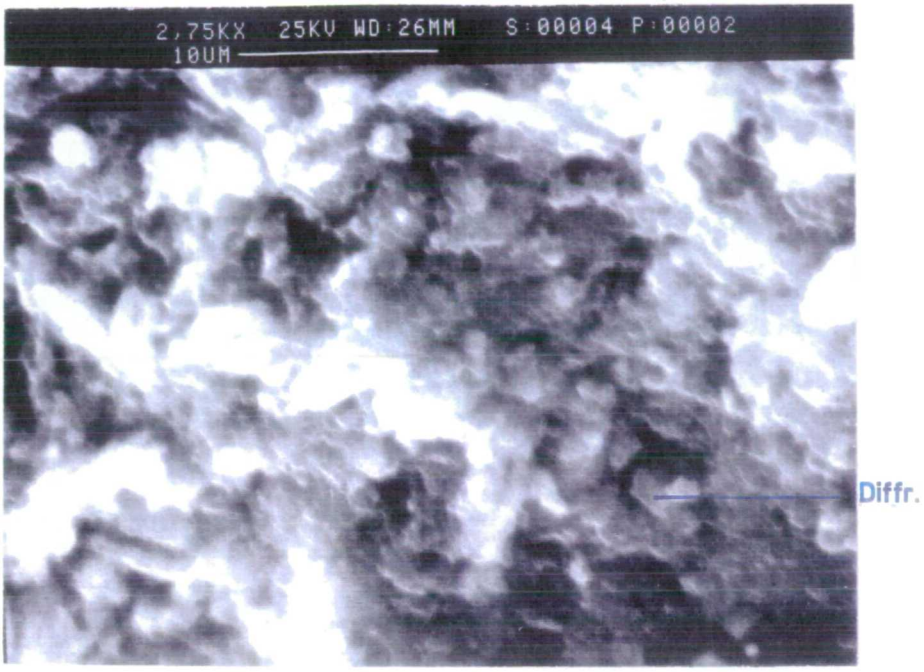

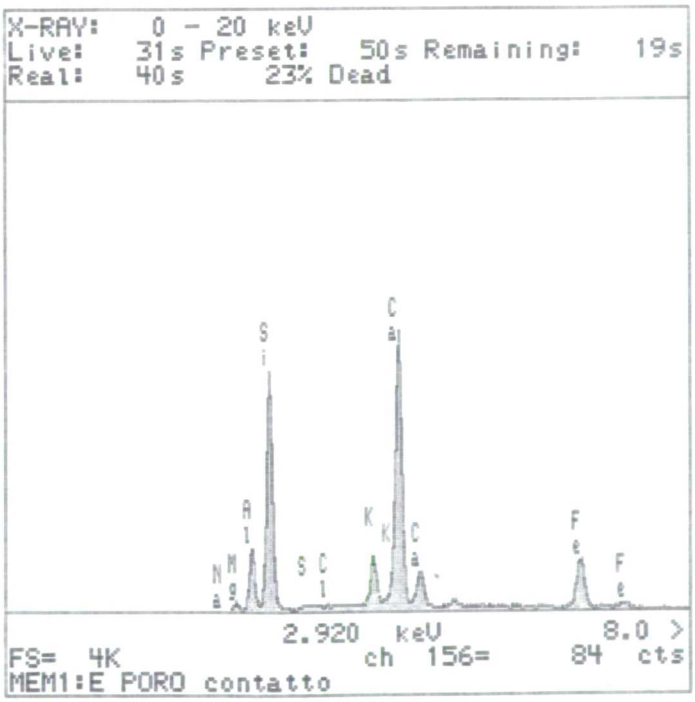

Fig. 5.57 - Reconstituted Pappadai Clay (compressed to 20 MPa): vertical fracture, group 3 (Table 5.9)

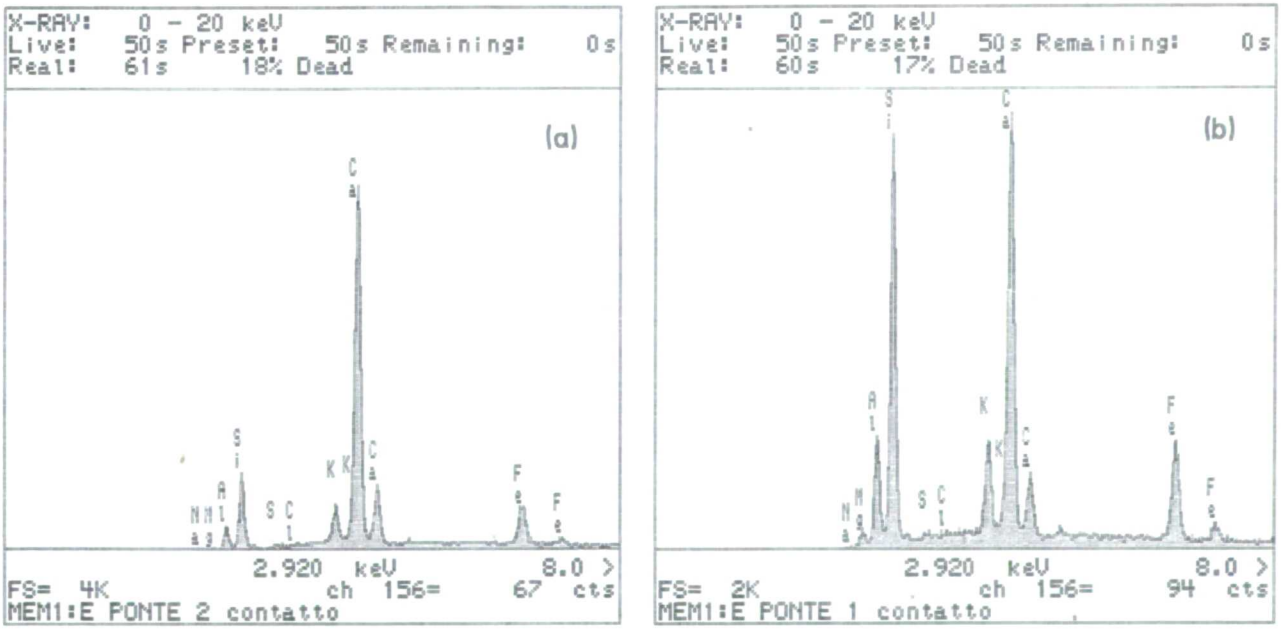

Fig. 5.58 - Reconstituted Pappadai Clay (compressed to 20 MPa): iso-orientated particles, group 3 (Table 5.9)

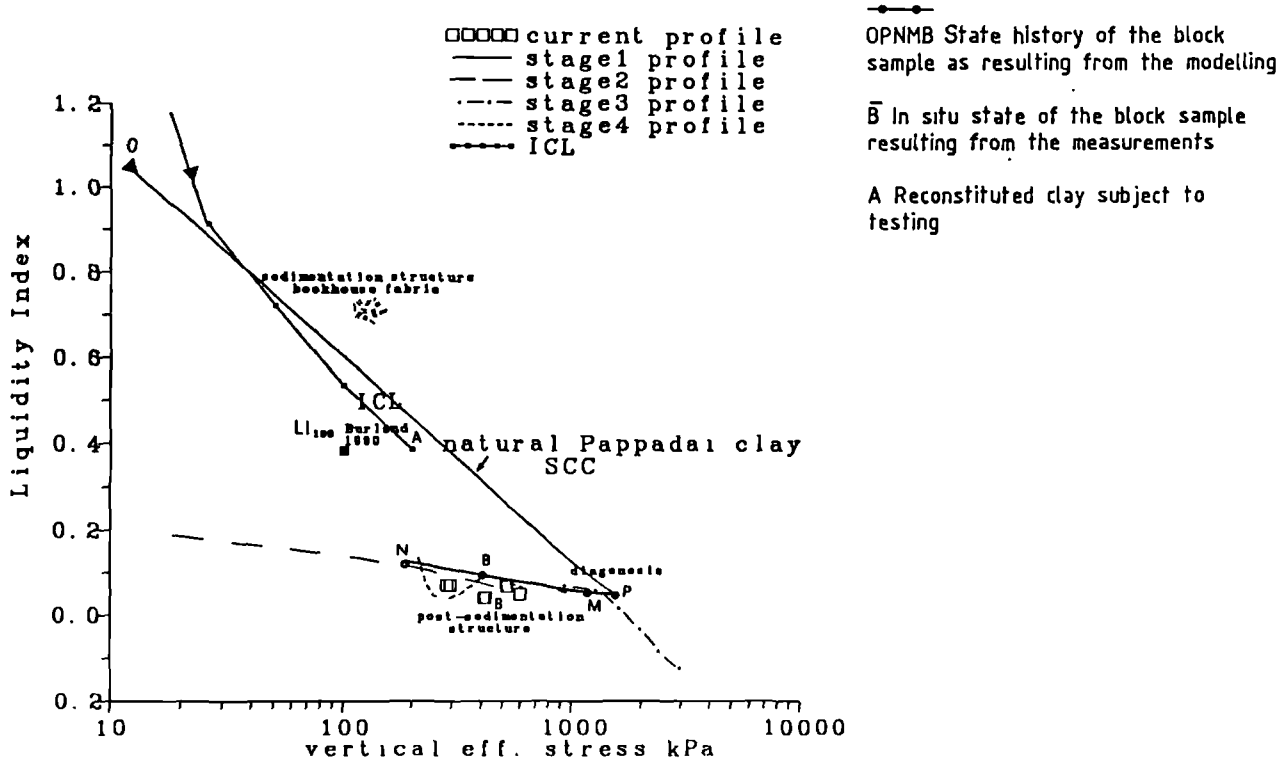

Fig. 5.59 State history of the natural and reconstituted Pappaday clay.

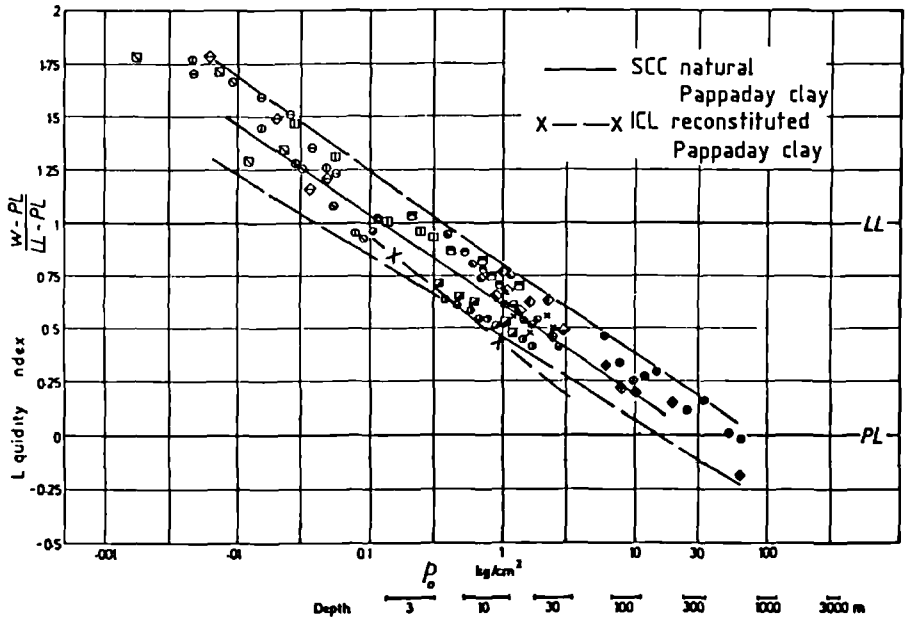

Fig. 5.60 In situ states of natural normally consolidated clays (after Skempton 1970) and sedimentation compression curves (SCC) of the natural and reconstituted Pappaday clay

CHAPTER 6

OEDOMETRIC COMPRESSION AND CONSOLIDATION BEHAVIOUR OF PAPPADAI CLAY

6.1 Introduction

As reported in Chapter 2, differences between the normalized behaviour of clays in the I_v-σ'_v plane arise from differences in the structure of the various clays, so that a general framework of clay behaviour should develop from a systematic study of the mechanical behaviour of clays, of their structure and of the behaviour of the same clay when reconstituted. Accordingly, in the present research the investigation of the natural and reconstituted Pappadai clay at the microscopic scale (see Chapter 5) was intended to complement the study of the mechanical response of the clay. The mechanical behaviour of both the natural and reconstituted Pappadai clay in laboratory tests is presented in the present chapter and in Chapter 8.

From the study of the literature (Chapter 2) it was deduced that many features of behaviour equally apply to all the clays, while the differences in behaviour mainly concern clay categories which have been classified in Table 2.1. Clays part of the same category exhibit behaviour which is basically similar as a result of similarities in the geological history and in the type of structure. The data presented in this chapter are used to investigate the general framework of behaviour of clays.

6.1 1 Objectives of the oedometer testing programme

Numerous oedometer tests were carried out to subject both the natural and the reconstituted Pappadai clay to different one-dimensional (1D) loading-unloading paths, and to study the effects of structure on the behaviour.

The oedometer test is well suited to such a study because of its simple test procedure and the well defined stress-strain conditions, which are uniform across the specimen The uncertainties in the strain paths which develop in triaxial specimens are more significant than in oedometer conditions, while in tests such as the direct shear or simple shear, uncertainties even exist concerning the stresses across the specimen (Bishop and Henkel 1962, Menkiti 1995) So the

oedometer test is probably the most useful by which to identify the basic structure-related differences in the behaviour of clays.

For reconstituted clay 1D compression and swelling define the intrinsic parameters such as e^*_{100}, C_c^* and C_s^* (Burland 1990), which are related to the basic parameters of the CSF. For the natural clay, 1D loading curves may show whether or not the CSF parameters apply to the natural clay behaviour.

This chapter examines the ICL up to very high stresses, and shows how far beyond the ICL is the gross yield point of the natural Pappadai clay. The effects on the clay behaviour of long-term diagenesis, occurring in the Pappadai clay after virgin compression, will be enlightened. Whether or not the post-sedimentation sensitivity of stiff clays compressed to yield, S_t(YSR=1) (Tables 1.1 and 2.1), compares with the distance of the yield point of the clay from the ICL, as for a sensitivity framework (Section 2.5.4) like the one in Fig.2 23, will be also demonstrated.

The behaviour of the natural clay beyond oedometric yield is shown in Section 6.6, investigated by means of a high pressure oedometer. The structural changes occurring in the clay during compression were in the first instance deduced from analysis of the test data, (Sections 6.5 and 6.6), but they were also checked by SEM, as reported in the next chapter.

The oedometer testing data were also used to investigate the applicability of the Terzaghi model (Sections 6.4 2 and 6.4.3) to represent the 1D consolidation behaviour of both the natural and the reconstituted clay. The Terzaghi hypotheses of linearity of the clay behaviour were compared with the non-linear strain-rate dependant behaviour observed for the two clays in 1D compression. The results of this comparison, and the strain-rate dependency of the behaviour of both the natural and the reconstituted clay are outlined in Sections 6.5.7 to 6.5.10 and 6.6

6.1.2. Testing Programme

The oedometer tests carried out on Pappadai clay are presented in Table 6 1 For the tests carried out on the undisturbed clay the name of the relative sample is reported in the table while the letter R is used to indicate reconst tuted clay samples

Both step-loading which will be denoted OED, and constant-rate-of-strain oedometer tests, which will be denoted CRS were carried out The CRS test procedure was used in the testing

programme with a high pressure oedometer which was assembled during the present research project (Section 6.2), and which permitted the study of the 1D compression behaviour of the clay under very high stresses (to 25MPa).

The OED and CRS tests differ fundamentally in the loading procedure, and consequently the stress profiles through the specimen at any time during the two tests are different. So the test data, e.g. the vertical total stress, the compression or change of specimen height and the base pore water pressure, where measured, were processed according to different integrations of the consolidation equation, which include different approximations. The theoretical solutions of the consolidation problem in the two cases are reviewed in Sections 6.4.2 to 6 4 4.

Three different designs of oedometer cell were used in the programme, which are described in Section 6.2.1; the design used in each test is specified in Table 6 1. The drainage boundary conditions for the oedometer specimens depended on the oedometer cell being used. The testing procedures followed in the individual tests are specified in Section 6 3 1. In the OED tests the apparatus permitted the measurement of the swelling pressure at the start of the test (Section 5.6.6, Table 5.3). In contrast in the CRS tests the high capacity of the apparatus did not permit a good control of the initial stage of the test. Different loading-unloading paths were followed in different tests, as specified in Table 6.1.

From the test data the compression curves of the clay in the e-σ'_v plane were derived, together with the variation with σ'_v of the compression index C_c, the oedometric stiffness M ($d\sigma'_v/d\varepsilon_v$), the coefficient of consolidation c_v and the vertical coefficient of permeability k. In Sections 6.5 and 6.6 the plots M-σ'_v, c_v-σ'_v, k-e are discussed and hypotheses concerning the changes of the clay structure associated with the variations of these parameters are proposed. From the OED test data the variation of the creep coefficient c_α with σ'_v was also derived. The influence of the structural viscosity on the clay behaviour was also investigated in the CRS test, which showed the strain-rate dependency of the clay

6.2. Apparatus and equipment used in the programme

6 2 1 Oedometer Cells

A basic conventional oedometer cell with double drainage was used in the initial set of OED tests This is referred to as Design 1 (D1) in Table 6 1, its dimensions are shown in Table 6 2 and

Fig 6.1. The ring is non-floating; it is clamped to the base via an outer confining steel ring which reinforces the lateral restraint on the sample.

The stress-strain conditions are assumed to be axi-symmetric, the friction stresses at the contact between the soil and the ring being assumed to be zero. The soil-steel contact at the inner surface of the ring was lightly lubricated with grease before testing, and the diameter : height of the sample is designed to be higher than 2 to reduce the friction effects (Bishop and Henkel 1962). The equations given in Section 4.7.3. for the stress-strain conditions of the soil element in the ground during 1D loading, i.e. eqs (4.15) to (4.18), are assumed to represent the soil stress-strain conditions during the oedometer tests. In the tests the volumetric strain ε_v equals the vertical strain and ε_v will be always referred to in the stress-strain equations in the following

In the Design 1 OED tests the pore water pressures in the specimen were not measured. In this type of test the effective stresses and strains experienced by the clay during consolidation are generally inferred from the settlement-time curve and the application of the Terzaghi theory for 1D consolidation, as discussed in Section 6 4 2. However, some of the hypotheses formulated by Terzaghi may sometimes not be realistic, so that Design 1 is limited in its usefulness to the conventional step loading (OED) tests Because of the lack of any pore pressure measurement, Design 1 is of limited value for CRS testing (Wissa et al.1971), as the assumption of zero pore water pressure through the specimen, sometimes adopted for these tests (Davison and Atkinson 1990), is incorrect for high strain rates and low coefficients of permeability k.

The high pressure oedometer tests necessarily had to be CRS tests because the load was applied in a motor driven loading frame. To do this the Design 1 oedometer cell was modified to measure the base pore water pressure, as shown in Fig.6.2. This new oedometer cell is referred to as Design 2 (D2) in Tables 6.1 and 6.2 This design also permitted the study of the discrepancies between the base pore water pressure changes during consolidation in OED tests and those predicted by the Terzaghi theory (Sections 6.5.7 to 6 5.10).

In Design 2 the specimen is seated on a brass base where an o-ring, seating in a groove located below the oedometer ring, ensures that the base is sealed when the o-ring is compressed by the oedometer ring, Fig.6 2(a) The hydraulic boundary condition at the base of the specimen are

$$du(z) / dz = 0 \qquad (6\ 1)$$

u being the excess pore water pressure and z the distance from the drainage boundary. The longest drainage path is equal to the height of the specimen in cell Design 2. A 38mm-diameter porous stone of medium pore size is embedded in the brass base (Fig.6.2(a)). The soil pore water communicates with a pressure transducer block (Fig 6.2). The valves at both the ends of the base pressure measuring system permit flushing of the system. A picture of one of the two Design 2 oedometer cells built during the project is shown in Fig 6.2(b). The system was carefully checked for leaks.

The system designed to measure the base pore water pressure (Fig 6 2) was sufficiently rigid for correct measurements to be made even in stiff soils. Before starting the testing programme with Design 2, its performance with soil was checked comparing the excess base pore water pressures u_b measured with time after a stress increment $\Delta\sigma_v$ with the u_b expected according to the Terzaghi solution of the consolidation problem :

$$u_b/\Delta\sigma_v = \Sigma_{(n=0\rightarrow\infty)}(2/M)[\sin(M)]\exp(-M^2T_v) \qquad (6.2)$$

where $M = [\pi(2n+1)/2]$ (6 3)

The value of c_v resulting from the Casagrande curve fitting construction (Section 6.4 2) was used in eq.(6.2). The comparison between the measured value of the pressure ratio $u/\Delta\sigma_v$ at the base of the specimen ($u_b/\Delta\sigma_v$) and the value of the ratio $u_b/\Delta\sigma_v$ from eq (6.2) was carried out at times before that the average degree of consolidation had reached 50%, which is when the Terzaghi theory best applies to the clay behaviour (see Section 6 4.2).

The value of $u_b/\Delta\sigma_v$ measured when loading soft clay was equal to 1 immediately after loading and was consistent with the predicted $u_b/\Delta\sigma_v$ value at all the other measurement times Values of $u_b/\Delta\sigma_v$ of 1 were never measured in the Design 2 oedometer cell when a stiff clay was tested, because of the very low values of c_v of the clay, which give rise to significant drainage before the full pressure response of the measuring system is achieved However already after five minutes the measured value of $u_b/\Delta\sigma_v$ was found to be consistent with the value resulting from eq.(6.2) On the basis of these observations it is considered that the apparatus correctly records the value of u_b.

Although great care was taken to de-air the porous stone before testing, and a careful flushing procedure was followed, the presence of air in the system was suspected more than once during testing with the Design 2 cell The tests in which this occurred are highlighted in Sections 6 5 and

6.6. Possible reasons for air in the system were trapping of air when the specimen was set up, the slight desaturation of some clay samples (see Table 6.1), or the cavitation of water in the u_b measuring system due to the high suctions of the undisturbed clay. This air would not have caused measurement errors if soft clays had been tested, but when air is compressed and dissolved in water, the local effective stress increase and pore water pressure drop are much more significant in stiff clays. It follows that the lack of saturation induces higher inaccuracies in the u_b measurements when testing stiff clays than when testing soft clays, and that the measuring system has to be calibrated for the type of soil being tested.

The problems of accurately measuring pore pressures for such a stiff clay as Pappadai clay were highlighted by the first series of tests, resulting in a redesign of the oedometer cell as shown in Fig 6.3. This cell is Design 3 (D3) in Tables 6.1 and 6.2. The brass base containing the u_b measuring system was remachined to fit the pedestal of a triaxial cell in which the oedometer base, specimen, ring and top cap were set up The u_b measuring system is connected by two metal tubes to the outlets of the cell pressure of the ordinary triaxial cell Immediately outside the cell the system is connected to a pressure transducer block and two valves. The two pipes forming the pore pressure measuring system in the ordinary triaxial cell are used to apply a constant cell pressure during the oedometer test, which acts as a back pressure for the oedometer soil specimen (Fig 6.3).

So in both the CRS and OED tests with Design 3 the soil was resaturated by means of a back pressure. Moreover, to avoid substantial cavitation of the base pressure measuring system when the specimen is set up, a 38mm diameter high air-entry porous stone is in place of the medium pore size stone. In Design 3 the vertical load is applied via the ordinary triaxial loading ram

Before carrying out the last set of CRS tests on the reconstituted soil the top cap of the Design 3 cell was remachined in order to reduce the bedding errors, as discussed in the following Section 6 3.2. After this operation Design 3 is shown as Design 3* (D3*) in Table 6 1

The main difference between the oedometer cells Design 2 and 3, and the CRS oed meter cells proposed first by Rowe and Barden (1966) and then by Wissa et al (1971) is that Des gns 2 and 3 are high pressure oedometers, with the load applied by a mechanical system, while in the cells designed by Rowe and Barden (1966) and Wissa et al (1971) the specim n is hydraulically loaded The present oedometers were designed to one-dimensionally compress the clay up to very high stresses, beyond large yield. In contrast, the hydraulic oedometers can be generally used only at low-medium pressures

The design of both the Rowe and the Wissa cells permits the application of a back pressure, but there are no case histories in the literature warning of the effects that even slight desaturation may have on the pore pressure measurement in CRS oedometer tests. Indeed, back pressures are not often used in CRS tests, e.g. Lerouil et al. (1983) and Lerouil et al.(1985). The importance of the use of back pressure in the CRS testing of stiff clays was recognized only after carrying out tests with Design 2 at high strain rates, as discussed in Section 6.6.

Davison and Atkinson (1990) had previously used a CRS oedometer formed of an oedometer seating inside a triaxial cell, though their design also was not intended for use at high pressures.

6.2.2 Application of the vertical load

During the OED tests loading frames such as those shown in Fig 6 4 were used with the three designs of oedometer cell used in the project. To set up the Design 3 oedometer within the frame in Fig.6.4 the rams "a" in the figure were modified as shown In Design 3 the vertical load was centred on the triaxial loading ram (Fig.6.4) which transferred to the oedometer top cap, Figs 6.3 and 6.5(a). Given the diameter of the triaxial loading ram (see Fig.6.5(a)) and the limited loads reached during the OED tests, there was no risk of buckling the triaxial ram.

Very high loads were reached in the tests with the high pressure oedometer, which uses the 10ton displacement-controlled loading frame shown in Figs.6.2 and 6.6. All the CRS tests reported in Table 6.1 were carried out with this loading frame. The sample is compressed between two vertically aligned steel rods, *T* and *P* in Fig 6.6. The top rod *T* is fixed, while the basal rod *P* is driven up by an electric motor. The gear box permits the use of different displacement rates, as shown in Table 6.1. A high capacity load cell is screwed onto the upper rod *T*, Figs 6.2 and 6.6.

Design 2 and 3 oedometer cells were centred on a rigid base platen, shown in Figs 6.2, 6 6 and 6.7, screwed to loading rod *P*. The vertical load was applied to the top cap of the Design 2 oedometer via the load cell with a spherical steel "ball" on the top cap, shown in Fig 6 2. Since the two loading rods *T* and *P* were aligned axially and were much stiffer than the soil being tested, the load is assumed to have been applied vertically and concentrically, as shown in the schematic diagram in Fig 6.8.

In Design 3 the triaxial loading ram was connected rigidly to the load cell (Fig.6.7). The load was transferred from the triaxial loading ram to the sample top cap as shown in Fig 6.5(b) in order to apply more uniform displacement even if some misalignment occurred between the different components of the loading system (Fig.6.9(a)). In this case the base of the loading ram provides reaction against the top cap tilting due to eccentric load. Moreover, the risk of buckling within this loading system (Fig 6.9(a)) is lower than for the loading system in Fig.6.9(b), i.e. the system used in the OED tests, as, if the load on the ram is not centred, due to the shape of the base of the loading ram in Fig.6.9(a) this ram is not free to move laterally

This is an important design consideration for an apparatus reaching high stresses. In considering safety the loading ram was assumed to be a free cantilever (see Appendix 6.1) With the diameter of the ram used of 15.79mm, a Euler stress of 794MPa was calculated, which is much higher than the stress of 314MPa assuming a perfectly concentric vertical load for the maximum stress reached in any test.

6 2.3 Measuring system

Both the OED and the CRS oedometer tests were data logged automatically. In the following the readings as collected are "raw" data; otherwise discussion refers mean data after correction for apparatus compliance and electrical noise (see Section 6 4.1).

Various automatic measuring systems were used during the testing programme. In the following the variables being measured and the transducers used in each type of oedometer test are listed.

- OED tests, Design 1 : vertical displacement measured by a transducer, Fig 6.4.
- OED tests, Design 3 · both the vertical displacement, u_b and the back pressure were measured by transducers, Fig.6 3.
- CRS tests, Design 2 : both the vertical displacement, u_b and the vertical load were measured by transducers, Figs 6.2 and 6.6.
- CRS tests, Design 3 : both the vertical displacement, u_b, the vertical load and the back pressure were measured by transducers, Fig 6.7.

The characteristics of the data loggers and of the transducers used are reported in Table 6 3. The accuracy of the transducers was principally governed by the electrical noise level which is reported in the table Oth r factors influencing the accuracy su h as non-l nearity drift and

temperature effects, were found not to be significant. The resolution of the transducers was in every case very much less than the noise. The sensitivities reported are for an input voltage of 10 Volts.

In both the OED and the slow CRS tests the pressure transducer used to measure u_b had a full scale output smaller than that of the transducer used in the fast CRS tests; the characteristics of the two pressure transducers are given in Table 6.3. Two types of displacement transducers were also used, LVDT's with large output, the others being of a resistive type. The load cell used in the high pressure oedometer had a very large capacity (70KN) and therefore a rather low sensitivity and resolution. Consequently the load could only be measured to an accuracy of about ±5N or about ±2.5kPa, as reported in Table 6.2.

Indeed, the main difficulty of setting up the high pressure oedometer was the need to match the requirement of a high capacity load cell with the necessity to measure small stress changes at small strain intervals. The accuracy finally obtained for the load cell readings permitted stress-strain increments to be observed which were small enough for an accurate calculation of the response of the clay.

One test was performed with a 4kN capacity internal load cell, as shown in Fig.6 10, using a dummy steel sample. The readings of the external high capacity load cell were compared with the readings of the internal load cell which was not affected by the friction where the loading ram passes through the top of the triaxial cell. Within the capacity of the internal load cell, the differences between the readings of the two load cells were as small as the noise affecting the readings of the high capacity load cell. In the measurement of the vertical strain, the overall accuracy of the measurement includes not only the accuracy of the displacement transducer (Table 6.3), but also the correction for the compliance of the apparatus. The latter is discussed in Sections 6.3.2 and 6.4.1.

6 3. Testing Procedures

6.3.1. Procedures followed in the soil testing

In the present section the oedometer test procedures are discussed In Table 6 1 the procedure followed for each test is indicated by the procedure number.

The OED tests were step-loading tests that, even if carried out with oedometer cells of different design, were all similar. Both the loading sequence and the duration of the loading steps could vary between the tests, as shown in Table 6.1 and Section 6.5, but these differences are not used to differentiate between the test procedures. Rather, the test procedures are related to the manner in which the equilibration stage was carried out. At the equilibration stage the suction present in the clay specimen is dissipated and the vertical effective stresses in the clay become equal to the applied σ_v. The voids ratio and effective stress reached at the end of the equilibration stage are reported as e_0 and σ'_{v0} in Table 6.1.

Procedures 1 to 6 were used with the OED tests on undisturbed clay. In Procedure 1 the clay swelling was restrained in order to keep the voids ratio constant; the swelling pressure of the clay was then equal to the applied vertical pressure, as discussed in Section 5.6.6 The clay specimen was initially loaded to σ_v of about 300kPa, then water was added to the oedometer cell and σ_v was increased until the immediate settlement reading (taken few seconds after loading) was higher than the compliance settlement measured in the compliance test. The values of the swelling pressures measured by this procedure are reported in Table 5.3.

With Procedure 2, σ_v was applied at about the average suction value measured for the clay sample with other techniques Water was added to the cell after the application of this σ_v ,which then coincided approximately with σ'_{v0}.

For Procedure 3 the equilibration stage was similar to the restrained swelling stage conventionally followed in routine oedometer tests. σ_v was increased when immediate negative displacements were recorded, otherwise the applied σ_v was left constant for 24 hours. Within this procedure the compliance of the apparatus are not taken into account in controlling the swelling of the clay. This procedure was applied in one test so as to compare the compression curves resulting from routine oedometer tests and those for tests in which clay swelling had not been permitted.

With both Procedures 4 and 5 the initial σ_v was greater than the suction, so that swelling did not occur, and compression immediately commenced. Procedures 4 and 5 differed as Procedure 4 was carried out with the Des gn 3 cell and Procedure 5 with the Design 2 cell. In Procedure 4, once σ_v was applied, the oedometer cell was filled with water and then the back pressure was applied

Procedure 6 was followed in the OED tests on reconstituted clay The initial σ_v value of the equilibration stage was then very low, about 20kPa, and was increased until the immediate

settlement was higher than the compliance settlement. Maximum swelling pressures of 30kPa were recorded for the reconstituted Pappadai clay.

The procedures followed in the CRS tests, i.e. Procedures 7, 8 and 9, are again distinguished depending on the manner in which the equilibration stage was carried out. Procedure 7 was applied in all the Design 2 cell CRS tests on undisturbed clay, apart from CRS 8 in which Procedure 7B was applied. In Procedure 7 the clay specimen was initially loaded to the average clay suction measured with other techniques. The σ_v value was increased if the compression recorded was lower than the corresponding compliance settlement A delay was allowed before starting CRS compression, to allow full equalisation of the sample and obtain a correct u_b measurement during the CRS compression.

During the equalisation period σ_v reduced because of the relative effects of stress relaxation of the loading system and compression of the sample. Consequently the clay could swell slightly. Thus the equilibration stage in the high pressure oedometer generally resulted in a complex soil-apparatus interaction. Nonetheless within about 8-12 hours a near constant value of σ_v was reached, with a small compression of the clay specimen. The readings recorded during the equilibration stage of test CRS5, reported in Fig 6.11, show typical equilibration stages with test Procedure 7. Sometimes the vertical stress was reinforced after the drop in σ_v due to the soil-apparatus interaction.

In Procedure 7B the clay was initially loaded to σ_v less than the clay suction, about 100kPa. The swelling of the clay interacting with the stiff loading system caused σ_v to increase, although its maximum value was lower than the suction. σ_v was then progressively reduced so that eventually σ'_v was significantly lower than the initial suction. This procedure was used to observe CRS compression of the clay after swelling from its intact state.

Procedure 8 was applied to the undisturbed clay, but with the oedometer cells Design 3 and 3*. The equilibration stage was equivalent to that developed with Procedure 7, but after the application of σ_v the triaxial cell was pressurized, the cell pressure working as a back pressure for the clay specimen (see Fig 6 3). In these tests back pressures of about 300kPa were used Finally, Procedure 9 was applied when testing the reconstituted clay with the high pressure oedometer and the cell Design 3 or 3*. In this case σ_v was first applied at a value lower than 40kPa. σ_v was then increased to about 80kPa while monitoring the compression, and only then was the water in the cell put under pressure

After the equilibration stage, a constant displacement-rate compression was applied by means of a gear motor; in tests CRS 6 and CRS R3 the displacement rate was changed during the test (Table 6.1), as shown in Section 6.6. In tests which were completed at the end of the compression stage, the oedometer cell was emptied of water and the sample quickly unloaded.

For those tests in which the sample was allowed to swell after the compression stage, dissipation was allowed before unloading. During this stage the excess pore water pressures, which had risen during compression, dissipated and the clay consolidated. However, due to the further consolidation of the clay and the soil-apparatus interaction, both the voids ratio of the clay and the σ'_v decreased. This is seen in Table 6.1, the maximum σ'_v reached during the CRS compression being higher than the σ'_v value at the beginning of unloading.

Swelling was generally carried out by step unloading. A negative displacement was applied, causing σ_v to decrease. An equilibration stage then followed during which drainage was allowed at both ends of the specimen. Again during this stage interaction between the swelling clay and the stiff loading system caused σ_v to increase. The next unloading step was commenced when both σ_v and the sample swelling had become constant. Fifteen hours were enough to allow equilibration. In Fig.6.12 the readings logged during an equilibration stage which lasted 45 hours are shown; after the first 15 hours the vertical load started oscillating due to temperature effects, but its average value changed very little.

Table 6.1 gives a summary of the experimental details of the CRS tests. Note that it was possible not to use the filter paper with the oedometer cells Design 3 and 3* because of the fine grading of the porous stone used in this design.

6.3.2. Apparatus compliance

The compliances of the various apparatus used in the OED tests were measured by performing tests with a dummy steel sample However the measured compliance compress ons do not necessarily coincide with the total errors affecting the settlement readings in the OED tests on soil Firstly, the compression of the filter paper disc is highly time-dependant In addition, the bedding of the real soil sample is not simulated when the dummy steel sample is compressed, and is not repeatable The correction of the compress on readi gs of the OED tests was therefore n t carried out subtracting the measured compl ance settlements Instead the Casagrande correct n

for the initial settlement d_o, computed as discussed in the following Section 6.4.2, was applied. The magnitude of the apparatus compliance however gives a good impression of the likely errors introduced, and for this reason is discussed here.

Compliance tests were carried out also for the high pressure oedometer. Again in each case the compliance tests were performed with a dummy steel sample replicating the conditions under which the soil was compressed. The CRS settlement readings were corrected by means of the measured compliance settlements, as outlined in Section 6.4.1, as there is no alternative way to correct the CRS raw data. The CRS data then may still be affected by a bedding error.

Sets of compliance tests were carried out with each one of the oedometer cells (Design 2, 3 and 3*) and those for Design 2 cell (Figs.6.2(b)) without filter paper discs are shown in Fig.6.13. The bedding error is quite repeatable, and the compliances differ only by an equivalent strain of ±0.13% over 50MN. For an initial voids ratio of 0.85 the error in the measurement of the voids ratio change during the whole test may thus be about ±0.002. The unloading behaviour during the same compliance tests is shown in Fig. 6 13(b). It is reasonably repeatable apart from an initial displacement which differs for the three tests, and causes a maximum random error in the voids ratio of ±0.04, though the shapes of the three unloading curves are very similar

Filter paper discs were used during CRS tests on soil with Design 2. The compliance test carried out with filter paper discs is shown in Fig 6.14(a), for the loading, and in Fig 6.14(b), for the unloading stage. The total compliance compression for a vertical load of 50MN was about 1.3 times the corresponding compliance compression when the filter paper discs were absent. In order to make the applied displacement rate and the actual displacement rate experienced by the soil more comparable, the compliance due to the compression of the filter paper discs were reduced in the later CRS tests with Design 2 by the use of filter paper discs loaded cyclically before testing. The result of the compliance test using the cycled filter paper discs is plotted in Fig 6.15.

Other compliance tests were carried out with oedometer cell Design 3, five of which are shown in Fig 6.16. The compressions shown in Fig 6 16(b) are particularly relevant to the CRS tests on the undisturbed Pappadai clay, which was usually initially loaded by σ'_v equal to the clay suction (procedures 7 and 8), i e. by a vertical force of about 1200N (see Table 6 2) During loading from 300N up to 50MN (Fig 6.16(a)) the maximum error in the strain measurement with Design 3 is about ±0 13% or, in terms of voids ratio, about ±0 002. For the CRS tests on the reconstituted clay, which started from very low pressures, an additional error of about 0 22% possibly affects the test results because bedding mainly occurred during compression up to a

vertical load of 300N, which is why in Table 6.4 the non-repeatable errors are similar for compressions above 300N and compressions above 1000N. The unloading curves recorded during the five compliance tests with Design 3 are shown in Fig.6.16(c). Although the curves start from different maximum loads, their shapes are very similar, but again a random error is recorded at the start of unloading. At maximum this is a strain of ±0.15% or ±0.003 in terms of voids ratio.

A final set of compliance tests was carried out with the oedometer cell Design 3*, whose results are reported in Fig. 6.17. Plots (a), (b) and (c) in the figure show the compliance compressions recorded after an initial compression to vertical loads of 0, 300 and 1000N respectively. The bedding settlements occurring up to 300N vertical load are again not repeatable, but the consequent error is lower than that occurring within the Design 3. The errors in the estimation of the compliance compression for the different system configurations are summarized in Table 6 4.

6.4. Processing the data: Methods used and Literature Review

6.4.1. Corrections applied to the raw data

The compressions measured directly in the oedometer tests include not only the soil compressions, but also the bedding compressions and the apparatus compliance As mentioned in Section 6.3 2 in the OED tests the compliance test results were not used to correct the data because they were found to be not sufficiently repeatable. In these tests both the bedding and most of the compliance settlement occur immediately after the application of the stress increment $\Delta\sigma_v$, that is at the commencement of primary consolidation, when the Terzaghi theory best fits the soil behaviour (Section 6.4.2). It is thus assumed that the Terzaghi theory can be used to distinguish the soil compression from the compliance and bedding settlements. Accordingly, the curve-fitting method proposed by Casagrande (1936-b) was applied to compute the sum of the bedding and compliance settlement (d_0) in the OED tests; the calculation of d_0 is explained in Section 6 4 2. In contrast, for unloading the strains were corrected using the compliance test data, since these are not subject to bedding errors.

As discussed in Section 6 3 2 and shown in Table 6 4, the compliance compression of the high pressure oedometer is fairly repeatable, so that the CRS test data were corrected by means of the compliance test data. The compliance curves used for the different apparatus in the processing are shown dotted in F gs 6 14 to 6 17

In the CRS tests on the undisturbed clay the continuous loading stage followed an equilibration stage, described in Section 6.3.1, during which high σ'_v values were reached. The voids ratio at the end of the equilibration stages, defined as e_0 in Table 6.1, were calculated allowing for any eventual swelling or consolidation that occurred during the equilibration stage, resulting from the difference between the compression readings and the compliance compression. The e_0 values of the CRS tests on the undisturbed clay may thus be slightly in error due to the non-repeatability of the bedding compression, though the data from the continuous loading stage of the CRS tests on the undisturbed clay are not influenced by bedding errors.

In contrast, the data from the initial part of the continuous loading stage in the CRS tests on the reconstituted clay, for σ_v below 140kPa, are probably affected by bedding errors. The errors affecting the strain results of all the CRS tests are summarized in Table 6.5. The strains measured during the unloading stages were corrected for compliance using the unloading curves in Figs 6.14 to 6.18.

Finally, with back pressure applied to cells Designs 3 and 3*, the force on the loading ram from the pressure in the cell (back pressure times 0.196) was subtracted from the load indicated by the external load cell.

6.4.2. Terzaghi's analysis of consolidation

The 1D consolidation data from the OED tests on the natural and reconstituted Pappadai clay were analysed according to Terzaghi's theory and the limitations of this theory in interpreting the clay behaviour were investigated as discussed in Section 6.5 In the following the equations of Terzaghi's model of 1D consolidation are briefly reviewed as they will be referred to in reporting the analysis of the OED test data.

Based upon the hypotheses of Terzaghi's model (Terzaghi and Peck 1967), the consolidation process is expressed by the differential equation :

$$c_v \partial^2 u(z,t) / \partial z^2 = \partial u(z,t) / \partial t \qquad (6\ 4)$$

where t is time, z is the depth from the drainage boundary and u(z,t) is the excess pore water pressure The coefficient of consolidation c_v is equal to

$$c_v = Mk/\gamma_w \qquad (6.5)$$

and is assumed to be constant according to the hypotheses of Terzaghi's model. The solution u(z;t) of eq.(6.3) by separation of variables (Taylor 1948) for consolidation under a stress increment $\Delta\sigma_v$ and constant water pressure at the drainage boundaries, emerged as a Fourier series:

$$u(X;T_v) = \sum_{n=0\to\infty} 2\Delta\sigma_v / M \sin(MX) \exp(-M^2 T_v) \qquad (6\ 6)$$

where M equals $(2n+1)\pi/2$. In eq (6.5) X and T_v (Terzaghi and Peck 1967; Taylor 1948) are :

$$X = z/H \quad \text{and} \quad T_v = c_v t/H^2 \qquad (6\ 7)$$

where H is the distance of the undrained boundary from the free drainage boundary (z=0) If Terzaghi's assumptions that the soil behaviour is linear elastic, not strain-rate dependant and of constant permeability do not hold in reality, then c_v may change during consolidation and the solution of the consolidation problem in eq (6.6) may be not accurate enough.

According to eq.(6.6) the average consolidation degree in terms of pore water pressures $U_p(T_v)$ is:

$$U_p(T_v) = \left[\int_0^1 (\Delta\sigma_v - u(X;T_v))\, dX\right] / \Delta\sigma_v = 1 - \sum_{n=0\to\infty} 2/M^2 \exp(-M^2 T_v) \qquad (6\ 8)$$

and because of the assumption of linear soil behaviour it is equal to the average degree of consolidation in terms of settlements $U_s(T_v)$:

$$U_p(T_v) = \left[\int_0^1 m_v(\Delta\sigma_v - u(X;T_v))\, dX\right] / m_v\Delta\sigma_v = U_p(T_v) \qquad (6.9)$$

where S is the soil compression in mm and m_v is the coefficient of 1D compressibility. So, for given boundary conditions, the model gives a unique expression of the average degree of consolidation of the soil stratum with time $U(T_v)$ $(=U_p(T_v)=U_s(T_v)$, Fig 6 18) and the soil compression completely defines the process of consolidation, controlled solely by the coefficient of consolidation c_v.

Terzaghi's model was applied to the OED test data using the Casagrande curve fitting method, which was found to give more consistent results than Taylor's root-time method For each loading step the initial compression d_0 due to apparatus compliance and the settlement related to the

average consolidation degree of 50% was calculated as shown in Fig.6.19 (Head 1986). The coefficient of consolidation for U% equal to 50% was calculated as:

$$c_v = 0.1036\ H^2/t_{50}\ [m^2/year] \qquad (6.10)$$

where H is the one defined above and is expressed in millimetres and t is time in minutes.
The oedometric stiffness, M (=1/m_v), was calculated as :

$$M = \Delta\sigma_v/[(S-d_0)/h] \qquad (6.11)$$

where h is the height of the specimen and S is the settlement recorded at the end of the compression step. The corresponding coefficient of permeability k was derived from eq.(6.4). c_v, M and k are model parameters, that is they are constants characterizing the soil behaviour according to Terzaghi's model. The extent to which these parameters differ from the true material behaviour will depend on the validity of the model's assumptions

In Section 6.5 the plots c_v-σ'_v, M-σ'_v and k-σ'_v, calculated as above from the OED test data both for the natural and the reconstituted Pappadai clay are compared. Although the degree of validity of the model may differ for the two clays, the differences between the values of c_v, k and M for the natural and reconstituted clay are presumed to be primarily the result of differences in soil structure, and the variation of the parameters with stress level is presumed to result from structural changes due to loading.

6.4.3. Limitations of the Terzaghi model

In this section the validity of the hypotheses of Terzaghi's theory is discussed on the basis of a review of studies of soil consolidation reported in the literature. In particular the section reviews the errors in the model predictions due to the assumption that the soil behaviour is linear elastic and not strain-rate dependant. These errors were further investigated within the analysis of the oedometer test results on Pappadai clay in order to interpret correctly the clay strain-rate dependency.

In the research it has been investigated whether Terzaghi's model prediction of the average consolidation degree $U_s(t)$ from compression data is consistent with the consolidation degree $U_p(t)$ from base pore water pressure data From eq (6 6), the values of $u_b(t)/\Delta\sigma_v$ expressed by eq (6 2)

can be derived so that for each time t, relative to a u_b value, the corresponding value of T_v for the Terzaghi model can be calculated. For these values of T_v expression (6 8) has been used to calculate $U_p(t)$. In Section 6.5.9 the curves U_p-t calculated as above are reported for tests OED 5 and 6, where u_b was measured.

From the compression data the curves U_s-t (eq.6.9) have been deduced (see Section 6.5.9). According to Terzaghi's assumptions of no strain rate dependency for the soil and of linear elasticity, the average consolidation degrees $U_s(t)$ and $U_p(t)$ should coincide. Therefore the difference between $U_s(t)$ and $U_p(t)$ gives an idea of the level of error inherent to the application of the above mentioned Terzaghi's assumptions and shows when the model better simulates the soil behaviour.

The effects of the change in oedometric stiffness M due to yielding on the shape of the consolidation curves U_s-t, U_p-t and $u_b/\Delta\sigma_v$-t have been studied by many authors (Davis and Raymond 1965, Mesri and Rokhsar 1974, Mesri and Godlewsky 1979, Davis and Raymond 1965). The soil non linearities have a particularly serious effect on the consolidation curves for loading steps in the region of the gross yield point, as shown in Figs 6 20 to 6.22

Lowe et al. (1969) showed that during oedometric compression following secondary compression the clay behaviour is strongly non linear (Fig.6.23(a)) as the values of M and c_v are very high soon after loading and decrease with time during consolidation (Fig 6.23(b)) In this case the Terzaghi's predictions would be in error. Lowe et al. hypothesized the occurrence of structural changes in the clay during secondary compression and considered these changes the cause of the increase of M and c_v at recompression. However the duration of the creep stages in the tests from Lowe et al. was rather short and therefore not sufficient to assume that micro-structural processes such as thixotropy had occurred, causing changes in the clay properties.

Leroul et al.(1985) recorded high stiffnesses at the start of compression steps in an end of primary test (EOP) (Fig 6 24), in which creep is not allowed for. As in the tests ageing had not occurred at all, thixotropic hardening and the other processes which develop during ageing were not the causes of the observed behaviour. Consequently Leroul et al (1985) suggested that the changes in stiffness were effect of the strain rate dependency of the clay behaviour, which they considered the principal cause of the general non linearity of the clay response during primary consolidation The M and c_v values from Terzaghi's theory are an average of the values truly experienced by the clay during primary consolidation, accordingly

On the basis of the experimental evidence discussed above the present research has started from the assumption that the soil behaviour is strain rate dependant and it should therefore be represented in the three-dimensional space e-σ'_v-$d\varepsilon_v/dt$. The c_v and M values calculated for the Pappadai clay from Terzaghi's model have been compared with the values calculated accounting for strain rate dependency (Sections 6.5 and 6.6) according to the consolidation analysis discussed in the following section.

However on the question of whether time is a variable on which the soil behaviour depends during primary consolidation there is not a general consensus of opinion. Terzaghi (1944), Crawford (1965), Gibson and Lo (1969), Bjerrum (1967), Mitchell (1976), Lerouil et al.(1983), Lerouil et al (1985) considered that the micro-structural factors controlling the soil straining during consolidation and creep can be the same, the structural viscosity being one of them. Consequently the clay behaviour is generally strain rate dependant. On the contrary Ladd et al (1977), Mesri and Godlewsky (1977), Mesri and Godlewsky (1979), Mesri and Choi (1985) and Jamiolkowski et al (1985) proposed that structural viscosity does not determine the soil response during either primary consolidation or creep.

The latter interpretation was first proposed on the grounds of observed values of c_α/C_c being constant for different clays at about 0.04±0 01 (Mesri and Godlewsky 1977). This was considered an indication of the fact that the secondary compression settlements [$c_\alpha\Delta\log(t)$] develop from mechanisms similar to the ones controlling the consolidation settlements to which C_c is mainly related. The authors then considered both the consolidation settlements and the creep settlements as effect of fabric deformations which do not include viscous phenomena The data later presented by Mesri and Choi (1985), showing that the primary consolidation strains of specimens of different sizes were not dependant on the primary consolidation duration, were considered to confirm this interpretation.

However, in contrast with this interpretation many experimental results are given in the literature which show that the soil behaviour is strain rate dependant (Crawford 1965, Burghignoli 1979; Lerouil et al. 1983, Hanzawa et al.1990) and that under any type of 1D compression it obeys a unique stress-strain law in the e-σ'_v-$d\varepsilon_v/dt$ space (Lerouil et al 1985). Two examples are shown in Figs 6 25 and 6 26.

Gibson and Lo (1961) used the simple physical model shown in Fig 6 27 to represent the soil skeleton and deduced a mathematical model for which the structural viscosity takes part into the soil response to loading A review of the basic equations representing the soil deformation

mechanism in this model is reported in Appendix 6.2. The authors did not consider in detail the precise inter-particle mechanisms involved. They assumed as elastic any part of the soil response other than the viscous one. The elastic springs have to represent all aspects of behaviour which are not viscous, that is modifications to either the fabric or the bonding of the soil structure. On the basis of a simple physical scheme, the model of Gibson and Lo then simulates the strain rate dependency of the soil behaviour during both primary consolidation and creep, as discussed in Appendix 6.2, and the validity of the model predictions, when checked against the experimental results, suggests that viscosity takes part into the soil response.

Following the work above primary consolidation and creep have been seen as part of the same process of soil straining. As shown in Appendix 6.2 the model of Gibson and Lo (1961) has been of use to interpret the connections between the creep behaviour of the soil and its strain rate dependency. During all the OED tests the creep coefficient c_α was measured as :

$$c_\alpha = \Delta e/\Delta \log t \qquad (6.12)$$

If c_α is constant with time, the creep strain rate $d\varepsilon_v/dt$ is equal to

$$d\varepsilon_v/dt_{creep} = c_\alpha/[(1+e_0)t] \qquad (6.13)$$

In Appendix 6.2 it is demonstrated that c_α should increase when both the soil compressibility b of the model from Gibson and Lo increases and the soil structural viscosity $1/\mu$ decreases (eqs.A.6 2.6 and A.6.2.7). At infinite time the creep strain rate is zero (eq.6.13) and the strain is (App.6 2) :

$$\varepsilon_{v\infty} = (a+b)\sigma'_v = m_v\sigma'_v \qquad (6.14)$$

Therefore the parameter b of the model from Gibson and Lo is part of the compressibility m_v and is then related to C_c It follows that c_α is expected to increase with both increasing m_v and C_c even for a model like the one from Gibson and Lo, which includes viscous behaviour Thus the c_α-C_c relationsh p cannot be used to demonstrate that the soil is not strain-rate dependent, as suggested by Mesri and Godlewsky (1977) The relationship between c_α and C_c has been investigated for the natural and the reconstituted Pappadai clay (Section 6 5 6)

6.4.4. Wissa's analysis of consolidation

The CRS and the OED test results have been examined to see if they fit a unique strain-rate dependency law, considering both the reconstituted and the natural material. The CRS test data were processed using a modification of the mathematical integration of the consolidation equation proposed by Wissa et al.(1971) :

$$c_v \, \partial^2 \varepsilon_v / \partial z^2 = \partial \varepsilon_v / \partial t \qquad (6.15)$$

Part of the assumptions of Terzaghi's model apply also to Wissa's solution of consolidation, but the formulation of eq (6.15) does not require either the soil behaviour to be linear in the $e\text{-}\sigma'_v$ plane nor that the soil behaviour is independent of strain-rate. Though eq.(6 15) requires c_v to be constant throughout the specimen at any time during consolidation.

The integration of eq.(6.15) given by Wissa et al.(1971) is reviewed in Appendix 6.3, where a modification of this integration procedure is presented. The revised version of the integration of eq.(6.15) yields the formulae :

$$\varepsilon_v = \Delta h(t)/h \qquad (6.16)$$

$$\sigma'_v = \sigma_v - 2/3 \, u_b \qquad (6\ 17)$$

$$M = \Delta\sigma'_v / \Delta\varepsilon_v \qquad (6\ 18)$$

$$k = 1/2 \, r h^2 \gamma_w / u_b \qquad (6.19)$$

$$c_v = 1/2 \, \Delta\sigma'_v \, h^2 / (\Delta t \, u_b) \qquad (6.20)$$

In these expressions r is the current average strain-rate and, as said above, h is the initial height of the specimen and $\Delta h(t)$ is the compression occurred by time t. Instead of assuming a constant r and c_v with time for all steps of the integration, as did Wissa et al (1971), it was found necessary to take c_v constant with time only in one step of the integration The formulae (6.16) to (6 20) differ only slightly from those of Wissa et al.(1971), but they are affected by an error which is less than that of Wissa's solution

The error arising from the hypothesis that c_v is constant with z, which is used in the definition of eq (6.15), is negligible providing u_b is less than 5% of the current σ_v (Wissa et al 1971).

In Appendix 6.3 it is shown that the expressions (6.16) to (6.20) are applicable to both oedometric consolidations at constant-rate-of-strain and to the case where the strain-rate is changing The data from the OED tests for which u_b was measured, OED 5 and 6, were then processed using eqs.(6.16) to (6.20). In the appendix the conditions for the applicability of these equations and the use of eventual correction factors are discussed in detail.

In addition to the errors discussed in Appendix 6.3, the error arising from the hypothesis of small strains may be significant for the CRS tests at high pressures, especially when testing reconstituted clay. If this error is not considered and providing the change in strain within the logging interval is designed to be small during the test, the values of M, c_v and k resulting from the processing of the CRS tests here proposed are believed to be reasonably accurate, and show the strain-rate dependency and non linearity of the soil behaviour during 1D compression For the CRS tests carried out on Pappadai clay care was taken to ensure that the increase of strain between successive readings was only about 0 03-0 05%.

During primary consolidation in the OED tests σ_v is constant, but both σ'_v and r change with time. The settlement and u_b data, logged at small time intervals in tests OED 5 and 6, were used in eqs (6.16) to (6.20) to deduce the continuous state paths experienced by the clay during primary consolidation. During primary consolidation the time dependent strain component .

$$\varepsilon_t^* = -r\, h^2/c_{v1}\; 2/\pi^2 \sum_{n=1\to\infty} \cos(n\pi X)\, n^2 \exp(-n^2\pi^2 T_v) \qquad (6.21)$$

which is part of the new $\varepsilon_v(z;t)$ solution reported in Appendix 6.3 (eq.A.6.3.19), may represent a significant contribution to strain. ε_t^* was instead neglected in the calculation of strain, with a consequent error. However the results of the processing of the OED test data (OED 5 and 6) were found to be consistent with the results of the CRS tests, in which this error is negligible. It follows that the use of the new solution to process OED tests in which the base pore water pressure is measured is rather accurate

The effects of strain-rate dependency on the compression curves in the ε_v-σ'_v plane is that usually examined (Crawford 1965, Lerouil et al 1983, Lerouil et al 1985) In the present work, the effects of strain-rate on other soil properties, such as the coefficient of permeability k, the stiffness M and the coefficient of consolidation c_v was examined too The studies in the literature have mainly considered the strain-rate dependency of soft clays, but few data have been presented for reconst tuted clays (Burghignoli 1979) and for stiff clays (Hanzawa et al 1990) The relationsh p between the strain-rate dependency of the clay behaviour and the c ay structural

features has never been investigated. The results of the present oedometer test programme were analyzed to investigate the strain-rate dependency of Pappadai clay and its comparison with the strain-rate dependency of the reconstituted clay.

Lerouil et al.(1983) and Lerouil et al.(1985) have shown that a unique law in ε_v-σ'_v-$d\varepsilon_v/dt$ space can describe the behaviour of soft clay under different types of oedometric loading This is shown by the unique state of the clay in the ε_v-σ'_v plane when subjected to a given σ'_v and a given current strain-rate $d\varepsilon_v/dt$, no matter whether strain is developing during primary consolidation, or secondary compression, or any other type of continuous loading

Suklje (1969) defined the compression curve in the e-σ'_v plane at constant rate of voids ratio change as "isotaca". Following Suklje (1969), Lerouil et al (1983) and Lerouil et al. (1985) identified a family of compression curves at constant strain-rate in ε_v-σ'_v plane for different soft clays, and showed that the state paths followed by the clay move from one to the other of these curves depending only on the current strain rate. In the following the term "isotaca" will be used for the compression curve in the e-σ'_v at constant strain-rate $d\varepsilon_v/dt$. This definition of isotaca does not differ significantly from the definition of Suklje, but it is more easily related to the rate of compression for comparisons of the strain-rate dependency of different clays. The isotacae of the natural and of the reconstituted Pappadai clay will be shown in Sections 6 6.5 to 6 6.7.

Although the strain-rate dependency is generally more evident during compression beyond yield, i.e. when the structure undergoes major changes and its stiffness reduces, there appears to have been no consideration of strain-rate dependency before and beyond yield, and its relation to either structural changes or to the changes in the clay mechanical properties. These relationships are addressed in the analysis of the present testing programme.

6.5. Discussion of the OED test results

In the OED and CRS tests various different loading paths were applied to the clay to investigate the clay's structural response, and the relation of the yield state and the state path to the variations of the parameters M, C_c, c_v, k, C_s and c_α As a consequence, a framework representing the oedometric behaviour of both the natural and reconstituted clay in e-σ'_v-$d\varepsilon_v$ dt space is defined, and the structural modifications interpreted, in Sections 6 6 and 6 7.

Nine OED tests were carried out on the undisturbed Pappadai clay, as summarized in Table 6.1. In tests OED 1, 2, 3, 5, 6, 8 and 9 the specimen was compressed from the undisturbed state of the clay in the laboratory. In test OED7 the clay was first swelled to 10 kPa, in order to measure the swelling index C_s of the clay before yield, and then recompressed to 4998 kPa, in test OED4 instead the clay was first swelled to 589kPa and then recompressed.

Tests OED4 and 7 were carried out to evaluate if swelling weakens the structure of the natural clay and then affects its response to compression. The clay was swelled from the highest σ'_v reached in compression in tests OED 3 and 5, and from just beyond yield (2940kPa) in test OED8, so as to evaluate how different levels of compression weaken the clay bonding. That bonding restrains the swelling of the clay has been often suggested in the literature, and the ratio C_s^*/C_s has even been proposed as a parameter of bond strength by Schmertman (1969) and Burland (1990).

The changes in structure occurring during compression were not only inferred from the mechanical response, but were also directly observed by the use of SEM, Chapter 7. Test OEDR was carried out on the reconstituted clay in order to compare the behaviour of the natural and reconstituted clay

6 5.1. Consolidation curves

In Fig.6.28 (a) to (i) the consolidation curves from the OED tests on the undisturbed clay are shown. The compressions shown in the figure are the raw data.

The Casagrande curve fitting technique could be satisfactorily applied to most of these curves to compute both d_0 and the Terzaghi coefficient of consolidation, c_v The application of the Casagrande curve fitting to the test consolidation curves is shown in Figs 6 29 and 6 30 for tests OED 5 and 6. For stress increment ratios $\Delta\sigma_v/\sigma'_v$ below 0 3 the consolidation curves do not show any flexure, as evident for the loading steps 1960-2548kPa in tests OED 5 and 6 (Figs 6 29 and 6 30), in these cases the Terzaghi parameter c_v could not be computed. The smaller the ratio $\Delta\sigma_v/\sigma'_v$, the smaller are the primary consolidation strain rates, so that at about a degree of consolidation of 60% the creep rate exceeds the primary cons lidation strain rate, and the flexure, predicted by the Terzaghi theory (which neglects creep) disappears

6.5.2 Compression curves and yield stresses

The compression curves starting directly from the undisturbed state of the clay are plotted in Fig.6.31. The compressibility of the clay increases dramatically at about σ'_v of 1500kPa and the coordinates of the gross yield state are :

$$0.8 < e < 0.82 \; ; \; 2350 < \sigma'_y < 2450 kPa$$

using Casagrande's construction (1936) to identify the yield point, though Casagrande actually proposed this construction to identify the preconsolidation stress of the clay; distinction between σ'_p and σ'_y was defined in Section 2.5. Beyond yield the compression curves follow a straight line very closely. The state of the clay examined by SEM, Chapter 7, is indicated in the figure.

The compression index C_c, plotted against σ'_v in Fig 6.32, is less than 0.05 below 1000kPa, and increases to 0.54 over the stress range 1000kPa-3000kPa. In tests OED 2 and 3 the compression curves started at the lowest voids ratio; they are initially parallel to the other curves and then join a common straight line beyond yield, Figs.6.31 and 6.33. Thus the natural clay follows a unique oedometric state path beyond yield. This aspect of behaviour cannot be seen in the ε_v-σ'_v plot, Fig.6.34, and thus analyzing the clay behaviour in terms of voids ratio may be more appropriate than carrying out the analysis in terms of strains ε_v.

As suggested by Janbu and Senneset (1979), σ'_y may be defined more objectively in the linear plot (Fig.6.33), where a value of σ'_y of 2600kPa is obtained for the state immediately before maximum compressibility. This value of σ'_y is higher than that derived from the Casagrande construction in Fig.6.31. In any case, for the natural Pappadai clay σ'_y is higher than its geological preconsolidation pressure σ'_p, which was about 1310kPa. The natural Pappadai clay thus has a YSR higher than its OCR, the former being about 6 and the latter about 3 2

This difference is the consequence of the structural changes undergone by the clay after virgin compression, in addition to the changes simply resulting from loading-unloading paths Earlier chapters have discussed the evidence supporting the hypothesis that the clay underwent long-term diagenesis, which is probably the main cause of the increase of the clay YSR with respect to the OCR. As anticipated in Sections 3 8 and 5.11, the Pappadai clay is seen to have a post-sedimentation structure, and lies in clay category 7, Table 2 1

6.5.3. Dependency of the state of the clay on strain rate

The importance of the e-σ'_v plot in developing a framework of clay behaviour is confirmed in the strain-rate dependency of the clay. In Fig.6.28 the strain rates $d\varepsilon_v/dt$ (equal to (dh/dt)100/h) recorded during consolidation steps (corrected for compliance) are plotted against time The plots show the strain-rate variation that the clay experiences during primary consolidation. The final strain rates for each loading step of the OED tests are reported in Figs.6.33 and 6.34. Before yield, the state points at the higher voids ratios, i e close to the continuous red curve in Fig 6.33, were all at strain rates in the range (3E-6%/min; 8E-5%/min). Beyond yield, all the state paths run very close to the red curve, and are at $d\varepsilon_v/dt$ about 3E-4%/min, apart from the final state of test OED9, which was at 5E-5%/min and which plots to the left of the red curve, and the final state of test OED2, which was at 1E-3%/min.

Thus beyond yield the red line in Fig 6.33 defines the compression curve for the undisturbed clay for a strain rate about 3E-4%/min, otherwise defined as the isotaca of the clay for $d\varepsilon_v/dt$ of 3E-4%/min and de/dt about 5.6E-6/min (Suklje 1969). In Fig.6 33, the state points at higher strain rate plot to the right of those at lower strain rates, as usually observed (Lerouil et al.1983; Crawford 1965). In Fig.6.34 the strain rate dependency of the clay is not as clear as in Fig.6 33. In the plot ε_v-σ'_v two are the lines beyond yield which join states at 3E-4%/min. The effects of the initial voids ratio of the clay on the ε_v-σ'_v curve obscures the basic behaviour of the clay in this plane. In conclusion, although other authors have often constructed their rheological models in the ε_v-σ'_v plane (Lerouil et al.1985), the data presented here show that is more appropriate to examine the clay response in the e-σ'_v plane.

6.5.4. Swelling data recorded in the OED tests

The behaviour of the natural clay when allowed to swell either before or beyond yield is shown in Fig 6.35. The swelling index, C_s, of the intact clay, measured on the swelling line from test OED7, is about 0 04 The swelling capacity of the clay increases with compressi n beyond yield, yield strongly weakens the clay bonding (Burland 1990) The bonding degradation arising from the compression of the clay to different values of σ'_v will be discussed further when comparing these data with the swelling data from the CRS tests on the natural and reconstituted clay

The state path followed by the clay during recompression after swelling in test OED7 plots to the left of the state path followed in test OED5 (Fig.6.35). The voids ratios of the two specimens coincide at σ'_v of 1176kPa, before the swelling of the OED7 specimen. The distance between the two compression curves, highlighted in the figure, is thus a consequence of the structural changes occurring during unloading.

6.5.5. Oedometric stiffness in OED tests

The values of oedometric stiffness M recorded in the OED tests are plotted against σ'_v in Fig.6.36. The stiffness of the undisturbed clay is about 70MPa, lying mid-way between the higher M values of those samples which underwent compression due to drying during storage (OED 2 and 3), and the M value of clay allowed to swell before compression (OED7) With compression the stiffnesses of the different samples reduced, and became progressively closer. The minimum values of M were recorded at σ'_v just beyond σ'_y Post-yield the clay specimens seem to exhibit equal stiffness for equal σ'_v, independent of their stress history.

6.5.6. Behaviour of the Pappadai clay during creep

The creep coefficients c_α recorded in the OED tests on both natural and reconstituted clay are plotted against σ'_v in Fig.6.37. The values of c_α of the clay compressed from its undisturbed state were less than 0.0025 at σ'_v below 2000kPa, and progressively increased with increasing σ'_v, reaching a maximum value of 0 023 at σ'_v of 1.5 σ'_y. The clay structure weakened by the unloading path prior to compression (OED7) exhibited similar c_α values to those of the natural clay for equal σ'_v. Thus the creep strain-rates seem not to be very sensitive to changes in structure occurring during unloading.

In Appendix 6.2 and Section 6.4.3 the dependency of c_α on both the stiffness and the structural viscosity of the clay have been discussed and theoretically derived within a model which assumes that viscosity takes part into the response of soils to loading Here the increase of c_α with increasing σ'_v, shown by all the test data, is in agreement with the model conclusions in App 6 2 (eq A 6 2.7).

The relationships between c_α, compressibility C_c, and stiffness M are shown in Fig.6.38. The plot of c_α against C_c in Fig.6.38(a) does not follow a unique straight line, as found empirically by Mesri and Godlewsky (1977); this is highlighted by the data from the test OEDR on reconstituted clay, which deviate from the trend followed by the undisturbed samples, which moreover appear to follow a curve rather than a straight line.

The relationship between c_α and the clay stiffness M is considered more fundamental than that between c_α and C_c. The c_α-M relationship was derived first on theoretical grounds in Appendix 6.2, where it is shown that c_α changes with both M and σ'_v. The c_α-M plot in Fig 6 38(b) shows that the relationship between c_α and M is not unique, accordingly (eq A 6 2 7).

The theoretical relationship between the measured values of c_α/σ'_v and the corresponding stiffnesses M (eq A.6.2.7) was explored in Fig.6.39 The data points c_α/σ'_v- M were found to follow a unique curve, irrespective of the clay structure and of the previous stress history of the soil. The deformation mechanism governing the creep behaviour of the natural, the reconstituted clay and the clay swelled to low stresses is found to be unique, given by the equation :

$$c_\alpha M^{1.058}/\sigma'_v = 0.248 \qquad (6.22)$$

Eq.(6.22) shows that the creep coefficient of clays increases with increasing pressure and decreasing stiffness of the soil, consistent with eq.(A 6.2 7) in App.6.2, derived from the model of Gibson and Lo (1961), although it has a different mathematical expression The main finding is that, even if the test data do not plot monotonically in Fig.639, but show some oscillation, in general they follow eq.(6.22), showing that it is unique for the Pappadai clay in any structural condition.

6.5 7. State paths during primary consolidation and strain-rate effects

The strain-rate dependency of the clay was investigated in the OED tests in which u_b was measured during consolidation, i e OED 5 and 6 (Figs 6 29 and 6 30) The strain rates d ring tests OED 5 and 6 are plotted against σ'_v in Fig 6 40 The state paths experienced by the clay specimens during primary consolidation and creep were computed applying the theory given in App.6 3, equations (6.16) to (6 20), and are plotted in Fig 6 41. In the same figure the step-loading compression curves from tests OED 5, 6, 2 and 9 are also shown

Tests OED 5 and 6 were carried out following identical procedures and loading steps, apart from the application of different back pressures, 300kPa in OED5 and 400kPa in OED6. The corresponding variations of u_b were very close (Figs.6.29 and 6.30). There was always a delay in the response of the pore water pressure measuring system, such that the maximum u_b was always recorded after about 5 minutes from the load application independently from both the value of $\Delta\sigma_v$ and the back pressure being applied. Presumably a transition stage occurred, during which the water in the measuring system got to equilibrium with the soil pore water; consequently only the pressures recorded after this stage can be considered representative of the soil pore pressures.

The ratio between u_b at peak and $\Delta\sigma_v$ was always about 0.5; slightly higher values were recorded in the final loading step. The e-σ'_v paths shown in Fig 6 41 were calculated from the point of maximum u_b onwards. A straight line is shown connecting the starting point of each consolidation step with the starting point of the computed state path. The state paths from the two tests almost coincide and plot far to the right of the compression curves connecting the final equilibrium states.

Despite the imperfections of the theory in App.6.3, the state paths fit into a credible framework of strain-rate dependency of the clay behaviour. In Fig 6.41 some strain rates recorded during tests OED 5 and 6 are reported as well as the isotaca shown in Fig 6.33. On the basis of the e-σ'_v-$d\varepsilon_v/dt$ data in Fig.6.41, the post-yield isotacae for the strain rates 1E-5 %/min, 1E-4%/min, 1E-3%/min, and 2E-2%/min can be identified. These isotacae outline to a first approximation a behavioural framework for the natural Pappadai clay in e-σ'_v-$d\varepsilon_v/dt$ space. The validity of the framework in the figure is confirmed by the CRS tests discussed in Section 6 6. The data in Fig 6.41 seem to show that strain rate also influences the behaviour of the clay before yield, although the isotacae are there less clear cut.

6.5.8. Variation of M with strain rate during primary consolidation

In Fig 6.42 the Terzaghi stiffnesses M for the OED tests shown in Fig.6.36, and the M values calculated for tests OED 5 and 6 with eq (6.18) are plotted The latter M values are plotted against σ'_v at the end of the relevant strain increment, while the Terzaghi M values are plotted against the average σ'_v for the corresponding loading step For that part of the consolidation preceding the maximum value of u_b in tests OED 5 and 6, the average value of M has been plotted against the σ'_v corresponding to the maximum u_b value Though the stiffnesses actually

exhibited by the clay at the very start of consolidation could not be computed, the average M values in this time interval are evidently influenced by the very high initial stiffness.

The state paths in Fig.6.41 and the M values in Fig.6.42 are consistent with those observed by Lowe et al. (1969) (Fig.6.23) and Lerouil et al. (1985) (Fig.6.24). As suggested in Section 6.4.3, the very high stiffness the clay exhibits at the start of compression does not necessarily rise from structural changes occurring during secondary compression, but rather it appears to be part of the effects of strain-rate. In tests OED 5 and 6 the duration of ageing was very limited and was not constant for the different loading steps, though the increases in strain rate at the start of loading were similar for the corresponding steps in the two tests, and the loading paths and the variations of M were similar. That the state paths shown in Fig.6 41 and the M values in Fig.6.42 are consistent with a framework of strain-rate dependency of the behaviour of Pappadai clay is emphasized by comparing these OED tests with the CRS tests (Section 6.6) Both before and beyond yield the clay stiffness strongly reduces with reducing strain rate during consolidation, from initial values in excess of 100MPa to about 2-5 MPa

6.5.9. OED test c_v values and inconsistencies of Terzaghi's model

The c_v values corresponding to the M values shown in Fig 6 42 are plotted Fig.6 43, where the continuous c_v plots for tests OED 5 and 6 were calculated using eq (6.20) The c_v values for Terzaghi's model were calculated by means of the Casagrande curve-fitting method, Section 6.4.2. Before yield the Terzaghi c_v values plot midway between the values of c_v at commencement of loading and the c_v values in the second part of primary consolidation. Beyond yield the Terzaghi c_v values are close to the c_v values in the second part of the consolidation stage. It can be seen in Fig.6.43 that the Terzaghi c_v values of the clay specimen subjected to unloading before yield (OED7), were lower than the c_v values logged in the other tests only before yield

The errors in Terzaghi's model due to the clay's non linear behaviour outlined above were investigated. The average degrees of consolidation U_s and U_p, calculated from the compression and the u_b measurements respectively (Section 6.4 3), were compared for tests OED 5 and 6, as shown in Fig 6 44. Since both the U_s-t and the U_p-t plots assume that M and c_v are constant they should coincide, but they do not, a result of the errors inherent in Terzaghi's theory

The discrepancy between the U_s t and U_p-t curves in Fig 6 44 resembles the difference between the trends of the U_s-t and u -t curves in Figs 6 20, 6 21 and 6 22 The incon stenc es in the

Terzaghi predictions in these latter figures are principally due to the change in stiffness of the clay over yielding. Fig.6.44 shows that a similar level of inconsistency is inherent in the Terzaghi predictions irrespective of the loading increments, and is related to the changes in stiffness M and c_v which arise from the changes in strain rate.

In Figs.6.45 and 6.46 the Terzaghi c_v values (Section 6.4.2; eq.6.10) for tests OED 5 and 6 are compared with the c_v values calculated as :

$$c_v (t) = T_v(u_b) H^2 / t \qquad (6.23)$$

$T_v(u_b)$ derives from eq.6.2 and is the same as the value of $T_v(u_b)$ used to calculate U_p. It is seen that different values of c_v can be derived from Terzaghi's model for the same loading stage. It has been found that Terzaghi's model under-predicts the duration of primary consolidation due to the use of constant c_v values which are higher than the c_v values of the clay in most part of the consolidation stage. The inconsistencies of Terzaghi's model highlighted above agree with the results of the theory in App.6.3.

6.5.10. Permeability coefficients from the OED tests

In Fig.6.47 both the coefficients of permeability k deduced from eq (6 5) using the Terzaghi c_v and M values and the k calculated for tests OED 5 and 6 with eq (6 19), i e according to the theory in App.6.3, are plotted against voids ratio. The two sets of data define a consistent linear reduction of the logarithm of k with decreasing voids ratio for values of e below 0 8, that is from about the average of the voids ratios at yield in the different tests

For values of e above 0.8, k appears to be constant, but a basic change in the relationship logk-e seems to occur at yield. The relation logk-e was further investigated using the CRS test results, as shown later. Fig.6.47 suggests that the permeability is not strain-rate dependent, as already observed by Lowe et al. (1969); the strain-rate dependency of k is returned to later

6 5.11. OED test on reconstituted clay

The consolidation curves and the corresponding strain rates for test OEDR are shown in Fig 6 48 The OEDR compression curve is plotted in Fig 6 49 together with the compression curve of the

clay reconstituted from a slurry (Fig.5.16). The data show that undrained unloading in the consolidometer caused some increase of voids ratio and reduction in effective stress, to about 20kPa. The voids ratio increase resulted from desaturation below 100%, see Table 6.1, and is consistent with extension fissures observed by SEM in this clay (see Section 5.9.4).

The ICL of Pappadai clay shown in Fig.6 49 is later extended to higher σ'_v values using CRS test results. The in situ state of the natural clay and the relative compression curves from the OED tests are also shown. These curves lie to the right of the ICL, beyond the geological preconsolidation state of the clay (P in the figure) showing the difference in the behaviour of the natural and reconstituted clay structure. The states of the clay investigated by SEM are also shown.

The ratio between the YSR and the OCR of the natural Pappadai clay, at present about 2, is a parameter representative of the mechanical effects of the long-term diagenesis The ratio between the yield stress σ'_y of the natural clay and the pressure on the ICL at the same voids ratio as the yield point of the natural clay Y, defined σ^*_e (Burland et al 1996) is about 3 5.

The values of the Terzaghi parameters M, c_v and k for the reconstituted clay are plotted in Figs.6.42, 6.43 and 6.50. Fig 6.51 shows that Terzaghi's model under-predicts the duration of primary consolidation for the reconstituted clay, a similar under-prediction has been found to apply also to the natural clay, as mentioned at the end of Section 6.5 9. The neglect of the strain-rate dependency thus results in similar errors with Terzaghi's model for both the natural and the reconstituted clay. Consequently, the reconstituted clay is expected to be as strain-rate dependant as the natural clay.

The stiffness measured for the reconstituted clay in the stress range of the OED tests is lower than that of the natural clay at any σ'_v (Fig 6 42)

6 6 Discussion of the CRS test results and comparison with the OED test results

In Table 6 5 the errors accumulated in the CRS compressions, which are additional to the bedding errors, are given In the CRS tests on the undisturbed clay the bedding errors affected the settlements in the equilibration stage, but not in the compression stage On the contrary for the reconstituted clay the bedding err rs affected the CRS compr n at σ_v bel w 130kPa Th e errors are allowed for in the f lowing discussion

The e_0-σ'_{v0} states reported in Table 6 1 refer to the end of the equilibration stage. The σ'_{v0} values of the tests carried out with procedure 7 are consistently close to the suction measurements in Table 5.3 and they confirm further these measurements.

As discussed in Section 6.4.4, the CRS test data were processed according to a revised version of the Wissa theory (Appendix 6.3). The steady state solution (eqs.6.16 to 6.20) was in general applicable since the time-dependent strain component expressed in eq 6.21 was found to be lower than 1E-4% throughout all the tests.

6.6.1. Clay stiffness M_0 at the start of CRS loading

At the beginning of all the CRS compression tests the compression was either zero or was very small. The values of e and σ'_v immediately before the start of significant soil compression, e_i-σ'_{vi}, are reported in Table 6.6. Very high stiffnesses were then measured before e_i-σ'_{vi}, much higher than the initial M values recorded in the OED tests, Fig 6.36. The very rapid increase in strain rate was probably the cause of the very high stiffnesses exhibited by the clay at the start of loading, an observation that could be of interest for studies of the stiffness of soils at very small strains. As will be demonstrated in Section 6 6 5, the clay stiffness is a function of both $d\varepsilon_v/dt$ and $d^2\varepsilon_v/dt^2$, and because of strain-rate changes, it can vary from zero to infinity. The M values reported in the following plots do not include these initial very high stiffnesses M_0.

6.6.2. Strain rates in the CRS tests

In Figs.6.52 and 6.53 the strain rates experienced by the undisturbed and the reconstituted clay (after correction of strain for compliance) are plotted against σ_v Note that, whereas for the OED test data the symbols represent data points for individual stages of loading, for the CRS tests the data are continuous and the symbols, where used, are simply to distinguish one test from another

The trends of strain-rate in the different tests were all similar, no matter what cell design was being used, this finding supports the validity of the compliance corrections

6.6.3 Pore water pressure response in CRS compression

In Fig 6.54(a) the values of u_b recorded in all the CRS tests on the undisturbed clay (apart from CRS6) are plotted against σ_v; the u_b data from tests on reconstituted clay are plotted in Fig 6.55. As expected, u_b values increase with strain rate and the shape of the u_b-σ_v plots match those reported for CRS tests on other clays (Fig 6.25, Lerouil et al.1985).

The u_b plots for tests at similar strain rates are consistent, except for tests CRS1 and 10, both carried out at about 0.025%/min. Test CRS11 was carried out with back pressure (Design 3) at a strain rate equal to that of tests CRS3 and CRS4, in order to check the validity of the u_b measurements in the slow tests with Design 2 (Section 6 2 1) Test CRS11 shows that the u_b measurements with Design 2 in tests at low strain rates were apparently accurate, and that if unrecognized errors affected u_b these would be very small with respect to σ_v

In contrast test CRS10, carried out with Design 3* to compare with the u_b measurements in the fast tests carried out with Design 2, showed that errors arising from poor system saturation can be significant in the fast CRS tests. Comparison of tests CRS1 and CRS10 shows that the discontinuous drops seen in u_b in test CRS1 did not occur in test CRS10 when the system had been saturated with back pressure. The drops in u_b in test CRS1 were probably caused by the presence of air bubbles in the pore water pressure measuring system.

Both the results of test CRS10 and an analysis of the general trend of the u_b-σ_v plots from all the tests (Figs.6.54 and 6.56), permitted the u_b data from test CRS1 to be corrected Beyond yield u_b generally increased almost linearly with σ_v; the u_b-σ_v plot of test CRS1 was thus corrected as shown in Fig.6.56, though the corrected u_b values of test CRS1 are still lower than those of test CRS10. This discrepancy will be shown to be consistent with the "softer" compression behaviour exhibited by specimen CRS10 The curve for test CRS1 in Fig 6 56 is corrected in this manner and all the following plots relate to the corrected test CRS1 These results are shown to be much more consistent with the other test results than the raw u_b data.

Thus tests with oedometer cell Des gn 2, used for much of the present research, are reliable, even though back pressure was not used, providing the test is slow Moreover, it is pos ible to correct the u_b data in the fast test CRS1 The u_b data from tests CRS7 and CRS9 were n t corrected because the u_b-σ_v plots were close to a straight line to σ_v of about 20MPa Whether the concave-upward shape of the u_b-σ_v plots at high σ_v is the result of err rs in measurement or is the real c av

response cannot be demonstrated. The general trend of the results, discussed in the following sections, shows that the u_b values recorded in test CRS9 are quite accurate, while the u_b values recorded in test CRS 7 at high values of σ_v are probably lower than the excess pore water pressures in the sample.

Figs. 6.54(b) and 6.55(b) show for all the tests, except the fastest tests CRS7, CRS9 and CRSR4, that, after an initial increase, u_b is nearly constant to σ'_v. Around yield the u_b-σ'_v plot bends upwards and becomes linear. This trend is common to both the natural and the reconstituted Pappadai clay, and can also be recognized in CRS tests reported in the literature (Lerouil et al 1983; Lerouil et al 1985).

This behaviour is of interest first because it shows that with overconsolidated clays the compression occurs at a constant excess pore water pressure, and that in the normally consolidated condition this increase is almost linear with increasing σ'_v. Second, this plot provides a useful means by which to identify the σ'_y of the clay. σ'_y cannot be recognized in the fast tests, probably because of the short time available for u_b to equalize before yield

6.6.4. Janbu and Senneset's (1979) correction

In Figs.6.57 and 6 58 the values of u_b/σ_v for tests on both natural and reconstituted clay are plotted against σ'_v . As can be seen this type of plot is useful to identify σ'_y, which can be related to the minimum ratio u_b/σ_v.

The u_b/σ_v values eventually exceeded 10 in fast tests CRS 1, 7, 9, 10 and R4 as the pore water pressure gradients through the specimen increased with compression These gradients conflict with the basic hypothesis of Wissa's theory (App 6 3) that c_v is constant through the specimen at any given time. Consequently σ'_v and c_v may be overestimated. The results of eqs.(6 17) to (6.20) were corrected for the error related to the high pore water pressure gradients in the specimen according to the theory from Janbu and Senneset (1979), who proposed the introduction of two correction factors α_m and α_c in eqs (6 17) to (6 20), as discussed in Appendix 6.3 and shown in eqs.(A.6.3.28) to (A 6 3 30)

In Fig 6.59 the values α_m and α_c from Janbu and Senneset are plotted against $du_b/d\sigma_v$, the curves used to correct the test data are also shown. The correction of σ_v and M by the coefficient α_m is

significant only if $du_b/d\sigma_v$ is higher than 0.3, so that it was applied only to some stages of tests CRS 7, 9 and 6. However, in no case did this correction have any significant effect, as seen for tests CRS7 and CRS9 in Fig 6.60. In contrast the correction applied to c_v and k using the coefficient α_c was found to be significant. The corrections of c_v in the fast tests were found to be about 10-20% of the value of c_v for the clay beyond yield.

These latter results show that the CRS testing and the data processing has to be carried out with great care for a correct interpretation of the clay behaviour in the CRS tests. In the fast tests even a slight desaturation of the pore water pressure measuring system can give rise to significant errors, while the pore pressure distribution through the specimen can violate the hypotheses of the Wissa theory.

The very low values of c_v recorded beyond yield for the Pappadai clay made the study of the behaviour of this clay at high strain rates very difficult The excess pore water pressures arising in the specimen during fast testing were so high that first the apparatus had to be equipped with transducers measuring very high pore water pressures, as discussed in Section 6 2 3, and second the above corrections had to be applied.

6.6.5 Behaviour of the natural clay in e-σ'_v-$d\varepsilon_v/dt$ and ε_v-σ'_v-$d\varepsilon_v/dt$ space

The compression curves from all the CRS tests on the undisturbed clay (except tests CRS 4, 6 and 10) are plotted in the e-σ'_v and in the ε_v-σ'_v planes in Fig.6.61. The clay behaviour was investigated in both these planes, as already done for the OED tests, because both these plots help to identify basic features of the clay behaviour. Errors in e_i values (Table 6.6) can shift the e-σ'_v curve, but not the ε_v-σ'_v curve, but at the same time the e-σ'_v plot can highlight features of clay behaviour which are dependent on e_i and so are not revealed in the ε_v-σ'_v plot.

In both the plots, Fig.6.61, the compression curves consistently shift to the right with increasing strain rate. In the e-σ'_v plot it is also evident that the curves, despite their different initial voids ratio, tend to converge post-yield, and to diverge at higher stresses, a feature already shown in Fig 6 33 by the OED test data.

The compression curves for the slow tests are shown in Fig 6 62. Test CRS8 was not plotted because it refers to a specimen unloaded prior to yield and then affected by the swe l g path

This figure thus shows the compression behaviour of the undisturbed clay compressed at slow rates from its in situ voids ratio. The compression curves in the figure define a new unique state path if tests CRS4 is excluded. Test CRS4 was in fact the only slow test not consistent with all the other test results, as will be discussed later in this section. The difference in strain rate between the various tests shown in Fig.6.62 is about 0.0025%/min and it does not seem in any way to affect the clay response. The narrow band comprising the curves from tests CRS 2, 3, 5 and 11 defines a unique state path, which can be recognized as that followed by the clay at about 0.003%/min strain rate.

Strain-rate differences about an order of magnitude give rise to appreciable and consistent effects on the clay's response, as shown in Fig.6.61 by the distances between the narrow band of compression curves from the slow tests and the curves from tests CRS1 (0.025%/min), 7 (0.12%/min) and 9 (0.07%/min).

This finding is confirmed in Fig.6.63 showing the curve from test CRS 6, during which strain-rate changes were imposed (Fig 6.52(c)), and tests CRS1, 5 and 11. During test CRS 6 the state of the clay shifts across the e-σ'_v plane as the strain rate is changed from 0 003%/min to 0.03%/min and back. The clay contracts with reducing effective stress as the strain rate is reduced. Creep strain-rates were also reached in this test, point C in Fig 6.63.

The clay response observed in test CRS6 is consistent with the behaviour shown by tests OED 5 and 6 when processed using the revised Wissa theory (Fig 6.41), where in any of these three tests $d\varepsilon_v/dt$ was changing. Test results similar to CRS6 have been shown for soft clays (Lerouil et al.1985), but have not been reported for either stiff clays or for reconstituted clays. The data shown in Fig.6 63 clearly define the strain rate dependency of the clay, since four tests, carried out in different ways, all identify the distance between clay states at strain rates differing by about one order of magnitude. Thus for Pappadai clay a framework of behaviour exists in e-σ'_v-$d\varepsilon_v/dt$ space, such that in the e-σ'_v plane each state of the clay is associated with a particular strain rate. These findings are shown consistently in both e-σ'_v and ε_v-σ'_v plots, Figs 6 61 and Fig 6.63. The success of the correction of the data for test CRS1, which was derived only from comparison of the u_b responses in the various tests (Section 6 6 3), is evident in Fig.6 64

Tests CRS4 (0 003%/min) and CRS10 (0 025%/min) (Figs 6 62 and 6 64) are inconsistent with the foregoing clay behaviour. In particular, CRS10 exhibited a behaviour (Fig 6 64) which suggests that the clay was probably disturbed during the sample preparation CRS4 test plots

close to the other slow tests for σ'_v below 6000kPa, but then diverges from the band of compression curves identified for the slow tests (Fig 6.62). It appears that random factors exist which have a similar influence to strain rate effects.

In Fig.6.65, in addition to all the CRS test data (except for those from tests CRS4 and 10), compression curves for constant $d\varepsilon_v/dt$ from the OED test data (Fig.6.41) are plotted. The consistency of the strain-rate dependency of the two sets of curves is excellent. Where the range of strain rates for the OED test data overlaps the strain rates relevant to the CRS tests, that is for 1E-3%/min<$d\varepsilon_v/dt$<1E-2%/min, the isotacae resulting from the OED test data almost coincide with the CRS curves for the same strain rates.

From the curves in Fig.6.65 the isotacae of the natural Pappadai clay I_1, I_2, I_3, I_4 and I_5 ·

I_1: 5E-5%/min; I_2: 3E-4%/min; I_3 3E-3%/min; I_4 3E-2%/min, I_5 1E-1%/min

shown in Fig.6.66 have been derived These isotacae govern the oedometric compression behaviour of the natural Pappadai clay in the e-σ'_v-$d\varepsilon_v/dt$ space. In Fig 6 67 the isotacae plotted with a linear scale in Fig 6 66 are plotted with a logarithmic scale.

The strain-rate dependency of clays before yield has not been comprehensively assessed in the literature. The results presented above show that compression curves at different strain rates already diverge before yield, so that even a stiff clay that has undergone diagenesis exhibits a strain-rate dependent behaviour before yield. The state paths for different strain rates thus result in different yield states.

The strain-rate dependency of Pappadai clay is more apparent beyond yield, as is generally observed for soft clays. The distance between the isotacae of Pappadai clay increases at yield and it increases further with increasing σ'_v beyond yield, as can be recognized in Figs 6 63 and 6 66 The increase of strain rate mobilizes increasing strength with increasing compression, since, as the strain-rate increases, the clay supports higher stresses for equal voids ratios, and vice-versa when the rate reduces The clay behaviour becomes increasingly strain-rate dependant with decreasing voids ratio.

It can be demonstrated that even the simple physical model used by Gibson and Lo (1969) requires the isotacae to diverge with decreasing stiffness as it happens beyond yield If eq at n

(A.6.2.9) in App.6.2 is considered, for a given change in strain rate $\Delta(d\varepsilon_v/dt)$, the change of strain rate concerning the viscous part of the clay structure (Fig 6.27) $\Delta(d\varepsilon_v/dt)$ is :

$$\Delta(d\varepsilon_v/dt) = \Delta(d\varepsilon_v/dt)\,[1 - ((\mu a+ba/dt+\mu b)-\mu b)/(\mu a+ba/dt+\mu b)] \qquad (6.24)$$

It follows that, when the clay stiffness reduces, both the compressibility coefficients a and b of the model increase, and the strain-rate change $\Delta(d\varepsilon_v/dt)$ corresponding to a strain rate difference $\Delta(d\varepsilon_v/dt)$ increases. Correspondingly, for eq (A.6.2.9) the response of the viscous part of the clay structure gives rise to a higher change of σ'_v, making the strain-rate dependency of the clay increase.

Thus, even if the interaction between the elasto-plastic and the viscous elements of structure did not change at yield, the fall in stiffness post-yield would necessarily increase the strain-rate dependency. With the Gibson and Lo model, because of the fall in stiffness at yield, both an increase of strain rate dependency of the clay behaviour and an increase in the c_α values are expected. Both these behavioural features are observed for Pappadai clay. However the model does not cover the behaviour of the clay at large strains, where the clay stiffness again increases, though the isotacae go on diverging.

The isotacae in Fig 6 66 are reference loci of the framework of strain rate dependency of the natural Pappadai clay. The clay state lies on one defined by its current strain rate and voids ratio. Consequently, the clay's stiffness M is dependent on both the strain rate and the strain acceleration the clay is subjected to. M can then change from zero to infinity with changing strain rate. The clay state is never quite permanent, although the distance between the isotacae reduces with reducing strain rate, so that the state is almost permanent at strain rates below 1E-6%/min. Indeed, given the low strain rates which may occur in situ, the compression curve representative of the soil behaviour in situ forms the left-hand boundary of the framework of isotacae, such as that derived by Lerouil et al (1985) on the basis of in situ test results

As strain-rate dependency is greater beyond yield, the question arises of whether the structural changes occurring during compression at different strain rates are different Since a clay state e-σ'_v can be reached following different e-σ'_v-$d\varepsilon_v/dt$ paths, it appears that the structural modification is not dependent on strain rate The modification of the structure is related to the voids ratio change only, while the compression stresses σ'_v necessary for the modifications to occur depend on the current strain rate

6.6.6. Reconstituted clay behaviour in the e-σ'_v-$d\varepsilon_v/dt$ and ε_v-σ'_v-$d\varepsilon_v/dt$ space

The CRS test compression curves for the reconstituted clay are plotted as e-σ'_v and ε_v-σ'_v in Figs.6.68 and 6.69. The slow-rate compression curves are about to coincide below 600kPa, particularly when possible strain-measurement errors are accounted for.

Test CRSR4 plots above the others from the initial state, showing that the clay response changes with strain rate. In test CRSR3 the clay state shifts with the changes of strain rate from the slow rate compression curves to the higher compression rate CRSR4 curve, and is consistent with what was observed for test CRS6 on the undisturbed clay. However at high strain rates the CRSR3 curve does not converge with CRSR4 as well as did the CRS6 with CRS1, and, in general, random factors other than strain-rate dependency apparently affect the response of the reconstituted clay in the CRS test more than was the case with the natural clay

The isotacae at the strain rates 3E-3%/min and 2 5E-2%/mn were chosen as intermediate between the test curves at the corresponding constant rate, the isotacae for both the reconstituted and the natural Pappadai clay are shown in Figs.6.70 and 6.71, to linear and logarithmic scales respectively. In the same figures the OEDR test results are also plotted, identifying the isotaca for 5E-5%/min.

6 6.7. Comparison of the strain-rate dependency of the natural and reconstituted clay

Figs.6.70 and 6.71 show that no matter whether the clay structure is reconstituted and consolidated in the laboratory, or if it developed as a consequence of geological events, affected by diagenesis and cementation, the clay behaviour is always strain-rate dependent and follows a particular framework of behaviour in the e-σ'_v-$d\varepsilon_v/dt$ space. The behavioural frameworks of the two clays are similar. In both cases strain-rate effects are observed both before and beyond yield, in both the yield point changes with strain rate, and the strain-rate dependency increases with compression beyond yield.

These findings support the concept of a general framework of clay behaviour since clays having very different structures exhibit similar fundamental features of behaviour This is emphasized by similarity of the magnitude of strain-rate dependency of the natural and the reconstituted clays, based on the similarities between the distances between the relative isotacae at any given voids ratio

6.6.8. Yield of natural and reconstituted clay

The yield states exhibited by the clay specimens during oedometric compression were primarily identified in the e-σ'_v and e-$\log\sigma'_v$ plots. σ'_y was identified in the ε_v-σ'_v plot only for the CRS tests. In the linear plot σ'_y was taken as the stress shortly before the clay exhibited maximum compressibility (Janbu and Senneset 1979), while in the logarithmic plot the Casagrande's (1936) construction was used.

Table 6.7 gives the σ'_y values derived from the OED curves, the CRS curves and the isotacae (I1 to I5; see Section 6 6.5) of the natural clay (Fig.6 66). For most tests the σ'_y values resulting from the different techniques were found to be slightly different. In any case, given the effect of strain-rate on σ'_y, this increases with increasing strain rate. The values of σ'_y from tests CRS8 and OED7 are not considered, as in these tests the specimens were unloaded before compression and other factors than strain-rate dependency caused difference between their yield stresses and those of other specimens

It may be deduced from Table 6 7 that the difference between the yield stresses exhibited in the e-$\log\sigma'_v$ plot by the clay in the OED compression and in CRS compression at 3E-2%/min was about 650kPa; this difference is equal to that between the σ'_y from isotacae I_1 and I_4. Table 6.7 can be used for comparison when deducing σ'_y from other relationships, such as the u_b-σ'_v, u_b/σ_v-σ'_v, the M-σ'_v, and c_v-σ'_v plots.

The yield stress exhibited by the reconstituted clay also changed with strain rate (Fig 6.71), from 190kPa for 3E-3%/min, to 210kPa for 2.5E-2%/min. The low value of σ'_y from test OEDR, 170kPa, was however affected by disturbance induced in the clay during specimen preparation.

6 6.9 Effects of swelling before compression on the compression behaviour of the natural clay

In Fig 6 72 test CRS8 is compared with two other tests carried out at the same strain rate While these tests followed procedure 7, test CRS8 followed procedure 8, with some swelling before the CRS compression stage (Table 6 1) Similarly, in Fig 6 35 (Section 6 5 4) the compression curve of test OED7, swelled to a very low value of σ'_v, is compared with the compression curve from test OED5

In CRS8 the unloading was limited and the state path passed close above the e_0-σ'_{v0} state during recompression, and then moved towards the gross yield point, exhibiting stiffnesses lower than those of clay not subject to unloading (CRS2 and CRS11 in the figure) In test OED7 the greater degree of swelling resulted in a state path which passed below the e_0-σ'_{v0} state, and progressed towards the gross yield point exhibiting low stiffness.

Figs 6.35 and 6.72 show that in both CRS8 and OED7 unloading caused the oedometric stiffness to decrease and the yield stress σ'_y to reduce, so that close to yield the state paths of these two tests lie below those of undisturbed clay not unloaded before compression. The effects of unloading on the σ'_y values can be seen in Table 6.7, where σ'_y values from the different tests are reported. The reduction of σ'_y due to unloading in test CRS8, measured by comparison with the yield stresses in tests CRS 2 to 5 and 11, was about 200kPa The reduction of σ'_y due to the unloading in OED7, by comparison with the yield stresses of the clay in the other OED tests, was of about 700kPa The reduction of σ'_y indicates that unloading weakens the clay structure, and that this weakening is more significant the greater is the unloading.

The unloading in test CRS8 was of similar magnitude to that which can occur in routine tests in which loading starts from stresses below the clay suction. Similar unloading also occurred in test OED4, whose results are shown in Fig 6.35. It thus appears that in routine tests higher compressibilities and smaller σ'_y values can easily occur

For limited unloading, such as in CRS8, soon after yield the recompression curve converges with compression curves of tests starting from e_0-σ'_{v0} on specimens not unloaded before compression When unloading prior to yield is greater, as in test OED7, the compression of the clay beyond yield is also affected, as the compression curve appears to plot below the other curves, even up to high stresses. Unloading to low stresses thus seems to affect the e-σ'_v state of the clay not only before, but also well beyond gross yield

Unloading is applied to the clay specimens before shear in the triaxial test when investigating the SBS of clay at high YSRs Although the unloading effects are not dramatic for the Pappadai clay, they show that there is an element of the clay structure which is meta-stable and is degraded before shearing in the specimens swelled to high YSRs In Section 2 5 6 the SBS of the natural clay which has not been compressed beyond gross yield has been defined as the current SBS of the clay, and the findings presented in this section show that the current SBS of the clay is necessarily related to a disturbed structure

6.6.10. Oedometric stiffness

The oedometric stiffnesses M presented in the following were calculated using eq.(6.18). No significant difference was found between the M values resulting from either the revised theory in App 6.3 or the original Wissa theory when the slow tests were concerned, as shown in Fig 6.73(a). Where the faster tests were concerned the results of Wissa's theory were found to overestimate the values of M, as shown for test CRS1 in Fig.6.73(b). In this case, the Wissa solution gave a stiffness 21% higher than that from the revised solution, at σ'_v of 10 6MPa. Had the original Wissa solution been used, the strain-rate dependency of Pappadai clay would have been overestimated.

The M values from both the OED tests and the CRS tests on the natural clay are both plotted against σ'_v in Fig.6.74. The M values at the start of the CRS tests were quite high, but they soon dropped to about 80MPa; thereafter they were constant or slightly decreasing, then fell to a minimum value, the immediate post-yield stiffness of the clay

Overconsolidated reconstituted clays usually exhibit a maximum stiffness before M decreases at yield, as shown in Fig.6.75(a) (Davison and Atkinson 1990; Janbu and Senneset 1979). Undisturbed Pappadai clay exhibits its highest pre-yield stiffness at the start of compression in both CRS and OED tests. These high stiffnesses (Fig 6.74) are less than the very high stiffnesses M_0 recorded in the CRS tests when loading started, that is at values of σ'_v lower than σ'_{vi} in Table 6.6. As discussed in Section 6.6.1, these very high stiffnesses have been considered to reflect the sudden strain-rate increase at the start of CRS loading and are not reported in Fig 6.74.

The high stiffnesses at the beginning of the plot in Fig.6.74 represent the current response of the clay structure to compression at constant strain rate. Clay recompressed after swelling in tests OED7 and CRS8 did not exhibit these initial high stiffnesses and the M-σ'_v plots for these two tests match typical plots for OC reconstituted clays, as in Fig 6.75. Evidently that part of the undisturbed clay structure which gives rise to high stiffness at the start of compression is weakened during swelling.

The OED and CRS test results show that before yield M increases with strain rate (Fig 6 74) Immediately beyond yield the M-σ'_v curves join a unique relation defining the increase of the clay stiffness with σ'_v at YSR equal to 1. This curve is a straight line when logarithmic axes are used, as shown in Fig 6 76(a) The test reported in the figure is test CRS8 which joins the rest of the

compression curves shortly beyond gross yield, and reaches the highest value of σ'_v. The stiffness of the natural clay beyond yield (M_{NC}) is then expressed by the equation :

$$M_{NC} = 0.187\ \sigma'^{1.432}_v \qquad (6.25)$$

The M values from tests on the reconstituted clay, shown in Fig 6 77 for tests CRSR2, R4 and OEDR, follow a trend similar to that in Fig.6.75(a). The strain-rate effects on stiffness observed for the natural clay are similar for the reconstituted clay. As with the natural clay, beyond yield the stiffnesses from the different tests on reconstituted clay all plot close to a unique curve, which again is a straight line when logarithmic axes are used, Fig.6.76(b). The equation for M_{NC} of the reconstituted clay is :

$$M_{NC} = 3\ 286\ \sigma'^{1.183}_v \qquad (6.26)$$

Thus in general, whatever the type of structure present in the clay, M_{NC} of the clay increases exponentially with vertical stress

In Figs.6 78 and 6.79 the stiffnesses recorded for the natural and the reconstituted clay are compared. Fig.6.79 shows that for a given voids ratio the stiffness of both the natural and the reconstituted clay increases with increasing strain rate, both before and beyond yield, although this increase is quite small. The increase of stiffness with strain rate in the M-e plot again shows that the isotacae of the clay diverge with compression, and that the strain-rate dependency of the clay increases.

The difference in stiffness arising from the differences in structure between the natural and the reconstituted clay are apparent in Figs.6.78 and 6.79. The clay disturbed by the swelling before compression in both tests CRS8 and OED7 is still stiffer than the reconstituted clay before yield (Figs 6 74 and 6.78). This finding is the first of many, discussed in the following sections, which demonstrate that part of the structural elements giving rise to the high current strength and stiffness of the natural clay are stable, and contribute to the clay strength even after disturbance and yield. Tests OED7 and CRS8 not only have yield states to the right of the ICL, but also have stiffnesses higher than the corresponding values of the reconstituted clay

Although beyond yield the structure of the natural clay is still stronger than that of the reconstituted clay, as its state e-σ'_v plots to the right of the ICL, at yield its st ffness falls and ev ntua v coincides with the stiffness of the reconst tuted clav at the same v ds rati as shown

in Fig.6.79. For a given strain rate the M_{NC}-e curve of the natural clay seems to coincide with the corresponding curve of the reconstituted clay. The M_{NC}-e relationships thus appear to be unique. This relationship is given by the equation :

$$M_{NC}\, e^{4.322} = 4000 \qquad (6.27).$$

Fig.6.80 shows the stiffnesses of the clay during two CRS tests, and during primary consolidation in tests OED 5 and 6 (see Section 6.5.7; Fig.6.42). While the differences in stiffness for compression at different constant strain rates have been shown to be quite small (Figs 6.74 and 6.79), Fig 6.80 shows that the changes of stiffness due to the strain rate changes are much more significant.

The clay stiffness is related within an overall framework in e-σ'_v-$d\varepsilon_v/dt$-$d^2\varepsilon_v/dt^2$ space, as confirmed by the results of the tests CRS6 and CRSR3 in Figs.6 81 and 6.82. The changes in M recorded for similar strain-rate changes in the two tests, on natural and reconstituted clay respectively, are equivalent. This finding gives further support to the similarity of the strain rate dependency of the natural and of the reconstituted clay. Moreover confirms that at the start of CRS loading, because of the sudden increase of strain rate, very high stiffness should be expected.

6.6.11. Compression indexes

The values of the compression index recorded during both the CRS and the OED tests on the natural and reconstituted clay are plotted against σ'_v and against voids ratio in Fig.6.83. The trends for the two clays are similar, showing that C_c increases over a small stress range which includes σ'_y. Thereafter C_c is first constant, and then decreases.

Beyond yield, the compression curves of both the natural and the reconstituted clay are linear on the logarithmic scale only in a limited range of stress, though this is the range of engineering interest.

For reconstituted Pappadai clay the average maximum compression index C_c^* is about 0 47, occurring from just beyond σ'_y to about 3 $3\sigma'_y$. For the natural clay, the average C_{cmax} is about

0.54-0.57 from 1.5 σ'_y to about 2.2σ'_y. Beyond yield the compression index of the natural clay is higher than that of the reconstituted clay at all values of σ'_v and voids ratio.

6.6.12. Coefficient of consolidation

The coefficients of consolidation c_v plotted in Fig.6.84 were calculated using eq.(6.20) of the revised Wissa theory and for the fast tests were corrected using the coefficient α_c (Section 6.6.4). The c_v values for the fast tests using the original Wissa theory were found to be higher than those from the revised theory (Appendix 6.3), as previously observed for the M values

The c_v values from both the CRS and the OED tests on the natural clay are plotted in Fig 6.85. The initial c_v values measured in the CRS tests were very high, partly because of the high clay stiffnesses at the start of compression, and partly because of the delay of the u_b measuring system in responding to the compression, as discussed in Section 6 6.3 However, the c_v values from the CRS tests rapidly drop to values which are entirely consistent with those measured in the OED tests (Fig.6 85).

For the reconstituted clay the c_v values rise to a maximum and only then drop to a minimum around yield (Fig.6.84), as is usually observed for overconsolidated clays (Davison and Atkinson 1990; Fig.6.75(b)).

c_v appears to be as strain-rate dependent as M (Fig.6.85). The c_v values resulting from the fastest tests, CRS 7 and 9, probably overestimate the true c_v of the clay for the corresponding strain rates, especially at high stresses, due to errors in the u_b measurements. However the relative position of the c_v values from the CRS tests, the c_v values calculated for the OED tests according to Terzaghi's theory, and the c_v values calculated by means of the revised Wissa theory for tests OED5 and 6, all show that c_v increases with strain rate (Fig 6 85).

Just beyond yield the c_v value of the natural clay is already very low, and it reduces further only slightly with increasing σ_v. The c_v of the reconstituted clay is always higher than that of the natural clay Compression beyond yield causes a decrease in c_v for the reconstituted clay that brings the c_v value down to those of the natural clay at very high stresses (Fig 6 84) Thus beyond yield, the structure of both natural and reconstituted clay at the same voids ratio exhibit equal stiffnesses, though they exhibit different strengths, different coefficients of consolidation

and, necessarily, different coefficients of permeability. The two structures are therefore still very different and are modified in different ways with post-yield compression.

6.6.13. Coefficient of permeability

In Fig.6.86 the values of the coefficient of permeability from both CRS and OED tests on the natural clay are plotted in logarithmic scale against voids ratio. Despite the logarithmic scale the k values from the CRS tests are very similar and define a narrow band.

The fall in k at the start of the CRS tests is probably related to the delay of the u_b measuring system in responding to compression. This is confirmed by the fact that in the tests using a back pressure, such as tests CRS11 and CRSR1 and R2 (Figs 6 86 and 6.87), the drop in k at the start of the compression was smaller, while in the fast tests, such as CRS7 and 9, the effects of the initial poor saturation of the system affected a larger part of the test At low voids ratios, only results of test CRS7 plot outside the general range and above the others, showing that u_b measured in this test at high σ'_v was rather low.

The coefficient of permeability appears not to be strain-rate dependent. Not only do the individual test data in Fig 6.86 show no relationship to the test strain rate, but moreover the OED test results plot both above and below the CRS test results. The logk-e plots resulting from the application of the revised Wissa theory (App.6.3) to the primary consolidation data of tests OED5 and 6 fall inside the band of k lines from the CRS tests.

Lowe et al. (1969), on the basis of the results from constant gradient oedometer tests (Fig.6.23), concluded that k seems not to be strain-rate dependant. Note also that the results shown here of the many different testing techniques and processing procedures used in the present research are mutually consistent, giving good support to the validity of the techniques and procedures, and to the validity of the findings so far presented.

The permeability of the natural clay before compression is about 2.5E-11m/s Fig 6 86 shows that from the average yield voids ratio of the clay, which is about 0 81, to the minimum voids ratio reached in the tests, about 0 35, during which the clay fabric is being compacted, the coefficient of permeability of the natural clay reduces according to the law:

$$k_{NC} = 10^{(-1\ 9 \cdot\ 3e} \qquad (6\ 28)$$

a straight line in the logk-e plot. As with the post-yield stiffness discussed in Section 6 6.10, the suffix NC is used here to indicate that the permeability beyond yield is being considered. All the data plot very close to this straight line. The coefficient of permeability of the clay at a voids ratio of 0.35 is about 5E-13m/s.

The logarithm of the coefficient of permeability of the reconstituted clay reduces beyond yield with voids ratio, following a smooth curve, as shown in Fig.6 87, although the k values measured in the CRS and OED tests on the reconstituted clay are not so consistent with each other as are the values measured for the undisturbed clay.

The linearity of the relationship between the logarithm of permeability and voids ratio has been commented on in the literature (Lambe and Whitman 1969) on the basis of in situ tests The laws governing the variation of the coefficient of permeability during the compression of clays have apparently never been examined in the literature, although the results of the present study show that these can be well defined by oedometer testing Of course the logk-e relationship is not necessarily a straight line, as for the reconstituted clay this relationship is not linear overall. Though the relationship is exactly linear for the natural clay Whether this is a general result for stiff clays, or peculiar to Pappadai clay, is not known.

In any case, k reduces with voids ratio, following a more or less exponential law only beyond yield. For both the natural and the reconstituted clay the data in Fig.6 87 show that at voids ratio prior to yield (above 1.2 for the reconstituted clay and above 0.8 for the natural clay), the measured coefficients of permeability were constant with e and σ'_v. This is shown in Fig.6.88 for some natural clay specimens; also the data from tests OED7, CRSR1, R2 and OEDR show that permeability is constant before yield. The constancy of k with changing e seems than to be a law generally applicable to overconsolidated clays

The variation of k with voids ratio is summarized in Fig 6 89 The clay is characterized by a constant coefficient of permeability at YSRs above 1, decreasing almost exponent ally with e at YSR of 1 The permeability of the reconstituted clay is h gher than that of the natural stiff clay at any voids ratio, the differences between the two permeability curves highlighting the differences between the structures of the two clays

The natural structure has a low permeab l ty not only because of its particle arrangements but also because of the chem cal condit ns characterizing the clay at the micro-level, part cularl the

existence of a calcite film which coats the particles at the inter-particle contacts, and fills some of the pores. Only high levels of compaction bring the reconstituted clay to the same values of permeability as the natural clay.

6.6.14. Swelling behaviour pre- and post-yield

The swelling lines plotted in Fig.6.90 were measured by unloading the specimens in steps in both OED and CRS tests. The states of the clay at the end of all the unloading steps are kinematically equivalent because the duration of unloading was always chosen to reach final strain rates of about 1E-4 - 1E-5 %/min.

The critical state framework of clay behaviour considers the swelling lines in the e-logσ'_v plane to be parallel, i.e. the swelling index C_s is independent of σ'_y. The swelling lines of the reconstituted Pappadai clay are close to linear, but they are not parallel. The values of C_s calculated for each unloading step are plotted in Fig 6.91.

Average values of C_s were calculated considering that part of the swelling line within 1 5 logarithmic cycles of the maximum pressure reached. For the reconstituted clay the average value of C_{s_n} calculated as above, on the swelling line at intermediate voids ratios (test OEDR), C_s^*, is about 0.072 (Fig.6.91) while the average swelling index measured on the swelling line after compression to high pressures (test CRSR1) is about 0.092. Thus the swelling index of the reconstituted clay is found to increase with decreasing voids ratio. However, within an engineering range of interest, with limited range of voids ratio, the swelling lines of the reconstituted clay may, with good approximation, be considered parallel. On the other hand the increase of C_s^* cannot be neglected when comparing the swelling behaviours of the natural and of the reconstituted clay. Such comparison is correct if the C_s values are measured in similar ranges of voids ratio.

The pre-yield swelling line of the natural clay (test OED7) is the most nearly linear, Figs 6 90 and 6.91, giving a swelling index of the natural clay in its current state of 0 038 The corresponding ratio C_s^*/C_{s_n} defined as swell sensitivity by Schmertman (1969), is equal to 2, higher if the swelling lines are compared at small stresses

Beyond yield the swelling index of the natural clay increases (Figs 6 90 and 6 91) The average values of C_s after loading to 3000kPa and 5000kPa are only slightly different and both are close

to C_s^*, i.e. 0.072 (Fig.6.91). Thus yield decreases the swell sensitivity C_s^*/C_s from above 2 to about 1 at voids ratios below 0.65.

Thus the bonding of the clay restrains swelling, and the swell sensitivity C_s^*/C_s may be an indicator of inter-particle bonding as proposed by Burland (1990). With the definition of bonding given in the first chapter (Section 1.5), the swell sensitivity is an indicator of the difference in strength between the bonding of the reconstituted and the natural clay. For the Pappadai clay, the increase of the swell sensitivity at yield suggests that a large part of the current bond strength of the natural clay is lost at yield. The degradation of the bonding progresses further with compression up to σ'_v of 5000kPa.

According to this interpretation, the natural and the reconstituted clay have similar bond strength at stresses above 5000kPa. In the writer's opinion these conclusions are likely to be only partly correct, because it is difficult, perhaps impossible, to discern the micro-structural features which control aspects of the clay's response from an analysis at the macro-level.

Post-yield the natural clay continues to exhibit higher strength than when reconstituted, as σ'_y for the natural clay is always higher than that of the reconstituted clay (Fig 6.90). The two clays probably have different fabrics and bonding which exist well beyond yield, and thus undergo different structural changes with compression. Both the increase of the swelling index of the natural clay and the decrease of its stiffness at yield simply suggest that there are meta-stable features of the natural structure which affect its stiffness and swelling capacity. These are weakened by unloading before yielding, and are certainly degraded by yield, since beyond yield the swelling and stiffness of the natural clay are similar to those of the reconstituted clay.

6 6.15. State of the natural and reconstituted clay at high stresses

The compression state path of the natural Pappadai clay lies to the right of that of the reconstituted clay up to very high values of σ'_v. The similarity of the M values for the two clays at equal voids ratios suggests that the state paths of the two clays converge only at very high stiffnesses, theoretically infinite In reality, the CRS compression curves of the two clays seem to converge, but not before σ'_v of about 40MPa, thirteen times the value of the yield stress of the natural clay.

Although part of the structure of the natural clay is meta-stable and degrades at yield, on the whole it exhibits quite stable behaviour and its higher strength with respect to the reconstituted clay is preserved, though is continually modified post-yield.

6.7. Framework for the oedometric compression behaviour of clays

Sections 6.5 and 6.6 outlined the response to oedometric loading of two clays with different structure. In this section these responses are discussed within a general framework of the behaviour of clays, in the light of the definitions and proposals given in Chapter 2.

6.7.1. Relationship between the geological history, the structure of the clay and its present state in the I_v-σ'_v plane

Natural Pappadai clay has been shown to be a stiff clay originally sedimented and normally compressed in situ as an uncemented clay of medium-low sensitivity (sedimentation sensitivity, see Table 1.1). At a time when it was subjected to relatively high stresses, either towards the end of virgin compression or once it was complete, the clay underwent ageing and diagenesis. The clay then had a post-sedimentation structure characterized by a higher strength due to the structural changes which had occurred under high stresses (Table 1 1). After virgin compression the clay was overconsolidated following unloading.

The precipitation of a calcite film, coating the clay particles and inter-particle contacts (see Section 5.10.3), was part of the long-term diagenetic processes that affected the clay strength This carbonate coating forms part of the clay bonding In the natural Pappadai clay the carbonate bonding is considered to be the result of an early stage in a cementation process, although a proper cement bonding does not exist, as seldom carbonate crystals between the particles are recognized by SEM.

In Fig 6 92 the isotacae of the natural Pappadai clay for strain rates 5E-5%/min, 3E-4%/min and 3E-3%/min (I_1, I_2, I_3), together with the state path followed by the clay unloaded prior to yield and then recompressed (OED7), have been plotted in the I_v-σ'_v plane. The figure also shows the isotaca of the reconstituted Pappadai clay for a strain rate of 3E-3%/min, and the compression of the reconstituted clay from slurry. The voids ratios used to normalize the Pappadai clay data are those recorded during compression of the reconstituted clay, they are equal to

$e_{100} = 1.27$ and $e_{1000} = 0.776$ (6.29)

These are higher than the values derived from the empirical relationships proposed by Burland (1990), which give 1.128 for e_{100} (Section 5.11) and 0.728 for e_{1000}. The compression data for the reconstituted clay are very close to the ICL of Burland (1990), which is also plotted in the figure and at high stresses lies only slightly above the measured reconstituted compression curve.

The present yield stress (σ'_y) of 2900kPa (isotaca I_3; see Table 6.7) is much higher than the vertical effective stress of 850kPa (σ^*_e) required to bring the reconstituted clay to the same voids ratio; the difference between σ'_y anf σ^*_e is a mechanical effect of the higher strength of the structure of the natural clay. The reconstruction of the state paths followed by the clay during its geological history, shown in Fig 5 59, shows that the sedimentation structure of the natural Pappadai clay was already stronger than that of the reconstituted clay Additionally, as discussed above, the clay was further strengthened diagenetically after virgin compression The strength acquired by the clay structure due to diagenesis is reflected by the difference between σ'_y and the preconsolidation pressure (σ'_p), 1310kPa, shown in Fig 6 92 This difference gives rise to a difference between the YSR (~6) and the OCR (~3.2) of the clay.

Burland et al.1996 suggest that for yield states lying between the ICL and the SCL in the I_v-σ'_v plane, the main difference between natural and reconstituted clay is due to differences in fabric, with only a limited influence of clay bonding. In contrast, the yield states to the right of the SCL are indicative of a highly sensitive material with brittle bonding The results obtained for Pappadai clay show that the type and strength of the bonding cannot be deduced solely on the basis of the location of the compression curve in the I_v-σ'_v plane. In spite of the fact that the bonding of the natural clay is far stronger than that of the reconstituted clay, natural Pappadai clay compression curve still plots to the left of the SCL (Burland 1990) Moreover, the results show that the bonding of Pappadai clay, which plots far to the right of the ICL, does not consist of a brittle cementation or other type of mechanical links between the particles

The Pappadai clay shows the level of increase of YSR that can arise from the diagenesis of the clay after burial. The compaction of the clay in s tu has been also shown to give rise to micro-chemical and micro-physical conditions which do not occur in the reconstituted clay during consolidation in the laboratory, and which result in the permeability of the natural clay being much lower than that of the reconstituted clay

6.7.2. A general Sensitivity framework for clays

In Section 2.5.4 it was demonstrated that for soft clays there exists a monotonic relationship between the ratio σ'_y/σ^*_e and the sensitivity of the clay consolidated to its yield stress S_t(YSR=1); this was defined the sedimentation sensitivity (Tables 1.1 and 2.1). This shows that for soft clays, irrespective of the structure present in the clay, the sedimentation sensitivity governs the location of the yield state in the I_v-σ'_v plane. Thus, all soft clays having the same SCC have the same sensitivity and therefore similar current state boundary surfaces and similar current behaviour (Section 2.5.6). Fig.2.23 summarizes this relationship between σ'_y/σ^*_e and the sensitivity S_t(YSR=1) of soft clays.

Compression data from the literature for both soft and stiff clays are reported in Fig.6.92, where they are compared with the behaviour of the Pappadai clay. The differences between the I_v-σ'_v state paths of the clays in the figure arise from their different structures. The values of both the ratio σ'_y/σ^*_e and the sensitivity at a YSR of 1 for these clays were extrapolated from the data reported in the literature, and are listed in Table 6 8

The value of S_t(YSR=1) in Table 6.8 for Pappadai clay was measured in the triaxial test programme discussed in Chapter 8. The values of the two ratios σ'_y/σ^*_e and p'_y/p^*_y are measured in oedometric and in isotropic compression respectively, p^*_y being the mean pressure on the isotropic compression line of the reconstituted corresponding to the volume at gross isotropic yield. These two ratios have about the same value for Pappadai clay. For Vallericca clay, Rampello et al.(1993) reported the isotropic compression curves of natural and reconstituted specimens, while Burland et al.(1996) reported the oedometric compression curves. The value of S_t(YSR=1) deduced from the data reported by Rampello et al. and that from the data reported by Burland et al. are different, although they are equal to the corresponding values of σ'_y/σ^*_e and p'_y/p^*_y. The same applies to Todi clay, for which values of the ratio σ'_y/σ^*_e and St(YSR=1) were deduced from both the data reported by Burland (1990) and Burland et al.(1996). It is not known why these discrepancies occur. The test data appear to be the same, but perhaps have been interpreted slightly differently by the various authors For London clay at Ashford Common (Webb 1965), the yield stress was not actually reported and the value used in Table 6.8 was deduced by F.Cotecchia (1990) and is probably lower than the actual value for this clay

The data in Table 6.8 and in Fig.6.92 seem to show that a monotonic relationship exists for these stiff clays between S_t(YSR=1) and σ'_y/σ^*_e,of the same type as that identified for soft clays in

Section 2.5.4 (Fig.2.23). From the soft sensitive Bothkennar clay, to stiff clays such as those illustrated in the table, the values of σ'_y/σ^*_e increase with increasing S_t(YSR=1), even though the clays have very different structures, origins and geological histories. The relationship between S_t(YSR=1) and σ'_y/σ^*_e seems to be unique and close to equality.

For the clays of categories 1 to 4 in Table 2.1 the ratio σ'_y/σ^*_e equals the ratio σ'_p/σ^*_e and the sensitivity S_t(YSR=1) is a sedimentation sensitivity (Fig.2 23). This is not the case for the stiff clays of categories 5 to 7, such as the Pappadai clay (category 7). For these clays the sensitivity S_t(YSR=1) appropriate for the general sensitivity framework outlined here is a post-sedimentation sensitivity.

Although the relationship between S_t(YSR=1) and σ'_y/σ^*_e identified here cannot be defined conclusively because of the lack of data relating to stiff clays, it is nonetheless regarded as the basis for the construction of a general framework of behaviour of natural clays. The St(YSR=1)-σ'_y/σ^*_e relationship applies to clays of any structure, and shows that there is an underlying equivalence of behaviour between clays of different structure but either equal sensitivity S_t(YSR=1), or equal σ'_y/σ^*_e. Clays of different structure, but having equal ratios σ'_y/σ^*_e, will be expected to have similar sensitivity S_t(YSR=1) and the size of their current SBS (see Section 2.5.6) will be expected to be similar, accordingly. The relationship between S_t(YSR=1) and σ'_y/σ^*_e would then be a powerful tool for modelling clay behaviour.

Fig 6.92 and Table 6.8 show that the S_t(YSR=1)-σ'_y/σ^*_e relationship holds, no matter whether the clay yields on the SCC, as for soft clays (see Table 2.1), or if it yields to the right of its original SCC, as for the Pappadai clay, and also for Boom clay and in general for clays of categories 5 to 7 (Table 2.1) Boom clay presently has a YSR of 2.3, which is higher than its OCR of about 1 (see Chapter 2; Horseman et al.1987, Coop et al 1995), and it is the current yield stress of the clay which is the parameter indicative of its behaviour. Thus it is confirmed that for stiff clays of type 5, 6 and 7 in Table 2.1 the location of their original SCC in the I_v-σ'_v plane is not relevant to their behaviour, as proposed in Section 2 5.3. Only the current σ'_y of the clay is of importance for the clay behaviour and for the response of the clay's post-sedimentation structure Unfortunately for the other stiff clays in Fig 6 92 and Table 6 8 which are all geologically overconsolidated, the available data are not sufficient to establish in which of the two categories, 4 or 7 in Table 2 1, they lie

The S_t(YSR=1)-σ'_y/σ^*_e relationship can probably be represented in the I_v-logσ'_v plane as a series of parallel lines which are loci of the yield points of clays of equal sensitivity S_t(YSR=1), as in the equivalent plot for soft clays in Fig.2.23. In the latter figure, the S_t lines are coincident with the SCCs of the clays. However confirmation of this framework will only be possible with further experimental data on the behaviour of stiff clays.

6.7.3. Sensitivity and structural stability of natural stiff clays

All the stiff clays in Fig 6.92 have a medium-low sensitivity. High sensitivities seem to apply only to soft clays which have undergone little fabric compaction (Table 2.1). The low sensitivity of stiff clays may be partly due to the fact that, if clays cemented during deposition and virgin compression are excluded, natural stiff clays tend to have low voids ratios (Fig 6.92), so that the strength of reconstituted clay subjected to the corresponding equivalent pressures is quite high. A clay having a strong bonding, such as the Pappadai clay, will thus be less sensitive than a clay having an open flocculated fabric and weaker bonding and plotting on or above the SCL, such as the Bothkennar clay (Fig.6.92).

6.7.4. The basic mechanics of natural and reconstituted clays pre- and post-yield

This section outlines the extent to which the basic mechanics of natural sensitive clays, compares with the mechanics of reconstituted clays pre- and post-yield. Further comparison of the behaviour of the natural and reconstituted clay, particularly normalization of the shearing behaviour, is discussed in Chapter 8.

In Section 6.6.7 it has been shown that a stiff clay such as Pappadai clay, whose oedometric compression line lies far to the right of the ICL in the I_v-σ'_v plane, can be as strain-rate dependent as the reconstituted clay. The changes in strain-rate have similar effects on the compression paths of the two clays Accordingly, the oedometric stiffnesses are similarly affected by the strain-rate variations, while the permeability of both clays is not strain-rate dependent The magnitude of the strain-rate effects changes when both the clays are at gross yield, this change is similar for the two clays

Data in the literature demonstrate that the oedometric behaviour of soft clays also is strain-rate dependent. It follows that, although the bonding and the fabric of clays may be different, a similar structural viscosity affects their stress-strain response.

In Sections 2.5.6 to 2 5.8 it was recognized that a "basically frictional" deformation mechanism seems to govern the stress-strain response of many natural clays as for the reconstituted clays.

Thus the basic features of the mechanics of clays, such as the influence of structural viscosity on the clay response, and the development of a frictional-like behaviour, seem to apply similarly to natural and reconstituted clays, irrespective of their difference in structure. These features of clay mechanics are unifying factors in a general framework of behaviour of clays.

Similarities were also found between the variations with σ'_v of the oedometric stiffness, the coefficient of consolidation and the coefficient of permeability of the natural and the reconstituted clay (see Sections 6.5 and 6 6) For both clays, critical changes in the relationships M-σ'_v, c_v-σ'_v, k-e occur at gross yield.

For both the natural and the reconstituted clay the oedometric stiffness M drops to a minimum value soon after yield and then increases linearly with σ'_v in the logarithmic plot (Fig 6.76), while the compression index C_c rises up to a maximum value and then remains constant up to a vertical stress of about 3 times σ'_y. For both the clays C_c decreases and C_s increases with increasing σ'_v beyond yield.

The M-e plot (Fig 6.79) shows that beyond yield the natural and reconstituted clay subjected to the same strain rate exhibit equal stiffness for the same voids ratio. The exponential relationship M_{NC}-e (eq 6.27) shown in Fig 6.93 applies to the behaviour of any specimen of Pappadai clay beyond yield, that is to the undisturbed specimens, to the specimens swelled before compression, and to the reconstituted specimens. In contrast the coefficients of permeability of the natural and of the reconstituted Pappadai clay at the same voids ratio differ both pre- and post- yield (Fig 6 87), although the relationships k-e are similar for the two clays (Fig 6 89)

Despite their equal oedometric stiffnesses and swelling indexes, the structures of the natural and reconstituted clay remain different up to high stresses beyond yield, as shown by the differe ces between their permeabilities and their yield stresses The data show that the state path of the natural clay plots to the right of the ICL, at least up to vertical stresses of ab ut 13 times the

yield stress σ'_y. The structure of the stiff clay thus remains stronger than that of the reconstituted clay well beyond yield.

The present research results also show that differences exist between the behaviour of natural sensitive clays and reconstituted clays, which arise from the different stability of their structures. The non-sensitive clays, such as reconstituted clays, are formed of stable components whose effects on the clay behaviour are permanent. In contrast the structure of sensitive clays has some meta-stable features which are lost with straining, and thus give rise to effects on the clay behaviour only before yield. Consequently, the sensitive clay exhibits changes in behaviour related to the degradation of these elements of structure which are not shown by the reconstituted clay.

Meta-stable features of the Pappadai clay degrade on unloading, so that both the stiffness M and the yield stress σ'_y of clay compressed after swelling are lower than those of the undisturbed clay. Gross yielding also causes a strong degradation of the meta-stable features of the Pappadai clay structure. Meta-stable features of the Pappadai clay bonding are degraded as demonstrated by the increase of the clay swelling index C_s with compression beyond σ'_y; the swelling index of the reconstituted clay C_s^* is instead not affected by the yielding process. The loss of meta-stable structural features with compression of the sensitive clays beyond yield is also generally shown by the reduction of the ratio σ'_y/σ^*_c, which in turns is related to the clay sensitivity, S_t(YSR=1) (see Section 6.7.2). Thus the difference in strength between the natural sensitive clay and the reconstituted clay progressively decreases beyond yield, though this difference may not become zero even at very high stresses.

Generally the degradation of the meta-stable features of the clay structure gives rise to more significant effects on the behaviour of natural soft clays than on that of stiff clays. The reduction in stiffness and sensitivity observed at yield for soft clays (see Sections 2 5.5 and 2.5 6) is in general more significant than for the stiff clays shown in Fig 6.92. This is consistent with the fact that stiff clays have lower sensitivities than soft clays.

It has been proposed by some authors (Rampello et al 1993; Coop et al 1995) that the difference in strength between a natural and a reconstituted clay is due to differences either in the clay fabric or in the clay bonding The writer considers that these proposals are incorrect since a given fabric can exist at a given pressure and specific volume only because an appropriate bonding exists in the clay Fabric and bonding cannot then be seen as distinguishing causes of clay behaviour Despite their different fabrics and bonding, natural and reconstituted clays have been shown to

follow a similar framework of behaviour, apart from those aspects of behaviour which result from the degradation of some meta-stable structural elements present in the sensitive clays. The structural elements in a sensitive clay which degrade with loading cannot be deduced from a study of the clay at the macro-level. This will be demonstrated in Chapter 7.

6.7 5. Normalization of the oedometric stiffness of Pappadai clay

The behaviour of reconstituted clays can be normalized with respect to volume, as discussed in Chapter 2. So it might be expected that the relationship between the oedometric stiffness and the yield stress ratio of the clay M-YSR can normalized similarly. In this section, normalization of the M-YSR relationship with respect to volume is shown to apply to the reconstituted Pappadai clay, but not to the natural clay, for which the introduction of an additional normalizing factor is necessary.

In Section 6 6.10 the M-σ'_v relationships from first loading of both natural and reconstituted clay specimens were discussed For both undisturbed and reconstituted specimens the clay states e_0-σ'_{v0} at the start of loading were all similar, except for the specimens of natural clay which had swelled before loading. The specimens were all initially at a YSR above 1 and were brought to YSR of 1 by compression beyond yield Thereafter they followed a compression curve e-σ'_v which may be defined as the oedometric normal compression line (NCL_{oed}) of the clay.

The NCL_{oed} curves of the undisturbed and reconstituted Pappadai clay are unique if the strain-rate dependency of the clay is neglected, as shown in Fig 6 94(a) The natural clay specimen which swelled before loading (OED7) was found not to reach the NCL_{oed} of the undisturbed clay as the clay structure had been disturbed by swelling (Figs. 6 35 and 6 94(c)).

Eqs 6 25 and 6.26 are the relationships between the oedometric stiffness of the clay on the NCL_{oed} line (M_{NC}) and the vertical effective stress (Fig 6 94(b)) for the natural and the reconstituted clay respectively

To examine the behaviour during unloading and reloading from different preconsol dation stresses two extra tests were carried out, test OEDRb on reconstituted clay and test OED10 on undisturbed clay In these tests the clay was loaded beyond yie d and then subjected to two further unloading-reloading cycles, a shown in Fig 6 95 Test OED10 shows that during recompress n after unloading from di erent p eco so da n stresses the state of the natural c ay j ins the

NCL_{oed} curve in the e-σ'v plane and the clay stiffness beyond yield M_{NC} plots on a unique curve in the M_{NC}-σ '$_v$ plane, as for reconstituted clay and for the idealized behaviour shown in Fig.6.94 (a) and (b).

The pre-yield change in stiffness with YSR, i.e. the M-YSR relationship, is uniquely related to a preconsolidation state e_y-σ'$_y$ on the NCL_{oed}. If the M-YSR relationships for compression related to different preconsolidation states have similar shapes, the M-YSR relationships can be considered the same, apart from a normalizing factor which depends on the state e_y-σ'$_y$ and on volume.

In order to normalize the relationship M-YSR for reconstituted Pappadai clay with respect to volume, the relationship M_{NC}-σ'$_v$ (eq.6.26) was used (Fig.6 76(b)) The oedometric stiffnesses in pre-yield states were normalized with respect to the value of oedometric stiffness M_{NC} that the soil will reach at its yield point e_y-σ'$_y$ (eq.6.26), so that the normalized stiffness of the clay when its state is on the NCL_{oed} line is unity.

The normalized stiffnesses were then plotted against the logarithm of the yield-stress ratio, YSR. For test OEDRb, both the first loading stiffnesses and the reloading stiffnesses for the two unloading-reloading cycles were normalized following the calculations above. The stiffnesses for the first loadings of the different tests, which are related to different strain-rates, when normalized with respect to M_{NC} were found to exhibit some scatter This finding suggested that strain-rate affects the M-YSR relationship. The stiffnesses were then normalized by an equivalent stiffness M_{NCeq}, which is the value of M_{NC} that corresponds to the yield void ratio (e_y) for the test being normalized, but on the NCL_{oed} line from a reference test, test CRSR2. The calculation of M_{NCeq} is shown in Fig.6.94(c). The stiffness of the reconstituted clay specimens normalized as above are shown in Fig.6.96. The data points from the first loading in both tests OEDRb and OED10 are indicated as 1 in the figures, while the data points from the reloading stages of the two tests are indicated as 2 and 3 (Figs.6.96, 6.97 and 6.98). In Fig 6.96 the M/M_{NCeq}-YSR data points for both the first loadings at different strain-rates of the reconstituted clay and the reloadings of test OEDRb lie close to one another. This suggests that the factor M_{NCeq} normalizes the M-YSR relationship both with respect to volume and with respect to the strain-rate Ideally, the normalization with respect to volume of stiffnesses from different loading stages would be better investigated using tests at a single strain-rate, and then M_{NC} could be used as a normalizing factor instead of M_{NCeq}. Fig 6.96 confirms that the behaviour of the reconstituted clay can be normalized with respect to volume.

Fig.6.97 shows the same normalization for natural samples. The equivalent values of σ'_y and M_{NC} for the different loadings are reported in Table 6.9, the reference NCL_{OED} line being the one from test CRS2. The data demonstrate the effect of changes in structure on the normalized stiffnesses. Both the first and second reloading stages of test OED10 lie significantly lower than the first loading stages of both test OED10 and of the other tests, as a result of the changes in structure following the first-yield of the clay. The fact that the first-loading stiffness of the natural soil does not agree with that for loading stages when the structure has been changed by loading beyond yield indicates that, in contrast to the reconstituted soil, it is not sufficient for the natural soil behaviour to be normalized simply with respect to volume, but it is necessary to normalize it also for changes in structure.

The data from test OED7 are for first-loading of the clay after swelling In this case swelling gave rise to the loss of metastable structural features, so causing the state path to lie to the left of those followed by other specimens If the stiffnesses from test OED7 are normalized by the equivalent stiffness M_{NCeq} (Fig 6.94(c)) the test data are divided by the value of stiffness that the clay should have exhibited soon after gross yield had the clay not been swelled before loading. The normalization used highlights the effects of the structural change occurred during swelling on the subsequent clay behaviour, as in Fig 6 97 the OED7 values of normalized stiffness lie close to the normalized stiffnesses of the reloading cycles of test OED10.

The M/M_{NCeq}-YSR relationships depend on the structural differences between the clay specimens. To normalize the stiffnesses for the changes in structure, the M/M_{NCeq} data were divided by the ratio σ'_y/σ^*_e, assuming that it is this ratio which expresses the effects of structure, as shown by the sensitivity framework discussed in Section 6.7.2.

The normalized data $(M/M_{NCeq})/(\sigma'_y/\sigma^*_e)$ are plotted in Fig 6.98 against YSR. All the data plot close to a unique curve, thus showing that this normalization successfully accounts both for the effects of volume and structure on the behaviour of the natural clay. It may be concluded that the M-YSR relationship for natural clays can be normalized if the effects of the structural changes with loading are allowed for normalized by means of the ratio σ'_y/σ^*_e

Test	Sample	Design cell	Filter paper	Average duration of the loading step (min) / $\Delta H/H_0$ (%/min)	w (%)	e	S_r (%)	e_0	σ'_{vo} End of the equilibration stage (kPa)	Loading Path	σ'_{vmax} (kPa)	Stress before unloading (kPa)
OED 1	P	D1	f.p.	1440	31,17	0,863	99		Sw P (Pr 1)	L	4981	
OED 2	1T	D1	f.p.	1440	30,19	0,844	98		Sw P (Pr 2)	L	7471	
OED 3	1T	D1	f.p.	1440	30,28	0,842	99		Sw P (Pr 1)	L & U	6232	6232
OED 4	P	D2	f.p.	1440	31,17	0,877	98		539 (Pr 3)	L & U	2156	2156
OED 5	P	D3	no	1440	32,18	0,882	100		1372 (Pr 4)	L & U	4998	4998
OED 6	P	D3	no	4000	31,69	0,876	99		1372 (Pr 4)	L	4998	
OED 7	P	D1	no	$\dot{\varepsilon}_f \sim \pm 3*10^{-5}$	32	0,887	99		1176 (Pr 5)	L & U & L	4900	1176
OED 8	P	D1	no	4000	31,3	0,866	99,3		882 (Pr 5)	L & U	2940	2940
OED 9	P	D1	no	> 4000	31,3	0,87	98,8		882 (Pr 5)	L	2940	
OEDR	R	D1	f.p.	4000	44,7	1,254	98		43 (Pr 6)	L & U	1995	1995
CRS 1	P	D2	f.p.	*0,028*	31,12	0,86	99	0,865	793 (Pr 7)	L	18000	
CRS 2	P	D2	f.p	*0,0053*	31	0,86	99	0,86	666 (Pr 7)	L	22000	
CRS 3	P	D2	f.p	*0,0037*	31,22	0,87	98,5	0,868	696 (Pr 7)	L	19000	
CRS 4	P	D2	f.p	*0,0025*	31,8	0,876	99,6	0,88	662 (Pr 7)	L & U	24800	23000
CRS 5	6B	D2	c f.p.	*0,0053*	30,9	0,86	99	0,856	642 (Pr 7)	L & U	29500	27500
CRS 6	1M	D2	c.f.p.	changing $\dot{\varepsilon}_v$	31,7	0,878	99	0,87	687 (Pr 7)	L	30000	
CRS 7	5B	D2	c.f.p.	*0,128*	30,16	0,8407	98,5	0,8407	685 (Pr 7)	L	20660	
CRS 8	5B	D2	c.f.p.	*0,0053*	30,81	0,854	99	0,856	254 (Pr 7B)	L	25700	
CRS 9	5B	D2	c f.p.	*0,068*	30,54	0,847	99	0,84	718 (Pr 7)	L	18800	
CRS 10	P	D3*	no	*0,025*	31,17	0,863	99	0,863	500 (Pr 8)	L	15200	
CRS 11	3B	D3	no	*0,0025*	31,18	0,864	99	0,863	500 (Pr 8)	L	20600	
CRS R1	R	D3	no	*0,005*	45,07	1,255	98,5	1,255	25 (Pr 9)	L & U	16300	15500
CRS R2	R	D3	no	*0,0025*	45,8	1,278	98,4	1,278	20 (Pr 9)	L	22000	
CRS R3	R	D3	no	changing $\dot{\varepsilon}_v$	44,95	1,288	96	1,285	18 (Pr 9)	L	19900	
CRS R4	R	D3*	no	*0,024*	45,15	1,283	96,5	1,283	39 (Pr 9)	L	15390	

P - prism, R - reconstituted, D - design, f.p. - filter paper, c.f.p. - cycled filter paper, $\dot{\varepsilon}_f$ - final strain rate (%/min), Pr - test procedure (see Section 6.3 1), Sw P - swelling pressure, L - loading, U - unloading

Table 6.1. Oedometer tests on Pappadai clay.

Oedometer Cell	Diameter D mm	Height H mm	D/H	Area sqcm	σ'_v (kPa) for 1N
D1 & D2	50	19	2.63	19.63	0.51
D3 & D3*	56	20	2.80	24.63	0.41

Table 6.2. Dimensions of the oedometer specimens.

Type of test	A/D convertor	TRANSDUCERS' SENSITIVITY				ELECTRICAL NOISE			
		Vertical Displac.	Pore Pressure	Load Cell	Cell Pressure	Vertical Displac.	Pore Pressure	Load Cell	Cell Pressure
OED Tests Design 2 & Design 3	PHILIPS	15mV/mm	34μV/kPa		30μV/kPa	+-3μm	+-0.5kPa		+-0.5kPa
CRS TESTS Design 2	CIL BOX	1.3mV/mm	0.3mV/kPa	0.13μV/N	-	+-7μm	+-0.7kPa	+-6N	-
		14mV/mm	34μV/kPa (5μV/kPa)*	0.13μV/N	-	+-3μm	+-0.5kPa	+-6N	-
CRS TESTS Design 3	MSL BOX	1.3mV/mm	33μV/kPa (5μV/kPa)*	0.2μV/N	64μV/kPa	+-1μm	+-0.5kPa	+-6N	+-0.5kPa

Table 6.3. Characteristics of the automatic measuring systems used in the oedometer tests; the annotation * refers to the pore water pressure transducer used in the fast tests.

Oedometer cell	Total error due to non-repeatable compliances from 0N to 50kN		
	settlement mm	strain %	void ratio
Design 2	+-0.025	+-0.13	+-0.002
Design 3	+-0.07	+-0.35	+-0.006
Design 3*	+-0.025	+-0.13	+-0.002
Oedometer cell	Total error due to non-repeatable compliances from 200-300N up to 50kN		
	settl. mm	strain %	void ratio
Design 2	+-0.025	+-0.13	+-0.002
Design 3	+-0.025	+-0.13	+-0 002
Design 3*	+-0.02	+-0.1	+-0 0015
Oedometer cel	Total eror due to non-repeatable compliances from 1000N up to 50kN		
	settl. mm	stra n °o	void ratio
Design 2	+-0.025	+-0.13	+-0.002
Des gn 3	+-0.025	+-0.13	+-0.002
Des gn 3*	+-0 01	+-0 05	+-0.001

Table 6 4. CRS tests : bedding errors and non-repeteable compliances of the high pressure oedometer

Test	Oedometer cell	$\varepsilon_v = \Delta H/H_o$ (%/min)	Bedding error (P < 300 N)		Total error accumulated during CRS compression stage of the test (P < 50 MN)		Error accumulated in the load interval 50 MN < P < 60 MN	
			ε_v (°o)	e	ε_v (%)	e	ε_v (°o)	e
CRS 1	D2	0.028	0	0	± 0.13	± 0.002		
CRS 2	D2	0.0053	0	0	± 0.13	± 0.002		
CRS 3	D2	0.0037	0	0	± 0.13	± 0.002		
CRS 4	D2	0.0025	0	0	± 0.13	± 0.002		
CRS 5	D2	0.0053	0	0	± 0.13	± 0 002	± 0.06	± 0.001
CRS 6	D2	0.0025 - 0.028	0	0	± 0.13	± 0.002	± 0.06	± 0.001
CRS 7	D2	0.128	0	0	± 0.13	± 0.002	± 0 06	± 0.001
CRS 8	D2	0.0053	0	0	± 0.13	± 0.002		
CRS 9	D2	0.068	0	0	± 0.13	± 0.002		
CRS 10	D3*	0.025	± 0 03	± 0.0005 (•)	± 0.05	± 0.001		
CRS 11	D3	0.0025	± 0 22	± 0.004 (•)	± 0.13	± 0.002		
CRS R1	D3	0.005	± 0.22	± 0.004 (°)	± 0.13	± 0.002		
CRS R2	D3	0.0025	± 0 22	± 0.004 (°)	± 0.13	± 0.002		
CRS R3	D3	0 0025 - 0.024	± 0.22	± 0.004 (°)	± 0.13	± 0.002		
CRS R4	D3*	0 024	± 0 03	± 0.0005 (°)	± 0.10	± 0.0015		

(•) - bedding error which affects the settlements during the equilibration stage of the CRS test and does not affect the settlements during the continuous compression stage. The voids ratio e_o in Table 6.1 may be affected by this error

(°) - bedding error which affects the initial part (P < 300 N) of the continuous compression stage of the test

Table 6.5 CRS tests : possible strain measurement errors.

Test	σ'_{v_e} end of equilibration stage (kPa)	σ'_{vi} (kPa)	e_i
CRS 1	793	1164	0.865
CRS 2	666	947	0.86
CRS 3	696	1100	0.868
CRS 4	662	799	0.876
CRS 5	642	730	0.86
CRS 6	687	716	0.87
CRS 7	685	941	0 85
CRS 8	254	497	0.865
CRS 9	718	931	0.85
CRS 10	500	647	0.863
CRS 11	500	742	0.864
CRS R1	38	40	1.255
CRS R2	39	43	1.278
CRS R3	20	25	1.285
CRS R4	39	39	1.283

Table 6.6. e_i-σ'_{vi} states at the start of the continuous CRS compressions.

Compression curves	Plot e - σ'_v σ'_y (kPa)	Plot ε_v - σ'_v σ'_y (kPa)	Plot e - log σ'_v (Casagrande's construction) σ'_y (kPa)
OED 1, 2, 3, 4, 5, 6, 8, 9	2600		2320 - 2400
CRS 2, 3, 4, 5	3000	3000	2850 - 2980
CRS 11	3000	2900	3000
CRS 1, 9	3080	3020	3060
CRS 7	4000	4000	3500
CRS 8	2800	2700	2600
OED 7	1850		1900
I_1: 5E - 5% /min	2430		2320
I_2: 3E - 4% /min	2558		2380
I_3: 3E - 3% /min	2900		2850
I_4: 3E - 2% /min	3080		3000
I_5: 1E - 1% min	4000		4000

Table 6.7. Values of σ'_y measured for the natural Pappadai clay.

	σ'_y/σ^*_e	p'_y/p^*_y	Sensitivity S_t (YSR=1)
Todi (*Burland*, 1990; *Rampello*, 1990)	1.6 ÷ 1.8		1.5
Todi (*Burland et al*, 1996)	2.25		2.3
Boom (*Coop et al.*, 1995)	1 5		1.55
London (*F.Cotecchia*, 1990; *Burland*, 1990; *Webb*, 1969)	> 2 (≃ 2.4)		1 9
Pappadai	3.5	3.2	3.1
Vallericca (*Burland et al.*, 1996)	2.47(*)		2.5
Vallericca (*Rampello et al.*, 1993)		≅ 3 3	≅ 3.3
Bothkennar (*Smith et al.*, 1993)	5		4 3 ÷ 5

Table 6.8. S_t(YSR=1)-σ'_y/σ^*_e data for various natural clays.

Test	σ'_y	$\sigma'_{y\,eq}$	Mnc eq.	σ^*_e/σ'_y
CRS2	3000	3000	17830	0.235
CRS8	2800	3020	17997	0.24
OED2	2600	3000	17830	0.273
OED5	2600	3000	17830	0.273
OED6	2600	3000	17830	0.273
OED7	1850	2800	17830	0.383
OED10 1 cycle	3070	3150	19000	0.33
OED10 2 cycle	6000	6200	50000	0.5

Table 6.9. Values of the equivalent oedometric stiffness $M_{NC_{eq}}$ and of the stress ratio σ'_y/σ^*_e used in the normalization of the oedometric stiffnesses.

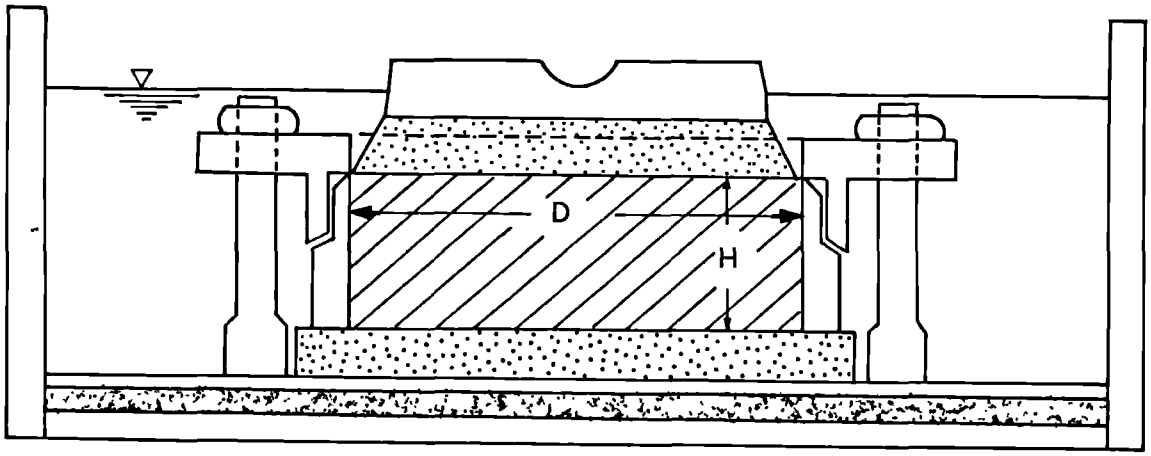

Fig.6.1. Oedometer cell Design 1.

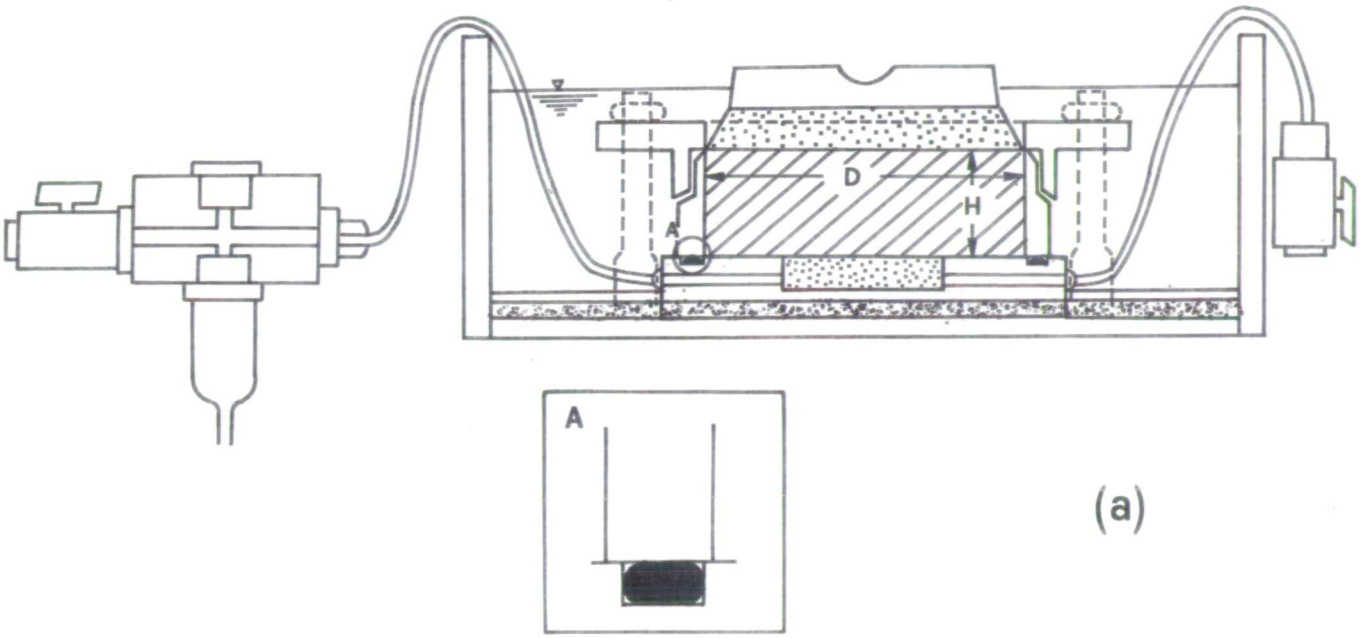

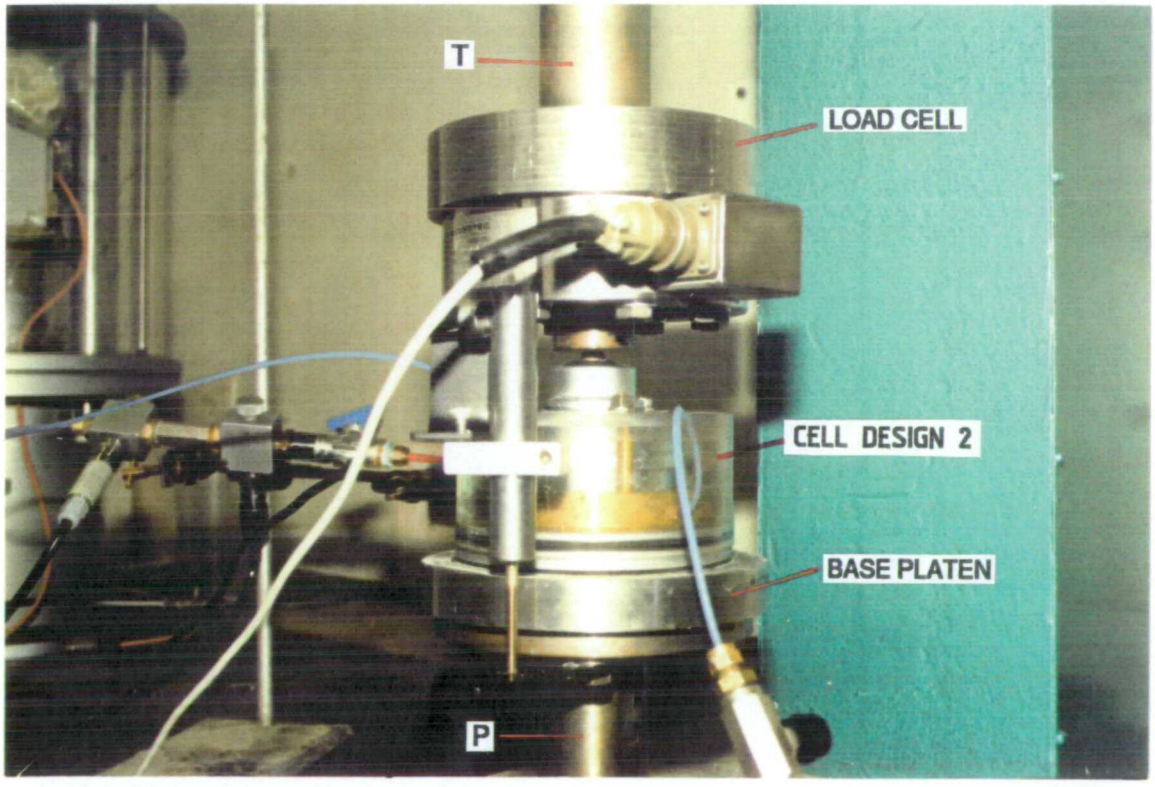

Fig.6.2. Oedometer cell Design 2 : (a) scheme; (b) cell set up within the high pressure oedometer.

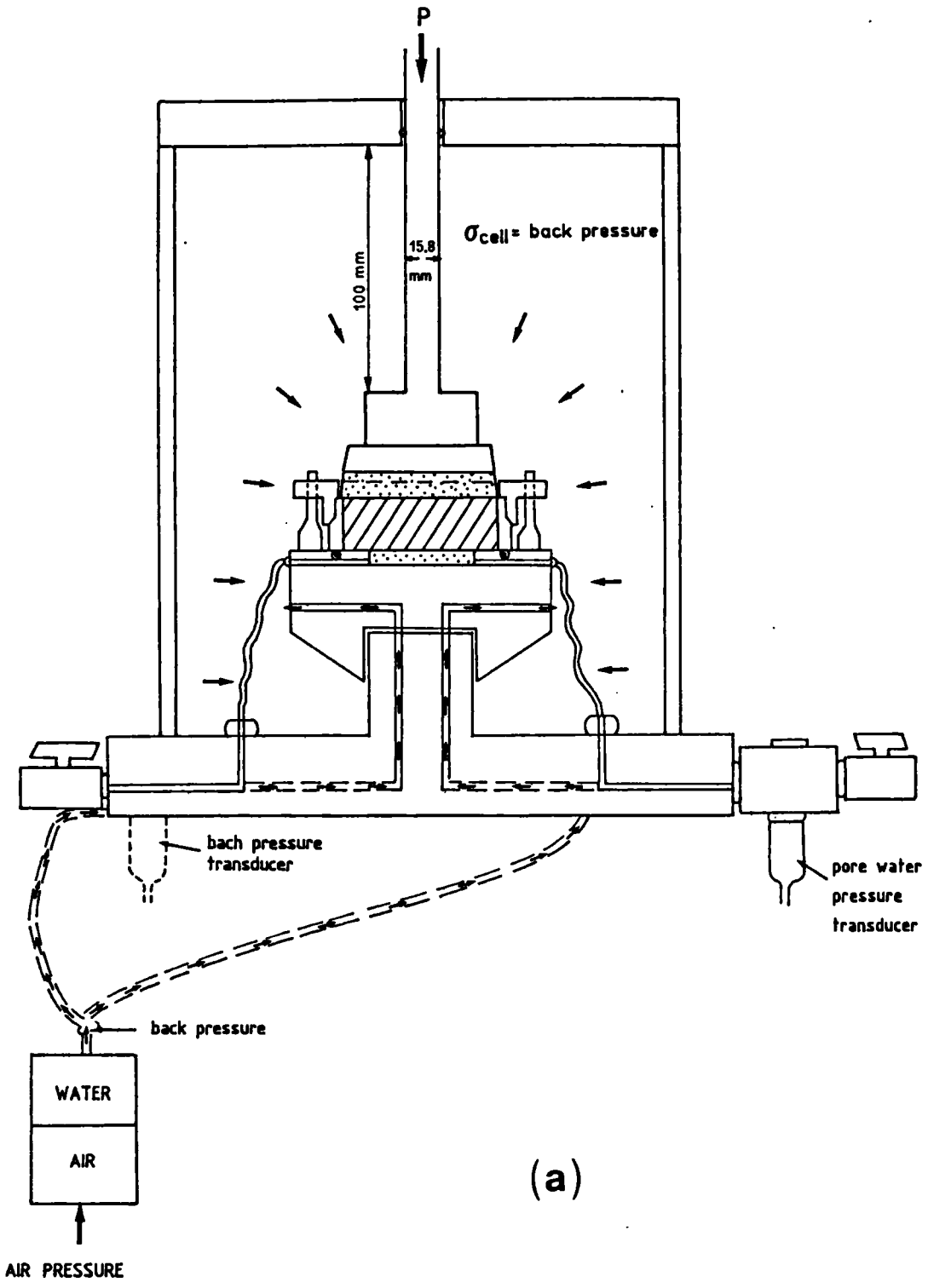

Fig.6.3. Oedometer cell Design 3 : (a) scheme; (b) cell set up within the OED loading frame.

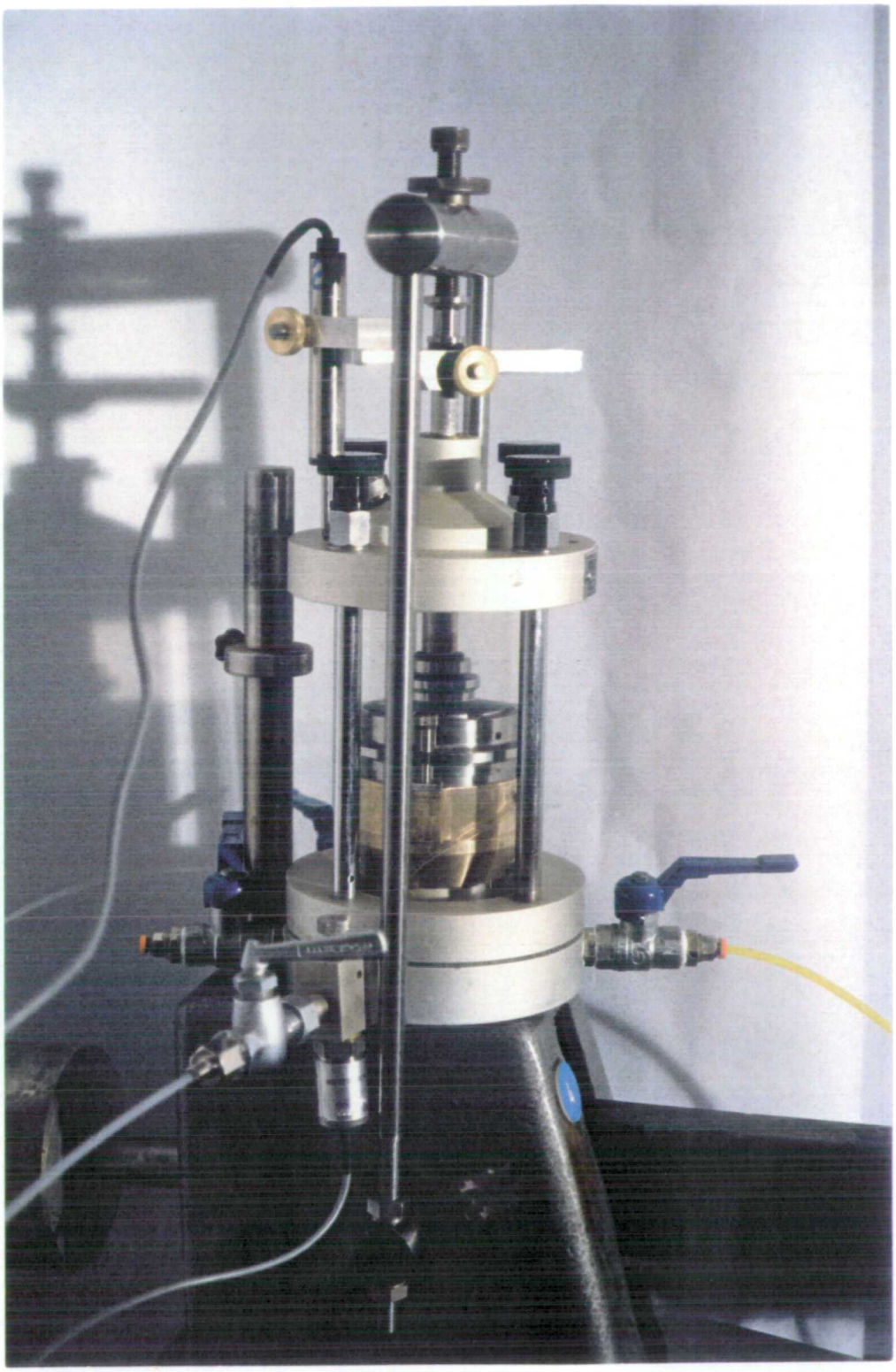

(b)

Fig.6.3. Oedometer cell Design 3 : (a) scheme; (b) cell set up within the OED loading frame.

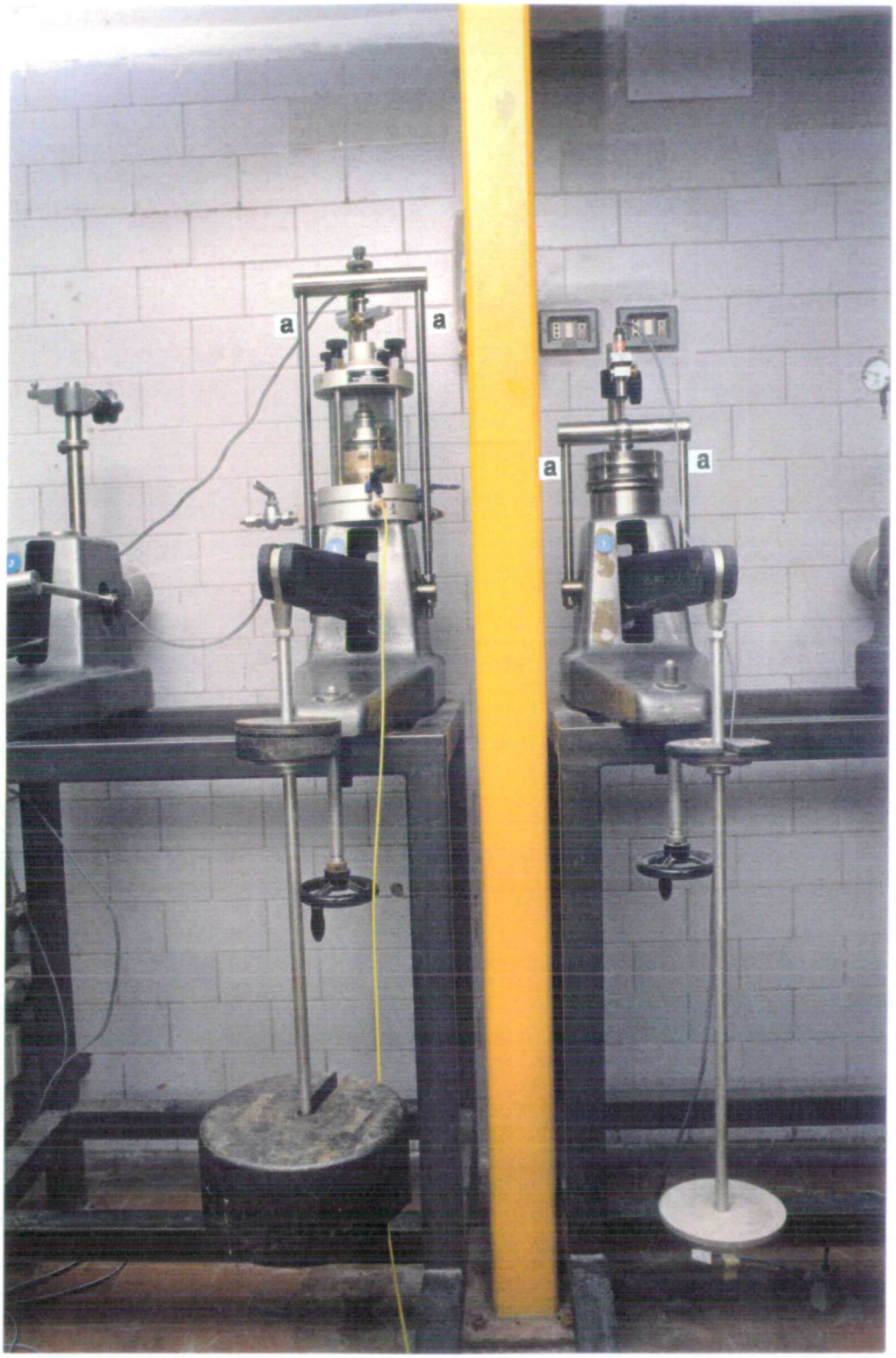

Fig.6.4. OED tests : loading frames with the oedometer cells Design 1 and 3.

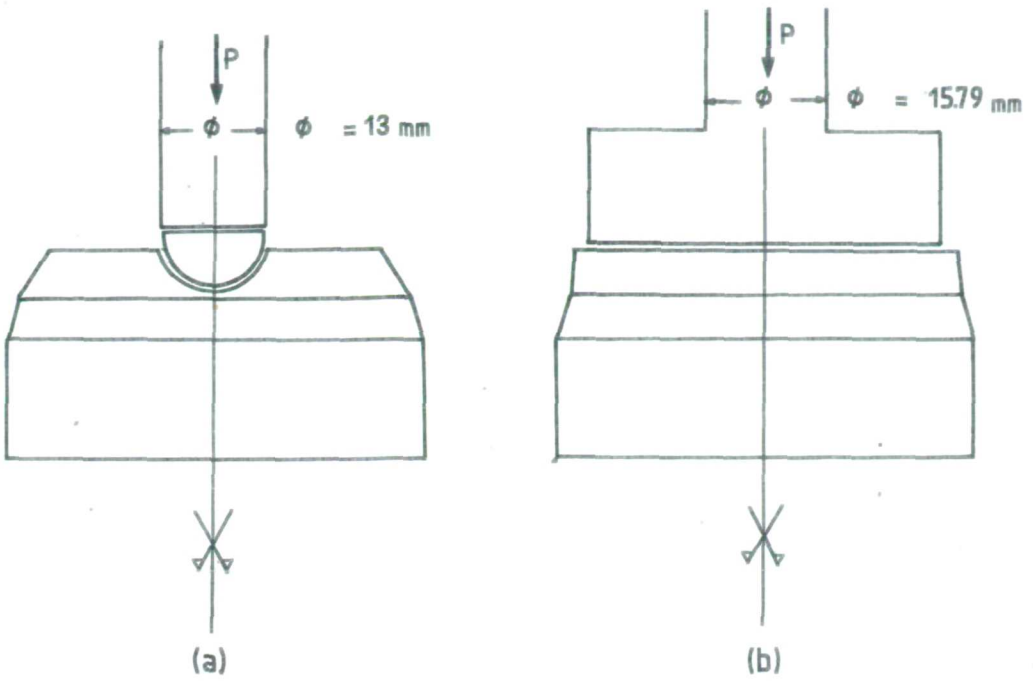

Fig.6.5. Application of the vertical load to the specimen in the oedometer cell Design 3 : (a) OED tests; (b) high pressure CRS tests.

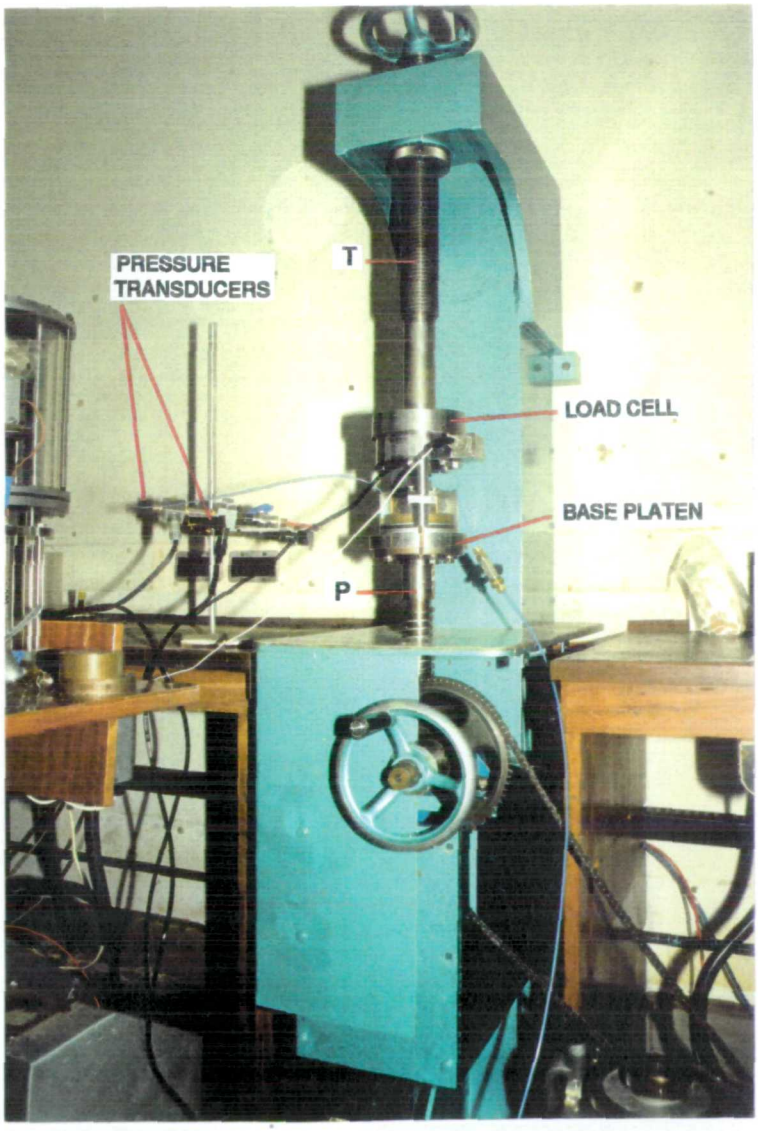

Fig.6.6. High pressure CRS test carried out with the oedometer cell Design 2.

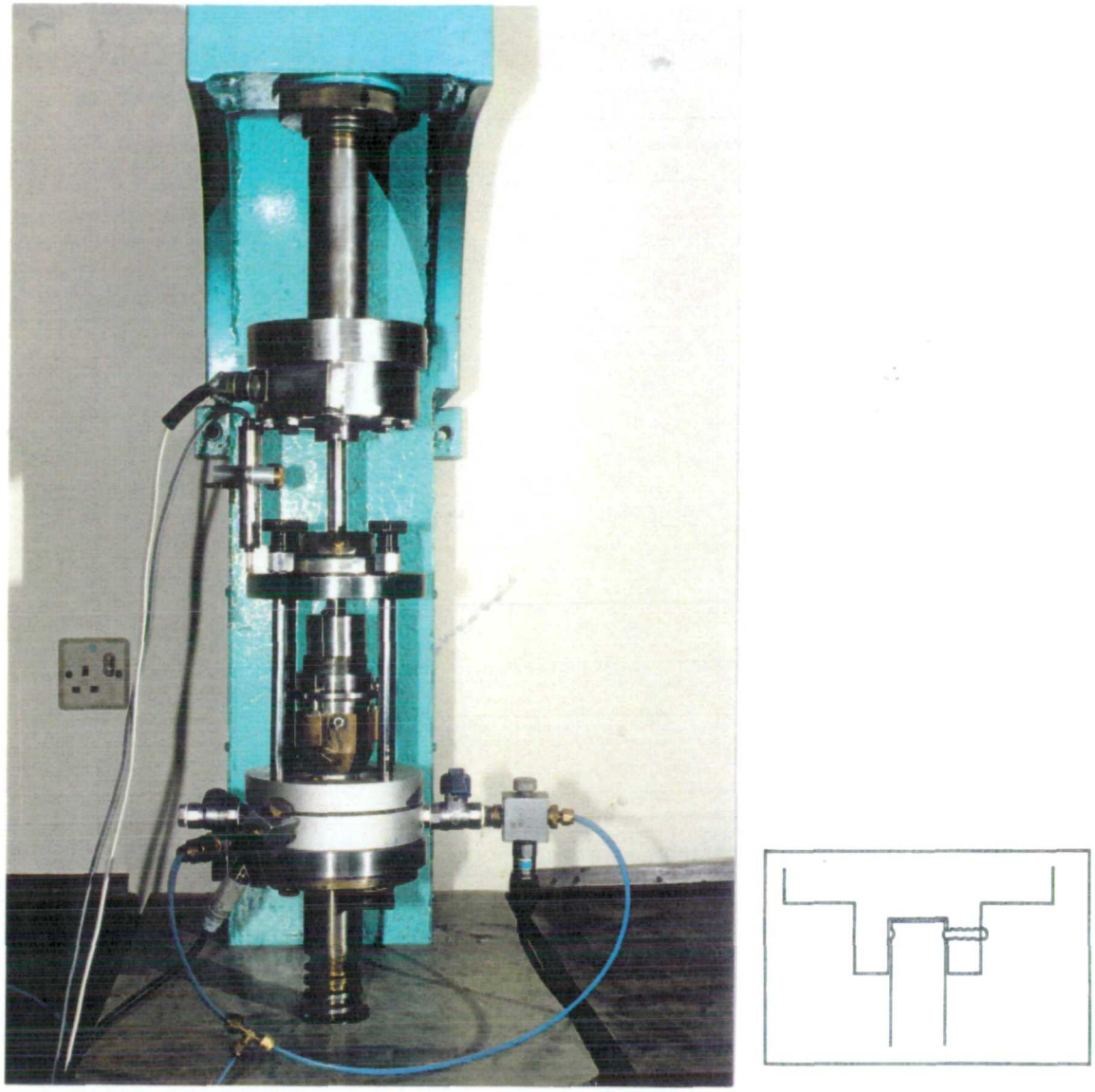

Fig.6.7. High pressure CRS test carried out with the oedometer cell Design 3; the detail sketch shows the connection between the loading ram and the load cell.

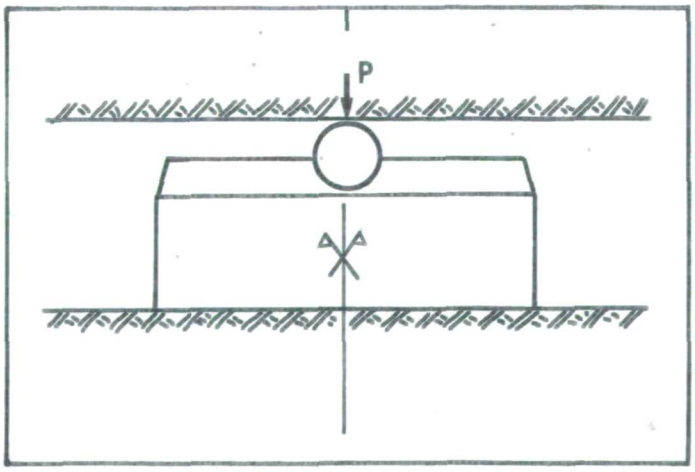

Fig.6.8. High pressure oedometer with cell Design 2 : application of the vertical load.

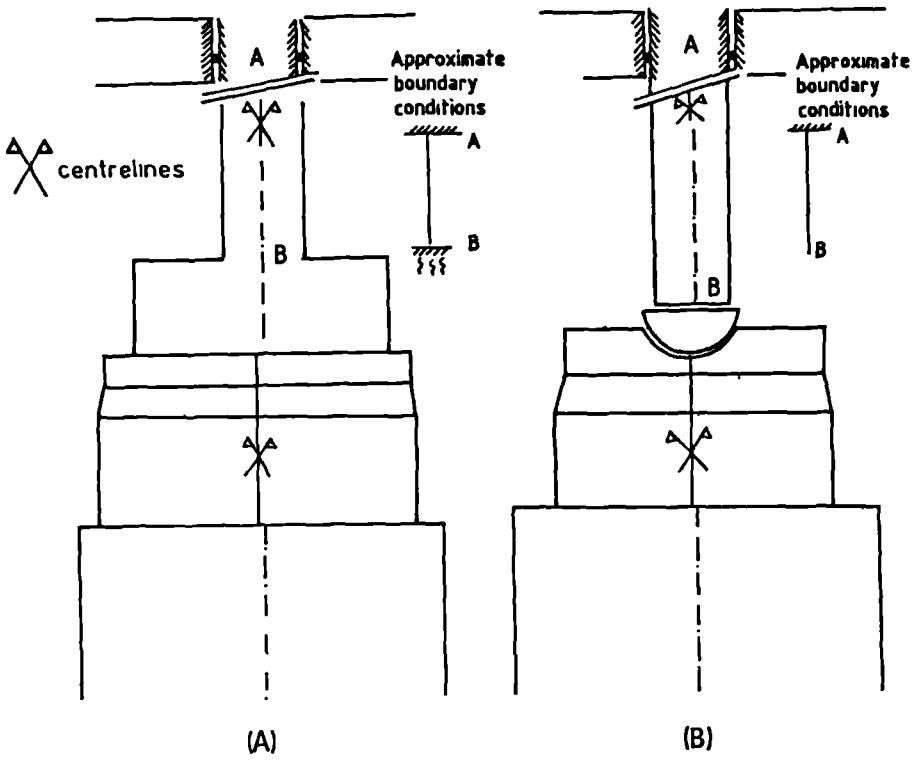

Fig.6.9. Oedometer cell Design 3 : eccentricity of the vertical load in the high pressure CRS tests (a) and in the OED tests (b); system (a) is safer against buckling of the loading ram.

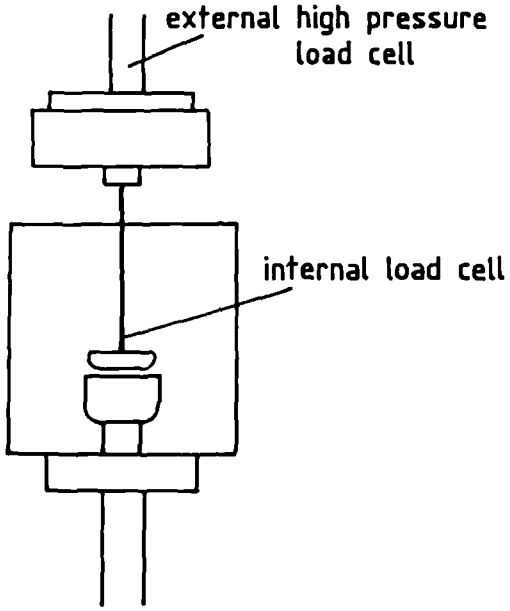

Fig.6.10. High pressure oedometer : measurement of the vertical load with both an external and an internal load cell.

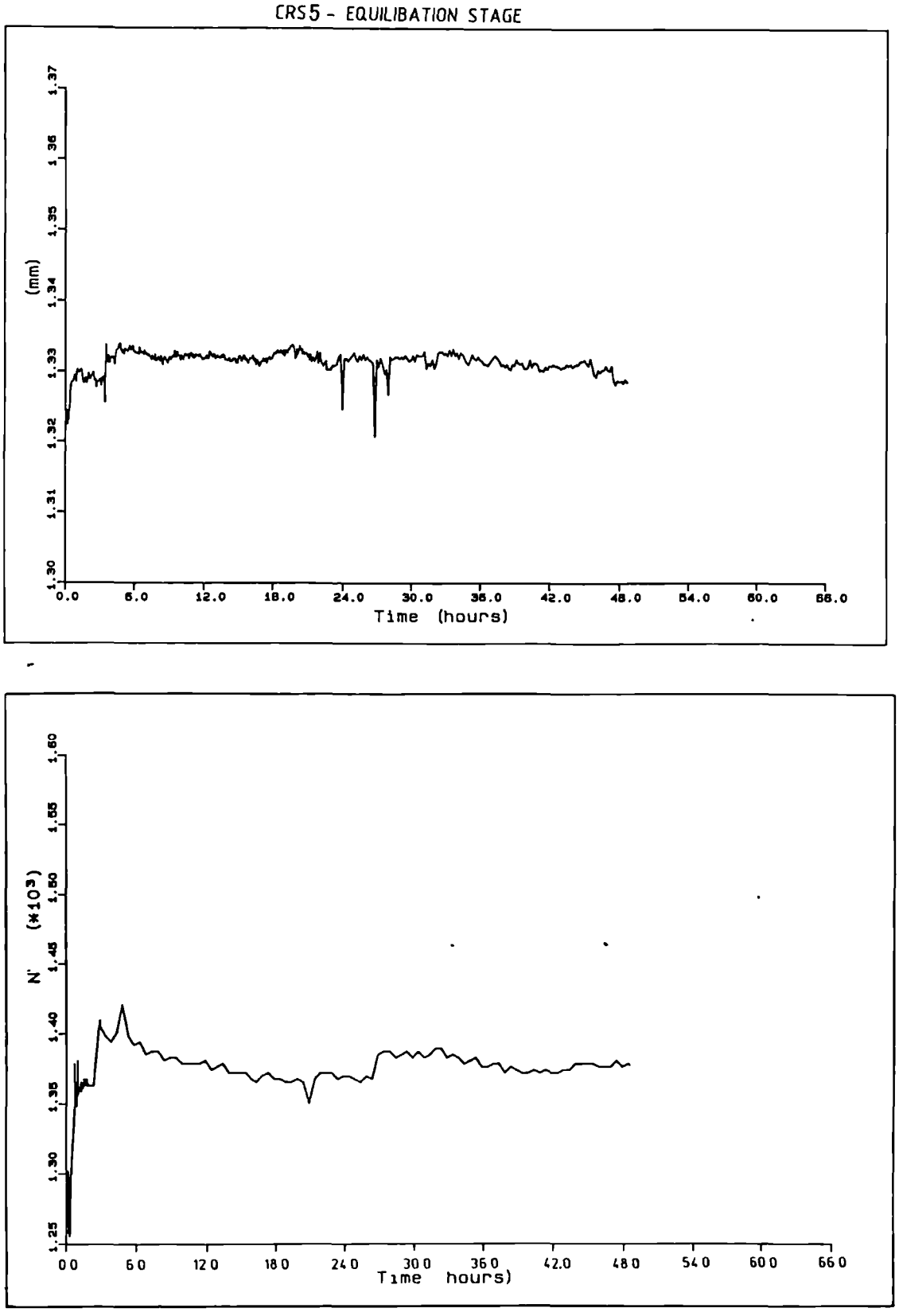

Fig.6.11. Typical equilibration stage at the start of the CRS tests (test CRS5).

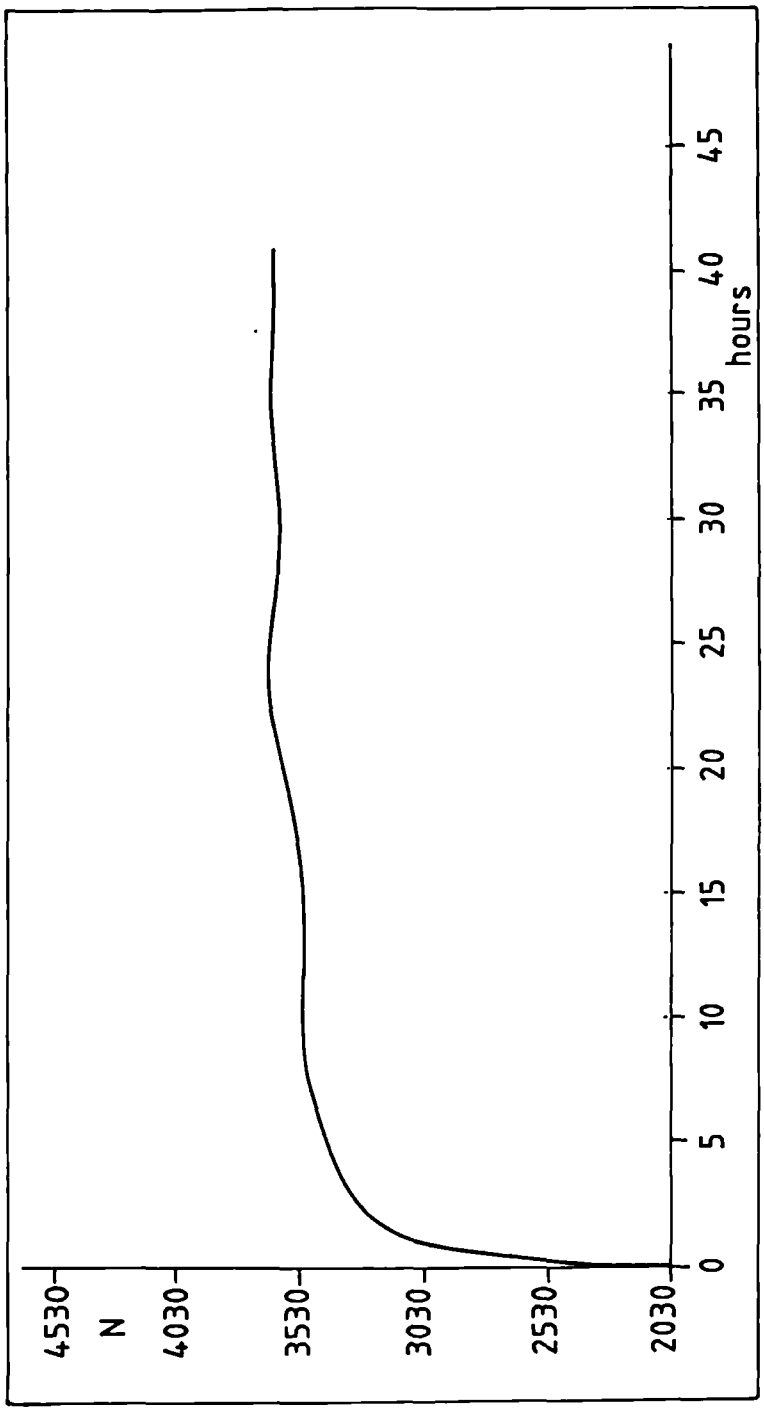

Fig.6.12. Typical equilibration stage after an unloading step in the CRS tests (test CRSR1).

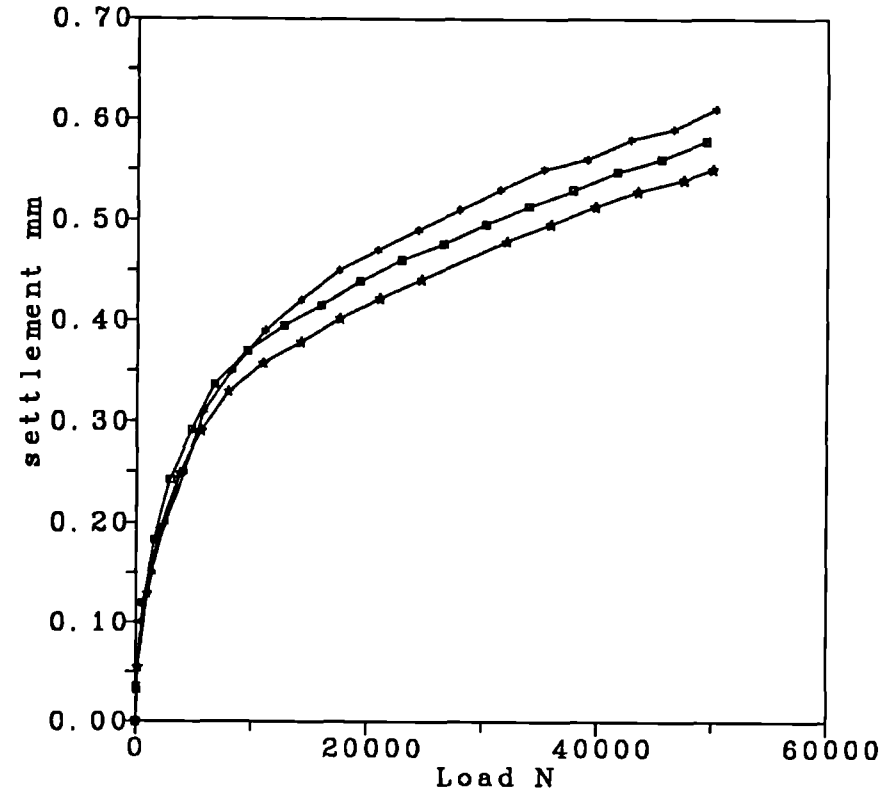

a

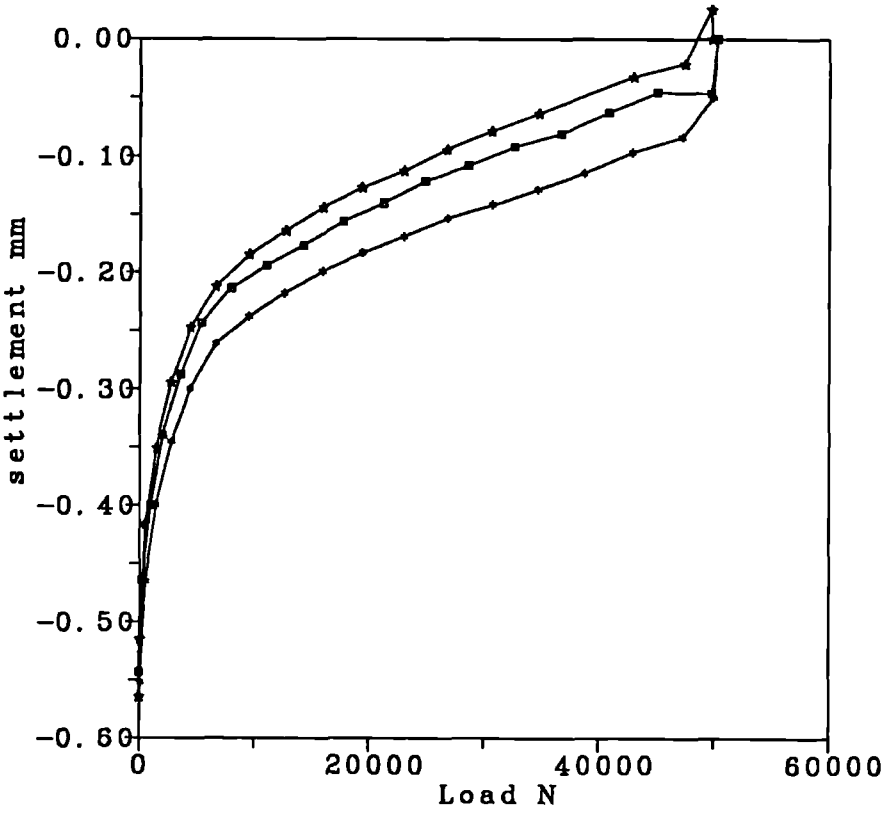

b

Fig.6.13. High pressure oedometer with cell Design 2 : compliance tests; no filter paper discs were present; (a) loading; (b) unloading.

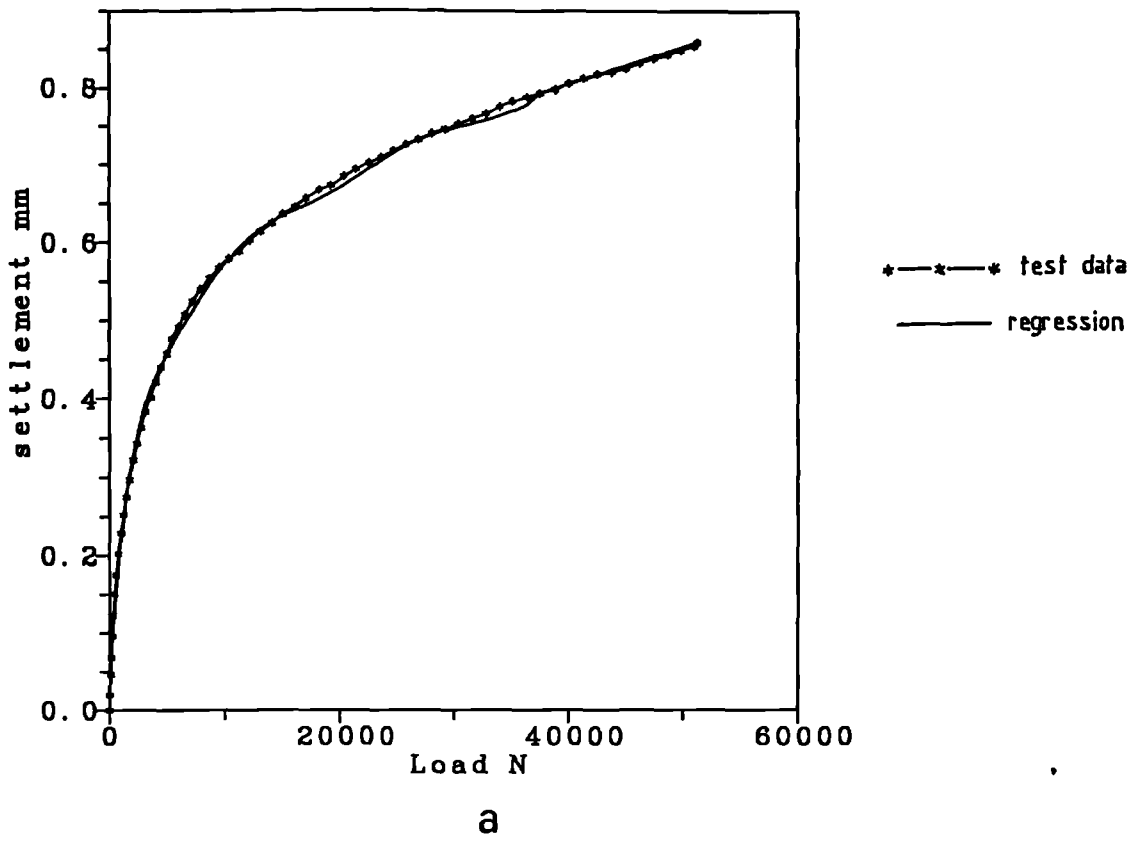

a

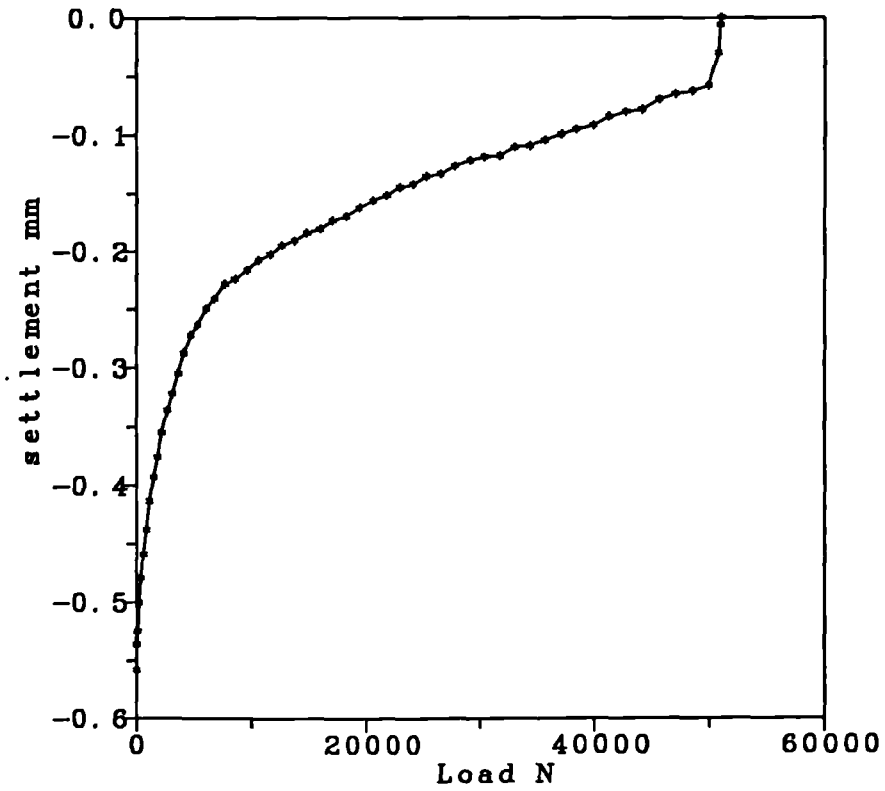

b

Fig.6.14. High pressure oedometer with cell Design 2 : compliance tests; filter paper discs were present; (a) loading; (b) unloading.

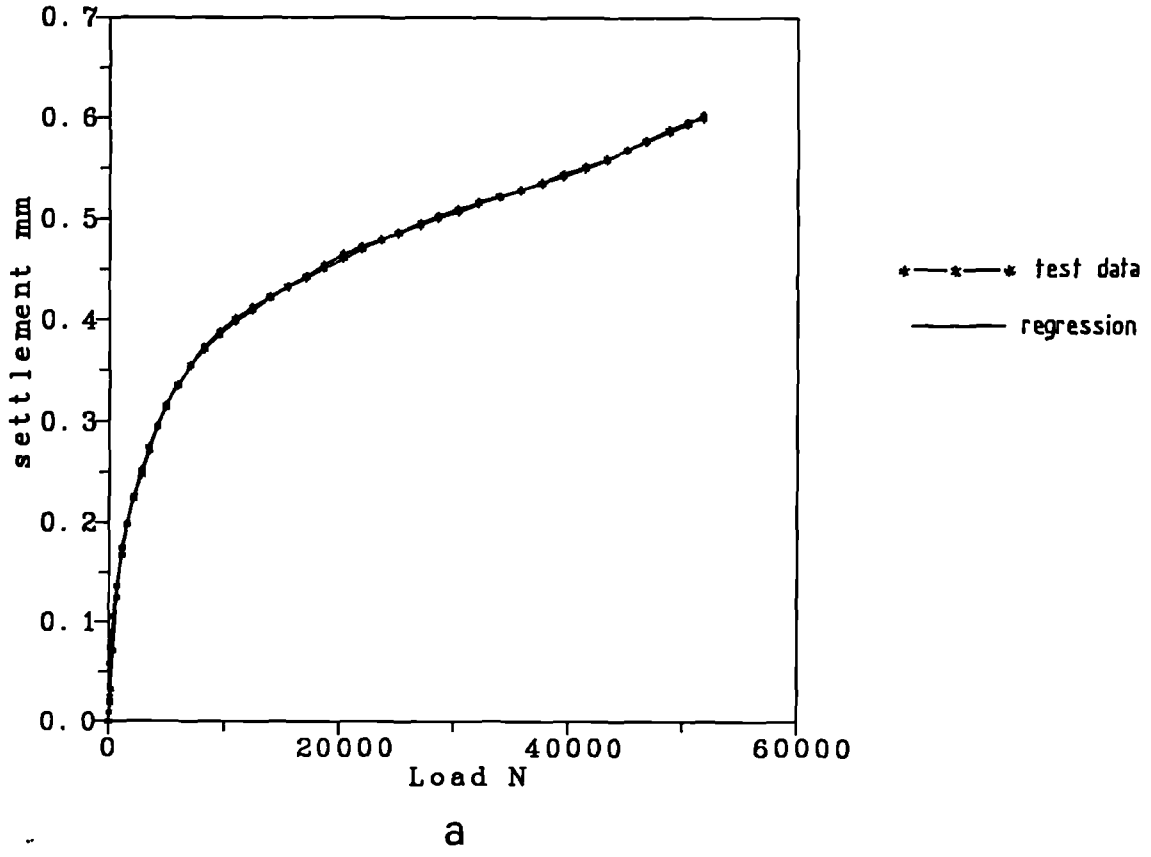

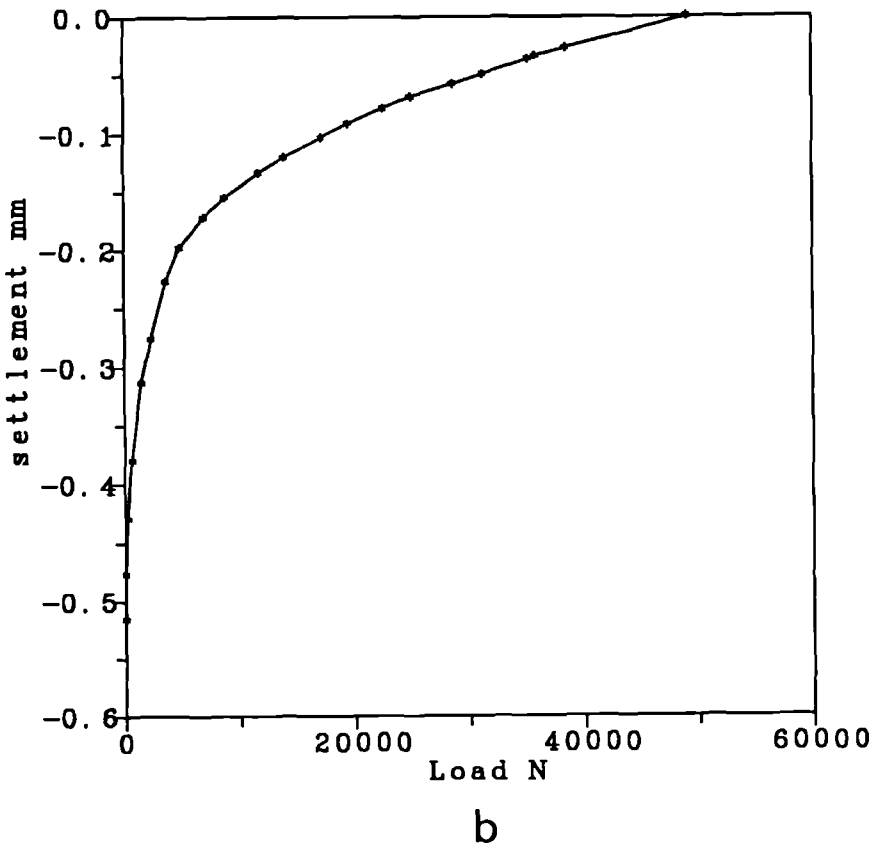

Fig.6.15. High pressure oedometer with cell Design 2 : compliance test; cycled filter paper discs were present (a) loading; (b) unloading.

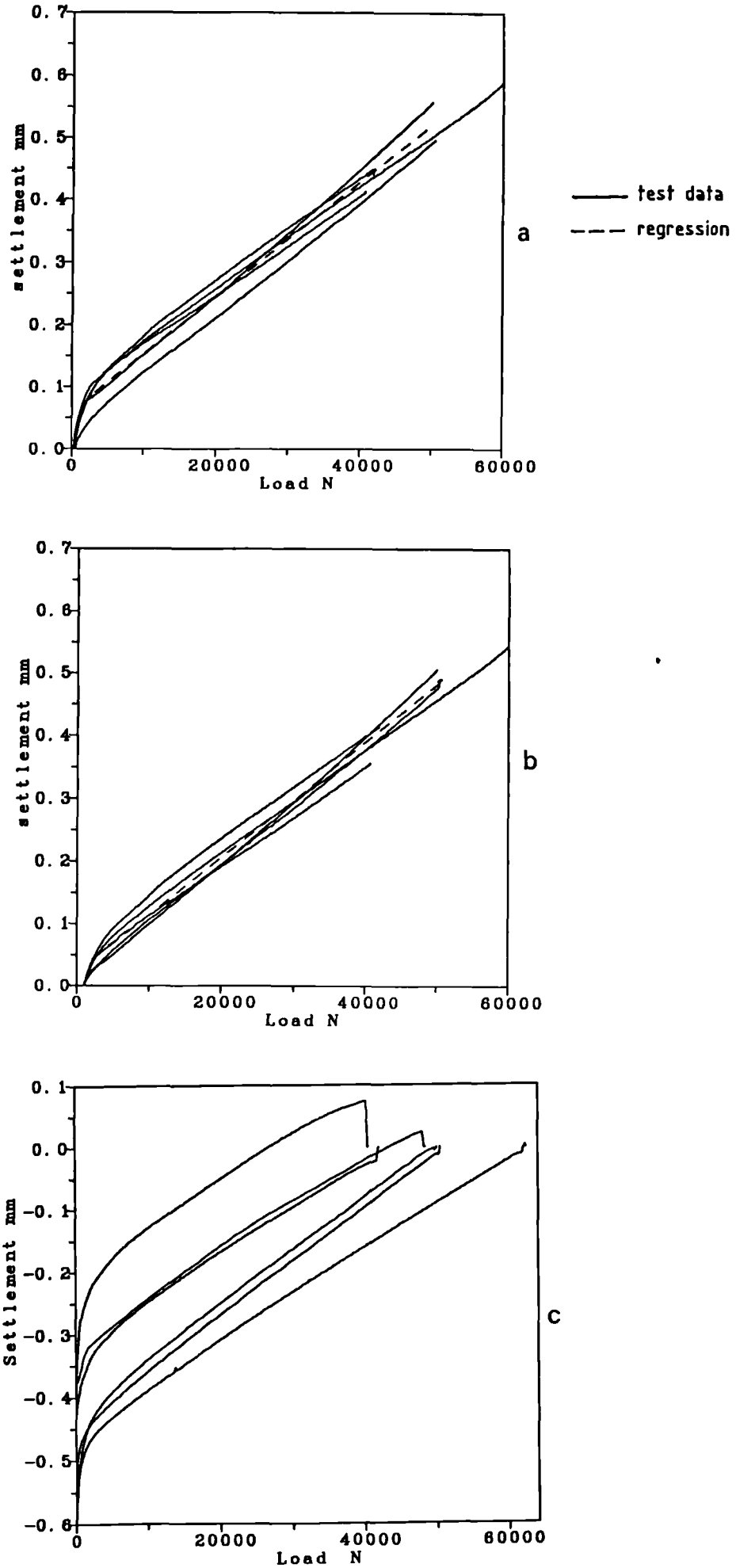

Fig.6.16. High pressure oedometer with cell Design 3 : compliance tests; no filter paper discs were present; (a) loading from 300N; (b) loading from 1000N; (c) unloading.

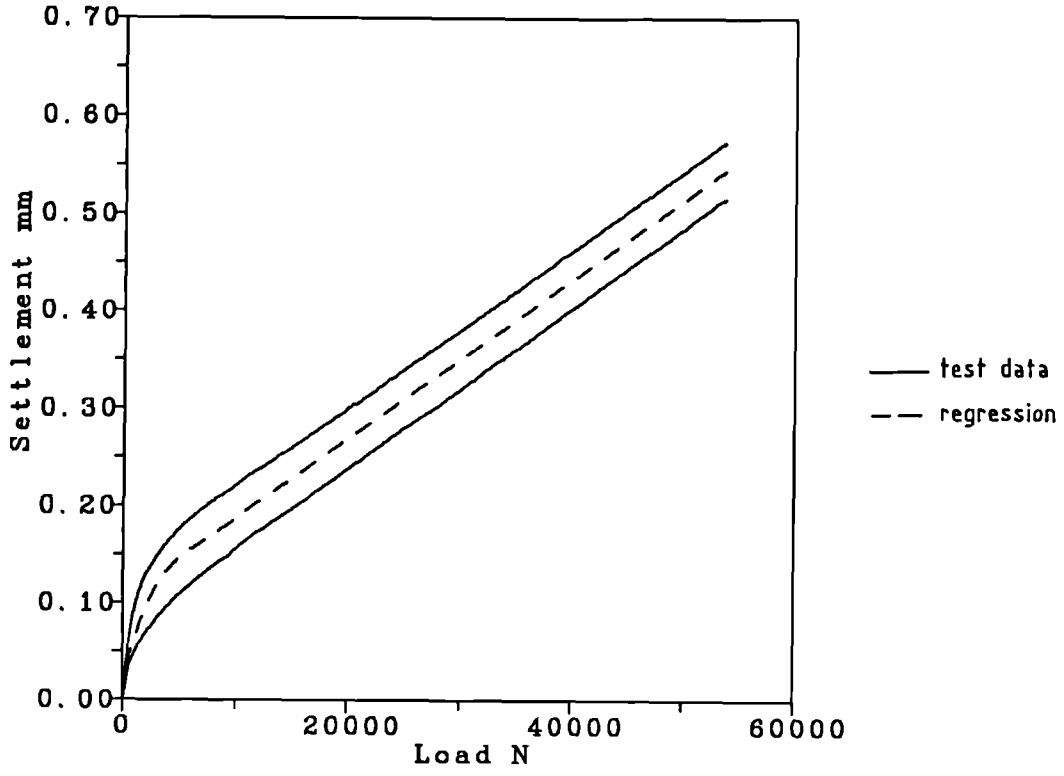

a

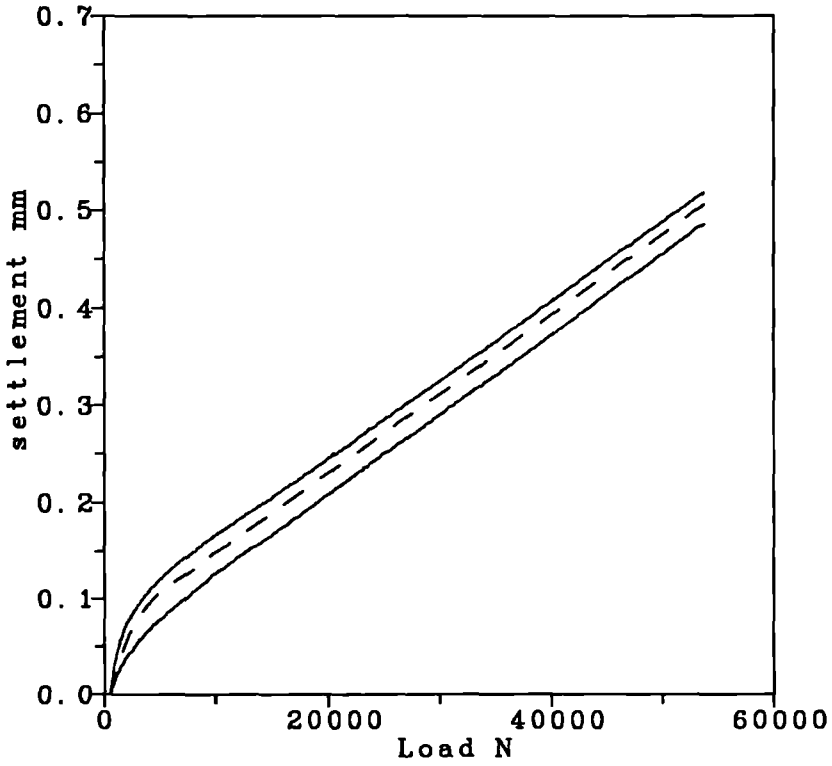

b

Fig.6.17. High pressure oedometer with cell Design 3* : compliance tests, no filter paper discs were present, (a) loading from 30N; (b) loading from 300N, (c) loading from 1000N; (d) unloading

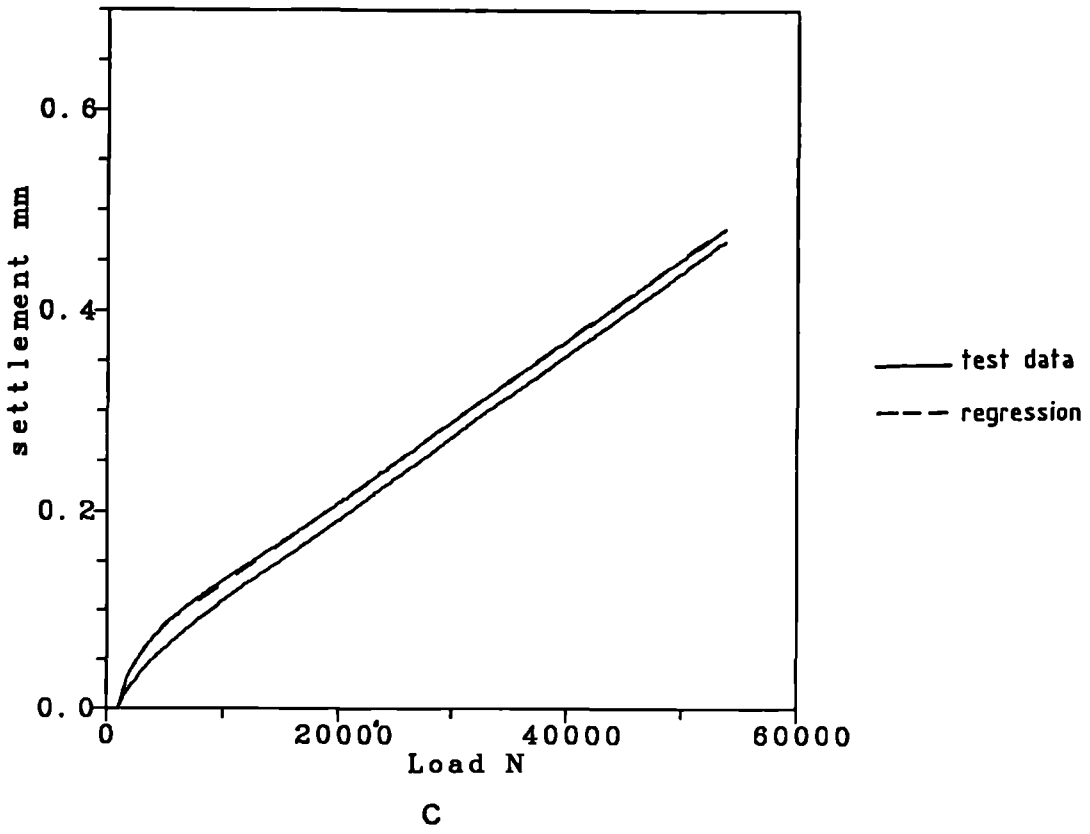

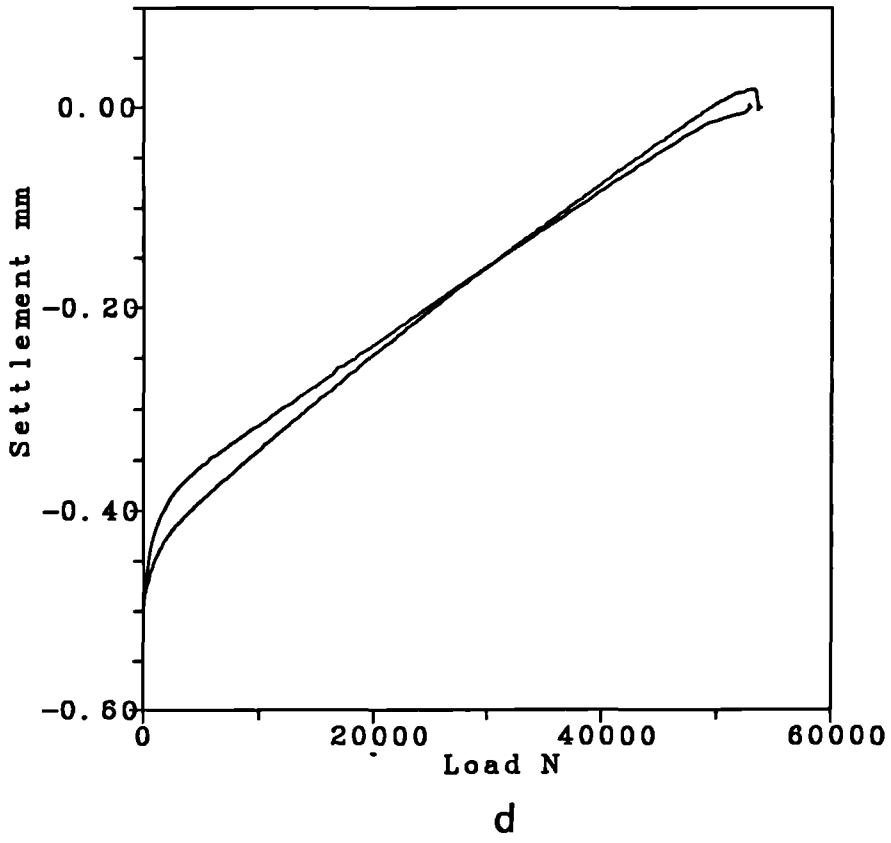

Fig.6.17. High pressure oedometer with cell Design 3* : compliance tests; no filter paper discs were present; (a) loading from 30N; (b) loading from 300N; (c) loading from 1000N; (d) unloading.

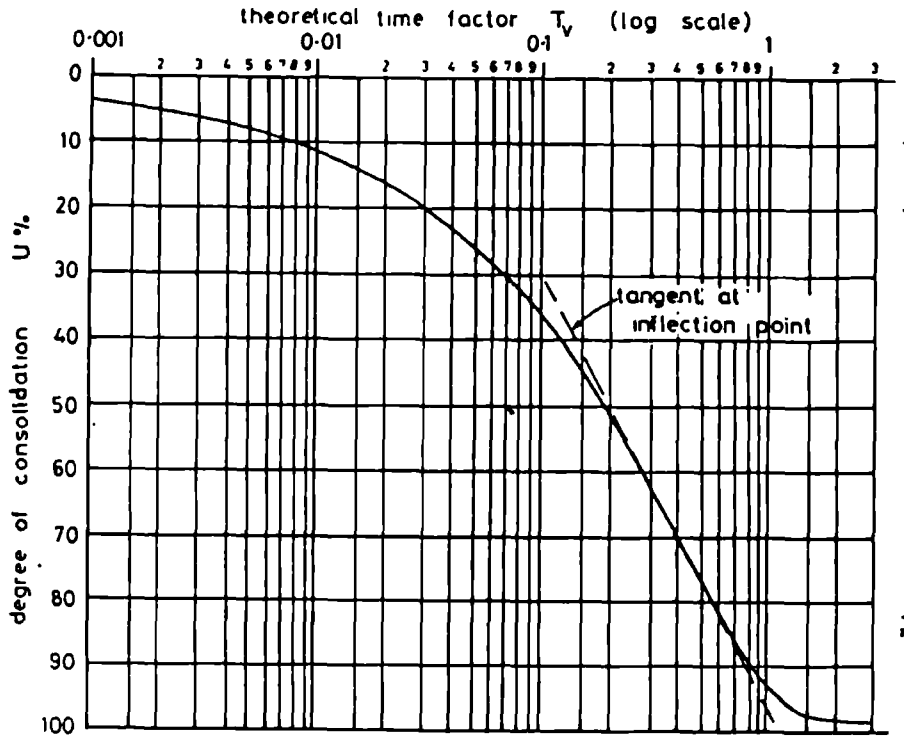

Degree of consolidation U %	Time factor T_v	$\sqrt{T_v}$
0	0	0
10	0.0077	0.0877
20	0.031	0.176
30	0.071	0.266
40	0.126	0.355
50	0 196	0.443
60	0.286	0.535
70	0 403	0.635
80	0.567	0.753
90	0 848	0.921
95	1.129	1.063
100	∞	∞

From Lowrie (1963)

Fig.6.18. Terzaghi model : U%-T_v relationship (after Head 1986).

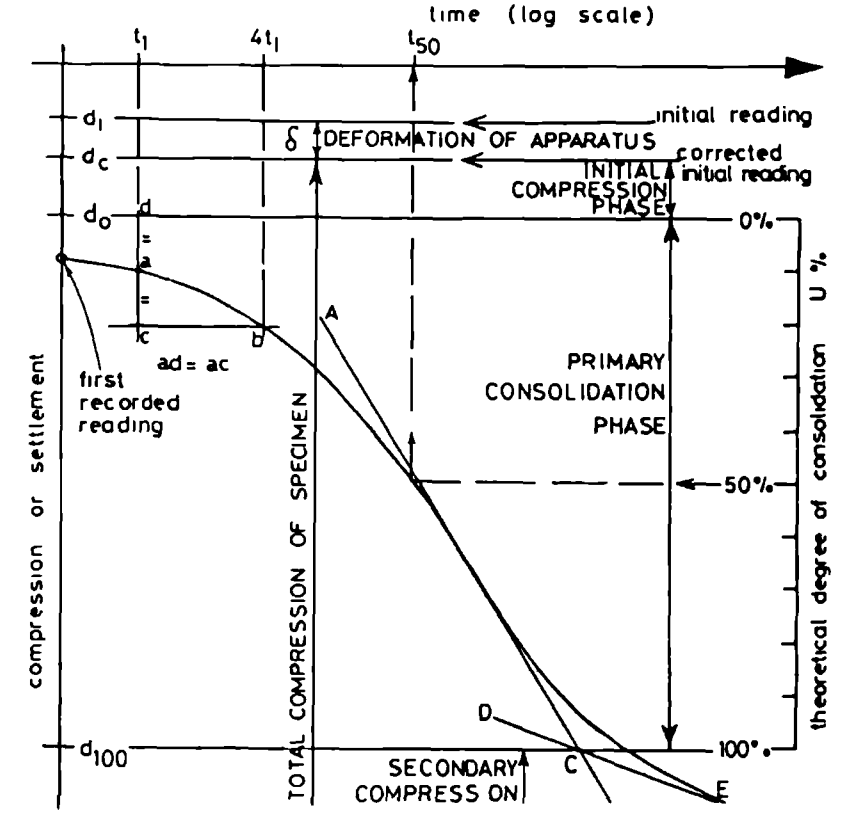

Fig.6.19. Casagrande curve fitting method (after Head 1986).

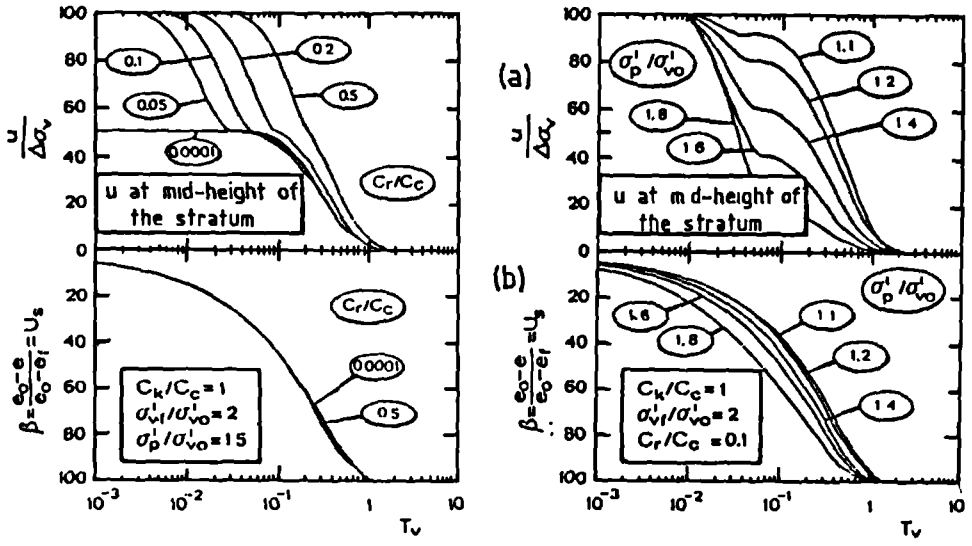

Fig.6.20. OC clay subjected to a load increment which includes σ'_p : (a) measured consolidation degree; (b) averagege consolidation degree U_s predicted by the Terzaghi model. Key : C_r recompression index; C_c compression index; σ'_p preconsolidation stress; σ'_{v0} initial vertical stress (after Mesri and Rokhsar 1974).

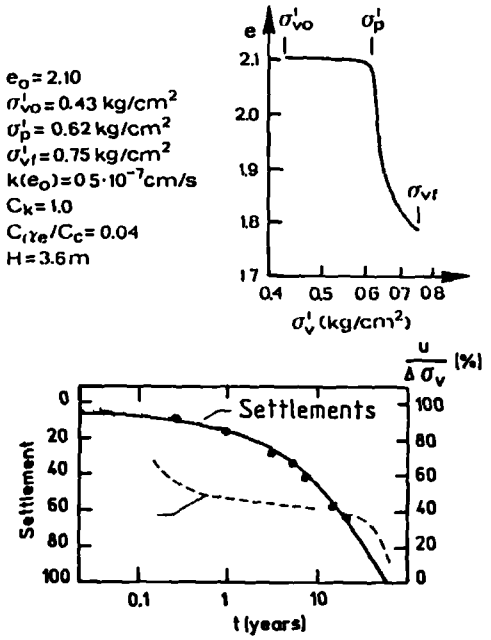

Fig.6.21. Consolidation of a clay stratum under a stress increment which includes σ'_p (after Mesri and Godlewski 1979).

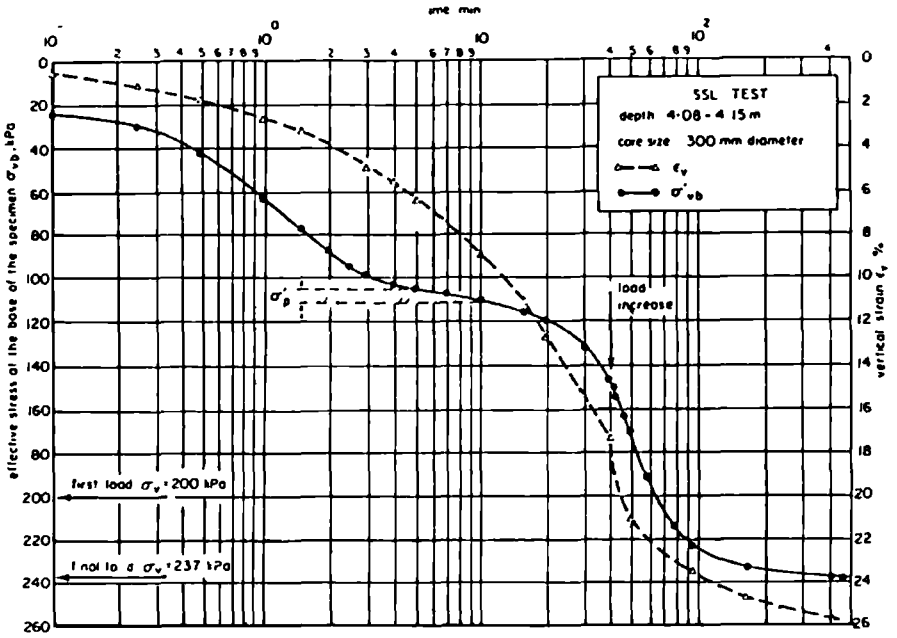

Fig.6.22. Average strain ε_v and base effective stress σ'_{vb} versus time for a single stage-loading test on an OC soil specimen (after Leroueil et al.1983).

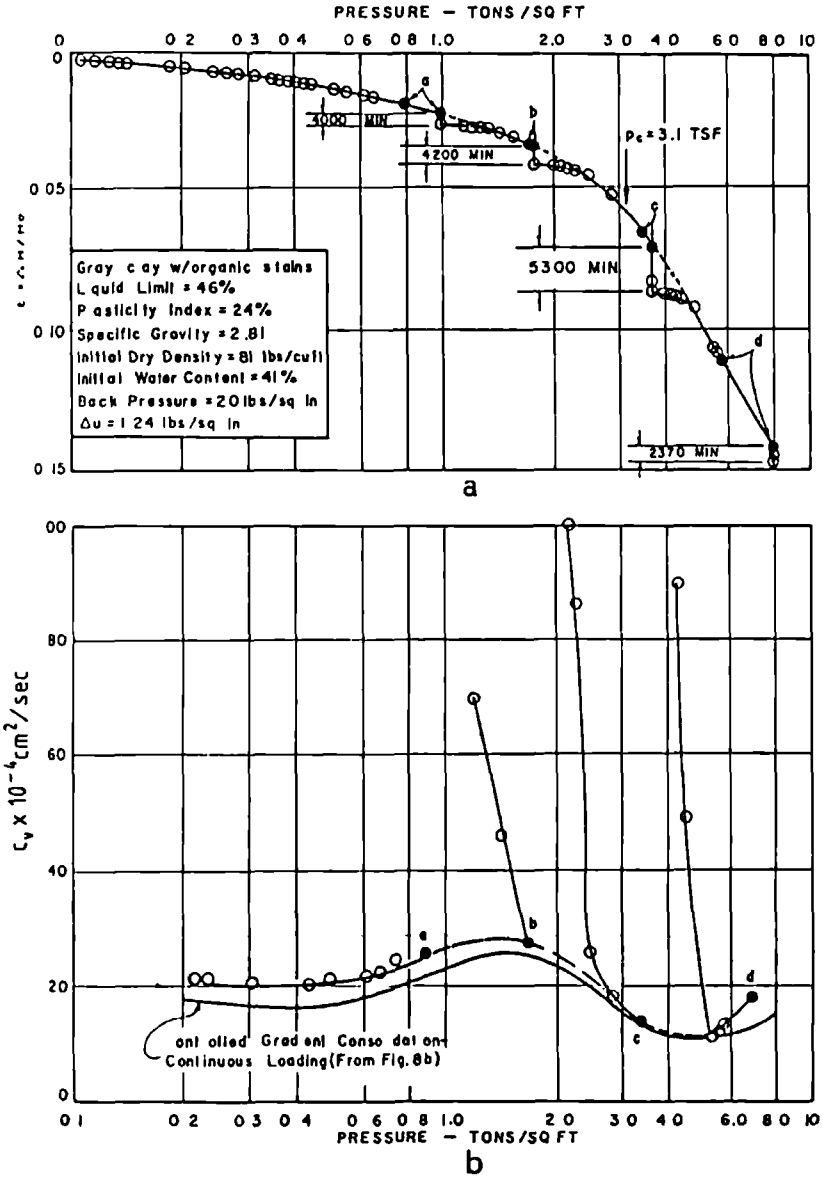

Fig 6 23. Ageing effects on both the compression curve and the c_v-σ'_v relationship of an OC marine clay (after Lowe et al.1969).

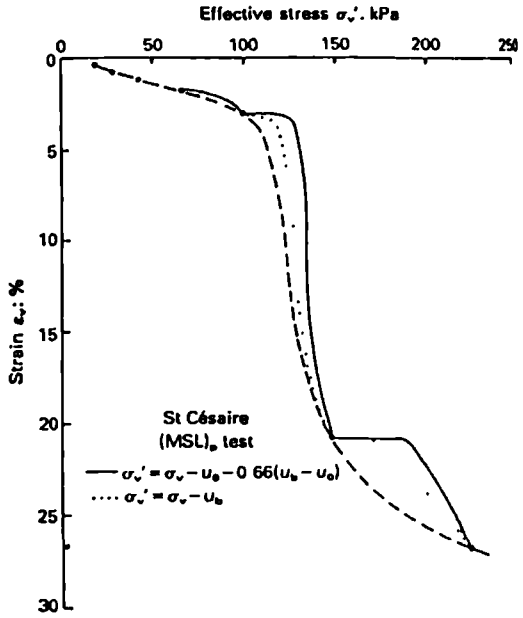

Fig.6.24. State path followed by a soft sensitive clay during an end of primary oedometer test (EOP) (after Lerouil et al.1985).

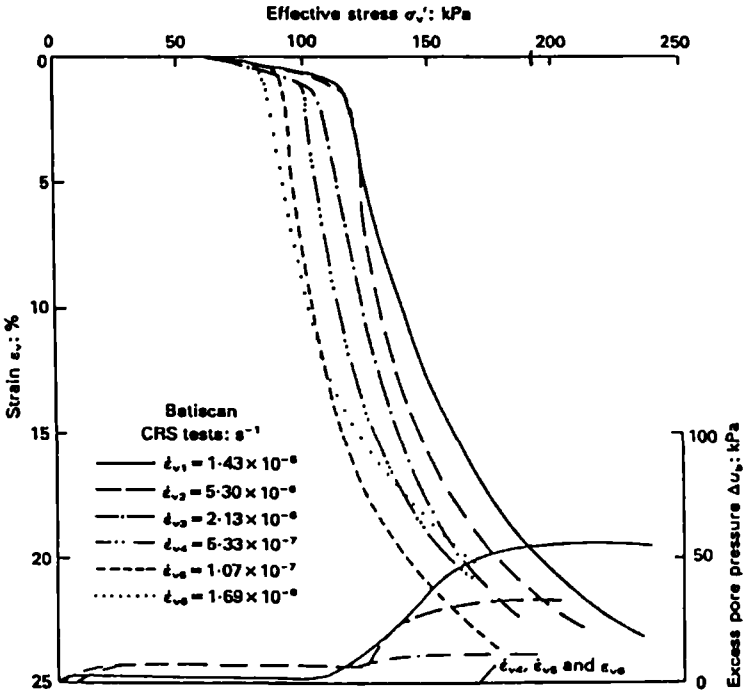

Fig.6.25. Strain rate dependancy of the behaviour of a soft sensitive clay (after Lerouil et al.1985).

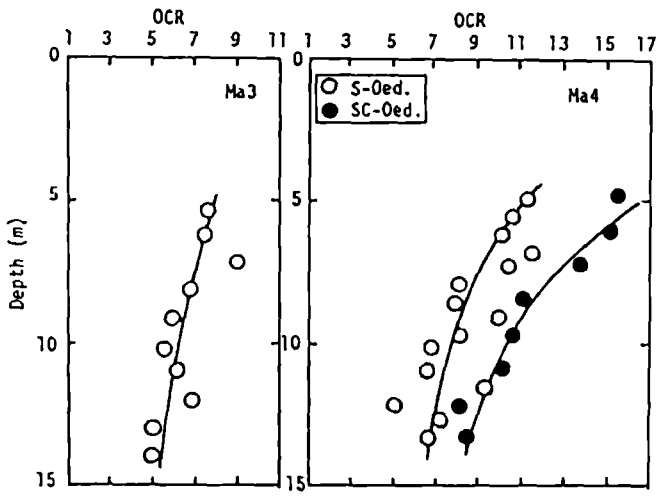

Fig.6.26. Values of YSR (OCR in the figure) measured on firm to stiff marine clays by means of both OED and CRS tests (after Hanzawa et al.1990); the S-Oed data are from OED tests and the SC-Oed data are from CRS tests.

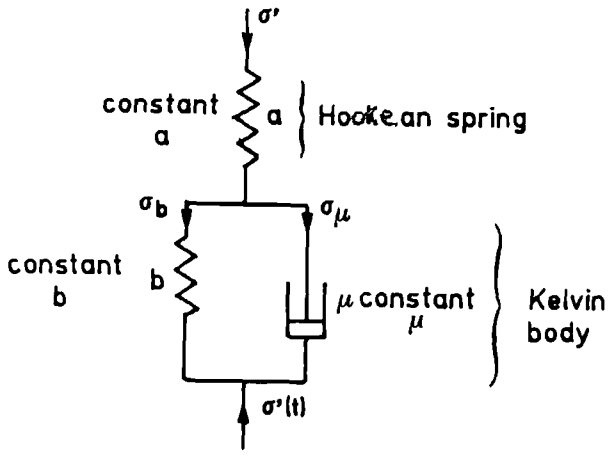

Fig 6.27. Model representation of soil skeleton in the 1D consolidation model of Gibson and Lo (1961).

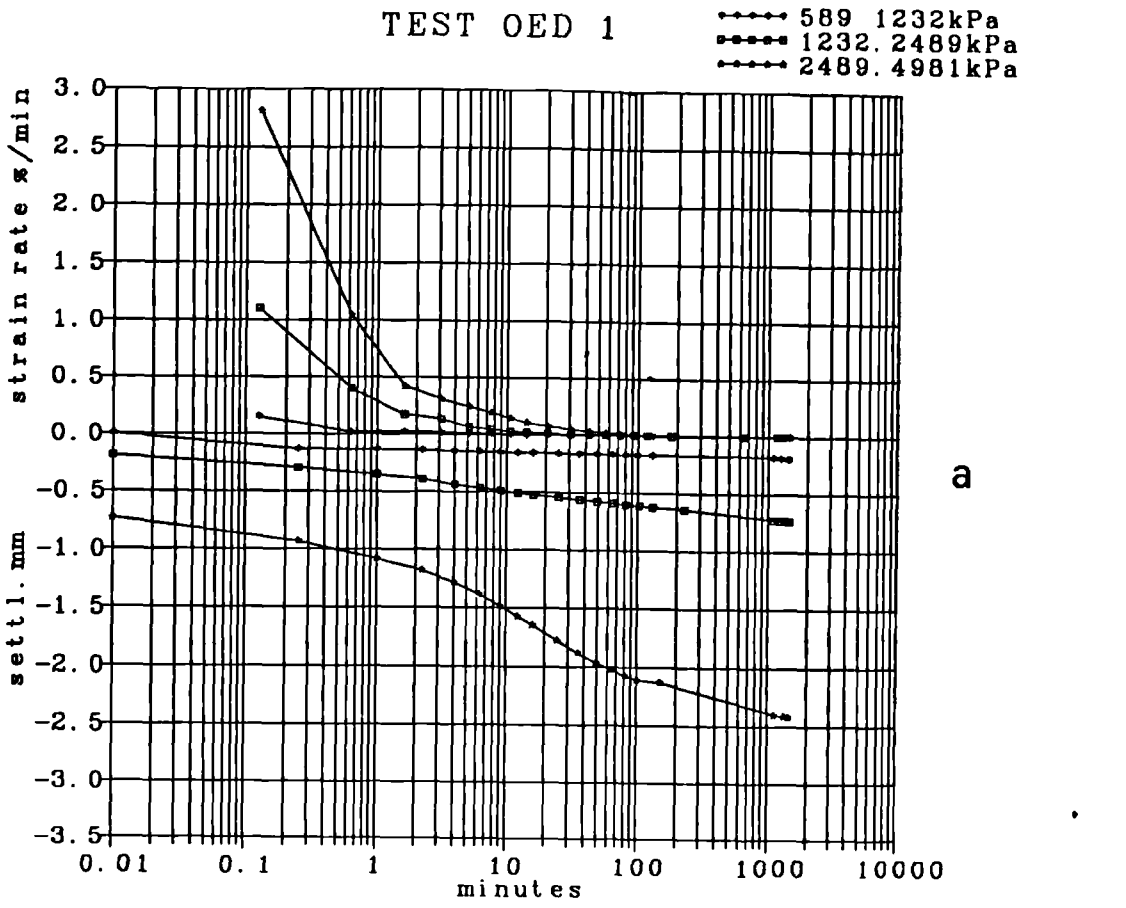

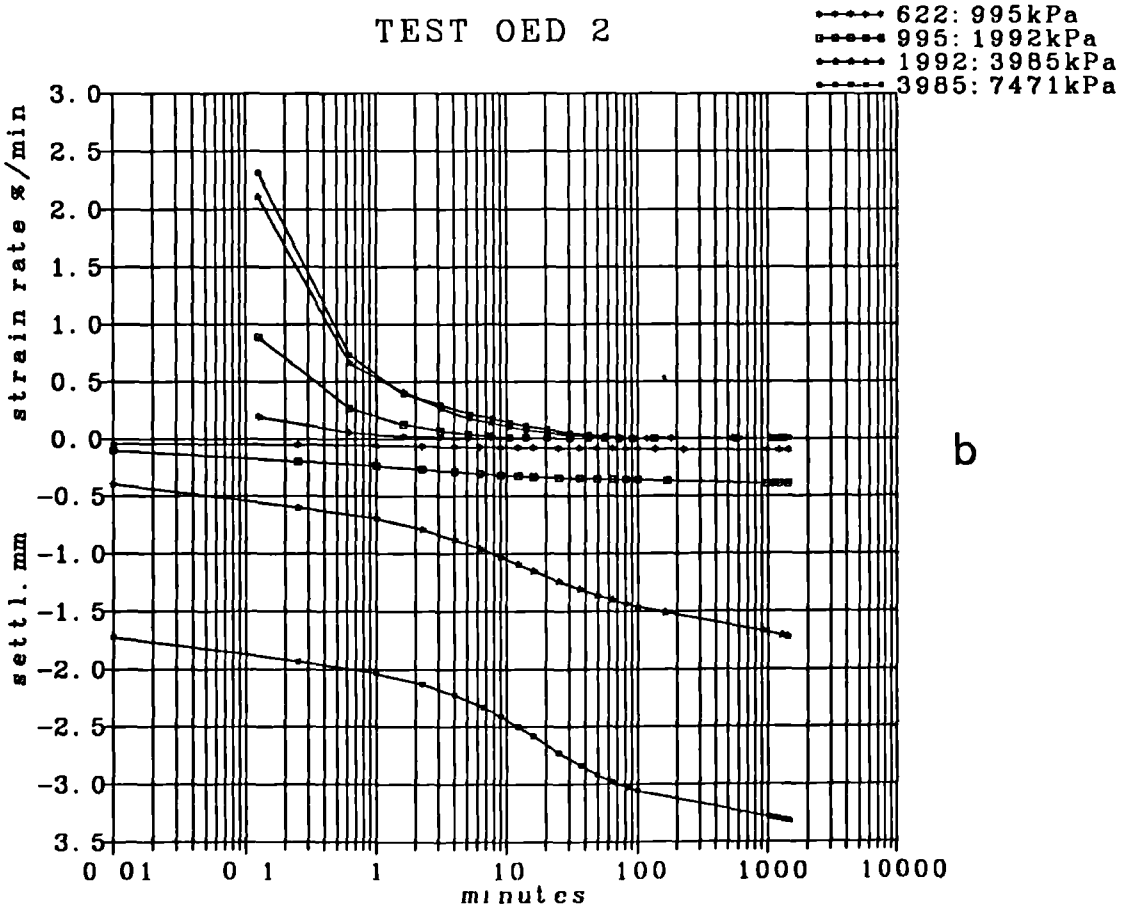

Fig.6.28. Consolidation curves and strain rates logged in the OED tests on the undisturbed Pappadai clay.

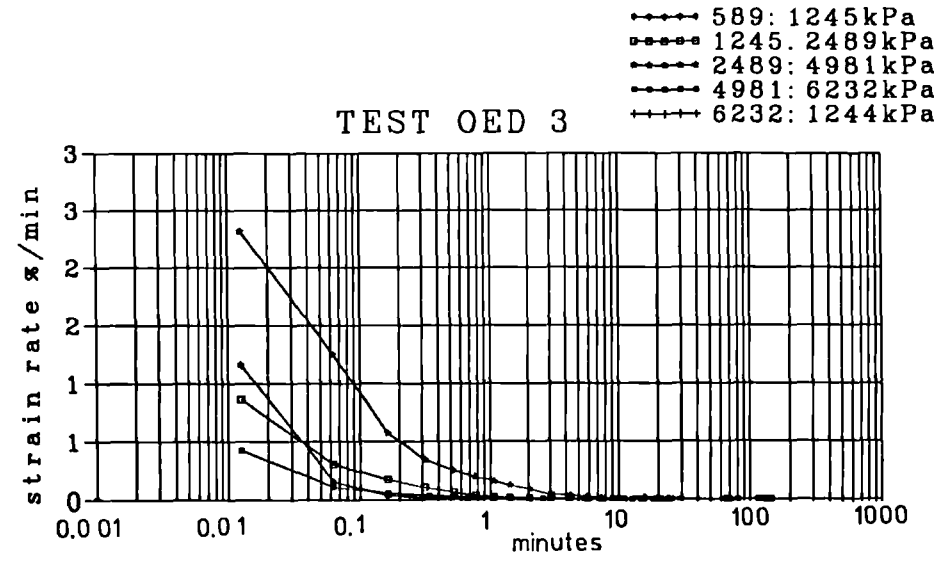

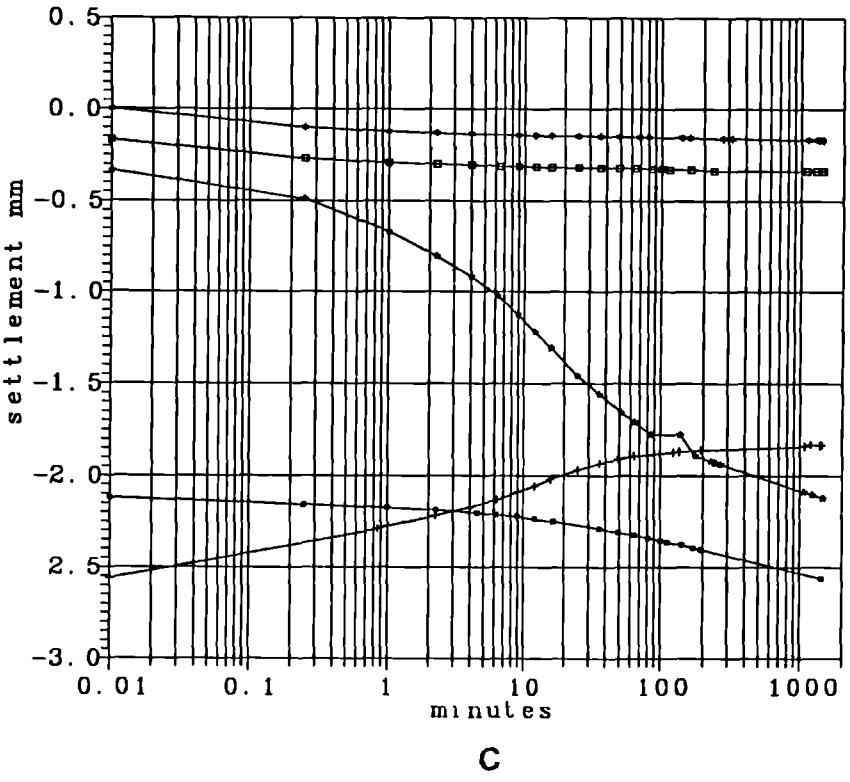

Fig.6.28. Consolidation curves and strain rates logged in the OED tests on the undisturbed Pappadai clay.

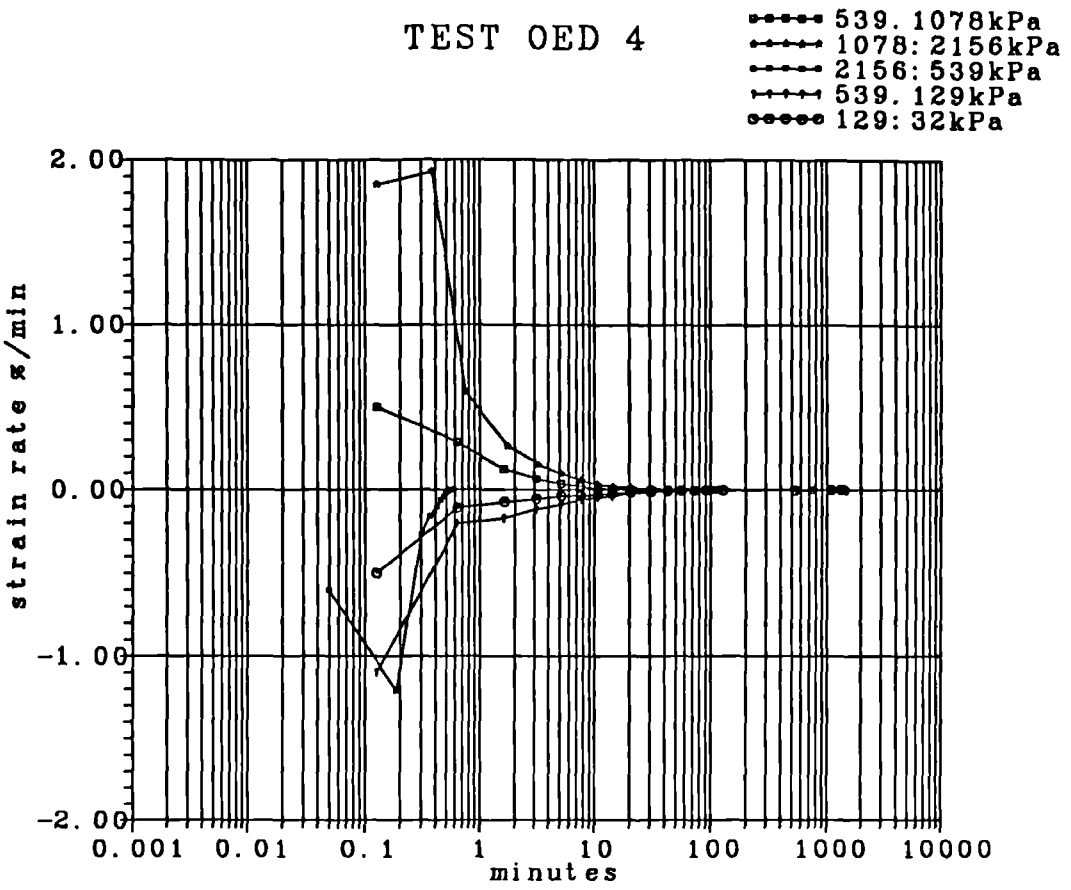

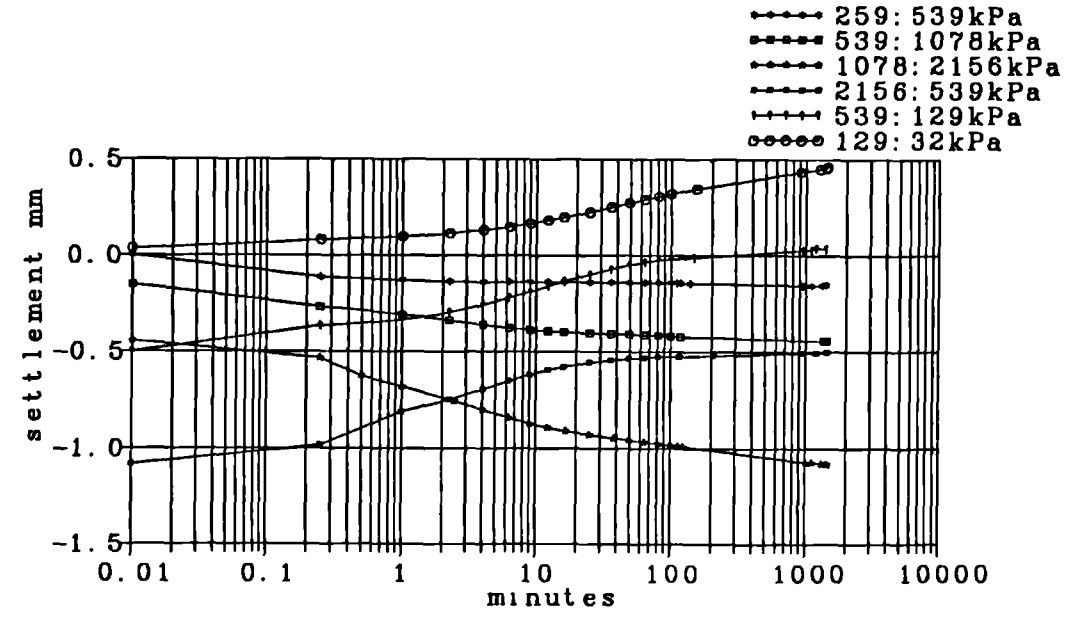

d

Fig.6.28. Consolidation curves and strain rates logged in the OED tests on the undisturbed Pappadai clay.

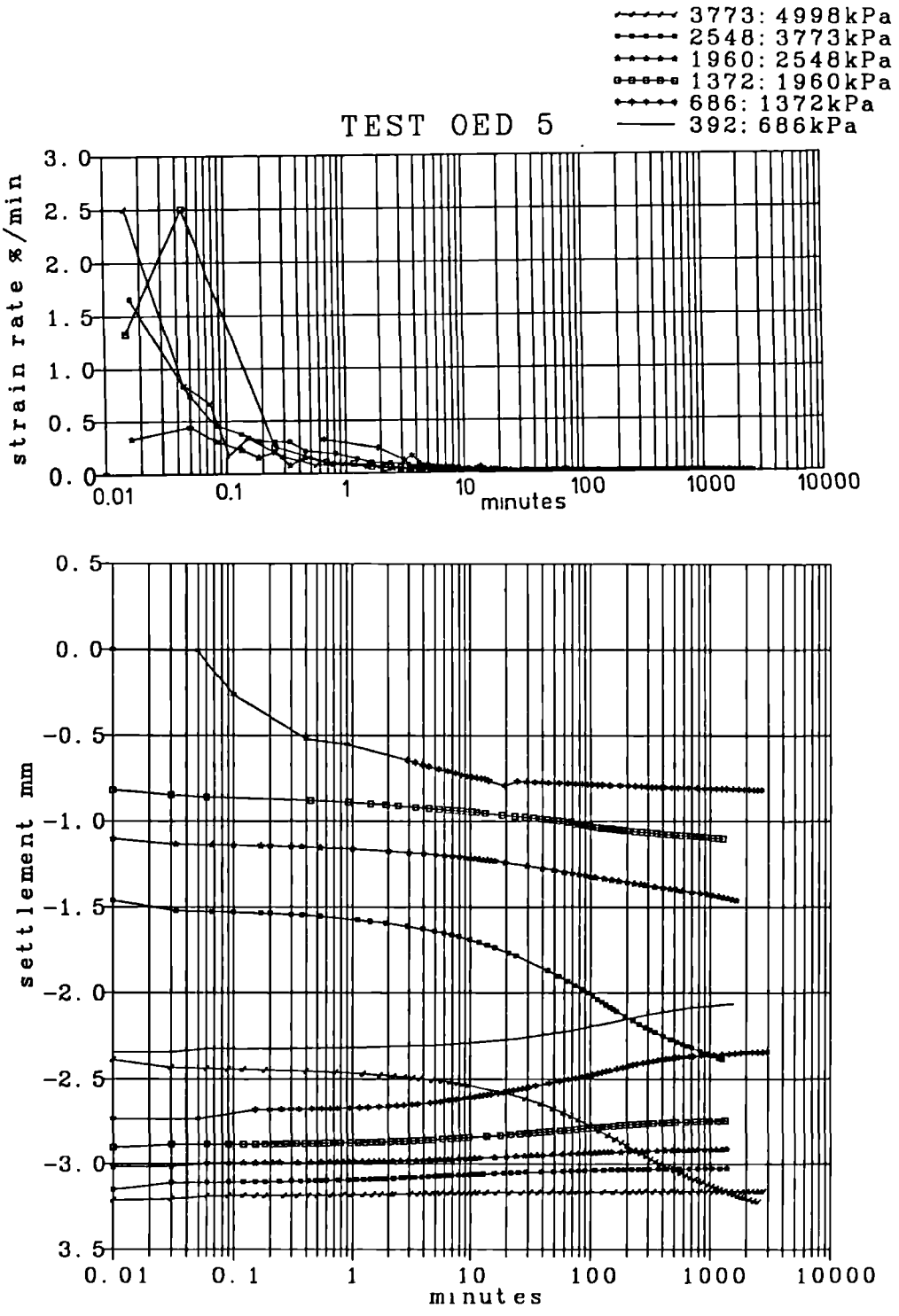

Fig.6.28. Consolidation curves and strain rates logged in the OED tests on the undisturbed Pappadai clay.

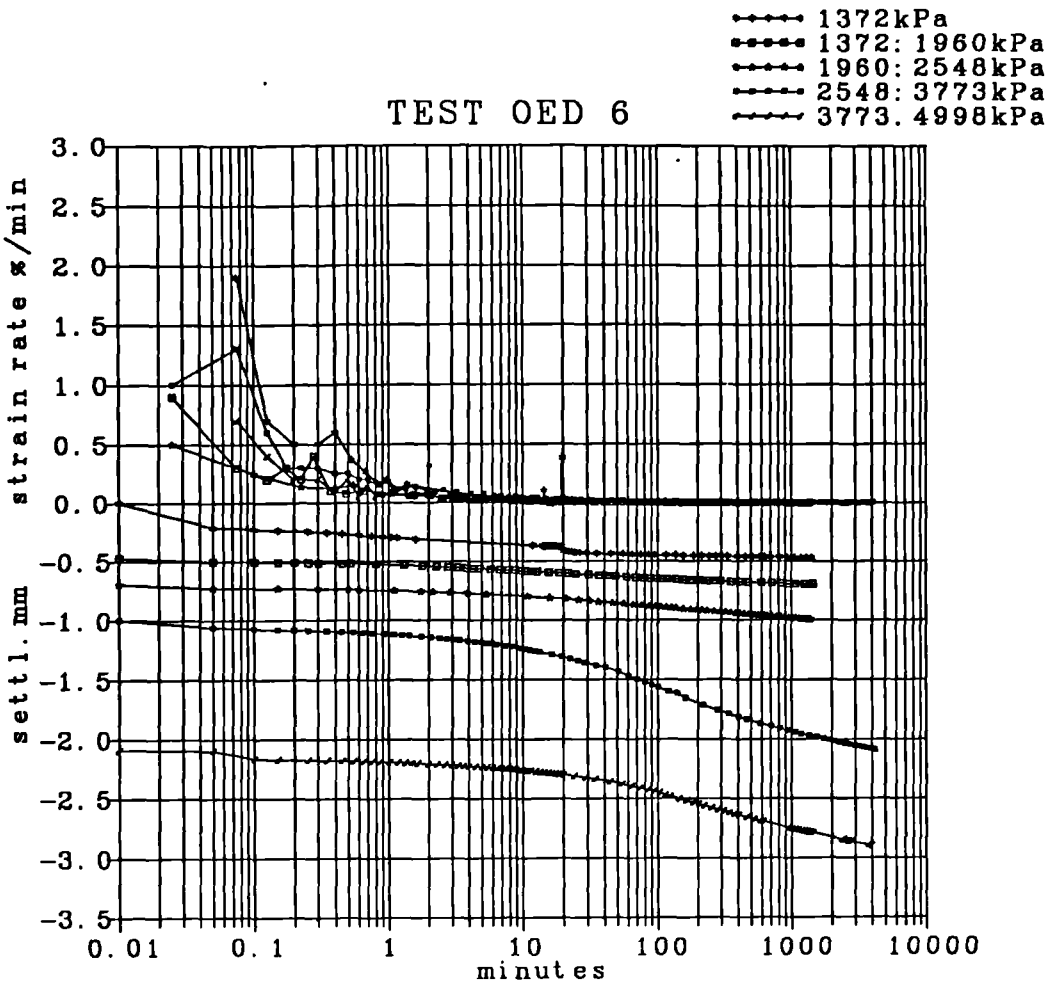

f

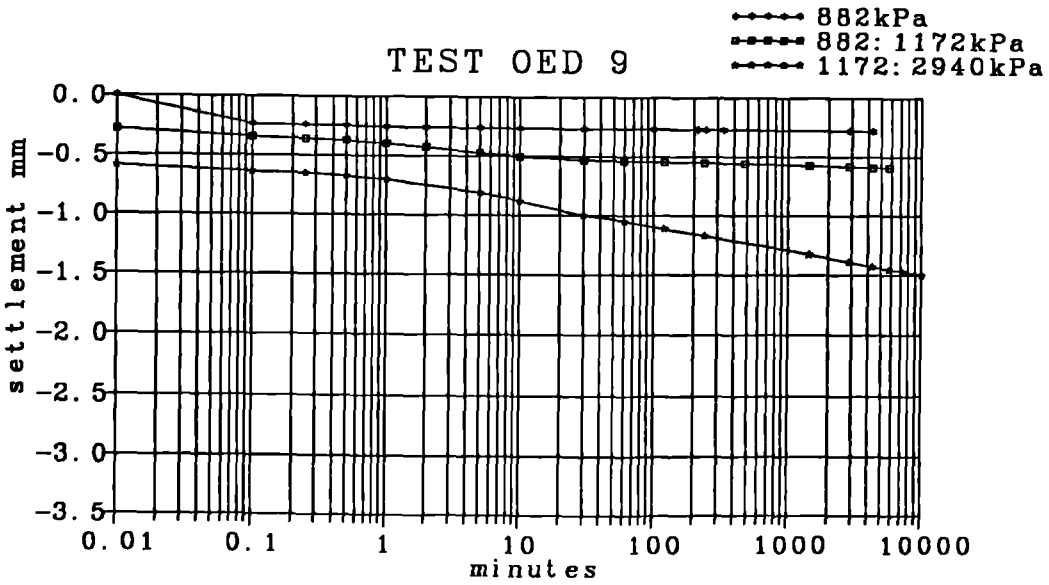

g

Fig.6.28. Consolidation curves and strain rates logged in the OED tests on the undisturbed Pappadai clay.

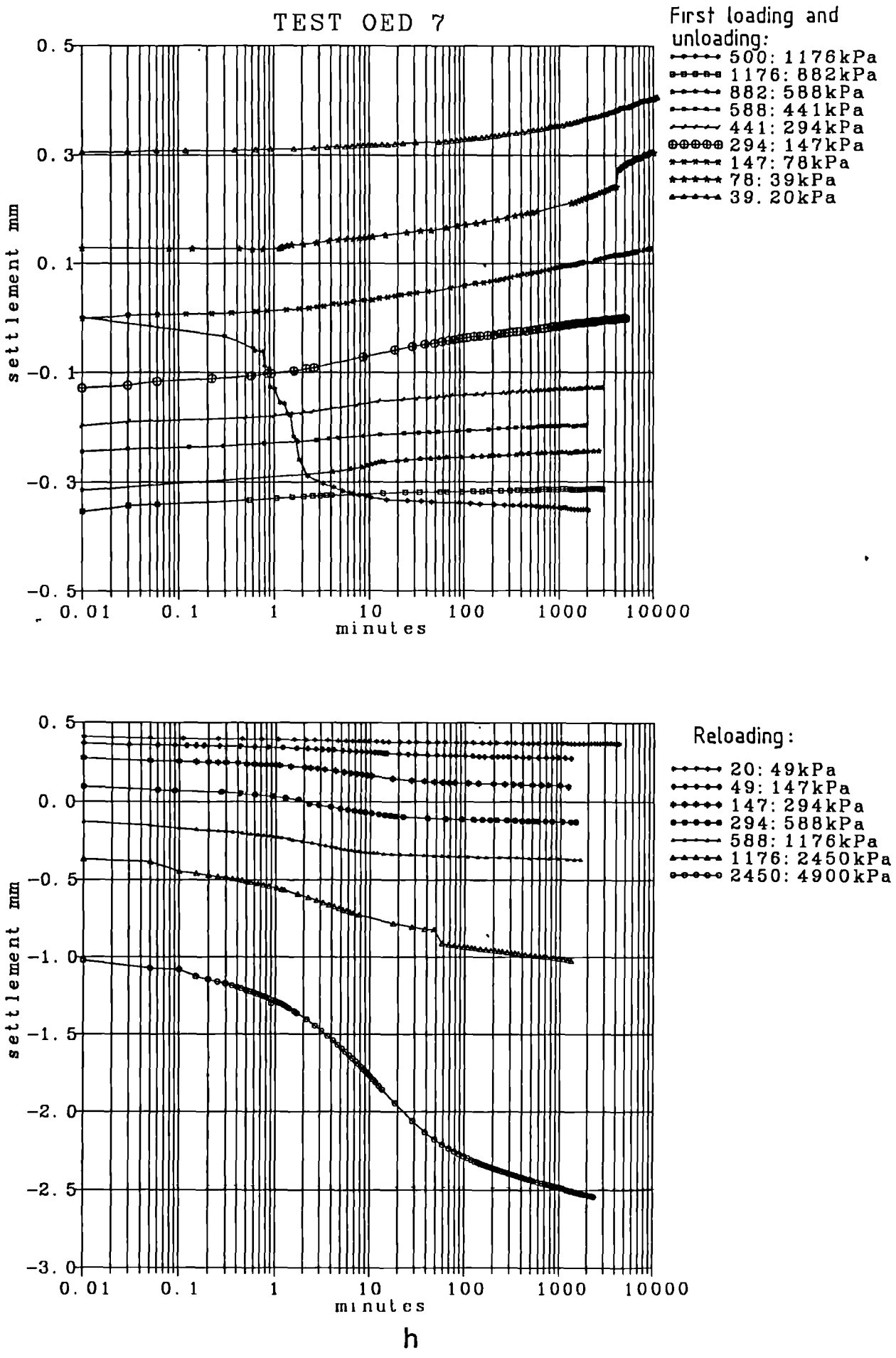

Fig.6.28. Consolidation curves and strain rates logged in the OED tests on the undisturbed Pappadai clay.

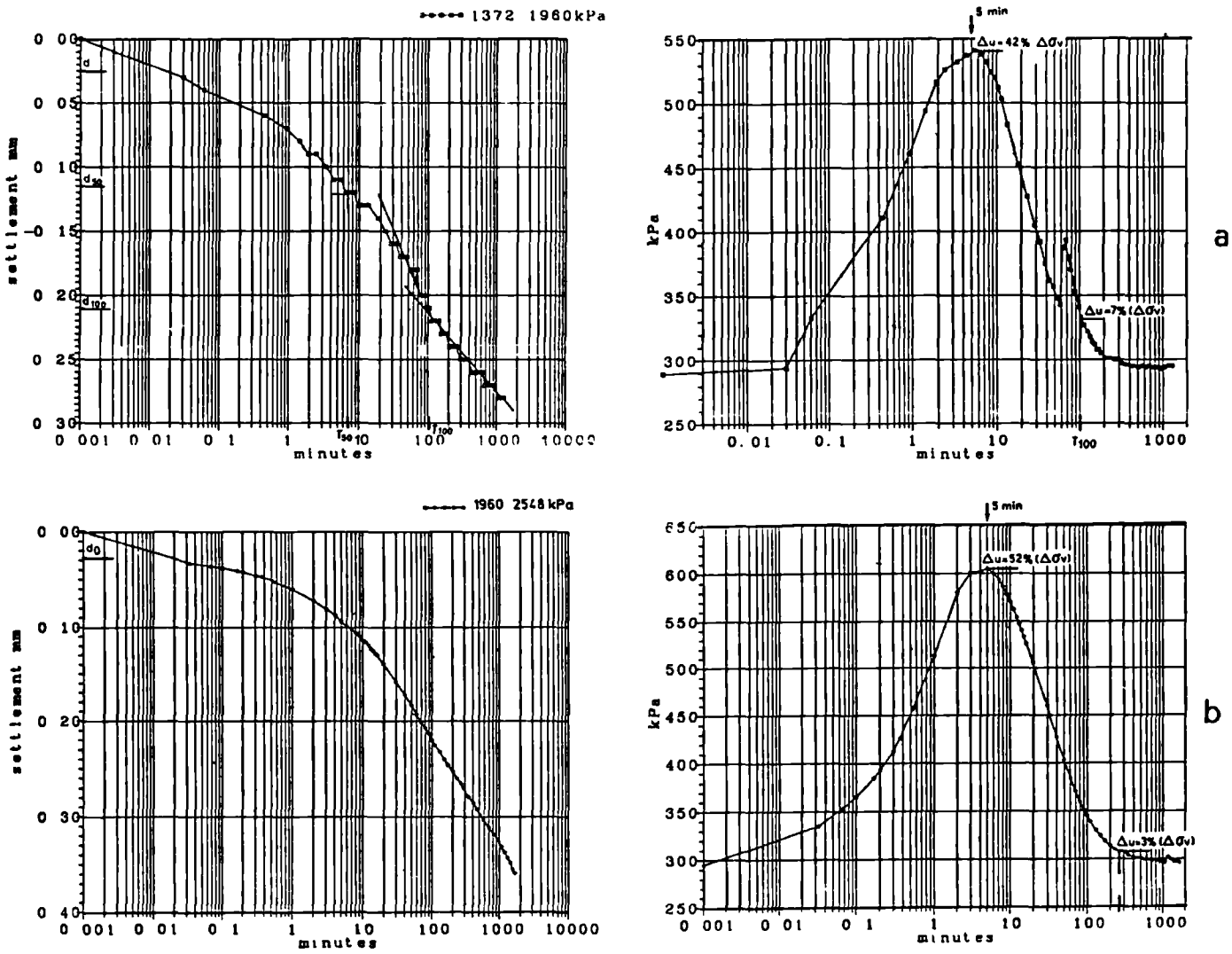

Fig.6.29. Test OED5 : raw settlements and base pore water pressures

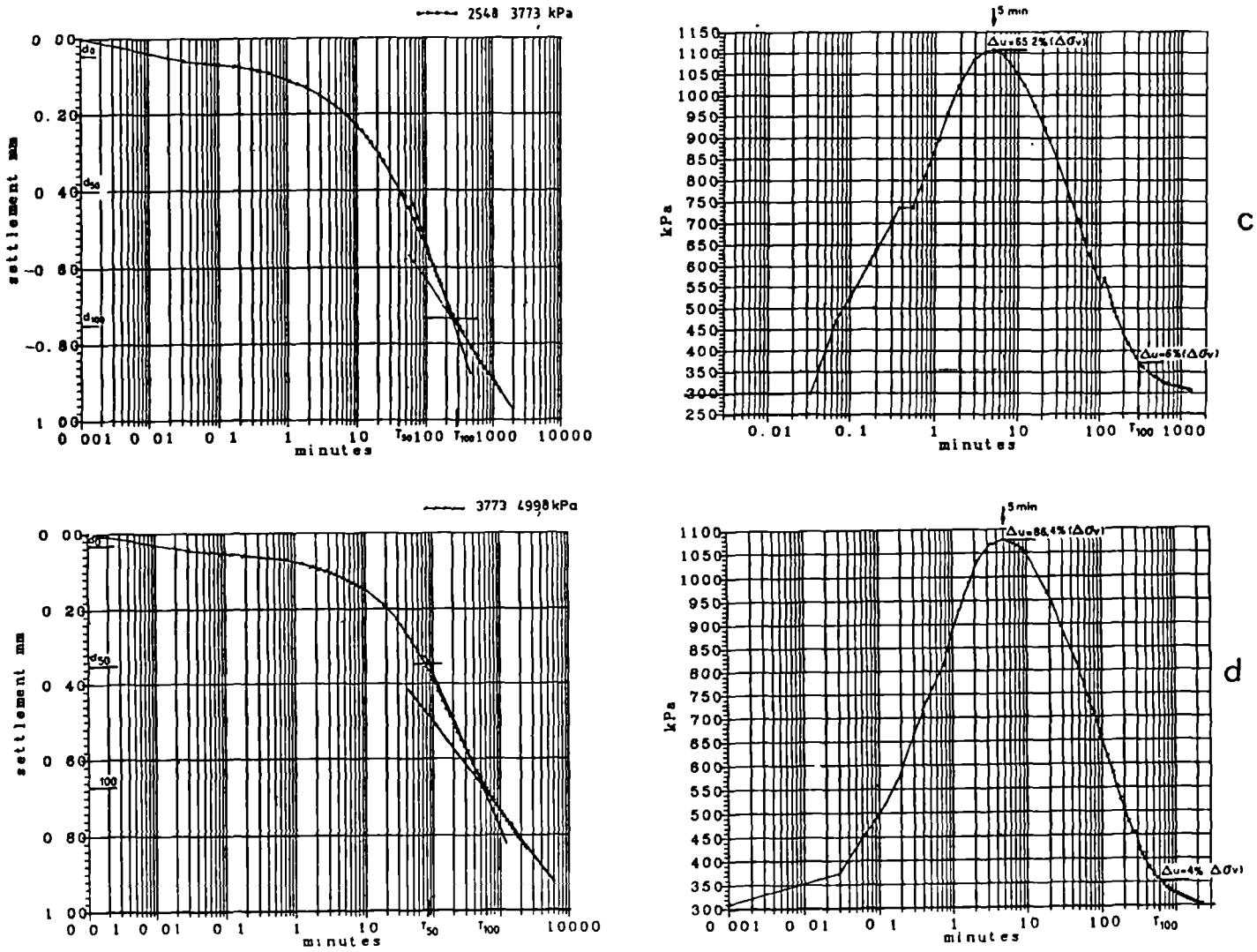

Fig.6.29. Test OED5 : raw settlements and base pore water pressures.

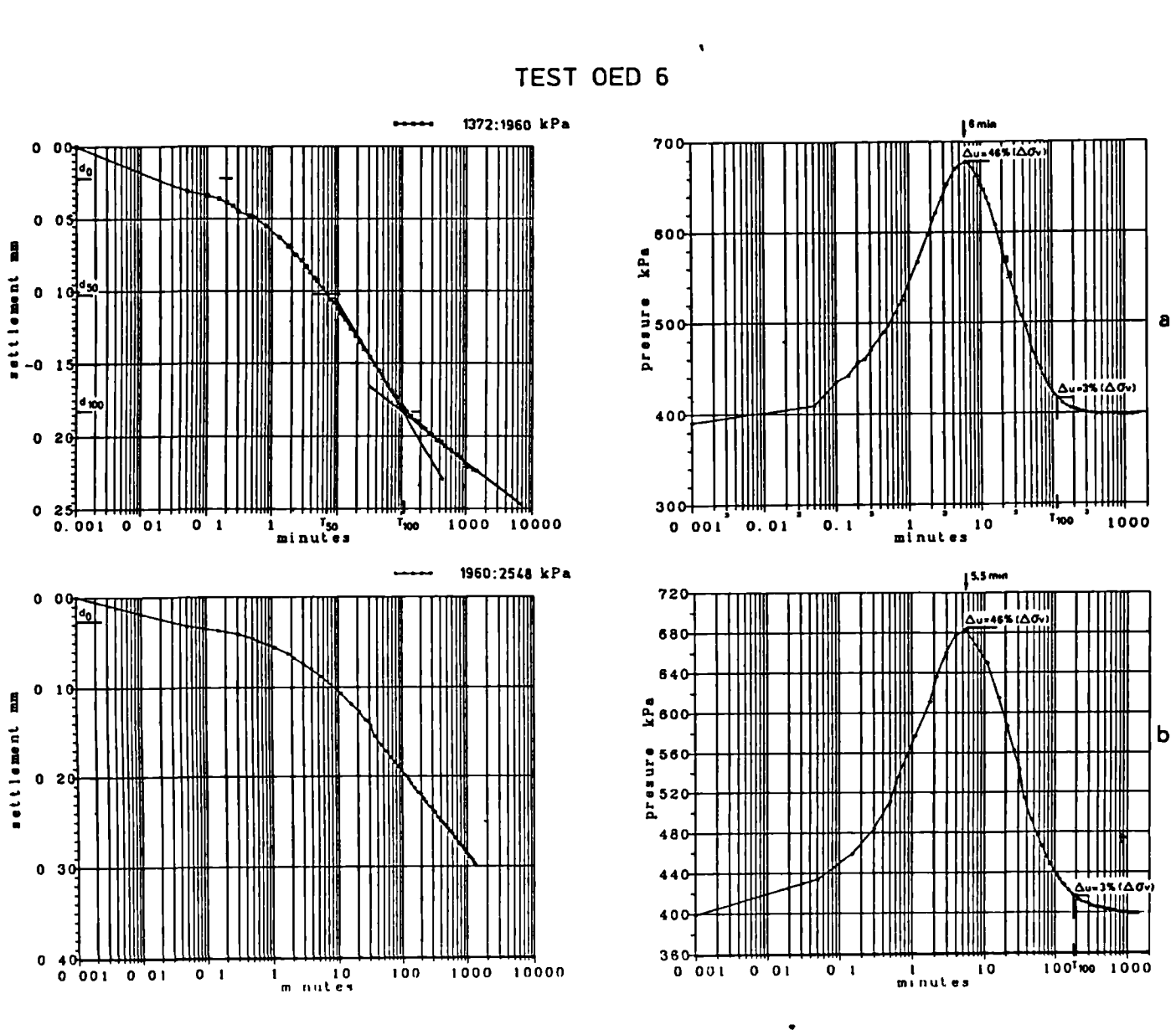

Fig 6.30. Test OED6 : raw settlements and base pore water pressures.

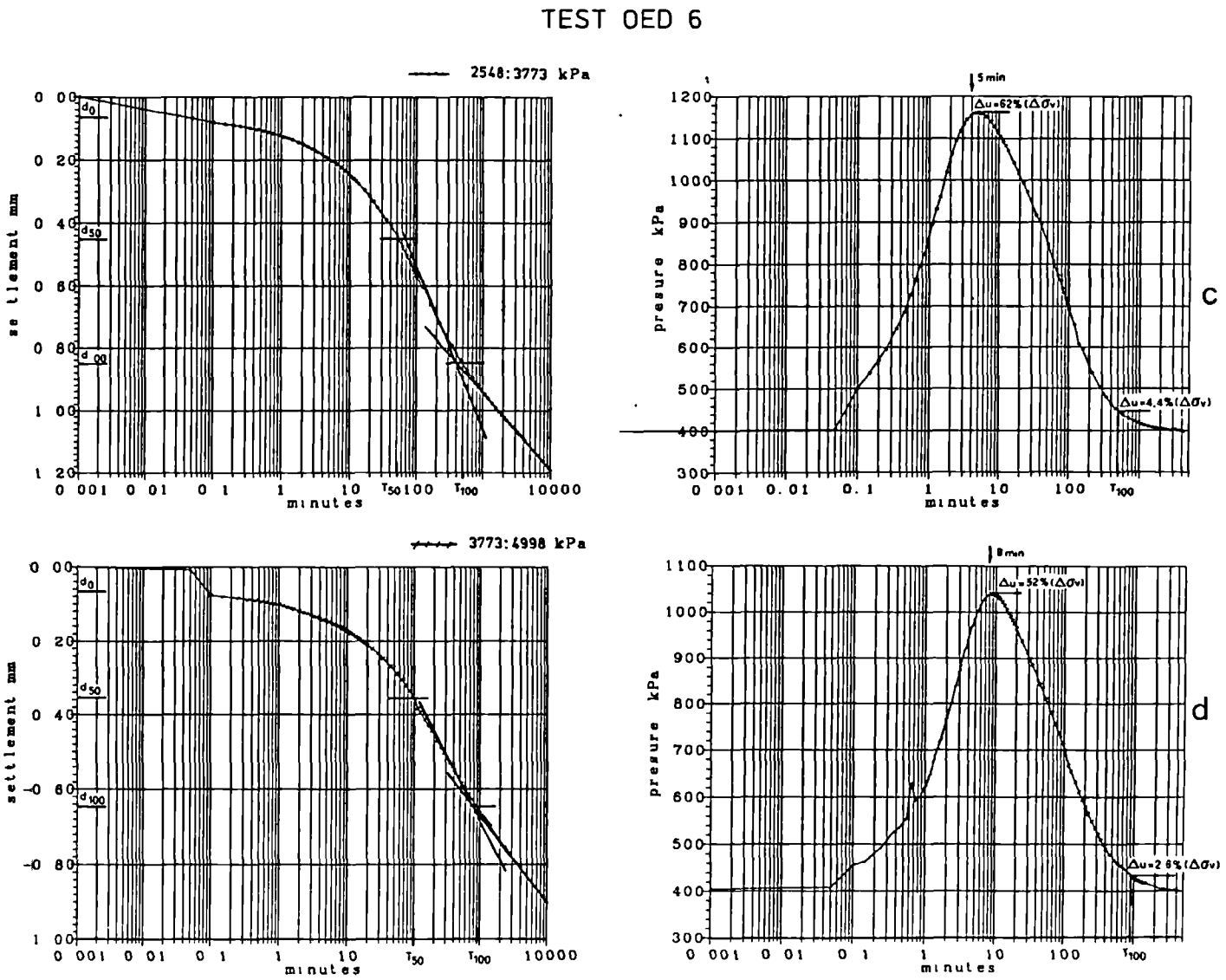

Fig.6.30. Test OED6 : raw settlements and base pore water pressures

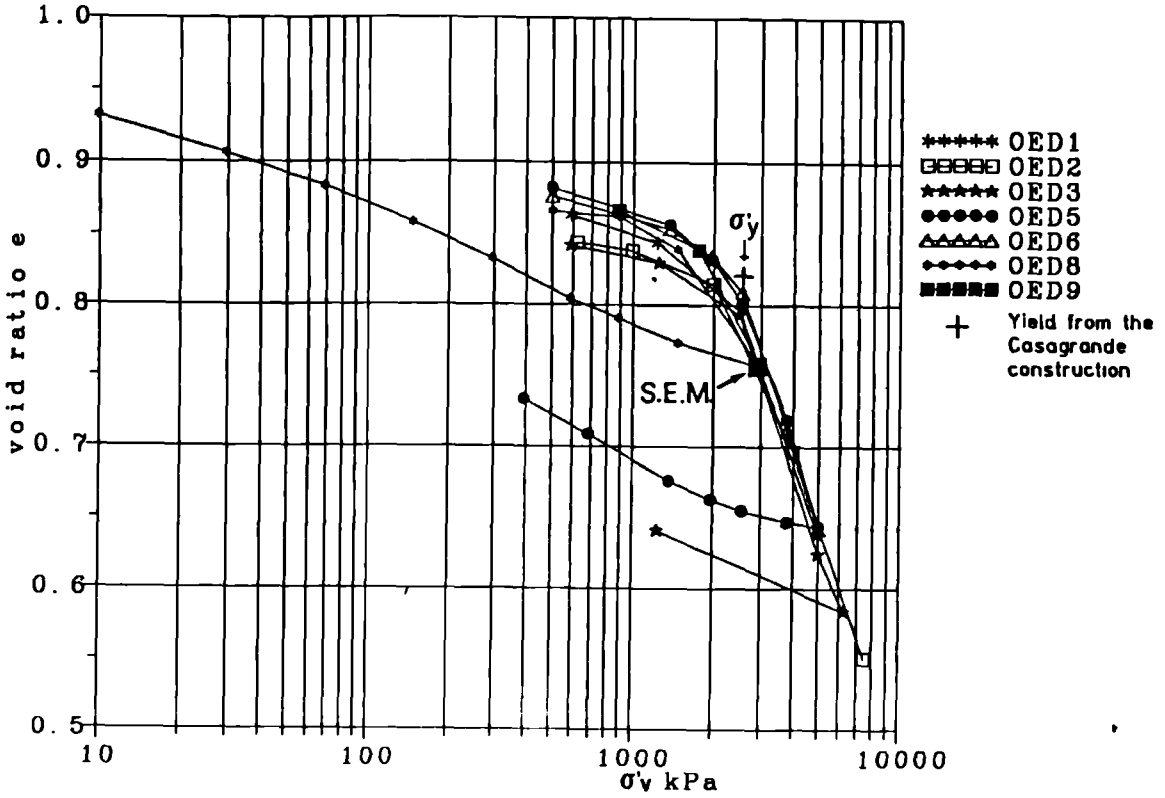

Fig.6.31. OED tests on the undisturbed clay : compression and swelling curves. σ'_y as measured by means of the Casagrande construction (1936); the OED9 specimen was subjected to SEM analysis after compression.

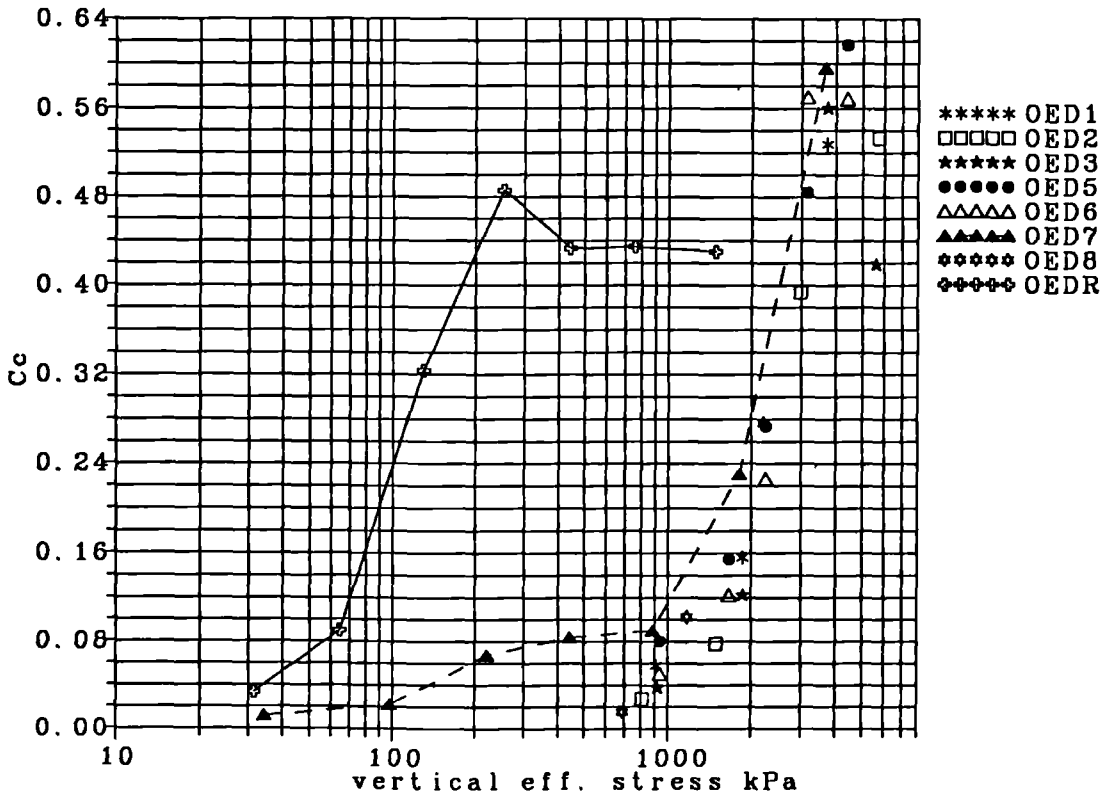

Fig.6.32. OED tests on the undisturbed and reconstituted clay : C_c values.

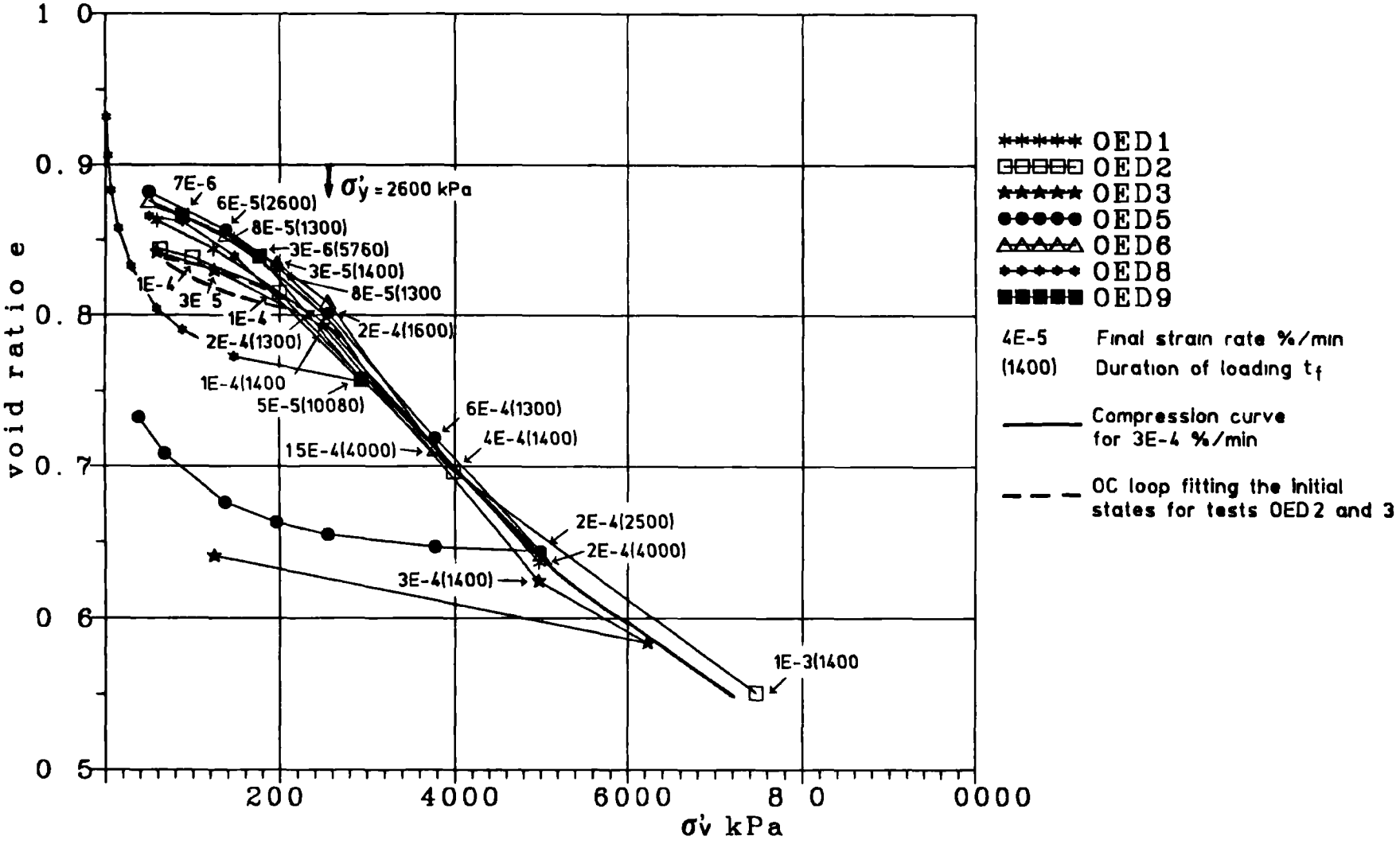

Fig.6.33 OED tests on the undisturbed clay : compression curves, duration of the loading steps and current strain rates. σ'_y as measured in the linear plots immediately before the points of minimum stiffness

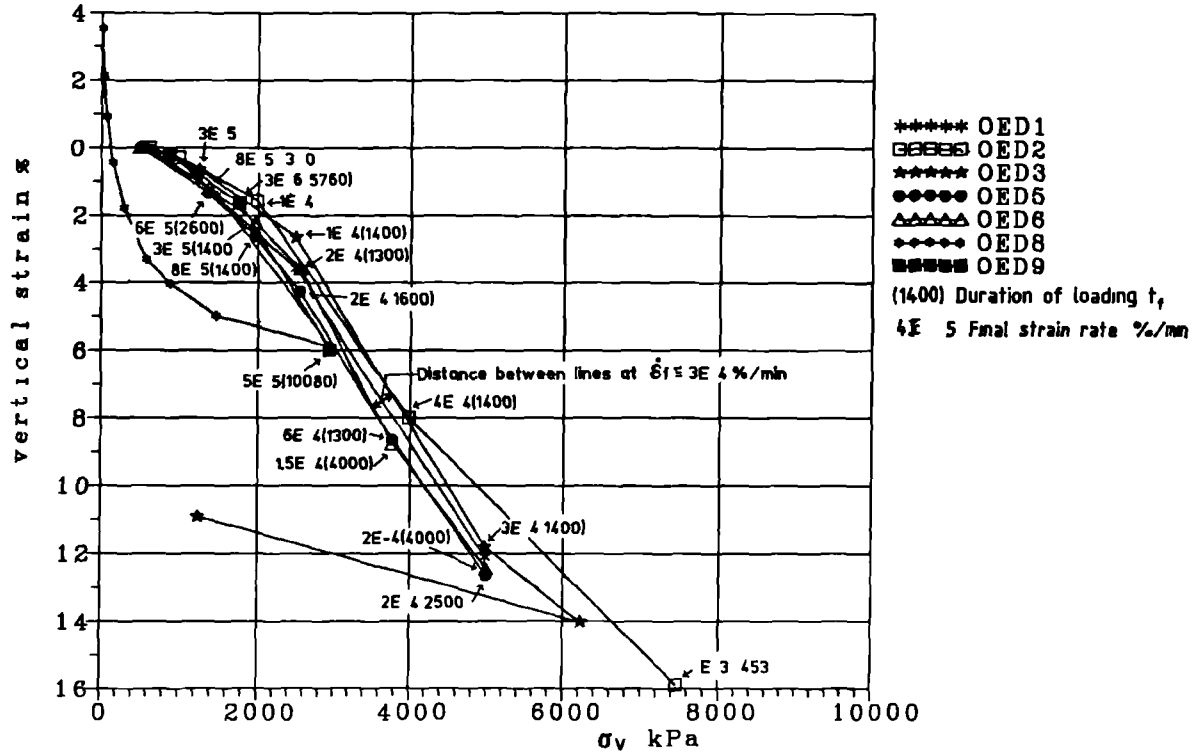

Fig 6 34 OED tests on the undisturbed clay. compression curves, duration of the loading steps and current strain rates

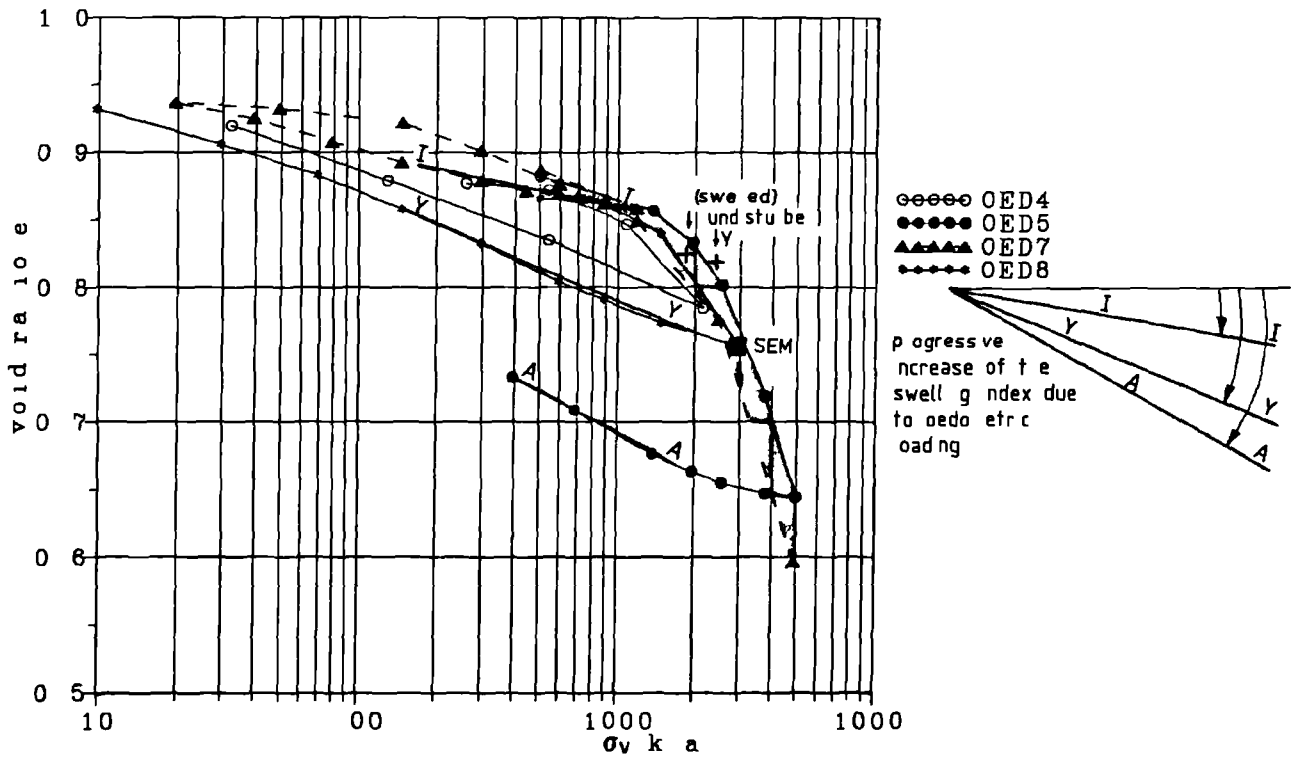

Fig 6 35 Natural Pappadai clay effects of swelling before compression on the OED compression curve and effects of the compression beyond yielding on the swelling index.

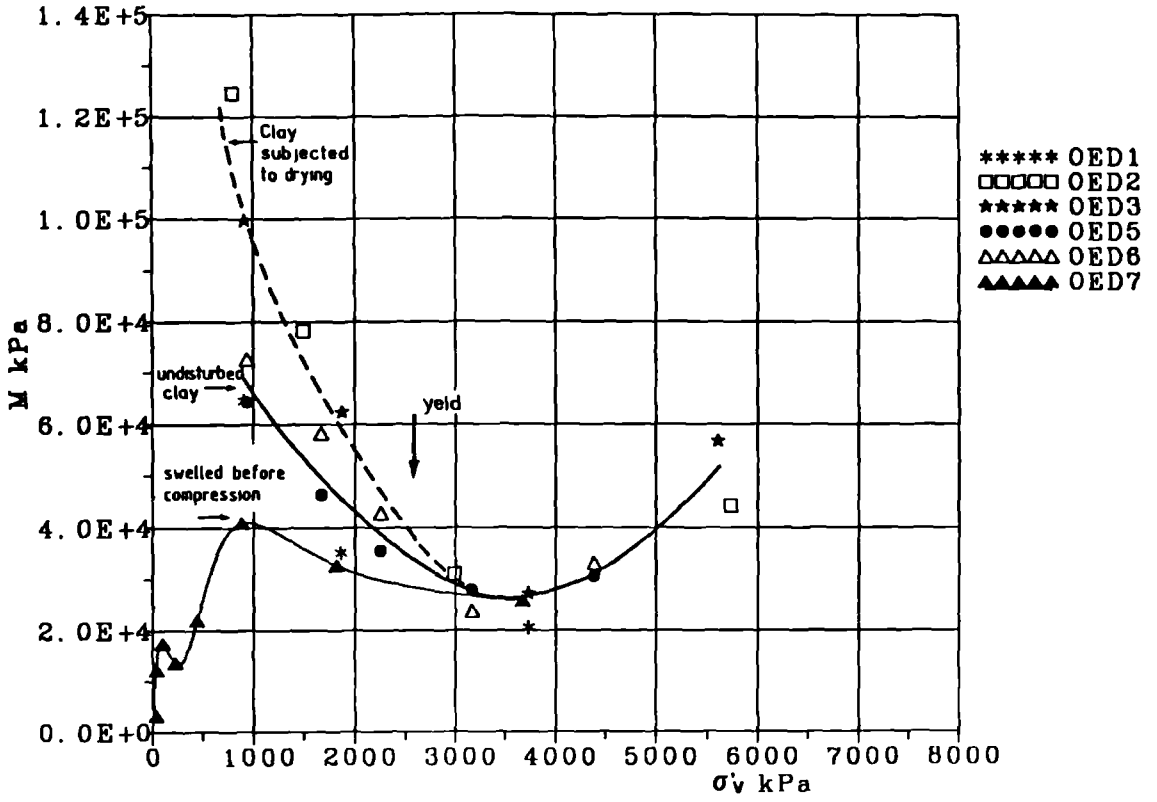

Fig.6.36. OED tests on the natural clay: measured oedometric stiffnesses M.

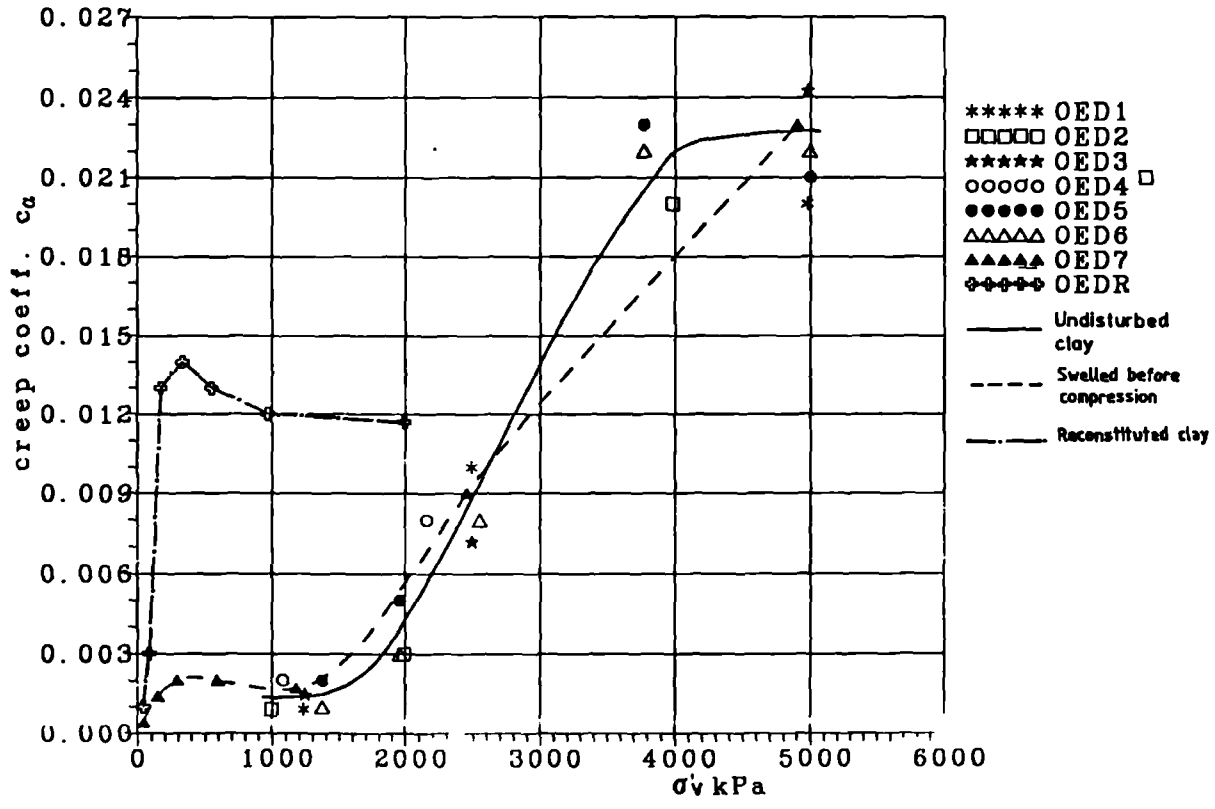

Fig.6.37. OED tests on the natural clay : c_α values.

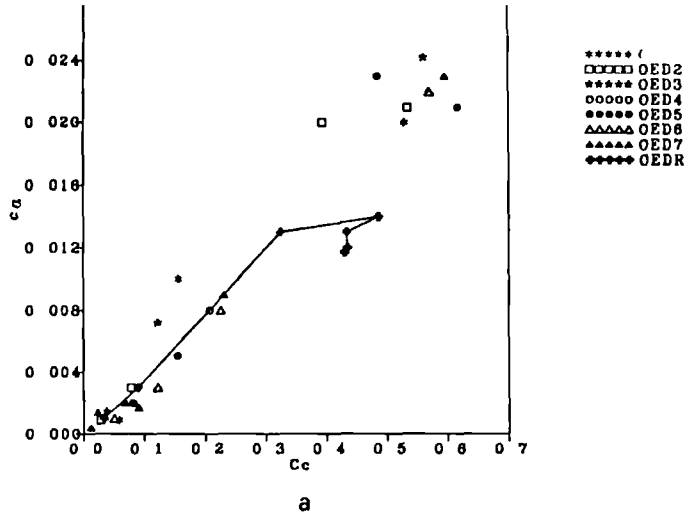

a

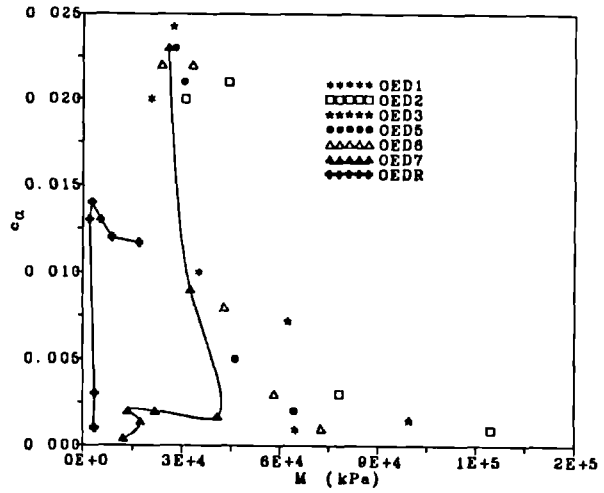

b

Fig.6.38. Natural Pappadai clay : variation of c_α with the compression index C_c (a) and the oedometric stiffness M (b).

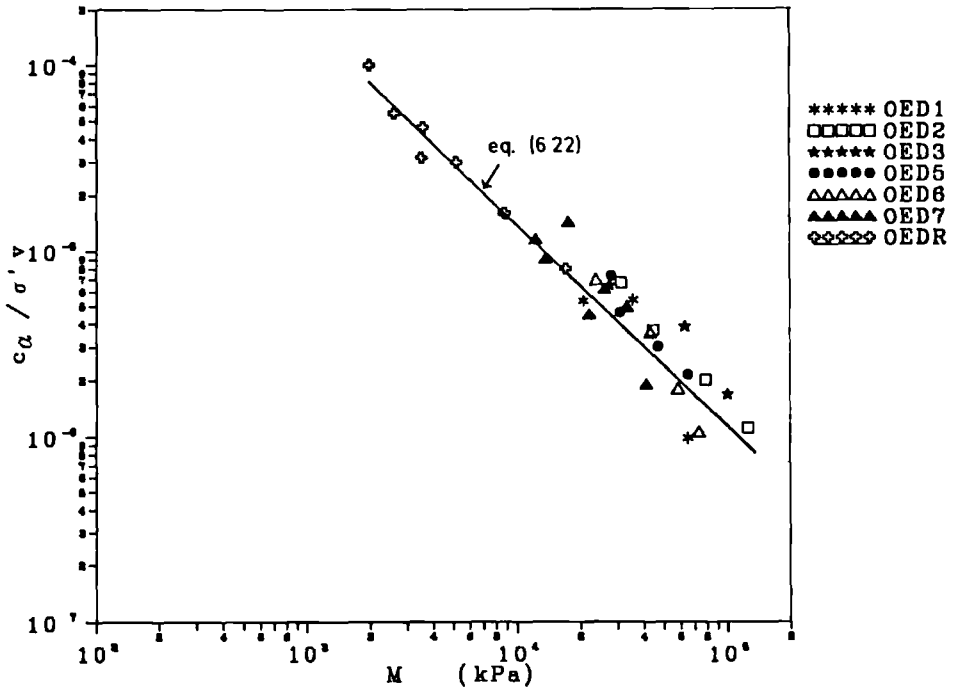

Fig.6.39. Natural Pappadai clay . c_α-σ'_v-M relationship.

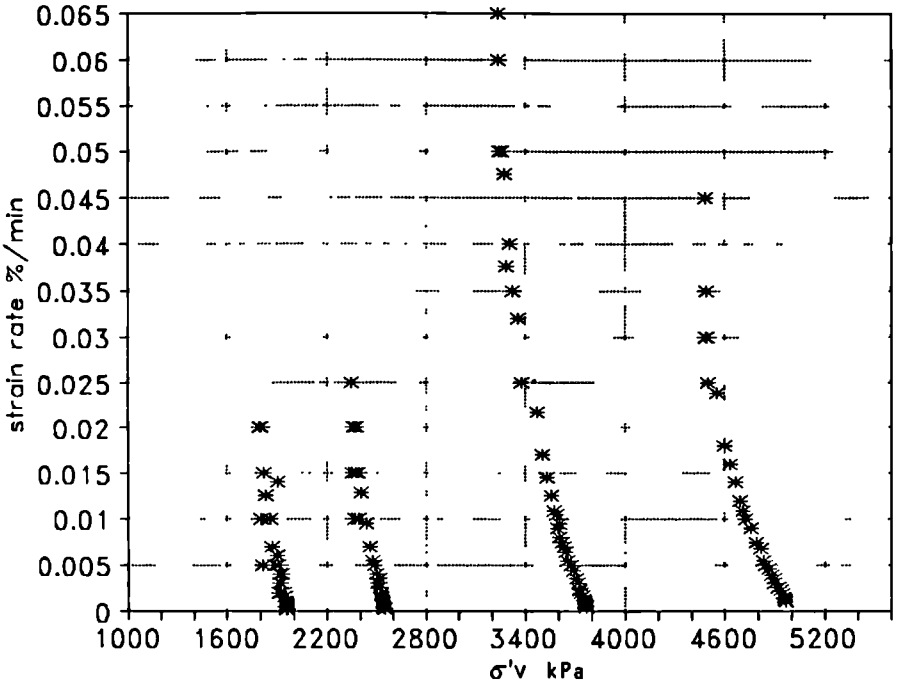

a

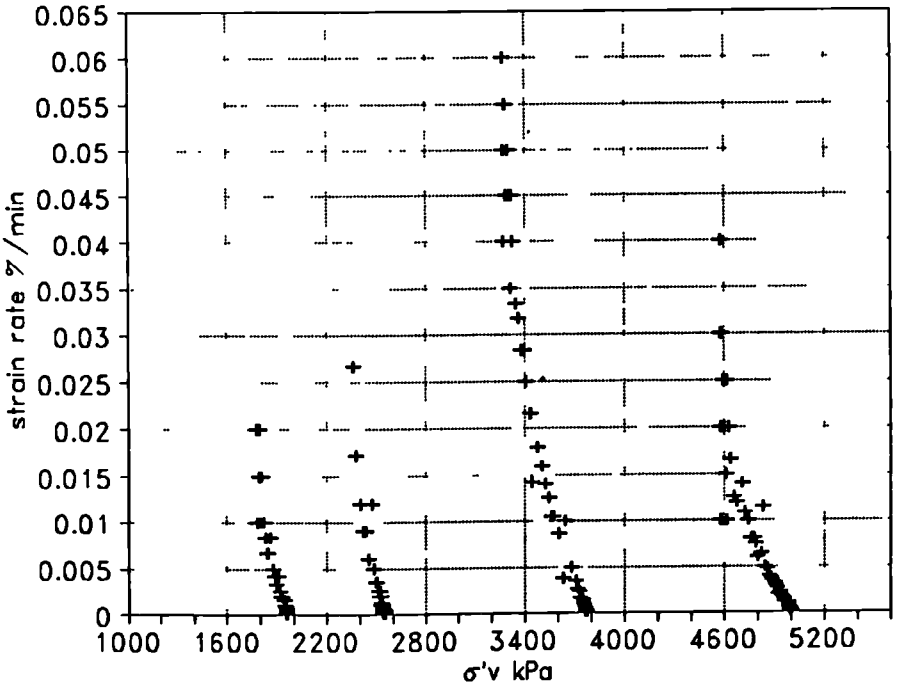

b

Fig.6.40. Tests OED 5 (a) and OED6 (b): strain rates; σ'_v as resulting from eq.(6.17).

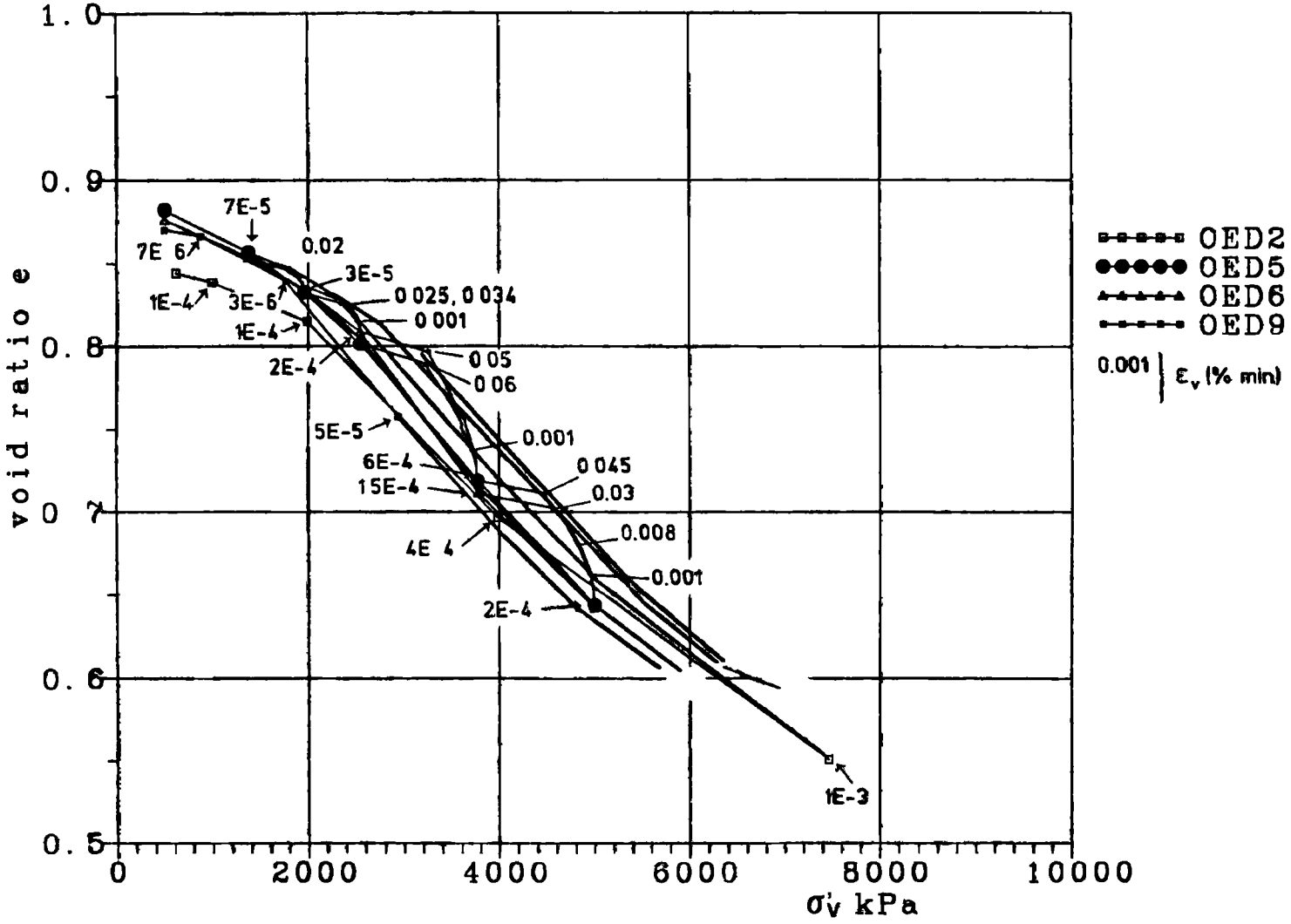

Fig.6.41. OED tests : black are both the compression curves relating the states at the end of the loading steps and the intermediate state paths (tests OED 5 and 6) during consolidation and creep. The red curves represent compressions at constant strain rate (isotacae).

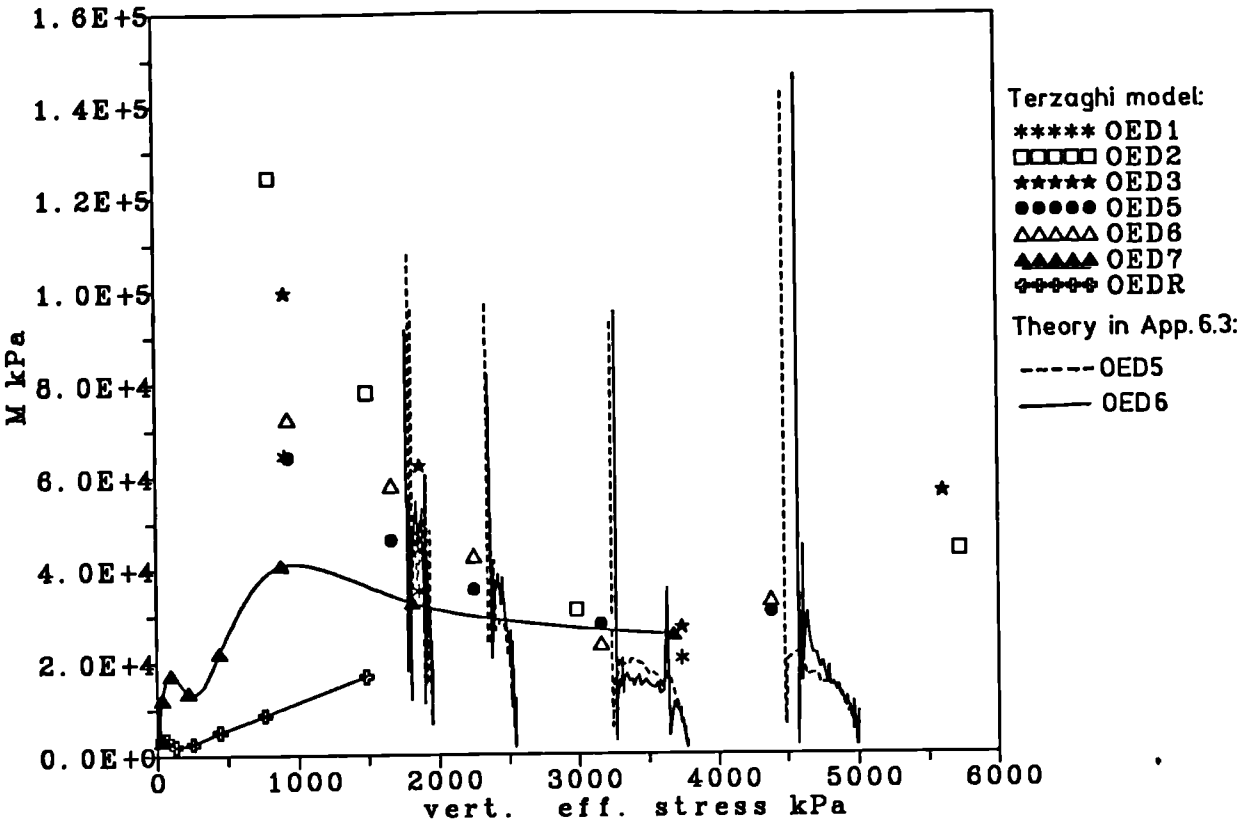

Fig.6.42. OED loading steps : average values of the oedometric stiffness M and variations of M during the single loading steps (tests OED 5 and 6; Appendix 6.3).

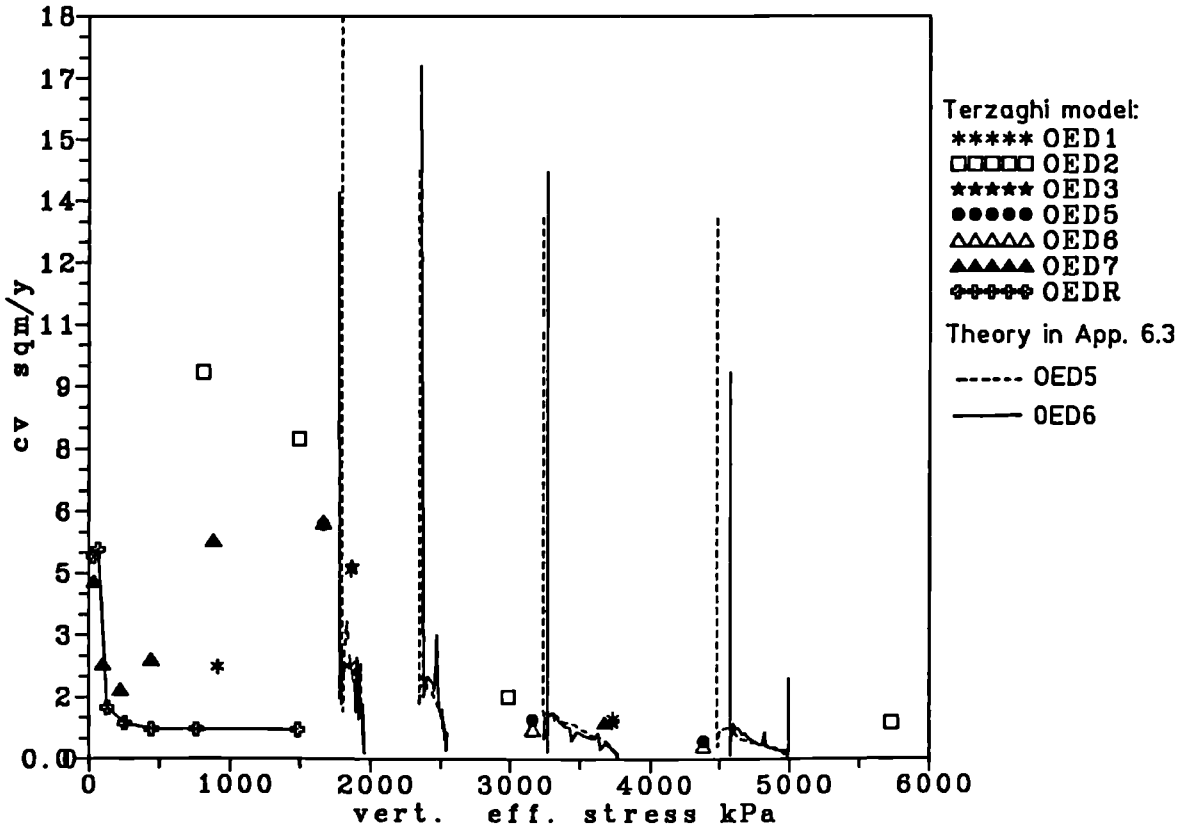

Fig.6.43. OED loading steps : values of c_v from the Terzaghi model and c_v variations in the single loading steps (tests OED 5 and 6; Appendix 6.3).

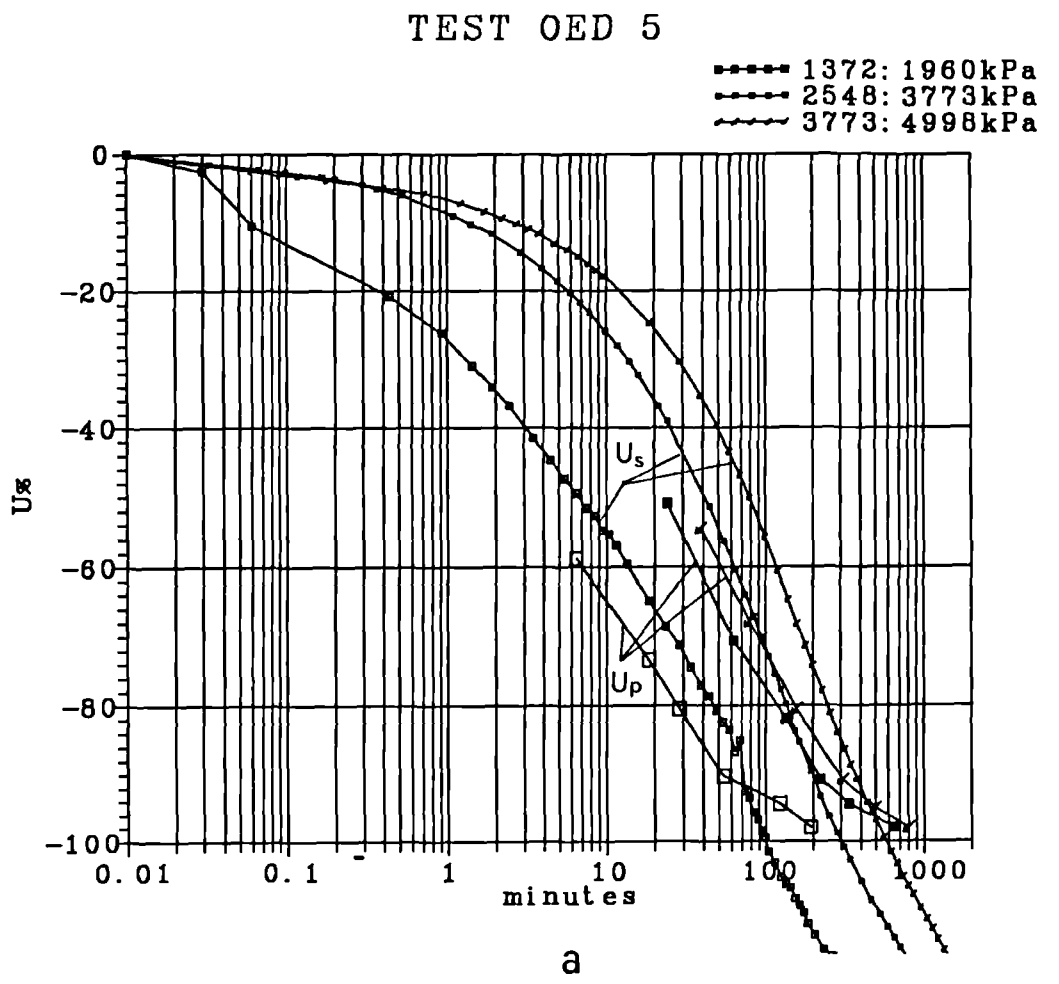

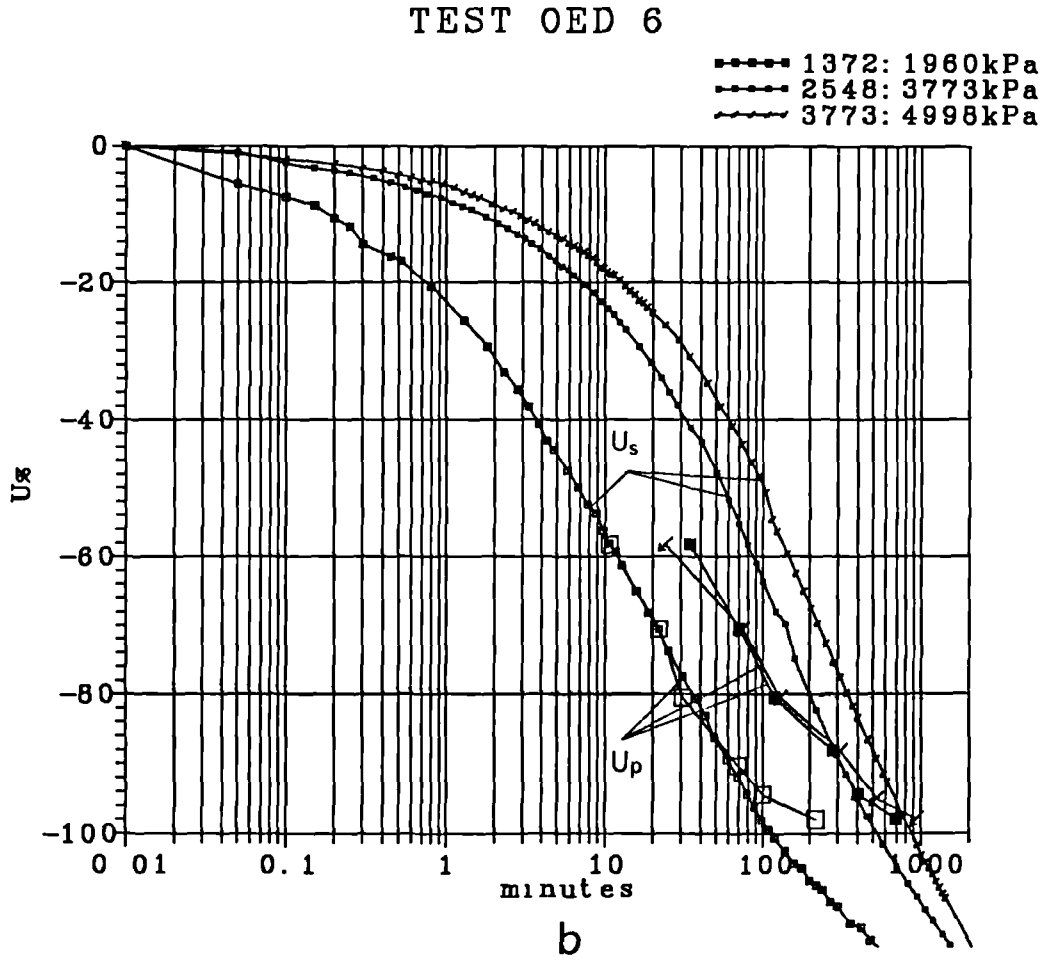

Fig.6.44 Discrepancy between the average consolidation degrees U_s% and U_p% of the Terzaghi model.

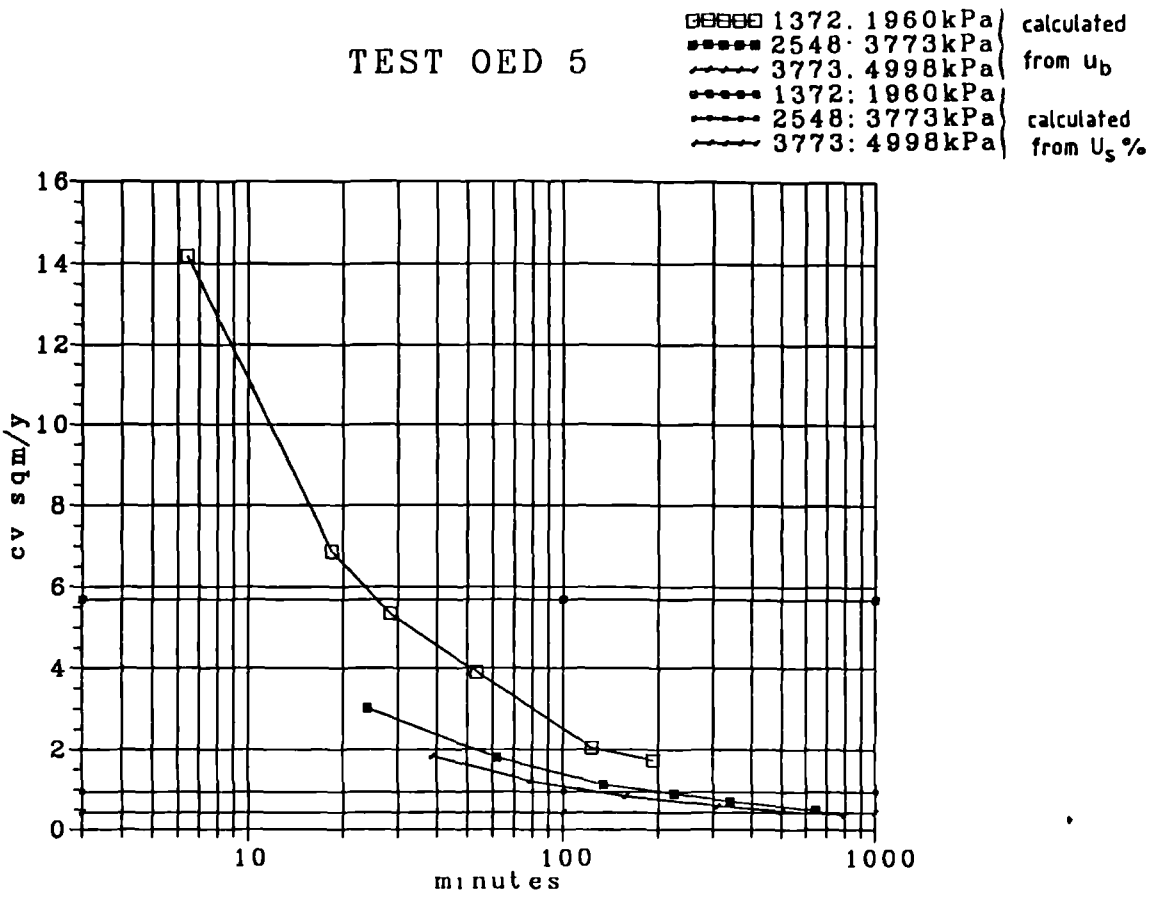

Fig.6.45. Terzaghi model : values of c_v (test OED 5) derived from either the average consolidation degree U_s% or the base pore water pressure (u_b).

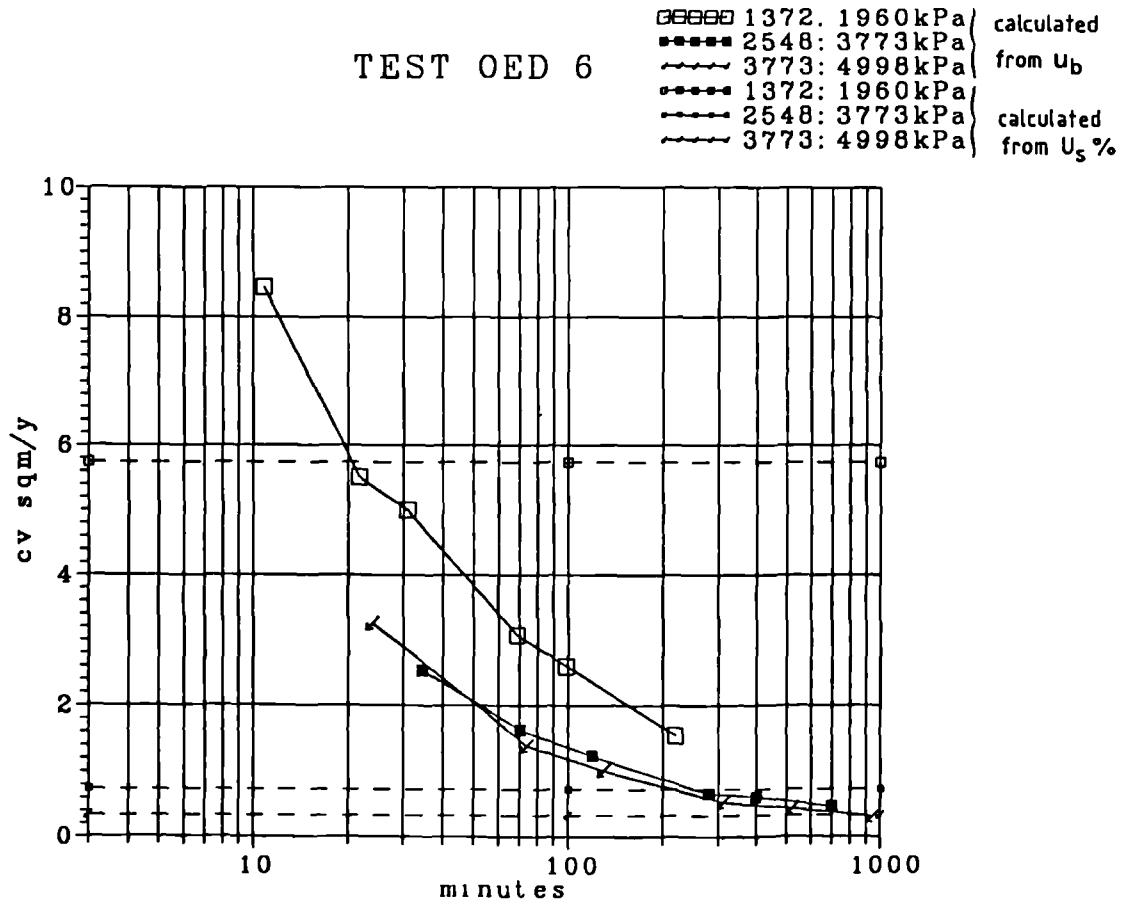

Fig.6.46. Terzaghi model : values of c_v (test OED 6) derived from either the average consolidation degree U_s% or the base pore water pressure (u_b).

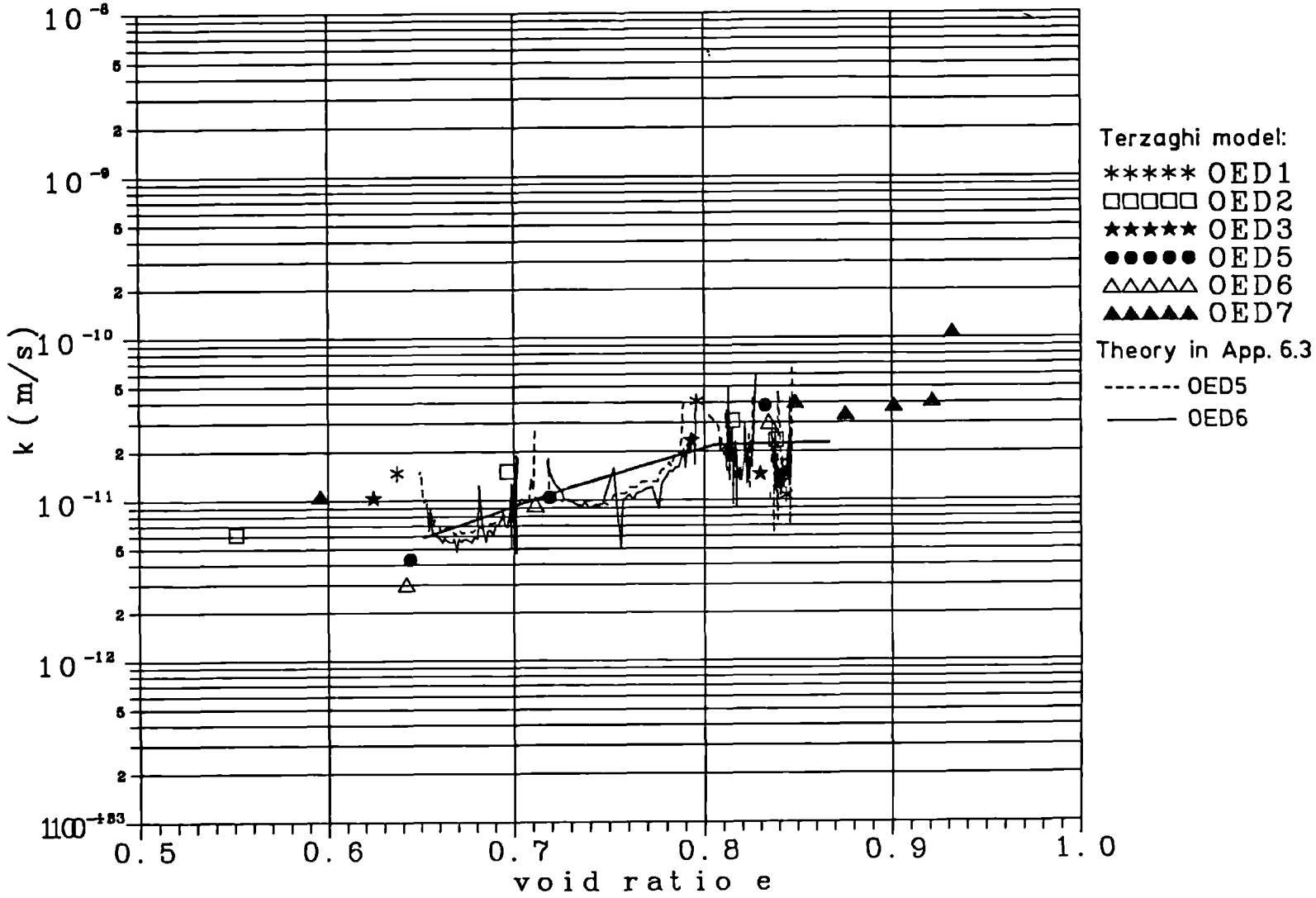

Fig.6.47. OED loading steps : k values from the Terzaghi model and variations of k in the single loading steps (tests OED 5 and 6 Appendix 6.3).

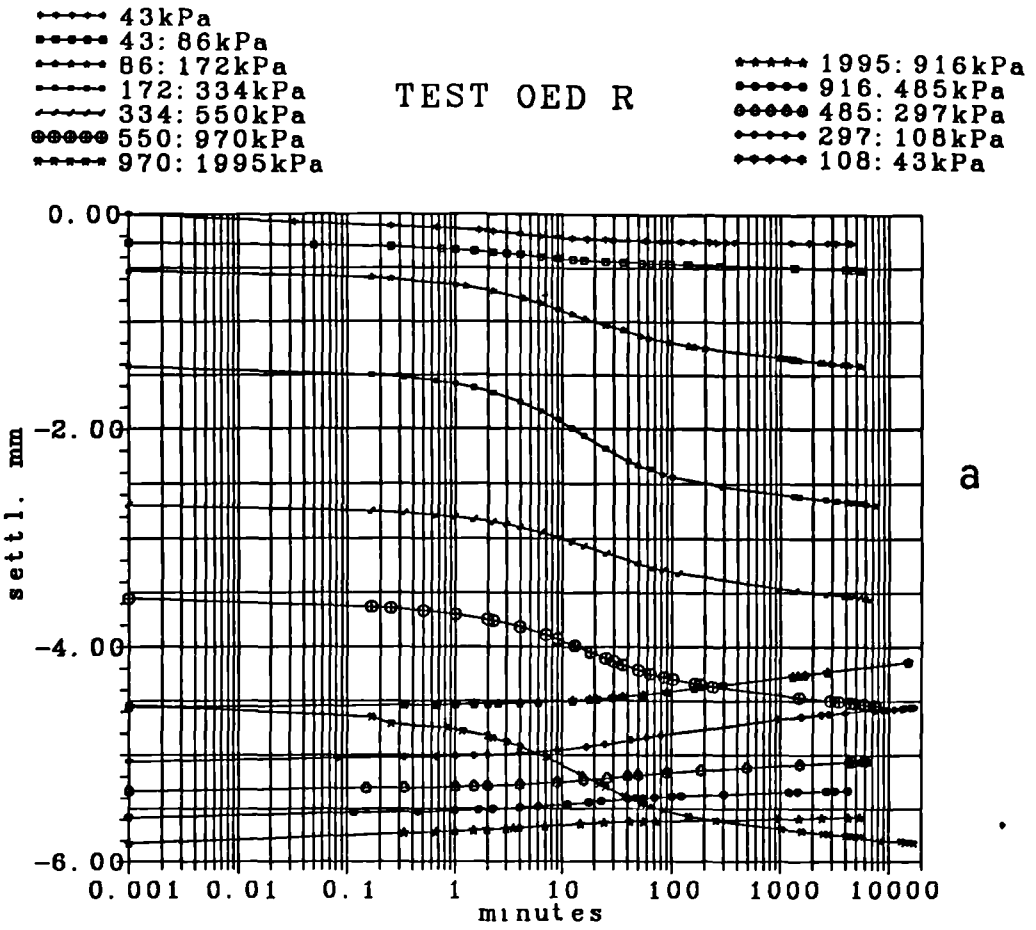

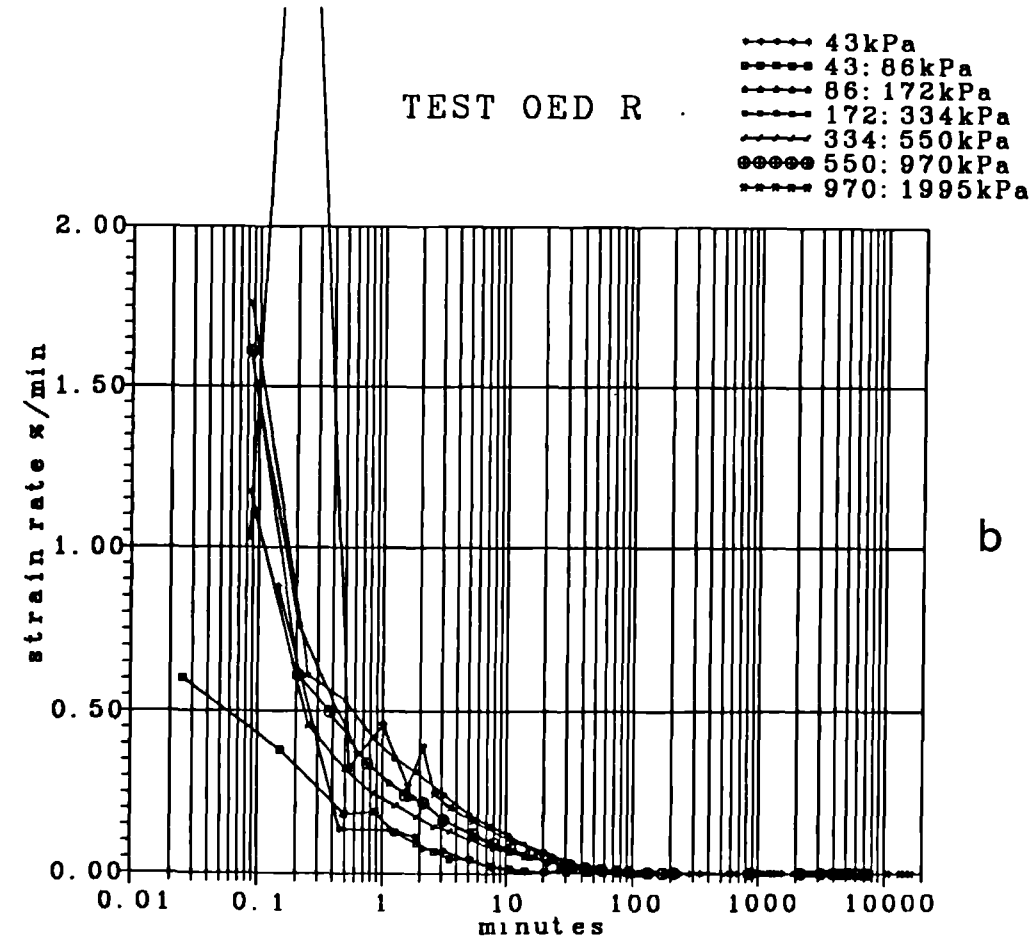

Fig.6.48. Reconstituted clay : (a) consolidation curves; (b) strain rates.

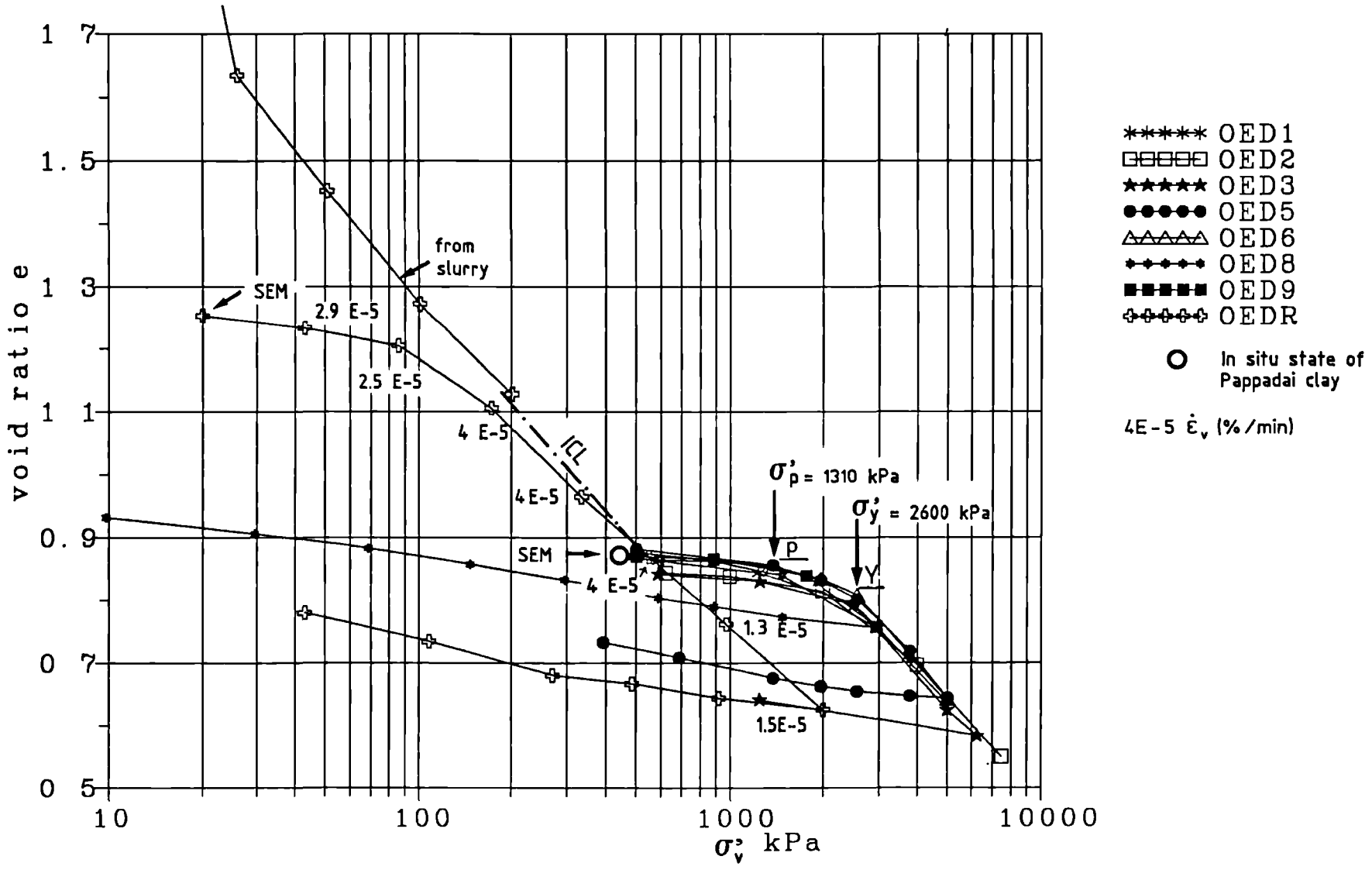

Fig.6 49. Natural and reconstituted clay : OED compression curves. The strain rates at the state points of the OEDR curve are reported.

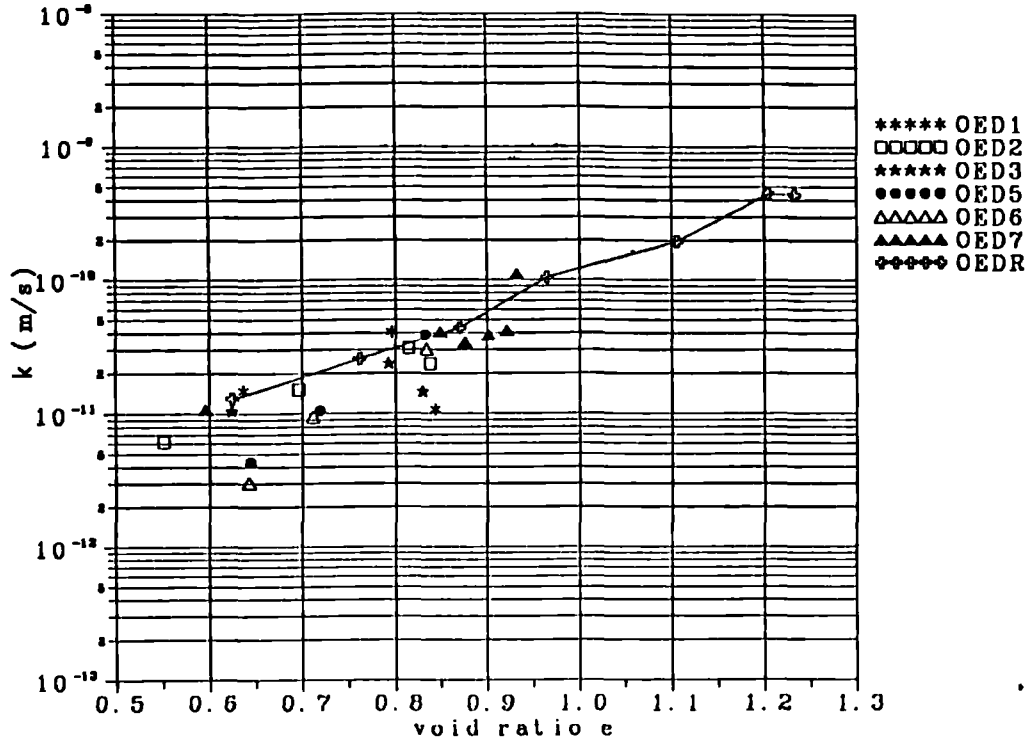

Fig.6.50. Natural and reconstituted clay : values of k from the Terzaghi model.

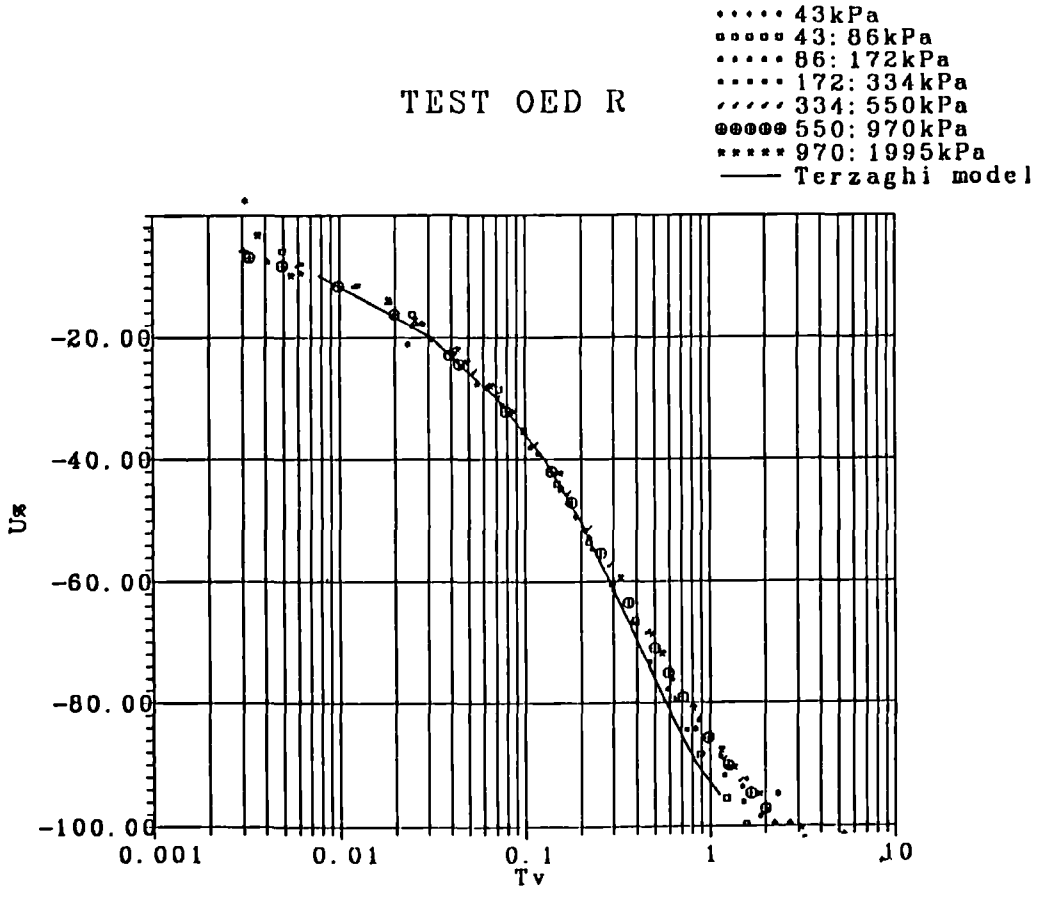

Fig.6.51. Reconstituted clay : comparison between the measured consolidation curves and the Terzaghi predictions.

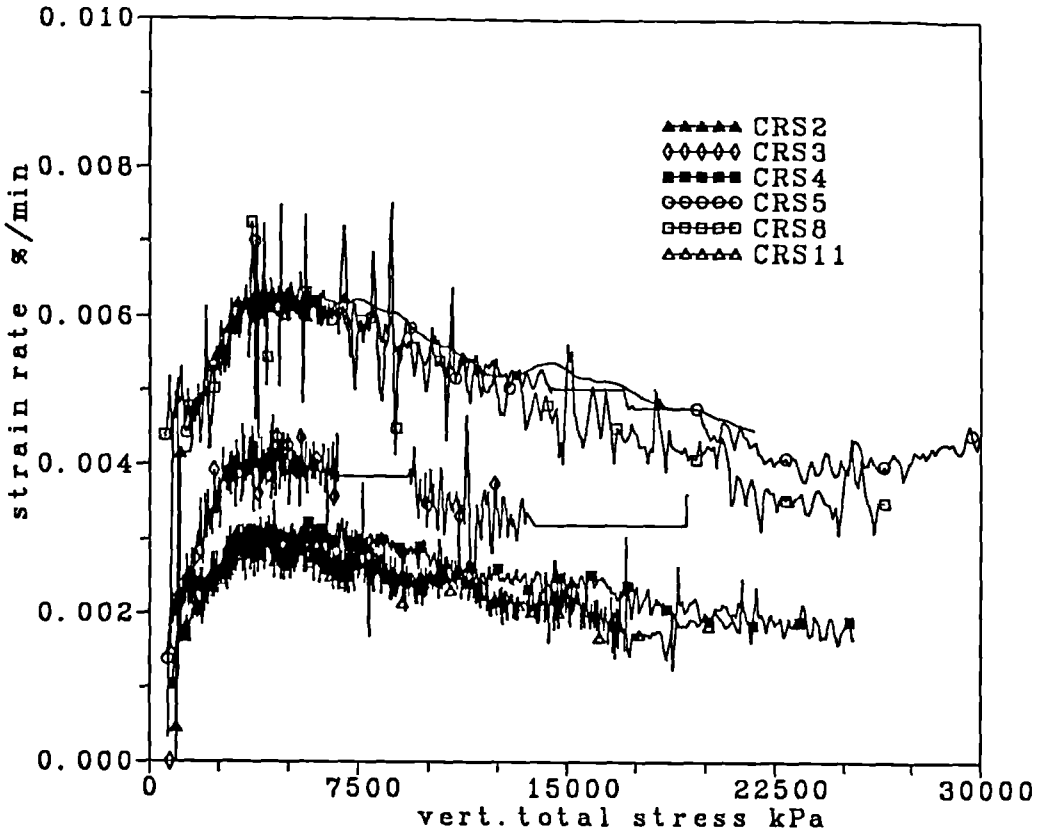

a

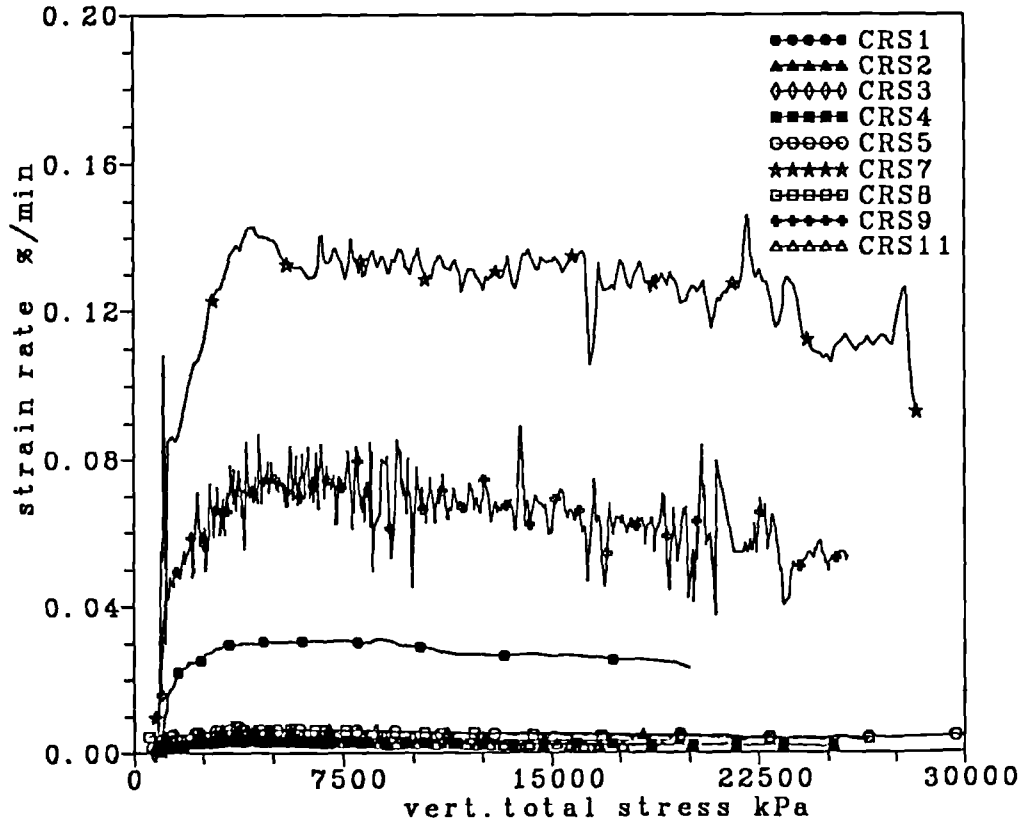

b

Fig.6.52. CRS tests on the undisturbed clay: strain rates; (a) slow tests, (b) all the tests and (c) test CRS6

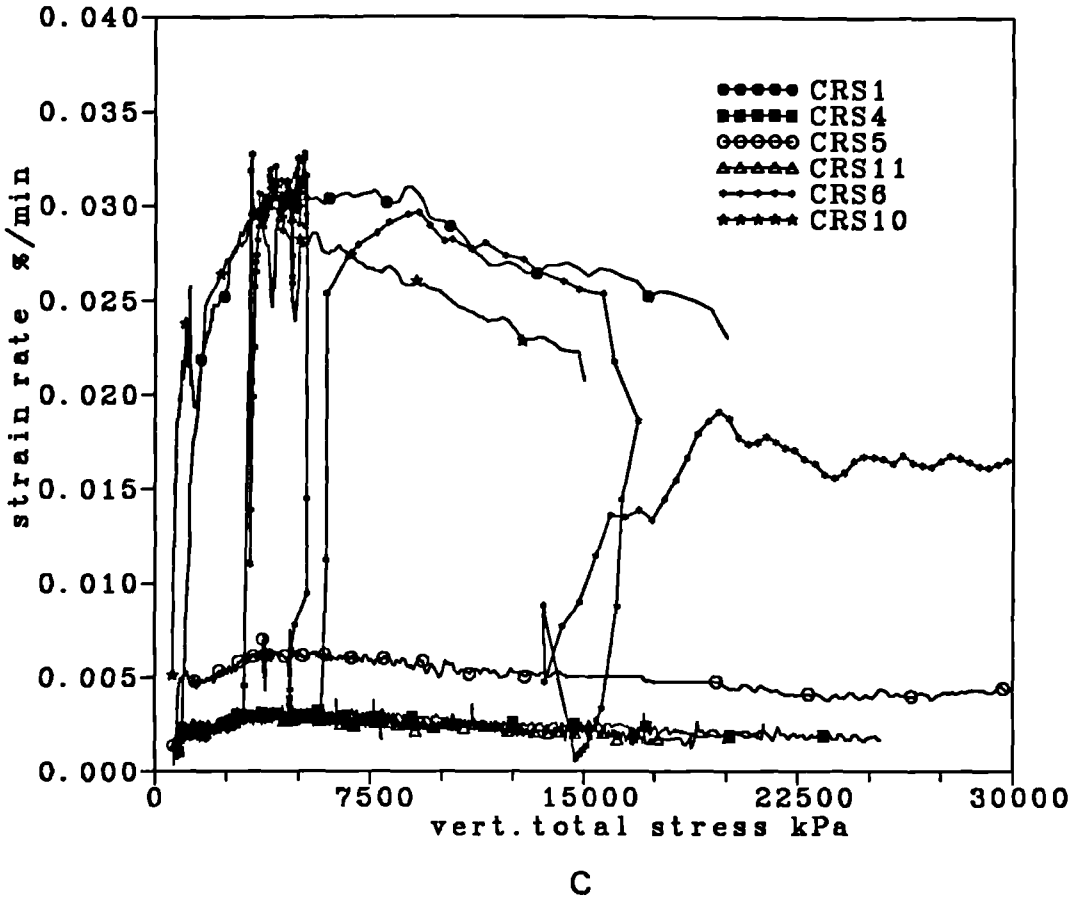

C

Fig.6.52. CRS tests on the undisturbed clay: strain rates; (a) slow tests, (b) all the tests and (c) test CRS6.

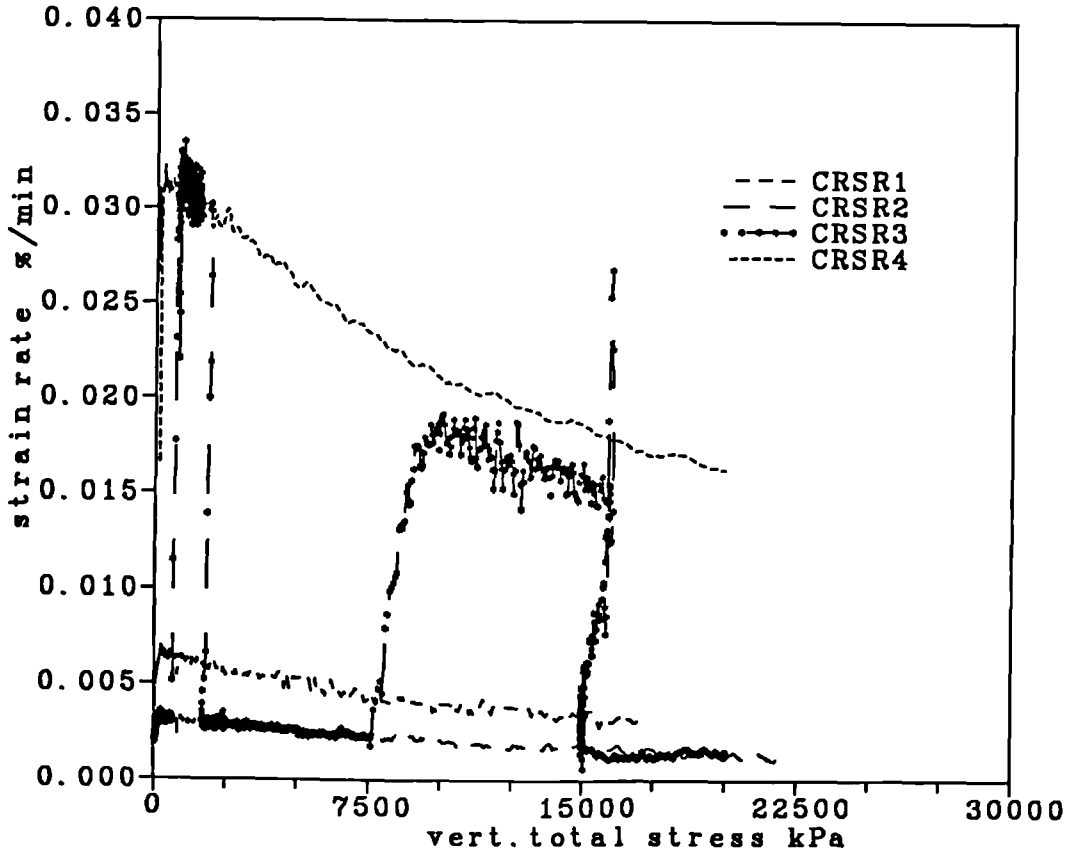

Fig.6.53. CRS tests on the reconstituted clay : strain rates.

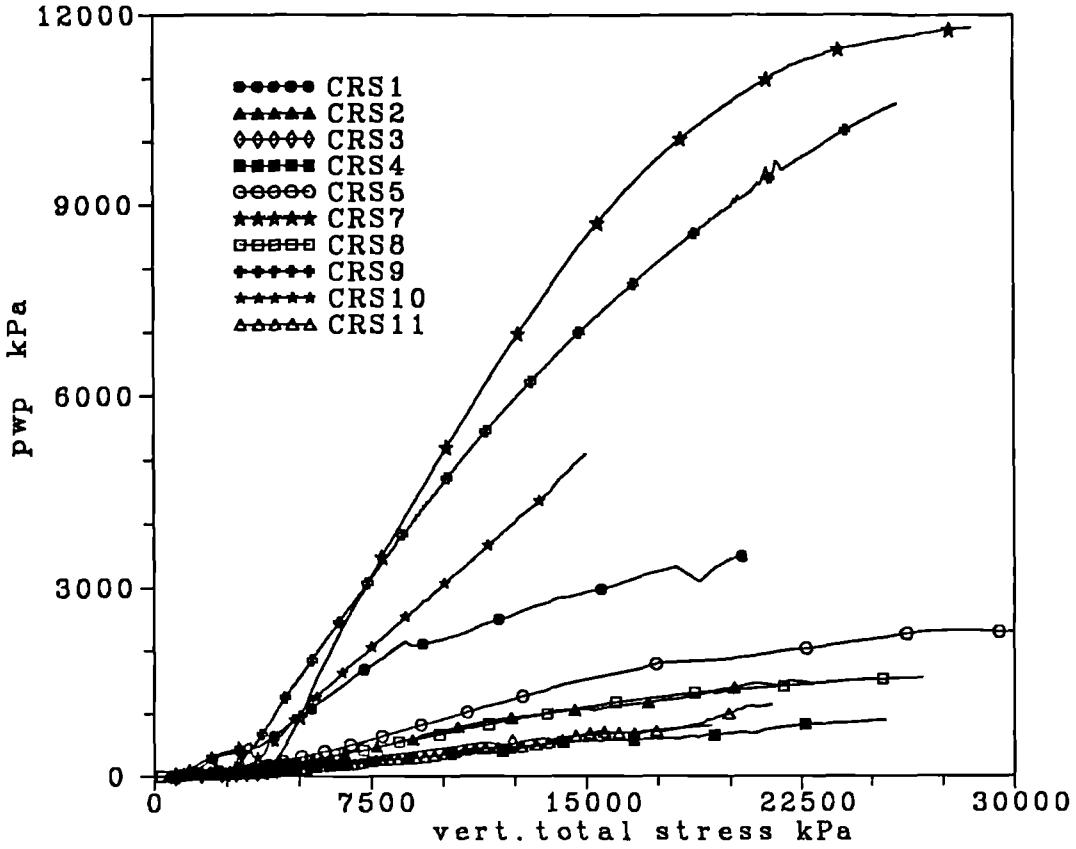

a

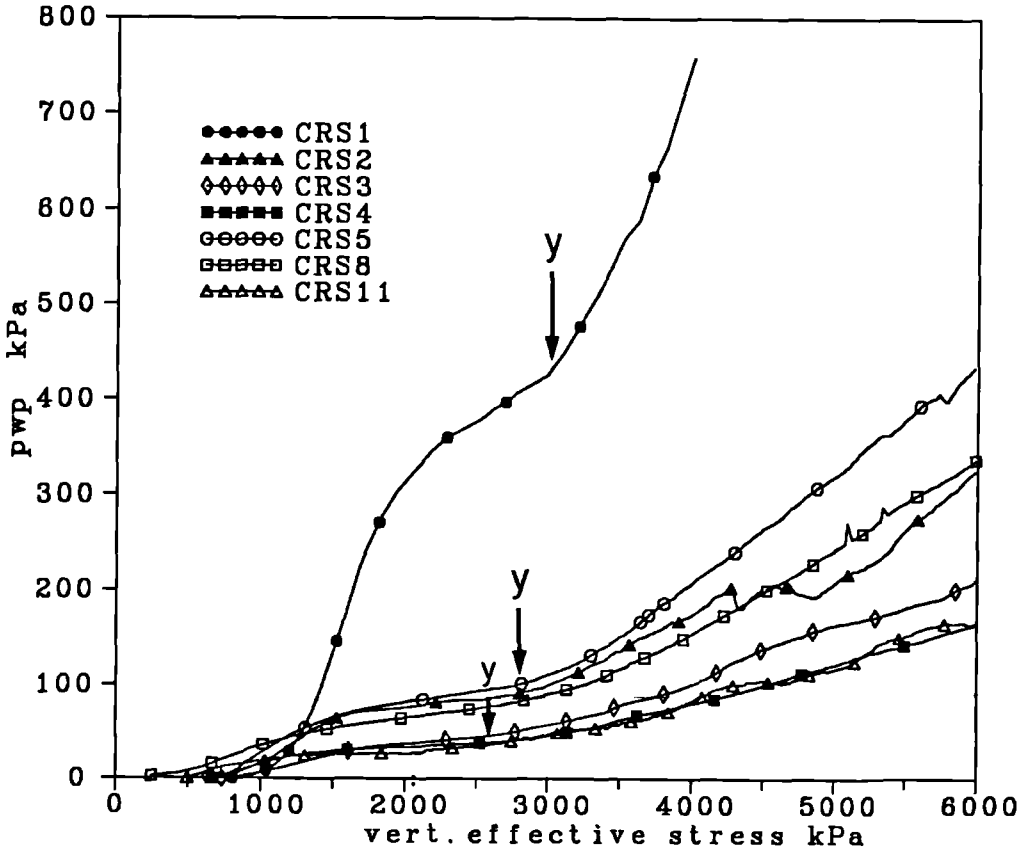

b

Fig.6.54. CRS tests on the undisturbed clay : (a) measured base excess pore water pressures u_b; (b) identification of the yield stress in the slow tests.

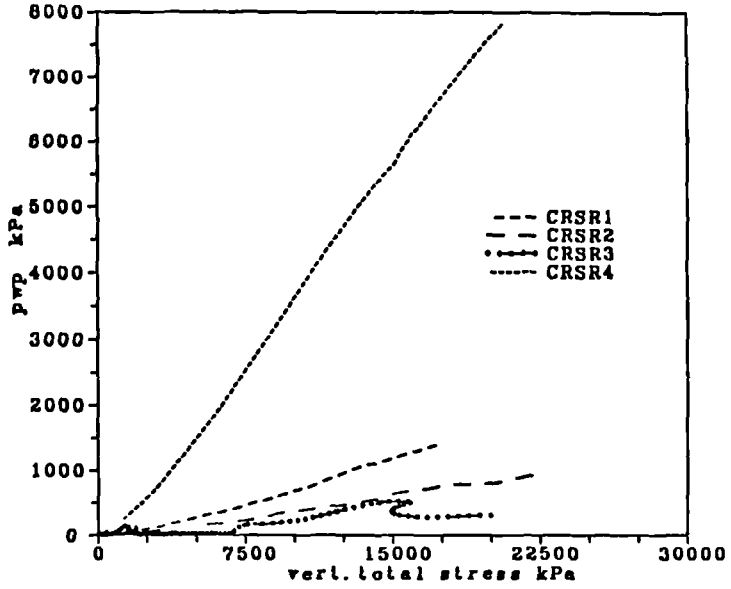

a

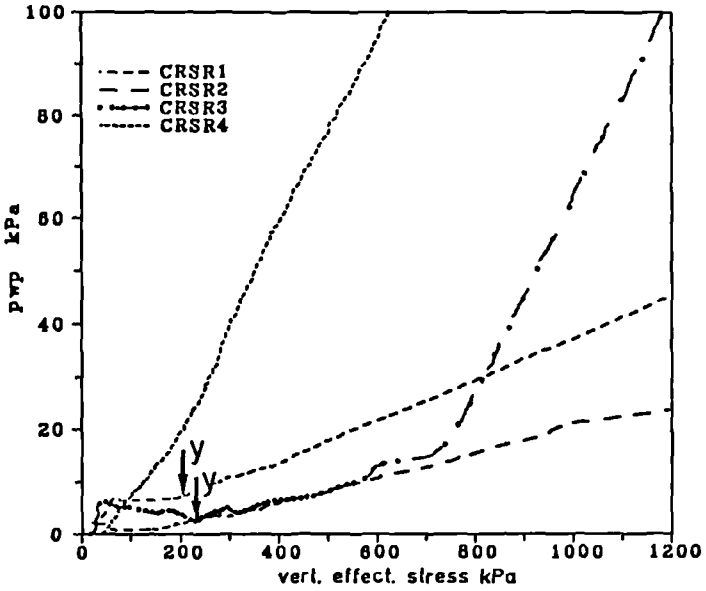

b

Fig.6.55. CRS tests on the reconstituted clay : (a) measured base excess pore water pressures u_b; (b) identification of the yield stress in the slow tests.

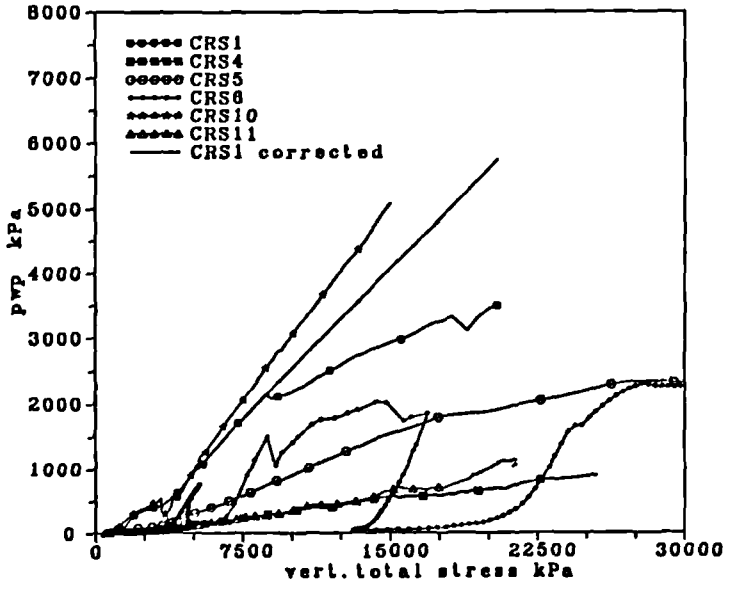

Fig.6.56. Effects on u_b of the strain rate changes in test CRS6. Correction of u_b in test CRS1.

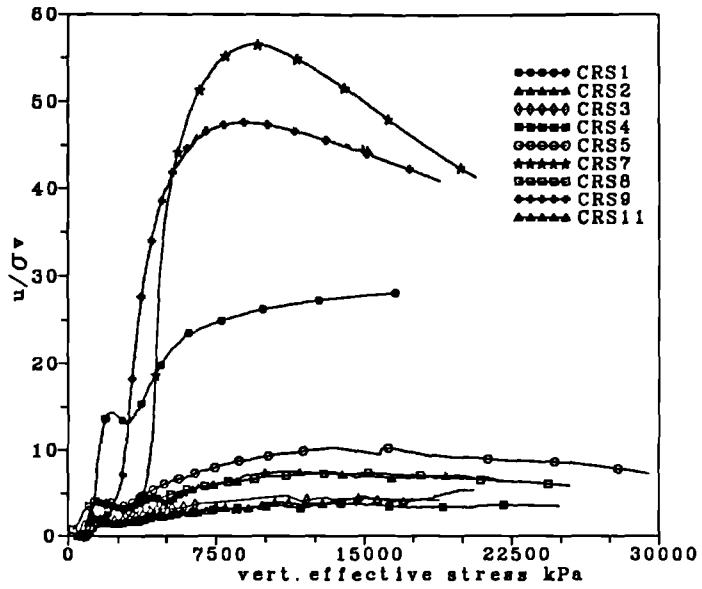

a

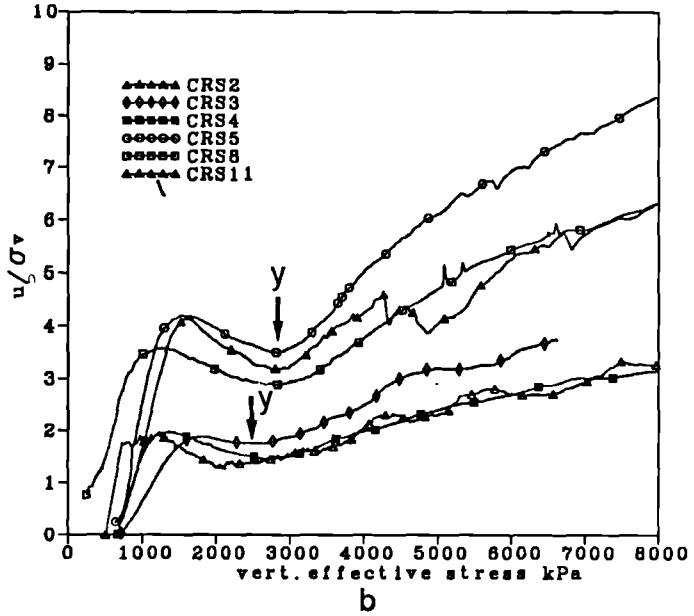

b

Fig.6.57. CRS tests on the undisturbed clay : (a) u_b/σ_v ratios; (b) identification of the yield stress in the slow tests.

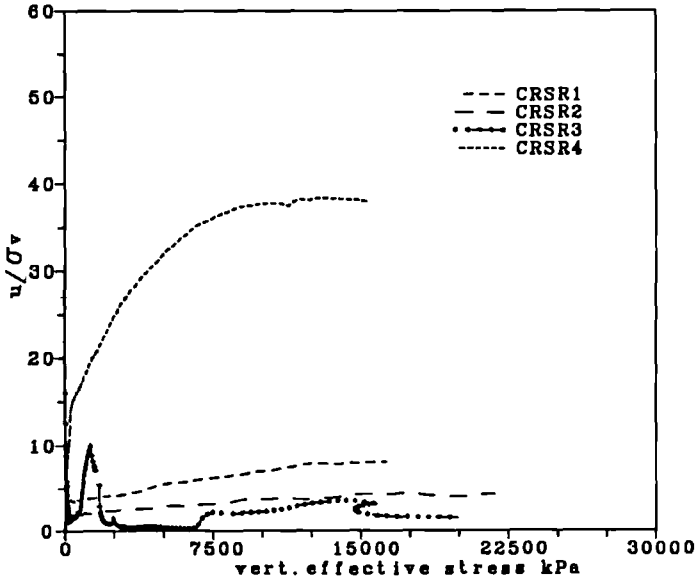

Fig.6.58 CRS tests on the reconstituted clay. u_b/σ_v ratios.

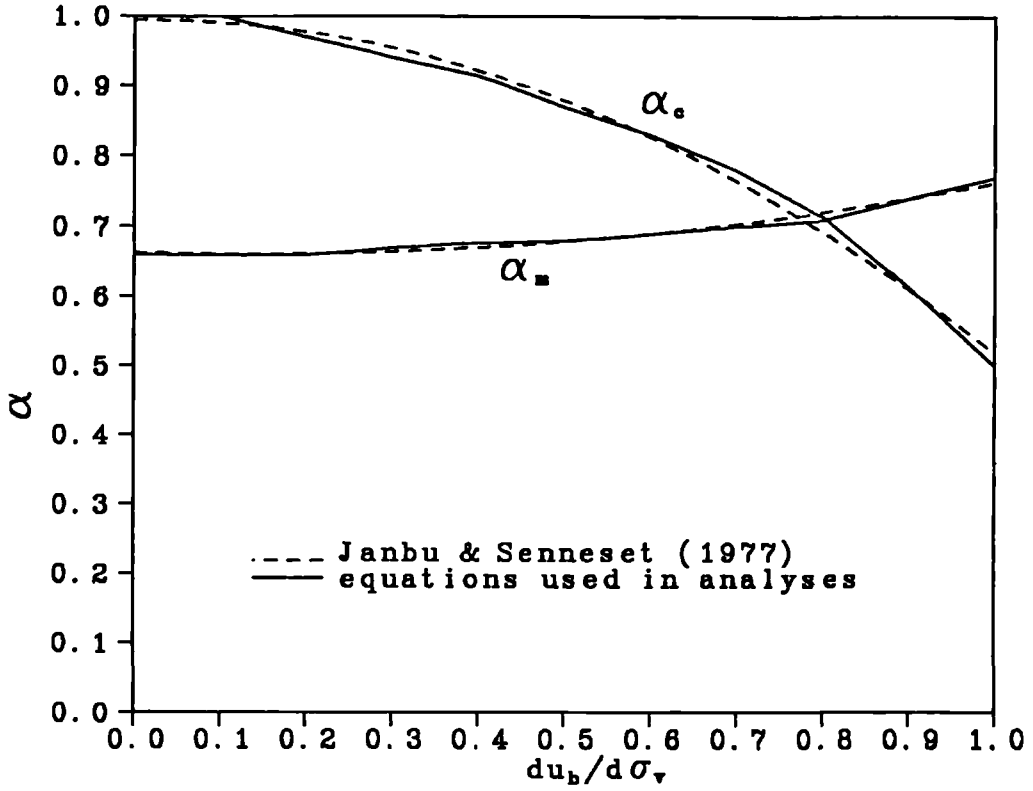

Fig.6.59. Correction coefficients α_m and α_c from Janbu and Senneset (1979).

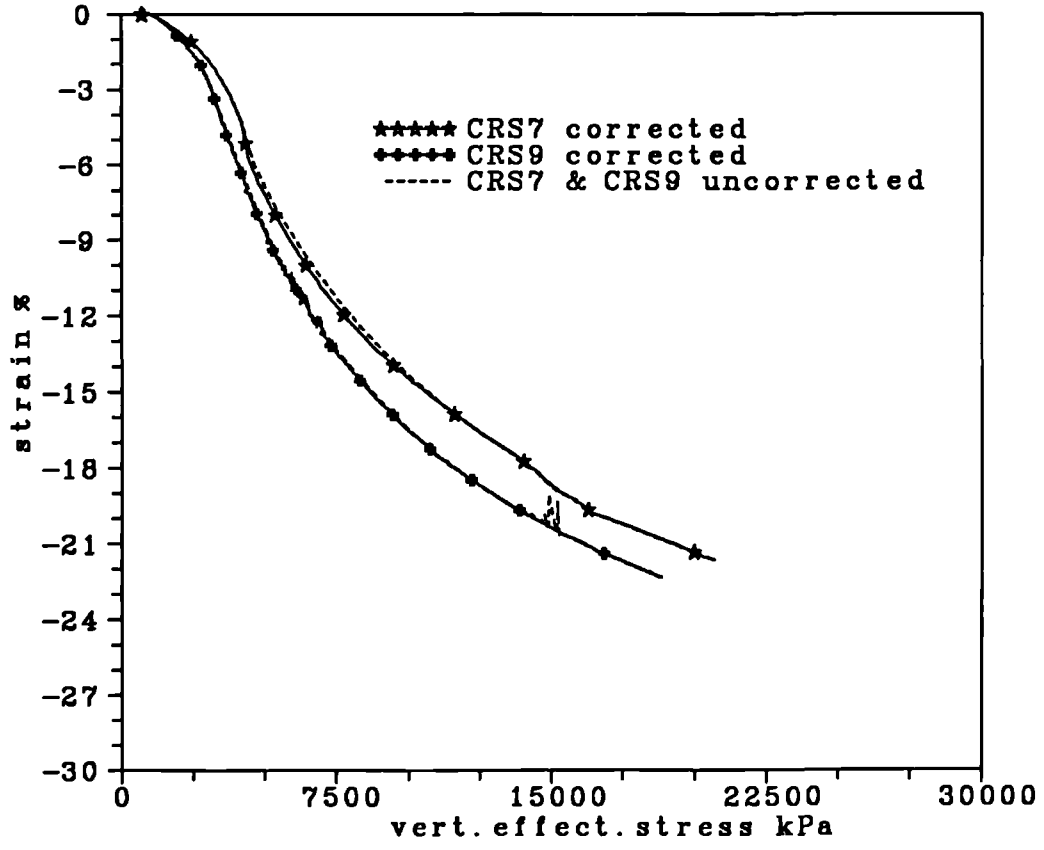

Fig.6.60. Compression curves from tests CRS 7 and 9 before and after the α_m correction .

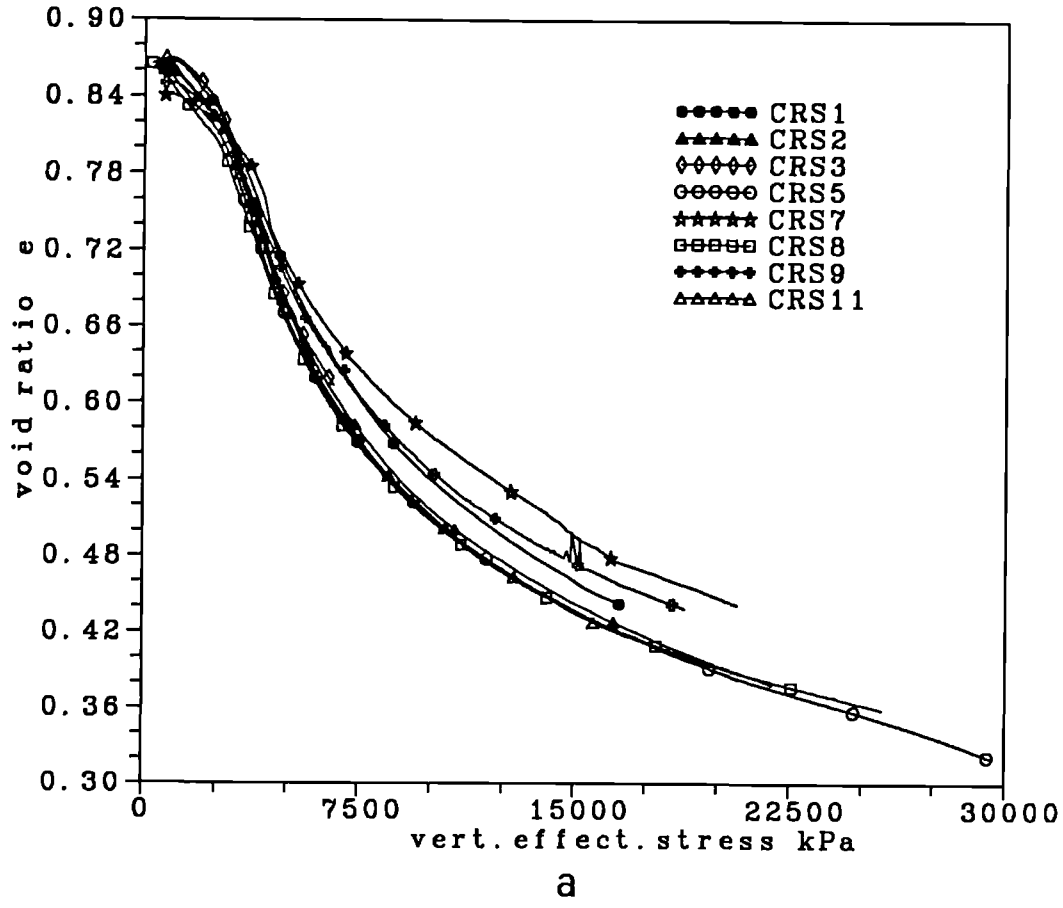

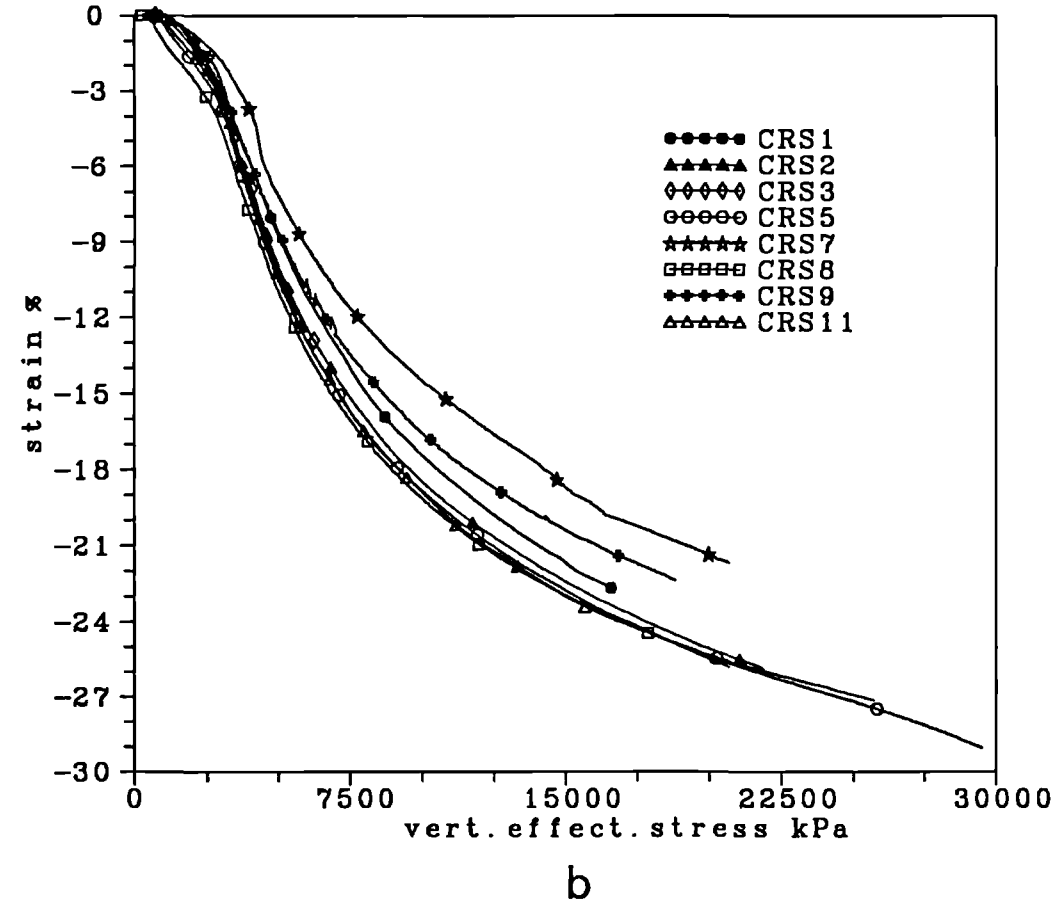

Fig 6 61. Undisturbed clay : CRS compression curves

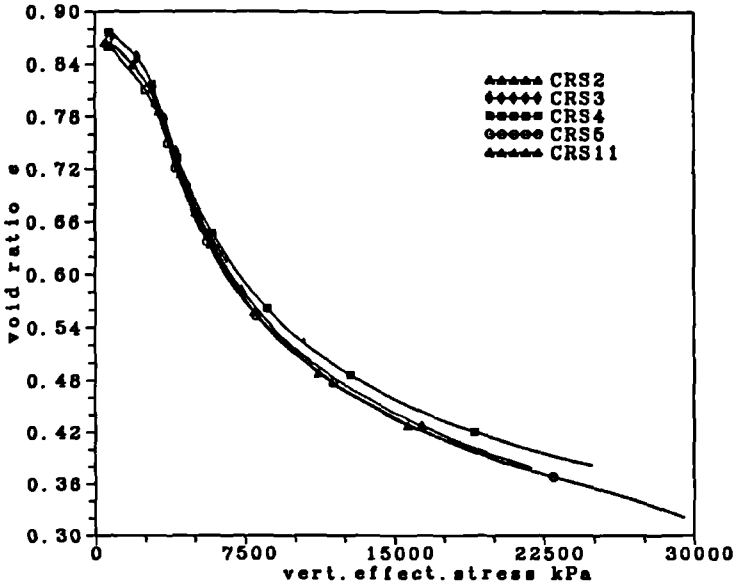

Fig.6.62. Undisturbed clay : slow CRS test compression curves (average strain rate 3E-3%/min).

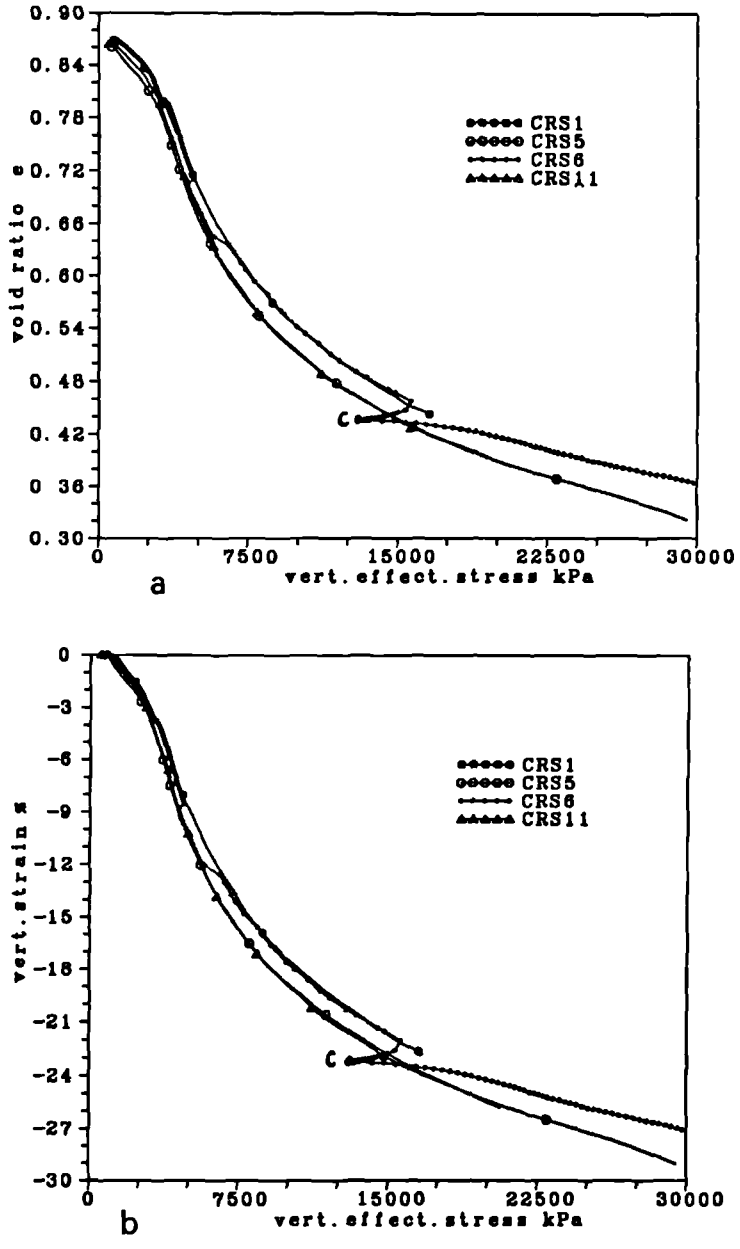

Fig.6.63. Effects of the change in strain rate (test CRS6) on the clay state path.

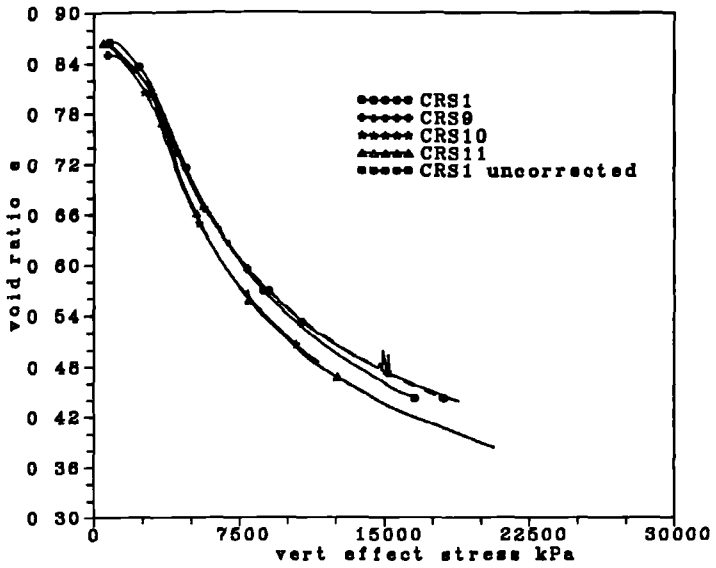

Fig 6 64 Effects of the correction of the base pore water pressure u_b on the CRS1 compression curve

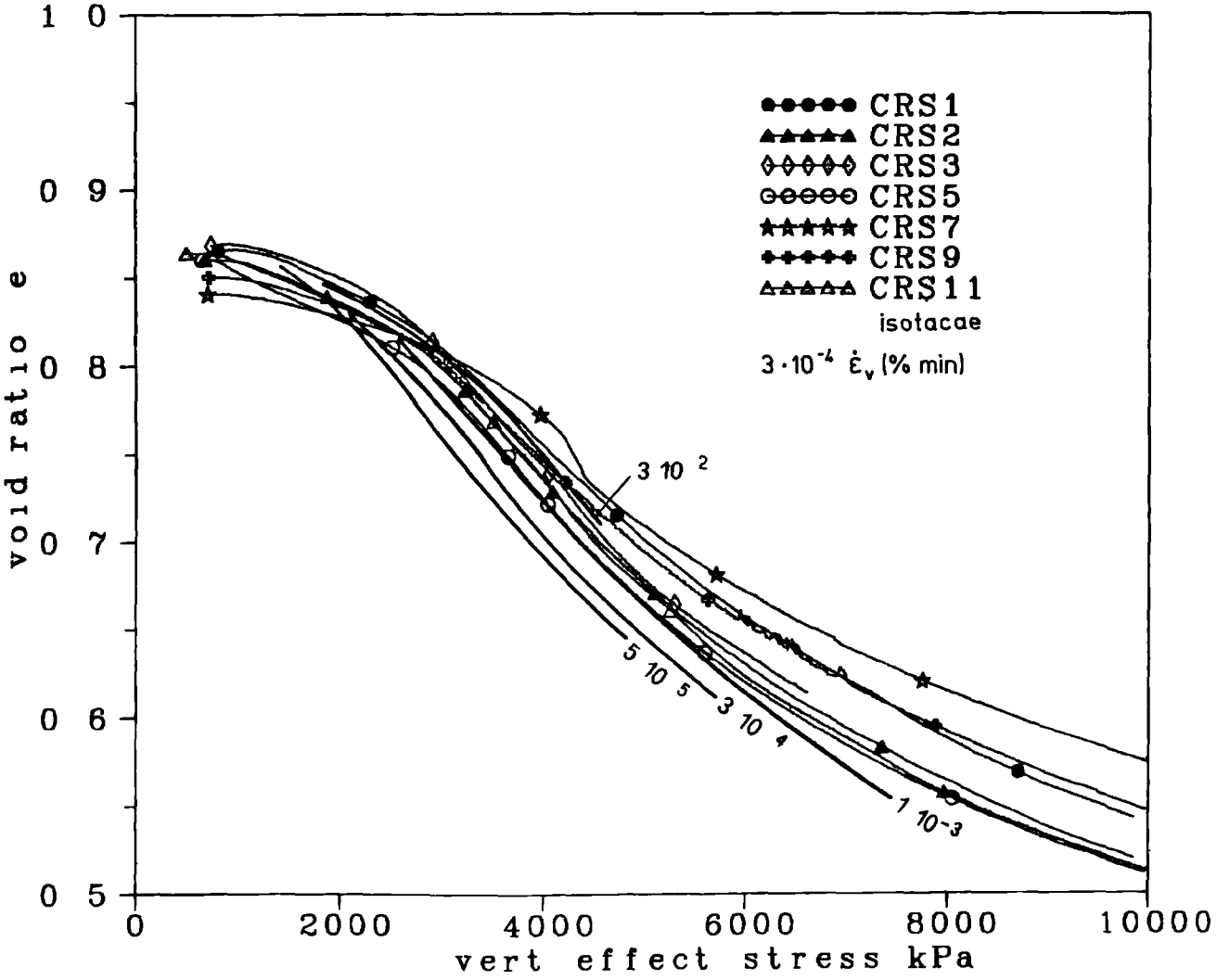

Fig 6 65 Undisturbed clay CRS compression curves and isotacae resulting from the study of the OED test data (see Fig 6 41)

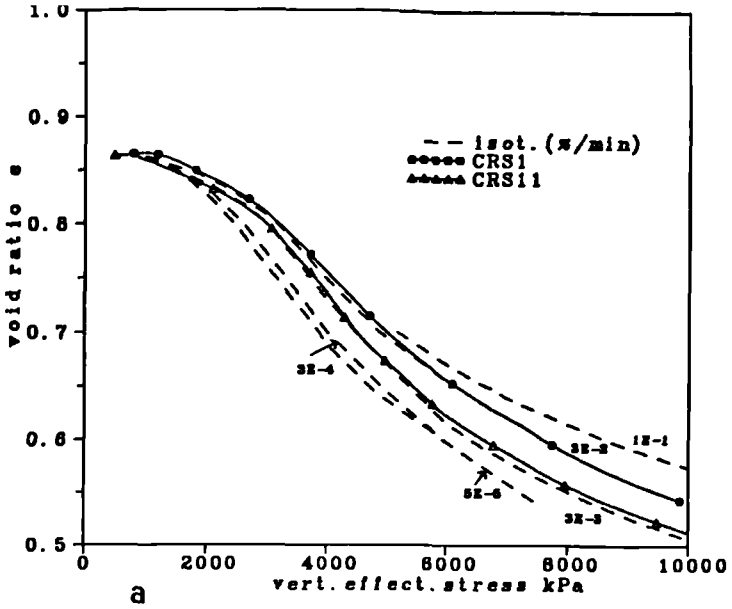

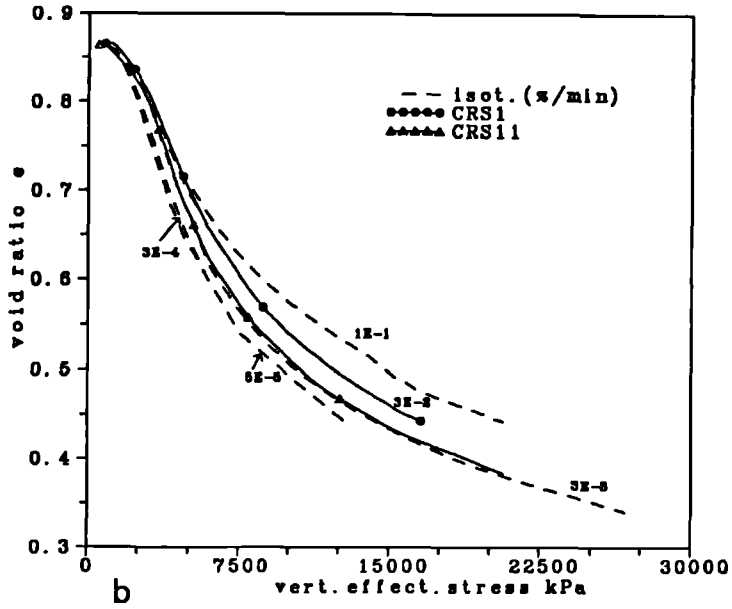

Fig.6.66. Undisturbed Pappadai clay : isotacae

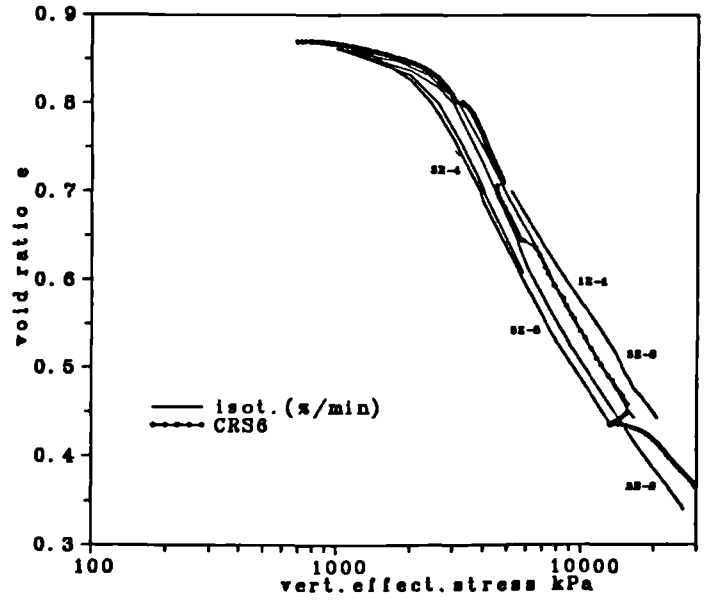

Fig.6.67. Undisturbed Pappadai clay : isotacąe and CRS6 compression curve.

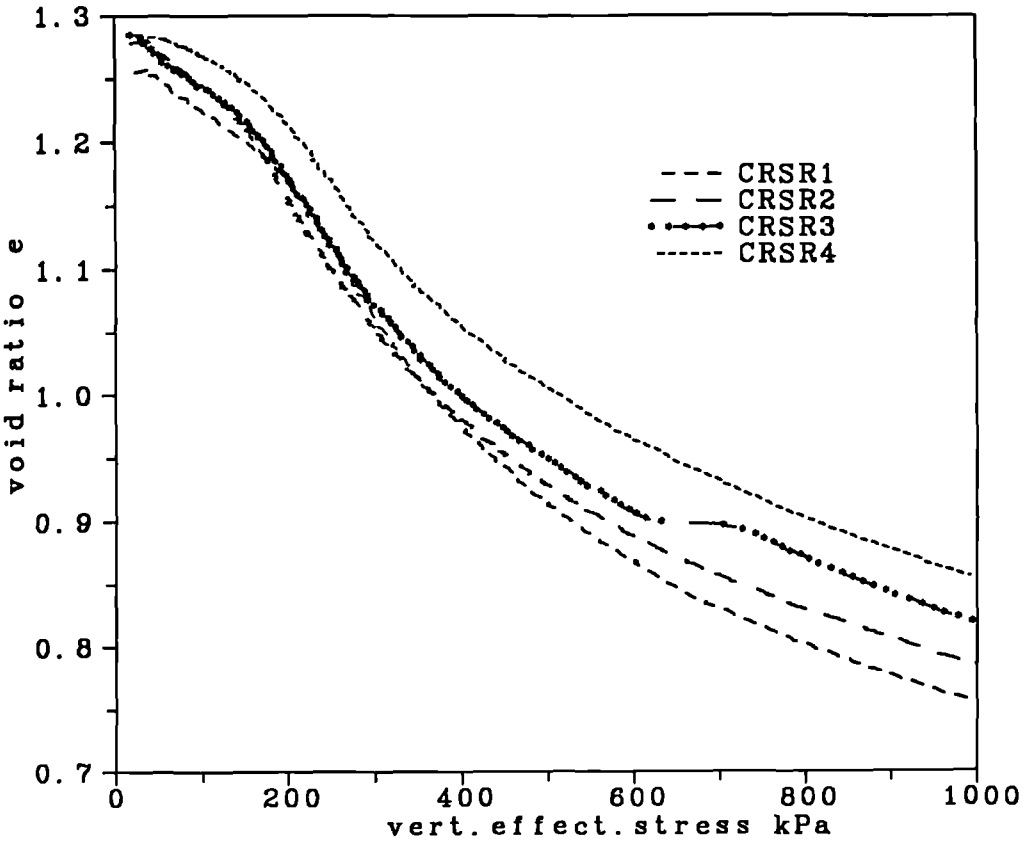

a

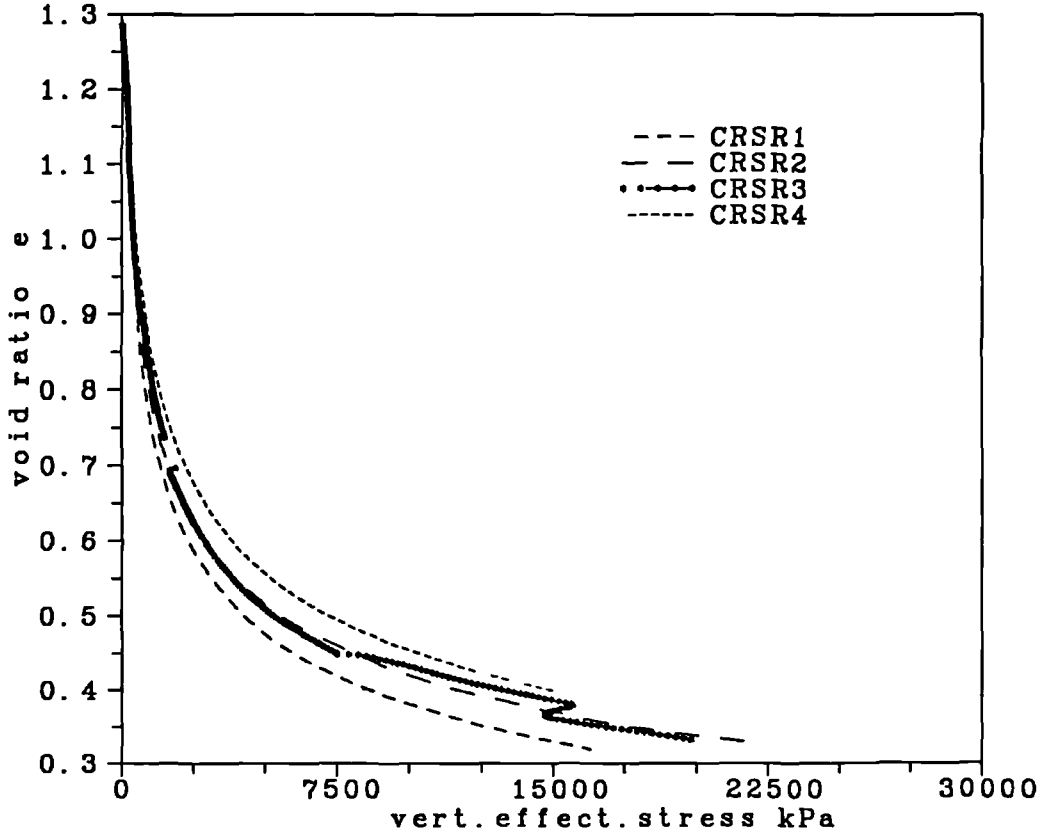

b

Fig.6.68. Reconstituted clay : CRS compression curves.

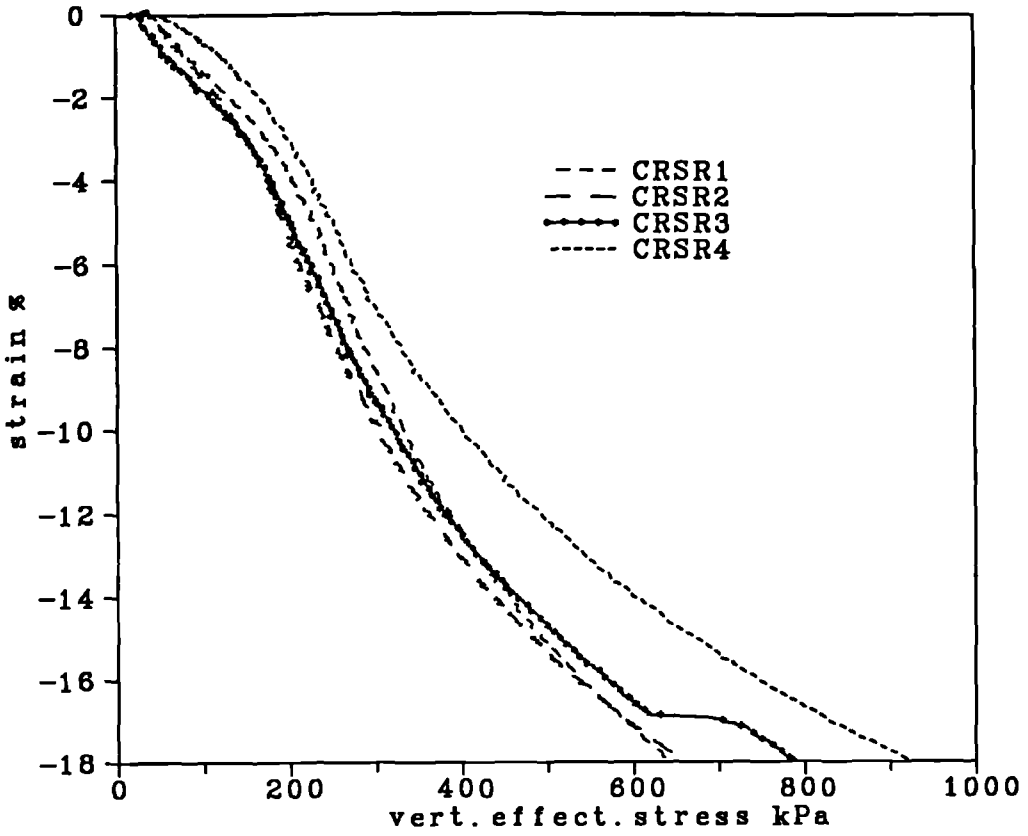

a

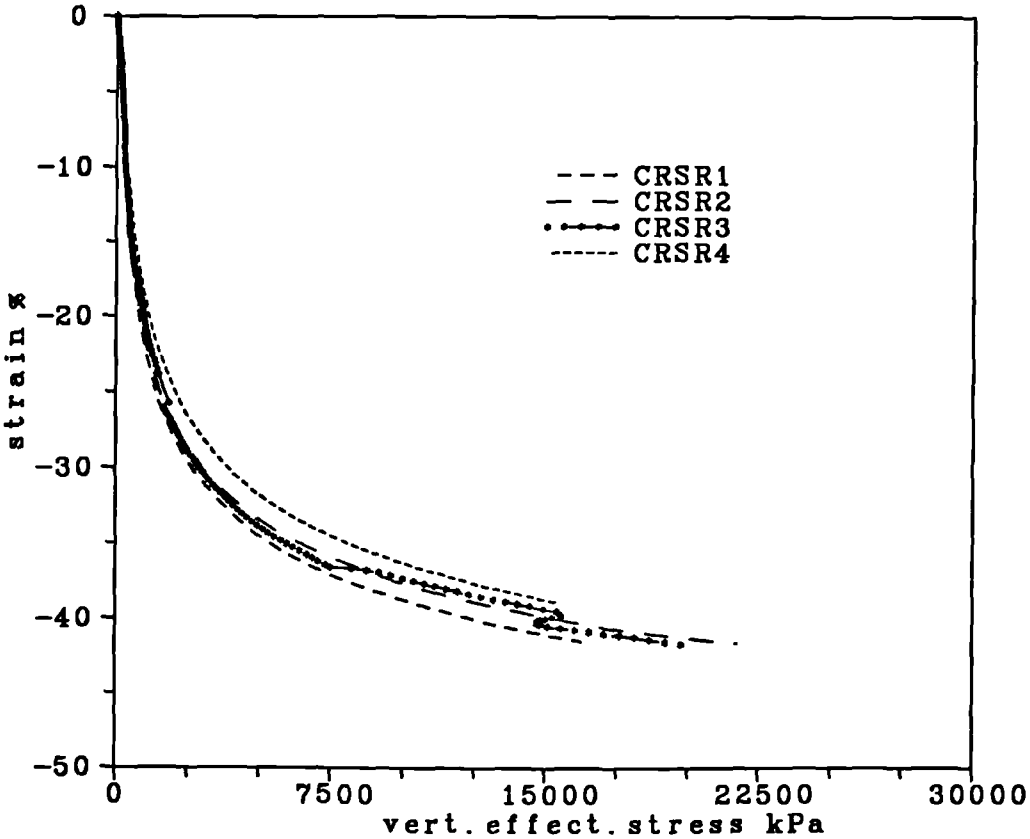

b

Fig.6.69. Reconstituted clay : CRS compression curves.

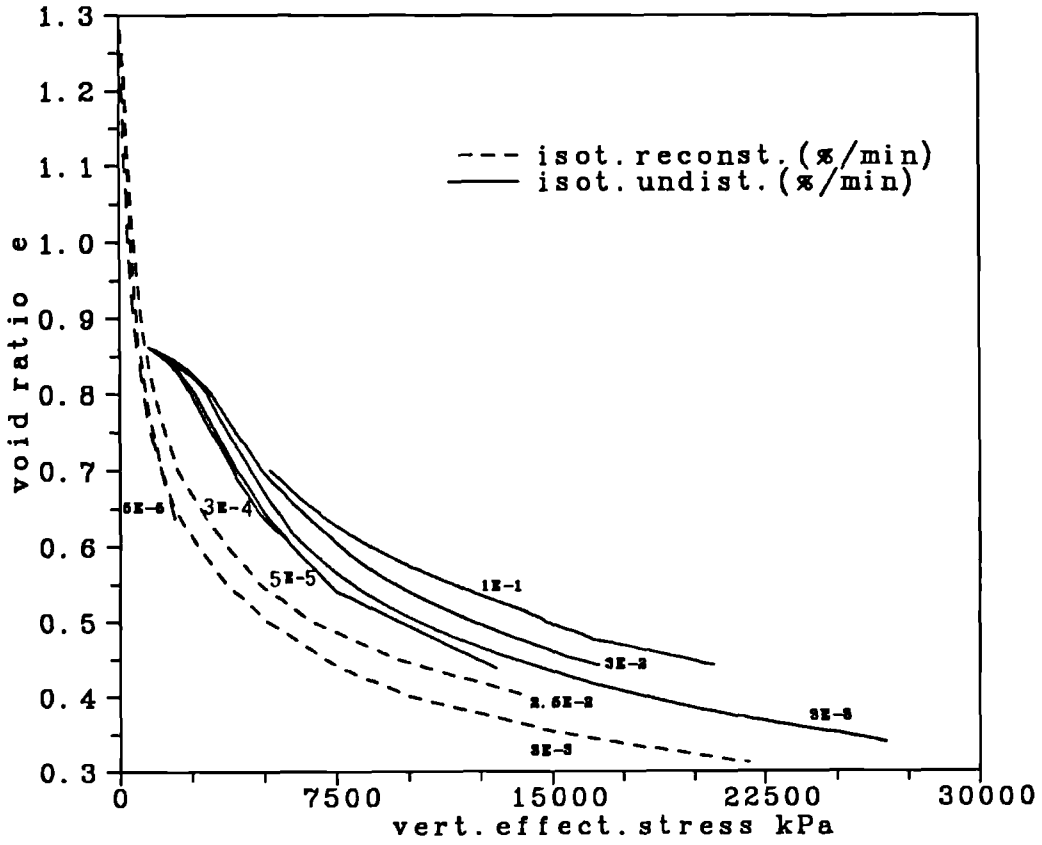

Fig.6.70. Framework of strain-rate dependancy of the natural and reconstituted Pappadai clay.

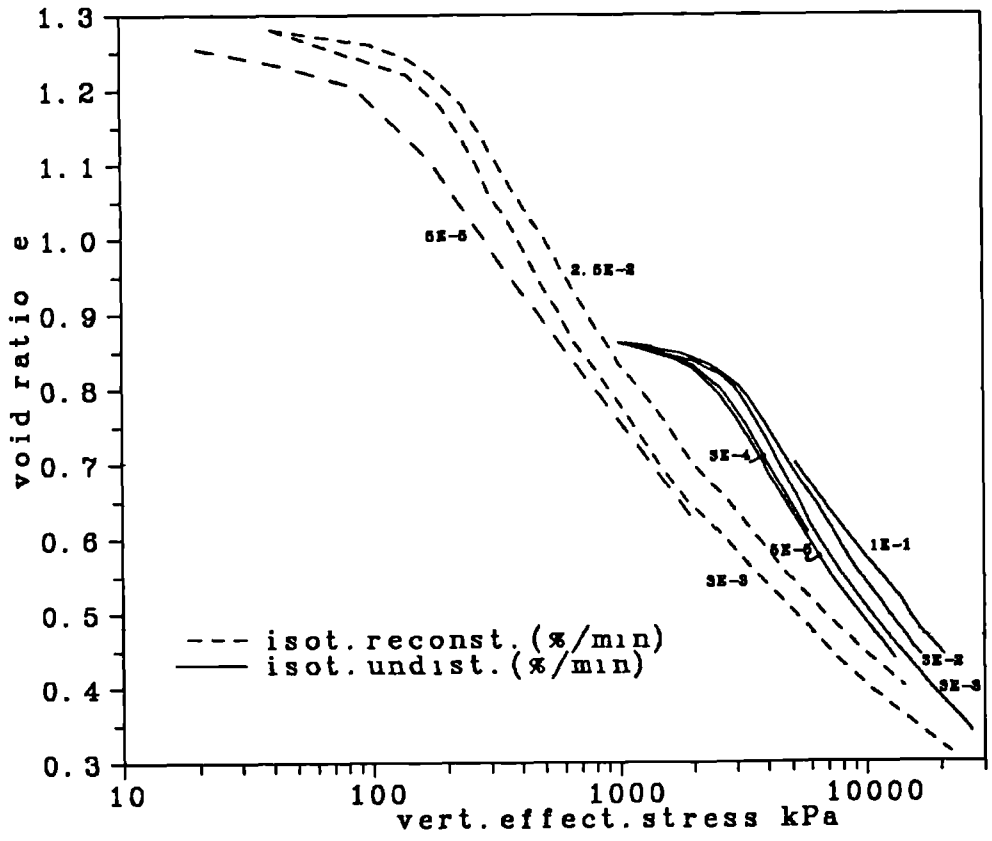

Fig.6.71 Framework of strain rate dependancy of the natural and reconstituted Pappadai clay

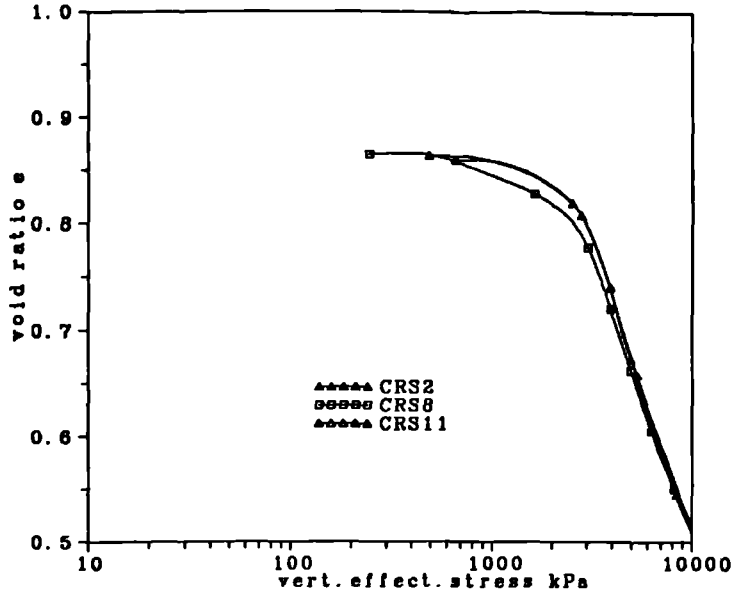

Fig.6.72. Effect of swelling before compression on the CRS compression of the natural clay.

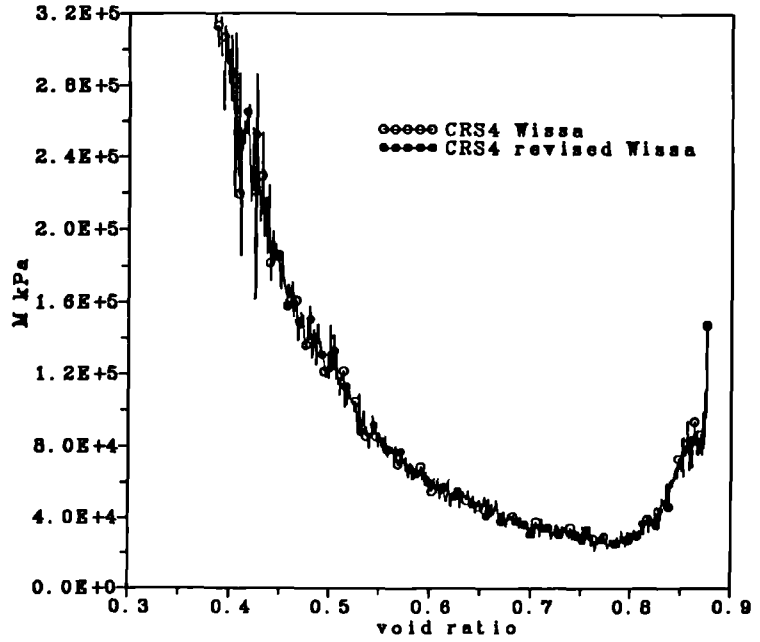

a)

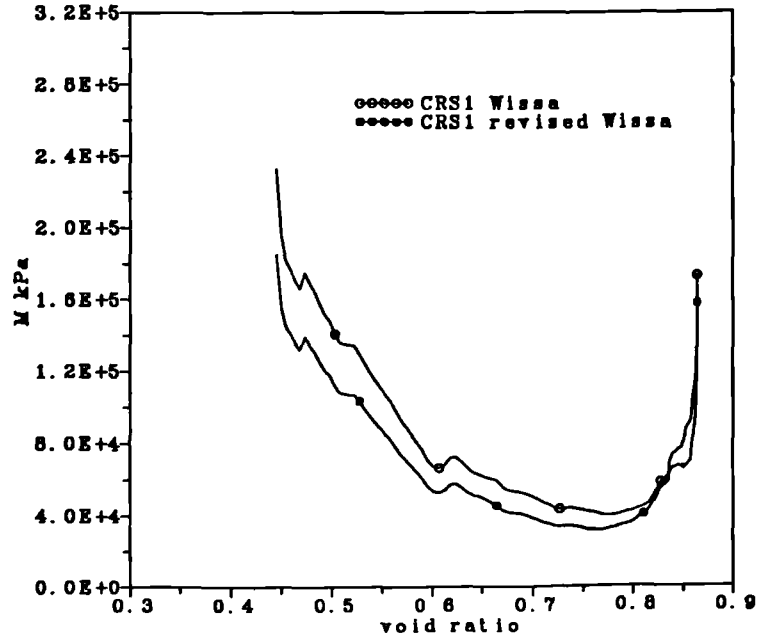

b)

Fig.6.73. M values from CRS tests calculated according to Wissa's solution and to the solution in App.6.3 : (a) slow tests; (b) fast tests.

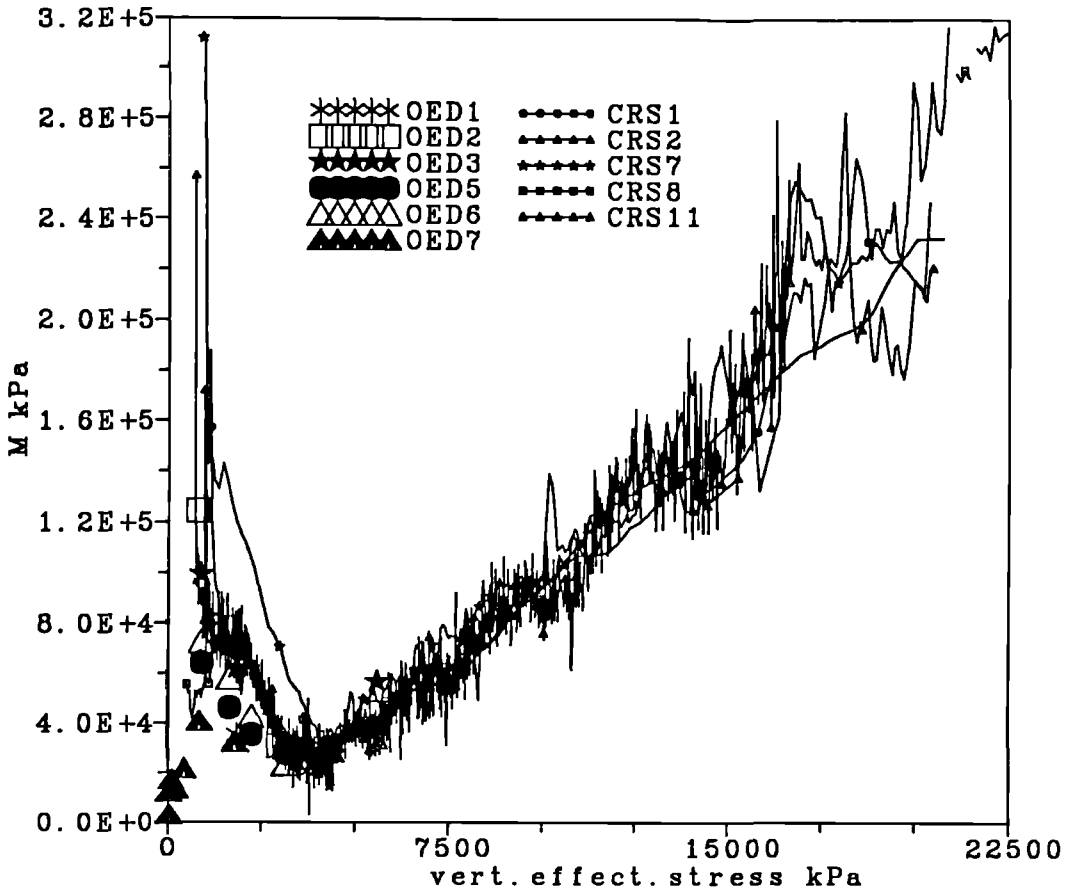

Fig.6.74. Oedometric stiffness M of the natural clay as resulting from the OED and CRS test results.

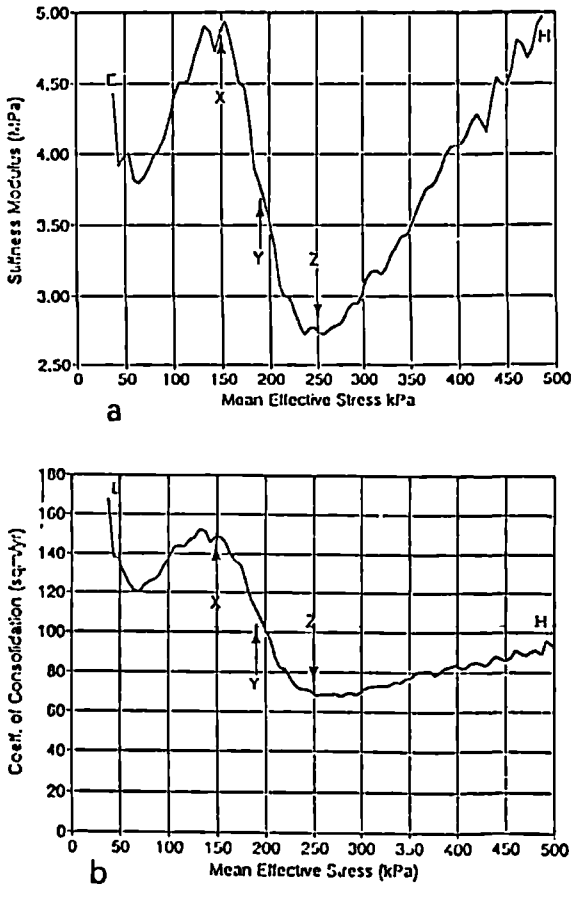

Fig.6.75. Values of M and c_v observed during the CRS compression of reconstituted kaolin clay (after Davison and Atkinson 1990).

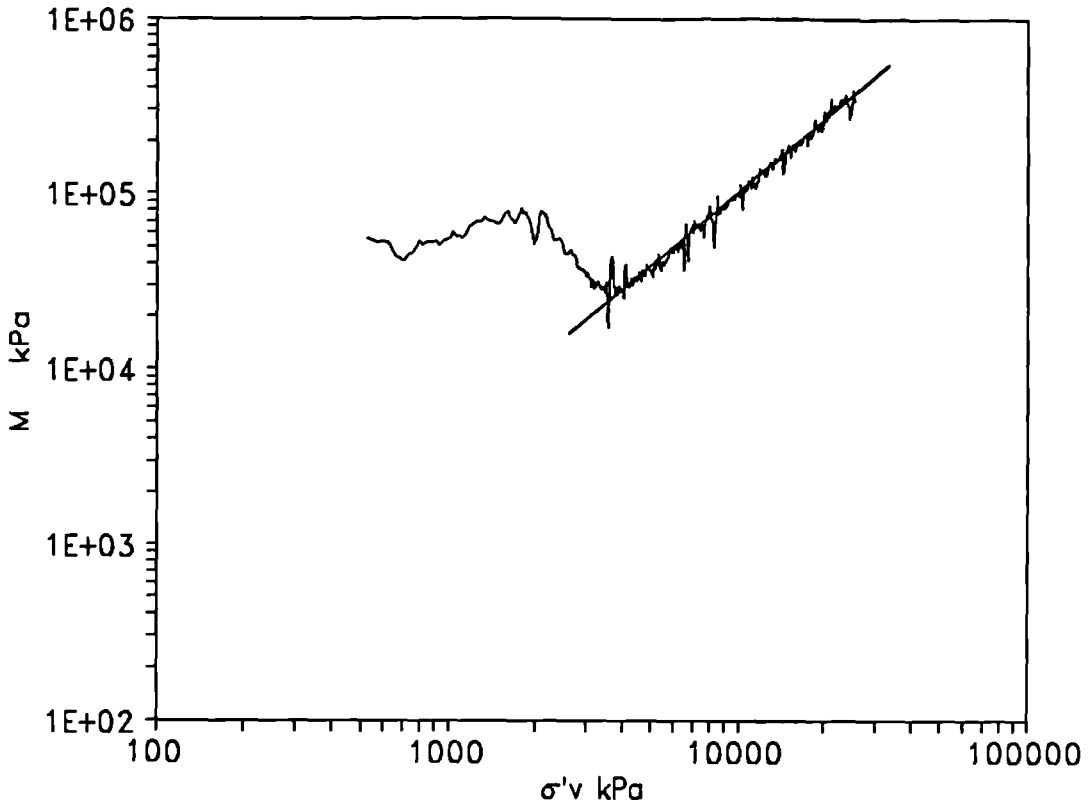

a

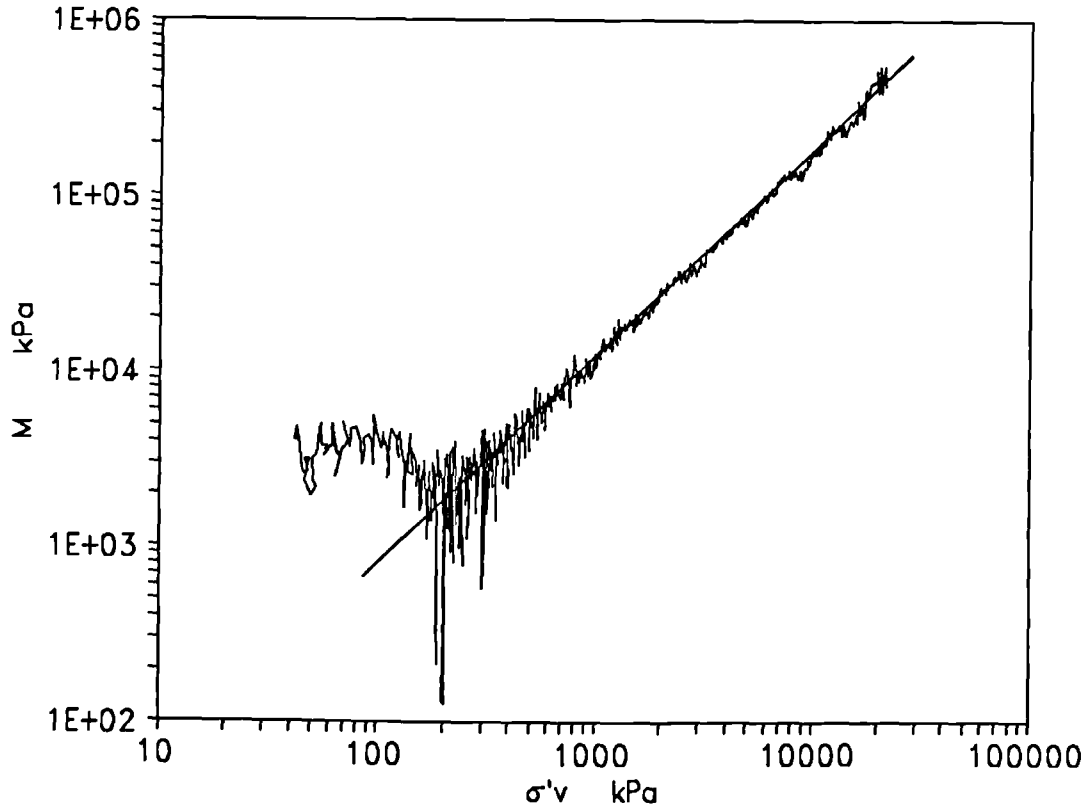

b

Fig.6.76. Exponential M-σ'_v relationships applying to (a) the natural clay and (b) the reconstituted clay.

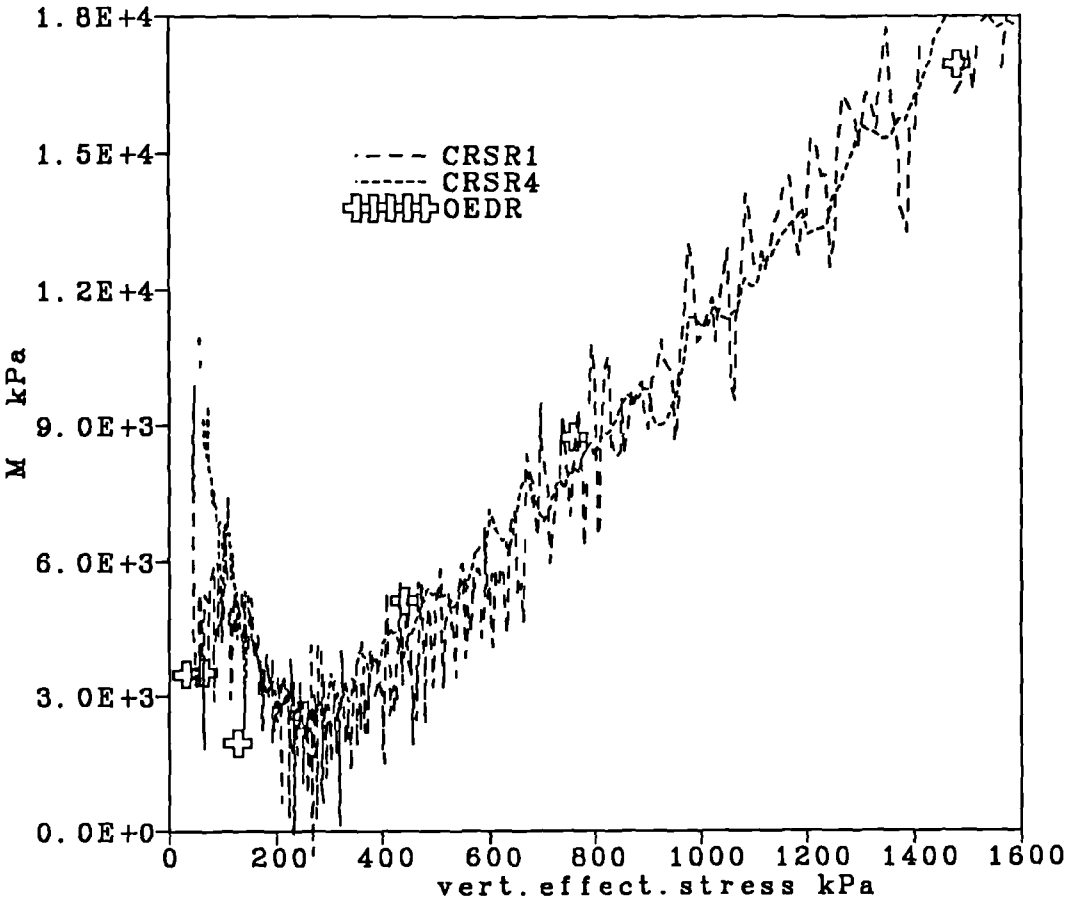

Fig.6.77. Oedometric stiffness M of the reconstituted clay as resulting from the OED and CRS tests.

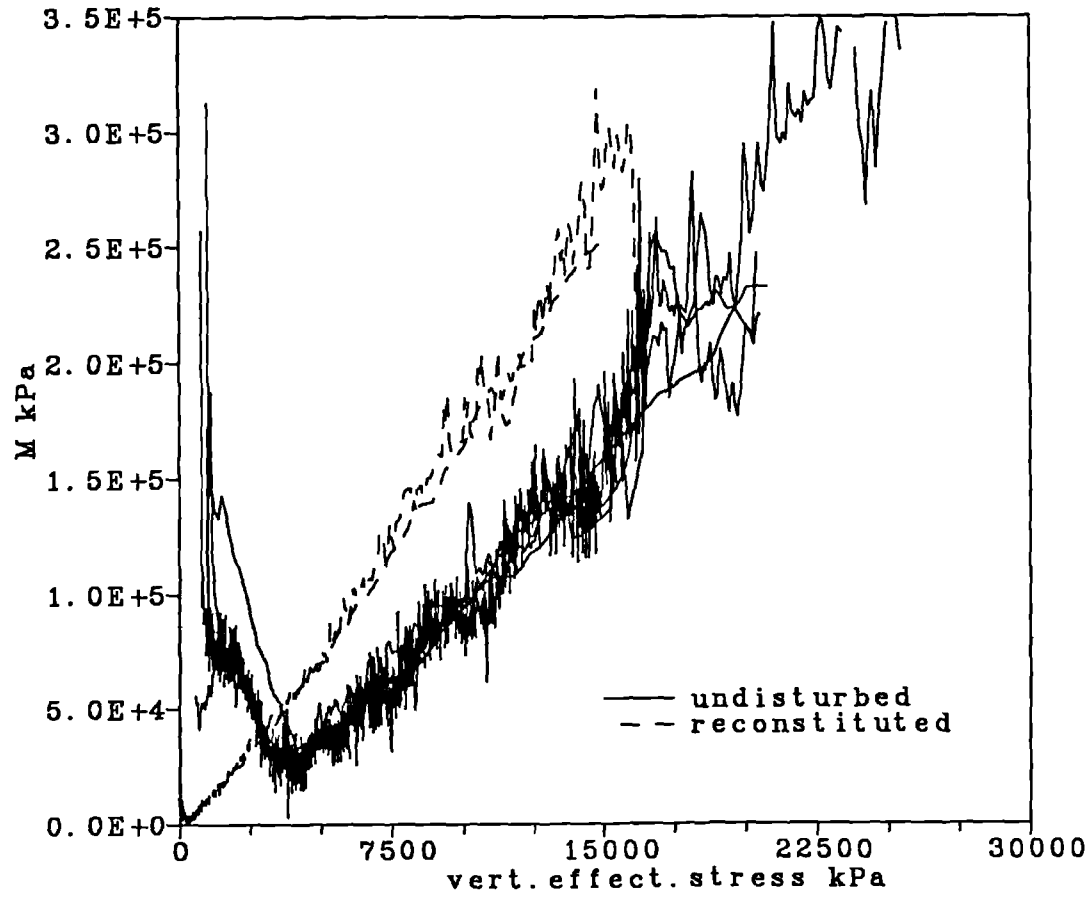

Fig 6 78 M-σ'_v data recorded for the natural and the reconstituted clay.

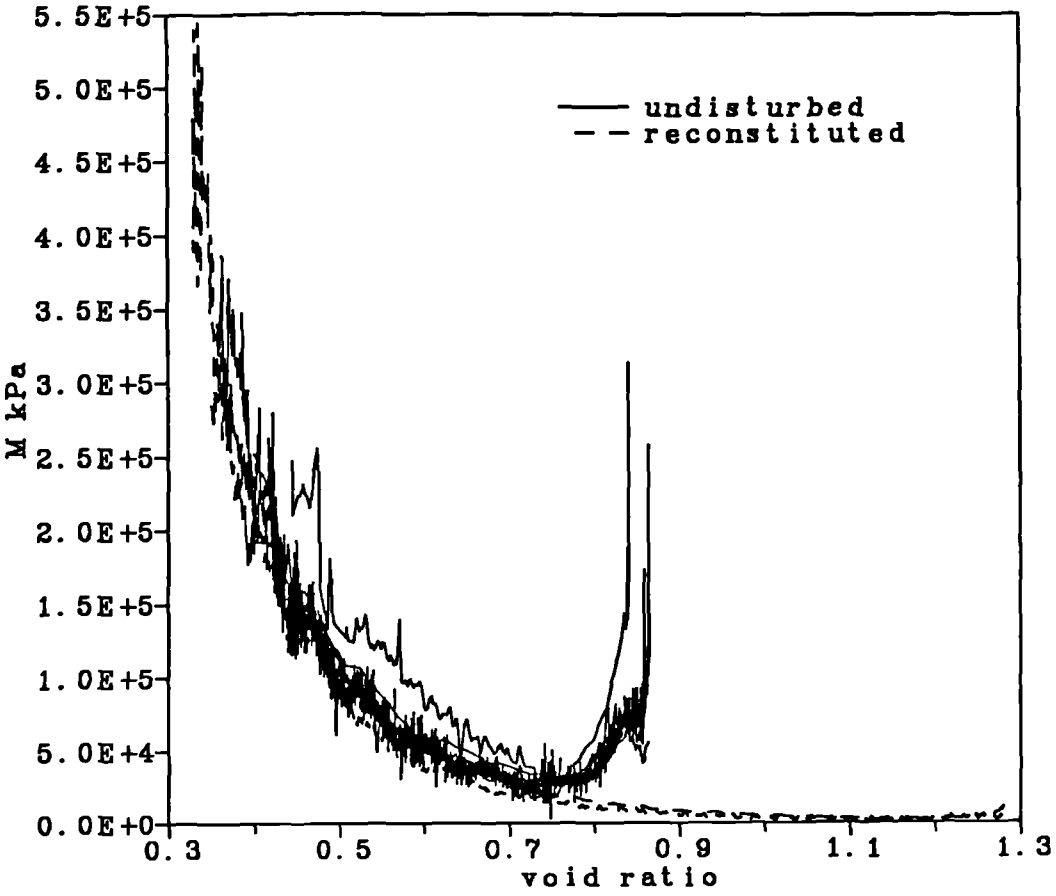

Fig.6.79. M-e data recorded for the natural and the reconstituted clay.

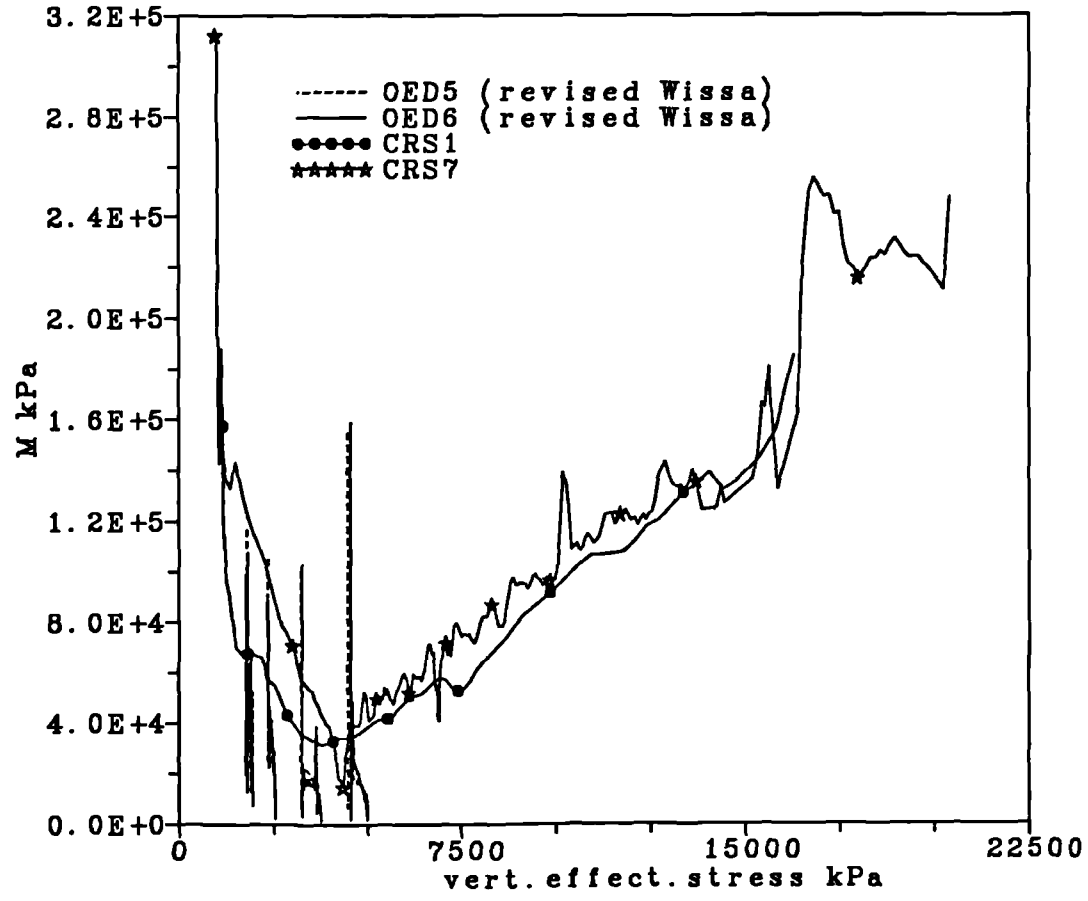

Fig.6.80. Comparison between the values of M in constant strain-rate compressions and the M values exhibited by the clay in the OED loading steps.

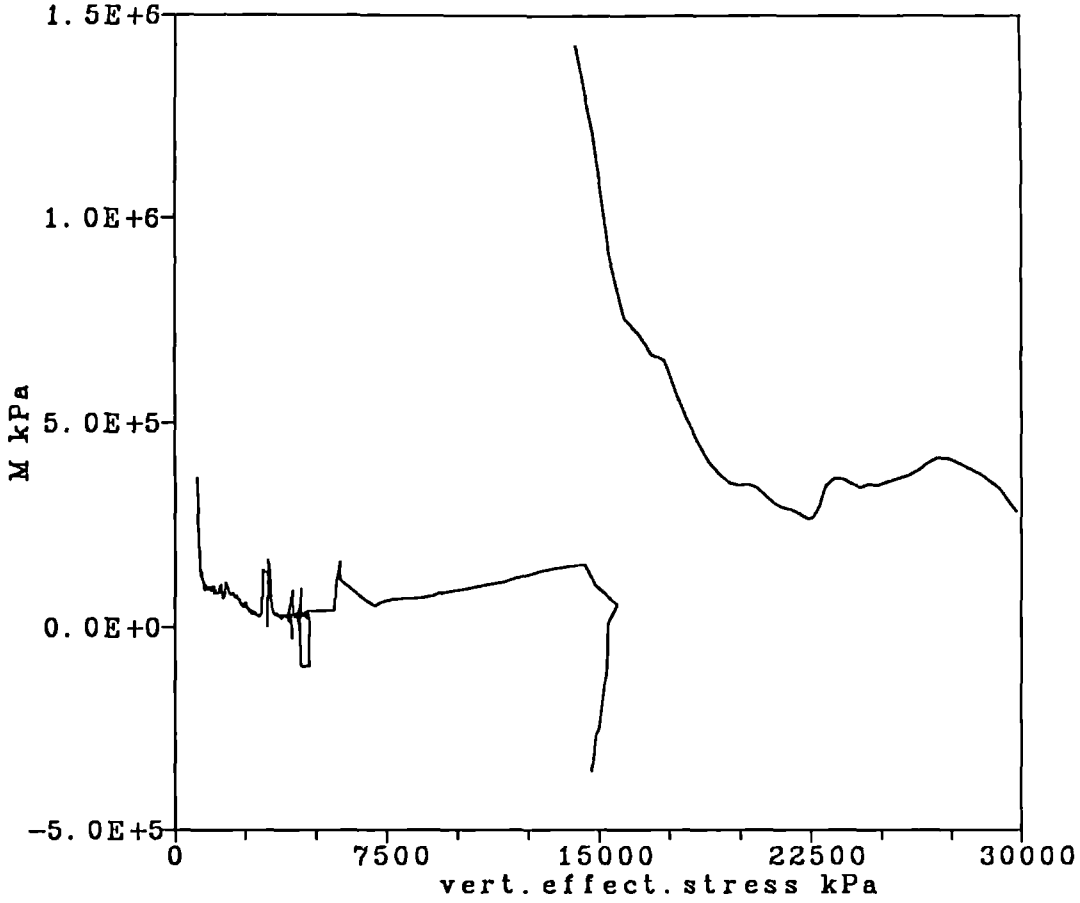

Fig.6.81. Variation of M during test CRS6 (undisturbed clay).

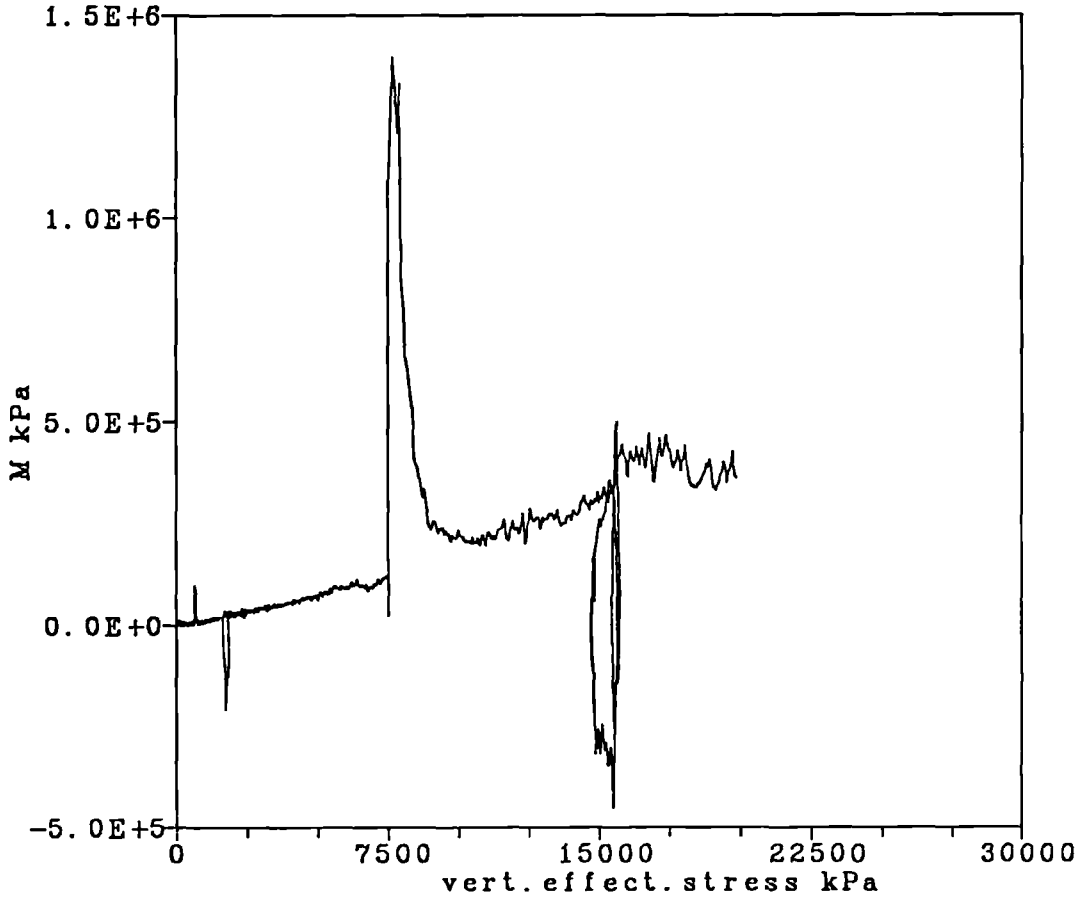

Fig 6.82. Variation of M during test CRSR3 (reconstituted clay).

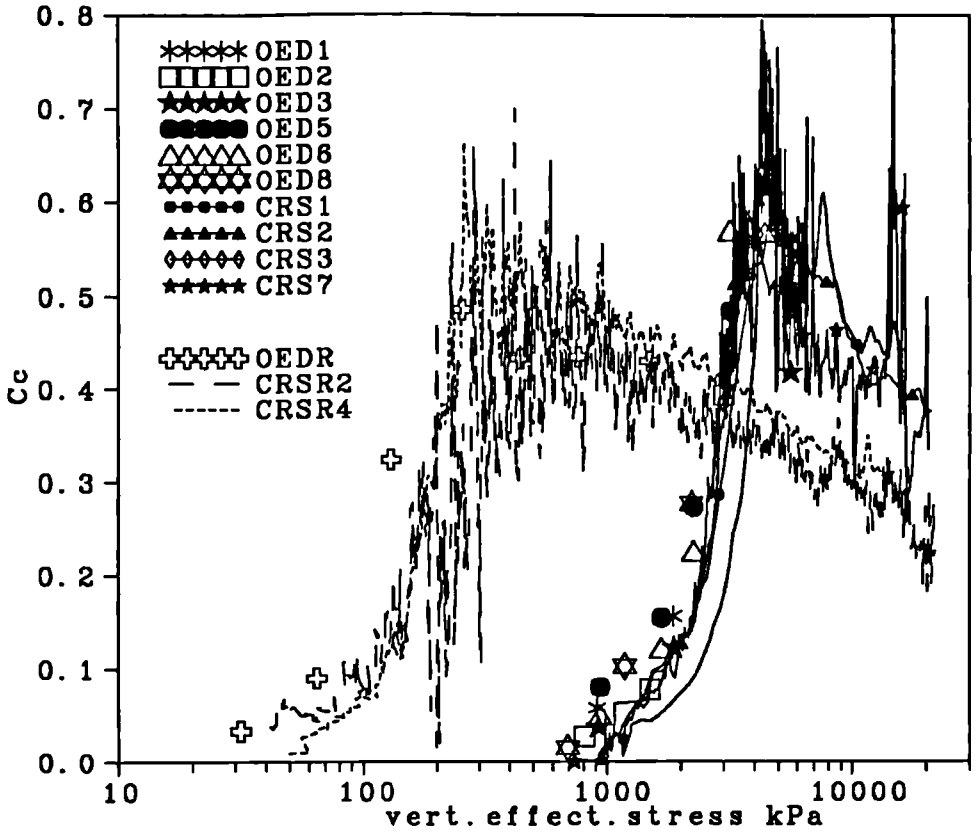

a

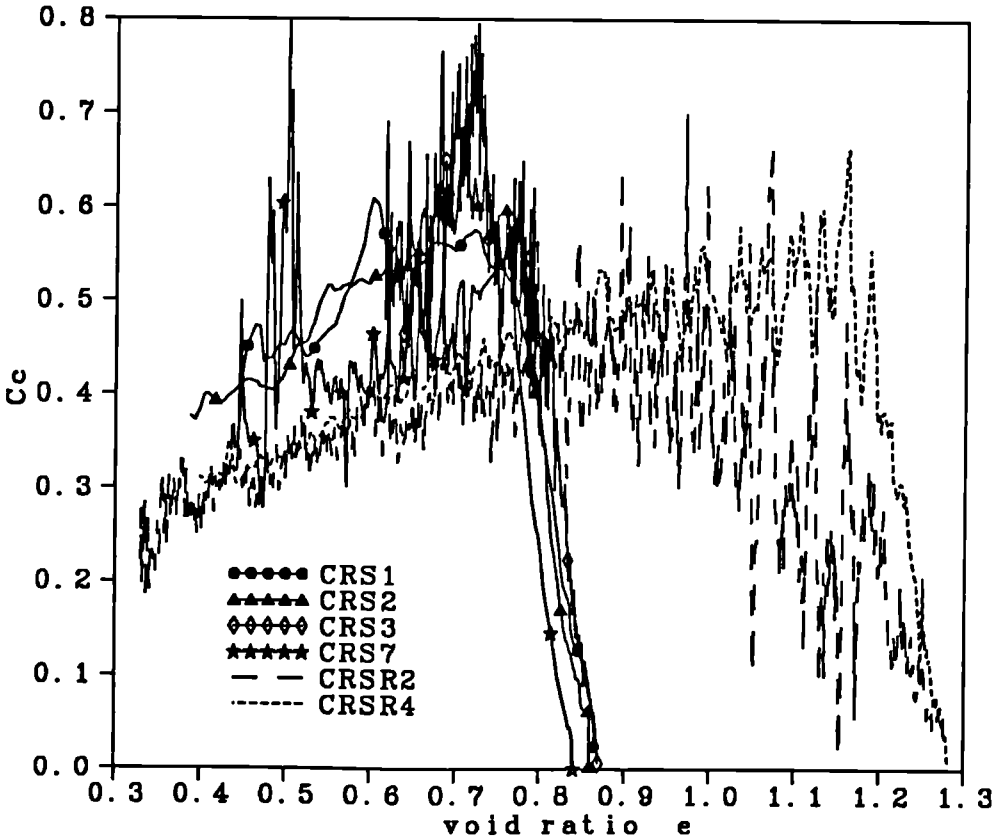

b

Fig.6.83. Natural and reconstituted Pappadai clay : values of C_c measured in the OED and CRS tests.

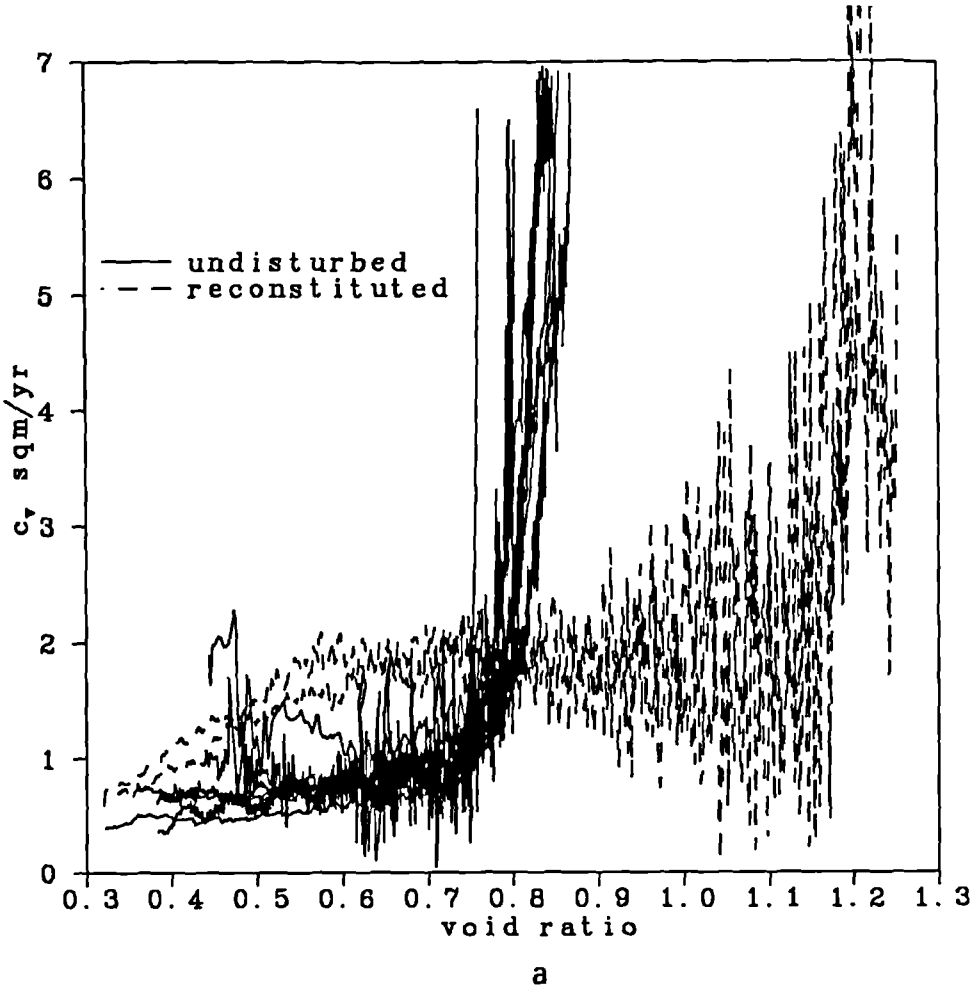

a

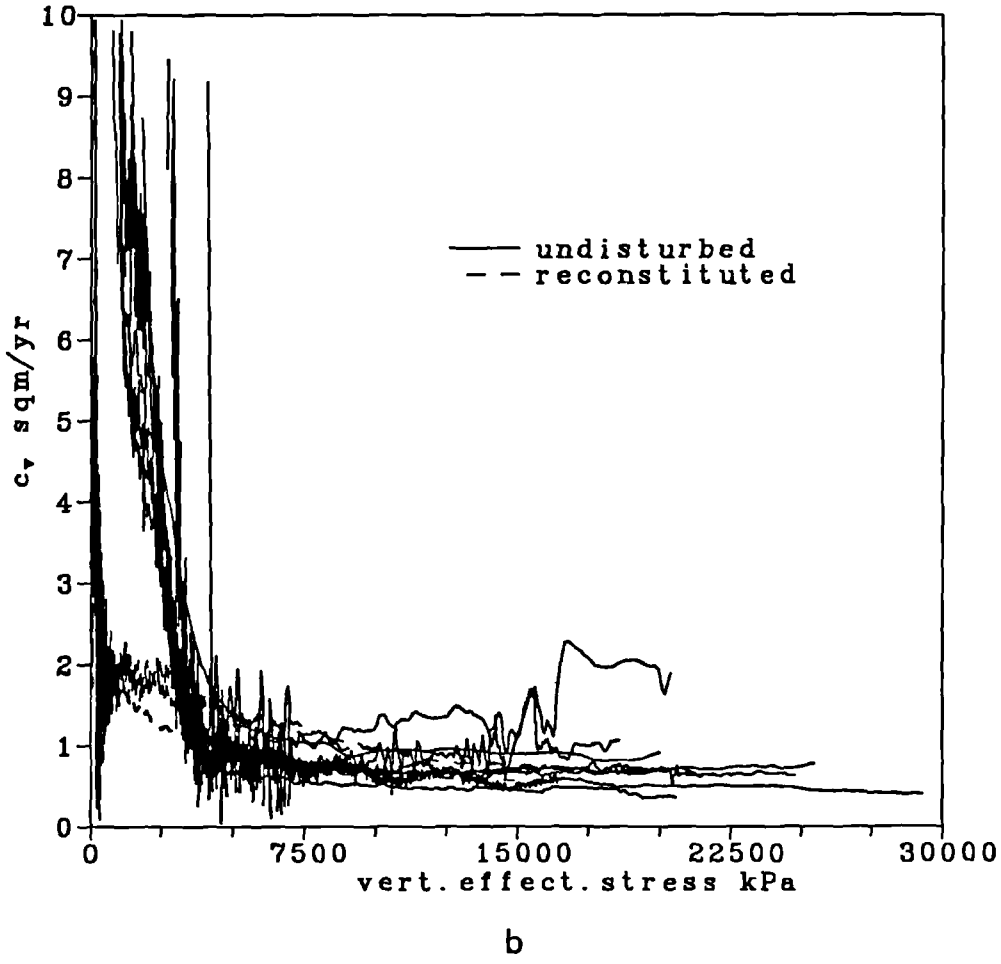

b

Fig.6.84. Natural and reconstituted Pappadai clay : values of c_v measured in the CRS tests.

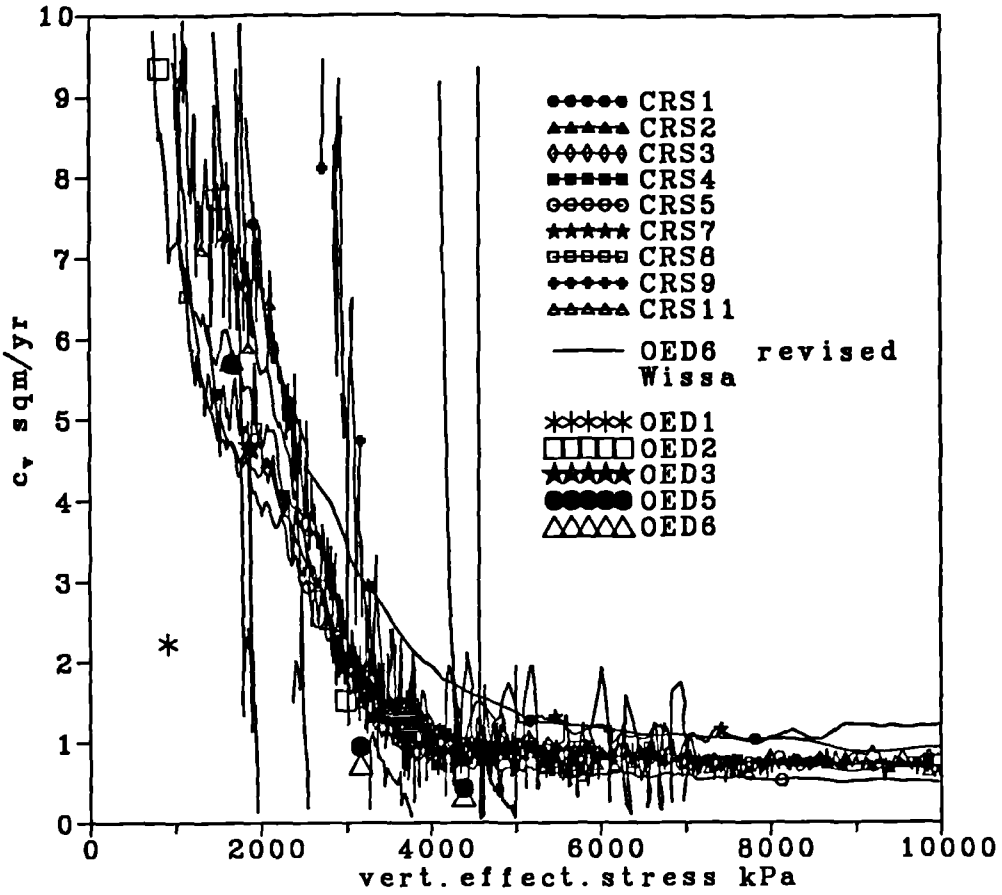

Fig.6.85. Natural clay : comparison between the c_v values measured in the OED and the CRS tests.

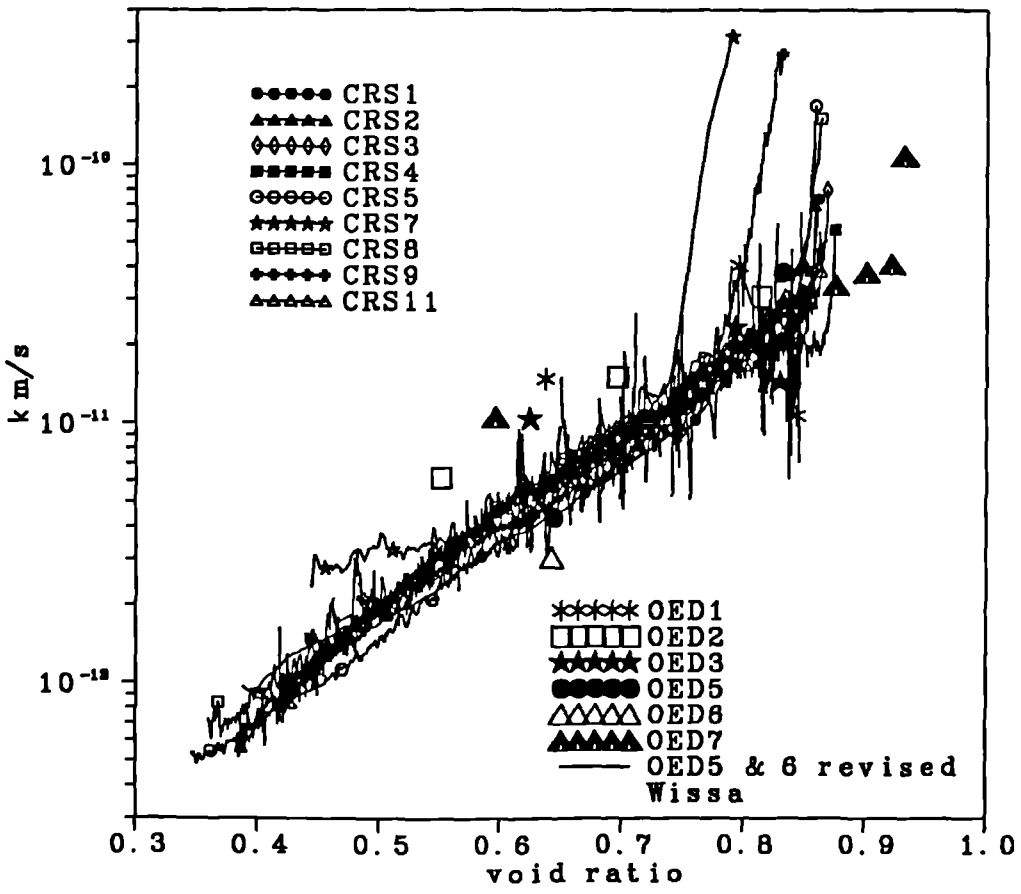

Fig.6.86. Natural clay : values of k measured in the OED and CRS tests.

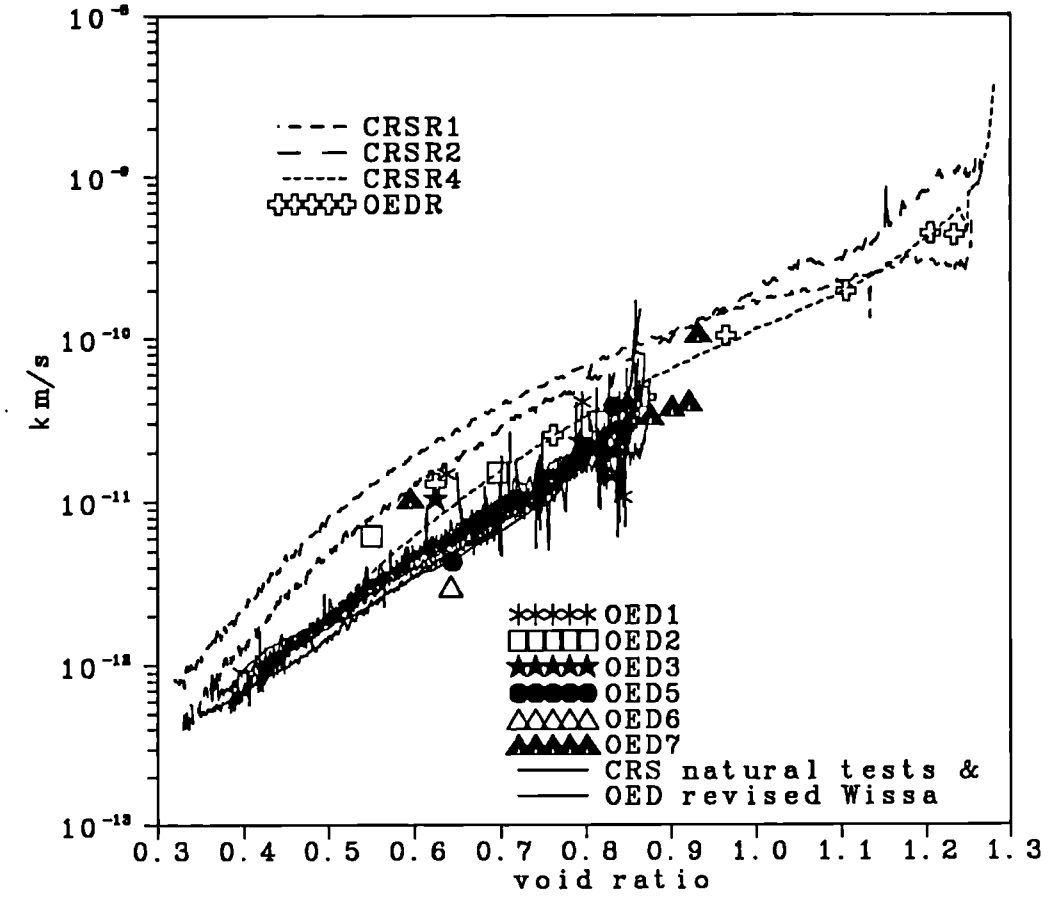

Fig.6.87. Comparison between the k-e relationships applying to the natural and the reconstituted clay.

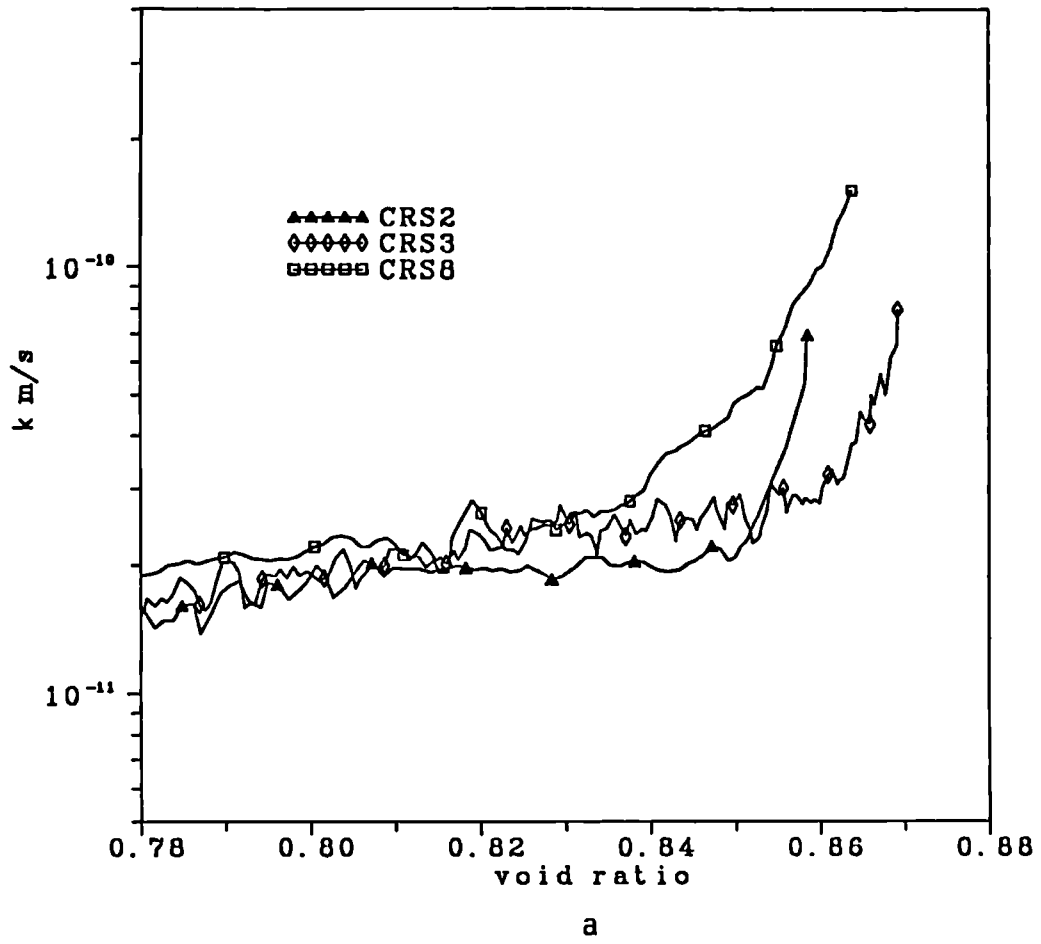

a

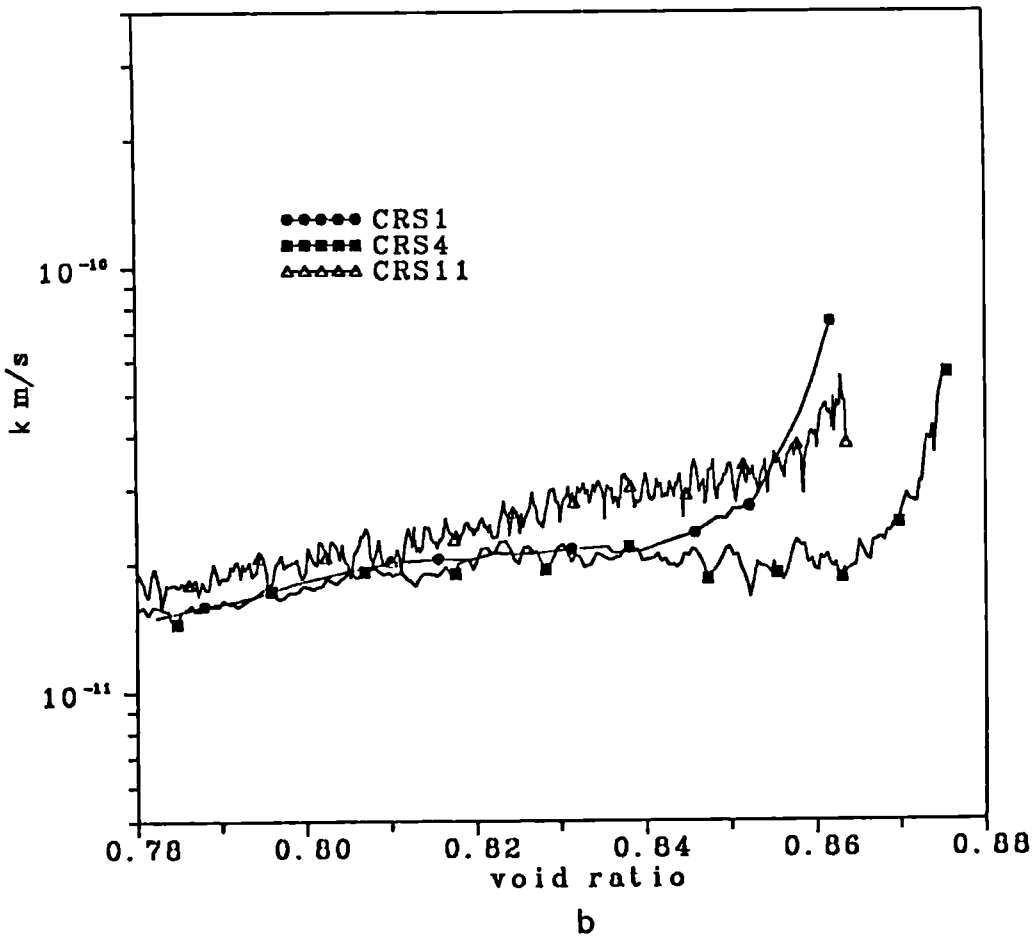

b

Fig.6.88. Constancy of k before yielding.

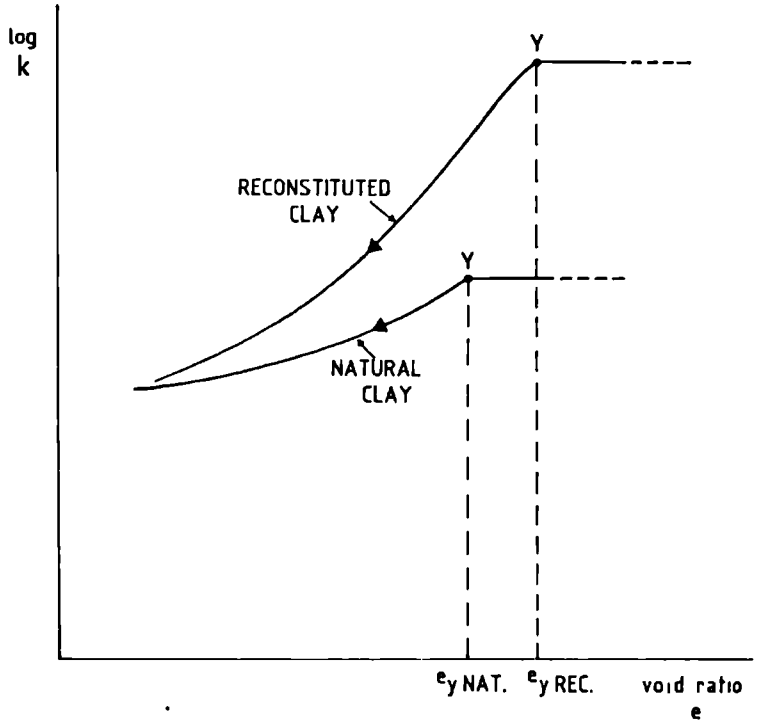

Fig.6.89. k-e relationships for clays.

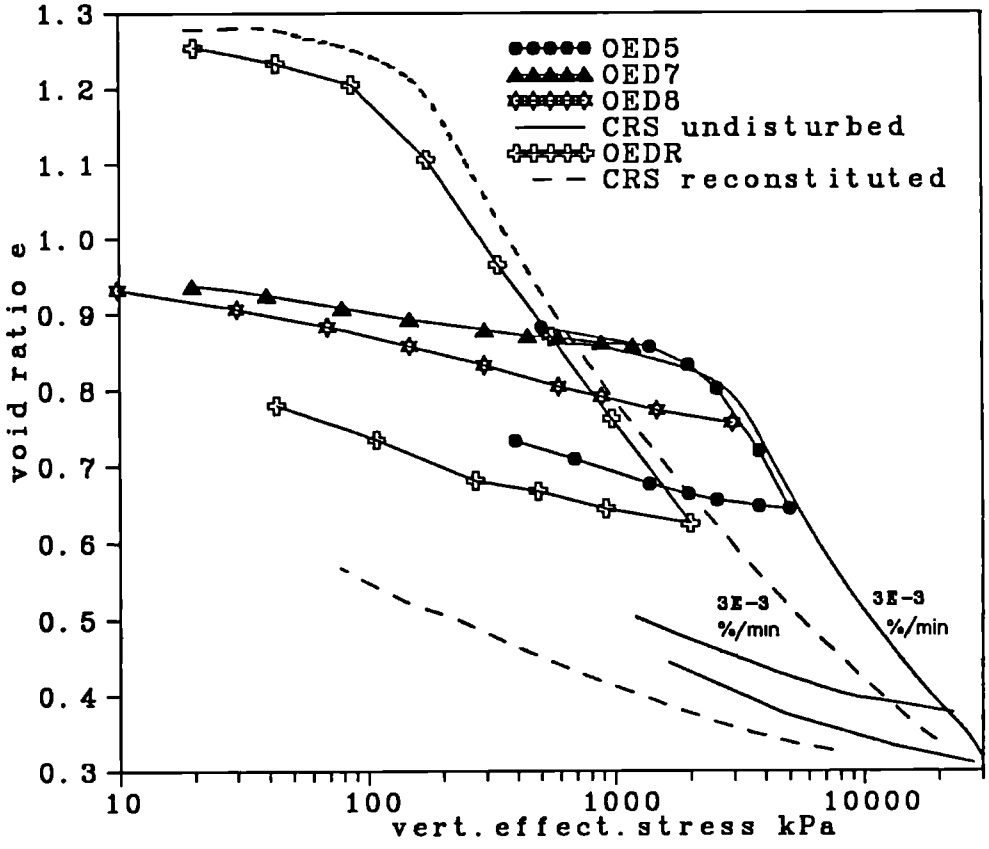

Fig 6 90. Compression behaviour of the natural and the reconstituted clay

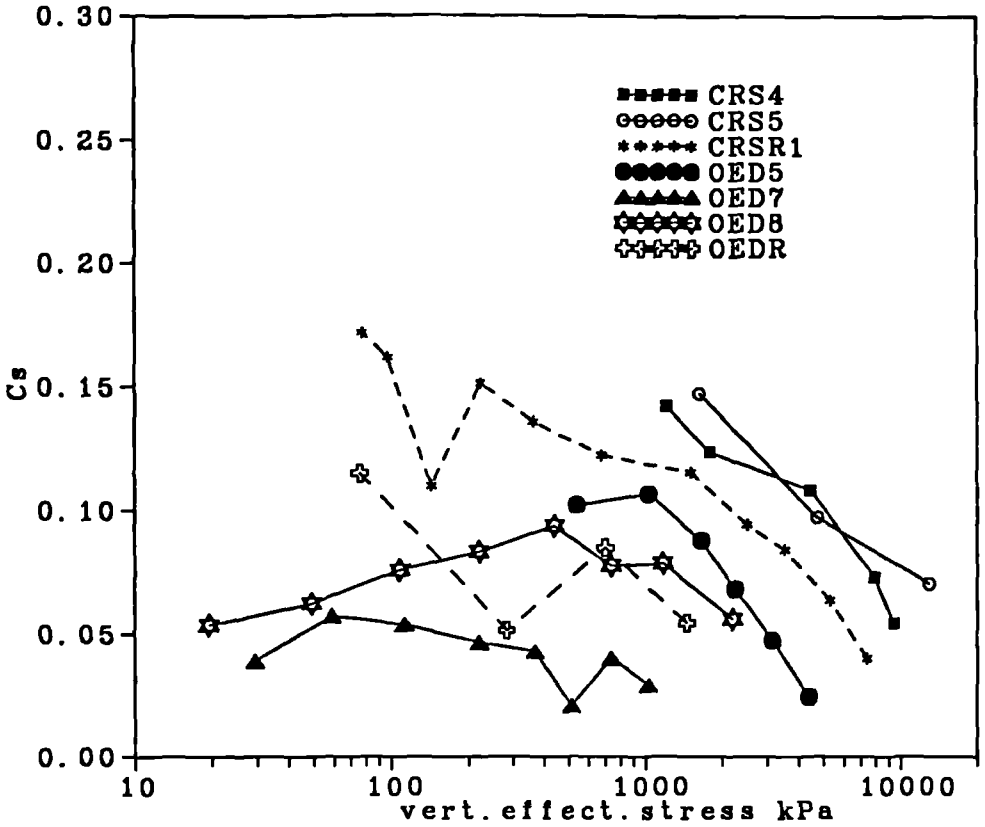

Fig.6.91. Natural and reconstituted clay : swelling index.

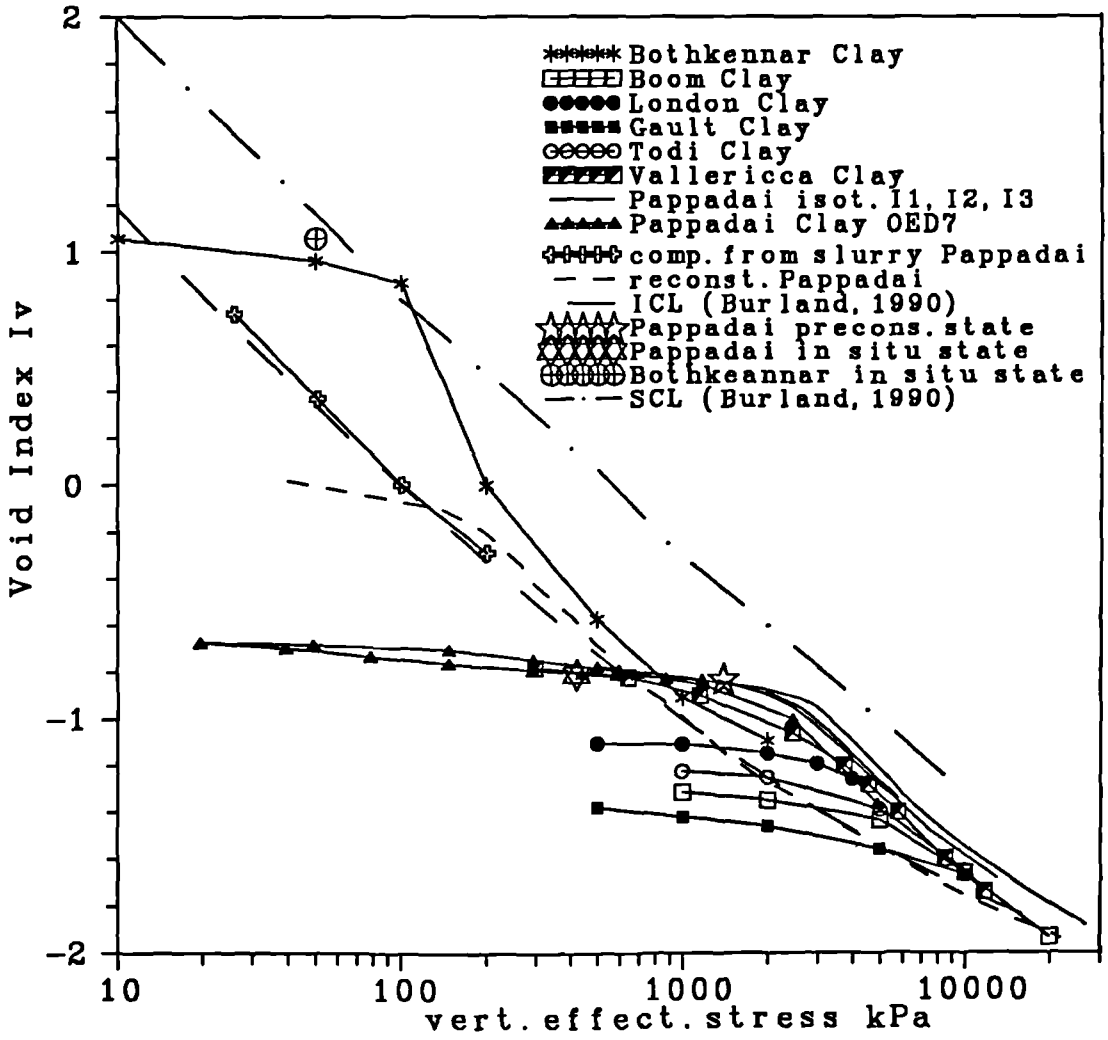

Fig.6.92. The ICL, the SCL (Burland 1990) and the normalized compression curves of natural clays of different origin and structure. Data from Webb (1964), Burland (1990), F.Cotecchia (1990), Rampello et al.(1993), Smith et al.(1993), Coop et al.(1995), Burland et al.(1996).

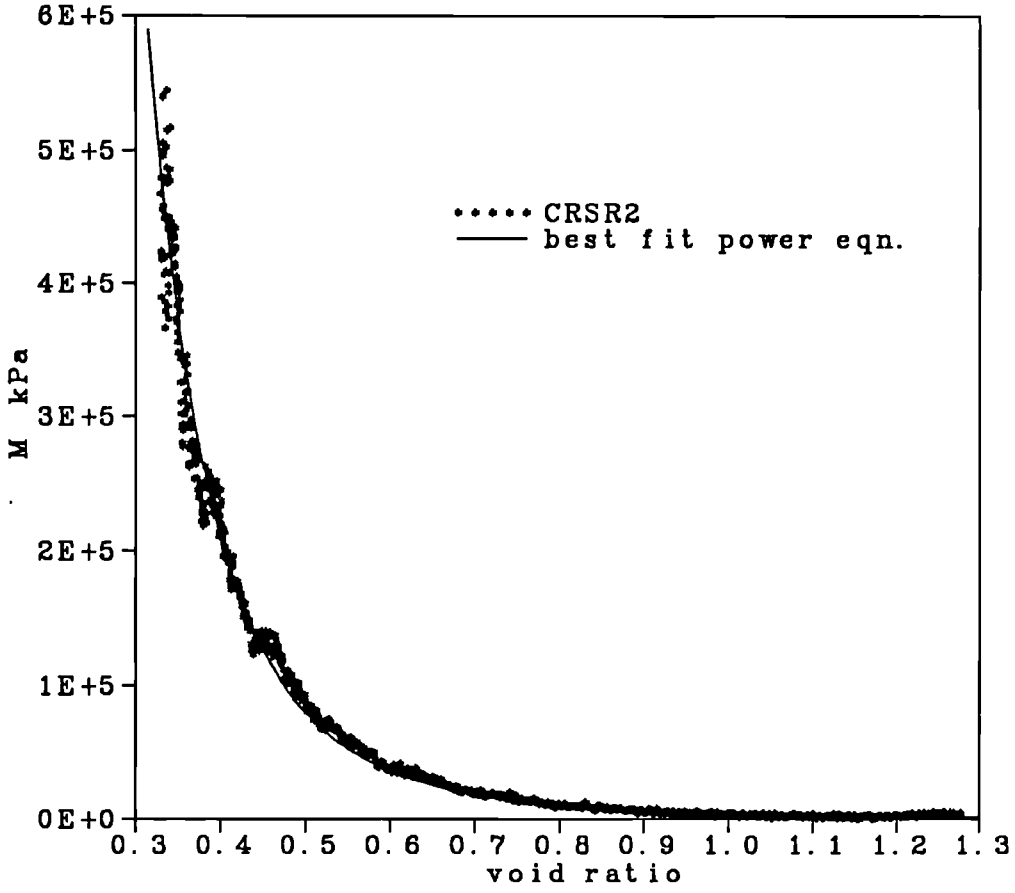

Fig.6.93. M-e relationship applying to both the reconstituted and the natural Pappadai clay beyond yield.

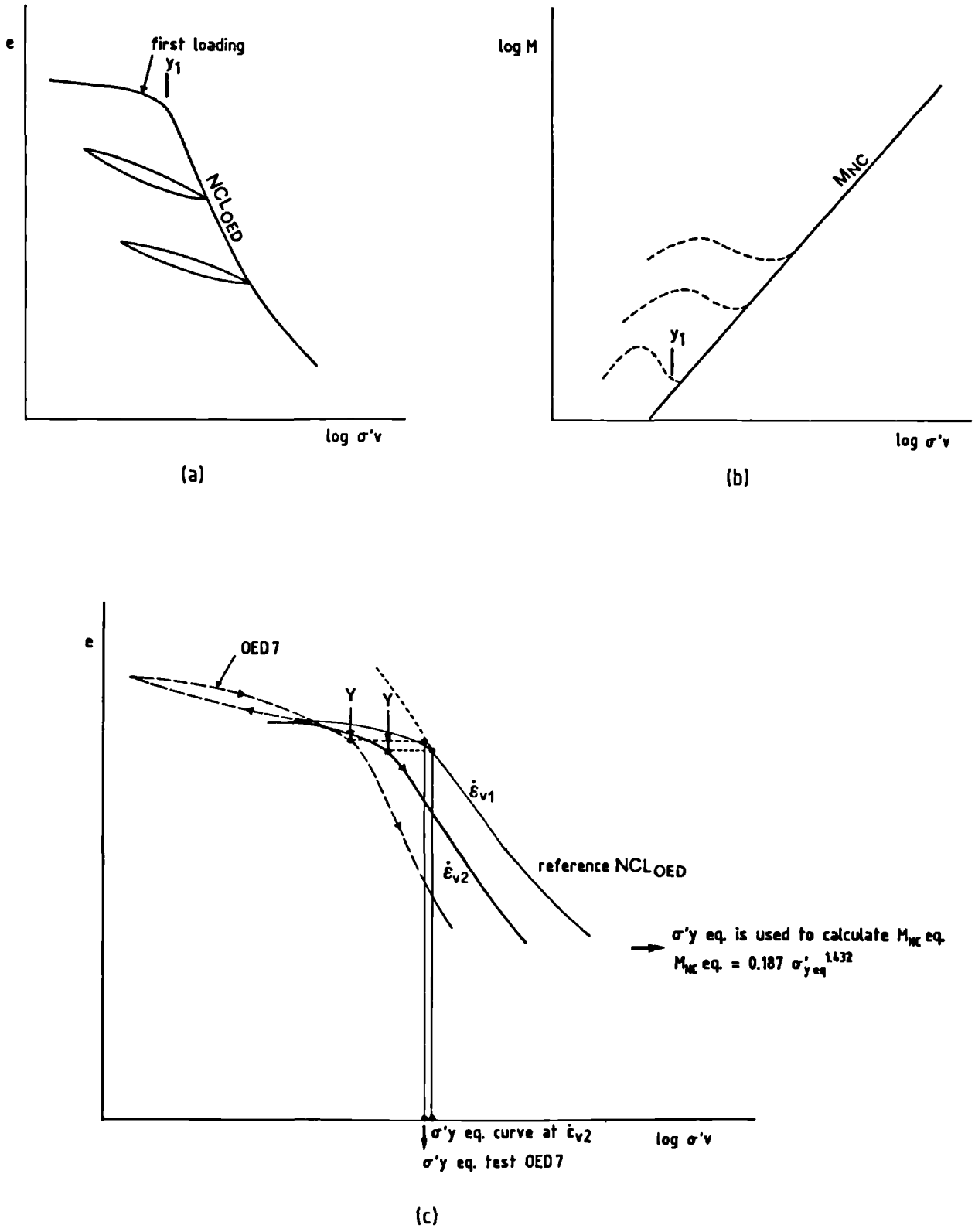

Fig.6.94. Idealized e-σ'_v (a) and M-σ'_v (b) behaviour of the natural and the reconstituted clay in oedometric compression; calculation of the normalizing factor M_{NCeq} (c).

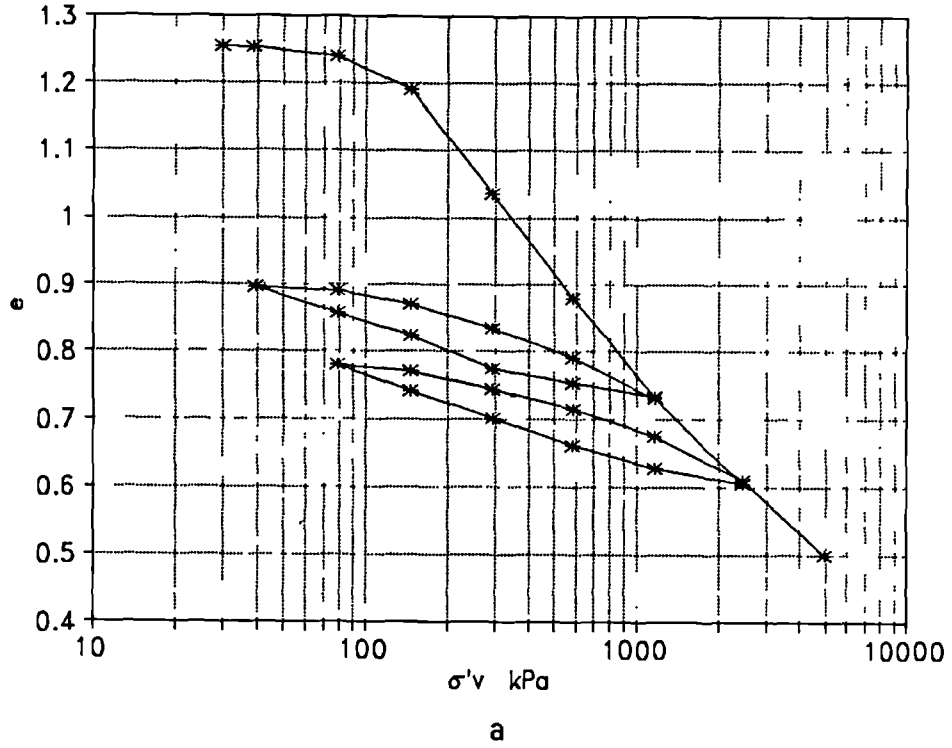

a

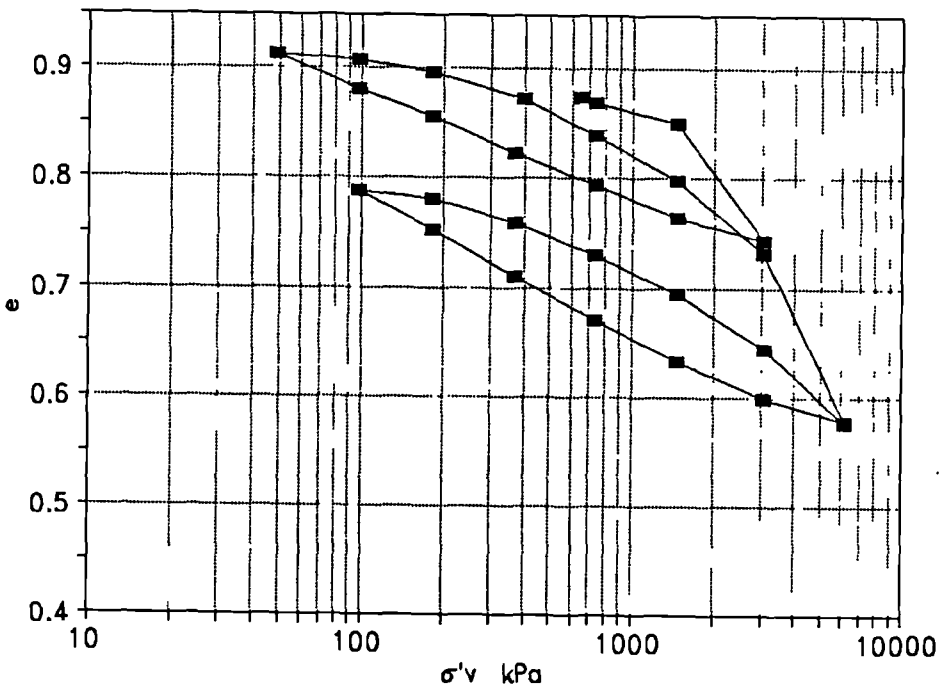

b

Fig.6.95. (a) Test OEDRb on the reconstituted clay and (b) test OED10 on the undisturbed clay.

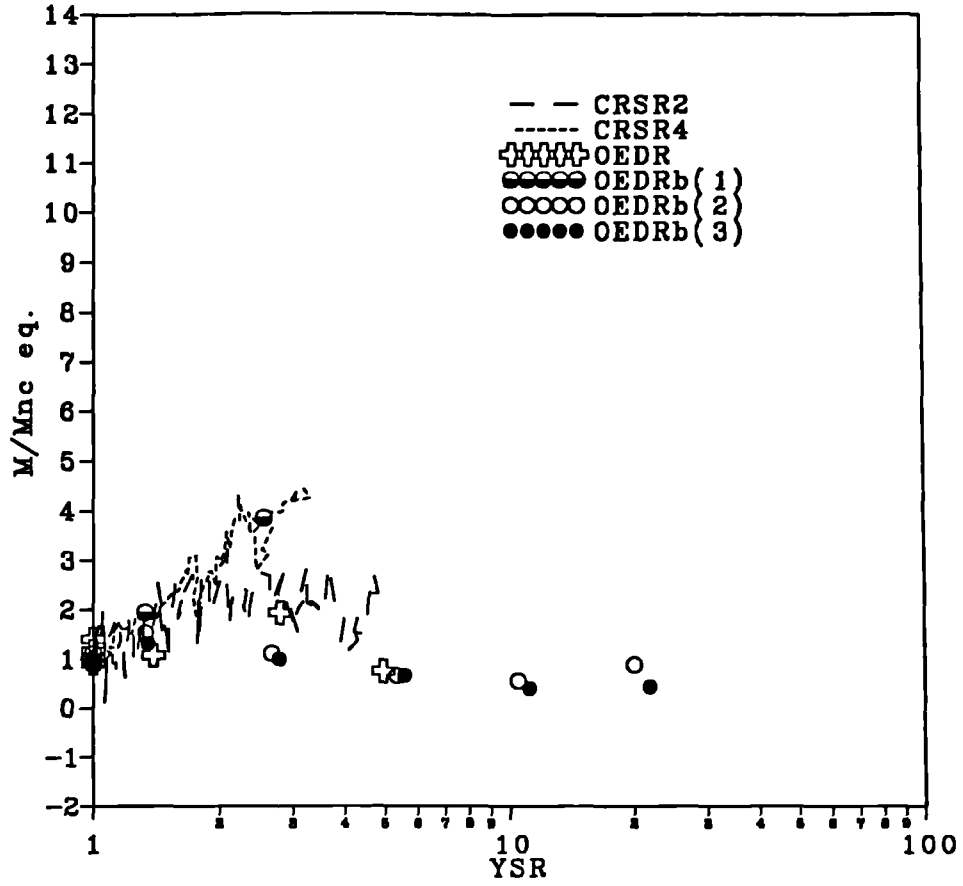

Fig.6.96. Oedometric stiffness of the reconstituted clay normalized with respect to volume.

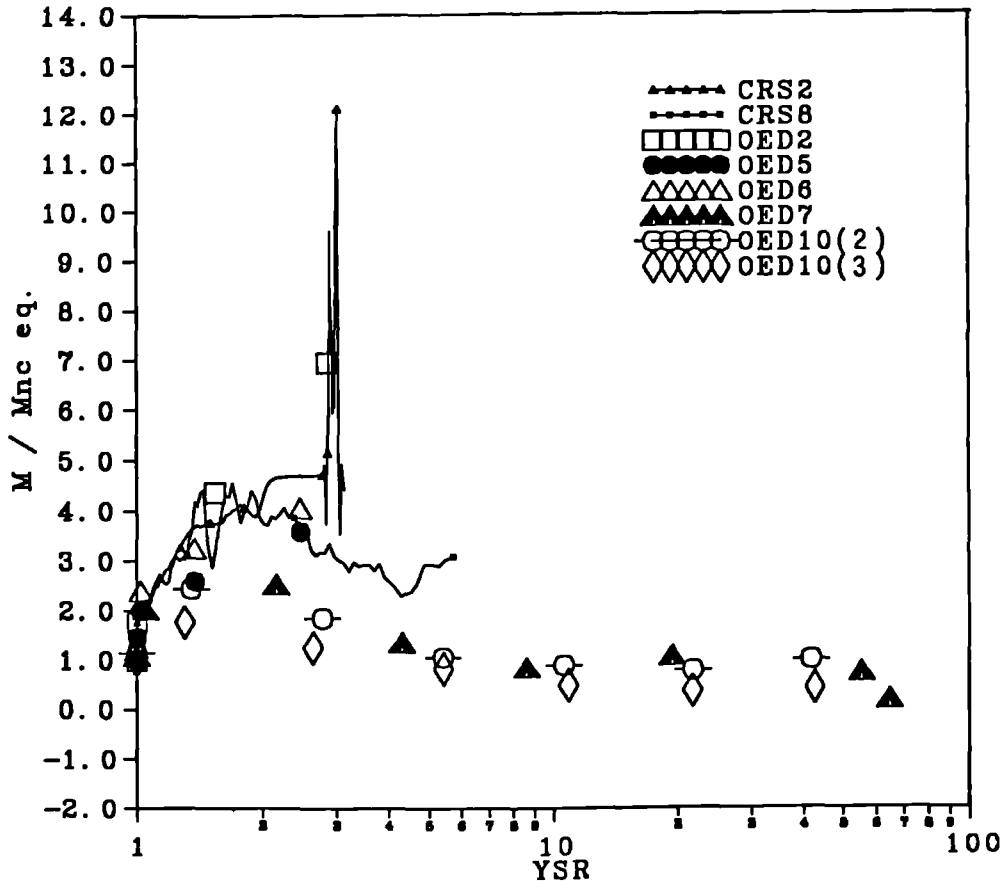

Fig.6.97. Oedometric stiffness of the natural clay normalized with respect to volume.

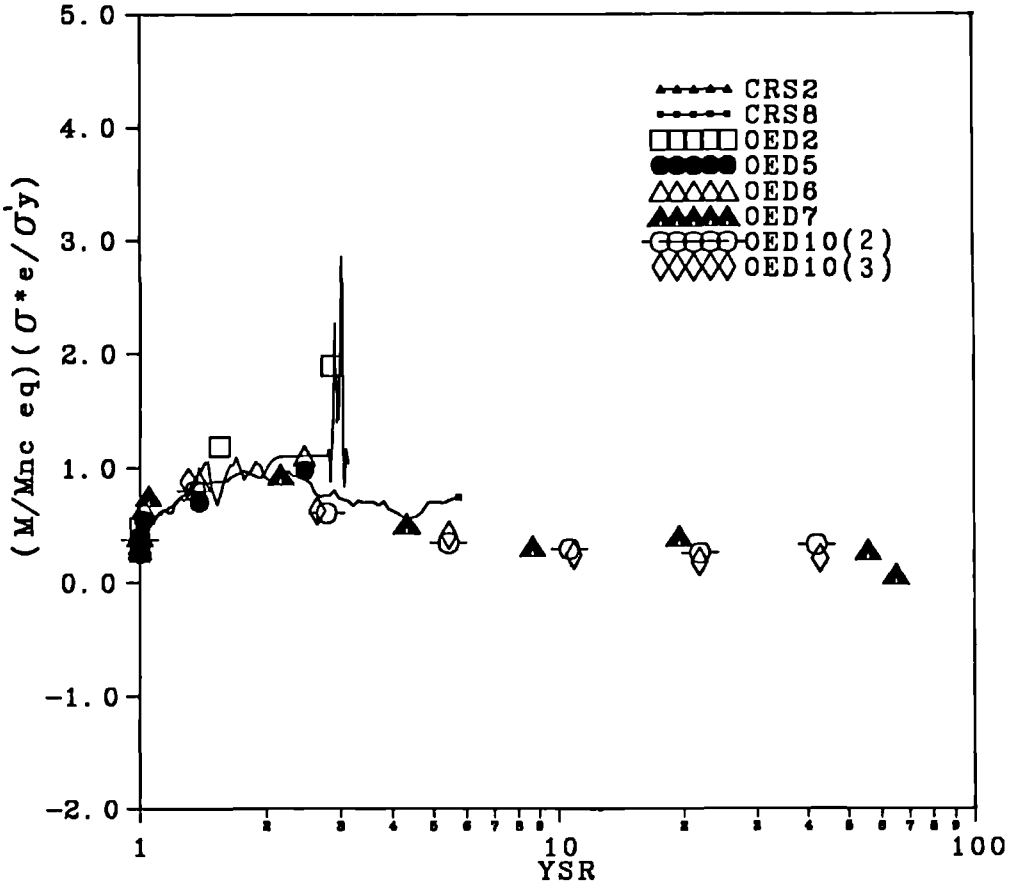

Fig.6.98. Oedometric stiffness of the natural clay normalized with respect both to volume and to the structural changes.

CHAPTER 7

CHANGES IN THE MICROSTRUCTURE OF THE CLAY DURING OEDOMETRIC COMPRESSION

7.1. Introduction

Chapter 6 presented the response to oedometric loading of both the natural and the reconstituted Pappadai clay, and proposed hypotheses concerning the changes in microstructure along the observed state paths. In this chapter the results of an SEM investigation of the microstructures of both the natural and the reconstituted clay during oedometric compressions to both intermediate and very high stresses are discussed. The microstructural changes are shown to be quite complex and to differ for the natural and reconstituted clay It is shown that it is not possible to postulate microstructural features and their modifications solely on the basis of the behaviour of the clay at the macro-level. Results of powder X-ray diffraction analyses are also presented to show the effects of the oedometric compression on the clay mineralogy

7.2. Clay samples examined by means of the SEM

In Sections 5.9.1 and 5 9 2 the procedures followed in the study of the microstructure of the natural and reconstituted Pappadai clay were discussed. The investigation was carried out by means of the SEM on samples of both the natural and the reconstituted Pappadai clay prepared by different techniques and analyzed in different laboratories, Table 5 9

The results of the analysis of the undisturbed clay (samples A in Table 5.9) and of the reconstituted clay consolidated from slurry to σ'_v of 200kPa (samples B in Table 5.9) were discussed in Sections 5 9 3 and 5.9 4. In this chapter the results of the analysis of samples C, D and E (Table 5 9) are discussed.

Samples C were created by fracturing a freeze-dried specimen of natural clay which had been compressed to 3MPa in test OED9 Similarly, samples D were natural clay compressed to 22MPa in test CRS2 and samples E were reconstituted clay compressed to 22MPa in test CRSR2. In the following the SEM samples C, D, E are referred to with the plural because for

each oedometer specimen, after compression and freeze drying, more samples were created by fracturing the specimen either horizontally or vertically.

The oedometer specimens subjected to the microscopic analysis were unloaded undrained in order to preserve the fabric acquired during compression At the end of compression the water was first extracted from the oedometer cell, and then the specimen was unloaded quickly. After freeze-drying and fracturing the samples were coated with either gold or carbon (see Table 5.9). The e-σ'_v states to which samples A to E correspond are indicated in Figs. 6.31, 6 49 and 6.71.

7.3. Fabric of the natural clay after oedometric yield

This section reports the study of the microstructure of samples C (Table 5 9) The clay fabric is mainly shown in SEM pictures of group 1. The fabric of samples C corresponds to a state point C in the e-σ'_v plane (C· e=0 75, σ'_v =3MPa) and resulted from the compression of sample A, from state point A (e=0.87, σ'_v ~0 65MPa) (see Fig 6 71)

During compression from A to C the clay underwent gross yielding, and the analysis of samples C was to observe what happens at gross yield in the clay The change in fabric following yield could be identified by comparing the fabrics of samples A and C, but the SEM was of no help in the study of the change in bonding

Figs.7.1 and 7 2 show global views of the fabric on vertical fractures through the clay after yield The fabric before yield shown in Figs 5 19 and 5 20 are at the same magnification as Figs 7 1 and 7 2, and may be compared After yield the fabric is more densely packed, although the large voids due to the presence of fossil shells are often preserved, as shown in Fig 7 2.

In the post-yield fabric the particle arrangements cannot easily be distinguished and the changes in particle arrangement in the different zones of the clay fabric are not as regular as in the undisturbed clay. The fabric changes are generally chaotic, different particle arrangements merging into each other so that their boundaries are ill defined Sub-vertical and sub-horizontal domains may be adjacent to and closely packed with flocculated and honeycomb fabrics These features are highlighted in the sketch in Fig 7 1, which refers to the photograph in the same figure.

In Fig.7.3 the fabrics of the clay before and beyond yield are compared at a higher magnification. Again the fabric beyond yield appears to be more densely packed, but less iso-orientated than the undisturbed fabric In the post-yield fabric some massive domains can be seen, which either bend in different directions or merge with areas of densely packed flocculated fabric, as highlighted in the sketch. In the undisturbed clay (Fig 7.3(a)) sub-horizontal iso-orientated domains are separated by an open flocculated fabric Both fabric types can be distinguished. These arrangements seem to be eliminated by the yielding process, being transformed into vortices of domains (see the sketch in Fig.7.3(b)), with no gaps separating the different fabric types. At some points circles of domains confine packings of random particles (Fig.7.3(b)) which may be effect of a flow of small particles to fill the large pores. The fabric transformations described above occur within an increment of vertical stress from about 700kPa to 3000kPa and a corresponding reduction in voids ratio of only 0.12.

The globigerinae shown in Fig.7.4 appear undamaged, as were many other shells observed in samples C. During the oedometric compression of the clay in the laboratory, as during the virgin compression of the clay in situ, the clay particles slide along the boundaries of the shells, which are then not damaged by the loading process (see Section 5.9). The fabric around the shells is strongly affected by the presence of these sand-size components.

The fabric on horizontal fractures through the clay is shown in Fig.7 5. Again, it appears more densely packed than the undisturbed fabric (see Figs 5 22, 5 23 and 5 26), but not as horizontally iso-orientated. A long thin stack of domains crosses the fabric horizontally in the middle of Fig.7.6, and is inter-bedded with particles arranged randomly; these features can be also observed in Fig.7.7, being highlighted in the sketch in Fig 7 6.

The highest magnification scans of the post-yield fabric in Figs.7.8 and 7.9 can be compared with the undisturbed fabric in Figs 5 28 and 5 31. Even at this magnification the post-yield fabric appears more densely packed and few voids can be distinguished Zones where small particle domains are densely and chaotically packed are frequent These masses of particles seem to form a very dense random fabric, a "chaotic mass" of particles, which may be regarded as the opposite of a stack of particles. This fabric type was not observed in samples A or B (see Section 5 9) and may be a peculiar effect of the yielding process In the centre of Fig 7 9 a "chaotic mass" of particles is seen, as also in Figs 7 7 and 7 8 Many coccoliths are trapped in the chaotic mass of particles shown in Fig 7 8(b)

The outlines of the particles in Figs.7.5 to 7.9 appear "fringed", giving a spongy appearance to the fabric. A similar appearance is associated with the presence of smectite particles in the undisturbed clay, but in samples C it is the state of the particles that gives rise to the spongy appearance. As the fabric changes occurring at yield have been shown to be complex and dramatic it is possible that the state of the clay particles is also affected by the yielding process.

In conclusion the yield of the clay causes substantial changes in the clay fabric. In the undisturbed clay the different fabric types can be distinguished from one another and often form a regular and repetitive architecture. Beyond yield this architecture is no longer recognizable. The original fabric has been destroyed and the particles compacted more densely. Comparison of pictures (a) and (b) in Fig.7.10, respectively showing the fabric of samples A and C (group 3 in table 5.9), confirms that the increase of density due to yield is not accompanied by an equivalent increase in particle orientation

7.4. Fabric of the natural clay under very high stresses

This section discusses the fabric of the clay when compressed by up to 22MPa vertical stress (samples D). Most of this analysis is based on SEM pictures of group 1, Table 5 9

In Fig.7 11 the fabric on a vertical fracture through the clay is shown Horizontal open fractures cross the clay. These are delimited by layers of perfectly orientated particles, as are evident in the enlargement in Fig.7.12. The horizontal surfaces of these planes are here defined as "fissility planes". The horizontal fractures are the effect of localized volumetric expansions of the clay during the unloading in the oedometer, even though the unloading was undrained Volumetric expansion occurred only between the "fissility planes".

This striking feature of the fabric highlights that, in the clay compressed to very high stresses, horizontal strata of perfectly orientated particles (c p o fabric) exist, which contain fissility planes It may be assumed that in samples D carbonate bonding no longer exists in the clay, so that the bonding between the particles is mainly of electrostatic and electromagnetic nature The observation that the volumetric expansion occurs only between the fissility planes and not elsewhere is then consistent with the fact that the bonding between particles in face to face contact, such as those forming the fissility planes, is weakest in the clay at high stresses (see Chapter 1)

The volumetric expansion of the clay necessarily resulted in cavitation of the pore water. It follows that the pore water did not sustain the suction developed in undrained unloading in those portions of the clay fabric where the bonding is weakest. A similar conclusion was drawn from the discussion reported in Section 5.9.4 concerning the extension fractures observed in the reconstituted clay.

Comparison of Fig.7.1 and Fig.7.13 shows that the degree of orientation of the fabric of the highly compressed clay is higher than that of the post-yield fabric, and that the clay porosity is much lower. It follows that the degree of orientation of the clay fabric is reduced during yield (see Section 7 3) and increases again in post-yield compression (see Figs.7.3(a), 7.3(b) and 7.14).

In Fig.7.14 an area of highly orientated fabric is shown. Perfectly orientated domains (c.p.o. fabric) form stacks which are interbedded between piles of mediumly to highly orientated domains. In addition the pictures of the fabric on horizontal fractures through the clay (Fig.7.15), and the high magnification pictures of the fabric on vertical fractures shown in Fig 7.16 indicate a highly orientated fabric. However the fabric shown in the lower half of Fig.7.14 is flocculated, and small stratified areas of flocculated fabric also appear to be interbedded with the sub-horizontally orientated domains; Figs.7.13 and 7.14 Zones of honeycomb fabric are shown in Fig 7 17; a sub-vertical framboid pyrite can be seen in the bottom left of the picture. The flocculated fabric shown in Figs.7.17 and 7.19 is as open as the fabric of the undisturbed clay.

Thus the compression of the natural clay to high stresses beyond yield does increase the orientation of the fabric, but only to a limited extent, as areas of flocculated fabric are either preserved or created during compression, and the fabric transformation is highly non uniform. It seems that oedometric compression changes the chaotic fabric created at yield into a regular alternation of stacks and areas of flocculated-honeycomb fabric. This fabric architecture resembles that proposed by Sfondrini (1977) for clay one-dimensionally compressed to medium-high pressures, shown in Fig.1.13(c). Fabric arrangements similar to this have also been recognized in the undisturbed normally consolidated Fiumicino clay Fig 1 13(a), in limited zones of undisturbed Pappadai clay, in the reconstituted Pappadai clay normally consolidated to 200kPa, in the normally consolidated sandy clay tested by Menkiti (1995), and in the normally consolidated kaolin tested by V.Cotecchia et al (1982) (see Chapters 1 and 5) The frequent occurrence of this fabric in one-dimensionally compressed clays supports the idea that one-dimensional compression does not simply induce iso-orientation of the clay particles, but in fact gives rise to complex non-uniform fabric changes

For clays normally consolidated to medium high stresses, compression creates stacks while preserving areas of open flocculated fabric which undergo little compaction (Figs 1.12 and 1.13(c)) Thus the increase in orientation arising from the 1D compression is a combination of the very high degree of orientation of the stacks and the very low degree of orientation of the flocculated fabric. Whether the compression of the normally consolidated clay to very high stresses changes the flocculated fabric into orientated fabric is not demonstrated by the data in the literature to date, and will be discussed in the following section on the basis of the results of the analysis of the reconstituted Pappadai clay after 1D compression to 22MPa.

The 1D compression of a natural clay which has been subjected to diagenesis, such as the Pappadai clay, can cause fabric changes which are even more complex than those described for normally consolidated clays. Not only is the compaction and reorientation of the clay fabric not uniform, but also it goes through stages, the first being the destruction of the original fabric at yield, and the second being the creation of a new fabric architecture.

The structure of the clay shortly after yield is more compressible than that before yield because of the weakening at yield of the clay bonding. This weaker structure finds itself subjected to high stresses while at high voids ratio. The 1D compression then appears to give rise to regular stacks of domains interbedded with areas of honeycomb fabric The latter fabric is very resistant and stiff due to the size of the electrostatic forces acting at the edge to face contacts between the particles within the honeycomb fabric This stiff fabric thus guarantees equilibrium with minimum deformation. The creation of this resistant fabric post-yield may be the reason why the natural Pappadai clay exhibits strengths higher than those of the reconstituted clay far post-yield, such that the natural clay lies to the right of the ICL to 25MPa vertical stress (see Sections 6.5 and 6 6). The question of whether the fabric changes observed in the natural Pappadai clay apply in general to stiff clays during oedometric compression cannot be answered here, as such an investigation has never been carried out for other stiff clays

Interbedding of stacks of particles and honeycomb fabric can be also recognized in clays which have undergone shearing The SEM pictures reported by Sfondrini (1977) for an Italian scaly clay, highly sheared during its geological history, the SEM pictures reported by V Cotecchia et al (1982) for a specimen of reconstituted clay after shearing to residual in the shear box, as well as the results of the application of tomography to a TRX specimen of Beauca re marl after shearing (Tillard-Ngan et al.1992) (see Chapters 1 and 2), are only some of the data in the literature which show that a resistant fabric such as that created by oedometric compression in

the Pappadai clay to high stresses, can result also from shearing paths. In this case the shearing planes coincide with the fissility planes which cross the stacks of particles.

Figs.7.18 and 7.19 show enlarged details of both orientated and flocculated fabric in the natural Pappadai clay at 22MPa vertical stress. The particle outlines appear to be even more fringed and folded than in the clay just after yield (samples C).

7.5. Fabric of reconstituted clay after compression to very high stresses

In this section the fabric of the reconstituted clay compressed to a vertical stress of 22MPa and a voids ratio of about 0.3 (samples E; Fig 6.71) is described.

Global views of the fabric on vertical fractures through the clay are shown in Figs 7 20 and 7 21 The striking feature of this fabric is its very dense packing. The increase in density of packing is evident in the comparison of these figures with Fig.5.41, which shows the reconstituted fabric at a voids ratio of 1.24 (sample B).

The fabric at low pressures is rather open, and it is easy to distinguish the different particle arrangements, though this is much more difficult in the very dense fabric of the clay compressed at high pressures. At low pressure the fabric shows (Fig 5.41) a medium-high degree of orientation, with open fractures between fissility planes, but in the highly compressed clay a fabric orientation is not apparent. In the highly compressed clay a medium degree of orientation is seen in Fig.7.21(b) only, which shows the fabric on an inclined fracture through the clay. The absence of open fractures between fissility planes, as in the clay immediately post-yield, also suggests the absence of highly orientated particles.

Undamaged globigerinae can be recognized in the clay at high pressure, in Fig 7 22 top left an undamaged coccosphere can be recognized. Thus even in very large compressions in the laboratory (40% vertical strain) carbonate shells may be not damaged

Fig.7.22 is most informative of those showing fabric of highly compressed reconstituted clay. Stacks of particles differently orientated and areas of flocculated fabric merge in with random or even chaotic particle assemblages. Thus for the reconstituted clay also the fabric changes are not uniform during compression The size of the orientated domains increases with compression, but

these are also distorted and merge with chaotic aggregates Thus 1D virgin compression to very high stresses may not give rise to an orientated fabric (Figs 7.22 and 7.23).

The fabric of reconstituted Pappadai clay at high stresses is more disordered than expected by Sfondrini (1977) (Fig.1.13(d)). Moreover, the fabric of the reconstituted Pappadai clay is much less orientated than the kaolin normally consolidated to 4.9MPa, Fig.1.12(e) (V.Cotecchia et al.1982). Presumably the mineralogical composition of the clay influences the fabric changes. With increasing compression, the fabric orientation of mono-mineralic clay seems greater than for clay formed of different clay minerals and having other constituents, e.g. fossils and crystals.

In the reconstituted Pappadai clay the small particles are either stuck on the surface of the large particle domains or penetrate into the domains (Figs 7.24 and 7.25). Chaotic packings of particles similar to the "chaotic masses" defined in Section 7.3 can also be recognized in the reconstituted clay at high pressure.

In conclusion the fabric of the reconstituted clay consolidated to 200kPa vertical stress seems to be more regular and orientated than that of the clay subjected to 22MPa vertical stress. At 22MPa the clay particles in open flocculated arrangements at 200kPa either form dense assemblages of random fabric or are stuck onto the large particle domains The fabric of the reconstituted clay at high pressure is more chaotic than that of the natural clay subjected to the same vertical stress, Fig.7.26. The creation of efficient and regular particle arrangements, as recognized in samples D (see Section 7 4), occurs during the post-yield compression of the natural stiff clay, and is probably related to the change in strength of the clay bonding at yield.

In the reconstituted clay at high pressure the surface of the clay particles appears to be more damaged than at 200kPa vertical pressure (see Fig.7.25). Thus compression seems to affect the particles of both the natural (see Section 7 4) and the reconstituted clay

7 6 Effects of oedometric compression on the mineralogy of the clay

Mineralogical analyses of the clay samples A to E in Table 5 9 were carried out to evaluate if the mineralogy of the clay was modified during oedometric compression. These analyses were carried out by the Mineralogy Section of the Geological Department of Bari University

The results of the analysis are reported in Table 7 1. The data for the undisturbed natural clay (sample A) are the same as those in Table 5.2(b), and the data for the reconstituted clay (sample B) are the same as those in Table 5.6. In Section 5 8 the difference between these two sets of data was considered to be the effect of an aggradation of the swelling clay minerals during the grinding of the clay.

The results of X-ray diffraction analyses are not well suited to discern small differences in the mineralogical content of different clay samples, as these analyses are principally qualitative and the errors affecting the percentages of the single minerals can be large. From the data in Table 7.1 the trends of the changes in mineralogy with compression of both the natural and the reconstituted clay can only be deduced hypothetically.

The natural clay seems to undergo only mild mineralogical changes, if any, when subjected to compression. Rather, with the reconstituted clay, an increase of non-swelling minerals seems to occur with compression (40% vertical strain) The percentage of swelling minerals reduces from about 16% to about 3%. Such a decrease is higher than the error of the measurement technique. Thus the swelling components of the reconstituted clay seem to undergo a collapse, i.e. transform from smectite into illite (see Chapter 1), greater than that of the swelling components of the natural clay. These different changes in the content of swelling minerals may be related to the different changes the fabrics of the two clays experience during compression.

Indeed the smectite particles undergo completely different rearrangement in the two clays, e g. different dislocations, distortions and compression, as shown in Sections 7.4 and 7.5. In the reconstituted clay, the smaller clay particles are found either stuck on the large particle domains or packed into very dense chaotic assemblages, while in the natural clay they are part of the open flocculated fabric which is interbedded with the stacks of domains.

Thus the occurrence of some aggradation of the swelling minerals (see Chapter 1) during the large compression of the reconstituted clay, although hypothetical, seems to be consistent with the results of the analysis of the SEM pictures discussed in the previous sections.

7 7 Conclusions

The changes in fabric occurring in both the natural and the reconstituted clay during oedometric compression have been shown to be very complex and the differences in microstructure between

the two clays, both at medium and at high stresses, have been illustrated and. These interpretations could not have been made by a study of the clay behaviour at the macro-level.
The yield of the natural Pappadai clay weakens the clay bonding and makes the fabric of the clay chaotic, erasing the features of the fabric architecture present before yield. Beyond yield the compression of the clay gives rise to a regular and resistant fabric, rather than to the "destructuration" which is usually assumed in the literature to occur in the post-yield compression of natural clays.

The compression of normally consolidated reconstituted clay consists of a non-uniform densification which does not necessarily give rise to an orientated fabric. On the contrary, it seems that the chaotic arrangement present in the reconstituted clay at high stresses is consistent with the high density of the clay as all the voids are chaotically filled with particles.

The structures of the natural stiff clay and of the reconstituted clay have been found to remain different beyond yield up to very high stresses The structural differences tend to diverge with compression rather than to become similar.

The main conclusion of the study of clay microstructure presented in this thesis is that is not correct to search for deterministic relationships between the structural features of clays and their effects on the clay behaviour. Natural and reconstituted clays have a different structure in any volume-stress state e-σ'_v, and it is not possible to define which of the features of the natural structure causes observed aspects of behaviour Nonetheless, while the differences in structure between the clays are complex, their behaviour at the macro-level is more similar (see Chapter 6 and 8). The structure of natural stiff clays which are not cemented was shown to be of medium-low sensitivity (Section 6.7.3); this finding is consistent with the observation, reported in this chapter, of the existence in the natural clay compressed to high stresses post-yield of a resistant structure different from that of the reconstituted clay at high stresses

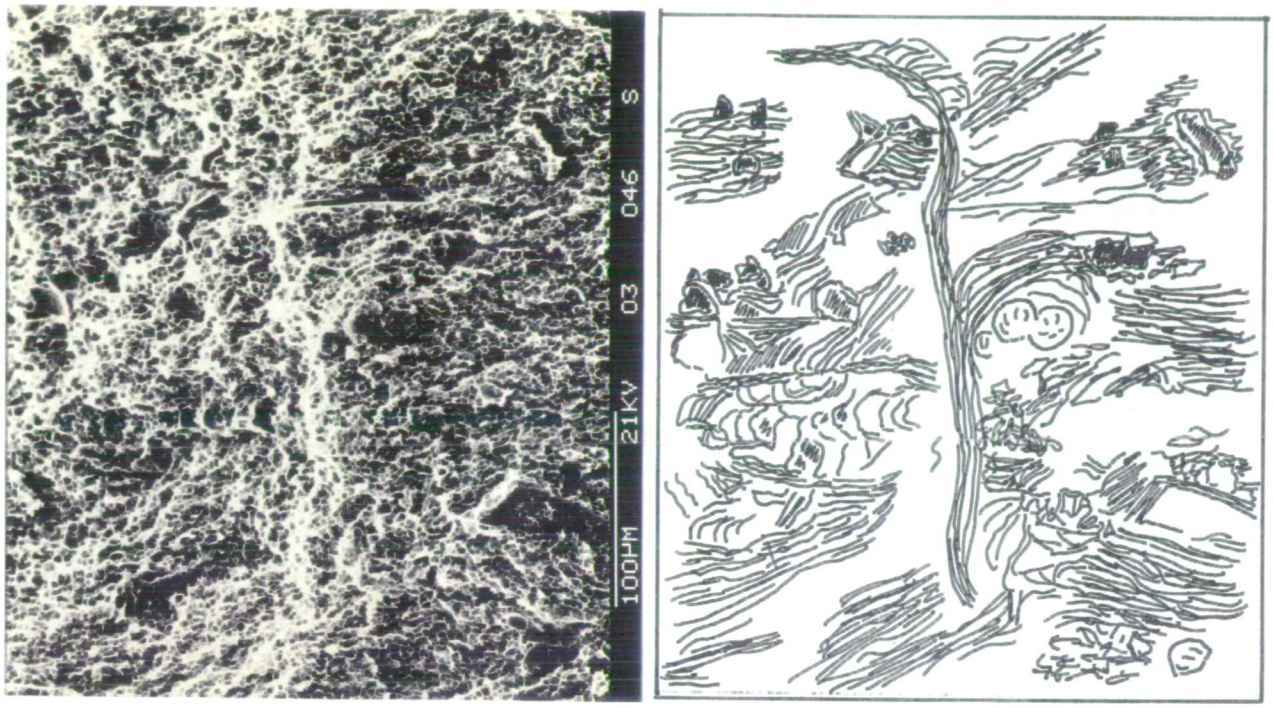

Fig. 7.1 - Natural clay compressed to a σ'_v of 3 MPa: global view of the fabric on a vertical fracture: the fabric appears densely packed but poorly orientated; group 1 (Table 5.9).

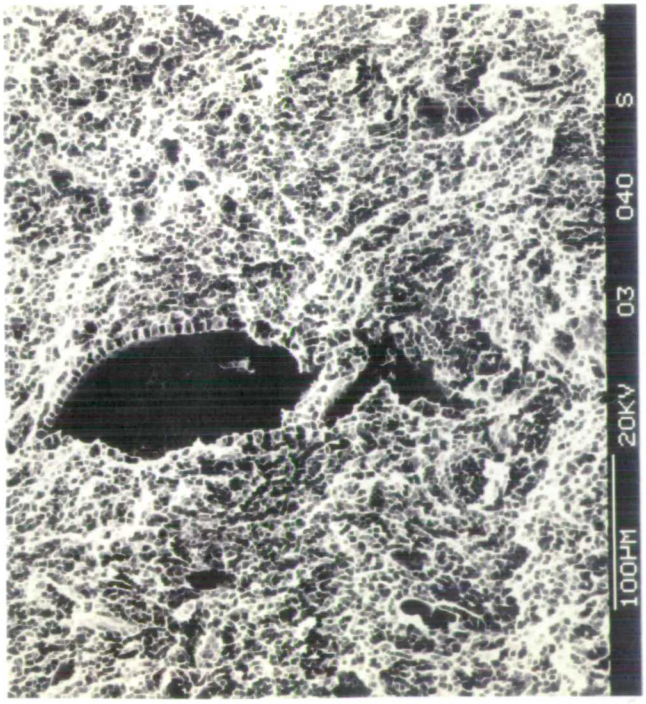

Fig. 7.2 - Natural clay compressed to a σ'_v of 3 MPa: vertical fracture; stacks of domains are inclined in different directions; empty macro-voids confined by fossil shells; group 1 (Table 5.9).

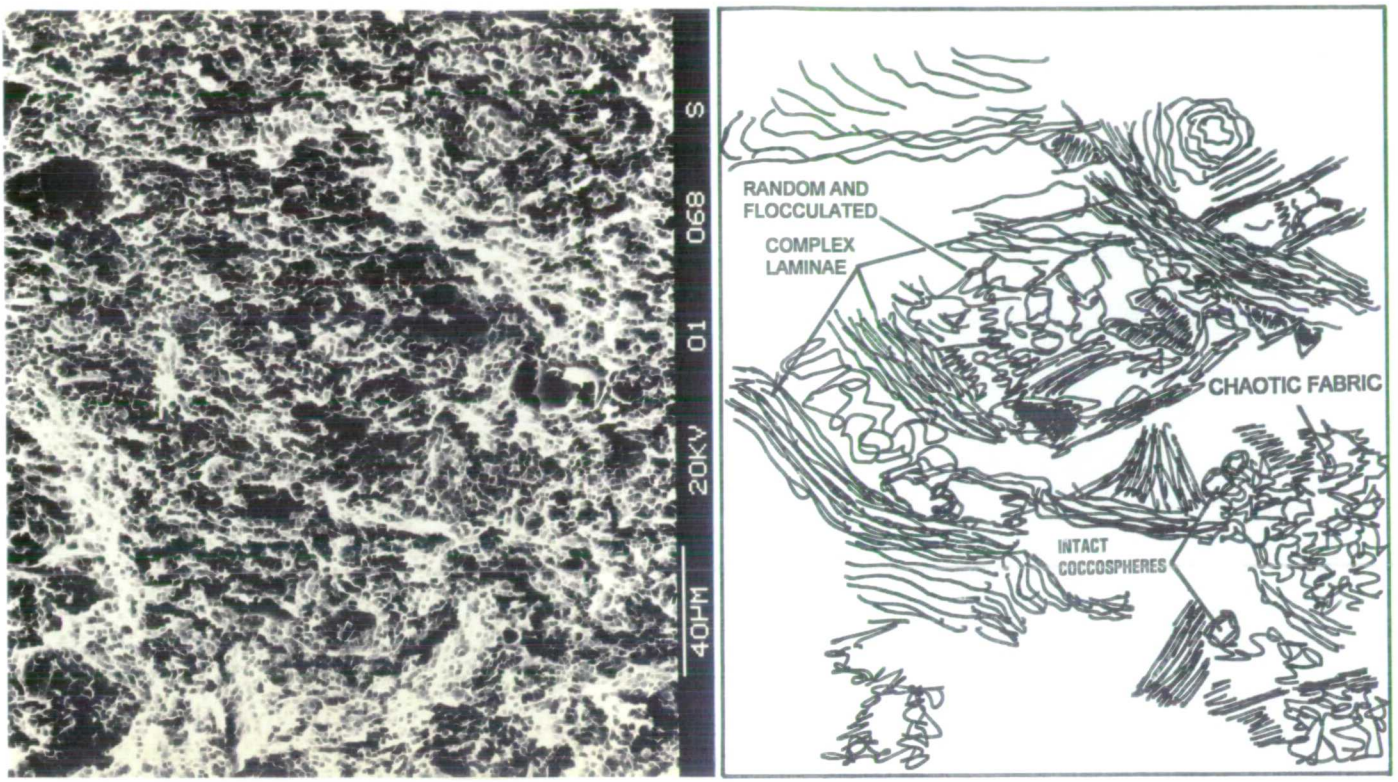

(a)

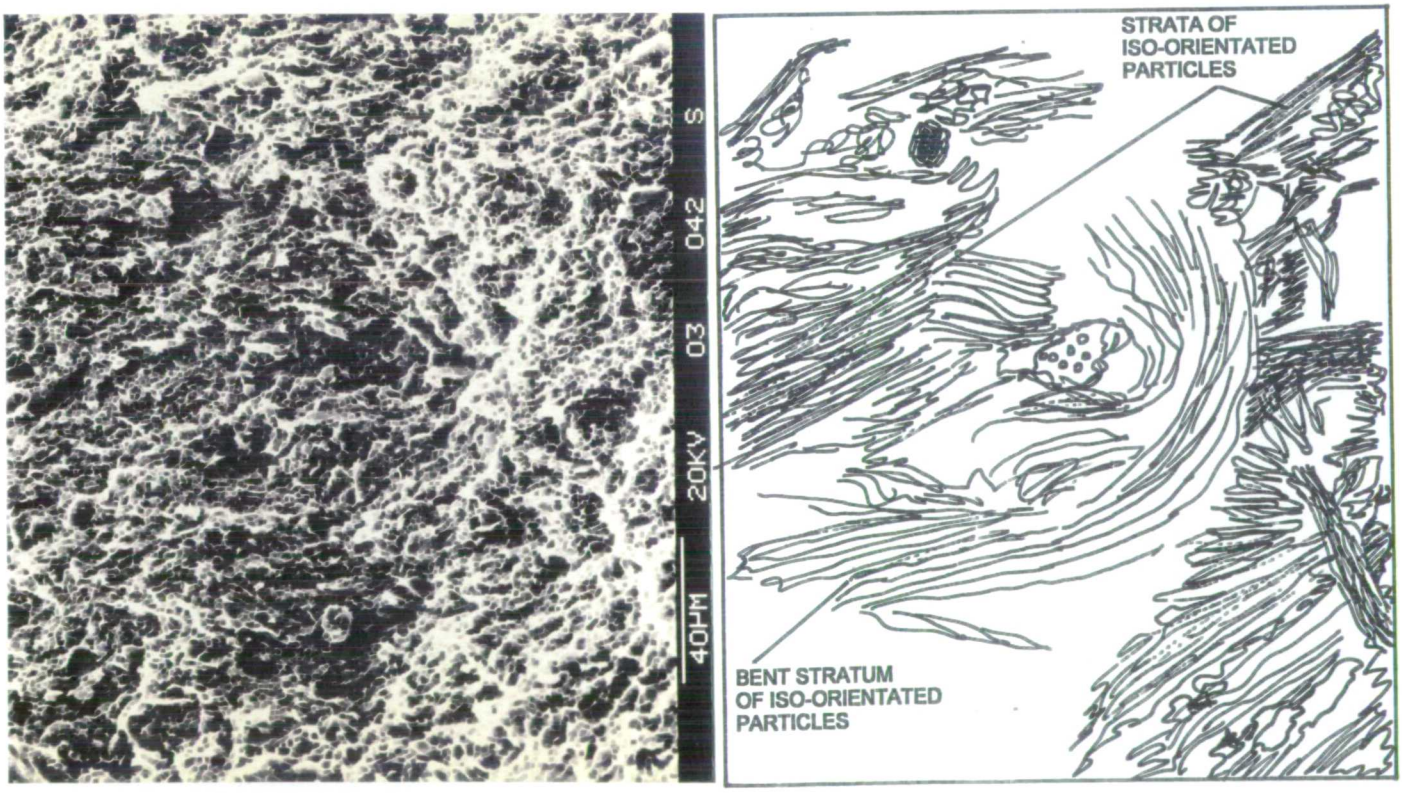

(b)

Fig. 7.3 - Natural clay compressed to a σ'_v of 3 MPa: vertical fractures; (a) stacks of domains following different directions confine areas of more open either random or more regularly flocculated fabric; at points the fabric is chaotic; various coccospheres can be seen on the right side of the picture; (b) the fabric is denser and with a higher degree of orientation than in (a); group 1 (Table 5.9).

(a)

(b)

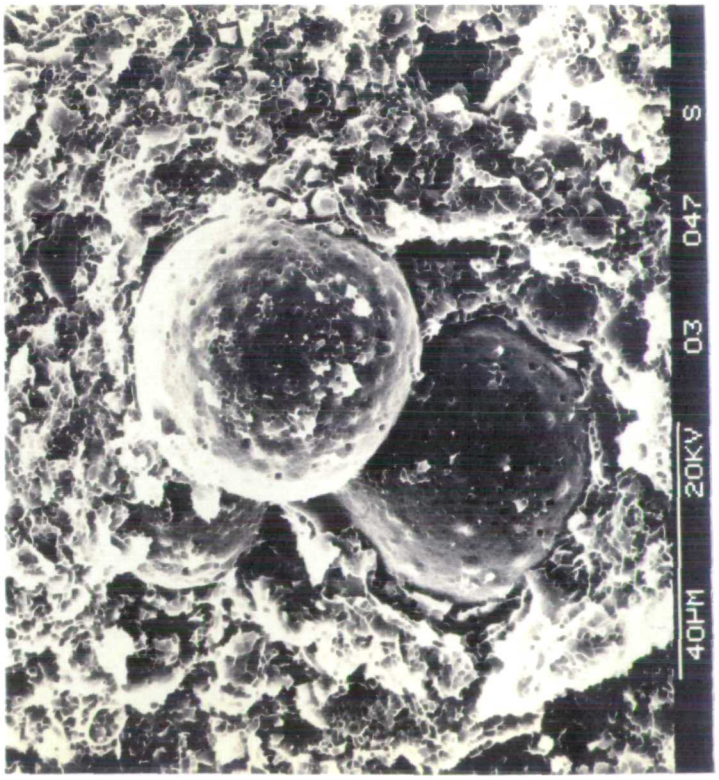

4

1

Fig. 7.4 - Natural clay compressed to a σ'_v of 3 MPa: vertical fractures; undamaged shells of globigerinae; group 1 (Table 5.9).

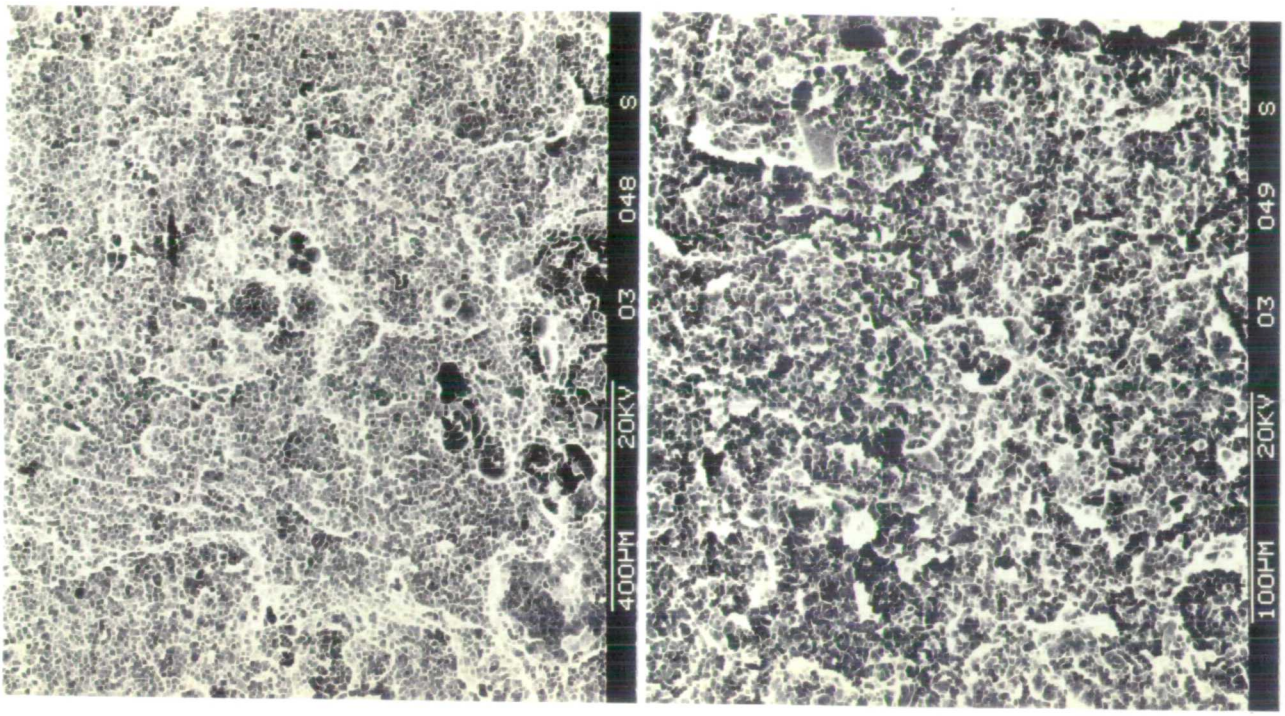

(a) (b)

(c)

Fig. 7.5 - Natural clay compressed to a σ'_v of 3 Mpa: horizontal fractures; in (a) a medium to low fabric orientation is shown; in (b) both intact and broken fossil shells appear; in (c) the fabric is chaotic, stacks of particles being interbedded with random particles and "chaotic masses" of particles; group 1 (Table 5.9).

Fig. 7.6 - Natural clay compressed to a σ'_v of 3 Mpa: vertical fracture; a long horizontal stack is interbedded between flocculated and chaotic fabric; group 1 (Table 5.9).

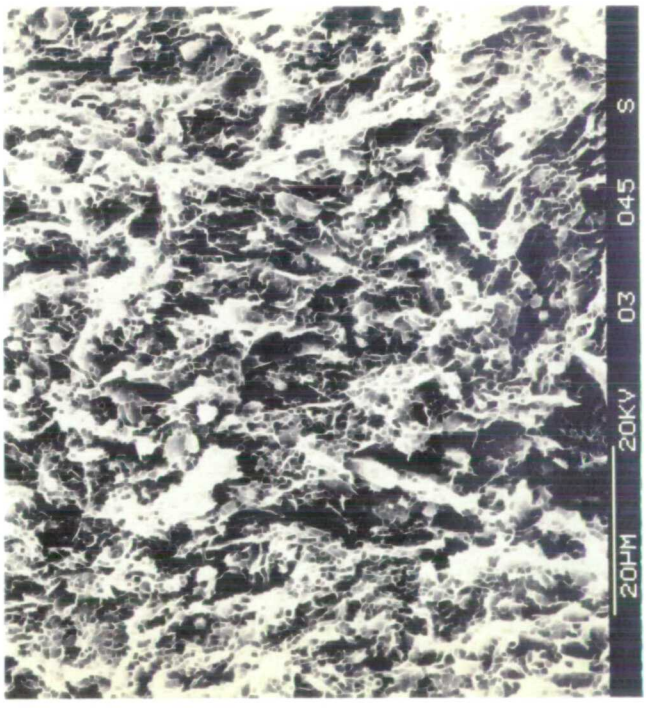

Fig. 7.7 - Natural clay compressed to a σ'_v of 3 MPa: vertical fracture; the fabric is more open and flocculated in the centre of the picture; "chaotic masses" of particles are seen in the bottom half and in the top right of the picture; group 1 (Table 5.9).

(a) (b)

Fig. 7.8 - Natural clay compressed to a σ'_v of 3 MPa: vertical fracture; chaotic densely packed fabric; coccoliths are shown; group 1 (Table 5.9).

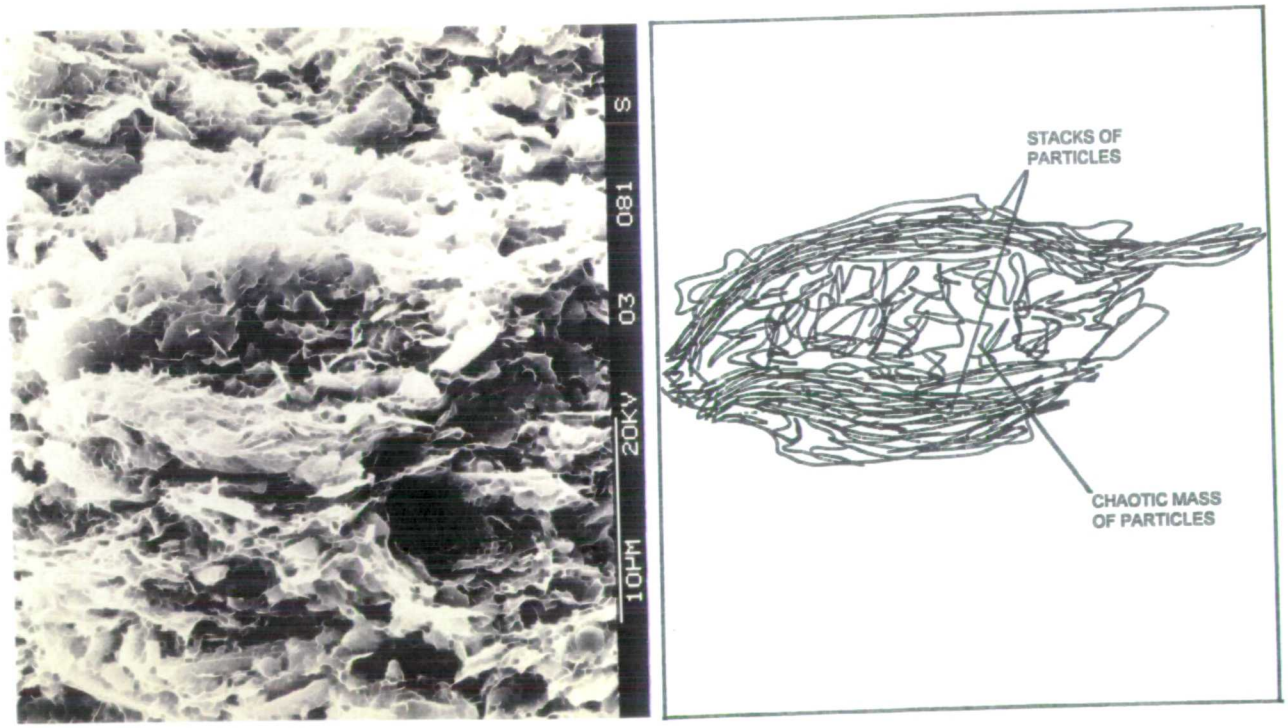

Fig. 7.9 - Natural clay compressed to a σ'_v of 3 MPa: vertical fracture; two stacks of iso-orientated particles confine a chaotic mass of particles; group 1 (Table 5.9).

(a)

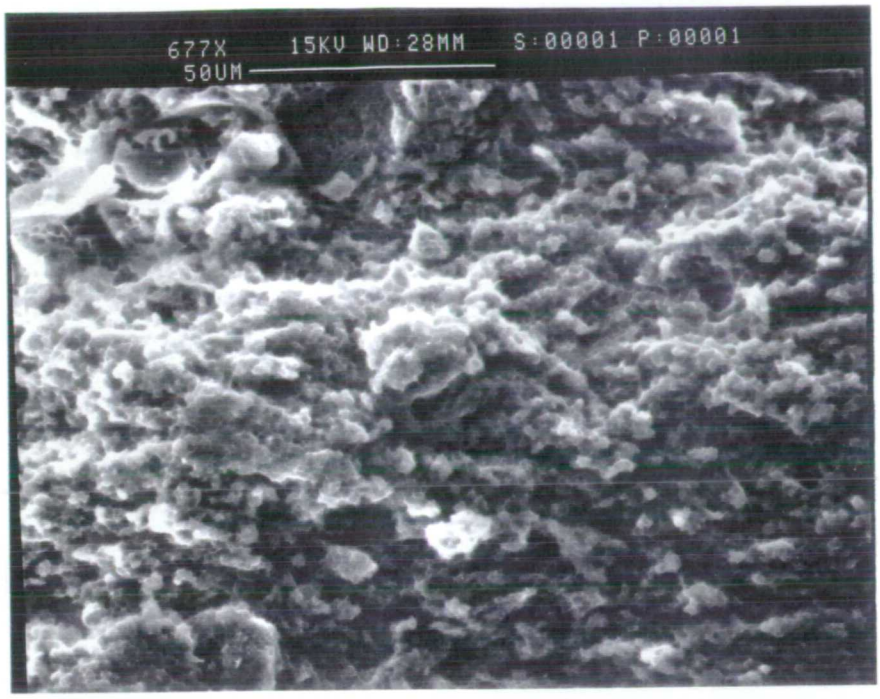

(b)

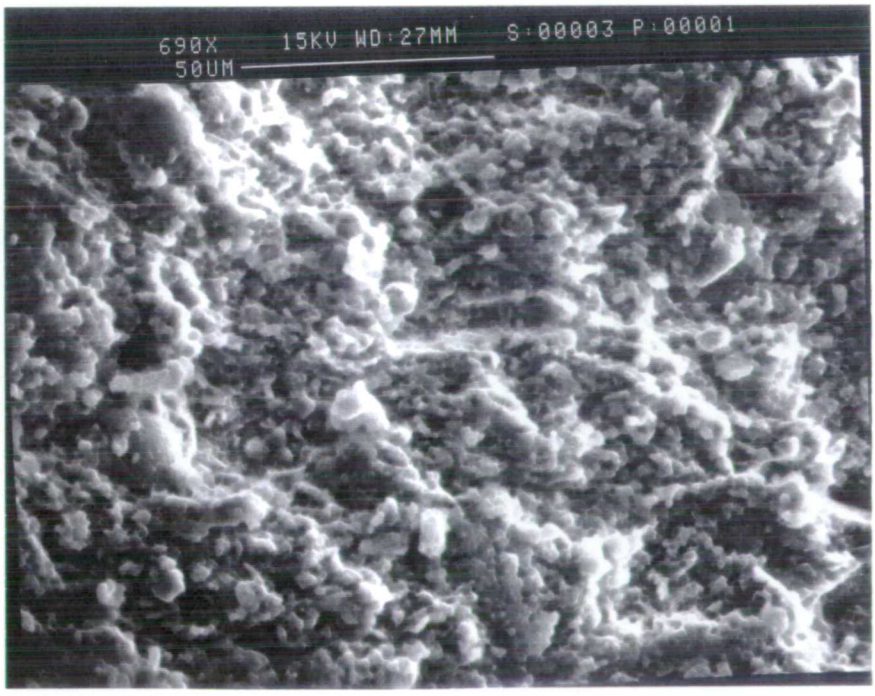

Fig. 7.10 - (a) Undisturbed natural clay before compression; (b) undisturbed natural clay compressed to a σ'_v of 3 MPa: vertical fractures; group 3 (Table 5.9).

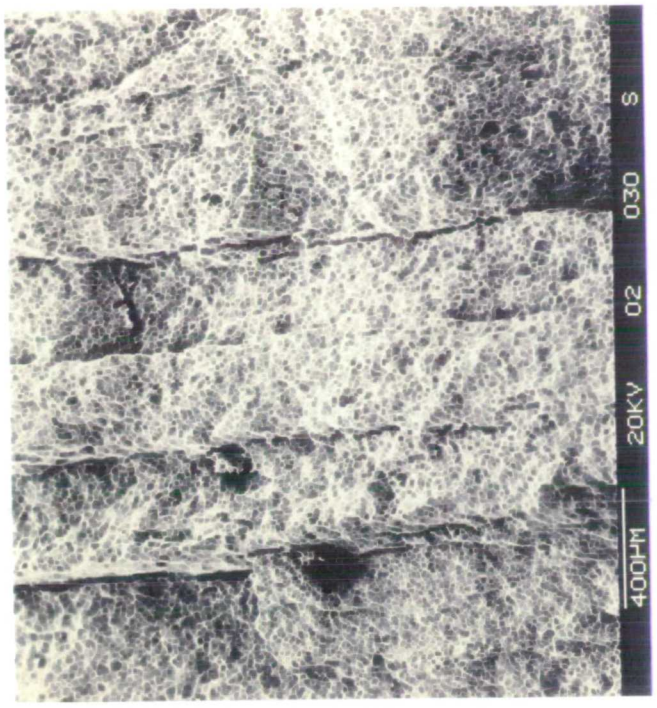

Fig. 7.11 - Natural clay compressed to a σ'_v of 22 MPa: fabric on a vertical fracture; the clay is crossed by horizontal extension fractures; group 1 (Table 5.9).

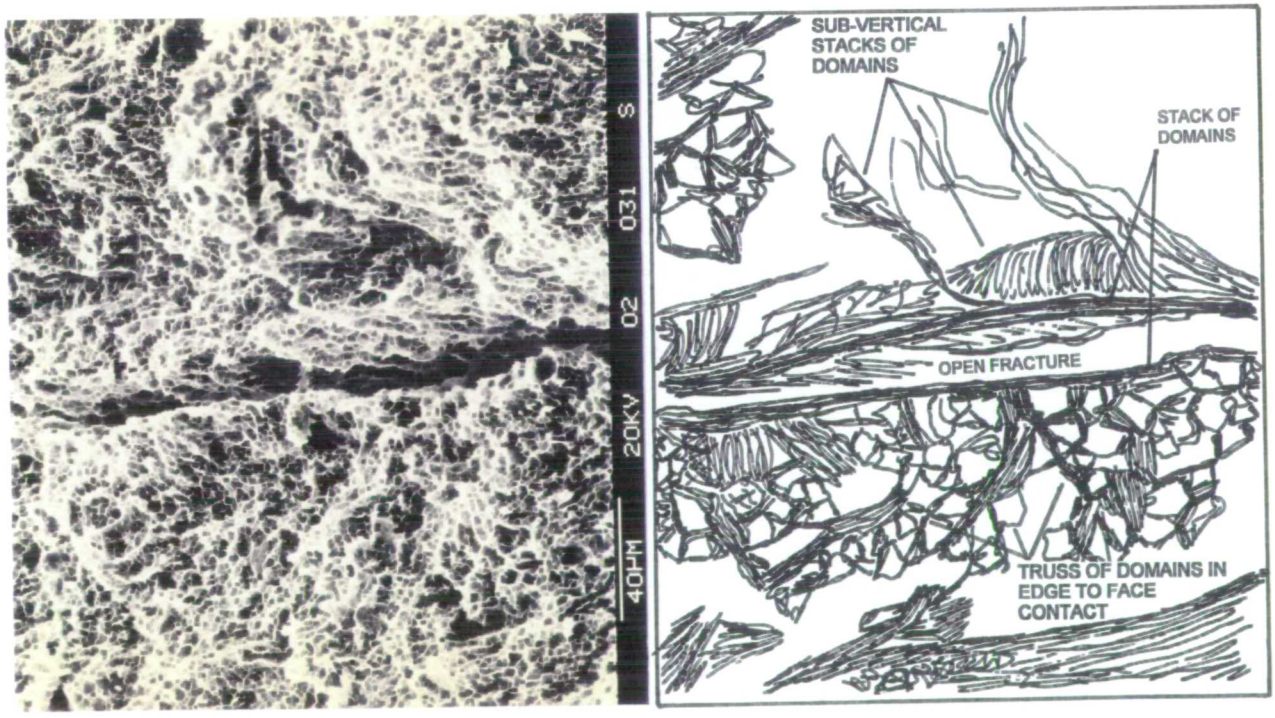

Fig. 7.12 - Natural clay compressed tσ a σ'_v of 22 MPa: vertical fracture; open horizontal fracture limited by two stacks of iso-orientated particles which are interbedded between flocculated fabrics; complex, but regular architecture: group 1 (Table 5.9).

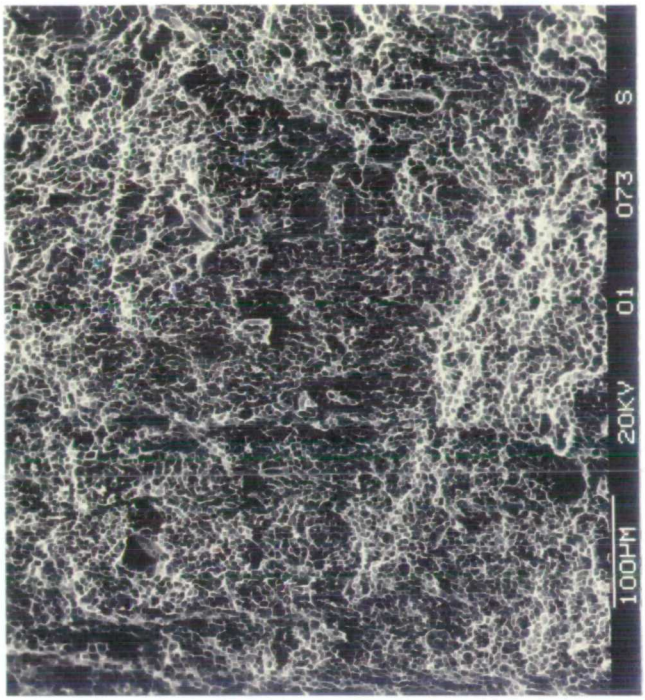

Fig. 7.13 - Natural clay compressed to a σ'_v of 22 MPa: vertical fracture; interbedding of denser iso-orientated fabric and more open flocculated one; group 1 (Table 5.9).

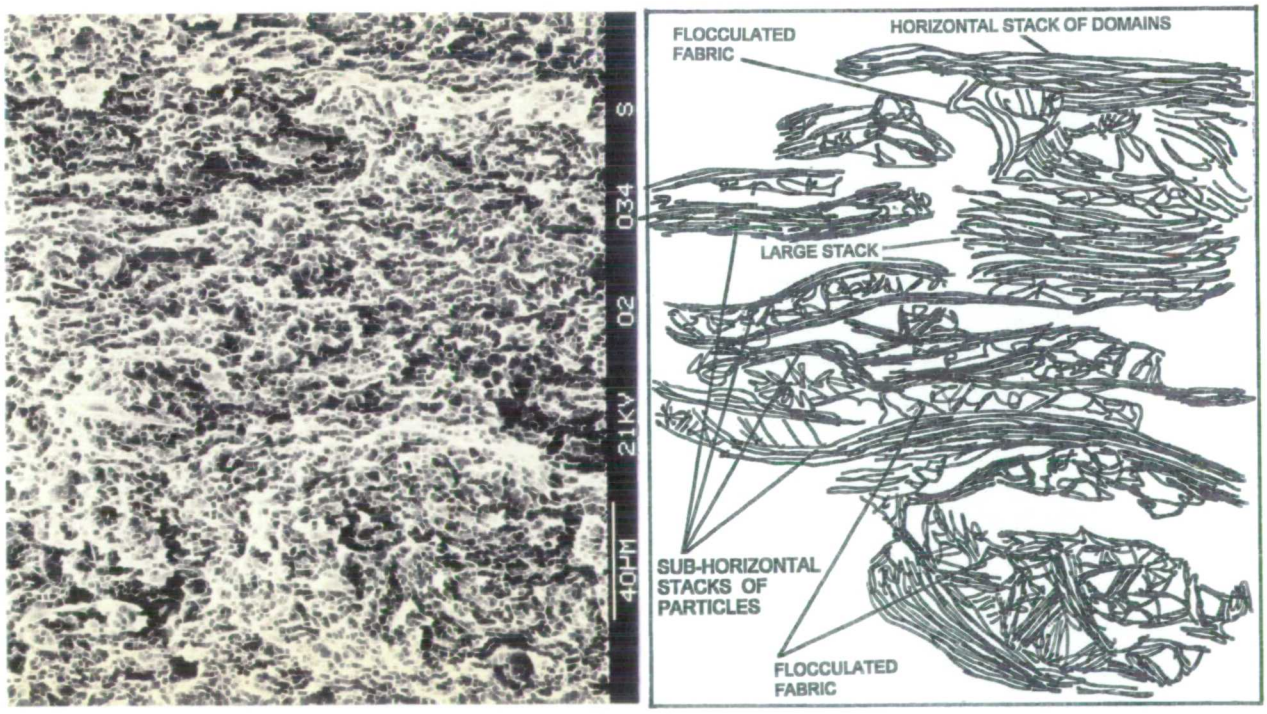

Fig. 7.14 - Natural clay compressed to a σ'_v of 22 MPa: vertical fracture; stacks of C.P.O. fabric within less orientated fabric; group 1 (Table 5.9).

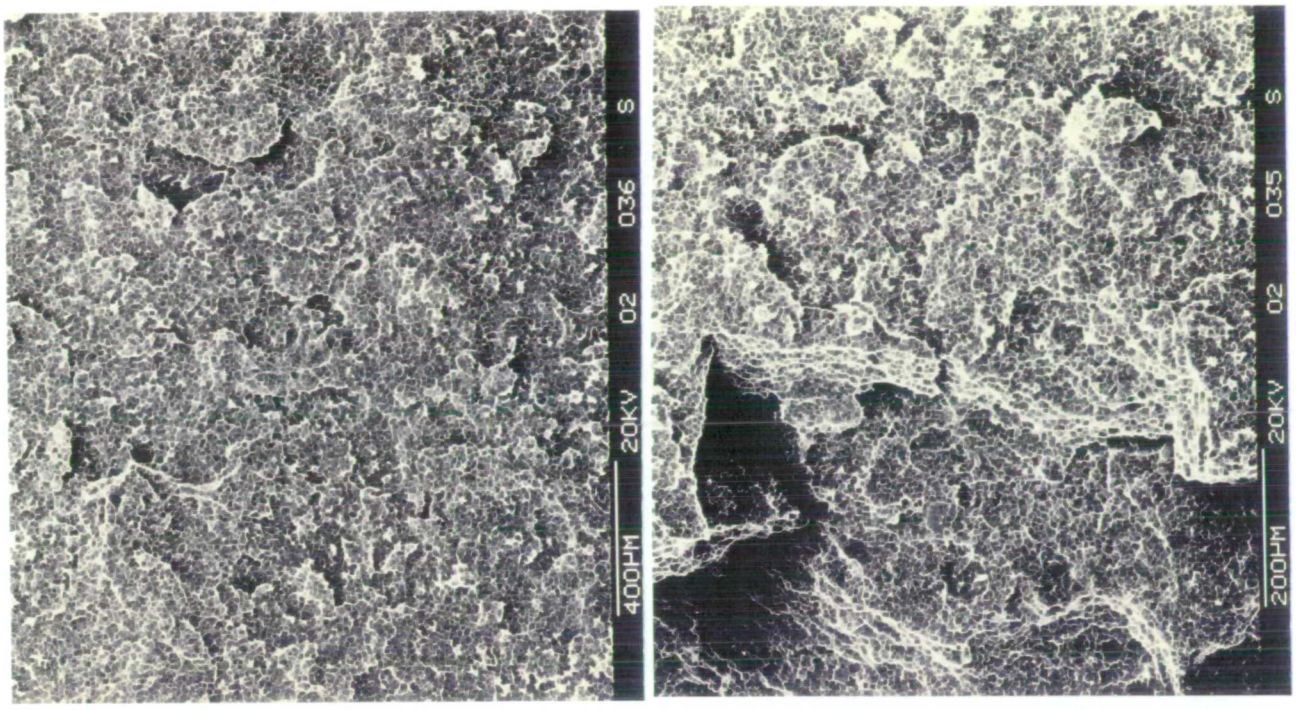

(a) (b)

Fig. 7.15 - Natural clay compressed to a σ'_v of 22 MPa: horizontal fractures; highly orientated fabric; in (a) a fissility plane is shown; group 1 (Table 5.9).

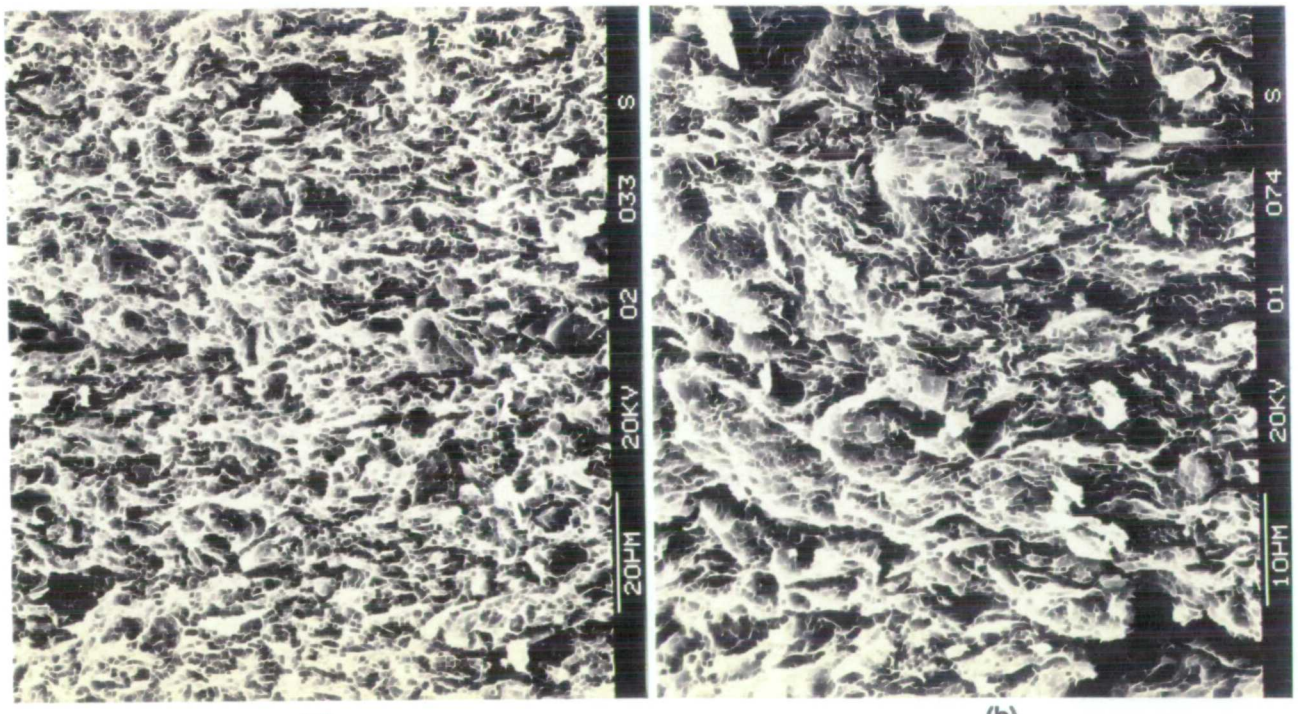

(a) (b)

Fig. 7.16 - Natural clay compressed to a σ'_v of 22 MPa: vertical fracture; the fabric is highly orientated, with many stacks of C.P.O. fabric; group 1 (Table 5.9).

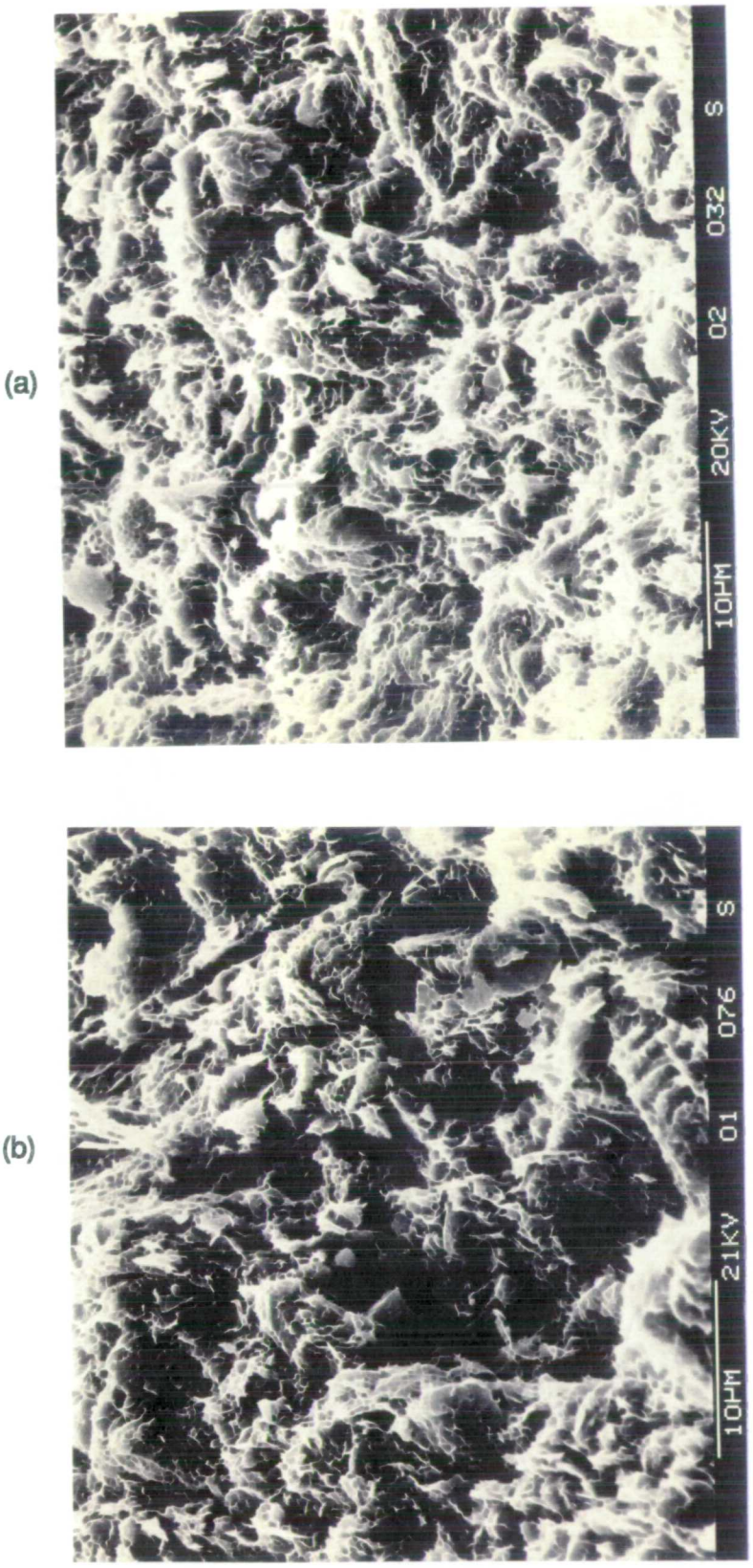

Fig. 7.17 - Natural clay compressed to a σ'_v of 22 MPa: vertical fracture; honeycombe resistant fabric; truss of domains in edge to face contact which sustain the horizontal stack of iso-orientated particles shown in Fig. 7.16; group 1 (Table 5.9).

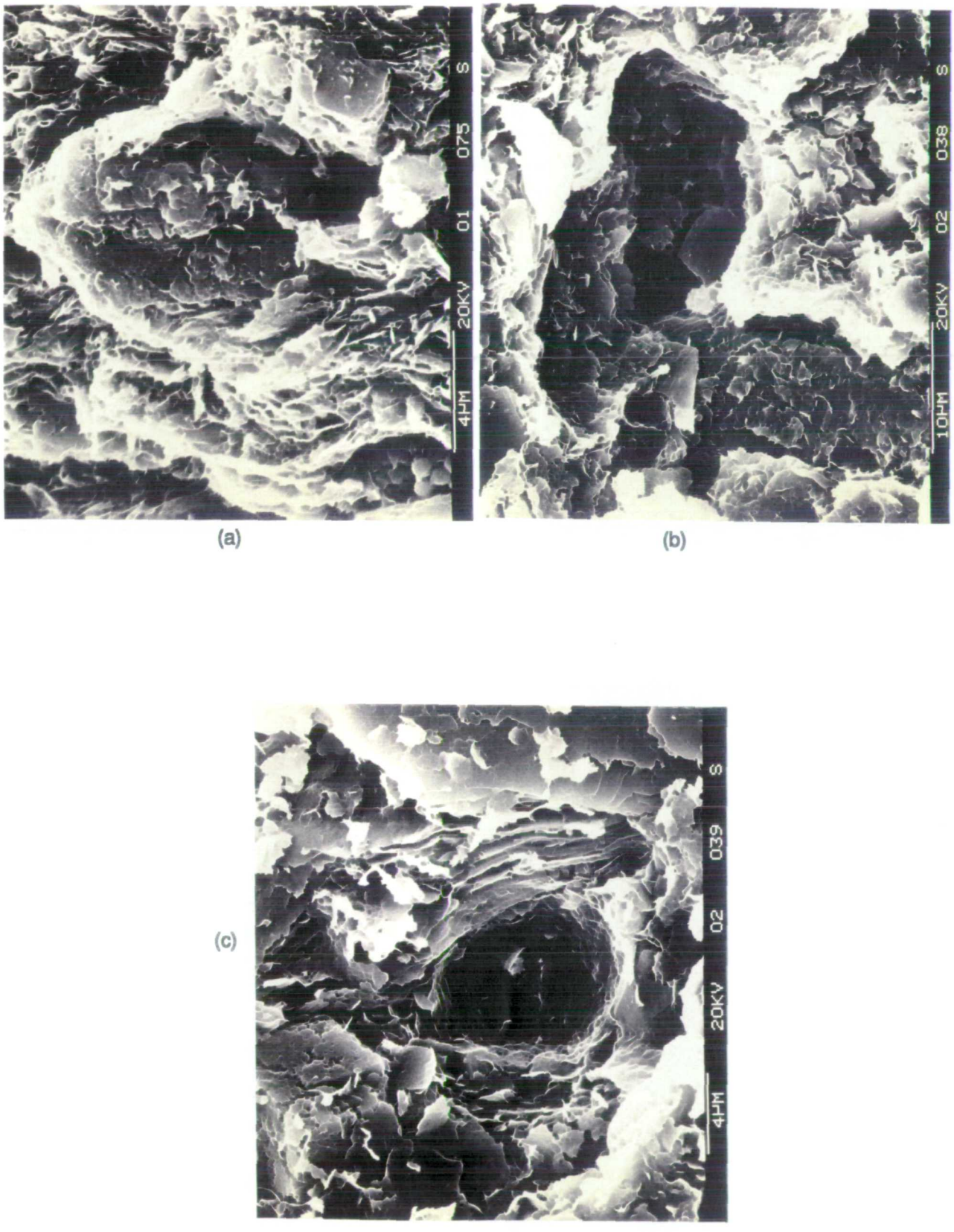

(a) (b) (c)

Fig. 7.18 - Natural clay compressed to a σ'_v of 22 MPa: details of orientated fabric; (a) vertical fracture; (b) and (c) horizontal fractures; group 1 (Table 5.9).

(a) (b)

(c)

Fig. 7.19 - Natural clay compressed to a σ'_v of 22 MPa: vertical fractures; details of flocculated fabric; many large voids between domains in edge to face contact; the particle outlines appear slightly fringed; group 1 (Table 5.9).

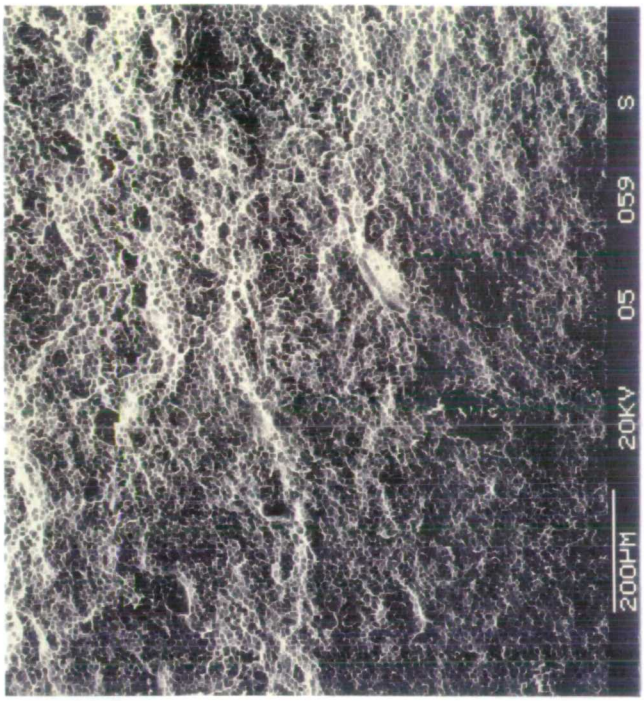

Fig. 7.20 - Reconstituted clay compressed to a σ'_v of 22 MPa: global view of the fabric on a vertical fracture; very densely packed fabric; some globigerina fossil shells can be seen; group 1 (Table 5.9).

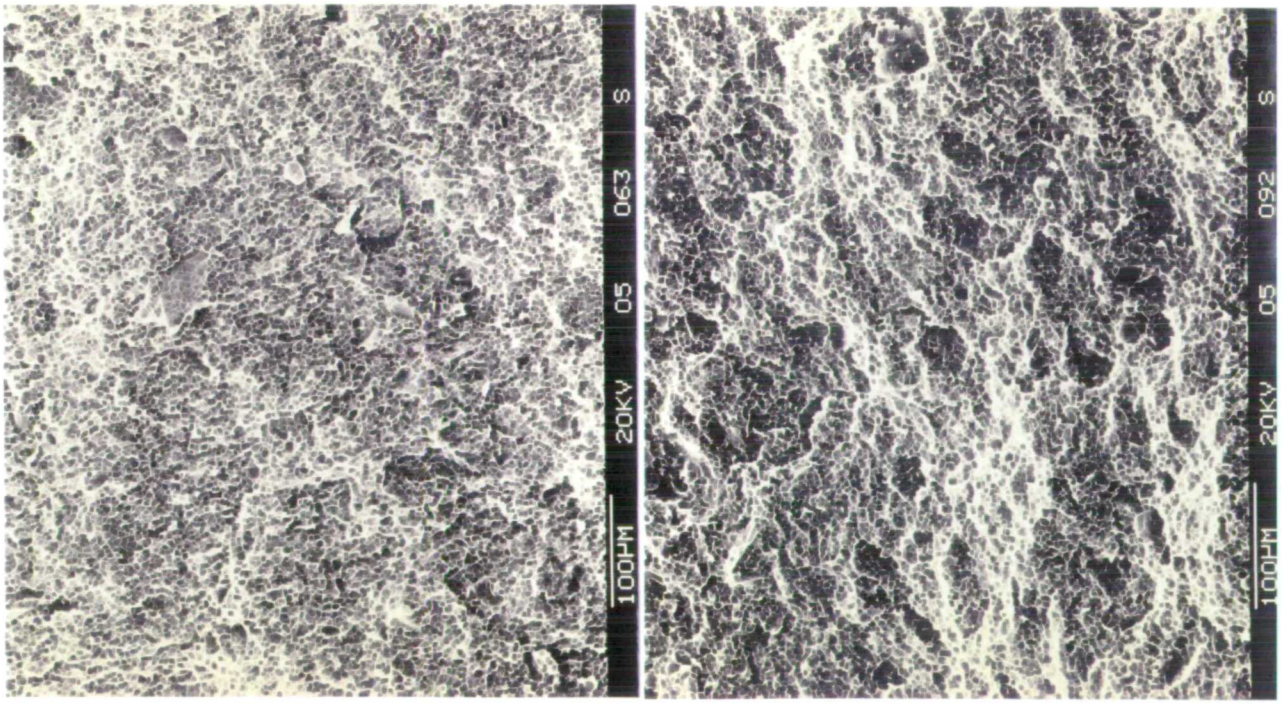

(a) (b)

Fig. 7.21 - Reconstituted clay compressed to a σ'_v of 22 MPa: fabric on fractures inclined to the horizontal; group 1 (Table 5.9).

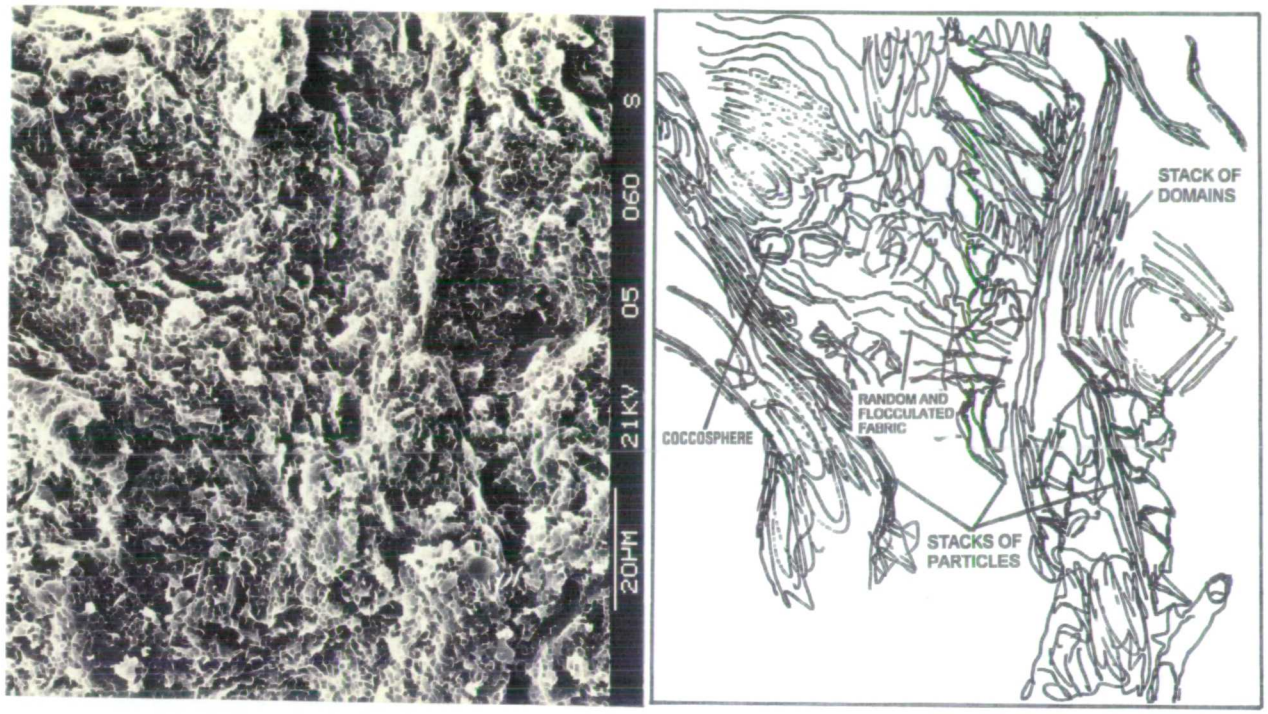

Fig. 7.22 - Reconstituted clay compressed to a σ'_v of 3 MPa: vertical fracture; stacks of iso-orientated particles following different directions interbedded with both areas of flocculated fabric and random chaotic fabric; group 1 (Table 5.9).

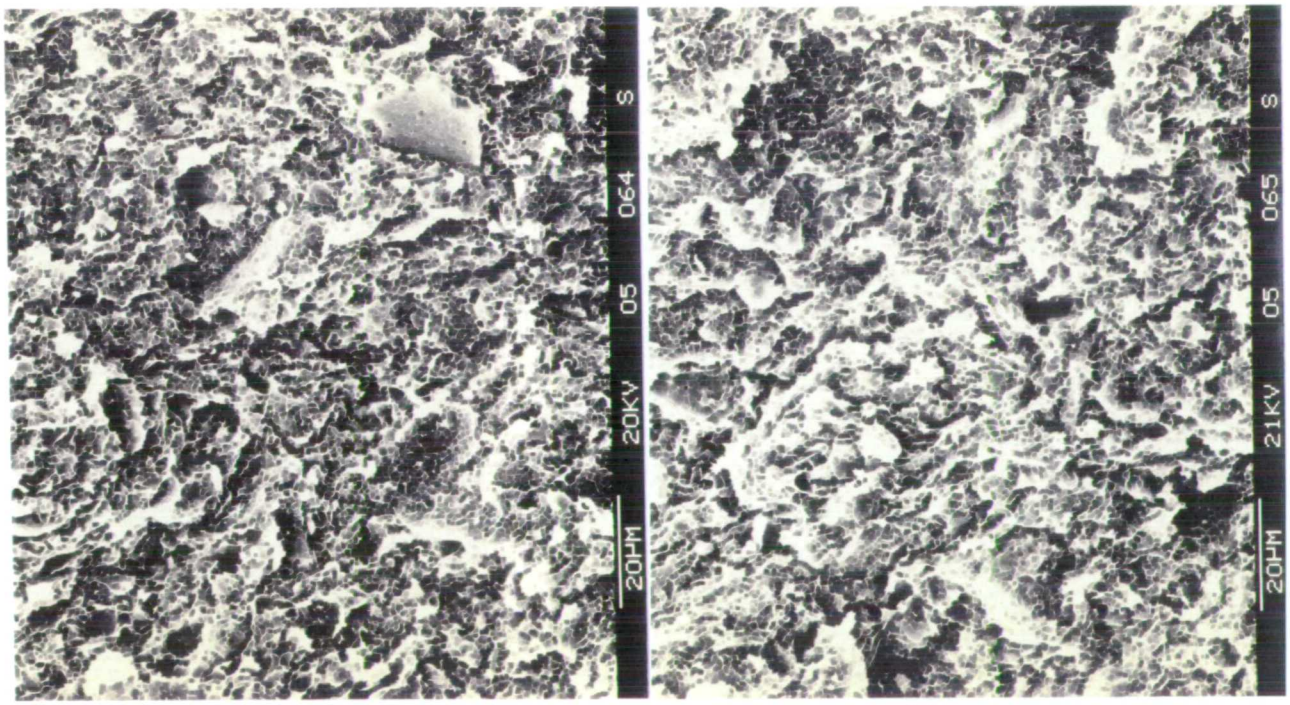

(a) (b)

Fig. 7.23 - Reconstituted clay compressed to a σ'_v of 22 MPa: highly dense fabric on vertical fractures; group 1 (Table 5.9).

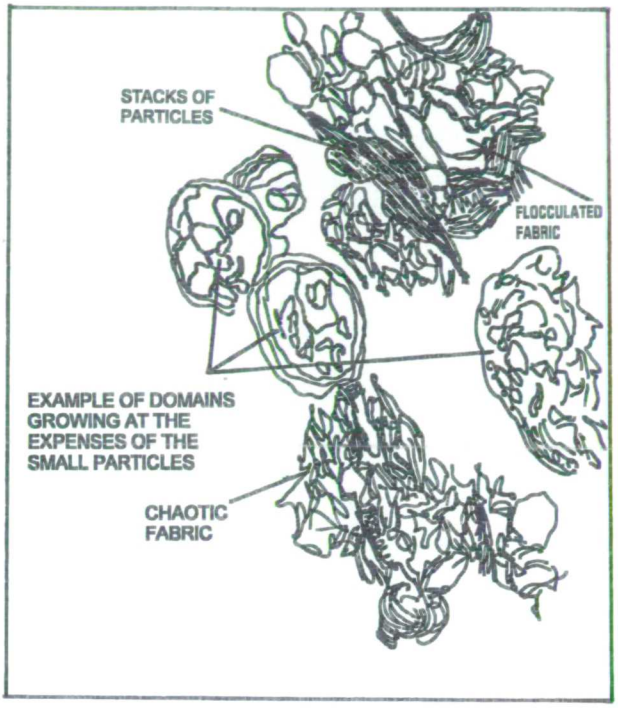

(a)

(b)

Fig. 7.24 - Reconstituted clay compressed to a σ'_v of 22 MPa: areas of chaotic fabric where the small particles are either stuck on the surface of the domains or penetrate into them; (a) densely packed fabric; (b) macro-void in areas of relatively more open fabric; group 1 (Table 5.9).

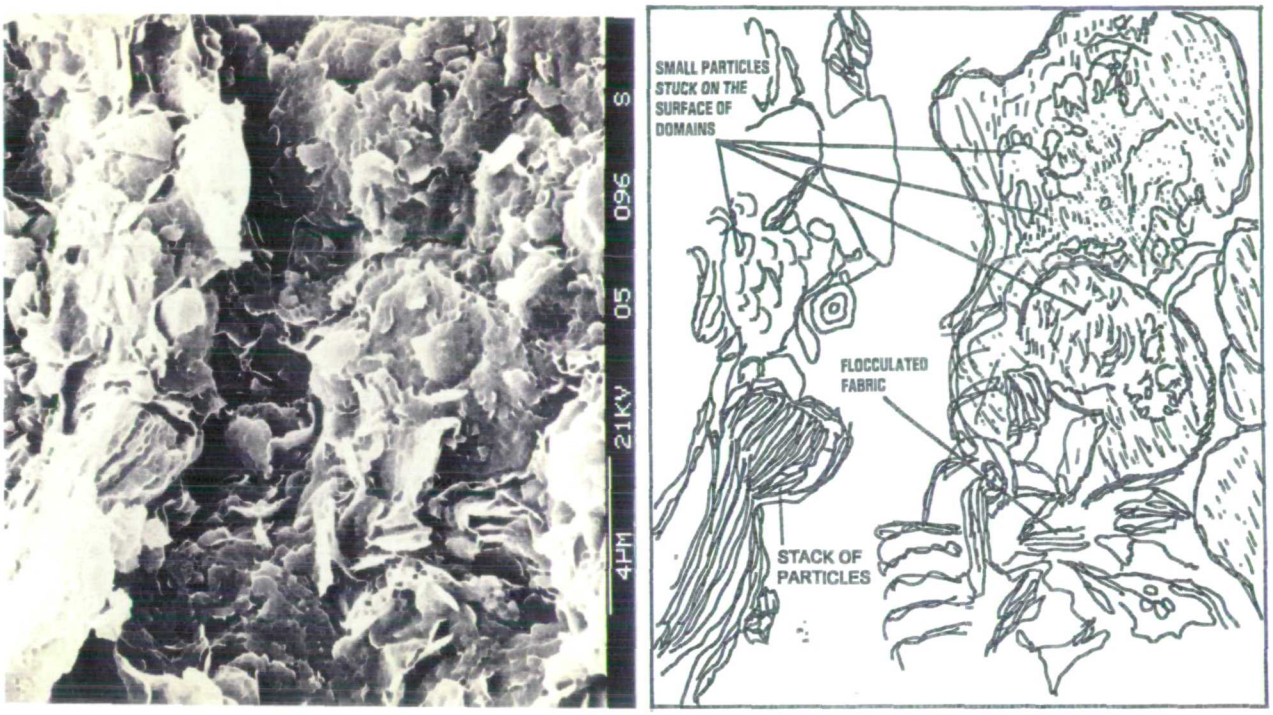

Fig. 7.25 - Reconstituted clay compressed to a σ'_v of 22 Mpa: domains grown at the expenses of the small particles; the particle surfaces appear damaged and their outlines fringed; group 1 (Table 5.9).

(a)

(b)

Fig. 7.26 - Comparison between the fabrics on vertical fractures of sample D (a), and of sample E (b), (see Table 5.9); the higher orientation of the fabric of sample D with respect to sample E is evident while the clay of sample E appears more densely packed; group 3 (Table 5.9).

CHAPTER 8
PAPPADAI CLAY : TRIAXIAL TESTING PROGRAMME

8.1. Introduction

8.1.1. Objectives of the triaxial testing programme

A series of triaxial tests was carried out to investigate the framework of behaviour of both natural and reconstituted clay in v-q-p' space, and to establish elasto-plastic constitutive laws for both clays. The tests were intended primarily to examine the yield function, the hardening rule and the flow rule of the soil at large strains.

The investigation addressed the definition of the gross yield surface of the soil. As discussed in Chapter 2, the gross yield surface separates the relatively stiff pseudo-elastic behaviour from the larger strains and coincides with a yield curve in the q-p' plane. Cam Clay-type models (Schofield and Wroth 1968; Roscoe and Burland 1968; Nova and Wood 1979) and other elasto-plastic strain-hardening models (Lagioia and Nova 1993) assume elastic behaviour before gross yield. Thus, the definition of the gross yield is an important element for these models, as it defines the point beyond which the elasto-plastic laws govern the soil behaviour The definition of the gross yield surface is also important for kinematic hardening models since it is the threshold for major plastic strains.

In Chapter 6 physical implications for gross yield of clays was discussed It was shown that the elimination of metastable structural features at gross yield of natural sensitive clays may result in clear-cut differences between their post-yield behaviour and that of reconstituted clay. In Chapter 7 the effects of gross yield in oedometric compression on the structural behaviour of the clay was demonstrated The investigation of the behaviour of both the natural and the reconstituted clay at gross yield during shear, which is presented in this chapter, further develops the study of the relationship between soil structure and clay behaviour.

The stresses at which gross yield (later also referred to as "yield") occurs must of necessity be estimated using empirical procedures, as there is typically a region of transition around the yield point Consequently, a degree of judgement must be exercised in selecting a yield stress As stressed by Graham et al (1988), it is important that the techniques used for defining the yield points do not themselves suggest spurious behaviour which is then assigned to the clay For instance, the gross yield curve of reconstituted clays lies on the SBS, whereas it has to be established whether or not this is the case for the natural clays If the range of states where yield develops includes boundary states the

natural and reconstituted clays have consistent behaviour. This approach is followed in the present analysis.

The CSF shows that yield curves in v-q-p' space and the SBS of the reconstituted soil can be normalized with respect to volume. As a consequence the Cam Clay-type models assume isotropic volumetric hardening. Models based on isotropic volumetric hardening have also been proposed for natural soils (Lagioia and Nova 1993) However, it has yet to be established whether the behaviour of the natural soil is isotropically hardening. Lagioia and Nova (1993) use an isotropic hardening model to simulate the behaviour of a calcarenite tested by Coop and Atkinson (1993). The model appears to simulate some of their data, though no experimental evidence is provided by Coop and Atkinson regarding the isotropic hardening of the calcarenite.

The soil behaviour is isotropically hardening if it can be normalized. In Chapter 6 it has been shown that the oedometric stiffness of the natural Pappadai clay is normalized by a factor accounting for both volume and structural changes beyond yield The triaxial test data were analysed similarly in order to investigate whether or not a suitable normalization of the shearing data existed

Mathematical expressions for the flow rule can be derived from the analysis of the plastic strain vectors in the q-p' plane. Though these flow rules may fit the data, they may not provide an interpretation of the physical behaviour of the soil, their use being confined to the particular soil tested. In contrast flow rules based on a physical interpretation are relevant to models of more general applicability. Cam Clay was the first model which prompted this approach to the study of soil behaviour. Its flow rule was originally defined as an expression of a frictional deformation mechanism, and was subsequently shown to describe the behaviour of the soil. In Chapter 2 a frictional deformation mechanism (eq.2.4) was found to apply to the behaviour of both natural soft clays and cemented granular soils (Fig.2 31) Its applicability to the behaviour of both reconstituted and natural Pappadai clay is examined here.

8 1 2 Testing programme

A series of tests was carried out on specimens of both natural and reconstituted Pappadai clay in triaxial stress path apparatus at Imperial College and at Politecnico di Bari Three tests were also carried out at City University with the kind help of Dr M R Coop The apparatus used and the procedures followed are described in Sections 8 2 and 8 3

Tables 8.1 and 8.2 list the initial water content, voids ratio and saturation degree of the specimens and other details of the various tests. Any additional equipment used during the tests (see Section 8 2.1) is also shown.

Most of the specimens were isotropically consolidated before shearing. Two tests were carried out on reconstituted specimens which had been isotropically normally consolidated to different values of p'. Two tests were carried out on reconstituted overconsolidated clay and one on K_0 normally consolidated clay.

Table 8.1 reports the values of the preconsolidation pressures p'_p, of the consolidation pressure p' and of the overconsolidation ratio R ($R= p'_p/p'$) for the different tests. Shearing was always carried out at a constant $\Delta q/\Delta p$ ratio of 1/3 and all tests on reconstituted clay were undrained, excepting drained test TR4.

Four undrained tests (TN1, TN2, TN4 and TN9) were carried out on unconsolidated undisturbed natural clay, the undrained strength of the undisturbed clay being measured (Table 8.2). In tests TN1, TN2 and TN9 an undrained isotropic loading was carried out before shearing (Section 5.6.4) to measure the suction of the clay which the strength was related to, but in Tests TN2 and TN9 only the suction was obtained from the high cell pressure applied in a high pressure apparatus (see Table 5.3 and Section 5.6 4). In test TN1 the applied cell pressure of 1000kPA was applied, but this was too low to limit the cavitation of the system, given the very high suction of Pappadai clay. In this test the system was resaturated by further application of cell pressure

The shearing stage of test TN9 was interrupted at an early stage due to a power failure. Thus in test TN2 only both the suction of the undisturbed clay and the corresponding strength were measured, the latter being approximately that of the clay in situ.

In test TN4 shearing was carried out rapidly with no pore water pressure measurement, keeping both top and bottom of the specimen dry. Also the c_u value measured in this test was approximately that of the clay in situ The influence of the test procedure on the measurement of c_u was assessed by comparing the results of tests TN2 and TN4 (see Section 8.6 10).

In all the remaining tests (Table 8 2) the specimens of natural clay were either isotropically consolidated or swelled prior to shearing, except for test TN21 which used strain-controlled K_0 compression, test TN21 was interrupted at an early stage due to a failure of the compressor Shearing was always carried out at a stress ratio $\Delta q/\Delta p$ of 1/3. The B values (Skempton 1954-a) measured after

resaturation and consolidation are reported in Table 8.2. B values as high as 100% were measured, the minimum B value accepted before shearing was 94%.

Table 8.2 shows the values of the yield stress ratio YSR_{is}, the ratio of the yield stress of the clay during isotropic compression p'_{yis} to the pre-shear consolidation stress p'. In tests TN12, TN13, TN17, TN21 and TN22 the specimens were compressed beyond isotropic yield before shearing, the object being to investigate the change in behaviour of the clay due to the change in structure occurring at yield. In these tests high pressure triaxial cells were used.

Due to the very low coefficient of consolidation of natural Pappadai clay post-yield, both consolidation and shearing stages took an incredibly long time, and system failures resulted in the loss of some tests. Major problems were encountered with both the resaturation stage and drained shearing The duration of the drained shearing stages was inferred from test TN14 in which a probe was used to measure the pore pressure at the mid-height of the specimen. The drained shearing rates ensuring complete drainage were found to be about 1/20 of the strain rates used in undrained tests. As a result, a complete triaxial test lasted, on average, 2.5 months. The long duration of the tests required accurate and time-consuming leak tests.

All the tests except test TN19 were carried out on vertically trimmed specimens. Test TN19 was run on a horizontally trimmed specimen, so as to investigate the effects of the intrinsic anisotropy on the strength of the unconsolidated clay. As discussed in Section 4 3 3 the c_u value measured in triaxial testing on horizontally trimmed specimens can be regarded as the strength measured in the triaxial closest to the c_u measured in situ by SBP testing. The various undrained shear strengths measured in the laboratory on unconsolidated specimens (tests TN2, TN4 and TN19) are compared to the SBP test results in Section 8.6.11.

8.2 Apparatus

A variety of different apparatus was used during the triaxial testing programme All had data-logging systems which monitored the transducers measuring force, pressure and displacement. In some instances the stresses or strains applied to the sample were manually adjusted, while others were automatically controlled The sample dimensions were usually 76mm in length by 38mm diameter

Each apparatus had both cell and pore pressure transducers, together with an internal load cell to measure the deviatoric force The pressure transducers were usually of a semi-conductor type manufactured by Druck, although different c pacity transducers were used for the different apparatus

This type of transducer has a very stiff response which is necessary for the accurate measurement of pore pressures in stiff soils during undrained loading. The pore pressure transducers were in all cases connected to the sample through drainage leads of sufficient rigidity as not to influence the measurements. The load cells were generally of Imperial College, though with a variety of capacities.

The volumetric changes of the sample were generally measured with a 50cc capacity Imperial College volume gauge. The movement of the piston of the gauge was monitored using a 25mm stroke displacement transducer either of a resistive type or a linearly variable differential transformer (LVDT). In all cases the volume gauge also acted as the air-water interface for the back pressure system, the base chamber being air filled and connected to the back pressure controller, while the top chamber was water-filled and connected to the sample drainage system. All drained tests were conducted under a constant back pressure to avoid errors due to the compliance of the drainage leads and volume gauge. The drainage and pore pressure measuring systems were generally connected only to the base pedestal, although in some cases a mid-height pore pressure probe (Hight 1982) was also used. The base pedestal in each apparatus had two drainage ports, one connected to the volume gauge and to the base pore pressure transducer and the other to a drainage tap. This arrangement allowed the base drainage system to be flushed during the test if it was suspected that air was entrapped within it. As with the back pressure the cell pressure was generally applied through an air-water interface, using a variety of types of regulator to control the air pressure.

Each apparatus had an externally mounted displacement transducer to measure axial displacement. In addition, in some tests an internal transducer was mounted directly on the sample. The external transducers were again of 25mm stroke and either of an LVDT or resistive type.

Another feature common to most of the apparatus was that the connection between the sample top platen and the load cell was made by means of a half ball seated in a conical notch in the platen as illustrated in Fig 8.1. This type of connection was used to reduce the possibility of eccentric loads or moments being transmitted into the sample, which for the stiff natural samples might influence the mode of failure and strength measured.

In the following, the various different pieces of apparatus are discussed in some detail, roughly in the sequence in which they were used. For convenience each is assigned a reference letter which has been used to identify the apparatus in Tables 8.1 and 8.2.

Apparatus A was a hydraulic triaxial cell (Bishop & Wesley 1975) used at Imperial College, with manual control of air pressure, shown in Figs 8.1(a) and 8.2. A third air pressure regulator and air-water interface provided control of the axial pressure in the base cylinder of the cell. Constant rate of

strain axial loading for the shearing stages was achieved by means of a motorised Bishop ram acting through a gear box which allowed the rate of displacement to be selected. The air-water interface on the cell pressure system was a two chambered bellofram type similar to the volume gauge, except that in this case the upper chamber had half the cross-sectional area of the lower so multiplying the applied air pressure by a factor of two (Fig 8.2). The maximum pressure was limited by the capacity of the triaxial chamber, which was 1200kPa. The base drainage system was provided with a high air entry porous stone to reduce the possibility of cavitation of the water within the drainage system while setting up the sample. This apparatus also used a mid-height pore pressure probe. The displacement transducers both on the volume gauge and for the measurement of the axial strain were of a resistive type. A CIL analogue-digital converter was used to which was connected a BBC micro-computer, Fig.8.3.

Apparatus B was also a hydraulic triaxial cell used at Imperial College. The system was similar to Apparatus A, with the same instrumentation, again with a mid-height probe, but in this case the axial strains were also measured by a pair of internal transducers of the pendulum inclinometer type (Ackerley et al. 1987). This apparatus did not have the cell pressure multiplying interface so that the maximum pressure was limited to the air compressor output of 800kPa. The principal difference with this apparatus was that the three air pressures were automatically regulated by means of Watson Smith electro-manostats. Logging of the transducers and control of the electro-manostats was performed by a Measurement Systems data-logger, again connected to a BBC micro-computer.

Apparatus C is two identical pieces of equipment constructed by the author at the Politecnico di Bari, one of which is shown in Fig 8.1(b) and 8.4. These were standard triaxial cells (Bishop & Henkel 1962) mounted in loading frames. The Wykeham Farrance triaxial chambers were made of a reinforced perspex with a capacity of 1700kPa. These were replaced for some tests by a steel chamber enabling the maximum cell pressure to be increased to 2800kPa, this limit being determined by the 1400kPa output of the compressor combined with the two times multiplying interfaces which were again used on the cell pressure systems. The cell and back pressures were both manually controlled, but only strain controlled axial loading was permitted by the loading frames The two times multiplying interfaces used on the cell pressure system in some tests doubled the oscillations of the air pressures acting at the air-water interface, thus causing an oscillation of the cell pressure applied to the specimen. This was reflected by an oscillation of the pore water pressure measurements in some undrained tests, as seen in the results of some of the tests carried out with apparatus C, see Section 8.6.2 The displacement transducers used on the volume gauge and for the measurement of the axial strain were all LVDTs, which were found to give better accuracy than the resistive type because of their higher output. Data-logging was handled by two CIL PC Super cards fitted into two IBM

compatible computers. These systems had no internal strain transducers nor mid-height probes. Again high air entry porous stones were used.

Apparatus D was a high pressure stress-path triaxial cell at City University. This was a conventional high pressure triaxial cell mounted in a 5-tonne capacity loading frame. An hydraulic cylinder between the cross-head of the frame and the axial loading ram of the cell provided the means of applying the stress-controlled axial load. The back-pressure system was as for the other triaxial apparatus with an Imperial College volume gauge. The cell pressure system was again based on controlled air pressure, but in this case, instead of acting through an air-water interface, the air pressure was fed into a pressure multiplier which delivered an output pressure approximately eight times the input, giving a capacity of 5MPa. A similar system provided the high pressure for the axial loading cylinder. In this apparatus the three air pressures were regulated by means of electro-pneumatic pressure converters also manufactured by Watson Smith. As with apparatus B, control of the pressures was achieved by means of a feedback loop. The readings of the transducers were data-logged, then compared with the values required using a control program and finally adjusted accordingly via the air pressure regulators. Again in this case the analogue-digital conversion for the logging of the transducers was performed by a PC Super card mounted in an IBM compatible computer. The same card also gave the three analogue outputs necessary to control the pressure converters. In this apparatus the internal load cell was manufactured by Maywood to a Surrey University design. The volume gauge displacements and external axial displacements were measured by LVDTs and a pair of Hall-effect local axial strain transducers (Clayton & Khatrush 1986) which were attached to the sample in tests TN21 and TN22. The sample in this apparatus was 50mm in diameter and 100mm in height The connection between the sample top platen and the load cell was made using a full ball-bearing seated in conical notches in both the platen and the base of the load cell. In addition to isotropic compression a one-dimensional compression test was also carried out in this apparatus on an undisturbed sample. To avoid the problem of apparatus compliance affecting the externally measured axial strain, and in the absence of a radial strain belt, the condition of zero radial strain was achieved by using a feedback loop to control the cell pressure so that the overall volumetric strain was maintained equal to the average local axial strain while the axial stress was increased at a constant rate (test TN21).

Apparatus E was another high pressure triaxial apparatus, but used at Imperial College. Again a conventional steel triaxial cell was mounted in a loading frame (Fig.8.5). While the back pressure was controlled by means of the usual electro-manostat, the elevated cell pressure was applied by an automated screw cylinder. This cylinder was driven by means of a computer controlled stepping motor Only strain-rate controlled axial loading was available on this apparatus The externally mounted displacement transducer and that attached to the volume gauge were both of a resistive type. This system had no internal instrumentation, but did have an internal load cell and as for the other high

pressure apparatus only base pore pressures were measured. Data-logging and control were performed by a Measurement Systems card communicating via an RS232 serial cable with an IBM compatible computer. The connection between the axial load cell and the sample in this case was made using a connector designed by Bressani (1990). A narrow pin attached to the base of the load cell entered into a hole of slightly greater diameter in the top platen. During initial deviatoric loading the load was transmitted through the head of the pin giving a point load but at large strains the pin and hole arrangement prevented rotation of the platen.

The final triaxial system used in this series of tests was Apparatus F, a hydraulic triaxial cell at the Politecnico di Bari This apparatus was controlled by means of screw cylinders produced by the GDS Ltd. and had a cell pressure capacity of 1700kPa Three controllers were used, for the axial pressure, cell pressure and back pressure, all connected via an IEEE parallel interface to an IBM compatible computer. The axial controller was not only to control the axial stress but also to apply a constant rate of strain during shearing. The back pressure controller also measured the volumetric changes of the sample through the movements of the screw cylinder. This apparatus had an internal load cell, an LVDT to measure the axial strains externally, and a separate pore pressure transducer in addition to that within the back pressure controller. Whereas the back-pressure controller was connected to the base drainage, the pore pressure transducer was connected via a drainage line to the top platen. No radial drainage filter was used, so that the latter transducer was used to check for incomplete drainage. The cell pressure was measured simply by the transducer inside the controller. This system also had a pair of miniature LVDTs (RDP model D5/200WRA) attached to the sample to measure the axial strains internally as described by Cuccovillo and Coop (1996). Each of the transducers external to the three controllers was logged using a GDS analogue-digital converter communicating with the computer.

8 2 1. Calibration and Accuracy

The load cells and pressure transducers were calibrated against a Budenberg dead-weight tester, and the displacement transducer was calibrated against micrometers. For the volume gauge either a burette or a previously calibrated Bishop ram was used. In all cases the calibrations were made over the range appropriate to a particular series of tests. Linear calibrations were used with the exception of some of the load cells and both types of local axial strain transducer.

The accuracy of a transducer is the product of a number of factors among which the more important are : electrical noise, drift, temperature sensitivity and deviation of the true reading from the chosen calibration line. In addition load and pressure transducers may suffer from hysteresis although this

was not found to be significant for any of the pressure transducers used here. Of the load cells, the Imperial College type exhibited a significant amount of hysteresis, and these were therefore cycled over their working range prior to use

The accuracy of the readings depends not only on the particular transducers used but also on the design of the apparatus, the temperature stability of the laboratory and the characteristics of the signal conditioning and data-logger. The stability of some of the systems used was established by leaving them under constant pressures over extended periods. In addition, before commencing a series of tests in any apparatus a leakage check was made on the drainage system by setting up a dummy sample and leaving it under constant cell and back pressures for several days while monitoring the volumetric change.

Given the diverse factors affecting accuracy and the variety of transducers and apparatus used it is difficult to specify single numbers which reflect precisely the accuracy of the readings, but the following are believed to be a reasonable guide. The pressure transducer readings had an accuracy of about ±0.5kPa in the standard pressure apparatus rising to ±2kPa in the two high pressure cells. The load cell accuracies were around ±1N, rising to about ±5N with the high pressure apparatus. At low strain levels the accuracy of the strain transducers is dominated by the electrical noise and the resolution of the transducers. For strains below 0.1% the axial and volumetric strains are believed to be accurate to about ±0.002%. The accuracy of displacement readings is not significantly different for the internal and external axial strain transducers, although the latter even when they have been corrected for the compliance of the apparatus are still subject to seating and bedding errors which introduce errors into the strains calculated for the sample. At large strains both the LVDT and resistive transducers gave accuracies of about ±0.5% of the current reading again for both axial and volumetric strains.

8 3. Test Procedures

The undisturbed specimens were hand trimmed on a lathe from the samples described in Section 5.5. This was done within one hour to minimise drying of the sample The moisture content of the trimmings was measured to determine the initial water content of the specimen The initial weight and dimensions of the trimmed specimen were also measured, and, after the test, the final total weight and water content were determined. The reconstituted specimens were trimmed by hand from blocks prepared in the same way as for the oedometer tests (Section 5 8)

The apparatus was prepared by de-airing the drainage leads and porous stone and taking zero readings for the pressure transducers and load cell prior to setting up the soil specimen. These readings were checked after the test to determine if there had been any significant drift of the transducer readings

Where possible a high air entry porous stone was used. Even so, to avoid the possibility of the undisturbed samples swelling during setting up as a consequence of cavitation of the water in the drainage system, a thin wire was placed between the specimen and the base porous stone as described in Section 5.6.4. As there was generally no provision for top drainage, no porous stone was used at the top of the sample.

No end filter papers were used, but in the drained shearing tests a radial drainage filter was placed around the sample to accelerate dissipation of the pore pressures In cases where radial drainage was used on reconstituted samples the rates of loading or loading step sizes were kept sufficiently small to avoid excessive pore pressure gradients and the consequent non-uniform compression that may occur Where a mid-height probe was used, the probe was placed in the middle of one of the windows of the Chinese lantern filter paper which had been cut larger than the others, so that a minimum drainage path length between the probe and the filter paper of 20mm was ensured. In this way the probe measurements correctly reflected the undissipated pore pressure in the sample.

Two membranes were generally used to avoid problems with punctures at the relatively high pressures used in the programme of tests. These were unsoaked to prevent any loss of suction in the natural samples Where a mid-height probe was used a special membrane was prepared, as shown in Fig.8 1, which had a latex collar built into the side of the membrane to receive the miniature pore pressure transducer. When placing the transducer in contact with the sample its tip was covered with wet kaolin to avoid loss of saturation. A pressure seal was achieved around the transducer body by two O-rings placed around the collar and by latex painted over the various component Prior to a series of tests the probe was saturated by leaving it under a pressure of about 400kPa in the triaxial chamber for about a week.

Each test on a natural sample generally started with a measurement of the suction. This was carried out as discussed in Section 5 6 4. This part of the test was not always successful (Section 5 6 4 and 8 1.2), particularly if the initial cell pressure was insufficiently high so that cavitation occurred in the drainage system. In some cases the measured suction was unusually high even if measurements of B showed the sample to have a high degree of saturation This was probably as a result of some drying during trimming. For example, Sandroni (1977) found that only two hours air drying of a sample of London clay increased the suction by 100kPa In other cases where samples were found to have both

apparently high suctions and B values below 95% it is probable that a small amount of air had been trapped in the drainage system during setting up.

When the sample was known to be incompletely saturated, after applying the undrained compression a back pressure of 200kPa was applied, giving an isotropic effective stress of 700kPa which is approximately the suction that should have been measured. This saturation stage was maintained until a B value greater than 95% was achieved, which was usually 48 hours. If a lower B value was obtained the base drainage system was flushed through under pressure using freshly de-aired water. In the case of test TN4 the sample was set up with a dry drainage system and so no pore pressure measurements were made

The reconstituted triaxial specimens generally had a higher degree of saturation than the oedometer ones and were not subject to a saturation phase. Instead, a total stress of around 80kPa was usually applied and the pore pressure allowed to stabilise. The test then commenced from whatever effective stress was measured

A number of tests on natural samples were unconsolidated before shearing as discussed in Section 8.1.2. The remaining natural samples and all reconstituted samples were consolidated and/or swelled prior to shearing. With the manually controlled apparatus step loading consolidation stages were used, but with the computer controlled apparatus continuous loading was used (test TN12, TN21, TN22, TNR1). The compression and swelling stages were usually isotropic, but in a few cases were one-dimensional. For the step loading stages a period of 48-72 hours was allowed for consolidation, while for continuous loading the rates of loading were such that the excess pore pressures in the sample were not significant.

Following compression or swelling the samples were sheared under a constant rate of strain, either drained or undrained but always with a constant cell pressure. The shearing was monotonic to failure. The rates of each shearing stage are shown in Tables 8 1 and 8 2 In general the maximum observed difference between the probe and base pore pressures was not greater than 3% of the total pore pressure change Rates of loading for tests without a mid-height probe were based on the observations from those tests where a probe was used

8 4 Data processing procedures

In this section the data processing is discussed. The results of this data processing are reported later

As discussed in Chapter 5 and Section 8.3, the water content w_0, voids ratio e_0, height h and volume V were measured before setting up the specimen. The vertical displacements logged by the external transducer were corrected for the compliance of each single apparatus. Compliance was measured by tests on steel dummy samples. The compliance was not repeatable at small strains, due to bedding errors and the initial compression of the internal load cell in the 0-6N load range.

The average axial strain during shearing ε_a was calculated as the ratio of the corrected displacement Δh to the height of the specimen at the start of shearing h_0. The value of h_0 was calculated assuming an isotropic strain during the isotropic (q=0) compression prior to shearing. After K_0 consolidation, h_0 was derived from local strain measurements. In the shearing stages, where local strain gauges were present, the axial strain was also calculated from the local strain measurements, which were not affected by the small strain-related errors in the measurement made by the external displacement transducers In the following sections mention will be made of the cases where the axial strain is determined from the local strain measurements

The volumetric strains ε_v were calculated as the ratio between the volume changes and the volume of the specimen V_0 before shearing. The shearing strain ε_s was calculated as.

$$\varepsilon_s = \varepsilon_a - \varepsilon_v /3 \qquad (8.1)$$

The current area of the specimen during shearing was calculated applying the right-cylinder correction (Bishop and Henkel 1962). The corrected area was used to calculate the q-p' state The definition of p' was based on the average of the base pore water pressure u_{base} and the pressure measured by the mid-height probe u_{probe}.

The area correction was applied until a complete kinematically-compatible mechanism of localized deformation emerged. In all the tests a failure surface formed rapidly and the prior formation of a shear band was not observed. After the formation of the failure surface the displacement mechanism consisted primarily of the sliding of two blocks along the failure surface Thus, the q-p' state was calculated using the expression proposed by Chandler (1966) for the cross-sectional area under the conditions shown in Fig 8 6 (a)

$$\text{Area} - D_{fs}^2 /2 \left[\pi/2 - \arcsin (\Delta h - \Delta h_{fs})/ D_{fs})\right] - (\Delta h - \Delta h_{fs}) \cot g\, \alpha \sqrt{[D_{fs}^2/4 -(\Delta h - \Delta h_{fs})^2(\cot g\alpha)^2\ 4]} \qquad (8\ 2)$$

where D_{fs} and Δh_{fs} are the d ameter of the specimen and the displacement at the time of f rmation of the fa lure surface respectively Eq 8 2 does not account for changes in volume of the c av blocks

Theoretically, it should be used in undrained tests only. However it was used also for the drained tests because of the limited extent of volume changes after failure surface formation (see Section 8 6.3).

The error in the overall calculation of the area during the test stems essentially from the assumption that the specimen was suddenly split into two sliding blocks when the failure surface was formed. By contrast, though the formation of the failure surface appeared brittle, there might have been a stage in the test when the specimen underwent a deformation as shown in Fig.8 6(b), though this deformation mode cannot easily be modelled. The expression used to calculate the vertical strain ε_v and the shearing strain ε_s was the same before and after the failure surface formation. Thus, the shearing strains ε_s were thereafter underestimated. In the following the data corrected for localization as above will be distinguished with the suffix loc

The plastic volumetric strain ε_v^p was calculated as the difference between the volumetric strain ε_v and the elastic volumetric strain ε_v^e. For the calculation of ε_v^e isotropic non-linear elasticity was assumed along the swelling lines (κ lines) in the v-p' plane Consequently, ε_v^p is equal to:

$$\varepsilon_v^p = \varepsilon_v - \kappa / v_0 \, (\ln(p'/p'_0)) \qquad (8.3)$$

v_0 and p'_0 being the specific volume and the mean effective pressure at the start of shearing, respectively. The excess pore water pressure due to plastic deformation u_p was calculated as follows:

$$u_p = u - q/3 \qquad (8\ 4)$$

The elastic shear strains ε_s^e were regarded as negligible given the high stiffness G of both the natural clay and the reconstituted clay at the testing p' Thus the plastic shear strains ε_s^p coincided with ε_s. The plastic strain increment ratio $d\varepsilon_v^p / d\varepsilon_s^p$ was derived from linear regression of the data. Similarly, the stiffness G was calculated from linear regression of the q-ε_s data.

8 5 Behaviour of the reconstituted clay

The results of the tests on reconstituted Pappadai clay are discussed in this section All the specimens were trimmed from the block of reconstituted clay consolidated from slurry to 200kPa vertical stress see Section 5 8) The applicability of the critical state framework to the behaviour of the clay will be examined, and the parameters derived. In accord with Burland (1990) the parameters and properties of the reconstituted clay, the intrinsic properties, will be indicated with an asterisk

8 5 1. Isotropic and K_0 compression

Continuous loading isotropic consolidation was carried out in test TR1 using automatic control, whereas incremental isotropic loading was applied in tests TR2, TR3 and TR4. The anisotropic consolidation loading in test TR5 was continuous

Isotropic compression data are plotted in Fig 8 7. The reconstituted specimens were initially overconsolidated due to the decrease in suction as a consequence of unloading in the consolidometer (see Sections 5 8). At p' higher than 200kPa the data appear to converge to a straight line The v-p' states of the clay at the end of the unloading stages in tests TR2 and TR3 are also plotted in the figure Prior to unloading the clay was compressed to a p' of 600kPa.

The strain increment ratio $d\varepsilon_v / d\varepsilon_a$ recorded in test TR1 is plotted against p' in Fig 8 8. The axial strain used to calculate this ratio matched the local strain measurements Even at a p' of 380kPa the strain ratio differed from three Apparently, the anisotropic structure of the clay (see Section 5.9 4) resulted in anisotropic deformations under isotropic stress compression to a p' much higher than that of the preconsolidation state. Based upon this finding, emphasis is placed on the high pressure data, so that the isotropic normal compression line (NCL_{is}) of the reconstituted clay is plotted slightly to the right of the low pressure data. The equation of NCL_{is} line in Fig.8.7 has the gradient λ^* equal to 0.204 and an intercept at p' of 1, N^*, equal to 3 16

The swelling line in Fig 8 7 has gradient κ^* equal to 0.046 κ^* was used in the calculation of the plastic volumetric strains ε_v^p (eq 8 3) of the reconstituted clay.

In Fig 8 9(a) the stress path followed during the consolidation of specimen TR5 is shown After an initially constant p' stress path, the stresses were increased keeping a constant value of K_0. The initial K_0 value was subsequently adjusted so as to keep the radial strain increment close to zero (Fig 8 9(b)) The strain ε_r in Fig 8 9(c) was derived from the volumetric strain and local axial strain measurements The local strain gauges gave similar readings and were always within 5% of each other

For p' between 100 and 180kPa, K_0 was kept constant at about 0 6, the corresponding strain increments $\Delta\varepsilon_r$ being roughly 0.1% only A sudden controller failure resulted in a drop of K_0, ε_r and p' (Fig 8 9) An overconsolidation of the specimen occurred accordingly (F g 8 1 The K_0 was raised again to 0.59 and the original ε_r was consequently re-established For p' lying between 200 and 270kPa, the radial strain increments were negligible Subsequently, K_0 was reduced to 0 53, but ε_r increased by 0 1% (Fig 8 9

The stage of the test closest to a post-yield compression at constant radial strain was that of p' within 200 and 250 kPa. The corresponding K_0 equalled 0.57. The K_0 normal compression line (NCL_{oed}) thus derived is plotted in Fig.8.10 (denoted with Anisot.compr.). This is parallel to the NCL_{is} line, with an intercept at p' equal to 1 of 3.105. The compression line resulting from oedometer test CRSR1 (see Section 6.6.6) is also plotted in Fig. 8.10, assuming a K_0= 0.57. The data at high pressures are found to lie very close to the NCL_{oed} line. This confirms the validity of both the NCL_{oed} line and the K_0 value of 0.57.

The NCL_{is} and NCL_{oed} lines of the reconstituted Pappadai clay are parallel ($\lambda^* = 0.204$), as provided for by the CSF. The value of λ^* is consistent with the value of C_c^* measured in the oedometer test (see Chapter 6) within the same range of voids ratio.

8.5.2. Stress-strain behaviour

The variations of the deviator stress q , of the stress ratio q/p' and of the excess pore water pressures u and u_p in the undrained tests are plotted against axial strain in Figs.8.11 to 8 14. In Fig.8.11(a) both the base pore water pressure u_{base} and the probe pressure measurements u_{probe} are plotted, showing the consistency of the pressure measurements generally achieved in the undrained tests.

In test TR1 the specimen was normally consolidated isotropically. As expected, the behaviour of the clay was contractant (Fig.8.11(a)) and strain-hardening, except for a mild softening at large strains. By the end of the test the pore water pressure was constant and the value of q/p' was equal to 0 95. This value should be close to the stress ratio at critical state of the clay.

The undrained shearing of the anisotropically normally consolidated specimen TR5 are shown in Fig 8.12. Again, the clay exhibited a contractant strain-hardening behaviour up to large strains. The stress ratio and plastic volumetric strain became constant by the end of the test and the clay reached a critical state. Thus, in this test the stress ratio at critical state was 0.91. The behaviour of the normally consolidated specimens TR1 and TR5 is in line with the critical state framework. However, the anisotropic structure of specimen TR5 affected the q-ε_a response A peak deviatoric stress occurred, which is not typical of an isotropically normally consolidated clay (Gens 1982, Rossato et al 1992).

The lightly overconsolidated specimen TR3 suffered localisation of strain while contracting and strain hardening The stress ratio q/p', corrected for localisation (eq 8 2), remained constant to an axial strain of 18%, at which stage the pore pressure had become constant Thereafter, the stress ratio decreased

(Fig.8.13). The localisation of strain in soil at critical state has been discussed in Section 2.3 and a similar process is thought to have occurred in test TR3, the critical state gradient being 0.87 in this case.

The behaviour of the overconsolidated clay in test TR2 (Fig 8.14) was dilatant in terms of the plastic component of pore pressure u_p, and strain-softening at axial strains beyond 11%. The strain-softening developed into the formation of a failure surface. The stress ratio for test TR2 was again corrected for localisation using eq.(8.2). At large strains both the stress ratio q/p'_{loc} and the plastic component of pressure u_{ploc} tend to a constant value, suggesting a stress ratio at the critical state of 0 9. The behaviour of this sample is therefore consistent with CSF (Section 2 2.2), the clay on the shear plane reaching a critical state with a higher specific volume than the rest of the sample.

In drained test TR4 strain-softening commenced well before the critical state stress ratio determined for the other tests, although no failure surface was evident. This conclusion was not changed significantly by the use of the area correction for strain localisation It seems possible that the strength measured in this test was affected by the shape of the specimen, whose height to diameter ratio had fallen to 1.38 at 20% axial strain, although usually shorter samples give higher strengths. At these larger strains the boundary conditions in the triaxial cause the stress state in the sample to be highly non uniform so that the calculation and corrections for q and p are no longer reliable.

8.5.3. Flow rule and stress ratio at critical state

To investigate the flow rule for the reconstituted clay, the plastic strain increment ratios $d\varepsilon_v^p / d\varepsilon_s^p$ during shearing were calculated as discussed in Section 8 4. These ratios are plotted against stress ratio for all the tests in Fig 8.15 The data from the two undrained tests on normally consolidated clay (TR1 and TR5) closely fit the linear relationship (Fig.8.15).

$$q/p' = 0.91 - 1.47\, d\varepsilon_v^p / d\varepsilon_s^p \qquad (8\ 5)$$

This is eq.(2.4) with values of the coefficients $M = 0.91$ and $A = 1.47$. This flow rule is much closer to the experimental data for the undrained tests than either the Cam-clay or Modified Cam-clay predictions which are also plotted.

The test data from the normally consolidated drained test (TR4) also closely fit eq (2 4 , with M=0 91, though with a lower value of A=0 53 (Fig 8 15). Due to the problems highlighted in the previous section these test data deviate from the linear relationship before reaching a critical state

Other relationships may exist which more accurately represent the flow rule, but a linear equation is not only more convenient for modelling, but also allows the simple physical interpretation of the behaviour as basically frictional (see Section 2.2.7). In Fig.8.16 the plastic strain increment ratio is plotted against p' for the isotropic compression stage of test TR1. The strains were shown not to be isotropic in Section 8.5.1. The compression seems to follow eq.(2.4) with values of $\mathcal{M}$ again of 0.91, but with A=1.0.

The stress-dilatancy data for the overconsolidated specimens (TR2 and TR3) initially oscillate around the zero dilatancy condition as would be expected for elastic behaviour However by the end of both tests the plastic strain increment ratio reaches a value of zero at a stress ratio of about 0.9.

In conclusion, a linear flow rule having a coefficient $\mathcal{M} = 0.91$ applies to the reconstituted clay beyond gross yield, though the factor A differs for drained and undrained tests and for compression, a feature that also applies to Lower Cromer Till (Section 2.4.2). The gradient of the critical state line for the reconstituted clay is therefore taken as 0.91, corresponding to a friction angle (ϕ'_{CS}) of 23°. Burland et al.(1996) observed a small reduction in the critical state friction angle with increasing stress level for some reconstituted marine and lacustrine clays, and Coop et al (1995) reported a much larger decrease for the reconstituted Boom clay. However there is no firm evidence of this effect with the Pappadai clay.

8.5.4. Critical State Line

The stress paths followed by the reconstituted clay are shown in Fig 8 17, where the critical state points for the individual tests are represented by an enlarged symbol. The lines for the maximum and minimum critical state stress ratios measured are also plotted, though a gradient of 0 91 appears generally applicable. The figure shows that test TR4 did not reach a critical state, as discussed above.

The v-p' state paths during shearing are plotted in Fig 8.18, together with the isotropic and K_0-compression lines. The final states of tests TR1 and TR2, which were consolidated isotropically, together with TR5 which was consolidated anisotropically, yield a unique line, parallel to the compression lines, with a gradient λ^* of 0 204 and an intercept Γ^* of 3 04 Although localization of strain occurred in overconsolidated test TR2, it is clear that post-yield internal drainage within the specimen was small Figure 8 17 shows that had test TR4 reached a critical state, p' would have been about 1150kPa. In figure 8 18 it is seen that this would have been consistent with the continuation of the state path to the critical state line (CSL) identified in the other tests

In conclusion, the behaviour of the reconstituted clay is consistent with the CSF. The spacing of the isotropic compression and critical state lines (N^*-Γ^*) of 0.12 is slightly smaller than the difference in the compression and swelling line gradients (λ^*-κ^*) of 0.16; with Cam-Clay behaviour they would be equal.

8.5.5. State Boundary Surface

To investigate the shape of the state boundary surface of the reconstituted clay the stress paths are normalized with respect to volume using of the equivalent mean effective stress p^*_e corresponding to the current specific volume of the specimen on the isotropic normal compression line.

The normalized stress paths are plotted in Fig 8.19. It would be expected that tests TR1 and TR4 should have had initial states which plotted on the isotropic normal compression line. The small discrepancies in this respect apparent in Fig 8.18 are assumed to result from inaccuracies of the water content measurements, and for the purposes of normalization the initial state has been assumed to lie on the line. The validity of this correction is confirmed by the close agreement of the normalized stress paths, which define a Roscoe surface for the reconstituted clay.

The stress path of the lightly overconsolidated specimen (TR3) rises to the Roscoe surface, and, after gross yield, follows it to a stress ratio close to the critical state, at which point strain localization and strain softening occurred as discussed earlier The stress path for the anisotropically consolidated specimen TR5 is also reasonably consistent with the Roscoe surface obtained from the other tests except for a small offset which is again likely to result from slight innaccuracy in the measurements during K_0-consolidation, but which cannot be easily corrected for.

The critical state lies at the end of the Roscoe surface. One test (TR2) on the dry side in addition allows a tentative identification of the Hvorslev surface It may be concluded that Fig 8 19 shows that the reconstituted clay exhibits the principal features of the CSF.

8.5.6 Normalized gross yield surface

The gross yield surfaces of the clay would be expected to be curves which plot along the state boundary surface in v-q-p' space. To investigate the shape of the gross yield curves, the gross yield stresses were normalized with respect to the current gross yield stress in isotropic compression, p'_p

This has been calculated as the intersection of the swelling line through the current v-p′ state and the isotropic normal compression line·

$$p'_p = \text{Exp}\,[(N^*-v-\kappa^*\ln p')/(\lambda^*-\kappa^*)] \qquad (8\ 6)$$

This normalization assumes that the soil is isotropically hardening, and that the point of intersection represents the gross yield that would be observed in isotropic compression for a particular yield curve. The normalized stresses are plotted in Fig 8.20. For tests TR1 and TR4 the whole stress paths are plotted, whereas for the overconsolidated specimens only the points of gross yield are shown. The normalised stress states are all close to a unique yield curve, showing that the yield behaviour of the clay can be normalised with respect to volume. It follows that the clay exhibits an isotropic volumetric hardening.

The plastic strain increment vectors for test TR4 are also plotted in Fig 8 20 (indicated as drained sh. vectors in the figure) along with a vector representing isotropic compression. These vectors appear to be near normal to the yield curve, except during compression and at the start of shearing, confirming that the q=0 compression was not isotropic in terms of strains (Section 8 5 1) Normality therefore appears to apply only to the later stages of shearing.

The coincidence of the yield curves and assumption of normality would suggest that the flow rule is the same for drained and undrained tests, though it was concluded in Section 8 5.3 that the flow rules were slightly different, but having the same linear frictional form.

8 6. Behaviour of the Natural Clay

In this section the results of the tests on the undisturbed specimens of the natural clay are discussed and are compared with the behaviour of the reconstituted clay The tests are detailed in Table 8 2.

8.6.1. Isotropic and K_0 compression

The states of the specimens after isotropic compression and swelling are shown in Fig 8 21, the scatter of the data is seen to be small A number of the tests reached elevated stresses in the high pressure apparatus

The use of internal local axial strain transducers in test TN22 showed the development of strain with increasing stress in isotr pic compression The ratio of the volumetric to axial strain increments is

plotted against the mean effective stress in Fig 8.22, yielding a ratio of three for p' above 2100kPa. This stress will be shown to be approximately the same as the yield stress in isotropic loading. In contrast to the reconstituted specimens which exhibited anisotropic strains even post-yield, the post-yield strains of the natural clay were isotropic.

For clarity in Fig.8.23 only the data from the high pressure tests (TN12, TN13 and TN22), one compression test at standard pressures (TN11) and a swelling test (TN5) are shown These have been used to define the isotropic compression and swelling lines. The isotropic normal compression line is straight, with a gradient λ of 0.254 and an intercept N, at p'=1kPa, of 3.77.

The straight line fitted to the pre-yield states in the figure has a gradient κ of 0.02 and an intercept at p'=1kPa of 2.02. The boundary envelope for the intact specimens, which is discussed later, refers to the behaviour of specimens with initial states close to this line.

The results of the K_0 compression carried out in test TN21 are also reported in Fig 8.23. This test was controlled by a feedback loop to keep the radial strain equal to zero as shown in Fig.8.24(a) The data from this test define the K_0 normal compression line for the natural clay which is parallel to the isotropic compression line, but with an intercept (v(p'=1)) of 3 74. The stress path is plotted in Fig 8.24(b), showing that at values of p' over 2000 kPa (which will later be shown to be the yield stress in K_0 compression), the value of K_0 became constant at about 0.63. Before yield K_0 first reduced, and then increased, as had been observed by others for various cemented soils (Chandler 1967; Coop and Atkinson 1993; Lerouil and Vaughan 1990).

The normal consolidation and swelling lines for both the natural and reconstituted clay are shown in Fig.8.25. The CSF appears to apply to both of the soils. The gradient of the normal compression line for the natural soil is higher than that for the reconstituted However, both are consistent with the values of C_c measured in the oedometer tests assuming a constant value of K_0. The only difference seen in Fig 8.25 between the behaviour of the natural and reconstituted clay is that, based on evidence from the oedometer tests (Section 6.6 14), the gradient of the natural clay swelling line increases after initial yield, becoming close to that of the reconstituted clay at a value of p' about twice the yield stress. Noting this the idealized swelling line for the natural clay at high pressures, also shown in Fig 8 25, has therefore been drawn parallel to the reconstituted swelling line. This increase of the value of κ beyond yield was accounted for in the analyses in the following sections

Both the isotropic and K_0 compression yield points of the natural clay plot far to the right of the ICL. The mean effective stresses at yield for isotropic compression (p'_{yis}) and K_0-compression (p'_{yK}) were calculated, using the Casagrande construction, as 226 and 2 0 kPa respectively The ratio of the

isotropic yield stress p'_{yi} to the equivalent pressure taken on the NCL_{is} line at the same specific volume as at yield (p^*_y) is 3.2 (Table 6.8). The corresponding ratio between p'_{yK0} and the equivalent pressure taken on the K_0-compression line of the reconstituted clay is 3 5. The latter value is equal to the same ratio expressed in terms of vertical stress (σ'_y/σ^*_e) measured in the oedometer tests (Table 6.8). The small difference between the isotropic and K_0-stress ratios is probably related to the difference in K_0 for the two clays. Either of the two ratios in terms of p' or that in terms of vertical stress could be used as a normalising factor to investigate the influence of structure on the behaviour of the clay (see Section 6.7.5).

8.6.2. Undrained stress-strain behaviour

The variation of the clay behaviour with changing isotropic yield stress ratio (YSR_{is}) is discussed in this section, and the influence of the post-yield structural changes is also described.

In Fig.8.26 two typical examples of the differences between base and probe pore pressure measurements are shown, these were always within 3% of one another

At values of YSR_{is} greater than 3 the clay exhibited a strongly dilatant behaviour after an initial contraction, similar to the reconstituted clay in the same YSR_{is} range. This is shown by the results of tests TN5, TN6 and TN7, plotted in Figs 8 27, 8.28 and 8.29 respectively. The difference between the total excess pore pressure (u) and the plastic component (u_p) represents the change in the pore pressure due to the elastic volumetric strain. The changes in u^p therefore reflect the plastic deformation of the clay. The size of the initial plastic contraction increases for reducing values of YSR_{is}, while the amount of the subsequent dilation decreases as the clay becomes more contractant. The value of u_p always starts to decrease before u, while the clay strain-hardens to gross yield.

Gross yield during shear is obtained from the curve of stress ratio (q/p') plotted against axial strain, taking the point immediately before significant reduction in the gradient of the curve. In cases when a sharp reduction in stress ratio was observed post-peak the gross yield point was taken as the peak. While for the drained tests there would be no difference between the use of the deviator stress or stress ratio plots to identify the yield points, in the undrained tests the yield state may plot either before the peak deviator stress or may not correspond to a sharp change in the gradient of the deviator stress·axial strain curve

This yield point is the first significant change in the clay behaviour during the test In Chapter 2 it was shown for both natural and reconstituted clays that when exhibiting dilatant behaviour the undrained

stress path touches the state boundary surface at the maximum stress ratio, after which the path follows the boundary (Atkinson and Richardson 1987; Sandroni 1977). The yield points are shown on the plots for each test, and the values of q/p'_y at yield are reported in Table 8 4.

In tests TN6, TN7 and TN5, yield occurred at the peak stress ratio, at a point corresponding to the maximum rate of reduction of u_p. In Section 8.6.5 this maximum gradient will be shown to be related to the maximum rate of dilation in terms of plastic strains, as would be the case for soils with frictional behaviour (eq.2.4). The maximum total excess pore pressure u occurs approximately at the peak stress ratio, as with reconstituted clays and for natural London clay (Sandroni 1977).

In these three tests, while the soil strain-softened in terms of stress ratio, the clay continued its plastic dilation as the deviator stress increased to peak, after which there is a substantial reduction in the deviator stress. For overconsolidated reconstituted clays the post-peak decrease of deviator stress during undrained shearing was attributed to the development of internal drainage within the sample, resulting in a volume increase and a strength decrease in the zone of strain localization (see Section 2.3). With the overconsolidated natural Pappadai clay it will be shown that this is not necessarily the cause of the reduction in strength post-yield since structural changes also contribute to this effect (see Section 8.6.5).

Localization of post-yield strains develops, at strains beyond the peak deviatoric stress, into a failure surface. In all natural clay tests a failure surface developed, and its formation corresponded to sharp discontinuities in the q-ε_a, q/p'-ε_a and u-ε_a curves, Figs.8.27 to 8.29. The formation of the failure surface, indicated with F.S. in the figures, gave rise to a sudden reduction in the deviator stress and in the total excess pore pressure u, but there is no corresponding effect on the values of u_p. Thus the post-peak decrease in pore pressure seems to be related to the elastic response of the soil in unloading, and should not be attributed to the plastic constitutive law of the clay.

The difference between the strain at the peak deviatoric stress and the formation of the failure plane increases with decreasing YSR_u, and thus with increasing mean effective stress, so that the tendency of the clay to dilate is smaller At low pressures the failure surface may develop soon after yield, so that its formation is sometimes difficult to distinguish from the brittle drop in deviatoric stress, as in test TN6 (Fig 8 27(a)) In any case the formation of the failure surface is subsequent to strain softening as this is the cause of localisation as discussed in Section 2 3

A significant drop in the total excess pore pressure occurred when the failure surface formed in tests TN6 and TN7, the drop reducing with decreasing YSR_u From the point at which the failure surface formed the stress invariants q and p' were calculated using the corrected cross-sectional area given by

eq.(8.2). The application of this correction had a significant effect on the test results. The values of q and q/p' resulting from calculation using the right cylinder area correction and also using the area corrected for localization are shown in Figs 8 27 to 8.29. The values of the inclination of the failure surface, $\alpha°$, are listed in Table 8.3. The use of eq (8.2) resulted always in values of q and q/p' (q_{loc}; q/p'_{loc}) which were significantly higher than those calculated with the right cylinder area correction while the values of u_p (u_{ploc}) reduced accordingly. The corrected data represent the stress-strain behaviour of the clay in the vicinity of the shear plane which was subject to large strains.

The values of q_{loc} and q/p'_{loc} tend to increase with increasing axial strain in many of the tests. Chandler (1968) showed this to be the effect of the restraint of the membrane to continued deformation of the specimen. He obtained a correction to the deviatoric stress which depended on the cell pressure and the deformation of the specimen after the formation of the failure surface This was used to correct the test data when necessary. The values of q_{loc} and q/p'_{loc} adjusted in this way remain almost constant after the drop resulting from the formation of the failure surface, (Figs 8 27, 8.29 and 8.30) while the values of pore pressure tend to reach constant values. The final values of q/p'_{loc} adjusted in this way are reported for all the tests in Table 8.4 ($q\ p_f$).

The behaviour of the clay at YSR_{is} = 2 4 (test TN2; Fig.8.30) was similar to that of the clay at YSR_{is} values greater than 3, but with a much smaller plastic dilation. The difference between the strain at peak stress ratio and the peak deviatoric stress was smaller than for the tests discussed above, so that after reaching the boundary surface the stress path drops away from it more quickly than for the tests at higher values of YSR_{is}. The formation of the failure surface occurred at about 1% axial strain after yield, following which the corrected u_p quickly stabilised and did not show the large decrease seen for the tests at higher values of YSR_{is}. As this test was carried out without consolidation, the measured strength of 500kPa represents in situ conditions, with an initial effective stress of 933kPa.

At a value of YSR_{is} of about 2 (test TN3) the clay behaviour changed, the strain softening becoming less pronounced and the plastic volumetric deformation tending to become contractant after the dilative stage. In both tests TN3 and TN1 the clay exhibited some plastic dilation after the initial contraction, and the peak stress ratio was followed by strain-softening during which at srains higher than 5% the plastic excess pore pressure again started to increase (Figs 8.31 and 8 32). As the strains at which the failure surface formed increased, the strain softening was less evident The formation of the failure surface gave rise to a decrease in the total excess pore pressure, while the plastic component again remained unaffected, demonstrating that the drop in total pore pressure is related simply to the elastic unloading as the strains localize, and not to the plastic constitutive behaviour of the soil

In test TN10 (Fig.8.33) it is evident that an incipient plastic dilation is terminated by plastic contraction which starts at around gross yield. In test TN11 (Fig 8.34) no dilative stage is seen, and the clay is continuously contractant to large strains. Although showing contractant behaviour, specimens with YSR_u values lower than about 1.8 are still strain-softening, giving rise to strain-localization and the subsequent formation of a failure surface at very large strains. At low values of YSR_u the behaviour of the natural clay is therefore qualitatively different from that of the reconstituted clay, where strain-hardening is always associated with plastic contraction.

In test TN12 (Fig.8.35) the clay was consolidated beyond isotropic yield, and during shear was contractant and exhibited strain-hardening to large strains However, this sample also strain-softened, and developed a failure surface at an axial strain of 19 5%. The specimen showed a peak deviatoric stress while still strain-hardening in terms of stress ratio. This behaviour is only seen with the reconstituted soil when K_0-compressed.

The tests on lightly overconsolidated and normally consolidated samples of natural clay suggest that part of the strain-softening of the natural clay reflects a loss in strength of the clay structure after gross yield. This is confirmed by the fact that a decrease in stress ratio also occurs when the clay contracts plastically, which, had it had a stable non-sensitive structure, is when it should have been strain-hardening. The behaviour of the natural clay beyond yield appears therefore not to be solely basically frictional. If this is the case the drop in deviator stress at high values of YSR_u is not only due to the development of local internal drainage, but also to a decrease in structural strength

Figures 8 36, 8.37 and 8.38 show the failed shapes of some of the specimens. It is evident that although all have a failure surface, the degree of barrelling increases as YSR_u reduces.

8.6.3. Drained stress-strain behaviour

Test TN14 (Fig.8.39) was performed to determine the correct axial strain rate which would allow complete drainage The sample, therefore, was equipped with a mid-height pore pressure probe The axial strain rate used to shear the sample were altered during the test so as to reduce the undissipated pore pressure Variations of the deviatoric stress due to the changes in strain rate may therefore be seen in the figure Before peak, for a strain rate in the range 0.2-0 7%/day, a difference in pore pressure of 25kPa between the base and mid-height was observed The increase of the strain rate post-peak did not significantly change this difference. For the other drained tests, which did not have a mid-he ght probe, a conservative strain rate of 0 2%/day was therefore chosen In retrospect this may have been too sl w, since although it helps to ensure complete drainage, the difference in strain rates

complicates the comparison with the undrained tests The rate chosen was an order of magnitude lower than that suggested by Gibson and Henkel (1954).

The stress ratio, q/p', and both the total and plastic volumetric strains during test TN14 are plotted against axial strain in Fig.8.39(b). The plastic volumetric strain ε_v^p was calculated as in Section 8 4 (eq 8 3). The value of κ used in the equation was dependent on the specific volume of the clay, because, as discussed earlier, the gradient of the swelling lines changes beyond yield. The following relationships were used to obtain κ :

$$\begin{aligned} \kappa &= 0.046-(0.046-0\ 02)/(1\ 84-1.64)(v-1.64) && v<1\ 84 \\ \kappa &= 0\ 02 && 1.84<v<1\ 88 \\ \kappa &= 0.02+(0.028-0\ 02)/(1.92-1.88)(v-1.88) && v>1\ 88 \end{aligned} \qquad (8.7)$$

According to these expressions beyond yield κ increases with respect to the pre-yield swelling coefficient, becoming equal to the κ^* at large pressures and specific volume v=1.64, and κ also increases at specific volumes above 1 84 due to the disturbance of the clay arising from swelling.

A smooth plastic volumetric contraction occurred in test TN14, although the clay was strain-softening and a failure surface formed at large strains. The oscillations in the plot result from temperature effects. After the formation of the failure surface, a correction to the deviatoric stress is applied for strain localization At the end of the test the sample appears to reach a constant volume.

A dilatant behaviour was recorded for the overconsolidated sample TN20 following an initial stage to 2% axial strain during which the plastic volumetric strain remained zero. Maximum dilation occurred at peak, as for a frictional material (Fig 8 40) The formation of a failure surface at about 1% axial strain after peak can be seen in both the stress-strain and the total volume change data, but again as for the undrained tests the plastic volumetric deformations do not appear to be influenced by the formation of the failure surface. Measurements using local axial strain transducers confirmed that the failure surface formed at this point, both of the gauges being located on the sliding blocks (see Fig 8 41) so that they registered little further deformation (Fig 8 40(b)). The pore pressure probe happened to be located on the failure surface (Fig 8 41), so that it recorded a sudden drop when the failure surface was created This confirms that the total volumetric dilation in the drained tests and the drop in total pore pressure in the undrained tests, which occur after peak, are associated with the formation of the failure plane Various authors (Maccarini 1987, Leroueil and Vaughan 1990, Aversa et al 1993) have considered that such post-peak dilative behaviour is proof that the soil structure influences the behaviour of the natural soil These data demonstrate that this conclusion is not correct

The behaviour of samples consolidated to YSR_u lower than 4 (TN15, TN16, TN17 and TN18) is always highly contractant, Figs.8.42 to 8.44. In test TN15 the clay exhibited a peak at small strains, but after this was only mildly strain softening At very large strains a failure surface formed, only after which did the rate of dilation reduce to about zero. The bulged TN15 specimen crossed by the failure surface is shown in Fig.8.45. In the other tests strain-hardening was recorded to large strains. Test TN16 was interrupted prematurely by an equipment failure, while in test TN18 (Fig.8.43) an accidental decrease in cell pressure diverted the total stress path so that the stress ratio rapidly reached a constant value, though a constant volume was not reached.

In test TN17 the sample was isotropically consolidated beyond yield, giving a contractant strain-hardening behaviour to 20% axial strain, after which the clay started to strain-soften with the subsequent formation of a failure surface As occurred in the high pressure test on the reconstituted sample (TR4), also in test TN17 the height to diameter ratio became very low at large strains, so that the observed drop in strength may not again be truly representative of the behaviour of the soil.

In conclusion, both the drained and undrained tests show the importance of shearing the sample to large strains to investigate whether or not it arrives at a critical state or not. The usual sample dimensions do not allow such an investigation at high pressures.

8.6.4. Critical States

The stress ratio is plotted against the plastic strain increment ratio to establish the flow rule for the natural clay in Figs.8.46 and 8 47. The flow rule at large strains is examined to understand whether the clay reached a critical state at which the plastic strain-increment ratio became zero at constant stress ratio. The plots for the undrained tests are shown in Fig 8 46, and those for the drained in Fig.8.47. In these plots the stress ratios are corrected for strain localization but not for membrane restraint, so that in some cases after the critical state is reached there is an artificial increase of the stress ratio at the end of the test The strain increment ratio cannot be corrected for localization, and so the values plotted are higher than those which would occur on the shear plane

In most of the undrained tests where a zero strain increment ratio was reached the stress ratio did not remain constant but continually decreased The values of q p' reached as the strain increment ratio became zero are reported as M in Table 8 4 The subsequent decrease may result from a reduction of the clay strength towards residual However Chandler (1968) showed that when samples shear along a discrete failure surface there is not only membrane restraint, but also a reduction of pore pressure resulting from the opening of a cavity underneath the membrane at the corner of the sliding block

Fig.8 48. This drop in pore pressure would result in an increase of the mean effective stress and so a reduction of the stress ratio. The failure surface formation is obvious from the stress-strain data, as is the consequent drop in pore pressure. The values of the drop in pore pressure which have been considered to be the result of this effect are indicated in Table 8.5. The corresponding corrected values of the final stress ratio ($\mathcal{M}_2$) are also reported in Tables 8.4 and 8.5. For the lowest pressure test, TN6, it is assumed that the high rate of plastic dilation is a real effect, since at the end of the test the strain increment ratio reduces to zero and no further decrease in stress ratio is seen. In Table 8.4 it is seen that the corrected values of stress ratio $\mathcal{M}_2$ are close to the values of $\mathcal{M}_1$, confirming that the low stress ratios recorded at the end of shearing q/p'_f (corrected for localization and membrane effects) are at least in part due to this pore pressure effect.

Figure 8.47 shows that only TN14, TN15 and TN20 among the drained tests approached a critical stress ratio. Test TN18 came closer to a critical state than is apparent in the figure, but the volumetric strain data were lost at the end of the test because of a failure of the transducer. For the drained tests the values of the stress ratio at critical state are given in Table 8.4 in the column for $\mathcal{M}_1$ No correction for the pore pressure effect is necessary, and so there are no $\mathcal{M}_2$ values

The values of $\mathcal{M}_1$ and $\mathcal{M}_2$ in Table 8.4 show that the average gradient of the critical state line for the natural Pappadai clay is 0.85, with a relatively small scatter of values between 0.78 and 0.93. This compares with a slightly higher value for the reconstituted soil of 0.91.

The undrained stress paths are plotted in Fig 8 49, together with the critical state points of both the drained and undrained tests, all corrected for localization, membrane restraint and pore pressure effects. The critical state line which best fits these data is also plotted. In Fig.8.50 the drained and undrained state paths are plotted in the v-lnp' plane, again with the critical state points. The critical states can be fitted with a straight line, parallel to the isotropic and K_0 compression lines, as shown in Fig.8.51. The state paths which do not arrive to a critical state seem also to approach this line. In these two figures the drained test critical state points are plotted only for those tests which clearly reached the critical state The critical state points are shown for all the undrained tests, though for those at low stress levels (TN6 and TN7) the critical state specific volume is inaccurate due to internal local drainage.

In conclusion, a critical state line is identified for the natural soil which is consistent with the CSF in that it is parallel to the compression lines, thus the natural clay arrives at a failure state at large strains which is entirely frictional. The critical state line for the natural clay lies to the right of the NCL_{ss} line Other authors have proposed that such a line should exist, but none so far has demonstrated its location (Smith et al 1992, Rampello et al 1993) The success in determining the location of the line is

due to the application of the corrections to the data, and to the fact that many of the tests yielded either on the wet side of critical or close to the critical state. The effect of structure on the critical state is evident, not so much in the observed friction angle, which is little changed, but in the large difference in the location of the critical state line of the natural clay and of the reconstituted clay in volume space (Fig.8.51).

8.6.5. Flow Rule

The analysis of the tests in Sections 8.6.2 and 8.6.3 suggests that the natural clay structure gives rise to peak strengths which are higher than those which would result for a frictional behaviour expressed by eq.(2.4) with the intercept M equal to the stress ratio at critical state. This is clearly the case since specimens yielding at stress ratios higher than that at the critical state (see q/p'_y in Table 8 4), although strain-softening, exhibit contractant behaviour. If the behaviour followed eq.(2 4) with friction M equal to the stress ratio at critical state, then if the clay exhibited contractant behaviour it should be strain-hardening to critical state. Thus the behavioural framework proposed in Chapter 2 (Fig 2.31) appears not to apply to Pappadai clay since the critical state line does not divide contractant from dilatant behaviour. Though some aspects of the clay behaviour prior to the critical state appear to be of a frictional type.

The plots of stress ratio against the plastic strain increment ratio (Figs.8 46 and 8.47) were made to identify the flow rule of the clay. In both drained and undrained tests the soil reaches a plastic strain increment ratio of zero prior to yield at a stress ratio which is always about 1.08, higher than the stress ratio at critical state. For a range of strains from below yield to beyond yield, but before the critical state, the relationship between the stress ratio and the plastic strain increment ratio is close to linear. In the undrained tests the gradient of this relationship is about 1 8, so that the flow rule for the clay is :

$$q/p' = 1.08 - 1.8\, d\varepsilon_v^p / d\varepsilon_s^p \qquad (8\ 8).$$

According to eq (8 8) the maximum stress ratio is reached by the specimens with dilatant behaviour at the point of maximum plastic dilation rate, as for a frictional behaviour

A linear equation is believed to be most convenient with which to represent the flow rule for the natural clay, though other relationships may exist which represent the flow rule more accurately For the natural clay, the data deviate from the chosen relationship at large strains, when they fall towards the critical state Thus the soil behaviour may be described as pseudo-frictional, following eq (8 8) in undrained conditions, changing to purely frictional behaviour at the critical state The intercept of

eq.(2.4) applying to the natural clay is the stress ratio of 1.08, which therefore divides the behaviour into contractive (wet) and dilative (dry), Fig.8.52. This will be more apparent in the following sections. If the clay yields at stress ratios above 1.08 its behaviour is dilatant, otherwise it is contractant. Specimens which yield at a ratio below 1.08, but above 0.85-0.9, follow the same flow rule with contractant behaviour to post-yield strains, and then finally deviate from the flow rule by strain softening to reach the critical state. This behaviour even holds for the specimen isotropically compressed beyond yield (TN12). Only specimens yielding at a stress ratio below 0.85-0.9 will show strain hardening behaviour to the critical state, although they may still obey the same flow rule up to high strains, as shown by the drained tests described in the following.

When the paths of the samples deviate from the flow rule given by eq (8.8), finally towards the critical state, the behaviour tends to be contractant. This is the reason why in some of the undrained tests an increase of plastic pore pressure was observed after a reduction due to plastic dilation. It is believed that this step, which occurs as the samples drop back to the critical state, results from progressive changes to the structure of the soil caused by yielding. In particular in tests TN1 and TN3 this contraction is responsible for the loop in the stress path (Fig.8.49).

In the drained tests, the relationship between stress and plastic strain increment ratios is again linear over much of the stress path, before and after yield. Again the intercept at zero dilation rate is 1.08, but the gradient is 0.72. Also with the reconstituted clay the flow rule is always linear, having the same intercept for both drained and undrained tests, but with a gradient greater than 1.0 for the undrained and less than 1.0 for the drained tests, as for the natural clay (Section 8.5.3). The principal difference between the flow rules for the natural and reconstituted clays is therefore in the intercepts, which results from the difference in structure of the two clays. The behaviour of the natural clay can therefore be considered to be frictional (eq.2.4), as for the reconstituted clay, but the friction parameter for natural structure, that is the intercept $\mathcal{M}$ in eq.(2.4), is different to that for the reconstituted structure and to the stress ratio of the natural clay at critical state ($\mathcal{M}$=0.85). The friction parameter of the natural clay, will be indicated with $\mathcal{M}_{nat}$ in the following. The flow rule for the natural clay therefore is :

$$q/p' = \mathcal{M}_{nat} - A d\varepsilon_v^p/d\varepsilon_s^p \qquad (8.9)$$

$\mathcal{M}_{nat}$ being equal to 1.08. It also appears that the friction parameter of the natural structure changes post-yield.

The behaviour of the natural clay during shear can be divided into three stages. At small strains the behaviour does not follow the flow rule of the second stage (eq 8.9) which applies to most of the test at

larger strains, including yield. In the third stage the soil behaviour no longer complies with the second stage flow rule, but goes to the critical state Consequently, the critical state line lies inside the state boundary surface of the soil (Fig.8.52), and, as will be shown later, all of the stress paths deviate inside the boundary surface when they move towards a critical state. This is true also for the undrained shearing of the clay compressed beyond isotropic yield. Only in test TN17, with the drained shearing of a sample compressed beyond isotropic yield, does the same flow rule apply as for the reconstituted soil. However even here the flow rule having an intercept 1 08 and gradient 0.72 still provides a good description of the behaviour of the soil (Fig.8.47).

The stress and plastic strain increment ratios during K_0 consolidation (TN21) are shown in Fig.8.53. When a constant stress ratio is reached following yield, a constant strain increment ratio is also reached, confirming that the frictional law eq (8.9) also applies to other stress paths for the natural clay.

8.6.6. Current yield surface of the clay

Table 8.4 shows the yield stress ratios q/p'_y for all the tests. To investigate the shape of the current gross yield curve of the natural clay (see Section 2 5.6), the shear yield stresses q_y-p'_y are normalized with respect to the yield mean effective stress in isotropic compression p'_{yis}, using two alternative definitions of the isotropic yield stress of the different specimens.

The normalized yield data are plotted in Fig.8.54. In one normalization p'_{yis} is assumed to be the same for all the specimens, and equal to the value actually measured in isotropic consolidation (2260kPa), as discussed in Section 8.6.1. This normalization assumes that all the intact specimens yield on the same curve

In the other normalization, p'_{yis} is assumed to correspond to the intersection point of the swelling line passing through the projection of the yield point on the v-p' plane with the NCL_{is} line The corresponding equation used of p'_{yis} is :

$$p'_{yis} = EXP[(N\text{-}v\text{-}\kappa \ln p)\ \lambda\text{-}\kappa)] \qquad (8\ 10)$$

The gradient of the swelling line κ of the in act clay was shown to equal 0 02 (Section 8 6 1) The values of λ and N were defined in Section 8 6 1 This normalization assumes that the yield curve depends on volume, as the normalizing factor p'_{yis} is related to both the stress state and the specific volume at yield The yield points corresponding to different swelling lines are considered to be located

on different yield curves. However, any errors in the water content measurements for the different specimens affect the normalized data.

The data from the first normalization appear to show more scatter, though the yield curves resulting from the two normalizations are quite close. The cupola-shape, identified in Chapter 2, also applies to the current yield curve of the natural Pappadai clay. In contrast to the commonly accepted view, the current yield curve of the natural clay is not oriented along the K_0 line. Graham et al.(1988) demonstrated the dependence of the orientation of the yield curve on the invariants and the normalization used to define it. Orientation along the K_0 line is only found in the *t*-s' plane.

8.6.7. Normalization of clay behaviour with respect to volume

The stress paths were normalized with respect to the equivalent pressure p^*_e, which corresponds to the current specific volume of the clay on the NCL_{is} line of the reconstituted clay. According to the definition of the NCL_{is} line given in Section 8.5.1, the expression for p^*_e was :

$$p^*_e = EXP[(3.16-v)/(0.204)] \qquad (8.11).$$

Tests TN12 and TN17 should have had initial states which plotted on the isotropic normal compression line. The small error which is apparent in Fig 8 50 is assumed to result from inaccuracies of the water content measurements, and for the purposes of normalisation the initial state has therefore been adjusted to lie on the NCL_{is} line of the natural clay.

In Fig 8.55(a) the normalized shearing stress paths and yield points for the specimens consolidated to states before isotropic yield are shown. The stress path followed by the clay in K_0 compression, the corresponding yield point, and the isotropic yield point are also shown. The shearing stress paths of the clay consolidated beyond isotropic yield before shearing are plotted in Fig 8 55(b), where they can be compared with the shearing yield points of the specimens consolidated to states prior to isotropic yield. The above figures enable to investigate whether the behaviour of the clay from gross yield onwards can be normalized with respect to volume, as is the case with the reconstituted clay

Based upon the undrained and K_0-stress paths and the isotropic yield point, the current state boundary envelope of the clay can be readily identified (Fig 8 55(a)) The drained stress paths appear to stop slightly below this envelope This may be ascribed in part to the effects of the very low strain rates used in the drained tests, Section 8 6.3 The state boundary envelope again has a cupola shape

The current state boundary surface of the clay and the state boundary surface of the natural clay join along the current state boundary envelope only, as discussed in Section 2.5.6. The state boundary surface of the natural clay in v-q-p' space encloses the states of the clay undergoing structural changes for changing specific volume. As is the case with the reconstituted clay, the gross yield points of the natural clay appear to lie on the SBS. Furthermore, the undrained stress paths of the dilating specimens rise along the state boundary surface for some distance beyond yield. Thereafter they drop to the critical state. The remaining drained and undrained stress paths barely reach the SBS of the natural clay and then rebound from it, unlike the stress paths of the reconstituted clay which lie on the SBS post-yield.

Fig 8.55(a) shows that the behaviour of the clay beyond gross shearing yield is not normalized by p^*_e. The normalized stress paths converge to a straight line of critical stress gradient (0.85) below the SBS They do not join at a critical state point in the q/p^*_e-p'/p^*_e plane due to the different gradients of the critical state line of the natural clay and of the NCL_{is} line of the reconstituted clay in the v-p' plane. Since the undrained stress paths fall to the critical state at constant volume, they cannot be normalized with respect to volume beyond gross shearing yield.

It can be concluded that the undrained behaviour of the clay beyond gross shearing yield does not exhibit volumetric isotropic hardening However, it cannot be determined whether the general gross yielding behaviour and the drained behaviour of the clay beyond shearing yield are isotropically hardening with respect to volume

The normalized stress paths of the specimens normally consolidated beyond isotropic yield (TN12 and TN17) define the size of the SBS of the natural clay at lower specific volumes. They are shown to plot within the current boundary envelope of the clay (see Fig.8.55(b)) Thus, unlike the SBS of the reconstituted clay, that of the natural clay is not normalized with respect to volume by the use of p^*_e However, another volume-related factor may come into play which normalizes the SBS of the natural clay, as discussed in detail in the following section

In Fig 8.55(b) the size of the SBS of the natural clay is compared to that of the reconstituted clay. Just as the distance between the NCL_{is} line of the natural clay and the NCL_{is} line of the reconstituted clay decreases with increasing pressure, the size of the SBS of the natural clay also becomes closer to that of the reconstituted clay The stress ratio p'_{ys}/p^*_y and the sensitivity of the clay are reduced with increasing pressure according to the sensitivity framework discussed in Section 6 7 2

The normalized stress paths of the specimens at values of YSR_{is} above unity (Fig 8 56) highlights features of the behaviour of the clay hinted at in the study of the flow rule in Section 8 6 5 The

specimens yielding at q/p'_y above 1.08 experience dilation, and a corresponding frictional increase of deviatoric stress along the SBS, following eq.(8.9). Subsequently, they leave the SBS and approach the critical state, either dilating or contracting. The specimens which contract after dilation follow a loop-shaped stress path (TN1 and TN3). As shown in Fig.8.56, it is these which yield at a stress ratio q/p'_y about 1.08, that is at a point on the SBS close to the intersection of the straight line of gradient 1.08 with the SBS.

The stress paths yielding at q/p'_y between 0.85 and 1.08 necessarily strain soften while contracting, in order to reach the critical state line inside the SBS. In the portion of the stress path where strain softening occurs, the flow rule of the soil differs from eq.(8.9), due to the structural changes which modify the friction of the soil from 1.08 to the critical state value of 0.85. Only those stress paths that yield at a stress ratio below 0.85, contract and strain harden to the critical state.

The behavioural framework of the natural clay is therefore divided into a dilative (dry) and a contractant (wet) side by the straight line of gradient $\mathcal{M}_{nat}$=1.08, and not by that of critical stress gradient $\mathcal{M}$=0.85 as would be the case for the reconstituted clay (see Figs.8.52 and 8.56).

8.6.8. Normalization with respect to volume and structural changes

The stress paths were normalized with respect to the equivalent pressure p'_{NC} corresponding to the current specific volume on the isotropic normal compression (NCL_{is}) line of the natural clay. The equation expressing p'_{NC} is :

$$p'_{NC} = EXP[(3.777-v)/(0.254)] \qquad (8\ 12).$$

All the normalized drained and undrained stress paths are shown in Fig. 8.57.

The p'_{NC} factor normalizes the stress paths with respect to volume. However, p'_{NC} is also affected by the changes in structure developing with decreasing volume. The variation of p'_{NC} represents the variation in strength of the clay structure with changing volume. Thus, for sensitive clays it accounts for the collapse of metastable structural elements in the clay together with the changes in specific volume. For this reason this normalization differs from that related solely to volume based on p^*_e

The p'_{NC}-normalized stress paths commencing beyond isotropic yield run closer to the current boundary envelope (Fig.8.57) than do the p^*_e -normalized stress paths (Fig 8 55(b)). However, stress paths TN12 and TN17 still remain slightly below the intact boundary envelope (Fig 8 57), posing the

question whether an accurate normalization of the SBS with respect to volume is actually feasible, even using p'_{NC}.

This doubt is reinforced by normalization of the stress paths with respect to p'_{ys} (eq 8 10). The latter was calculated using the same κ values as for eq.(8.7). The normalized stress paths are shown in Fig 8.58, where the normalized yield curves for the natural clay related to different isotropic yield stresses can be identified. The data in Fig 8.57 identify constant volume sections of the SBS of the natural clay, whereas the data in Fig 8 58 define yield curves on the SBS relating to different isotropic yield pressures. If the SBS could be normalized with respect to volume, unique curves would then be obtained in Figs.8.57 and 8.58.

In addition, the normalizations discussed here show that the behaviour of the clay during drained shearing beyond gross yield cannot be normalized with respect to volume. The post-yield shearing stress paths join at the critical state point which is located inside the SBS, as clearly shown in the figures.

In Section 6.7, the oedometric stiffness behaviour of the natural clay was normalized by a factor accounting for both volume and structural changes, $\sigma'_y(\sigma'_y/\sigma^*_e)$. The normalized deviator stresses in Figs 8.57 and 8.58 were thus further normalized by the factors p'_{NC}/p^*_e and p'_{ys}/p^*_y respectively. In Fig 8.59 the ratio p'_{NC}/p^*_e has been denoted as X_{NC} and in Fig 8.60 the ratio p'_{ys}/p^*_y has been indicated with X_y. This further normalization appears better to identify a locus which represents the normalized state boundary surface of the natural clay in Fig 8 59, and a curve in Fig 8 60 which represents the normalized yield curve of the clay.

It follows that the gross yield behaviour of the natural clay is isotropically hardening The size of the gross yield curve varies not only with volume but also with the changes of structure occurring in the clay with changing volume. Both the normalizing factors p'_{ys} and p'_{ys}/p^*_y, the same as the two factors p'_{NC} and p'_{NC}/p^*_e, include the structural changes of the clay, and enable the behaviour of the clay to be normalized with respect to structure. The ratios p'_{NC}/p^*_e and p'_{ys}/p^*_e in particular reflect the changes in sensitivity of the clay as discussed in Section 6.7.2.

The stress paths after shearing yield remain closer to the yield curve in Fig 8 60 than they do in Fig 8 58 The drained stress paths on the wet side appear to converge in a narrow band, though the normalizations used in Figs 8 59 and 8 60 show that the behaviour of the clay beyond gross shearing yield is not isotropically hardening.

8.6.9. Normalized stiffnesses of natural and reconstituted clay

For each of the shearing stages tangent shear moduli G were calculated by means of a linear regression over a fixed number of data points. Up to 21 points were used, which was considered a sufficiently small interval relative to the total number of data points which was typically over 500. The stiffnesses thus calculated are then plotted against the strain at the centre of the interval of regression. Examples from three tests are shown in Figs 8 61 and 8.62. Where internal gauges were used the agreement with the external readings corrected for apparatus compliance was generally good, indicating that the bedding and seating errors were small, the former probably as a result of the relatively high confining stresses used in these tests.

Fig.8.63 shows an attempt to compare the undrained stiffnesses of the natural and reconstituted soils. This comparison must first account for the different confining stresses used. Among others Viggiani and Atkinson (1995) have investigated the influence of p' on the undrained shear modulus of normally compressed soils at very small strains G_0 (Section 4.7.3) and have concluded that the relationship may be represented as the function:

$$G_0 = A p'^n \qquad (8.13)$$

where the coefficients A and n vary with strain level. They are typically determined for any particular soil by comparing the undrained stiffnesses over a range of confining stresses for normally consolidated samples, or for samples with the same overconsolidation ratio. In this case there were insufficient such tests to derive the values of these coefficients directly, and values of n have therefore been estimated by means of the correlation presented by Viggiani and Atkinson between n and the plasticity index for a variety of reconstituted soils. Because of the relatively high plasticity of this clay, the estimated values of n of 0.91 at a shear strain of 0.02%, 0.94 at 0.06% and 0.98 at 0.2% would be insensitive to any error in this correlation. These factors have been used to normalize the stiffness data for the influence of the confining stress as shown in Fig 8.63 The data have then been plotted against a parameter representing the state of the soil. For the reconstituted samples this is simply the overconsolidation ratio for isotropic stresses (R in Table 8.1). For the natural samples, the yield stress ratio YSR_u has been used (see Table 8 2)

The data in Fig 8 63 show that after normalization there is no difference between the small strain stiffnesses of the natural and reconstituted clays, in contrast to the large strain behaviour This is consistent with similar comparisons of stiffnesses made by Rampello and Silvestri (1993) for Vallerica clay and by Coop et al (1995) for Boom clay In these two cases there was reason to believe that the disturbance due to sampling had erased any possible effect of structure on the small strain

stiffness of the clays. In both cases block sampling had been used, but the Vallerica clay had been sampled from a quarry face, while the Boom clay samples were taken from the face of a deep tunnel. The sampling of the Pappadai clay probably subjected the soil to considerably less disturbance, but there is still no apparent influence of structure on the small strain behaviour.

Another interesting feature of the data is that the relationship between the normalized stiffness and R or YSR is not linear when log.log axes are used, as would be generally expected. A closer examination of the data presented by Viggiani and Atkinson, Coop et al., and Rampello and Silvestri shows that their data do not extend to sufficiently high values of R or YSR to confirm the linear relations they have assumed; their data also might be better fitted by a curve.

The stiffness of the horizontal sample (Test TN19) is significantly greater than that of the other samples. Also shown in Fig 8 63 is a data point representing the stiffness measured by the pressuremeter for an unload-reload loop carried out during the test at the depth from which the soil samples were recovered. This stiffness has been normalised for the in situ mean effective stress and is plotted against the in situ value of YSR, again based on isotropic yielding The pressuremeter modulus, which is for a shear strain of 0 2% lies well above the triaxial data for vertically tested samples at this strain level but is very similar to the stiffness of the horizontal sample.

8.6.10. Intrinsic anisotropy

The stress-strain and pore water pressure data from test TN19 are shown in Fig 8 64. This test was carried out on a horizontally trimmed specimen consolidated to a mean effective stress at about the average suction measured for the undisturbed clay The consolidation stresses for tests TN2, TN4 and TN5 on vertically trimmed specimens were also close to the suction values of the undisturbed clay (see Table 8.2). Therefore, the comparison between the results of "horizontal" test TN19 and those of tests TN2, TN4 and TN5 shows the effects of the micro- and macro-anisotropy of the clay on its stress-strain behaviour. The micro-anisotropy of the clay results from the horizontal orientation of the fabric discussed in Section 5.9, while the lamination of the clay (see Section 3.4) gives rise to what has been defined as macro-anisotropy of the clay

The undrained strengths measured in tests TN2, TN4, TN5 and TN19 were 501kPa, 556kPa 506kPa and 514kPa respectively It appears that the undrained strength c_u of natural Pappadai clay is not affected by the clay intrinsic anisotropy Support for this conclusion is provided by the undrained strength measured in situ in the self-boring pressuremeter tests carried out approximately at 25m depth down borehole A (see Section 4 6 2 and Fig 4 2 , which were 43 kPa and 5 0kPa This value is

expected to be closer to the strength of the horizontally trimmed specimen, as discussed in Sections 4.3.3 and 8.1.2. However the strength data from all the above mentioned tests were surprisingly consistent.

However, the intrinsic anisotropy of the clay appears to affect significantly its stress-strain behaviour. The horizontally trimmed specimen strain-hardens to large axial strains, when strain-softening occurs which develops into the formation of a failure surface. The stress-strain curves shown in Fig 8.64 for the horizontally trimmed specimen exhibit a clear difference compared to those in Figs.8.29 and 8.30, for vertically trimmed specimens.

As discussed in the previous section the stiffness of the horizontally trimmed specimen is higher than that of the vertically trimmed ones, this being consistent with the in situ stiffness in the SBP tests. However at large strains both the horizontally and vertically trimmed specimens reach the same critical stress ratio of about 0 85-0.9, as shown in Fig.8.64.

8.7. Behavioural framework of the natural clay

The natural clay in isotropic and K_0 normal compression and swelling exhibits similar behaviour to that predicted by the critical state framework, enabling the CSF parameters λ and κ to be defined.

Three stages of behaviour are identified during shear. In the first stage, the clay behaviour can be either modelled as pseudo-elastic or kinematically hardening, and when interpreted as elasto-plastic it follows a flow rule different from that which applies to the second stage.

In the second stage, the clay flow rule is of a frictional nature, described by eq.(8.9). This stage includes gross yield. The flow rule varies with the type of stress path due to differences in the coefficient A of eq (8.9). However, the same friction property applies to the different stress paths, which is thus recognized as the friction $\mathcal{M}_{nat}$ of the natural clay In q-p' plane a straight line through the origin having a gradient equal to the friction stress ratio $\mathcal{M}_{nat}$ divides the behavioural framework into a dry and a wet side (Figs 8 52 and 8 56), where the clay exhibits dilating and contractant behaviour respectively $\mathcal{M}_{nat}$ has been measured as 1 08 for the natural Pappadai clay This is higher than the stress ratio at critical state of both the natural ($\mathcal{M}$=0 85) and the reconstituted clay ($\mathcal{M}$=0 9)

In the third stage, which covers the clay behaviour at large strains, the clay does not follow the stage two flow rule Its behaviour is strain softening towards a critical stress ratio close to that of the

reconstituted clay (0.85-0.9). The final friction stress ratio of the clay $\mathcal{M}$ is therefore smaller than the friction stress ratio of the natural clay at gross yield $\mathcal{M}_{nat}$.

Because of the drop towards critical state in the third stage, the behaviour of the clay beyond gross yield is not that of isotropic volumetric hardening. Gross yield occurs on the SBS, as with the reconstituted clay. However, unlike the reconstituted clay, the SBS of the natural clay lies above the critical state line. However the SBS of the natural clay can be normalized by means of a factor accounting for both the volumetric and structural changes of the clay. The behaviour of the natural clay at gross yield therefore appears to be isotropically hardening.

Test	w_0 %	e_0	S_{ro} %	Consolidation	p'_p (kPa)	R	p' before shearing (kPa)	e before shearing	Shearing	$d\varepsilon_a/dt$	Apparatus	Mid-height pwp probe	L.s.g.**
TR1	44.93	1.258	98	Isotropic	424	1.06	399	0.919	U	3%/day	B	yes	yes
TR2	44.0	1.27	95	Isotropic	600	2.4	250	0 869	U	2%/day	C	no	no
TR3	44.7	1.258	97.5	Isotropic	600	1.33	450	0 839	U	2%/day	C	no	no
TR4	45.1	1.250	99	Isotropic	800	1	800	0 825	D	0.5%day	C	no	no
TR5	45.12	1.264	98	Anisotropic	450	1	450	0 823	U	3%/day	F	yes*	yes

** *Internal local strain transducers*
* *Top pwp independent from base pwp*

Table 8.1. Triaxial tests on reconstituted Pappadai clay.

TEST	Sample	w_0%	e_0	S_{ro}%	Consolidation	YSR_{in}	p' before shearing (kPa)	e before shearing	Shearing	$d\varepsilon_a/dt$	Apparatus	B% before shearing	Mid-height pwp probe	L.s.g.*
TN1	P	31.1	0.87	98	no	1.95	1150	0 865	U	4 8%/day	A	94%	yes	no
TN2	P	31.3	0.873	99.6	no	2.42	933	0 873	U	4%/day	D	96%	no	no
TN3	P	30.6	0.857	98	isotropic	2.167	1042	0 862	U	4.3%/day	A	96%	yes	no
TN4	P	31.53	0 87	99 8	no	/	(650-900)	0 87	U	9%/day	A	/	no	no
TN5	P	31.97	0.878	99 9	isotropic	3.22	700	0.8945	U	4%/day	A	97%	yes	no
TN6	5B	30.57	0 857	98 0	isotropic	7.50	300	0 907	U	7%/day	A	94%	yes	no
TN7	8B	30.79	0.862	98.1	isotropic	4 52	500	0.898	U	4%/day	A	94%	yes	no
TN8	P	30 58	0.857	98 0	isotropic	5.013	450	0 900	U	4%/day	C	94%	no	no
TN9	P	31.5	0.872	99 1	no	/	900	0 872	/	/	/	95%	no	/
TN10	P	29.8	0 843	97	isotropic	1 74	1300	0.843	U	4.5%/day	C	94%	no	no
TN11	P	32.3	0 885	100	isotropic	1.40	1600	0.856	U	5%/day	C	94%	no	no
TN12	3T	31 328	0.868	99	isotropic	1	3800	0 677	U	0 8%/day	E	94%	no	no
TN13	2T	31.7	0 870	98	isotropic	/	3800	0 692	/	/	E	/	no	no
TN14	3B	31 756	0.862	98	isotropic	4.52	500	0.875	D	0 2-0 6%/day	B	95%	yes	yes
TN15	P	30.93	0 866	98	isotropic	2 825	800	0 8725	D	0 189%/day	C	98%	no	no
TN16	P	31.075	0 868	98 2	isotropic	1 73	1300	0.84	D	0 189%/day	C	100%	no	no
TN17	P	30 165	0 850	97	isotropic	1	2500	0.766	D	0 189%/day	C	94%	no	no
TN18	P	31 33	0 877	98	isotropic	1 50	1500	0 839	D	0 4%/day	C	94%	no	no
TN19	P	30.74	0 863	98	isotropic	/	680	0 863	U	4 5%/day	C	94%	no	no
TN20	2T	32 6	0.888	100	isotropic	9 04	250	0 888	D	0 3%/day	B	94%	yes	yes
TN21	5T	30 87	0 879	96	anisotropic	/	2707	0.879	/	/	D	94 %	no	yes
TN22	8M	31 44	0 872	99	isotropic	/	2877	0 872	/	/	D	/	no	yes

* *Internal local strain transducers*

Table 8.2. Triaxial tests on undisturbed Pappadai clay.

TEST	α°
TN1	53
TN2	52
TN3	52
TN5	52
TN6	63
TN7	58
TN10	60
TN11	52
TN12	53
TN14	54
TN15	53
TN16	/
TN17	53
TN18	/
TN20	61

Table 8.3. Triaxial tests on the undisturbed clay : inclination of the failure surfaces.

TEST		YSRis	(q/p')y	(q/p')f	M1	M2
U	TN1	1.95	1.22	0.89	0.89	0.89
N	TN2	2.42	1.24	0.75	0.82	0.81
D	TN3	2.17	1.20	0.80	0.86	0.86
R	TN5	3.22	1.39	0.80	0.90	0.90
A	TN6	7.50	1.93	0.88	<.92	0.88
I	TN7	4.52	1.54	0.80	0.86	0.85
N	TN10	1.74	1.04	0.75	0.78	0.78
E	TN11	1.40	0.93	0.70	0.79	0.73
D	TN12	1.00	0.93	0.78	0.80	0.78
D						
R	TN14	4.52	1.14	>.93	0.93	-
A	TN15	2.82	0.95	0 81	0.81	-
I	TN16	1.73	0.70	/	>.80	-
N	TN17	1.00	/	/	/	-
E	TN18	1.50	0.63	0.84	0.84	-
D	TN20	9 04	1.47	0.92	>.92	-

Table 8.4. Triaxial tests on the undisturbed clay : yield and final stress ratios.

TEST	pwp correction	M2
TN1	35kPa	0.89
TN2	75kPa	0.81
TN3	60kPa	0.86
TN5	100kPa	0.9
TN7	40kPa	0.85
TN10	30kPa	0.78
TN11	35kPa	0.73

Table 8.5. Triaxial tests on the undisturbed clay : corrections applied to the final pore water pressure values and corrected final stress ratios.

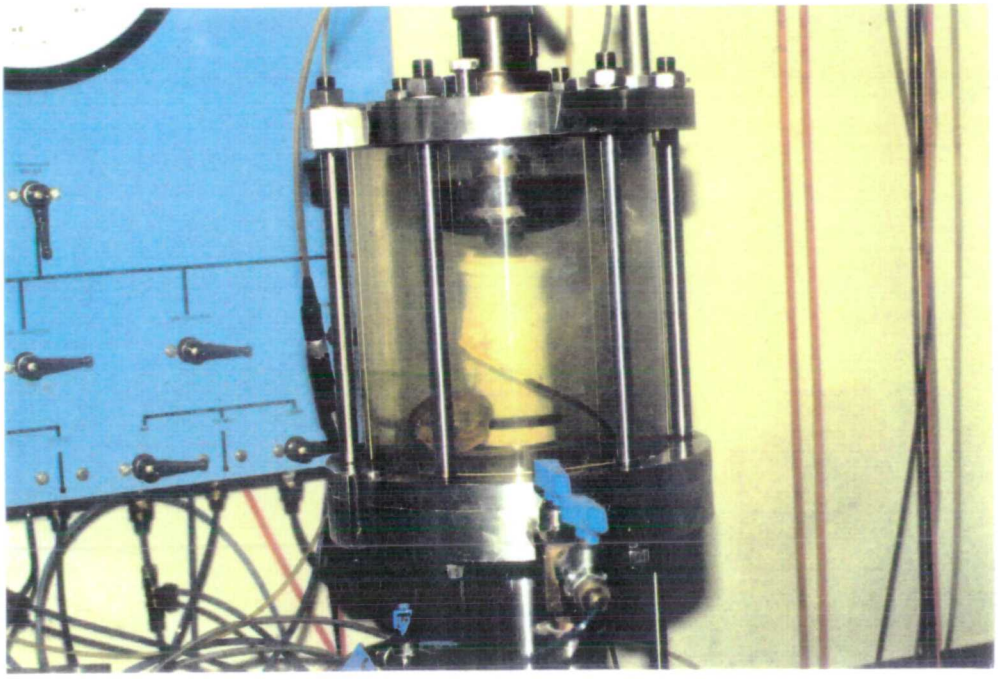

a)

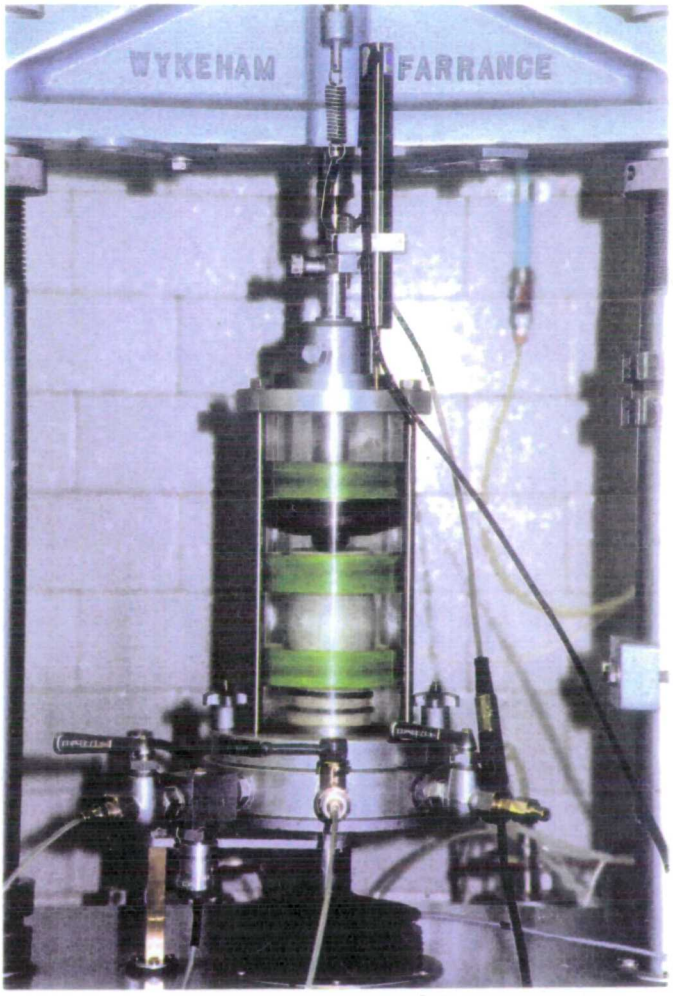

b)

Fig.8.1. Half ball connection between the sample top platen and the load cell : triaxial apparatus A (a) and C (b).

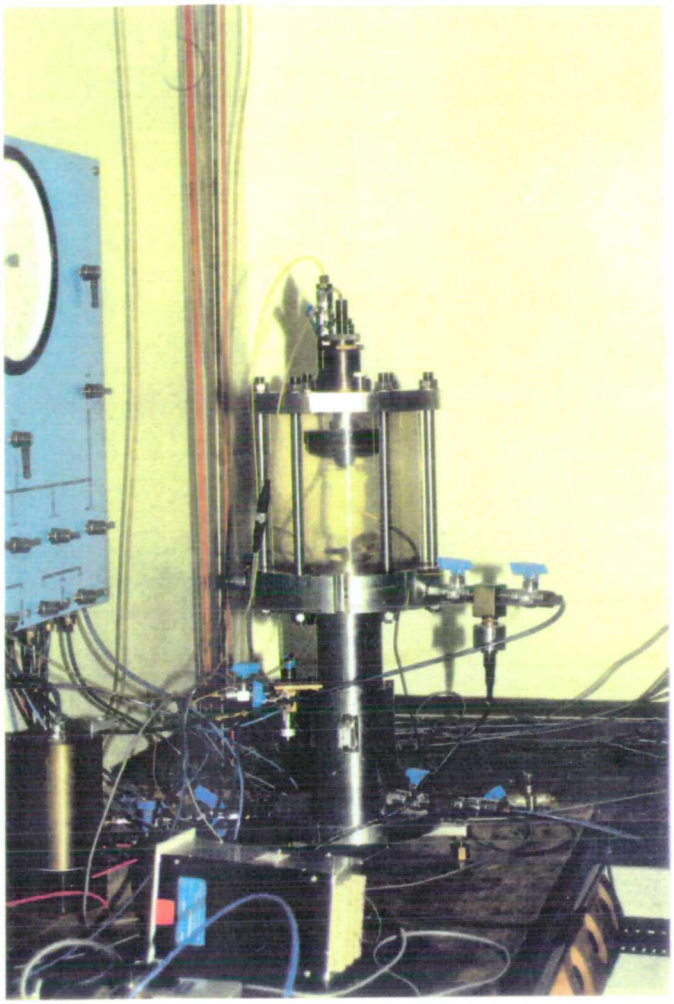

Fig.8.2. Triaxial apparatus A.

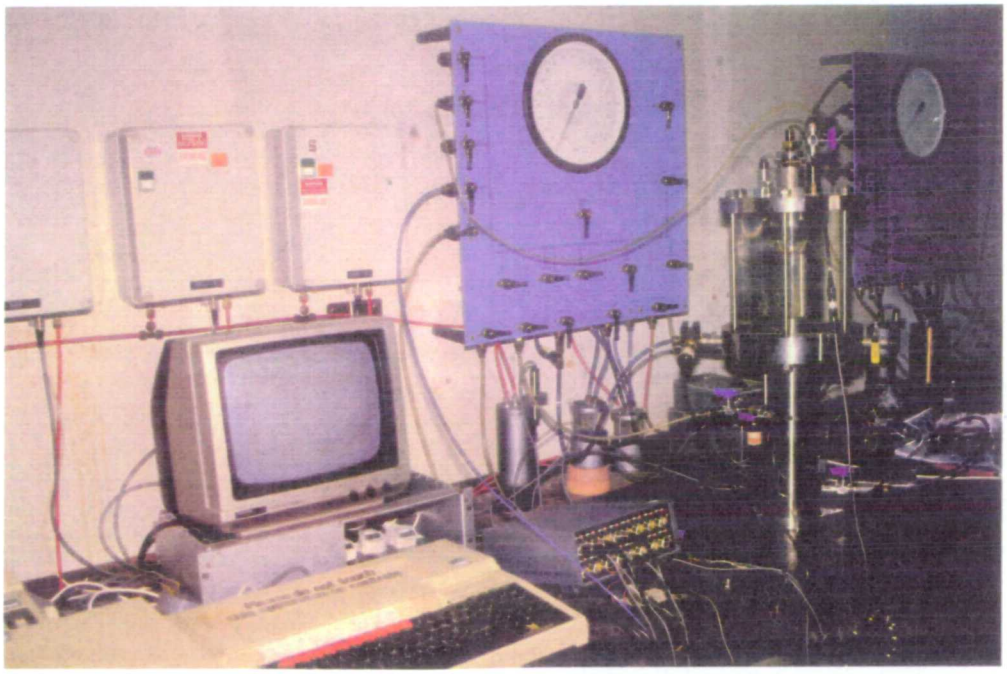

Fig.8.3. Triaxial apparatus A : data logging system.

Fig.8.4. Triaxial apparatus B.

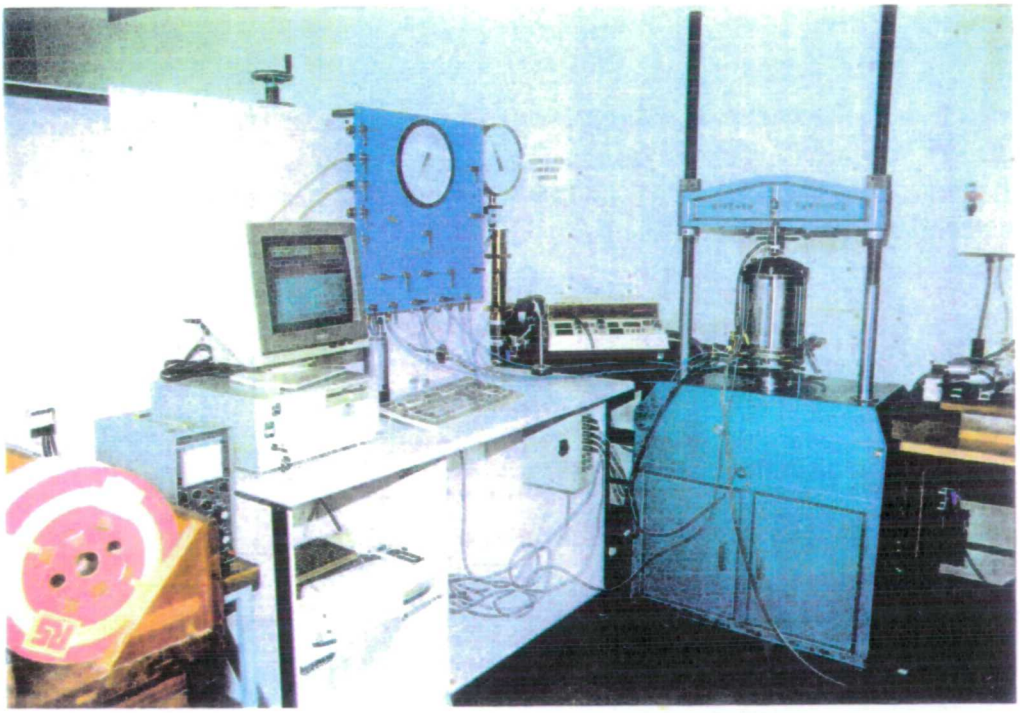

Fig.8.5. Triaxial apparatus E.

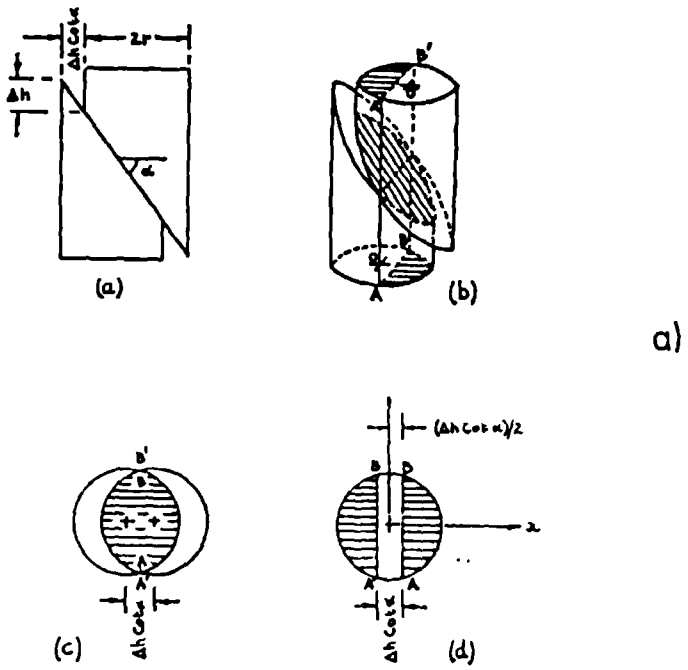

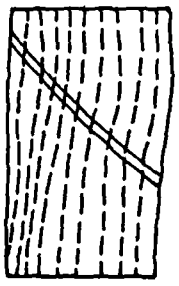

b)

Fig.8.6. (a) Specimen with preformed failure plane at axial displacement Δh (eq.8.2; after Chandler 1966); (b) bulging and progressive shear band formation before the development of a failure surface.

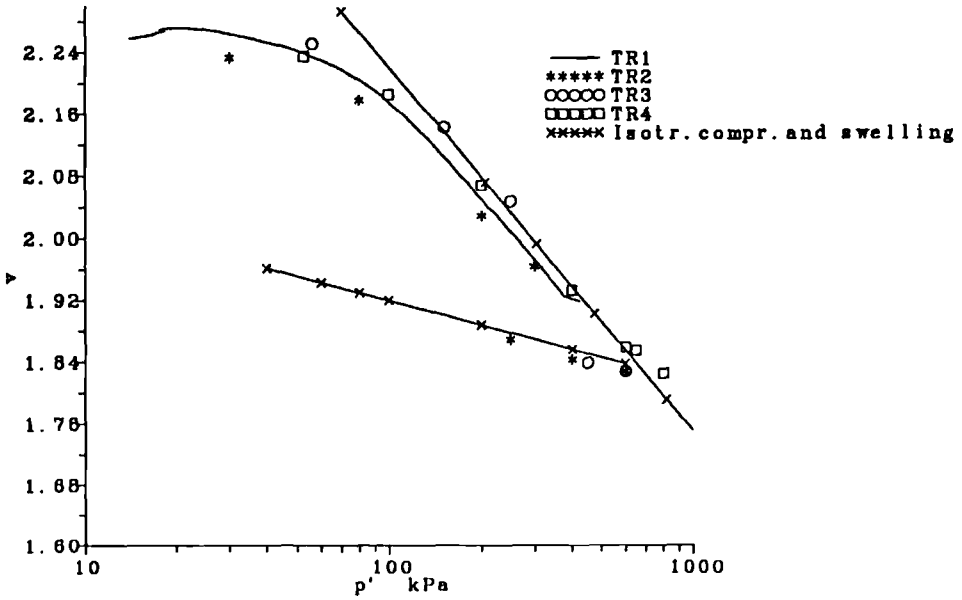

Fig.8.7. Reconstituted clay : isotropic compression and swelling states.

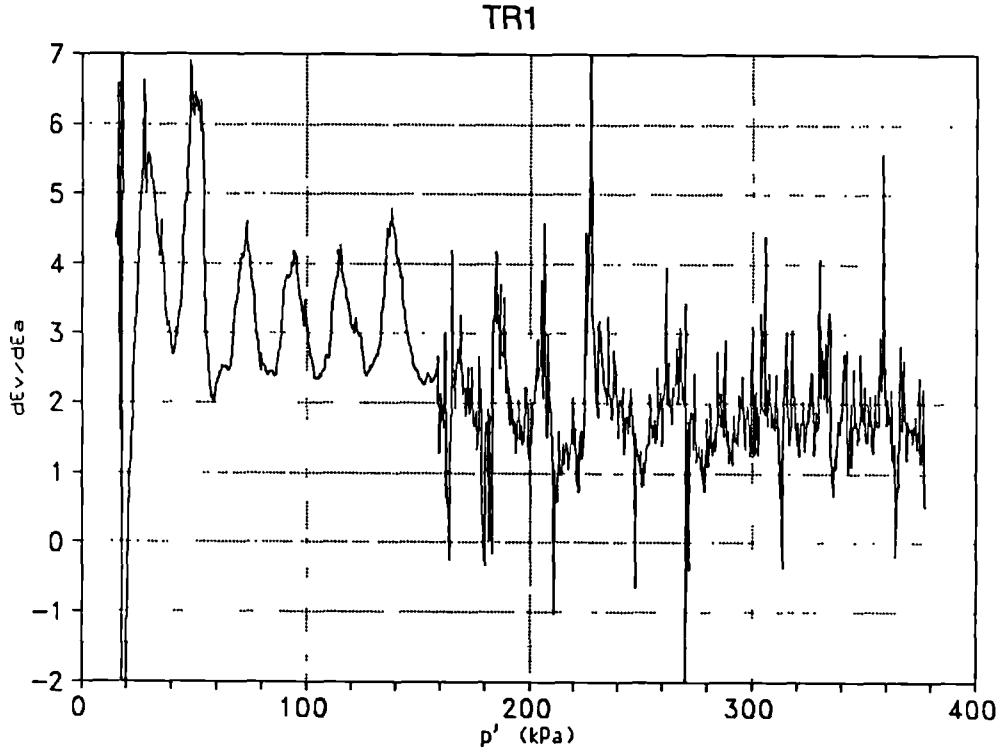

Fig 8.8. Anisotropic strains recorded during the isotropic stress compression of the reconstituted clay (test TR1).

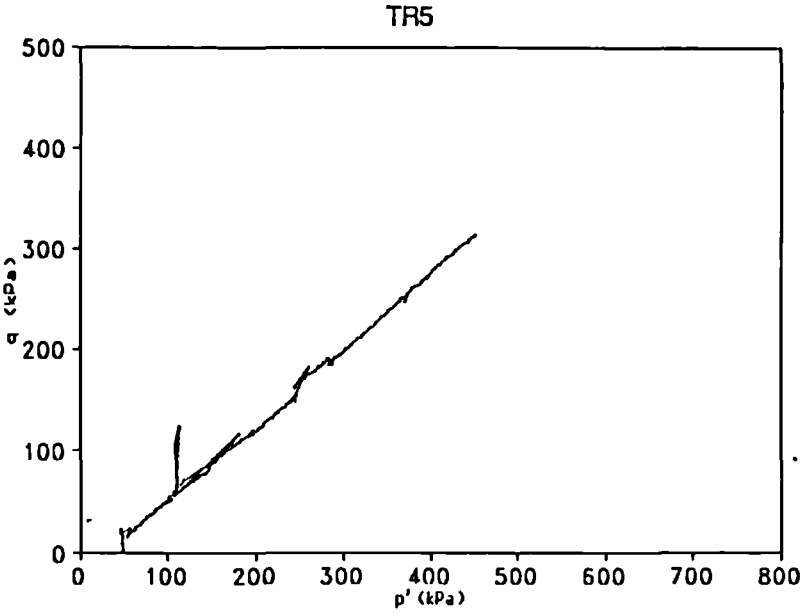

a)

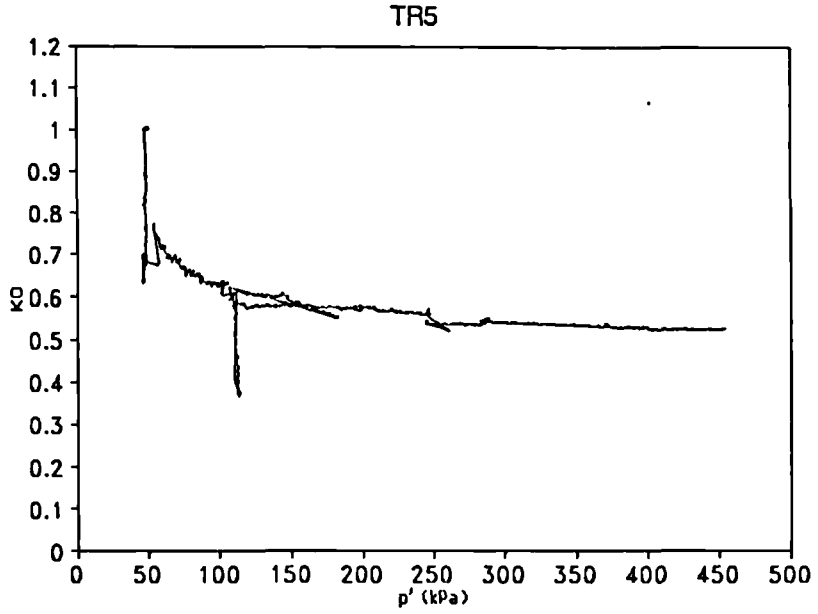

b)

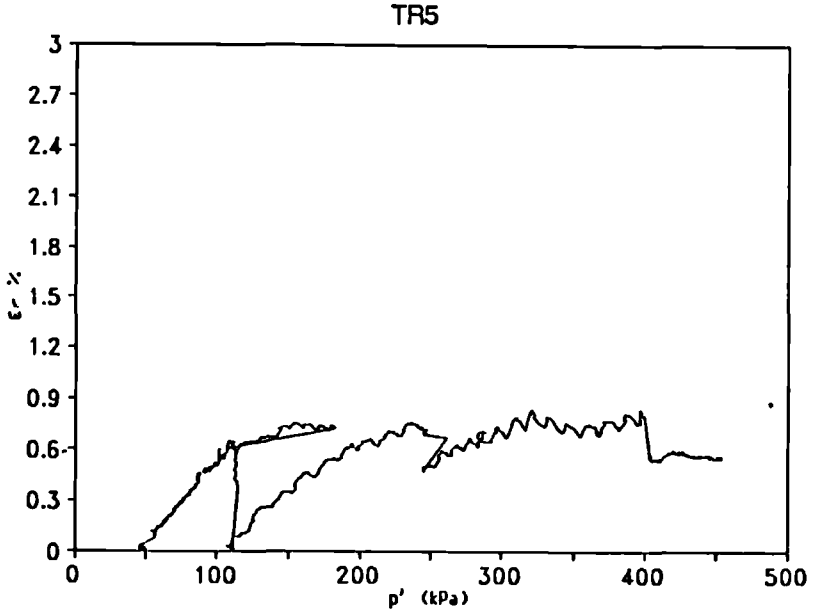

c)

Fig.8.9. Anisotropic compression of the reconstituted clay (test TR6).

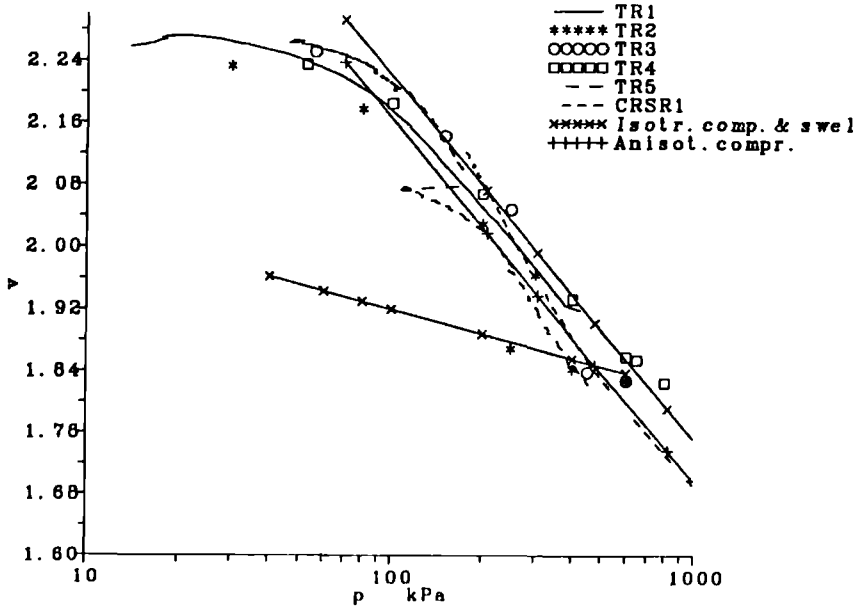

Fig.8.10. Reconstituted clay : states in isotropic and anisotropic compression and swelling.

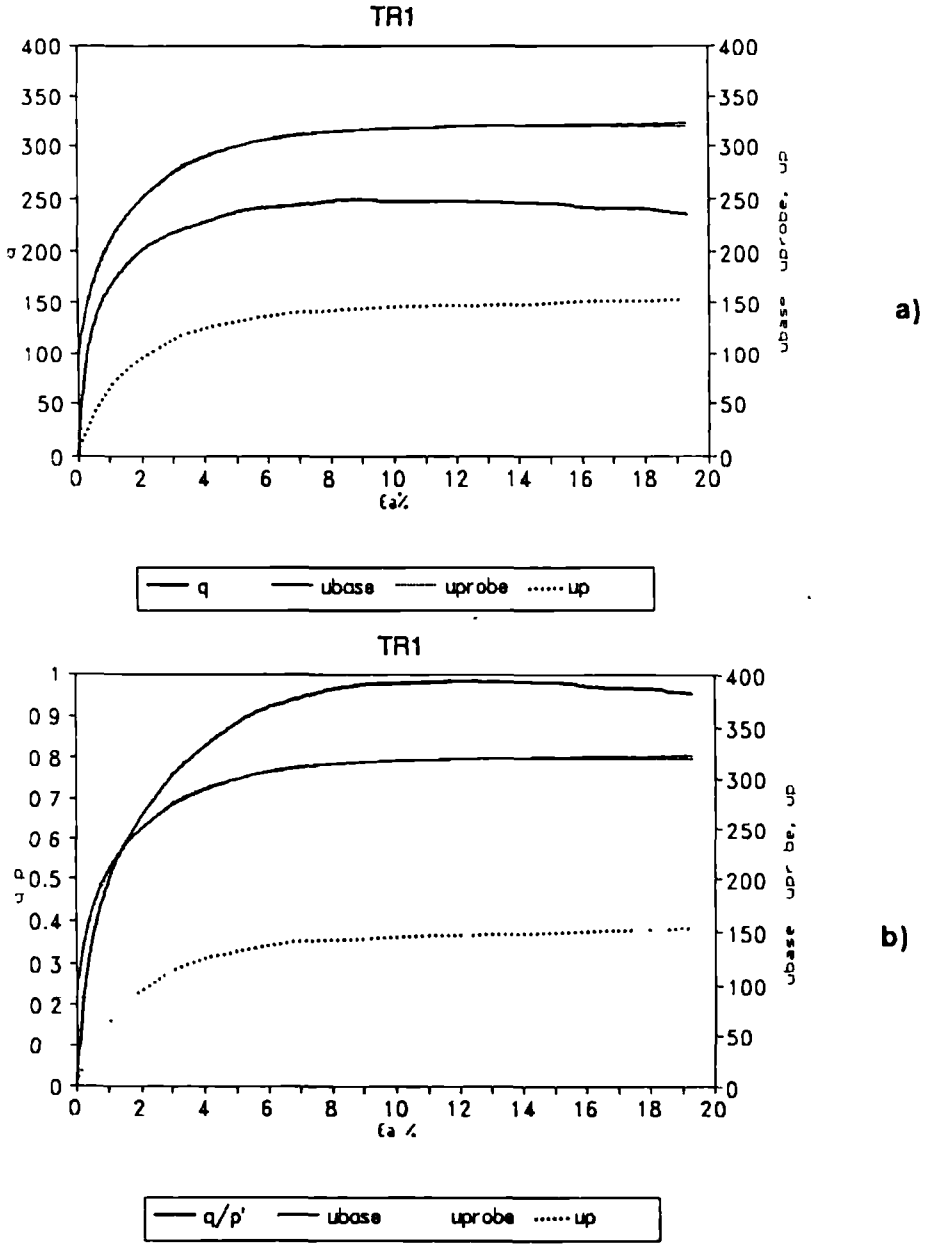

Fig 8.11. Reconstitu ed clay · stress strain behaviour of isotropically normally consolidated specimen.

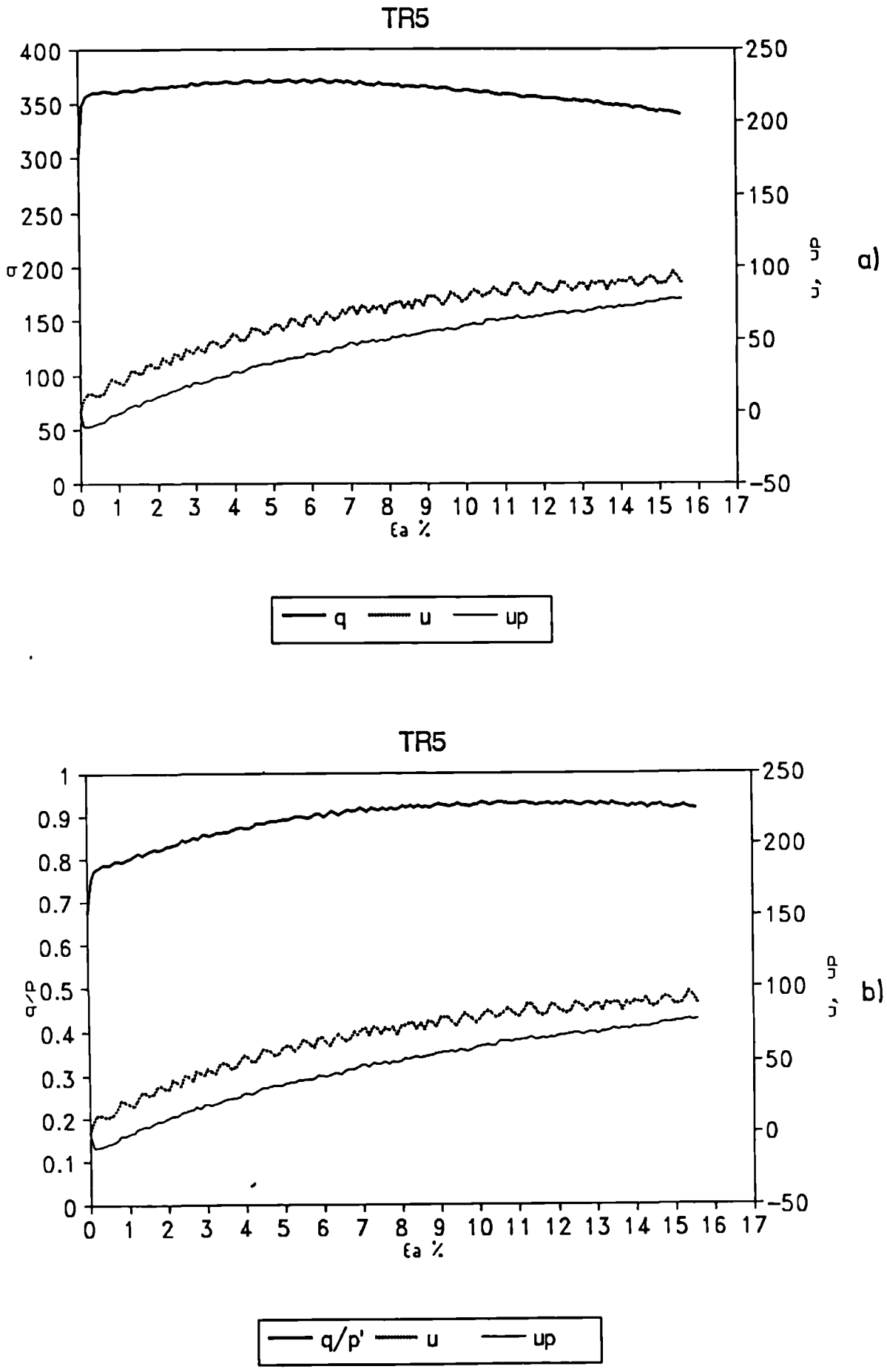

Fig.8.12. Reconstituted clay : stress-strain behaviour of anisotropically consolidated specimen.

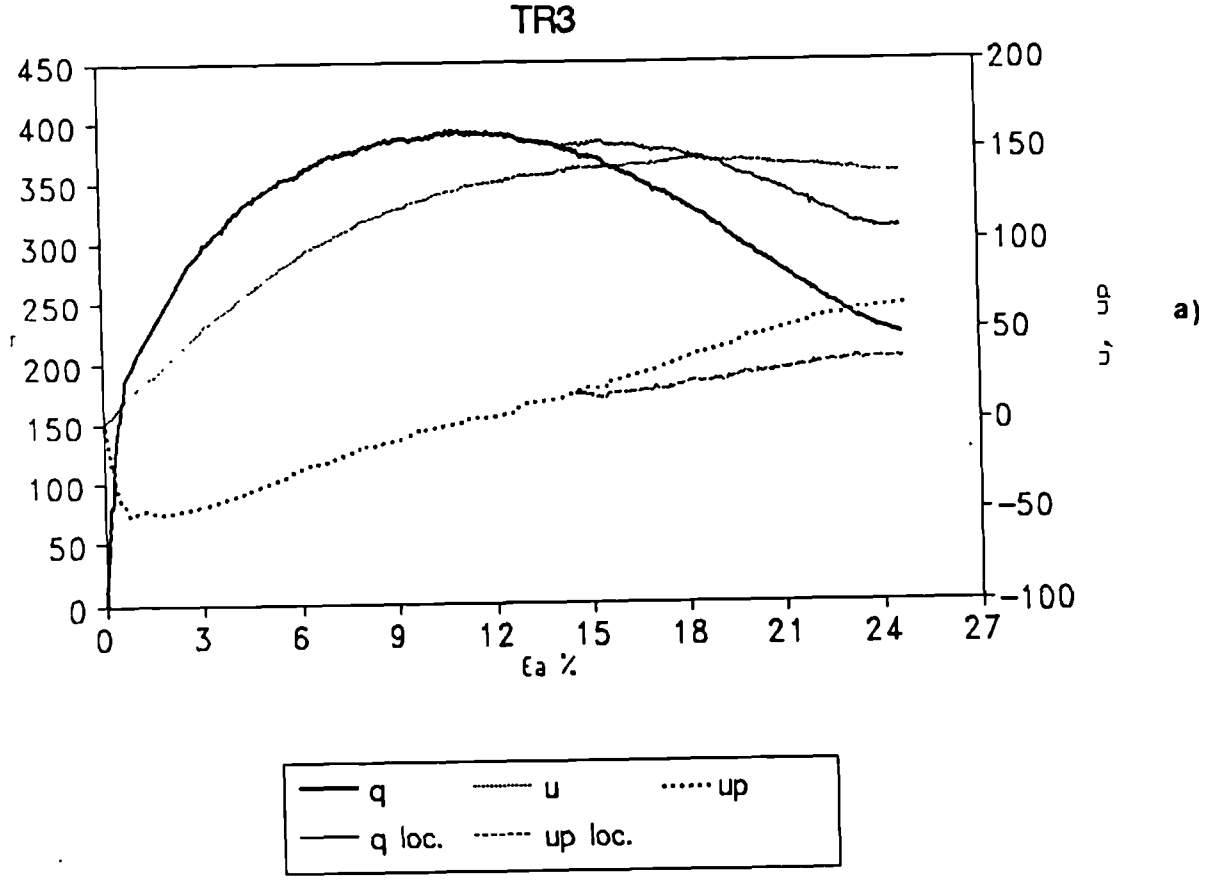

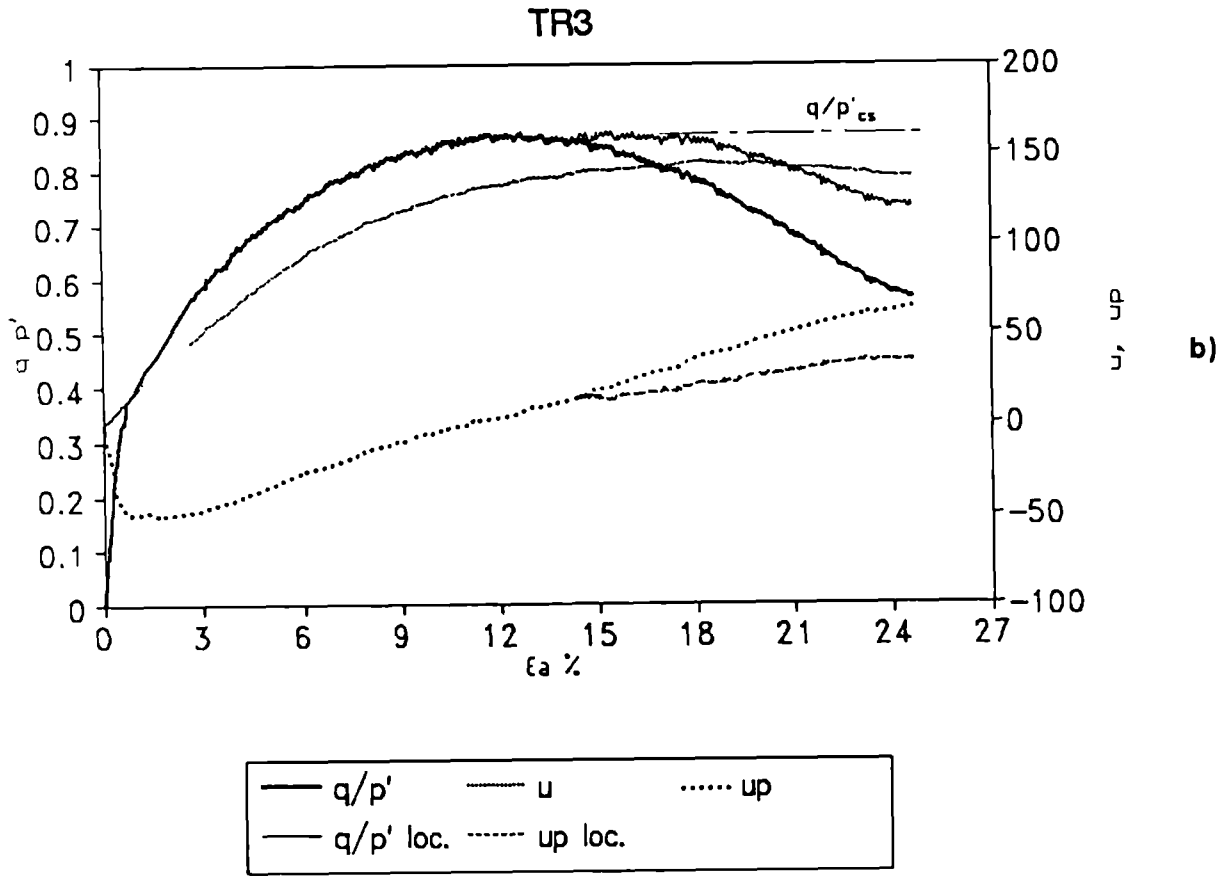

Fig.8.13. Reconstituted clay : stress-strain behaviour of isotropically overconsolidated specimen R=2.4), before and after correction for localization ($q_{loc.}$,q/p'_{loc}, u^p_{loc}).

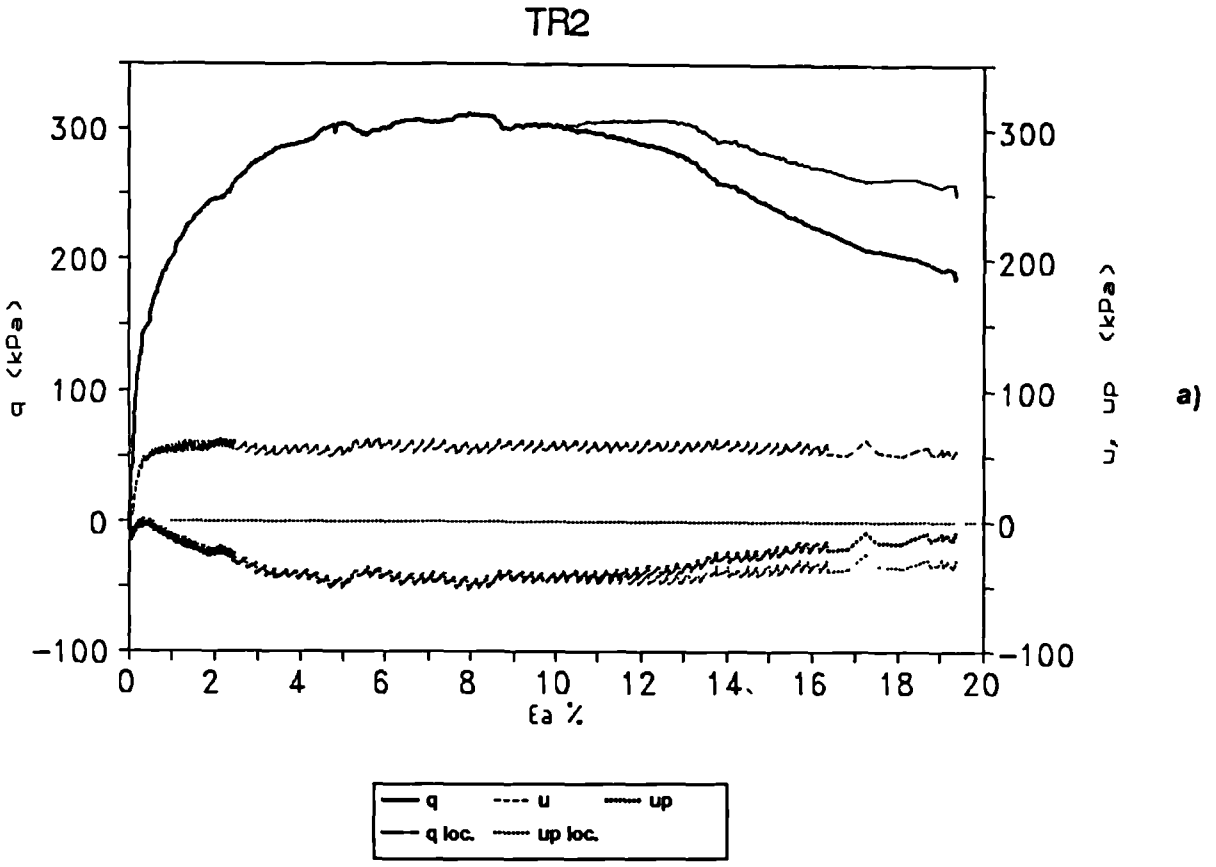

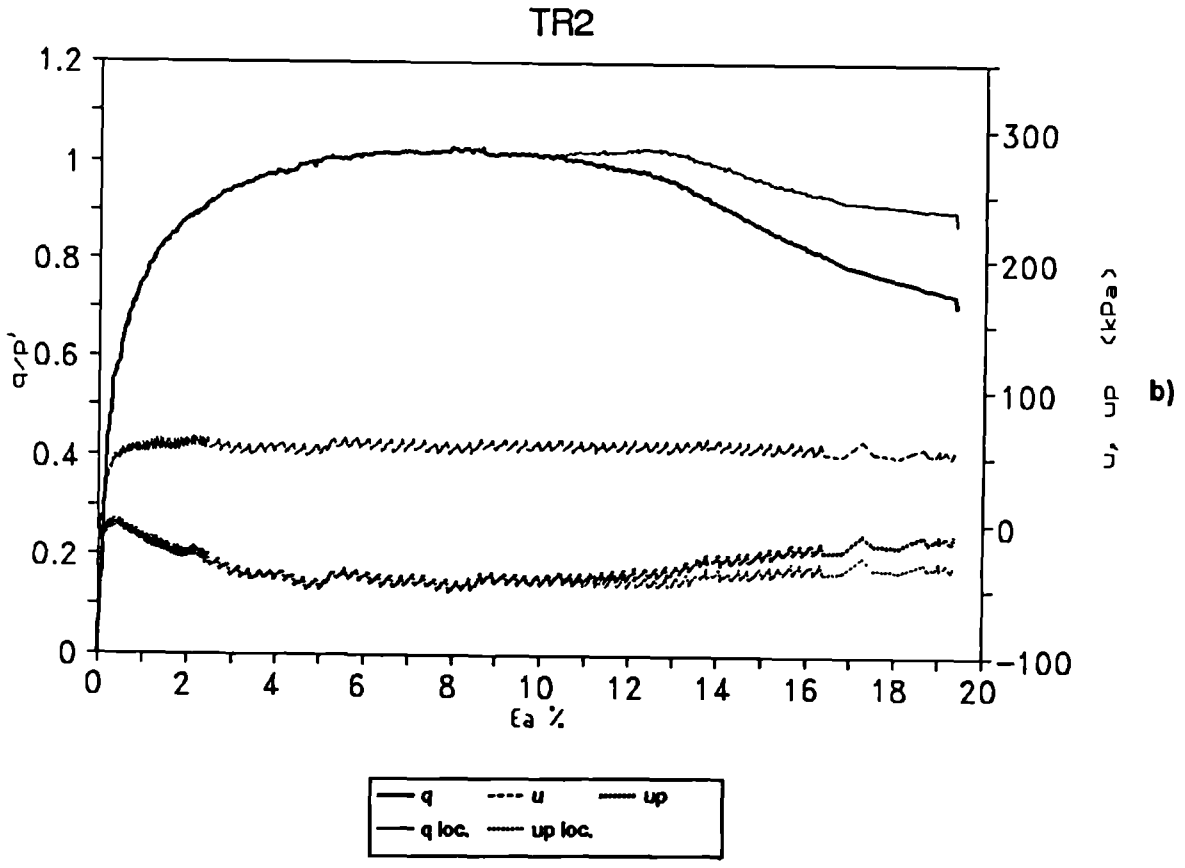

Fig.8.14. Reconstituted clay : stress-strain behaviour of isotropically overconsolidated specimen (R=4.5), before and after correction for localization ($q_{loc.}$, $q/p'_{loc.}$, u^p_{loc}).

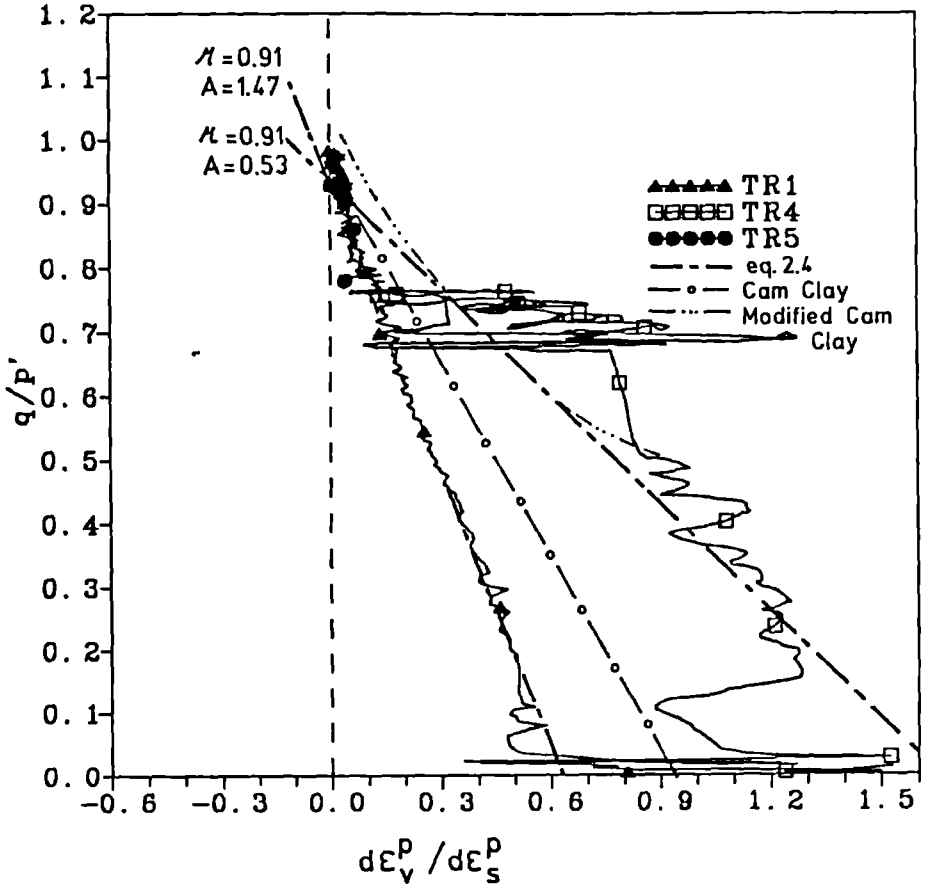

Fig.8.15. Reconstituted clay : flow rules.

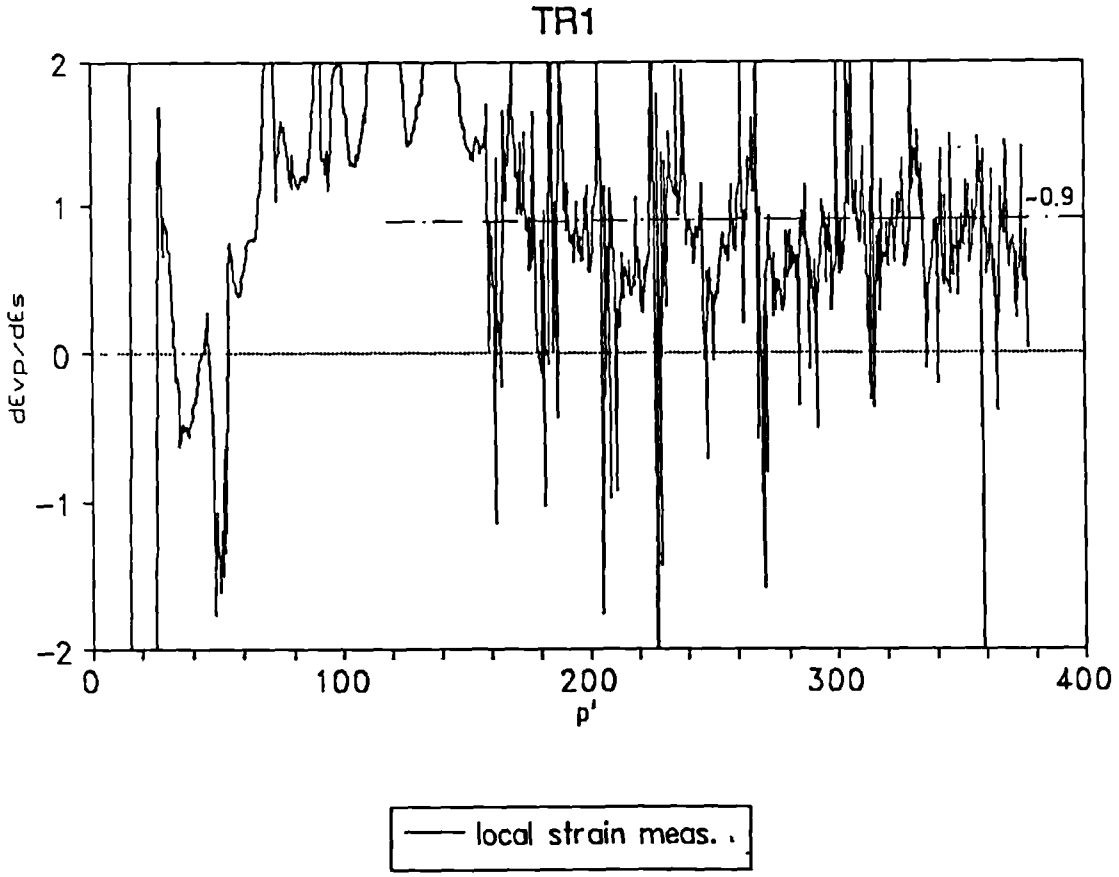

Fig 8 16. Reconstituted clay · plastic strain ratios in isotropic compression.

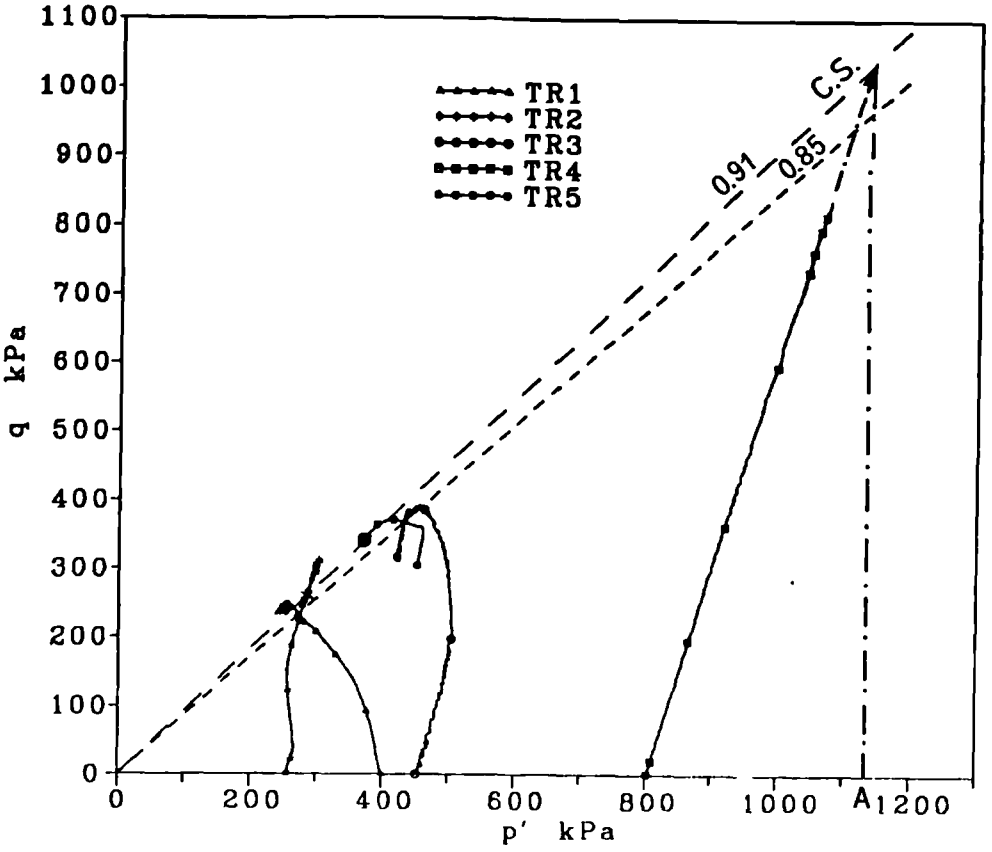

Fig.8.17. Reconstituted clay : stress paths and critical state line.

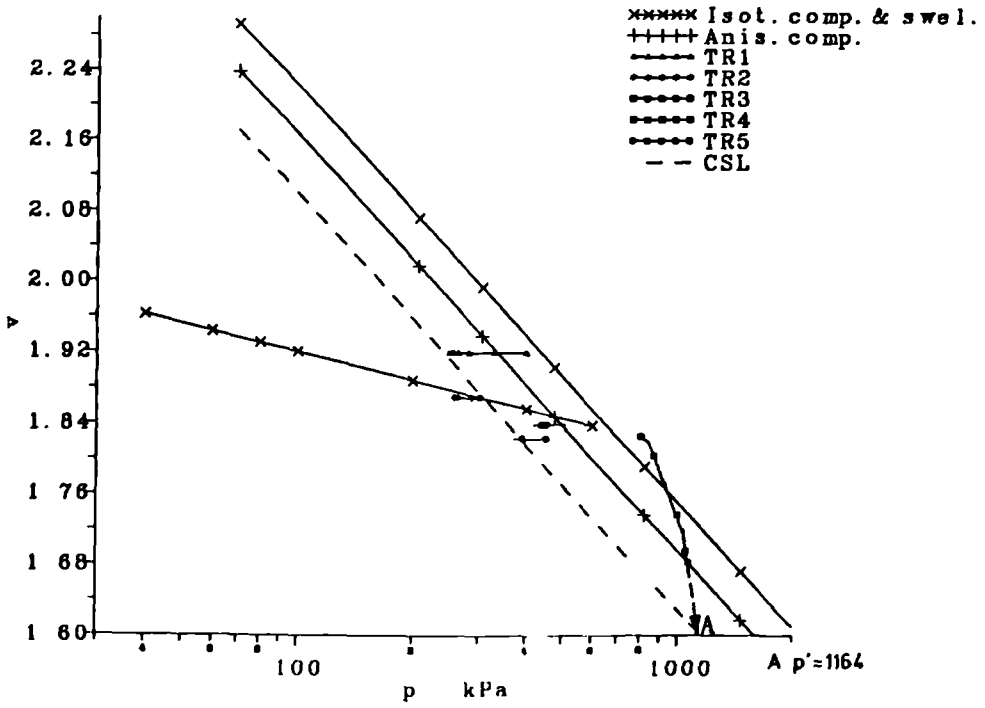

Fig.8.18. Reconstituted clay : v-p' state paths and critical state line.

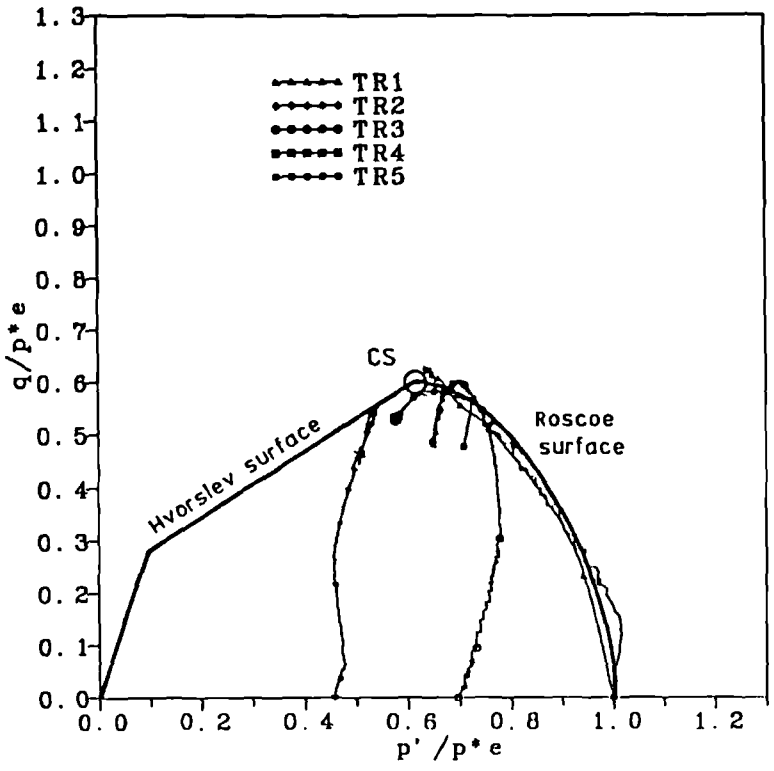

Fig.8.19. Reconstituted clay : normalized stress paths and state boundary surface.

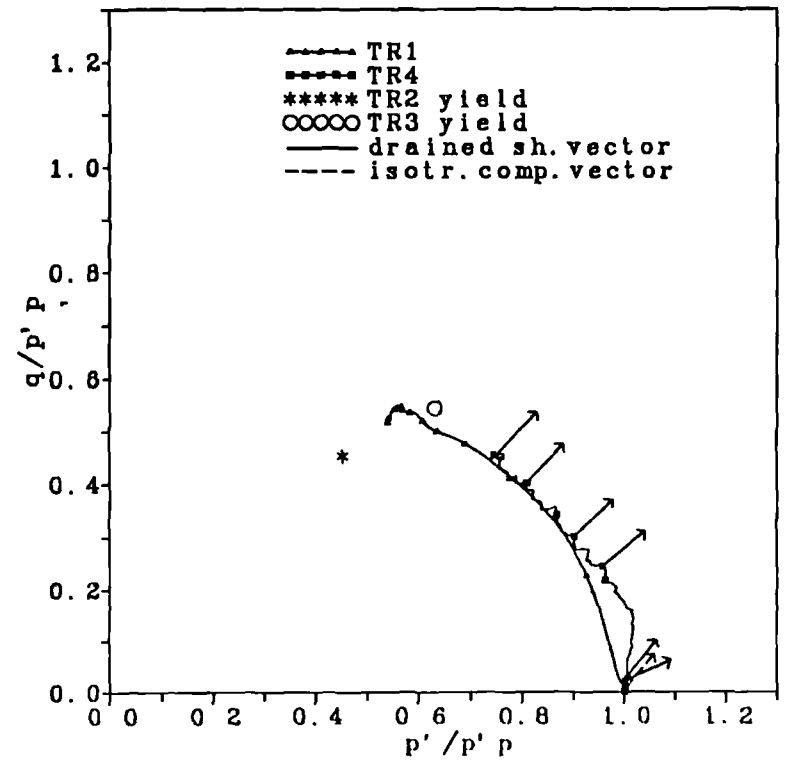

Fig.8.20. Reconstituted clay : normalized yield curve and plastic strain vectors.

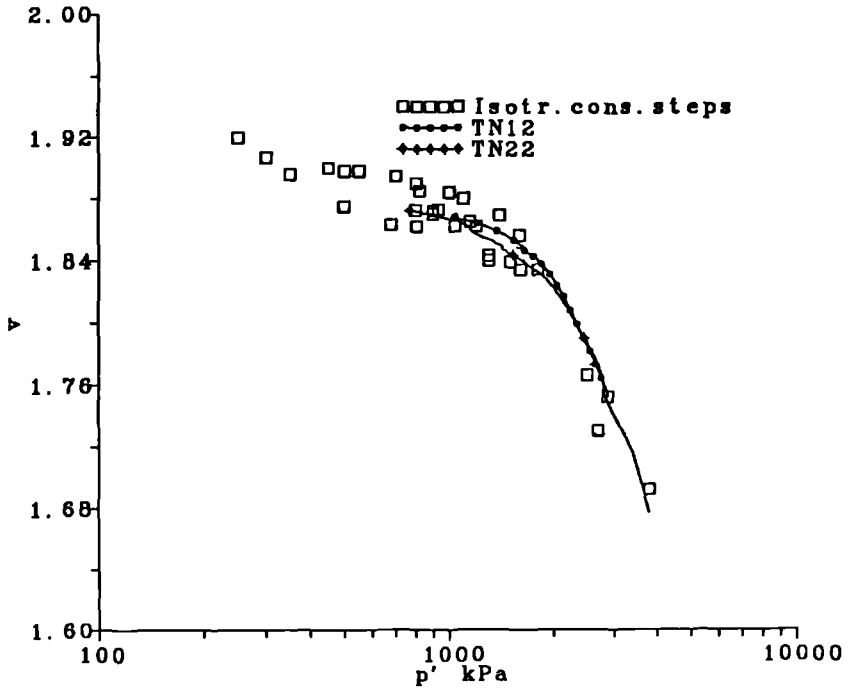

Fig.8.21. Undisturbed clay : isotropic compression and swelling states.

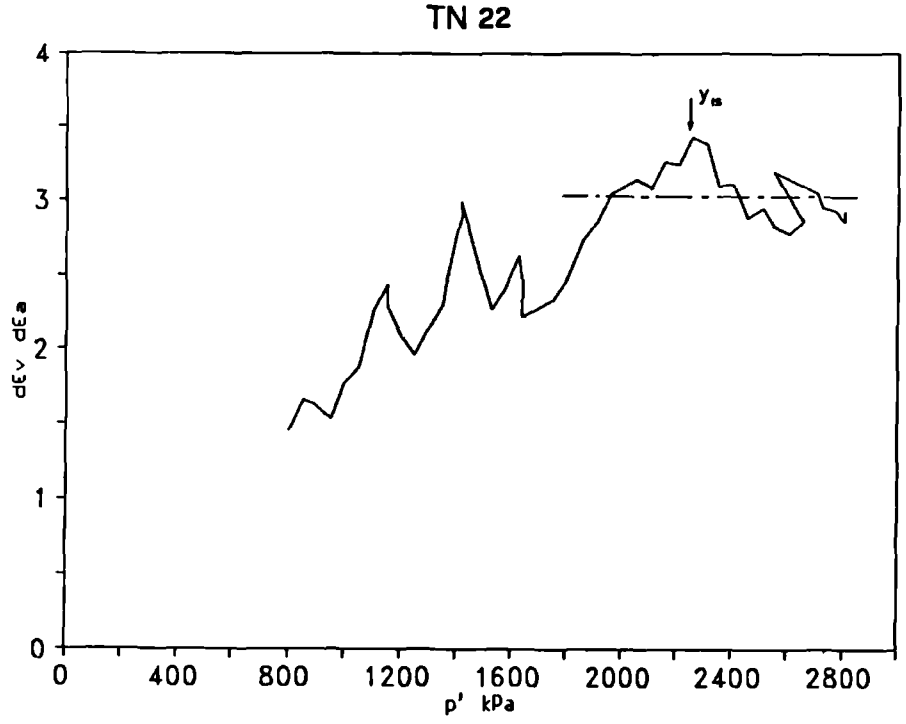

Fig.8.22. Undisturbed clay : strain ratios in isotropic compression.

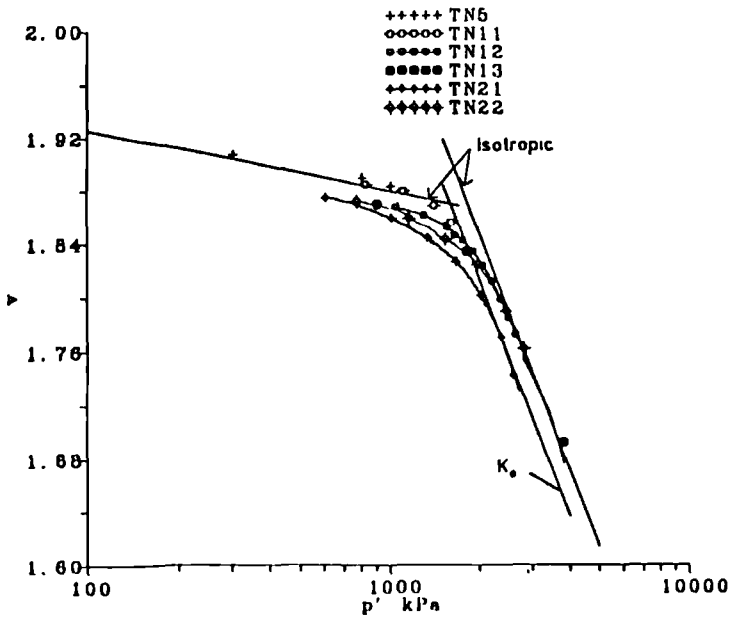

Fig.8.23. Undisturbed clay : isotropic and K_0 compression lines.

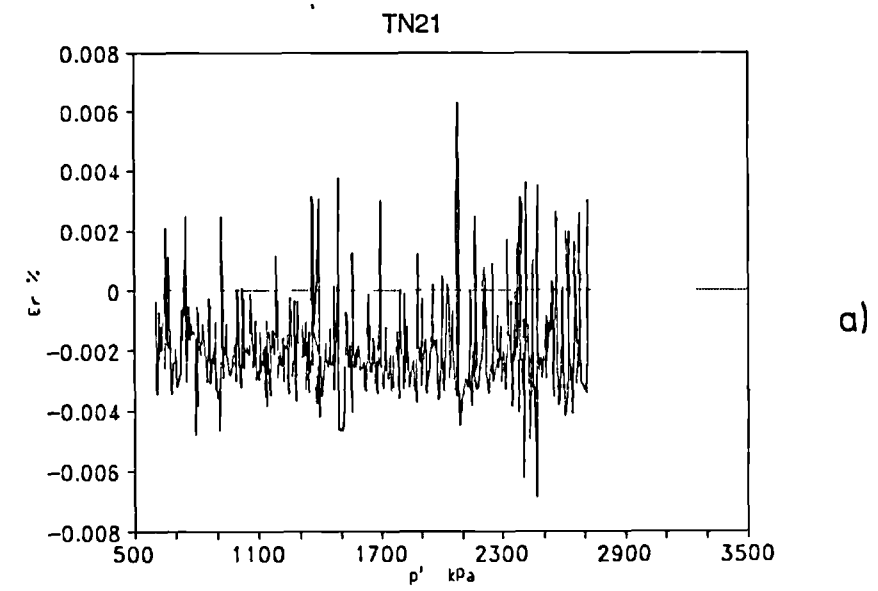

a)

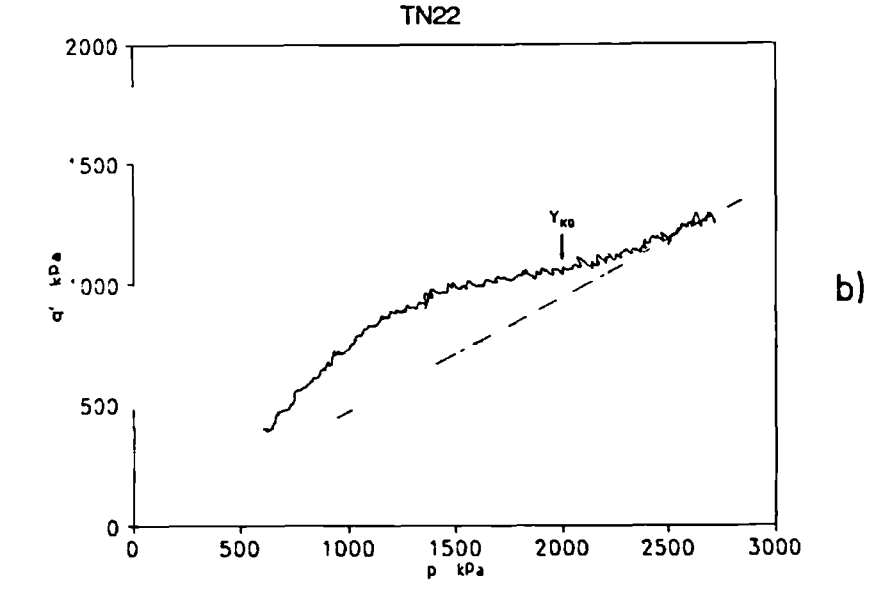

b)

Fig.8.24. K_0 compression of the undisturbed clay : (a) radial strains, (b) stress path.

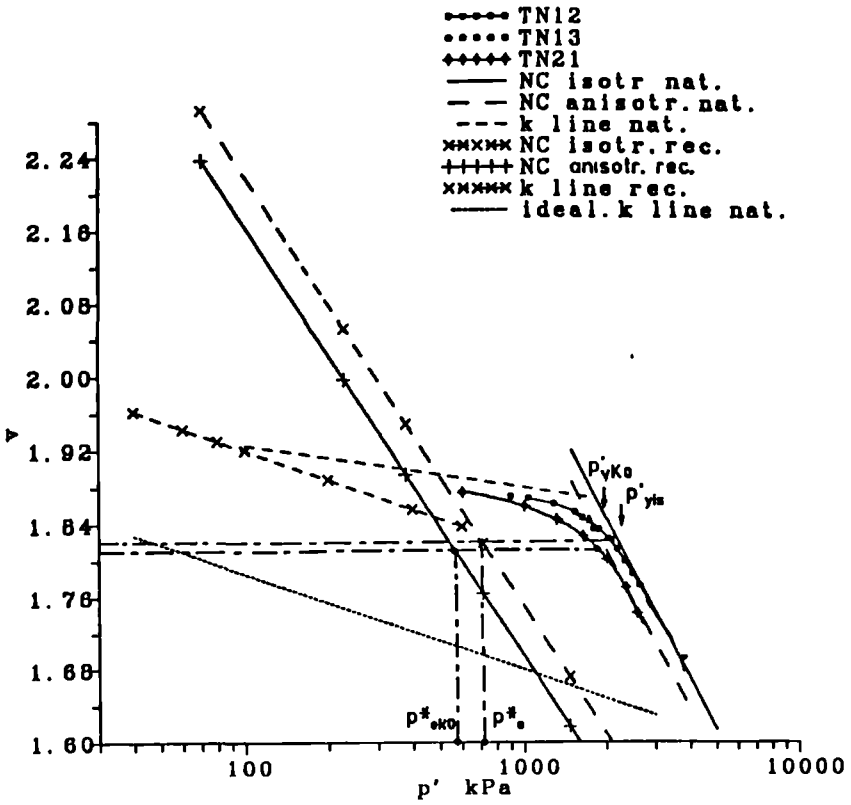

Fig.8.25. Natural and reconstituted Pappadai clay : isotropic and K_0 compression and swelling behaviour.

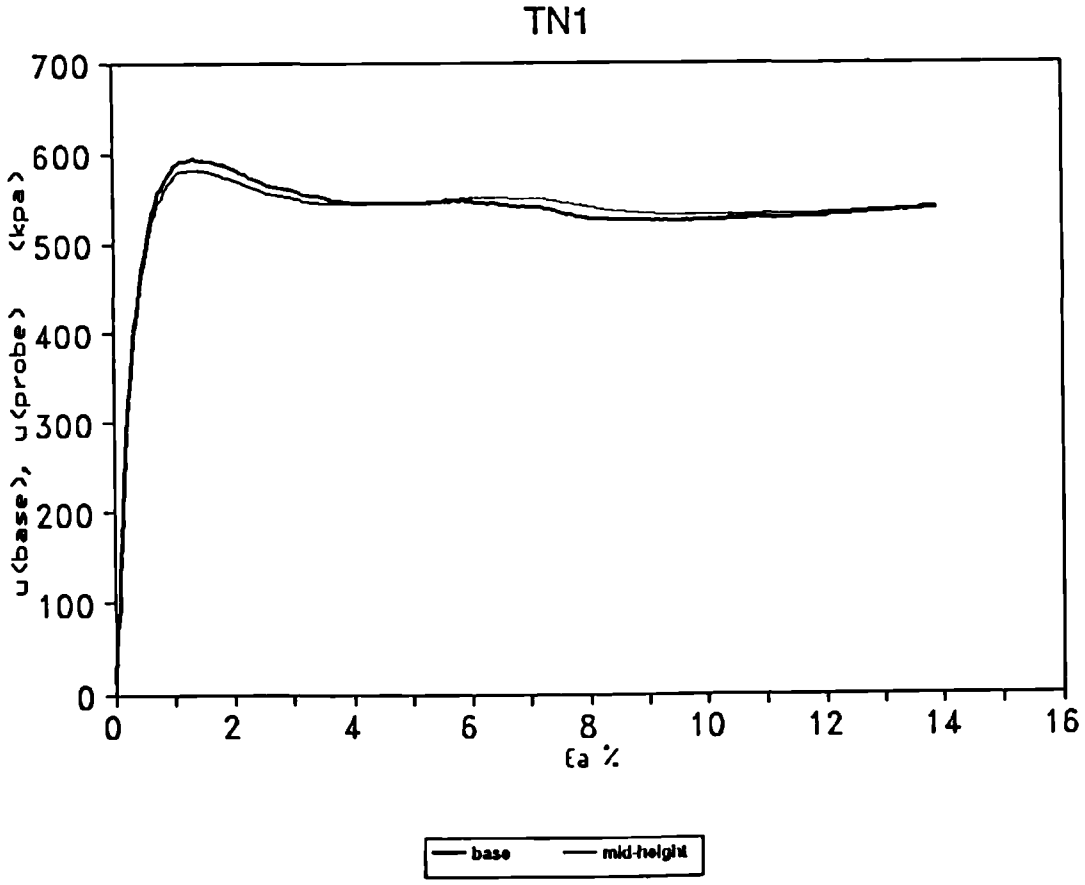

Fig.8.26. Undisturbed clay : typical differences between the measurements of pore water pressure at the base and at mid-height of the specimen.

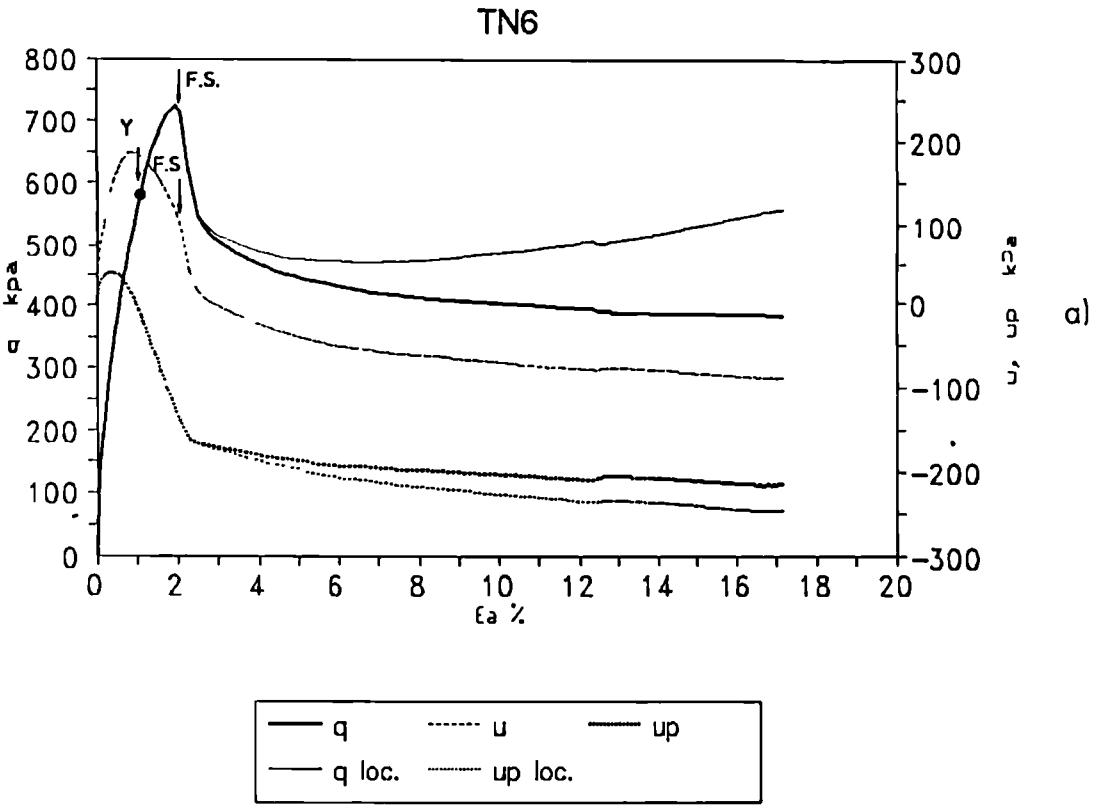

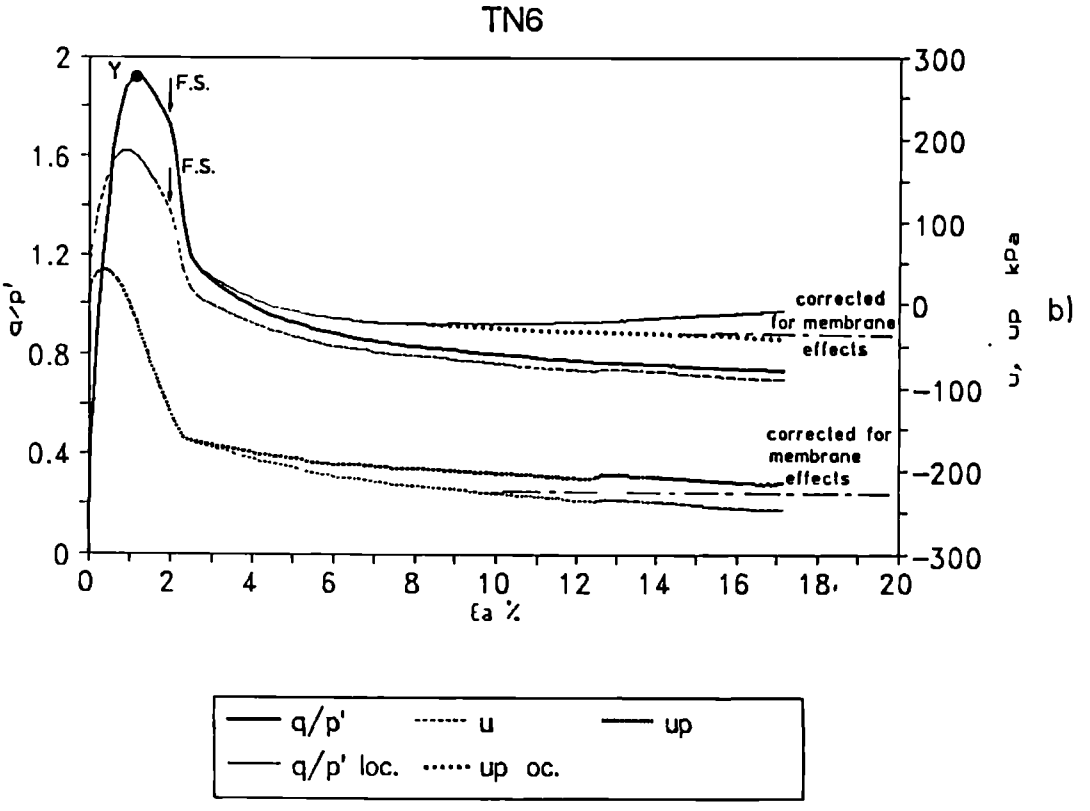

Fig.8.27. Undisturbed clay (YSRis=7.5) : undrained stress-strain behaviour before and after correction for localization (q_{loc} , $q/p'_{loc.}$, $u^{P}_{loc.}$).

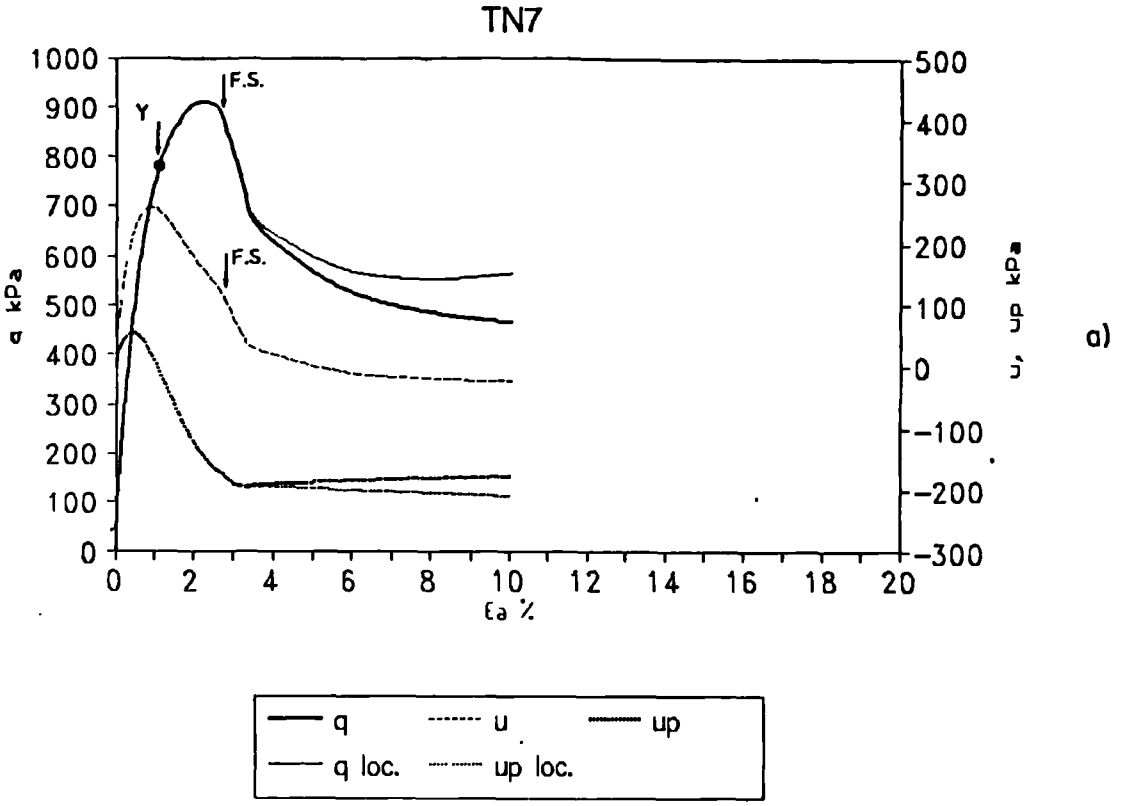

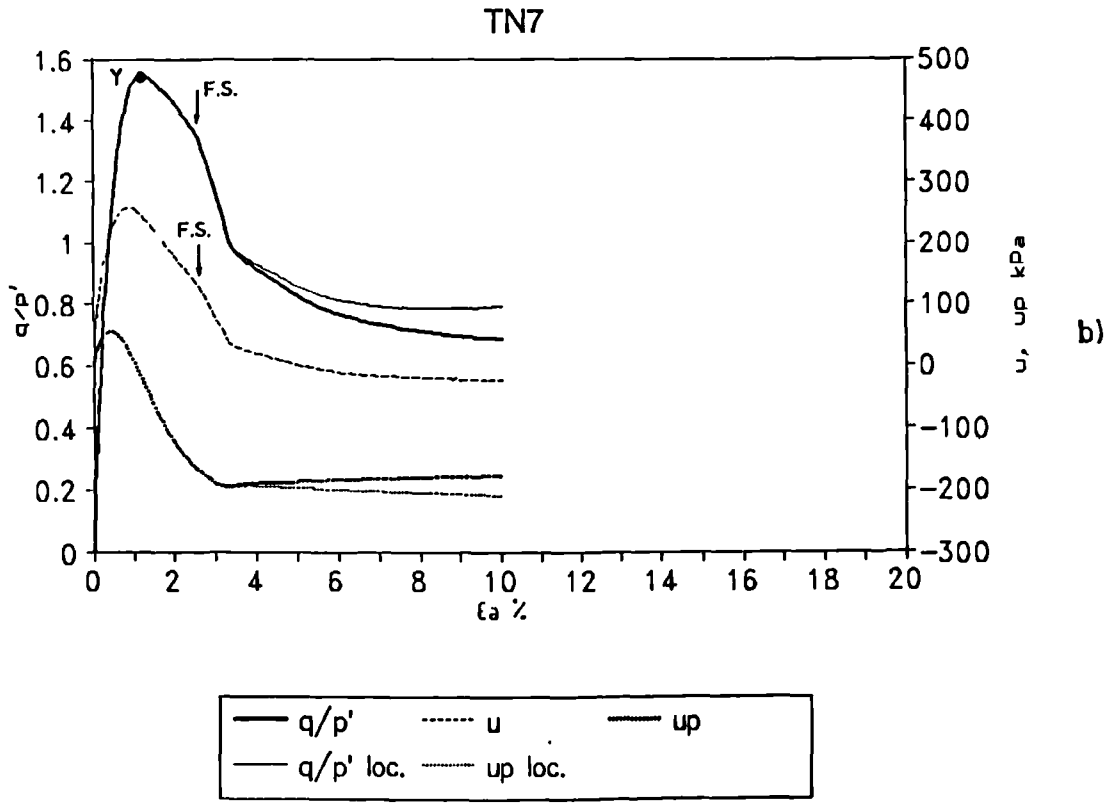

Fig.8.28. Undisturbed clay (YSRis=4.52) : undrained stress-strain behaviour before and after correction for localization ($q_{loc.}$, $q/p'_{loc.}$, $u^{p}_{loc.}$).

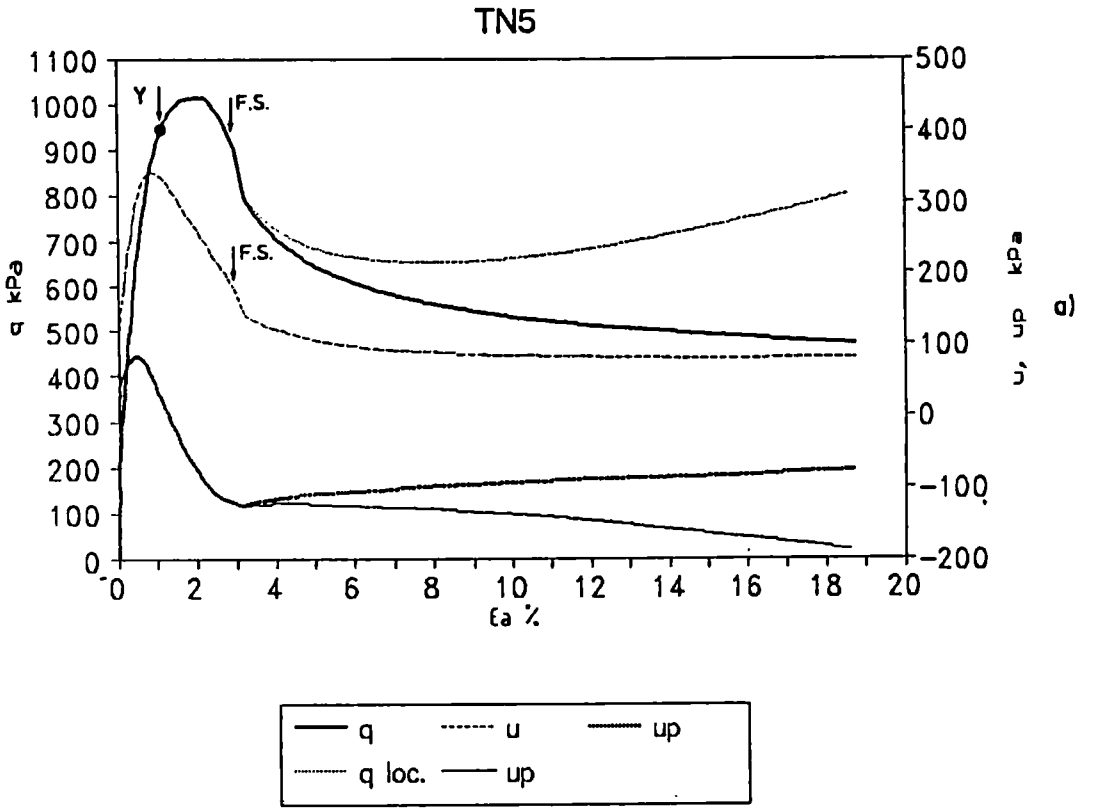

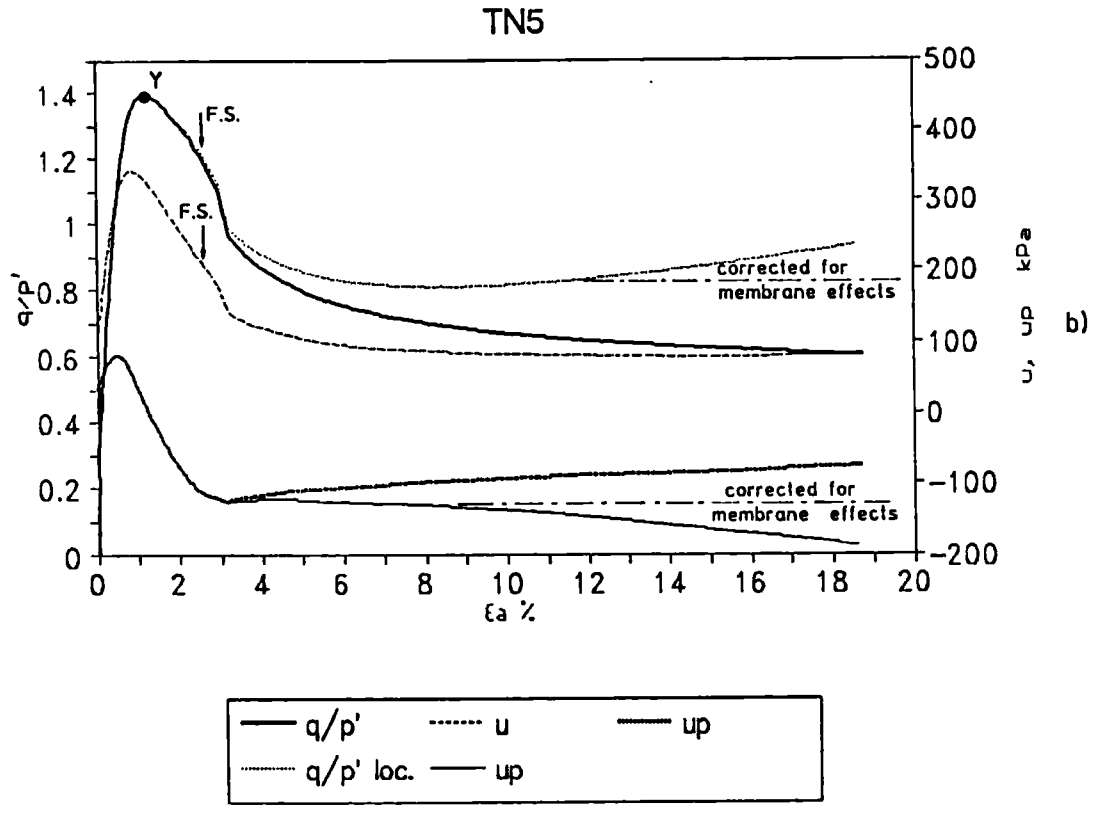

Fig.8.29. Undisturbed clay (YSRis=3.22) : undrained stress-strain behaviour before and after correction for localization ($q_{loc.}$, $q/p'_{loc.}$, $u^{p}_{loc.}$).

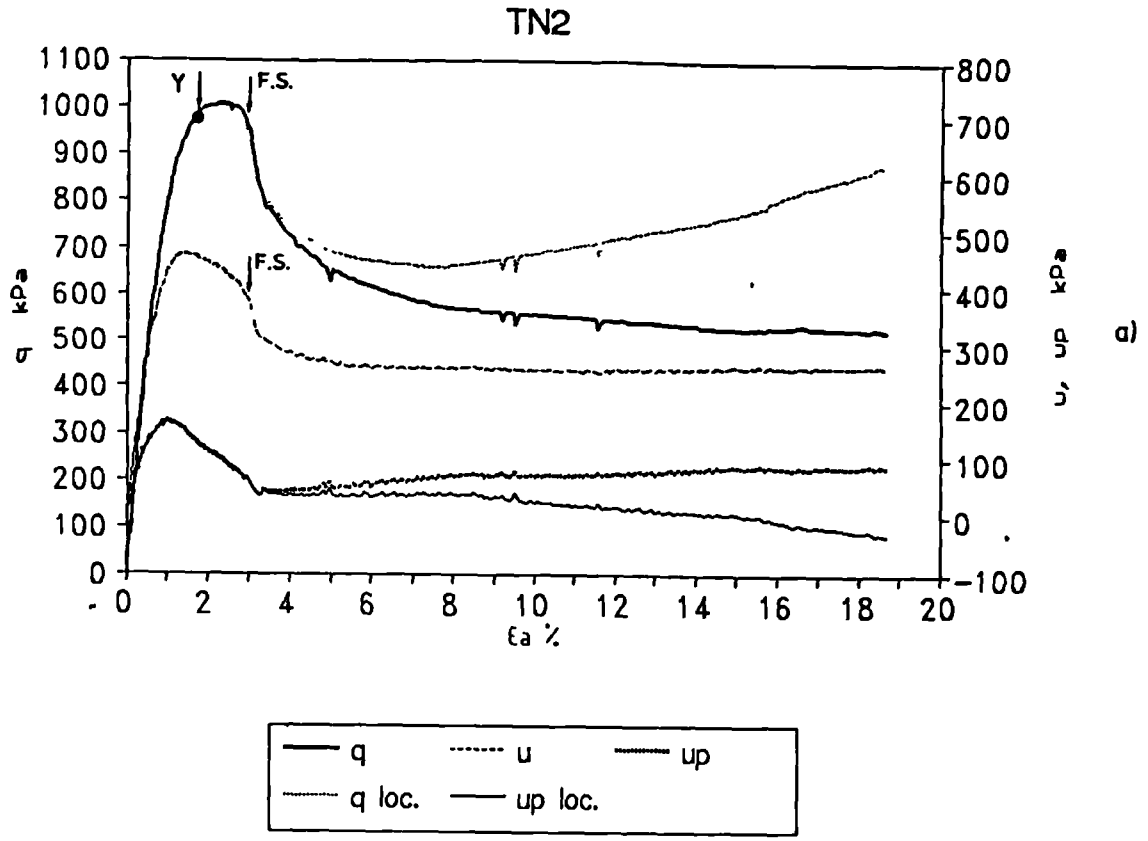

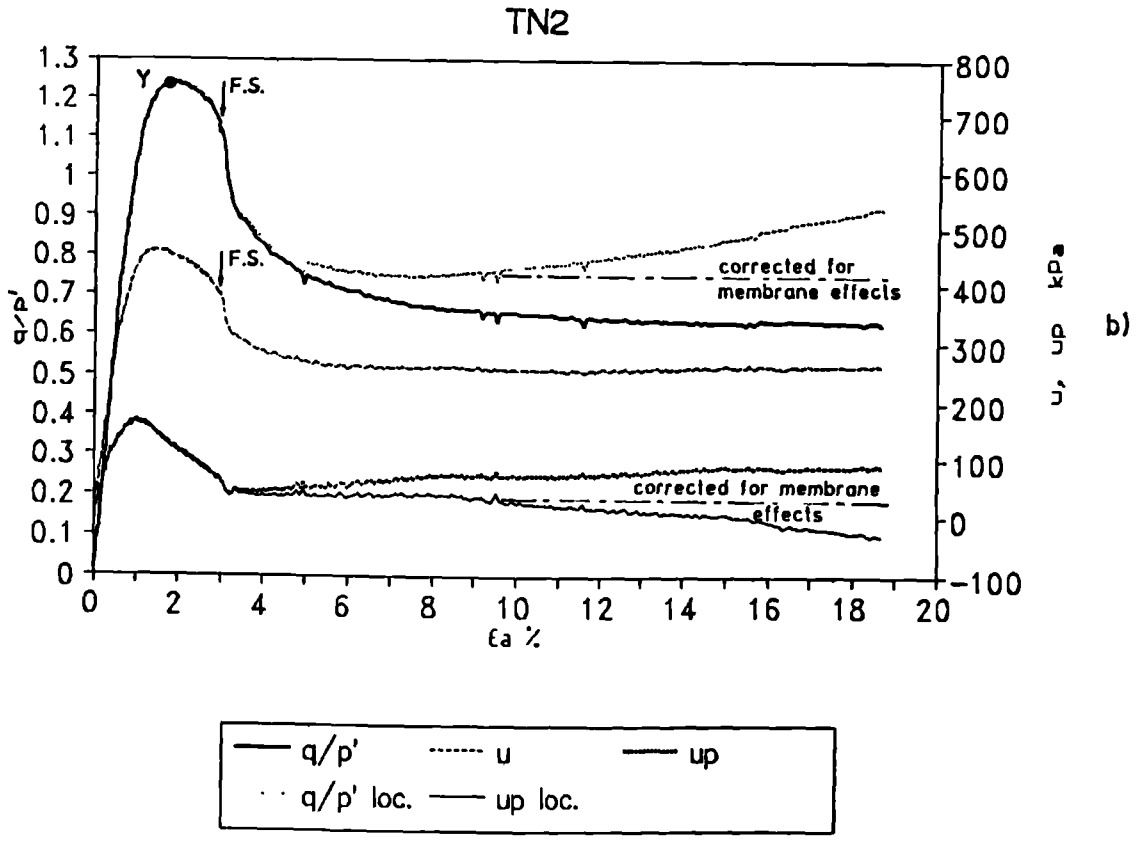

Fig.8.30. Undisturbed clay (YSRis=2.42) : undrained stress-strain behaviour before and after correction for localization ($q_{loc.}$, $q/p'_{loc.}$, $u^p_{loc.}$).

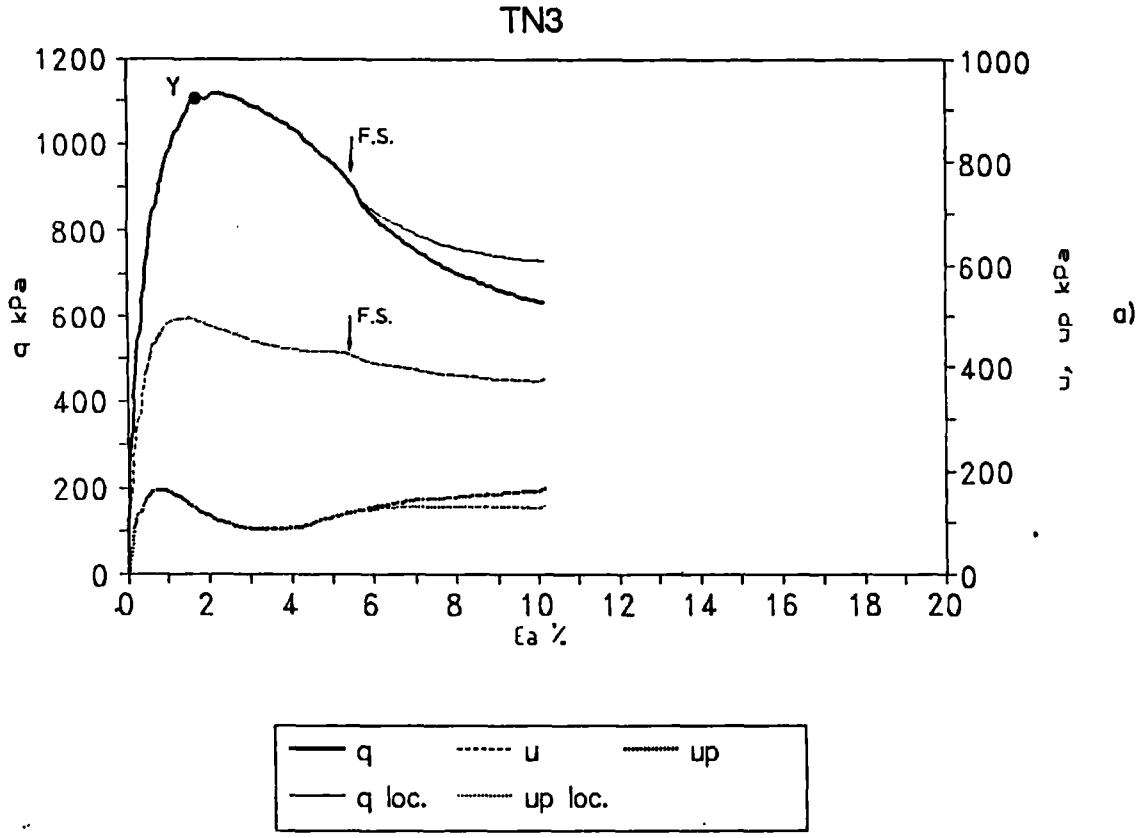

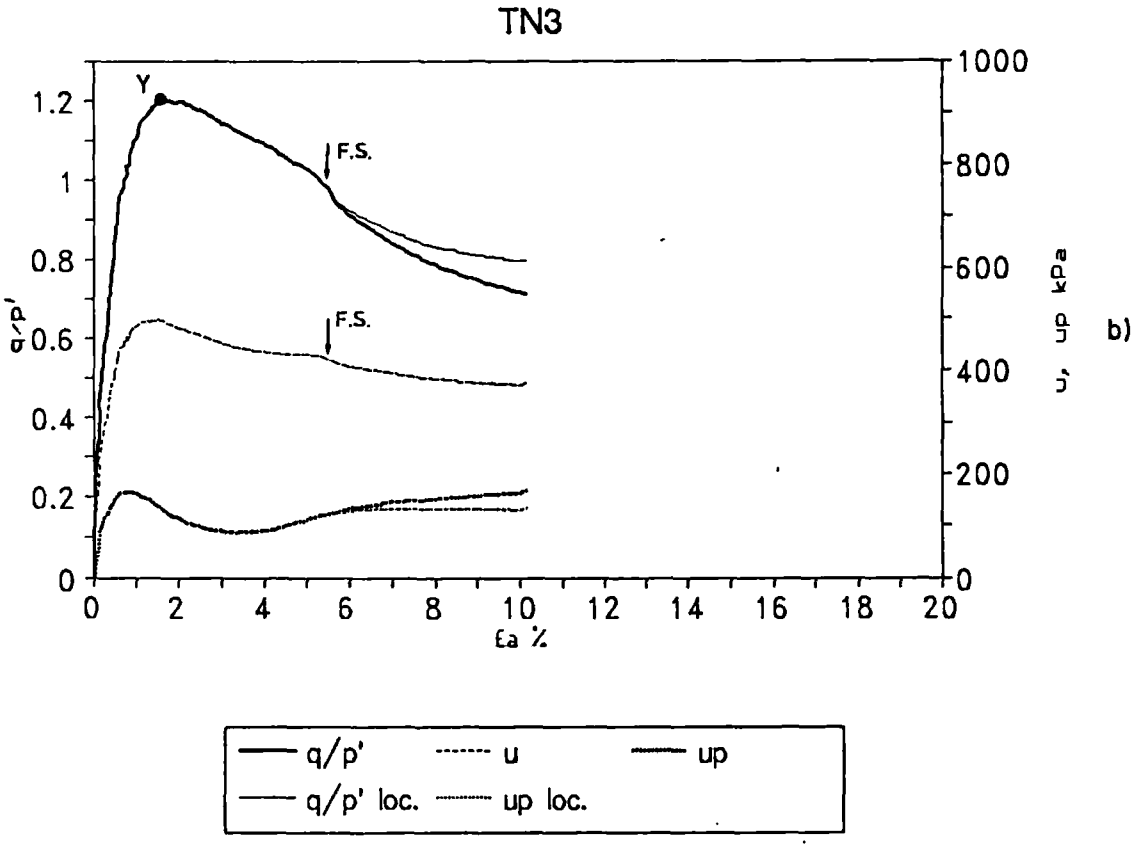

Fig.8.31. Undisturbed clay (YSRis=2.167) : undrained stress-strain behaviour before and after correction for localization ($q_{loc.}$, $q/p'_{loc.}$, $u^{p}_{loc.}$).

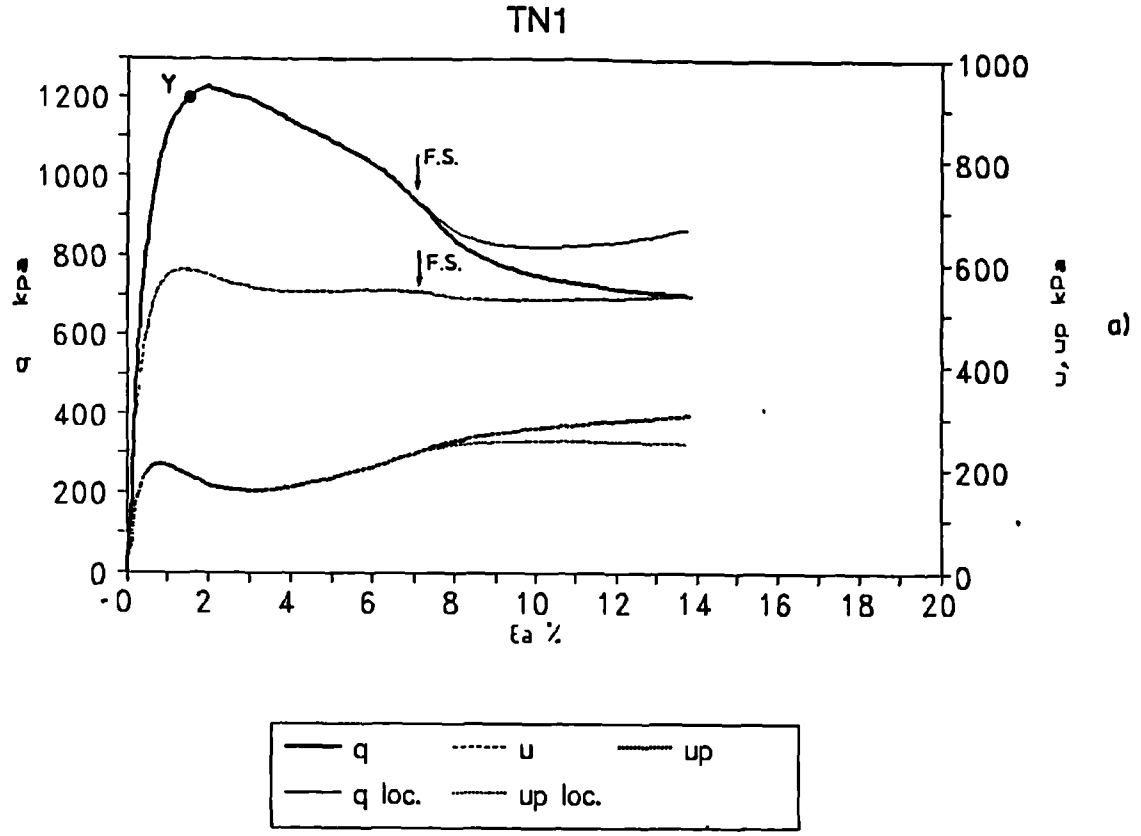

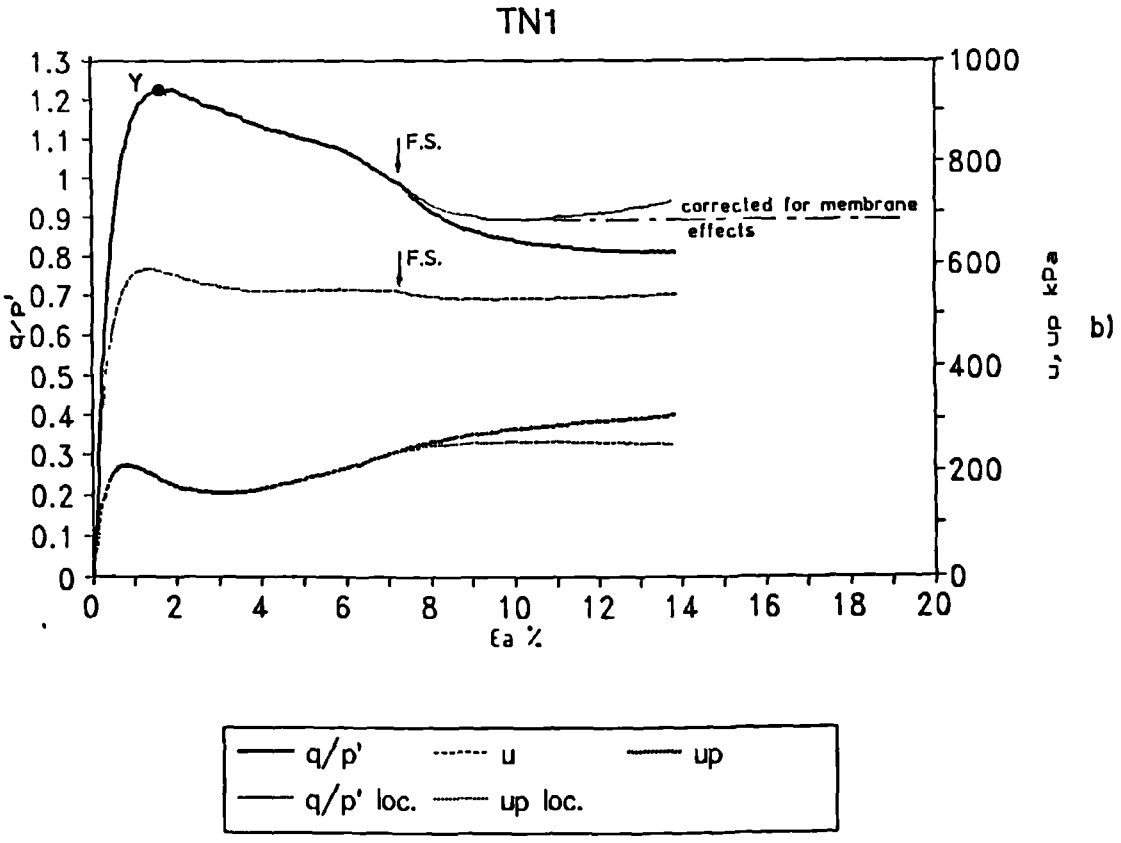

Fig.8.32. Undisturbed clay (YSRis=1.95) : undrained stress-strain behaviour before and after correction for localization ($q_{loc.}$, $q/p'_{loc.}$, $u^{p}_{loc.}$).

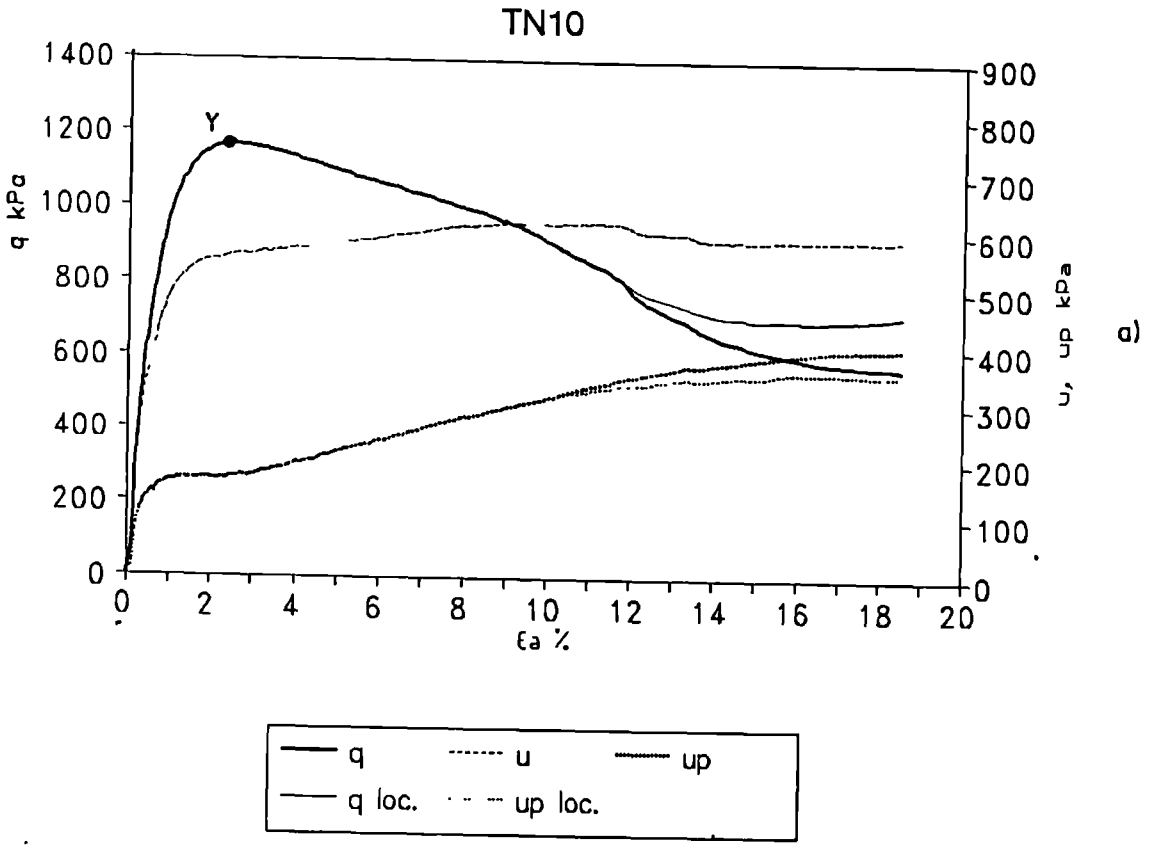

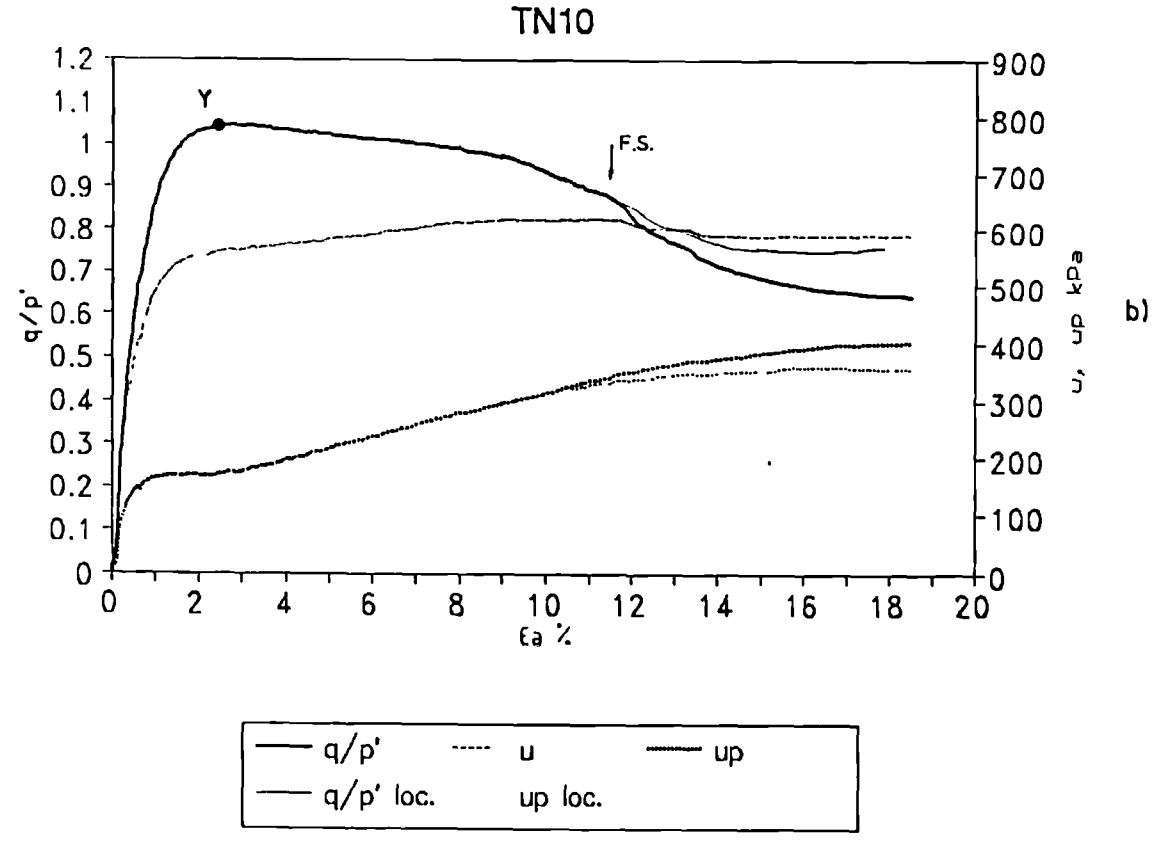

Fig.8.33. Undisturbed clay (YSRis=1.74) : undrained stress-strain behaviour before and after correction for localization $q_{loc.}$, $q/p'_{loc.}$, u^{p}_{loc})

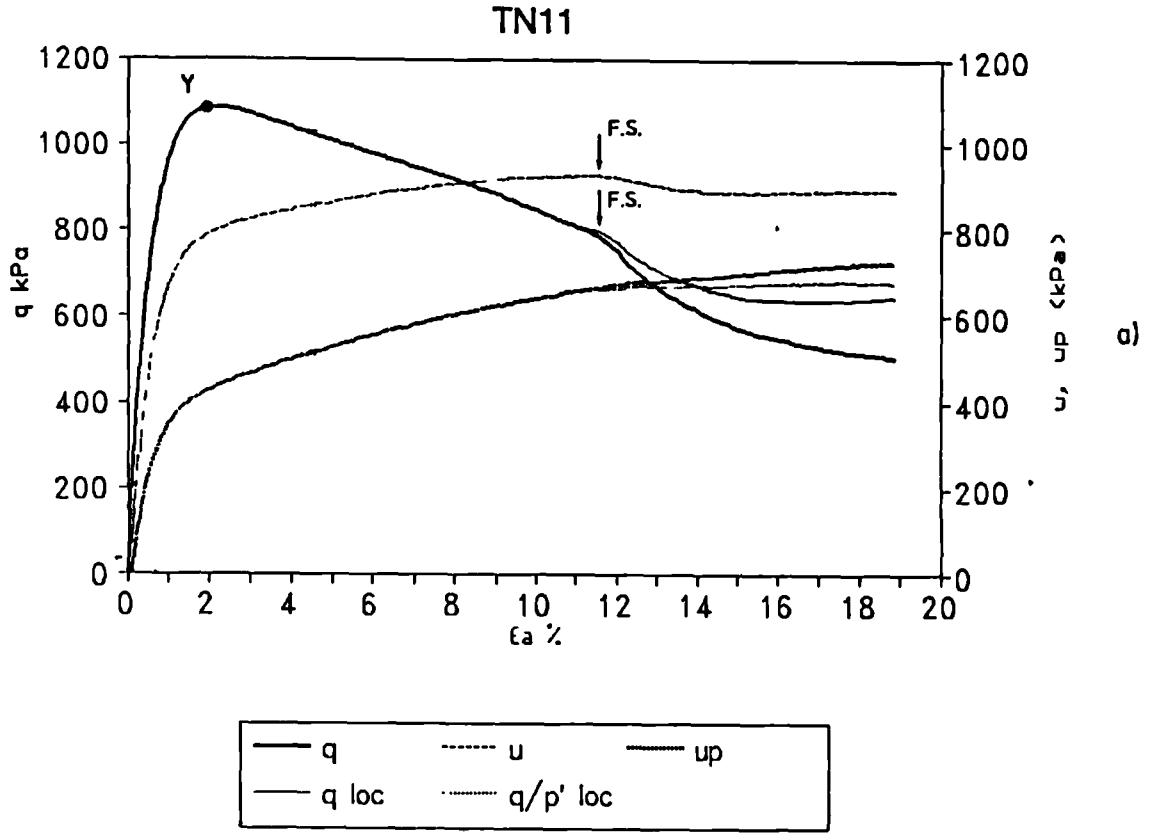

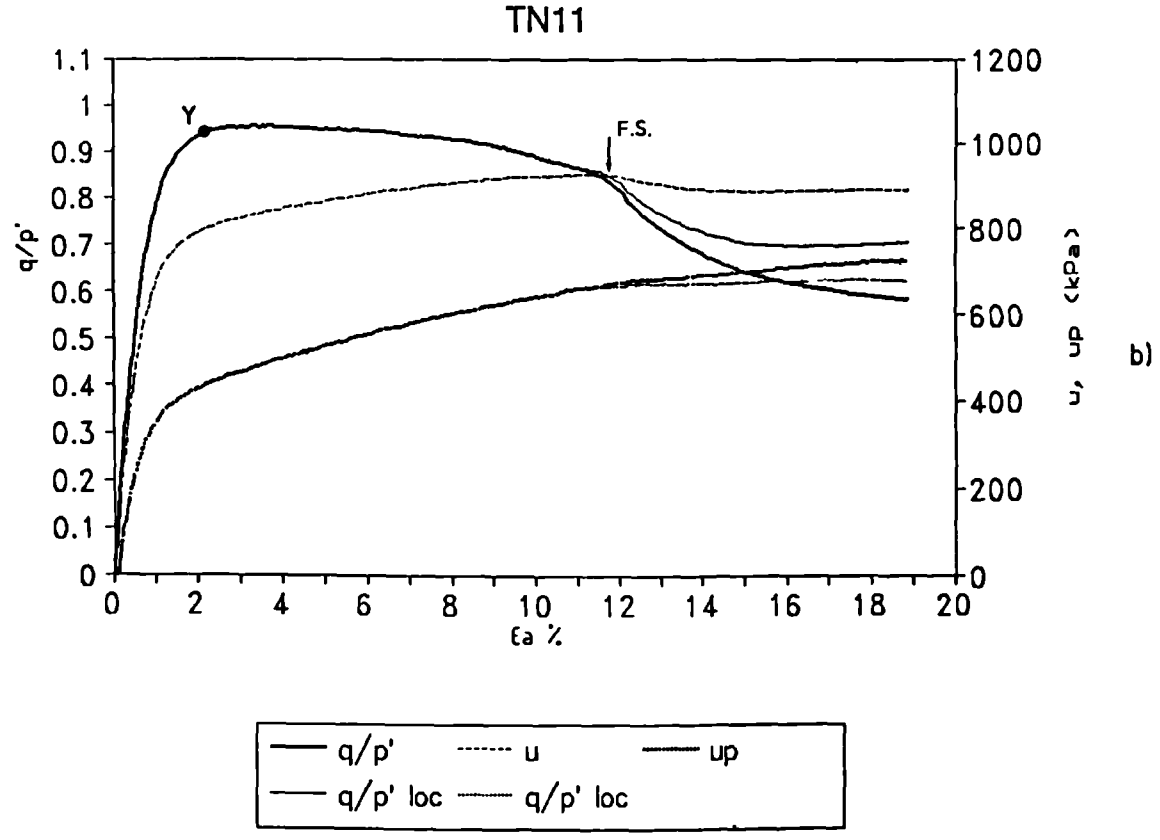

Fig.8.34. Undisturbed clay (YSRis=1.4) : undrained stress-strain behaviour before and after correction for localization ($q_{loc.}$, $q/p'_{loc.}$, $u^{p}_{loc.}$).

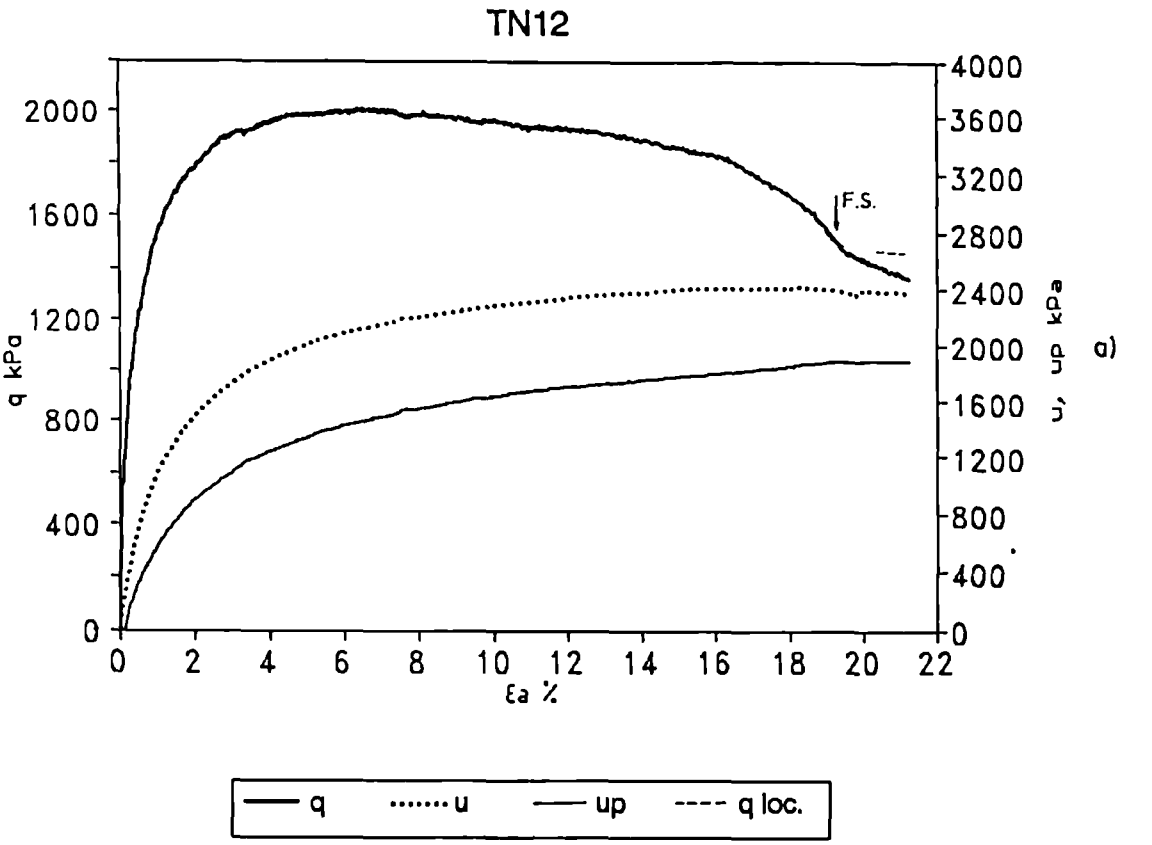

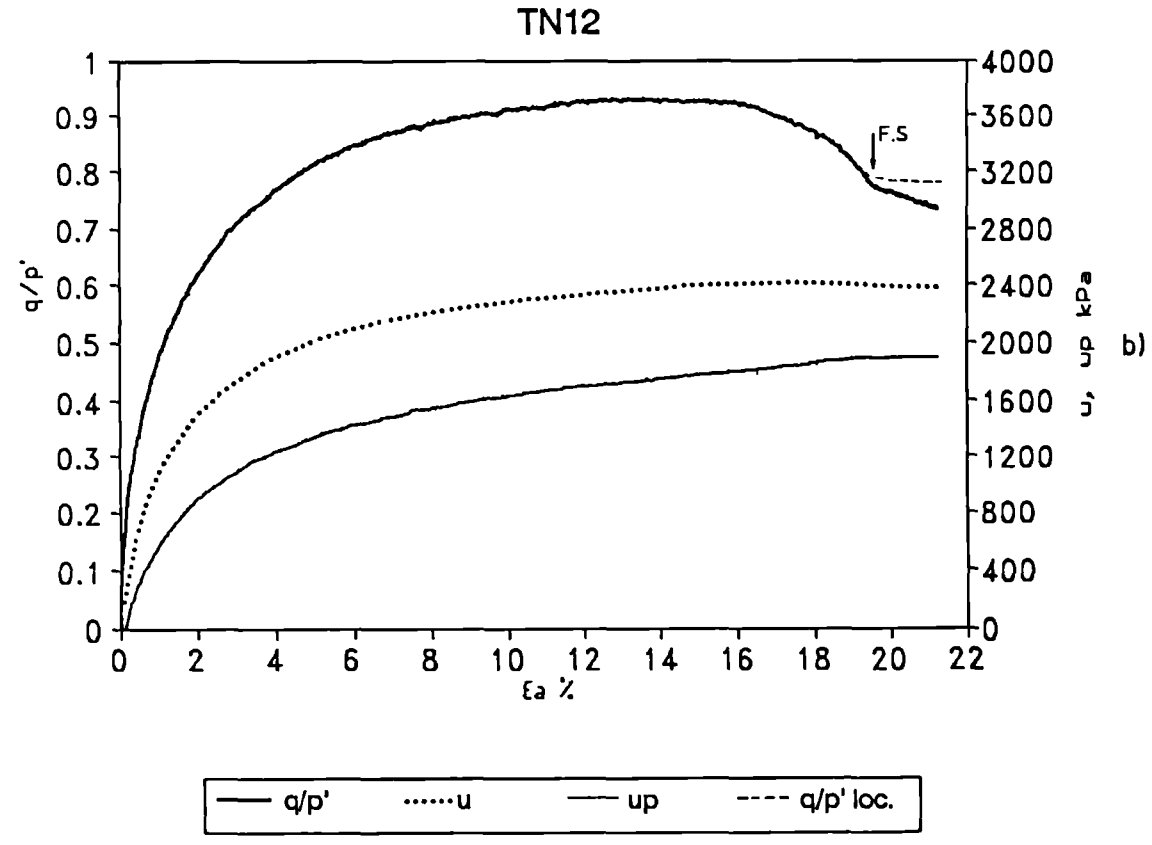

Fig.8.35. Undisturbed clay compressed beyond isotropic yield : undrained stress-strain behaviour before and after correction for localization ($q_{loc.}$, q/p'_{loc}).

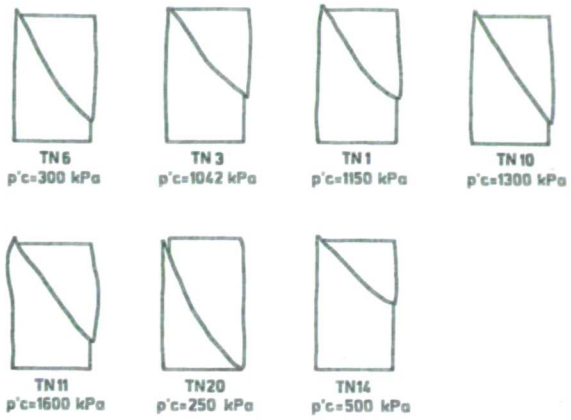

Fig.8.36. Shape of undisturbed clay specimens after shearing to large strains.

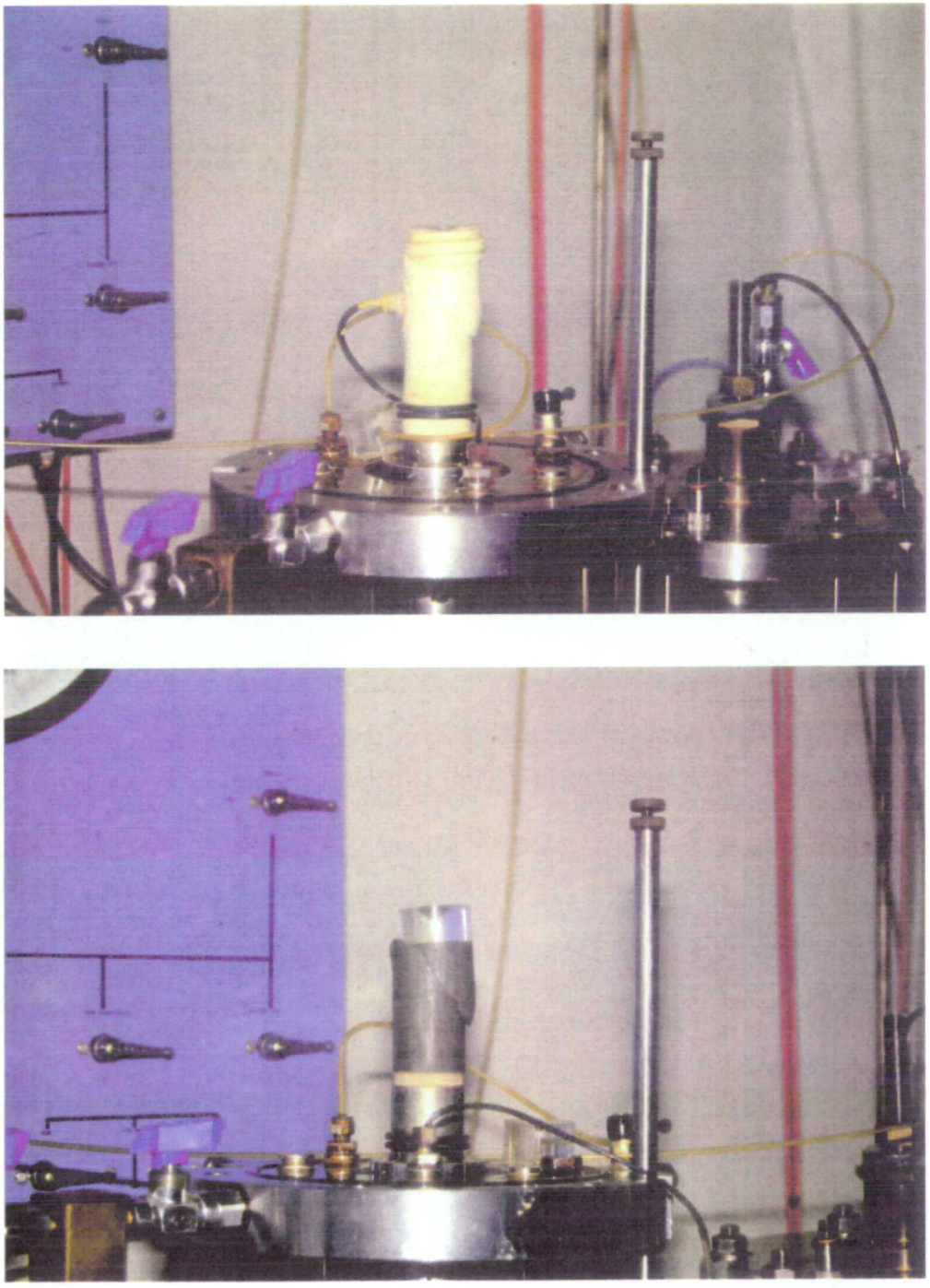

Fig.8.37. Undisturbed clay after undrained shearing to large strains : specimen TN2.

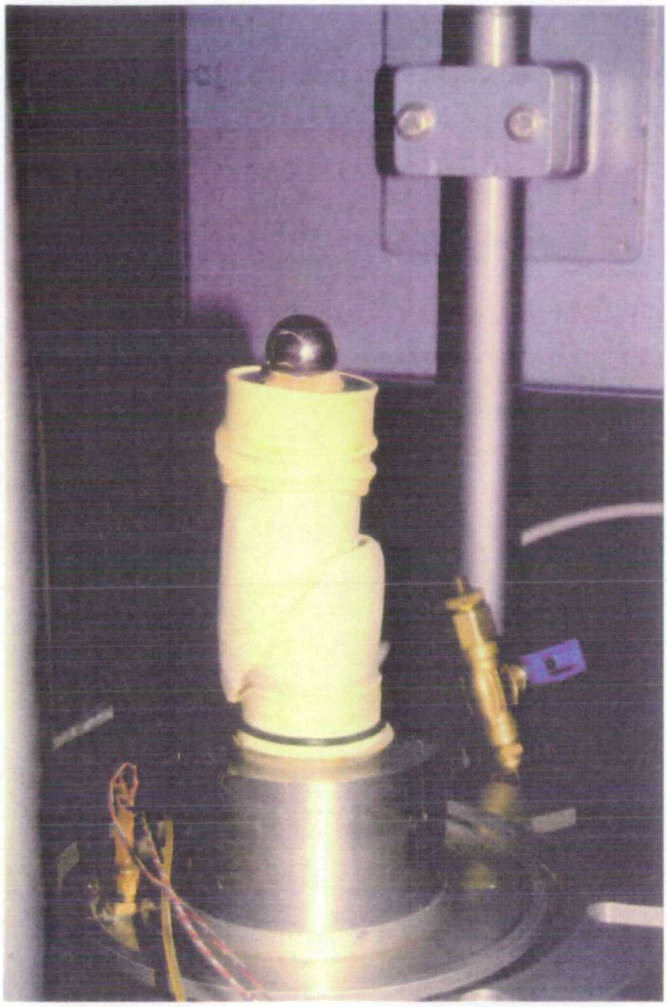

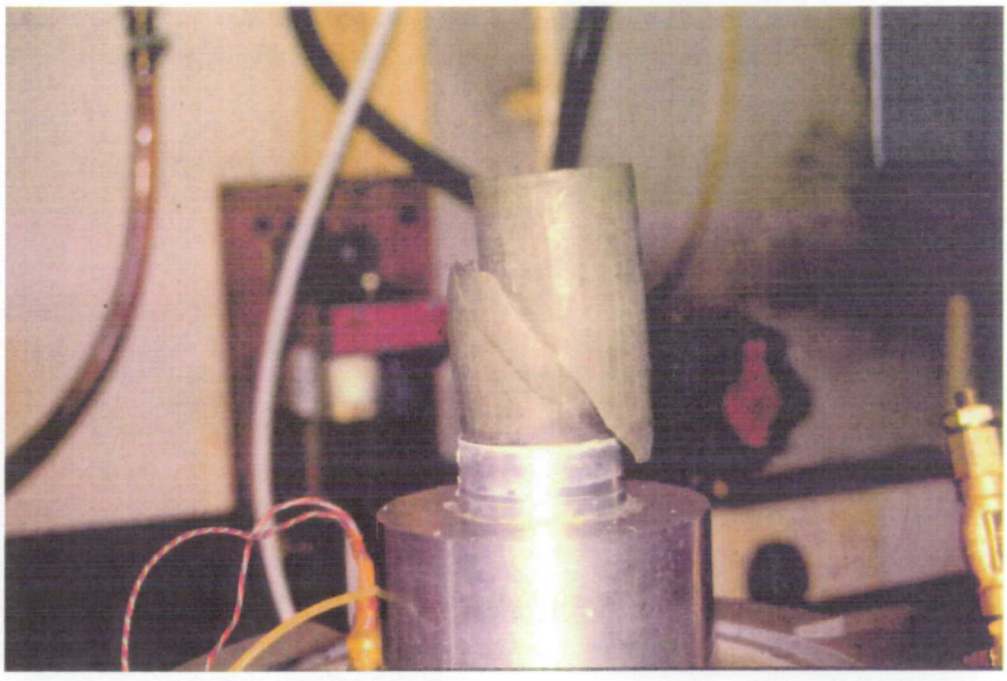

Fig.8.38. Undisturbed clay after undrained shearing to large strains : specimen TN1.

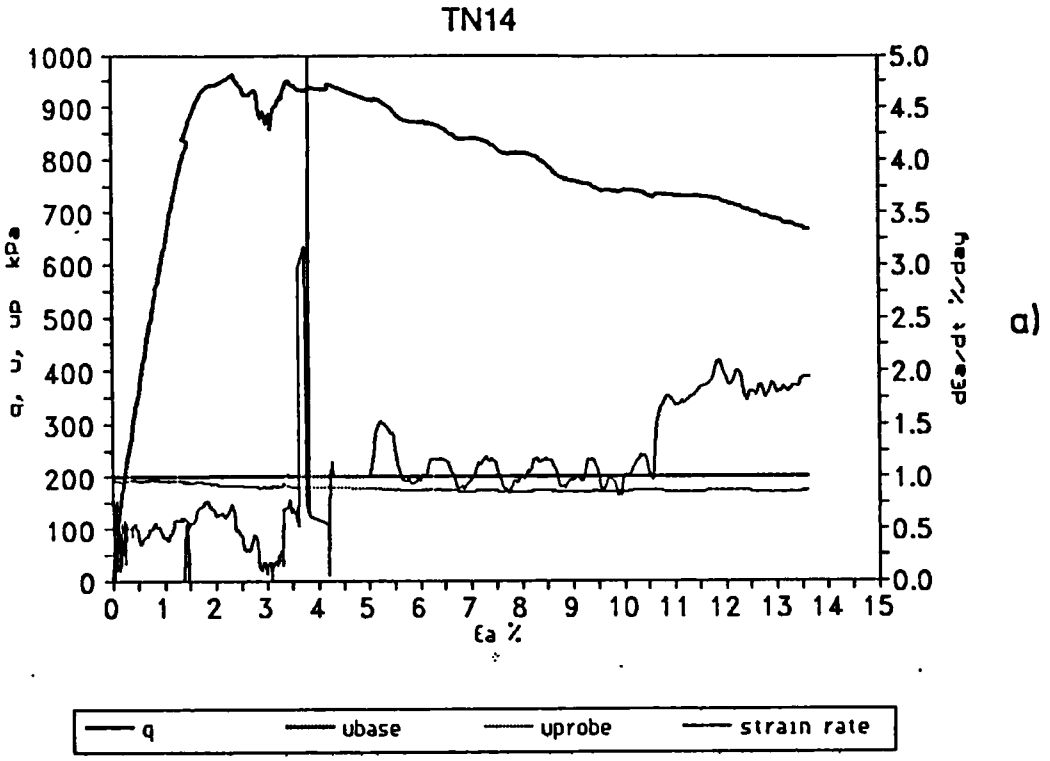

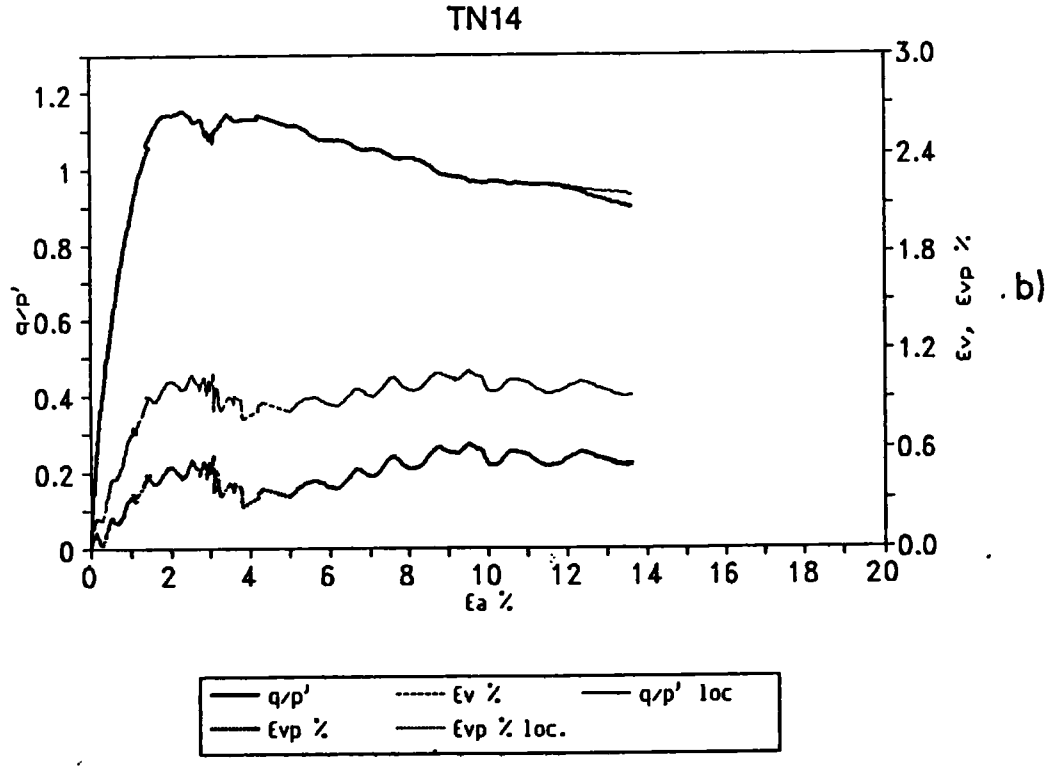

Fig.8.39. Undisturbed clay (YSRis=4.52) : drained stress-strain behaviour and strain rates.

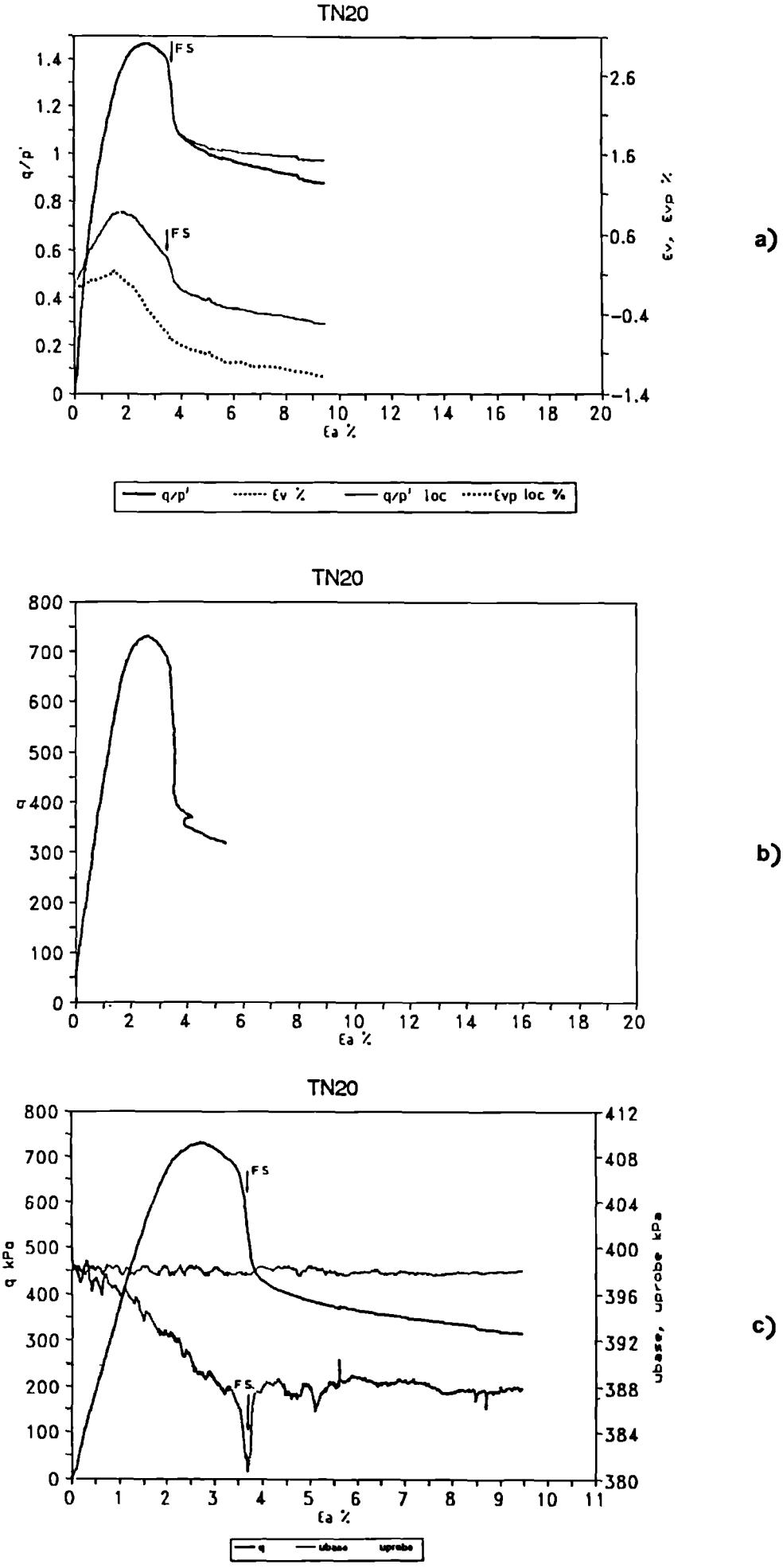

Fig.8.40. Undisturbed clay (YSR_{is}=9.04) : (a) drained stress-strain behaviour before and after correction for localization (q/p'_{loc}, $\varepsilon_v^{\sim}{}_{loc}$); (b) stress strain curve accord g to the local strain measurements; (c) local dilation at the formation of the failure surface.

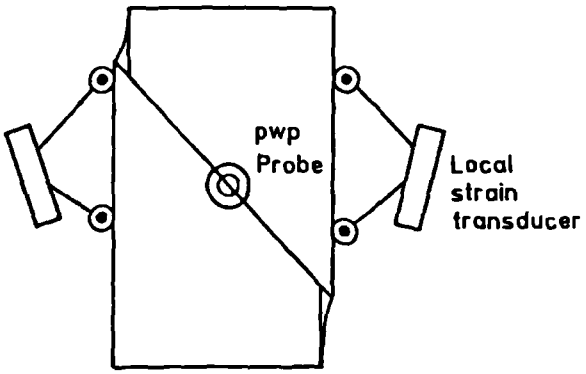

Fig.8.41. TN20 specimen : location of both the local strain transducers and the mid-height probe after the failure surface formation.

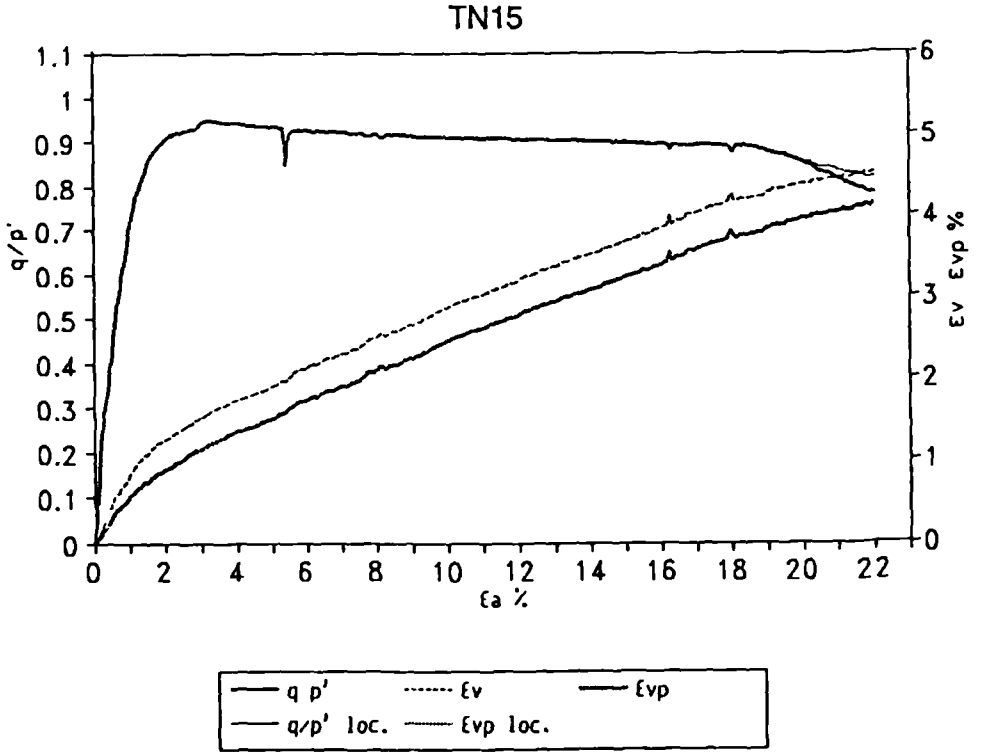

Fig.8.42. Undisturbed clay (YSR_{is}=2.825) : drained stress-strain behaviour before and after correction for localization ($q/p'_{loc.}$, $\varepsilon_v{}^p{}_{loc.}$).

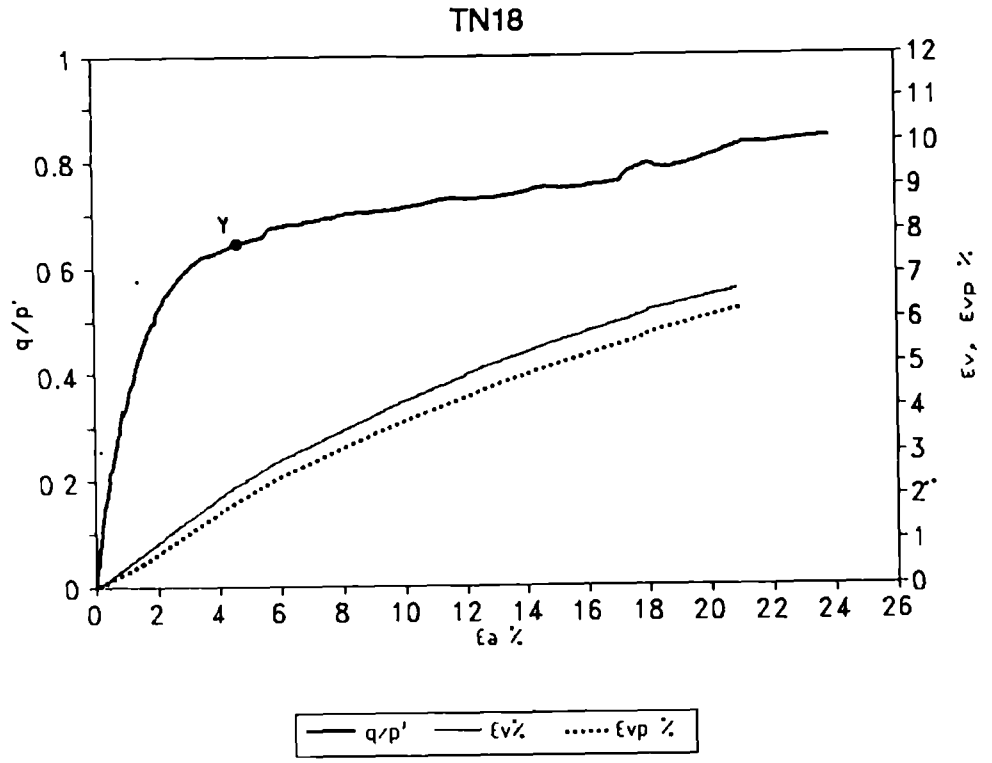

Fig.8.43. Undisturbed clay (YSRis=1.5) : drained stress-strain behaviour.

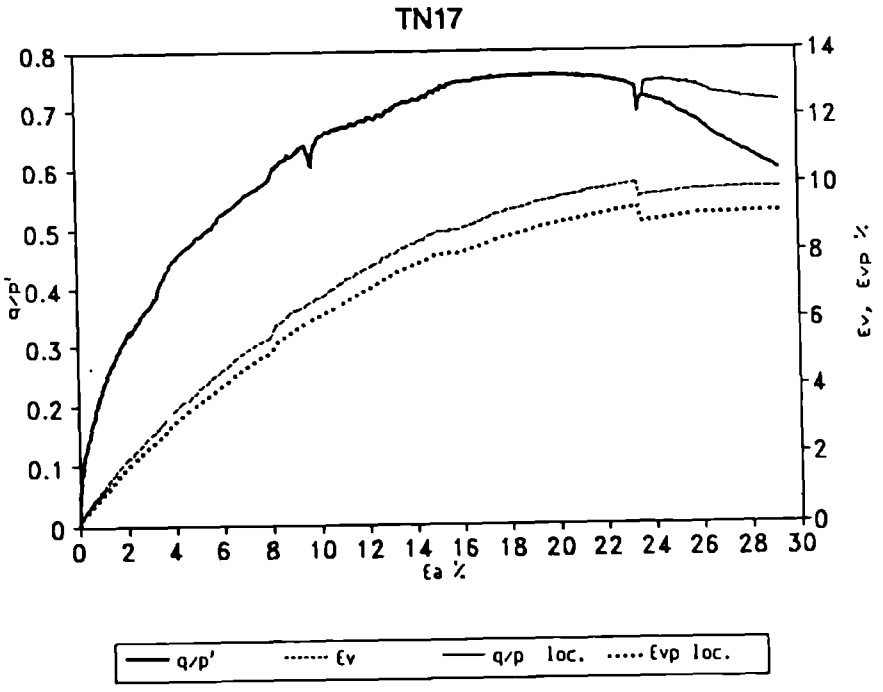

Fig.8.44. Undisturbed clay compressed beyond isotropic yield : drained stress-strain behaviour.

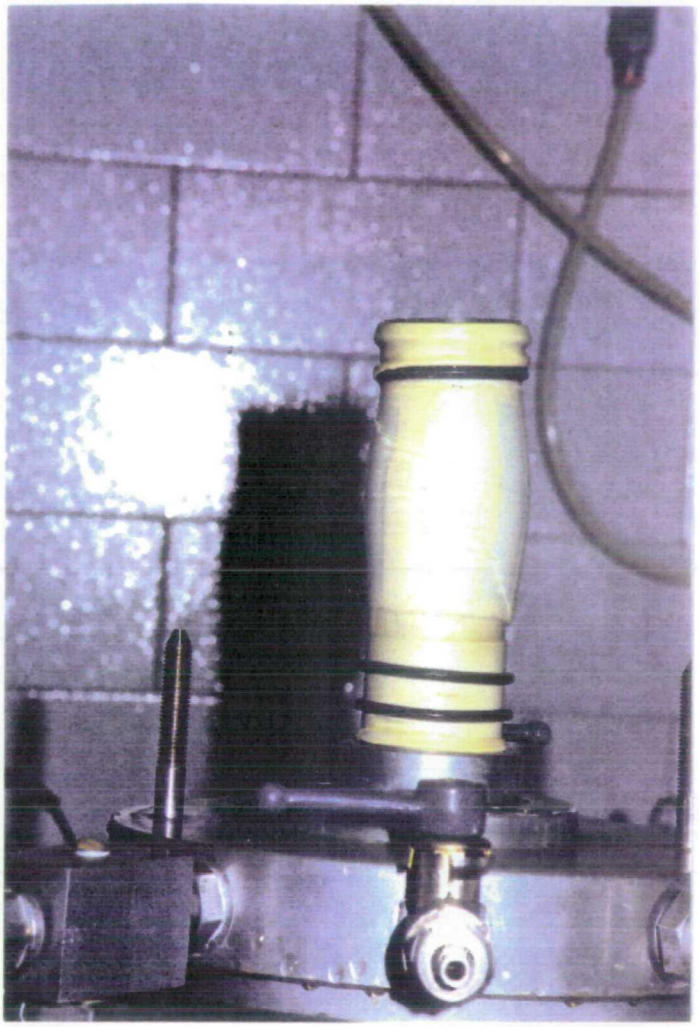

a)

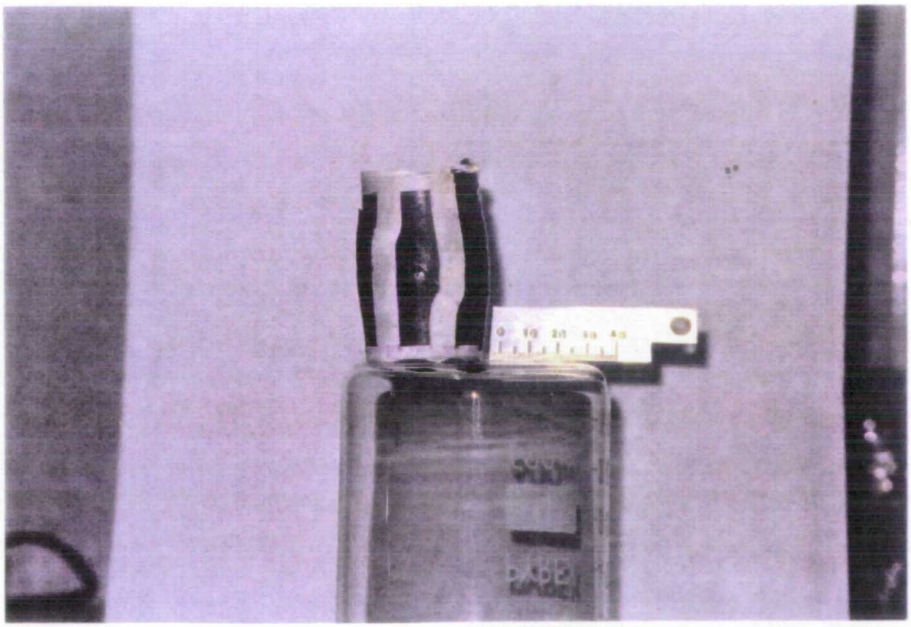

b)

Fig.8.45. Undisturbed clay after drained shearing to large strains : specimen TN15.

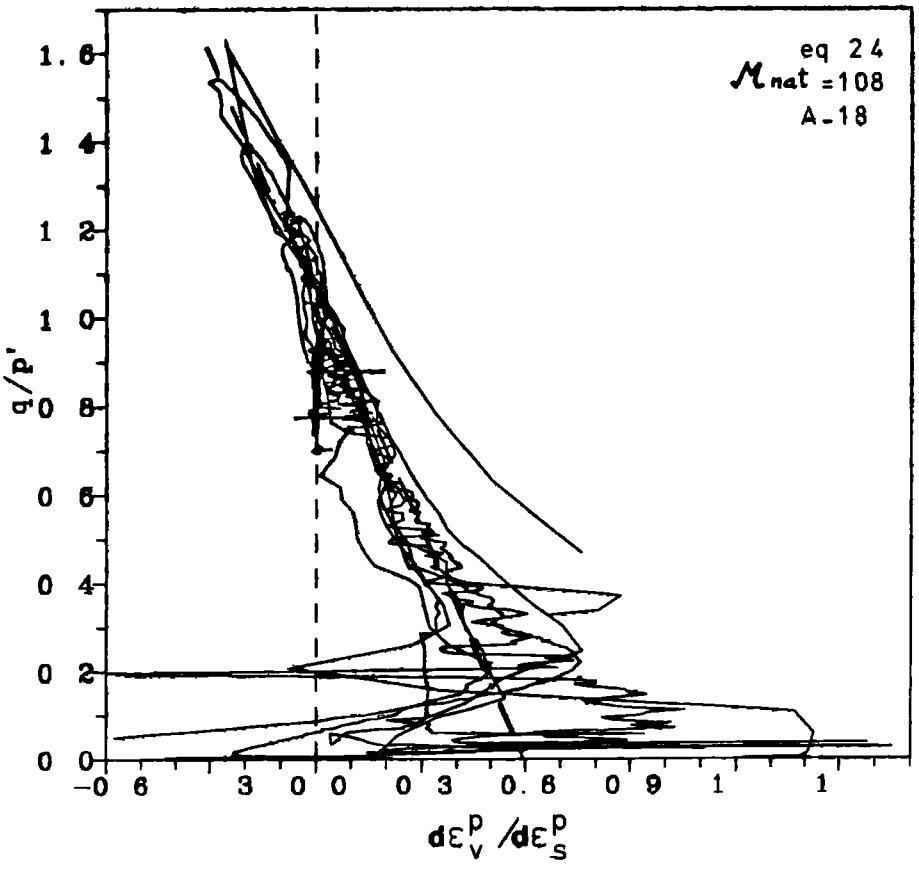

Fig 8 46 Flow rule of the undisturbed clay in undrained shear

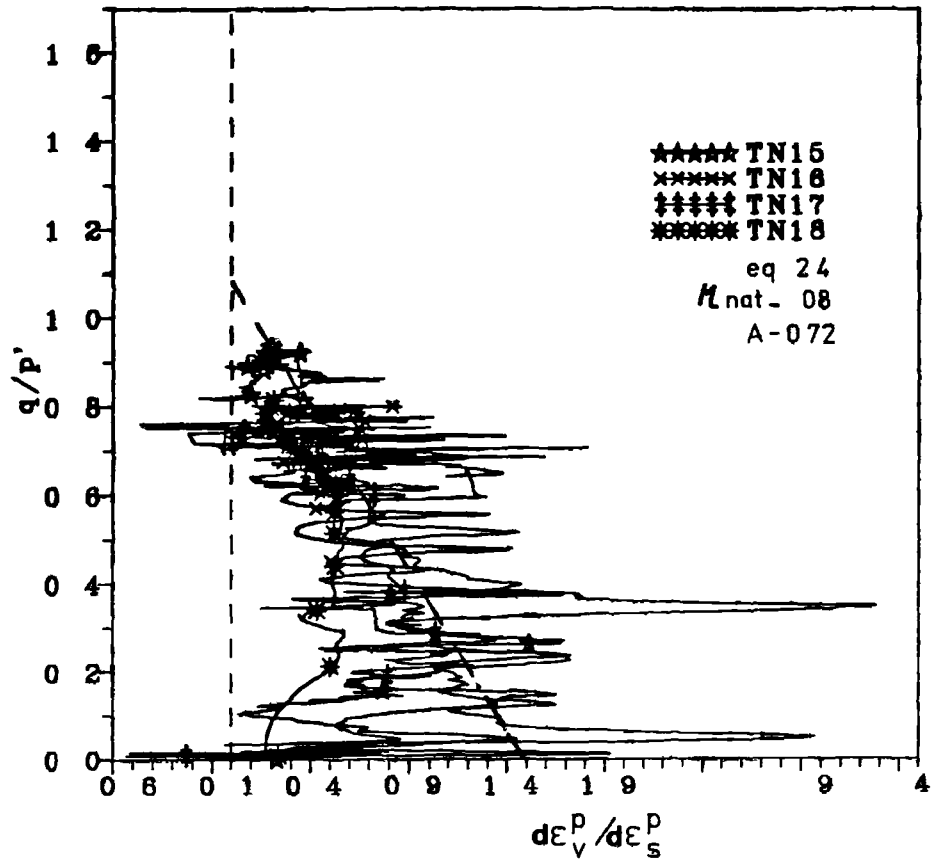

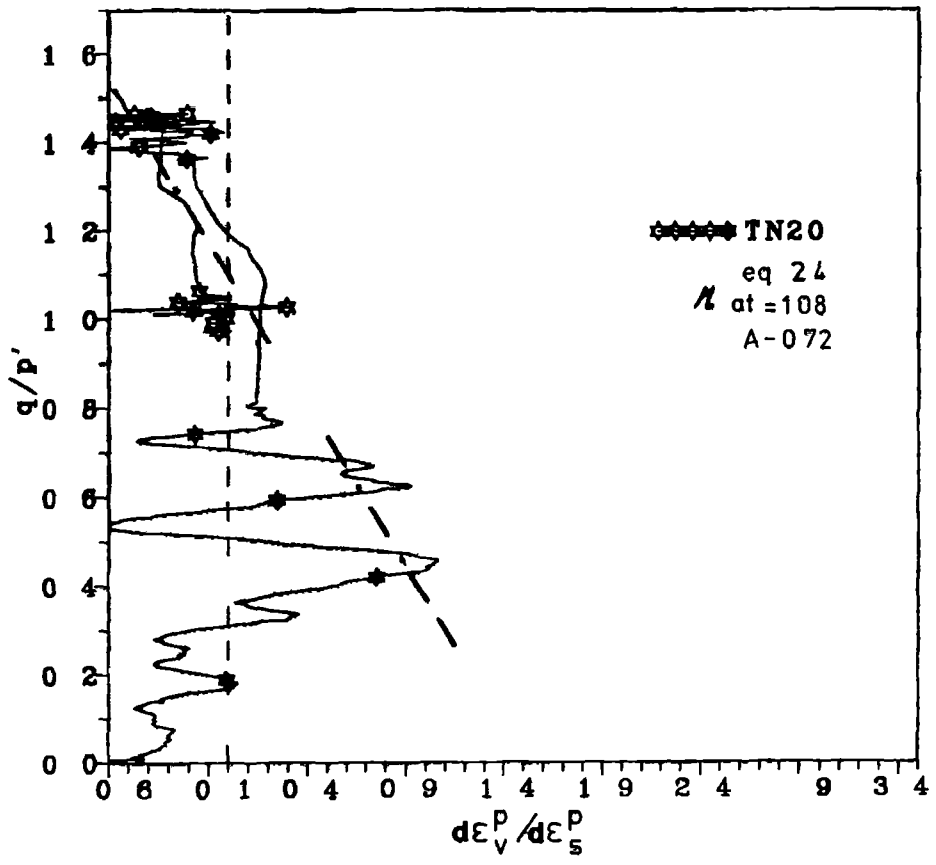

Fig 8 47 Flow rule of the undisturbed clay in drained shear

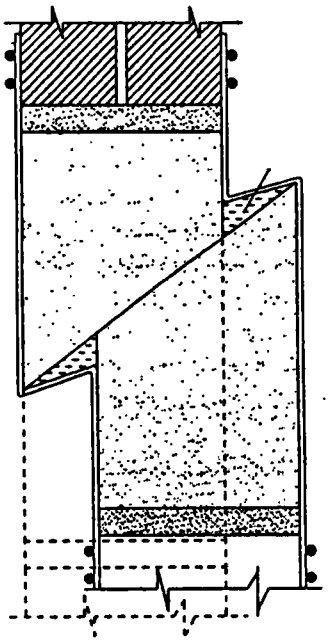

Fig.8.48. Undrained shearing : fictitious dilation of the specimen causing a drop of pore water pressure after the formation of the failure surface.

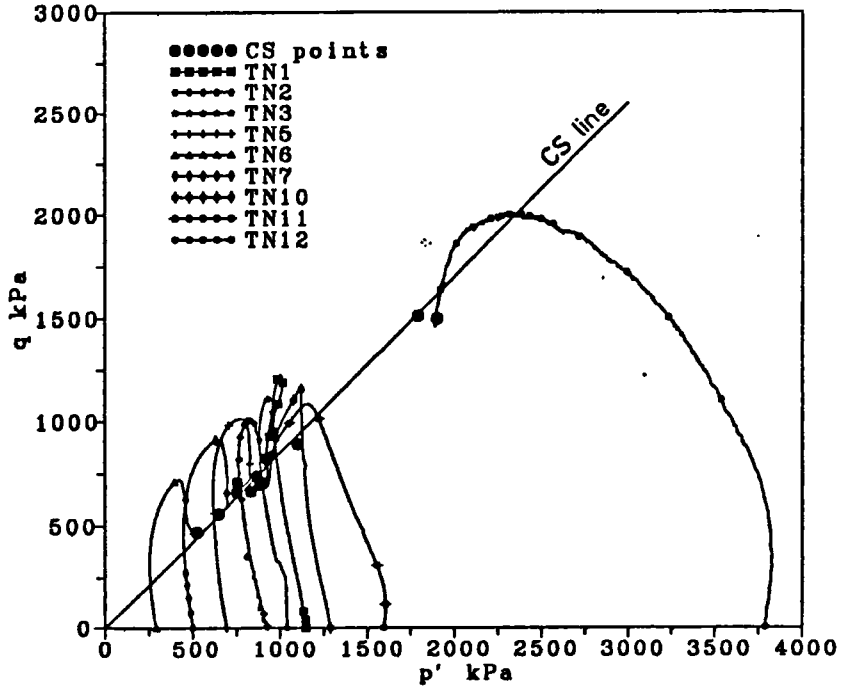

Fig.8.49. Undisturbed clay : undrained stress paths and critical state line.

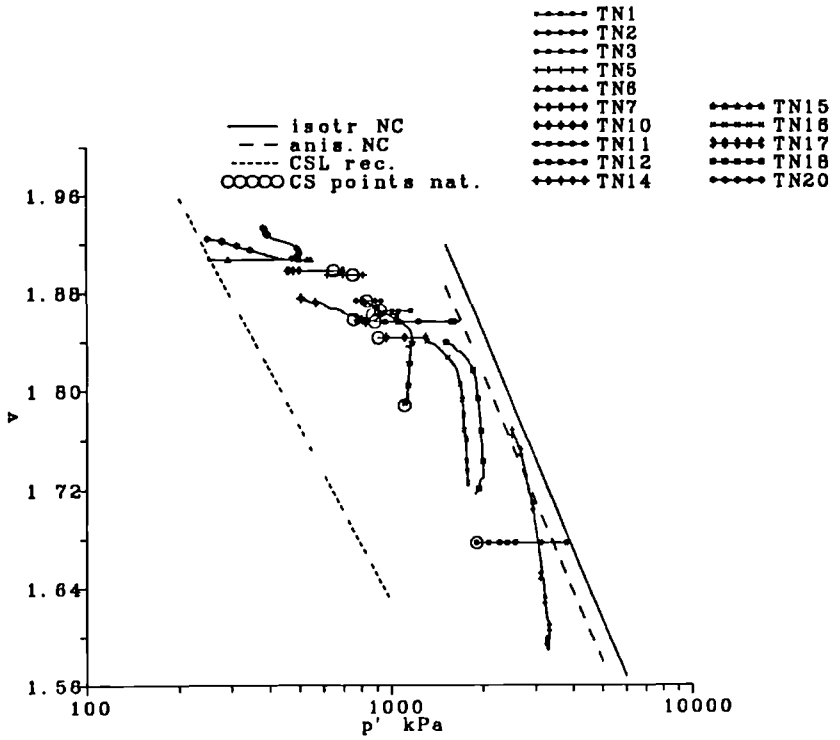

Fig.8.50. Undisturbed clay : v-p' state paths and critical states.

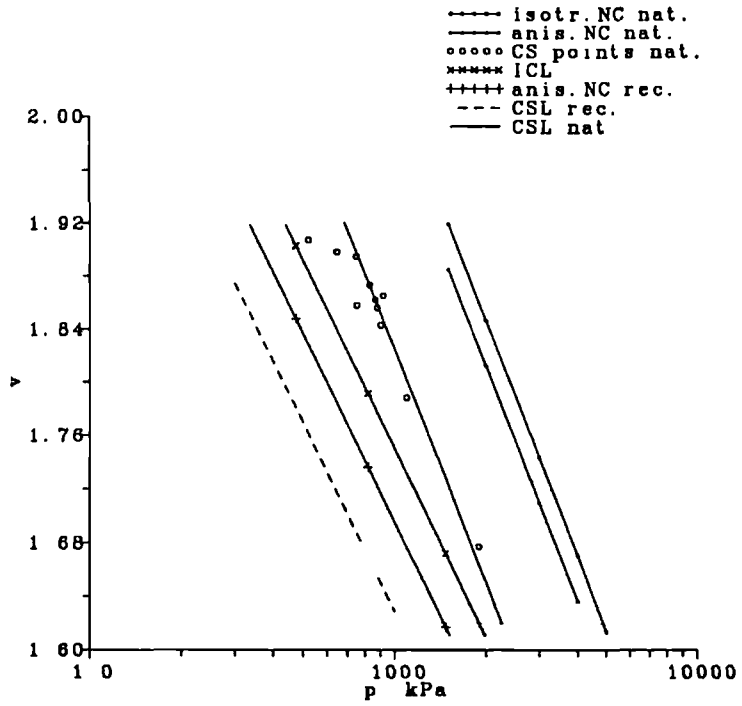

Fig 8.51. Isotropic and K_0 normal compression lines and critical state lines (constant η lines) of the natural and reconstituted Pappadai clay.

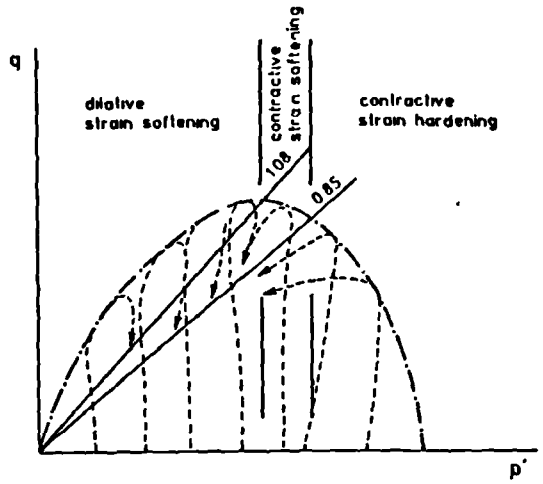

Fig.8.52. Behaviour of the undisturbed Pappadai clay in relation to the location of yield with respect to both the straight line of gradient 1.08 and the critical state line.

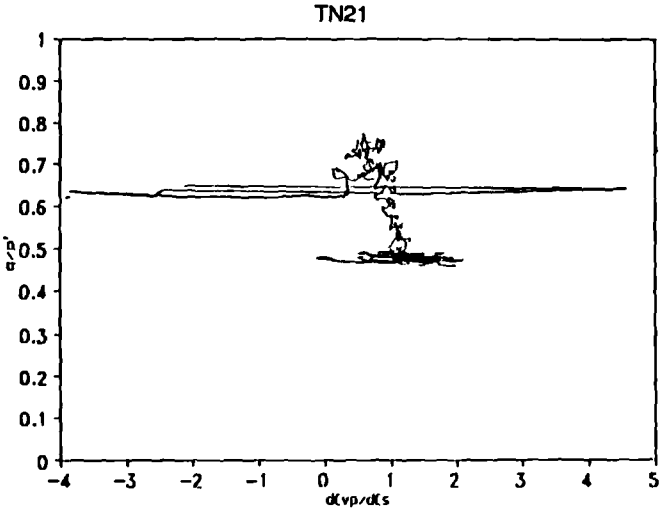

Fig.8.53. Plastic strain ratios during the K_0 compression of the undisturbed clay.

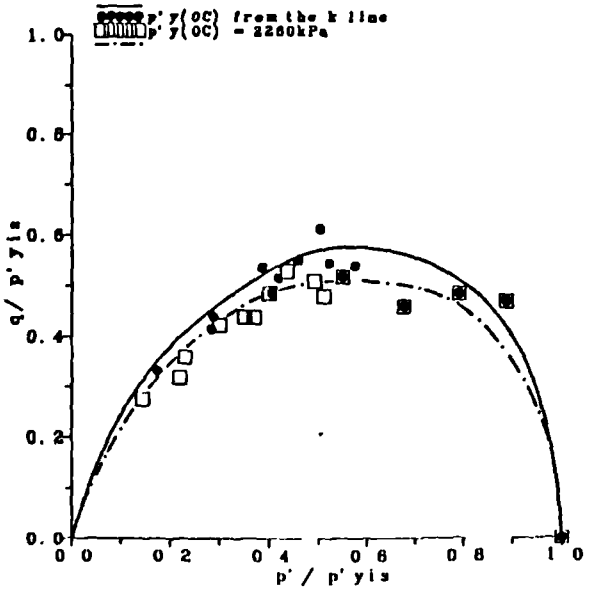

Fig.8.54. Current yield curve of the undisturbed clay : the yield states have been normalized with respect to two alternative values of p'_y.

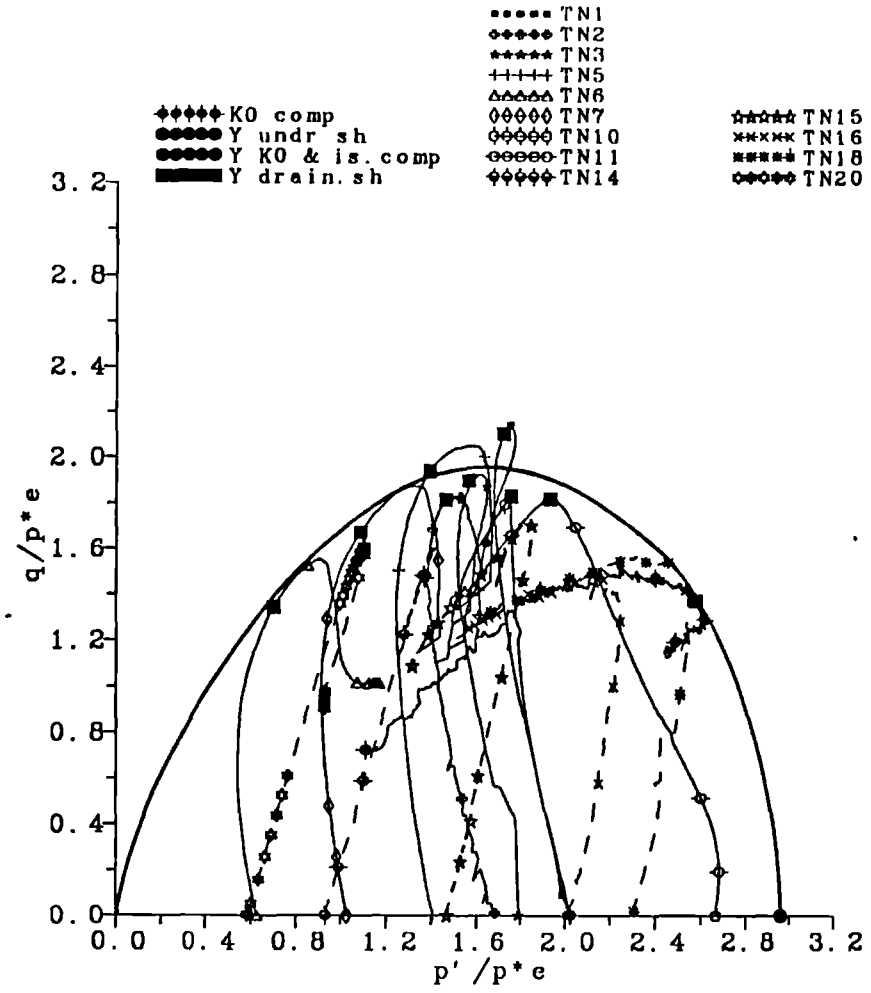

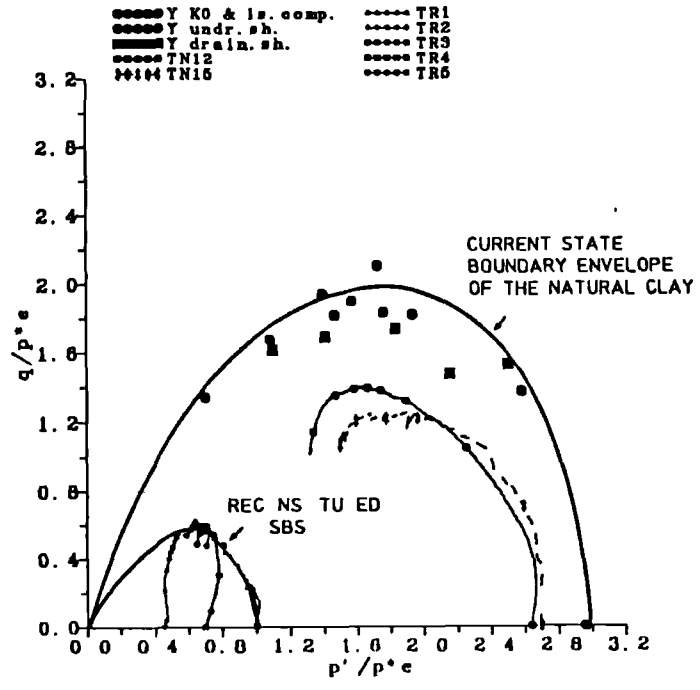

Fig.8.55. Stress paths normalized with respect to the equivalent pressure p_e^* : (a) natural clay specimens consolidated to states before isotropic yield; (b) natural clay specimens consolidated to states beyond isotropic yield and reconstituted clay specimens

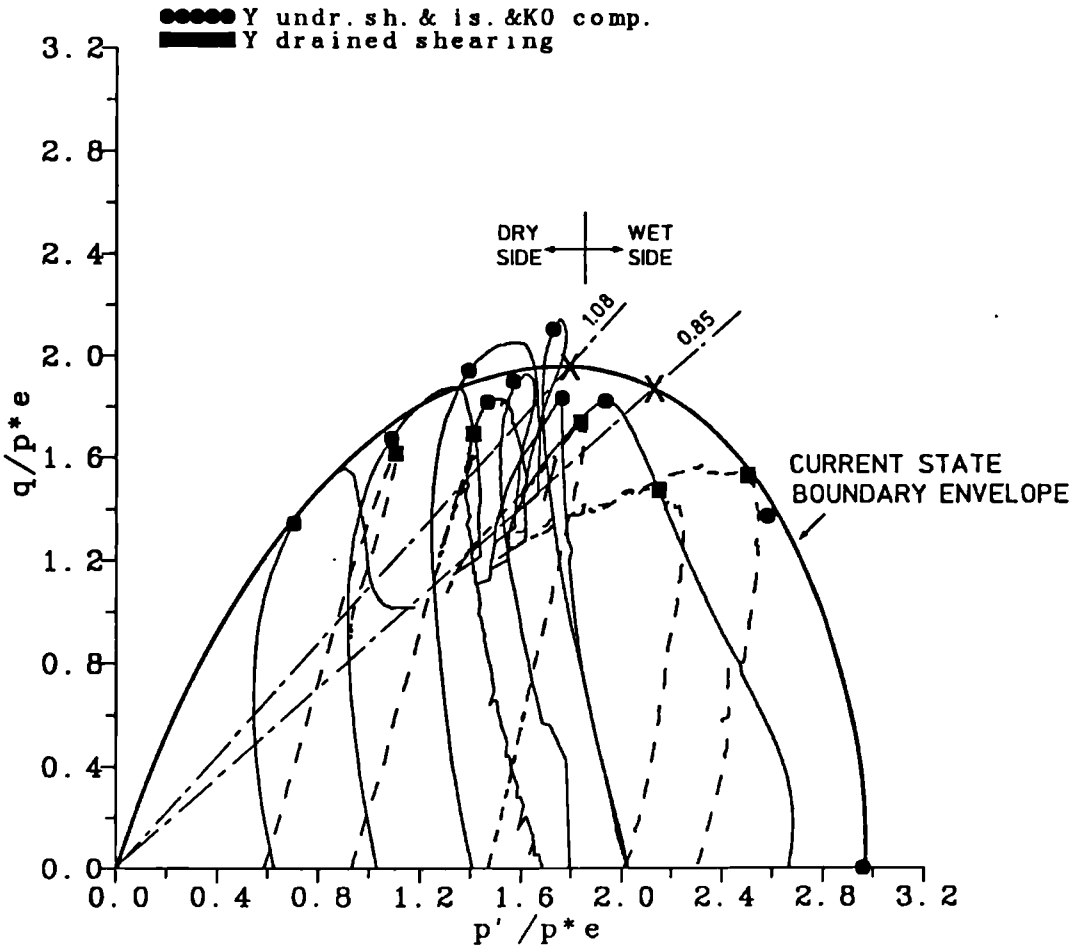

Fig.8.56. Normalized stress paths of the natural clay consolidated to states before isotropic yield and dry and wet sides of the natural clay framework of behaviour.

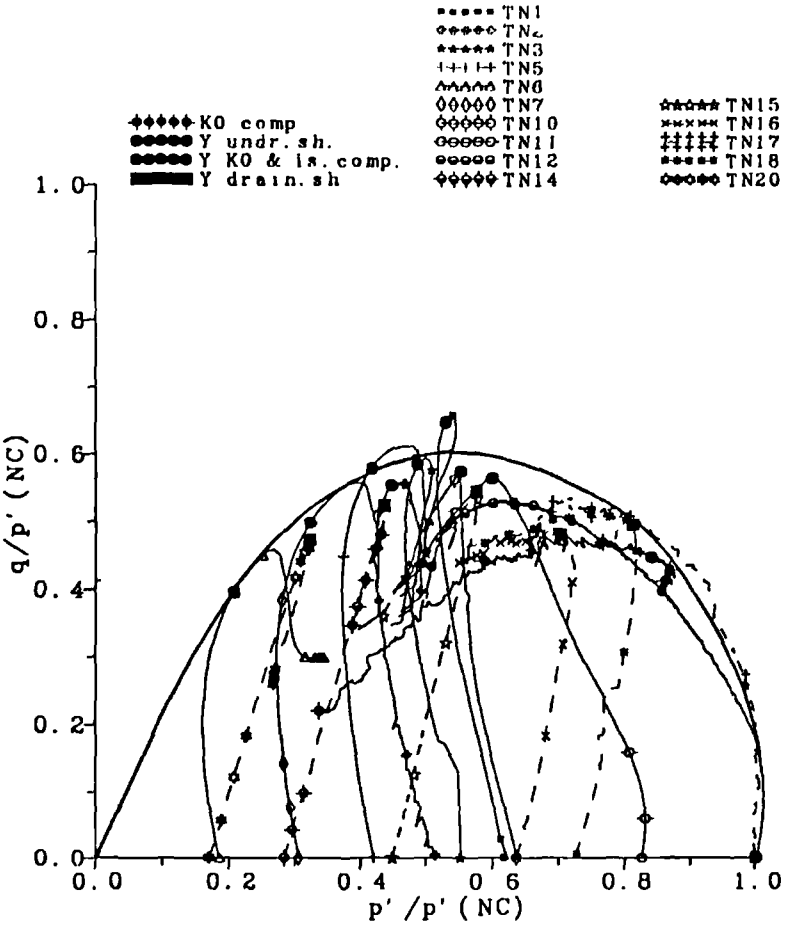

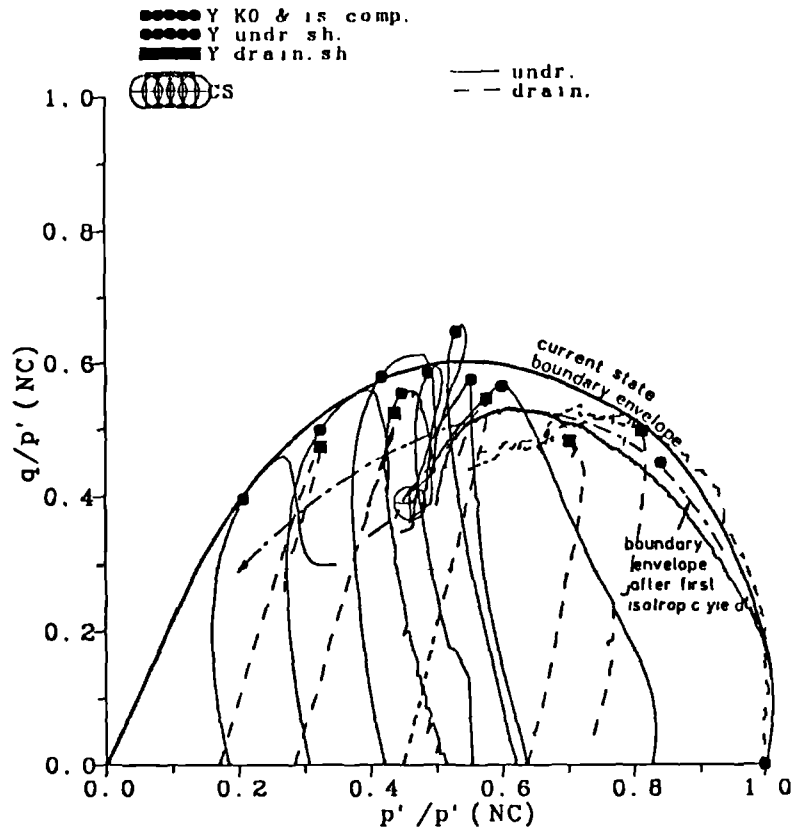

Fig 8 57. Natural clay : stress paths normalized with respect to volume by means of the pressure p_{NC}.

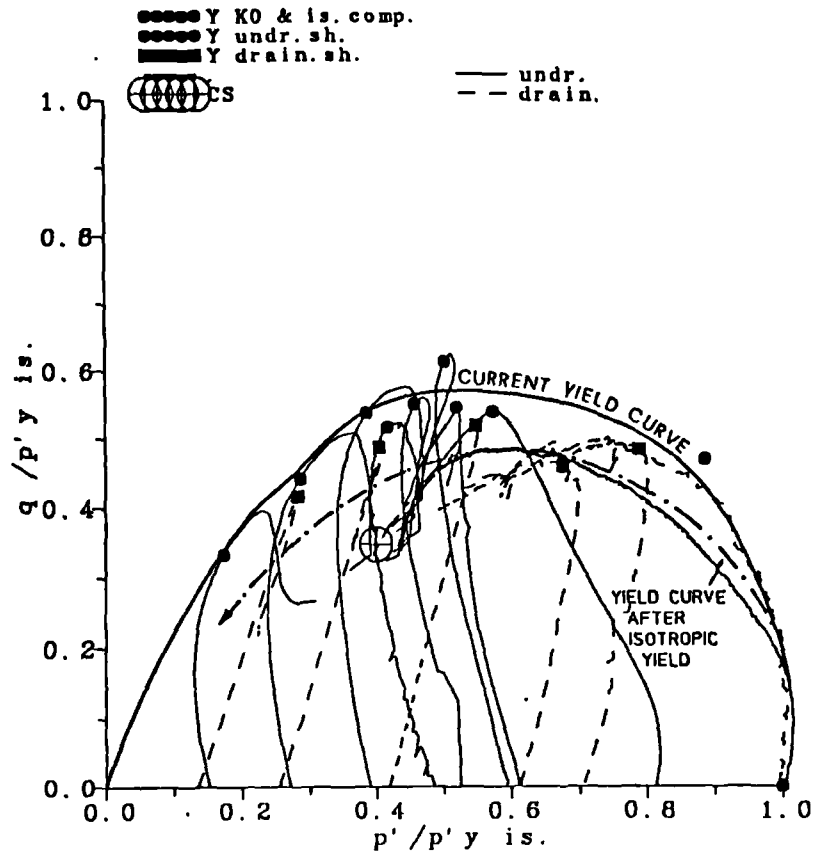

Fig.8.58. Natural clay : stress paths normalized with respect to volume by means of the yield pressure p'_{ys}.

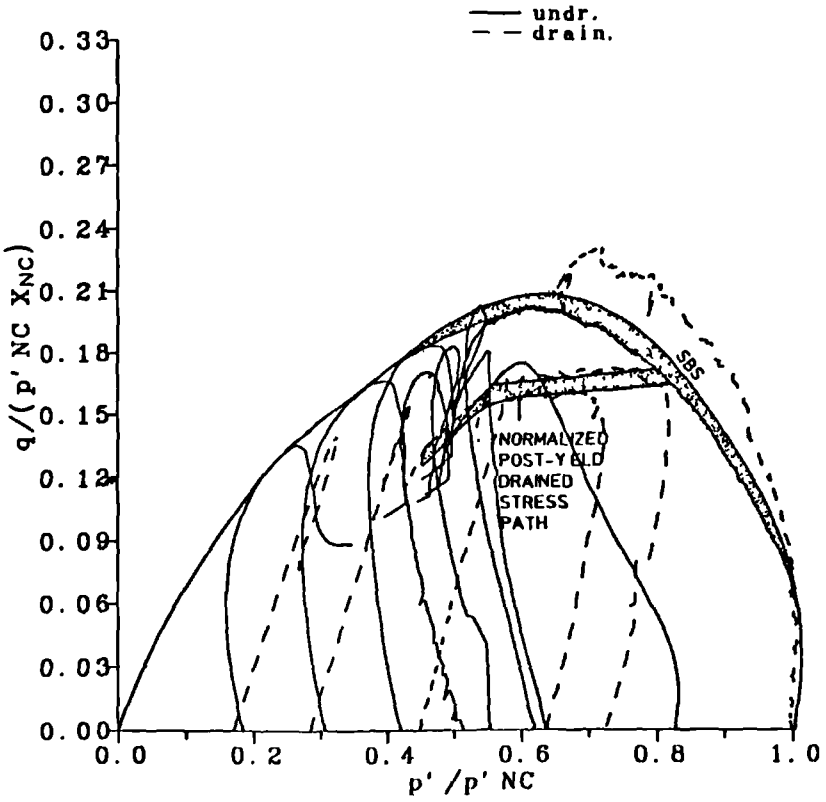

Fig.8.59. Natural clay : stress paths normalized with respect to volume and structure by means of the pressure p'_{NC} and the stress ratio $X_{NC}(=p'_{NC}/p^*_e)$.

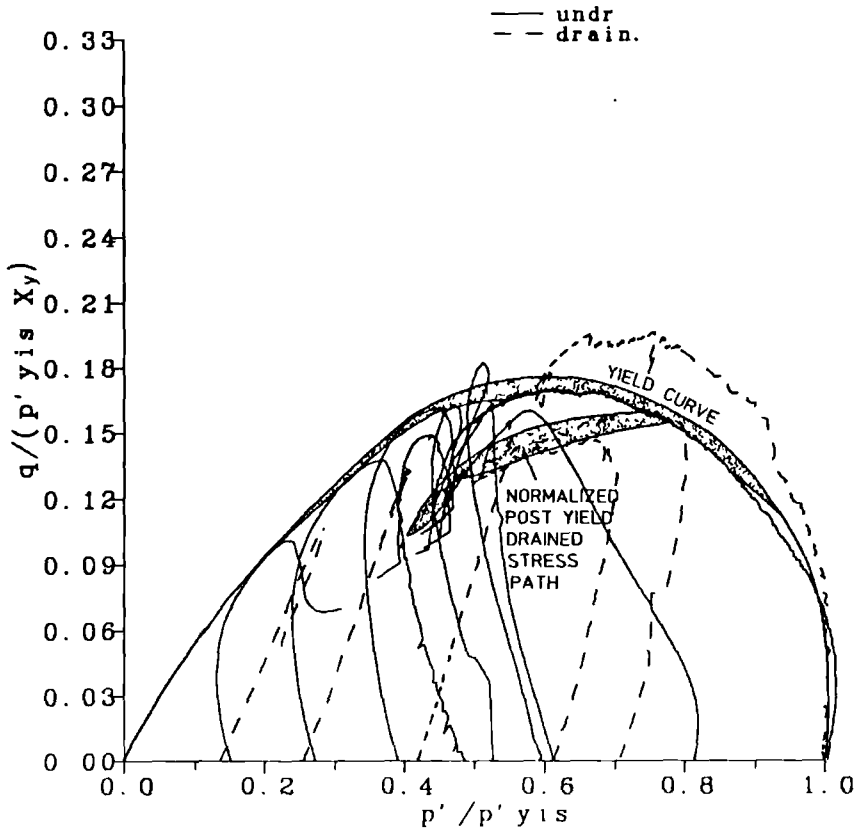

Fig.8.60. Natural clay : stress paths normalized with respect to volume and structure by means of the yield pressure p'_y and the stress ratio $X_y=(p'_{yis}/p^*_c)$.

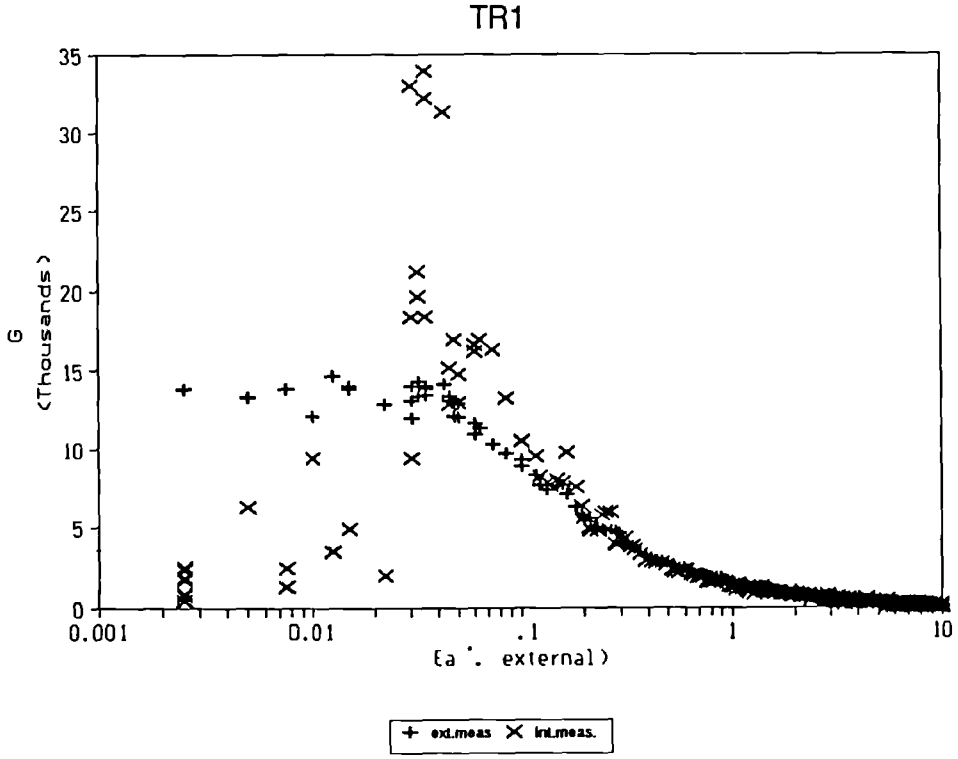

Fig 8.61. Reconstituted clay : shear stiffness measurements

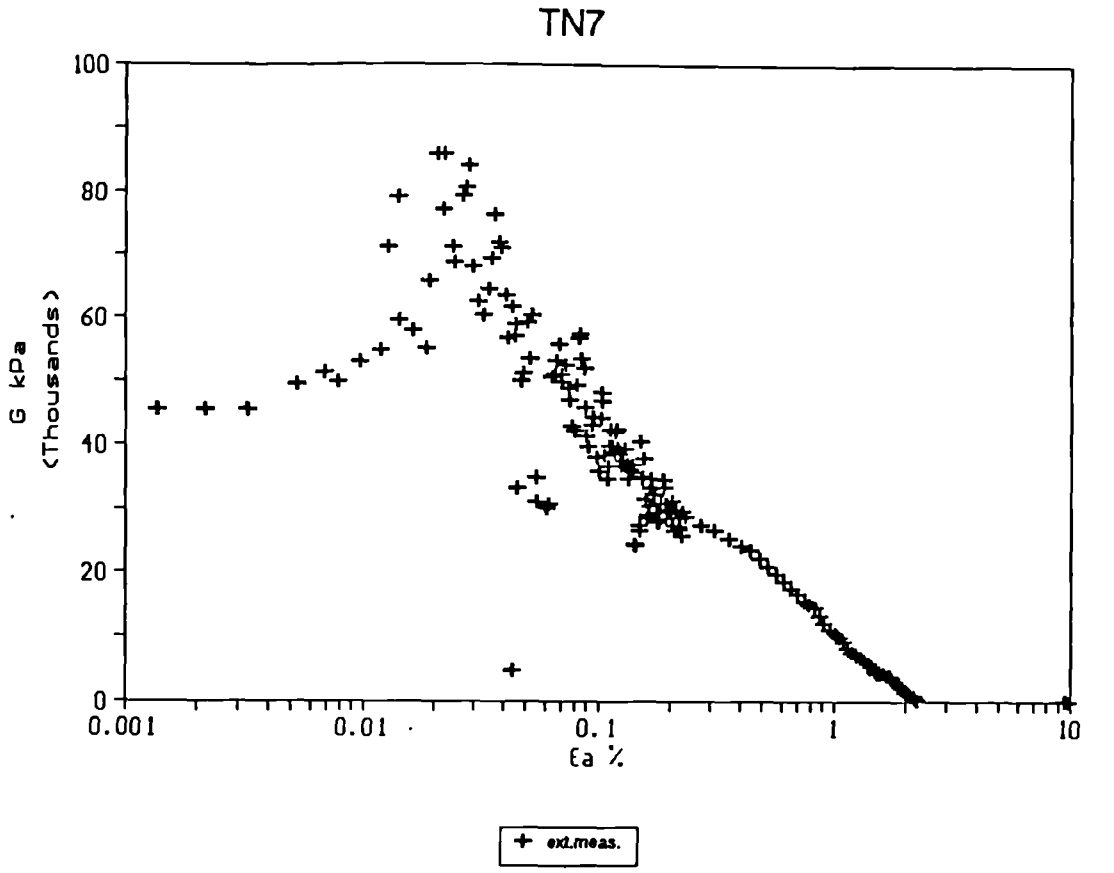

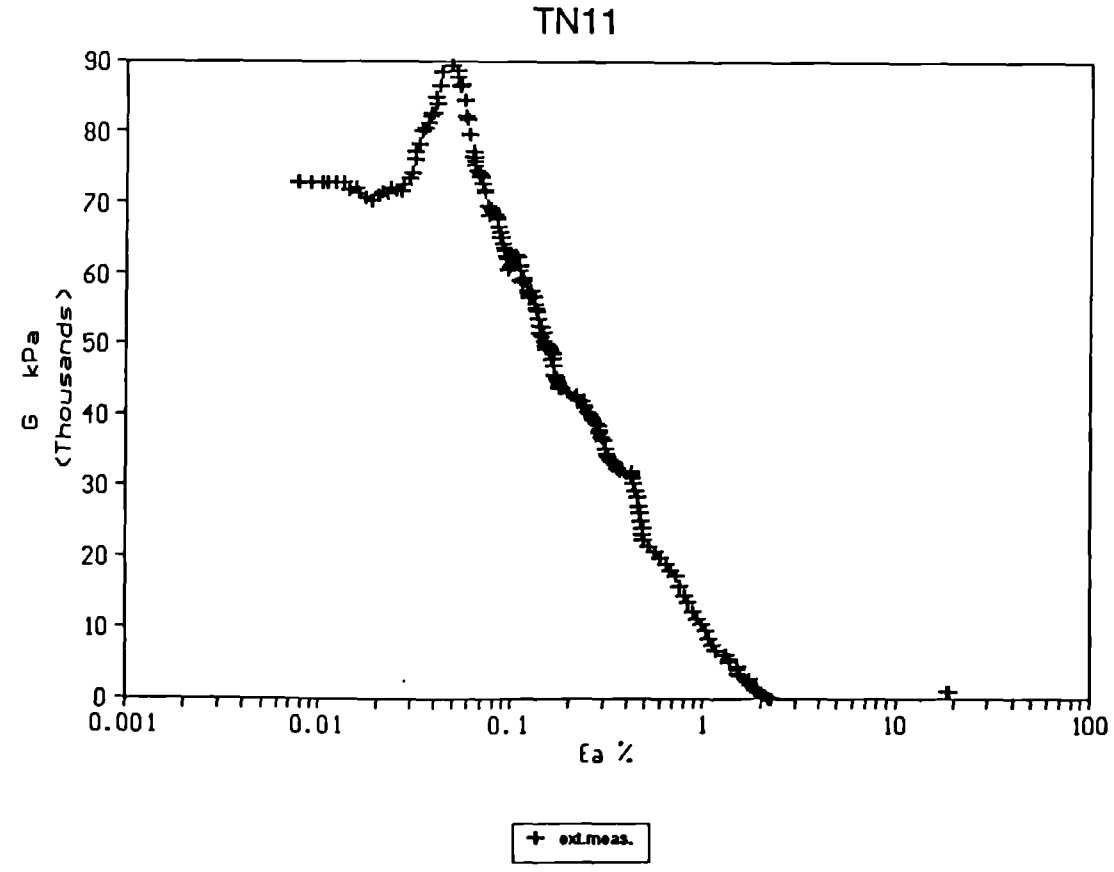

Fig.8.62. Natural clay : shear stiffness measurements.

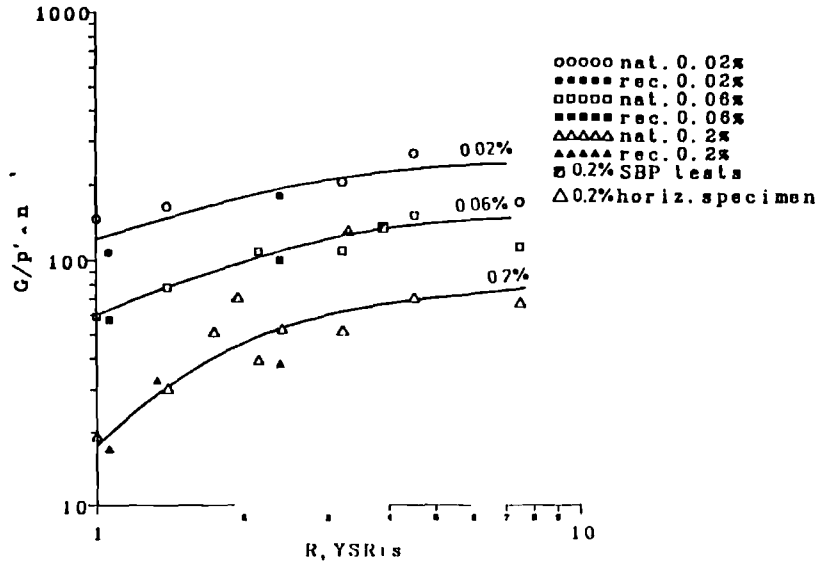

Fig.8.63. Relationship between the normalized shear stiffness and the yield stress ratio for both the natural and the reconstituted clay.

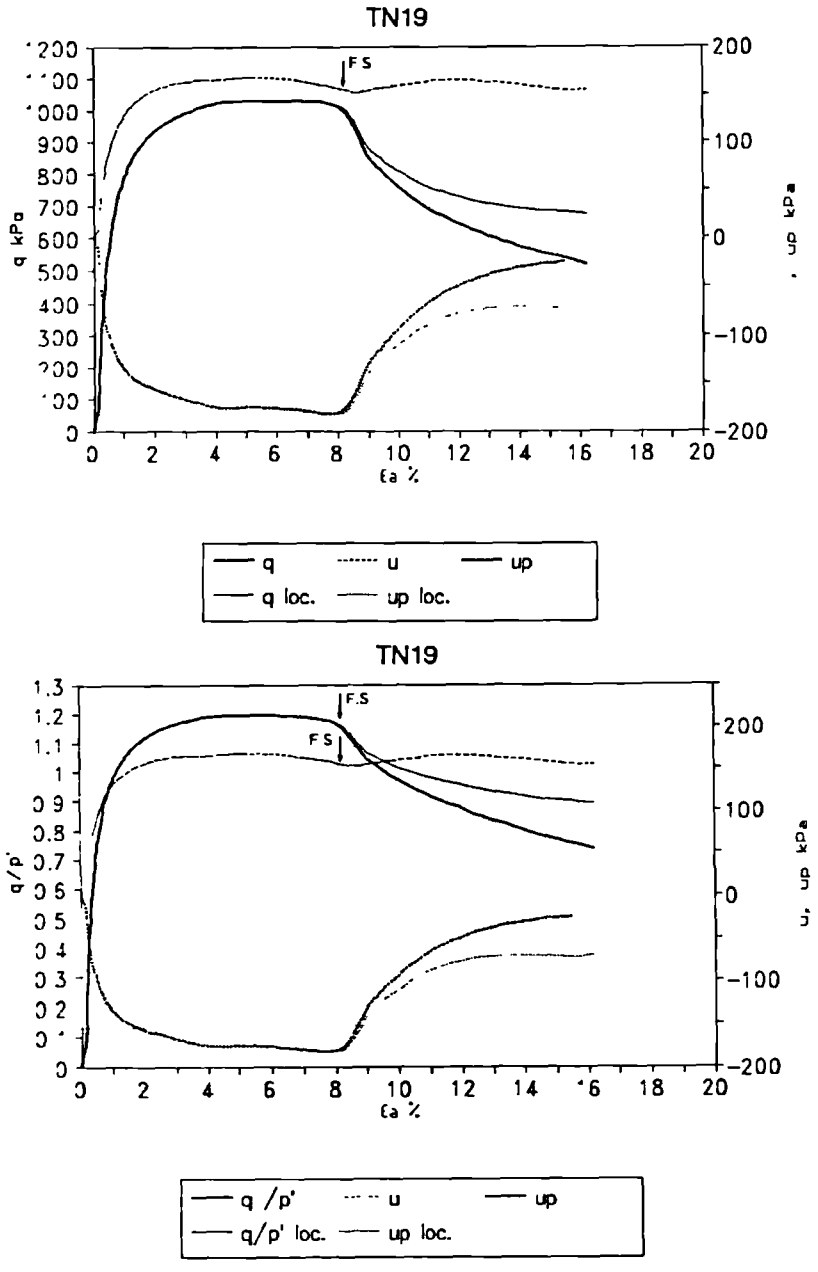

Fig 8.64. Horizontally trimmed specimen of undisturbed clay : stress-strain behaviour before and after correction for localization (q_{loc}, q/p'_{loc}, $u_{ploc.}$).

CHAPTER 9

CONCLUSIONS

9.1. A framework for the behaviour of clays

9.1.1. A novel approach to the structural effects on clay behaviour

The long-term objective of the present research was to construct a simple framework representing the general behaviour of clays, which would extend the present understanding of the critical state behaviour of reconstituted clays to the behaviour of undisturbed natural clays. In such a framework the similarities of behaviour of clays of different origins, composition and structure need to be defined and the differences related by numerical parameters. As the behaviour of a clay is the consequence of its structure, the differences in behaviour between clays should therefore be related to parameters representative of differences in clay structure.

With this objective, the work presented in this thesis started with a detailed review of clay structure, leading to definitions of structure, fabric and bonding of clays. This review also resulted in a novel approach to the comparison of natural and either reconstituted or remoulded clays. Clays have generally been distinguished as "structured" or "non-structured" and considered as following laws of behaviour and mechanisms of deformation which differ fundamentally. In contrast, it is shown that the differences between the structure of remoulded clays and natural sensitive clays is not necessarily the type of soil fabric, but the nature, stability and strength of the bonding. In remoulded and reconstituted clays the bonding is basically of an electrostatic and electromagnetic nature and is stable, whereas with natural sensitive clays bonding may include other meta-stable components.

Remoulded clays have been shown to possess both dispersed and flocculated fabrics. The reconstituted and natural Pappadai clay, investigated by means of the scanning electron microscope (SEM), are both shown to be of a bookhouse type at medium pressures, although the two clays are very different. Both undergo complex changes during compression, the nature of which is also different

Eliminating the distinction between structured and non-structured soils has permitted the use of an approach which treats natural and reconstituted clays simply as clays of different structure,

both represented by different elements of the same framework of general clay behaviour. Consequently, the similarities in behaviour between natural and reconstituted clays have been explored, developing the hypothesis that since only some elements of structure differ, many aspects of their behaviour should be similar. Thus, the general applicability of the basic features of the CSF to both natural and reconstituted clays has been investigated.

The stability of the bonding is the principal difference between natural sensitive and reconstituted or remoulded clays, and so the relationship between this structural difference and the differences in the macro-behaviour of the clays has been particularly considered. The sensitivity of the clay is an effect of the stability of the clay bonding, a sensitive clay being formed by metastable bonding. Sensitivity is therefore proposed as a numerical parameter representing the differences between clay structures This allows the construction of a behavioural framework for clays. Basic deformation mechanisms common to natural and reconstituted clays have been identified, and the differences in behaviour have been related to the clay sensitivity, as summarized in the following sections.

9.1.2. Classification of clays

A classification of clays is proposed, based upon two main categories of structure, on aspects of the clay response in the I_v-σ'_v plane (YSR), and on the clay's stress history (OCR).

Clay structure is divided into two main categories, each related to the history of the clay; that is, whether it has been formed during normal-consolidation, the "sedimentation" structure, or whether it includes elements developed at a later stage, the "post-sedimentation" structure. All natural clays must have one or other of these two structures

Clays having a sedimentation structure are necessarily geologically normally consolidated (OCR=1) and also exhibit a YSR of 1 in the Iv-σ'_v plane, unless they have been cemented during virgin compression. Among these clays, three categories may be distinguished based upon the ratio between the values of YSR and OCR. This ratio is greater than 1 only for those clays with a cemented sedimentation structure (type 5 in Table 2.1). For clays with an uncemented sedimentation structure a distinction is made between soft clays (type 1) and stiff clays (type 3).

For clays with a post-sedimentation structure and having a value of OCR about equal to the YSR, geological unloading seems to be the only event which can cause a change in structure after

virgin compression. These clays therefore revert to their original sedimentation structure when recompressed and would be expected to fit the same behavioural framework as clay types 1 and 3 (Table 2.1). Both soft clays (type 2) and stiff clays (type 4) may fall in this category.

Consideration of the structural changes which may take place in clays after virgin compression suggests two further categories of clays, type 6 and 7 in Table 2.1, where some phenomenon in addition to, or instead of, simple geological unloading has affected the clay structure. It has been demonstrated that these clay types (6 and 7), which may geologically be either normally or overconsolidated, exhibit a gross yield stress on recompression which is higher than the geological preconsolidation pressure. The behaviour of these clay types thus depends on the YSR value rather than the OCR, and necessarily reflects the clay stress history differently from that of clay types 1 to 4.

Leached clays are considered to form a separate category, type 8 in Table 2.1.

In the proposed classification, reconstituted clays may be any of types 1 to 4. Undisturbed Pappadai clay has been demonstrated to be of type 7, on the basis of the results of the comparative studies of the geological history of the clay, its mineralogy, its present in situ state, its present microstructure, and of its response to oedometer testing in the laboratory.

Different clay categories may be expected to have similar patterns of behaviour. For example types 1 to 4 should behave similarly. Types 6 and 7 should also be similar in their behaviour, but different to that of types 1-4. However, the proposed classification attempts to cover all the natural clay types in order to define a general framework for the behaviour of clays.

The data presented in the literature for the behaviour of soft clays and cemented soils are shown to be more comprehensive than for stiff clays, so that the study of Pappadai clay adds significantly to the knowledge of stiff clay behaviour.

9.1.3. Framework of clay behaviour in the I_v-σ'_v plane

Sensitivity is an additional factor which may cause differences in clay behaviour. This reflects the presence in the clay of more or less stable structural elements. Clays of sensitivity greater than unity have a structure more resistant than that of the reconstituted clay, and are shown to plot to the right of the reconstituted clay in the I_v- σ'_v plane. A monotonic relationship is found between

the values of sensitivity of clays at yield, S_t(YSR=1), and the ratio of the yield stress to the equivalent pressure on the ICL (σ'_y/σ^*_e). This relationship is demonstrated to be universal since it applies to clays falling in all categories shown in Table 2.1, despite differences in structure and geological history.

Clays of different type, but having equal sensitivity at yield, all yield on the same line, which is almost parallel to the ICL in the I_v-logσ'_v plane (Fig 6 92). This finding suggests that the differences in behaviour between clays depend on the metastable structural elements present in the clay. This research has shown that the differences between the behaviour of a natural clay and of the equivalent reconstituted clay can be related to either the value of the clay sensitivity S_t(YSR=1) or to the ratio σ'_y/σ^*_e, which are thus two mutually dependant numerical parameters both indicating the effects of structure on the clay's behaviour.

Based upon the S_t(YSR=1)- σ'_y/σ^*_e relationship, a framework based on sensitivity has been defined in the I_v-logσ'_v plane, in which a series of parallel lines define the yield loci for clays of given sensitivities. For soft clays (types 1 and 2, Table 2.1) these lines also represent the sedimentation compression curves of clays of equal sensitivity (Fig.2.23), as soft clays yield on the sedimentation compression curve. The distance between the SCC and the ICL is therefore representative of the strength of their current structure at yield (the sedimentation structure). This distance is expressed by the ratio σ'_y/σ^*_e, which in these cases (types 1 and 2) is equal to the ratio of the preconsolidation pressure σ'_p to the equivalent pressure. This should also be the case for stiff clay types 3 and 4, although few data exist in the literature for these materials. For categories 1 to 4 the geological preconsolidation pressure is therefore related to the clay sensitivity and thus is a parameter of the clay behaviour. In contrast, for stiff clay types 5 to 7 the geological preconsolidation pressure is not representative of the current strength of the clay, as the yield stress is higher than the preconsolidation pressure, and it is the yield stress to which the clay behaviour must be related.

For clays which were not cemented during either deposition or virgin compression the difference between the geological preconsolidation and yield stresses indicates the existence of metastable elements in the clay structure, which developed after virgin compression resulting in an increase of the clay strength (types 6 and 7). This has been fully demonstrated for the Pappadai clay.

The development of long-term diagenetic processes in the Pappadai clay is demonstrated by the results of mineralogical analyses, the study of the clay microstructure by means of the SEM and

the comparison of the results of a modelling of the clay state history and the state of the clay measured in situ at present. The precipitation of a calcite film coating the clay particles and inter-particle contacts during diagenesis is shown by chemical micro-analysis of the natural Pappadai clay. This carbonate coating resulted from an early stage of a cementation process and at present forms part of the clay's bonding.

Thus in the natural Pappadai clay elements of structure exist which were acquired after virgin compression and which affect its current behaviour. A yield stress σ'_y higher than the geological preconsolidation stress has been measured in oedometer testing. This is the result of the structural changes which occurred in the clay after virgin compression, and results in the observed difference between YSR and OCR.

The analyses of the behaviour of Pappadai clay in the I_v-σ'_v plane, of its microstructure, and of its geological history, demonstrated that the location of the clay yield stress in the Iv-σ'_v plane may change during the history of the clay and that there is not a unique relationship between the clay's structural features and the location of the yield stress. Consequently, the type and strength of the clay bonding cannot be deduced solely from the location of the compression curve with respect to the ICL or SCL in the I_v-σ'_v plane, as suggested by various authors in the literature (see Section 6.7.1). The geological processes may change a non-sensitive sedimentation structure into a strongly bonded post-sedimentation structure which nonetheless has a yield stress which plots between the ICL and the SCL, and therefore has a medium to low sensitivity.

The distance between the yield stress and the ICL of the clay does not therefore necessarily increase with the strength of the clay bonding. On the contrary, stiff clays have been found mainly to lie between the ICL and the SCL in the sensitivity framework, and thus to have medium to low sensitivity. The open flocculated structure of soft clays is likely to be more sensitive than clays which have become stiff due to compression to high stresses, and which therefore have voids ratios which are low and to which also a high strength of the reconstituted clay corresponds.

For all clay types a higher value of σ'_y/σ^*_e results in a decrease in behavioural stability and a corresponding increase of post-yield compressibility. Therefore the post-yield compressibility is related solely to the value of the sensitivity (or the ratio σ'_y/σ^*_e). With further compression post-yield the metastable elements of the clay structure are degraded and the clay sensitivity falls, so that the post-yield compression curve crosses different constant sensitivity lines. This is not the

case for the reconstituted clays, which have a sensitivity of unity and whose behaviour is not affected by changes in sensitivity during loading

9.1.4. Similarities in the patterns of behaviour of clays

Despite the difference between natural sensitive clays and reconstituted clays, similar behavioural laws apply to these clays as demonstrated by both a study of the literature and results of the present investigation of the natural and reconstituted Pappadai clay.

Oedometric compression of the strongly bonded Pappadai clay, is as strain rate dependent as is that of the equivalent reconstituted clay. Data in the literature similarly show that natural soft clays are strain-rate dependent. A similar structural viscosity seems therefore to affect the stress-strain response of all clays, despite their different categories and sensitivities. A unique exponential law consistent with this hypothesis is shown to relate the creep coefficients of both the natural and the reconstituted Pappadai clay to the vertical effective stress and the oedometric stiffness (eq.6.22). The bonding of the natural Pappadai clay does not seem to change the basic mechanism of behaviour at the micro-level.

Similarities were also found between the variations with σ'_v of the oedometric stiffness, the coefficient of consolidation and the coefficient of permeability of both the natural and reconstituted clay. For both the clays critical changes were observed in the relationships at yield, although the size of these changes differed due to the loss of structural strength which in the natural clay occurs only at yield.

Similar but different exponential relationships between the post-yield oedometric stiffness and the vertical effective stress (eqs.6.25 and 6.26) are found to apply to the natural and the reconstituted clays, and a same equation even applies to both clays for the relationship between the post-yield stiffness and the voids ratio (eq 6.27).

The coefficient of permeability of both the natural and the reconstituted clays is found to be constant at values of YSR greater than one, and for both clays tends to follow exponential relationships with the voids ratio for post-yield compression (eq 6.28).

The post-yield compression index of both natural and reconstituted clays is found to decrease with increasing pressure, while the swelling index increases with compression under increasing stresses.

The magnitude of the variations of these parameters during compression differs for natural and reconstituted clays as they are affected by the changes in sensitivity of the clay occurring with compression. However, for all clays these variations are similar and even follow similar laws, irrespective of the clay's sensitivity.

The investigation at the micro-level of both the natural and reconstituted Pappadai clays has demonstrated that they retain different structures to very high stresses; this is consistent with the location in the I_v-σ'_v plane of the natural clay which plots to the right of the reconstituted even to very high stresses, with only a slow convergence. While the yielding process changes the clay structure, this is not sufficient for it to converge towards that of the reconstituted clay, in contrast to what has been observed by other authors for cemented sands. The comparison of the behaviour of the natural and reconstituted clay may therefore be seen as the comparison between a sensitive and a non-sensitive clay with the same mineralogy.

The similarities in the behaviour of the natural and reconstituted clays reinforce the idea that common basic deformation mechanisms drive the response of both sensitive and non-sensitive clays, so that the framework of clay behaviour is universal.

Further support to this hypothesis is derived from the behaviour of the natural and reconstituted clay during shearing. The shearing behaviour of reconstituted clays may be explained within the critical state framework as being purely frictional, since a simple frictional flow rule, such as eq.(2.3), describes completely both the contractive strain-hardening and the dilative strain-softening of the clay. The stress ratio at the critical state, M is the frictional parameter of the clay. Depending on the value of the yield stress ratio with respect to M_{nat} the clay exhibits either a contractive (wet) or a dilative (dry) behaviour.

The present results demonstrate that although the large strain behaviour of both reconstituted and natural clays is frictional, the law expressed by eq (2.3) does not always fit the data and a similar equation, introducing a coefficient A, generally gives better agreement (eq.2.4). It is often necessary to modify the value of the coefficient A to interpret the soil behaviour, as a result of the different effects that different structural changes have on the flow rule, although this still remains of a frictional type. Thus the deformation mechanism expressed by eq.(2.4) is regarded as

"basically frictional", and it follows that both reconstituted and natural soils exhibit a frictional deformation at large strains, even though the resulting clay behaviour is also affected by other structural events.

A literature survey shows that eq.(2.4) applies to both anisotropically consolidated and aged reconstituted soils, as well as to soft natural clays. For a given clay, coefficient A appears to vary with the stress path, as the structural changes taking place with loading are different in each case. However, whatever the value of A, eq.(2.4) always describes the stress-strain behaviour. Soft sensitive clays contract or dilate depending on the value of the yield stress ratio with respect to the critical stress ratio. Consequently a "dry" zone and a "wet" zone are identified in the framework for soft sensitive clay behaviour, as with reconstituted clays, and as shown in Fig.2.31(d). The gross yield points are shown to be boundary states for soft sensitive clays as for reconstituted clays in the CSF.

According to these findings many basic features of the critical state framework and of the Cam Clay model are applicable to the behaviour of soft sensitive clays, that is clay types 1 and 2 in Table 2.1. The analysis of the experimental evidence of the behaviour of cemented soils reported in the literature shows that soil type 5 (Table 2.1) has a basically frictional deformation mechanism at large strains, so that eq.(2.4) again applies (see Fig.2.31(c)).

The demonstration of the applicability of the basic principles of the CSF to the behaviour of clay types 1 to 6 (Table 2.1) is limited by the necessity of relying on data from the literature. The applicability of the CSF was investigated in some detail for clay type 7, which includes the natural Pappadai clay.

Both the reconstituted and natural Pappadai clay fit the CSF in isotropic and anisotropic compression and swelling, and the parameters λ and κ have been calculated for both the clays. A basically frictional flow rule thus applies at large strains to all the state paths followed by the two clays, whether in compression or shear. This is given by eq.(2.4) for the reconstituted clay and eq.(8.9) for the natural clay. For both soils the values of the coefficient A were found to be constant for a given stress path, and indeed it is the stress path which influences A more than whether the soil is natural or reconstituted.

During shear the clay follows the frictional flow rule at large strains both before gross yield and along part of the state path beyond yield. The gross yield points of the natural clay were also found to be boundary states, as for the reconstituted clay. Therefore the gross yield curve of the

natural clay in v-q-p' space lies on the clay state boundary surface (SBS) as in the Cam Clay model. A "cupola" shape has been established for the yield curve and SBS of the natural clay, as is also the case for anisotropically consolidated reconstituted clay, so as to include the response of specimens with anisotropic structure. The basic elements of the Cam Clay model are therefore applicable to a large part of behaviour of the natural Pappadai clay, although with a modified version of the frictional linear flow rule.

The behavioural framework of the natural Pappadai clay is separated into a "wet" and a "dry" side by the point of intersection of the straight line of gradient $\mathcal{M}_{cst}$ through the origin (the friction line) and the SBS (Figs.8.52 and 8 56). The behavioural framework of the stiff Pappadai clay is therefore similar to those for reconstituted soils, cemented soils and soft sensitive clays.

The behaviour of natural clays up to gross yield, and for part of the state path beyond yield, depends, as for the reconstituted clay, on the clay's YSR. Generally at YSRs of about 2 the clay behaviour starts to change from contractant to dilatant. Relationships establishing the dependency of behavioural parameters on the OCR, which generally apply to reconstituted clays, have been found to apply also to the natural clay provided the YSR is substituted for the OCR. For example, the value of K_0 measured in situ for the clay forming the undisturbed block sample is close to the K_0 value from the K_0-OCR relationship applying to soft and reconstituted clays if YSR is used instead of OCR. This finding confirms the interpretation of the behaviour of clays with YSR different from the OCR (types 5 to 7 in Table 2 1) which was anticipated from the definition of the sensitivity framework in the I_v-σ'_v plane, as this suggested that for these clays the behaviour should not be dependant on the geological preconsolidation pressure.

Finally, the interpretation of localization phenomena developed for reconstituted clays is also shown to fit the "dry" side behaviour of natural clays. Localization phenomena affect the peak strength of the clay in undrained shearing, but not the values of the peak stress ratios. Therefore the SBS resulting from undrained tests is consistent with that from drained tests.

9.1.5. The differences between the behaviour of clays

In addition to the similarities in behaviour reviewed above, the research also shows differences between the behaviour of natural and reconstituted clays which arise basically from the differences in their structural stability.

The higher strength of the natural Pappadai clay structure affects the size of the SBS and of the oedometric and shearing stiffnesses, as might be expected. A novel finding of interest is the difference measured between the friction stress ratio, which governs the frictional behaviour of the natural clay at gross yield, $\mathcal{M}_{nat}$ (eq.8.9), and the friction stress ratio of the reconstituted clay at the critical state, $\mathcal{M}$. The difference in structure between the two clays therefore also seems to affect the basic frictional behaviour of the clay.

The literature review shows that the friction stress ratio of both natural cemented soils and soft clays does not seem to differ from the critical state line gradient of the reconstituted soil. However, given the small difference between the values of $\mathcal{M}_{nat}$ and $\mathcal{M}$ measured for the natural Pappadai clay, it is possible that similar differences apply also with natural soft clays.

However, the most significant differences between the behavioural framework of the natural and reconstituted clay are in the shearing behaviour of the soil beyond yield at large strains and in the post-yield compression behaviour A careful analysis of the triaxial test data at large strains, corrected for the effects of localization of the specimen post-rupture, shows that the mode of deformation of natural Pappadai clay beyond yield is towards a critical state. The stress ratio at critical state is found to be equal to that of the reconstituted clay, and so is lower than the friction stress ratio controlling the behaviour of the clay at intermediate shear strains, including yield. It is shown, however, that while the natural and reconstituted critical state lines are coincident in the q-p plane, the two clays tend to different critical states in terms of volume. The critical state line of the natural clay lies to the right of the ICL in the v-lnp' plane, although it is still parallel to the other λ lines of the natural clay framework.

Because of the difference between $\mathcal{M}_{nat}$ and $\mathcal{M}$ all the natural clay specimens strain-soften to reach the critical state beyond yield at large strains, and the critical state line is located inside the SBS of the natural clay At large strains the purely frictional behaviour which is observed up to and immediately after gross yield, no longer applies. The location of the critical state line with respect to the SBS may be considered to be the main difference between the behavioural frameworks of the natural and the reconstituted clays, as it is this which causes the deformation mode of the natural soil deviate significantly from that of the reconstituted Contractant soils, on the wet side of the framework, start strain-softening at very large strains, deviating from a frictional mode of deformation Dilatant soils strain-soften from $\mathcal{M}_{nat}$ to $\mathcal{M}$, again deviating from the behaviour expected of a frictional material.

It is thus concluded that the behaviour of natural stiff clays does not comply with the CSF when approaching the critical state at very large strains. A review of the existing literature leaves it uncertain whether this also applies to natural soft clays.

In compression beyond yield the metastable elements of the natural clay structure are degraded. This gives rise to differences between the behaviour of the reconstituted and that of the natural clay. For example, as a direct consequence of the degradation of the metastable bonding, the value of the swelling index increases. Another fundamental effect is that, while the behaviour of reconstituted clays in compression before and beyond yield can be normalized with respect to volume, the behaviour of the natural Pappadai clay cannot be. For example the oedometric stiffness of the natural clay does not depend solely on the YSR and specific volume of the clay, as is the case for the reconstituted clay. The size of the SBS of the natural clay also changes with compression beyond yield according to a normalizing factor which does not depend solely on volume.

Nonetheless it has been demonstrated that the behaviour of the natural clay is still isotropically hardening. The size of the SBS of the clay, the same as the size of the relationship between the clay's oedometric stiffness M and YSR, changes with compression only. However these relationships depend not only on volume, but also on the structural changes that occur within the clay during compression, that is on the loss of the metastable structural elements. The factor which is best suited to normalize the clay behaviour with respect to the effects of these structural changes is the ratio σ'_y/σ^*_e.

The behaviour of the natural clay has been normalized with respect to volume by referring to the post-yield isotropic compression line of the natural clay, v-p'_{NC}. The normalizing pressure p'_{NC} is used for the natural clay in the same way as the equivalent pressure p^*_e is used for the reconstituted clay. The use of p'_{NC} rather p*e to normalize the natural clay behaviour is consistent with the interpretation of these two clays as two different and independent soils which have different sensitivities. It is the value of p'_{NC} and not that of p*e which is representative of the clay's current volume, and therefore this has to be used in the normalization. At the same time, the change in the value of the ratio σ'_y/σ^*_e is a direct effect of the change in the clay's sensitivity, and therefore of the structural changes occurring in the clay with compression. This factor has been proved to be successful in normalizing the clay behaviour.

In conclusion, the structural changes occurring with compression beyond yield affect the behaviour of the natural sensitive clay, but not that of the reconstituted clay. Consequently, for

natural clays, the framework of behaviour of similar samples compressed in situ to different volumes, which has been defined as the current behavioural framework of the clay, is different from the behavioural framework of undisturbed samples from one depth compressed in the laboratory to different volumes, which has been defined as the behavioural framework of the natural clay. This difference does not exist for reconstituted clays. The current behaviour of the natural clay is isotropically hardening solely with respect to volume, as for the reconstituted clay The behavioural framework of the natural clay diverges from the current framework at gross yield, and is isotropically hardening with respect to both volume and the structural changes. The shearing behaviour of the natural clay ceases to be isotropically hardening beyond yield, when the clay strain-softens to reach the critical state.

9.2. Geological history, structural features and v-p' state history of Pappadai clay

The research has provided an accurate interpretation of the geological history of Pappadai clay, a marine clay which forms part of the sub-Apennine blue clays. A knowledge of the geological events experienced by the clay is fundamental to the interpretation of the clay's current structural features at the micro-level, and therefore in the identification of the origins of those aspects of the clay behaviour which differentiate Pappadai clay from other clays. From the geological history of the clay it is recognized to have a post-sedimentation structure (Table 1.1), demonstrating that diagenesis affected the clay structure and that the clay has been geologically unloaded, so that the clay falls within the clay category 7 in Table 2.1. The mechanical behaviour of Pappadai clay therefore illustrates the behaviour of this type of clays in the general framework.

The deposition environment of the clay has been characterized on the basis of both a literature review as well as a detailed analysis of the in situ soil properties. By means of a palaeontological analysis it is shown that the clays currently present at Pappadai were deposited in the isolated Montemesola Basin about 1.2-1 3 million years ago. The sequence of soil strata deposited during the transgression is characterized and the stratum from which the block sample was taken has been shown to be formed in the quietest stage of the transgression. The clay was deposited in still water, about 100 metres deep, with reducing conditions at the sea bed which is demonstrated by the presence of framboid pyrite in the clay The clay is currently laminated as post-depositional mixing did not occur in the depositional environment, and its macro-structure is therefore strongly anisotropic. However this anisotropy does not affect the clay's strength. The lamination is due to the intermittent intense deposition of coccoliths which are seen in the microscopic analysis of the clay

An alternating deposition of finer and coarser material during the transgression has been identified from both the clay fraction and Atterberg limit profiles. The activity profile shows that the various clay strata at Pappadai, although of different granulometries, are formed of predominantly similar mineralogies, though there is a slight reduction of activity with depth This is consistent with the results of the mineralogical analyses of the clays, which showed a reduction of the swelling minerals with depth, with a corresponding increase of the illites, chlorites and intergrades. The falling proportion of swelling minerals thus shows that aggradation of the swelling minerals occurred at Pappadai due to their compression under burial. The occurrence of these and other diagenetic processes in the Pappadai clays is further confirmed by microstructural analysis.

It is proposed that the natural Pappadai clay originally had a bookhouse primary fabric due to the high content of active minerals. This was compressed by an overlying stratum of clays, about 170 metres thick, which caused the compaction of the bookhouse fabric. The results of this compaction are observed with SEM.

The clay was not cemented at deposition or during virgin compression despite its high carbonate content. The carbonate content in the Pappadai clay is mainly composed of detritus, first recognized in the analysis of the relationships between the carbonate content, the clay fraction and the plasticity index of the soils. This is also confirmed by the SEM analysis of the clay fabric. The absence of calcite crystals at the inteparticle contacts has shown that a proper carbonate cement is not present in the clay, though an amorphous calcite film coats the clay particles, showing that the clay does possess a carbonate bonding. This is the result of a mild cementation processes developed in the clay when it was under high in situ pressures, that is after deposition and compression. The Pappadai clay is therefore currently strongly bonded due to diagenetic effects, including carbonate bonding, which developed either during or after the final stages of virgin compression.

This interpretation of the history of the clay structure is confirmed by modelling the state history of the clay. The closeness of the measured and calculated values for the current volumetric states of the clay in situ demonstrates that the assumption of an uncemented structure of medium sensitivity for the Pappadai clay during virgin compression is correct, as must be also the hypothesis of the geological unloading and reloading history of the clay. From the LI profile observed at Pappadai it is shown that deep drying occurred after the erosion of the top 120 metres of clays, which was followed by a rise of the water table up to the present level. The similarity of

the shapes of the LI profile resulting from the modelling of these events and the actual LI profile demonstrates the validity of the reconstructed geological history of the clay From this the value of the geological preconsolidation pressure of Pappadai clay may be accurately derived, and the clay's OCR at the sampling depth is calculated as 3.1.

The modelling of the clay's response during the loading-unloading history, carried out assuming that the natural clay behaved as the reconstituted clay, predicts K_0 values in situ lower than those measured. It is demonstrated that the bonding acquired by the clay following virgin compression is the cause of the higher than expected K_0 values of the natural clay.

9.3. Structural changes occurring in the clay with compression

The natural clay fabric, which appears well packed and well orientated at low magnifications, is in fact far less orientated when observed at higher magnifications. The natural compression of the clay is such as to give rise to particle orientation only in some areas of the fabric, preserving flocculated particle arrangements in other areas. The presence of coarse particles is a cause of the lack of orientation.

The existence of contiguous areas of orientated and flocculated fabric can also be recognized in the one-dimensionally consolidated clay, showing that one-dimensional consolidation of clays gives rise to non-uniform changes of fabric. In some areas the strain localizes and the maximum compaction of the clay particles develops to form stacks of parallel particles. In other areas the volumetric deformation is much less pronounced and the particle aggregates remain flocculated and some pore space is preserved. The observation of areas of one-dimensionally consolidated clay fabrics formed of stacks and regularly alternated flocculated particle arrangements is confirmed by data in the literature.

The changes of fabric due to oedometric compression is very different for the natural and the reconstituted clays. Yield of the natural clay erases the features of the fabric present in the clay before yield, the post-yield fabric being chaotic and irregular. Further compression then reorganizes the fabric, creating a new regular fabric architecture, which again consists of alternating stacks of perfectly orientated particles and areas of flocculated fabric. In contrast, the compression of the reconstituted clay gives rise to a non-uniform compaction of chaotic particle arrangements which seems to reflect the very low porosities of the reconstituted clay at high pressures.

The structure of the natural stiff clay and of the reconstituted clay are therefore different at all stages, and their features actually tend to diverge with increasing compression. The fabric developing in the natural clay with compression beyond yield appears to be very resistant, and it is probably this fabric that also allows the natural clay exhibit a strength higher than that of the reconstituted even at large strains. This new finding supports the approach to structure proposed in the present research, which considers the comparison between natural and reconstituted clays as that between clays of different structure and therefore different sensitivity, rather than between structured and unstructured clays.

9.4. Strain-rate dependency of clays

The study of strain-rate dependency is important in the recognition of similarities between the basic deformation mechanisms of clays of different structure. The discovery of similar strain-rate dependencies for the strongly bonded natural Pappadai clay and the reconstituted clay demonstrates that structure does not change the effects of viscosity on the stress-strain behaviour of the clay.

In order to investigate accurately the strain-rate dependency a revised version of the Wissa theory for consolidation is developed, which is generally more applicable than the original theory. This new theory has been used to interpret the consolidation behaviour of the clay during both CRS and conventional oedometer tests. The primary consolidation in the conventional oedometer tests is also interpreted by using the Terzaghi theory, and the effects of the errors of this theory due to the assumption of no strain-rate dependency are investigated. This investigation has proved to demonstrate the validity of the revised Wissa theory

Strain-rate effects are observed with both the natural and the reconstituted clay, both before and beyond yield. The strain-rate dependency increases with compression beyond yield up to very large strains. The oedometric stiffness of the clay, M, is dependent on both strain-rate and the strain-rate change, and, because of the latter effect, M can vary from zero to infinity. As a result of this the coefficient of consolidation of the clay is also shown to vary, while the clay's coefficient of permeability remains unaffected by the strain-rate.

The analysis of the clay's secondary compression in conventional oedometer tests results in the definition of a unique relationship between the creep coefficient c_α of the clay, the clay stiffness

M, and the effective vertical pressure. This relationship therefore confirms that the mechanisms giving rise to the strain-rate dependency are similar for both natural and reconstituted clays.

9.5. Future Work

The general framework of behaviour of clays proposed in this thesis needs to be further checked by studies of other natural and reconstituted clays using the same approach followed in the present research. There are many sophisticated experimental studies of clay behaviour in the literature which, once complemented by a study of geological history and microstructure, would usefully add to the development of the general behavioural framework proposed here.

Although the literature review shows that frictional behaviour generally applies to soft sensitive clays, it would be of interest to examine if the linear flow rule found for Pappadai clay is generally applicable and whether the friction ratio of natural clays $\mathcal{M}_{nat}$ is generally affected by the clay structure as with the Pappadai clay, or is simply equal to the stress ratio at the critical state. It should be also checked whether the coefficients A of the linear flow rule follow the same pattern of variation observed for the Pappadai clay.

Equally of interest is an understanding of whether the strain-rate dependency is always unaffected by structure, as found here. This can be done by the development for other clays of compression test programmes similar to that presented here.

The framework of behaviour of the natural Pappadai clay should be completed by means of other tests on specimens isotropically compressed beyond yield, and then unloaded to values of YSR greater than one. These data would help to check the isotropic hardening of the SBS of the natural clay.

The high pressure oedometer constructed during the research could be further developed by improving the loading and the strain measurement systems. Both strain-controlled and stress-controlled tests could be carried out if loading were applied by means of a high pressure hydraulic cylinder in line with the loading ram. This would allow both more accurate control of the load in the equilibration stages of the CRS tests, and the development of high pressure OED tests. To eliminate bedding errors and compliance effects the use of small-strain transducers located inside oedometer cell Design 3* is suggested. These should measure the displacement of

the loading plate at the top of the specimen with respect to the fixed steel ring confining the specimen.

REFERENCES

Ackerley S.K., Hellings J.E. and Jardine R.J. (1987), Discussion on : A new device for measuring local axial strains on triaxial specimens, Geotechnique 37, No.3, pp.413-417.

Allmann M.A. and Atkinson J.H. (1992), Mechanical properties of reconstituted Bothkennar Clay, Geotechnique 42, pp.289-302.

Anagnostopoulos A G , Kalteziotis N., Tsiambaos G.K. and Kavvadas M. (1991), Geotechnical properties of the Corinth Canal marls, Geotechnical and Geological Engineering, pp.1-26.

Atkinson J.H. and Bransby P.L. (1978), The Mechanics of Soils. An introduction to Critical State Soil Mechanics, Mc Graw-Hill Book Co., London.

Atkinson J.H. and Richardson D. (1987), The effects of local drainage in shear zones on the undrained strength of the overconsolidated clay, Geotechnique 37, No.3, pp.393-403.

Atkinson J.H., Richardson D. and Stallerbrass S.E. (1990), Effects of recent stress history on the stiffness of overconsolidated soils, Geotechnique 40, No.4, pp.531-540.

Aversa S., Evangelista A., Lerouil S.and Picarelli L. (1993), Some aspects of the mechanical behaviour of structured soils and soft rocks, Proc. Conf. on Geotechnical Engn. of Hard soils-Soft rocks, Athens, Balkema, pp.359-366.

Balasubramaniam A.S. (1969), Some factors influencing the stress-strain behaviour of clay, PhD Thesis, University of Cambridge.

Baldi G., Hight D.W. and Thomas G.E. (1988), A revaluation of conventional triaxial test methods, Advanced Triaxial of Soil and Rock, ASTM STP 977, R.T.Donaghe, R.C.Chaney and M.L.Silver, Eds., ASTM, Philadelphia, pp.219-263.

Bishop A.W. and Henkel D.J. (1962), The measurement of soil properties in the triaxial test, Edward Arnold LTD (London).

Bishop A.W., Webb O.L. and Lewin P.I. (1965), Undisturbed samples of London Clay from the Ashford Common Shaft: strength-effective stress relationships, Geotechnique 15, pp.1-31.

Bishop A.W.and Wesley L.D. (1975), A hydraulic triaxial apparatus for controlled stress path testing, Geotechnique 25, No.4, pp.657-670.

Bjerrum L. (1967), Engineering geology of Norwegian normally-consolidated marine clays as related to settlements of buildings, Geotechnique 17, No.2, pp.81-118.

Blith F.G.H. and de Freitas M.H. (1984), A geology for engineers, 7th Edition 1984, Eduard Arnold LTD, London.

Bolt G.H. (1956), Physico-chemical analysis of the compressibility of pure clays, Geotechnique 6, No.1, pp.86-93.

Bressani L.A. (1990), Experimental properties of bonded soils, PhD thesis, University of London.

Brooker E.W. and Ireland H.O. (1965), Earth pressure at rest related to stress history, Canadian Geotechnical Journal, Vol.1, No.1, pp.1-15.

BS 1377 - Methods of testing for soils (1975), British Standards Institutions, London.

Burghignoli A. (1979), An experimental study of the structural viscosity of soft clays by means of continuos consolidation tests, Proc. of the 7th ECSMFE, Vol.2, pp.23-28.

Burland J.B. (1990), On the compressibility and shear strength of natural clays, Geotechnique 40, No.3, pp.329-378.

Burland J.B., Rampello S., Georgiannou V.N. and Calabresi G. (1996), A laboratory study of the strength of four stiff clays, Geotechnique, in print.

Campanella R.G. and Vaid Y.P. (1972), A simple K0 - triaxial cell, Canadian Geotechnical Journal, Vol.9, No.3, pp.249-260.

Canestrari F. and Scarpelli G. (1993), Stress-dilatancy and strength of Ancona Clay, Proc. of the Conf. on Geotechnical Engn.of Hard soils-Soft rocks, Athens, Balkema, pp.417-424.

Casagrande A. (1936-a), Characteristics of cohesionless soils affecting the stability of slopes and earth fills, Journal of the Boston Soc. Civ. Eng., pp.257-276.

Casagrande A. (1936-b), The determination of the preconsolidation load and its practical significance, Proc. 1st ICSMFE, Harvard University Cambridge, Mass., Vol.3, D34, pp.61-64.

Chandler R.J. (1966), The measurement of residual strength in triaxial compression, Geotechnique 16, No.3, pp.181-186.

Chandler R.J. (1967), Discussion, Proc. Geotechnical Conf. Oslo2, pp.177-178.

Chandler R.J. (1968), A note on the measurement of strength in the undrained triaxial compression test, Geotechnique 18, pp.261-266.

Chandler R.J. (1972), Lias clay: Weathering processes and their effect on shear strength, Geotechnique 22, pp.403-431.

Chandler R.J. and Gutierrez C.I. (1986), The filter-paper method of suction measurement, Geotechnique 36, No.2, Technical note, pp.235-238.

Chandler R.J. and Apted J.P. (1988), The effects of weathering on the strength of London Clay, Quarterly Journal of Engineering Geology, London, Vol.21, pp.59-68.

Ciaranfi N., Nuovo G. and Ricchetti G. (1971), Le argille di Taranto e di Montemesola (Studio Geologico, Geochimico e Paleontologico), Boll.Soc. Geol. It., pp.293-314.

Ciaranfi N., Pieri P. and Ricchetti G. (1988), Note alla carta geologica delle Murge e del Salento (Puglia Centromeridionale), Mem.Soc.Geol.Italia, 41, pp.449-460.

Clarke B.G. and Allan P.G. (1989), A self-boring pressuremeter for testing weak rock, Proc 12th ICSMFE, Rio De Janeiro, Vol.1, pp.211-214.

Clarke B.G. (1992), Introduction to pressuremeters, choice of a testing system and an overview of systems currently available, Technical Seminar on Pressuremeters for Design in Geotechnics, Chorleywood, Hertfordshire.

Clarke B.G. (1992-a), Interpretation of data for the assessment of design parameters from tests in clays and rocks, Technical Seminar on Pressuremeters for Design in Geotechnics, Chorleywood, Hertfordshire.

Clarke B.G. (1992-b), The interpretation of self-boring pressuremeter tests to produce design parameters, Technical Seminar on Pressuremeters for Design in Geotechnics, Chorleywood, Hertfordshire.

Clayton C.R.I. and Khatrush S.A. (1986), A new device for measuring local axial strains on triaxial specimens, Geotechnique 36, No.4, pp.593-597.

Coop M.R. (1990), The mechanics of uncemented carbonate soils, Geotechnique 40, No.4, pp.607-626.

Coop M.R. and Atkinson J.H. (1993), The mechanics of cemented carbonate sands, Geotechnique 43, No.1, pp.53-67.

Coop M.R., Atkinson J.H. and Taylor R.N. (1995), Strength, yielding and stiffness of structured and unstructured soils, Proc. 11th ECSMFE, Copenhagen 1, pp.55-62.

Coop M.R. and Cotecchia F. (1995), The compression of sediments at the archaeological site of Sibari, Proc. 11th ECSMFE, Copenhagen 8, pp.19-26.

Cotecchia F. (1990), Study of the relationships between the undrained shear strength of clay and its overconsolidation ratio. Analysis of the application of these relationships to the undrained shear strength values of six soft clays and two highly overconsolidated natural clays, Msc Dissertation, Imperial College, University of London

Cotecchia V., Federico A. and Trizzino R. (1982-a), Microtessiture di sedimenti argillosi. Analisi delle tipologie e terminologie, ed applicazione nel campo della geotecnica, Geologia Applicata e Idrogeologia, Vol.17, pp.1-34.

Cotecchia V., Federico A. and Trizzino R. (1982-b), Microtessiture di sedimenti argillosi. Esperimenti su Kaolinite e Bentonite ed esempi di sedimenti argillosi dell'Italia Meridionale, Geologia Applicata e Idrogeologia, Vol.17, pp.53-78.

Cotecchia V., Melidoro G., Romanazzi L. and Spilotro G. (1977), Osservazioni sul comportamento geotecnico delle Argille di Taranto determinato da alcuni caratteri geologici, Geologia Applicata e Idrogeologia, Vol.12, pp.311-323.

Cotecchia V., Monterisi L., Sembenelli P. and Claps G.A. (1993), La costruzione dell'invaso Pappadai in Puglia, Quarry and Construction, N.10, October, pp.87-97.

Cotecchia V. and Tafuni N. (1996), in preparation.

Crawford C.B. (1965), The resistance of soil structure to consolidation, Canadian Geotechnical Journal, Vol. II, no. 2, pp.90-97

Cuccovillo T. and Coop.M.R. (1996), The measurement of local axial strains in triaxial tests using LVDT's, Geotechnique, Technical note, in print.

Davis E.H. and Raymond G.P. (1965), A non linear theory of consolidation, Geotechnique 15, No. 2, pp.161-173.

Davison L.R. and Atkinson J.H. (1990), Continuous loading oedometer testing of soils, Quarterly Journal of Engineering Geology, London, Vol. 23, pp.347-355.

Dell'Anna L. and Laviano R. (1991), Mineralogical and Chemical classification of Pleistocene clays from the Lucanian Basin (Southern Italy) for the use in the Italian tile industry, Applied Clay Science, 6, pp.233-243.

Del Prete M. and Valentini G. (1991), Le caratteristiche Geotecniche delle Argille Azzurre dell'Italia Sud-Orientale in relazione alle differenti situazioni stratigrafiche e tettoniche, Geologia Applicata e Idrogeologia, Vol.6, pp.197-215.

De Marco A, Moresi M. and Nuovo G. (1981), Le argille dei bacini di Taranto e di Grottaglie-Montemesola : caratteri granulometrici, mineralogici e chimici, Società Italiana di Mineralogia e Petrografia, 37, pp.241-266.

Desrues J. (1992), Strain localisation in geomaterials: experimental basis, Programma di Istruzione Permanente, Politecnico di Milano.

Gens A. (1982), Stress-strain and strength characteristics of a low plasticity clay, PhD Thesis, London University.

Gens A. and Potts D.M. (1982), Application of critical state models to the prediction of the behaviour of a normally consolidated low plasticity clay, Proc. Int. Symp. of Numerical Models in Geomechanics, Zurich, 13-17, pp.312-323.

Gens A. and Potts D.M. (1982), A theoretical model for the describing the behaviour of soils not obeying Rendulic's principle, Proc. Int. Symp. of Numerical Models in Geomechanics, Zurich, 13-17, pp.24-32.

Georgiannou V.N., Burland J.B. and Hight D.W. (1990), The undrained behaviour of clayey sands in triaxial compression and extension, Geotechnique 40, No.3, pp.431-449.

Ghionna V. et al. (1983), Evaluation of self-boring pressuremeter, Proc. Int. Symposium on In situ Testing, Paris, Vol.2, pp.294-301.

Gibson R.E. and Henkel D.J. (1954), Influence of duration of tests at constant rate of strain on measured drained strength, Geotechnique 1, No.4, pp.6-32.

Gibson R.E. and Anderson W.F. (1961), In situ measurements of soil properties with pressuremeter, Civ. Engng. Public. Wks. Rev. Vol.56, No.658, pp.615-618.

Gibson R.E. and Lo K.Y. (1961), A theory of consolidation for soil exhibiting secondary compressions, Report No. 41, Norwegian Geotechnical Institute, pp.3-16.

Graham J., Crooks J.H.A. and Bell A.L. (1983), Time effects on the stress-strain behaviour of natural clays, Geotechnique 33, No.2, pp.327-340.

Graham J., Crooks J.H.A. and Lau S.L.K. (1988), Yield envelopes: identification and geometric properties, Geotechnique 38, No.1, pp.125-134.

Griffith F.J. and Joshy R.C. (1990), Clay fabric response to consolidation, Applied Clay Science, 5, pp.37-66.

Hanzawa H., Smith K. and Kurihara M. (1990), Shear strength and consolidation yielding stress of Pleistocene clay found at Izumi-Hill of Osaka district, Soils and Foundations, Vol.30, No.1, pp.129-141.

Hawkins A.B. and Mc Donald C. (1992), Decalcification and residual shear strength reduction in Fuller's Earth Clay, Geotechnique 42, No.3, pp.453-464.

Head K.H. (1980) Manual of soil laboratory testing, 3 Vols., London, Plymouth, Pentek.

Henkel D.J. (1956), The effects of overconsolidation on the behaviour of clays during shearing, Geotechnique 6, pp.139-150.

Henkel D.J. (1960), The relationships between the effective stresses and water content in saturated clays, Geotechnique 10, pp.41-54.

Hight D.W. (1982), A simple piezometer probe for the routine measurement of pore pressure in triaxial tests on saturated soils, Technical Note, Geotechnique 32, No.4, pp.396-401.

Horseman S.T., Winter M.G. and Entwistle D.C. (1987), Geotechnical characterization of Boom Clay in relation to disposal of radioactive waste, Luxembourg: Office for Official Publications of the European Community.

Hvorslev M.J. (1937), Uber die Festigkeitseigenschaften Gestorter Bindiger Boden (On the strength properties of remoulded cohesive soils), Thesis, 159 pages, Copenhagen.

Jaky J. (1944), The coefficient of earth pressure, J.Soc. Hungarian Archit. Engrs.

Jamiolkowsky M., Ladd C.C., Germain J.T., Lancellotta R. (1985), New developments in field and laboratory testing of soils, Proc. 11th ICSMFE, San Francisco, Vol.2, pp.57-153.

Janbu N. and Senneset K. (1979), Interpretation procedures for obtaining soil deformation parameters, Proc. of the 7th ECSMFE, 1, pp.185-188.

Janbu N., Tokheim O. and Senneset K. (1981), Consolidation tests with continuous loading, Proc. 10th ICSMFE, Stockholm 1, pp.645-654.

Jardine R.J. (1992), Some observations on the kinematic nature of soil stiffness, Soils and Foundations, Vol.32, No.2, pp 111-124.

Jezequel J.F., Lemasson H. and Touze J. (1968), Le pressiometre Louis Menard: Quelques problemes de mise en oevre et leur influence sur les valeurs pressiometriques, Bulletin de LCPC, No.32, pp.97-120.

Lacasse S., Berre T. and Lefebvre G. (1985), Block sampling of sensitive clays, Proc.11th ICSMFE, San Francisco, Vol.2, pp.887-892.

Ladd C.C. and Lambe T.W. (1963), The strength of undisturbed clay determined from undrained tests, ASTM, STP 361, pp.342-371.

Ladd C.C., Foot R., Scholosser F. and Poulos H.G. (1977), Stress deformation and strength characteristics: State of the Art report", Proc. 9th ICSMFE, Tokio, pp.421-494.

Lagioia R. and Nova R. (1993), A constitutive model for soft rocks, Proc. Conf. on Geotechnical Engn. of Hard soils - Soft rocks, Athens, Balkema, pp.625-632.

Lambe T.W. (1953), The structure of inorganic soils, Proc. A.S.C.E., 79, Separate n.315

Lambe T.W. and Withmann R.V. (1969), Soil Mechanics, John Wiley & Sons Inc., New York.

Leonards G.A. and Ramiah B K. (1959), Time effects in the consolidation of clay, ASTM Special technical publication No.254, pp.116-130.

Lerouil S., Tavenas F., Brucy F., La Rochelle P., Roy M. (1979), Behaviour of destructured natural clays, Proc.A.S.C.E. 105, GT6, pp.759-778.

Lerouil S., Sanson L and Bozozuk M. (1983), Laboratory and field determination of preconsolidation pressure at Gloucester, Canadian Geotechnical Journal 20, No.3, pp.477-490.

Lerouil S., Tavenas F. and Locat J. (1984), Discussion on : Correlations between index tests and the properties of remoulded clays - Carrier W.D. and Beckman J.F., 1984 (Geotechnique). Geotechnique 35, No.2, pp.223-226.

Lerouil S., Kabbaj M., Tavenas F. and Bouchard R. (1985), Stress-strain rate relation for the compressibility of sensitive natural clays, Geotechnique 35, No.2, pp.159-180.

Lerouil S. and Vaughan P.R.(1990), The important and congruent effects of structure in natural soils and weak rocks, Geotechnique 40, No.3, pp.467-488.

Leroux A.(1975), Les differentes textures. Leur influence sur le comportment des sols argileux et marneux, Geologia Applicata e Idrogeologia, Vol.10, pp.67-85.

Loudon P.A. (1967), Some deformation characteristics of Kaolin, PhD Thesis, University of Cambridge.

Lowe J., Jonas E. and Obrician V. (1969), Controlled gradient consolidation test, Jour. Soil Mechanics and Found. Div. ASCE, Vol. 95, SM1 Jan. 1969, pp.77-97.

Lupini J.F., Hight D.W. and Cavounidis S. (1980), Some observations of microfabric and their role in understanding soil behaviour, Rivista Italiana di geotecnica, No.2, pp.112-123.

Maccarini M. (1987), Laboratory studies of weakly bonded artificial soil, PhD Thesis, University of London.

Maire R.J. and Wood D.M. (1987), Pressuremeter testing, methods and interpretation, Ciria, Project 335, Butterworths, London.

Marhinho F.A.M. (1994), Shrinkage behaviour of some plastic soils, PhD thesis, University of London.

Mayne P.W. and Kulhaway F.H. (1982), K0-OCR relationships in soil, Proc.ASCE, 108, GT6, pp.851-872.

Menkiti C.O. (1995), Behaviour of clay and clayey-sand with particular reference to principal stress rotation, PhD thesis, University of London.

Mesri G. and Rokhsar A. (1974), Theory of consolidation for clays. Proc. ASCE, 100, GT8, pp.889-904.

Mesri G. and Godlewsky P.M. (1977), Time and stress-compressibility interrelationship, Proc. ASCE, 103, GT5, pp.417-430.

Mesri G. and Godlewsky P.M. (1979), Time and stress-compressibility interrelationship, Discussion, Proc.ASCE (May), GT1, pp.106-113.

Mesri G. and Choi Y.K. (1985), The uniqueness of the End of Primary (EOP) void ratio - effective stress relationships. Proc. 9th ICSMEF, San Francisco, pp.587-590.

Mitchell J.K. and Houston W.N. (1969), Causes of clay sensitivity, Proc. ASCE, SM3, pp.845-871.

Mitchell J.K. (1976), Fundamentals of soil behaviour, New York, Wiley.

Mokni M. (1992), Relations entre le comportement en masse et la localisation de la deformation dans le materiaux granulaires, These de doctorat, UJF-INPG.

Nova R. and Wood D.M. (1979), A constitutive model for sand in triaxial compression, Int. Journal for Numerical Methods in Geomechanics, 3, pp.255 278.

O'Brien N.R. and Slatt R.M. (1990), Argillaceous Rock atlas, Springer Velag.

Ogniben L. (1969), Schema introduttivo alla geologia del confine calabro-lucano, Memorie della Società Geologica Italiana, 8.

Palmer A.C. (1972), Undrained plane strain expansion of a cavity in clay: a simple interpretation of the pressuremeter test, Geotechnique Vol.22, No 3, pp.451-457.

Parry R.H.G. (1958), Correspondence on " On the yielding of soils", Geotechnique 8, pp.184-186.

Parry R.H.G. (1960), Triaxial compression and extension tests on remoulded saturated clay, Geotechnique 10, pp.166-180.

Pender M.J. (1978), A model for the behaviour of overconsolidated soil, Geotechnique 28, No.1, pp.1-25.

Pickles A.R. (1989), The application of critical state soil mechanics to predict ground deformations below an embankment constructed on soft alluvium, PhD Thesis, City University, London.

Push R. (1966), Quick clay microstructure, Engineering Geology, Vol.1, No.6, pp.433-443.

Rampello S. (1993), Compressibilità di campioni indisturbati e ricostituiti di alcune argille consistenti, Gruppo Nazionale di Coordinamento per gli studi di Ingegneria Geotecnica, CNR, Attività di Ricerca anno 1992-93.

Rampello S., Viggiani G. and Georgiannou V.N. (1993), Strength and dilatancy of natural and reconstituted Vallericca Clay, Proc. Conf. on Geotechnical Engn. of Hard soils-Soft rocks, Athens, Balkema, pp.761-768.

Rampello S. and Silvestri F. (1993), The stress-strain behaviour of natural and reconstituted samples of two overconsolidated clays, Proc. Conf. on Geotechnical Engn. of Hard soils-Soft rocks, Athens, Balkema, pp.769-778.

Rendulic L. (1936), Pore-index and Pore-water Pressure, Baningeenieur 17, pp.559.

Ricchetti G. (1967), Osservazioni preliminari sulla geologia e morfologia dei depositi quaternari nei dintorni del Mar Piccolo (Taranto), Atti Acc.Gioenia in Catania, S.6, 18,1967, pp.123-130.

Ridley A.M. (1993), The measurement of soil moisture suction, PhD thesis, London University.

Roscoe K.H., Schofield A.N. and Wroth C.P. (1958), On the yielding of soils, Geotechnique 8, pp.22-53.

Roscoe K.H. and Poorooshasb H.B. (1963), A theoretical and experimental study of strain in triaxial compression tests on normally consolidated soils, Geotechnique 13, No.1, pp.12-38.

Roscoe K.H. and Burland J.B. (1968), On the generalized stress-strain behaviour of wet clay, In Engineering Plasticity (J.Heymann and F.A.Leckie, eds), Cambridge University Press, Cambridge, pp.535-609.

Rosenqvist I.T. (1963), The influence of physico-chemical factors upon the mechanical properties of clays, Norwegian Geotechnical Institution, Publ. n.54, pp.1-19.

Rossato G., Ninis N.L. and Jardine R.J. (1992), Properties of some kaolin-based model clay soils, Geotechnical Testing Journal, GTJODJ, Vol.15, No.2, pp.166-179.

Rowe P.W. (1962), The stress-dilatancy relation for static equilibrium of an assembly of particles in contact, proc. R. Soc. A., 264, pp.500-527.

Rowe P.W. and Barden L. (1966), A new consolidation cell, Geotechnique 16, pp.162-170.

Samuels S.G. (1975), Some properties of the Gault Clay from Ely-Ouse Essex water tunnel, Geotechnique 25, No.2, pp.239-264.

Sandroni S. (1977), The strength of London Clay in total and effective stress terms, PhD Thesis, London University.

Schmertmann J.H. (1969), Swell sensitivity, Geotechnique 19, No.41, pp 530-533

Schmidt B. (1966), Discussion on: Earth pressure at rest related to stress history, Canadian Geotechnical Journal, Vol.3, No.4, pp.237-242.

Schofield A.N. and Wroth C.P. (1968), Critical State Soil Mechanics, Mc Graw-Hill Book Co., London.

Schreiner H.D. (1988), Volume change of compacted highly plastic clays, PhD thesis, London University.

Sfondrini G. (1975), Caratteri microtessiturali e microstrutturali di alcuni sedimenti argillosi connessi con la natura e il tipo delle sollecitazioni subite, Geologia Applicata ed Idrogeologia, 10, parte 2, pp.87-124.

Sides G. and Barden L. (1970), The microstructure of dispersed and flocculated samples of kaolinite, illite and montmorillonite, Canadian Geotechnical Journal, 8, pp.391-399.

Skempton A.W. and Bishop A.W. (1950), Measurement of shear strength of soils, Discussion by A.W.Bishop, Geotechnique 2, No.2, pp.113-120.

Skempton A.W. and Northey R.D. (1952), The sensitivity of clays, Geotechnique 3, No.1, pp.30-53.

Skempton A.W. (1953), The colloidal activity of clays, Proc. 3rd ICSMFE, Zurich, 1, pp.57-61.

Skempton A.W. (1954), The structure of inorganic soil, Proc.ASCE, SM3, Vol.80, No.478, pp.19-22.

Skempton A.W. (1954-a), The pore-pressure coefficients A and B, Geotechnique, Vol.4, pp.143-147.

Skempton A.W. (1961) Horizontal stresses in an overconsolidated Eocene clay, Proc. 5th ICSMFE, Paris 1, pp.351-357.

Skempton A.W. and Sowa V.A. (1963), The behaviour of saturated clays during sampling and testing, Geotechnique, Vol.13, No.4, pp.269-290.

Skempton A.W. (1970), The consolidation of clays by gravitational compaction, Q.J. Geological Soc. No.125, pp.373-411.

Smart P. and Tovey N.K. (1981), Electron microscopy of soils and sediments: examples, Oxford University Press, pp.178.

Smart P. and Tovey N.K. (1982), Electron microscopy of soils and sediments: techniques, Oxford University Press, pp.264.

Smith P.R. (1992), The behaviour of natural high compressibility clays with special reference to consolidation on soft ground, PhD Thesis, London University.

Smith P.R., Jardine R.J. and Hight D.W. (1992), On the yielding of Bothkennar clay, Geotechnique 42, pp.257-274.

Suklje L. (1969), Rheological aspects of soil mechanics, London, Wiley-Interscience.

Tavenas F. and Lerouil S. (1985), Discussion, Proc. 11th ICSMFE, San Francisco 5, pp.2693-2694.

Taylor D.W. (1948), Fundamentals of soil mechanics, John Wiley and Sons, New York.

Tchalenko J.S. (1967), The influence of shear and consolidation on the microscopic structure of some clays, PhD thesis, London University.

Terzaghi K. (1925), Erdbaumechanik auf Bodenphysikalischer Grundlage, Leipzig, Deuticke, 399 pp.

Terzaghi K. (1944), Ends and means in Soil Mechanics, Engineering Journal (Canada), Vol 27, pp.608.

Terzaghi K. and Peck R.B. (1967), Soil Mechanics in Engineering Practice, John Wiley and Sons, New York.

Tillard-Ngan D., Desrues J., Raynaud S. and Mazerolla F. (1992), Strain localisation in the Beaucaire marl, Structure and Mechanical Behaviour of Geomaterials, pp.1-16.

van Eekelen H. and Potts D.M. (1978), The behaviour of Drammen Clay under cyclic loading, Geotechnique 28, No.2, pp.173-196.

Veniale F. (1983), Consolidamento e stabilizzazione dei terreni argillosi mediante diffusione di sali (KCl), Ingegneria Ferroviaria, Vol.6, pp.1-9.

Veniale F. (1985), The role of microfabric in clay soil stability, Miner. Petrogr. Acta, Vol.29-A, pp.101-119.

Veniale F. (1993), Private Communication.

Viggiani G., Rampello S. and Georgiannou V.N. (1993), Experimental analysis of localization phenomena in triaxial tests on stiff clays, Proc. Conf. on Geotechnical Engn. of Hard soils-Soft rocks, Athens, Balkema, pp.849-856.

Viggiani G. and Atkinson J.H. (1995), Stiffness of fine-grained soil at very small strains, Geotechnique 45, No.2, pp.249-265.

Webb D.L. (1964), The mechanical properties of undisturbed samples of London Clay and Pierre shale, PhD thesis, London University.

Wenk H.R. (1976), Electron-Microscopy in Mineralogy, Springer Velag, Berlin Heidelberg New York.

Wiewiora A., Sanchez-Soto P.J., Aviles M.A., Justo A. and Perez-Rodriguez J.L. (1993), Effect of grinding and leaching on polytypic structure of pyrophyllite, Applied Clay Science, 8, pp.261-282.

Windle D. and Wroth C.P. (1977), The use of a self-boring pressuremeter to determine the undrained properties of clays, Ground Engng, Vol.10, No.6, pp.37-46.

Wissa A.E.Z., Christian J.T., Davis E.H. and Heiberg S. (1971), Consolidation at constant rate of strain, Proc. ASCE, 97, SM10, pp.1393-1413.

Wroth C.P. (1958), Shear behaviour of soils, PhD Thesis, Cambridge University.

Wroth C.P. (1984), The interplay of in situ soil tests, Geotechnique 34, No.4, pp.449-489.

APPENDIX 6.1

Design of the loading ram in the high pressure oedometer

In the present appendix the calculation is reported which was carried out to check the design of the loading ram of the Design 3 oedometer cell for safety against buckling. This calculation refers to the ram used in the cell during the CRS tests with the high pressure oedometer whose diameter D was 15.79 mm. The boundary conditions for the loading ram during the high pressure tests were as shown in Fig.A.6.1.1(a). To check the design for safety the ram was assumed to be a free cantilever (Fig.A.6.1.1(b)), which represents a conservative boundary condition. The condition (b) in the figure is equivalent to the condition indicated as (c), the latter being the one used for the calculation of the Euler stress. The expression of the Euler stress σ_e is as follows:

$$\sigma_e = \pi^2 E I / [(L)^2 \mathcal{A}] \qquad (A.6.1.1)$$

where E, L, I and $\mathcal{A}$ are defined in the following:

E : Young's modulus of steel, equal to 206KN/sqmm;

L : length of the beam, i e. 20cm as shown in Fig. A.6.1.1(c);

I : moment of inertia ($= \pi D^4/64$);

$\mathcal{A}$: area of the ram, equal to 1 96sqcm.

The Euler stress for the beam in Fig A.6 1.1(b) is then equal to:

$$\sigma_e = 791 \text{ MPa} \qquad (A.6\ 2\ 1)$$

σ_e would give rise to a load of 158 kN on the ram in Fig 6 5(b) (Design 3), that is much higher than the capacity of the load cell used in the tests, i.e. 70 kN. The loads which had to be reached during testing were then far below the ones causing buckling of the ram.

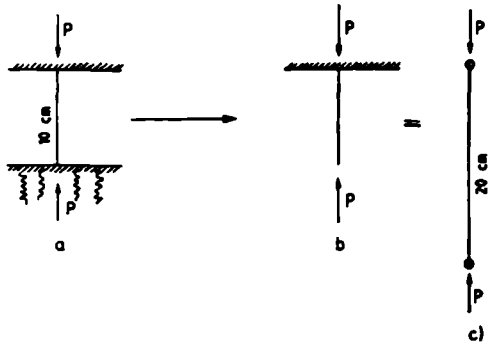

Fig A.6.1.1. Loading ram of the oedometer cell Design 3 : boundary conditions assumed in the calculation of the Euler stress.

APPENDIX 6.2

Use of the Gibson and Lo model (1961) to interpret the behaviour of soil during creep and the strain-rate dependency of the soil

Gibson and Lo (1961) presented a mathematical model of 1D consolidation applying to soils exhibiting secondary compression. The model representation of the soil skeleton that they used is shown in Fig 6.27; this is formed of a Hooke an spring in series with a Kelvin or Voigt body. In the figure the constants a, b and μ representing the parameters of behaviour of the three elements forming the rheological model are shown.

(*a*) Soil compression under a step increment of load

Gibson and Lo outlined the process of consolidation as follows. When a stress increment σ is applied to the clay element, because of primary consolidation the transferral of stress to the soil skeleton is delayed and the effective stress increases with time: $\sigma'(t)$. Hence the compression of spring a in Fig.6.27 is gradual and is fully accomplished only when the applied stress has become fully effective. Under $\sigma'(t)$ the Kelvin body compresses, the load being initially fully taken from the Newtonian dashpot μ and then progressively transferred to the spring b. This process of transference corresponds to the secondary compression which occurs under the current sustained $\sigma'(t)$. Only after long time the full effective stress will be taken through springs a and b, the dashpot sustaining no load. Gibson and Lo expressed the process of transferral of load from μ to b with the relationship:

$$\sigma'(t) = \varepsilon_c/b + (d\varepsilon_c/dt)/\mu \qquad \text{(A.6.2.1)}$$

where ε_c is equal to the strain of the Kelvin body. The corresponding total settlement of the soil element is equal to the sum of the settlement related to ε_c and the settlement related to the strain in a, ε_a ($=\sigma'(t)/a$).

In the present research the equation (A.6.2.1) from Gibson and Lo (1961) was used to investigate the stress-strain relationship of the soil during creep. After primary consolidation σ' becomes

almost constant with time and equal to σ, being negligible the excess pore water pressure still present in the soil At this stage eq (A 6 2 1) becomes ·

$$\sigma' = \sigma = \varepsilon / b + (d\varepsilon_c / dt)/\mu \qquad (A\ 6\ 2\ 2)$$

which is here considered to represent the stress-strain relationship of the Kelvin body during creep At this stage the compression of the Hookean element is complete and the strain increment $\Delta\varepsilon_c$ is the only source of settlement for the soil. $\Delta\varepsilon_c$ can be considered equal to the soil strain increment $\Delta\varepsilon$. The strain rate of the soil during creep can be consequently derived from eq.(A 6 2 2) as ·

$$d\varepsilon / dt = (\sigma' - \varepsilon_c / b)\ \mu \qquad (A.6\ 2\ 3)$$

The strain rate during creep then depends on both the constants b and μ which are respectively related to the soil stiffness and structural viscosity. From eq.(A.6.2.3) a relationship between the creep coefficient c_α and the soil stiffness and viscosity was derived as follows During creep the soil strain increments are equal to:

$$d\varepsilon = c_\alpha\ d\log(t) / (1+e_0) \qquad (A\ 6\ 2.4)$$

where c_α is usually assumed to be constant. Then the creep strain rate is given by the equation :

$$d\varepsilon/dt = [c_\alpha /(1+e_0)]\ d\log(t)/dt = c_\alpha /[(1+e_0)t] \qquad (A\ 6\ 2\ 5)$$

showing that the strain rate reduces with time. From eqs.(A.6 2.3) and (A.6 2 5) an expression for c_α can be derived, which is :

$$c_\alpha /[(1+e_0)t] = (\sigma' - \varepsilon_c/b)\ \mu \qquad (A\ 6\ 2\ 6)$$

If in eq (A.6.2.6) the compressibility of the element b is replaced with its stiffness M_b and the structural viscosity is defined as $1/\mu$ equal to β, than c_α can be expressed as

$$c_\alpha /[(1+e_0)t] = (\sigma' - \varepsilon_c M_b)/ \beta \qquad (A\ 6\ 2\ 7)$$

Eq (A 6 2 7) then defines the dependency of c_α on the applied stress σ', on the clay stiffness and structural viscosity c_α is expected to be smaller for stiffer soils and for soils of higher viscosity and to increase with increasing stress and when the compressibility of the soil increases

(*b*) Soil compression under a controlled strain rate

When a strain rate $d\varepsilon/dt$ is applied to the soil element, the Hookehan spring responds with a stress $\sigma_a'(t)$ equal to $\varepsilon_a(t)/a$, where ε_a is the strain in the Hookehan spring when the soil element is subjected to ε. In the Kelvin body two different stresses arise in the two elements, which are :

$$\sigma_b'(t)= (\varepsilon- \varepsilon_a)/b \quad \text{and} \quad \sigma_\mu'(t) = [d(\varepsilon-\varepsilon_a)/dt]/\mu \qquad \text{(A 6.2.8)}$$

whose sum is equal to σ'_a. The stress increment then necessary for a strain increment ε is :

$$\sigma'(\varepsilon) = \sigma'_a(\varepsilon) = (\varepsilon- \varepsilon_a)/b + [d(\varepsilon- \varepsilon_a)/dt]/\mu \qquad \text{(A.6.2 9)}$$

Eq.(A.6.2.9) shows that if the soil is represented by the three element rheological model in Fig 6 27, the compression curve of the soil ε-σ' depends on the current strain rate $d\varepsilon/dt$ the soil is experiencing.

APPENDIX 6.3

Theoretical solution of CRS one-dimensional consolidation

In this appendix the solution of CRS consolidation according to Wissa et al (1971) is briefly reviewed. In addition, a solution similar to that given by Wissa, but which reduces the error intrinsic to its hypotheses is proposed.

The basic differential equation of the Wissa's solution

$$c_v \, \partial^2\varepsilon_v / \partial z^2 = \partial\varepsilon_v / \partial t \qquad \text{(A.6.3 1)}$$

assumes that the strains are small, and c_v is constant, with z being the distance from the drainage boundary as shown in Fig.A.6.3.1. Equation (A.6.3.1) was reformulated by Wissa making the displacement v explicit as follows :

$$\partial^3\mathcal{V} / \partial X^3 = \partial^2\mathcal{V} / \partial X \partial T_v \qquad \text{(A.6.3.2)}$$

where : $\mathcal{V} = v/H$, $T_v = c_v t/H^2$ and X= z/H, H being the distance of the undrained boundary from the free drainage boundary at the start of consolidation. H coincides with the initial height of the sample h if the sample drains only from one side (Fig.A.6.3.1). For simplicity T_v will be referred to as T in the following.

The solution of equation (A.6.3.2) for a unit constant step displacement $\mathcal{V}(0,T)=1$ applied at T=0 is :

$$\mathcal{V}(X;T) = (1-X) - \Sigma_{n=1\to\infty} [2\sin(n\pi X) \exp(-n^2\pi^2 T)] / n\pi \qquad \text{(A.6.3.3)}$$

in which c_v is constant not only with z, but also with T. Wissa used the following superimposition integral :

$$\mathcal{V}(X;T) = \int_0^T \mathcal{V}(X,T-\tau) \, \partial\mathcal{V}(0;T) / \partial T \, d\tau \qquad \text{(A.6.3.4).}$$

$\partial\mathcal{V}(0,T)/\partial t$ (reported simply as $\partial\mathcal{V}/\partial t$ in the following) is equal to the current average strain-rate down the specimen r. Wissa et al. assumed r to be constant and $\mathcal{V}(0,T)$ to be equal to rt (= $T[rH^2/c_v]$). Wissa et al. then integrated equation (A.6.3.4) over the entire T assuming that both c_v

and r are constant with T and therefore $\partial \mathcal{V}/\partial T$ is equal to $rH^2 c_v$ A graphic representation of the process underlying the superimposition integral (A 6 3 4) is shown in Fig A 6 3 2 In Fig A 6 3 2(a) an ideal representation is reported of the function $\mathcal{U}(X,T-\tau_n)\partial\mathcal{U}\partial T$ according to Wissa et al., as c_v and r were assumed to be constant with T The function $\mathcal{U}(X,T-\tau_n)\partial\mathcal{U}\partial T$ is plotted against T for different τ_n In order to explain the integration process used by Wissa et al and the way it may be modified, the integral A 6 3.4 for $T=T_i$ is interpreted as sum of the products $[\mathcal{U}(X,T-\tau_n)\partial\mathcal{U}\partial T]\ \Delta\tau$ Following this approach the result of the integration A 6 3 4 is $\Sigma_{n=0\rightarrow i}\ [\mathcal{U}(X;T-\tau_n)\partial\mathcal{U}\partial T]\ \Delta\tau$, in which τ_0 equals zero, τ_n equals $(\tau_{n-1}+\Delta\tau)$ and τ_i equals Ti This schematic solution of the integral A.6.3.4 is shown in Fig.A 6.3.2(a) according to Wissa's hypotheses.

The Wissa's solution of integral (A 6.3.4) is then :

$$\mathcal{U}(X;T) = rH^2/c_v\ [(1-X)T - 2\Sigma_{n=1\rightarrow\infty} \sin(\pi nX)(1-\exp(-n^2\pi^2T)) / n^3\pi^3] \qquad \text{(A.6 3 5)}$$

The strain function from Wissa et al. was then as follows :

$$\varepsilon_v(X;T) = rH^2/c_v\ \{T + (3X^2-6X+2)/6 - [2\Sigma_{n=1\rightarrow\infty} \cos(\pi nX)\exp(-n^2\pi^2T)/n^2\pi^2]\ \} \qquad \text{(A.6 3 6)}$$

which shows that at any z the CRS consolidation gives rise to a permanent strain component ε_p as well as to a time dependent strain component ε_t:

$$\varepsilon_p = rH^2\ (3X^2-6X+2) / (6c_v) \qquad \text{(A 6 3 7)}$$

$$\varepsilon_t = -rH^2/c_v\ [2\Sigma_{n=1\rightarrow\infty} \cos(\pi nX)\exp(-n^2\pi^2T) / n^2\pi^2]$$

in addition to the average strain rt

The assumption of a constant c_v with time during the CRS test is the least adequate among all Wissa's assumptions with respect to the real behaviour of clays, especially if the consolidation develops in a large stress interval For times when steady conditions have been reached and thus the strain component ε_t is negligible, from equation (A.6.3.6) Wissa et al.(1971) derived the equations :

$$\Delta\varepsilon_v\ (t_i-t_{i-1}) = r\ (t_i-t_{i-1}) \qquad \text{(A.6.3 8)}$$

for the strain increment in the time interval $t_i - t_{i-1}$, and the equation :

$$\Delta\varepsilon_v (0\text{-}H) = rH^2 \quad (2c_v(t)) \qquad \text{(A 6 3 9)}$$

for the strain difference between the top and bottom of the specimen at a given time t.

From these equations, disregarding that c_v had been assumed to be constant, Wissa et al.(1971) none-the-less derived a c_v changing with time during the test, which for linear elastic behaviour was as follows:

$$c_v(t) = \Delta\sigma_v(t)\, H^2 / (2\Delta t\, u_b(t)) \qquad \text{(A.6.3.10)}$$

However, this equation is somehow inconsistent with the integration which yields the equation (A.6.3.5). The error concerning Wissa's assumption of $c_v(t)$ being constant can be limited as illustrated here below

The superimposition integral can be split into a sequence of integrals for successive time intervals $0\text{-}T_1$, $T_1\text{-}T_2$,..$T_{i-1}\text{-}T_i$. Equation (A.6.3.5) can be used with no significant error as integration of (A 6.3.4) in an initial small time interval $(0,T_1)$, where c_v and r can be assumed to be constant. The c_v and r values used in the integration in this interval would than be c_{v1} and r_1 The gradient $\partial\mathcal{U}\partial T$ (at X=0) for this integration would then be equal to r_1H^2/c_{v1}(see Fig A.6 3 2(b)) This integration would give rise to the displacement function $\mathcal{V}_1$ (T) :

$$\mathcal{V}_1(X;T) = \int_0^T \mathcal{U}(X;T-\tau)\partial\mathcal{U}\partial T\, d\tau = r_1H^2/c_{v1}\ [(1-X)T - 2\Sigma_{n=1\to\infty} \sin(\pi nX)(1-\exp(-n^2\pi^2T))/n^3\pi^3] \qquad \text{(A.6.3.11)}$$

for $0<T<T_1$.

For $T>T_1$, the displacement functions $\mathcal{V}_1$, generated in the time interval $0\text{-}T_1$, gives rise to the displacement component (see Fig A 6 3 2(b)) :

$$\mathcal{V}_1(X;T) = \int_0^{T_1} \mathcal{U}(X;T-\tau)\partial\mathcal{U}\partial T\, d\tau = r_1H^2/c_{v1}\ \{ (1-X)T_1 - 2\Sigma_{n=1\to\infty} \sin(\pi nX)[\exp(-n^2\pi^2(T-T_1)) - \exp(-n^2\pi^2T)]/n^3\pi^3\} \qquad \text{(A.6.3 12)}$$

In the successive time interval T_1-T_2, eq (A 6 3 4) can be integrated using the c_{v2} and r_2 values corresponding to the new time interval, giving the second displacement function $\mathcal{V}_2(X,T)$

$$\mathcal{V}_2(X,T) - r_2H^2/c_{v2}\,[(1-X)(T-T\,) - 2\Sigma_{n=\ \to\infty}\,\sin(\pi nX)(1-\exp(-n^2\pi^2T-T_1))/\,n^3\pi^3] \qquad (A\ 6\ 3\ 13)$$

for $T_1<T<T_2$, and the function

$$\mathcal{V}_2(X;T) = r_2H^2/c_{v2}\,\{(1-X)(T_2-T_1) - 2\Sigma_{n\ 1\to\infty}\sin(\pi nX)[\exp(-n^2\pi^2(T-T_2))$$
$$-\exp(-n^2\pi^2(T-T_1))]\,/\,n^3\pi^3\} \qquad (A.6.3.14)$$

for $T>T_2$.

The displacement at any time T in the interval T_1-T_2 is given by the sum of the displacement functions $\mathcal{V}_1$ (eq A.6.3.12) and $\mathcal{V}_2$ (eq.A.6.3.13) both calculated in T, with an approximation which is later discussed. In fact, the strain function generated in the first interval $\mathcal{V}_1$ gives rise to a displacement contribution at T higher than T_1, which is expressed by eq.(A 6 3 12).

Thus, the general expression of the displacement $\mathcal{V}$ for any $T=T_i$ will be :

$$\mathcal{V}(X;T_i) = \int_0^{\tau_1} \mathcal{V}(X,T-\tau)\,\partial V/\partial T\,d\tau + \int_{\tau_1}^{\tau_2} \mathcal{V}(X;T-\tau)\,\partial V/\partial T\,d\tau + \ldots\ \ldots\ldots$$
$$\ldots\ldots + \int_{\tau_{i-1}}^{\tau_i} \mathcal{V}(X;T-\tau)\,\partial V/\partial T\,d\tau \qquad (A\ 6\ 3.15)$$

in which the values of c_v and r used in the different time intervals are different Eq (A 6.3 15) becomes :

$$\mathcal{V}(X;T_i) = [(r_1H^2/c_{v1})T_1 + (r_2H^2/c_{v2})(T_2-T_1) + (r_3H^2/c_{v3})(T_3-T_2) + \ldots(r_iH^2/c_{vi})(T_i-T_{i-1})](1-X) -$$

$$- (r_iH^2/c_{vi})\,2\Sigma_{n\ 1\to\infty}\,\sin(\pi nX)/n^3\pi^3 + (r_1H^2/c_{v1})\,2\Sigma_{n\ 1\to\infty}\,\sin(\pi nX)\,\exp(-n^2\pi^2T_1)/\,n^3\pi^3 -$$

$$- \ [2\Sigma_{n=1\to\infty}\sin(\pi nX)\exp(-n^2\pi^2(T-T_1)/n^3\pi^3]\,(r_1H^2/c_{v1}-r_2H^2\,c_{v2}) \ - \qquad (A.6\ 3.16)$$

$$- \ [2\Sigma_{n=1\to\infty}\sin(\pi nX)\exp(-n^2\pi^2(T_1-T_2)/n^3\pi^3]\,(r_2H^2/c_{v2}-r_3H^2/c_{v3}) \ - \ldots\ldots\ldots$$

$$. \ - \ [2\Sigma_{n=1\to\infty}\sin(\pi nX)\exp(-n^2\pi^2(T_i-T_{i-1})/n^3\pi^3]\,(r_{i-1}H^2/c_{vi-1}-r_iH^2/c_{vi})$$

In this solution of the consolidation problem c_v and r have been assumed to be constant only in the integration of eq (A.6 3.4) in the intervals T_{i-1}-T_i (see Fig. A.6.3.2 (b)). Thus the integration

still bears an error because, where the assumption of c_{vi} and r_i constant in the relative time interval causes a negligible error that tends to zero with the decreasing size of the time interval, for T higher than T_i the displacement function $\mathcal{V}_i$ is derived assuming c_v and r still equal to c_{vi} and r_i. The error associated with this approximation is nonetheless thought to be smaller than that associated with the integration from Wissa et al (1971) of eq (A.6 3 4) which assumes c_v and r constant for any T over the whole interval (0;T).

Equation (A.6.3.16) is still based on the Wissa's other assumptions, including c_v constant down the specimen and small strains. The first of these two assumptions is acceptable if the ratio between the excess base pore water pressure u_b and the vertical stress (u_b/σ_v) is kept below about 5% during testing (Wissa et al.1971).

The accuracy of the solution here proposed (eq.A.6.3.16) increases the smaller the time intervals T_{i-1}-T_i. For small time intervals, the components of eq (A.6 3 16) :

$$[2\Sigma_{n=1\to\infty}\sin(\pi nX)\exp(-n^2\pi^2(T_i-T_{i-1}) / n^3\pi^3] \quad (r_{i-1}H^2/c_{vi-1} - r_iH^2/c_{vi}) \qquad \text{(A.6.3.17)}$$

are close to zero and the equation can be simplified to give

$$\mathcal{V}(X;T_i) = H^2 [(r_1/c_{v1})T_1 + (r_2/c_{v2})(T_2-T_1) + (r_3/c_{v3})(T_3-T_2) +....(r_i/c_{vi})(T-T_{i-1})] \quad (1-X) -$$
$$- (r_iH^2/c_{vi})\, 2\Sigma_{n=1\to\infty} \sin(\pi nX)/n^3\pi^3 + (r_1H^2/c_{v1})\, 2\Sigma_{n=1\to\infty} \sin(\pi nX) \exp(-n^2\pi^2T_i)/ n^3\pi^3 \quad \text{(A.6.3.18)}$$

The gradient with respect to X of the displacement in eq (A 6.3.18) gives the strains as follows:

$$\varepsilon_v (X;T)= H^2 [(r_1/c_{v1})T_1 + (r_2/c_{v2})(T_2-T_1) + (r_3/c_{v3})(T_3-T_2) +... (ri/c_{vi})(T-T_{i-})] +$$
$$+ (r_iH^2/(6c_{vi})) (3X^2-6X+2) - (r_1H^2/c_{v1})\, 2\Sigma_{n=1\to\infty} \cos(\pi nX) \exp(-n^2\pi^2T)/ n^2\pi^2 \qquad \text{(A.6.3.19)}$$

This equation, which can be compared to Wissa's eq (A 6 3 6), can be applied in tests where both c_v and r change with time When the time dependent strain component ε_i^*:

$$\varepsilon_i^* = - (r_1H^2/c_v)\, 2\Sigma_{n=1\to\infty} \cos(\pi nX) \exp(-n^2\pi^2T_i)/ n^2\pi^2 \qquad \text{(A 6 3 20)}$$

becomes negligible the steady state solution of the consolidation problem can be applied, which is

$$\varepsilon_v(X;T_i)= H^2 [(r_1/c_{v1})T_1 + (r_2/c_{v2})(T_2-T_1)+(r_3/c_{v3})(T_3-T_2)+...(ri/c_{vi})(T_i-T_{i-1})] +$$
$$+ (r_iH^2/(6c_{vi})) (3X^2-6X+2) = \Delta H(t_i)/H_0 + (r/6c_v) H^2(3X^2-6X+2) \qquad (A.6.3.21)$$

where r and c_v are the current ones at time $t = t_i$

Both equations (A 6.3.19) and (A.6.3.21) were used to process the test data to give the results in Chapter 6. In particular, for all the tests the steady state solution could be applied because the strain component ε^*_t was always found to be negligible

For the steady state solution, $\varepsilon_v(z;t)$ varies parabolically with z as for the steady solution from Wissa et al.(1971). The formula for the average vertical strain ε_{av} is:

$$\varepsilon_{av} = \Delta H(t)/H = \Sigma_{n=1\rightarrow i}\, r_n\, (t_n - t_{n-1}) \qquad (A\ 6.3.22)$$

and assuming a linear behaviour of the soil in the strain interval defined by the strains at the top and the base of the soil specimen at time t.

$$\Delta\varepsilon_{v\ TOP\text{-}BASE} = rH^2/(2c_v) \qquad (A\ 6\ 3.23)$$

the average vertical stress σ'_{av} is as follows :

$$\sigma'_{av} = \sigma_v - 2u_b/3 \qquad (A\ 6.3\ 24)$$

From eqs.(A.6.3.22) and (A.6.3.24) the average coefficient of oedometric deformability $m_v(t)$ is derived as follows:

$$m_v = \Delta\varepsilon_{av}/\Delta\sigma'_{av} \qquad (A\ 6\ 3\ 25)$$

From eq (A.6.3.23) the expression for the permeability coefficient k(t) can be derived

$$k = rH^2\gamma_w/(2u_b) \qquad (A\ 6\ 3\ 26)$$

From eq A 6 3 25 and A.6.3 26 the coefficient of consolidation c_v can be obtained

$$c_v = k/(m_v\gamma_w) = \Delta\sigma'_{av}\, H^2\ (2\Delta t\, u_b) \qquad (A\ 6\ 3\ 27)$$

The equations A.6.3.22-A.6.3.27 are slightly different from those proposed by Wissa et al.(1971) (eq.A.6.3.10). In Chapter 6, the test results obtained with the procedure proposed here and with Wissa's solution are compared. When Wissa's solution can be applied without significant difference with the here proposed procedure, its error is smaller than the one initially assumed for it.

The equations A.6.3.22-A.6.3.27 are consistent with those reported by Janbu and Senneset (1979) and Janbu et al.(1981) for continuous loading compressions. Janbu and Senneset (1979) proposed the inclusion of some correction factors in equations A.6.3.23-A.6.3.27 when the pressure-load ratio $du_b/d\sigma_v$ is high. The formula proposed by Janbu and Senneset are the following:

$$\sigma'_{sv} = \sigma_v - \alpha_m u_b \qquad \text{(A.6.3.28)}$$

$$M = (d\sigma'_v/dt - \alpha_m du_b/dt)\, H/(dH/dt) \qquad \text{(A.6.3.29)}$$

$$c_v = \alpha_c\, (d\sigma'_{sv}/dt)\; H^2/\,(2u_b) \qquad \text{(A.6.3.30)}$$

In Fig.A.6.3.3 α_m and α_c are plotted against the pressure-load ratio. The correction factors from Janbu and Senneset were applied to the test data when required, as explained in Chapter 6.

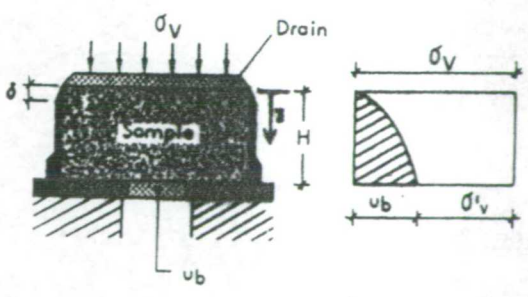

Fig.A.6.3.1. Pore water pressures in the oedometer specimen.

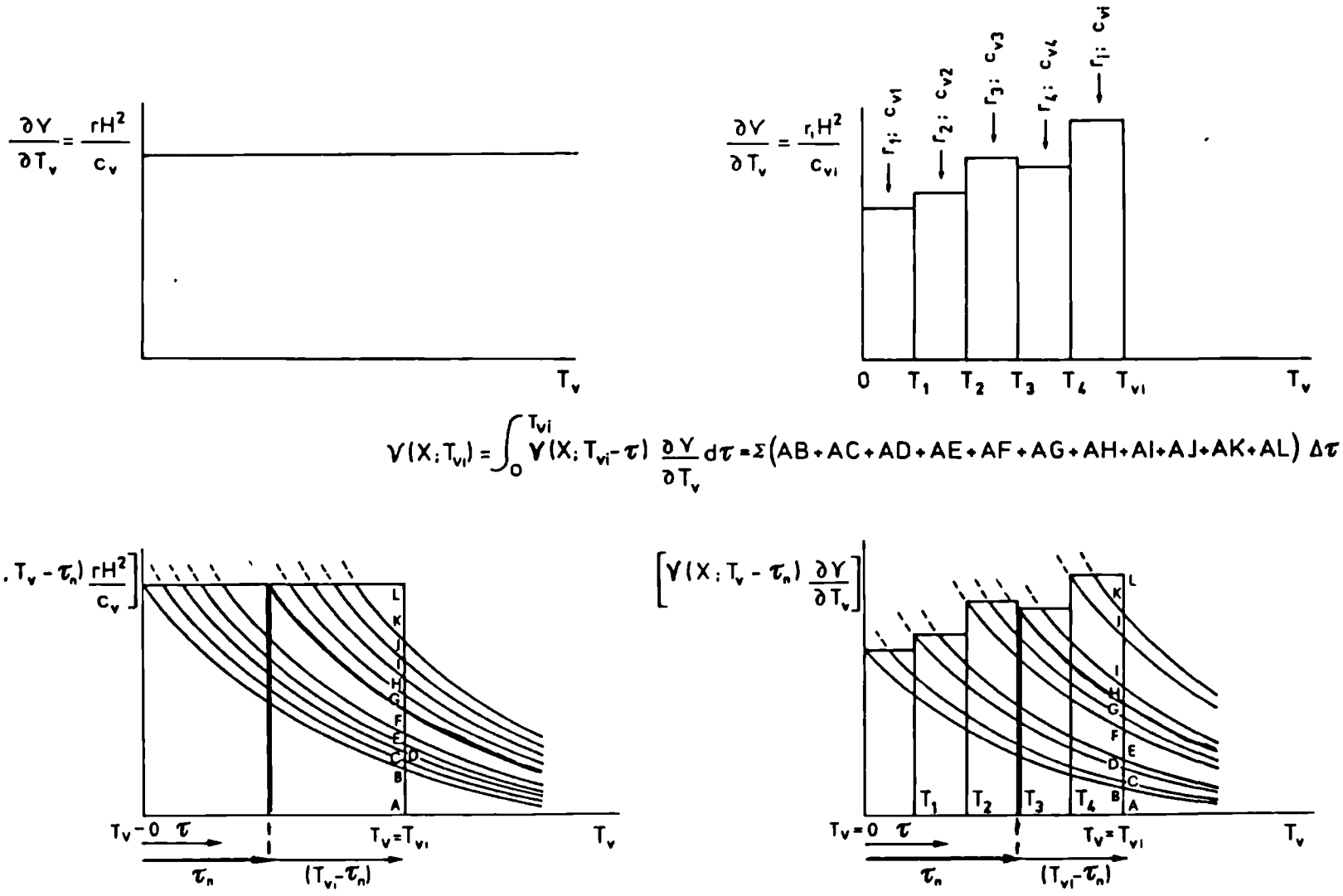

Fig A.6 3.2. Integration of the CRS consolidation integral (A 6.3.4) : (a) integration proposed by

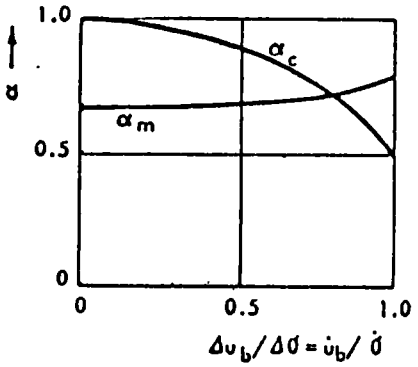

Fig.A.6.3.3. Correction factors α_m and α_c proposed by Janbu and Senneset (1979).